Opening ceremony, IUS Awards, and Plenary Talk

CONGRESS HALL

Monday, July 22 2013, 08:30 am - 10:00 am

Plenary I-1

Cancer and the Acoustic Bubble

Peter Burns[1]; [1]*University of Toronto, Toronto, ON, Canada*

Background, Motivation and Objective
Statement of Contribution/Methods
Results/Discussion

Tissue Engineering, neurostimulation and drug delivery

CONGRESS HALL

Monday, July 22 2013, 10:30 am - 12:00 pm

Congress Hallair: **Christopher Hall**
Philips Research North America

IUS1-A1-1

Engineering of Tissues with Ultrasound

Denise Hocking[1,2], Diane Dalecki[2,3]; [1]*Department of Pharmacology and Physiology, University of Rochester, USA,* [2]*Rochester Center for Biomedical Ultrasound, University of Rochester, Rochester, NY, USA,* [3]*Department of Biomedical Engineering, University of Rochester, Rochester, NY, USA*

Background, Motivation and Objective

Developing new technologies that enable the repair or replacement of diseased or injured tissues and organs is a major focus of tissue engineering. The successful production of complex tissues requires recreating the biologically-active extracellular environment that stimulates tissue assembly. Recent advances in the field of tissue engineering include the engineering of skin, cartilage, and bladder, all of which are relatively thin tissues that can rely on diffusion for the delivery of oxygen and nutrients. The development of more complex tissues has been limited by the need for techniques that can rapidly organize cells and proteins within large three-dimensional scaffolds, and the need to create vascular networks within tissues to maintain viability and function.

Statement of Contribution/Methods

To address these challenges, we are developing ultrasound-based technologies to spatially organize cells and extracellular matrix proteins within tissue-engineered constructs. One of these technologies takes advantage of the acoustic radiation forces associated with ultrasound standing wave fields to spatially pattern cells within collagen-based hydrogels. A second technology uses ultrasound to noninvasively control the microstructure of collagen within engineered tissues.

Results/Discussion

Ultrasound standing wave field-induced spatial patterning of endothelial cells leads to extracellular matrix collagen remodeling and the rapid formation of a vascular network throughout the volume of the three-dimensional hydrogel. Using this technology, the spatial patterning of cells can be controlled noninvasively through proper design of the ultrasound field. By changing the initial density of the cell bands during hydrogel formation, the technology can produce vascular networks having two distinct morphologies – one that resembles peripheral vascular networks (i.e. arterioles and venules) and one that more closely resembles capillaries. Investigations also demonstrate the capability of ultrasound to spatially pattern various collagen microstructures within engineered tissue noninvasively, via a thermal mechanism. These changes in collagen microstructure were produced using both ultrasound standing wave fields and traveling wave fields. Thus, ultrasound technologies can be used to enhance the level of complexity of extracellular matrix microenvironments and cellular functions achievable within three-dimensional engineered tissues.

IUS1-A1-2

Localization of Ultrasound Induced In Vivo Neurostimulation in the Mouse Model

Randy King[1], **Julian Brown**[2], Kim Butts Pauly[3]; [1]*Bioengineering, Stanford University, Stanford, CA, USA,* [2]*Neurobiology, Stanford University, Stanford, CA, USA,* [3]*Radiology/Bioengineering, Stanford University, USA*

Background, Motivation and Objective

Developments in the use of ultrasound to stimulate neural activity have raised the possibility of using ultrasound as a new investigative and therapeutic tool in brain research. Until now there has been little evidence demonstrating a clearly localized effect in the brain. Here we report distinguishable effects in sonicating rostral and caudal regions of the motor cortex.

Statement of Contribution/Methods

A total of ten CBL-7 mice were employed in this study, in which two EMG electrodes were placed approximately 2-3 mm apart, into the base of the tail and in the neck region, in order to record the bioelectric potential difference across the muscle tissue. The ultrasound was generated by a single element, focused transducer with a center frequency of 500 kHz. A coupling column was fitted to the transducer and filled with degassed water. Ultrasound gel was used to couple the end of the transducer column to the head of the animal. The transducer was fixed to a three-axis positioning system. For all experiments the transducer was positioned 2mm from the surface of the animal's head which allowed free movement of the transducer over the animal's head.

Results/Discussion

Motor responses, measured by normalized EMG (Fig. 1) in the neck and tail regions, changed significantly when sonicating the different areas of motor cortex. Response latencies varied significantly according to sonication location (Fig. 2) suggesting that different neural circuits were activated depending on the precise focus of the ultrasound beam. Our findings present good evidence for being able to target selective parts of the motor cortex with ultrasound neurostimulation in the mouse, a step that should set the stage for developing new applications in larger animal models including humans.

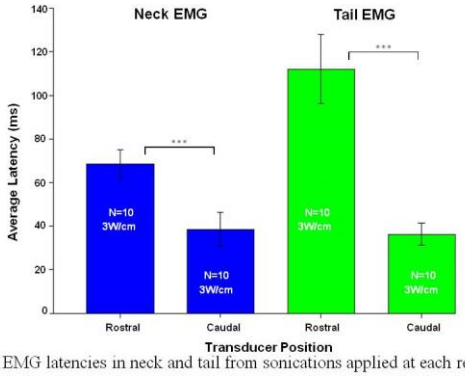

Figure 2: EMG latencies in neck and tail from sonications applied at each region of the brain. Latencies were larger when the transducer was in the rostral position compared to the caudal posterior. This was true for both signals from the neck and tail EMGs. The difference was statistically significant. The error bars represent the standard error. (*** p-value < 0.01)

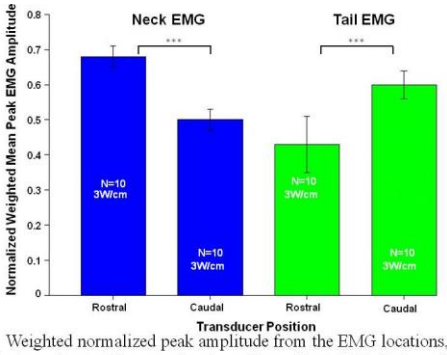

Figure 1: Weighted normalized peak amplitude from the EMG locations, neck and tail, with the transducer at the rostral and caudal positions. With the transducer at the rostral region of the head, the neck EMG had a higher average normalized peak amplitude than the caudal region. When sonicating the caudal position, the EMG amplitude in the tail was larger. The difference was statistically significant (*** p-value < 0.01). Error bars represent the standard error.

IUS1-A1-3

Transcranial ultrasound neuromodulation of the contralateral visual field in awake monkey.

Youliana Younan[1], **Thomas Deffieux[1]**, Nicolas Wattiez[2], Mickael Tanter[1], Pierre Pouget[2], Jean-Francois Aubry[1]; *[1]Institut Langevin, ESPCI ParisTech, CNRS UMR7587, INSERM U979, France, [2]Insitute of Brain and Spinal Cord, UMRS 975 INSERM, CNRS 7225, UMPC, Paris, France*

Background, Motivation and Objective

In this work, we investigated the effect of low intensity pulsed focused ultrasound in the brain of two awake Maccaca Mulatta monkeys using the antisaccade (AS) paradigm. The objective of the study was to determine if transcranial ultrasound has an effect on behavioural tasks in awake animal involving a specific brain structure.

Statement of Contribution/Methods

Two Maccaca Mulatta monkeys (Y and L) were trained to perform antisaccade (AS) movements where they initially have to fix a central stimulus on a screen and then refrain from looking at an appearing peripheral target but instead initiate as soon as possible a saccade towards the opposite direction. The eye movements are tracked using an infra-red eye tracker (Eyelink 1k, SR-Research, Ontario, Canada) and then analyzed to estimate the antisaccade latencies.

In order to investigate the effect of low intensity focused ultrasound, a continuous 100 ms sonication pulse (derated pressure estimated at 0.35 ± 0.05 MPa, ISPTA 13.46 ± 3.78 mW/cm2) was focused at the frontal eye field (identified according to stereotaxic coordinates) using a 320 kHz transducer (H115, Sonic Concept, Bothell, WA, USA).

In a series of 23 independent experiments, animals performed 3 blocks of AS training per session: a baseline 100 trials block of AS (50 left/50 right); a 400 trials block composed of 360 trials without focused ultrasound (180 for each side) and 40 trials with focused ultrasound (20 for each side); a last block of 100 trials, as post-test.

Results/Discussion

Ipsilateral mean AS latencies with ultrasound stimulation were significantly (t-test ;monkey Y: p=.0345, monkey L: p= .0311) increased compared to the non-stimulation condition (monkey Y: +14ms; monkey L: +15 ms). This effect is consistent with previous findings of transcranial magnetic stimulation studies of the frontal eye field of non human primates[1].

The study demonstrates the feasibility of using focused ultrasound to causally modulate behaviour in awake non-human primate brain. Focused ultrasound neurostimulation could potentially lead to a new noninvasive neurostimulation tool with a better resolution and a larger volume of targeting than transcranial magnetic stimulation.

[1] *Frontal non-invasive neurostimulation modulates antisaccade preparation in non-human primates*. Valero-Cabre A, Wattiez N, Monfort M, François C, Rivaud-Péchoux S, Gaymard B, Pouget P. PLoS One. 2012;7(6), p. e38674.

IUS1-A1-4

Evaluation of a rabbit carotid artery model for dissolving clots using pulsed focused ultrasound and rtPA under MRI monitoring.

Christakis Damianou[1,2], Venediktos HadjiSavvas[1], Nicos Mylonas[3], Kleanthis Ioannides[4]; *[1]MEDSONIC LTD, Cyprus, [2]Cyprus University of Technology, Cyprus, [3]Frederick University, Cyprus, [4]Polikliniki Igia, Cyprus*

Background, Motivation and Objective

The potential of using focused ultrasound combined with the thrombolytic drug recombinant tissue plasminogen activator (rt-PA) under magnetic resonance angiography (MRA), to dissolve clots in the carotid of a New Zealand rabbit in vivo is evaluated.

Statement of Contribution/Methods

A spherically-focused transducers of 5 cm diameter; focusing at 10 cm and operating at 1 MHz was used. The transducer was placed inside a custom made plastic holder which is coupled to the. A pulsed ultrasound protocol was used that maintains a tissue temperature increase of less than 1ºC in the clot (called safe temperature). The temperature was acquired using a thermocouple which is placed near the clot.

Results/Discussion

Different animal models were evaluated, and it was concluded that the carotid model is the best because it is easily accessible to ultrasound and it is sufficiently visible to MRI using MRA. Initially the artery was opened using rt-PA alone. With rt-PA alone 50 % of the artery was opened in about 120 mins. It was found that the time needed for opening 50 % of the artery using rt_PA and Focused ultrasound was decreased with acoustic intensity. With an intensity (20 W/cm2 SATA) that is not causing artery heating (less than 1ºC) the time needed to open 50% of the artery is 50 mins. The proposed protocol was monitored using Magnetic Resonance Angiography (MRA) every 1 min. Transducer registration was achieved using MRI visible marking on the transducer holder.

Focused ultrasound has the potentials to dissolve clots that are injected in the carotid of rabbits in vivo. The procedure is safe because with the protocols used the artery temperature was less than 1 oC. With focused ultrasound the time needed to open the artery is decreased. MRA clearly shows the opening of the artery. The acquisition of MRA is slow (1 min) but since the procedure takes close to 50 mins this is not causing any problem.

IUS1-A1-5

Delivery of Zoledronate is Highly Improved by Low Intensity Continuous Ultrasound in a Breast Cancer Bone Metastases Model

Sophie Tardoski[1,2], Jacqueline Ngo[2], Philippe Clézardin[2], David Melodelima[3]; *[1]INSERM U1032, LabTau, Lyon, Rhône-Alpes, France, [2]INSERM U1033, France, [3]INSERM U1032, LabTau, Rhône-Alpes, France*

Background, Motivation and Objective

Bone metastases occur in 70% of advanced breast cancer. Zoledronate (ZOL) acts as an inhibitor of osteoclasts-mediated bone resorption. Antitumoral effects of ZOL have been described only in vitro at high doses, incompatible with a clinical use. Here we report the feasibility of using low intensity continuous ultrasound (C-US) to enhance the delivery of ZOL in tumor cells in an in vivo model.

Statement of Contribution/Methods

First, in vitro experiments were performed in order to measure the penetration of ZOL into tumor cells by mass spectrometry. Then, 69 mice bearing breast cancer bone metastases were randomized into 5 groups for an in vivo study. A single dose of ZOL was combined with a daily application of low intensity C-US. This dose of ZOL was calculated equivalent to the 4-mg clinical dose. A transducer working at a frequency of 2.9 MHz was used. The free field acoustic power was 7 watts applied for 30 minutes to produce thermal effects in bone tumors. US treatments were performed each day for fifteen days. Efficacy of treatments was measured by radiography (area of the osteolytic lesions), histomorphometry (Tumor Burden/Soft Tissue Volume: TB/STV) and immunohistochemistry.

Results/Discussion

In vitro, mechanical effects of US and generated-hyperthermia enhance the penetration of ZOL of at least 3 times compared with no US. In vivo, it was found that US alone did not have any inhibitory effect on bone destruction (7.4±2.7 mm^2) when compared to vehicle-treated animals (6.6±1.6 mm^2, p=0.65). A statistically significant decrease of bone destruction and skeletal tumor burden was found in mice that received a daily treatment of continuous US with ZOL (1.3±0.4 mm2, TB/STV=11%) compared with vehicle (6.6±1.6, TB/STV=62%) and, more importantly, with ZOL alone (TB/STV=46%). Tumor cells proliferation was decreased by 70% in animal who received ZOL and daily US. In this group, angiogenesis was reduced by 75% compared to ZOL alone. US exposure conditions have not created cavitation. The temperature in tumors was 42±2,8°C during US treatment. No lesions were observed in surrounding tissues.

Low intensity continuous ultrasound in combination with a single dose of ZOL decrease bone osteolysis and tumor burden, supporting by a significant decrease of proliferation of tumor cells and angiogenesis. US enhance membrane cell permeability and acoustic radiation force as well as the bioavailability of ZOL for tumor cells. Importantly, clinical doses of ZOL and US were used, suggesting that clinical application of such therapy is possible.

Clinical applications of elasticity imaging

M4

Monday, July 22 2013, 10:30 am - 12:00 pm

Congress Hallair: **Kathy Nightingale**
Duke University

IUS1-A2-1

Shear wave quantitative elasticity of the cervix during pregnancy

Marie Muller[1], Dora AitBelkacem[1], Mahdieh Hessabi[2], Jean-Luc Gennisson[1], Mathias Fink[1], Dominique Cabrol[2], Mickaël Tanter[1], Vassilis Tsatsaris[2]; *[1]Institut Langevin, CNRS, ESPCI, INSERM, Université Paris Diderot, Paris, France, [2]Maternité Port-Royal, hôpital Cochin, APHP, Université Paris-Descartes, Fondation PremUP, Paris, France*

Background, Motivation and Objective

The quantitative and objective assessment of cervical stiffness has great potential for the estimation of preterm delivery risk, as well as for the prediction of the success of labor induction. Various methods can be used in vivo for cervical assessment such as vaginal digital examination or static elastography but to our knowledge, none of them can provide a quantitative, absolute and independent evaluation of cervical stiffness in vivo. In this study, such values were obtained in pregnant patients in vivo by using dynamic Shear Wave Elastography (SWE).

The objectives of this study were: i) to assess the range of normal elasticity values throughout the pregnancy, ii) to evaluate the intra and inter-operator reproducibility of the measurement and iii) to evaluate the potential of SWE for the discrimination of pre-term delivery threat.

Statement of Contribution/Methods

In SWE, radiation force is used to generate shear waves locally within tissue. Shear wave propagation is then followed using an ultrafast ultrasound scanner (5000 frames/s, Aixplorer, Supersonic Imagine, France), and a time-of-flight algorithm is applied to retrieve shear wave displacement, and shear modulus. In this study, stiffness of the lower anterior part of the cervix was quantified over a 8 mm diameter region of interest, during vaginal ultrasound examination in 63 pregnant women.

Results/Discussion

These are the preliminary results of a prospective study. The elastic modulus of the cervix was found to decrease significantly throughout the pregnancy. Among all patients, cervical stiffness varied from 11.75 kPa +/- 3.81 kPa at the end of the first trimester (12 to 14 weeks of gestational age (GA)) to 6.03 kPa +/- 1.15 at the end of the third trimester (38 to 41 weeks of GA). The difference between stiffness values measured with the first trimester and the third trimester populations was statistically significant ($p<0.001$). For patients diagnosed with preterm labor, stiffness values measured during the second trimester were found around 6.73 kPa +/- 1.27 kPa, significantly lower than the values measured in normal patients in the second trimester ($p<0.005$).

This study provides for the first time a database for absolute elastic modulus values of the cervix throughout the pregnancy. Stiffness was observed to decrease with GA, which is consistent with the results previously obtained using a cervicotonometer (1). Cervical stiffness is reduced in patients with preterm labor threat. Further studies are needed to evaluate the interest of this technique in clinical practice.

1: Cabrol D. Cervical distensibility changes in pregnancy, term, and preterm labor. Semin Perinatol. 1991 Apr;15(2):133-9.

Funding sources : PremUp Foundation, Région Ile de France

IUS1-A2-2

Correlation between the shear wave speed in tendon and its elasticity properties

Chia-Lun Yeh[1], Po-Ling Kuo[1], Pai-Chi Li[2]; *[1]BEBI, National Taiwan University, Taiwan, [2]Electrical Engineering, National Taiwan University, Taipei, Taiwan*

Background, Motivation and Objective

Tendon problems are commonly seen. Although ultrasound imaging can be used for clinical diagnosis, only structural changes can be monitored and the ability to differentiate the pathological state is limited. On the other hand, tendon mechanical properties have been considered the gold standard in evaluating tendon functions. Therefore, noninvasive assessment of mechanical properties of tendon is of particular interest in rehabilitation medicine. The relationship between the shear wave speed and elasticity is complicated in tendon due to the anisotropy from the organization of collagen fiber network. In this study, correlation between the changes of shear wave speed and alteration of elastic properties under different degree of loading are investigated both in normal and diseased models. The long term objective of this research is to replace the invasive elasticity measurement by using shear wave elasticity imaging of tendon.

Statement of Contribution/Methods

By using a motor with a linear stage and a load cell, elastic properties of normal and diseased tendon under different degrees of loading are directly derived based on fitting the slope of stress-strain curve. The collagenase enzyme is used to develop the diseased model. A fully programmable array imaging system with a linear transducer of 5MHz is utilized to measure the shear wave speed at the same loading condition. The trend between the shear wave speed and elastic properties in different degrees of loading are analyzed.

Results/Discussion

Results of elasticity measurement under different degrees of loading (figure A) are highly correlated with the shear wave speed (figure B) in both normal and diseased models. Comparisons of results in normal and diseased models are shown in figure C and figure D, respectively. The correlation coefficients between the wave speed and elastic modulus in normal and diseased models are 0.98 and 0.99, respectively. It is shown that the change of elasticity properties under different degrees of loading can be measured by shear wave propagation speeds. Based on the results, the changes of shear wave speed in tendon have the potential to be used to represent the real elastic property changes. Our findings may provide a new strategy for tendon function investigation in clinical practice.

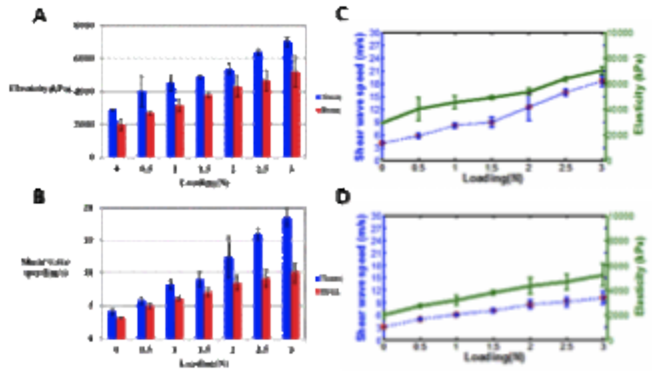

Figure (A) Elastic modulus and (B) shear wave speed under different loadings (C) Shear wave speed (blue) and elastic modulus (green) of (C) normal and (D) diseased tendons

IUS1-A2-3

How the measurement depth influences the liver stiffness assessment using shear wave elasticity imaging (SWE)

Congzhi Wang[1], Jian Zheng[2], Jie Zeng[2], Zeping Huang[2], Rongqin Zheng[2], Hairong Zheng[1]; *[1]Institute of Biomedical and Health Engineering, Shenzhen Institutes of Advanced Technology, Shenzhen, Guangdong, China, People's Republic of, [2]The Third Affiliated Hospital of Sun Yat-sen University, Guangzhou, Guangdong, China, People's Republic of*

Background, Motivation and Objective

Many techniques have been used to evaluate the elastic properties of tissues. The reliable measurement procedure of transient elastography (TE) and acoustic radiation force impulse imaging (ARFI) have been reported in previous studies, which provide important references for the clinical practice. However, to the best of our knowledge, the reliable measurement procedure of real time shear wave elasticity imaging (SWE) technique was still not studied systematically. The purpose of this study was to evaluate the influence of measurement depth on liver stiffness assessment with SWE and to find a reliable measurement depth for performing tissue quantification on liver.

Statement of Contribution/Methods

Measurements were performed on a standard elasticity phantom and livers of 88 healthy volunteers using a commercial SWE device (Aixplorer system, SuperSonic Imagine). In phantom study, the measurement depth from the probe surface was set to be from 0-1 cm to 8-9 cm (totally 9 levels) and at each level measurements were repeated 10 times. In human study, the measurement depth was also set to be 1 cm interval, and 5 measurements were repeated at each depth from 2-3 cm to 7-8 cm (totally 6 levels). The measurement success rates (SR) and the coefficients of variation (CV) of repeated measurements at different depths were calculated and the results were studied statistically using SPSS.

Results/Discussion

In phantom study, the SRs were all 100% from 0-1 cm to 7-8 cm depth. However, at the depth larger than 8 cm the SR was 0. The CV was larger at 0-1 cm depth (9.8%) than at the other depths (from 0.6% to 3.8%). For healthy subjects, the SRs at the depth from 3-4 cm to 6-7 cm were higher than at the other depths. The shear modulus of liver and the CVs at different depths were found to have statistically significant differences (P <0.001). The shear modulus was significantly larger at 6-7 cm and 7-8 cm depths than at the other depths. And the CVs at the depth from 2-3 cm to 4-5cm were significantly lower than at the other depths. According to our results, the most reliable depths of liver stiffness assessment using SWE technology were 3-4 cm and 4-5 cm, which had the highest SR and the lowest CVs. This could be a reference in clinical applications for getting more reliable results using SWE device on liver.

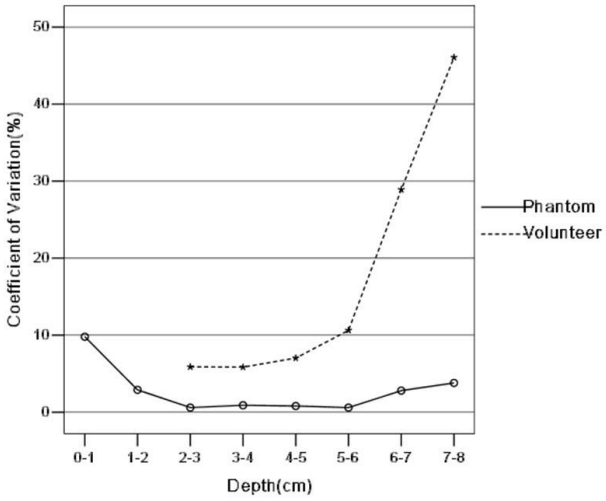

IUS1-A2-4

Assessing liver fat fraction by ARFI induced shear wave attenuation: a preliminary result

Liexiang Fan[1], John Benson[1], Lisa Clark[2], Jessica Lam[2], Abdullah Al Turki[2], Cesar Patino-Ochoa[2], Claude Sirlin[2]; *[1]Ultrasound, Siemens Healthcare, Issaquah, WA, USA, [2]Liver Imaging Group, Dept. of Radiology, University of California San Diego, San Diego, CA, USA*

Background, Motivation and Objective

Nonalcoholic fatty liver disease (NAFLD), the most common liver disease in American adults and children, is characterized by excess hepatic fat accumulation as well as hepatic fibrosis. MRI accurately measures the proton density fat fraction (PDFF) as a biomarker of hepatic fat content, but MRI is not widely available. AN US-based technique to quantify liver fat would advance clinical care. This study investigated the correlation in human liver in vivo between acoustic radiation force impulse (ARFI) induced shear wave propagation parameters and MRI PDFF.

Statement of Contribution/Methods

10 human adult subjects spanning a wide range of hepatic fat content were enrolled in this pilot study under IRB at University of California San Diego. Each subject underwent an MRI and ultrasound scan on the same day. Hepatic PDFF was measured using a 3T MRI scanner. Shear wave propagation data were obtained using Siemens Acuson S3000 Virtual Touch Quantification (VTQ) feature with the 6C1HD abdomen transducer. In the 10 subjects, PDFF measurements ranged from 4.1% to 28.8% and VTQ shear velocities from 0.64 to 1.55m/s. Offline processing was conducted on the collected shear wave displacement data in a region of interest (ROI) of 10 mm tall and 5mm wide. The time duration and sampling rate of the displacement data was 12 milliseconds and 4.8 kHz. After the displacement was averaged over the ROI height dimension, the shear wave magnitude (peak value) and the shear wave center frequency and bandwidth at multiple locations along the propagation direction were calculated. The attenuation slope and intercept of magnitudes and the median values of center frequencies and bandwiths were calculated in each ROI. To obtain shear wave dispersion, a filter bank with 10 center frequencies evenly distributed in the range from 50 to 275 was applied to the shear wave displacement data. Shear velocity was estimated for each filtered narrow band shear wave and the dispersion slope obtained. For the 10 subjects, shear wave parameters were then correlated to MRI-PDFF.

Results/Discussion

Significant correlations were found between the MRI-PDFF and the shear wave magnitude attenuation slope and intercepts ($r = 0.83$, $p < 0.003$; and $r = 0.85$, $p < 0.002$) and between MRI-PDFF and shear wave bandwidth ($r = 0.75$, $p < 0.01$). The correlation between shear wave center frequency and velocity dispersion was weak ($r = 0.17$, $p<0.63$; and $r = 0.39$, $p<0.26$) in the small number of subjects enrolled in this study.

This pilot study shows proof of concept that shear wave attenuation can objectively quantify fat content in liver. Future study will be to test these variables in subjects with liver biopsy, so that the fat content and the fibrosis content can be quantified and correlated with both the attenuation and shear velocity. It may be possible to combine the shear velocity and the attenuation to predict both fat and fibrosis degree in liver using US technology.

IUS1-A2-5

Material Characterization of In Vivo and Ex Vivo Porcine Brain using Shear Wave Elasticity

Caryn Urbanczyk[1], Mark Palmeri[1], Cameron Dale Bass[1]; *[1]Duke University, Durham, NC, USA*

Background, Motivation and Objective

Shear Wave Elasticity Imaging (SWEI) quantifies material properties such as shear modulus by relating it to transverse wave propagation speed, estimated via time of flight based reconstruction. It has been used noninvasively in liver[1,2]. We use SWEI in brain (*in vivo, in situ, in vitro*), to study effects of environmental variables including intracranial pressure, temperature and confinement. Alteration of key properties provides modelers and scientists a more accurate *in vivo* picture and may be employed clinically as an indicator of pathology.

Statement of Contribution/Methods

Shear waves were generated, and IQ data in 4:1 parallel receive was collected with a Siemens ACUSON S2000 scanner and AcuNav 10F catheter transducer focused to 10mm, operating at 6.15MHz (F/# 1.4). Off-axis motion was tracked in a 10 x 4mm region of interest (ROI) for 4ms. Under isotropic, elastic assumptions, displacements were calculated with the Loupas phase shift estimator and shear wave speeds (SWS) were estimated with a RANSAC algorithm, which ignores erroneous motion by iteratively removing outlying data points. *In vivo* surgery was minimally invasive. The transducer was inserted through a drilled hole in the temporal skull, preserving the dura. Sagittal plane images were acquired in B-mode and SWEI. After euthanasia, *in situ* SWEI images were taken with the skull intact and then with the calvarium open. *In vitro* specimens were removed from the skull and placed in a saline bath at either 20°C or 37°C for imaging. *In situ* and *in vitro* measurements were used to discern boundary effects on tissue response and compare physiological and experimental states.

Results/Discussion

Shear modulus *in situ* and *in vitro* were 50% and 22% higher than *in vivo*, respectively ($p<0.01$), suggesting that confinement by the skull impacts nonlinear strain hardening. Varied temperature *in vitro*, yielded white matter shear moduli of 3.22±1.20kPa at 22°C and 2.63±.92kPa at 37°C ($p<0.05$), suggesting that to obtain biofidelic material properties in a lab setting, samples must be tested at body temperature. *In vivo* shear modulus did not show significant differences with changes in ICP from 5–40mmHg. Normalized *in vivo* shear modulus for all subjects was 3.06±.49kPa. This is comparable to published results in constrained livers[2].

1. Palmeri et al. Ultra Med Biol, 2008 34:4 546–58
2. Rotemberg et al. Phys Med Biol, 2012 57:2 329-42

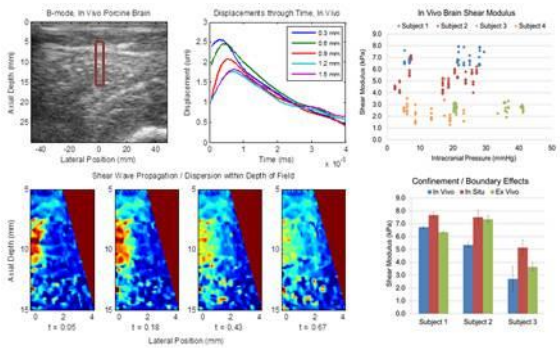

Identifying Malignant and Benign Breast Lesions Using Vibroelastography

Hani Eskandari[1], Septimiu Salcudean[1], Robert Rohling[1,2], Ali Baghani[1], Samuel Frew[1], Paula Gordon[3], Linda Warren[3]; [1]*Electrical and Computer Engineering, University of British Columbia, Vancouver, Canada,* [2]*Mechanical Engineering, University of British Columbia, Vancouver, Canada,* [3]*Faculty of Medicine, University of British Columbia, Vancouver, Canada*

Background, Motivation and Objective

Vibroelastography (VE) is a method for mapping tissue mechanical properties using a multifrequency shear wave approach. The method uses ultrasound to image steady-state motion within tissue while an actuator applies surface vibrations. In prior work, VE has been shown successful in reconstructing relative stiffness, absolute shear modulus and viscosity. In this paper we report for the first time, the efficacy of VE in differentiating between malignant and benign breast lesions.

Statement of Contribution/Methods

A total of 60 subjects with breast lesions have been tested. The study was approved by the Clinical Research Ethics Board and informed consent was collected from every subject. The VE system comprised an ultrasound machine (Ultrasonix Medical Corp.), a voice coil actuator, controller circuitry, a computer application to capture raw data and a program to compute and display real-time elasticity maps on the screen. In most cases, the applied vibration comprised a waveform with the following frequency components: 21, 42, 63, 84, 105 and 126Hz. Sampling of the tissue motion at higher frequencies was made possible using the bandpass sampling technique. The steady-state displacement profile in the underlying tissue was measured using a correlation-based motion tracking algorithm and absolute elasticity was reconstructed from the spatial wavelength of the displacements. The snap-on design of the actuator made it possible to seamlessly incorporate the VE exam into the clinical workflow. The subjects recruited had BIRADS scores of 3, 4 and 5. Elasticity images were shown in real-time on the screen while echo data was stored for offline VE analysis. After the VE exam, the subjects underwent core-needle biopsy. The pathology report was used as the ground truth to measure the efficacy of the VE technique.

Results/Discussion

An example VE image of a BIRADS 5 lesion with a biopsy-proven invasive ductal carcinoma (IDC) is shown below. The VE results indicate that both benign fibroadenoma (FA) and IDC result in the hardening of the tissue; however, IDC exhibits higher values of elasticity compared to a benign lesion which can be captured using absolute elasticity maps provided by VE. Statistical analysis performed on the first 7 subjects (3 IDC and 4 FA) show 100% sensitivity and 75% specificity for breast VE. A full statistical analysis of the results will be reported.

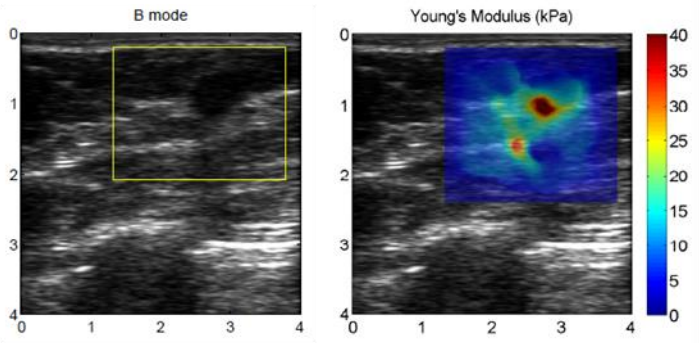

B-mode and elasticity images of an invasive ductal carcinoma.

Medical signal processing

M5

Monday, July 22 2013, 10:30 am - 12:00 pm

Congress Hallair: **Svetoslav Nikolov**
BK Medical Aps

IUS1-A3-1

Real time deconvolution of in-vivo ultrasound images

Jørgen Arendt Jensen[1]*; [1]Center for Fast Ultrasound Imaging, Dept. of Elec. Eng., Technical University of Denmark, Kgs. Lyngby, Denmark*

Background, Motivation and Objective

The axial resolution in medical ultrasound is directly linked to the emitted ultrasound frequency, which, due to tissue attenuation, is selected based on the depth of scanning. The resolution is determined by the transducers impulse response, which limits the attainable resolution to be between one or two wavelengths. This can be improved by deconvolution, which increase the bandwidth and equalizes the phase to increase resolution under the constraint of the electronic noise in the received signal.

Statement of Contribution/Methods

A fixed interval Kalman filter based deconvolution routine written in C is employed. It uses a state based model for the ultrasound pulse and can include a depth varying pulse and spatially varying signal-to-noise ration. An autoregressive moving average (ARMA) model of orders 8 and 9 is used for the pulse, and the ARMA parameters are determined as a function of depth using a minimum variance algorithm using averaging over several RF lines. In vivo data from a 3 MHz mechanically rotating probe is used and the received signal is sampled at 20 MHz and 12 bits. In-vivo data acquired from a 16th week old fetus is used along with a scan from the liver and right kidney of a 27 years old male.

Results/Discussion

The deconvolved image of the fetus is shown in the figure below on the right along with the original image on the left. The resolution is increased and the contrast is maintained or increased in the amniotic fluid surrounding the fetus and in the smaller black structures (vessels/cysts) to the right of the fetus. The axial resolution has been determined from the in-vivo liver image using the auto-covariance function. From the envelope of the estimated pulse the axial resolution at Full-Width-Half-Max is 0.581 mm corresponding to 1.13 λ at 3 MHz, which is typical for a high-resolution clinical system. The algorithm increases the resolution to 0.116 mm or 0.227 λ corresponding to factor of 5.1. The basic pulse can be estimated in roughly 0.176 seconds on a single CPU core on a Intel i5 CPU running at 1.8 GHz. An in-vivo image consisting of 100 lines of 1600 samples can be processed in roughly 0.1 seconds making it possible to perform real-time deconvolution on ultrasound data by using dual or quad core CPUs for frame-rates of 20-40 Hz. The C implementation can thus attain real-time processing of images for an increased resolution without affecting the perceived contrast and noise.

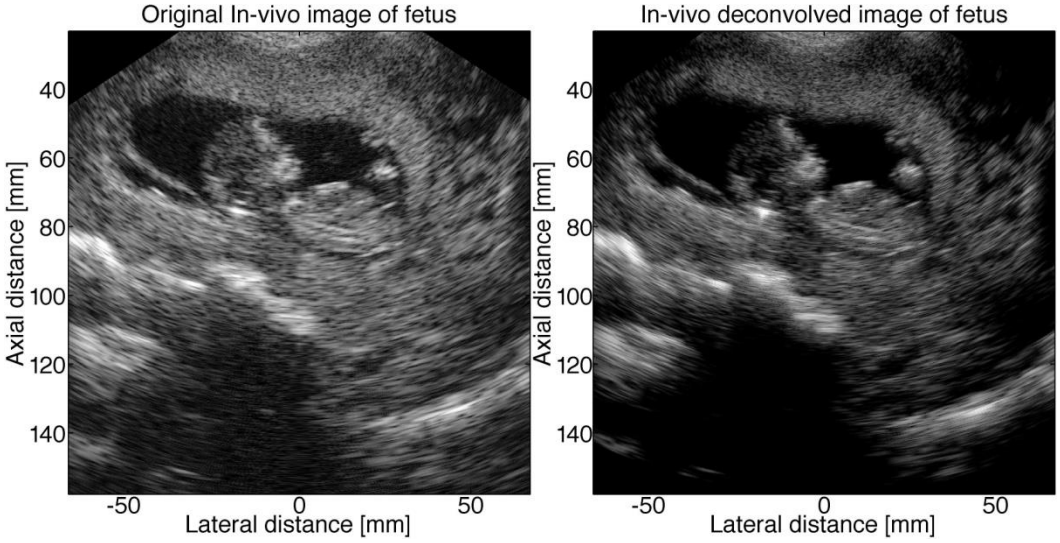

IUS1-A3-2

Range Side-lobe Inversion for Dual-Frequency Harmonic Imaging with Chirp Excitation

Che-Chou Shen[1], **Chun-Kai Peng**[1]*; [1]National Taiwan University of Science and Technology, Taipei, Taiwan*

Background, Motivation and Objective

Dual-frequency harmonic imaging (DHI) is capable of simultaneous harmonic detection at both fundamental frequency (f0) and second harmonic frequency (2f0). To achieve DHI, dual-frequency (DF) composite waveform is utilized for transmit and the resultant 2f0 second harmonic signal and f0 frequency-difference harmonic signal are received for imaging. When chirp excitation is utilized to improve signal-to-noise ratio (SNR) in DHI, however, range side-lobe artifacts occur at both imaging frequencies because of inevitable spectral overlap between the two chirp-encoded harmonic signals. Even with narrow signal bandwidth, DHI still suffers from fourth-order harmonic interference.

Statement of Contribution/Methods

In this study, it is proposed that the image artifacts in DHI can be removed by manipulating the transmit phase of DF chirp waveform for range side-lobe inversion (RSI). For an original DF chirp waveform with f0 and 2f0 transmit phases of 0° and 0°, a modified counterpart with f0 and 2f0 transmit phases of 90° and 90° will lead to the inversion of the 2f0 second harmonic signal while the f0 frequency-difference harmonic signal remains unchanged. In other words, the original and the modified chirp harmonic signals have their

range side-lobes inverted and therefore they can be combined to remove the side-lobe artifacts. The DF chirp waveform with f0 and 2f0 transmit phases of 0° and 180° is also another feasible solution for side-lobe inversion. Hydrophone measurement and B-mode imaging are performed to verify the side-lobe reduction in chirp-encoded DHI.

Results/Discussion

Results indicate that the RSI technique effectively reverses the range side-lobe and suppresses the side-lobe level when either the summation or difference of echoes from the original and the modified chirp transmit waveforms is utilized for imaging. Fig.(A) shows that f0 and 2f0 harmonic signal envelopes have lower side-lobe with RSI technique. B-mode harmonic images in Fig.(B) also show that the anechoic cyst is less contaminated by side-lobe artifacts when the RSI technique is adopted. The corresponding side-lobe magnitude (SLM) decreases from -30 dB to -37 dB. It is concluded that, at the cost of an additional transmit to reverse the range side-lobe, the RSI technique provides a solution for chirp-encoded DHI to achieve SNR improvement together with reduced image artifacts.

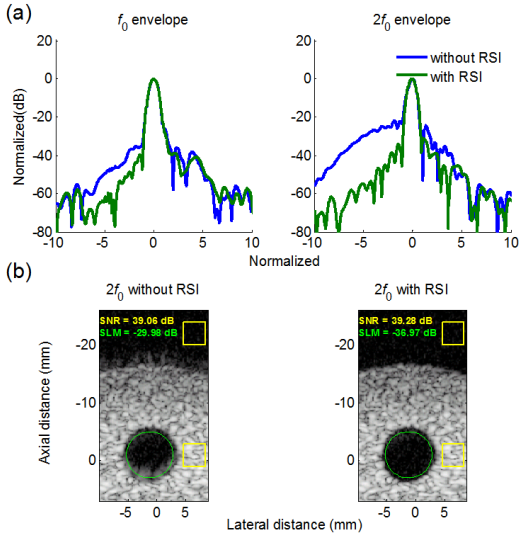

IUS1-A3-3

Extraction of Spectrally Overlapped Second Harmonic using the Fractional Fourier Transform

Sevan Harput[1], Muhammad Arif[2], James McLaughlan[1], Peter R. Smith[1], David M. J. Cowell[1], Steven Freear[1]; *[1]School of Electronic and Electrical Engineering, University of Leeds, Leeds, United Kingdom, [2]Biomedical Engineering, Mehran University of Engineering & Technology, Jamshoro, Sindh, Pakistan*

Background, Motivation and Objective

Tissue harmonic imaging provides better spatial resolution by producing the image with the second harmonic (SH) generated by nonlinear propagation. However, the spectral overlap between the transmitted signal and received SH signal results in image artifacts. Conventional filtering techniques such as a bandpass filter can separate the SH at the expense of reduced bandwidth and image resolution. The fractional Fourier transform (FrFT) demonstrated to be a good candidate for filtering linear frequency modulated (LFM) signals overlapping in both time and frequency domains.

In this study, a filtering method based on the estimated signal parameters of the SH component is proposed. The estimated chirp rate of the SH is used to calculate the FrFT transformation order, which achieves the maximum compression for the SH. Increasing the compression efficiency allows the application of narrower filtering windows over the signal, therefore the complete cancellation of range sidelobe levels and image artifacts is possible.

Statement of Contribution/Methods

The validity of the proposed method was verified by in-vitro measurements on a wire phantom with a medical ultrasound probe. The phantom was built with 4 wires located at a depth of 42, 50, 60, and 70 mm in tissue mimicking material. A 3.5 MHz centered LFM chirp with a bandwidth of 3 MHz was used for excitation. The SH was received by the same probe at 4-10 MHz.

To separate the fundamental and the SH components, the received signal was transformed into the FrFT domain by using the estimated SH chirp rate. In the FrFT domain, the SH component was extracted by applying a filter window. After filtering, the extracted SH was transformed to the time domain using the inverse FrFT and compressed by a second harmonic matched filter.

Results/Discussion

Second harmonic image of the wire phantom is shown in the figure (left) with image artifacts due to spectral overlap. The figure (right) shows the same image filtered with the proposed method before forming the image, where no image artifacts are visible.

Results show that the range sidelobe levels of the compressed SH can be completely removed by filtering in the FrFT domain. When compared with the previously reported filtering techniques, a further reduction in sidelobe levels are achieved in this work for second harmonic imaging with chirp excitation without reducing the system frame-rate and bandwidth.

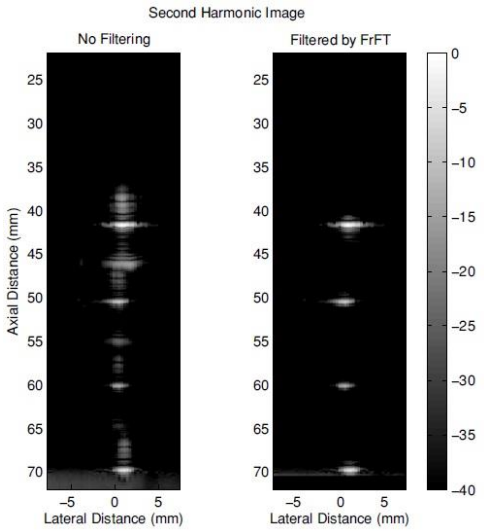

IUS1-A3-4

Arbitrary Waveforms using a Tri-State Transmit Pulser

John Flynn[1], Peter Kaczkowski[1], Ken Linkhart[1], Ronald Daigle[1]; [1]*Verasonics, Inc, Redmond, WA, USA*

Background, Motivation and Objective

Arbitrary waveform synthesis is used in several medical ultrasound applications, including high frame rate acquisition employing orthogonal pulses, large time-bandwidth pulses for increased penetration, and time reversal-based imaging and therapy. Conventional hardware for arbitrary waveform transmission uses multi-bit Digital to Analog Converter (DAC) circuits and linear amplifiers. Alternatively, tri-state encoded pulse trains can energize the transducer, producing analog waveforms with usable fidelity at the transducer output. However, the simplicity of tri-state pulse circuitry presents an encoding design challenge for arbitrary waveform synthesis. The present study examines methods of encoding a tri-state pulser having precise timing control available over waveform edges to approximate arbitrary waveforms under the constraints of commercial hardware circuitry.

Statement of Contribution/Methods

The study was performed in both simulation and experiment, using the Verasonics Research System. The waveform specification provides choice of edge transition times for very long pulse trains at a 250 MHz clock. Three classes of waveforms are examined: a linear FM (LFM) sweep, a set of orthogonal pulses, and an arbitrary waveform simulating a received signal in a time-reversal application. Each is given "ideal" precision, and stored as a sampled analog waveform. Using an empirical model of the transducer dynamics, encoding methods produce a tri-state pulse sequence so the acoustic medium is ensonated with an analog of the desired waveform. We evaluate heuristic algorithms as well as minimum-mean-square-error (MMSE) equalizer-based structures for their fidelity in reproducing the desired waveforms in the medium.

Results/Discussion

As expected, the tri-state waveforms contain many more harmonics than the multi-bit DAC waveforms would prior to filtering by a transducer dynamics. However, the post-filtered waveforms are significantly closer to each other in the acoustic medium. An example of the MMSE encoder performance is shown in the figure, where a windowed LFM sweep is applied to a hypothetical 5MHz transducer with 80% bandwidth. Here the MMSE-based encoder demonstrates practical LFM reproduction by generating a tri-state pulse sequence with -26 dB of error energy against the analog specification, at the modeled acoustic output.

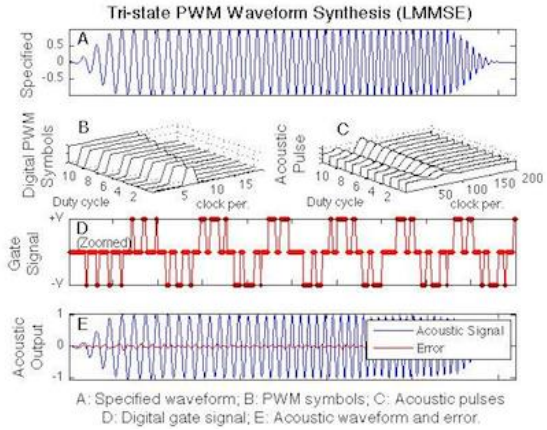

A: Specified waveform; B: PWM symbols; C: Acoustic pulses
D: Digital gate signal; E: Acoustic waveform and error.

IUS1-A3-5

Compressive Sensing Ultrasound Imaging using Overcomplete Dictionaries

Oana Lorintiu[1], Hervé Liebgott[1], Olivier Bernard[1], Denis Friboulet[1]; [1]*Université de Lyon, CREATIS ; CNRS UMR5220 ; Inserm U1044 ; INSA-Lyon ; Université Lyon 1, France*

Background, Motivation and Objective

Compressive sensing (CS) is a recent theory allowing the recovery of a signal sampled below the limit set by Shannon's theorem. The application of CS to medical ultrasound (US) imaging is a very recent field and the few existing studies mostly focus on fixed sparsifying transforms. In contrast to previous work, we propose a new approach based on the use of learned overcomplete dictionaries. Such dictionaries allow for much sparser representations of the signals since they are optimized for a particular class of images such as US images.

Statement of Contribution/Methods

The principle of CS can be summarized as follows. Let x be an N-pixels image sampled using a so-called "sensing" basis Φ, resulting in $y=\Phi x$ with y of $R^{M\times N}$, M<N. The CS theory assumes that x has a sparse representation in some model basis which, in this case, will be an overcomplete dictionary rather than a fixed basis. Let x_p of R^n , n<N, be a patch of an image x and D of $R^{n\times K}$ be an overcomplete dictionary, with n<K, such that $x_p=Dv_p$. Application of CS implies learning D such that v_p is a sparse representation of the patch p in D with at least T_0 non-zero entries. Assuming the sensing basis Φ is incoherent with D, we will then be able to recover the original image patches from the linear measurements y.

In this study, the dictionary D was learned using 8×8 patches extracted from the image to be reconstructed. This training was performed using K-SVD, due to the efficiency and ease of implementation of this algorithm.

Results/Discussion

Experimental beamformed RF signals were acquired using Ultrasonix MDP system scanning a CIRS Model 054GS US phantom. CS reconstruction was performed by removing 25% to 75% of the original samples according to a uniform law. The accuracy of the reconstruction was measured using the mean absolute error.

The obtained accuracies were in the ranges $[1.6, 3.1].10^{-4}$, $[2.1, 4.9].10^{-4}$ and $[7.9.10^{-6}, 2.1.10^{-4}]$ using Fourier, Daubechies wavelet basis and K-SVD dictionary respectively, showing the potential of the overcomplete dictionaries. Figure 1, shows a reconstruction example, the sparsity as a function of the dictionary and the resulting accuracy as a function of the subsampling rate.

This study demonstrates the high potential of learned overcomplete dictionaries for CS in US imaging. Future work will consist in showing the generality of overcomplete dictionaries.

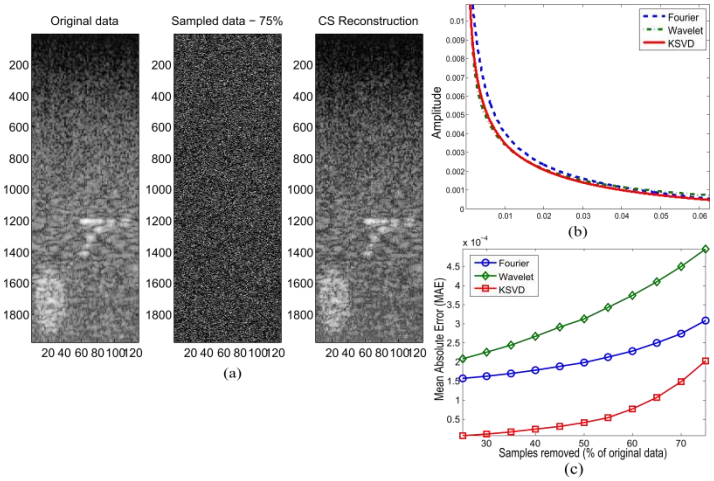

(a) Example of log-envelope beamformed images computed from original data and CS reconstruction from 25% of the original data using K-SVD, (b) Coefficients sparsity in Fourier, Wavelets basis and K-SVD dictionary, (c) MAE calculated for the beamformed RF signals after CS reconstruction using Fourier, Wavelets and K-SVD.

IUS1-A3-6

Effects of heart rate on the pulse waveform measured at the left common carotid artery

Yuka Komagata[1], Tomohisa Mase[1], Yuki Ikenaga[1], Mami Matsukawa[1], Masashi Saito[2], Takaaki Asada[2], Yoshiaki Watanabe[1]; *[1]Wave Electronics Research Center, Doshisha University, Japan, [2]Murata Manufacturing Co., Ltd., Japan*

Background, Motivation and Objective

Pulse wave evaluation is simple and useful for screening arteriosclerosis. The pulse wave is composed of two kinds of displacement waves: incident and reflected waves. In our former study, pulse wave measurement was performed on the skin of the neck near the left common carotid artery using a commercial piezoelectric transducer. Because the attenuation of the reflected wave during propagation changes due to the stiffness of the artery, we have proposed a method to extract the reflected wave from the observed pulse waves. A good correlation between the age and the maximum amplitude of the measured reflected was observed (R^2=0.65). However, the data showed a dispersion, which seemed to come from the difference in the personal conditions, blood viscosity, heart rate etc. In this study, we then focused on the effect of heart rate on the pulse waveform.

Statement of Contribution/Methods

Pulse wave and blood flow velocity on the neck were measured simultaneously from 12 male subjects in their 20s to 60s. A piezoelectric sensor was used to measure the pulse wave. Blood flow velocity was measured using an ultrasonic Doppler system (AplioSSA-700A, Toshiba Medical Systems, Japan). The reflected wave was extracted from the pulse wave following the technique of Saito [1]. We then divided pulse waves and blood flow velocity waves into three blocks, from the half of the initial upstroke to the peak (T_1), from the peak to the incisura (T_2), and from the incisura to the end (T_3). We then obtained the time interval of three blocks.

Results/Discussion

In all data, the interval T_3 only depended on the heart rate. We then normalized T_3 into 0.8 seconds. Fig. 1 shows examples of the pulse and reflected waves. There were few differences between the maximum amplitudes of reflected waves obtained from the original and normalized waves. The result suggests that the effect of heart rate on the reflected wave was small. Actually, changes of heart rate showed very small effects on the intervals of T_1 and T_2, where reflected wave and the initial wave usually overlapped. Considering the characteristics of heart rate and pulse wave, the small effects on the reflected waves are reasonable. Therefore, even if *in vivo* measurement, the effect of heart rate does not seem to be a main cause of the dispersion.

[1]: M. Saito, IEEE, TUFFC. (2012) vol. 59, pp. 2411-2419

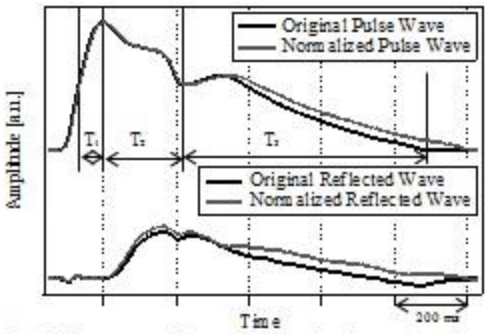

Fig. 1 Comparison between original and normalized waves.

NDE - Phased Arrays

NH

Monday, July 22 2013, 10:30 am - 12:00 pm

Congress Hallair: **Robert Addison**
Retired for Rockwell Scientific Company

IUS2-A-1

Ultrasonic array imaging of composite components

Paul Wilcox[1], Chuan Li[2], Damien Pain[2], Bruce Drinkwater[2]; [1]*Mechanical Engineering, University of Bristol, Bristol, Avon, United Kingdom,* [2]*University of Bristol, United Kingdom*

Background, Motivation and Objective

As carbon fibre composite becomes more widely used for primary structural components in aerospace applications, the reliable detection of small defects and other material anomalies in thick-sections is increasingly important. Composites present challenges for inspection in terms of the type of defects (e.g. delaminations, porosity, resin-rich regions, fibre-waviness), the nature of the material (in particular, heterogeneity on multiple scales and anisotropy) and the geometry of components. The objective of this work is the development of array imaging techniques specifically tailored to defect detection in composite components.

Statement of Contribution/Methods

The starting point is Full Matrix Capture (FMC) of ultrasonic data from an array. In isotropic materials the Total Focusing Method (TFM) of imaging using FMC data yields images close to the theoretical diffraction limit in terms of resolution. However in composite materials this is not the case as velocity anisotropy, multiple-scattering and angle-dependent backscatter from ply-interfaces corrupt images. In a contact inspection of a planar component, the authors have previously shown how the TFM method may be tailored for this case by anisotropy correction combined with optimisation of aperture angle and frequency filter. In the current paper, this approach is extended to the immersion inspection of non-planar composite components. Here the material properties are no longer translationally invariant and ultrasonic rays follow curved paths. An efficient numerical model based on Dijkstra's method to find the shortest duration routes is developed and validated against finite element predictions.

Results/Discussion

Accounting for ray path curvature in imaging is shown to significantly improve results. This is demonstrated both via simulation and experiment. To make the technique viable for practical use it is necessary to be able to compute ray-paths very rapidly and a technique for achieving this is shown. The extension to 2D arrays is discussed.

IUS2-A-2

A Design Methodology for 2D Sparse NDE Arrays using an Efficient Implementation of Refracted-Ray TFM

Jerzy Dziewierz[1], Anthony Gachagan[1]; [1]*Centre for Ultrasonic Engineering, University of Strathclyde, Glasgow, United Kingdom*

Background, Motivation and Objective

2D sparse ultrasonic NDE array designs would benefit from a real-time simulation package in which the array transducer parameters and inspection scenario were fully integrated to optimise the array design for a specific application. Importantly, this process is not straight-forward for many applications, due to the conflicting requirements of conventional array theory (inter-element spacing and element beam characteristics) and the physical demands of the inspection scenario (refraction at non-planar interface).

Statement of Contribution/Methods

A novel algorithm has been developed that allows extremely efficient calculation of the total time of flight of an acoustic ray through two layer media, taking into account the effects of refraction through a 3D surface. The approach has been implemented on GP-GPU hardware, and embedded within the Total Focussing Method imaging algorithm. This new software module supports arbitrary location of probe elements, array element directivity, arbitrary curved interface between two media, arbitrary transmit/receive sequences and any 1D/2D/3D image size for reconstructing the ultrasonic image from raw RF ultrasonic data.

Results/Discussion

The measured performance for the implemented algorithm is >23 GPaths/second on a Fermi-class GPU. For example, a 640x960 pixel image and 128-element probe requires ~5e9 transmit-receive path calculations and the GP-GPU system performs the entire calculation in 0.22 seconds (subject to data acquisition and other constraints).

An example 2D array design is presented for the inspection of composite material, with the principal design objective to maximise the array aperture to ensure greatest volumetric coverage from a single inspection point. The final array configuration comprised 128 array elements, within a 35mm aperture, with each array element 1.5mm in diameter. Moreover, this array operated through a column of water and provided coverage of an area roughly equivalent to 40mm in diameter. The array transducer has been fabricated and tested on composite fan blade samples with a thickness variation between 5mm and 50mm and shown to detect simulated defects and impact damage locations.

Fig.1: PSF Reconstruction using sparse array and TFM imaging algorithm trough refracting, curved interface.

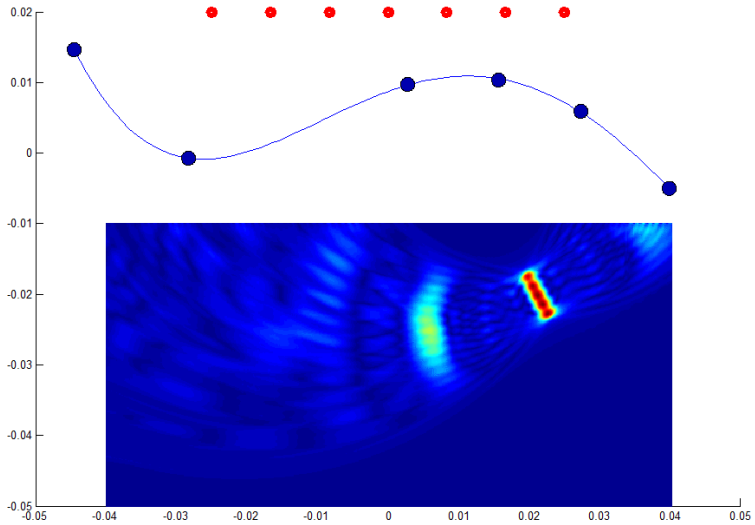

IUS2-A-3

Efficient computation of delay law for imaging structure with a complex surface

Jie Zhang[1], Bruce Drinkwater[1], Paul Wilcox[1]; [1]*University of Bristol, United Kingdom*

Background, Motivation and Objective

Ultrasonic array immersion inspection can be used for detect defects in a structure with a com-plex surface, where a water layer is used to couple ultrasonic waves from an array probe into the structure. A high resolution image can be formed by using an imaging algorithm, e.g., the total focusing method (TFM), for a full matrix capture (FMC) array data. In this case, one difficulty is that the focal laws are not easily calculated. The imaging speed depends on the complexity of the surface and the total number of image pixels. In order to increase imaging speed for on-line in-spection application, this paper presents an efficient way to compute delay law without compro-mising the measurement accuracy. This includes extracting surface geometry from the ultrasonic data and optimizing key parameters for delay law estimation.

Statement of Contribution/Methods

In the proposed imaging process, the surface geometry is first measured by forming an image in the couplant layer. This leads to a set of discrete points that define the surface profile. The prop-agation delay from an array element to a point in the component is determined by a grid search of candidate ray-path through each surface point to identify the one that yields the shortest trav-elling time according to Fermat's principle. Time delays in the components are first generated on a coarse mesh and then these values are linear interpolated to find the time delays to each image pixel. The computed delay laws are finally used to reconstruct the structure image.

An analytical model is developed to build the relationship between estimated delay law errors and array inspection configuration. These errors are mainly caused by incorrect or insufficient points defining the surface and the linear interpolation process. The errors manifest as an ampli-tude reeducation of signals from targets in the structure. Experimental measurements performed on 3 aluminum samples with the same curved surface and 3 defects of the same size but different locations were used to validate the analytical model of delay law error. The validated model is then used to determine the optimum parameters for delay law calculation.

Results/Discussion

The proposed analytical model of delay law error was validated by the experimental results. The finding is that a surface can be adequately described by points spaced at 0.5 mm and that delay laws can be computed on a grid spaced at 1 mm. With these parameters, the reduction in ampli-tude of a point target in the structure can be guaranteed to be less than 1 dB.

IUS2-A-4

Time Reversal Techniques for Multitarget Identification

Franck Assous[1], Marie Kray[2], **Frederic Nataf**[3]; [1]*Ariel University, Israel,* [2]*Mathematisches Institut, Universität Basel, Basel, Switzerland,* [3]*LJLL, UPMC and CNRS, Paris, France, France*

Background, Motivation and Objective

Since the seminal paper by M. Fink et al., time reversal is a subject of very active research. The main idea is to take advantage of the reversibility of wave propagation phenomena such as it oc-curs in acoustics, elasticity or electromagnetism in a non dissipative unknown medium to back-propagate signals to the sources that emitted them. Number of industrial applications have alrea-dy been developped: touchscreen, medical imaging, non destructive testing and underwater communications. However, the resolution of these applications is restricted by the diffraction limit.

Statement of Contribution/Methods

We have designed a method named TRAC (Time Reversed Absorbing Conditions, [1]) that enables to go far beyond the diffraction limit without knowing the physical properties of the tar-gets. This is made possible by introducing time reversed absorbing conditions in time reversal techniques. Using multiple illuminations, TRAC is able to exceed the diffraction limit.

[1] Assous F., Kray M., Nataf F. and Turkel E., Time Reversed Absorbing Condition: Applica-tion to inverse problem, Inverse Problems 27 (2011).

Results/Discussion

An example of a geometric configuration is depicted on the left figure. A source-receiver array illuminates the targets at a distance of several wavelenghts and then record the scattered waves. From these data, we generate the right figure. The number of peaks enables us to count the num-ber of targets although they are located in a disk of radius smaller

than the Rayleigh diffraction limit λ/2. Hard, soft and penetrable inclusions are treated in the same way by the method. It ge-nerates resolution beyond the diffraction limit even in presence of high level of noise on the data.

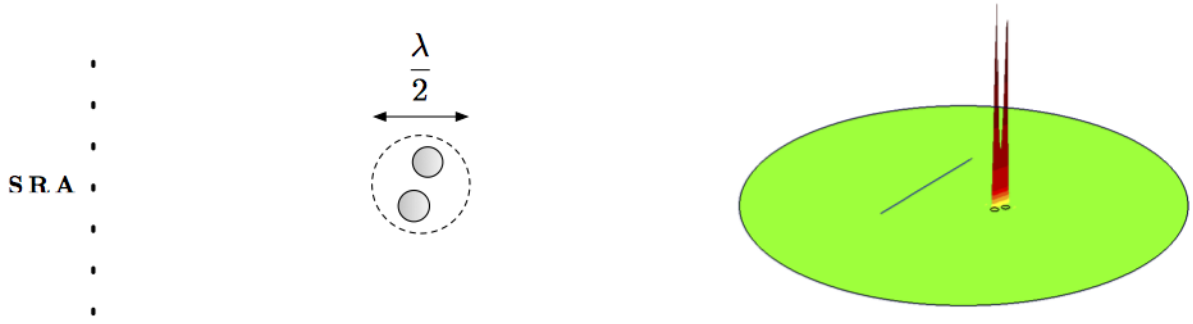

IUS2-A-5

Simultaneous measurement of thickness and sound velocities of each layer in multi-layered structures

Sebastian Kümmritz[1], Elfgard Kühnicke[1], Mario Wolf[1]; [1]*Solid-State Electronics Laboratory, TU Dresden, Dresden, Saxony, Germany*

Background, Motivation and Objective

Layered systems are part of numerous structures, e. g. asphalt in road construction, solidification processes of melts, circuit boards etc. The precise thickness and the elastic properties of the single layers can obtain important information about the state of the whole system.

Conventionally, one of the properties (thickness, sound velocity) of each layer has to be known to determine the other property using the time of flight. Unfortunately, in many applications none of these parameters is available. A procedure for the simultaneous and nondestructive determination of sound velocity and thickness is currently not known.

Statement of Contribution/Methods

In this contribution, a novel nondestructive and noninvasive approach for the simultaneous measurement of sound velocity and thickness of each layer in a multi-layer structure is introduced. Because the focus position of an ultrasound transducer depends on the sound velocity in the medium, the basic idea is to use it as an additional piece of information. To vary the focus position, an annular array is used. All its elements can send and receive independently, which enables synthetic focusing. An iterative algorithm which varies the set of delay times for different sound velocities and different focus positions has been developed.

If the chosen sound velocity and focus position for the calculated set of delay times match to the actual position of boundary surface and sound velocity in the layer, the echo signal takes its maximum. This is the procedure for one layer. For multi-layer systems, the determination of sound velocity and thickness is carried out layer by layer.

If the focus extension is small, the maximum of the reflected signal appears, when the focus is positioned on the boundary surface. For a larger focus extension (e. g. for measurements at a big distance), the echo signal takes its maximum when the focus is positioned in front of the surface. Sound field simulations give the dependence of the focal extension and the distance between the reflector and the focal point causing maximal echo amplitude. They also deliver the focal position as a function of material parameters, thicknesses and the sequence of the layers.

Results/Discussion

With this method the thicknesses and sound velocities of different two-layer structures were determined with accuracies below two percent. First studies for systems with more than two layers are presented.

IUS2-A-6

Ultrasonic imaging of a turbine blade model using a 360° synthetic-aperture-focusing-technique and reverberation suppression

Thomas Scharrer[1], Andreas Koch[1,2], Stefan J. Rupitsch[1], Alexander Sutor[1], Helmut Ermert[1,2], Reinhard Lerch[1]; [1]*Chair of Sensor Technology, University of Erlangen, Erlangen, Germany*, [2]*High Frequency Engineering Research Group, Ruhr-University Bochum, Bochum, Germany*

Background, Motivation and Objective

Nowadays, non-destructive testing of turbine blades is often based on X-ray Computed Tomography (X-ray CT). But, due to an intense X-ray absorption in specific directions, the material cannot be completely penetrated and consequently, several projections are missing in the measurement data. Therefore, a new approach is developed to complement these absent projections with information gained by ultrasonic testing. However, with respect to substantial refraction effects and an irregularly shaped specimen, ultrasonic testing in immersion technique is impeded. Emerging refraction effects and reverberation signals cause a poor ultrasound image quality and inhibit an adequate detection of the desired structural information. Here, we present an adapted 360° synthetic-aperture-focusing-technique (SAFT) based on a virtual point source, which eludes influences of refraction effects of the specimen´s surface. To reduce signal reverberation artifacts, data is filtered by means of principle component analysis (PCA) and predictive deconvolution (PD).

Statement of Contribution/Methods

The procedure can be divided into five major steps. (i) First, data is acquired successively along a path at constant distance to the surface of the specimen, i.e. wave propagation direction is always perpendicular to the surface of the device (Fig. 1). (ii) In a next step, surface echoes are eliminated by a subspace analysis and projection filter. (iii) Afterwards, the obtained data is filtered by a predictive deconvolution algorithm to reduce reverberation signals. (iv) Subsequently, the processed data is converted into an analytic signal and in a last step, (v) the 360° synthetic-aperture-focusing-technique is applied to the aperture, which is determined by the data acquisition procedure.

Results/Discussion

To demonstrate the potential of this method, several structures within a simplified model of a turbine blade (Fig. 1; width: 100 mm, height: 25 mm) were imaged. The comparison of images produced by an adapted 360° SAFT with unfiltered data (Fig. 2) and with filtered data (by means of PCA and PD; Fig. 3) shows that image quality is increased. Accordingly, an adapted 360° SAFT with an irregular shaped aperture in combination with a sufficient reverberation suppression approach shows great potential in ultrasonic imaging of turbine blades for data fusion.

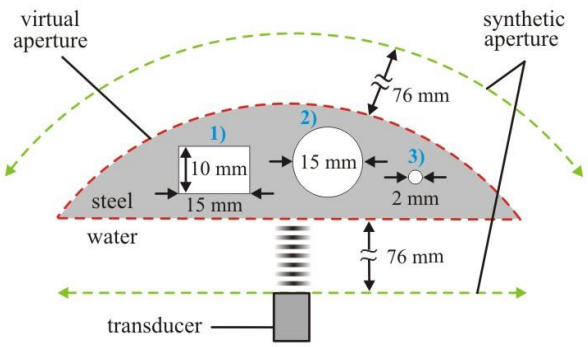

Fig. 1: Schematic measurement setup

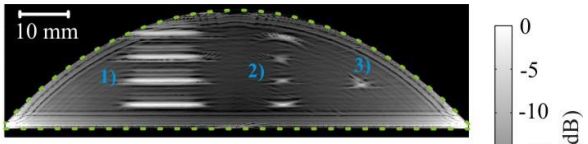

Fig. 2: Unfiltered SAFT processed data

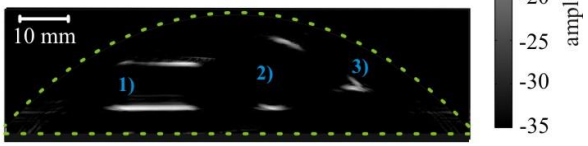

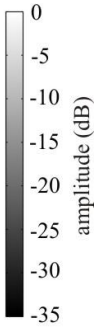

Fig. 3: Filtered SAFT processed data

Ultrasonic motors 1

T1

Monday, July 22 2013, 10:30 am - 12:00 pm

Congress Hallair: **Joerg Wallaschek**
Leibniz Universitaet Hannover

IUS3-A-1

A nano emulsion generator using a microchannel and a bolt clamped type transducer

Takefumi KANDA[1], Yusuke KIYAMA[1], Koichi SUZUMORI[1]; [1]*Graduate School of Natural Science and Technology, Okayama University, Okayama, Okayama, Japan*

Background, Motivation and Objective

The aim of our study is to obtain antitumor substance emulsion which has a droplet • fs diameter of 200 nm or less. In our previous research presented in 2010 IUS, we reported a microchannel device oscillated by 2.3 MHz plate type vibrator. The system realized a flow, silent and small system. By using the system, we succeeded in generating o/w (oil in water) emulsion of antitumor substance. However the system needs much higher power to increase the ratio of oil phase against water phase. This is because the oil-phase contains the drug. In this study, we have used a bolt clamped type small transducer to oscillate ultrasonic vibration against the microchannel.

Statement of Contribution/Methods

For a generation of emulsion, two syringe pumps to supply oil-phase and water-phase, a T-type microchannel plate and an ultrasonic device were used. First, by the T-type microchannel, micron-sized emulsions are generated. Then the micron-sized emulsions were sonicated by the ultrasonic vibration and nano-sized droplets are obtained. In the ultrasonic device, the microchannel is 0.711 mm wide and 0.65 mm deep. The oscillating frequency of our ultrasonic device is over 2 MHz. This is because the microchannel • fs depth is shallow, and it needs a high frequency to oscillate a standing wave. In our new device, we designed a small bolt clamped type transducer to apply higher pressure against the micron-size droplets. The cross sectional pattern of the ultrasonic microchannel device and the bolt clamped type transducer was designed by using FEM as a unit. The fabricated device is shown in the photo. The left plate is the microchannel plate and the right device is the transducer.

Results/Discussion

The distribution of the generated droplets • f diameter was measured with a dynamic light scattering (DLS). In our previous study, the peak of diameter was in 100 nm when the flow rates of the water-phase and the oil-phase were 100 and 5 µl/min. However the oil-phase has a high viscosity and we could not increase the ratio by our previous devise. With our new device, the peak of diameter was in 100 nm when the flow rates of the water-phase and the oil-phase were 100 and 12 µl/min. We have succeeded in obtaining higher oil-phase ratio against the water-phase with our new oscillating system.

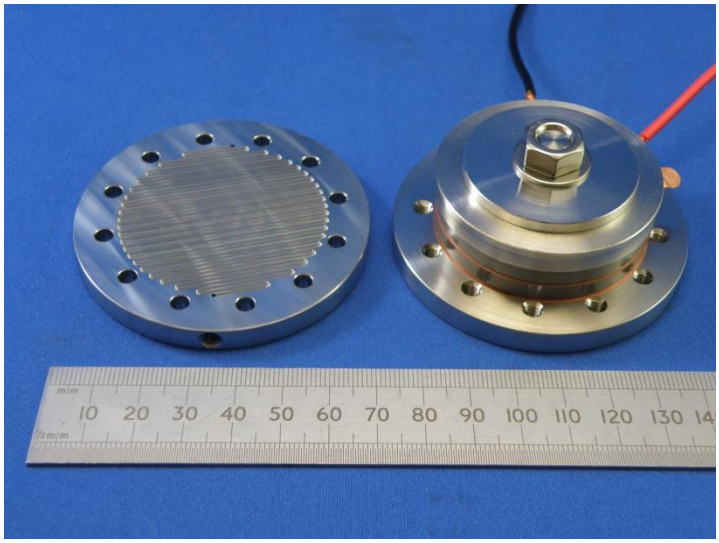

IUS3-A-2

Ultrasonic motor using thrust bearing for friction drive with lubricant.

Takaaki Ishii[1], Hiroki Yamawaki[2], Kentaro Nakamura[3]; [1]*Mechatronics, University of Yamanashi, Kofu, Yamanashi, Japan,* [2]*University of Yamanashi, Japan,* [3]*Precision and Intelligence Laboratory, Tokyo Institute of Technology, Yokohama, Kanagawa, Japan*

Background, Motivation and Objective

Using lubricant is one of the solutions to obtain high efficiency and good motor characteristics. In order to use lubricant effectively, high contact pressure is required. In this report, we propose using thrust bearing for friction drive of the ultrasonic motor, instead of the conventional friction material. High contact pressure is expected between balls and flat surface. At the same time, the contact points keep changing by rotating the bearing balls, hence the low wear of the balls is expected. Improved lubrication is also expected by rotating the balls.

Statement of Contribution/Methods

A hybrid transducer type ultrasonic motor is used for this experiment. The thrust bearing is placed between a rotor and a stator as shown in figure 1(a). The diameter of the motor is 30 mm. Figure 1(b) shows the thrust bearing used for the experiment. The hybrid transducer type ultrasonic motor is driven by two electrical inputs to excite elliptical motion

on the friction surface. PZT for longitudinal vibration and PZT for torsional vibration are excited. Three kinds of lubricants with two kinds of viscosities are used for bearing lubrication. Two methods of rotor-output-type and bearing-output-type are used to obtain output torque.

Results/Discussion

Fundamental characteristics of the hybrid transducer type ultrasonic motor using thrust bearing were obtained for the first time. Figure 2 shows one of the results obtained under the pre-load of 300 N. The maximum rotation of 10 r.p.m., the maximum torque of 0.123 Nm and the maximum driving efficiency of 2.7 % were successfully achieved by the bearing-output-type motor using high traction fluid with viscosity of 100 cSt.

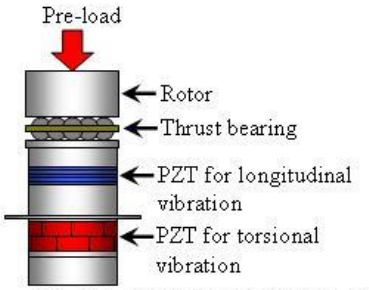

Fig. 1(a) Schematic illustration of the proposed motor.

Fig. 1(b) Thrust bearing used for the motor.

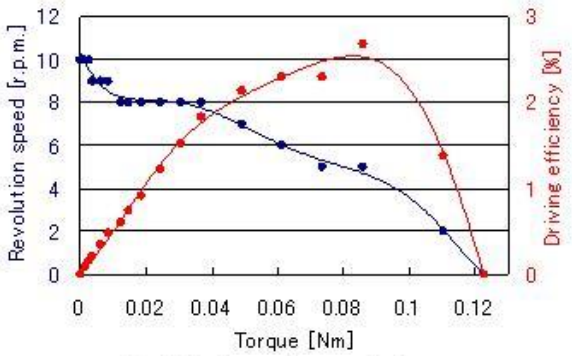

Fig. 2 Motor characteristics.

IUS3-A-3

Piezo Impact Type MEMS Rotary Actuator and Application to Millimeter Size AI Controlled Robot

Minami Takato[1], Tatsuya Ogiwara[1], Shinpei Yamasaki[1], Ken Saito[1], Fumio Uchikoba[1]; [1]*Precision Machinery Engineering, Nihon University, Funabashi, Chiba, Japan*

Background, Motivation and Objective

Micro robots have been studied for various applications. These robots require small size body and small size actuator, for example, electromagnetic actuators, shape memory alloy (SMA) actuators, piezoelectric actuators, and so on. Previously, we developed insect type MEMS micro robots. These robots were fabricated by MEMS (Micro Electro Mechanical Systems) technology and shape memory alloy based artificial muscle wires. The micro robot had six legs and the robot performed foot step walking. However, the artificial muscle wire actuator had problems of large power consumption and slow motion speed. In this study, we propose a piezo impact type MEMS rotary actuator for micro robot application. Applied robot is a millimeter size and controlled by an artificial intelligence system.

Statement of Contribution/Methods

In the rotary actuator, a multilayer piezoelectric element was arranged the outside of the rotor. The arranged piezoelectric element was expanded by electrical pulses. When the impact caused by the expansion was added to the rotor, the rotary motion was generated. The frame of this actuator was fabricated by MEMS technology. Fig. 1 shows the structure of the piezo impact type MEMS rotary actuator. Developed rotary actuator was applied to millimeter size robot which has six legs and link mechanism. Driving pulses were generated by the AI hardware neural networks.

Results/Discussion

The rotation speed of the rotary actuator showed 80 rpm when the applied frequency was 18 kHz. The dimensions of the micro robot which has the piezo impact type MEMS rotary actuator were 4 mm, 4.6 mm and 3.6 mm, width, length and height, respectively. Fig. 2 shows the fabricated micro robot. The locomotion speed achieved 128 mm/min.

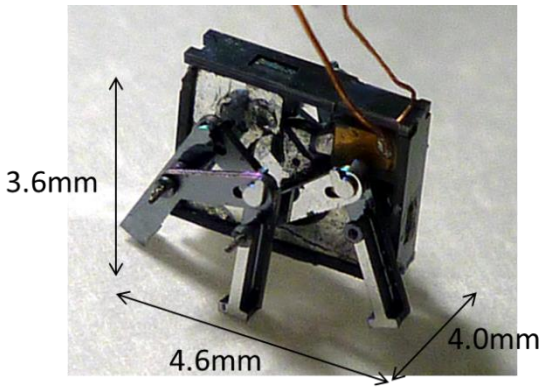

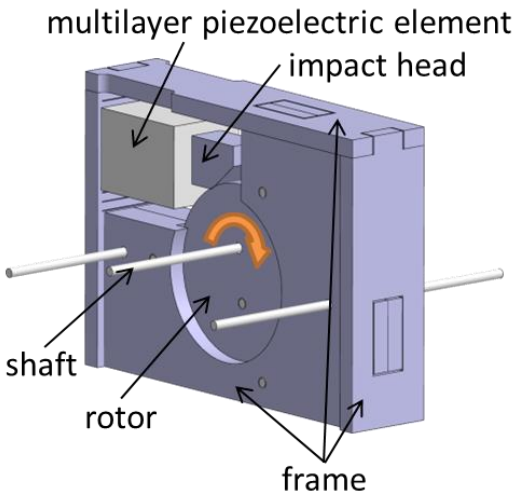

IUS3-A-4

Evaluation of Piezoelectric Materials for Cryogenic Ultrasonic Motor

Daisuke Yamaguchi[1], Takefumi Kanda[1], Koichi Suzumori[1]; [1]*Graduate School of Natural Science and Technology, Okayama University, Okayama, Okayama, Japan*

Background, Motivation and Objective

In advanced area of scientific research, a cryogenic temperature environment is used for important measuring condition. The cryogenic temperature is near the liquid helium temperature, from 20 to 4.2 K. Previous actuators located in the cryogenic temperature had limitation of application because output of these actuators was low. Our objective is achieving the ultrasonic motor that has high output at cryogenic temperature. In our previous study, the efficiency of the motor was low under ultralow temperature condition. In this study, to increase the driving performance, ferroelectric materials were used as the piezoelectric material for cryogenic ultrasonic motor.

Statement of Contribution/Methods

The piezoelectric performances of ferroelectric materials were evaluated. To measure the piezoelectricity of various ferroelectric materials from room temperature to 4.5 K, a resonance-antiresonance method was used. Additionally, the ultrasonic motor using these ferroelectric materials were fabricated. The motor has bolt-clamped Langevin-type transducer. The transducer was designed to decrease the thermal stress by falling temperature.

Results/Discussion

Figure (a) shows the relationship between the piezoelectricity and the temperature. PMN-PT single crystal has higher piezoelectricity than PZT ceramics under cryogenic temperature condition. The motors using each material were fabricated and evaluated. The efficiency of the motor using PMN-PT single crystal was 44 times larger than that using PZT ceramics at 4.5 K.

(b) Cryogenic Ultrasonic Motor

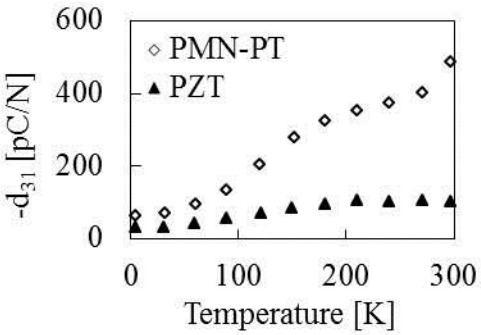

(a) Piezoelectricity of materials

IUS3-A-5

Design and Analysis of a Nonrational B-Spline Profiled Horn for High Displacement Amplification

Hai-Dang Nguyen[1], **Dung-An Wang**[1]; [1]*Graduate Institute of Precision Engineering, National Chung Hsing University, Taichung, Taiwan*

Background, Motivation and Objective

Parametric curves, such as Bezier and B-spline curves, may be used to describe the profiles of horns for high displacement amplification and ease of machining of ultrasonic horns.

Bezier curve is generated by using the vertices of a defining polygon and the Bernstein basis functions. From a mathematical point of view, the flexibility of Bezier curve is limited by its two characteristics. First, the number of polygon vertices fixes the order of the polynomial which defines the curve. Second, a local change within a curve is inhibited due to the global nature of the Bernstein basis. Therefore, a parametric curve, such as B-spline curve, defined by a nonglobal basis which allows the degree of the curve to be changed without changing the number of the defining polygon vertices can be used to describe the profile of horns for higher displacement amplification.

In this paper, we develop a new horn with a nonrational B-spline profile for high displacement amplification.

Statement of Contribution/Methods

Methods:

The optimal designs of the horns are sought by a multiobjective optimization algorithm. Prototypes of horns are fabricated by a numerical control (NC) machining process. Displacements and resonant frequencies of the horns are obtained by a laser displacement sensor. The experimental results are compared with the optimized solutions. Performance of the developed horn is compared with traditional horns and other parameter curve profiled horns.

Contributions:

1.The displacement amplification of the proposed horn is 41.4% and 8.6% higher than that of the traditional catenoidal horn and a Bezier horn, respectively, with the same length and end surface diameters.

2. The developed open uniform nonrational B-spline horn has larger displacement amplification than the Bezier horn and the commonly used catenoidal horn, and much lower stress concentration than the NURBS horn and the stepped horn.

Results/Discussion

Based on the finite element analyses, the stepped horn and the Non Uniform Rational B-Spline (NURBS) horn may give high displacement amplifications, but their high stress concentration near the abruptly changing section makes them prone to failure. The developed open uniform nonrational B-spline horn has larger displacement amplification than the Bezier horn and the commonly used catenoidal horn, and much lower stress concentration than the NURBS horn and the stepped horn. Prototypes of the horn have been fabricated and tested to verify the effectiveness of the proposed new horn. The displacement amplification of the proposed horn is 41.4% and 8.6% higher than that of the traditional catenoidal horn and a Bezier horn, respectively, with the same length and end surface diameters. The proposed horn may be more suitable than the classical stepped and catenoidal horns and other parametric curve profiled horns in application where high displacement amplification and low stress concentration are required.

IUS3-A-6

Ultrasonic friction reduction applied to agricultural tillage

Wiebold Wurpts[1], **Jörg Wallaschek[1]**; [1]*Institute of Dynamics and Vibration Research, Leibniz Universität Hannover, Germany*

Background, Motivation and Objective

In agricultural tillage the friction forces between the soil and the grubber's tine are a limiting factor in the extension of the toolsize. To overcome this problem, the use of ultrasonic dither is proposed and investigated. The piezoelectrically excited grubber is driven in a longitudinal vi-bration mode. Due to the vibrations a significant decrease of the effective friction is gained.

Statement of Contribution/Methods

In this contribution we first review the basic effect of friction reduction by superimposed ultrasonic vibration. We then evaluate the effective friction reduction for the case of vibrations in the sliding direction as well as for vibrations perpendicular to the sliding direction.

In the center of the contribution is the design of an ultrasonic grubber for applications in agricul-ture. The grubber tine is excited by a piezoelectric transducer as depicted in Fig.1a). Mounting of the transducer as well as impedance matching of transducer and grubber tool were studied in detail and a prototype grubber system, including the power electric supply, was designed and built. It was tested in the field with a mobile test rig that allowed to make measurements of the system's behavior with different soils and velocities. Fig.1b) shows the typical behavior of the pulling force with and without ultrasonic excitation. Depending on the parameters a reduction of the friction forces in the order of 50% was achieved. The level of friction reduction was studied as a function of different velocities and soils.

Results/Discussion

Finally the nonlinear dynamics of the system was investigated. The measurements showed, that the phase minimum and the shape of the phase diagram strongly depended on the amplitude of vibration. These effects were modeled and explained with a piezoelectric equivalent circuit that was extended by a Coulomb friction element. An analytical solution, which was obtained by the method of harmonic balance provides a good explanation of the observed nonlinear behavior.

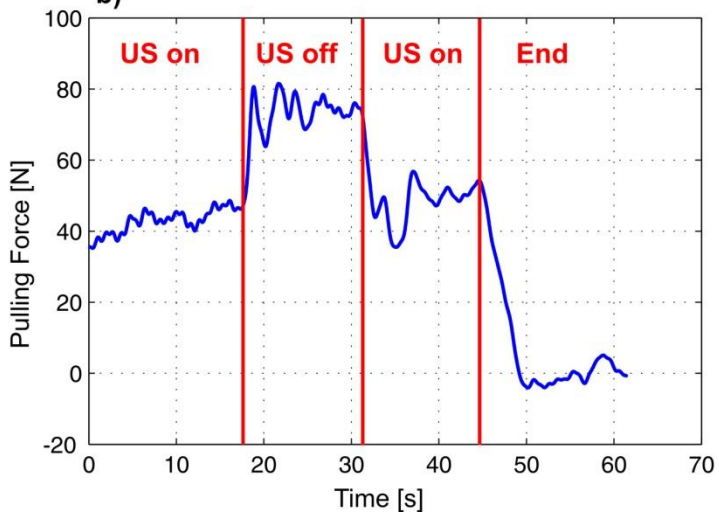

BAW & FBAR

T2

Monday, July 22 2013, 10:30 am - 12:00 pm

Congress Hallair: **Paul Bradley**
Avago Technologies

IUS4-A-1

Miniaturization of BAW Devices and the impact of Wafer Level Packaging Technology

Gernot Fattinger[1], Paul Stokes[1], Alexandre Volatier[1], Fabien Dumont[1], Robert Aigner[1]; [1]*TriQuint Semiconductor, Apopka, FL, USA*

Background, Motivation and Objective

As wireless mobile applications continue to drive shrinkage of the individual components, consequently a corresponding decrease in required footprint and component thickness needs to go along with it. Over the last years, single-band PAD front-end module foot-prints have been steadily decreasing at an average rate of about 30% year-over-year in terms of area. Similarly, standalone duplexers shrunk over the last ten years at about 25% per year in required foot-print area. Although technology improvements can allow for radical BAW die shrinkage, the packaging technology that comes along with the BAW die needs to contribute it's share to maintain this trend.

Statement of Contribution/Methods

The first part of this paper deals with the steps that have been taken to shrink the foot-print of the BAW die itself, acoustic portion as well as the surrounding areas. Some of the most important items along these lines are partial integration of formely external matching components on the BAW die, methods to selectively reduce coupling of resonators for improved slope steepness, and additional (more than two) resonator frequencies on the same die.

In the second part a novel concept for a BAW wafer-level packaging approach will be presented, which results in some enhanced electrical performance, as well as in a significant reduction in the required real-estate of final products (front-end modules as well as discrete parts).

Results/Discussion

The historical shrinkage of BAW die and the associated drivers will be discussed on the example of a B2/B25 Rx die (see fig.1).

Similarly, we will demonstrate the impact of wafer-level packaging (fig.2) on the miniaturization of devices on the example of a B2/B25 BAW duplexer. Advantages and limitations will be discussed.

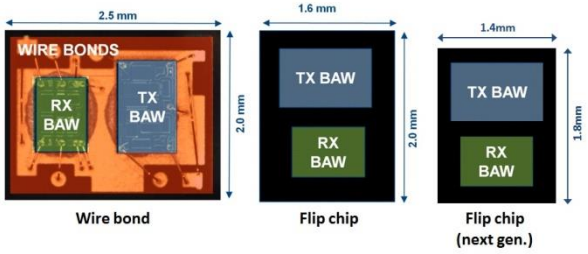

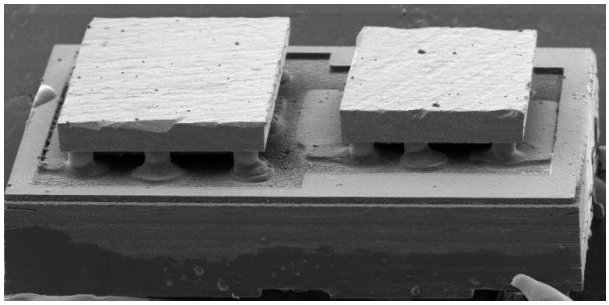

IUS4-A-2

Laterally Coupled BAW Filter using Two Acoustic Modes

Johanna Meltaus[1], Tuomas Pensala[1]; [1]*VTT Technical Research Centre of Finland, Espoo, Espoo, Finland*

Background, Motivation and Objective

Thin-film bulk acoustic wave (BAW) resonators with lateral acoustic coupling have been shown to produce passband (PB) response with a matched bandwidth (BW) of 5% at 1980 MHz [1]. In a solidly-mounted resonator (SMR) filter operating in the first-order thickness-extensional mode (TE_1), there is an unwanted response below the PB from the second-order thickness-shear (TS_2) mode, since the IDT geometry induces coupling to the TS_2 mode. In this paper, we study using that mode to further increase the filter BW.

Statement of Contribution/Methods

Laterally coupled BAW (LBAW) filters were fabricated onto an acoustic reflector comprising two W-SiO_2 pairs, with AlN as the piezolayer, Mo bottom electrode and Al top electrode. Dispersion characteristics of the stack was designed such that the TE_1 and TS_2 modes have a frequency separation of ~35 MHz at 2 GHz (1.8%), bringing the two modes sufficiently close in frequency so that the coupled resonances arising in each of them can be combined to produce a passband response. Interdigital coupled resonators with varied number of resonator electrodes *N*, electrode width *W* and gap width *G* were used. Electrical frequency responses were measured with a vector network analyser.

Results/Discussion

Both acoustic plate wave modes (TE_1 and TS_2) produce coupled (even and odd) resonances, four resonances in total compared to two in a conventional LBAW. Frequency separation of the resonances depends on the dispersion and on the resonator geometry. With a suitable combination of parameters, the resonances form a wide BW filter response. The best results were achieved with N=31, W=9 µm and G=1.5 µm, with BW roughly 10% at 2 GHz. There were notches in the PB at the frequencies between the TS_2 and TE_1 modes. Overall insertion loss (IL) level in the PB was 5 dB.

The results demonstrate the principle of using two acoustic plate wave modes to form a wideband response in a laterally coupled SMR BAW filter. Some tuning of the design parameters is needed to improve the PB shape and IL level. Dispersion properties have a major role, because the frequency separation of the two modes should be carefully designed to avoid notches in the PB. Resonator geometry can then be used to tune the separation of the coupled resonances so that a wideband response is obtained. Compared to

an LBAW filter using only the TE_1 mode, the optimum IDT width is larger, leading to relaxed processing parameters. The large BW makes possible to trade off BW for other parameters, such as suppression or transition width.

[1] J. Meltaus and T. Pensala, "Laterally Coupled BAW Filters with 5% Bandwidth", in Proc. 2010 IEEE IUS, pp. 966-969

IUS4-A-3

Temperature Compensated FBAR Duplexer for Band 13

Qiang Zou[1], Frank Bi[1], Genichi Tsuzuki[1], Paul Bradley[1], Rich Ruby[1]; [1]*Avago Technologies, USA*

Background, Motivation and Objective

As LTE (Long Term Evolution) supersedes CDMA/wCDMA in Cell Phones and new frequency bands are being created, more stringent requirements are being forced onto the front-end radios in handsets. And, most of these requirements impact the duplexer. One example is the Band-13 (B13) proximity to the public safety band (PSB), where PSB is used for low-power, on-scene response radios. The uplink of B13 covers 777.5 to 787 MHz, but the PSB covers 769 to 775 MHz. The guard band between these two is only 2.5 MHz. Almost all piezoelectric based duplexers have a Temperature Coefficient equal or greater than 30 ppm/C such that, over temperature, even with a 0% wide roll-off, the duplexer transmit band will 'bleed' into the PSB. The potential risk of interference to the PSB radios requires all cell phones using B13 to reduce power by as much as 8 to 12 dB when transmitting. A 'perfect' duplexer offering 20 dB or more additional rejection would eliminate the need to back off power in a hand set in the presence of psb radios.

Statement of Contribution/Methods

To enable co-existance (i.e. no interference) between B13 and the PSB, one needs to create a zero temperature drift resonator with sufficiently high Q to make the transmit filter (of the duplexer). To meet the A-MPR (Additional Max Power Reduction, the duplexer must roll off by at least 20 dB in the 2 MHz. This was done using a temperature compensated, FBAR resonator in the transmit portion of the duplexer. Temperature compensation was accomplished using an oxide layer in the active acoustic stack. To meet the 2 MHz guard band (actually closer to 2.5 MHz), the Tx filter roll-off error budget was split between process variation, frequency drift over temperature, and roll-off.

Results/Discussion

Two fundamental difficulties were overcome. The first was to create a zero drift resonator (ZDR) that was stable and repeatable over a wide temperature range. The second requirement is to ensure that the Q of the ZDR was sufficiently high to guarantee a roll-off of less than 1.5 MHz in the Tx filter. This required a manufacturable Q in the range of 2200 or higher. Figure 1 shows the filter response of a B13 duplexer using high-Q, ZDR resonators. The B13 duplexer Tx filter shows 2.7 dB or better worst-case insertion loss from 777.5 to 787 MHz and a rejection of 20 dB or better 1.5 MHz 775 MHz and below. The additional 1 MHz was used for process variation and over-temperature drift.

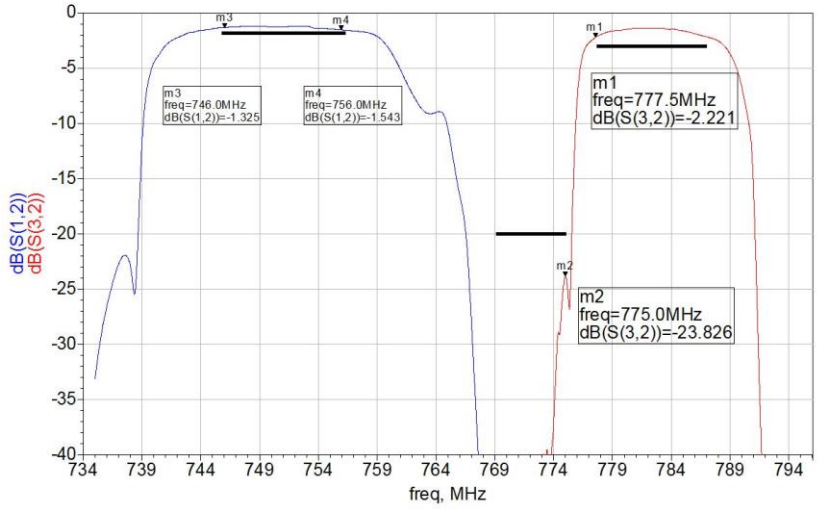

IUS4-A-4

3rd type of FBARs?

Victor Plessky[1], Sylvain Ballandras[2], Valery Grigorievsky[3], Ventsislav Yantchev[4]; [1]*GVR Trade SA, Switzerland,* [2]*FreC'N'Sys, France,* [3]*IRE RAS, Russian Federation,* [4]*Dept. Solid State Electronics, Uppsala University, Sweden*

Background, Motivation and Objective

Different « layered structures » were proposed in the past combining the advantageous features of substrate (e.g. low SAW attenuation in sapphire) and good piezoelectric properties and high quality of piezoelectric (e.g. AlN) films. Unfortunately, achievable piezo-coupling constant K^2 is in most cases very small. Meanwhile in FBARs AlN films excited in thickness mode demonstrate K^2 >6%. The reason for so low K^2 in layered structures is in the structure of displacement in acoustic waves and in a fact that the main energy of the wave is still concentrated in passive substrate. Also, the oscillations under 2 electrodes of each pair in the IDT have opposite phase. The solid uniform piezoelectric film resists to development of such motion mode.

We propose here a transducer structure usable in different microacoustic components which allows for much stronger coupling with the same combination of substrate and piezo-film.

Statement of Contribution/Methods

Microacoustic device is proposed comprising

· substrate suitable for propagation of acoustic waves in X-direction with low loss,

·metal layer deposited on said substrate and

·microacoustic transducers (resonators) created in form of piezoelectric (AlN, ZnO, etc.) bars with cross-section dimension in X-direction smaller than a half of wavelength of any acoustic wave in substrate material at operation frequencies and having top conducting electrodes.

The thickness of the piezoelectric layer is close to λp /4 or λp /2 of the bulk wave excited in said resonators. The resonators being placed periodically and separated (centre-to-centre) by a distance in X-direction smaller than 1/2 wavelength of any acoustic wave in substrate material are connected to the balanced source of voltage +/- V .

Results/Discussion

The period of the structure is chosen to favor the interaction between a surface mode and a localized bulk resonance of the AlN bars considered as single resonators arranged in a periodic grating. Taking for estimation the SAW velocity VSAW ~ 5000 m.s-1 for the Sapphire and the longitudinal velocity in AlN V_{AlN} ~ 11000 m.s-1, we have following rough estimates to get a resonance frequency f=1GHz:

- Pitch (period) p =λ/2 =2.5 µm,

- Metal (Al) thickness hAlu =1000 – 2000 Å (not critical here)

- AlN layer thickness (supposing it is close to λ/4) h_{AlN} ~ 2.5µm or (for λ/2) h_{AlN} ~ 5.0µm . We have simulated both cases. The principal results are that the resonator grating always provides larger coupling factors than the solid layer one, and that a mode can occur exhibiting a coupling which can overcome 4.2% depending on the layer thickness. In this mode the resonances in narrow FBARs are coupled through the substrate. Actually a new type of FBARs is described, wherein the isolation from the substrate is provided by the resonators periodicity $<\lambda_{Bulk}$ /2 killing the bulk wave radiation in substrate. The coupling can be easily adjusted. The mode we see may be treated as not a SAW, but as a system of coupled FBARs.

IUS4-A-5

Dispersion of Lamb waves Propagating Under Periodic Metal Grating in AlN Plates

Natalya Naumenko[1]; [1]*Acousto-Optical Research Center, National University of Science and Technology "MISIS", Moscow, Russian Federation*

Background, Motivation and Objective

Lamb wave resonators using AlN plates are a promising class of devices for high-frequency applications in wireless communication systems. Lamb waves are usually excited by IDTs and reflected by electrodes of periodic metal grating or resonator edges. The behavior of Lamb waves under periodic metal grating in not yet well understood. There exist simple models for estimation of Lamb wave velocities as functions of plate thickness. Recently FEM-analysis based on commercial COMSOL software was applied to simulation of admittance of Lamb wave resonators, and electromechanical coupling was calculated for resonators using modes s_0 and a_0 [1]. To develop reliable simulation tools for Lamb wave resonators, other important aspects, which have not been reported previously, should be investigated: reflection coefficient as function of geometrical parameters, generation of higher-order modes and interaction between the modes in a wide frequency range etc.

Statement of Contribution/Methods

The main parameters required for simulation of resonator performance can be extracted from the dispersion curve Δs(f) of Lamb wave resonator, i.e. normalized wave number versus frequency dependence. The numerical technique SDA-FEM-SDA, which was developed for analysis of SAW resonators sandwiched between multilayered half-spaces with arbitrary thickness of each layer, has been recently successfully applied to simulation of dispersion in Lamb wave resonators using AlN/SiO_2 structures[2]. Here the same technique is used for analysis of dispersion in AlN resonators, in a wide frequency range.

Results/Discussion

Dispersion was simulated for AlN resonators with thicknesses h/2p=0.1 and h/2p=0.5, and Al electrode thickness h/2p =0.004, in frequency range from zero to $f=V_L/2p$, where V_L is the longitudinal BAW velocity in AlN. The behavior of Lamb waves in the grating looks more complicated than that of common SAW because of guiding in a plate of finite thickness. Due to the lossless nature of Lamb waves, velocity changes continuously with frequency even when crosses the cut-off BAW velocity. The modes s_0, a_0 and higher-order Lamb waves interact with each other and build a complicated pattern in the 2D space (f,Δs). The number of modes grows with increasing AlN thickness. When h_{AlN}=1p, interactions between the counter-propagating modes s_0 a_0 and a_1 build the stopbands at λ=2p, 3p and 4p. Each stopband is characterized by own reflection coefficient and resonance of admittance at one of the stopband edges. The velocities of the found modes vary between 4500 and 18000 m/s, with typical k^2 of high-velocity modes about 0.4%. Each mode is characterized by integer number of half-wavelengths within plate thickness, h=nλ/2. It is confirmed by the displacements simulated for the analyzed modes.

[1] F.Di Pietrantonio, M.Benetti, D.Cannata, R. Beccherelli, and E. Verona, IEEE Trans., UFFC-57, No. 5, pp.1175-1182, 2010.

[2] N. Naumenko, in Proc. 2011 IEEE Ultrason. Symp.

IUS4-A-6

Full Vectorial measurement of 2nd harmonic of an FBAR Resonator

Farhad Bayatpur[1], Siamak Fouladi[1], Jong-hoon Lee[1], Dong Shim[1], David Feld[1]; [1]*AVAGO Technologies, San Jose, CA, USA*

Background, Motivation and Objective

We have performed a 1-port measurement of the phase response of the 2nd harmonic emissions of a thin film bulk acoustic (FBAR) resonator. This phase measurement is the difference in phase between the emitted 2nd harmonic waveform to that of the incident waveform. We are not aware of any such measurement prior to this work and with it we have the full vectorial representation of the measured 2nd harmonic response. This vectorial representation is useful for two reasons: (1) To understand the 2nd harmonic behavior of a filter comprised of multiple resonators where interference between vectors takes place, and (2) in understanding the 2nd harmonic responses in the RF front ends of radios where the weak 2nd harmonic vectors of various components -- filters, switches, and other components -- interact with one another.

Statement of Contribution/Methods

Investigators have routinely reported measurements of the 2nd harmonic magnitude response of resonators, but the phase measurement presents a challenge because it requires an elaborate measurement setup with a sophisticated calibration procedure. Using Agilent's non-linear vector network analyzer we were able to measure not only the standard S-parameters of a resonator but at the same time the magnitude and phase of the weak second harmonic.

Results/Discussion

Fig. 1 is a measurement of the 2nd harmonic magnitude response of a resonator referenced to the fundamental frequency (dotted line). Also plotted is the response from our non-linear model (solid line). Fig. 2 shows the measured and modeled phase (dotted & solid). We briefly discuss the measurement setup but we focus on comparing measurement with our non-linear model. We hope this work will lead to the vectorial measurement of intermod products (IMD3) in situations where two or more tones mix.

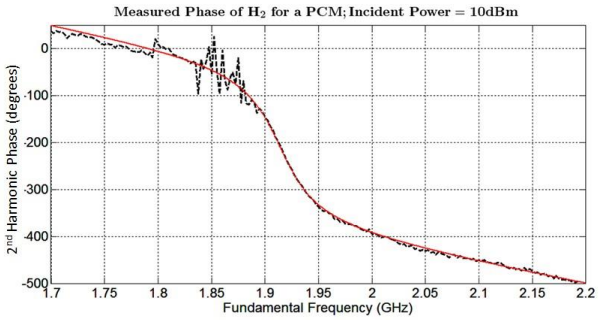
Measured Phase of H_2 for a PCM; Incident Power = 10dBm
2nd Harmonic Phase (degrees)
0
-100
-200
-300
-400
-500
1.7
1.75
1.8
1.85
1.9
1.95
2
2.05
2.1
2.15
2.2
Fundamental Frequency (GHz)

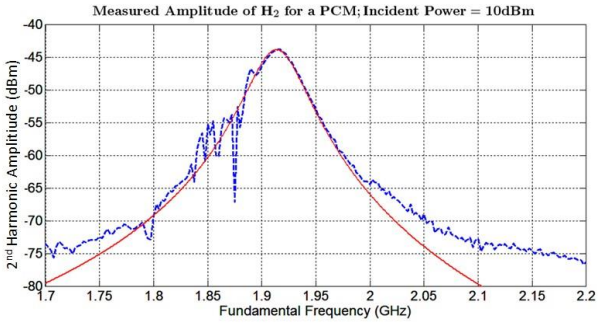
Measured Amplitude of H_2 for a PCM; Incident Power = 10dBm
2nd Harmonic Amplitiude (dBm)
-40
-45
-50
-55
-60
-65
-70
-75
-80
1.7
1.75
1.8
1.85
1.9
1.95
2
2.05
2.1
2.15
2.2
Fundamental Frequency (GHz)

Sonoporation and drug delivery

CONGRESS HALL

Monday, July 22 2013, 02:00 pm - 03:30 pm

Congress Hallair: **Paul Dayton**
UNC Chapel Hill and NC State University

IUS1-B1-1

Basic studies on sonoporation with size- and position-controlled microbubbles adjacent to cells

Nobuki Kudo[1], Yuto Tanaka[1], Kazuaki Uchida[1]; *[1]Graduate School of Information Science and Technology, Hokkaido University, Japan*

Background, Motivation and Objective

We have been studying a sonoporation technique in which cells with adjacent microbubbles are exposed to a single shot of short-pulsed ultrasound. This technique is useful for studying cell damage caused by direct mechanical stress of bubble activities and the following repair process. Here, we introduce a new sonoporation system that can control the sonoporation effect by controlling the size and position of a bubble adjacent to a cell using optical tweezers.

Statement of Contribution/Methods

An inverted-type microscope with an ultrasound exposure system was equipped with optical tweezers. A CW laser of 1065 nm in wavelength and 2 W in maximum optical output was used for the light source. A holographic phase pattern (Fig. 1a) displayed on a phase-only spatial light modulator (X10468, Hamamatsu photonics) was illuminated by a Gaussian beam from the light source and generated a Laguerre-Gaussian (LG) beam. This beam has a dark spot at the center and is used to trap a microbubble that has a refractive index lower than that of the surrounding water (Fig. 1b).

Results/Discussion

Results of basic experiments showed that the tweezers can trap bubbles of 1-5 μm in diameter suspended in water, and the minimum optical power for trapping 2-μm bubbles was around 10 mW. Figures 1c • |1f show a typical sonoporation process of a cell with a bubble manipulated by the optical tweezers. The bubble of desired size was trapped by the LG beam and dragged up along the cell membrane (Fig. 1c), indicating that the optical tweezers have sufficient strength to drag a microbubble up the cell surface. The cell and bubble (Fig. 1d) were irradiated by a single shot of short-pulsed ultrasound, and the resulting cell membrane damage (Fig. 1e) and following repair process (rapid resealing by vesicle accumulation, Fig. 1f) were observed at the bubble position. This experimental method is useful to find the optimal conditions for efficient sonoporation using size- and position-controlled adjacent microbubbles.

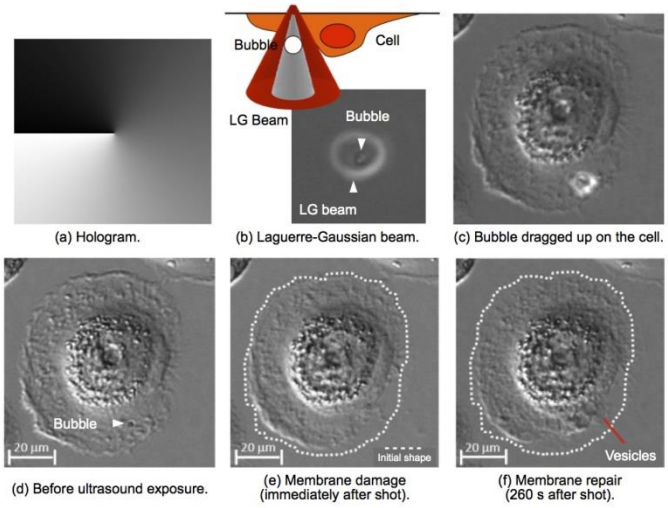

Figure 1. Sonoporation of a cell with an adjacent bubble controlled by optical tweezers.

IUS1-B1-2

Liposome Release from an Oscillating Microbubble

Ying Luan[1], Guillaume Lajoinie[2], Heleen Dewitte[3], Ine Lentacker[3], Tom van Rooij[1], Hendrik Vos[1], Antonius van der Steen[1,4], Michel Versluis[2], Nico de Jong[1,4]; *[1]Erasmus Medical Center, Netherlands, [2]University of Twente, Netherlands, [3]Ghent University, Belgium, [4]Interuniversity Cardiology Institute of The Netherlands, Netherlands*

Background, Motivation and Objective

Microbubbles (MBs) with drug-carrying liposomes attached to the bubble shell have been identified as a highly efficient drug delivery vehicle under the application of ultrasound (US) [1]. Earlier, we have observed US-triggered detachment of liposomes from the MB surface on a microsecond scale [2]. However, further characterizing the release with respect to MB dynamics is essential to understand the release process and control the drug delivery using liposome-loaded (loaded) MBs. Here we present a study to resolve and quantify the liposomes release during MB oscillations on a time scale of nanoseconds.

Statement of Contribution/Methods

1) To qualitatively resolve the liposome release, 24 loaded MBs with DiI-labeled liposomes were investigated. Imaging of the release dynamics was performed with the Brandaris 128 camera at 1 Mfps in fluorescence mode. For each MB, a single US burst of 100 cycles at a frequency of 1 MHz was applied, with an acoustic pressure of 200 kPa. 2) To quantify the release as a function of the bubble oscillations, another 48 loaded MBs were studied. The same US setting was applied on MBs as in 1), except that the acoustic

pressure was ranging from 100 to 300 kPa. The amplitude of oscillations relative to the initial radius was derived from the radius-time curve. Laser-induced fluorescence images on the same MBs were captured before and after US application separately by a Photron camera. The amount of release was quantified based on the image intensity, defined by I_r/I_0, where I_r represents the integrated pixel intensity (IPI) in the area of release after US, and I_0 is the IPI in the MB projection area before US.

Results/Discussion

Qualitatively, 80% of the investigated 24 MBs show a liposome release within the first 10 cycles of the burst (Figure a). Quantitatively, there was a clear threshold for the occurrence of the release at a relative oscillation amplitude of 0.15. In addition, the relative amount of liposome release increases with the amplitude of oscillations, and goes up to 95% for an MB having relative oscillation amplitude of 0.35 (Figure b). In conclusion, the release of drug-loaded MBs can be controlled by US.

[1]I. Lentacker et al. Mol. Ther., vol. 18, pp. 101-8, 2010.

[2]E. C. Gelderblom, PhD thesis: "Ultra-high-speed fluorescence imaging," Enschede, 2012

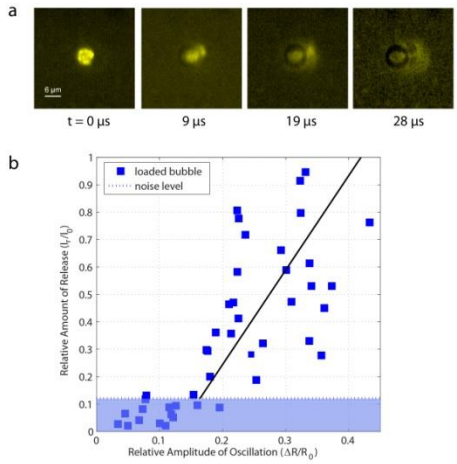

Figure a. liposome release from a loaded MB. b. Quantification of release as a function of the relative amplitude of oscillations for 48 loaded MBs.

IUS1-B1-3

Ultrastructural sonoporation bioeffects: Comparative study on two human cancer cell lines

Aya ZEGHIMI[1], Jean-Michel ESCOFFRE[1], Ayache BOUAKAZ[1]; [1]*Inserm UMR-930 Imagerie & Cerveau, Université François Rabelais, Tours, France, Tours, France*

Background, Motivation and Objective

Sonoporation increases transiently the cell membrane permeability, enabling the therapeutic compounds internalization into the cells. Several investigations reported heterogeneities in the permeabilization and transfection efficacy depending on the ultrasound (US) settings and cell type. Here, we compare the sonoporation effects on two human cell lines, glioblastoma and breast cancer using scanning electron microscopy (SEM).

Statement of Contribution/Methods

Adherent U-87 MG and MDA-MB-231 cells were insonated at 1 W/cm2, during 60 s at 20% or 10% duty cycle, in the presence of BR14® microbubbles, injected at a microbubble-cell ratio of 5. SYTOX® Green, a non-permeant fluorescent dye was used at 1µM, to quantify the membrane permeabilization by flow cytometry. The ultrastructural changes of the cell membrane morphology were monitored by SEM.

Results/Discussion

Flow cytometry results show that the percentage of permeabilized U-87 MG cells reaches 60%, while this value doesn't exceed 40% for MDA-MB-231 cells. These results indicate that the percentage of permeabilized cells depends on the cell type. SEM observations were carried out to elucidate the differences in permeabilization rate between the 2 cell lines.

The SEM analysis reveals that control cells show regular plasma membrane morphology. Their insonation in the presence of BR14® induce the formation of dark holes on their membrane surfaces (named here pore-like structures). However, the quantitative analysis of the SEM micrographs highlights noticeable differences in morphological changes post-sonoporation between the two cell lines. Thus, the mean number of pore-like structures is more abundant on U-87 MG than on MDA-MB-231 membrane (645 vs 290). In addition, the mean size of pore-like structures depends on the cell line. Indeed, the mean size on MDA-MB-231 cells is 40 ± 1.2 nm (30-60 nm) while this value reaches 80 ± 0.9 nm (10 to 160 nm) for U-87 MG cells.

In conclusion, the study confirms that the pore-like structures observed post sonoporation are directly associated to the cell permeabilization level. Moreover, the observed differences in the permeabilization levels between both cell lines could be attributed to the differences in the number and size of pore-like structures that were seen on the cell membrane. This sensitivity to the sonoporation may be due to the fibroblastic nature of the U-87 MG cells.

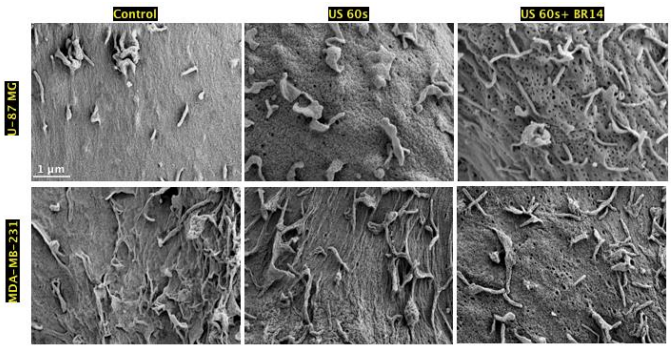

Fig 1: SEM photomicrographs showing plasma membrane morphology of both human cancer cell lines U-87 MG and MDA-MB-231, for three conditions: control cells and insonified cells either in the absence or presence of BR14® microbubbles.

Acknowledgment

This project was funded by the EU Project SONODRUGS (NMP4-LA-2008-213706). The authors are grateful to the Bracco Research Geneva, for supplying the contrast agents and to Rustem Uzbekov for discussions.

IUS1-B1-4

Comparing nanodroplets and microbubbles for enhancing ultrasound-mediated gene transfection

Robert Paproski[1], **Roger Zemp[1]**; [1]*University of Alberta, Canada*

Background, Motivation and Objective

Ultrasound exposure to cells can facilitate gene transfection due to sonoporation. Microbubbles can increase the efficiency of ultrasound-mediated transfection but are relatively large (2-4 µm) and cannot extravasate. The inner gas of perfluorobutane microbubbles can be turned into liquid through pressurization, creating nanodroplets which may be more effective at accumulating in tumors due to their smaller size. Perfluorobutane nanodroplets can phase change back into microbubbles with ultrasound which can be used as cavitation nuclei for sonoporation. Our objective was to compare perfluorobutane nanodroplets and microbubbles for their ability to enhance ultrasound-mediated transfection in vitro and in vivo.

Statement of Contribution/Methods

Microbubbles were made by shaking a lipid stock in a tube with a perfluorobutane headspace. Nanodroplets were created by pressurizing the microbubbles. Transfection experiments were performed by incubating confluent HEK293 cells in 24-well plates with 12 µg/mL pEGFP-C1 with or without 2% (v/v) microbubbles or nanodroplets. Cells were sonicated with 1 MHz ultrasound (0.76 mechanical index) for 10 – 100,000 cycles and transfection efficiency was determined by flow cytometry the following day. Bioluminescence imaging was used to assess in vivo transfection due to intramuscular injection of luciferase plasmids with or without microbubbles / nanodroplets and ultrasound.

Results/Discussion

Ultrasound alone only demonstrated significant transfection with 100,000 cycles ultrasound (1.5 ± 0.3 %). Ultrasound with microbubbles displayed a relatively linear increase in transfection efficiency with increasing ultrasound cycles. Compared to microbubbles, nanodroplets displayed significantly less transfection with 100 cycles ($P < 0.05$, presumably due to most nanodroplets not being converted yet into microbubbles) but similar levels of transfection at 1000 and greater cycles of ultrasound. Compared to 10,000 ultrasound cycles without contrast agent, addition of microbubbles and nanodroplets increased transfection efficiency 23- and 32-fold, respectively. In vivo imaging demonstrated markedly significant increases in luciferase expression in muscle tissues when both ultrasound and contrast agents are used compared to either treatment alone or untreated locations.

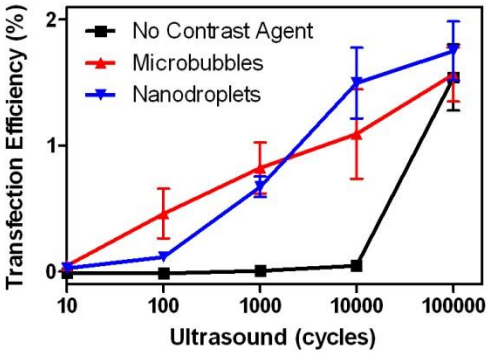

IUS1-B1-5

Precision drug delivery with ultrasound and microbubbles: mechanisms, applications and (progress to) translation to clinics

Ayache Bouakaz[1]; [1]*Université François Rabelais, INSERM U930, TOURS, France*

Background, Motivation and Objective

Targeted drug delivery (delivery of a drug to a spatially localized site in the human body) is one of the most ambitious goals of modern therapy. The strict localization of the pharmacological activity of a drug to the site of pathology would result in a significant reduction in systemic drug toxicity. This would enable the ability to deliver increased doses

of drug to desired tissue, and thus would result in an increase in treatment efficacy and safety. Although a great amount of work is conducted worldwide on the research of various targeted drug delivery systems, clinical applications of site-targeted delivery are still very limited. In recent years, new promising possibilities for targeted drug delivery have been discovered based on the combination of ultrasound (US) and microbubbles.

Statement of Contribution/Methods

Sonoporation consists of the interaction of US waves and gaseous microbubbles used as contrast agents. The result of this interaction is a transient permeabilization of the cell membrane allowing for the uptake of drugs or DNA, and other therapeutic compounds from the extracellular environment. The membrane alteration is temporary but leads to a permanent trap of the compound inside the cell after US exposure. The first experiments on sonoporation date back to 1980s, Various US exposure conditions have been tested blindly including frequencies ranging from the kHz to the MHz. Sonoporation has also been evaluated using high pressure amplitude US waves. Since then and with the recent introduction of contrast agents, higher frequency US with cavitation enhanced by microbubbles have been sought to induce a range of effects on cells. Extensive examinations have been carried out to evaluate the efficiency of US in combination with contrast microbubbles in inducing cellular uptake. Although these result and finding were achieved in a controlled in-vitro environment, diagnostic US scanners were also useful for therapeutic applications of sonoporation particularly with the guidance of treatment afforded by the imaging mode.

Results/Discussion

Today, the mechanisms involved in the sonoporation process and the cell membrane permeabilization remain poorly identified. Although no consensus has been reached, several scenarios have been hypothesized, including the formation of pores, further stimulation of endocytotic pathways and occurrence of membrane wounds. Elucidating the mechanisms responsible for delivery of compounds to the cells and the kinetics of permeabilization are essential in order to improve and control this therapeutic strategy. This invited talk will focus on the current knowledge of the mechanisms of sonoporation and drug delivery using US and microbubbles. We will also discuss the current therapeutic applications of microbubbles and future progress and potential translational use into clinics.

3D and vector velocity imaging

M4

Monday, July 22 2013, 02:00 pm - 03:30 pm

Congress Hallair: **Jørgen Jensen**
Technical University of Denmark

IUS1-B2-1

3D Intra-cardiac flow estimation using speckle tracking: a feasibility study in synthetic ultrasound data

Hang Gao[1], Brecht Heyde[1], Jan D'hooge[1,2]; *[1]Cardiovascular Imaging and Dynamics, Department of Cardiovascular Sciences, KU Leuven, Belgium, [2]Medical Imaging Laboratory, Norwegian Institute for Science & Technology, Norway*

Background, Motivation and Objective

In recent years, echo particle image velocimetry (EPIV) has been proposed to characterize intra-cardiac flow fields non-invasively. To date, these methods remain 2D. As volumetric cardiac ultrasound has become more readily available and as this may avoid some of the problems inherent to 2D imaging (i.e. out-of-plane flow), the aim of this study was to test whether EPIV could be extended to 3D using synthetic data sets.

Statement of Contribution/Methods

A typical inflow velocity profile and a dynamic volume change profile combined with a 3D anatomical model of the left ventricle (LV) were used to build a realistic computational fluid dynamics (CFD) flow vector field (Fluent 12.1, ANSYS). 3D B-mode image sequences were acquired using a fast ultrasound simulator (COLE) of virtual contrast bubbles moving along this 3D flow field. The simulated US system was equipped with a two-dimensional phased array transducer transmitting a Gaussian pulse with a -6dB relative bandwidth of 65% (frequency = 4.5MHz; sampling frequency = 50MHz; 60×60 degrees opening angle; frame rate = 113 Hz; image size 120×60×60mm). Inter-frame motion during diastasis was estimated by volumetric speckle tracking (kernel 2.2×16.4×16.4mm; search region 10.8×22.4×21.2mm; overlap 40%×90%×90%) using 3D normalized cross-correlation as a similarity metric. Cubic spline interpolation was embedded for subsample motion estimation prior to median filtering (6.34×4.73×4.75mm) of the resulting velocity vector field. Regression and correlation coefficients of the estimated velocity amplitudes with the CFD reference ground truth were calculated.

Results/Discussion

The figure shows the estimated velocity field (a), the CFD reference (b) as well as the point-wise velocity vector errors (c) during diastasis together with the color coded velocity amplitude. The averaged point-wise velocity vector error was 0.02 m/s. The correlation coefficient of the velocity amplitudes was 0.88 and the regression line was shown in panel (d). This simulation study showed the feasibility of extending EPIV to 3D in order to measure 3D intra-cardiac flow fields. More thorough investigation during the whole cardiac cycle is ongoing.

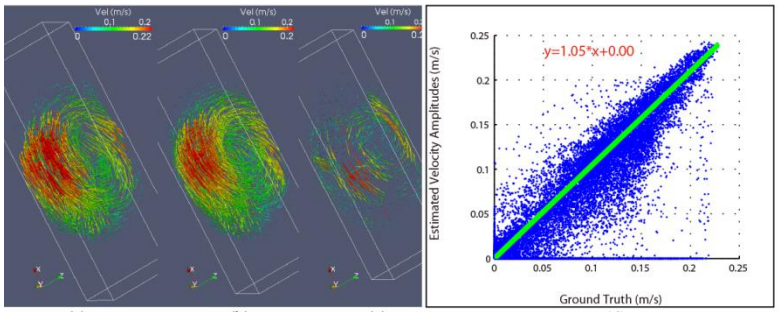

IUS1-B2-2

3-D Velocity Tensor Imaging in Two Orthogonal Planes

Michael Johannes Pihl[1], Jørgen Arendt Jensen[1]; *[1]Center for Fast Ultrasound Imaging, Dept. of Elec. Eng., Technical University of Denmark, Kgs. Lyngby, Denmark*

Background, Motivation and Objective

This paper presents examples of 3-D velocity tensor imaging (VTI) obtained using the 3-D Transverse Oscillation (TO) method, which estimates all three spatial velocity components. 3-D VTI has a high temporal resolution and does not require reconstruction opposed to MRI using ECG gating. This paper demonstrates that the 3-D TO method is suitable for performing real-time 3-D VTI.

Statement of Contribution/Methods

A carotid artery flow phantom is connected to a CompuFlow 1000 flow system (Shelley Medical Imaging Technologies, Toronto, Canada), which is set to drive a constant flow rate of 10 ml/s. The phantom is scanned using a 3.5 MHz 32x32 element 2-D phased-array transducer (Vermon S.A., Tours, France) connected to the experimental ultrasound scanner SARUS. Flow data are acquired in two sectorial scan planes orthogonal to each other: *ZX* and *ZY*. The transducer is orientated to yield a cross sectional view (*ZX*) and a longitudinal view (*ZY*) of the vessel. The main flow direction is expected to be in the *y* direction. Each plane covers a depth of 4 cm and consists of 15 flow lines spanning a sector of 30 degrees. The three estimated velocity components are rotated and scan converted accordingly. Using 32 emissions per velocity estimate, a frame rate of 20 Hz can be obtained.

Results/Discussion

One frame of the three velocity components v_x, v_y, and v_z for both planes are shown in the figure. The velocity components v_x and v_z are almost 0 cm/s for both planes as expected due to the transducer orientation. For the top row, v_y is the out-of-plane motion, which the 3-D TO method makes it possible to measure. As the blue colors indicate, an out-of-plane motion is estimated. At the center of the vessel, the mean and standard deviation of the velocity magnitude based on 10 frames are 38.9±5.2 cm/s compared to the expected 39.8 cm/s. The standard deviation relative to the peak velocity is 13%. Integrating the out-of-plane velocity component yields a volumetric flow rate of 9.97 ml/s compared with

the expected 10 ml/s. For the bottom row, mainly v_y shows estimated velocities different from 0 cm/s. The colors indicate velocities ranging from 0 cm/s to approximately -40 cm/s. The red area is due to aliasing. The results demonstrate that 3-D VTI is feasible using the 3-D TO method, and that a temporal resolution of at least 20 Hz can be achieved allowing for dynamic studies of complex flow phenomena and heart rate variability.

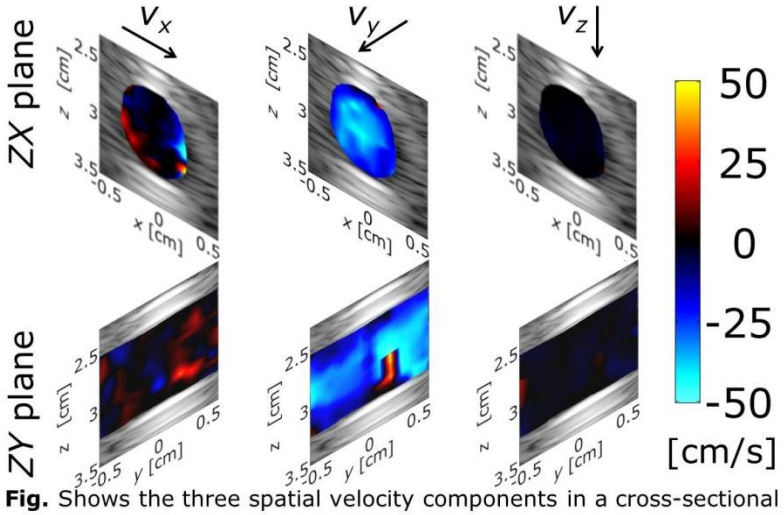

Fig. Shows the three spatial velocity components in a cross-sectional plane (top row) and a longitudinal plane (bottom row) of the vessel.

IUS1-B2-3

Full 3D vascular atlas of the rat brain via Ultrafast Doppler Tomography

Charlie Demene[1], Ana Ricobaraza[2], Anastasia Vorontsova[1], Bruno-Felix Osmanski[1], Sophie Pezet[2], Zsolt Lenkei[2], Mickael Tanter[1]; *[1]Institut Langevin, ESPCI ParisTech, CNRS UMR7587, Inserm U979, Universite Paris7, Paris, France, [2]Laboratoire de Neurobiologie, ESPCI ParisTech, CNRS UMR7637, Paris, France*

Background, Motivation and Objective

The emergence of functional Ultrasound (fUS) Imaging based on Ultrafast Doppler to detect changes of cerebral blood volume in the rat brain correlated with a functional activity opens a new field of application for Ultrasound: its use as a routine tool in neuroscience to study the working brain. As a consequence there is a need for a reference atlas of the typical vascular slices observed via fUS, in connection with the reference anatomical structures. In this study, we propose a tomographic method for the construction of this high resolution atlas, with a complete voxel representation of the blood volume in the whole brain with an unprecedented resolution (100µmx100µmx100µm) and a 3D meshing of the detected vessels.

Statement of Contribution/Methods

N=5 Rats were used to reduce inter-individual variance, and underwent a complete craniotomy fixed in a stereotactic frame, on an anti vibration table. A 15 MHz ultrasound probe mounted on a four degree of freedom set of motors localized in stereotactic coordinates was used to acquire coronal, sagittal and intermediate slices. The main issue is the resolution which is high in the imaging plane (80 µm) but low in the elevation plane (400 µm). To reduce the point spread function, particularly in the elevation plane, 18 different vertical imaging planes, rotated of 10° compared to each other, were used. For each plane, 70 different slices, 200µm apart along the transverse translation were imaged. For each slice an Ultrafast Doppler ultrasound acquisition, consisting in 400 repetitions, at a 500Hz frame rate, of a 15 angle compound plane wave emission, was done. The complete acquisition of this 1260 Doppler images data set was achieved in less than 3 hours. The fusion of these images was then computed to improve the resolution. A reconstruction algorithm based on a segmentation of the vascular structures and a meshing using marching cubes was performed to obtain a 3D vascular network. Comparison with histological data was conducted by labeling and visualization of blood vessels with a lipophilic carbocyanine dye.

Results/Discussion

High quality Ultrafast Doppler images were obtained from the acquisition, enabling to observe precisely the 3D architecture of blood vessels inside the rat brain. From the referenced fusion volume, a slice in any orientation can be easily obtained with a good resolution, enabling the design of new imaging protocols for functional imaging: previously, fUS imaging was only performed in coronal and sagittal slices because the imaged structures were easier to recognize. It is now possible to choose an arbitrary imaging slice, for the need of an experiment with two remote cerebral structures, and to verify on the fly the pertinence of the visualized slice by comparison with the atlas. The 3D angiographic mesh is the first reconstruction of this kind for the study of the rat brain. Data and 3D viewer will be soon freely available for reference and academic use.

IUS1-B2-4

In vitro Validation of an Accuracy Feedback Method for Ultrasonic Vector Flow Mapping in 3D Velocity Field

Tomohiko Tanaka[1], Rei Asami[1], Ken-ichi Kawabata[1], Kunio Hashiba[1], Takashi Okada[2]; *[1]Hitachi Ltd., Japan, [2]Hitachi Aloka Medical Ltd., Japan*

Background, Motivation and Objective

Vector flow mapping (VFM) is a promising and clinically handy tool for obtaining 2D flow vectors in the left ventricle (LV). VFM estimates azimuth velocities by using color Doppler velocities under a non-trivial assumption that the flow is planar in the imaged plane. Due to the planar flow assumption, through-plane (TP) velocity is the dominant error source, and TP velocity depends on the angle of the flow direction and the imaged section, indicating that VFM errors vary for each measurement. To resolve this issue, we proposed an method to provide the VFM accuracy feedback for each measurement [1]. Given that uncertainty of certain VFM measurements is fed back, quality of diagnosis can be improved by rejecting, or retaking, VFMs with large uncertainties. We had shown the validity of the method for case with small TP flows, but further examination of the 3D velocity fields is needed to establish this method. In the present study, the method was experimentally validated for cases with large and small TP flows using an LV phantom.

[1] Tanaka et al. IEEE IUS (2012)

Statement of Contribution/Methods

An in vitro experimental phantom [1] developed by our group was used to validate the proposed method. The flow vectors inside the LV phantom (Fig. 1(a)), which were pulsated by controlling the external pressure, were measured by both VFM and optical stereo PIV (particle image velocimetry), which gives accurate 3D velocity components in a plane.

The estimated VFM accuracy with the proposed method was compared with the accuracy measured by stereo PIV. Two imaged planes, one parallel and the other perpendicular to the valve alignment (Fig. 1(b)), were examined to investigate the effects of the TP velocities.

Results/Discussion

Fig. 1(c) shows the correlation of VFM errors between estimated and measured VFM errors. Each result (shown as a dot) was calculated by using vector data in two frames, and 5-beat data sets were examined. When TP velocities were small in plane A, the error range was less than 0.05 m/s, while a larger error range was observed with large TP velocities in plane B. However, the estimated errors correlated well with the measured ones regardless of TP velocities. It can be concluded that the VFM accuracy feedback method is applicable for 3D flow fields. Further results will be presented.

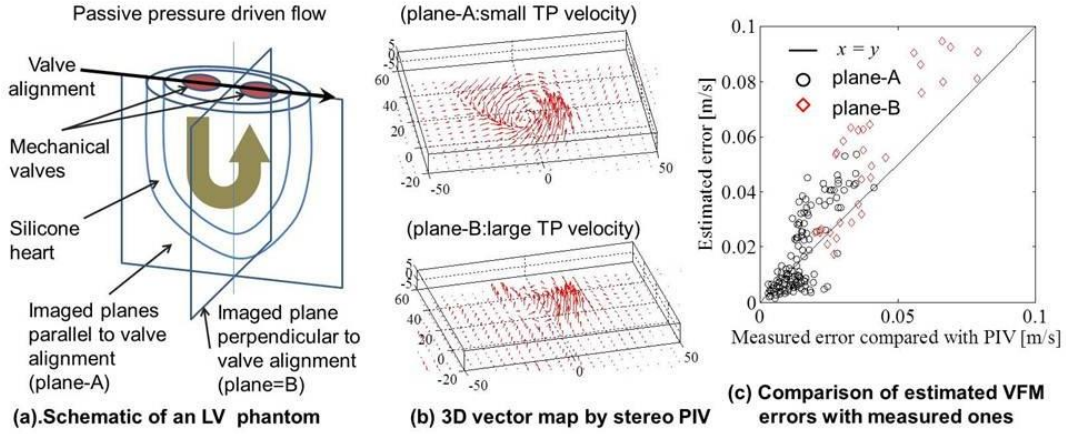

Fig. Correlation of VFM errors between estimated errors by ultrasound and measured errors by PIV for case with small and large through-plane velocities.

IUS1-B2-5

In vivo out-of-plane Doppler imaging based on ultrafast plane wave imaging

Bruno-Félix Osmanski[1], Gabriel Montaldo[1], Mathias Fink[1], Mickael Tanter[1]; [1]*Institut Langevin, ESPCI ParisTech, CNRS UMR7587, Inserm U979, Universite Paris 7, Paris, Ile de France, France*

Background, Motivation and Objective

Retrieving the blood flow velocity vector (VV) on 2D acquisitions transverse to the vessel (fig a) could improve the quantification of flow rate in large vessels. The *in plane* component is easily computed using the Doppler frequency shift. The main problem is to retrieve the angle α between the probe and the vessel to compute the out of plane component. Here, we study the case where the VV is contained is the plane (z,y) and explore the combination of a technique called spectral broadening with the high spatio temporal sampling of ultrafast plane wave imaging (UPWI) which permit a Doppler spectrum (DS) quantification of flows in each pixel to retrieve the out of plane component of the blood flow VV in 2D. Moreover, UPWI permits a fast calibration method of DS spectral broadening avoiding approximations of a complex theoretical analysis.

Statement of Contribution/Methods

The calibration is performed on a agar phantom. The transducer array (8MHz) is moved with a 5 cm/s speed with an angle α (fig b). We measure the spectral broadening of DS in a 2D plane for 20 different angles from 1° to 20° then using the scaling property of DS we can compute its spectral broadening for every speed for the set of angles acquired. Figure c shows an example of calibration spectrum. The inverse problem consists in retrieving the absolute speed from a measure of the DS.

Results/Discussion

First, the technique was tested retrieving VV of Poiseuille flow and accelerated moving phantom for several speeds and angles. Then, the carotid artery of N=5 healthy volunteers was imaged at an ultrafast frame rate (5kHz) using plane wave transmits during a complete cardiac cycle (1s). Longitudinal (i. e. the VV direction is in the imaging plane which allows to measure the absolute VV by evaluating the angle between the VV and the probe) and transverse acquisitions were performed. Figure d shows that we can retrieve the same absolute VV in time on both acquisitions. Using transverse vessel imaging also allows to compute two dimensional space profile of the blood flow VV (fig e), we see that spatial distribution of the VV in the carotid artery is not circular so this technique can improve the studying of VV spatial gradient. This quantitative technique for out-of-plane VV measurement could be an asset in many configurations for which the longitudinal view is not available such as for example in the aorta during transcostal examination.

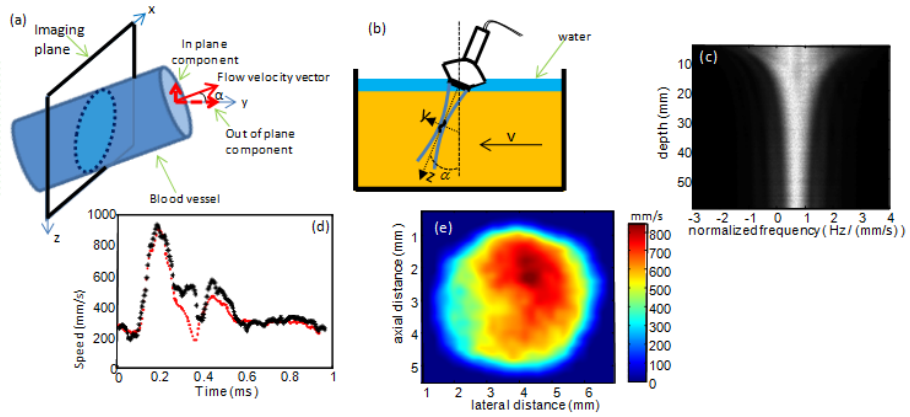

Figure: (a) Description of transverse imaging of a blood vessel, (b) Experimental set-up for the spectrum calibration, the imaging plane is orthogonal to the figure, (c) Example of calibration spectrum (α=4°), we notice that the DS width is varying with the depth due to the elevation focus of the probe, (d) Time speed profile obtained with the transverse (black) and the longitudinal (red) acquisition on a region of interest , (e) Two dimensional speed profile obtained with a transverse acquisition at the time 270ms.

IUS1-B2-6

High-Frame-Rate Color-Encoded Speckle Imaging for Visually Intuitive Rendering of Complex Flow Dynamics

Billy Y. S. Yiu[1], Alfred C. H. Yu[1]; [1]*Medical Engineering Program, The University of Hong Kong, Pokfulam, Hong Kong*

Background, Motivation and Objective

Realization of flow imaging at high frame rates can undoubtedly benefit the visualization of complex flow patterns with significant spatiotemporal variations. It would be even better if fluid motion can be coherently rendered through parallel display of both flow trajectory and flow speed. Driven by these motivations, we have developed a new high-frame-rate ultrasound flow visualization technique called color-encoded speckle imaging (CESI). It provides a visually intuitive interpretation of complex flow through a hybrid display format that shows both flow speckle pattern and color-encoded velocity mapping.

Statement of Contribution/Methods

CESI works by integrating two key principles: 1) using broad-view data acquisition schemes to obtain image data at frame rates well beyond the video range; 2) deriving and displaying both flow speckles and velocity estimates from the acquired broad-view data. We have realized CESI on a channel-domain research platform that consists of a programmable transmit core (SonixTouch), a pre-beamformed data acquisition tool (SonixDAQ), and a high-performance GPU-array processor (for flow signal processing). Plane wave compounding was implemented (5 steering angles, ranging from -10 to +10 degrees), and these parameters were used: 10 kHz PRF (yielding 2000 fps frame rate for 5 steer angles), 3-cycle transmit pulse, and 7 MHz frequency. Speckle and velocity were estimated using a sliding window method and the lag-one autocorrelation algorithm. The performance of CESI was evaluated in the context of monitoring complex flow dynamics inside a carotid bifurcation flow phantom with 25% eccentric stenosis at the ICA inlet (developed via investment casting). Cineloops were generated in both the CCA and the bifurcation region.

Results/Discussion

With 2000 fps frame rate and parallel rendering of speckles and velocities, CESI was capable of visualizing various fast-changing flow dynamics (both spatially and temporally) in a stenosed carotid bifurcation with 72 bpm pulses. Not only was CESI able to track flow acceleration and deceleration, it was also effective in depicting flow jet formation and progression as well as the development of recirculation zones (see figure). These are new visualization features beyond what color flow imaging is capable of providing. They demonstrate that CESI can more intuitively render complex flow dynamics.

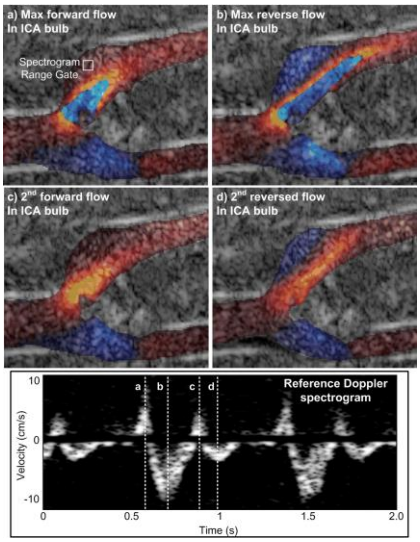

Soft tissue characterization I

M5

Monday, July 22 2013, 02:00 pm - 03:30 pm

Congress Hallair: **James Miller**
Washington University in Saint Louis

IUS1-B3-1

In Vivo Measurements of the Shear wave Velocity and Attenuation in the Pancreas

Ivan Nenadic[1], Matthew Urban[1], James Greenleaf[1]; [1]*Mayo Clinic, USA*

Background, Motivation and Objective

Pancreatic cancer is the fourth most common cause of cancer-related deaths in the United States with the one- and five-year survival rates of 25% and 6% respectively. In 80% of the cases patients report pain in the advanced metastatic stage of the disease with no well-established biomarkers for the disease. We have been investigating the use of shear wave vibrometry to quantify mechanical properties of 4 excised pig pancreases. In addition, we performed in vivo transabdominal measurements of shear wave velocity and attenuation of the pancreas in a pig.

Statement of Contribution/Methods

Ultrasound radiation force was focused in the pancreas to excite impulsive shear waves. Pulse-echo ultrasound was used to track the motion of the tissue and cross-spectral analysis to calculate tissue displacement as a function of time and propagation distance, u(x,t). A two-dimensional fast Fourier transform (2D FFT) of u(x,t) yielded the k-space whose coordinates are the wave number (k) and frequency (f). Shear wave velocity (c) at any frequency was calculated by finding the peak at that frequency in the 2D FFT and dividing the frequency (f) coordinate by the wave number (k) coordinate ($c = f/k$). The shear wave attenuation (α) at the given frequency was obtained using the equation $\alpha = (\pi/\sqrt{3})$ x FWHM, where FWHM is the full width at half-maximum of the peak along the k-axis. A fully programmable ultrasound system (Verasonics, Inc. Redmond, WA, USA) operating a linear array probe (L7-4Philips Healthcare, Andover, MA) was used to excite 400 μs impulse in the pancreases and track the motion by compounding flash imaging at 10 kHz from three different angles. First, we studied shear wave propagation at several different locations in 3 excised porcine pancreases and repeated each measurement 5 times. In addition, we submerged an excised pig pancreas in a formalin bath and measured the shear wave velocity and attenuation every 20 minutes for a total of 100 minutes. Measurements in the in vivo pig pancreas were performed both trans-abdominally and with an open abdomen allowing a direct acoustic access to the organ. In the formalin and the in vivo studies, shear wave velocity and attenuation were measured at 100 Hz.

Results/Discussion

The group velocities in the three excised pancreases ranged from around 0.65 m/s to around 1.1 m/s with the largest standard deviation around 9% of the mean. The formalin studies showed that the velocity increased from 0.5 m/s at t = 0 minutes to 1.1 m/s at t = 100 minutes, while the attenuation decreased from around 400 Np/m to around 200 Np/m. The formalin studies suggest that shear wave vibrometry can track changes in pancreatic shear wave velocity and attenuation. In vivo transabdominal values of shear wave velocity and attenuation at 100 Hz were $c = 1.07$ m/s and $\alpha = 173$ Np/m. The in vivo open-abdomen values were $c = 1.14$ m/s and $\alpha = 170$ Np/m. These results demonstrate the feasibility of using shear wave vibrometry to assess mechanical properties of the pancreas.

IUS1-B3-2

Detecting Cervical Softening with Shear Wave Speed Estimation

Lindsey C. Carlson[1], Helen Feltovich[1,2], Mark Palmeri[3], Alejandro Munoz Del Rio[1], Michael H. Wang[3], Timothy J. Hall[1]; [1]*Medical Physics, University of Wisconsin, Madison, WI, USA,* [2]*Maternal Fetal Medicine, Intermountain Healthcare, Park City, UT, USA,* [3]*Biomedical Engineering, Duke University Pratt School of Engineering, Durham, NC, USA*

Background, Motivation and Objective

Spontaneous preterm birth is the leading cause of neonatal morbidity and mortality. The cervix must soften, shorten, and dilate to allow for delivery of a fetus, but premature changes may lead to premature birth. Although the cervix plays a critical role in parturition, there exists no objective method to evaluate its stiffness/softness. Our goal is to develop a safe, reliable, non-invasive method to assess cervical softness. The aim of our current work is to determine the sensitivity in shear wave speed (SWS) for distinguishing normal non-pregnant cervices with those that have been artificially ripened using a prostaglandin agent.

Statement of Contribution/Methods

Hysterectomy specimens were obtained from 22 subjects, 7 of whom received a prostaglandin agent (misoprostol) the night prior to surgery to ripen/soften the cervix. Specimens were bivalved, placed in saline solution, and scanned with a Siemens Acuson S2000 system using a 9L4 linear array transducer aligned parallel to the endocervical canal. SWS measurements were taken at 5 locations along the canal (10-30mm from external os) with 5 replicate measures at each location to increase precision. SWS estimation was performed using an iterative random sample consensus (RANSAC) method. Two-sided t-tests and receiver operating characteristic (ROC) curves were obtained for mean medial SWS in the anterior and posterior sides. Areas under the curve (AUC), 95% confidence intervals and odds ratio (OR) were computed, and the former were compared via N=2000 bootstrap replicates.

Results/Discussion

The SWS estimates were significantly lower ($p<0.001$) for specimens treated with misoprostol (2.11 +/- 0.45 m/s and 2.66 +/- 0.56 m/s for anterior and posterior, respectively) compared to the unripened group at the medial location (3.45 +/- 0.95 m/s and 3.58 +/- 0.89 m/s for anterior and posterior, respectively). Anterior SWS had good discriminatory ability (AUC=0.9, 95% CI: 0.72-1.00) and was significantly associated with ripening (OR=0.47, p=0.038). Posterior SWS was marginally significant (OR=0.126; p=0.10) and had lower discriminatory ability (AUC=0.8), although it was not significantly different from that of anterior SWS (p=0.52). There is a statistically significant difference in SWS estimates between hysterectomy specimens that are treated with a prostaglandin agent and untreated specimens. SWS estimation is an effective quantitative tool that has potential for applications to preterm birth.

Acknowledgements:

This work was supported by NIH grant R21HD063031.

IUS1-B3-3

Spatial Variability of Shear Wave Speed Estimation in Non-Pregnant Cervix

Lindsey C. Carlson[1], Helen Feltovich[1,2], Mark Palmeri[3], Alejandro Munoz Del Rio[1], Michael H. Wang[3], Timothy J. Hall[1]; *[1]Medical Physics, University of Wisconsin, Madison, WI, USA, [2]Maternal Fetal Medicine, Intermountain Healthcare, Park City, UT, USA, [3]Biomedical Engineering, Duke University Pratt School of Engineering, Durham, NC, USA*

Background, Motivation and Objective

Cervical remodeling in pregnancy begins with softening soon after conception, and later becomes markedly softer and also shortens and dilates to allow delivery of a fetus. Preterm birth may be linked to premature softening and changes in cervical structure, but currently there is no objective tool to clinically assess the softness/stiffness of the cervix. Our objective is to develop a safe, reliable, non-invasive method to monitor the state of the cervix. Due to known cervical heterogeneity, careful analysis of spatial variability in shear wave speed (SWS) estimates is essential for *in vivo* studies. The aim of our current work is to use SWS estimation to assess cervical softening as a function of location in hysterectomy specimens.

Statement of Contribution/Methods

Hysterectomy specimens (n = 22) from nonpregnant women were bivalved into anterior and posterior halves and placed in an isotonic solution. A Siemens Acuson S2000 system was used to scan each specimen with a 9L4 linear array transducer aligned parallel to endocervical canal. SWS estimates were obtained in five positions along the canal (10-30mm from the external os) with 5 replicate measures at each location. The shear wave speeds were estimated using an iterative Random Sample Consensus (RANSAC) method. Linear mixed models were used to model SWS as a function of anterior/posterior half, location (fixed effects) and cervix (random effects) with a $p < 0.05$ (two-sided) criterion for statistical significance.

Results/Discussion

An average of all specimen shear wave speed estimates showed an increase in shear wave speed from distal to proximal end. In multivariate analysis, SWS varied by location ($p < 0.001$). In addition, location interacted with anterior/posterior side ($p = 0.014$). The posterior side showed a larger gradient in average SWS than the anterior side.These results demonstrate there is a significant stiffness gradient along the endocervical canal that can be characterized using shear wave speed estimation. This tool provides a non-invasive, quantitative means for assessing the softness of the uterine cervix.The dependence of SWS on location will need to be taken into account when assessing pregnant cervixes for premature softening.

Acknowledgements:

This work was supported by NIH grant R21HD063031.

IUS1-B3-4

Ultrasonic attenuation imaging in a rodent thyroid cancer model

Omar Zenteno[1], Billy Ridgway[2], Sandhya Sarwate[2], Michael Oelze[2], Roberto Lavarello[1]; *[1]Sección Electricidad y Electrónica, Pontificia Universidad Católica del Perú, San Miguel, Lima, Peru, [2]Department of Electrical and Computer Engineering, University of Illinois at Urbana-Champaign, Urbana, IL, USA*

Background, Motivation and Objective

The incidence of thyroid cancer has increased significantly over the last decades. Although advances in ultrasonic imaging have made malignancies more likely to be detected, current ultrasonic imaging markers do not provide a sufficient level of diagnostic accuracy to replace fine needle aspiration biopsy. Recent studies suggest that ultrasound parameters derived from backscatter coefficients may allow differentiating among different types of thyroid tumors and normal tissues. In this work, the potential of attenuation coefficient (AC) estimates to differentiate among different types of benign and malignant thyroid tissues in a rodent model ex vivo was explored.

Statement of Contribution/Methods

The model consisted of mice having different predispositions to developing thyroid abnormalities. A sample set of 24 excised mice thyroids were scanned using a 40-MHz, f/3 single element transducer. According to the results of the histo-pathologic classification, the experimental dataset contained six animals that developed papillary thyroid carcinoma (PTC), five that developed follicular variant papillary thyroid carcinoma (FV-PTC), five that developed c-Cell adenoma (c-Cell) and eight that did not develop thyroid abnormalities (control). AC slope maps were generated with a spectral log difference method using 0.5mm by 0.5mm data blocks. Outliers of each slice due to artifacts in AC estimation were discarded using the Thompson Tau method. Finally, a Kruskal-Wallis test was conducted to analyze if statistically significant differences in the mean AC slope among the four groups existed.

Results/Discussion

An example of the attenuation maps obtained from a control and a c-Cell thyroid is shown in Fig 1a. The Kruskal-Wallis distribution chart of the 24 samples is shown in Fig 1b. The median and interquartile range for each group were 1.41 and 0.19 dB/cm-MHz for the control group, 1.60 and 0.20 dB/cm-MHz for c-Cell, 1.28 and 0.45 dB/cm-MHz for PTC and 1.40 and 0.06 dB/cm-MHz for FV-PTC, respectively. These values are consistent with previous reports of attenuation in thyroid tissues. The Kruskal-Wallis test reported statistically significant differences between the c-Cell group and the other groups of study ($p<0.05$). These preliminary results suggest that the AC may be used to discriminate the c-Cell samples among these specific pathological groups.

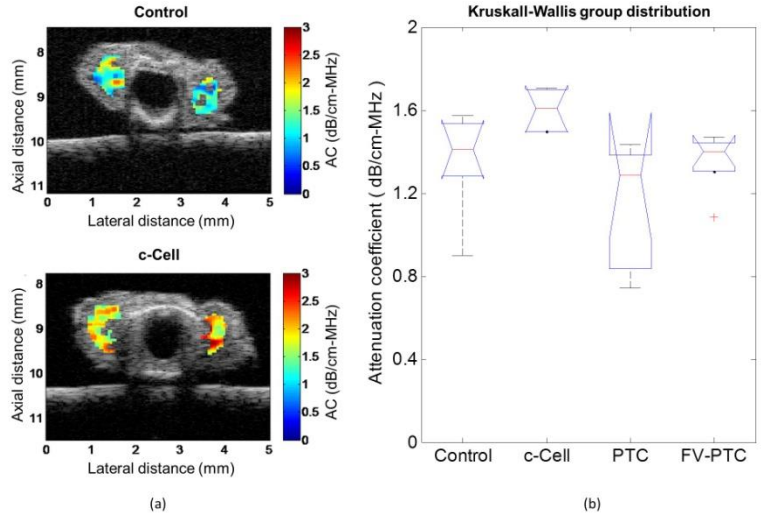

IUS1-B3-5

In Vivo Human Assessment of Bladder Elasticity and Compliance using Ultrasound Bladder Vibrometry (UBV) and Comparison with Urodynamic Studies

Ivan Nenadic[1], Mohammad Mehrmohammadi[1], Matthew Urban[1], Azra Alizad[1], James Greenleaf[1], Douglas Husmann[1], Lance Mynderse[1], Mostafa Fatemi[1]; *[1]Mayo Clinic, USA*

Background, Motivation and Objective

Bladder stiffens with age and various pathological processes. Urodynamic studies (UDS) are currently considered the gold standard in clinical assessment of bladder compliance and are based on measuring the detrusor pressure as a function of catheter filling. UDS are accompanied with pain, traumas and infections during and after the procedure in both men and women. We have been investigating the use of Ultrasound Bladder Vibrometry (UBV) for noninvasive measurement of bladder wall elasticity in patients. In this study, we present in vivo patient assessment of bladder elasticity and compliance using UBV and compare it to UDS.

Statement of Contribution/Methods

In UBV, ultrasound radiation force is focused at the bladder wall to excite impulsive anti-symmetric Lamb waves. Pulse-echo ultrasound is used to track tissue motion, and cross-spectral analysis of the received echoes is used to calculate the wall displacement. Fourier-space analysis of the displacement is used to calculate the change of Lamb wave velocity as a function of frequency, i.e., the Lamb wave dispersion. The Lamb wave dispersion equation is fit to the dispersion data to estimate bladder elasticity. Six patients with healthy and neurogenic bladders undergoing routine UDS evaluations at the Mayo Clinic were recruited for our study. All studies were performed under a protocol approved by the institutional review board (IRB). A programmable ultrasound scanner system (Verasonics, Inc. Redmond, WA, USA) operating a curved array probe was used to excite a 400 µs impulse in the bladder wall and track the motion with plane wave imaging at 2 kHz.

Results/Discussion

Results of UBV and UDS measurements in a neurogenic patient bladder are shown in Figure 1a and 1b, respectively. Both methods show that the bladder compliance does not change significantly until 225 mL at which point both the UDS and UBV curve show a significant increase in detrusor pressure and elasticity, respectively. Similar measurements were performed in 3 patients with healthy bladders and 3 patients with neurogenic bladders. Healthy bladders were more compliant than the neurogenic bladders as their bladder elasticity does not increase significantly over the full range of bladder capacity. The results presented in this study demonstrate the potential of UBV serving as a surrogate to UDS studies.

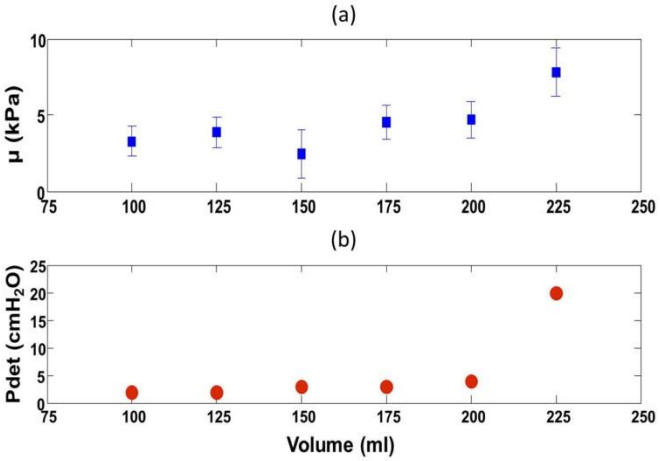

IUS1-B3-6

A new approach to ultrasonic detection of malignant breast tumors

Nishant Uniyal[1], Hani Eskandari[1], Purang Abolmaesumi[1], Samira Sojoudi[1], Linda Warren[2], Paula Gordon[2], Robert N. Rohling[1], **Septimiu E. Salcudean[1]**, Mehdi Moradi[1]*;* *[1]University of British Columbia, Vancouver, Canada, [2]BC Women's Hospital, Vancouver, Canada*

Background, Motivation and Objective

Mammography is the routine method of screening for breast cancer. However, the recall rate for biopsy after mammography is very high and almost 75% of the biopsies turn out to be benign. Breast ultrasound could be used as a supplement to improve the radiologic evaluation of breast tumors. B-mode ultrasound has a high sensitivity, however rather low specificity. We work towards alternative ultrasound-based solutions for breast lesion characterization to separate malignant and benign lesions, in order to improve on the currently used BIRADS scoring system. Ultrasound vibroelastography [1] and RF time series [2] analysis are among the technologies that we have developed and are studying for this purpose. In this work we report results of the RF time series analysis used for classification of breast lesions in 12 patients. They were recruited with consent, after a mammography finding, into our IRB approved elastography study during which RF time series data is also collected.

Statement of Contribution/Methods

In RF time series analysis, the tissue typing parameters are extracted from the temporal changes of the echo signals without applying motion to the probe or the tissue. Imaging for this work was performed with an L14-5/38 ultrasound transducer, at a center frequency of 10 MHz and a depth of 4 cm, sampling rate of 40 MHz. We obtain vibroelastography (results reported in a separate abstract by Eskandari *et al.*) and then RF time series at a frame-rate of 98 frames per second. In 2.6 s, we obtain 256 frames from the area marked by the radiologist as suspicious of cancer. Then a biopsy core is obtained for pathology analysis. The area of the suspicious finding is divided into 1 mm^2 regions and from each region, seven parameters are extracted. These are the fractal dimension and six spectral features described in [2]. A Support Vector Machine (SVM) with radial basis function kernel is used for classification with leave-one-patient-out cross validation. Posterior class probability of each ROI is estimated using a maximum likelihood estimation to determine the parameters of a sigmoid probability function on the training data. The posterior malignancy class probability is used for generating cancer maps and the ROC curves.

Results/Discussion

We report an area under ROC curve of 0.79 using the SVM classifier. Six out of seven patients with malignant breast lesions and 4 out of 5 with benign lesions were correctly classified, with success defined as correct classification of at least 80% of the 1 mm^2 regions. The sensitivity and specificity of the method are 86.7% and 84.5%, respectively. This is the first report of RF time series analysis for breast cancer detection and shows the potential of the method for enhancing the ultrasound-based assessment of breast lesions.

Support: NSERC I2I (PIs: Salcudean-Rohling) and NSERC Strategic (PI: Abolmaesumi).

[1] Salcudean, et al., MICCAI, LNCS 4190, pp. 389-396, 2006.

[2] Moradi, et al., IEEE TBME, vol. 56, no. 9, pp. 2214-2224, 2009.

Compressed Sensing and Phased Arrays

NH

Monday, July 22 2013, 02:00 pm - 03:30 pm

Congress Hallair: **Jafar Saniie**
Illinois Institute of Technology

IUS2-B-1

Compressed beamforming in ultrasound imaging

Yonina Eldar[1], Tanya Chernyakova[2]; [1]*Technion, Haifa, Israel,* [2]*Technion, Israel*

Background, Motivation and Objective

Sonography techniques use multiple transducer elements for tissue visualization. Signals detected at each element are sampled prior to digital beamforming. The required sampling rates are up to 4 times the Nyquist rate of the signal and result in considerable amount of data, that needs to be stored and processed. A developed technique, based on the finite rate of innovation model, compressed sensing (CS) and Xampling ideas, allows to reduce the number of samples needed to reconstruct an image comprised of strong reflectors. A significant drawback of this method is its inability to treat speckle, which is of significant importance in medical imaging. Here we build on previous work and show explicitly how to perform beamforming in the Fourier domain. Beamforming in frequency exploits the low bandwidth of the beamformed signal and allows to bypass the oversampling dictated by digital implementation of beamforming in time. We show that this allows to obtain the same beamformed image as in standard beamforming but from far fewer samples. Finally, we present an analysis based CS-technique that allows for further reduction in sampling rate, using only a portion of the beamformed signal's bandwidth, namely, sampling the signal at sub-Nyquist rates.

We demonstrate our methods on in vivo cardiac ultrasound data and show that reductions up to 1/25 over standard beamforming rates are possible.

Statement of Contribution/Methods

Results/Discussion

IUS2-B-2

Compressive sensing of full field images in Lamb waves inspections

Luca De Marchi[1], Giampaolo Cera[1], Guido Masetti[1]; [1]*University of Bologna, Italy*

Background, Motivation and Objective

Lamb wave testing for structural health monitoring often relies on analysis of wavefields recorded through scanning laser Doppler vibrometers (SLDVs) or ultrasonic scanners. A representative measurement might contain 1000x1000 spatial data measurement locations to image an area of about 1 m^2. So about 10^6 measurement locations. Moreover, at each measurement location several time samples of the acquired waveform must be collected. In the inspections of large structures, this means a very large set of data to store in memory, and also a quite time-consuming process. In this paper, a Compressive Sensing (CS) framework to minimize measurement locations and data size while preserving the informative content is presented.

Statement of Contribution/Methods

CS is a novel paradigm that has emerged in recent years [Donoho, IEEE TIT, 2006]. CS theory states the possibility of reconstructing a signal by feeding a limited number of measurements into an L1 norm minimization procedure. As a prerequisite, the signal must be sparse, i.e., it should be well-approximated by a linear superposition of a few atoms of an appropriate basis. Within this perspective, we propose to perform and assess CS reconstruction of ultrasonic data using the recently introduced Warped Curvelet Frames representation, which exhibits advantageous properties for sparsely representing Lamb wave acquisitions [De Marchi, IEEE TUFFC, 2012].

The proposed approach allow to recover full wavefield data with high fidelity from a small set of traces acquired in randomly selected locations.

Results/Discussion

Full wavefield data obtained experimentally, with a scanning laser Doppler vibrometer from a 3-mm thick Aluminium plate, were used to validate the proposed approach. An example of curvelet-based recovery is presented in Fig. 1, which shows the results of decimating, and then reconstructing, vibrometer measurement data. Aside from sparsity in the curvelet domain, and the group velocity curves for Al plates to design the warped representation, no prior information was used during the recovery. The proposed approach allows to reduce the measurement locations required for exact signal recovery to less than 34% of the original sampling grid. The explanation of this success in data reduction lies in the curvelet's ability to locally approximate the 3D geometry of the data.

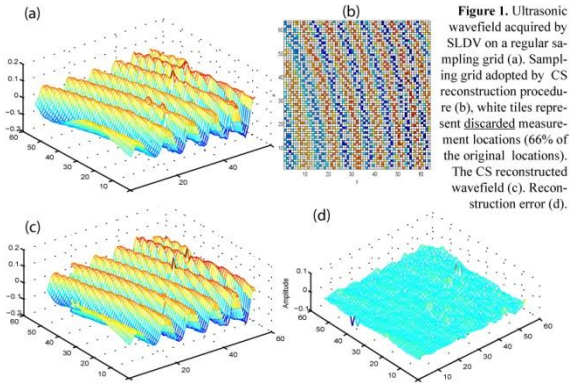

Figure 1. Ultrasonic wavefield acquired by SLDV on a regular sampling grid (a). Sampling grid adopted by CS reconstruction procedure (b), white tiles represent discarded measurement locations (66% of the original locations). The CS reconstructed wavefield (c). Reconstruction error (d).

IUS2-B-3

Compressive Sensing with Frequency Warped Compensation for Damage Detection in Composite Plate

Alessandro Perelli[1,2], Sevan Harput[2], Luca De Marchi[1], Steven Freear[2]; [1]*Department of Electrical, Electronic and Information Engineering - DEI, University of Bologna, Bologna, Italy,* [2]*School of Electronic and Electrical Engineering, University of Leeds, Leeds, United Kingdom*

Background, Motivation and Objective

This work focuses on an ultrasonic guided wave structural health monitoring (SHM) system development for composite plate inspection. An in-situ monitoring system that can inspect large areas and communicate remotely is highly computational demanding due to both the huge number of piezoelectric sensors needed and the high sampling frequency. To address this problem, a general approach for low rate sampling Compressive Sensing (CS) is developed as a viable technique for the efficient acquisition that exploits the sparse representation of dispersive ultrasonic guided waves in the frequency warped basis.

Statement of Contribution/Methods

CS is an alternate framework to the traditional Nyquist acquisition framework. CS can be viewed as a scheme for simultaneous sensing and compression where the rate of data acquisition need only be proportional to the sparsity of the signal. The assumption is that a signal x can be represented as a sparse linear combination of elements from a fixed, known basis Ψ. In this study the compressive acquisition of Lamb wave signal for damage detection in carbon fiber materials is studied; this new framework is based on the Warped Frequency Transform to achieve a sparse representation of the signal. In particular a random modulator acquisition module and reconstruction stage is developed to obtain the sparse reflection due to the damage in the warped domain.

Results/Discussion

As a result, a detection procedure to locate defect-induced reflections was demonstrated and simulated in PzFlex® by Lamb waves propagating in a 1 meter^2 carbon fiber (2 layer 0°/90°) with 4 piezoelectric transducers at a distance of 0.25 m from the edge and f_{CS} = 150 kHz. The active monitoring was performed by a chirp excitation at 10-100 kHz on one element and by three sensors on the top of the surface as shown in Fig. 1(a). The acquisition CS framework sampling at 150 kHz was realized in Matlab® with the reconstruction algorithm. The corresponding coordinates provide the distance traveled by the incident wave and the total distance of the wave reflected by the defect as shown in Fig. 1(b). The proposed method is suitable for defect detection in SHM applications.

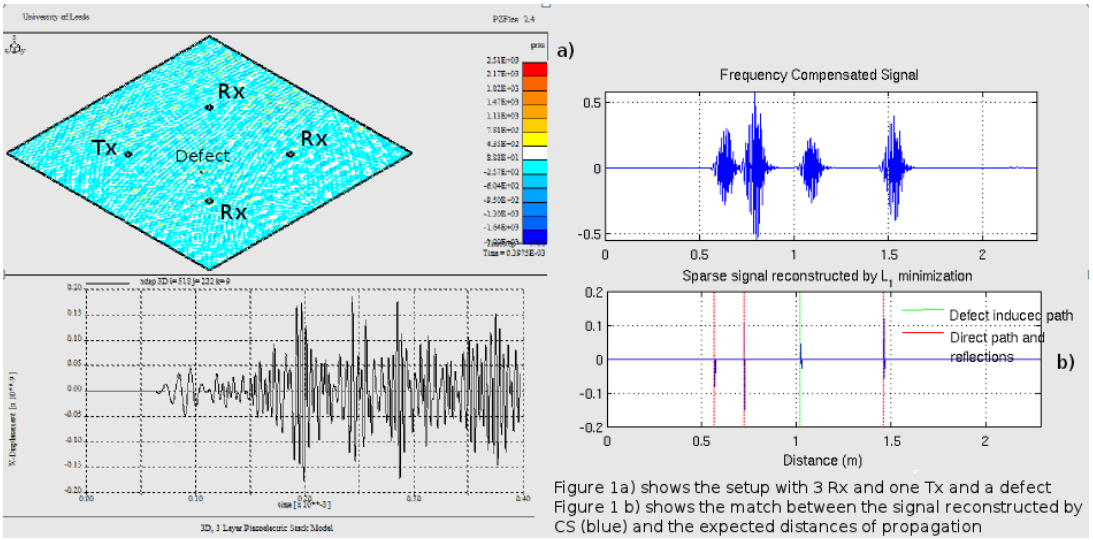

Figure 1a) shows the setup with 3 Rx and one Tx and a defect
Figure 1 b) shows the match between the signal reconstructed by CS (blue) and the expected distances of propagation

IUS2-B-4

Bulk wave FSAT for 2D optic fiber endoscopic echography

Nicola Testoni[1], Luca De Marchi[2], Nicolò Speciale[2], Massimo Ruzzene[3]; [1]*Department of Civil, Environmental and Materials Engineering (DICAM), University of Bologna, Bologna, Italy,* [2]*Department of Electrical, Electronic and Information Engineering (DEI), University of Bologna, Bologna, Italy,* [3]*School of Aerospace Engineering, Georgia Institute of Technology, Atlanta, GA, USA*

Background, Motivation and Objective

Piezoelectric transducers have long dominated US transducer technology, and current state-of-the-art arrays includes high-quality linear, convex and phased array probes. One noticeable limitation of these systems is the hardware complexity stemming from the phased array beamforming principle of operation, which requires a large number of individually controlled emitting/receiving elements and the associated wiring and multiplexing circuitry. Such complexity hampers the possibility of manufacturing compact and miniaturized probes.

Statement of Contribution/Methods

In this work a simpler and promising solution will be presented. Extending Frequency Steering Acoustic Transducer (FSAT [1]) theory to bulk waves (BW), beam steering will be achieved by a single element transducer. Thanks to the proposed approach, it will possible to control US BW direction by patterning the distribution of active materials on the probe surface as shown in Fig.1a. The BW FSAT will allow to discriminate between different transmission angles as a function of the frequency of the acoustic signal traversing the transducer as depicted in Fig.1b-c. The frequency steering concept can advantageously be combined with micromachining technologies to fabricate miniaturized US probes on fiber optic terminations [2,3].

Results/Discussion

The discussed probe will be free of mechanical moving parts and immune from electromagnetic interference. It will allow for an angular scanning in the range [18-90°] and will be characterized by a very wide bandwidth, both in transmission and in reception, above 50 MHz, providing a theoretical depth resolution of about 15 µm. Numerical and preliminary experimental results show that angular resolution is also satisfying for a single element, unfocused actuator: half-power beam width is 13° in the elevation direction over the whole steering range, while it is lower than 20° in the lateral direction for steering angles lesser than 56°, quickly and steadily dropping below 10° for steering angles lesser than 38°.

[1] IEEE TUFFC 58(7), pp. 1430-1441, 2011.

[2] Proc. IEEE Sensors, pp. 1156-1160, 2010.

[3] J. Opt. Soc. Am. B 29(8), pp. 2016-2020, 2012.

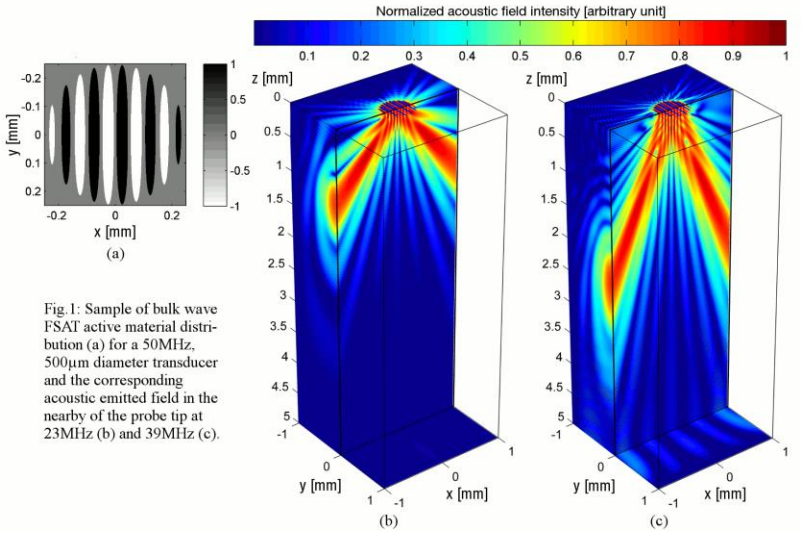

Fig.1: Sample of bulk wave FSAT active material distribution (a) for a 50MHz, 500µm diameter transducer and the corresponding acoustic emitted field in the nearby of the probe tip at 23MHz (b) and 39MHz (c).

IUS2-B-5

Guided Wave Enhancement Phased Array Beamforming Scheme using Recursive Feedback

David M. Charutz[1,2], Sevan Harput[2], David M. J. Cowell[2], Etai Mor[1], Steven Freear[2]; *[1]NDT, SOREQ NRC, Yavne, Israel, [2]Ultrasound group, School of Electronic & Electrical Engineering, The University of Leeds, Leeds, West Yorkshire, United Kingdom*

Background, Motivation and Objective

Guided waves are well established and beneficial tools of ultrasonic nondestructive evaluation applications. Using a phased array it is possible to ensure selectivity, both in terms of the mode and the direction of the wave (Rose *et al.* IEEE TUFFC v46 n3 1999). Yet, there is a growing need to improve both selectivity and power efficiency of the incoming ultrasonic wave. The aim of this study is to improve on the identification of cracks in thin plates and pipes. In this work, a novel adaptive beamforming technique for guided waves is developed. The method is based on a recursive feedback algorithm which optimizes the individual excitation waveforms to increase the total energy at a desired mode, and enhance a uni-directional propagation of the ultrasonic wave.

Statement of Contribution/Methods

In practical applications it is likely that the nature and composition of the object to be examined is not fully known. The proposed technique consists of an in-situ examination paradigm that overcomes this kind of circumstance. Unlike bulk waves, surface waves produced with a phased array can be sampled by the elements of the transducer array before they leave its spatial range of influence. This in turn suggest a recursive scheme made of n iterations, where n is the number of elements in the array, at which in every step i the first i elements transmit, and element $i+1$ receives the signal. In the next step, element $i+1$ will start transmitting with the very same signal that has just been acquired. The outcome of this n-loop is an optimal superposition of contributions, and the overall wave will propagate dominantly to one direction. This can be represented mathematically by solving the eigenvalue problem $(\boldsymbol{K}^{H}\boldsymbol{K}-\lambda\boldsymbol{I})\,\boldsymbol{t}=\boldsymbol{0}$ where $\boldsymbol{K}$ is a vector of the response of the last element to the transmitted signal of the other elements of the array.

Results/Discussion

The uni-directional beamforming achieved by this method is demonstrated in Fig. 1(a) on a 2.54mm thick aluminium plate at 0.75 MHz, using finite element analysis performed with *PZFlex* software. The selectivity of the proposed method is evident from the difference between Fig. 1 (b) and (c). In the latter case the ultrasonic wave amplifies the A_0 mode, with a small contribution of the S_0 mode. As the algorithm uses feedback, no a-priori information is required of the structure. This is ideally suited for complex structures such as composites and layered geometries.

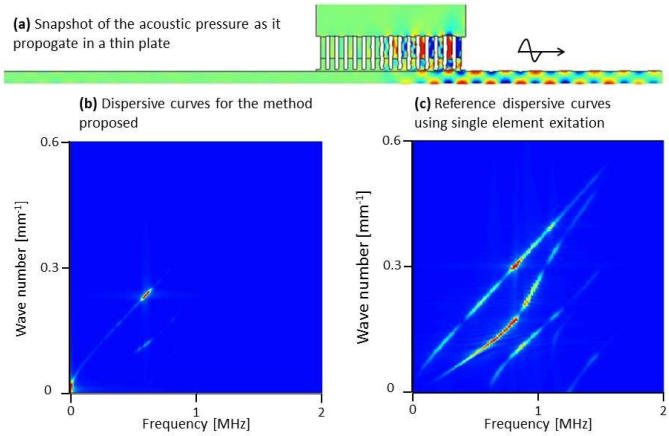

Figure 1: **(a)** A snapshot of the propagated wave at time t = 30ms **(b)** Dispersive curves calculated by FFT in time and space of the plate's surface displacements; the dominance of A_0 mode can be clearly seen, and **(c)** Reference dispersive curves for the same setup, but with *a single element* excitation; wave propagation with A_0 together with S_0, A_1, S_1, S_2 can be seen.

MUT Modeling

T1

Monday, July 22 2013, 02:00 pm - 03:30 pm

Congress Hallair: **Levent Degertekin**
Georgia Institute of Technology

IUS5-B-1

An Accurate Equivalent Circuit for the Clamped Circular Multiple-Electrode PMUT with Residual Stress

Firas Sammoura[1,2], Katherine Smyth[3], Sang-Gook Kim[3]; [1]*Microsystems Engineering Division, Masdar Institute, Abu Dhabi, United Arab Emirates,* [2]*MI/MIT Cooperative Program, MIT, Cambridge, MA, USA,* [3]*Department of Mechanical Engineering, MIT, Cambridge, USA*

Background, Motivation and Objective

Thickness-mode piezoelectric resonators have enabled ultrasonic medical diagnostic sensors. The labor-intensive manufacturing processes (dicing and bonding) limit the practicality of micro-scale piezoelectric transducers. In ultrasonic devices operated based on plate flexural mode such as cMUTs and pMUTs, MEMS fabrication technologies can be utilized and the mechanical impedance can be closely matched to the imagining medium resulting in improved bandwidth (BW). Whereas, cMUTs suffer from high DC voltage, small gap height, and low output pressure capability, pMUTs are not bound to these limitations. As such, pMUTs can be better ultrasonic transducers when proper models and designs are available.

Equivalent circuit models are very important in order to predict and optimize the BW, resonant frequency, input impedance, and the output pressure under various acoustic loads. CMUT elements were described by 1-D model parameters, and the predicted results fitted well with FEM simulation. Recently, there have been efforts to model pMUTs and extract circuit model parameters; however, no explicit lumped element model was derived for a clamped circular pMUT.

The objective of this work is to theoretically develop a circuit model representation of a clamped unimorph circular pMUT with multiple electrode architecture using Green's function solution. The explicit expressions for the circuit parameters include the influence of the process-related residual stress. The derived model is verified using FEM.

Statement of Contribution/Methods

The clamped plate shape function is solved analytically using a novel Green's function technique under both pressure and voltage excitation, where the residual stress in each layer is accounted for. The electromechanical admittance matrix relating the velocity vector (volumetric velocity and current) to the forcing vector (pressure and voltage) is then derived.

Results/Discussion

Figure 1(a) shows a circular unimorph pMUT plate of radius b with a stack of n layers, while Fig. 1(b) shows m concentric ring electrodes excited by a voltage Vm. As the derived admittance matrix is bilateral, the system is represented by the simple circuit lumped element equivalent model as shown in Fig. 1(c). The circuit parameters can be explicitly expressed as shown in Fig. 1(d). PMUT performance as predicted by this model is within 5% of the FEM simulated data.

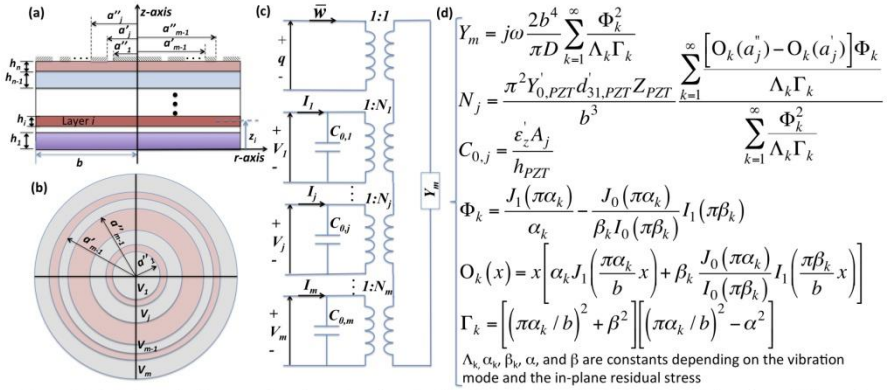

Figure 1: (a) A schematic diagram of a unimorph stack pMUT in d_{31} mode with n layers, where the i^{th} layer has a thickness h_i and is at a distance z_i from the reference axis. The plate has a radius b and the top electrode is patterned with m circular/ring electrodes, such that the inner and outer radii of the j^{th} electrode are designated as a'_j and a''_j, respectively, (b) Top view showing the concentric ring electrode, where each is excited by a voltage V_j, (c) The basic electric network representation of a unimorph circular pMUT with m-electrodes, and (d) Lumped element parameters including input capacitance $C_{0,j}$, transformer ratio N_j, and mechanical admittance Y_m.

IUS5-B-2

An advanced equivalent circuit for a piezoelectric micro-machined ultrasonic transducer and its lumped parameter measurement

Yub Je[1], Haksue Lee[2], Kyounghun Been[1], Hongmin Ahn[1], Wonkyu Moon[1]; [1]*Department of Mechanical Engineering, Pohang University of Science and Technology, Pohang, Gyungbuk, Korea, Republic of,* [2]*Agency for Defense Development, Changwon, Gyungnam, Korea, Republic of*

Background, Motivation and Objective

A piezoelectric micromachined ultrasonic transducer (pMUT) has mainly been investigated for raging and imaging applications, such as medical imaging and nondestructive testing. In a pre-vious study by the authors, it was shown that the electroacoustic efficiency of a pMUT can be improved to over 80% in air by using a thin-film structure, and a pMUT array was investigated as a high-intensity sound generator in air. For such applications, a theoretical model of the pMUT is necessary for precise prediction of the pMUT characteristics. An equivalent circuit model called the Van Dyke circuit model has been widely used for representing the characteristics of piezoelectric transducers. However, an advanced model derived from the unimorph piezoelectric structure is required when considering design issues of the pMUT. Obtaining precise material properties is also required since material properties vary according to the fabrication conditions in micromachining.

Statement of Contribution/Methods

In this work, we developed an advanced equivalent circuit model for air-coupled pMUT. The lumped parameters and the radiation impedance of the unimorph piezoelectric transducer, consisting of an edge-clamped circular plate with a piezoelectric layer on its top surface, were derived and applied to the equivalent circuit model. Design issues pertaining to the electromechanical efficiency of the pMUT, such as parasitic impedance and electrode resistance, were also identified in the equivalent circuit model. The developed equivalent circuit was verified by comparing with the measured admittance curves of the pMUT unit sample.

Results/Discussion

The model-produced admittance curves were compared with the measured admittance curves of the pMUT unit sample in the figure. The pMUT unit sample with a circular silicon radiating plate (radius of 610 microns, thickness of 15 microns) and a PZT layer on its top surface (radius of 200 microns, thickness of 3 microns) was used for measurements. By using the lumped parameters extracted from the measured admittance curves, the material properties of the silicon layer and PZT layer was obtained. The agreement between the calculated lumped parameters and the measured lumped parameters was satisfactory with errors below 10%.

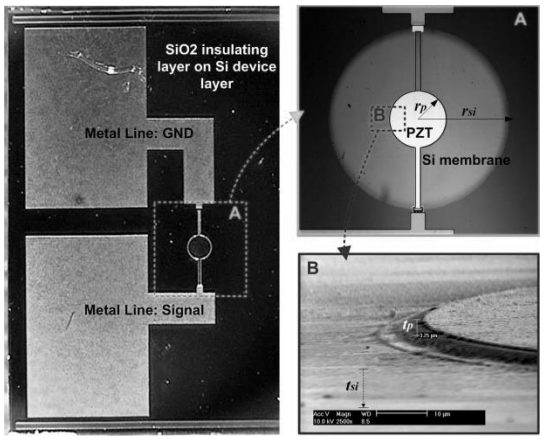

IUS5-B-3

Fully Parametric Large Signal Collapsed Mode Model for CMUTs

Elif Aydogdu[1], Kagan Oguz[1], Hayrettin Koymen[1], Abdullah Atalar[1]; [1]*Electrical and Electronics Engineering, Bilkent University, Ankara, Turkey*

Background, Motivation and Objective

Lumped element modeling, a fast and accurate simulation tool [1], has been used to predict the CMUT performance in uncollapsed mode. However, the collapsed mode was not included, as its mechanical formulation is not convenient for obtaining analytical expressions of lumped parameters. In [2], a collapsed mode model was developed for the first time, by adapting discrete calculations of bending to lumped parameters. This model was able to simulate transmit mode operations, but it was not accurate enough. Moreover, a new model was needed when the physical parameters are changed. In this work, we obtain a fully parametric model with higher accuracy, and it can simulate a CMUT of any physical dimension both in transmit and receive mode operations.

Statement of Contribution/Methods

The bending profile of collapsed membrane is numerically calculated at different levels of static excitation, utilizing Timoshenko equation [3]. The exact electrical force distribution across the membrane is used in the equation, in order to have accurate results. Equation is arranged so as to be expressed in normalized versions of static pressure, applied voltage and geometric dimensions. For different values of these normalized values, 840 solutions are obtained, and lumped parameters of the electrical model are defined by fitting polynomials to those solutions. The self radiation impedance of collapsed membrane [4] is also calculated as a function of normalized contact radius and introduced in the model. The model accepts all the physical and operational parameters of CMUT as input, and performs transient simulation of mechanical and electrical operation much faster than that can be obtained with FEM.

Results/Discussion

Merging our model with the uncollapsed mode model [1], a single CMUT operation is fully predicted under any excitation regime. Obtained results are compared with FEM simulations to verify the accuracy. A single CMUT of 30µm radius, 1.4µm membrane thickness, 0.27µm effective gap height is driven in water with the pulse as shown in the figure. Its response at collapse and snapback are correctly predicted by the lumped element model, as verified by the FEM result.

[1]H. Koymen, et.al., IEEE Trans. UFFC, 59, p.1791-99, 2012.

[2]S. Olcum, et.al., IEEE Trans. UFFC, 58, p.1468-77, 2011.

[3]S.Timoshenko et.al., McGraw Hill, 1959

[4]A. Ozgurluk et.al., IEEE Trans. UFFC, 59, p.1301-08, 2012

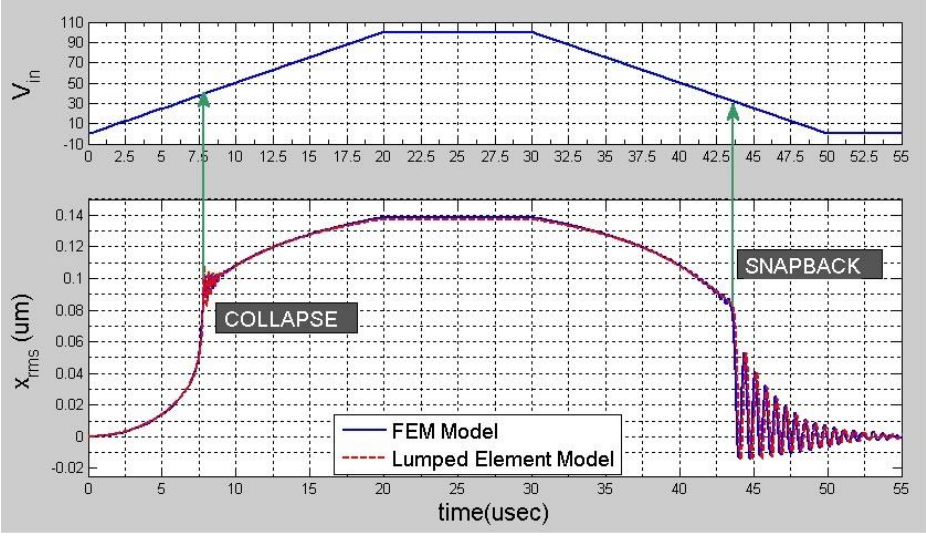

IUS5-B-4

Finite element analysis of mechanically amplified CMUTs

Alexander Unger[1], Maik Hoffmann[1], Min-Chieh Ho[2], Kwan-Kyu Park[2], Butrus T. Khuri-Yakub[2], Mario Kupnik[1]; *[1]Brandenburg University of Technology (BTU), Cottbus, Germany, [2]Stanford University, Stanford, USA*

Background, Motivation and Objective

We introduce the possibility of improving a single-cell capacitive micromachined ultrasonic transducer (CMUT), by simply adding a hollow conical-shaped structure (horn), on top of the plate. The main objective is to improve both transmit and receive sensitivity by increasing the average displacement of the plate, *i.e.* by lowering the center-to-average displacement ratio. In particular, the latter parameter inherently is limited in a bending plate operated device. In receive mode, the force due to the impinging sound pressure wave is concentrated to the center of the plate resulting in larger signals. For larger commercially available piezoelectric-based bending plate devices, this approach has been proven to be successful (M. Kota, patent US 5495766, 1996).

Statement of Contribution/Methods

To test the idea we start with an already fabricated wafer-bonded single-cell CMUT, operating at 50 kHz. It has a 55-µm-thick single-crystal silicon plate with a diameter of 4 mm. By fabricating our own punching tools, we test what thicknesses and diameters for the horns can be achieved for this CMUT and whether they can be properly glued to a flat surface. From these tests we obtained feasible geometries for an axially symmetric 2D model (ANSYS) of the plate in a rigid baffle, including the surrounding air, meshed in a quarter-circle with absorbing boundary. Then we use a pre-stressed static-, modal- and harmonic analysis at 90% of pull-in voltage (245 V) to investigate the CMUT without and with various horn designs by calculating all relevant parameters. The model helps identifying the final geometry of the horn (thickness, diameter and opening angle of the horn) before it is glued to the real CMUT plate for validating the model with measurements (electrical impedance, frequency, displacement ratios, transmit and receive sensitivity, and sound pressure levels).

Results/Discussion

We succeeded in fabricating various designs of horns with thicknesses ranging from 100 µm to 300 µm and with two diameters (2380 µm and 3180 µm). For example, the calculations for the smaller diameter, 200-µm-thick horn, with an opening angle of 156° reveal, that the frequency reduces from 50 kHz down to 20 kHz. The center displacement improves by a factor of 12 from 360 nm to 4.4 µm. The average displacement improves by a factor of 23 from 114 nm to 2.6 µm. Hence, the center-to-average displacement ratio reduces from 3.2 to 1.7, which results in a boost of calculated surface sound pressure level of 19.3 dB SPL RMS. The total mass and effective mass of the CMUT plate increases by a factor of 2.2 and 3.9, respectively.

The idea of gluing a horn on top of a CMUT plate is very promising. In contrast to other non-uniform CMUT plate designs the static DC operation point of the CMUT is barely affected and not only the effective mass significantly increases, but due to the specific shape of the horn, also the average displacement improves. In general, we observe a positive effect in both transmit and receive sensitivity.

IUS5-B-5

Circuit Theory Based Analysis of CMUT Arrays with Very Large Number of Cells

Huseyin Kagan Oguz[1], Abdullah Atalar[1], Hayrettin Köymen[1]; *[1]Electrical and Electronics Eng. Dept., Bilkent University, Ankara, Turkey*

Background, Motivation and Objective

Many applications require capacitive micromachined ultrasonic transducers (CMUTs) to be used in the form of large arrays to attain better performance. To benefit from its full potential, it is necessary to use analysis tools that are capable of handling multiple CMUT cells. In this regard, finite element analysis (FEA) tools become unfit for use, because in arrays with a large number of cells, it is often practically impossible to use.

Statement of Contribution/Methods

In our recent work, we investigated the effects of mutual acoustic interactions between the cells of CMUT arrays and shown that the performance of the array is influenced with this phenomenon[1]. We connected each cell in the array to a radiation impedance matrix that contains the mutual radiation impedance between every pair of cells, in addition to their self radiation impedances. Note that it is crucial to couple every cell in the array, otherwise the solution becomes misleading. In this way, we obtained a practical way of analyzing the performance of large arrays using the circuit theory principles. However, efficient analysis of very large arrays is still challenging, since a typical CMUT array may contain 100,000 cells, which makes it computationally cumbersome.

Results/Discussion

The figure shows the acoustic force, F_i, and velocity, U_i, of the individual cells at the radiation interface of an array, where the large square matrix is the radiation impedance matrix, **Z**. To partition the problem we electrically drive a single element in the array and keep the rest undriven but biased and with their electrical ports terminated with a load. As in figure, to represent the loads due to the undriven cells ($\mathbf{Z_{tr}}$), **Z** can be partitioned and rearranged in a reduced form of size NxN, where N is the number of cells in the electrically driven element and N+M (M»N) is the total number of cells in the array. In this way, only the driven element can be simulated by coupling its cells through this reduced impedance matrix. This method considerably reduces the number of cells and the size of **Z** at the expense of calculating the inverse of the complex symmetric matrix ($\mathbf{Z_{tr}+D}$). Under small signal regime, the separately calculated responses of elements can be added using superposition principle to find the total response.

[1] H.K.Oguz, A.Atalar, H.Köymen "Equivalent Circuit-Based Analysis of CMUT Cell Dynamics in Arrays", accepted in IEEE Trans. UFFC

$$\begin{bmatrix} F_1 \\ \vdots \\ F_N \\ \hline F_{N+1} \\ F_{N+2} \\ \vdots \\ F_{N+M} \end{bmatrix} = \left[\begin{array}{ccc|ccc} & \mathbf{A} & & & \cdots & \mathbf{B}^{\mathrm{T}} \\ & & & & \cdots & \\ \hline & \vdots\ \mathbf{B}\ \vdots & & & \mathbf{D} & \end{array}\right] \begin{bmatrix} U_1 \\ \vdots \\ U_N \\ \hline U_{N+1} \\ U_{N+2} \\ \vdots \\ U_{N+M} \end{bmatrix}$$

$$\Rightarrow \begin{bmatrix} F_1 & \cdots & F_N \end{bmatrix}^{\mathrm{T}} = \left[\mathbf{A} - \mathbf{B}^{\mathrm{T}} \left(\mathbf{Z_{tr}} + \mathbf{D}\right)^{-1} \mathbf{B}\right] \begin{bmatrix} U_1 & \cdots & U_N \end{bmatrix}^{\mathrm{T}}$$

IUS5-B-6

Model Based Drive Signal Optimization of CMUTs in Non-Collapse Operation and its Experimental Validation

Sarp Satir[1], Toby Xu[1], F. Levent Degertekin[1]; [1]*Georgia Institute of Technology, USA*

Background, Motivation and Objective

A model based transmit optimization method for CMUT arrays operated in conventional imaging mode is presented. For the large signal analysis we use the transient CMUT array model presented in [1]. The model is based on separation of electrostatic nonlinear relationships that govern CMUT operation and boundary element method to effectively calculate the linear acoustic array response, and greatly reduces the computational load for nonlinear transient analysis. Using the model, the transmitted pressure can be simulated for different drive signal configurations. The transmit behavior can be optimized iteratively and the optimal drive signal that results in maximum achievable pressure output can be identified in a short time given the CMUT array geometry and drive signal constraints.

Statement of Contribution/Methods

A 15 MHz, 60% FBW CMUT array element with 16 membranes and 50 nm gap is modeled, fabricated and tested (Fig.1(left)). Through iterative simulations, the transmit behavior of the transducer for the full range of different drive signals is explored as a function of DC bias, pulse width, and amplitude for unipolar and bipolar pulsed operation. The case where the TX and RX elements are the same is also investigated where the 90% of the collapse voltage is applied to the transmitting element for optimal receive sensitivity.

Results/Discussion

Through experimental and simulation results, it is shown that for a CMUT element operating in the non-collapse mode, the maximum possible pressure output is generated when the transducer is driven with no DC bias and a short pulse that results in full gap swing. With DC bias the same pressure level can be achieved using proper asymmetric bipolar pulses. Full swing is achievable for different pulse amplitude and width combinations, however the pulse width can be selected to maximize the transmit sensitivity in Pa/V. It is shown that a 45 V, 30 ns pulse maximizes the transmitted pressure for this particular device. In Fig.1(middle), the pressure output 2.2 mm away from the device for no DC bias and 45 V, 30 ns unipolar pulse is compared to simulation results, which show a good match over the frequency range of interest. For given pulse amplitude, the effect of pulse width on the pressure output is shown in Fig.1(right), where the measured optimal pulse width for the array is shown to be 35 ns for 30 V pulse with no DC bias, in agreement with simulations.

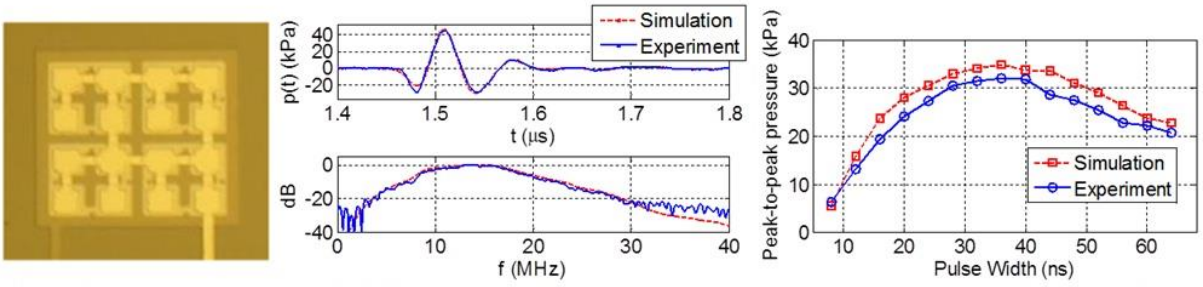

Fig. 1. (left) The array has 2.2μm thick, 35μm square membranes with 25μm electrodes. The elements have 50nm gap and 200nm isolation layer. Membrane pitch is 45μm. (middle) Pressure 2.2 mm away from the array when the CMUT array is driven with a 45 V, 30 ns unipolar pulse and no DC bias. (right) Pressure as a function of pulse width for 30 V unipolar pulse and no DC bias

[1] S. Satir *et al.*, "Transmit Optimization of CMUTs in Non-Collapse Mode using a Transient Array Model," *IUS* 2012

Devices for High Temperature

T2

Monday, July 22 2013, 02:00 pm - 03:30 pm

Congress Hallair: **omar elmazria**
Université de Lorraine - CNRS

IUS4-B-1

Wireless temperature monitoring in an electrolytic galvanizing plant

Rene Fachberger[1], Christoph Werner[1]; [1]*Sensideon, Wels, Upper Austria, Austria*

Background, Motivation and Objective

Surface acoustic wave (SAW) transponder systems are perfectly suited for various wireless sensing and radio frequency identification (RFID) applications in harsh industrial environments. In surroundings with elevated temperatures and hazardous substances like in the steel industry the advantages of SAW transponders come clearly into effect, especially when sensing of moving or rotating items is required.

A wireless SAW transponder system was developed to monitor the temperature of rotating rollers of an electrolytic galvanizing plant. The exact knowledge of the roller temperature of an electrolytic galvanizing plant is an important process parameter that could be used for an in-line quality control of the galvanized sheets. Preliminary measurements on the rollers with optical methods (laser and infrared) did not succeed.

Statement of Contribution/Methods

The rollers as well as the transponders are exposed to hot sulfuric acid, and rotate with a maximum tangential velocity of 2 m/s. The system is designed without an external trigger and can be attached without much effort. The measurements have been carried out within an electrolytic galvanizing plant during the normal production process without interfering.

Results/Discussion

With the newly developed SAW sensor system the temperature could be interrogated wirelessly over a distance of 0.5 meters in the first try. The sensor survived the durability test with a period of three weeks representing one maintaining circuit of the rollers without any damage. In the paper the system design and the results of the measurements are presented.

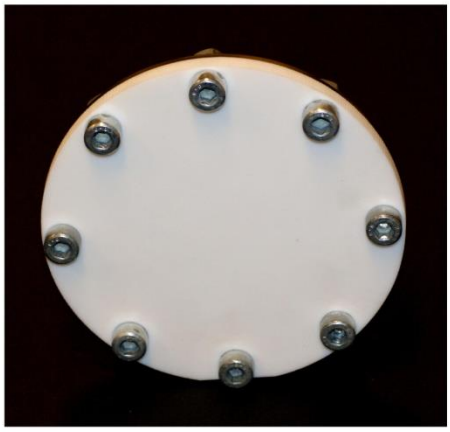

Fig. 1: First prototype of the SAW transponder covered in a protective housing to resist the hot sulfuric acid.

IUS4-B-2

Capacitively Coupled IDT for High Temperature SAW Devices

Scott Moulzolf[1], Roby Behanan[1], Robert Lad[1], **Mauricio Pereira da Cunha**[1]; [1]*LASST, University of Maine, Orono, ME, USA*

Background, Motivation and Objective

The University of Maine has developed surface acoustic wave (SAW) sensors that are operational at temperatures up to 1000°C for wireless sensing applications in harsh environments. The sensors utilize ultrathin film (~130 nm) Pt-based nanocomposite electrodes patterned on langasite ($La_3Ga_5SiO_{14}$) substrates. One major technical challenge for the long-term high-temperature sensor stability is the reliability of bond wire interconnects. Typically, thin Pt wires (~25µm diameter) are welded directly to the ultrathin SAW busbar electrodes to connect with a cable or antenna. Pt diffusion from the wire during welding and high temperature operation, particularly above 1000°C, alters the nanocomposite film composition, which leads to premature failure in the area surrounding the bond.

Statement of Contribution/Methods

In this work, a method to overcome the interdiffusion problem and increase the bond strength has been developed. Namely, capacitive coupling was used to make the electrical connections to the interdigital transducer (IDT) on the SAW devices. Conformal pinhole free Al_2O_3 layers were deposited using atomic layer deposition (ALD) on top of SAW device electrodes to serve as the series capacitor dielectric layer, as well as a diffusion barrier and protective capping layer for the IDT bus-bar electrodes. Thick film Pt bond pads were printed on the dielectric layer as the top electrode of the capacitor structure. The thick film pads also provided a robust bonding surface for thicker (up to 0.1mm) Pt wires.

Results/Discussion

The inset in the figure shows an SEM image of the area near a Pt wire bonded to a $PtRh/ZrO_2$ electrode film after heating at 1025°C in air for 4 hrs. Agglomeration is observed throughout the film, but the darker area adjacent to the wire is agglomerated into isolated islands, which appears darker in the SEM image due to charging from the electron beam. Away from the wire, the agglomerated film (lighter area) is still conductive, which demonstrates that Pt diffusion adjacent to the wire is detrimental. The plot shows a measured $|S_{11}|$ frequency response at room temperature of a capacitively coupled $PtRh/ZrO_2$ single port SAW resonator with a 50 nm Al_2O_3 layer that was heated at 1000°C for 3 hrs. The data demonstrates that the capacitive coupling architecture enables noncontact coupling to a SAW device and can survive extreme environments.

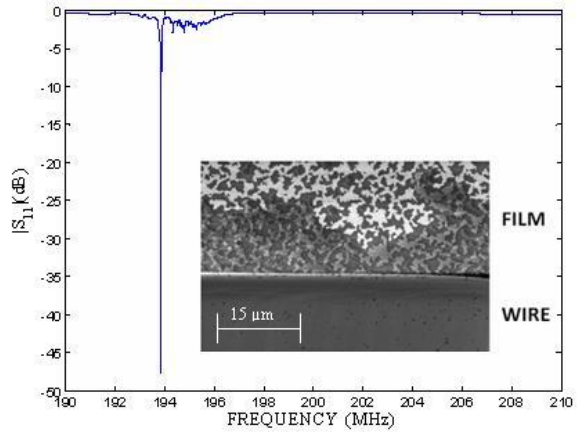

IUS4-B-3

Thermoelastic effects in Pt IDTs. Impact on the behavior of high-temperature LGS-based SAW devices

Thierry Aubert[1], Pascal Nicolay[2], Frédéric Sarry[3]; *[1]Laboratoire SYMME, Université de Savoie, Annecy-le-Vieux, France, [2]CTR AG, Villach / St. Magdalen, Austria, [3]Institut Jean Lamour, UMR 7198, CNRS - Nancy University, Vandoeuvre-lès-Nancy, France*

Background, Motivation and Objective

Recent research, in particular from Pereira da Cunha's group, have established that SAW devices based on langasite (LGS) crystals enable wireless sensing up to at least 800°C. Subsequently, the design of high-performing LGS-based SAW sensors fulfilling specific purposes will require efficient simulation. To do so, it is needed first to determine a reliable high-temperature LGS constants set. However, accurate simulation will be achieved only if all relevant second-order physical phenomena that impact the behavior of LGS-based SAW devices at high temperatures, are also identified and considered. The aim of this study is precisely to determine if thermoelastic effects in platinum (Pt) IDTs should be considered as such.

Statement of Contribution/Methods

SAW devices based on different LGS cuts and Pt electrodes with various relative thicknesses h/λ have been simulated using FEMSDA and COM tools developed by K. Hashimoto. All the calculations were made with LGS constants reported by Bungo *et al.* [1]. To take account of thermoelastic effects in the IDTs, temperature dependence of Pt elastic coefficients and density were considered, using Collard and Papadakis' data [2-3]. Finally, the fractional frequency change (FFC) of the considered devices was calculated from room temperature to 700°C. Comparison with recent experimental data from [4] was done.

Results/Discussion

Calculations show that, when thermoelastic effects in Pt IDTs are fully considered in the simulations, the FFC at high temperatures becomes strongly dependent on the Pt relative thickness (Fig. 1). This result fits very well with experimental observations. This phenomenon is related to the strengthening of mass-loading effect with temperature (which is a consequence of the 30%-decrease of Rayleigh-wave velocity in Pt between the ambient and 700°C). Therefore, considering thermoelastic effects in Pt IDTs is mandatory to achieve accurate simulations of SAW devices at high temperatures. Besides, it was observed that the FFC dependence on Pt relative thickness is influenced by the LGS cut. This will be discussed in more details in the proceeding.

[1] A. Bungo *et al.*, *Proc. IEEE Ultrasonics Symp.*, 1999.

[2] S. M. Collard and R.B. McLellan, *Acta metall. Mater.*, 1992.

[3] E. P. Papadakis, *Mater. Sci. Eng.*, 1972.

[4] J. Bardong *et al.*, *IEEE Trans. on UFFC*, Apr. 2013.

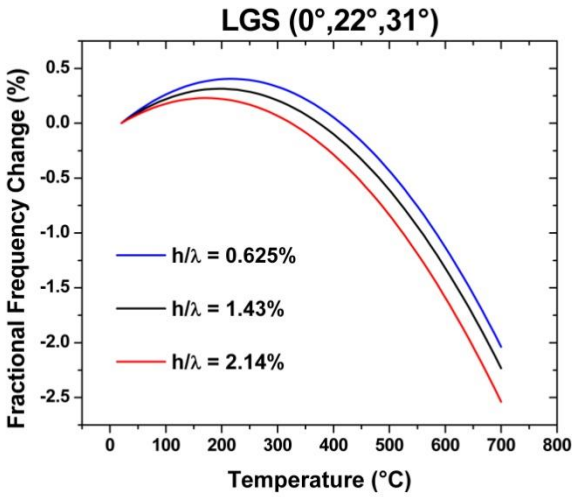

IUS4-B-4

Surface Transverse wave (STW) resonators on langasite

Victor Plessky[1], Ventsislav Yantchev[2], Valery Grigorievsky[3], William Daniau[4], Sylvain Ballandras[5], Weibiao Wang[6]; *[1]GVR Trade SA, Switzerland, [2]Dept. Solid State Electronics, Uppsala University, Sweden, [3]IRE, Russian Federation, [4]FEMTO-ST, France, [5]frec|n|sys SAS, TEMIS Innovation, France, [6]Nanjing Electronic Devices Institute, China, People's Republic of*

Background, Motivation and Objective

The need for developing high temperature remotely controlled passive SAW sensors on langasite (LGS) to answer industry demand is growing high with the arising of new materials supporting temperature in excess of 500°C preserving their piezoelectric properties. The Surface Transverse Wave (STW) cut of LGS with the Euler angles (0°,22°,90°) [1], provides temperature stable delays of STW combined with an electromechanical coupling coefficient larger than that of STW on (YXlt)/36°/90°cut of quartz. As for quartz, excellent Q-factor was expected for resonators based on STW on LGS. For high temperature sensors refractory Pt (or Ir) electrodes are necessary. However, recent attempts to develop such resonators resulted in mediocre Q factors of the order of 1'000 in place of expected Q>10'000 for the 434 MHz ISM frequencies. Here we try to explain this results and to find the ways to solve this problem.

Statement of Contribution/Methods

We demonstrate that for the used relative thickness of Pt $h/\lambda \approx 1\%$ to 2% on the above cited cut of LGS there is no waveguiding of the STW that is the STW energy is not located under the electrode grating and is radiated into the busbars. That explains the mediocre Q-factors obtained previously. 3D accurate modeling of the waves propagation in periodic finite aperture gratings is possible using FEM/BEM software. For modeling of periodic waveguide structure we also have used the COMSOL software as well as recently developed 3D FEM/BEM tool [3] – both results are close and will be presented.

Results/Discussion

The effect of losing waveguiding can be explained by the concave shape of the slowness curve in the busbar area, that is by the strong decrease of the wave velocity with derivation of the propagation direction from 0X axis. As a result, for relative thickness Pt electrodes $h/\lambda < 3\%$ the radiation conditions for the STW propagating in the electrode grating are met. This is the "banana" effect [2], except that is happens directly at the resonance. COMSOL simulation for $h/\lambda = 1.7\%$, p=6 μm shows that the wave is guided more by bus-bars than under the electrode grating. In practice, with rather wide busbars, it gives poor or no guiding for STW and poor Q-factor for the resonator losing energy into busbars. A few ways to solve the problem are proposed. One can use more thick Pt with the relative thickness h/λ greater than about 3%. Then the phase velocity of STW in periodic grating at the resonance is strongly slows down due to high reflectivity of the heavy electrodes and usual waveguiding conditions are satisfied.

[1] J. Koskela, et al, "Surface transverse waves on langasite" Appl. Phys. Lett. 72, 2665 (1998)

[2] J. Koskela, et al.,"Mechanism for acoustic leakage...", Appl. Phys. Lett., V.75, No 17, OCT, 1999, p. 2683

[3] S. Ballandras et al. . "A mixed finite element/boundary element approach... " Journal of Applied Physics, 105, 014911, 2009

IUS4-B-5

Fabrication of a 4.4 GHz oscillator using SAW excited on epitaxial AlN grown on a Sapphire substrate

Roland Salut[1], Arnaud Claudel[2], Gilles Martin[1], William Daniau[1], Didier Pique[2], Sylvain Ballandras[3]; *[1]FEMTO-ST, France, [2]SPADE SAS, France, [3]Frec'n'Sys, France*

Background, Motivation and Objective

The fabrication of SAW resonators for boarded frequency sources still receives a strong interest because of their remarkable properties: low phase noise (down to -180 dBc/Hz at 500 MHz), temperature stability and minimization of 1/f noise by proper technological process. However, the need for frequency multiplication to reach higher radio-frequency bands yields degradation of the oscillator properties. Therefore the possibility for directly reaching frequencies up to 8 GHz is considered by several groups.

Statement of Contribution/Methods

In this work, SAW resonators have been built on an epitaxial Aluminum Nitride layer grown on a high quality C-oriented Sapphire substrate. The AlN layer was grown at temperature in excess of 1000°C directly onto a 2-inch Sapphire substrate without any interfacial layer. Two-port resonators have been fabricated using E-beam lithography, with narrow gaps between the transducers to minimize propagation losses. A first run was achieved with a 643 nm period, and a second test was implemented reducing this value down to 605 nm.

Results/Discussion

The first run provided resonators operating at 4.43 GHz with Q factors higher than 2800 (fig.1). The maximum Q factor was 3280 at 4.43 GHz yielding a QF product very close to 1.5.1013 (insertion losses 15 - 20 dB). These data are compatible with the fabrication of a feed-back loop oscillator with only one amplifier stage. The resonators have been inserted in an oscillator loop and their phase noises have been characterized, yielding -95 dBc at 10 kHz from the carrier and a noise floor of -157 dBc/Hz at 2.5 MHz (fig.2). These outstanding results were again observed for the second run at 4.71 GHz with a Q of 3150 and insertion losses of 15-20 dB. Work is in progress to design and fabricate high frequency resonators up to 8 GHz.

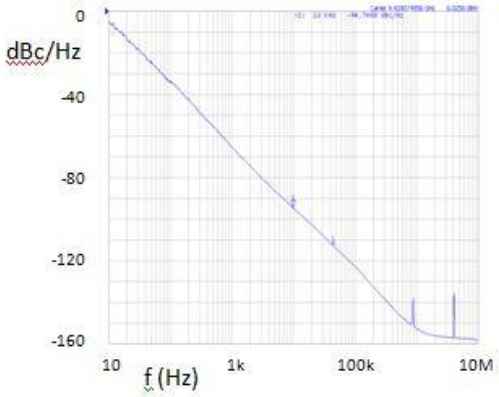

Fig 2: Phase noise measurement of the oscillator at 4.43 GHz

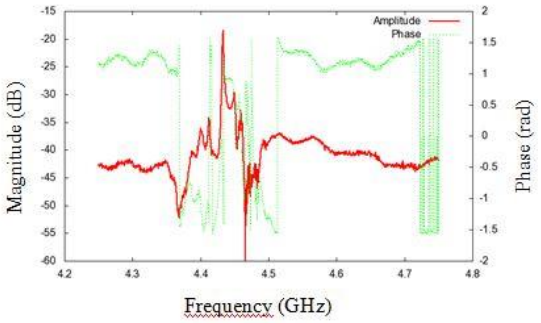

Fig 1: Characterization of a resonator centered on 4.43 GHz (Q = 2900)

IUS4-B-6

An optimized set of temperature coefficients for LGS

PASCAL NICOLAY[1], THIERRY AUBERT[2]; *[1]Wireless Sensors, CTR AG, Villach / St. Magdalen, Austria, [2]Université de Savoie, Annecy, France*

Background, Motivation and Objective

Langasite (LGS) is a well-known and very promising material for SAW applications at very high temperature. It has been extensively studied and many possible applications have been proposed. However, in order to take full advantage of the existing CAD tools and develop the next high-performing LGS-based SAW sensor for high temperature applications, experts need a more accurate set of temperature coefficients (TCs) of LGS material constants. Indeed, even the best available set does not allow precise prediction of the Fractional Frequency Change (FFC) above 300°C. Our objective was precisely to derive a new set of optimized TCs, in order to predict the FFC up to at least 800°C with a very high accuracy.

Statement of Contribution/Methods

The set of optimized coefficients was derived using a simulated annealing (SA) optimization procedure. A specially designed Rayleigh-wave simulation tool was used to compute the wave properties at high temperature, for each new set of test values provided by the SA-algorithm. The wave simulation was based on the Campbell and Jones approach. The starting point was a set made of the best constants and corresponding TCs identified in the literature (including the thermal expansion coefficients). Experimental data for three different cuts in the range [0-800°C] were set as targets for the optimizer and therefore used to compute the error to be minimized. The Euler angles of these reference cuts were (0,22,31), (0,90,0) and (0,138.5,26.6). The resulting optimized set of TCs was subsequently tested on other cuts, for which experimental data were also available: (0,144,24) and (0,90,90).

Results/Discussion

The new set of optimized TCs allowed for an astonishingly accurate prediction of the FFC in the range [0-800°C], for each of the afore-mentioned cuts. Results for two selected cuts are shown in Fig. 1. It is stressed that the cut (0,144,24) was not used in the optimization procedure but computed afterwards, with the new set of optimized TCs. The new set of TC will be discussed in detail in the paper. It was notably observed that only the TCs of the stiffness constants needed to be tuned. Among these TCs, only the one for C66 needed to be more than slightly corrected in the first order. However, much bigger corrections were needed for all of the second order coefficients.

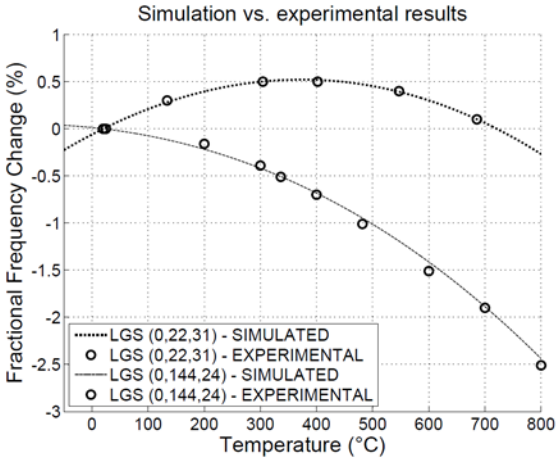

Cardiac strain imaging

CONGRESS HALL

Monday, July 22 2013, 04:30 pm - 06:00 pm

Congress Hallair: **Elisa Konofagou**
Columbia University

IUS1-C1-1

4-D echocardiography assessment of local myocardial strain using 3-D speckle tracking combined with shape tracking

Colin Compas[1], **Emily Wong[2]**, Xiaojie Huang[1], Smita Sampath[1], Ben Lin[1], Prasanta Pal[1], Xenophon Papademetris[1], Karl Thiele[3], Donald Dione[1], Lawrence Staib[1], Albert Sinusas[1], Matthew O'Donnell[2], James Duncan[1]; *[1]Yale University, USA, [2]University of Washington, USA, [3]Philips Medical Systems, USA*

Background, Motivation and Objective

In 4-D echocardiography, displacement estimates obtained solely from multi-dimensional speckle tracking can exhibit large variances and peak hopping, making it challenging to accurately calculate myocardial strains (Fig. 1a). 3-D phase-sensitive speckle tracking can produce sensitive estimates along the axial direction, but typically provides poorer estimates in orthogonal directions and at tissue boundaries. Shape tracking provides complimentary information, as it effectively tracks the myocardial boundaries and is not dependent on beam orientation. We propose a method combining 3-D speckle tracking with 3-D shape tracking using a quality-based radial basis function approach.

Statement of Contribution/Methods

Echocardiographic data (3D+t) were acquired in an open chest canine at six weeks following surgical coronary occlusion using a commercial 2-D phased array. 3-D phase-sensitive correlation-based speckle tracking was performed between consecutive volumes of the radiofrequency data, using a 3-D kernel approximately the size of one speckle. 3-D shape tracking was applied using generalized robust point matching, which determines the trajectory of feature points on the segmented myocardial surfaces using local curvature descriptions. An adaptive multi-level radial basis function method was used to combine information from the two tracking methods, utilizing confidence metrics to weight the contribution of each estimate to generate a dense 3-D displacement field throughout the myocardium. A multi-level approach was used to capture smaller scales of motion in regions of fine deformation variation and high tracking confidence. Cardiac coordinate strains were calculated from displacements derived from the combined method, and compared to magnetic resonance (MR) tagging measurements.

Results/Discussion

The 3-D combined approach produced displacement estimates with greatly reduced variance and peak hopping compared to 3-D speckle tracking alone. Lower radial strains were observed in the myocardial infarct region (Fig. 1b), corresponding to reduced local contractility. Strong correlations were observed for both radial and circumferential strains between the combined method and estimates from MR tagging studies on the same animals, with correlation values greater than 0.8 for 90% of the strain curves analyzed in 30 anatomical segments.

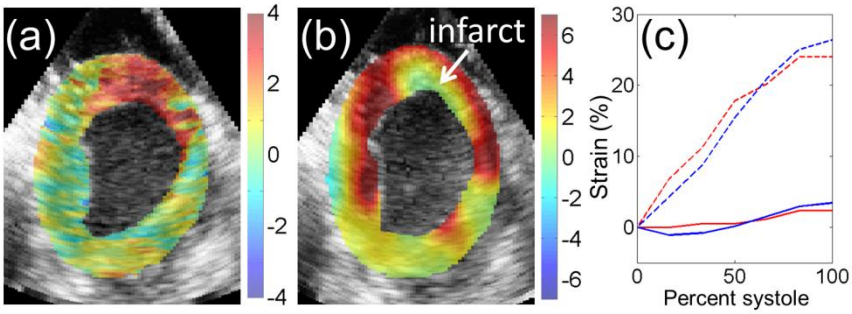

Figure 1. Maps of (a) myocardial axial displacements from 3-D speckle tracking and (b) resultant radial strains (defined relative to the heart coordinate system) from the combined 3-D method near peak systole. (c) Radial strain curves integrated over the systolic interval from the combined 3-D method (blue) compared to MR tagging results (red) in the infarct zone (solid lines) and normal tissue region (dashed lines) ($R > 0.95$).

IUS1-C1-2

Acute and Chronic myocardial infarct differentiation using Atrial Kick Induced Strain (AKIS) imaging

Brett Byram[1], Lauren Oliveri[1], Patrick Wolf[1], Gregg Trahey[1]; *[1]Duke University, USA*

Background, Motivation and Objective

There are 470,000 cases of recurrent myocardial infarction (MI) every year in the US. Diagnosis of recurrent MI is a challenge because conventional methods like ECG or cardiac enzymes are non-diagnostic or slow. MI diagnosis by ultrasound assessed wall motion abnormalities is almost immediately sensitive to a patient's first infarct. However, wall motion has not been shown to differentiate between acute and chronic MI, which is necessary for recurrent MI.

Statement of Contribution/Methods

Accurate differentiation of chronic MI from healthy tissue has been demonstrated using atrial kick induced strain (AKIS) imaging of the ventricles. The ventricles expand quickly during active filling inducing passive strain at the end of ventricular diastole, which is unique because the ventricles are fully relaxed. Strain induced during this period can serve

as a proxy for passive mechanical stiffness allowing for differentiation such as with stiff chronic MI or soft acute MI (consistent with literature stiffness characterization) relative to healthy myocardium. Differentiation of acute and chronic MI using passive stiffness is demonstrated using AKIS.

AKIS images of MI were formed from volumetric IQ data acquired at 100 Hz. The data were acquired using the Siemens SC2000 and 4Z1c matrix array operating at 2.8MHz (Siemens Healthcare, Mountain View, CA). Chronic MI data were acquired from dogs with infarcts older than one year (N=3) with two dogs yielding sufficient quality data. Acute MI data were acquired from dogs with infarcts less than 15 minutes old caused by left anterior descending artery occlusion (N=2). Cardiac motion was estimated using Bayesian speckle tracking with a big to small multiple kernel size strategy. Strain was estimated using the typical regression approach. Images were made of the axial strain magnitude.

Results/Discussion

AKIS image metrics were calculated on acute and chronic infarcts. (Statistics are not reported due to small study numbers). Contrast and contrast-to-noise ratio (CNR) are reported with healthy myocardium used as the background quantity. The chronic infarcts had contrast of 0.81 and 0.87 and CNR of 2.9 and 1.6. The acute infarcts have contrast of -3.3 and -3.9 and CNR of 2.3 and 2.8. The reversal in contrast between acute and chronic infarcts demonstrates differentiation and is depicted graphically in the example figure of an acute and chronic MI.

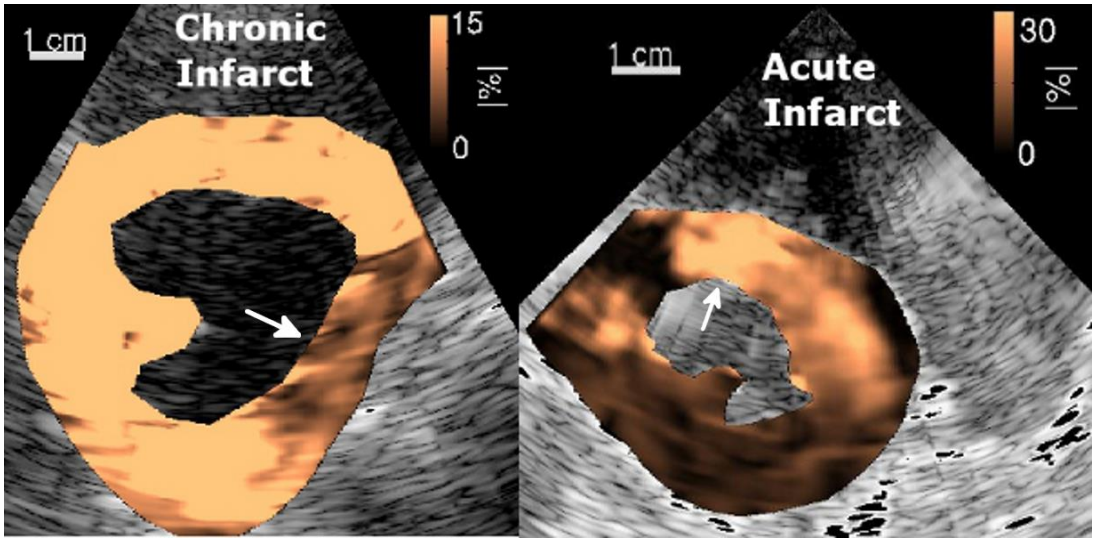

IUS1-C1-3

Performance Analysis of Two-Dimensional Cardiac Strain Estimation Using Different Beamforming and Temporal Resolution in Vivo

Ethan Bunting[1], Jean Provost[2], Elisa Konofagou[1]; *[1]Columbia University, USA, [2]ESPCI ParisTech, France*

Background, Motivation and Objective

Increased motion estimation rate (MER) has been shown to decrease decorrelation errors and improve cardiac strain estimation. However, achieving high MERs in cardiac imaging often comes at the cost of reducing the field of view, depth, or spatial resolution, or requires acquisition over multiple heart cycles. Two new types of sequences—temporally unequispaced acquisition sequence (TUAS) (Provost et al., Phys. Med. Biol., 2011) and the unfocused beam sequence (Provost et al., Phys. Med. Biol., 2012)—have recently been developed by our group, enabling high MERs within a single heartbeat while minimizing tradeoffs. Although both of these sequences rely on different beamforming methods, each have successfully been used in vivo to achieve accurate axial strain estimation. In this study, a comparison between the two beamforming methods is performed, and the ideal MER for cardiac imaging is explored for both axial and lateral strain estimation.

Statement of Contribution/Methods

Using a 64-channel Verasonics® system, pre-beamformed radiofrequency (RF) data was acquired over a single heartbeat in an in vivo human heart using the TUAS and unfocused sequences. TUAS uses multiple, conventionally focused transmits per frame, while the unfocused sequence uses a single, diverging transmit per frame. A delay-and-sum algorithm was used for each technique to reconstruct 128 lines per frame from the pre-beamformed RF signals. MERs achieved by TUAS were 67, 131, 272, 544, 815, and 1631 Hz, and MERs achieved by the unfocused sequence were 1000 and 2000 Hz. Axial and lateral incremental displacements were computed using a 1-D cross-correlation and lateral recorrelation and a least-squares strain opera-tor was used to estimate strains. After normalization of the strains by MER, the probability distribution of the SNRe was computed and then integrated for each strain value to calculate the probabilistic expected value of the SNRe for both methods.

Results/Discussion

For both methods, axial and lateral strains exhibited a gradual increase in the expected SNRe with strain up to a certain value, beyond which the SNRe dropped significantly. The peaks of the expected SNRe curves shifted to higher strains at higher MERs; however, the highest expected SNRe value occurred at different MERs for different strains. There was a 227% increase in expected SNRe at higher MERs in axial strain estimation compared to a 30% increase for lateral. For both axial and lateral strains, TUAS performed better than the unfocused sequence at similar MERs by approximately 149% and 23% respectively. These results indicate that different MERs should be employed depending on the strain in order maximize the expected value of the SNRe across the entire image. In terms of beamforming, the focused transmits of TUAS led to higher SNRe than the unfocused case. These results indicate that both the MER and beamforming can have significant effects on the SNRe of the estimated strains.

IUS1-C1-4

Three-Dimensional Fusion of Shear Wave Imaging and Electro-Anatomical Mapping for Intracardiac Radiofrequency Ablation Monitoring

Peter Hollender[1], Stephen Rosenzweig[1], Stephanie Eyerly[1], Patrick Wolf[1], Gregg Trahey[1,2]; *[1]Biomedical Engineering, Duke University, Durham, NC, USA, [2]Radiology, Duke University, Durham, NC, USA*

Background, Motivation and Objective

Transcatheter ablation (TCA) is a common treatment for atrial fibrillation (AF) and other cardiac arrhythmias. Electroanatomical mapping (EAM) gives electrophysiologists the ability to construct a 3-D shell of anatomy and local activation time to guide radiofrequency ablation (RFA) lesion placement. Intracardiac echo (ICE) is used during TCA to visualize the myocardium-catheter contact in real-time. Acoustic radiation force impulse (ARFI) imaging and shear wave imaging (SWI) have shown promise for assessing ablation lesion dimensions by imaging the local mechanical properties of tissue, with ablated tissue presenting as a region of low compliance. These 2-D images can identify the transmurality of lesions and their extent in the lateral imaging plane, but cannot individually determine the out-of-plane extent of the lesions. This work uses the spatial tracking of the EAM system to register a series of ARFI-SWI images in 3-D space, and combines the data into a volumetric map of myocardial stiffness.

Statement of Contribution/Methods

Data were acquired on a Siemens SC2000 ultrasound scanner, using custom pulse sequences to generate on-demand, ECG triggered ARFI and SWI images with a SoundStar ICE imaging catheter. A Biosense-Webster CARTO3 EAM system was used to both map the atria and track catheter positions in canine subjects. Prior to ablation, the target myocardium was imaged with a series of ARFI and SWI images, steered in the elevation plane to sample the tissue every 1-2 mm. The center of the target region was then ablated for 60 seconds, after which the tissue was imaged again. Post-procedure, the catheter position data were reconstructed to orient each stiffness estimate in 3-D. Estimates were then linearly interpolated onto a 3-D volume, bound by the total imaging field of view, the endocardium (from the EAM), and the epicardium (from ICE).

Results/Discussion

The image fusion system was able to reconstruct volumes of ARFI and SWI elasticity estimates that are highly registered to the 3-D cardiac anatomy. Following RFA, the maps showed a region of increased stiffness consistent with the location of the ablation, as seen in the figure, and confirmed by post-mortem pathology staining. A real-time version of this system may be able to reduce TCA procedure times and the total amount of ablation energy needed by providing detailed feedback on the 3-D extent of ablation lesions.

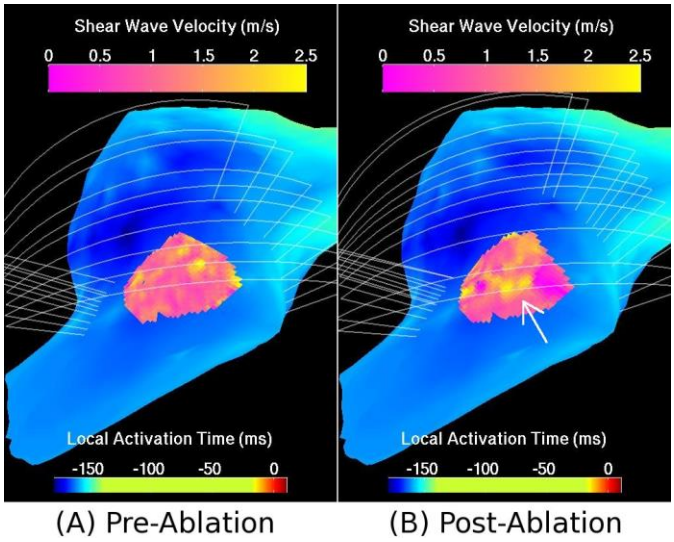

IUS1-C1-5

Intracardiac Myocardial Elastography at high temporal resolution in canines and humans in vivo

Julien Grondin[1], Elaine Wan[1], Alok Gambhir[1], Hasan Garan[1], Elisa Konofagou[1]; [1]*Columbia University, USA*

Background, Motivation and Objective

Intracardiac echocardiography (ICE) is routinely used during radio-frequency (RF) ablation procedures for abnormality identification and procedural guidance. Combining ICE with an insight into the mechanical properties of the myocardium can provide additional information during the ablation procedure. ICE has been used in previous studies to estimate strain rates using tissue Doppler imaging (Wang, J Am Soc Echo. 2006). However, these studies could not achieve high temporal resolution in a large field of view to depict the mechanical function of a heart chamber within a single heartbeat. The objective of this study was to demonstrate initial feasibility of imaging myocardial strains in vivo within the same imaging plane as ICE at high temporal resolution.

Statement of Contribution/Methods

A normal canine and a human subject with atrial tachycardia were studied in vivo. The studies were approved by the Institutional Animal Care and Use Committee and an Institutional Review Board of Columbia University, respectively. A 5.8-MHz center frequency ICE probe inserted into the femoral vein was used to image the heart with an unfocused beam transmit method to achieve high frame rates (1200 frames per second) and the channel data were acquired on a clinical ultrasound system (Z.one ultra, Zonare, Mountain View, CA) during 620ms. The RF signals were reconstructed off-line on a 9cm depth and 90° field of view region with a delay-and-sum algorithm and axial cumulative displacement estimation was performed using 1-D cross-correlation using a window size of 2.6mm and 95% overlap. Axial cumulative strains were obtained from the axial displacements using a least-squares estimator with a kernel of 5.1 mm.

Results/Discussion

In the canine, the average cumulative axial displacement of the posterior-lateral wall of the left ventricle during systole was approximately 5mm and the cumulative strain was approximately 12% due to radial thickening. In the right ventricle, the average cumulative axial displacement of the lateral-apical wall during diastole was approximately 4mm and the cumulative strain was approximately -7% due to radial thinning. In the human subject, cumulative displacement of the lateral wall of the right atrium during systole was approximately 2mm and the cumulative strain was approximately -3% due to longitudinal shortening. The lower strain values may be attributable to the tachycardia.

Myocardial Elastography using ICE was shown feasible in vivo at high temporal resolution. This initial feasibility of may offer new prospects in RF ablation guidance when fully integrated with ICE.

This study was supported by NIH R01EB006042 and R01HL114358.

IUS1-C1-6

A Comparison of Intracardiac ARFI and SWI for Imaging Radiofrequency Ablation Lesions

Peter Hollender[1], Lily Kuo[1], Virginia Chen[1], Stephanie Eyerly[1], Gregg Trahey[1,2]; [1]*Biomedical Engineering, Duke University, Durham, NC, USA,* [2]*Radiology, Duke University, Durham, NC, USA*

Background, Motivation and Objective

Transcatheter ablation (TCA) is commonly used to treat cardiac arrhythmias. The procedure involves generating a series of discrete radiofrequency ablation (RFA) lesions in the myocardium to destroy or isolate arrhythmogenic conduction pathways. Lesion placement is typically guided by electroanatomical mapping (EAM) and real-time imaging of the catheter tip with intracardiac echo (ICE) or fluoroscopy. The duration, power, and temperature of the ablation are used to control lesion formation, but feedback regarding the size, transmurality and continuity of lesions could improve the efficacy of the procedure. Intracardiac acoustic radiation force impulse (ARFI) and shear wave imaging (SWI) are novel ultrasound-based imaging methods that show promise for assessing RFA lesions by imaging the local mechanical compliance of the myocardium. This work compares the two imaging modalities' ability to resolve lesion boundaries.

Statement of Contribution/Methods

Sections of canine and porcine heart were either mounted in a saline bath or imaged *in vivo*. Sets of RFA ablation lesions were generated on the endocardial surface with variable gaps between them, using a Biosense Webster Stockert 70 RF Generator and a ThermoCool irrigated ablation catheter at 25W for 60 seconds. A Siemens AcuNav 10Fr ICE transducer was used to image the tissue at a depth of 1 cm along the axis of the RFA lesions. Custom pulse sequences, running on a Siemens Acuson SC2000 ultrasound scanner, were used to acquire both ARFI and SWI images. Both sequences used 32 ARF transmit locations over a 45° field of view (FOV). The ARFI sequences use focused tracking pulses for 16 kHz displacement tracking, while the SWI sequences used spherical wave transmits and parallel receive focusing to image and track the entire FOV at 16 kHz. Multiple images were acquired to record a 3 cm lateral FOV along the axis of the ablation lesions. After imaging, each segment of tissue was sliced and stained with triphenyltetrazolium to determine the size and spacing of the lesions.

Results/Discussion

The figure shows compiled ARFI and SWI images of two ablation lesions with a gap between them that is 1.5 mm wide at the narrowest point, which is consistent with histological staining. SWI and ARFI similarly image the lesions (SNR ~0.5), while SWI images the gap with higher SNR than ARFI (1.25 vs 0.8). CNR was marginally higher for SWI than ARFI (0.8 vs 0.65).

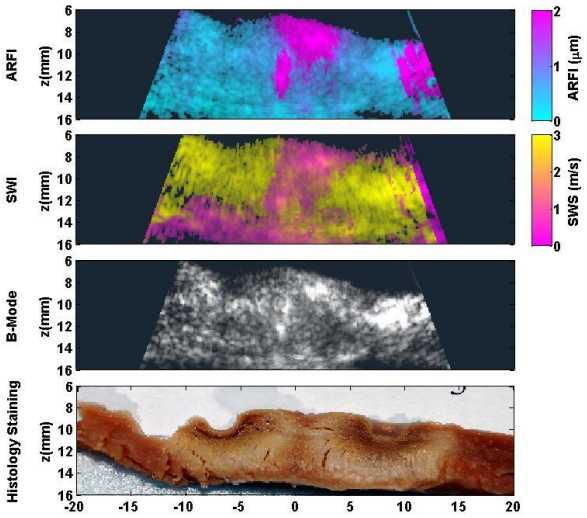

High intensity focused ultrasound and cavitation

M4

Monday, July 22 2013, 04:30 pm - 06:00 pm

Congress Hallair: **Greg Clement**
Harvard Medical School

IUS1-C2-1

Feasibility of HIFU cardiac therapy and monitoring using shear-wave imaging with a dual mode intracardiac catheter

Wojciech Kwiecinski[1], Jean Provost[1], Mathieu Legros[2], An Nguyen[2], Rémi Dufait[2], Mathias Fink[1], Mickaël Tanter[1], Mathieu Pernot[1]; [1]*Institut Langevin, ESPCI ParisTech, CNRS UMR7587, INSERM U797, Paris, France,* [2]*Vermon, Tours, France*

Background, Motivation and Objective

Atrial fibrillation (AF) is the most common cardiac arrhythmia and is the cause of 15-20% of strokes. Atrial arrhythmias such as AF can be treated by creating continuous, transmural ablation lines in the heart to isolate or eliminate electrically abnormal regions. However, clinically available systems based on radio-frequency ablation are associated with high recurrence rates in part because they cannot be used to create transmural lesions nor monitor their extent. We have shown previously that local tissue elasticity estimation with Shear-Wave Imaging (SWI) leads to a precise mapping of thermal lesions. In this work, we have developed and validated ex vivo a novel non-contact dual-mode ultrasound catheter, which can perform High-Intensity Focused Ultrasound (HIFU), Bmode and Shear-Wave Imaging (SWI) to create transmural lesions and monitor their extent in real-time.

Statement of Contribution/Methods

A 64-element intracardiac transducer (6 MHz, 64 elements, 0.2 mm pitch, Vermon, France) mounted on catheter (9F, 3-mm diameter) was designed and built for dual mode imaging and therapy. Fresh porcine ventricular (n=10, 10*30*30mm3) and atrial (n=6, 2*30*30mm3) samples were studied in a 37°C bath. The ultrasonic transducer was positioned to perform SWI on the samples. Shear waves were generated remotely with the probe and recorded (10000 frames/s, 3 shear wave generations per sample, 300 µs bursts) with an ultrafast scanner prototype (Supersonic Imagine, France) to map the shear modulus in 2D. This prototype was used to perform both transmit/receive imaging sequences and transmit HIFU sequences (up to 4W/cm2 per channel). HIFU lesions were then induced using the same probe by emitting a focused beam during 10s interrupted every second during 50ms in order to perform SWI imaging. The shear modulus maps were then processed and the elasticity ratio between pre and post treatment was compared against gross pathology for validation.

Results/Discussion

The total acoustic output power was measured with an acoustic radiation force balance. A total acoustic power of 2.6 W corresponding to an acoustic intensity of 11±0.2W/cm2 at the surface of the probe was measured during 10 s of emission without any detectable overheating effects. After 10 s of emission, thermal lesions were created. Thermal lesions of approximately 3 mm x 2 mm were visible on the shear modulus maps but not on B-mode images. The stiffening was found to increase from 31kPa±12kPa to 82kPA±30kPa at the boundary of the ablated zone and up to 150±43kPa in the core of the lesion. After comparison with gross pathology, a stiffness ratio of 2.6±0.46 between pre and post treatment on the 2-D elasticity maps was found to determine accurately the lesions boundaries.

We have demonstrated the feasibility of both thermal ablation and monitoring using the same ultrasonic catheter in ex-vivo samples. This direct therapy/imaging association could lead to a precise and reliable atrial fibrillation treatment.

IUS1-C2-2

Clinical evaluation of a toroidal HIFU Transducer designed for the treatment of liver metastases during an open procedure

David Melodelima[1,2], Jeremy Vincenot[1], Aurelien Dupre[2], Yao Chen[2], Michel Rivoire[2], Jean-Yves Chapelon[1]; [1]*LabTAU, INSERM, France,* [2]*Centre Leon Berard, France*

Background, Motivation and Objective

An ultrasound device that uses a toroidal HIFU transducer guided by ultrasound imaging was evaluated clinically for the treatment of colorectal liver metastases during an open procedure. Our long-term objective is to associate HIFU with hepatic resection. Here we report clinical results obtained on 18 patients. The principal objective was to validate the effectiveness, accuracy, tolerance and safety of the HIFU treatment. In addition, the response to HIFU was assessed using ultrasound imaging and compared with histological analysis.

Statement of Contribution/Methods

18 patients with liver metastases and scheduled for elective surgical resection of their tumors were included. The transducer has a toroidal shape with a diameter of 70 mm and is divided into 256 emitters of 0.13 cm2 each. The radius of curvature is 70 mm to enable treatment of the deepest regions of the liver. The operating frequency was 3 MHz. A 7.5 MHz ultrasound imaging probe was placed in the centre of the device to guide the treatment. The imaging plane was aligned with the HIFU focal zone. Two single thermal ablations were created in each patient after laparotomy and just before the planned liver resection.

Results/Discussion

36 HIFU lesions were performed. Consistent with our previous experience, the demarcation between ablated and non-ablated tissue was apparent in ultrasound images as a hypoechoic boundary and a central hyperechoic zone. The dimensions measured on ultrasound imaging were correlated (r=0.92) with dimensions measured during histological analysis. The average coagulated volume obtained from a 40 s total exposure in the liver was 5.6 ± 2.6 cm3 (1.9 – 11.4) with an average diameter of 21.6 ± 4.5 mm (12.0 – 28.0) and an average depth of 28.4 ± 6.3 mm (20.0 – 43.0). Patients have tolerated the treatment well. There was no hemodynamics and respiratory changes. No HIFU-related complications occurred during surgery and 30 days postoperatively. The HIFU device can enable the treatment of 94% of the liver volume.

This HIFU treatment using a toroidal transducer is feasible, safe and well tolerated. The treatment is characterized by its brevity (40 seconds for one single ablation of 5-6 cm3). This device is capable of achieving selective ablation of predefined liver regions. Ultrasound imaging evidence of complete ablation of the target region can be taken to infer histological success.

IUS1-C2-3

Preliminary ex vivo experiments of linear cardiac ablation using an ultrasound-guided transesophageal HIFU device

Elodie Constanciel[1], William Apoutou N'Djin[1], Francis Bessière[2], Mathieu Pioche[3], Philippe Chevalier[2], Jean-Yves Chapelon[1], Cyril Lafon[1]; *[1]Inserm, U1032, LabTau, Lyon, F-69003, France ; Université de Lyon, Lyon, F-69003, France, [2]Hospices Civils de Lyon, Hôpital cardiologique Louis Pradel, F-69000, France, [3]Hospices Civils de Lyon, Hôpital Edouard Herriot, F-69000, France*

Background, Motivation and Objective

Atrial fibrillation (AF) is the most frequent cardiac arrhythmia. Endocardial ablation is currently performed to treat this disease. The main target of this procedure is to isolate the pulmonary veins (PV) by thermal ablation. However transmural lesions are difficult to obtain and this invasive technique is less helpful for patients with well-settled AF. High-Intensity Focused Ultrasound (HIFU) devices have been designed to improve the transmurality of the lesions but they all require invasive interventions. Transesophageal HIFU probes are in development but none of them integrate imaging system to guide the procedure. Here an ultrasound-guided transesophageal HIFU device is presented that was designed to perform a complex procedure, the HIFU «mini-Maze». It was made with a 3 MHz 8-ring HIFU transducer including in its center a 5 MHz 64-element imaging transducer. Preliminary simulation investigations showed the ability to focus the ultrasound (US) beam over a broad range of depths from 17 to 55 mm to perform lesions in various areas, while preserving intervening tissues. The aim of the present *ex vivo* study was to demonstrate experimentally the feasibility to achieve precise transesophageal cardiac ablation under US guidance.

Statement of Contribution/Methods

The first trial was performed on *ex vivo* veal heart and pig esophagus. A hyperechoic cylindrical landmark, 5-mm in diameter, was inserted inside the cardiac tissue as a target comparable in size with a PV. After locating the target region on the 2D transversal US image provided by the on-board imaging system, HIFU exposures were performed transesophageally on the surface of the myocardium following a 2D coronal treatment planning (perpendicularly to the US image plane). Multiple elementary lesions were juxtaposed linearly in- and out-of-image-plane to trace an ablation barrier surrounding the vein-shaped target. The second trial was carried out *ex vivo/in situ* on a 40-kg pig. In realistic anatomical conditions, transesophageal HIFU exposures were performed in interventricular septum under 2D US guidance to create an in-plane single line of ablation.

Results/Discussion

Well-delimited pattern of ablation lines could be created transesophageally in heart, while protecting the interleaving tissues. No damage was detected macroscopically on esophageal tissues. On-board US imaging allowed accurate location in real-time of specific structures in cardiac tissues and enabled completing dedicated treatment planning accordingly. It was also showed that homogeneous linear lesions could be obtained transesophageally in deep seated heart tissues under realistic anatomical conditions. These preliminary experiments gave encouraging results for future development of a real HIFU Mini-Maze procedure. *In vivo* tests are ongoing to confirm that ultrasound-guided transesophageal HIFU devices can contribute significantly to AF treatment.

[Supported by ANR TecSan Grant No. ANR-11-TECS-004]

IUS1-C2-4

Ultrasound Thermography In Vivo: A new model for calculation of temperature change in the presence of temperature heterogeneity

Mahdi Bayat[1], John R. Ballard[1], Emad S. Ebbini[1]; *[1]Electrical and Computer Engineering, University of Minnesota, USA*

Background, Motivation and Objective

Speckle tracking is widely used in ultrasound thermograhy and has been shown to have high sensitivity and spatial resolution, especially when used at relatively high frame rates. It is being routinely used in providing estimates of in vivo tissue heating in response to sub-therapeutic HIFU beams (as a form of image guidance in advance of the application of therapeutic HIFU). Previous derivations have shown that thermal strain may be estimated using time accumulation and axial differentiation of the incremental tissue displacement. However, ignoring the spatial dependency of the temperature change in already heated tissues can result in erroneous negative temperature change values. A new formulation of the temperature change estimation accounting for nonuniform baseline temperature is presented.

Statement of Contribution/Methods

A new derivation of temperature change estimation based on speckle-tracking estimation of axial echo shifts is presented which accounts for the nonuniform temperature baseline. The new derivation results in the following model for echo shift due to change in tissue temperature,

$\Delta\tau_z = 1/c(2(\alpha-\beta)\Delta T + 2\alpha z \Delta T_z)$

where $\Delta\tau_z$ is the axial derivative of displacement, α and β are thermal expansion and change in speed of sound coefficients respectively and ΔT_z is the axial derivative of change in temperature and it is assumed to be a function of both time and space in general. The solution of this equation can be found as the output of a differentiator-integrator filter in the axial direction with the displacement field as the input. RF data obtained during a sub therapeutic HIFU shot in the hind limb of a Copenhagen rat partially submerged in a temperature controlled degassed water bath was used to verify the performance of this new approach.

Results/Discussion

A 3.5 MHz array was used to produce localized subtherapeutic heating ≈10mm under the skin with 750 msec duration. Figure 1 shows the axial-temporal temperature profile using the echo strain method (a) and the new method (b). The new method effectively removes the negative temperature artifacts that can be clearly seen in the echo strain estimate of temperature change.

The axial extent of the focal heating estimated using the new method is ≈2mm which is consistent with the extent of the focal spot for the HIFU transducer. The *in vivo* results demonstrate the robust estimation of temperature change using ultrasound.

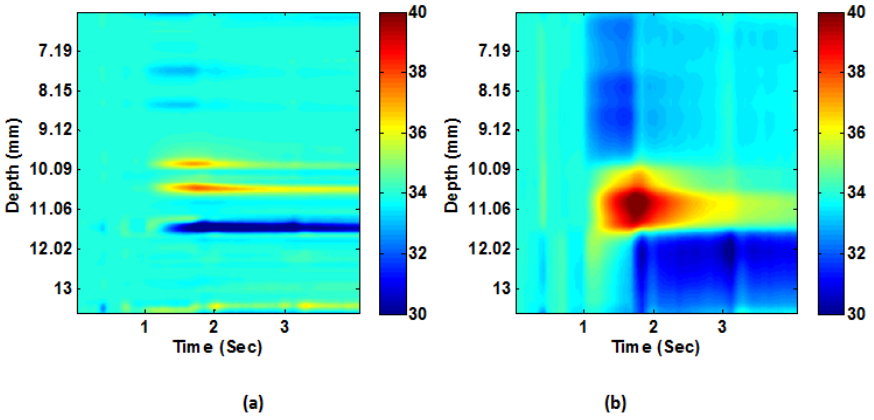

Figure 1: Axial-temporal distribution of temperature in a lateral point close to the heating focus (a) old method (b) new method

IUS1-C2-5

Non-invasive toroidal HIFU transducer for increasing the coagulated volume in depth

David Melodelima[1], Jeremy Vincenot[1], Anthony Kocot[1], Jean-Yves Chapelon[1]; [1]*LabTAU, INSERM, France*

Background, Motivation and Objective

A first toroidal-shaped HIFU device, developed for the treatment of liver metastases during surgery, has been previously described to be used as a tool for assisting liver resection. It was shown that this HIFU prototype allowed the creation of large HIFU lesions in the liver. Currently, this device is tested clinically for the treatment of liver metastases. The selected approach for the first evaluation of this toroidal HIFU treatment is surgical laparotomy. Here we report in vitro results obtained using a second version of this toroidal transducer. Unlike the previous prototype, the transducer is developed based on the interior volume of a torus. The aim is to verify whether the use of this geometry combined with electronic beam steering is capable of creating large volumes of ablations in depth in soft tissues without damageing intervening tissues (skin-fat-muscle).

Statement of Contribution/Methods

A toroidal transducer operating at 2.5 MHz was used. The radius of curvature was 70 mm with a diameter of 67 mm. An ultrasound-imaging probe was placed in a central circular opening of 26 mm in diameter. The transducer was also divided into 32 rings of 78 mm2 each. Using a 32 channels amplifier with a phase resolution of 1.4 degrees, it was possible to change the diameter (0 to 14 mm) and depth (75 to 95 mm) of the focal zone in order to maximize dimensions of lesions. Numerical simulations were performed in order to evaluate the feasibility of producing ultrasound ablation in the liver after passing through an abdominal wall of ten millimeters. In vitro studies have also been conducted. Experiments were performed in 8 bovine livers purchased from a local butcher. Livers were cut into samples with dimensions matching those of a sample holder (6.5 cm × 6.5 cm). The thickness of the samples was 10 cm. Intervening tissues were composed of skin-fat-muscle taken from pigs at the butchery and were placed at the top of the liver sample. The thickness of intervening tissues was between 10 and 12 mm in order to reproduce the in vivo conditions more closely. Twenty HIFU lesions were created at 20 mm in depth in tissues.

Results/Discussion

Each HIFU lesion was created in 55 seconds. HIFU lesions have an average width of 15.0 ± 1.7 mm and an average length of 26.7 ± 2.9 mm. The average distance between the skin and the beginning of the HIFU lesion was 34.4 ± 4.9 mm. On average 20.8 ± 4.0 mm of liver tissues were spared. In both sets of experiments, the maximal temperature in intervening tissues during treatment was 40°C. No lesions were observed in skin, fat, muscle or intervening liver tissues. The transducer described in this study is able to produce large zones of ablation in depth without creating any damage in intervening tissues. Based on these results, the potential clinical usefulness has to be further validated based on preliminary in vivo studies that will demonstrate the feasibility, efficiency and tolerance of this treatment.

IUS1-C2-6

Cavitation with confocal transducers

R. Andrew Fowler[1], Jean-Louis Mestas[1], Adrien Poizat[1], Françoise Chavrier[1], Cyril Lafon[1]; [1]*LabTAU, Inserm U1032, University of Lyon, Lyon, Rhone-Alpes, France*

Background, Motivation and Objective

Inertial cavitation has been shown to be useful in many therapeutic applications such as drug delivery, tissue ablation, and gene therapy; thus controlling this phenomenon is of great therapeutic interest. However, the stochastic nature of cavitation initiation and evolution often proves problematic for predicting the location and extent of inertial cavitation. Traditional solutions to this problem have been to use dedicated detection apparatuses, or to use injectable microbubbles (MBs) which act as nuclei for the initiation of cavitation. In this work, we study the efficacy of using two transducer confocal ultrasound system for the controlled generation of inertial cavitation as compared to a single transducer without the use of MB. The advantages of such a system are twofold: the system is simplified by eliminating the need for cavitation detection, and this system can be used for applications in which MB use is not feasible.

Statement of Contribution/Methods

Ultrasonic setup consisted of two 1.1MHz spherical transducers with focal length and diameter of 50mm, aimed confocally at 110°. The cavitation driven radical formation was determined chemometrically by the use of hydroxyterephthalic acid (HTA) oxidation assay with fluorescence measurements on a fluoromax-5 (Horiba Jobin Yvon). Acoustic measurements were performed with an FOPH2000 fiberoptic hydrophone (RP Acoustics). Simulated linear pressure fields were calculated by solving the Rayleigh integral for the case of focused radiators in C. Cavitation bubble evolution was observed using a Phantom v12.1 high speed camera (Vision Research).

Results/Discussion

For the same average electrical power, comparative HTA studies showed a 6.5-fold increase in HTA concentration for the confocal setup over the case with just a single transducer of 50mm diameter, confirming greater cavitation effects. Simulated results show that -3dB focal areas for a single transducer gave a continuous focal area of 19mm², compared to a focal area of 3.5mm² distributed in discontinuous lobes for the confocal setup. High speed camera imaging shows bubbles stabilized in the focal zone in a pattern qualitatively similar to the interference pattern measured with a fiberoptic hydrophone, supporting the hypothesis that interference created by beam crossing stabilizes the bubble cloud. For a 400V drive voltage, the pulse from the single transducer had a p+/p- ratio of 31/12 MPa, and the confocal system had 17/15MPa, demonstrating less non-linear propagation with the confocal system, increasing peak negative pressure, and diminishing the harmonic content of the pulse. Our system has been shown to produce cavitation in a robust fashion compared to a single transducer system without the use of MBs in vitro and ex vivo. Future experiments in vivo are planned.

Work supported by the European Union through the Eurostars program (project E!6173) and Caviskills

Photoacoustic imaging and contrast agents

M5

Monday, July 22 2013, 04:30 pm - 06:00 pm

Congress Hallair: **Georg Schmitz**
Ruhr-Universität Bochum

IUS1-C3-1

Molecular imaging of glioblastoma cells using functionalized nanorods and a high resolution optoacoustic microscope

Wolfgang Bost[1], Marc Fournelle[1]; [1]*Biomedical Ultrasound Research, Fraunhofer IBMT, St. Ingbert, Germany*

Background, Motivation and Objective

In optoacoustic imaging the contrast potential can be significantly enhanced by auxiliary nanoparticulate contrast agents showing a high optical absorption in the near-infrared (NIR) region of the electromagnetic spectrum, where tissue is relatively transparent.

Functionalized polymeric nanoparticles containing entrapped gold nanorods as potential optoacoustic contrast agents for glioblastoma multiforme have been developed and evaluated. The suitability and targeting efficiency of the nanomaterial has been investigated on a single cell level using a microscopic based high resolution optoacoustic imaging platform.

Statement of Contribution/Methods

Gold nanorods (GNRs) were produced following a seed-growth method and optimized for absorption at 1064 nm fundamental wavelength in order to allow their use as optoacoustic contrast agents based on Nd:YAG lasers. For specific binding to glioblastoma cells, the nanorods were functionalized with the peptide Chlorotoxin (Cltx), known to have a high binding affinity to such tumor cells. For enhancement of biocompatibility, the nanorods were entrapped in a PLGA copolymer (GNR-PNP kindly provided by Prof. Comes-Franchini from University of Bologna).

For molecular imaging of the chosen cell model, our high resolution optoacoustic microscope was used. The platform is based on an inverted optical microscope (Olympus IX81) and includes a microchip Nd:YAG laser (Teem Photonics) with sub-nanosecond pulses at 1064 nm and 4 kHz repetition rates. Further, an inhouse-constructed focused 400 MHz ZnO transducer is integrated for detection of laser-induced ultrasound signals. A fast scanning unit allows acquisition of 3D data that are digitized with a 4 GSamples/s AD-converter board. Prior to the actual measurement of the glioblastoma cells, the system resolution was characterized using 1,6 µm gold beads and a lateral resolution of 2,5 µm was obtained.

The binding affinity of the developed nanosystem towards glioblastoma cells was investigated using conventional optical phase contrast microscopy and high resolution optoacoustic microscopy. GNR-PNP-Cltx were incubated for 20h with U87MG cells at a concentration of 5 µg/ml of gold and imaged in both modalities. For control experiments, U87MG cells without NP-incubation and U87MG cells incubated with control particles (GNR-PNPs) at a gold concentration of 5µg/ml were used.

Results/Discussion

No differences in cell morphology between untreated cells, cells incubated with GNR-PNPs and cells incubated with GNRs-PNPs-Cltx could be observed in optical mode. On the contrary, a clear difference was recognizable using optoacoustic microscopy. Control cells that had not been incubated with contrast agents did not show any optoacoustic signal. Incubation with GNRs-PNPs led to a minor signal, while for cells incubated with GNR-PNPs-Cltx, stronger and more abundant signals were detected.

IUS1-C3-2

Transrectal photoacoustic-ultrasonic imaging enhancement through interstitial irradiation and targeted nanoparticles

Trevor Mitcham[1], Tatiana Marques[1], Dev Chatterjee[1], Sunil Krishnan[1], Thomas Pugh[1], **Richard Bouchard**[1]; [1]*MD Anderson Cancer Center, Houston, Texas, USA*

Background, Motivation and Objective

Given that prostate cancer is the second leading cause of cancer deaths in the United States, enhanced contrast and sensitivity provided by transrectal imaging would improve clinical options for cancer diagnosis and therapy in the prostate. Transrectal photoacoustic-ultrasonic (TR-PAUS) imaging is capable of imaging metallic implants with superior contrast and of probing molecular attributes of tissue. TR-PAUS imaging enhanced with interstitial irradiation (i.e., to increase local fluence) and targeted nanoparticles has the potential to allow for intraoperative, local tissue assessment (i.e., oxygen saturation or presence of targeted nanoparticles) during needle-biopsy or brachytherapy-implantation procedures in the prostate.

Statement of Contribution/Methods

A BPL9-5/55 transrectal probe connected to a Sonix RP ultrasound system was modified to include seven 800-micrometer optical fibers that were coupled to an Nd:YAG tunable laser (A). An interstitial, single-fiber irradiation source was added to provide local irradiation (D). TR-PAUS imaging acquisitions were conducted in a tissue-mimicking phantom or excised bovine prostate with embedded Ti targets. PA imaging of gold nanorods (AuNRs; 810-nm peak) targeting the LHRH receptor in PC-3 human prostate cancer in a murine model was achieved with a Vevo LAZR PAUS system (680, 734, 758, 810, & 950 nm) to demonstrate potential transrectal feasibility.

Results/Discussion

A clinical imaging system was integrated with a TR-PAUS probe to provide seed visualization (B) with contrast improvements (over US) in excess of 25 dB @ 1064 nm. Although this system is capable of delivering >100 mJ per pulse @ 1064 nm, an interstitial irradiation source was also integrated to provide >15 mJ (@ 1064 nm) of local irradiation (E - US; F - PA), which could provide irradiation for local assessment of oxygenation during a needle biopsy procedure. LHRH-targeted AuNRs were successfully imaged and segmented using correlation-based methods (C - PAUS image @ 810 nm). The contrast provided by TR-PAUS enhanced with an interstitial source shows tremendous potential in assisting in diagnostic procedures (e.g., needle biopsy) and during therapy guidance (e.g., visualization of brachytherapy seeds), while the utilization of targeted nanoparticles could further improve the sensitivity and clinical translatability of these technologies.

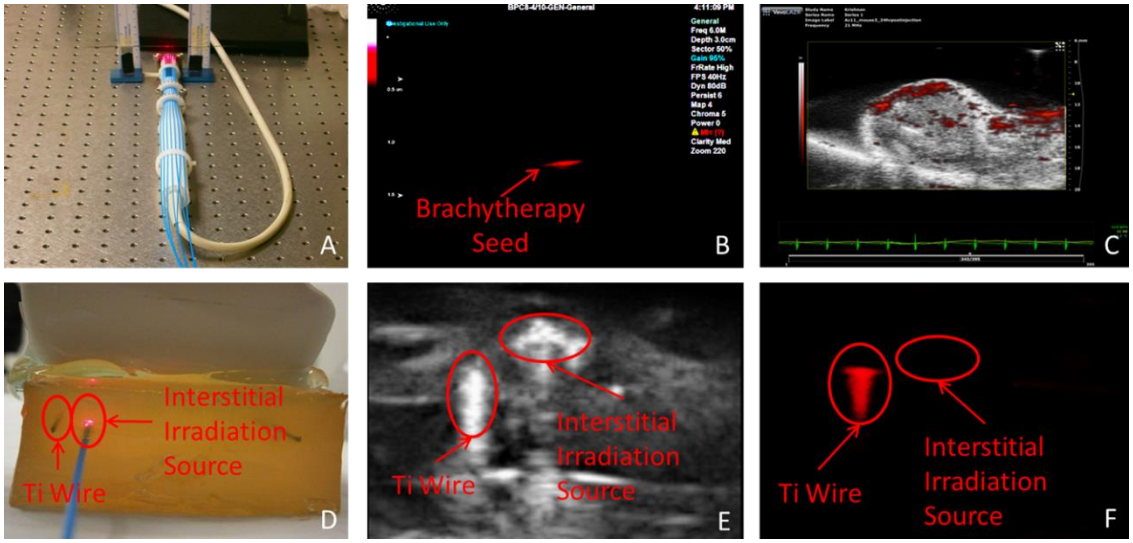

IUS1-C3-3

Nonlinear ultrasound/photoacoustic contrast enhancement by ultrasound probing of laser pulse induced bubbles with gold nanospheres coated emulsion beads

Chen-wei Wei[1], Kjersta Larson-Smith[2], Ivan Pelivanov[1,3], Camilo Perez[4], Jinjun Xia[1], Danilo Pozzo[2], Thomas Matula[4], Matthew O'Donnell[1]; *[1]Bioengineering, University of Washington, Seattle, USA, [2]Chemical Engineering, University of Washington, Seattle, USA, [3]International Laser Center, Moscow State University, Moscow, Russian Federation, [4]Applied Physics Lab, University of Washington, Seattle, USA*

Background, Motivation and Objective

Labeled microbubble contrast agents make ultrasound (US) an attractive modality for molecular imaging, providing low-cost, non-ionizing, real-time, and non-invasive detection of specific molecules or diseased cells with sub-mm spatial resolution. Also, photoacoustic (PA) imaging, which uses US sensing of pulsed laser-generated acoustic waves, provides high optical-contrast molecular imaging with targeted nanoparticles and can easily integrate with US imaging systems. In this study, a new technique using a composite contrast agent is proposed to increase specific contrast in integrated US/PA molecular imaging.

Statement of Contribution/Methods

The composite particle has an emulsion bead core with a surface-assembled monolayer of gold nanospheres (GNSs), which efficiently absorbs optical energy under laser irradiation and promotes a phase transition of the emulsion bead to form a transient bubble. Much stronger PA signals are also generated by the phase transition process than those from thermal expansion, the most common mechanism of laser-sound conversion. Furthermore, delivering a US beam to probe the laser-induced bubbles creates harmonic signals, enabling nonlinear contrast-enhanced US imaging. The emulsion bead sample and a control sample of clustered GNSs with the same optical absorption were tested in a tube phantom with the experimental setup including a fiber bundle delivering laser pulses to induce bubbles, an array transducer transmitting probe US pulses, and a broadband PVDF transducer to detect nonlinear harmonics. US-alone, laser-induced PA-alone, and simultaneous US/laser probing signals were recorded for comparison.

Results/Discussion

Fig. 1 shows the received signals at different probe conditions using control linear GNS clusters (top row) and emulsion beads (bottom row). The PA signal amplitude of the emulsion bead increases by three times compared to that of the cluster GNS sample, indicating enhanced PA sensitivity. Also, by subtracting the single probe US and PA signals from the dual-probing (US+PA) signal, the nonlinear residue signal of the emulsion bead sample exhibits 19.7 dB increase in magnitude compared to that of the control linear sample. The proposed technique can greatly enhance the sensitivity and specificity of both US/PA molecular imaging by locally activating nonlinear contrast agents in targeted regions.

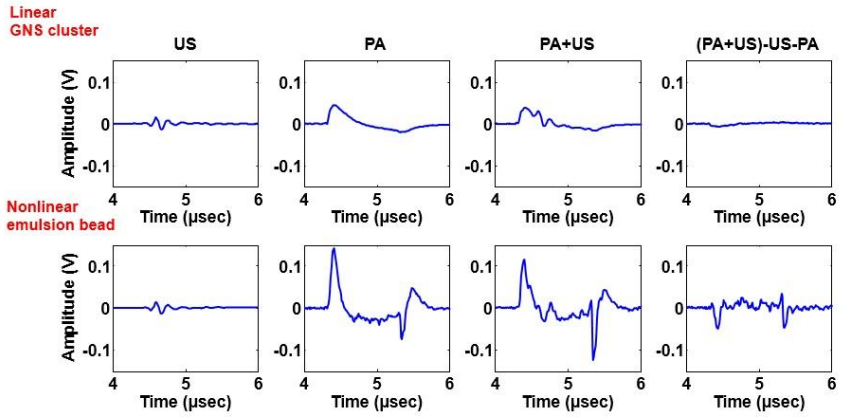

Fig. 1. Received signals at different probe conditions for two samples: test dispersion of GNS clusters (top row) and emulsion beads (bottom row). The average magnitude of the differential signal between dual-probing (US+PA) and single probe US and PA signals of the nonlinear emulsion sample is about 10 times larger than that of the control linear GNS cluster sample, representing contrast enhancement from the nonlinear harmonics by US probing of laser-induced bubbles.

IUS1-C3-4

Emulsion-aided laser clot disruption using a portable low-cost high-repetition rate fiber laser with simultaneous photoacoustic imaging

Jinjun Xia[1], Chen-wei Wei[1], Camilo Perez[1], Michael Lombardo[2], Kjersta Larson-Smith[2], Ivan Pelivanov[1,3], Danilo Pozzo[2], Thomas Matula[4], Matthew O'Donnell[1]; *[1]Bioengineering, University of Washington, USA, [2]Chemical Engineering, University of Washington, USA, [3]International Laser Center, Moscow State University, Russian Federation, [4]Applied Physics Lab, University of Washington, USA*

Background, Motivation and Objective

Previously, we have shown that an emulsion-based photoacoustic (PA) contrast agent can enhance clot disruption using a low-repetition rate (20 Hz) laser running at 700 nm wavelength. However, a compact, low-cost, high-repetition rate fiber laser is much more attractive for clinical translation in laser-induced imaging and therapy applications. The objective of this paper is to study the feasibility of using this type of laser for emulsion-aided clot disruption with simultaneous photoacoustic imaging.

Statement of Contribution/Methods

The fiber laser used operates at 1064 nm wavelength, with mJ pulse energy level and variable pulse width (10 ns -250 ns) at a kHz repetition rate. The 1064 nm laser is the most widely available and economical laser, making it a practical solution for clinical translation. The emulsion-based composite particle includes an emulsion bead core assembled with a single layer of gold nanospheres on the surface for enhanced optical absorption. Its optical absorbance spectrum is shown in figure 1(a). A home-made clot phantom with a Young's modulus similar to a typical human artery clot was used as the test object. The emulsion and clot were loaded adjacently in a 1.6 mm diameter PETF tube pressurized to mimic a human artery. Phantoms were placed in a water tank equipped with a light delivery system. Laser pulses with 30 ns pulse duration and 5 mJ/cm2 fluence at repetition rates over 1 kHz were used to both disrupt the clot and image the disruption process at a high frame rate. Laser illumination induced a rapid liquid-gas phase transition and generated strong acoustic waves for photoacoustic imaging and clot breaking.

Results/Discussion

Results indicate that high-repetition rate, low pulse energy illumination is potentially very effective for clot disruption in vasculature systems. Figure 1(b) shows an example of the PA signal mean amplitude change with time in the tube region filled with emulsion during the clot disruption process. The curve clearly reflects the change in PA signal concomitant with clot breakage. Clot disruption was also confirmed visually. These results strongly suggest that clot disruption and PA imaging with a compact fiber laser as a light source is possible for therapy and imaging applications. This technique represents an attractive translational path for peripheral vessel and intravascular applications of simultaneous photoacoustic imaging and therapy.

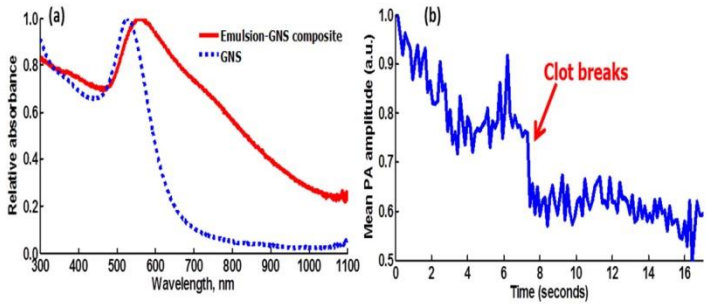

Figure 1. The relative absorbance spectra of emulsion-gold nanosphere (GNS) composite and pure GNS (a), and mean PA amplitude change with time in the tube region filled with emulsion-GNS composite solution (b). In (a), the classic spectrum of GNS has been red shifted and broadened by clustering in the emulsion, which enables operation at multiple wavelengths in the near IR. Even though the absorption at 1064 nm is 68% less than at 700 nm, our results demonstrate that the absorption is sufficiently large for effective photoacoustic imaging and therapy at this wavelength.

IUS1-C3-5

Numerical modeling of photoacoustic generation by metallic nanoparticles : source extension and thermoelastic based non-linearities

Amaury Prost[1], Emmanuel Bossy[1]; *[1]Institut Langevin, ESPCI ParisTech, CNRS, INSERM ERL U979, Paris, France*

Background, Motivation and Objective

Metallic nanoparticles have proved to be valuable contrast agents for photoacoustic imaging due to their large absorption cross-sections and their spectral selectivity, and are already widely used in the biomedical field. Yet the emission of photoacoustic waves from such particles involves various coupled physical mechanisms. It has been shown recently [Chen et al., SMALL, 2012, 8(1)] that the dominant contribution to the photoacoustic signal for usual conditions of illumination (nanosecond pulse) is generated by the medium surrounding the particles. In this work, our objective is to theoretically investigate the local and transient thermal phenomenons, in particular to describe the extent of the emission zone and explain non-linearities that have been reported experimentally.

Statement of Contribution/Methods

In this work we perform a numerical resolution of the thermal and photoacoustic wave equations for uncoated gold nanospheres immersed in water, based on semi-analytical and finite-difference in time domain approaches. The varying physical parameters are the diameter of the spheres, the pulse energy and duration, the medium equilibrium temperature. Within the thermoelastic regime, our numerical approach allowed to take into account the temperature variations of thermodynamic coefficients such as the coefficient of thermal expansion, as opposed to analytical formulation.

Results/Discussion

We demonstrate that the spatial extent of the contributing layer is mostly dependent on the duration of the laser pulse, and increases with it. For particle diameter varying from 20nm to 80nm and for a laser pulse duration of 5 ns, the spatial extent is about 50nm. Taking into account the temperature-dependence of the coefficient of thermal expansion, we predicted significant non-linearities of the photoacoustic signal amplitude as a function of laser fluence (fig), in agreement with experimental results. Finally, we show that the importance of the non-linearities is highly dependent on the frequency at which the photoacoustic signals are detected(fig).

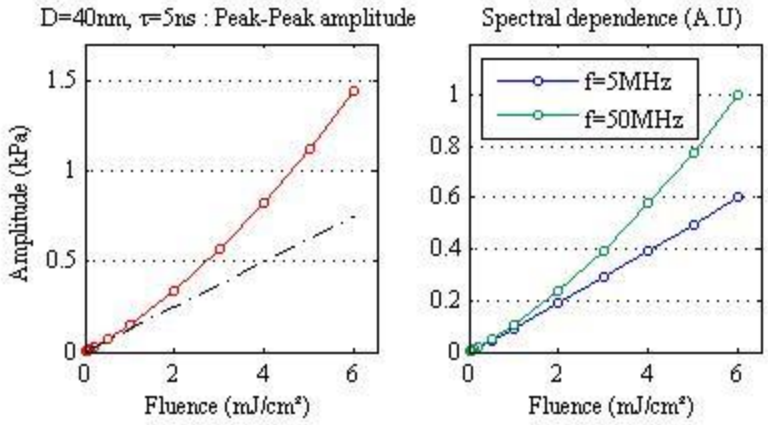

IUS1-C3-6

Vaporization, Photoacoustic and Acoustic characterization of PLGA/PFH particles loaded with optically absorbing materials

Yang Sun[1], Chengcheng Niu[1], Yanjie Wang[2], Eric Strohm[2], Zhigang Wang[1], Haitao Ran[1], Yuanyi Zheng[1], **Michael Kolios[2]**; *[1]Second Affliated Hospital, Institute of Ultrasound Imaging, Chongqing Medical University, Chongqing, China, People's Republic of, [2]Physics, Ryerson University, Toronto, Ontario, Canada*

Background, Motivation and Objective

Poly (lactide-co-glycolic acid) (PLGA) is an FDA approved biocompatible and biodegradable material that is widely used in implantation and drug delivery applications. It can be used as a carrier for various chemotherapeutic drugs, imaging agents and targeting moieties. Perfluorocarbon (PFC) liquids have been used in various biomedical applications, and can be activated (liquid core converted to gas) via laser irradiation through the incorporation of optically absorbing nanoparticles (NPs) or dyes into the droplets. PLGA particles were synthesized with NPs and/or dyes within the PLGA shell and liquid PFC within the core. These particles were characterized using ultrasound (US) and photoacoustic (PA) methods to optimize the particle composition.

Statement of Contribution/Methods

Dyes (DiI, Rhodamine) and NPs (gold, iron oxide) were incorporated into 1-6 µm diameter PLGA/PFH particles using a double emulsion evaporation method. The optical vaporization threshold and optimum composition were investigated using US and PA and a 375 MHz transducer. PA measurements used a 532 nm laser focused to a 5 µm spot size, with a maximum energy per pulse of 450 nJ. The PLGA/PFH particles were incubated with MDA cells for 2 hours to investigate particle toxicity, and to assess the vaporization threshold with the PLGA particles incorporated within cells.

Results/Discussion

The strongest PA signal measured was from DiI-loaded PLGA/PFH particles with gold NPs (see figure). During exposure, the PA signal from dye-loaded PLGA/PFH particles decreased due to photobleaching, while the PA signal from NP-loaded particles remained constant. The vaporization threshold was less than 100 mJ/cm^2; these particles were used in the in-vitro cell experiments. These particles were internalized by MDA cells after incubation for 2 hours, confirmed via fluorescence and electron microscopy imaging. The DiI/gold loaded PLGA/PFH particles were vaporized, forming a bubble while inside the cells resulting in cell destruction (see figure). This work demonstrates different PLGA/PFH particles are usable as PA contrast agents and theragnostic agents. Combining the NPs with DiI enabled identification via fluorescence, and increased the PA signal while reducing the vaporization threshold. When incorporated within cells, PLGA particles can be used as both imaging and therapy agents.

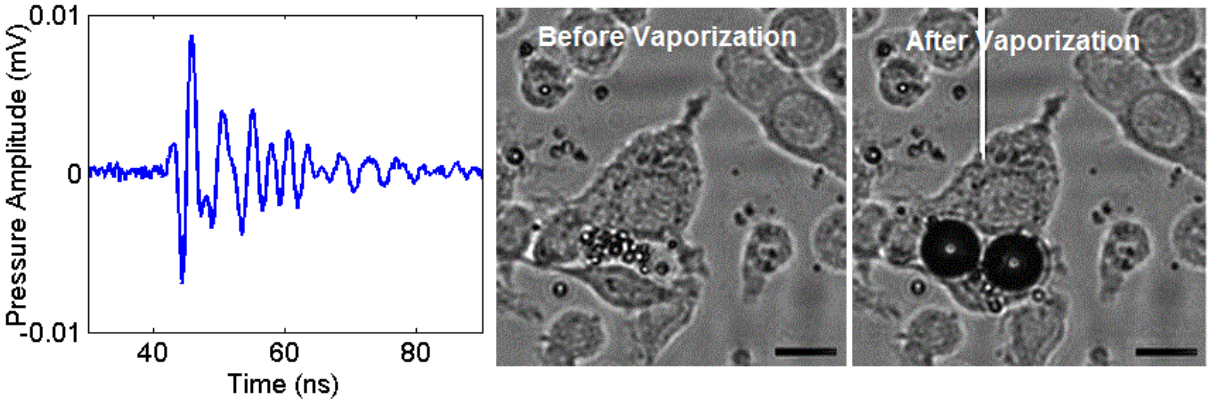

Guided Waves

NH

Monday, July 22 2013, 04:30 pm - 06:00 pm

Congress Hallair: **Walter Arnold**
Saarland University

IUS2-C-1

Guided Wave Attenuation in Cylindrical Bars Surrounded by Soil

Masanari Shoji[1], Takashi Sawada[1]; *[1]NTT Energy and Environment Systems Laboratories, Nippon Telegraph and Telephone Corporation, Musashino-Shi, Tokyo, Japan*

Background, Motivation and Objective

In ultrasonic guided wave NDE of a structure surrounded by a solid medium, guided wave attenuation caused by energy leakage into the medium is an important property that has a significant effect on the inspection range and/or signal-to-noise (SN) ratio. Thus far, this property has been investigated mainly for bars embedded in grout and epoxy to carry out ultrasonic NDE of architectural structures, but has scarcely been examined for bars embedded in soil. In this work, guided wave attenuation in cylindrical steel bars surrounded by soil has been studied through calculation.

Statement of Contribution/Methods

First, characteristic equations of guided waves (L, T and F modes) in cylindrical bars surrounded by a solid medium are presented, and then the attenuation dispersion curves of L(0,m) modes and T(0,m) modes of cylindrical steel bars surrounded by soil are computed and analyzed for various material properties of soil (density, bulk longitudinal wave velocity and bulk shear wave velocity).

Results/Discussion

Figure 1 shows the attenuation dispersion curves of the L(0,m) modes. Each mode has rather complex frequency dependence. Because the relation between attenuation-radius and frequency-radius does not depend on the radii, the attenuation of each mode has larger frequency dependence for smaller diameter bars. Figure 2 illustrates the attenuation dispersion curves for various possible bulk shear wave velocities of the surrounding soil. Each mode exhibits a specific variation of the attenuation with respect to the bulk shear wave velocity of soil. The results indicate that selecting the appropriate guided wave mode and frequency with consideration of the attenuation and the soil material properties is essential for proper ultrasonic guided wave NDE of bars surrounded by soil.

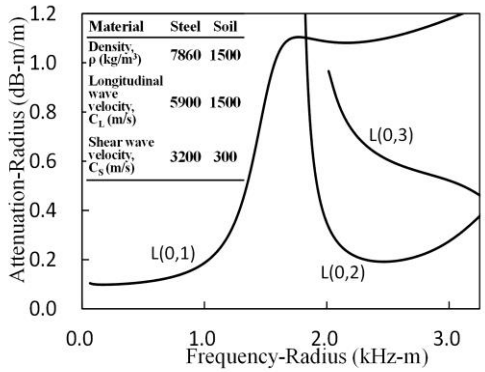

Fig. 1 Attenuation of L(0,m) modes as function of frequency-radius product in cylindrical steel rod surrounded by soil.

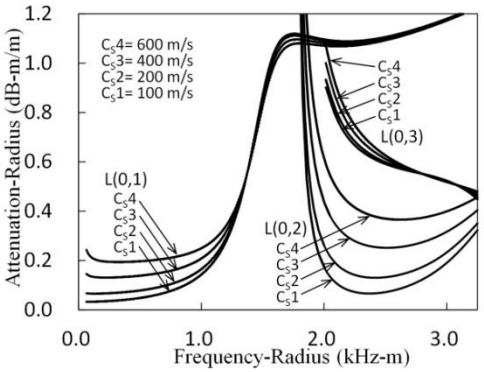

Fig. 2 L(0,m) mode attenuation as function of frequency-radius product for four values of bulk shear wave velocity (C_S) in soil. Other material properties were the same as shown in Fig. 1.

IUS2-C-2

AN ULTRASOUND METHOD FOR PIEZOCERAMIC FIBERS CHARACTERISATION

Robert Dittmer[1], Thomas Rödig[2], Andreas Schönecker[2]; *[1]Materials Science, TU Darmstadt, Germany, [2]IKTS Dresden, Germany*

Background, Motivation and Objective

PZT fibers are used in 1-3 composites to obtain high end ultrasound transducers. The advantages refer to adjust the acoustic impedance, bandwidth and the sensitivity. The performance of the ultrasound 1-3 composites transducer depends mainly on the properties of the piezoelectric fibers. Consequently the electrical, mechanical and electromechanical properties of single fibers have to be determined. The brittle nature of the ceramic fibers and their high aspect ratio limit the use of known standard measurement methods applicable for bulk piezoceramics.

Statement of Contribution/Methods

A novel non-destructive and contactless method developed at IKTS is based on ultrasound guided waves in solids. The piezoelectric fiber itself is used for generating and receiving ultrasound waves. Mechanical contact points and consequently source of errors between transducer and wave path are avoided. For electromechanical coupling two pairs of ring electrodes is applied. One set of the ring electrodes is placed on the end and the other set is placed in the middle of the long fiber (>100 mm). The fiber segments between the two pairs of ring electrodes are poled in parallel to the fiber direction. Applying a pulse voltage on the pairs of ring electrodes at the end of the fiber leads into an ultrasound wave traveling along the fiber as a quasi longitudinal wave.

Results/Discussion

The novel method requires a set of different measurements, e.g. delay time (pulser-receiver and transmission) and echo signal amplitude under different electrical boundary conditions of the poled and electrical contacted segment in the middle of the fiber. Depends on the electrical boundary conditions the Young's Modulus YE and YD meaning the short-circuit-conditions and open-circuit-conditions, respectively, can be determined. Applying the known piezoelectric equations the electromechanical properties k33 und d33 can be calculated. For calculation purposes Only the density the fiber and the dielectric constant of the poled fiber segment is needed for calculation purposes. Both values can be determined using known standard measurement methods.

For comparison standard electrical measurement methods are applied to 1-3 composites made of PZT fibers. Additionally laser vibrometer measurements carries out the fiber deformation caused by ultrasound. For evaluation and further investigations an electromechanical model of single fibers under ultrasound wave loads was developed and used for the interpretations of the measurements results.

The novel characterization method is designed for single fiber measurements. The results can be used for materials development, PZT fiber production and quality control. Optimized piezoelectric fibers will significantly enhance the performance of 1-3 composites as well as ultrasound transducer made of 1-3 composites.

IUS2-C-3

Space Tether Produced to Strength Specification

Anni Toppila[1], Henri Seppänen[1,2], Timo Rauhala[1], Göran Maconi[1], Sergiy Kiprich[3], Jukka Ukkonen[1], Martin Simonsson[4], Pekka Janhunen[2], Edward Hæggström[1,5]; *[1]Department of Physics, University of Helsinki, Helsinki, Finland, [2]Finnish Meteorological Institute, Helsinki, Finland, [3]National Science Center Kharkov Institute of Physics and Technology, Institute of High Energy Physics and Nuclear Physics, Kharkov, Ukraine, [4]4Centre for Image Analysis (CBA) and SciLifeLab, Uppsala University, Uppsala, Sweden, [5]University of Helsinki, Helsinki Institute of Physics, Finland*

Background, Motivation and Objective

We show that an active feedback combined with real-time measurements permits us to manufacture thin metallic space tether with less than 0.1‰ failed bonds. The failure criterion is less than 50 mN maximum sustainable pull strength.

E-sail, or the electric solar wind sail is a new space propulsion concept that utilizes the solar wind momentum to produce thrust. The propellant-less E-sail consists of multifilament tether; three 25 µm in diameter wires bonded to one 50 µm in diameter wire by ultrasonic wire-to-wire bonding. Recently we produced a continuous 1 km long e-sail tether including more than 90.ooo wire-to-wire bonds. While 99.5‰ of the bonds were attached [1], there was no way to tell how many of the bonds fulfilled the 50 mN pull force criterion.

Statement of Contribution/Methods

An ultrasonic non-destructive real-time method is created, to measure the bond strength. Combined with the active feedback of the ultrasonic bonder the setup can produce bonds to quality specification. In our test run 10000 bonds is produced to specification. After the production, each bond's maximum sustainable pull strength is tested by destructive pull testing.

Results/Discussion

Our results show that less than 0.1‰ of the bonds fail the criterion whereas without the active feedback the failure rate was 0.5‰. This kind of production to specification can reduce the necessity to carry quality assurance off line. To our knowledge ultrasonic wire bonding has not been done to specification before.

Caption: Prediction of bond quality is conducted since initiation of bonding with a constant time interval. The target predicted bond quality is represented by the black line and it is allowed to fluctuate within the blue area. At t = 5 the prediction falls outside the allowed region causing an intervention to occur, which retrieves the predicted quality to an acceptable level. The gray dots show how the bond quality would have evolved without the intervention.

[1] Automatic 4-wire Heytether production for the electric solar wind sail, International Microelectronics Assembly and Packing Society Topical Workshop and Tabletop Exhibition on Wire Bonding, Radisson SAS hotel San Jose airport, Jan 22-23, San Jose, California, USA, 2013.

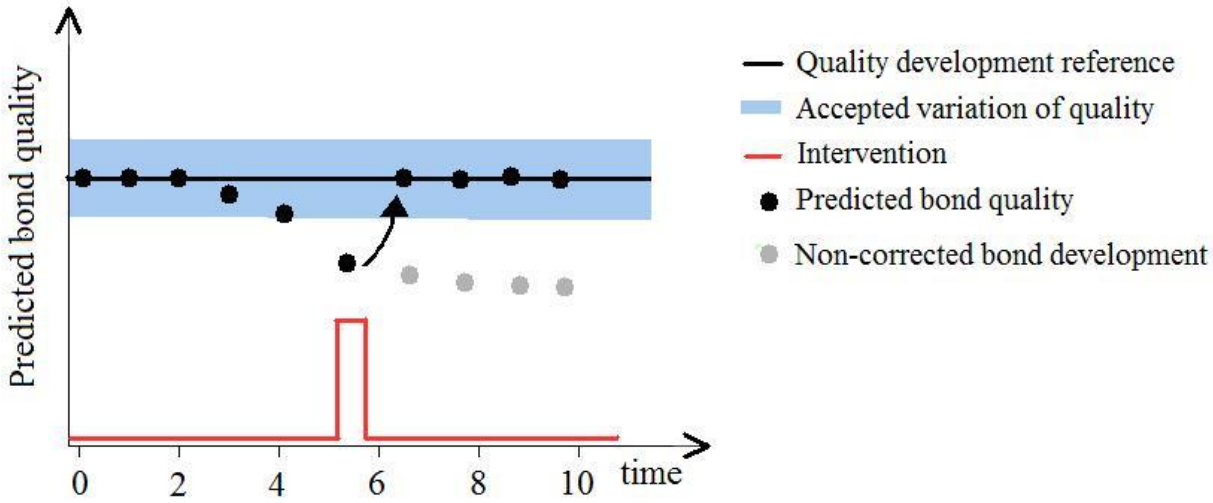

IUS2-C-4

Influence of flow speed on guided waves in a liquid filled pipe

Bixing Zhang[1], **Hanyin Cui**[1], Jianzhong Shen[1], Jon Trevelyan[2]; *[1]Institute of Acoustics, Chinese Academy of Sciences, China, People's Republic of, [2]Durham University, United Kingdom*

Background, Motivation and Objective

Liquid-filled pipes are widely used in industries such as power and nuclear plants with harsh environments. These pipes must be regularly inspected for the structure integrity. Elastic guided waves are suitable for long-range inspection of pipes, since they can guide the ultrasonic energy propagating along the axial or circumferential directions, and they are sensitive to material properties and geometries of pipes. In this paper, the influences of liquid flow speed and temperature on guided modes in steel pipes filled with flowing high temperature liquid metals are investigated. The aim is to choose the suitable guide modes, which are non-sensitive to the flow speed and temperature of the inner liquid, for the development of a nondestructive evaluation method to inspect liquid-filled pipes.

Statement of Contribution/Methods

The dispersion equation of guided waves propagating in a cylindrical pipe carrying flowing liquid is theoretically obtained by the transformation between two cylindrical coordinates. Dispersion curves of longitudinal and flexural guided modes are then numerically simulated by applying bisection technique to calculate the dispersion equation, so that to find the proper guided modes slightly affected by the liquid flow speed. Lab experiments are carrying out to compare with theoretical dispersion curves.

Results/Discussion

Fig.1 shows the numerical group velocity dispersion curves of the second order longitudinal mode, shorted as L(0,2), in two water-filled steel pipes with water flow speeds equal to -3 and 3 m/s, respectively. When frequency is less than 40 kHz, group velocity differences between two dispersion curves, as represented by the dotted line in the right vertical axis of Fig. 1, are trivial. It is concluded that the L(0,2) mode is a suitable mode for inspection of pipes containing flowing liquid. In the low frequency range, this mode is slightly dispersive, group velocity distinguishable, and not sensitive to the flow speed and high temperature of the liquid inside a pipe.

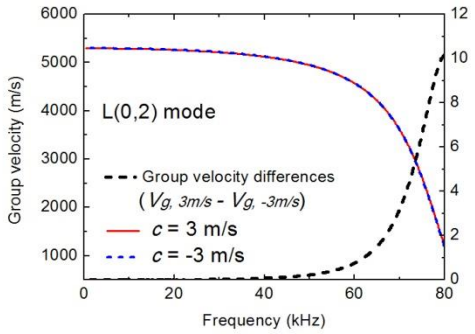

IUS2-C-5

Ultrasonic density measurement of polymer melts in extreme conditions

Regina Rekuvienė[1], Rymantas Kaþys[1], Reimondas Ðliteris[1], Elaine C. Brown[2], Adrian L. Kelly[2], Ben R. Whiteside[2]; *[1]Prof. K. Barðausko ultrasound research institute, Kaunas University of Technology, Kaunas, Lithuania, [2]IRC in Polymer Science&Technology, Bradford University, Bradford, United Kingdom*

Background, Motivation and Objective

In line real time monitoring and measurement of density of manufactured products is very important in various industrial applications, especially during extrusion of polymer melts. In this case measurements must be performed in very complex conditions, for example at high tem-perature (up to 4000C), high pressure (up to 10 MPa) and high chemical activity of the medium, mechanical impacts. Such extreme conditions limit the number of measurement techniques which can be used. The objective of this work was to develop and investigate an in line ultra-sonic density measurement technique of polymer melts.

Statement of Contribution/Methods

The proposed technique is based on transformation of the acoustic impedance of the measured liquid, which is realized by means of the λ/4 (λ is the wavelength) acoustic matching layer between the measured medium and the ultrasonic transducer. The conventional ultrasonic transducers cannot withstand a high temperature; therefore transmission of ultrasonic waves is performed via ultrasonic waveguides with a low thermal conductivity. The λ/4 acoustic matching layer is placed on the tip of the waveguide, contacting the medium under a measurement. Match-ing layers made off different materials with various acoustic impedances were investigated both theoretically and experimentally.

It is very important to select a proper geometry and material of the waveguide. Therefore numerical investigation of ultrasonic wave propagation in cylindrical and tapered waveguides with λ/4 acoustic impedance matching layers using two different modeling techniques- 2D finite element and 3D finite difference (Wave 3000) techniques was performed.

Numerical modeling of the ultrasonic wave propagation in titanium and steel waveguides revealed a complicated character of the wave propagation. In order to reduce trailing waves the tapered geometry waveguide should be used. The investigations showed that material of the waveguide influences not only waveforms of the ultrasonic signals, but also sensitivity and accu-racy of density measurements. The results obtained by the numerical modeling show, that tita-nium is most suitable as a waveguide material.

Results/Discussion

The proposed technique was verified experimentally using the following reference liquids with different densities: ethyl alcohol, distilled water and sugar water solutions (30%, 60%, 70%). The range of density measurement is 0.8-1.4 g/cm3.

The instrument has been installed on a 38mm diameter single screw extruder in the labo-ratories in Bradford University and used to measure values of and fluctuations in polymer melt density in real-time during single screw extrusion of polyethylene, polypropylene, polystyrene and flexible PVC.

The part of this work was sponsored by the European Union under the Framework 7 pro-ject POLYSENSE “Development of a low cost in-line polymer inspection system to improve the use of recycled materials in plastics processing industry”.

IUS2-C-6

Detection of a Subsurface Flaw with the Total Internal Reflection Ultrasonic Sensor

Alexander Yurchenko[1], Vadim Danilov[1], Yuriy Pilgun[1], Eugene Smirnov[1]; *[1]Department of Quantum Radiophysics, Taras Shevchenko National University of Kyiv, Ukraine*

Background, Motivation and Objective

The well-known fact that flaws located immediately below the surface are difficult to detect with ultrasonic techniques [1] challenges researchers to seek new methods specifically aimed at detecting such defects. Resent research [2] studied a novel Total Internal Reflection Ultrasonic Sensor (TIRUS) exploiting a phenomenon of frustrated total internal reflection of an ultrasonic wave in the sensor body caused by an object under test being in contact with the sensor. The sensor feasibility was proved for the case of flaws located at the surface of the tested objects. The current paper deals with detection of a defect under the surface of the tested specimen.

Statement of Contribution/Methods

The idea behind the TIRUS is illustrated in Fig. 1. It is made of a single crystal TeO2 prism and operates as a two-port device whose transfer function is affected by a flaw beneath the surface of a tested object. An ultrasonic shear horizontal wave excited by the input transducer travels to the interface between two solids, the sensor and the tested object. A reflected wave is received by the output transducer. If the angle of incidence of the wave incident at the interface is greater than the critical angle, evanescent wave arises in the surface layer of the tested object. A flaw present in the field of the evanescent wave affects it and hence affects the reflected wave in the sensor body increasing measured insertion loss of the sensor.

Results/Discussion

In the experiment, the sensor designed to operate at the frequency of 27 MHz was applied sequentially to a flawless object of fused quartz and then to a defected object of the same material. The artificial "defect" of the latter was a layer of epoxy resin under a thin (~70 micrometers in thickness) plate bonded to a solid piece of fused quartz. A result of measurements of the sensor transfer function shows that it changes distinctively for the sensor in contact with the surface of the plate compared to that for the sensor in contact with the flawless object. Thus, the TIRUS capability to detect subsurface flaws has been proved.

1. A. Matzkanin, H. T. Yolken, "Selecting a Nondestructive Testing Method: Ultrasonic Testing", The AMMTIAC Quarterly, Vol. 2, No 3, p. 9-13, 2008.

2. "Total Internal Reflection Ultrasonic Sensor for Detection of Subsurface Flaws: Proof of Concept", Final Tech. Report, March 2010, http://www.dtic.mil/dtic/tr/fulltext/u2/a527212.pdf

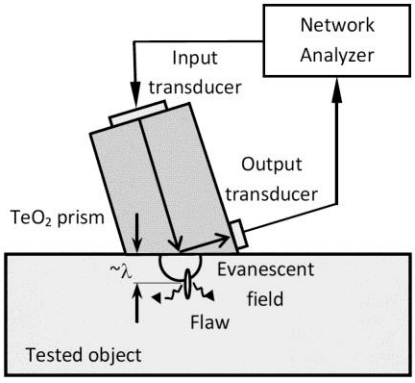

Acoustic Manipulation and Force

T1

Monday, July 22 2013, 04:30 pm - 06:00 pm

Congress Hallair: **Sandy Cochran**
University of Dundee

IUS5-C-1

Ultrasonic Manipulation Systems: From Simple Tweezing to Sonic Screwdrivers and Beyond

Christine Demore[1], Peter Glynne-Jones[2], Yongqiang Qiu[1], Zhengyi Yang[1], Han Wang[1], Bruce Drinkwater[3], Martyn Hill[2], Mike MacDonald[1], Gabriel Spalding[4], Sandy Cochran[1]; [1]*Institute for Medical Science and Technology, University of Dundee, Dundee, Scotland, United Kingdom,* [2]*School of Engineering Sciences, University of Southampton, Southampton, United Kingdom,* [3]*Department of Mechanical Engineering, University of Bristol, Bristol, United Kingdom,* [4]*Department of Physics, Illinois Wesleyan University, Bloomington, IL, USA*

Background, Motivation and Objective

Ultrasonic manipulation has arisen out of a requirement to move particles and cells within fluidic systems. Simple systems, using single element transducers attached to microfluidic channels, have found applications such as concentrating particle flows. However, a much greater level of sophistication in manipulation can be achieved and a much broader range of applications becomes feasible with dynamic reconfiguration of the ultrasound field. In parallel to the versatility that has been realised with optical tweezing systems using matrix array-like spatial light modulators to generate complex optical fields, electronically controlled array-based systems can provide a step-change in ultrasonic manipulation. These array based systems require advances in both the design and fabrication of arrays suited to specific applications, and in the electronics and algorithms to control the tailored acoustic fields. This paper reports the development of array-based ultrasonic manipulation systems, and discusses what becomes possible with electronically controlled ultrasonic tweezers.

Statement of Contribution/Methods

Two general classes of ultrasound manipulation systems, based on their mode of operation and means of manipulating particles, are introduced. The first generates an ultrasound standing wave within a microfluidic chamber, trapping particles using forces arising from gradients in the potential and kinetic energy densities of the ultrasonic field. Progressing from single element to 1D array devices enables, for example, controlled positioning along the length of a capillary as well as trapping along the axis of the microfluidic channel. The second class of system extends the dexterity by making use of propagating beams to generate an acoustic radiation force on objects in the field. Using 2D array with even moderate element counts (~1000 elements) enables the formation of complex ultrasonic beams that can carry both linear and angular momentum, and be used to rotate objects in the field as well as move them along the beam axis.

Results/Discussion

Arrays and control systems for both manipulation within resonant microfluidic chambers and with propagating ultrasonic beams are presented in this paper. The controlled manipulation of cell agglomerates along a capillary with a bespoke 1D array is shown, and the design considerations of 2D arrays suitable for manipulation within a plane are discussed. For manipulation with propagating ultrasound waves, a clinically approved focused ultrasound surgery system with a 2D array (ExAblate 2100, InSightec, Israel) is used. This system is used to demonstrate a "Sonic Screwdriver", in which the helical wavefronts from a vortex beam both lift and spin a rubber disc that is large relative to the wavelength. Finally, the fundamental physics that can be understood, and the possible applications of the acoustic fields that can be generated with 2D array configurations are discussed.

IUS5-C-2

Ultrasonic tactile sensor array for tissue elasticity measuremen

Kyungrim Kim[1], Xiaoning Jiang[1]; [1]*Department of Mechanical & Aerospace Engineering, North Carolina State University, Raleigh, NC, USA*

Background, Motivation and Objective

Tactile sensing is important in minimally invasive surgery (MIS) since the surgeon is not able to directly perceive target's shapes, locations and applied force. For open surgery, tactile sensing is still required to detect invisible targets that are embedded or enclosed by other tissues. For these reasons, various tactile sensors have been developed to obtain the target tissue's tactile information including force and elastic properties. However, those methods usually measure the force and the elasticity separately and/or indirectly which can be complicated and time consuming, or they are not able to measure both parameters at once. In this paper, a novel ultrasonic tactile sensor array using piezoelectric resonators was investigated for force and tissue elasticity measurements.

Statement of Contribution/Methods

A 6×6 face-shear mode PMN-PT piezoelectric sensor array was designed, fabricated and characterized for force and tissue elasticity measurements. By detecting the target materials' acoustic impedance change, the shear moduli of targets (or composition) and the magnitude of applied force can be estimated in a simple and rapid manner. Gelatin and water mixtures with different weight ratios were used for fabrication of tissue mimicking phantoms with shear moduli of 120 kPa - 430 kPa. Electrical impedance shift of resonators was measured using an impedance analyzer. External forces ranging from 0.1 N to 1.0 N were applied to the resonators for the force sensing test and the electric impedance was measured.

Results/Discussion

The electrical impedance shift of the resonator at resonance was found to be 45 % which was nearly close to the modeling result. This shift was corresponding to the shear modulus difference of tissue phantoms. The array test result showed that the array was able to distinct and image tissue phantoms with different shear moduli or compositions. From the force sensing test, the relationship between the electric impedance and the force was verified. It was found that the amount of electrical impedance shift increased (~ 30 %) as the magnitudes of applied stress increased (4 kPa - 40 kPa). The results reveal that the proposed novel sensing technique is promising for a number of biomedical applications including tactile sensors for MIS, novel artificial skins for surgical robotics and biological sensors for the cell or tissue stiffness sensing.

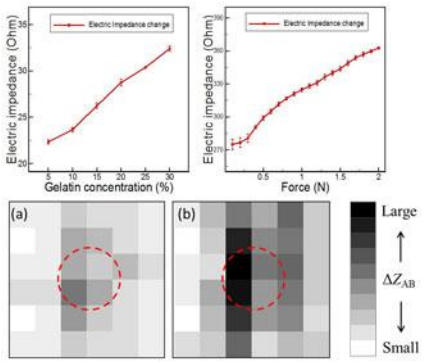

IUS5-C-3

Design basis of large scale acoustic separators

Hans Cappon[1,2], Karel Keesman[2,3]; *[1]HZ University of Applied Sciences, Netherlands, [2]Wetsus Centre of Excellence for Sustainable Water Technology, Netherlands, [3]Wageningen University, Netherlands*

Background, Motivation and Objective

Acoustic separation devices are able to separate water and particulate matter by means of ultrasound. These devices have been miniaturised in recent years for sensing and characterisation of particles (acoustophoresis), whereas up-scaling has received little attention. The last commercial acoustic separator, called BioSep, is already over a decade old. Previously published work showed that detailed numerical modelling of acoustic separators is possible and valid [1],[2], and that a prediction of particle retention efficiency can be made. This study is the next step in the design process, evaluating the basic choices to be made for a high efficiency separator.

Statement of Contribution/Methods

Before actually optimizing a separator a sound choice of a basic design should be established. This study presents the process of obtaining a basic design based on flow characteristics inside the separation chamber, on acoustic analysis within the chamber and calculated particle trajectories combining these two analyses into a third simulation. Using these, the effect of the flow direction with respect to the transducers on particle retention was studied. Moreover, changes to the flow by means of separator chamber partitioning is introduced as well as the effect on the particle displacement. Finally, adequate criteria for subsequent optimisation are evaluated.

Results/Discussion

The results show that it is possible to obtain a basic separator design with high particle retention by numerical analysis by positioning the piezoelectric transducer surfaces perpendicular to the flow direction and introducing chamber partitioning with multiple flow lanes to obtain laminar flow. The average particle displacement was found to be related to acoustic pressure, showing large retention at pressures above 1 MPa (for 10 µm, 1100 kg/m3 particles and a flow speed of 3.5 cm/s), thus providing a comprehensible criterion for subsequent optimisation.

References

[1] H. Cappon, K. Keesman, Numerical modelling of piezoelectric transducers using physical parameters, IEEE Transactions on Ultrasonics Ferroelectrics and Frequency Control 59 (5) (2012) 1023–1032.

[2] H. Cappon, K. Keesman, Numerical modeling, calibration and validation of an ultrasonic separator, IEEE Transactions on Ultrasonics, Ferroelectrics and Frequency Control (2013).

IUS5-C-4

Zebrafish egg manipulation using ultrasound microbeam transducer

Kwok Ho Lam[1], Fan Zheng[1], Ying Li[1], Qifa Zhou[1], Kirk K. Shung[1]; *[1]NIH Transducer Resource Center and Department of Biomedical Engineering, University of Southern California, Los Angeles, CA, USA*

Background, Motivation and Objective

As there is a growing demand for the reduction of adult animal testing, the use of Zebrafish eggs/larvae as model organisms in scientific research is growing in interest rapidly. Devices for such organism manipulation have attracted much attention in recent years. Nevertheless, existing techniques are either expensive or time consuming. Previously, tightly focused ultrasound microbeam has been reported to be capable of manipulating a single microparticle. The goal of this research is to develop an ultrasound microbeam device that can manipulate a single Zebrafish egg which can be as large as 1.5 mm diameter. This is for the first time that the utilization of acoustic microbeam for manipulating such large organism is reported.

Statement of Contribution/Methods

In order to allow the microbeam to form a steep intensity gradient for enhancing the trapping capability, the f-number (f# = focal length / aperture size) of the device was designed to be very small. A 60 MHz lithium niobate single crystal single-element ultrasonic transducer with an f# of 0.6 was developed. The f# of the transducer is the smallest ever reported on the study of ultrasound microbeam. The transducer design was modeled with PiezoCAD in which the single crystal was ~ 45 µm thick with an aperture size of 1.6 mm. In fabrication, the transducer was press-focused at a focal length of 1.0 mm to obtain the designated f#. Pulse-echo measurement was employed to evaluate the basic transducer performance. Fish egg manipulation experiment was performed in water provided by the supplier (Caroline Biological Supply Company). The motions of fish egg were recorded via a CCD camera combined with a microscope.

Results/Discussion

Although the f# fabricated approaches the physical limit, the device exhibits high sensitivity in pulse-echo results. Its measured centre frequency and -6 dB bandwidth were found to be ~ 60 MHz and ~ 50 %, respectively, which agree well with the simulation. Fish egg manipulation experiment demonstrated that the microbeam device can manipulate a single fish egg within the range of tens of millimeters as shown in Fig. 1. This preliminary result shows the ultrasound microbeam is versatile that can manipulate the particles or

organisms not only in micron scale, but also in millimeter scale. The study also suggests the potential of ultrasound microbeam for organism sorting and artificial insemination applications.

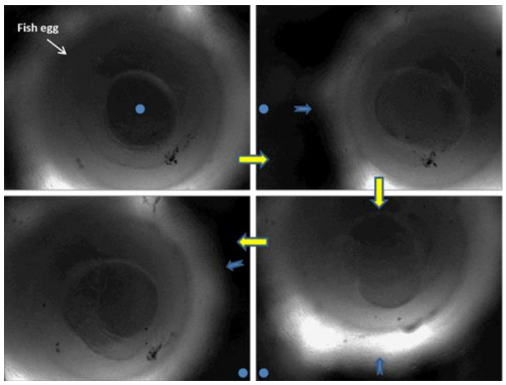

Fig. 1: Example of Zebrafish egg manipulation. A single fish egg was manipulated along the movement of the 60-MHz press-focused transducer. The bright circular shape is the projection of the transducer. A blue dot is given as a reference point to show the location change of the fish egg. (The capturing frame rate was 10 frames/second.) The magnification of the existing lens is too high. The low magnification lens will be ready soon so that the motions should be much better and clearer in the movie during the oral presentation.

IUS5-C-5

Design of Stepped Exponential Horns for Acoustic Energy Transfer Systems

Maurice Roes[1], Marcel Hendrix[1], Jorge Duarte[1]; [1]*Eindhoven University of Technology, Eindhoven, Netherlands*

Background, Motivation and Objective

The energy transfer efficiency and the power transfer capability are the most important measures of the performance of an acoustic energy transfer (AET) system, or for any contactless energy transfer system in general. Energy transfer in an air-based AET system is heavily influenced by the large mismatch in acoustic impedance that can exist between the transmitting transducer and the medium on one hand, and the receiving transducer and the air on the other hand. A well-designed horn acts as an acoustics impedance transformer that can be used to overcome these problems. In this research, stepped exponential horns (figure 1) are designed and optimised for an existing AET system. The shape of a stepped exponential horn consists of a stepwise change in the radius, followed by a section of which the radius flares out exponentially.

Statement of Contribution/Methods

The horns are modelled both analytically and using finite element (FE) modelling. For the sake of simplicity, the horn walls are modelled in the FE model as perfectly reflecting surfaces. The horns are assumed to be sufficiently rigid to be able to neglect their structural mechanical properties.

To obtain maximum power transfer, the dimensions of the horns are optimised using the FE model. The analytical models (which are based on the Webster horn equation) have too poor accuracy in some situations for this optimisation. This is due to deviation from the small flare-rate assumption that is made for the derivation of the analytical models. The optimisation yields separate designs for the transmitter and receiver horns. The resulting horns were CNC milled out of solid aluminium and fitted with PX051 piezoelectric transducers (produced by EMCT SA) for experiments.

Results/Discussion

The received power is P_r = 255mW, at an efficiency of η = 9.9% at a distance of R = 10cm in FE simulations, which is a major improvement over previous results. For comparison, FE simulations of the same transducers without horns give an output power of P_r = 406µW at η = 0.39%

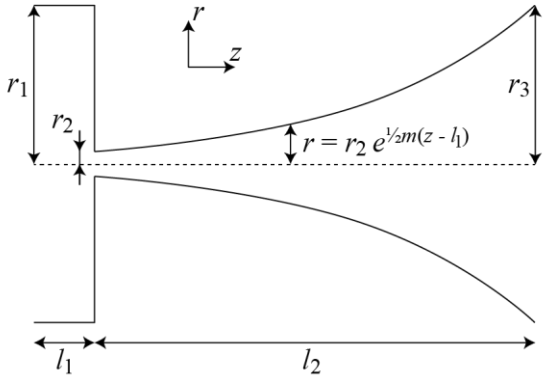

Optical and electromagnetic interactions 1

T2

Monday, July 22 2013, 04:30 pm - 06:00 pm

Congress Hallair: **John Larson**
Avago Technologies

IUS3-C-1

Surface acoustic waves control with external magnetic field in $TbCo_2$/FeCo films

Ivan Lisenkov[1,2], Alexey Klimov[1], Vladimir Onoprienko[1,2], Vladimir Preobrajenski[3,4], Philippe Pernod[4], Sergey Nikitov[1,2]; *[1]Kotelnikov Institute of Radio-engineering and Electronics, Russian Academy of Sciences, Moscow, Russian Federation, [2]Moscow Institute of Physics and Technology (State University), Dolgoprudny, Moscow, Russian Federation, [3]Wave Research Center, A. M. Prokhorov General Physics Institute, Russian Academy of Sciences, Russian Federation, [4]Institut d'Electronique, de Microelectronique et de Nanotechnologie, Ecole Centrale de Lille, Lille, France*

Background, Motivation and Objective

The effect of giant magnetostriction makes possible controlling stiffness of materials using external magnetic fields. Despite of called 'giant', the changes of stiffness in absolute values, which can be obtained with reasonable values of magnetic fields, are generally very small. In our work we show both theoretically and experimentally, that spin reorientation transition (SRT) effect in uniaxial magnetostrictive materials can significantly increase the value of elasto/magnetic interaction. We show possibility to control Rayleigh surface acoustic wave (SAW) velocity by applying external magnetic field in materials with SRT.

Statement of Contribution/Methods

We consider propagation of Rayleigh SAW in a sandwiched structure consisting of -YZ-cut of $LiNbO_3$ as a substrate with $TbCo_2$/FeCo layers placed on its top. The layers were fabricated in a bias magnetic field, thus uniaxial magnetic anisotropy was formed. The layer thickness is 200 nm, formed by 40 interchanging layers of $TbCo_2$ and FeCo, 5 nm each, saturation magnetization is about 120 Oe. The easy axis of the film lies in plane of the film and the magnetic field is applied along the hard axis. A sample was placed between two interdigital transducers fabricated on a substrate. Rayleigh SAW velocity deviation dependence is measured by phase locking technique. Effective stiffness of $TbCo_2$/FeCo is calculated by minimizing total energy of both magnetic and elastic subsystems in an equilibrium state and applying perturbation theory. Rayleigh SAW propagation characteristics are calculated by solving equation of motion and applying boundary condition on the free surface of the layer and on layer/substrate interface.

Results/Discussion

In Figure we present measured and calculated Rayleigh SAW velocity deviation dependence versus applied external magnetic field. The magnetic field changes from saturation to zero. It is seen, that propagation characteristics control is possible by using the external magnetic field. The maximum of Rayleigh SAW velocity deviation in applied magnetic field from its value at the zero magnetic field appears near saturation the value of magnetic field, where SRT occurs. In our work we have estimated parameters of magnetostrictive layers needed for effective magnetic field detection by measurement acoustic wave dispersion.

The work is supported by RFBR grants #12-07-00203 and #12-07-91703

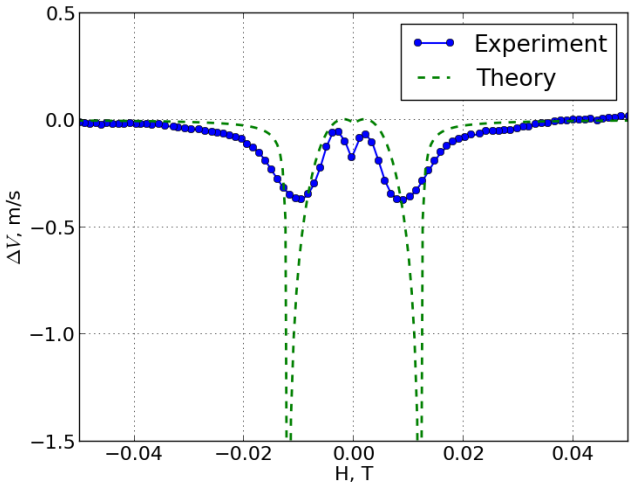

IUS3-C-2

Theoretical and Experimental Study of Multilayer Piezo-magnetic Structure Based Surface Acoustic Wave Devices for High Sensitivity Magnetic Sensor

Huan Zhou[1], Abdelkrim Talbi[1], Noura Gasmi[1], Nicolas Tiercelin[1], Olivier Bou Matar[1]; *[1]International Associated Laboratory LICS/LEMAC, IEMN UMR CNRS 8520, PRES Lille Nord de France, ECLille, Villeneuve d'Ascq, France*

Background, Motivation and Objective

Recent developments in physics and technology made possible to elaborate new magneto-electro-elastic materials such as multilayered piezoelectric piezomagnetic composites. The large magnetoelectric coefficient of these composites, compared to the one of single phase materials, has attracted recently a large amount of studies. These structures are now widely used in the development of sensors, actuators, magnetic-electric energy converting devices, and solid state memories.

Statement of Contribution/Methods

This study addresses the experimental and theoretical investigations of piezomagnetic acoustic waves propagating along the surface of piezoelectric substrate combined with a magnetostrictive thin film. The main objective of this work is to design high sensitivity surface acoustic wave resonator for the development of a magnetic sensor.

Results/Discussion

The investigated device consists of a 200 nm magnetostrictive film, composed of 20 bilayers of TbCo2/FeCo, deposited on a Y-cut LiNbO3 substrate (Fig. 1). A delay line was fabricated using two interdigitals transducers to generate and detect the SAW propagating in the X direction. Both generalized Rayleigh and shear horizontal modes are generated in the substrate. The easy axis of the magnetostrictive film was chosen parallel to the propagation direction of the SAW. Fig. 2 shows an example of the measured velocity change as a function of a magnetic field. The maximum sensitivity is achieved at low magnetic field amplitude. To optimize the design of the sensor we developed an original numerical method to compute propagation constants and mode shapes of elastic waves in piezoelectric-piezomagnetic composites. The comparison of the numerical results with the experimental ones, obtained on the designed system, is very good.

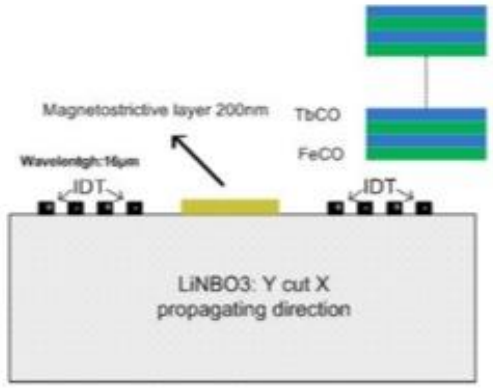

Fig. 1: Schematic view of the device.

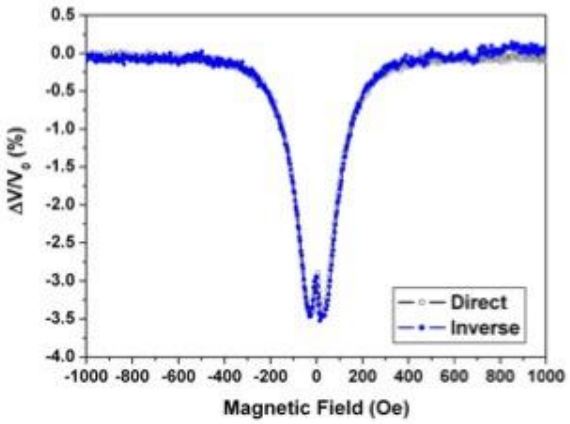

Fig. 2: Velocity change versus applied magnetic field for the first shear mode.

IUS3-C-3

Acoustically Driven Magnetic Excitations in BAW Resonators with Magnetic Layers

Natalia Polzikova[1], Sergey Alekseev[1], Iosif Kotelyanskii[1], Alexander Raevskiy[1]; [1]*Kotelnikov Institute of Radioengineering and Electronics RAS, Moscow, Moscow, Russian Federation*

Background, Motivation and Objective

An acoustic wave drives magnetization dynamics in a ferromagnet via the magnetoelastic interaction if the acoustic wave frequency is in resonance with the spin system at a given effective magnetic field (magneto acoustic resonance – MAR). The interest to the microwave BAW resonator with ferrite layers arises from the possibilities of frequency tuning by an external magnetic field. Furthermore, last time the nonmagnetic excitation of magnetic oscillations and acoustically generate spin current for spintronic applications have drawn a lot of attention [K. Uchida et al, Nature Mater.10, p.737 (2011)].

Statement of Contribution/Methods

In the composite resonator considered magnetic oscillations, including spin wave resonance in thin films, could be excited and detected by electroacoustic transducer. In previous works [N.Polzikova et al, JAP, v.113, p. 17C704 (2013); S.G Alekseev et al., IEEE IUS, (2012)] we have reported the tuning of resonator frequencies in the rather small range of ± 0.25 MHz in comparison with intermodal separations $\Delta = f_{n\pm1}-f_n = \pm 3$MHz. In present paper we report the development of the theory and experiment of the HBAR based on Al-ZnO-Al (piezoelectric transducer) / yttrium iron garnet (YIG) epitaxial film (magnetostrictive media) on gadolinium gallium garnet substrate (Fig.1a). The change of BAW resonance position is caused by the rearrangement of acoustic and spin wave dispersion in the ferrite film. For the excitation of the transversal BAW thin ZnO films with the c-axis 40°-45° tilted with respect to the YIG- substrate normal were sputtered.

Results/Discussion

Near the MAR frequencies the tuning of resonator frequency f_n=2.530 GHz in the range of ±2 MHz due to the external magnetic field is experimentally obtained (Fig.1b). This range is compared with intermodal distance Δ. For comparison, the calculated curves are also depicted by blue lines. Also we report the further development of the theory of a composite acoustic resonator, which includes multiple layers of magnets, alternating with nonmagnetic dielectrics/ ferro(piezo)electrics. The different resonant structures with magnetic layers, as HBAR, SMR and FBAR, are considered.

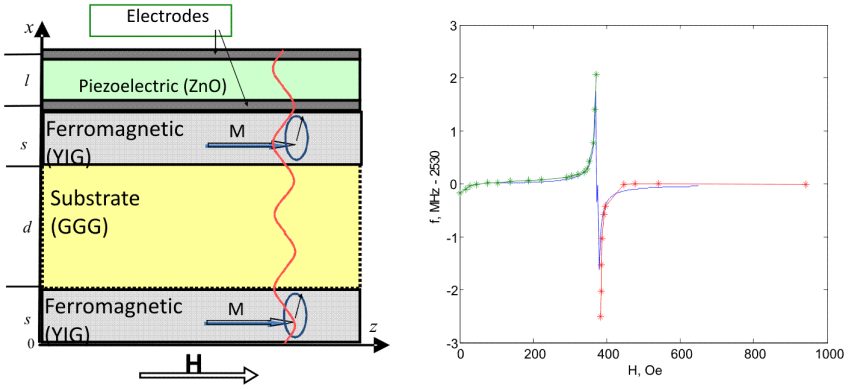

(a) (b)

Fig.1. The layout of composite resonator (a) and frequency shift $f(H)= f_n(H)-2530$ (MHz) versus applied magnetic field (b). Green and red – measured, blue-calculated.

IUS3-C-4

Shear and longitudinal GHz elastic properties in GaN single crystals determined by Brillouin scattering method

Hayato Ichihashi[1], Takeshi Sugimoto[1], Takahiko Yanagitani[2], Shinji Takayanagi[1], Mami Matsukawa[1]; *[1]Doshisha University, Japan, [2]Nagoya Institute of Technology, Japan*

Background, Motivation and Objective

In recent years, GaN resonators and SAW devices have attracted attention because they are compatible with GaN IC technology. However, the experimental temperature characteristic of acoustic velocities which determines the temperature stability of the resonators has not been reported for GaN. In case of conductive piezoelectric material such as GaN, the relaxation process due to piezoelectric stiffening effect may be observed by GHz acoustic velocity measurements. In this study, we measured acoustic wave velocities of GaN single crystals in the GHz at the wide temperature range by a Billouin scattering technique.

Statement of Contribution/Methods

Acoustic velocities of longitudinal (around 20 GHz) and shear (around 10 GHz) wave propagating along c-axis in two types of GaN single crystal samples with different resistances (conductive sample: 2×10^{-4} Ω·m, and semi-conductive sample: $1\text{-}5\times10^{-2}$ Ω·m) were measured. A Tandem Fabry-Perot interferometer (JRS), Ar ion laser (wave length: 514.5 nm, spot diameter: 50 μm, 43 mW near the sample) and the reflection induced ΘA geometry [1] were used in a Brillouin scattering measurement system. The temperature of samples was controlled using a stage (LK-600PM, Linkam) during the experiments. The measurement errors of the longitudinal and shear wave velocities were ±8 m/s and ±4 m/s, respectively.

Results/Discussion

Figure 1 shows velocities as a function of temperature. Longitudinal and shear wave velocities of the conductive sample showed similar tendency and constantly decreased with the temperature coefficients of -13 ppm/ºC and -6 ppm/ºC normalized at room temperature, respectively. In case of the semi-conductive sample, the temperature coefficients of longitudinal and shear wave were -15 ppm/ºC and -20 ppm/ºC in the region from 80ºC to 340ºC. The ratios between shear and longitudinal waves were observed to be constant. In these samples, relaxation processes due to piezoelectric stiffening effect was difficult to observe. However, we found a slight nonlinear behavior in both longitudinal and shear wave data in the low temperature region.

[1] J.K. Kruger, et, al: J. Phys. D: Appl. Phys. 31 1913 (1998)

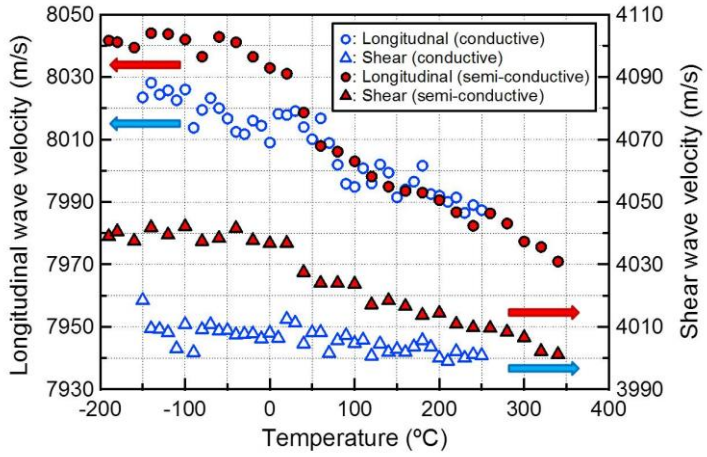

Fig. 1 Temperature dependences of longitudinal and shear wave velocities in two GaN single crystals with different resistances.

IUS3-C-5

Temperature dependence of X-ray diffraction on the LGS crystal modulated by SAW

Dmitrii Irzhak[1], Luc Ortega[2], Dmitry Roshchupkin[1]; [1]*Institute of microelectronics technology and High purity materials RAS, Russian Federation,* [2]*Laboratoire de Physique des Solides, Univ. Paris-Sud, CNRS, Orsay, France*

Background, Motivation and Objective

Investigations of the temperature dependences of crystals acoustic properties are generally based on a study of the frequency response function. The use of x-ray diffraction on a crystal modulated by acoustic wave allows to reveal the relationship of the frequency response function and the deformation of the crystal lattice. This work presents the results of the study of x-ray diffraction on a crystal $La_3Ga_5SiO_{14}$ (LGS) modulated by surface acoustic wave (SAW) heated up to 400 C°.

Statement of Contribution/Methods

In the case of X-ray diffraction on a crystal modulated by SAW, additional diffraction satellites appear on the rocking curve [1]. The angular distance between two adjacent diffraction satellites (δθ) depends on the interplanar spacing of the crystal (d) and the wavelength of SAW (Λ):

$$\delta\theta = d/\Lambda.$$

Example of the x-ray rocking curve obtained for the LGS crystal modulated by 4 mkm SAW ((100) reflection, x-ray energy E=11 keV) is shown on Fig. 1. As the SAW amplitude increases additional diffraction satellites intensity and they amount also increas, while the main Bragg peak falls.

It was shown [2] that in the case of strong X-ray absorption dependence of diffraction satellites intensity vs the SAW amplitude can be calculated with using of simple equation taking in to account crystal lattice deformation caused by acoustic wave propagation and the SAW amplitude. It is allowed to calculate the crystal lattice deformation field change for the investigated temperature range.

Results/Discussion

As a result of this studies it was found that the resonant frequency of SAW excitation varies from 580 MHz to 583 MHz for the temperature range from 20 C° to 400C°. This corresponds to a SAW velocity changing from 2320 m/s to 2332 m/s. According to this it is possible to calculate the temperature coefficient of the SAW velocity for Y-cut of LGS crystal, X-direction of SAW propagation : $1.36 \cdot 10^{-5}$ 1/C°. Also it was found that features of the crystal lattice deformation field changes with the temperature growth.

[1] IA Schelokov, DV Roshchupkin, DV Irzhak, R Tucoulou, Journal of applied crystallography 37 (1), 52-61 (2004)

[2] A.I. Erko, D.V. Irzhak, L. Ortega, D.V. Roshchupkin, Int. Synchrotron Radiation Conference, Novosibirsk, pp.2-7 (2008)

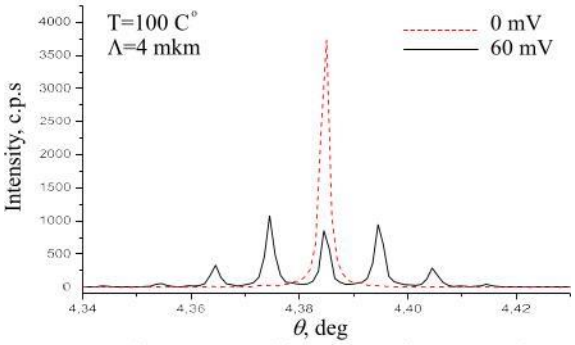

Fig. 1. X-ray rocking curves of LGS crystal modulated by SAW

IUS3-C-6

Noise Tolerance in Wavelength-Selective Switching of Optical DQPSK Pulse Train by Collinear Acoustooptic Devices

Nobuo Goto[1], Yasumitsu Miyazaki[2]; [1]*The University of Tokushima, Japan,* [2]*Aichi University of Technology, Japan*

Background, Motivation and Objective

Wavelength-selective switching and signal processing of WDM optical packets are required in photonic networks. The authors have studied on weighted acoustooptic (AO) switches and on their application to optical packet routing and optical label recognition of high bit-rate packets.[1] In this paper, we clarify noise tolerance in switching of optical differential quadrature phase-shift-keying (DQPSK) pulse trains.

Statement of Contribution/Methods

We consider 40 and 100G symbol/s DQPSK pulse trains having 75 and 150GHz bandwidth, respectively. As the symbol rate increases, AO switching induces distortion of pulse shape and the phase, which results in decrease of bit error rate (BER). Since BER can be regarded as most important measure in optical packet transmission and processing, the obtained results will be useful in designing wavelength-selective processing systems for photonic networks. Fig.1(a) shows an example of weighted AO switch consisting of an asymmetric optical directional coupler and a SAW tapered waveguide proposed by our group. In addition to this switch, we also consider a Butterworth-type weighted AO switch consisting of a lossy SAW directional coupler proposed by Song.[2] The BER of the switched DQPSK pulse trains with these two kinds of AO switches is numerically analyzed by the Monte-Carlo method.

Results/Discussion

The AO interaction length of the tapered SAW device and Butterworth-type device is 20.0 and 42.72mm, respectively. The full-width at half maximum (FWHM) of the AO devices is about 185GHz. Simulated BER is shown in Fig.1(b). The decrease of BER at 100G symbol/s is due to wavelength selectivity in AO switching. Although the Butterworth-type device provides a flat-top pass band characteristics, the switched pulse train was distorted more than that with the tapered SAW waveguide device due to the nonlinearity of the phase in the filtering response, which results in the increase of the BER.

This work was supported in part by JSPS KAKENHI (24360150).

[1]N. Goto and Y. Miyazaki,"Theoretical study of the switching characteristics of 40 and 100G bps pulse trains by weighted collinear acoustooptic switches", Jpn. J. Appl. Phys. vol.51, 07GA06-1--6, 2012.

[2]G.-H. Song and S.-Y. Shin,"Design of corrugated waveguide filters by the Gel'fand-Levitan-Marchenko inverse-scattering method", J. Opt. Soc. Am. A vol.2, no.11, pp.1905-1915, 1985.

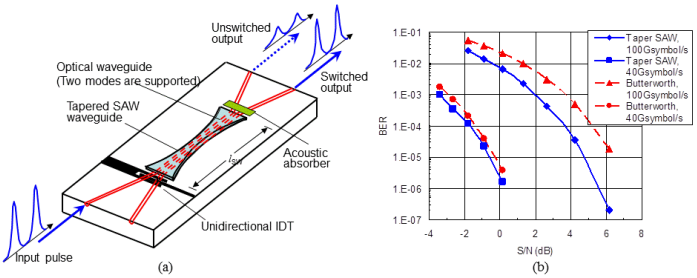

Fig.1 (a) Routing of optical pulse train by weighted collinear AO device with a tapered SAW waveguide, and (b) simulated result of BER for two kinds of AO switches.

Contrast agents and imaging

Forum Hall

Monday, July 22 2013, 01:00 pm - 04:30 pm

Congress Hallair: **Steven Freear**
University of Leeds

IUS1-PA1-1

Correction of nonlinear imaging artefacts in contrast enhanced ultrasound

Yesna Yildiz[1], Robert J. Eckersley[2], Meng-Xing Tang[1]; [1]*Imperial College London, United Kingdom,* [2]*Kings College London, United Kingdom*

Background, Motivation and Objective

Contrast enhanced ultrasound (CEUS) imaging with microbubbles has shown to be a promising tool in a wide range of clinical applications including cardiovascular diseases and cancer. The detection of these agents over background tissue relies on the nonlinear echo signals assumed to specifically originate from microbubbles. However, this assumption is violated when nonlinear propagation of ultrasound in tissue containing bubbles distorts the ultrasound pulse causing the tissue echoes to become nonlinear, resulting in misclassification of tissue as bubble echoes. This type of artifact is common and significantly affects imaging both qualitatively and quantitatively. This paper proposes a method to correct for this artifact.

Statement of Contribution/Methods

The method makes use of the simultaneous availability of ultrasound B-mode data and contrast specific image data. It is assumed that B-mode image contains mostly tissue signal and the CEUS image mostly microbubble signal. Ultrasound image formation is described as a convolution between a tissue scattering distribution (TSD) and the point spread function (PSF) with added measurement noise.

The proposed method estimates the underlying TSD by deconvolving the known PSF from RF data. This tissue signal is in turn convolved with a nonlinear PSF to generate nonlinear tissue echoes (artifact) which are then removed from the CEUS image to generate a corrected microbubble specific image.

The proposed method was tested both in simulation and on laboratory phantoms. Using a clinical scanner, RF data of a tissue mimicking material (TMM) with nonlinear propagation through water was acquired. The PSF of the scanner was measured using a metal wire.

Results/Discussion

Figure 1a shows a simulated RF line of pulse inversion signal from tissue before and after correction. Very good cancellation of nonlinear tissue echoes is achieved in the presence of noise (SNR=36dB) in simulation as shown.

Figure 1b displays a pulse inversion RF line of measured nonlinear TMM signal, estimated nonlinear signal and corrected signal. The reduction in nonlinear TMM signal is about 50% or higher. Perfect cancellation is not expected due to system noise and preliminary experimental results suggest that further reduction is feasible with improved estimations of the TSD and a spatially varying PSF.

Figure 1 a (left) and b (right)

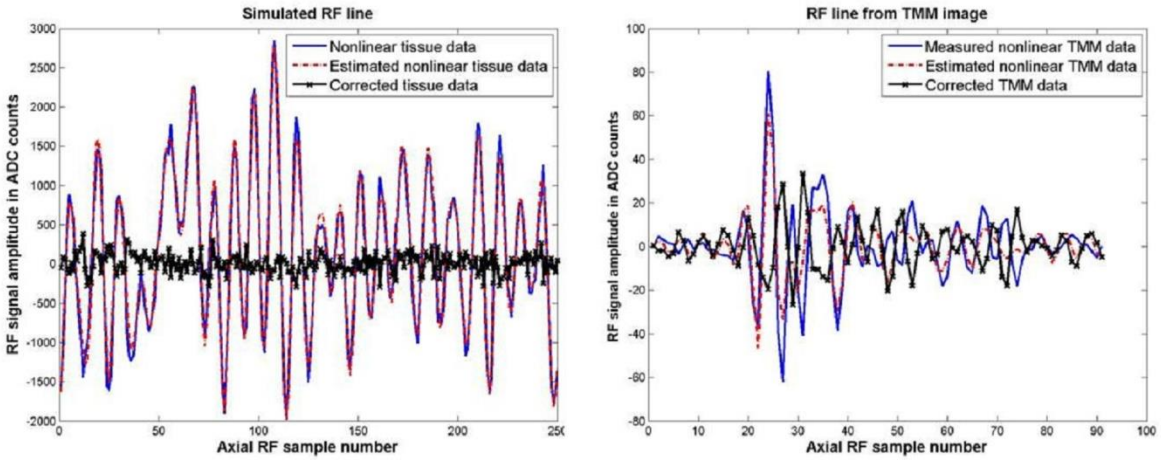

IUS1-PA1-2

Characterising Microbubble Surface Charge using a Microfluidics Approach

Fairuzeta Ja'afar[1], Mengxing Tang[2], Valeria Garbin[3], John Seddon[1]; [1]*Chemistry, Imperial College London, London, United Kingdom,* [2]*Bioengineering, Imperial College London, London, United Kingdom,* [3]*Chemical Engineering, Imperial College London, London, United Kingdom*

Background, Motivation and Objective

Medical ultrasound is a widely established, powerful tool for diagnostic imaging applications. Combined with the use of microbubble contrast agents, it has been shown to be a promising tool for drug delivery and therapeutic applications. Microbubbles (MBs) are small (typically less than 8μm in diameter) gas cores stabilised by a biocompatible shell and suspended in an aqueous dispersion. For lipid-based MB shells, changing the lipid type to be cationic, anionic or neutral can affect the bulk MB-cell interactions. This in turn can have an overall effect on the MBs' suitability as a therapeutic agent. It is therefore important to be able to characterise the surface charge of the MB shell accurately. Current electrophoretic light scattering (ELS) methods for determining MB surface charge rely on measuring MB electrophoretic mobility in an electric field and calculating its zeta

potential. However, there are limitations to this method as it does not account for MB buoyancy. In this study, we sought to determine the surface charge of some commercial MBs (SonoVue™, Optison™ and Definity™) by employing a relatively cheaper microfluidics approach.

Statement of Contribution/Methods

Using ibidi™ microchannels, we applied variable electric potential across our MB suspension and tracked MB movement under bright-field microscopy. By tracking MB mobility over time, MB surface charge can then be determined by the direction of MB movement and quantified by calculating the MB zeta-potential. We then compared our findings with the widely-used ELS method.

Results/Discussion

We found that for the more buoyant MBs, ELS measurements would not give an accurate value for MB surface charge. Our approach presents a cheaper alternative for determining MB surface charge, while accounting for MB buoyancy and ensured MB integrity in an electric field.

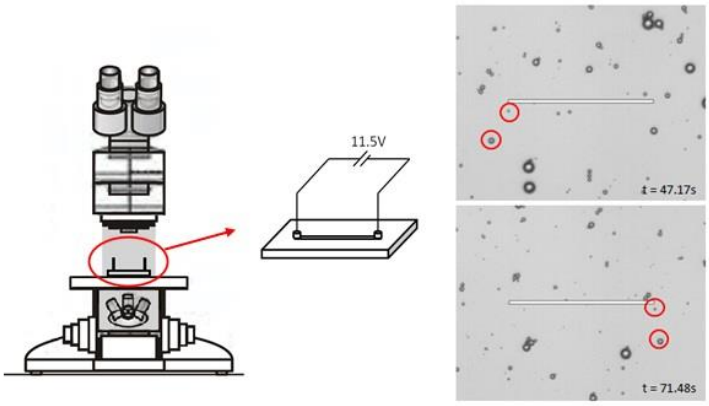

Figure 1 - Schematic representation of experimental setup. MB suspension was flowed into an ibidi™ microchannel (channel dimensions: L=5cm, w=0.5cm, h=200µm) and a potential of 11.5V was applied. MB movement over time was then recorded to determine MB surface charge. Right: Images of SonoVue™ MBs movement in an applied over time (Scale bar represents 100µm).

IUS1-PA1-3

Acoustical response of DSPC versus DPPC lipid-coated microbubbles

Tom van Rooij[1], Ying Luan[1], Antonius F.W. van der Steen[1,2], Nico de Jong[1,2], Klazina Kooiman[1]; *[1]Biomedical Engineering, Erasmus MC, Rotterdam, Netherlands, [2]Interuniversity Cardiology Institute of the Netherlands, Utrecht, Netherlands*

Background, Motivation and Objective

Microbubbles (MB) are promising ultrasound contrast agents for molecular imaging and therapy. The influence of the lipid coating on MB shell properties is ongoing [1]. This study compares the acoustical response of two types of lipid-coated MB with different shell composition. The main component was DSPC or DPPC (2 C-atoms less than DSPC), leading to respectively a heterogeneous or homogeneous lipid distribution, i.e. different surface microstructures [2].

Statement of Contribution/Methods

Two types (DSPC and DPPC) of MB (mol %: DSPC or DPPC 59.4; PEG-40 stearate 35.7; DSPE-PEG(2000) 4.1, DSPE-PEG(2000)-biotin 0.8) with a C_4F_{10} gas core were made by sonication [3]. Dynamics were captured using the Brandaris 128 high-speed camera at 10 Mfps. Ultrasound signals were single bursts of 8 cycles at 50 kPa. The frequency was swept from 1-4 MHz. Shell properties were calculated using the method of Van der Meer [4].

Results/Discussion

We investigated 15 DSPC and 14 DPPC MB (2-10 µm in diameter). Both MB types did not significantly shrink under insonification, indicating good stability. We found similar resonance frequencies for both MB, with values in line with Luan [5]. The subharmonic resonance frequency decreased with diameter and subharmonics were observed in 13% of DSPC and 71% of DPPC MB (Fig a,b), which may suggest a different surface tension. Second harmonics were present in ~60% for both MB.

The elasticity (~10 N/m) and shell damping coefficient (~0.2) were not significantly different between both MB. Shell viscosities were ~10^{-8} kg/s, but showed different trends (Fig c). For DSPC, viscosity increased with dilatation rate while this decreased for DPPC. Interestingly, the smallest DSPC and largest DPPC MB suggest the directional trends. Previous work on BR14 (DSPC) [4] showed a trend opposite to our DSPC MB and for DPPC MB with slightly different composition, no clear trend was observed [5]. This could be due to other lipids in those MB.

In conclusion, we showed that different lipid coatings can result in different acoustic responses. The higher subharmonic response suggests that DPPC MB may be better for non-linear imaging.

[1] Kwan et al, Adv Colloid Interface Sci 183:82 2012; [2] Kooiman et al, IEEE Proceedings 2012; [3] Klibanov et al, Invest Radiol 39:187 2004; [4] van der Meer et al, JASA, 121:648 2007; [5] Luan et al, Ultrasound Med Biol 38:2174 2012

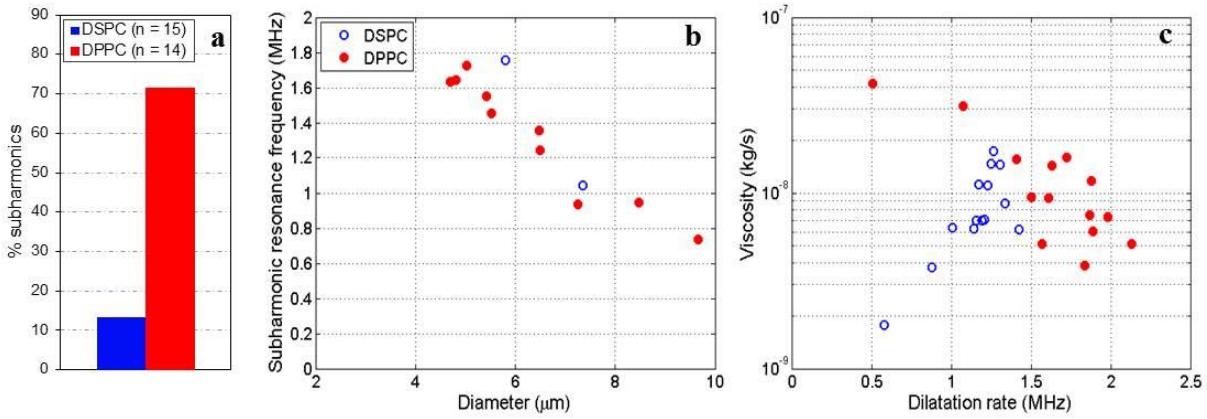

This work is supported by NanoNextNL of the Dutch Government and 130 partners.

IUS1-PA1-4

Nonlinear dynamics of polymer shell ultrasound contrast agents at 8-32 MHz ultrasonic excitations

Amin Jafari Sojahrood[1], Raffi Karshafian[2], Eleanor Stride[3], Michael C. Kolios[2]; *[1]Physics, Ryerson University, Canada, [2]Ryerson University, Canada, [3]Oxford University, Biomedical Engineering, United Kingdom*

Background, Motivation and Objective

The response of polymer shell ultrasound contrast agents (PSUCAs) at frequencies < 5 MHz has been shown to be associated with shell rupture and formation of free gas bubbles. Recently, it was shown that PSUCAs produce significant subharmonic (SH) response at higher frequencies (20-40 MHz) which is not consistent with the formation of free bubbles. Despite the high control over the manufacture of PSUCAs, there is limited knowledge on the response of PSUCAs to ultrasonic excitation, especially at higher excitation frequencies.

Statement of Contribution/Methods

The dynamics of individual PSUCAs in response to 30 cycle 8-32 MHz excitations with pressure amplitudes ranging ~70 kPa - 2.5 MPa was studied by experimental observations using a Vevo 770 ultrasonics imaging instrument. In each case a very dilute solution of PSUCAs were used to minimize the interaction between the PSUCAs. The RF signal of the individual UCA oscillations were extracted and analyzed. Numerical simulations of the Hoff and Marmottant model were used to explain the experimental observations.

Results/Discussion

The results of this study show that PSUCAs can undergo stable linear and nonlinear oscillations with substantial amplitude. 2nd and 3rd order super harmonic (SUH) oscillations were observed with 8-16 MHz excitations. Figs 1a-b show the 2nd order SUH backscatter and its frequency response. SH oscillations were observed for all of the investigated frequencies. Figs 1c-d show the ½ order SH backscatter and its frequency response. Higher order SHs were detected for frequencies above 20 MHz. Figs. 1e-f show the 1/5 order SH backscatter and its frequency response. Finally, compression only behaviors were detected mainly resulting in linear oscillations. Figs g-h show a compression only backscatter with its frequency response. The results of the numerical simulations with Hoff and Marmottant model correctly predicted the generation of the SUHs and ½ SHs. However, the generation of the higher order SHs and compression only behavior were only explainable by the Marmottant model.

Results of this study show the feasibility of the substantial nonlinear oscillations in the oscillations of the PSUCAs. Further investigations are needed to be carried out to fully realize the potential of the application of PSUCAs within the field of medical ultrasound.

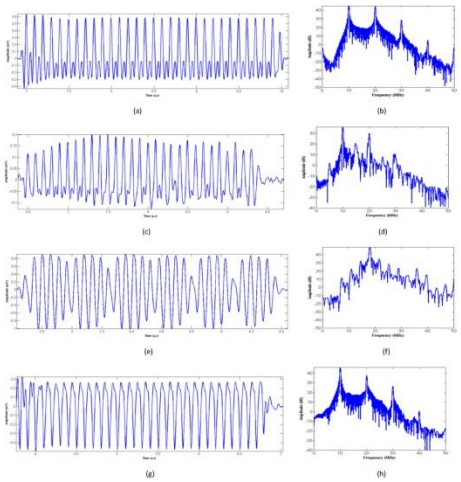

Figure 1: Left column: Backscatter from individual polymer shell UCAs: a) 2nd order super harmonic oscillations at 10 MHz, c) ½ order SH oscillations at 10 MHz, e) 1/5 order SH oscillations at 20 MHz g) compression only oscillations at 10 MHz, Right column: b-h The frequency spectrum of the signal show in the left column.

IUS1-PA1-5

Rician inverse Gaussian model of scattering in ultrasound contrast media

Vladimir Slavik[1], Radim Kolar[1,2], Radovan Jirik[1,3], Vratislav Harabis[1,2]; [1]*Department of Biomedical Engineering, Faculty of Electrical Engineering and Communication, Brno University of Technology, Brno, Czech Republic,* [2]*International Clinical Research Center, Center of Biomedical Engineering, St. Anne's University Hospital, Brno, Czech Republic,* [3]*Institute of Scientific Instruments of the ASCR, v.v.i., Brno, Czech Republic*

Background, Motivation and Objective

This contribution continues our previous experiment with Nakagami distribution. Here, we describe statistical analysis of 1st and 2nd harmonic signals backscattered from contrast media using Rician inverse Gaussian (RiIG) envelope model. This model was proposed in recent works as a possible alternative to other distributions. Knowledge of statistics of the scattered signal may contribute to perfusion analysis.

Statement of Contribution/Methods

To evaluate a range of ultrasound contrast agent (UCA) concentrations, a measurement setup was designed - a water tank with the SonoVue UCA solution contained in a plastic bottle. Radiofrequency (RF) data were collected using a conventional ultrasound scanner (GE Vingmed System Five), bandpass-filtered for 1st and 2nd harmonic components, respective images reconstructed from these datasets, and a number of regions of interest selected for processing. Finally, the RiIG distribution was fitted to histograms from these regions, using Matlab Global optimization toolbox.

We also tested the influence of simulated attenuation by multiplication of image values with $a(x) = exp(-bx)$ such that the attenuation factor bx reached maximal values of 1,2,3,5 and 10 at the distant edge of image.

Results/Discussion

Analysis of resulting RiIG distribution parameters shows that the differences between parameters estimated from 1st and 2nd harmonic images are statistically insignificant. The RiIG distribution has three parameters: while α and β do not follow any properties of the changing concentration, parameter δ shows logarithmic dependence on concentration in range of 3.125 - 50 mg/l (see figure below; note the log scale of x axis). This parameter influences dispersion and mean value of the distribution. Increasing UCA concentration results in a stronger backscattering signal, shifting the probability density function of acquired image to higher values and increasing its spread, because of greater variability of the scatterers. Taking into account simulated attenuation, we observed that the range and shape of the dependency remain stable, although the actual range of parameter δ decreases with increasing attenuation.

This analysis contributes to our previous results, where the Nakagami distribution showed similar dependence of the shape parameter on UCA concentration in a smaller, partially overlapping, concentration range.

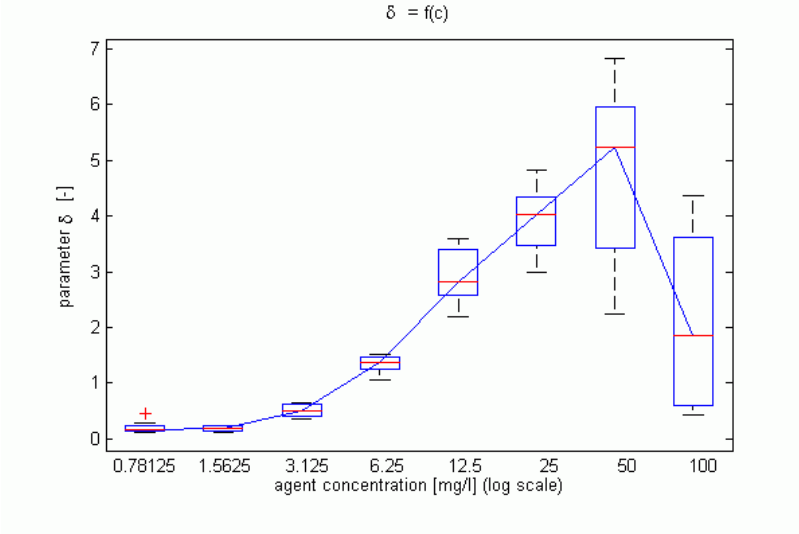

IUS1-PA1-6

Effects of microbubble interaction on occurrence of subharmonics

Shoma Kanazawa[1], Akira Tsuruoka[2], Toshihiko Sugiura[2]; [1]*Mechanical Engineering, Keio University, Japan,* [2]*Keio University, Japan*

Background, Motivation and Objective

Microbubbles irradiated by ultrasound show nonlinear oscillation and reflect harmonic and sub-harmonic signals. Microbubbles are used as ultrasound contrast agents by using harmonic signals, but harmonic signals are also reflected from biological tissues. On the other hand, subharmonic signals are not almost reflected from biological tissues. So it is important to use subharmonic signals, though it is not clarified enough how to generate subharmonic signals. In this study, we investigated effects of microbubble interaction on occurrence of subharmonics.

Statement of Contribution/Methods

Our analytical model is shown in Fig.1. Effects of interaction between two bubbles have nonlin-earities and depend on the distance of two bubbles and their radius ratios. For different values of these parameters, we numerically calculated the Rayleigh-Plesset equations with these interaction terms added and investigated occurrence conditions of subharmonics.

Results/Discussion

Fig.2 shows unstable regions which indicates occurrence conditions of subharmonics with respect to the transmit frequency and the pressure amplitude. Results obtained by changing the distance of two bubbles are shown in Fig.2(a) and results obtained by changing the radius ratio of two bubbles are shown in Fig.2(b). If the distance of two bubbles is smaller, the transmit frequency generating subharmonics is lower (see Fig.2(a)). Moreover, if the radius of the neighboring bubble is larger, the transmit frequency generating subharmonics is lower (see Fig.2(b)). As above, occurrence conditions of subharmonics depend on the distance of two bubbles and their radius ratios.

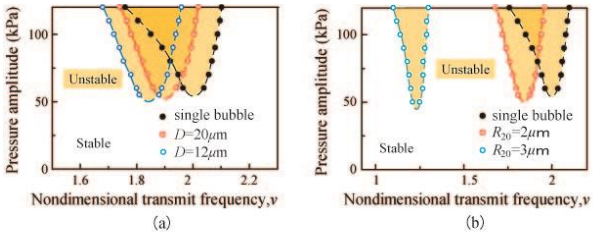

Fig.2: Occurrence regions of subharmonics: (a) changing with the distance of two bubbles, and (b) changing with the radius ratio of two bubbles (R_{20}:initial radius of bubble2)

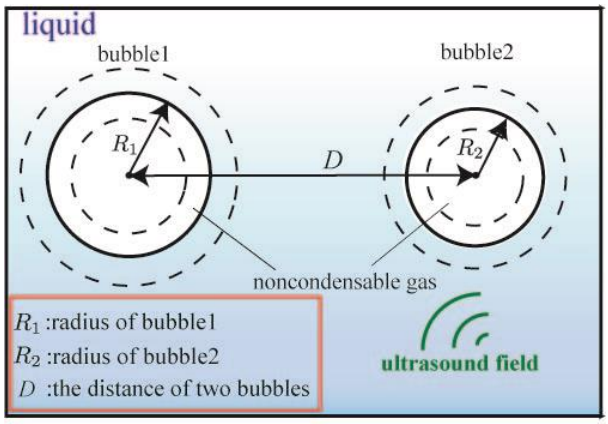

Fig.1: Analytical model

IUS1-PA1-7

Enhanced ambient pressure sensitivity of the subharmonic signal from ultrasound contrast microbubbles

fei li[1,2], feiyan cai[1], long meng[1], Qiaofeng Jin[1], Hairong Zheng[1], Deyu Li[2,3]; *[1]Paul C. Lauterbur Research Center for biomedical imaging, Shenzhen Institutes of Advanced Technology, Chinese Academy of Sciences, China, People's Republic of, [2]School of Biological Science and Medical Engineering, Beihang University, China, People's Republic of, [3]State Key Laboratory of Virtual Reality Technology and Systems, China, People's Republic of*

Background, Motivation and Objective

The microbubble ultrasound contrast agent (UCA) has been well recognized as a potential noninvasive tool for the blood pressure measurement. A decrease in subharmonic amplitude of 9 to 12 dB has been reported for Levovist, Optison, Definity, Sonazoid, and SonoVue for ambient overpressure values around 180 mmHg. However, a pressure resolution of 3mmHg is desirable in medical diagnostics, it is still necessary to enhance the ambient pressure sensitivity for the method based on the subharmonic amplitude as a function of local pressure. The purpose of this study was to improve the ambient pressure sensitivity of the subharmonic amplitude by optimizing acoustic parameters in *in vitro* experiments.

Statement of Contribution/Methods

The commercial UCA in this study was SonoVue, which had a resonance frequency f_0 = 2MHz. The acoustic scattering measurement was conducted to determine the subharmonic amplitude at different overpressures. Tone bursts of 64cycles were transmitted at a pulse repetition frequency of 1000Hz. Two different driving frequencies, f, of 4MHz ($2f_0$) and 1.33MHz ($2/3f_0$) were used in the measurement. The acoustic pressures, P_a, at the focus were 350kPa, 450kPa, and 500kPa, respectively. The ambient pressure inside the water tank was monitored by a pressure sensor, and controlled by an air pump. For each measurement, the average of subharmonic amplitudes of 50 received signals was calculated in the computer by fast Fourier transform (FFT). The mean values and standard deviations for five sets of measurements were calculated at each overpressure.

Results/Discussion

As shown in Table I, when the driving frequency is 4MHz, as the acoustic pressure increases to 500kPa, the subharmonic amplitude reduces by 19.8dB, and when the acoustic pressure is 350kPa, as the driving frequency decreases to 1.33MHz, the subharmonic amplitude reduces by 17.6dB. The two observed subharmonic reductions are more than the reported values. The results demonstrated the effect of the mechanical index ($MI=P_a/f^{1/2}$) on the ambient pressure sensitivity of subharmonic amplitude, and indicated the existence of a MI threshold (≈0.23) at which the sensitivity can be enhanced significantly, and an excellent linear correlation between the overpressure and subharmonic amplitude also can be achieved. It may be caused by the microbubble destructive mechanism of acoustic dissolution.

Table I. Comparision ambient pressure sensitivity of subharmonic amplitude with different acoustic parameters between 0mmHg and 180mmHg.

Pa (kPa)	*f* (MHz)	MI	Subharmonic reduction(dB)	Sensitivity (mmHg/dB)	Linear correlation(r^2)
350	4	0.175	2.6	-67.98	0.5322
450	4	0.225	10.9	-16.44	0.8285
500	4	0.25	19.8	-9.1	0.9919
350	1.33	0.30	17.6	-10.21	0.9633

IUS1-PA1-8

Tumor vascular structure and its influence on model selection for VEGFR2-targeted microbubble studies

Thomas Payen[1], Alexandre Dizeux[1], Delphine Le Guillou-Buffello[1], Eva Compérat[2], Olivier Lucidarme[3,4], S. Lori Bridal[1]; *[1]Laboratoire d'imagerie paramétrique, UPMC Paris6 - CNRS UMR 7623, Paris, France, France, [2]Department of Anatomopathology, GH Pitié-Salpêtrière,Assistance Publique-Hôpitaux de Paris, France, [3]Department of Radiology, GH Pitié-Salpêtrière,Assistance Publique-Hôpitaux de Paris, France, [4]Functional Imaging Laboratory, INSERM 678, France*

Background, Motivation and Objective

Non-invasive assessment of VEGFR2 with ultrasound is very promising for monitoring therapeutic responses in cancer. Tumor models, however, can vary significantly in terms of baseline vascular distribution and levels of VEGFR2 expression. The characterization of these aspects is important to correctly interpret modifications observed by ultrasound contrast imaging in terms of the underlying tumor evolution. The goal of this work is to improve understanding of the influence of tumor vascular structure on contrast-enhanced imaging for flow and VEGFR2 assessment.

Statement of Contribution/Methods

This work compares two highly vascularized tumor models with different structural characteristics, Lewis lung carcinoma (3LL) and CT26 colon carcinoma. Each cancer model was grafted subcutaneously in ten mice and the tumor development was monitored for 16 days. Functional imaging with a clinical ultrasound system (Acuson Sequoia 512, Siemens, 7MHz, CPS) was performed every 3 days from day 5 using SonoVue (Bracco SA, Milan, Italy). Immunohistology was performed at different time points to assess vascular distribution, necrosis and expression of VEGFR2.

Results/Discussion

Functional imaging using the bolus tracking method showed that 3LL tumors present a strong homogeneous enhancement (Figure). CT26 tumors consistently demonstrated two distinct zones: the center with no uptake of microbubbles and the periphery with high enhancement. CD31 staining revealed a fine homogeneous vascular network in 3LL tumors and a more chaotic vascularization in the CT26 model with a less-stained central zone. Necrosis was shown to be low and equivalent in both models. VEGFR2 expression was lower in 3LL than in CT26.

Dark central cores in functional imaging are commonly interpreted as necrosis. The fact that the cores of the CT26 tumors were not necrotic suggests that other factors limit the relative distribution of contrast in this model.

Based on histological results assessing VEGFR2 density, the CT26 model appears to be the better choice for a subsequent study using VEGFR2-targeted microbubbles. However, non-perfused zones must be excluded from measurement regions to assess the attached VEGFR2-targeted microbubbles during therapy in the CT26 model.

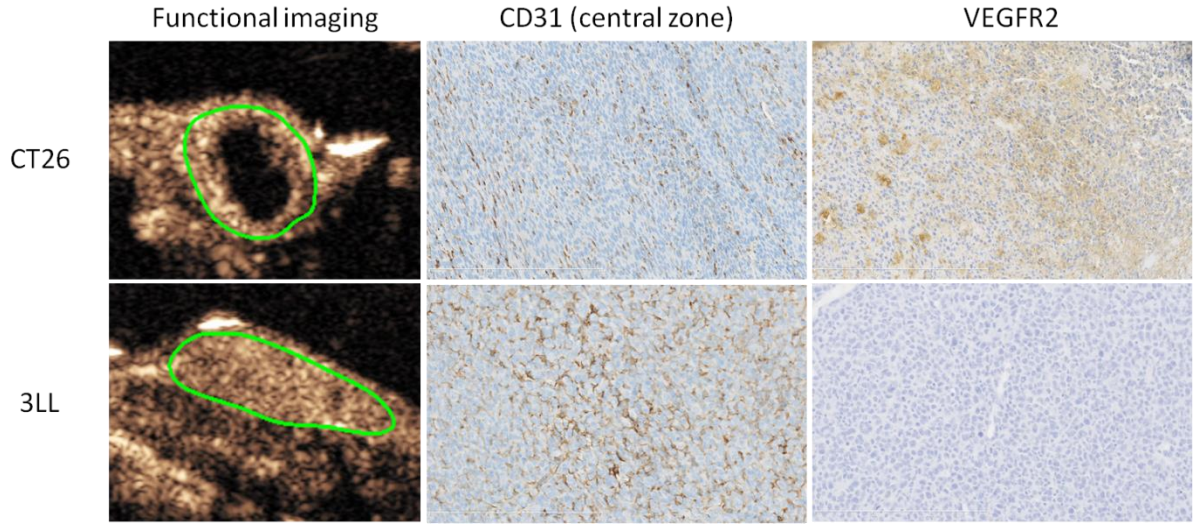

Monday, July 22 2013, 01:00 pm - 04:30 pm

IUS1-PA1-9

Vibration modes in a pendulums ring: analogy with gas microbubbles surface modes

Jennifer CHALINE[1], Victor SANCHEZ MORCILLO[2], Noé JIMENEZ[2], Ayache BOUAKAZ[1], Serge DOS SANTOS[1,3]; *[1]Equipe 5, UMR Inserm U930 and Université François-Rabelais, TOURS, France, [2]IGIC, Universidad Politecnica de Valencia, GANDIA, Spain, [3]ENIVL, BLOIS, France*

Background, Motivation and Objective

Under specific ultrasound activation, microbubbles undergo nonlinear oscillations and present surface patterns. The bubble dynamics can thus be described with a space-dependent function and can be developed on the basis of spherical harmonics depicting spatial vibrational modes. Such a behavior concerns many nonlinear systems when subjected to an external force, like bubbles, drops or macromolecules well modeled with coupled oscillators. In this study, the surface oscillatory behavior of a microbubble is investigated through an analogue macroscopic experiment of coupled pendulums parametrically excited by a vertical force. The objective of our work is to select optimal excitation conditions of the bubble for imaging and therapeutic applications.

Statement of Contribution/Methods

Based on a discrete nonlinear model of coupled pendulums [1] and the continuous model developed by Marmottant et al. [2], vibration modes are investigated theoretically and experimentally. The experimental setup was improved and consists of a ring with a diameter of 62 cm, on which 54 pendulums of mass 6 g are fixed with nylon strings forming a "V" shape with the vertical axis. The coupling is obtained by overlapping the strings and fixing them with a node. The excitation system consists of a loudspeaker driven by a waveform generator through an audio amplifier. The sinusoidal excitation varies from 1 Hz to 4 Hz with amplitudes varying from 0.5 Vpp to 3.5 Vpp.

Results/Discussion

Calculations and symmetry analysis applied to the equation of the continuous and the discrete models allow finding dimensionless similarity variables. Experiments show surface modes with localized oscillations up to n=12 where n is the mode number. Moreover, results show modes oscillating at subharmonics of the parametric excitation and the emergence of a band gap between 2.5 Hz and 3.2 Hz (Fig. 1c) in which no vibration mode is observed. The same mechanisms seem to be at the origin of surface vibration modes

of the pendulums ring and microbubbles. Such acousto-mechanical analogy of macroscopic behavior and microscopic surface modes provides important insights for the comprehension of coated microbubble's dynamics for both imaging and therapeutic applications.

[1] S. Dos Santos et al., IEEE International Ultrasonics Symposium Proceedings, 648-351, 2011
[2] P. Marmottant et al., J. Acoust. Soc. Am. 118, 3499–3505, 2005

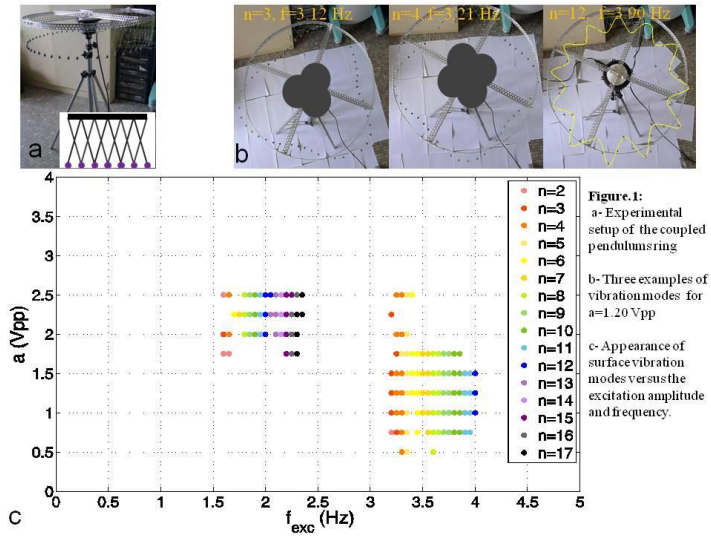

Figure.1:
a- Experimental setup of the coupled pendulums ring

b- Three examples of vibration modes for a=1.20 Vpp

c- Appearance of surface vibration modes versus the excitation amplitude and frequency.

Elastography methods

Forum Hall

Congress Hallair: **Hiroshi Kanai**
Tohoku University

IUS1-PA2-1

Effect of aperture size on plane-wave ultrasound strain estimation

Narasimha Reddy Vaka[1], Hendrik H.G. Hansen[1], Anne E.C.M Saris[1], Chris L de Korte[1]; [1]*MUSIC- Department of Radiology, Radboud University Nijmegen Medical Center, Nijmegen, Netherlands*

Background, Motivation and Objective

Ultrasound strain imaging (elastography) is a well known technique for estimation of the local mechanical properties of tissue. Plane wave insonation followed by Fourier beam forming techniques (which map the temporal echo spectrum to the spatial frequency spectrum) has shown to yield high frame rates, when compared to conventional imaging. The aim of this study is to compare the accuracy of strain estimation (SE) using plane wave insonation with Delay and Sum (DAS) for different apodization (AP) settings and to compare it with Fourier Based (FB) reconstruction.

Statement of Contribution/Methods

Ultrasound radio frequency (RF) element data were simulated for a vascular phantom at two different states of deformation for a linear array transducer (3-11 MHz, fs = 39 MHz, pitch = 135 [mu]) in plane wave transmission mode using Field II software. Beamformed RF data were constructed using AP-DAS and FB reconstruction. From these data, axial and lateral strains were estimated using a normalized iterative 2D cross correlation technique. Performance of axial and lateral strain estimation was quantified for varying F-numbers (0.5, 1, 2, 3, 4 and 5) by determining the root mean squared error (RMSE) of the strain results with respect to the ground truth. Furthermore, strain results after DAS reconstruction without apodization (non-AP DAS) were compared to those obtained with FB.

Results/Discussion

Apodization has an effect on the axial and lateral strain estimation results, see figure. For axial strain estimation, an F-number of between 1 and 3 was found to be optimal. This is in the same range as regularly used in B-mode imaging. However, for lateral strain estimation, a higher F-number was beneficial: RMSE decreased for an F-number up to 5. Comparing the strain estimation between FB and non-AP DAS, axial strain RMSE is 0.0098 and 0.0085, and lateral strain RMSE 0.0124 and 0.0078, respectively. However, qualitative assessment of the strain images shows better performance of FB than non-AP DAS in some regions. Consequently, incorporation of region/depth-dependent apodization in the FB method is required. The main benefit for using FB approach instead of DAS is to reduce the computation complexity. Computation performed by Matlab shows a decrease of ~10 times in computational load with FD, when compared to DAS. This factor might be significantly improved by implementation in C++.

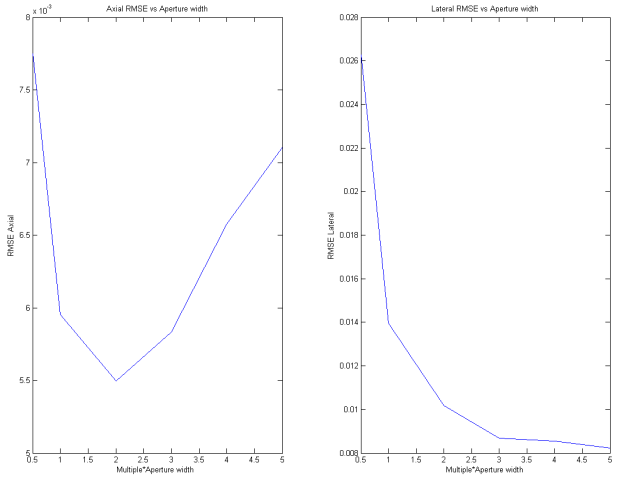

IUS1-PA2-2

The effects of surrounding media on the shear wave propagation in plates as related to the dispersion velocity

Luiz Henrique A. Vasconcelos[1], Ivan Nenadic[1], Bo Qiang[1], Matthew Urban[1], James Greenleaf[1]; [1]*Mayo Clinic, USA*

Background, Motivation and Objective

The calculation of dispersion curves and, therefore, the rheological properties is possible by analyzing how the different phase velocity modes behave in the medium of interest. In organs such as the liver, breast and kidney, the geometry of the organ is such that the shear wave propagation in the middle of the organ does not feel the effects of the boundaries, and can be treated as an infinite medium. In thin organs such as the spleen, myocardium, arteries, bladder and pancreas, the geometry and boundary conditions strongly effect shear wave propagation. In addition, shear wave propagation in “thin” organs is affected by the mechanical properties of the tissues surrounding those organs. In order to obtain the proper mechanical properties of such boundary sensitive organs, an analytical solution for the dispersion curves in a plate surrounded by semi-infinite solids was derived and validated. Shear wave propagation in a solid plate surrounded by gelatin was used to demonstrate the experimental feasibility of the method.

Statement of Contribution/Methods

The wave potential fields and displacement functions for the inner layer and the semi-infinite layers were derived using the stress-strain relation for isotropic materials and applying the Navier's equation. Since the displacement is continuous, one can use the boundary conditions to match the equations for two contact surfaces. This results in a system of eight equations with eight unknowns, which can be written as an 8 by 8 matrix. In order to have nontrivial solutions, the determinant of the matrix must be zero which yields the dispersion equations for the given geometry. In order to validate the derived dispersion equations, the dispersion curves were compared to those obtained using the commercial software DISPERSE 2.0.16d (Imperial College, London, United Kingdom). The method was also compared to the dispersion curves obtained from Finite Element Analysis (FEA) of a plate surrounded by a semi-infinite solid obtained using ABAQUS 6.10 (SIMULIA, Providence, RI). In these simulations Shear Modulus values of 25 and 36 kPa for the plate, and a range of 4 to 121 kPa for the surrounding, were used. A fully programmable ultrasound system (Verasonics, Inc. Redmond, WA, USA) operating a linear array probe (L7-4Philips Healthcare, Andover, MA) was used to excite 400 µs impulse in a thin solid plate surrounded by gelatin and track the motion by compounding flash imaging at 10 kHz from three different angles. Fourier space analysis was used to calculate the wave dispersion in the solid.

Results/Discussion

The analytical dispersion curves were in excellent agreement with those obtained using DISPERSE and FEA simulations for all the combinations of shear moduli for the thin layer and the surrounding medium. The experimental data show a good agreement with the theoretical predictions suggesting that the properties of the surrounding media effect the wave dispersion in thin organs.

IUS1-PA2-4

Coded Excitation Scheme for Acoustic Radiation Push Pulse Compression

Kengo Kondo[1], Makoto Yamakawa[2], Tsuyoshi Shiina[3]; *[1]Center for the Promotion of Interdisciplinary Education and Research, Kyoto University, Kyoto, Japan, [2]Advanced Biomedical Engineering Research Unit, Kyoto University, Kyoto, Japan, [3]Graduate School of Medicine, Kyoto University, Kyoto, Japan*

Background, Motivation and Objective

Shear wave elasticity imaging using acoustic radiation force has spread widely in these years. It consists of exciting a shear wave by a "push pulse" and tracking the shear wave by ultrafast imaging. It radiates at several hundred micro seconds, which is about 100 times higher than the pulse used in imaging.

Statement of Contribution/Methods

We propose a new pushing-and-tracking sequence, coded push pulse excitation, which can decrease energy density of the push pulse with respect to time by shortening the burst duration or reducing the amplitude without degrading the signal-to-noise ratio (SNR) of the observed shear wave propagation. Of course, an ensemble averaging procedure can also improve SNR, however it takes a long time to observe the shear wave, therefore the procedure is impractical for real-time measurement.

Assuming linear tissue deformation with excitation enables tissue displacement to be coded by push pulses. Coded displacement can be decoded by post-processing, and the decoded displacement is equivalent to the result of short-time, high-amplitude excitation. Such sequences can be achieved by interleaving push and track pulses (Fig. 1 (a)-(b)). The push pulse energy is dispersed to coding bits. The shear waves caused by the bits are superimposed, but decoding compresses push pulses. The proposed scheme enables us to implement coded excitation of push pulses and it can be employed with various coding methods already used in ultrasound imaging and other applications such as Golay codes, Barker codes, and m-sequences.

Results/Discussion

The proposed method was validated by phantom experiments. A 16-bit Golay code experiment demonstrated that the duration of push pulse excitation could be reduced to one quarter of its original level without SNR degradation (Fig. 1 (c)-(e)). The 16-bit coding was comparable to that obtained by ensemble averaging 16 times (Fig.1 (f)). The experiment was also indicated that one half amplitude of the normal excitation was needed to achieve the same levels of SNR by 16-bit Golay code. In addition, Barker codes and m-sequences enabled shorter acquisition time than Golay code, although there were some decoding artifacts. However, the error was small compared to the peak, thus it would have little effect on shear wave elasticity imaging that estimates shear wave velocity by measuring time-of-flight.

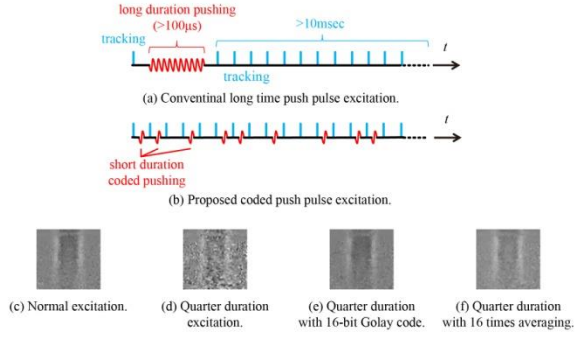

Figure 1. (a)-(b) Schematic of push pulse excitation.
(c)-(f) Displacement map at 4 ms after excitation.

IUS1-PA2-5

Axial displacement tracking in transient elastography using neighboring local minima maxima in Radio Frequency (RF) signals

Yassine MOFID[1], Melouka Elkateb[1], Caroline Chartier[1], Cecile Bastard[2], Stephane Audiere[2], Veronique Miette[2], Frederic Ossant[1,3]; *[1]Inserm U 930, Universite Francois-Rabelais de Tours, PRES Centre-Val de Loire Universite, Tours, France, [2]Echosens Company, Paris, France, [3]CHRU de Tours, Tours, France*

Background, Motivation and Objective

Dynamic elastography is an ultrasound (US)-based technique used for noninvasive measurement of the soft tissues elasticity in-vivo. In this context, different methods are developed with combining two systems: a system able to generate a vibration and an ultrafast US imaging system. The excitation could be mechanical (e.g. transient elastography (TE)) or induced by the US radiation force (e.g. ARFI). However, these methods have a common point: the application of an ultrafast imaging system to track internal displacements of the shear wave (SW) generated by the vibration. Most algorithms used to estimate local displacements are based on cross-correlation (CC) technique. Two principal parameters must be defined: a kernel length and an overlapping percent. These parameters limit the spatial resolution (SR) and the elastographic signal to noise ratio (SNRe) and affect the SW front reconstruction and so the velocity (Vs) esti-mation which is calculated as the slope of the SW front as used in TE for homogeneous media.

In this work, we propose an algorithm based on detection of neighboring local minima maxima (MM) of successive RF signals since the US acquisition is ultrafast (e.g. PRF 80 kHz) to obtain a local delay inferior than half-period of the RF signal . This algorithm permeated to reach a high SR (half of wavelength) with a good SNRe which is helpful for thin media (few mms) investigation such as the skin. In this case, the elastogram quality is linked only to acoustic SNR and anymore to windowing parameters.

Statement of Contribution/Methods

Technically, when local MM were located in successive RF signals, a parabolic interpolation was applied to estimate the corresponding time delay (displacement) independently of RF sampling. A linear interpolation was then applied to perform an elastogram with defined spatial axis.

Results/Discussion

Figure 1 shows the displacement field (SW front reconstruction) using TE: A high frequency transducer (15 MHz, 200 MHz sampling) induced a sinusoidal vibration (400 Hz) in a homogeneous phantom (16 kPa). Three elastograms are presented using: local MM (Fig1-a), CC with optimal windowing (Fig1-b) and CC with high SR (close to MM) (Fig1-c). SR, SNRe in a SW front homogeneous region and Vs values are indicated in the legend. The good performance of the MM algorithm was clearly quantified for SR, SNRe and Vs estimation.

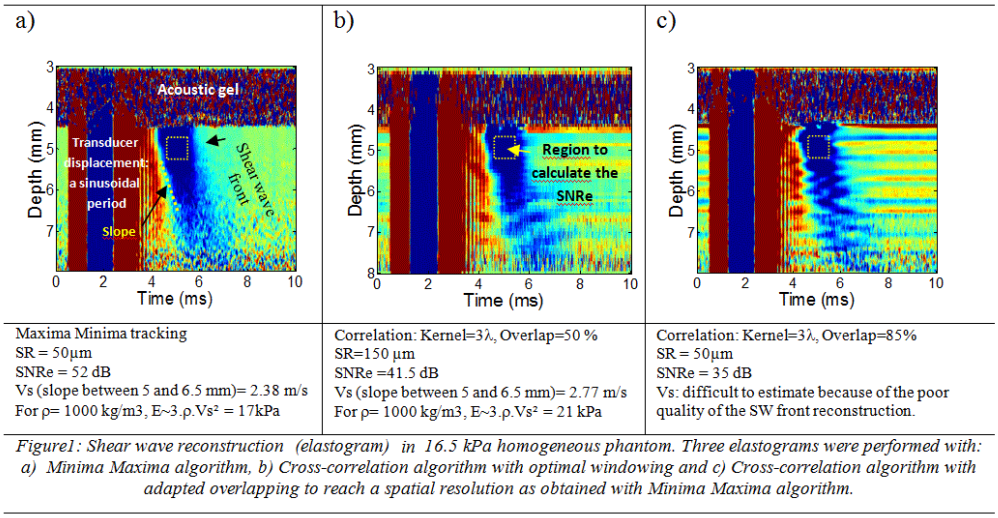

Figure1: Shear wave reconstruction (elastogram) in 16.5 kPa homogeneous phantom. Three elastograms were performed with: a) Minima Maxima algorithm, b) Cross-correlation algorithm with optimal windowing and c) Cross-correlation algorithm with adapted overlapping to reach a spatial resolution as obtained with Minima Maxima algorithm.

IUS1-PA2-6

How shear wave celerity depends on tissue stress tensor ?

Frederic PATAT[1], Fournier Joseph[2], Plag Camille[2], Defontaine Marielle[2], Calle Samuel[2], Remenieras Jean-Pierre[2]; *[1]Inserm-U930-CICIT-Universite F. Rabelais, TOURS, France, [2]Inserm U930 - Université François-Rabelais, Tours, France*

Background, Motivation and Objective

The question of the nonlinear behavior of biologic tissues remains very important with no unique and general answer since everything depends on the type and level of the applied mechanical stress. There are 2 sources of nonlinearity in acoustics: first is simply linked to the material and needs an accurate enough model of its response, second is due to the fact that basically the equations of acoustics are nonlinear. Recent developments of shear wave elastography use the measurement of shear wave celerity. It is therefore of great interest to consider the relationship between this celerity and a constant stress tensor applied to the tissue. Applied to muscle or tendons for instance, we could either measure the material stress or characterize nicely some of its mechanical key parameters (eventually nonlinear). The question we address is then: how the nonlinearity of acoustics equation can explain the dependence of shear wave celerity with tissue stress?

Statement of Contribution/Methods

We considered a general homogeneous Hookian material defined by its Cijkl 4th order elastic tensor being submitted to a constant T0 stress tensor. Linearized equations of acoustics do not couple those quantities. However, when the true strain deformation tensor is considered, the treatment of the equation involves the Piola Kirhchoff stress tensor and we come out with a modified Christoffel equation. Within the second order approximation, we then show it is sufficient to replace Cijkl by a modified tensor C*ijkl depending on T0.

Results/Discussion

The impact of traction for acoustic wave celerity for anisotropic material or orthotropic material like tissues is simple and will be fully given. It perfectly explains why a very soft tissue like muscle with a relaxed shear module of let us say 4 kPa is strongly influenced by contraction where T0 can reach 300 or 400 kPa (see fig). Our result is that the intrinsic nonlinearity of acoustics can fairly contribute to tissue hardening under stress.

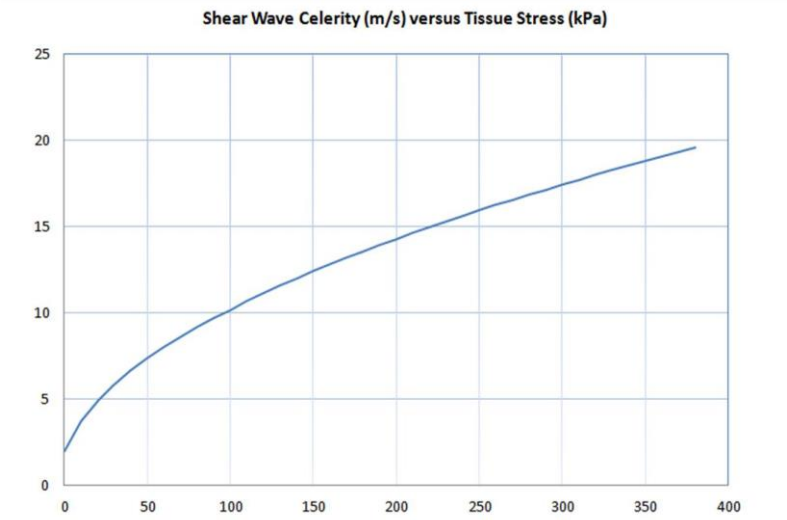

IUS1-PA2-7

Effects of Phase Aberration on Acoustic Radiation Force-Based Shear Wave Generation

Carolina Amador[1], Sara Aristizabal[1], Matthew Urban[1], James Greenleaf[1]; [1]*Physiology and Biomedical Engineering, Mayo Clinic College of Medicine, Rochester, Minnesota, USA*

Background, Motivation and Objective

Tissue elasticity is measured by shear wave elasticity imaging methods using acoustic radiation force to create the shear waves. Reliable tissue elasticity measurements are achieved with strong shear waves. Phase aberration and tissue attenuation can hamper the generation of shear waves for *in vivo* applications. In this study we explored how phase aberration affects ultrasound focusing for creating shear waves and evaluate the resulting shear wave amplitude and the shear wave velocity.

Statement of Contribution/Methods

Various phantom studies to explore how shear waves were affected by phase aberration were conducted. For these experiments, a Verasonics ultrasound system (Verasonics, Inc., Redmond, WA) equipped with a linear, a curved linear, and a phased array transducer (L7-4, C4-2 and P4-2, Philips Healthcare, Andover, MA) was used. Measurements were made 40 mm depth in a calibrated elastic phantom (CIRS, Inc., Norfolk, VA). In the experiments an excised piece of swine belly tissue was used. This tissue sample consisted of the skin, subcutaneous fat, and muscle. The different layers were separated and placed in different combinations on top of the elastic phantom to evaluate the shear wave produced when transmitting through the different layers. The skin alone, fat alone, muscle alone, a double fat layer, and a combination of skin, fat, and muscle were tested. The ultrasound frequency used for three transducers was varied to evaluate the resulting shear waves with the different tissue layers; 2.50, 3.00, 3.46, 4.09, 4.50, and 5.00 MHz for linear array; 1.5, 2.00, 2.50, and 3.00 MHz for curved linear array; 1.5, 1.73, 2.0, and 2.50 MHz for phased array. The shear wave amplitude and shear wave speed measured were evaluated.

Results/Discussion

The temporal peaks of particle velocity for all experiments are shown in Figure 1. The shear wave amplitude decreased with the introduction of the layers. With the L7-4 transducer decreasing the ultrasound frequency was important for maintaining a focused beam for creation of shear waves. Analysis of shear wave production with real tissue layers showed that large fat layers and com-binations of skin, fat, and muscle defocused the ultrasound beam most, thereby decreasing the shear wave amplitudes. This study was supported in part by NIH grants DK092255 and DK082408.

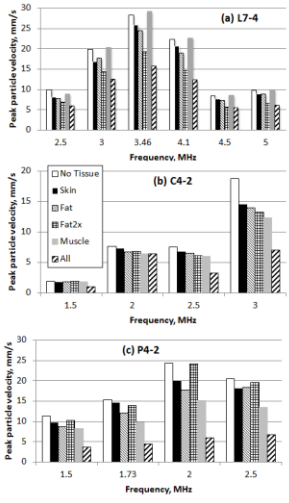

Figure 1: Temporal peak of particle velocity for (a) L7-4 linear array, (b) C4-2 curved linear array and (c) P4-2 phased array transducer.

IUS1-PA2-8

Observation of Shear Wave Dispersion Based on Optical Detection

Yi Cheng[1], Sinan Li[1], Robert Eckersley[2], Daniel Elson[3], Mengxing Tang[1]; *[1]Department of Bioengineering, Imperial College London, United Kingdom, [2]Department of Biomedical Engineering, King's College London, United Kingdom, [3]Institute of Biomedical Engineering and Department of Surgery and Cancer, Imperial College London, United Kingdom*

Background, Motivation and Objective

Shear wave dispersion in tissue is closely related to tissue mechanical properties and can be measured ultrasonically to permit tissue characterization. However, this is limited by the sensitivity of ultrasound signal to tissue motion. In this work, we proposed a highly sensitive optical method to measure shear waves dispersion with a CCD camera.

Statement of Contribution/Methods

A tissue mimicking phantom was exposed simultaneously to a 532 nm CW laser and a 5 MHz focused ultrasound transducer which was stimulated by amplitude modulated burst with 200 to 500 Hz modulation frequencies. Shear waves were generated by the acoustic radiation forces and subsequently interacted with diffused light within the phantom and tracked by a CCD camera which was aligned with the laser axis (Fig 1a). Voigt model was then applied to estimate tissue elasticity and viscosity.

Results/Discussion

According to Voigt model (Fig 1b), with 95% confidences bounds, shear elasticity of phantom is 7.32 +/- 0.41 kPa and viscosity is 1.52 +/- 0.21 Pa.s, which are within biological tissue range and close to our previous elasticity measurement results (Ref 1).

In this work, optical based method was applied to track shear waves at different frequencies and local tissue elasticity and viscosity at centimeter depth were estimated with Voigt model. Compared with ultrasound based method, this method is more sensitive to tissue displacement and hence potentially has higher sensitivity on shear wave tracking, but is limited by penetration depth.

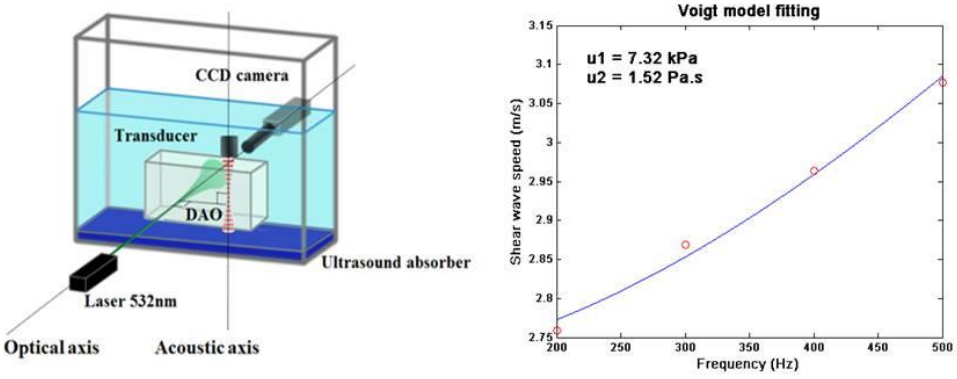

(a) (b)

Figure 1 (a) Experiment set-up. DAO: the distance between optical and acoustic axis. (b) Calculated shear wave speeds at different frequencies (dots) and the Voigt model fitting (solid line). (Ref 1)

1. Y. Cheng, et. al, Ultrasound in Medicine & Biology, vol. 38, p.1637-45, 2012

IUS1-PA2-9

Exact Viscoelastic Green's Functions of the Voigt-model-based Navier's Equation

Sheng-Wen Huang[1], Hua Xie[1], Jean-Luc Robert[1], Shiwei Zhou[1], Vijay Shamdasani[2]; *[1]Philips Research North America, Briarcliff Manor, NY, USA, [2]Philips Healthcare, Bothell, WA, USA*

Background, Motivation and Objective

Acoustic radiation force based ultrasound shear wave elastography (SWE) is a non-invasive tool for extracting quantitative tissue viscoelasticity information. While in SWE's reconstruction aspect shear modulus has received more attention than viscosity, shear viscosity is equally important in the forward problem dealing with viscoelastic response of tissue to acoustic radiation force.

The Voigt model has been shown to well model tissues' viscoelastic properties. Bercoff et al. [1] derived a Green's function for an infinite isotropic viscoelastic soft solid described by the Voigt model and Navier's equation. That solution assumes low viscosity and is not exact.

Statement of Contribution/Methods

Following the Lame's theorem approach described in [2], we have derived exact Green's functions of the Voigt-model-based Navier's equation (different from viscoelastic scalar wave equations) that can handle high viscosity. To avoid difficulties in finding analytical solutions as a function of position and time, we sought for solutions that are either a function of spatial frequency and time or of position and temporal frequency. Green's functions of position and time can be obtained from these exact solutions via inverse Fourier transform. The expressions are to be presented in the conference.

Results/Discussion

The figure below compares the z displacement profiles obtained using the Green's function in [1] (blue) and ours (green and red, close to each other). The green curves were obtained from the Green's function of position and temporal frequency with high sampling range and rate to avoid aliasing and serve as the gold standard. We assumed a tissue of 2 kPa shear modulus and 2 Pas shear viscosity (close to values in normal liver), and a short point push force along the z direction at the spatial origin. The significant deviation of the approximation given in [1] from the exact solutions shows that our formulations are better choices for the SWE forward problem. They can help develop SWE reconstruction algorithms to achieve more accurate estimate of shear modulus and viscosity for clinical diagnosis.

[1] J. Bercoff et al., "The role of viscosity in the impulse diffraction field of elastic waves induced by the acoustic radiation force," IEEE Trans. UFFC, vol. 51, pp. 1523–1536, 2004.

[2] K. Aki and P. G. Richards, Quantitative Seismology. University Science Books, 2nd edition, 2009.

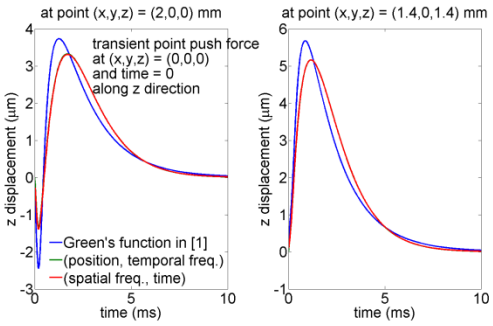

IUS1-PA2-10

Two-dimensional simulations of displacement accumulation incorporating shear strain

Matthew Bayer[1], Timothy Hall[1]; [1]*Medical Physics, University of Wisconsin-Madison, Madison, Wisconsin, USA*

Background, Motivation and Objective

The measurement of elastic nonlinearity of tissues has the potential to provide additional diagnostic information for breast cancer, but requires large tissue deformations that challenge motion tracking algorithms. To track large deformations, tracking methods must accumulate displacement estimates from smaller sub-deformations into a final large-deformation displacement map. Although this accumulation process has been used and studied previously, its statistics have not been fully investigated. Often it is assumed that the errors in consecutive displacement estimates are independent, but the results of 1D simulations conducted by the authors have recently shown that this assumption is likely in error. The present work extends these previous results to a 2D model and includes the effects of shear strain as well as normal strain.

Statement of Contribution/Methods

The ultrasonic imaging process was modeled as the convolution of an idealized 2D point spread function (PSF) with scatterers randomly distributed in a 2D space. The scatterers were subjected to either normal strain or simple axial shear strain in small steps of about 0.12% for normal strain and 0.06 degrees for shear strain. At each step an image was formed, and displacement estimation was performed for image pairs with varying amounts of strain between them. The variance of these estimates was measured both individually and after accumulation as a function of step size, data kernel size, and electronic noise level. Their mutual covariance was also examined.

Results/Discussion

These 2D simulations largely confirm the previous 1D results. The accumulated error variance showed significant effects of correlation between consecutive estimates. They are not independent. Strain-induced errors tended to have positive covariance, reinforcing one another under accumulation, while electronic noise-induced errors tended to have negative covariance, partially canceling under accumulation. The effects of normal strain and shear strain were qualitatively similar, except for their response to kernel size. Kernels that are longer axially perform better under axial shear strain but more poorly under normal strain, while kernels that are wider laterally perform more poorly under axial shear and better under normal strain. For a kernel size of about one PSF area, and with zero electronic noise, the error-inducing effects of 1% normal strain was found to be equivalent to 0.2 degrees of axial shear strain.

The authors gratefully acknowledge support from NIH grants T32CA0009206 and R01CA140271.

IUS1-PA2-11

Neighborhood Weighted Phase Root Seeking Algorithm with Temporal Stretching for Displacement and Strain Estimation

Golam Kibria[1], Sharmin Ara[1], Mohammad Haque[1], Soo Lee[2], **Kamrul Hasan**[1,2]; [1]*Department of Electrical and Electronic Engineering, Bangladesh University of Engineering and Technology, Bangladesh,* [2]*Department of Biomedical Engineering, Kyung Hee University, Korea, Democratic People's Republic of*

Background, Motivation and Objective

In ultrasonic elastography, the post-compression signal is considered to be a compressed and time-shifted version of the pre-compression signal. In conventional phase root seeking (PRS) algorithm, displacement of identical tissue segments in the pre- and post-compression signals is calculated by seeking the zero phase of the cross-correlation between the corresponding analytic pre- and post-compression RF echoes. The strain image is then estimated from this displacement field neglecting the compression effect of the post-compression signal. As the correlation function is not suitable for matching two delayed signals with different temporal scaling, the resulting strain image is erroneous. Though the algorithm performs well for low applied strain, the quality of the image falls significantly with increasing strain. Moreover, the continuity of the displacement and also the strain field cannot be guaranteed because of using only the interrogation window and its counterpart from the post-compression signal.

Statement of Contribution/Methods

In order to overcome the limitations of the conventional PRS based algorithms, we propose two modifications. First, we stretch the post-compression window in each iteration of phase root seeking so that the time-scaling discrepancy between the pre- and post-compression signals is reduced. The stretching factor can be adaptively calculated from the estimated strain of the previous segment. Second, we estimate the zero-lag position for each segment from the weighted average of the cross-correlation phases in the neighborhood region. Strain is then estimated from the displacement field by the least-squares approach.

Results/Discussion

The performance of the proposed algorithm is evaluated using quantitative indices, e.g., MSSIM, SNRe and CNRe, for the FEM simulation phantom. The results demonstrate that proposed technique significantly improves the quality of the strain image compared to that of the PRS algorithm. For example, the improvement in terms of MSSIM, SNRe and CNRe indices are found to be 0.48, 1.8, and 23.13, respectively for 2% strain; 0.53, 4.6, and 23.06, respectively for 3% strain; and 0.5, 6.6, and 19.48, respectively for 4% strain. The strain images generated by the conventional PRS and proposed methods for 2% applied strain are presented in the uploaded figure.

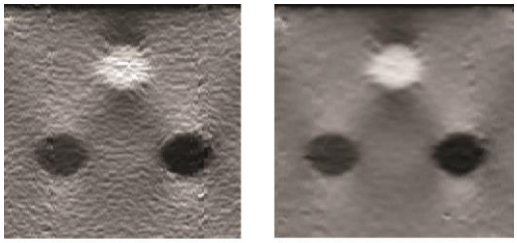

IUS1-PA2-12

Acoustic radiation force creep-recovery: theory and finite element modeling

Carolina Amador[1], Bo Qiang[1], Matthew Urban[1], Shigao Chen[1], James Greenleaf[1]; [1]*Physiology and Biomedical Engineering, Mayo Clinic College of Medicine, Rochester, Minnesota, USA*

Background, Motivation and Objective

In viscoelasticity theory, creep is a slow, progressive deformation of a material under constant stress. The removal of a constant stress elicits a response just as the imposition of the constant stress does, this response is called recovery. A method to quantify viscoelastic properties in a model-independent way by using time-dependent creep-recovery response induced by acoustic radiation force push pulse has been proposed to study tissue viscoelasticity. In this study a finite element method is used to model the recovery deformation induced by acoustic radiation force. Experimental data was obtained from tissue mimicking phantoms.

Statement of Contribution/Methods

The acoustic intensity fields associated with a creep-recovery excitation were simulated using Field II. A three-dimensional finite element model (FEM) was constructed in Abaqus/CAE 6.01-EF1 (Dassault Systèmes S.A., Vélizy-Villacoublay, France). A 500 μs push excitation focused at a depth of 25 mm from the surface of a linear array transducer was used and the effects of different parameters (material properties described by Voigt model, mass density and geometry) on the recovery displacement and strain were analyzed. For the experiments, a Verasonics ultrasound system (Verasonics, Inc., Redmond, WA) equipped with a linear array transducer (L7-4, Philips Healthcare, Andover, MA) was used. Acoustic radiation force recovery was measured in two 10% polyvinyl alcohol (PVA) phantoms with 30% and 40% polyethylene glycol (PEG) concentration. The recovery strain at the focus was evaluated as well as the group velocity and phase velocities of the shear waves resulting from the radiation force application.

Results/Discussion

From the FEM study, the effect of material viscosity (μ_2) in strain recovery is illustrated in Fig. 1(a) for 1 Pa·s and Fig. 1(b) for 3 Pa·s with fixed Elastic modulus (μ_1) of 5 kPa. A Voigt model was fit to phase velocities of PVA phantoms found using a shear wave measurement for the 30% PEG phantom μ_1 was 9.2 kPa and μ_2 was 2.64 Pa·s, for the 40% PEG phantom μ_2 was 12 kPa and μ_2 was 5.19 Pa·s. Fig. 1(c) and Fig. 1(d) illustrate the normalized recovery strain for the PVA phantoms. The experimental results resemble those from the FE model. The normalized recovery strain is more likely to converge to Voigt model when viscosity is high. This study was supported by NIH grants EB002167, EB002640 and DK082408.

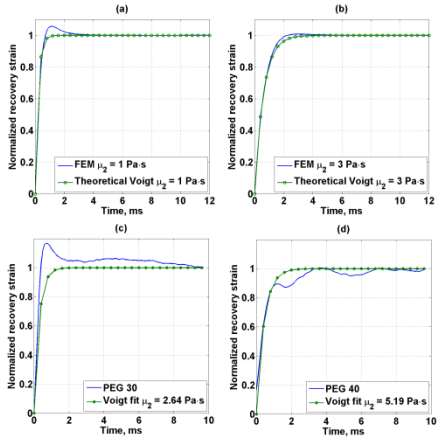

Fig. 1. Normalized recovery strain from FEM and theoretical Voigt model with μ_1 = 5 kPa and (a) μ_2 = 1 Pa•s, (b) μ_2 = 3 Pa•s. Normalized experimental recovery strain and Voigt model strain from fitting parameters to shear wave dispersion for (c) PEG 30 and (d) PEG 40.

Ultrasound simulation and computed tomography

Forum Hall

Monday, July 22 2013, 01:00 pm - 04:30 pm

Congress Hallair: **Nebojsa Duric**
Karmanos Cancer Institute

IUS1-PA3-1

A GPU-based implementation of the spatial impulse response method for fast calculation of linear sound fields and pulse-echo responses of array transducers

Tom Bruyneel[1], Alejandra Ortega[2], Ling Tong[2], Jan D'hooge[2]; [1]*Trisco IT Consultancy, Sint-Denijs-Westrem, Oost-Vlaanderen, Belgium,* [2]*Cardiovascular imaging & dynamics, Katholieke Universiteit Leuven, Leuven, Flemish-Brabant, Belgium*

Background, Motivation and Objective

A commonly used program for the simulation of linear sound fields and pulse-echo responses of transducers is FieldII which is based on the spatial impulse response (SIR) method. However, with the introduction of 2D array transducers, the complexity of the simulations leads to long computation times. Modern hardware is aimed at executing a high number of tasks across parallel computing nodes, which is particularly suited for linear problems. The aim of this work was therefore to develop a simulation tool extensively making use of parallelization to speed up the simulation process.

Statement of Contribution/Methods

OpenMP was used to divide the task of calculating the pressure fields or pulse echo responses according to the SIR methodology across several CPU cores. Hereto, the collection of observation points was divided in equal parts, each assigned to a thread. The calculations were further optimized by using GPU acceleration through OpenCL. In this way, the SIR can be calculated for hundreds of points in parallel across many GPU cores. The GPU handles the computation of the SIR for each crystal; afterwards the CPU handles only the convolutions required to obtain the pressure/pulse-echo responses. As such, a fast and scalable simulation tool was obtained as simply adding OpenCL devices will automatically result in further speed up of the simulations.

In order to benchmark the developed simulator, the pressure field of a 32x32 element phased array transducer (9.28x9.28mm) transmitting a Gaussian pulse (2.5MHz; 50% bandwidth) focused at 60mm was simulated in an azimuth-axial plane using both the GPU-based tool and FieldII. Simulations were done on a PC with a Quad Core Intel® Xeon® Processor, 12GB RAM and 32 compute units with a total of 2048 stream (GPU AMD Radeon™ HD 7970 GHz).

Results/Discussion

The figure shows the sound fields generated with the GPU-based SIR tool (left) and FieldII (right). Despite slight differences, which are likely due to different approximations used in each of the simulators, the pressure fields were very comparable. The simulation time in FieldII was 309.94 min (i.e. >5h) while in the proposed tool it was only 4.43min implying a total speed up of ~70. The proposed tool may thus play an important role in the future design of 2D arrays and 3D beam forming.

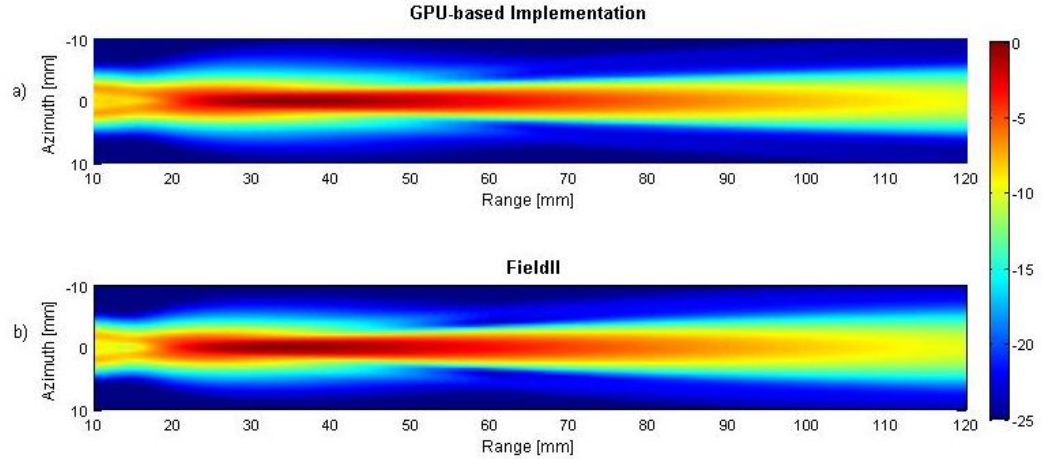

Figure. Pressure fields generated with the GPU-based implementation (a) and with FieldII (b)

IUS1-PA3-2

Simulating Ultrasonic Pulse Echo Registration including Multiple scattering, Attenuation and Nonlinearity

Libertario Demi[1], Erwin J. Alles[2]; [1]*Lab. of Biomedical Diagnostics, Eindhoven University of Technology, Eindhoven, Netherlands,* [2]*Joint Department of Physics and CR-UK & EPSRC Cancer Imaging Centre, Institute of Cancer Research and Royal Marsden NHS Foundation Trust, Sutton, Surrey, United Kingdom*

Background, Motivation and Objective

The advantages of nonlinear ultrasound propagation are exploited in an ever increasing number of applications. As a consequence, much research is devoted to the development of numerical methods capable of modeling nonlinear pressure wave fields propagating through (inhomogeneous) biomedical tissue. These tools are essential to assist in the design and optimization of ultrasound transducers and to investigate novel ultrasound modalities or devices.

Statement of Contribution/Methods

The Iterative Nonlinear Contrast Source (INCS) method [1] is an accurate full-wave method for modeling three-dimensional nonlinear acoustic wave fields propagating through biomedical soft tissue containing arbitrary inhomogeneities in the coefficient of nonlinearity, in the attenuation and in the speed of sound. This method is directionally independent and can deal with large three-dimensional domains measuring hundreds of wavelengths and periods. Here, we present the first synthetic harmonic ultrasound images generated with INCS.

Results/Discussion

The INCS method has been applied to compute the three-dimensional nonlinear acoustic pressure wave field generated by a 160 element linear array propagating through an inhomogeneous medium. The array is excited with a 1 MHz Gaussian modulated pulse, resulting in a pressure at the transducer surface equal to 2 MPa. Simulations have been performed up to the 3rd harmonic component. The simulated pressure field propagates through a medium containing inhomogeneities in the coefficient of nonlinearity, attenuation and speed of sound of magnitudes representative for biomedical tissue. The obtained scattered wave field, which includes multiple scattering, has been utilized to generate synthetic fundamental and harmonic ultrasound images of the insonified volume. The images are created using a delay-and-sum aperture focusing scheme. Results show the applicability of the INCS method as a simulator for ultrasound harmonic imaging systems.

[1] L. Demi, M.D. Verweij and K.W.A. van Dongen, Modeling Three-Dimensional Nonlinear Acoustic Wave Fields in Media with Spatially Varying Coefficient of Nonlinearity, Attenuation and Speed of Sound", to appear in Proc. IEEE Int. Ultrason. Symp., (2012).

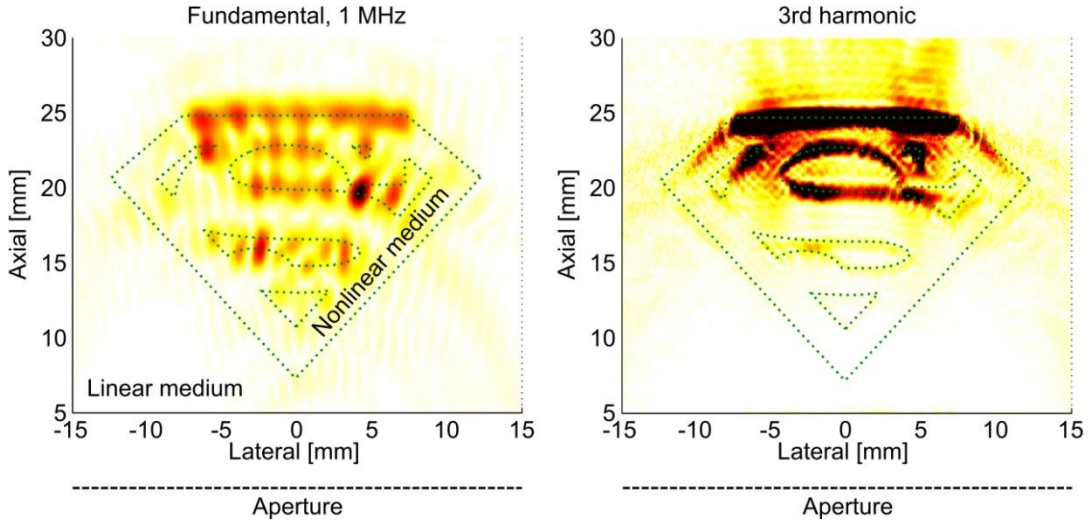

IUS1-PA3-3

Acoustic Beam Simulator with Aberration, Power Law Absorption, and Reverberation Effects

Thomas Szabo[1], Pedro Nariyoshi[2], Robert McGough[2]; *[1]Biomedical Engineering, Boston University, Boston, MA, USA, [2]Electrical and Computer Engineering, Michigan State University, USA*

Background, Motivation and Objective

Present ultrasound imaging simulations rely on pulse-echoes from amplitude-weighted point scatterer models rather than a model based on wave propagation. Aberration has been most often modeled as a phase screen adjacent to the aperture rather than as a distributed effect.

Statement of Contribution/Methods

A more realistic model which accounts for diffraction, absorption, reverberation, and aberration effects has been implemented. Based on two layer measurements of fat and muscle in abdominal walls[1], the new model projects the layer data three-dimensionally to their correct physical locations so that spatially local heterogeneous aberration effects vary with array geometry to the field point. Frequency-dependent effects in the original data are removed and combined with wave propagation effects calculated along ray paths from a multilayer time domain model that includes material impulse response functions[2] for power law media and reverberations. The net result is a set of temporal functions that can be convolved with diffraction responses from the FOCUS software program [3] for more efficient simulations.

Results/Discussion

Beam contours calculated for a 5 MHz, 76 element linear array demonstrate that beam quality has greater local dependence on combined propagation and aberration effects than shown in earlier work. Compared to phase screen simulations, beams have more pronounced asymmetries and shifts. This new scalable model for beam and eventual image simulation, which includes aberration, absorption and reverberation effects, is adaptable to different array geometries, frequencies, waveforms, and tissue combinations.

[1]L.M. Hinkelman,T.D.Mast,L.A.Metlay and R.C. Waag.,"The effect of abdominal wall morphology on ultrasonic pulse distortion, Part 1: Measure-ments,",J. Acoust. Soc. Am. vol. 104, p. 3635-3649, 1998.

[2]T. L. Szabo, "The material impulse response for broadband pulses in lossy media," Proceedings of the IEEE 2003 Ultrasonics Symp.,(03CH37476C, IEEE New York), pp 748-751, 2003.

[3](http://www.egr.msu.edu/~fultras-web)

IUS1-PA3-4

Simulation based evaluation of different speed of sound reconstruction methods for Ultrasound Computer Tomography

Neslihan Ozmen-Eryilmaz[1], Robin Dapp[2], Michael Zapf[2], Hartmut Gemmeke[2], Nicole Ruiter[2], Koen W.A. van Dongen[1]; *[1]Laboratory of Acoustical Wavefield Imaging, Delft University of Technology, Delft, Netherlands, [2]Institute for Data Processing and Electronics, Karlsruhe Institute of Technology, Karlsruhe, Germany*

Background, Motivation and Objective

Ultrasound Computer Tomography for breast imaging is gaining popularity due to its low cost and high efficiency. In addition, current studies show that it can successfully detect tumors in dense breasts whereas mammography might miss them. In this work, we compare three different imaging methods to detect breast tumors by reconstructing speed of sound profiles.

Statement of Contribution/Methods

Three reconstruction methods were investigated: Bent-Ray Time-of-Flight Tomography, Born Inversion and Contrast Source Inversion (CSI). Time-of-Flight Tomography uses bent rays com-puted by approximating the Eikonal equation to obtain a non-linear inverse problem. The Eikonal equation is the infinite frequency limit of the wave equation and is able to account for refraction. The inverse problem is then solved by an adapted numerical minimization algorithm with Total Variation regularization. With Born Inversion, the wave-based inverse problem is first linearized, and successively solved using an iterative scheme. CSI solves the full wave-based inverse problem, and updates the contrast and the contrast sources using conjugate-gradient directions by minimizing a cost functional.

Results/Discussion

To test the methods, noise-free synthetic measurement data was computed using a full wave method. The breast model was based on an MRI scan of a cancerous breast and typical speed of sound values of the breast tissues are included. The 2D simulation included multiple scattering, refraction, diffraction and interference, and not noise and attenuation. There reconstruction methods were applied on the same data sets, and the results are shown in Fig. 1. The root-mean-squared errors (RMSE) were approximately equal to 14.9 m/s, 38.1 m/s and 6.4 m/s for Time-of-Flight Tomography, Born Inversion and CSI, respectively. Time-of-Flight Tomography and CSI allow for speed of sound reconstructions, where Born Inversion only localize the object. Moreo-ver, CSI method outperforms the ray based method with respect to accuracy at the cost of an increase in computational load (hours versus minutes).

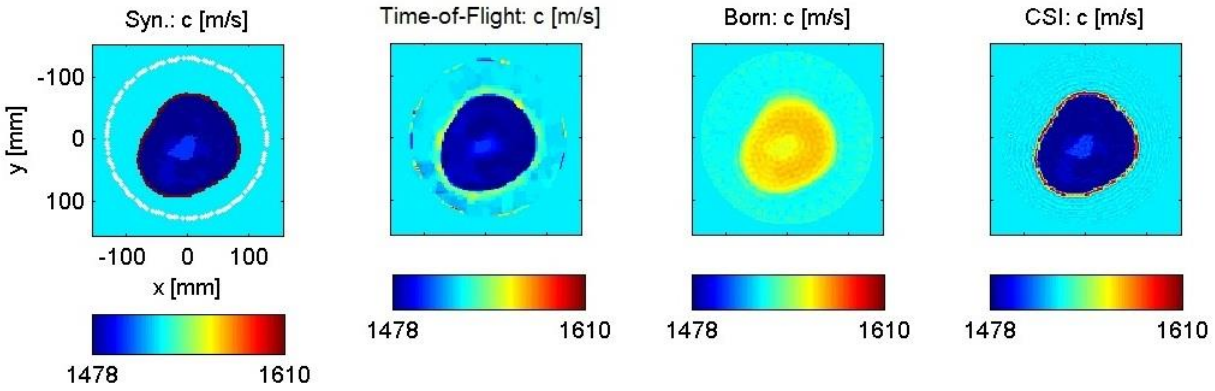

Fig. 1: Speed of sound reconstructions of a two-dimensional cancerous breast model, from left to right: breast model, Time-of-Flight, Born Inversion and CSI.

IUS1-PA3-5

Evaluation of phase aberration correction for a 3D USCT

Ernst Kretzek[1], Robin Dapp[1], Michael Zapf[1], Matthias Birk[1], Nicole Ruiter[1]; [1]*Institute for Data Processing and Electronics (IPE), Karlsruhe Institute of Technology (KIT), Germany*

Background, Motivation and Objective

3D ultrasound computer tomography (3D USCT) promises reproducible high-resolution images for early detection of breast tumors. A new 3D USCT prototype has been developed with an optimized aperture in form of a semi-ellipsoid to maximize the isotropy of the 3D PSF, the image contrast and the illumination. The prototype provides three different modalities (reflectivity, speed of sound (SOS), and attenuation) using 2041 transducers. In this setup, with a diameter of 26 cm and height of 16 cm, ultrasound can travel over long distances up to 52 cm. Phase aberrations (PA) due to SOS variations cause many pulses not to overlap in the reflectivity reconstruction. Previous research showed that image quality could be increased performing PA correction. Yet, no quantitative error assessment was done. The aim of this work is to use a ray trace based simulation to quantify the image degradation caused by PA for the 3D USCT aperture.

Statement of Contribution/Methods

A simulation based on ray tracing was used to assess errors in the reflectivity image reconstruction. The environment consists of two regions with different SOS, see Fig. 1 a): The water with cw=1500 m/s and the region of a hemispherical approximated breast with cb=1460 m/s. A point scatterer represents a small cancer cell. The simulation generates A-scans including the PA due to SOS variations, which were used for image reconstruction. The quality of the resulting images was then evaluated by measuring the position of the point scatterer, the contrast (maximum value) and the resolution (FWHM). As reference the reconstructed image for cb=1500 m/s, see Fig. 1 b) is used. To determine the average SOS value for every path through the SOS volume the Bresenham algorithm was applied.

Results/Discussion

Several negative influences for image quality could be determined caused by PA for two SOS regions. In comparison to reconstruction without aberrations (cb=1500 m/s, Fig. 1b)), the point scatterer's maximum moved by 1.2 mm (cb=1460 m/s, Fig. 1 c)). The contrast decreased by factor 22.7 and FWHM was widened by 53%. Performing PA correction, the focal point was only 0.1 mm off, the contrast increased to factor 0.73, and the FWHM widened only 5%, see Fig. 1 d). The presented simulation showed that PA correction significantly restored reconstructed image quality. Furthermore we validated the PA correction with experimental data, see Fig. 1 e) and f).

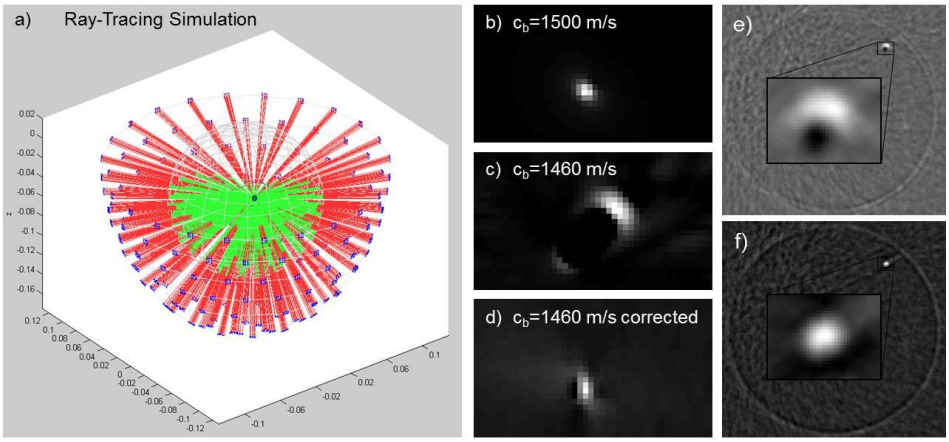

Fig. 1: a) Simulation of ultrasound propagation paths from emitters to one point scatterer and back to receivers. Aperture (emitters and receivers) in blue. Rays simulate the propagation of ultrasound in water (red) and in breast (green). Reconstruction of simulated point scatter without (b), with (c) different speed of sound regions and with phase aberration correction (d). Reconstruction of experimental data without (e) and with (f) phase aberration correction.

IUS1-PA3-6

Ultrasound Tomography for Breast Imaging: Initial results using the SoftVue scanner

Nebojsa Duric[1,2], Peter Littrup[1,2], Olivier Roy[1,2], Steve Schmidt[1,2], Cuiping Li[1,2], Roman Janer[2], Xiaoyang Chen[2], David Kunz[2], Lisa Bey-Knight[1], Jefferey Goll[2], William Greenway[2]; *[1]Karmanos Cancer Institute, Detroit, MI, USA, [2]Delphinus Medical Technologies, Plymouth, MI, USA*

Background, Motivation and Objective

We discuss the application of ultrasound tomography (UST) to breast imaging, based on data obtained with a recently developed imaging device named SoftVue. The motivation for this work derives from current limitations of standard breast imaging techniques. For women with dense breast tissue, for example, who are at the highest risk for developing breast cancer, the performance of mammography is at its worst. Improved cancer detection for women with denser breasts would decrease the proportion of breast cancers diagnosed at later stages, which would significantly lower the mortality rate.

Statement of Contribution/Methods

The SoftVue scanner was installed at the Karmanos Cancer Institute, Detroit, USA in November 2012. Following an approved protocol, we imaged both healthy patients and patients with benign and malignant disease. Data were obtained in coronal planes, starting at the chest well with a ring-shaped transducer that surrounds the breast. The transducer was translated downward in 3 mm intervals until the entire breast was scanned. Tomographic inversion algorithms were used to reconstruct images of reflection, sound speed and attenuation, yielding three image stacks per patient. The image stacks were analyzed to determine the effectiveness of SoftVue in differentiating benign from malignant masses.

Results/Discussion

The reflection images generated by SoftVue revealed complex and highly detailed parenchymal patterns, as shown in the figures below (bilateral image slices on left, averaged unilateral slices on the right). Such images proved highly effective in detecting spiculation and architectural distortion, two important attributes of malignant masses. The addition of sound speed and attenuation data improved the ability of SoftVue to characterize malignant masses.

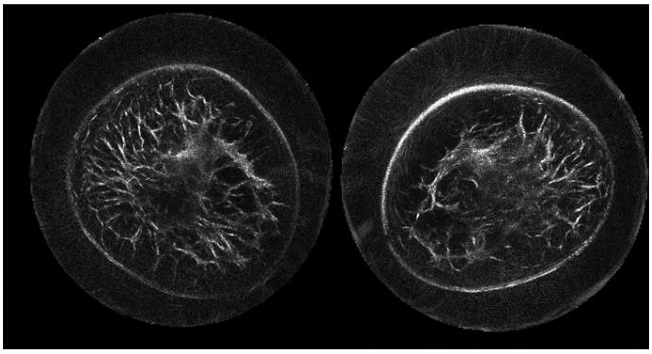

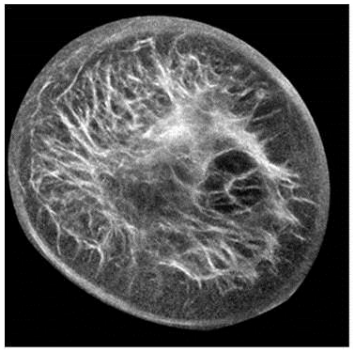

Bioeffects and metrology

Forum Hall

Monday, July 22 2013, 01:00 pm - 04:30 pm

Congress Hallair: **Jonathan Mamou**
Riverside Research

IUS1-PA4-1

Measuring the photo detector frequency response for hydrophone calibration using laser interferometry

Youichi Matsuda[1], Tsuneo Kikuchi[1]; [1]*National Metrology Institute of Japan / AIST, Japan*

Background, Motivation and Objective

The signal to noise ratio of a photo detector frequency response calibration system was improved for high frequency measurements. A photo detector was calibrated up to 40 MHz using the system to extend the frequency range of our hydrophone calibration system using laser interferometry. Recently, high frequency ultrasound above 20 MHz is used to improve image resolution in ultrasonic diagnostic equipment. Hydrophone calibration using ultrasonic far-field is difficult at the frequencies above 20 MHz because ultrasound attenuation increases with increasing frequency. We have designed and developed a 1 mm radius plane transducer and have realized ultrasonic far-field at a 50 mm propagation distance at 40 MHz. The amplitude sensitivity of a membrane hydrophone was measured using ultrasonic far-field of the transducer from 10 MHz to 40 MHz using laser interferometry. The laser interferometer frequency response should be compensated for accurate hydrophone calibration. It has been calibrated using our twice-modulated light system in the frequency range from 0.5 MHz to 20 MHz. In this study, the signal to noise ratio of the twice-modulated light system was improved for high frequency measurements. The photo detector frequency response of our hydrophone calibration system was measured from 10 MHz up to 40 MHz with a frequency interval of 1 MHz.

Statement of Contribution/Methods

The frequency response of the photo detector was measured using the twice-modulated light system up to 40 MHz. A linearly polarized 15 mW He-Ne laser was the calibration light source. The laser beam intensity was modulated twice using two acousto-optic modulators operated at two signal frequencies at f1 and f2. The amplitude components of frequencies f1 - f2 and f1 + f2 are always identical for the twice-modulated light. Therefore, the ratio of the photo detector frequency response at the frequencies f1 - f2 and f1 + f2 can be derived by comparing these two amplitude components of the photo detector output voltage. The photo detector frequency response can be measured by scanning the two signal frequencies of f1 and f2 appropriately. In this study, the laser beam was expanded five times using a beam expander and was focused on to the modulators using the plane-convex lens with a 150 mm focus length to improve the signal to noise ratio at high frequency range.

Results/Discussion

The photo detector frequency response of our hydrophone calibration system was measured in the frequency range from 10 MHz up to 40 MHz with a frequency interval of 1 MHz. The photo detector showed a relatively flat response in the frequency range. Relative standard deviation of the measured frequency response was improved from 4 % to 1 % at 40 MHz. Measurement uncertainty of the photo detector frequency response will be evaluated.

IUS1-PA4-2

Novel thermochromic-doped polymers for rapid visualization of ultrasonic intensity distributions

Bajram Zeqiri[1], Ian Butterworth[1], Pierre Gelat[1], Malcolm Norris[2]; [1]*Acoustics and Ionising Radiation Division, National Physical Laboratory, Teddington, Middlesex, United Kingdom,* [2]*Acoustics Polymers Ltd, Mitcheldean, Gloucestershire, United Kingdom*

Background, Motivation and Objective

Due to the close link between time-averaged acoustic intensity and tissue heating, knowing the spatial distribution of the former is key with regard to safety and efficacy of clinical ultrasound procedures, particularly therapeutic. Conventional techniques rely on spatially mapping acoustic pressure using miniature hydrophones; characterization which is time-intensive and demanding in terms of the cost and complexity of the measurement system. There is therefore a need for simpler techniques, ideally low cost, to aid in the development, testing and validation of equipment performance.

Statement of Contribution/Methods

Thermochromic (TC) pigments, materials which change colour in response to temperature, have found some application in terms of visualising intensity distributions, albeit it a qualitative level. This paper describes studies investigating the potential of a novel implementation of the TC technique that might provide a basis for quantitative visualisation of the acoustic field, to determine key properties such as the beam nonuniformity ratio and effective radiating area, important quantities relevant to physiotherapy ultrasound equipment. TC materials exhibiting three “switch” temperatures in the range 31ºC to 60ºC have been employed. The particular novel implementation of these visualisation tools has been to embed the TC crystals within a background polyurethane rubber matrix whose acoustic properties can be refined to boost ultrasound attenuation, leading to a rapid temperature increase generated through ultrasound absorption. Another important feature of the polyurethane materials is their low thermal conductivity, which means that the spatial distribution of heating, related to the local acoustic intensity, can be “locked in” for further processing and analysis.

Results/Discussion

A range of implementations of the TC and polyurethane matrices will be presented, from solid tiles designed for use with clinical physiotherapy devices, to thin membranes for application to High Intensity Focused Ultrasound equipment. The potential of the TC technique as a rapid and cost effective first-line check of equipment performance will be discussed. Results of Finite Element modeling of the polyurethane tiles will also be described.

Fig. 1: Thermochromic tile image obtained from a 3 MHz physiotherapy ultrasound treatment head operating at a time-averaged intensity level of 2 W cm-2 for 20 seconds. The image has been acquired 10 seconds after exposure had ceased and illustrates a central “hot-spot” of acoustic intensity along with a lower level ring of intensity. The width of the heated area shown in the figure is nominally 25 mm in diameter.

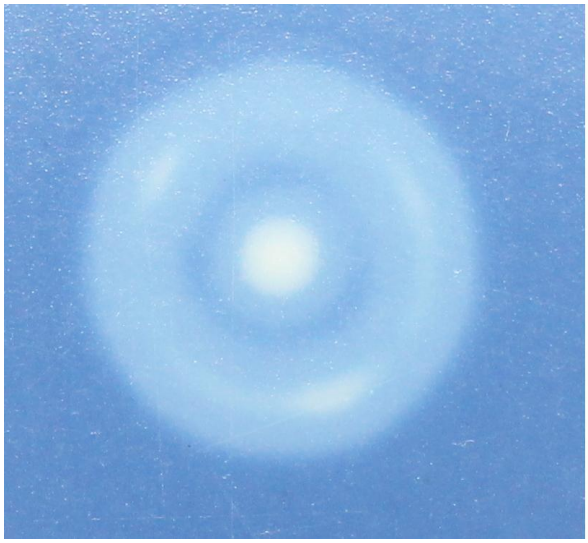

IUS1-PA4-3

Development of In Vivo Measurement System for Temperature Rise in Animal Tissue under Exposure to Ultrasound with Acoustic Radiation Force

Naotaka Nitta[1], Nobuki Kudo[2], Tomoo Kamakura[3], Yasunao Ishiguro[4], Hideki Sasanuma[4], Nobuyuki Taniguchi[4], Iwaki Akiyama[5]; *[1]Human Technology Research Institute, National Institute of Advanced Industrial Science and Technology (AIST), Tsukuba, Ibaraki, Japan, [2]Laboratory of Biomedical Engineering, Graduate School of Information Science and Technology, Hokkaido University, Sapporo, Hokkaido, Japan, [3]Graduate School of Informatics and Engineering, The University of Electro-Communications, Choufu, Tokyo, Japan, [4]Jichi Medical University, Shimotsuke, Tochigi, Japan, [5]Faculty of Life and Medical Sciences, Doshisha University, Kyotanabe, Kyoto, Japan*

Background, Motivation and Objective

Acoustic radiation force (ARF) has been recently used for the tissue elasticity measurement and imaging. The typical ARF technologies use longer pulse durations (PD) and higher acoustic pressures than conventional ultrasound devices. Consequently, since it is predicted that the temperature rises are also higher, in vivo measurement of temperature rises in animal experiments is important. However, when a thermocouple is used, there are some problems such as lack of thermocouple sensitivity, viscous heating error and position mismatch of a temperature sensing part (apex of thermocouple) and a focal point. In this study, to overcome these problems, a temperature measurement system for animal experiments is presented. The performance was investigated by using a tissue mimicking material (TMM) and an extracted porcine liver.

Statement of Contribution/Methods

The temperature measurement system for animal experiment is composed of the ultrasound irradiation and temperature measurement parts. The ultrasound irradiation part includes a custom-made focused transducer (2.5 MHz, focal depth: 35 mm, f-number: 2), function generator and power amplifier. On the central axis of transducer, a puncture hole (φ2 mm) is prepared for inserting a thin wire thermocouple (Chino, φ0.15 mm, K type) into the target. Since the hole axis corresponds to the beam axis, the position error of temperature sensing part to the focal point is minimized. After the apex of thermocouple is placed on the focal point by using a cylindrical puncture needle, and only the needle is pulled out. In the temperature measurement part, to improve the sensitivity of thermocouple measurement, the output voltage of thermocouple via a reference junction compensator is amplified by a low-noise preamplifier (40 dB) and acquired by using a high-speed digitizer at a rate of 500 kS/s and 16 bits. After the high-frequency noise of acquired voltage data is suppressed by a low-pass filer and the viscous heating error is removed on the basis of curve fitting technique, the temperature data is finally obtained.

Results/Discussion

The performance of temperature measurement system was evaluated using a TMM, which was based on IEC60601-2-37. Series of ultrasound pulses with each PD of 0.3 to 10 ms, MI of 0.7 to 3.4, pulse repetition time (PRT) of 10 s were irradiated to the TMM during total measurement time of 200 s. As a summary, a linear relationship between the spatial peak-pulse average intensity ($I_{sppa.3}$) and the peak temperature rise was observed. The temperature rise per unit intensity (TPI) was 0.22 °C/W/cm^2. As reference, the theoretical TPI calculated under same conditions as the TMM was 0.21 °C/W/cm^2. Moreover, for the extracted porcine liver, the TPI was 0.33 °C/W/cm^2. These results indicate that the system is capable of measuring the temperature rise accurately and discriminating the difference of acoustic absorption coefficients, and is a promising tool for animal experiments.

IUS1-PA4-4

Ultrasound-enhanced Delivery of Antibiotics and Anti-inflammatory Drugs into the Eye

Marjan Nabili[1], Hetal Patel[1], Sankaranarayana Mahesh[2], Ji Liu[2], Craig Geist[2], Vesna Zderic[1]; *[1]Electrical and Computer Engineering, George Washington University, USA, [2]Ophthalmology, George Washington University, USA*

Background, Motivation and Objective

Millions of people suffer from variety of ocular diseases which in some cases lead to vision impairment and eventually blindness. Topical administration of drugs through cornea is the preferred method for drug delivery, but cornea's barriers makes delivery of sufficient amount of drugs a challenging task.

Statement of Contribution/Methods

Initial study was carried out using unfocused ultrasound transducers in ultrasound- and sham-treated rabbit corneas *in vitro* using a standard diffusion cell set-up. Ultrasound application (frequencies of 400 KHz-1 MHz, intensities of 0.3-1.0 W/cm^2, and exposure duration of 5 min) was studied to investigate corneal permeability of ophthalmic drugs, Tobramycin and Dexamethasone Sodium Phosphate, and Sodium Fluorescein, a drug mimicking compound. Light microscopy observations of histology slides were used to determine ultrasound-induced structural changes in cornea. For *in vivo* study, an eye-cup filled with Dexamethasone Sodium Phosphate was placed on cornea. Ultrasound at frequencies of 400 KHz and 600 KHz, and intensity of 0.8 W/cm^2 was applied for 5 min. Drug concentration in aqueous humor samples, collected after 60 min, was determined using chromatography methods. Corneas were dissected and fixed for histological observations.

Results/Discussion

Our *in vitro* results showed that increase of 32-47% , 46-126% ($p<0.05$) and 32-109% ($p<0.05$, except for 1 MHz ultrasound application) in corneal permeability for Tobramycin, Sodium Fluorescein, and Dexamethasone Sodium Phosphate, respectively, was achieved at different ultrasound-treatment parameters as compared to sham-treated samples. For *in vivo* study, increase in drug concentration in aqueous humor samples was 2.8 times ($p<0.05$) at frequency of 400 KHz and 2.4 times ($p<0.01$) using 600 KHz frequency, both at 0.8 W/cm^2 intensity and 5 min of ultrasound application, as compared to sham treated samples. Histologic analysis showed some structural changes that were limited to epithelial layers of cornea and were observed at all applied ultrasound parameter combinations.

In conclusion, ultrasound application provided enhancement of drug delivery, increasing the permeability of the cornea, and has a potential to provide effective and safe method for ocular drug delivery in treatment of eye infection and inflammation. Ultrasound appeared to be most effective at lower frequencies and higher intensities.

IUS1-PA4-5

A Nano-Mechanical Study on the Influence of Ultrasound Exposure on Cellular Elasticity

Michael Conneely[1], David McGloin[1], Pamela Robertson[2], W.H. Irwin McLean[2], Paul A. Campbell[1]; *[1]Division of Physics, University of Dundee, United Kingdom, [2]Molecular Medicine, University of Dundee, United Kingdom*

Background, Motivation and Objective

Ultrasound (US) has for some time been identified as a method of effecting change at the cellular level. Long established in the medical field as an indispensable imaging modality, currently however there is much promise for its [non-thermal] therapeutic potential, such as in targeted drug delivery where it can be exploited to mediate the transport of molecules into or across tissues and membranes. Of key importance for the therapeutic application of US is a safe dose threshold, particularly in light of recent publications highlighting the genotoxic potential of US via the induction of DNA double strand breaks through purely mechanical mechanisms (Y. Furusawa et al.). In a previous preliminary study we sought to examine the mechanical effects of US on live cells, where we observed marked increases in cellular elasticity post US exposure.

Statement of Contribution/Methods

Compelled by the results of our preliminary work, here we have undertaken live-cell investigations on the MCF-7 human breast cancer cell line, expanding on the experimental parameter space previously used in order to examine the dependency of mechanical induced effects with incident US power and exposure times. Sonication was performed using Sonidel KP-SS2Y 2mm transducer driven by a Nepagene KTAC-4000 and quantitative cell elasticity measurements were done pre and post US exposure using a JPK NanoWizard scanning force microscope (JPK Instruments, Berlin, Germany). Force-distance curves were recorded (Figure 1) using 10µm spherical indenter's and Young's modulus values were determined by using a Hertz model fit.

Results/Discussion

Correlating with our early data we observe marked increases in cellular elasticity both on and off nucleus with US exposure (see histogram figure 1). By varying US power and exposure times we note in some instances a divergence in the induced elasticity change between the on and off nucleus region, where, at low powers and shorter exposure times the off nucleus region exhibits a tendency to maintain an elasticity value close to its pre exposure value while the nucleus will exhibit a higher elasticity.

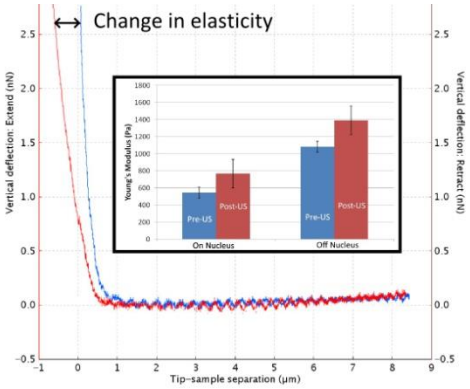

IUS1-PA4-6

Ultrasound as a Repulsive Cue for Neuronal Development: Real-Time Morphological Observations In-Vitro

Yaxin Hu[1], Wenjing Zhong[1], Jennifer M. F. Wan[2], Alfred C. H. Yu[1]; *[1]Medical Engineering Program, The University of Hong Kong, Pokfulam, Hong Kong, [2]School of Biological Sciences, The University of Hong Kong, Pokfulam, Hong Kong*

Background, Motivation and Objective

A core event in neuronal development is the outgrowth of neurite branches from a neuron's cell body. It is known that, by presenting physical or chemical cues to the extracellular environment, neuronal development can potentially be modulated. In this work, we seek to investigate the use of ultrasound in modifying neuronal development behavior. We hypothesize that ultrasound, when applied at low intensity and pulsed settings, can possibly serve as a physical cue that operates like mechanical stimulation.

Statement of Contribution/Methods

Our study was carried out on a customized platform that allows real-time imaging of neuronal morphology. Pulsed ultrasound (1 MHz frequency, 20 or 100 cycle pulse lengths, 500 or 2500 Hz PRF) was applied through a waveguide at a 45 degree angle with respect to the microscope's field of view, which is aligned to the center of a 100mm polystyrene cell dish. Three different peak acoustic pressures (measured in-situ) were used: 0.13, 0.40, 0.84 MPa (correspond to SPTA intensities of up to 1.168 W/cm2 for our given pulsing parameters). In this work, N2a mouse neuroblastoma was used as the cell model; they were first induced to differentiate into neuronal-like cells using retinoic acid (for 24 h), after which they were seeded onto the cell dish for real-time morphological observations. Ultrasound exposure was applied over a 10 min period, and the resulting morphological behavior was recorded using a video camera (from start of exposure to 100 min after exposure). A subset of experiments was conducted in the presence of Gd3+ stretch-sensitive ion channel blockers or EGTA calcium ion chelators to examine the potential involvement of mechanotransduction.

Results/Discussion

Neurite retraction and cell body shrinkage were found over the exposure period (see figure). The effect was dependent on acoustic intensity: peak acoustic pressure was found to be a more important contributing factor than pulse duration. The morphological changes were found to be non-destructive; indeed, post-exposure neurite outgrowth and

neuritogenesis were respectively observed in neurite-bearing and neurite-less cells (see figure). The morphological changes were suppressed if stretch-activated ion channels were blocked or if calcium ions were chelated. Overall, our results show that ultrasound can potentially influence how neuronal cells develop.

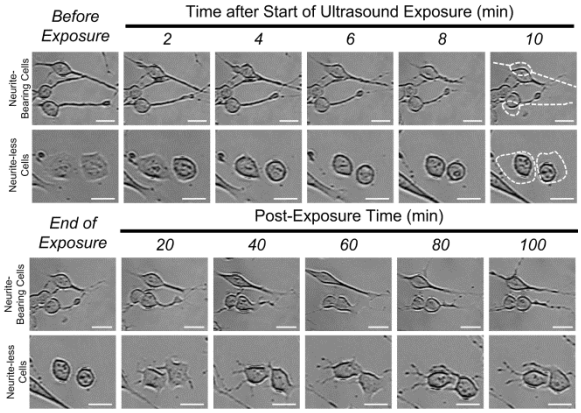

Soft tissue characterization I

Forum Hall

Monday, July 22 2013, 01:00 pm - 04:30 pm

Congress Hallair: **Michael Oelze**
University of Illinois

IUS1-PA5-1

Acoustic characteristics of fatty and fibrotic liver measured by an 80-MHz and 250 MHz scanning acoustic microscopy

Tadashi Yamaguchi[1], Kenta Inoue[2], Hitoshi Maruyama[3], Jonathan Mamou[4], Kazuto Kobayashi[5], Yoshufumi Saijo[6]; *[1]Reseach Center for Frontier Medical Engineering, Chiba University, Chiba, Japan, [2]Graduate School of Engineering, Chiba University, Japan, [3]Department of Gastroenterology and Hepatology, Chiba University, Japan, [4]Lizzi Center for Biomedical Engineering, Riverside Research, USA, [5]Honda Electronics, Japan, [6]Graduate School of Biomedical Engineering, Tohoku University, Japan*

Background, Motivation and Objective

Ultrasound imaging is ideally suited for early-stage assessments of liver steatosis and fibrosis, but conventional ultrasound images based on backscatter do not display quantitative tissue information because conventional ultrasound does not incorporate modeling of the complex interactions between ultrasound and liver tissue in normal and diseased states.

Statement of Contribution/Methods

Two normal, two fatty, and two fibrotic rat livers were harvested, fixed, and embedded in paraffin. From each specimen, a single, central, 10-µm thin section was placed on a microscope slide and scanned in two dimensions (2-D) using a modified scanning acoustic microscope (AMS-50SI; Honda Elec.) incorporating transducers operating at 80 and 250-MHz center frequencies. RF echo signals were digitized with 8-bit precision at a sampling frequency of 2-GHz.

2-D images of speed of sound (SOS) and attenuation were obtained as sizes of 2.4 mm × 2.4 mm and 0.6 mm × 0.6 mm using the 80 and 250-MHz transducers, which have 20- and 4-µm spatial resolutions, respectively. All images contained 300 × 300 pixels.

Results/Discussion

Figure 1 displays the 2-D image of the SOS (Fig. 1a) and the Azan-stained histology image (Fig. 1b) of the fibrotic liver. On these images, fibers with thicknesses of 10-µm (or smaller) are easily visualized on the peripheries of the liver lobules; they have a relatively high SOS value of approximately 1700 m/s and appear blue on the Azan-stained histology image.

The SOS and the attenuation values were calculated by averaging all values within 11 regions of interest (ROIs) from each 2-D image of all six livers. At 250-MHz, the SOS and attenuation values of normal, fatty, and fibrotic livers were 1622±32, 1591±20, 1700±44 m/s and 5.70±0.62, 8.38±0.51, 7.90±1.00 dB/mm respectively. The differences in SOS and attenuation values among liver types were greater at 250 MHz than at 80 MHz because of the improved spatial resolution, which allowed more-optimal placement of ROIs to contain only fatty or fibrotic tissue.

These studies show that fine-resolution measurements allowed by very-high-frequency ultrasound can provide accurate measurements of acoustic properties of different tissue constituents. These measurements can effectively characterize liver state, in particular for non-alcoholic steatohepatitis (NASH) liver in which fat and fibers are intermingled.

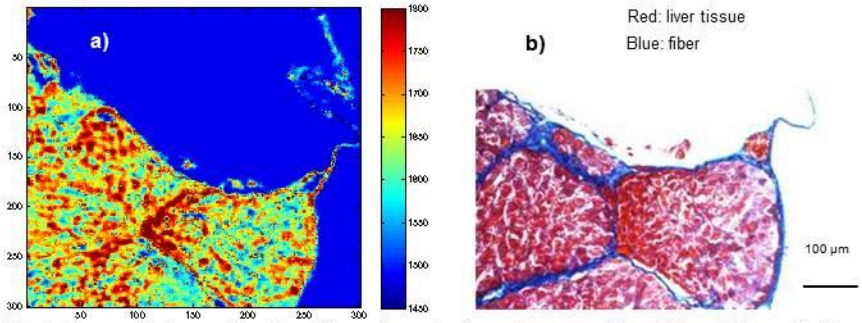

Fig.1: Illustrative results from a fibrotic rat liver. a) speed-of-sound measured from 10-µm thin section by 250-MHz center frequency transducer. b) Azan stained corresponding pathological image of 4-µm thin section.

IUS1-PA5-2

RSNA/QIBA: Shear wave speed as a biomarker for liver fibrosis staging

Timothy Hall[1], Andy Milkowski[2], Brian Garra[3], Paul Carson[4], Mark Palmeri[5], Kathy Nightingale[5], Other Authors[6]; *[1]Medical Physics, University of Wisconsin, Madison, WI, USA, [2]Ultrasound Division, Siemens Healthcare, USA, [3]Division of Imaging & Applied Mathematics, OSEL - CDRH Food and Drug Administration, USA, [4]Radiology, University of Michigan, USA, [5]Biomedical Engineering, Duke University, USA, [6]http://qibawiki.rsna.org/index.php?title=Ultrasound_SWS_tech_ctte, USA*

Background, Motivation and Objective

The Radiological Society of North America (RSNA) has created a Quantitative Imaging Biomarker Alliance (QIBA) to advance the conversion of "imaging systems" into "measurement systems". The goal is to create QIBA/UPICT (Uniform Protocol for Imaging in Clinical Trials) protocols that specify methods for data acquisition, analysis and interpretation as well as QIBA Profiles that will provide specific claims of what can be accomplished by following the QIBA Protocol. The next step is to then validate the profile across imaging systems with phantoms and volunteers through collaborative efforts.

We are developing a protocol and data analysis methods to allow direct comparison of shear wave speed (SWS) measurements in liver for staging fibrosis. Several systems that measure SWS in the liver are commercially available, and several peer-reviewed manuscripts report the ability to differentiate among fibrosis stages. Providing a common SWS estimate among systems would make these studies more clinically viable and speed adoption of the technology.

Statement of Contribution/Methods

The first phase of our study involves SWS estimation in pairs of phantoms that are nearly completely elastic (little loss component). These phantoms are homogeneous cylinders and one of each pair is relatively soft and one relatively stiff (compared to liver). The phantoms were distributed among at least eleven sites for measurements on commercial clinical imaging systems as well as experimental systems under development in some labs. Prior to distribution to those sites, all phantoms were measured in a single lab with a single system to assess the between-phantom component of variance (see figure 1). Each lab had at least three participants scan each phantom at least three times to estimate the bias and components of variance in SWS estimates among systems. In addition, several test samples of the same phantom materials were manufactured for independent material property assessment with dynamic mechanical testing equipment. Magnetic resonance elastography scans of the phantoms are included.

Results/Discussion

A comprehensive analysis of the group SWS measurements is underway. The sources and magnitudes of bias and variance among systems, operators and laboratories will be reported. This study will be followed by similar studies on phantoms with lossy media that more closely mimic living tissues.

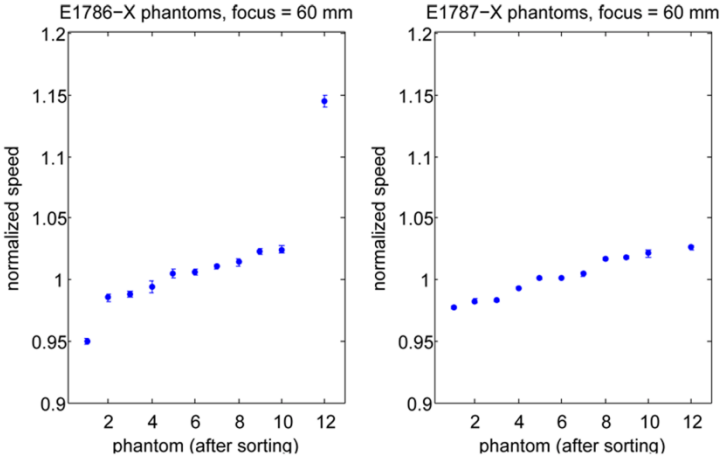

Figure 1: Normalized shearwave speed measurements made in a single laboratory from 22 zerdine phantoms fabricated by CIRS, Inc. (Norfolk, VA) (softer group (left) and stiffer group(right)) used for calibration experiments across 11 laboratories.

IUS1-PA5-3

Influence of heterogeneities on ultrasound attenuation for liver steatosis evaluation (CAP™): relevance of a liver guidance tool

Magali Sasso[1], Stéphane Audière[1], Laurent Sandrin[1], Véronique Miette[1]; [1]*R&D, Echosens, Paris, France*

Background, Motivation and Objective

Controlled Attenuation Parameter (CAP) [1] is a measure of the liver ultrasound attenuation developed to assess steatosis on the Fibroscan® - vibration controlled transient elastography device for the clinical evaluation of liver stiffness-. CAP performance was assessed in clinical studies[1,2,3,4], always showing satisfactory results. However, CAP is based on the hypothesis that liver parenchyma is homogeneous whereas it is not everywhere (blood vessel, nodules, etc.).

The objective of this work is to determine the influence of heterogeneities on CAP and to show the clinical relevance of a liver guidance tool, based on the statistical properties of ultrasound signals, developed to target the homogeneous parenchyma.

Statement of Contribution/Methods

Influence of heterogeneities was assessed on:

Simulations using Field II: Simulations were performed in the Fibroscan® configuration and run in media with overall attenuation varying from 100 up to 350 dB/m at 3.5 MHz (normal range up to massive steatosis). Hypo or hyper echogenic (+/- 3,6 and 12 dB) heterogeneities were embedded (size: 2-10 mm, depth: 25-65 mm) so as to cover heterogeneities usually observed in liver parenchyma;

Tissue mimicking phantoms: acquisitions were performed in homogeneous and heterogeneous parts of 2 phantoms: model G403GS (Gammex), a custom-made phantom (ATS) with hyper and hypo echogenic inclusions with different sizes at different depths;

Clinical data: 30 patients from 3 steatosic groups (no / moderate / massive steatosis) were assessed using the Fibroscan®. Each acquisition zone was tagged as homogenenous / heterogeneous by 2 expert operators (blind evaluation, with consensus if discordant).

For each acquisition, CAP and the liver guidance tool values were assessed.

Results/Discussion

Preliminary results show that the size, amount and characteristics of heterogeneities influence CAP (cf. Fig 1). Relative difference reach 50% and in that case CAP does not represent the liver parenchyma which may induce false diagnosis. The liver guidance tool allows the detection of homogenous parenchyma zone and its use in clinical practice is promising to enhance liver steatosis evaluation using Fibroscan®.

1. Sasso et al., UMB, v. 36, p. 1825-35, 2010

2. Sasso et al., J Viral Hep, v. 19, p. 244-53, 2012

3. Myers et al., Liver Int, v. 32, p. 902-10, 2012

4. de Ledinghen et al., Liver Int, v. 32, p. 911-18, 2012

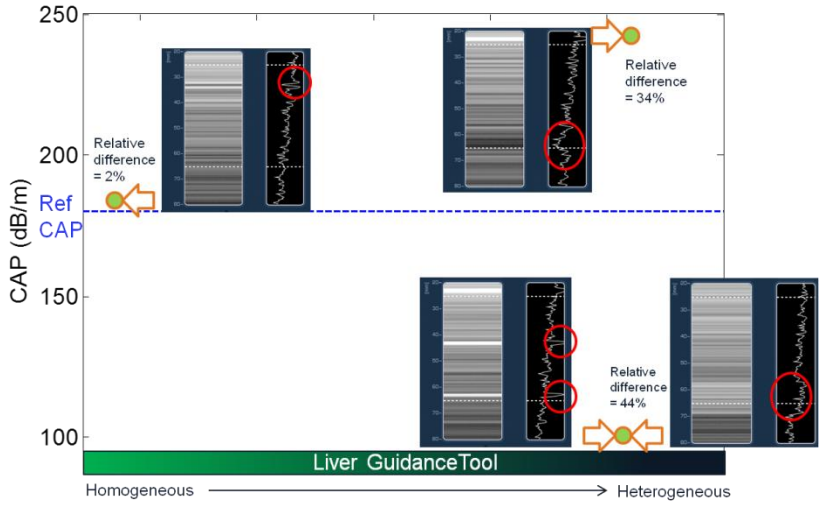

IUS1-PA5-4

Quantitative evaluation method of liver fibrosis using multi-Rayleigh model with three echo envelope components

Tatsuya Higuchi[1], Shinnosuke Hirata[1], Tadashi Yamaguchi[2], Hiroyuki Hachiya[1]; [1]*Graduate school of Science and Engineering, Tokyo Institute of Technology, Meguro-ku, Tokyo, Japan,* [2]*Research Center for Frontier Medical Engineering, Chiba University, Japan*

Background, Motivation and Objective

The realization of the quantitative diagnosis method of liver fibrosis using ultrasound echo signal is highly required. The probability density function of ultrasonic the echo amplitude from a homogeneous medium with high scatterer density, such as normal liver, can be approximated by Rayleigh distribution. As liver fibrosis progresses, the amplitude distribution of the echo signal deviates from Rayleigh distribution. In our study, we proposed a quantitative method for liver fibrosis staging based on new echo envelope model.

Statement of Contribution/Methods

In our previous model, the approximation accuracy is insufficient at region with low intensity part like a hypo-echoic nodule or a blood vessel. We examined multi-Rayleigh model with three Rayleigh distributions. Each Rayleigh distribution corresponds to the distribution of echo amplitude from low intensity parts, normal and fibrous tissue respectively. Parameters of multi-Rayleigh model with three components were estimated by expectation maximization (EM) algorithm using clinical data. Clinical data were classified into F0 (normal liver), F2 (moderate hepatitis), F3 (late hepatitis), and F4(liver cirrhosis) in accordance with the new-Inuyama classification based on the result of biopsy. We also showed quantitatively that proposed model can be modeling the amplitude distribution of liver fibrosis echo data with low intensity parts adequately using K-L divergence, that is an index of the difference between two probability distributions.

Results/Discussion

Figure shows the estimated fibrous indices of Multi-Rayleigh model with three components using clinical data. Multi-Rayleigh model with three components has two fibrous indices. One is a parameter corresponding to the rate of fibrous tissue in the ROI, and the other is a parameter corresponding to the degeneration degree of fibrous tissue. In Figure, the angle along the circumference is the rate of fibrous tissue, and the radius is the degeneration degree of fibrous tissue. Fibrous index was estimated stably and it is found that this value increases as the liver fibrosis progresses.

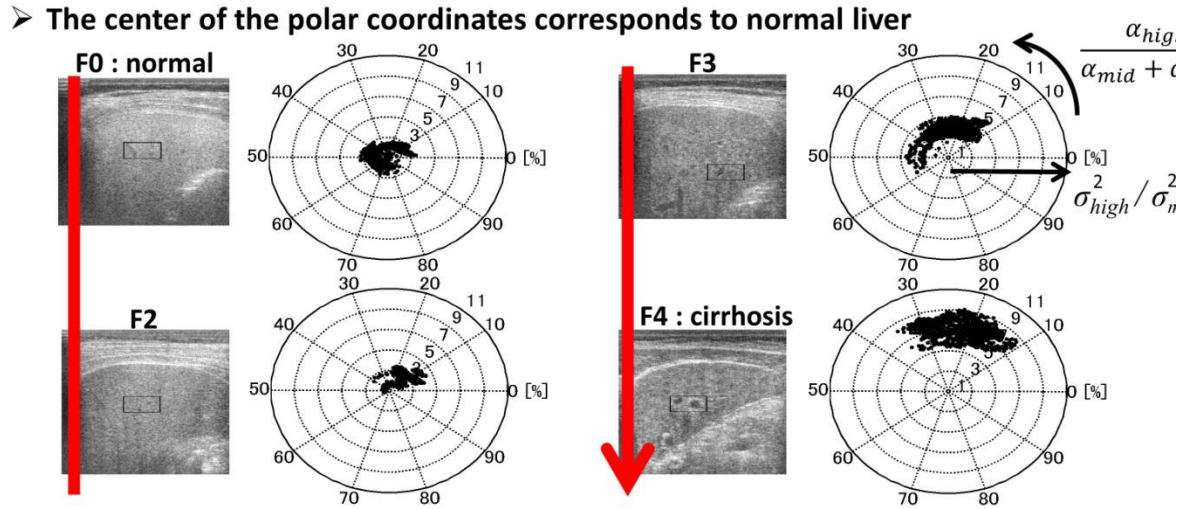

IUS1-PA5-5

Effect of Scanning Direction on the Statistical Parameters of Ultrasonic Signals Backscattered from the Annular Pulley and Tendon

Yi-Hsun Lin[1], Chih-Chung Huang[2], Tai-Hua Yang[3], Shyh-Hau Wang[1], Fong-Chin Su[3]; *[1]Computer Science and Information Engineering, National Cheng Kung University, Tainan, Taiwan, [2]Fu Jen Catholic University, Taiwan, [3]Biomedical Engineering, National Cheng Kung University, Taiwan*

Background, Motivation and Objective

Previous study has demonstrated that quantitative parameters estimated from backscattering signals are capable of characterizing pulley and tendon tissues for being applied to diagnose the trigger finger syndrome. Yet, the probability density functions of the envelope signals were found to vary significantly between signals acquired from the axial and sagittal views of samples. To extensively explore possible causes, measurements were performed, using a 30 MHz high-frequency ultrasound incorporated with theoretical considerations, to further comprehend the effect of ultrasonic scanning direction on the estimation of statistical parameters from backscattering signals of the annular pulley and tendon.

Statement of Contribution/Methods

The *ex vivo* experiments began with the preparations of pulley and tendon tissues excised from the first annular pulley region of cadavers. The tissue samples were then immersed in a saline solution tank. The ultrasound system was arranged to allow the scanning of tissues from the direction parallel to the fiber axis, at 0^o, to that of perpendicular direction, at 90^o, where the increment of scanning angle is 5^o. Statistical parameters, including Nakagami parameter (m) and scaling parameter, were estimated from regions of the acquired backscattering signals. Histological slices were also made for results verification.

Results/Discussion

B-mode images in Fig. 1(a) are the annular pulley and tendon tissues corresponding to the scanning directions of 0^o and 90^o. The scaling parameters associated with pulleys and tendons of different scanning angles did not vary significantly; while those of the corresponding m tended to decrease exponentially, as shown in Fig. 1(b). The m of tendon tended to decline with the increase of scanning angle, and which is faster than that of pulley. Specifically, the m parameters of pulley and tendon tissues decreased respectively from 1.06 ± 0.10 to 0.88 ± 0.07 and from 1.04 ± 0.07 to 0.54 ± 0.14. The empirical results are consistent with Nakagami statistical distribution, and which demonstrate that m could be applied to quantitatively assess the degree of fiber orientation for tissue characterization. It is also feasible to combine m parameter with the scanning direction consideration for further diagnosing the trigger finger syndrome.

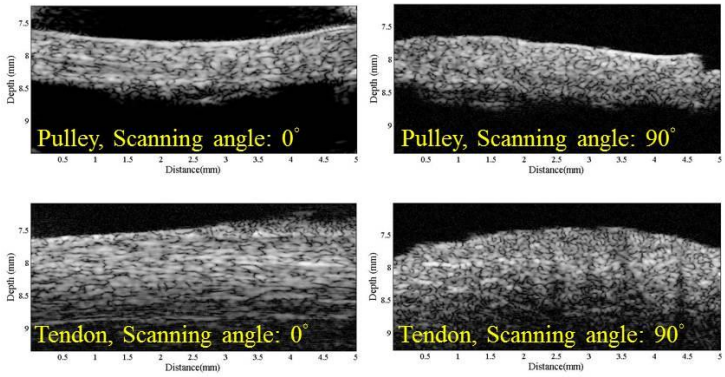

Fig. 1(a)

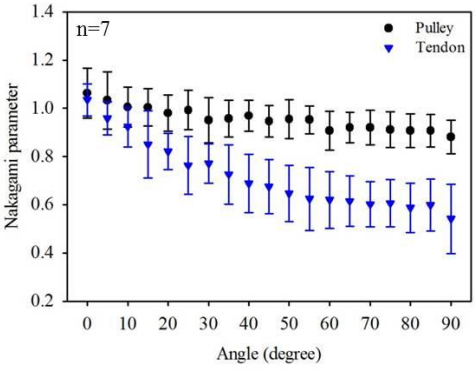

Fig. 1(b)

IUS1-PA5-6

Modeling volume power spectra for collections of spheres in finite containers

Adam C. Luchies[1], **Michael L. Oelze**[1]; *[1]Department of Electrical and Computer Engineering, University of Illinois at Urbana-Champaign, USA*

Background, Motivation and Objective

When modeling the power spectrum for a collection of randomly positioned scatterers, the assumption is usually made that the incoherent component of the spectrum is much larger than the coherent component. With this assumption, scattering form-factor models such as the Gaussian, fluid-filled sphere, etc. can be fitted to the power spectrum of scattered ultrasound signals for the purpose of estimating parameters such as the scatterer size. The accuracy of the assumption concerning incoherent and coherent component spectrum magnitudes was studied using simulations of spheres in a finite container.

Statement of Contribution/Methods

A collection of spheres with a specific number density was simulated and the volume power spectrum was computed by taking the 3D Fourier Transform and squaring the modulus. Realizations of spheres with random positions within a cubical or spherical container were simulated and the resulting volume power spectra were averaged to study the expected value of the power spectrum versus different number densities of spheres. These results were compared to the volume power spectrum for a single sphere (i.e., the fluid-filled sphere form factor). A single sphere volume power spectrum is expected if no coherent component in the spectrum exists.

Results/Discussion

For low number density, the volume power spectrum for a collection of spheres matched the fluid-filled sphere form factor. As volume fraction increased, the volume power spectrum became biased for low values of ka compared to the power spectrum for a single sphere. For a 2% volume fraction, the relative percent error (RPE) between the on-axis experimental spectrum and the spectrum for a single sphere was -3% and -12% for ka=0.5 and ka=1.0, respectively. For a 20% volume fraction, the RPE was 240% and 77% for ka=0.5 and ka=1.0, respectively. The source of this bias can be attributed to the interaction of sphere positions. As more spheres are placed in the container, their positions become less random, increasing the effect of the coherent component relative to the incoherent component. The simulations also indicated that that the container shape affected the shape of the volume spectrum. When using a cube as the container for the collection of spheres, asymmetry was observed in the volume power spectrum. Specifically, peaks were present on-axis in k-space that were not present off-axis nor in the power spectrum for a single sphere. When changing the container to a sphere, the volume power spectrum was symmetric and the on-axis peaks observed for the cube container were not present. The results of this study indicate that when modeling the effects of scattering using single scattering approximations, a large number density may yield a significant coherent component in the power spectrum and the shape of the scattering volume must be taken into account. The work was supported by NIH Grant R01-EB008992.

IUS1-PA5-7

Time domain analysis of causal and noncausal fractional wave equations

Xiaofeng Zhao[1], **Robert McGough[1]**; [1]*Electrical and Computer Engineering, Michigan State University, East Lansing, MI, USA*

Background, Motivation and Objective

The attenuation of ultrasound propagating in human tissue follows a power law with respect to frequency. Power law attenuation is described by several wave equations with fractional derivatives, where some models are causal, and some are noncausal. To demonstrate the similarities and differences in the time domain responses predicted by causal and noncausal models, the Green's functions for two related fractional wave equations are calculated numerically and the results are compared.

Statement of Contribution/Methods

Comparisons between related causal and noncausal Green's functions yield similar results in the farfield region, yet significant differences are evident in the extreme nearfield region. This is demonstrated by numerically evaluating the noncausal and causal Green's functions for the power law wave equation and for the Caputo fractional wave equation, respectively, and comparing the results for fat with a power law exponent of y=1.5.

Results/Discussion

Simulation results show that, although the attenuation closely matches over a wide range of ultrasound frequencies, the time domain responses for these two fractional wave equations differ in the nearfield region. Furthermore, the noncausal features of the numerically calculated time domain response, if present, are only evident in the extreme nearfield region. Simulation results also show that, in the far field, the causal and the noncausal Green's functions converge to the same time domain result. The results of these simulations therefore indicate that, in the context of power law attenuation, causality is essentially a nearfield phenomenon, and the time responses for these causal and noncausal Green's functions are approximately the same in the farfield region. [Supported in part by NIH grant R01 EB012079].

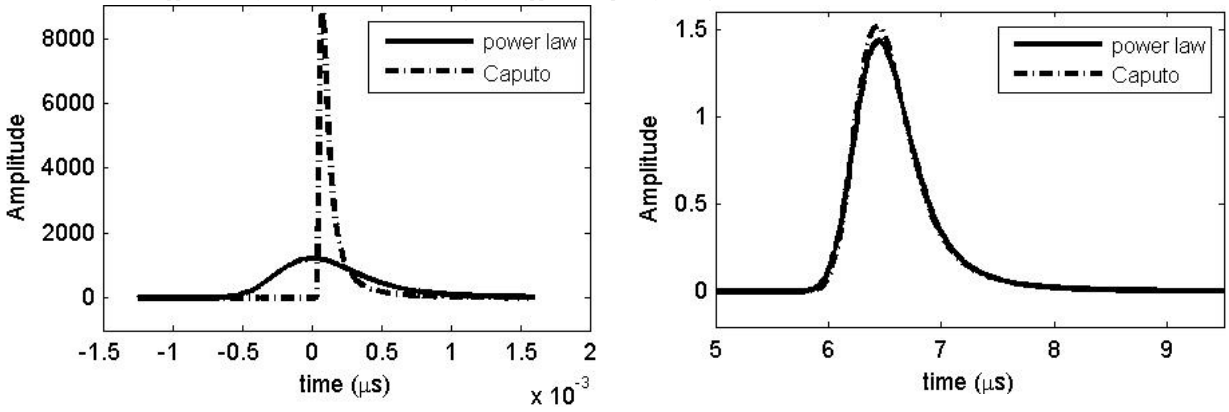

IUS1-PA5-8

Estimation of quantitative ultrasound parameters derived from backscatter coefficients using plane wave compounding – A comparative simulation study

Roberto Lavarello[1]; [1]*Sección Electricidad y Electrónica, Pontificia Universidad Católica del Perú, San Miguel, Lima, Peru*

Background, Motivation and Objective

Quantitative ultrasound (QUS) based on backscatter coefficient (BCS) estimation has shown potential for tissue characterization. Even though beamforming using plane wave compounding (PWC) has shown advantages for echographic, Doppler, and elastographic imaging, to this date PWC has not been evaluated for the purpose of BSC estimation. The objective of this study is to analyze through simulations the performance of BSC-based QUS when using PWC versus single focus beamforming.

Statement of Contribution/Methods

Simulations were performed with FIELD II using a 6.5 MHz, 128-element array with 0.3 mm element pitch. Beamforming was produced both with a single focus at 3 cm and with PWC with 60 transmission angles, with the focal number set to two in both cases. BSCs were estimated using the reference phantom method. The reference and sample phantoms had a concentration of 16 scatterers/mm^3 with backscatter cross-sections corresponding to fluid spheres with diameters of 35 and 70 μm, respectively. Both the effective scatterer diameter (ESD) and concentration (ESC) were derived from the estimated BSCs. The effects of noise and mismatches Δc in the sound speed of sample and reference phantoms were assessed by (1) corrupting the pre-beamformed data with additive Gaussian noise corresponding to peak echo signal-to-noise ratios (eSNRs) of down to 20 dB in the beamformed data, and (2) simulating sample phantoms with Δc between -4% and 4%.

Results/Discussion

In the presence of noise, the use of PWC allowed producing estimates with a lower, more uniform variance than the use of a single focus (i.e., PWC ESD and EAC standard deviations of less than 15% and 3 dB, respectively versus single focus ESD and EAC standard deviations of more than 40% and 20 dB, respectively for a peak eSNR of 20 dB). In the presence of phantom sound speed mismatch, PWC produced ESD estimates with a slightly larger (i.e., up to 5%) bias. Even though in the noiseless case single focus beamforming outperformed PWC by up to 6 dB in terms of ESC estimation bias away from the focal region, this improvement was compromised in the presence of noise. For illustration, Figs. 1a-1b show the ESD and EAC estimation errors, respectively, for a peak eSNR of 20 dB and $\Delta c = 0$ and Figs. 1c-1d show the ESD and EAC estimation errors, respectively, with noiseless data and $\Delta c = 4\%$. These results suggest that PWC may provide benefits to BSC-based QUS imaging.

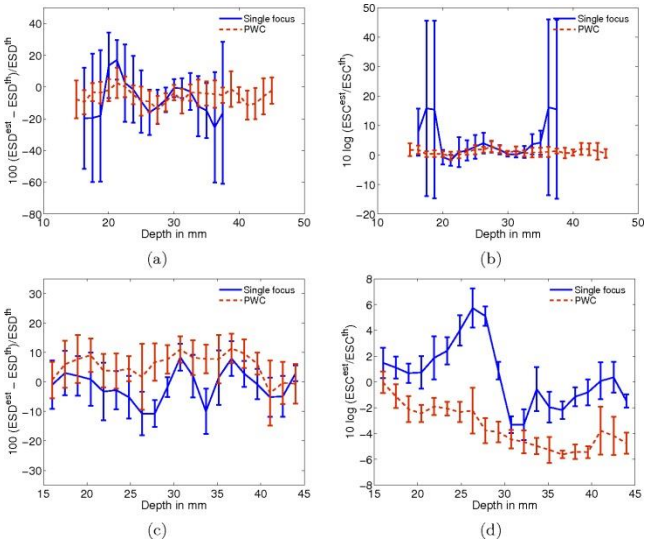

IUS1-PA5-9

Characterization of scatterers concentration in cataract lens using Nakagami distribution by ultrasounds

Miguel Caixinha[1], Danilo Jesus[1], Elena Velte[2], Mário Santos[1], Jaime Santos[1]; *[1]Department of Electrical and Computer Engineering, University of Coimbra, Coimbra, Portugal, [2]Department of Physics, University of Coimbra, Coimbra, Portugal*

Background, Motivation and Objective

Cataract affects more than 20 million people in the world. Its formation is associated with the increase of the protein aggregation in the lens eye. In the early stages the protein aggregates act as light scatterers and in advance stages these aggregates increase in size preventing the light propagation through the eye. This work aims to analyze the protein aggregates spatial distribution, concentration, and average dimension, for different stages of cataract formation, and to explore their impact in the ultrasound attenuation.

Statement of Contribution/Methods

Fifty porcine lenses with different degrees of induced cataract were sliced to analyze the protein aggregates properties. Cataract was induced by lens immersion in an ethanol:2-propanol:formalin solution over time ranging from zero (lens without cataract) to 180min (lens with total cataract), every 20min. Slices of 2 mm in thickness were extracted from two different regions (nucleus and cortex), to locally analyze the scatterers distribution and concentration. A 25MHz focused ultrasonic transducer provided the backscattering signals used to estimate the frequency dependent attenuation and the Nakagami parameter m. The slices were also imaged using very high frequency acoustic microscopy (C-Scan) and conventional microscopy. The information provided by both types of the images were compared and correlated with the Nakagami parameters calculated from the ultrasound backscattering signals.

Results/Discussion

The variation of the Nakagami parameters, scatterers distribution and average sizes, allowed to establish valid correspondences with the attenuation, in the two considered regions (nucleus and cortex) and for different degrees of cataract.

A good correlation was found between the Nakagami parameter and the attenuation in the two considered regions (nucleus and cortex) for all immersion times ($p<0.001$). Concerning to the scatterers distribution and Nakagami parameters, statistically differences were found between those two regions.

The results obtained by the high frequency C-Scan and microcopy images are in good agreement concerning the protein aggregates distribution, which was confirmed by the good correlation found between local attenuation and the identified regions of high scatterers concentration ($p<0.001$).

The results suggest that the interpretation of backscattering signals by the Nakagami distribution, when combined with the knowledge of the physical scatter properties are challenging for obtaining a distribution map of cataract hardness by a noninvasive way.

IUS1-PA5-10

Performance of an Adaptive Multitaper Method for the Reduction of Coherent Noise in the Spectral Analysis of Ultrasound Backscattered Echoes

Ivan Rosado-Mendez[1], Timothy Hall[1], James Zagzebski[1]; *[1]Department of Medical Physics, University of Wisconsin-Madison, Madison, Wisconsin, USA*

Background, Motivation and Objective

This work is a simulation-based investigation of the performance of an adaptive multitaper (aMTM) method of spectral estimation for reducing apparent coherence from limited samples of random scatterers. The motivation is to create high spatial resolution, low-noise parametric images of Quantitative Ultrasound (QUS) parameters that assume incoherent scattering. The aMTM is compared to conventional PSD estimation methods and the dependence of coherence noise reduction on scatterer density and pulse bandwidth is studied.

Statement of Contribution/Methods

Pulse-echo simulations convolved a Gaussian-envelope, 6MHz acoustic pulse with 3000 independent realizations of one-dimensional assortments of randomly distributed scatterers (diffraction and attenuation are ignored). The pulse bandwidth was varied between 25% and 100% and the scatterer density varied between 2 to 20 scatterers per pulse length. The PSD for a waveform was estimated as the average of individual PSDs from gated segments of a subset of the independent realizations. Individual PSD estimates were computed with the periodogram using low-leakage tapering functions, Welch's method with different subsegment length and overlap ratios, and Thomson's multitaper method with $3<NW<13$. We investigate a window-length/bandwidth adaptive NW criterion (the aMTM) when estimating PSD-derived parameters such as the backscatter coefficient. The bias, standard deviation, and mean squared error (MSE) of the PSD estimates were computed when reducing the window size from 1 to 50 pulse lengths axially and 1 to 50 averaged realizations laterally. For a particular MSE value, the window size leading to equal contributions of the bias and coherence noise was determined and the diagonal of this window (D_w) was used as a criterion for comparison among PSD estimation methods.

Results/Discussion

Welch's and the multitaper method led to 71% and 72% reductions in (D_w) compared to that of the periodogram regardless of the tapering function. The aMTM reduced (D_w) by 11% compared to the optimum Welch's estimator (25% subsegment length and 75% overlap ratio). These values did not vary with different pulse bandwidths or scatterer densities above 10 scatterers per pulse lengths, agreeing with existing theoretical models. The proposed criterion for automated NW selection successfully adapted to the high bias or coherent noise scenarios showing the advantage of the aMTM for the spectral analysis of incoherent backscattered signals.

IUS1-PA5-11

A Multitaper, Generalized Spectrum Technique for Detection of Periodic Structures in Tissue: Comparison with conventional methods.

Ivan Rosado-Mendez[1], Lindsey Carlson[1], Timothy Hall[1], James Zagzebski[1]; [1]*Department of Medical Physics, University of Wisconsin-Madison, Madison, Wisconsin, USA*

Background, Motivation and Objective

Quantifying features related to acoustic scatterer periodicity can provide useful information to monitor tissue structural changes, but their detection is hindered by apparent coherence from random scatterers. This work compares the use of the periodogram-based Generalized Spectrum (pGS) , a multitaper Generalized Spectrum (mtGS), and the Singular Spectrum Analysis (SSA) for detecting periodicity in backscattered echo signals when reducing the ROI size.

Statement of Contribution/Methods

A phantom with Rayleigh scatterers and an array of 100µm-diameter nylon fibers spaced 400µm apart was scanned with a Siemens S2000 using a linear array transducer. Radiofrequency (RF) echo signals from the fiber plane were obtained and GS-estimates were made either by the pGS or by a multitaper strategy with Slepian sequences. Spectral components corresponding to periodic structures were identified by peaks in the GS Collapsed Average. SSA was implemented by obtaining eigenvalues and eigenvectors of the autocovariance matrix of signal segments. The periodic component of the RF signal was reconstructed using pairs of eigenvectors with similar eigenvalues. The frequency of the periodic component was estimated from the maximum value of its power spectrum. Histograms of frequency components detected by each method were constructed. The conspicuity of the 1.9MHz peak (corresponding to the fiber spacing) was measured as the ROI size was reduced from 20 to 2 pulse lengths.

Results/Discussion

Histograms (Fig.1) of the frequency components detected with (a)SSA, (b)pGS, and (c)mtGS show the mtGS improves detection of the relevant frequency components (1.9MHz and its harmonic) compared to pGS and SSA by reducing the presence of spurious components. The minimum window size to detect periodicity was 3.6, 5.2 and 10 pulse lengths for the pGS, mtGS and SSA, respectively. Results motivate use of the multitaper GS particularly for creating parametric images based on detection of periodic structures.

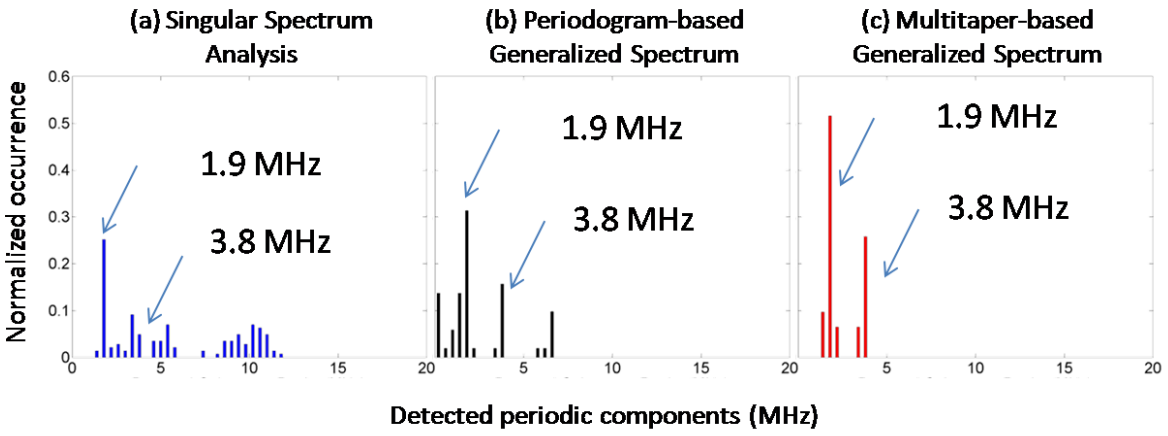

NDE Signal Processing

Forum Hall

Monday, July 22 2013, 01:00 pm - 04:30 pm

Congress Hallair: **Ramazan Demirli**
Villanova University

IUS2-PA1-1

Performance evaluation of 3D compression for Ultrasonic nondestructive testing applications

Pramod Govindan[1], **Jafar Saniie[1]**; *[1]Electrical and Computer Engineering, Illinois Institute of Technology, USA*

Background, Motivation and Objective

Ultrasonic imaging applications require large volumes of data. Therefore, it is essential that the signal has to be compressed without degrading the signal quality or inadvertently damaging desirable signal features. The objective of this study is to design 3D compression and evaluate the degree of compression of ultrasonic data as a function of data integrity.

Statement of Contribution/Methods

For high-definition data and detecting small and transient features within the signal, the signals are often sampled at much higher rate than one analytically may require capturing the essence of the signal. Sampling at a rate higher than Nyquist will ensure a high SNR. However, this oversampling generates huge amount of data with a lot of redundant information. The signal compression involves removing the redundant and irrelevant components of the signal. An efficient method is Discrete Wavelet Transform (DWT), which is used for ultrasonic compression applications due to its high energy compaction properties. Another method is by decimation where the redundant information is removed, and this may cause degradation of time resolution. However, the decimated signal may need to be interpolated when certain signal features with fine time resolution are required. The shift-properties of Fourier Transform are used to recover the decimated samples and to reconstruct and interpolate the signal.

Results/Discussion

A volumetric image of 128 x 128 x 2048 samples (33 MB of data) is used for the analysis of results. This experimental data was generated by using a 5 MHz, 0.5 inch diameter broadband transducer. A 2 inch by 2 inch surface of a steel block was used for the test. 128 A-scans (each A-scan has 2048 sample points) are taken along both the spatial (y and z) directions. The study of correlation properties between A-scans indicates that there is a high correlation between neighboring A-scans. Through extensive evaluation of ultrasonic A-Scans, we have found that many of the wavelet coefficients have almost zero energy and, therefore, can be ignored resulting in a total 3D compression of up to 98% with a Peak Signal-to-Noise Ratio (PSNR) of 20 dB. The study of variation of PSNR with the compression ratio shows that the PSNR can be improved (from 20 dB to 23 dB) by a marginal reduction in the compression ratio (from 98 to 95 %). Further this study shows the compression can be maximized by the proper selection of wavelet basis. Various compactly supported wavelet basis are experimented and found that Daubechies basis gives best compression with high quality reconstruction compared to other basis like Haar, Coif and Symlet. In summary, ultrasonic signal compression is performed by using 2 methods – DWT and decimation. Both give high compression ratio with a high quality reconstruction. By carefully choosing the right wavelet basis according to the signal characteristics, maximum compression can be achieved without degrading the quality of reconstruction.

IUS2-PA1-2

Image Compilation in multi-transducer Ultrasonic System

Aryaz Baradarani[1], **Fedar Seviaryn[1]**, Roman Maev[1]; *[1]Institute for Diagnostics Imaging Research, University of Windsor, Windsor, Ontario, Canada*

Background, Motivation and Objective

The objective of the presented work is to develop an algorithm to process ultrasonic data collected by a multi-channel acoustical microscope which has several focussed transducers mounted on one mechanical scanner. Its parallel operation allows significant reduction in scanning time as each transducer performs scanning of fracture of total area. The resulting image is formed as combination of partial data sets acquired by the channels. The assembly procedure shall overcome mechanical instability of the transducer frame, difference in parameters of individual transducers and general image distortion.

Statement of Contribution/Methods

The described procedure was realized in the prototype of advanced fingerprint reading system. Set of four spherically focused 50 MHz acoustic lens operating in pulse-echo mode was mounted on unique cylindrical scanner accommodating specific geometry of the finger. Each transducer is connected to an independent pulser, receiver and digitizer channel. The spiral lens trajectory eliminates repeatable acceleration, reduces vibration and allows constant data flow on maximal rate. The sequential operation of lenses creates interlaced volume of data which stored in form of 3D cube for each channel. Afterward data processing includes compensation of transducer shaking, leveling of parameters for individual scans and adaptive extraction of C-scans. Further overlapping of partial C-scans with interpolative adjustment gives the output image.

As an application, this technology has been demonstrated in providing high quality acoustic image of fingerprint including different levels of information: fingerprint pattern, sweat porous locations, and dermis structures. These additional characteristics can significantly facilitate fingerprint based identification task.

Results/Discussion

The novel scanner accommodating several transducers was designed, built and tested. General principles developed during this work can be applied for other configurations with data acquisition from multiple acoustic transducers. Advanced data processing algorithm, developed and adapted for specific fingerprint application in this paper, provides proper function of multi-transducer system and compensates mechanical imperfections of the real device. The obtained high quality fingerprint images indicate the effectiveness of the approach whereas the results compare favorably to the current best paper-print fingerprint images.

IUS2-PA1-3

3D Locating system for Augmented Reality glasses using coded ultrasounds

Riccardo Carotenuto[1]; *[1]DIIES, Università Mediterranea di Reggio Calabria, Reggio Calabria, Italia, Italy*

Background, Motivation and Objective

Augmented Reality (AR) is the new frontier of the human-machine interfaces. Giants of consumer electronics (Google, Microsoft, Apple, Canon, etc.) are currently working on prototypes of glasses with head mounted displays that superimpose additional information to the real world scene. AR systems need to know the point of view of the user with a high degree of accuracy, in order to correctly superimpose supplemental information to the scene.

In past works, the author presented different prototypes of locating systems based on airborne ultrasounds, fast and accurate enough for the implementation of touchless gestural interfaces. In this work, the development of a first prototype of a modified locating system well suited to work in conjunction with AR glasses is reported.

Statement of Contribution/Methods

The prototype is composed of four wideband microphones fixed to a glasses frame, of a set of beacons, and of a central unit. Each microphone has its own signal conditioning circuitry, while there is only one shared circuitry for the RF coding and emission, together with a small battery. The beacons emit a sequence of ultra-acoustic (in the 20 – 48 kHz band) coded bursts in the space region containing the microphones. When the microphones are reached by the acoustic coded signal, a return signal is sent back through a coded RF transmission channel to a central unit that computes the positions of the microphones. The RF signals are acquired by the central unit, which carries out the distance computation and then the microphones location by applying an ad hoc algorithm to identify and discard possible false signals due to echoes and environmental noise.

Results/Discussion

A working prototype of the absolute 3D position and orientation system has been realized, using four microphones fixed to a commercial glasses frame (see figure). The locating system uses an improved ultrasound signal coding for immunity to noise and a new geometrical processing method for robust rigid body position and orientation computing. The measured positioning standard deviation was about 6 mm in all the three spatial directions within a range of 300 cm.

All the computations are carried out by the central unit, and the simple remote device circuitry can be easily realized with low cost ASIC and low power consumption. The achieved rate of 25 Hz is fast enough for the majority of the intended AR applications.

IUS2-PA1-4

A New Sonar Localization Strategy Using Receiver Beam Characteristics

Francesco Guarato[1], James Windmill[2], Anthony Gachagan[2]; [1]*Centre for Ultrasonic Engineering, Electronic and Electrical Engineering, University of Strathclyde, Glasgow, United Kingdom,* [2]*Electronic and Electrical Engineering, University of Strathclyde, Glasgow, United Kingdom*

Background, Motivation and Objective

Sonar systems aiming to reproduce echolocation often comprise an emitter and two receivers through which a broadband signal is produced and echoes from targets around the source are collected. The time between sound emission and reception for each receiver is often used to determine the location of the target whereas knowledge of the system's directivity characteristic has rarely been considered. In this work, the emitter has a flat response within a limited set of orientations, while the receivers are designed with two shapes to make their beam patterns directional. Subsequently, the emitted acoustic signal is reflected back to the receivers and filtered through the beam pattern of each, thus altering the amplitude of the echo depending on frequency and direction. This feature is used discern the incoming signal's orientation.

Statement of Contribution/Methods

The received echoes can be modeled to include the emitted signal, receiver beam pattern filtering, air absorption and attenuation. It is possible to remove all of these contributions, except the information related to the beam pattern filtering, by dividing the two received signals to produce a ratio, for each frequency component of the signal. This ratio of the received signals is then compared to the corresponding ratio calculated from the acoustic beam pattern of the two receivers, and defined over the whole set of orientations. Target orientation is estimated as the one providing the closest match, across the frequency spectrum, between the ratio derived from the beam patterns at that orientation and the ratio associated with the simulated received echoes. A corresponding comparison can be carried out by calculating the difference of the received echoes across the frequency spectrum and the difference of the two beam patterns, this being defined over the whole set of orientations. In order to allow a comparison of the two obtained differences, the received signals have also been divided by the emitted signal, while attenuation due to distance and air absorption cannot be excluded using the difference technique.

Results/Discussion

Several target locations were chosen to test the localization method through a simulation program. The target distance is calculated from time of flight: therefore, distance was considered to be known and the simulations only performed estimates of target orientation. 25 orientations spanning the beam pattern domain (60 degrees in the elevation direction, 90 degrees along the azimuth) were estimated in noisy conditions (SNR between 15dB and 50dB) and using 2 different beam patterns: an acoustic simulation of the *Phyllostomus discolor*'s left ear; and an ideal beam pattern with linear attenuation over orientations in the azimuth and elevation. The accuracy in estimating target orientation strongly depends on the beam pattern shape across the frequency spectrum, with error values between the true and the estimated orientations range from 0.1 to 5 degrees achieved.

IUS2-PA1-5

A Novel use of Signal Processing tools for fault detection in IC Engines

Sreedhar Puliyakote[1], Dr. Krishnan Balasubramaniam[1]; [1]*Mechanical Engineering, Indian Institute of Technology,Madras, Chennai, Tamil Nadu, India*

Background, Motivation and Objective

Condition Monitoring of Internal combustion engines is becoming more and more crucial as the engine designers try to achieve better fuel efficiency and/or more power while adhering to the stringent pollution control norms practiced today. Most of the condition monitoring practices follows a periodic maintenance model or in case of cheaper engines, none at all. Keeping in mind the importance of continuous monitoring of critical parts of engine like piston rings and cylinder liner there are a number of real time condition monitoring methods in practice.

Statement of Contribution/Methods

Our work deals with an unconventional use of signal processing tools on Acoustic Emission (AE) from engine cylinder liner to identify or enhance the features associated with various faults commonly found in critical engine components. Experimental data is obtained from a small petrol engine in which various fault conditions are recreated. Signals collected from the engine running with bad piston, worn out piston rings and under lubricant oil level were analyzed.

Results/Discussion

A novel unconventional signal processing method involving wavelet transform is used to analyze the signals under these fault conditions. The results are compared with existing popular signal processing tools like FFT and STFT. Figure1 below shows a comparison of STFT spectrogram and scalogram obtained using the novel wavelet algorithm applied on a signal acquired under lubricant oil starvation. This method offers a unique and reliable way for online monitoring of IC engines for early warning of impending faults.

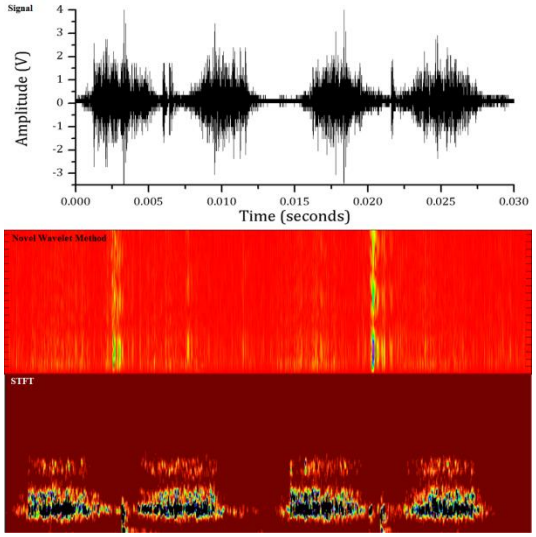

NDE Transducers

Forum Hall

Monday, July 22 2013, 01:00 pm - 04:30 pm

Congress Hallair: **Kentaro Nakamura**
Tokyo Institute of Technology

IUS2-PA2-1

Parametric evaluation of NDE pulsed ultrasonic responses including relevant realistic inductive and non-linear piezoelectric & electronic phenomena

Abelardo Ruiz[1], **Antonio Ramos[2]**, J. Luis San Emeterio[3], Halim Azbaid[4]; *[1]Lab. Ultrasonic Systems, CSIC, Spain, [2]Lab. Ultrasonic Systems, CSIC, Madrid, Spain, [3]CSIC, Spain, [4]CSIC, Madrid, Spain*

Background, Motivation and Objective

Global behaviour on high-voltage (HV) equipment for ultrasonic NDE depends on complex effects from Driving-Receiving (D/R) electronics [1]. But, usually, these effects are only included for analysis with too simplified approaches. Further, reactive & Non-Linear Influences (NLI) of front-end electronics strongly modify responses. In fact, practical NDE systems contain inductances and semiconductors

Non-ideal aspects in NDE commercial units, need still careful analyses to properly know their quantitative implication on final inspection data. Efficiency, axial resolution and dynamic range are greatly influenced by piezoelectric and front-end hardware stages. Here, accurate models, including realistic inductive phenomena and NLI of piezoelectric & electronic stages, are applied to numerically predict global pulsed ultrasonic responses in HV practical NDE units.

Statement of Contribution/Methods

A global pulse-echo (P-E) modeling in PSPICE format is proposed to analyze Time & Frequency Responses (TFR), in HV driving pulses and P-E signals of practical NDE systems, with: a) an equivalent circuit including a quadratic approach [2] for mechanical losses in piezoceramics; b) relevant non-ideal frequency-dependent effects of reactive nature and NLI in spike generators. 2) The possible responses fan in the electrical behavior of pulsed D/R stages is found, by means of an extensive parametric analysis of key aspects, damping resistor (Rd) and energy-discharge capacitor (Cd), in HV pulsers under distinct inductive tuning

Results/Discussion

1) P-E performance for damping and inductive matching combinations is found. 2) Influence of Cd is analyzed under light & strong damping conditions (L&S DC). 3) TFR of spikes & echoes are evaluated; an useful merit figure for pulses, involving amplitude & bandwidth (Fig. 1), is computed and tested. 4) Some key simulated and experimental results are compared with very good agreement.

- Significant NLI (from piezoelectric losses and HV driving) on NDE responses, are accurately quantified, showing they must be included in a real modelling of new NDE ultrasonic designs. Effects of inductive tuning and Cd value (for L&S DC) show a relevant influence on spike & echo pulses.

[1] A. Ramos et al. IEEE Trans. UFFC, 47, 4, 2000, pp. 826-835

[2] A. Ramos et al. Ultrasonics 44, 2006, pp. e995–e1000

Fig.1. (Spectral Peak - Bandwidth) Product for L&S DC

.

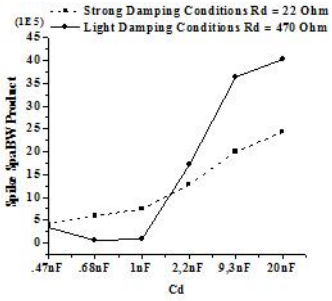

IUS2-PA2-2

Transducer Excitation with Switched-Mode Encoded Signals for Harmonic and Amplitude Control Verified Using the Leach Model

Robert H. Ingham[1], Robert James[1], Peter R. Smith[1], David M.J. Cowell[1], Steven Freear[1]; *[1]Ultrasound Research Group, School of Electronic & Electrical Engineering, University of Leeds, Leeds, West Yorkshire, United Kingdom*

Background, Motivation and Objective

Switched-mode, Class D amplifiers are convenient alternatives to Class A or Class A-B designs for multi-channel ultrasonic transmitter systems. Class D circuits generate square-wave excitations with undesired harmonic content. This increases Total Harmonic Distortion and causes harmonic leakage effects in harmonic imaging. For a bipolar switched-mode signal the third harmonic is of greatest magnitude at 33% of the fundamental.

Previous literature has demonstrated elimination of the third harmonic using a three-level bipolar signal and by choice of a switching angle at Π/6. This can be extended for use with multi-level signals, where several harmonics can be cancelled with additional switching angles. A single switching angle chosen to suppress a desired harmonic will encode a train of pulses of fixed width. Such a pulse train generates uniform pressure amplitude. For many applications it is desirable to produce pulses that are shaped or tapered.

Our previous work has shown that pulse-width modulation (PWM) within the excitation sequence can shape the pressure waveform. Described herein is a novel multi-level switched-mode encoding scheme that permits simultaneous control of both pressure amplitude and harmonic content for class D output stages.

Statement of Contribution/Methods

Multi-level switched-mode sequences are designed by comparing a specifically derived 'carrier' signal to a desired signal. An example encoded sequence, a 6-cycle 5-level Gaussian weighted tone, is shown in Figure. 1.

SPICE modelling enables complete system evaluation in both the electrical and acoustic domains.

The use of an electro/acoustic SPICE model provides a basis for full analysis of the performance of the encoding scheme, and opportunity for system optimization by considering aspects such as MOSFET performance, transducer response, and acoustic propagation.

Results/Discussion

Spectral analysis shows that the encoding method successfully suppresses the third harmonic within the pre-transducer encoded switched-mode. Amplitude control is demonstrated by comparison with an ideal 'analogue' 6-cycle Gaussian-weighted excitation sequence passed through the Leach model. Results show that the encoded sequence is an accurate representation of the ideal 'analogue' signal after propagation.

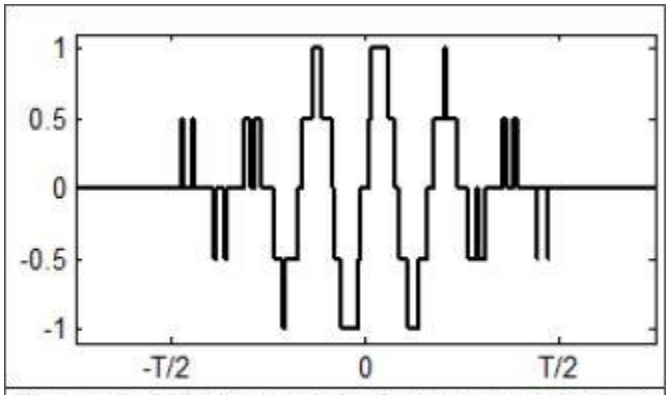

Figure 1: Switched-mode Gaussian pulse with harmonic and amplitude control.

IUS2-PA2-3

A vibrating stylus as two-dimensional PC input device

Riccardo Carotenuto[1], Giousè Caliano[2], Nicola Lamberti[3], Alessandro Stuart Savoia[2], Antonio Iula[4]; *[1]DIIES, Università Mediterranea di Reggio Calabria, Reggio Calabria, Italia, Italy, [2]Dip. di Ingegneria, Università Roma Tre, Roma, Italy, [3]Dip. di Ingegneria Industriale, Università di Salerno, Salerno, Italy, [4]Scuola di Ingegneria, Università della Basilicata, Potenza, Italy*

Background, Motivation and Objective

With the advent of tablet PCs and smartphones, multi-touch or stylus-based input solutions are perceived as being more user-friendly. Over the past 30 years, several solutions, based on different types of optical and acoustical interactions, have been shown in literature and by patents. Our objective is to make surfaces, which have not been designed for this use, input devices for natural writing or drawing, using a low cost vibrating stylus capable of transmitting acoustical waves to fixed sensors.

Statement of Contribution/Methods

The prototype is composed of a vibrating stylus, a number of miniaturized wideband microphones in fixed positions and a central processing unit. The stylus cyclically vibrates and emits coded ultrasound bursts, namely in the 20 – 48 kHz band, which propagates in a solid medium through a contacting rubber tip. The medium is homogenous, has a plain surface, and can be, for example, the glass screen of a TV set, a classroom blackboard, a desktop, etc. The ultra-acoustic coded signal reaches each microphone, and a central unit is capable to accurately compute the time difference of arrival by exploiting the good correlation properties of the coded signal. The central unit, knowing the speed of the sound in that medium (through an initial set-up session), computes the position of the vibrating tip of the stylus, applying an ad hoc algorithm to identify and discard possible false signals due to internal reflections, multipath interferences, and environmental noise.

Different stylus vibrating structures were investigated: longitudinal and flexural Langevine vibrators, and a new flexural bimorph vibrating structure derived from an acoustic fiber.

Results/Discussion

A working prototype has been realized using different vibrating structures. The measured positioning standard deviation was about 1 mm in all the two spatial directions, within a range of 80 cm. In the figure, the microphones setup and one of the investigated stylus vibrator are shown.

Coded ultrasound signals highly improve the noise immunity and allows accurate timing detection, using cross correlation. All the computations are carried out by the central unit, and the simple stylus driving circuitry can be easily integrated and battery operated. The achieved location rate of 25 Hz is fast enough for the majority of the intended 2D drawing applications.

IUS2-PA2-4

Reciprocity-based method for magnitude and phase calibration of hydrophone sensitivity

Everande Oliveira[1], Rodrigo Costa-Felix[1], Joao Machado[2]; *[1]Laboratory of Ultrasound, Inmetro, Brazil, [2]Program of Biomedical Engineering, Federal University of Rio de Janeiro, Brazil*

Background, Motivation and Objective

Two-transducer reciprocity is a traditional, long time validated and well known transducer calibration method used in the calibration of hydrophone sensitivity magnitude. The method uses a reciprocal auxiliary transducer, whose transmission and reception sensitivities are related by a reciprocity parameter. Typically, reciprocity calibration is done at discrete frequencies. Reasonable simple measurement setup is used, once it demands basically electrical measurements. Other methods for measuring hydrophone complex sensitivity have been described, and some examples, with intrinsic drawback, include: optical methods, nonlinear acoustic wave propagation, and time-delay spectrometry. The present work proposes a novel method for magnitude and phase calibration of hydrophone sensitivity based on the reciprocity method.

Statement of Contribution/Methods

The present paper contributes with a method for magnitude and phase calibration of hydrophone sensitivity that combines advantageous properties of a pulse-echo measurement and the two-transducer reciprocity, avoiding the need of a calibrated device. The pulse-echo measurement uses an auxiliary transducer plus a flat reflector immersed in a water tank and allows to determine the transducer complex transmit transfer function. Thereafter its on-axis pressure waveform is obtained, given the excitation signal and the propagation medium properties. Next, the reflector is replaced by the hydrophone placed with the same distance from the auxiliary transducer and aligned with its axis of symmetry. Then, the hydrophone complex receive sensitivity is calculated knowing its incident pressure and output waveform signals. The method was tested with a 0.4mm of active element diameter PVDF membrane hydrophone (UC1604, Precision Acoustics, UK), previously calibrated in magnitude by the National Physical Laboratory (NPL), UK. A 3 MHz auxiliary transducer (A382S, Olympus-NDT, MA, USA) with 12,7mm of active element diameter was used, excited by a burst signal with 6,6 µs duration and repetition frequency of 100 Hz.

Results/Discussion

The hydrophone sensitivity at 3 MHz was determined with magnitude of 77.3 nV/Pa (7% of uncertainty) and phase of -163 degrees. The measured magnitude sensitivity is identical, within 4%, to that certified by the NPL (6% of uncertainty). The hydrophone was not calibrated by NPL regarding phase sensitivity, and therefore no comparison could be done for phase. Even so, the experiment was repeated in order to determine the phase measurement precision, which provided repeatability of less than 4 degrees. The results achieved in this work are considered to be metrological acceptable, since they have a good intra-laboratorial agreement in phase calibration (less than 4 degrees) and an inter-laboratorial agreement within the declared uncertainties in magnitude (less than 4%).

Acknowledgments: the authors thank the financial support provided by CNPq and FAPERJ.

IUS2-PA2-5

High Temperature Immersion Ultrasonic Probes

Takuo Inoue[1], Kazuki Iwata[1], Makiko Kobayashi[1]; *[1]Kumamoto University, Japan*

Background, Motivation and Objective

The inspection of inside opaque liquid such as molten metals is difficult so that periodical inspection has been operated during off-line without opaque liquid. However, in order to assure the safety, condition-based monitoring becomes important. Ultrasonic pulse-echo technique is often used to perform nondestructive testing to their simplicity, speed, economy and capability to probe the interior of an opaque material. However, condition-based monitoring requires high temperature durability. For example, viewing under sodium at temperatures up to 600℃ was reported in order to inspect in-vessel structures in nuclear reactor.

Sol-gel composite materials could be good candidates for those applications because of high temperature durability. In the past research, sol-gel composite films were fabricated onto buffer rods (delay line) to facilitate the measurement system for high temperature, though it made the system bulky and signal contains the reflected echoes from buffer rods so that the length of buffer rods needed to be carefully chosen in order to overlap the desired signals.

Statement of Contribution/Methods

Therefore in this research, sol-gel composite, between lead ziroconate titanate (PZT) piezoelectric powder and PZT sol-gel was fabricated onto 200µm thick stainless steel substrate without delay line. PZT/PZT was firstly used for feasibility study purpose. The film thickness and the diameter were ~100µm and ~30mm, respectively. Then the stainless steel substrate with PZT/PZT film with co-axial cable connection was attached with ~35mm stainless steel tube by soldering and it became an immersion ultrasonic probe.This stainless tube was a protection case from the liquid.

Results/Discussion

The experiment was first carried out in water at room temperature. The above mentioned probe was immersed into water bath at together with a ~4mm thick ceramics disc onto an ~35mm thick aluminum block. The typical ultrasonic measurement result in time domain was given in Fig. 1.The reflected echoes from the front and back surfaces of ceramics and

aluminum samples were clearly observed. It is noted that ceramics sample was engraved and porous so that the reflected echoes from the surface were multiple and the sound velocity was low.The experimental results in oil bath at 150°C will be demonstrated.

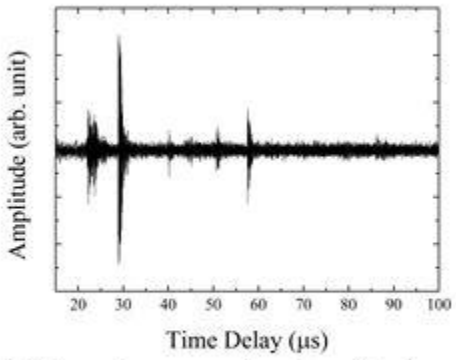

Fig. 1: Ultrasonic response in water with ~4mm thick ceramics and 35mm thick aluminum samples.

IUS2-PA2-6

Dual-layer ultrasonic transducer used for touch sensing

Adit Decharat[1], Sanat Wagle[1], **Frank Melandsø[1]**; [1]*Department of Physics and Technology, The University of Tromsø, Norway*

Background, Motivation and Objective

The use of two or more piezoelectric layers in ultrasonic transducers may in addition to increasing the overall sensitivity, facilitates many interesting applications. Some examples are Barker coded sequences generated from multi-layer polyvinylidene fluoride (PVDF) transducers [*Q. Zhang, P.A. Lewin, and P.E. Bloomfield, IEEE Ultrasonics Symposium, p. 1341-1344, 1995*], and 3D imaging obtained from a dual-layer of polyvinylidene fluoride-trifluoroethylene [P(VDF-TrFE)] and PZT with a crossed electrode design [*Y. Chen, M. Nguyen, and J. T. Yen, IEEE Ultrasonics Symposium, p 2400-2403, 2010*].

Statement of Contribution/Methods

In the current work, a dual-layer ultrasonic transducer made from P(VDF-TrFE) has been developed and explored as a touch sensor. The proposed multi-element touch sensor drives two or more sender (Tx) elements simultaneously in opposite phases to increase the sensitivity. To test out these ideas a prototype illustrated under was build, using a single Kapton polyimide (PI) circuit to carry the electrode pattern for four Tx and four receiver (Rx) elements with diameters around 1 mm. Films of P(VDF-TrFE) are casted from the fluid phase on both sides of the PI film, and then metalized on top, after solvent evaporating and annealing. Finally a polymer or elastomer cover layer is deposited on the upper side to provide acoustic delay, and at the same time, maintain sufficient acoustic discrimination (e.g. caused by modifying the boundary condition and/or deforming the material) when a finger or touch pen is pressed against the surface (see figure).

Results/Discussion

The proposed dual-layer design has shown several benefits compared to a similar single layer transducer, e.g. for simplifying the external electronics and reducing the transient current induced during pulse firing. Thus a transient current down to the level imposed by the acoustic reflections has been achieved when driving two or four Tx-elements in opposite phases that facilitate use of long wave trains (in coded or chirped form) to increase the sensitivity. Both wide-band pulses and longer chirped sequences show promising results for frequency ranges from 5 MHz to 30 MHz. The number and sizes of sensor elements can easily be changed in the suggested design, and enhanced bandwidth can probably be achieved by replacing the standard Kapton copper electrodes with thinner sputtered electrodes.

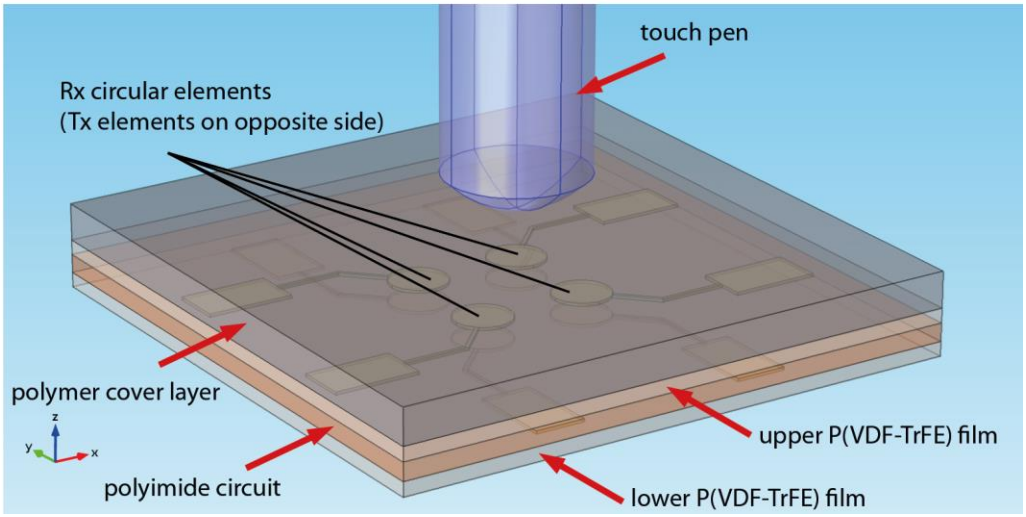

Ultrasonic motors 2

Forum Hall

Monday, July 22 2013, 01:00 pm - 04:30 pm

Congress Hallair: **Takefumi KANDA**
Okayama University

IUS3-PA1-1

An ultrasonic motor using transmission line with oblique slits driven by a Langevin transducer.

Takaaki Ishii[1], Masayuki Takada[2], Yuki Kubota[2], Hidetoshi Ohuchi[2]; [1]*Mechatronics, University of Yamanashi, Kofu, Yamanashi, Japan,* [2]*University of Yamanashi, Japan*

Background, Motivation and Objective

A micro-ultrasonic motor has usually small torque and small revolution speed because of its small size transducer. If large size transducer is used for small output part, we can expect high performance micro-ultrasonic motors. In this report, bolt-clamped Langevin transducer with 30 mm in diameter is used to drive the rotor with 5 mm in outer diameter. The structure, driving principle and fundamental characteristics of the motor are discussed.

Statement of Contribution/Methods

The longitudinal vibration excited by the transducer is amplified by the stepped horn and its vibration travels along the flexible transmission line with 2 mm in diameter attached on the top of the stepped horn as shown in figure 1(a). The oblique slits shown in figure 1(b) convert the longitudinal vibration to torsional vibration, and then the elliptical motion drives the rotor near the end of the transmission line. The slit angle is 45 degrees, width is 1mm and the depth is 0.5 mm. In order to drive the ultrasonic motor, two electrical input signals are usually required to excite the elliptical motion. However, in our experiment, only one electrical input to the transducer can excite the elliptical motion because of the slit structure. The single phase drive is successfully obtained by our proposed slit structure. The radial bearing is used for the rotor. Inner ring of the bearing is pressed by the spring and outer ring of the bearing is directly used for the rotor.

Results/Discussion

One of the fundamental motor characteristics is obtained as shown in figure 2. The maximum rotation speed of 182 r.p.m., the maximum torque of 0.086 mNm and the maximum driving efficiency of 0.083 % were successfully achieved for the first time.

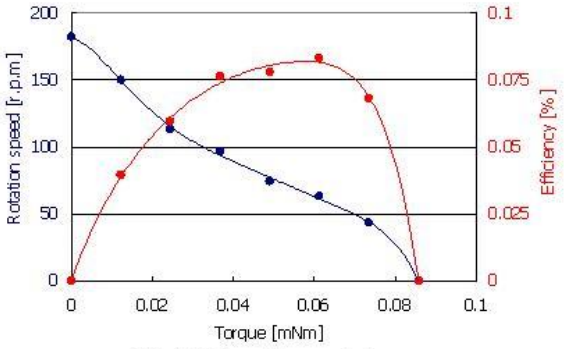

Fig. 2 Motor characteristics.

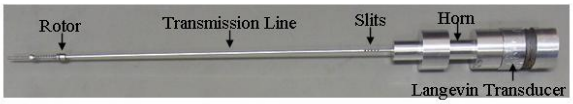

Fig. 1(a) Overview of the motor

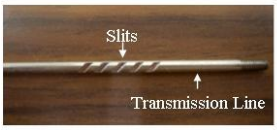

Fig. 1(b) Closed view of the slits

IUS3-PA1-2

High-speed Microscopic Observation of the Elliptical Motion in a Ultrasonic Motor

Tomoaki Mashimo[1], Midori Takaoka[2], Kazuhiko Terashima[2]; [1]*Toyohashi University of Technology, Toyohashi, none, Japan,* [2]*Toyohashi University of Technology, Japan*

Background, Motivation and Objective

Elliptical motions generated by stators are a key driving principle of travelling wave ultrasonic motors. Much of modeling study deals with the amplitude of an elliptical motion to predict the motor output, but none of the existing models have been compared with the real elliptical motion. It is due to that the amplitude and frequency of the elliptical motion are too small (a few microns) and fast (more than 40 kHz), respectively, to measure the real elliptical motion.

Statement of Contribution/Methods

Recent improvement of high-speed cameras is remarkable and the frame rate of the high-speed cameras has reached to an ultrasonic range. In this study, we observe an elliptical motion generated by a travelling wave ultrasonic motor by using a high-speed camera with a microscope (high-speed microscope) that can capture images with an ultrasonic frequency and a few micron amplitudes. It has a frame rate of 230,000 fps with a resolution of 160 x 32 pixels, which enables the observation of the ultrasonic vibration. The use of the high-speed microscope clarifies the dynamic and steady vibration amplitudes of the elliptical motion. Another advantage of using the high-speed microscope is that it can easily observe the elliptical motion of the ultrasonic motor in which the stator contacts with the rotor. We examine how the elliptical motion is related to the ultrasonic motor characteristics, such as the torque and rotational speed while the ultrasonic motor rotates at steady state.

Results/Discussion

Figure shows successive five frames of the elliptical motion captured by the high-speed microscope when the AC voltages (A = 110 Vrms, fr = 46 kHz, ϕ = 90 degrees) are applied to the ultrasonic motor. From the frame rate of 230,000 fps and the resonant frequency of approximately 46 kHz, the high-speed microscope can capture about four frames per one cycle of the elliptical motion. A marker, which is circled in the figure, generates an elliptical motion clockwise in the five flames. In the experiments, we clarify the

relationship of the elliptical motion with the motor input such as the amplitude, frequency, and phase of applied AC voltages. Important characteristic of the ultrasonic motor design is the relationship of the motor output with the preload between the stator and rotor. The experiment clarifies how the elliptical motion is changed by increase of the preload.

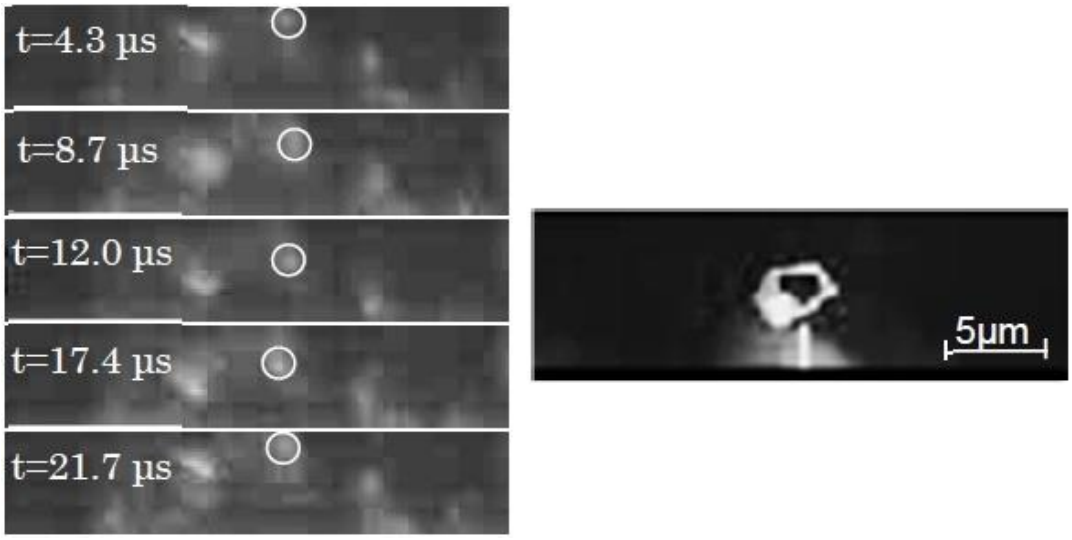

IUS3-PA1-3

Analysis of a Linear Piezoelectric Motor Driven by a Single-Phase Signal

Shine-Tzong Ho[1], Yan-Jhang Shin[1]; [1]*Department of Mechanical Engineering, Kaohsiung University of Applied Sciences, Kaohsiung, Taiwan*

Background, Motivation and Objective

A new linear piezoelectric motor is presented called the semi-elliptical ultrasonic motor, as shown in Fig.1. The composite structure of the stator is formed by two multilayer piezoelectric actuators clamped in an elastic body. The linear ultrasonic motor using normal vibration and tangential vibration modes of a semi-elliptical shape stator was fabricated and studied in this research. The geometric design of the stator has been computed with the help of the finite element analysis.

Statement of Contribution/Methods

In dynamic analysis, the semi-elliptical stator is analyzed by the impedance analysis method. Then, the equivalent circuit model is established to describe the relations between the system parameters and the dynamic characteristics of the motor, as shown in Fig.2. Based on the model, it can be explained theoretically why the piezoelectric motor can be driven by a single phase signal.

Results/Discussion

The semi-elliptical ultrasonic motor prototype was fabricated for the experimental evaluation. In experiments, the impedance curves of the stator were calculated and compared with the measurement. Also, the simulated elliptical trajectories on the stator were compared with the measurement. The experimental results all agree with the simulation. The performance of the prototype motor was measured and the results were discussed. The prototype motor achieved maximum moving speed of 88 mm/s and the maximum output force of 1.96 N when applying a sine wave of 16Vp driving voltage.

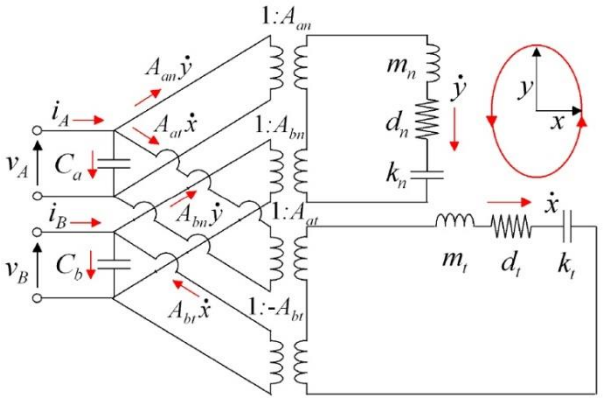

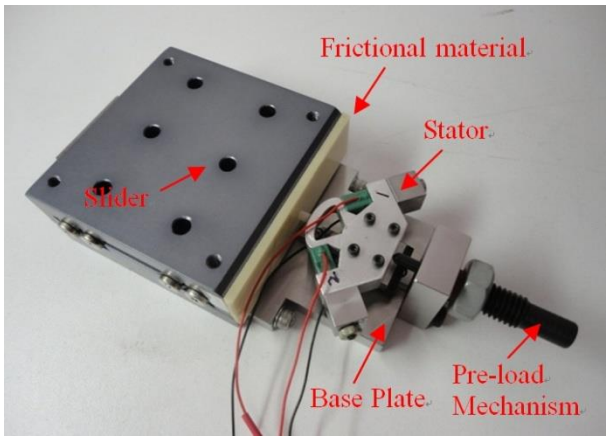

IUS3-PA1-4

A Hybrid Ultrasonic Squeeze Film and Magnetic Levitation Actuator for Machine Guideways

Sebastian Mojrzisch[1], Igor Ille[1], **Jörg Wallaschek**[1], Berend Denkena[2]; [1]*Institute of Dynamics and Vibration Research, Leibniz Universität Hannover, Hannover, Germany,* [2]*Institute of Production Engineering and Machine Tools, Leibniz Universität Hannover, Garbsen, Germany*

Background, Motivation and Objective

In applications that require high precision and acceleration of the supported member, non-contact bearings are frequently used. A novel active non-contact bearing system is given by ultrasonic levitation bearings. The working principal is based on ultrasonic squeeze film levitation. Due to the excellent dynamic response behavior, this kind of bearing system is well suited for dynamically loaded applications like machine guideways.

In this article we present a novel hybrid ultrasonic/magnetic levitation actuator for machine guideway applications. This arrangement is beneficial due to the repulsive and attractive forces of each physical phenomena. The combination simplifies guideway constructions significantly.

Statement of Contribution/Methods

Starting from analytical models of each effect, a combined system model is developed. Besides of steady state solutions, the dynamic behavior of the new hybrid actuator is investigated. Moreover, the driving method of the employed ultrasonic transducer is discussed in detail. As shown by the authors an auto-resonant driving of the ultrasonic transducer is required in order to ensure stable levitation force and fast dynamic response of the system. In this context the non-linear characteristics of the system are investigated by averaging methods in order to describe the hybrid system's behavior under changing levitation gab conditions.

Results/Discussion

The prototype actuator is depicted in Fig. 1. This actuator shows a self-stabilizing mechanism, which means that the levitation is stable without a feedback control of the levitation gab distance. This is achieved by saturation effects of the magnetic part, which appears when the levitation gab becomes small. In order to take advantage of the dynamic properties of the actuator, a position feedback is implemented. This controls the actuator's levitation height as well as the bearing's damping and stiffness, respectively. The paper is concluded by an outlook to future applications of the novel hybrid actuator in machine guideways along with more compact actuator designs.

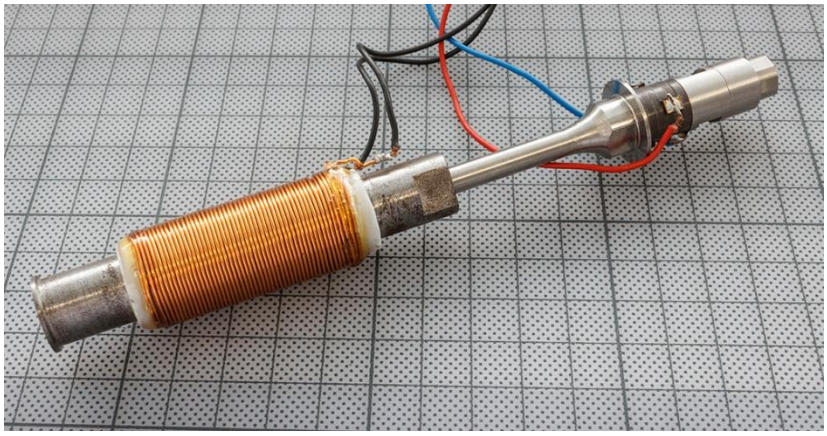

IUS3-PA1-5

Ultrasonic Dewatering in Minute Holes

Masaya Takasaki[1], Takanori Endo[2], Takeshi Mizuno[2]; [1]*Saitama University, Saitama, Saitama, Japan,* [2]*Saitama University, Japan*

Background, Motivation and Objective

Printed-circuit boards are widely used for miniaturizing electronic equipments. According to the demand, diameter of holes in the boards is decreasing. There is a problem in their fabrication processes, in which they should be cleaned in water. After the cleaning process, water remains in the small holes. The remained water contains chemical material and/or dusts and might cause damage of the boards in the future. Conventionally, air pressure has been used to remove the water in the boards. But the method is not valid for holes that have bottoms inside neither for much smaller holes. Heating could be an alternative method, but this method might leave chemical material in the water and cause deflection of the board.

Statement of Contribution/Methods

In this research, a new dewatering method has been proposed. The method utilizes standing wave of ultrasonic wave in air. An experimental apparatus was organized to observe the ultrasonic dewatering and consisted of a Langevin type ultrasonic transducer and a reflector.

Results/Discussion

Proposed dewatering was observed successfully and recorded by a high-speed camera. The sound pressure in the standing wave was measured by a microphone. A condition for successful dewatering was discussed with reference to the distribution of the sound pressure.

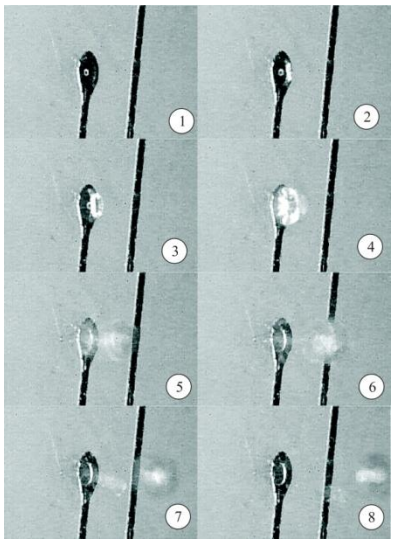
1
2
3
4
5
6
7
8

Optical and electromagnetic interactions 2

Forum Hall

Monday, July 22 2013, 01:00 pm - 04:30 pm

Congress Hallair: **Vincent Laude**
Centre National de la Recherche Scientifique

IUS3-PA2-1

Magnetoelastic properties of some uranium intermetallic antiferromagnets as studied by high-field ultrasound measurements

S. Zherlitsyn[1], A.V. Andreev[2], S. Yasin[1], Y. Skourski[1], A.A. Zvyagin[3], J. Wosnitza[1]; *[1]Helmholtz-Zentrum Dresden-Rossendorf, Germany, [2]Institute of Physics ASCR, Czech Republic, [3]B.I. Verkin Institute for Low Temperature Physics and Engineering of the National Academy of Science, Ukraine*

Background, Motivation and Objective

Uranium intermetallics of the composition UT2X2 and UTX where T is a transition metal and X is Si or Ge exhibit a large variety of magnetic states starting from antiferromagnetic (UCr2Si2, UCo2Si2 and UCu0.95Ge), complex ferrimagnetic (UNi2Si2) and ferromagnetic (UCu2Si2) structures through Pauli paramagnets (UFe2Si2), and, finally, to URu2Si2, a heavy-fermion superconductor featured by so-called hidden order. It is crucial to clarify a role of the magnetoelastic couplings in physics of the uranium intermetallic compounds. Ultrasound technique is known to be a highly sensitive probe for the magnetoelastic interactions. Access to high magnetic fields combined with the ultrasound technique can shed new light on various physical phenomena in the uranium intermetallic compounds.

Statement of Contribution/Methods

We report on recent studies of the magnetoelastic properties of uranium intermetallic antiferromagnets UCo2Si2 and UCu0.95Ge. Since the uranium intermetallics demonstrate a large magnetic anisotropy, the ultrasound investigations have been performed on the single crystals in pulsed magnetic fields up to 63 T in a wide temperature range between 1.5 and 300 K. The measurements have been carried out using a phase-sensitive detection technique based on a standard pulse-echo method in the frequency range from 40 to 107 MHz.

Results/Discussion

We have investigated UCo2Si2, an antiferromagnet with ordering temperature TN = 83 K. We have observed a metamagnetic transition to a ferrimagnetic state at 45 T (at 1.5 K) for the magnetic field applied along the c-axis. The sound velocity and sound attenuation exhibit sharp anomalies in the vicinity of both the spontaneous and the field-induced magnetic phase transitions. Our analysis suggests that the changes in the sound velocity and sound attenuation are predominantly determined by a renormalization of the exchange interactions due to the sound waves.

Studies of magneto-acoustic characteristics of the UCu0.95Ge have been performed in pulsed magnetic fields applied along the main crystallographic directions. Along the a-axis, a first-order phase transition has been observed at 61 T. For the field applied along the c-axis, the first-order phase transition occurs at a much lower magnetic field (38 T). These field-induced transitions as well as the magnetic ordering at TN = 48 K are accompanied by pronounced anomalies in the sound velocity and sound attenuation. The field-temperature phase diagrams are constructed for both directions of the magnetic field. The results of our theoretical analysis within the framework of the mean-field approximation qualitatively agree with the observed behavior of magnetic and magneto-acoustic characteristics of UCu0.95Ge.

Our studies show that the magnetoelastic interactions play a very important role in UCo2Si2 and UCu0.95Ge compounds.

IUS3-PA2-2

The Influence of the External Magnetic Field on Acoustic Properties of Magnetic Elastomers

Iren Kuznetsova[1], Boris Zaitsev[2], Alexander Shikhabudinov[2], **Irina Borodina[2]**, Elena Kramarenko[3], Vladimir Kolesov[1], Gennadiy Stepanov[4]; *[1]Kotel'nikov Institute of RadioElectronics and Engineering of RAS, Moscow, Russian Federation, [2]Saratov branch, Kotel'nikov Institute of RadioElectronics and Engineering of RAS, Saratov, Russian Federation, [3]Physics Department, Moscow State University, Moscow, Russian Federation, [4]State Institute of Chemistry and Technology of Organoelement Compounds, Moscow, Russian Federation*

Background, Motivation and Objective

At present attention of researchers is excited by magnetically controlled elastomers. These materials present the polymeric matrixes with embedded magnetic nano and microparticles. It is known that magnetically controlled elastomers may be reversibly deformed by the applied magnetic field and may change their texture depending on the magnetic field direction. Such materials are characterized by low acoustic impedance and may be used for matching the piezoelectrics and low-impedance media. They also may be utilized in piezoelectric structures for development of the magnetically controlled devices for signals processing. The purpose of this work is the investigation of the acoustic properties of magnetically controlled elastomers and the analysis of the influence of the external magnetic field on their properties.

Statement of Contribution/Methods

The materials under study present the silicon matrix with embedded microparticles (2-5 mkm) of carbonyl iron of 20% mass concentration. The growth process allowed to get the samples of two types: unstructured and structured by the magnetic field. For carrying out the measurements the samples of aforementioned materials with diameter of 12 mm and thickness of 2-4 mm were made. The frequency dependencies of the phase and insertion loss of output signal connected with passing the ultrasound through the sample were measured by the meter of S-parameters Agilent E5071C. The obtained data allowed to estimate the elastic constants and viscosity coefficients of the materials under study. We also developed the experimental stand for the investigation of the external magnetic field on the velocity of the longitudinal bulk acoustic wave (BAW) in pointed above elastomers. This stand allowed to change the magnetic field from 0 up to 10 kOe with the step of 0.5 kOe. In experiment we measured the dependence of the change in the output signal phase on the magnetic field intensity. The experiments were carried out at the different orientations of magnetic field.

Results/Discussion

As a result of the performed experiments it has been found that with the increase of the frequency the elastic constant of magnetically controlled elastomers increases. It has been also shown that with the increase in the magnetic field intensity the velocity of BAW increases. The maximum fractional change in velocity is equal ~ 2.5% for structured samples at the magnetic field intensity of 10 kOe. Analysis has shown that the value of change in the velocity of BAW for structured samples is more compared to the unstructured ones. Besides it has been found that the reaction on the magnetic field applied to structured samples in contrast to unstructured ones depends on the number of magnetization acts. The

analysis has allowed to make the conclusion that for unstructured samples the change in BAW velocity is mainly defined by the electrostriction effect. For structured samples the nonsymmetric ΔE –effect presents in addition to the electrostriction effect.

IUS3-PA2-3

Impedance Spectroscopy in Laser Calorimetry of Nonlinear-Optical Crystals

Oleg Ryabushkin[1,2], **Aleksey Konyashkin[1,2]**, Daniil Myasnikov[1,2], Valentin Tyrtyshnyy[1,2], Oleg Vershinin[1,2], Dmitriy Nikitin[1,2]; *[1]NTO "IRE-Polus", Fryazino, Moscow region, Russian Federation, [2]Moscow Institute of Physics and Technology, Dolgoprudnyy, Moscow region, Russian Federation*

Background, Motivation and Objective

Laser calorimetry is standardized technique for optical absorption measurement. Both optical absorption α and heat transfer h^T coefficients of crystal can be determined using nonstationary heat conduction equation in case temperature distribution inside crystal and surrounding air is known. As a rule in this method kinetics of air temperature is measured near the crystal surface when laser radiation passes through the crystal. Impedance spectroscopy can be applied for accurate crystal temperature measurement during its interaction with laser radiation. The equivalent temperature Θ_{eq} of nonlinear-optical crystal is directly measured using crystal's piezoelectric resonance (PR) frequency Rf dependence on temperature [1].

Statement of Contribution/Methods

It was shown that uniform crystal heating results in linear Rf shift with temperature Tc: $\Delta Rf(\Delta Tc) = K^{prt}\Delta Tc$ [1]. Coefficient K^{prt} value depends on selected PR mode. For linear case of crystal heating by laser radiation its equivalent temperature change with power P is $\Delta\Theta_{eq}(P) = [Rf(P)–Rf(0)]/K^{prt}=\beta P$, where β is optothermal coefficient of the crystal [1]. When laser radiation heats the crystal its equivalent temperature kinetics is measured using Rf dependence on time t: $Rf(t)=[Rf(0)–Rf(P)]\exp(–t/\tau)+Rf(P)$. Here Rf(P) corresponds to the PR frequency stationary value at fixed power P. Both heat transfer and optical absorption coefficients are obtained using values of Rf kinetics characteristic time τ, crystal mass M, heat capacity C, crystal surface area S and length L: $h^T=(MC)/(S\tau)$; $\alpha L=h^T S\beta$. In order to measure Rf(t) the external probe electric field frequency *f* is changed stepwise in time as it is shown on the left figure. In each time interval when *f* is fixed the PR frequency Rf equals to *f* at time moment t_i when measured electrical admittance phase is at its minimum.

Results/Discussion

Widespread nonlinear-optical lithium triborate (LBO) crystal was used in experiment with CW Yb-doped fiber laser. Right figure shows measured kinetics of Rf together with obtained data for LBO. Combination of laser calorimetry with impedance spectroscopy is a powerful tool for precise measurement of crystals optical absorption and heat transfer coefficients.

[1] O.A. Ryabushkin et. al, "Equivalent temperature of nonlinear-optical crystals interacting with laser radiation," J. Eur. Opt. Soc., Rapid Publ. 6, 11032 (2011).

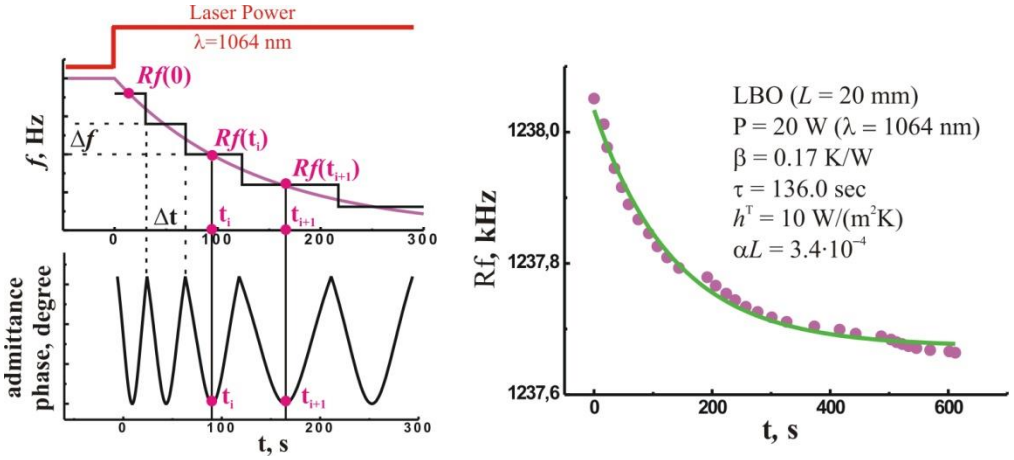

IUS3-PA2-4

new telluride alloys for efficient acousto-optic devices of near, middle and far ir-region

Liudmila Kulakova[1]; *[1]Russian Academy of Sciencies, Ioffe Physico-Technical Institute, Sankt Petersburg, Sankt Petersburg, Russian Federation*

Background, Motivation and Objective

It is known that many of acousto-optic devices are based on monocrystalline TeO_2. Large value of acousto-optic quality (M_2) of this material is due to large M_2 value of tellurium (Te). Unfortunately because of strong anisotropy of physical properties of TeO_2 crystals fabrication of acousto-optic sells is very expensive. So we used Te as basic element for fabrication of Si-Te alloys transparent in wide (λ: 2.1μm ÷ 18μm) IR-region. Record-breaking value of M_2 had been revealed in $Si_{20}Te_{80}$ [1]. Further, improvement of optical and acoustic properties of telluride alloys we realized in the $Ge_{19}Se_9Te_{72}$ alloy [2, 3].

The problems of energy saving initiated search of new effective alloys on the basis of the tellurium, allowing to promote in the IR range of short-wave area, including λ ~ 1,5 μm, that provides not only expansion of AO devices optical range, but also essential increase of their efficiency ($\eta \sim M_2/\lambda^2$) in this area.

Statement of Contribution/Methods

We have fabricated and studied optical, acoustic and acousto-optic properties of new Ge-Se-Te- S and Ge-Se-Te glassy alloys.

Results/Discussion

The analysis of the data obtained has resulted in the following conclusions. (i) It is shown that the basic tellurium matrix governs, to a great extent, the elastic, optical and acousto-optic properties of telluride glasses. (ii) Shift of optical absorption edge in the short-wave area has been found at decrease of Te content. (iii)$Ge_{25}Se_{15}Te_{60}$ has been found to be the highest quality alloy and exhibits important advantage in comparison to the promising acousto-optic $Si_{20}Te_{80}$ alloy studied previously [1]. The acousto-optic efficiency of diffraction increases almost twice at its optical absorption edge (λ=1.69 mcm). (iv) Moreover, the $Ge_{27}Se_{18}Te_{55}$, $Ge_{30}Se_{20}Te_{50}$ and $Ge_{30}Se_{25}Te_{45}$ alloys are not of less interest: at rather high efficiency (comparable with that one for $Si_{20}Te_{80}$) their optical absorption edge shifts up to λ ~ 1,4μm. Owing to these properties, and also because of low acoustic

attenuation, these alloys are worthy competitors of the $Si_{20}Te_{80}$ alloy in the fabrication of modulators and deflectors for wide IR range of the spectrum including $\lambda \sim 1{,}5\mu m$ (transparency aria of the TELECOM standard)

This study was supported by the Russian Foundation for Basic Research (Gr.N 11-02-00729) and scientific programs of Presidium of the Russian Academy of Sciences.

References

[1] L.A.Kulakova, B.A.Matveev,. J. of Non-Crystalline Solids, **266-269**, 969-972, (2000)

[2] L. A. Kulakova, B. T. Melekh, V. I. Bakharev, and V. Kh. Kudoyarova. Semiconductors, 37, No. 7, pp. 795–799 (2003).

[3] L.A. Kulakova, V. Kh. Kudoyarova, B. T. Melekh, V. I. Bakharev. - J. Non-Cryst. Sol., **352** (9-20), p. 1555, (2006)

IUS3-PA2-5

Anisotropic Diffraction of Acoustic Waves in Crystals Used in Acousto-Optic Dispersive Delay Lines

Natalya Naumenko[1], Sergey Chizhikov[1], Vladimir Molchanov[1], Konstantin Yushkov[1]; *[1]Acousto-Optical Research Center, National University of Science and Technology "MISIS", Moscow, Russian Federation*

Background, Motivation and Objective

Acousto-optic (AO) dispersive delay lines are a modern class of photonic devices for femtosecond pulse shaping in high-power laser systems. The design of these devices is based on acoustic properties of highly anisotropic crystals. Architecture of AO interaction in the dispersive delay lines is mainly determined by the energy drift of elastic waves caused by anisotropy. On the other hand, anisotropic diffraction spreading of acoustic beams affects spectral bandwidth of the devices and degrades efficiency of AO coupling. Most often the dispersive delay lines are built on paratellurite TeO2. Extremely low phase velocity of the slow shear bulk acoustic wave (BAW) in TeO2 results in a low quick-action of the devices. Meanwhile, some novel applications in ultrafast optics require pulse processing with high repetition rates. Lithium niobate (LN), in which shear BAW propagates 4-6 times faster than in TeO2, looks promising as a material for AO dispersive delay lines with pulse repetition frequency up to 100 kHz. One of the problems to be solved is investigation of diffraction of acoustic waves in suitable directions.

Statement of Contribution/Methods

Anisotropic diffraction of BAWs propagating in arbitrary direction of a crystal is characterized by the planar tensor of anisotropy coefficients K_{ij}, which is similar to the scalar anisotropy parameter used for surface waves. Two nonzero eigenvalues of the tensor, K_{11} and K_{22}, refer to eigenvectors confined in the plane normal to the propagation direction and describe anisotropic BAW diffraction. In the far field they characterize the elliptical cross section of initially round acoustic beam. Tensor K_{ij} describes the curvature of the BAW slowness surface, which can be elliptical, hyperbolic, parabolic or conical. K_{ij} depends on the propagation direction and can be derived explicitly via differentiation of Christoffel equation with stiffened elastic modules, which take into account piezoelectric effect.

Results/Discussion

The calculated diffraction coefficients were compared for pure shear BAWs propagating in the symmetry planes of TeO_2 and LN. For shear waves propagating in YZ plane of LN, K_{11}, which characterizes diffraction in the same plane, is close to isotropic value, while K_{22}, which shows diffraction along X-axis, varies in a wide range. Hence, it is possible to combine BAW velocity about 4000 m/s with full autocollomation of acoustic beam along X-axis provided that AO coupling efficiency is 60% of its maximum value. Such combination of parameters looks promising and makes LN more preferable than TeO2 for AO dispersive delay lines with pulse repetition frequencies up to 100 kHz. Low attenuation and low diffraction of acoustic waves in LN, i.e. higher beam quality, enables design of AO dispersive delay lines with higher interaction length for increase in spectral resolution, optical delay, and AO coupling efficiency. Our recent research is aimed at design and fabrication of optimized AO devices based on LN

IUS3-PA2-6

Modeling of Non-Coherent O-CDMA Data Transmission System with Walsh Coding Functions Using Multi-Frequency Acousto-Optic Matched Filtering

Valery Proklov[1], Oleg Byshevski-Konopko[1], Valery Grigorievsky[1]; *[1]IRE RAS, Russian Federation*

Background, Motivation and Objective

Recently in optical telecommunications the two basic ideologies dominate – the time division multiple access (TDMA) and the wavelength division multiplexing (WDM). However, the interest of specialists to the most perspective principle – the optical code division multiple access (O-CDMA) on the analogy of the well-known CDMA radio systems, approved for 3G, 4G and next generations [1], [2] emerged only recently. In this concern the development of non-coherent O-CDMA data transmission systems based on a spectrum domain coding/decoding principles, specially with use of a multi-frequency acousto-optic filters (MAOF), seems to be very actual [3], [4].

Statement of Contribution/Methods

In this work the computer simulation of the possible parameters of O-CDMA system using three identical MAOFs – one is for the optical spectral encoding and other two are for the balanced decoding has been considered. There were proposed also the 16-bit Walsh family as a set of coding functions and the geometry of collinear AO light diffraction by shear acoustic wave in X-cut crystal $CaMoO_4$ with wave length resolution 1.27 nm near the wave length 600 nm.

Results/Discussion

The simulation results show that the system is operable at a frequency separation of adjacent spectral lines not less than two-fold the Rayleigh criterion when a ratio of the appropriate signal autocorrelation function to the sum of all cross correlations provides a choice of threshold for the automatic decision about the meaning of the received bits. There was shown also that at an appropriate choice of spectral acoustic signals in a proper MAOF filters the considered system can work in asynchronous data transmission regime with the following potential characteristics - a range of light wavelengths is 600-740 nm, intervals between the neighbor spectral lines is about 8 nm, number of simultaneously served subscribers (channels) - 16, and estimated bit rates per each channel is up to $2x10^9$ bits/second.

This work was supported by the Russian Basic Research Foundation, Project # 10-02-00029-a and #12-07-00186-a.

[1] K.S.Gilhousen, et al., "On the Capacity of a Cellular CDMA System", IEEE Trans. On Veh. Tech., vol. 40, N 2, pp. 303-311, May 1991.

[2] M. Kavehrad, Fellow, IEEE, and D. Zaccarh, "Optical Code-Division-Multiplexed Systems Based on Spectral Encoding of Noncoherent Sources", J. Lightwave Technology, Vol.13, N.3, March 1995

[3] Hinkov, V. Hinkov, K. Iversen, O. Ziemann, "Feasibility of optical CDMA using spectral encoding by acoustically tunable optical filters", Electronics Letters, v.31, no. 5, p. 384, 1995

[4] V.V.Proklov, "Acousto-optic integrated circuits for incoherent spectral encoding/decoding in all-optical network with asynchronous data transmission" (Invited) - Proceedings the ISTC-Samsung Forum: Partnership development in Russia/CIS, Moscow, October 9-10, 2001, p. 42.

IUS3-PA2-7

Acoustic-optical Properties of Silicon Crystals in Visible Range of Spectrum

Farkhad Akhmedzhanov[1]; [1]*Physics, Samarkand state university, Samarkand, Samarkand, Uzbekistan*

Background, Motivation and Objective

It is well known an acoustic-optical interaction is lacking in absolutely transparent crystals. In this connections the greatest interest are presented acoustic-optical investigations in the optical range, in what the crystal is not transparent. Evidently, the geometry of the experiment must be different from that for transparent crystal because the crystal thick a few nanometers will absorb the incident light completely. In order to carry out similar experiments, it is necessary to use the additional crystal with a small light absorption coefficient at applied wavelength.

Statement of Contribution/Methods

At present work the acoustic-optical properties of Si crystal have been investigated at light wavelength 632.8 nm, in which it is nontransparent.To observe the diffracted light by acoustic waves the crystal of gallium phosphide (GaP) was used as the buffer sample because it is transparent in visible range of spectrum. The experimental geometry has been changed so that we could observe the diffraction of light in an opaque silicon crystal at a given wavelength. The single crystal of pure GaP was formed to have a pair of opposite faces polished to ensure entrance and exit the light wave. Also, at least one of the faces of this pair was perpendicular to the propagation direction of acoustic wave, which is excited in the silicon sample at fixed frequency by piezoelectric transducer of quartz. Another face of buffer crystal (under an angle of 90.degree) provides the physical contact with the investigated Si crystal.

Results/Discussion

At the experiment we observed the light diffracted on the transversal acoustic waves in Si crystal. It was detected the diffracted light intensity is much more powerful in comparison with that for GaP crystal. Acoustic-optical efficiency M2 has been calculated from the values of optic coefficients and elastic constants for appropriate directions of sound and light. The results have been shown the possibility of determination of photoelastic properties of nontransparent crystals by Bragg diffraction method in visible range of spectrum. At that rate, the very high intensity of diffracted light can be obtained in comparison with the light diffraction observed in transparent crystals.

IUS3-PA2-8

Impact of the deposition process on the elastic properties of thin films measured by ultrafast acoustics

Arnaud Devos[1,2], Arnaud Le Louarn[2], Patrick Emery[2]; [1]*ISEN, IEMN, Lille, France,* [2]*MENAPiC, Lille, France*

Background, Motivation and Objective

The elastic properties of materials currently used by the microelectronic industry are poorly known. More and more applications require the knowledge of Young modulus or mass density of such materials especially in thin-films (MEMS, BAW resonators, strained MOS transistors…). So there is a need for a better understanding of mechanical properties at sub-micron scale.

The materials these nano/microstructures are made of may strongly depend on the deposition/fabrication process. For example, due to the use of fast elaboration processes at moderate temperatures, thin film materials are often in metastable states, with no equivalent bulk structures. Most of the thin films are polycrystalline materials and their elastic properties are averaged over all the grains.

If such a dependence of elasticity on material growth process can be seen as a problem, it can also be very useful for tuning the elastic properties of thin-film for some specific applications. For that one needs some dedicated characterization techniques able to reach accurately elastic properties at nanoscale.

Statement of Contribution/Methods

We use the ultrafast acoustic technique to measure some elastic properties of thin films. This laser technique implements a sonar at nanoscale by generating and detecting an acoustic wave in the sample. It offers a unique way of measuring elastic properties of thin-layer in a non-destructive way using ultrashort optical pulses.[1]

For several years we have shown that the capabilities of the ultrafast acoustic technique can be enhanced if one uses several laser wavelengths or colors. More parameters are measurable, for example thickness and sound velocity are simultaneously reachable and the measurement accuracy can be significantly enhanced using this so-called colored picosecond acoustic technique.[2]

[1]. A. Devos, R. Cote, G. Caruyer, and A. Lefevre, Appl. Phys. Lett. 86, 211903 (2005).

[2]. A. Devos, J.-F. Robillard, R. Côte et P. Emery, Physical Review B 74, 6, 064114 (2006)

Results/Discussion

We present various results obtained on different materials among which silica and diamond. Series of thin-films are studied using ultrafast acoustics and elastic properties are measured. According to the deposition technique we measure significantly different sound velocities and Young moduli. Elastic properties are found to be strongly dependent on the realization process.

Ultrasonic Arrays

Forum Hall

Monday, July 22 2013, 01:00 pm - 04:30 pm

Congress Hallair: **Scott Smith**
GE Global Research

IUS5-PA-1

Development of Miniaturized Linear Arrays for Integration with Interventional Tools

Robert Ssekitoleko[1,2], **Christine Demore[1]**, Jack Hoyd-Gigg Ng[3], Marc Desmulliez[3], Sandy Cochran[1]; *[1]Institute for Medical Science and Technology, University of Dundee, Dundee, Scotland, United Kingdom, [2]Department of Bioengineering, University of Strathclyde, Glasgow, United Kingdom, [3]MIcroSystems Engineering Centre, Heriot-Watt University, Edinburgh, United Kingdom*

Background, Motivation and Objective

High resolution ultrasound (HRUS) transducer arrays enable imaging with resolution suitable for both visualizing tissue structure and for tissue characterization, with significant potential application in oncology, gastroenterology and neurosurgery. Devices operating above 15 MHz are capable of resolving features below 200 µm; increasing the operating frequency further, high resolution characterisation of tissues becomes feasible. However, clinical application of HRUS is currently challenging due to the limited penetration depth with increasing frequency and limited access. Since the device dimensions scale with imaging wavelength, it becomes feasible to integrate miniaturised high frequency arrays arrays within interventional tools. Although there are many design and fabrication challenges associated with miniaturising arrays and transducer packaging, such a device would create opportunities for efficient and effective characterisation of tissue, leading to in vivo pathology.

Statement of Contribution/Methods

In this paper, we report the development of miniature linear arrays suitable for integration with biopsy needles that can be positioned at the tissue region of interest to overcome the constraints of attenuation at high frequencies. Microfabrication and precision micromachining techniques have been developed to make small wafer scale processing feasible, minimising manual handling of the devices. PMN-PT 1-3 composites are used to take advantage of the enhanced performance of piezocrystal materials, consequently limiting fabrication process temperatures. Matching and backing layers of loaded epoxies are cast on the electrode front and back surfaces of the composite. A polyimide flexible printed circuit has been patterned with fine-pitch traces using an ultrasonic etching technique. This flexible cable is twisted into a helical structure to fit within the core of the biopsy needle, and connected to the array elements with low temperature bonding techniques. The array elements are defined by dicing after connecting to the flex circuit, although photolithographic patterning is feasible.

Results/Discussion

Prototype arrays operating at up to 15 MHz, with 100 µm element pitch and small enough to fit within a 2 mm diameter biopsy needle have been fabricated. Impedance and pulse-echo responses from these arrays validate the fabrication process and demonstrate functionality. The twisted polyimide flex circuit design permits large numbers of channels and electrode traces while minimising volume for cabling. A range of low temperature bonding techniques suitable for high density interconnect with flexible circuits are discussed. The extension of the fabrication processes to higher frequency arrays, and higher element count arrays, as well as limitations of the processes are discussed.

IUS5-PA-2

Design, Fabrication and characterization of a bi-frequency co-linear array (7.5MHz/15MHz)

Xiaoning Jiang[1], Jianguo Ma[1], Xuecang Geng[2]; *[1]North Carolina State University, USA, [2]Blatek, Inc., USA*

Background, Motivation and Objective

Ultrasound imaging with high resolution and large field of depth is important in disease diagnosis, surgery guidance and post-surgery assessment. Conventional ultrasound imaging arrays work at a particular frequency, with -6dB fractional bandwidth of < 100%, limiting the resolution or field of depth in many ultrasound imaging cases. In this paper, a 7.5 MHz/15MHz bi-frequency co-linear array is reported with bandwidth of 5MHz-20 MHz, which can be significant in a broad range of biomedical ultrasound imaging applications.

Statement of Contribution/Methods

A bi-frequency co-linear array with 64 elements were designed, followed by fabrication and characterization. KLM model was used to calculate single element transmitting sensitivity and impulse response simulation. The Field II simulation package in MATLAB was used for acoustic field modeling to determine the approximate resolution and detection ranges, as well as the field pattern during scanning and dynamic focusing. For fabrication, 15 MHz 1-3 composite was prepared, and two layer of 15 MHz composite plates will be bonded together with matching, backing and flex circuit layers forming the co-linear array acoustic stack. A number of characterizations will be performed to evaluate the arrays during prototyping and post assembly. Specifications such as element capacitance, dielectric loss, the time-domain response, bandwidth, electrical impedance, crosstalk, directivity, and insertion loss could be performance benchmarks for such evaluations. All array tests will follow Blatek array test procedures.

Results/Discussion

Key design parameters of the 7.5MHz/15MHz co-linear array include: pitch of 100 um, kerf width of 21 um, elevation and azimuth length of 6.4mm, and 64 elements. KLM modeling shows that the -6dB fractional bandwidth of a single 7.5 MHz and 15 MHz element can be > 70%. Field II modeling shows that reasonably good focus can be obtained at the depth up to 15mm- 22 mm. Beam steering at +/- 40 degree was demonstrated in Field II simulations. The co-linear array is being assembled, and the extensive characterizations will be reported in the full paper. The reported bi-frequency co-linear array holds great potential for medical imaging with high resolution and large field of depth.

IUS5-PA-3

Variable-size elements in 2D sparse arrays for 3D medical ultrasound

Bakary Diarra[1,2], Marc Robini[1], Hervé Liebgott[1], Christian Cachard[1], Piero Tortoli[2]; *[1]CREATIS, Université de Lyon ; CNRS UMR 5220 ; INSERM U1044 ; Université Lyon 1 ; INSA-Lyon, Villeurbanne, France, [2]Electronics and Telecommunications Dept., Università degli Studi di Firenze, Florence, Italy*

Background, Motivation and Objective

3D ultrasound imaging using 2D arrays is one of the most challenging recent innovations in medical ultrasound. The electronic control of the probe elements allows the beam steering in all directions, making possible volumetric acquisitions. Usually, 2D array elements are aligned on a regular mid-wavelength (pitch<λ/2) grid giving rise to grating lobes. An irregular elements placement allows reducing the grating lobes and the use of elements of size greater than λ/2 to improve the signal-to-noise ratio. We propose an irregular positioning strategy with variable-size elements to maintain large beam directivity, increase the probe energy and reduce the grating lobes.

Statement of Contribution/Methods

The method proposed in this paper consists in randomly choosing the size of the 2D array elements in an interval around λ/2. This new strategy is combined with the irregular placement of the elements [Diarra et al. 2012 IEEE Ultrasonics symposium] to further reduce the grating lobes. The use of both small and wide elements permits to find a good tradeoff between probe energy and directivity. An optimization step, based on a carefully designed simulated annealing, is used: the cost function includes the classic beam features (main lobe width and side lobes). Simulations based on Field II have been run for: (i) a sparsely-filled 2D array with elements of size λ/2 on a 64x16 regular-grid (reference), (ii) a non-grid sparse array with elements of size λ/2, and (iii) a non-grid sparse array with variable-size elements. The footprint of the 3.5 MHz probe and the final number of activated elements (128) are the same in all cases.

Results/Discussion

Fig.1 displays the beam profiles obtained without steering and for a 30° steering angle; it illustrates the improvement obtained with the new approach in terms of grating and side lobes reduction. In the absence of steering (Fig. 1(b)), the grating lobes are reduced by 10 and 25 dB compared to the non-grid and sparse arrays, respectively. In the case of a 30° steering angle (Fig. 1(c)), this reduction is about 8 dB compared to the non-grid array and 25 dB compared to the sparse array. The -6 dB width of the main lobe is 5° for the three arrays; the side-lobe level is -39 dB for the two non-grid arrays (with fixed- or variable-size elements), whereas it is -35 dB for the reference array. Complementary results will be presented to further validate the proposed method.

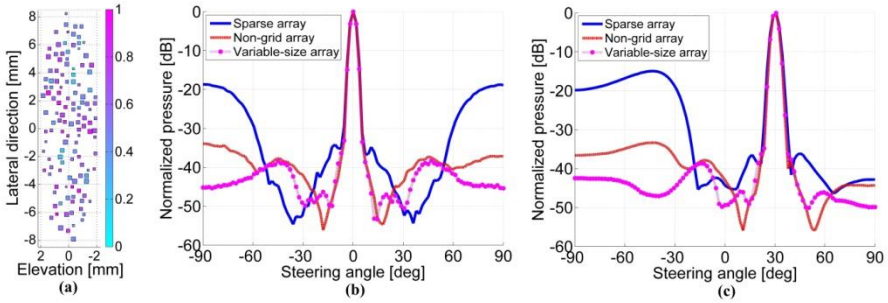

Fig. 1. (a) The non-grid sparse array with variable-size elements (the element size is in [4λ/10, 8λ/10] and the color bar represents the apodization coefficients after optimization). Unsteered (b) and steered (c) beam profiles for sparse array (continuous line), non-grid sparse array with fixed-size elements (dashed line) and non-grid array with variable-size elements (dotted line).

IUS5-PA-4

Micromachined High-Frequency ZnO Ultrasonic Linear Arrays

Jinying Zhang[1,2], Weijiang Xu[2], Gang Han[1], Julien Carlier[2], Xinming Ji[3], Shuming Chen[1]; *[1]School of Computer, National University of Defense Technology, Changsha, China, People's Republic of, [2]Departement Opto-Acousto-Electronique, I.E.M.N., UMR CNRS 8520 University of Valenciennes, Valenciennes, France, [3]ASIC and System State Key Lab, Department of Microelectronics, Fudan University, Shanghai, China, People's Republic of*

Background, Motivation and Objective

High-frequency (>100 MHz) ultrasonic array transducers can efficiently provide the necessary spatial resolution for use in corneal epithelium and skin epidermis visualizations, small tissue differentiations and other medical applications where high quality subsurface imaging is required. A number of researchers have focused their efforts on the fabrication methods of zinc oxide (ZnO) high-frequency transducers. ZnO single-element transducers have been widely used for acoustic microscopy applications in the frequency range of 100 MHz to 1GHz. Unlike high-frequency single-element transducers, one of the major challenges in developing high-frequency array transducers is the patterning of small-scale features within the array.

Statement of Contribution/Methods

Among the approaches to fabricate ZnO arrays, such as dice-and-fill, interdigital pair bonding, laser micromachining and so on, wet etching is much easier to carry out cheap and expeditious batch production. To realize ZnO arrays, the development of ZnO wet etching techniques with high etching rates, high selectivity over mask materials, highly anisotropic etch profiles, and smooth side-walls is essential. In this work, we develop a recipe to fabricate very-small-pitch array transducers based on wet etching of ZnO films on silicon substrate.

Results/Discussion

We use a controllable wet etching to fabricate 300 MHz c-axis ZnO-based linear array transducers. This method makes it possible to define the lateral element dimensions and positions with the resolution offered by photolithography techniques. Fig.a is the novel ZnO array by anisotropic etching using NH_4Cl solution (concentration: 10 wt%). It has a pitch of 13 μm and a kerf width of 6 μm. Fig.b presents a close-up detail of the side-wall profiles in this novel array. Moreover, the characteristics of the transducer are measured and compared to the theoretical predictions obtained by finite element method. The measured and simulated electrical impedances (Z) are illustrated for central element in a fabricated 15-element ZnO array. The real part of Z is around 200 Ω at 300 MHz. The paper also shows the measured and simulated crosstalk of adjacent and second adjacent elements in this ZnO array. The maximum magnitude is -53 dB in air at 300 MHz. The results indicate that the device has desired performances.

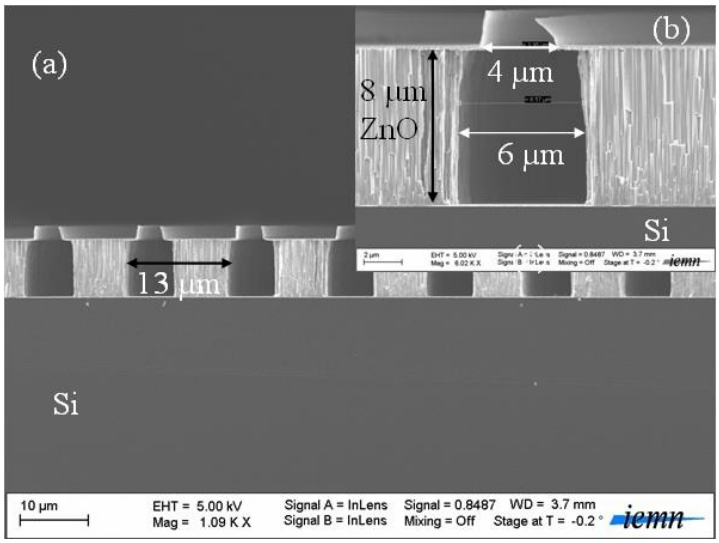

IUS5-PA-5

Fabrication and Performance of a 10 MHz Annular Array Based on PMN-PT single crystal for Medical Imaging

Jue PENG[1,2], Zhenhua HU[1,2], Hu TANG[1,2], Xin CHEN[1,2], Tianfu WANG[1,2], Siping CHEN[1,2]; *[1]Department of Biomedical Engineering,School of Medicine, Shenzhen University, National-Regional Key Technology Engineering Laboratory for Medical Ultrasound, Shenzhen, Guangdong, China, People's Republic of, [2]Guangdong Key Laboratory for Biomedical Measurements and Ultrasound Imaging, China, People's Republic of*

Background, Motivation and Objective

Most of high frequency focused ultrasound transducers in use today are spherically curved, single element transducers. These transducers have a limited axial depth of field (DOF) and a narrow geometric focus region, the image quality is dramatically deteriorated out of the focal zone. For the clinical ophthalmologic application, the B-mode/depth (B/D) scan method is not desirable because the transducer is moved in the axial direction, increasing the possibility of damaging the surface of the cornea. Annular array devices can provide the unique attribute of providing a much larger focal region through element-to-element time delay while retaining the image resolution.

The relaxor-based ferroelectric single crystal (1-x)Pb(Mg1/3Nb2/3)O3-xPbTiO3 (PMN-PT), although possessing extraordinary piezoelectric properties, are rarely reported being used for this purpose because it is difficult to separate PMN-PT single crystal into annular elements by dicing saw. In this paper, we report the development of an eight channel phased annular array based on a PMN-PT single crystal for medical imaging. Individual elements were created by ultraviolet laser ablation techniques.

Statement of Contribution/Methods

The array designed here had a total active aperture diameter of 7 mm with eight equal area (4.85 mm2) elements separated by 50µm kerfs. The desired central frequency was 10MHz. After the poling process, the PMN-PT sample was then cut by a commercial laser micromachining system M355-2E UV Laser Marker. Interconnection between ultra-fine coaxial cables and piezoelectric was accomplished by using 50 ¦Ìm copper wires soldered directly onto the individual elements. The cylindrical brass housing was then placed around the array, and partially filled with insulating epoxy with tungsten powder mixed to create an acoustically loss backing material. Finally, a prefabricated acoustic matching layer (8.8 Mrayls) was bonded to the exposed bottom electrode on the front face of the transducer.

Results/Discussion

The annular phased array was tested in a deionized water tank at room temperature in pulse/echo mode. The measured pulse/echo waveforms and the built-in fast Fourier transform spectrum are displayed. The measured results show that the central frequency was 10MHz, and the -6dB bandwidth as wide as 78%. The average two-way insertion loss at the central frequency of 10MHz was about -27dB. The improved lateral resolution and depth of field from the 50µm aluminum wire phantom image were observed, in which the axial and lateral resolutions at 12 mm depth are found to be 702µm and 188µm, respectively. Ultrasonic images of cattle eyes also were obtained with the 10-MHz annual array transducer. In the anterior portion of cattle eye it can be seen that the cornea and iris are well distinguishable. This eight element annular transducer is promising for ophthalmology and dermatology ultrasonic imaging and other high frequency ultrasonic diagnostics applications.

IUS5-PA-7

Reverse-Row-Column Method for Increasing Focusing Volume of 2D CMUT Array

Albert Chen[1], Lawrence Wong[1], John Yeow[1]; *[1]Systems Design Engineering, University of Waterloo, Waterloo, on, Canada*

Background, Motivation and Objective

Microfabrication technology has allowed miniature transducers, namely capacitive micromachined ultrasonic transducers (CMUTs), to be integrated in a dense array for high quality 3D imaging. However, with the increase of array count, the issue of circuit bulkiness and complexity increases dramatically. To counter this problem, a handful of techniques based on sparse array and synthetic aperture were created to simplify the electronics and drivers for high-density 2D arrays and real-time 3D imaging. Meanwhile, another promising method, the row-column (RC) addressing scheme, can also be adopted for simplifying the 2D array architecture. One of the main advantages of the RC array includes an ultra-fast scan rate similar to that of a 1D phase array. Secondly there is a dramatic reduction of interconnects. Given an N × N elements array, the total interconnects for a RC array is 2N instead of N2. As a result, the bulkiness of the front-end electronics can be minimized and the need for multiplexing and/or a large number of micro-coaxial cables can be avoided. However, RC array has the inherent inability to scan the volume above or below the transducer. Since an acoustic beam cannot be electronically steered in the elevation direction, transmit focusing in the elevation direction is limited by the natural focusing.

Statement of Contribution/Methods

This work reports a novel Reverse-Row-Column method, which virtually rotates the RC array orthogonally to achieve transmit beam steering in both directions without altering the transducer array. The implementation is achieved mainly by adding electrical switches such that each row and column can be connected to either the transmitter or receiver circuitry. Simulations were performed to map the theoretical focal volume, given the CMUTs' parameters. A custom-built circuitry was designed to implement the novel method. A custom-built fast imaging system was used to drive a 32 x 32 element RC CMUT array.

Results/Discussion

The imaging system successfully demonstrates a significant increase in scanning volume in the elevation direction. Strategically-placed Scatterers were able to help visualize the scanning volume shapes. Special circuitry and focusing design considerations are discussed for ensuring the bias voltage and pulsers are reconnected properly at each virtual rotation to minimize scan time and system perturbation.

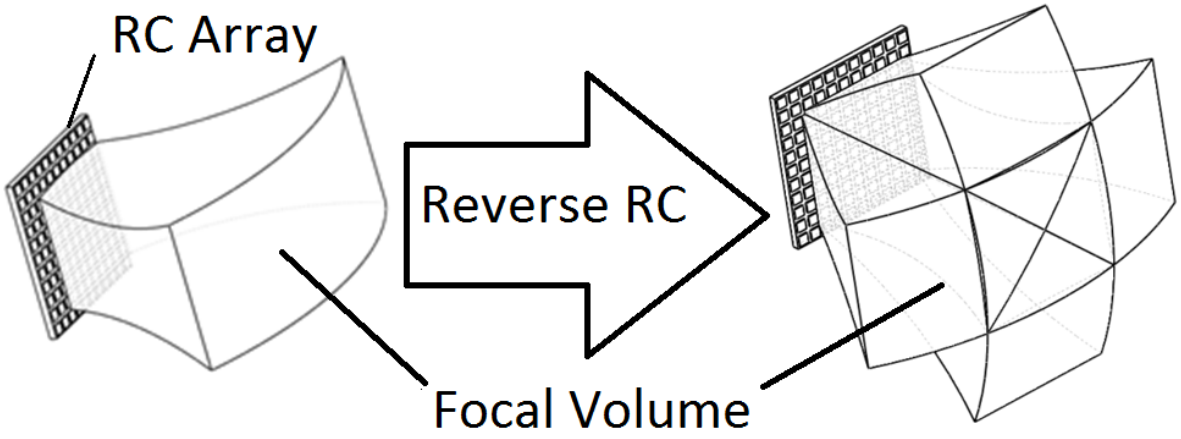

IUS Student Poster Competition

Forum Hall

IUS-SPC-1

08:00 am **Ultrasonic imaging of tightly closed cracks by linear phased array with global preheating and local cooling and the estimation of crack closure stress**

Koji Takahashi[1], Yoshikazu Ohara[1], Kazushi Yamanaka[1]; [1]*Materials Processing, Tohoku University, sendai, Japan*

Background, Motivation and Objective

We have developed a closed crack imaging method, subharmonic phased array for crack evaluation (SPACE) and verified it [Y. Ohara, et al., APL **90** (2007) 011902]. However, the selectivity of closed cracks might be degraded when SPACE used short-burst input waves. So we have developed load difference phased array (LDPA) and verified it in a fundamental experiment by a servohydraulic testing machine [Y. Ohara, et al., Ultrasonics **51** (2011) 661]. However, it was not practical because of its big size. As a practical method, local cooling (LC) by cooling spray was proposed [P. B. Nagy, et al., Rev.Prog.QNDE **14** (1995) 1979]. However, the tensile thermal stress is insufficient to open tightly closed crack. In this study, to increase the thermal stress, we propose global preheating and local cooling (GPLC) and verify it by linear phased array (PA). We also estimate crack closure stress with a heat transfer analysis.

Statement of Contribution/Methods

In GPLC, the top surface of specimen is locally cooled with cooling spray after global preheating, resulting in a tensile thermal stress by a principle similar to that of a three-point bending test. The thermal stress can be increased by increasing GP temperature since it depends on the temperature difference ΔT between the top surface and the crack area. Here we applied LC and GPLC to a closed crack with 11.3 mm depth and imaged it by PA. Furthermore, we analyzed temperature distribution within the specimen by 1D heat transfer analysis as a measure of thermal stress, and estimated the crack closure stress.

Results/Discussion

The closed crack was not observed in the PA image before LC (Fig. 1 (a)). By applying LC, the crack was imaged at a depth of 9.6 mm (Fig. 1 (b)). However, it was still smaller than the actual one. This shows that the thermal stress is insufficient. Then, we applied GPLC. As a result, the crack was imaged at a depth of 11.3 mm (Fig. 1 (c)). This is the same as the actual one. Thus, we demonstrated that GPLC is effective in opening the tightly closed crack. Furthermore, we compared the change in crack depth d and ΔT obtained by the heat transfer analysis with cooling time t (Fig. 2). ΔT took a maximum at t = 4-6 s, and gradually decreased at $t \geq$ 7s. This behavior agrees with that of d. Also, by assuming the thermal stress at t = 4-6 s to be the crack closure stress, we estimated it by substituting the temperature distribution into an equation of thermal bending stress.

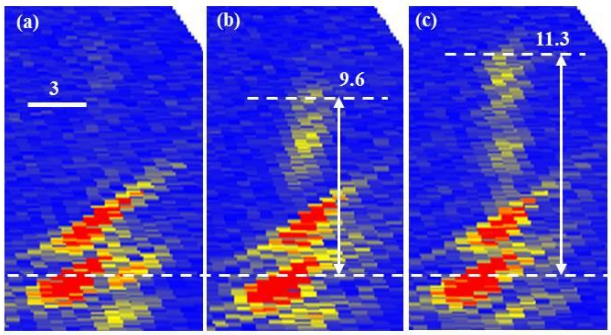

Fig. 1 PA images of closed crack :
(a)Before cooling, (b)LC, (c)GPLC.

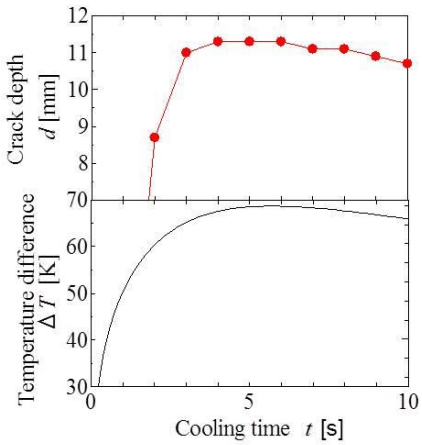

Fig. 2. Crack depth by experiment d
and Temperature difference by analysis ΔT.

IUS-SPC-2

08:00 am **Performance evaluation of reconfigurable FPGA based embedded ARM processor for ultrasonic imaging**

Spenser Gilliland[1], Pramod Govindan[1], Thomas Gonnot[1], Jafar Saniie[1]; [1]*Electrical and Computer Engineering, Illinois Institute of Technology, USA*

Background, Motivation and Objective

The objective of this study is to evaluate the performance of an FPGA based embedded ARM processing system for the implementation of signal processing in the fields of ultrasonic imaging and nondestructive testing. The embedded processor has many advantages including the integration of various components within the system through the use of hardware-software (HW/SW) co-design. Architectural advancement of FPGAs with embedded processors are capable of meeting the real-time processing requirements for all practical applications.

Statement of Contribution/Methods

A Reconfigurable Ultrasonic System-on-Chip Hardware (RUSH) platform is developed to implement ultrasonic signal processing algorithms in embedded software and reconfigurable hardware. In this study, we evaluate and optimize the execution time of three ultrasonic signal processing algorithms (i.e., parametric echo estimation, frequency diverse flaw detection, and joint time-frequency distribution) on a Xilinx Virtex-5 FPGA with an embedded Microblaze processor and a Xilinx Zynq 7020 FPGA with an embedded ARM processor. The Zynq combines an ARM dual-core processing unit with the FPGA fabric which makes it ideal for ultrasonic signal processing applications since it

provides a significant boost to the software execution capabilities. Additionally, due to the wide adoption of embedded ARM devices, it is more convenient to acquire code development tools and technical support for ARM based devices.

Results/Discussion

A real-time frequency-diverse ultrasonic flaw detection application with a repetition rate of 1000 measurements/sec using split-spectrum processing (SSP) is implemented in both hardware and software using optimized IP Cores on the RUSH platform. The SSP execution time for 2048 samples using the ARM processor embedded within the Zynq is only 5 ms, whereas the same algorithm requires 160 ms using the Microblaze processor within the Virtex-5. Parametric echo estimation using the chirplet signal decomposition (CSD) algorithm on the Microblaze processor takes one second to estimate one echo; while the ARM processor estimates 100 echoes per second. Time-frequency distributions including Wigner-Ville distribution (WVD) and short-time Fourier transform (STFT) require a computation time of less than 50 ms for 2048 points on the ARM processor. Our study proves that the Zynq FPGA with an ARM processor computes the ultrasonic algorithms almost 30 times faster than the Virtex-5 FPGA with a Microblaze processor. The ability to quickly port the RUSH platform to the Zynq was enabled by the use of portable applications which require simple recompilation to port to a new platforms. The performance improvement of moving to newer and faster FPGAs clearly demonstrates the advantages of using portable reconfigurable platforms for ultrasonic imaging and signal processing applications.

IUS-SPC-3

08:00 am **Laser ultrasonic velocity measurement for Phase transformation investigation in Ti alloy (Ti-6% Al-4% V)**

Saeid Zamiri[1,2], Bernhard Reitinger[1], Jürgen Roither[1], Siegfried Bauer[3], Peter Burgholzer[1,2]; *[1]Research Center for Non Destructive Testing GmbH (RECENDT), Linz, Austria, [2]Christian Doppler Laboratory for Photoacoustic Imaging and Laser Ultrasonic, Linz, Austria, [3]Department of Soft Matter Physics, Johannes Kepler University, Linz, Austria*

Background, Motivation and Objective

Titanium (Ti) alloys sustain highest demands, e.g. in aerospace industries. The mechanical properties of Ti with different percentages of aluminum and vanadium strongly depend on the microstructure and further the change of microstructure with temperature (Phase transformation). Therefore monitoring the phase transformation of Ti is essential and is carried out by using a nondestructive method. We monitor the Phase transformation in a Ti alloy by using a laser ultrasonic (LUS) method based on two wave mixing interferometer which has the key benefits of being fast and contactless with high resolution.

Statement of Contribution/Methods

We will report on monitoring the phase transformation temperature in Ti alloy (Ti-6% Al-4% V) about 1000°C by using a simple contactless LUS method based on two waves mixing in a fast BSO photorefractive crystal. In our LUS laboratory setup, a reference beam and a phase modulated signal beam interfere inside the BSO crystal. Due to the modulated refractive index in the crystal, a grating is formed and the two beams are coupled, and further the reference beam is diffracted in the speckled signal beam direction. The diffracted beams were focused with a lens on a broadband and fast photo-receiver. The experiments were carried out on 1.5 mm thick Ti sheets with 100 mm length. The samples were heated up by applying high current (0-30A) up to a temperature of 1200°C. To generate the ultrasonic bulk waves, picoseconds pulses from a 1064 nm Nd:YAG pulsed laser were focused on the sample backside. The detected bulk waves on the opposite side of the sample (measurement in transmission geometry) with the longitudinal and shear waves are shown in the Figure 1.

Results/Discussion

With the mentioned contactless and fast method it was possible to detect the phase change of Ti-6-4 from α to β phase. From the figure the phase change shows as the temperature increases the ultrasonic wave velocity decreases (time of flight increases) up to 980°C which shows the start of the phase change region in Ti. At 980°C to 1020°C the bulk wave velocity is approximately constant which indicates the process of the phase transformation from α to β phase. Above 1050°C to 1200°C the bulk wave velocity reduces very slowly.

Fig1. Phase change of Ti-6-4 from α to β phase versus Temperature (room to1200°C)

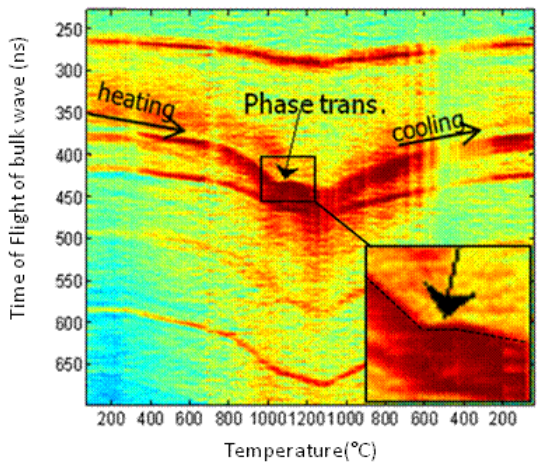

IUS-SPC-4

08:00 am **Optoacoustic Elastography for Tissue Biomechanical Property Characterization Using a Ring Transducer**

Teng Ma[1], Rui Li[2], Wenjuan Qi[2], Qifa Zhou[1], Zhongping Chen[2], K. Kirk Shung[1]; *[1]Department of Biomedical Engineering, University of Southern California, Los Angeles, California, USA, [2]Beckman Laser Institute & Medical Clinic, University of California, Irvine, Irvine, California, USA*

Background, Motivation and Objective

Elastography, capable of quantitatively providing the biomechanical properties information of tissue, plays a key role in the clinical diagnosis, such as cancerous tumor detection and atherosclerotic plaque characterization. Phase-resolved optical coherence elastography (PR-OCE) possesses superior resolution, high imaging speed with the capability of providing point-by-point elastogram mapping. Acoustic radiation force (ARF) generated by high-intensity ultrasound bursts, offers the dynamic excitations with the benefits of directly and remotely inducing the localized displacement of tissue within the region of interest. Different methods of beam forming are capable of producing ARF such as AM

beam geometry and confocal dual beam geometry. In this work, we successfully differentiate the biological tissues with different biomechanical properties utilizing a ring transducer with AM beam geometry in PR-OCE system, which demonstrates the feasibility and superiority to move this imaging system into clinical application.

Statement of Contribution/Methods

The PR-OCE vibration detection system is similar to a previous publication using an 890 nm spectral domain OCT system with the minimum phase being detected of 1.5mrad. The sample is excited by a 4MHz focused ring transducer driven by a 500 Hz AM modulated square wave. The transducer has a focal width of 1.2 mm and length of 1.5 mm at a working distance of 49mm. This featured confocal configuration enables the 2D scanning within the insonation field, in which we assume the ARF induced particle displacements are evenly distributed. The instantaneous axial velocity of vibration can be extracted from the phase shift information measured PR-OCE system to characterize the biomechanical properties. We imaged the cancerous kidney tissue, and the results are confirmed by the histology.

Results/Discussion

The 3D OCT intensity image in Fig.1 (a) provides a general morphological view of the sample. However, in Fig1 (b), the OCE image displays regions with different vibration phase contrast, where the red area indicates the stiffer cancerous tumor tissue, and the green area indicate the softer fat tissue. The fused OCT and OCE image is shown in Fig1(c). The 2D OCE image Fig1 (d) clearly agrees with the histology image Fig.1 (e) in its capability of distinguishing the cancerous tumor tissue on both sides with the middle soft tissue.

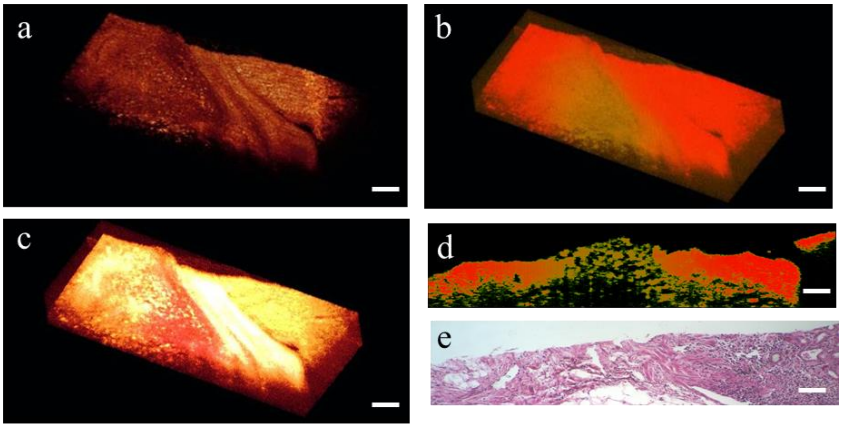

Figure.1 (a) 3D OCT intensity structural image of kidney tissue. (b) 3D OCE phase image under ARF excitation. (c) Fused OCT and OCE image. (d) 2D B-scan OCE image corresponding to the across blue line in (b). (d) Histology image Scale bars:100um.

IUS-SPC-5

08:00 am **A 32x32 Integrated CMUT Array for Volumetric Ultrasound Imaging**

Anshuman Bhuyan[1], Chienliu Chang[2], Jung Woo Choe[1], Byung Chul Lee[1], Amin Nikoozadeh[1], Omer Oralkan[3], Yagi Takayuki[2], Butrus Khuri-Yakub[1]; *[1]Stanford University, USA, [2]Canon Inc., Japan, [3]North Carolina State University, USA*

Background, Motivation and Objective

Volumetric ultrasound imaging is very important in medicine due to the diagnostic potential it can offer to physicians. Two-dimensional transducer arrays are desirable to capture 3D images. However, large 2D arrays require appropriate interface circuits to reduce the number of backend cables as well as to improve the noise performance. In this paper, we demonstrate volumetric imaging by use of a 32×32 array IC directly integrated with a 32×32 capacitive micromachined ultrasonic transducer (CMUT) array using flip-chip bonding technology.

Statement of Contribution/Methods

The 32×32 CMUT array is designed to operate at a center frequency of 5 MHz with a transducer element pitch of 250 µm. Previous work (Bhuyan et al, ISSCC 2013) shows integration of four 16×16 ICs to a 32×32 CMUT array by use of an interposer. However, the larger 32×32 IC enables direct flip-chip bonding with the CMUT array without the interposer layer, thereby reducing parasitics. It also allows for compact assembly making it possible to build probes with a smaller form factor. Each IC channel has the capability to either transmit or receive. The receive circuitry consists of a transimpedance amplifier and a buffer for signal conditioning of the echo. The transmit circuitry consists of a pulser, shift-registers, and digital logic to enable transmit beamforming. Each element in the array can be excited with a high voltage unipolar pulse of up to 60 V. We packed all the circuitry pertaining to one transducer element within a 250 µm × 250 µm space (i.e., same as the CMUT array element size). For pulse-echo 3D imaging, we use all elements (except diagonals) for transmit and diagonal elements for receive to reduce the number of backend cables without significantly degrading the image quality.

Results/Discussion

The CMUT-IC assembly measure 9.1 mm × 9.1 mm. Each receive channel has a bandwidth of 20 MHz and a transimpedance gain of 200 kΩ. The power per receive channel is 4.5 mW. A circuit board is designed to interface the frontend CMUT-IC assembly to the backend system consisting of an FPGA and a data acquisition system. Wire-phantoms were used in the imaging experiment. We have successfully demonstrated real-time volumetric imaging at a rate of 3 volumes per second and up to a depth of 75 mm. This work is funded by the NIH. Intersil Corporation provided support for fabrication of the ICs.

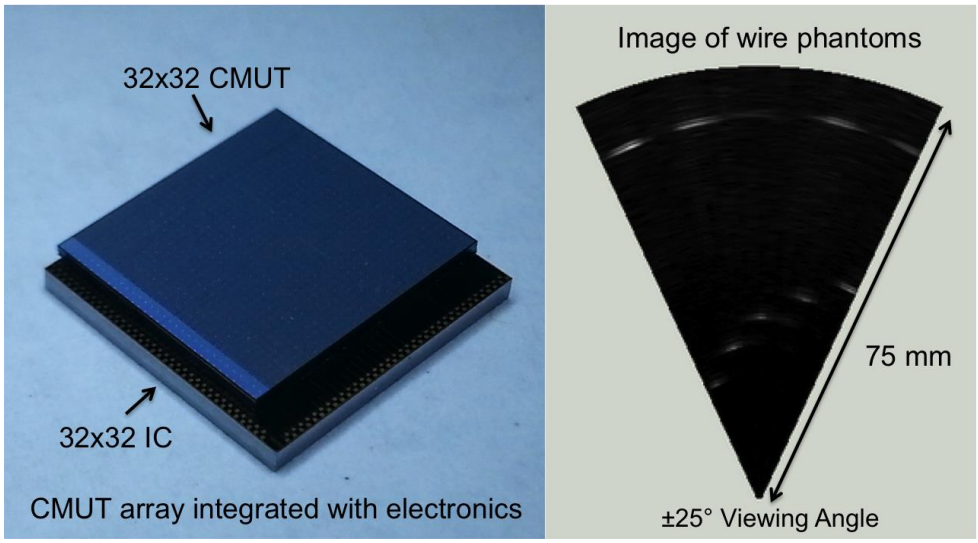

IUS-SPC-6

08:00 am **Towards Backscattering Tensor Imaging (BTI): Analysis of the Spatial coherence of ultrasonic speckle in anisotropic soft tissues**

Clément Papadacci[1], Mathieu Pernot[1], Mickael Tanter[1], Mathias Fink[1]; [1]*Institut Langevin, CNRS, ESPCI, Paris, France*

Background, Motivation and Objective

The assessment of fiber architecture is of major interest in the progression of myocardial disease. Recent techniques such as MR Diffusion Tensor Imaging or Ultrasound Elastic Tensor Imaging (ETI) can derive the fiber directions by measuring the anisotropy of water diffusion or tissue elasticity, but these techniques present severe limitations in clinical setting. We propose to investigate the anisotropy of the backscattered ultrasound field. The spatial coherence of the backscattered field was previously shown to vary with the fibers direction in composite solid materials. In this study, we measure the spatial coherence of ultrasonic speckle in skeletal muscles and myocardial tissues, determine the fibers directions and compare it to ETI.

Statement of Contribution/Methods

Acquisitions were performed using a linear transducer array (6MHz, 128 elements, 0.2mm pitch, Vermon) connected to an ultrasonic scanner (SuperSonic Imagine) mounted on a rotation device with angles from 0° to 355° by 5° increments to image ex vivo bovine skeletal muscle and porcine LV myocardial samples. At each angle, a focused ultrasonic pulse was transmitted and the backscattered echoes recorded. After backpropagation, the autocorrelation of the signals received on the transducers was performed by pairs to compute the spatial correlation function. The coherence factor was measured as the integral of the correlation function over 40 elements. Shear Wave Imaging was performed at each angle by imaging at 8,000 frames per second the propagation of a shear wave induced by the acoustic radiation force of a focused ultrasound burst (300µs).

Results/Discussion

The coherence varied by a factor of 3 with the probe angle in skeletal muscle and myocardium. In skeletal muscle, maximal/minimal coherence was found for the probe parallel/perpendicular to the fibers. In myocardium, the coherence was assessed across the entire myocardial thickness, and the position of maxima and minima varied transmurally due to the complex fibers distribution. The shear wave speed (3.9 m/s across the fibers to 5.9 m/s along the fibers) variation with the probe angle was found to follow the coherence variation. Spatial correlation can thus reveal the anisotropy of the ultrasonic speckle in skeletal muscle and myocardium. BTI could be used on any type of ultrasonic scanner for non invasive evaluation of myocardial fibers.

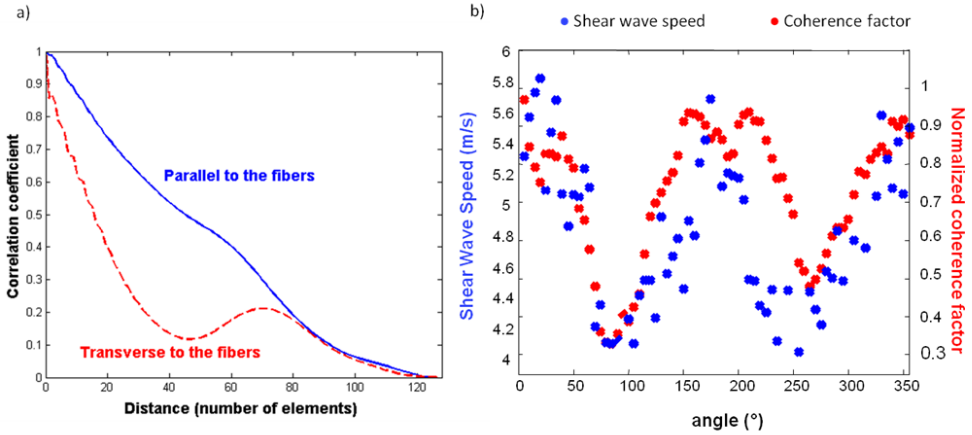

Figure: a) spatial correlation functions when the probe is set parallel and transverse to the fibers. b) Variation of the coherence factor and shear wave speed with the probe angle.

IUS-SPC-7

08:00 am **Compensation of the Combined Effects of Absorption and Dispersion in Plane Wave Pulse-Echo Ultrasound Imaging Using Sparse Recovery**

Martin Schiffner[1], Georg Schmitz[1]; [1]*Chair of Medical Engineering, Bochum, NRW, Germany*

Background, Motivation and Objective

Conventional strategies for fast image acquisition, e.g. coherent plane wave (PW) compounding or synthetic aperture focusing (SA), are based on physical models that emphasize a lossless medium. However, absorption is a major effect in biological tissues and exhibits a power law dependence on frequency. This dependence is accompanied by a frequency-dependent phase velocity of the ultrasound waves that strongly distorts the shape of broadband pulses (dispersion, cf. (a)).

In this study, we extended our concept for PW pulse-echo ultrasound imaging (UI) based on sparse recovery (SR) [1] to compensate for the combined effects of absorption and dispersion. Our goal was to significantly improve the image quality in fast image acquisition.

Statement of Contribution/Methods

We formulated a linear inverse scattering problem (ISP) to recover spatial fluctuations in compressibility in a specified field of view from measurements of the scattered sound. The governing wave equation contains convolutional loss operators to account for absorption and dispersion based on a time causal model. For excitation, multiple steered broadband PWs were emitted. We adopted a sparse recovery strategy to regularize the ill-posed ISP, i.e. we assumed that there exists a sparse representation of the fluctuations in compressibility in a known basis. We investigated various wavelet bases and block transforms.

For experimental validation, we acquired pulse-echo measurement data from a commercial tissue phantom (A) and a human thyroid (B, *in vivo*). Recovered images were compared to those generated by SA (128 wave emissions), delay-and-sum (DAS; 11 PW emissions), and minimum variance (MV, 11 PW emissions) algorithms.

Results/Discussion

Using only two steered PW emissions and a Daubechies-20 wavelet basis for sparse representation, our concept outperformed SA, DAS, and MV in terms of lateral -6 dB-widths and image contrast (cf. (b) to (f)).

Our SR-based concept in combination with a realistic physical model for wave propagation significantly improved the image quality in comparison to conventional strategies for fast image acquisition. It could thus be beneficial in applications that crucially depend on short acquisition times, e.g. cardiac UI and flow UI.

[1] M.F. Schiffner and G. Schmitz, "Fast Image Acquisition in Pulse-Echo Ultrasound Imaging Using Compressed Sensing", Proc. IEEE IUS, 2012

Financial support by Ziel2.NRW 2007-2013 co-financed by ERDF, grant no. 005-0908-0117.

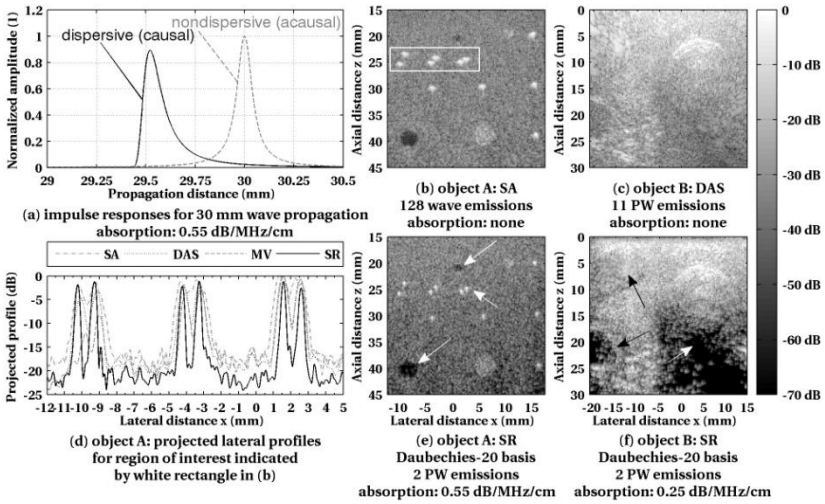

IUS-SPC-8

08:00 am **Ultrasound-induced bioorthogonal chemistry in-situ using composite droplets**

Marine Bézagu[1], Claudia Errico[1], Victor Chaulot-Talmon[1], Stellios Arseniyadis[1,2], Olivier Couture[1,2], Mickael Tanter[1,3], Janine Cossy[1], Patrick Tabeling[1]; [1]*ESPCI ParisTech, Paris, France,* [2]*CNRS, France,* [3]*INSERM, France*

Background, Motivation and Objective

Drug-delivery would undoubtedly become much more powerful if the drug could be prepared at the focus of an ultrasound scanner. In this context, we previously proposed the use of composite droplets comprised of a nanoemulsion of water within a perfluorohexane matrix (4 µm in diameter) for the encapsulation of large payloads, which could be delivered *in-vivo* with an ultrasound scanner (Couture *et al. Medical Physics*, **2011**, 2012). We hypothesized that these droplets could be used to isolate two reactants (**A** and **B**) from one another and deliver them upon vaporization of the perfluorocarbon matrix, thus allowing the *in situ* generation of a new product (**C**) (Figure 1). The steep threshold of release (1.7 MPa PNP at 5 MHz) of these droplets allows the triggering of a chemical reaction with a **high spatial** (mm) and **temporal resolution** (ms).

Statement of Contribution/Methods

The demonstration was achieved by encapsulating a solution of **A** (azidocoumarin) in DMSO into composite droplets of perfluorohexane and releasing the content into the external flow containing **B** (reactive alkyne). Most importantly, the product of the reaction of **A** and **B** is fluorescent (ex: 350 nm, em: 430 nm). The two solutions (**A** encapulsated + **B** in solution) were injected in a microfluidic channel where a 2.25 MHz transducer was focused. A single pulse of 20 cycles was emitted while a camera (10 fps) mounted on a fluorescent microscope (10X, DAPI) recorded the fluorescence induced during the reaction.

Results/Discussion

Within the microfluidic channel, a single acoustic pulse was able to vaporize several droplets, leading to the release of their content in the surrounding medium. As shown below, in the following 100 ms upon release, the fluorescence intensity within the focus zone was multiplied by a factor of 2.9 (**A** + **B**). As the fluorescence is specific to the reaction product, this demonstrates the subsequent formation of the latter after ultrasound release.

In summary, we managed to remotely induce a chemical reaction with ultrasounds by releasing an encapsulated reactant locally into a flow containing its reactive partner. This reaction was limited temporally, following the 10 ms pulse, and spatially, within the focus of the transducer. We expect that such targeted chemistry could lead to the localized release of prodrugs or to the localized production of drugs in-vivo that are either too toxic or unstable to be injected.

Figure 1. Microscope images of the ultrasound-induced chemical reaction. The release pulse happened between the first and second images (100 ms apart). a) t= −100 ms; b) t= 0, c) t= +100 ms; d) t= +200 ms.

IUS-SPC-9

08:00 am **New Quantification Methods for Carotid Intraplaque Neovascularization in Contrast Enhanced Ultrasound (CEUS)**

Zeynettin Akkus[1], Gonzalo Vegas Sanchez-Ferrero[2], Guillaume Renaud[1], Stijn C.H. van den Oord[3], Arend F.L. Schinkel[3], Nico de Jong[1], Antonius F.W. van der Steen[1]; *[1]Biomedical Engineering-Thoraxcenter, Erasmus MC, Netherlands, [2]Image Processing Laboratory, University of Valladolid, Spain, [3]Department of Cardiology, Thoraxcenter, Erasmus MC, Netherlands*

Background, Motivation and Objective

Carotid intraplaque neovascularization (IPN) has been associated with progressive atherosclerotic disease and plaque vulnerability. Therefore, its accurate quantification might allow early detection of plaque vulnerability. CEUS can detect these small microvessels. To quantify IPN, we developed quantitative methods which are perfusion analyses based on time intensity curve (TIC) and maximum intensity projection (MIP), vascular structure analysis (VSA), and statistical segmentation (SS).

Statement of Contribution/Methods

Plaque region of interest (ROI) is manually drawn and motion compensation is applied before each analysis. In TIC and MIP, we examine perfusion dynamics and regions within plaques. In VSA, we detect and track contrast spots to examine microvessels network. In SS, we classify plaque intensities into different components for quantification of IPN. Through an iterative expectation-maximization algorithm, plaque pixels are initially labeled into artifacts, contrast, intermediate and background class. Next, spatiotemporal and neighborhood information is used to relabel intermediate class pixels, remove artifacts and correct false-contrast. From the applied analyses, we derived several parameters – MIP based IPN surface area (MIPNSA), MIP based IPN surface ratio (MIPNSR), SS based IPN surface area (SSIPNSA), plaque mean intensity, mean plaque contrast percentage, and number of microvessels (MVN) – and compared them to visual grading of IPN by two independent physicians. We analyzed 45 carotid arteries with stenosis. To verify if SSIPNSA improves the suppression of artifacts, we analyzed 8 plaques twice, with saturation artifacts included and excluded from the ROI.

Results/Discussion

MIPNSA (r=0.719), SSIPNSA (r=0.698), MIPNSR (r=0.484) and MVN (r=0.538) were found to be significantly correlated to visual scoring ($p<0.01$). The MIPNSA & SSIPNSA parameters gave the best distinction between visual scores. SSIPNSA (3.9±3.2 mm2 with vs. 3.8±3.2 without artifact) gave slightly higher areas but proved less sensitive for artifacts than MIPNSA (9±3.3 with vs. 3.2±2.9 without). If there are artifacts within plaque ROI, SSIPNSA will suppress artifacts and gives more reliable results than MIPNSA (fig. 1). MIPNSA, SSIPNSA, MIPNSR and MVN may thus have the potential to replace qualitative visual scoring and to measure the degree of carotid IPN.

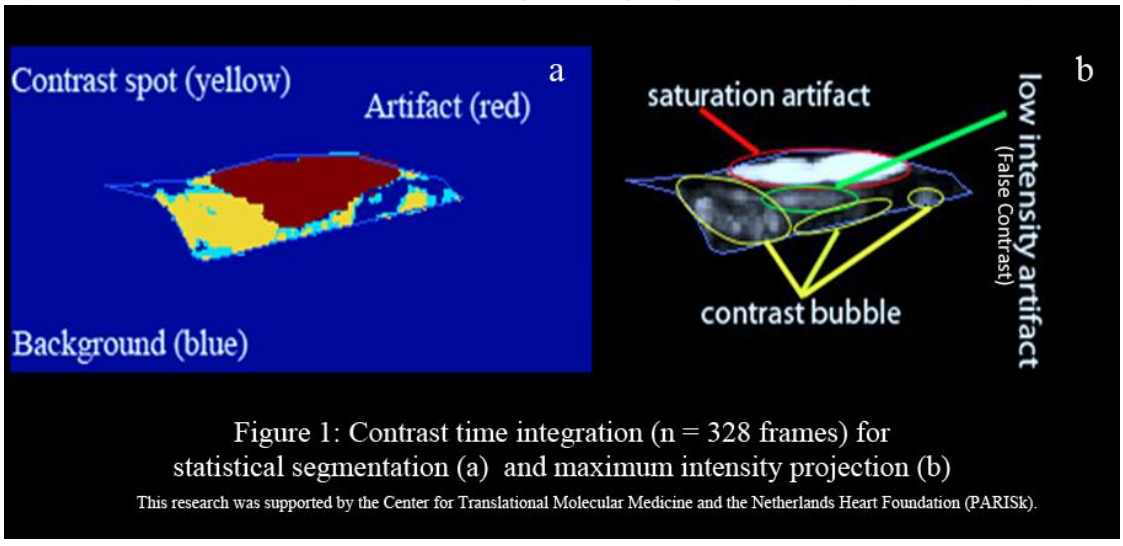

Figure 1: Contrast time integration (n = 328 frames) for statistical segmentation (a) and maximum intensity projection (b)

This research was supported by the Center for Translational Molecular Medicine and the Netherlands Heart Foundation (PARISk).

IUS-SPC-10

08:00 am **Leaky Wedge Acoustic Waves in Single-Crystal Silicon**

Alexey Lomonosov[1,2], **Pavel Pupyrev**[1,3], Peter Hess[2], Andreas Mayer[3]; *[1]General Physics Institute, RAS, Moscow, Russian Federation, [2]Institute of Physical Chemistry, University of Heidelberg, Germany, [3]HS Offenburg - University of Applied Sciences, Gengenbach, Germany*

Background, Motivation and Objective

Wedge acoustic waves are guided by the apex of an edge formed by two intersecting planar surfaces of a solid elastic medium. In ideal wedges, these waves are non-dispersive like surface acoustic waves in homogeneous halfspaces. In isotropic media, their speed is lower than the Rayleigh wave velocity. Potential applications include NDE, sensors, and actuators.

In anisotropic media, the existence of leaky surface acoustic waves is a well-known phenomenon widely used in signal-processing devices. Very recently, their analogs at the apex of an elastic silicon wedge have been found in experiments using laser-ultrasonics [1].

Statement of Contribution/Methods

With a laser-operated mode-selective transducer developed for these purposes, surface acoustic wave (SAW) pulses and acoustic pulses localized at the apex of the wedge were excited. In addition to a wedge-wave pulse (WW) with low speed, a pseudo-wedge wave pulse (p-WW) was found with a velocity higher than the velocity of shear bulk waves, propagating in the same direction. (An example is shown in the figure below.) Several geometries in the highly anisotropic silicon crystals were investigated with wedge angles of 90° and 70.5°.

With a probe-beam deflection technique, the propagation of the WW pulses was monitored on one of the surfaces of the wedge at variable distance from the apex. In this way, their depth structure and the leakage of the p-WW could be visualized directly.

Calculations were carried out using FEM and a method based on a representation of the displacement field in Laguerre functions. Based on the latter, an "apex-projected density of states" was calculated, where the p-WW emerge as sharp peaks.

Results/Discussion

The speeds of the wedge wave and p-WW pulses were confirmed in the calculations. A detailed analysis of the strain distribution of the wedge and pseudo-wedge pulses on the surfaces of the wedge is given. Especially, the interaction of p-WW pulses with the surface and bulk waves is demonstrated.

This work is supported by Deutsche Forschungsgemeinschaft (Grant No. Ma 1074/11).

[1] A. M. Lomonosov, P. Hess and A. P. Mayer, Appl. Phys. Lett. 101, 031904 (2012).

Figure: Retarded time as function of propagation distance.

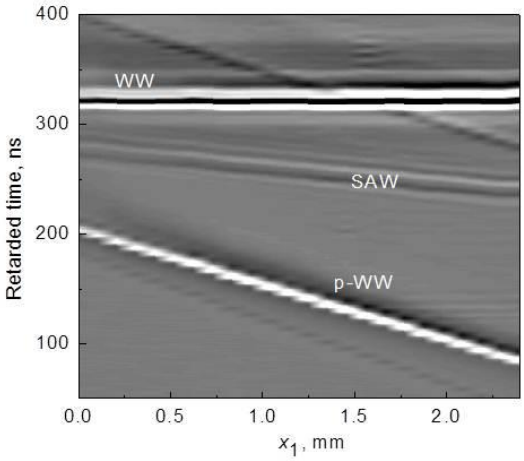

IUS-SPC-11

08:00 am **Polarity control of c-axis oriented ZnO films and application to polarity-inverted ZnO multilayer resonators**

Ryosuke Hashimoto[1], Takahiko Yanagitani[2], Ryo Ikoma[1], Shinji Takayanagi[1], Masashi Suzuki[2], Hiroyuki Odagawa[3], Mami Matsukawa[1]; *[1]Doshisha University, Japan, [2]Nagoya Institute of Technology, Japan, [3]Kumamoto National College of Technology, Japan*

Background, Motivation and Objective

Physical constants, such as nonlinear optical coefficient and piezoelectric constant, are reversed in sign between Zn- and O-polar ZnO. Polarity control of ZnO is therefore important for optical and piezoelectric devices. Generally, the polarity of ZnO is controlled by using an epitaxial technique. In this study, we report a method for controlling polarity of ZnO by adjusting the amount of ion bombardment and substrate temperature during sputtering deposition.

Statement of Contribution/Methods

ZnO films were grown on the Al/Ti/SiO_2 substrates by an RF magnetron sputtering technique. The amount of ion bombardment inside the glow discharge is larger than that of the outside [1]. We set the substrate inside or outside the glow discharge to induce or reduce the ion bombardment. The substrate temperatures were adjusted from 70 to 400 ºC. Au top electrode was evaporated on each ZnO film to fabricate a HBAR (high overtone bulk acoustic resonator) structure. Sign of the polarities of the ZnO films were determined by sign of the piezoelectric response when compression stress is applied to the sample. k_t values were estimated by a conversion loss of the HBAR. Finally, we fabricated two types of polarity-inverted ZnO multilayer resonators consisting of O-polar on Zn-polar or Zn-polar on O-polar ZnO structure. Zn-polar and O-polar ZnO films in this structure were grown outside the glow discharge at 150°C and 400°C, respectively.

Results/Discussion

Fig. 1 (a) shows polarities and k_t values of ZnO films grown at different substrate temperatures. Zn-polar ZnO films were grown below 150°C, whereas O-polar ZnO films were grown above 300°C. Around 250°C, the polarity of ZnO films might be determined by the amount of ion bombardment to the substrate. Fig. 1 (b) and (c) show conversion losses of polarity-inverted ZnO multilayer resonators consisting of (b) O-polar on Zn-polar and (c) Zn-polar on O-polar ZnO structure. Fundamental thickness extensional modes (L_1) resonances were suppressed and second-overtone modes (L_2) resonances were strongly excited. These results indicate that two layered ZnO resonators have O-polar on Zn-polar or Zn-polar on O-polar ZnO inverted polarity structure as expected. We demonstrated that this method could control polarity of ZnO without epitaxial technique.

[1]S. Takayanagi, et al., *Appl. Phys. Lett*., 101(2012) 232902.

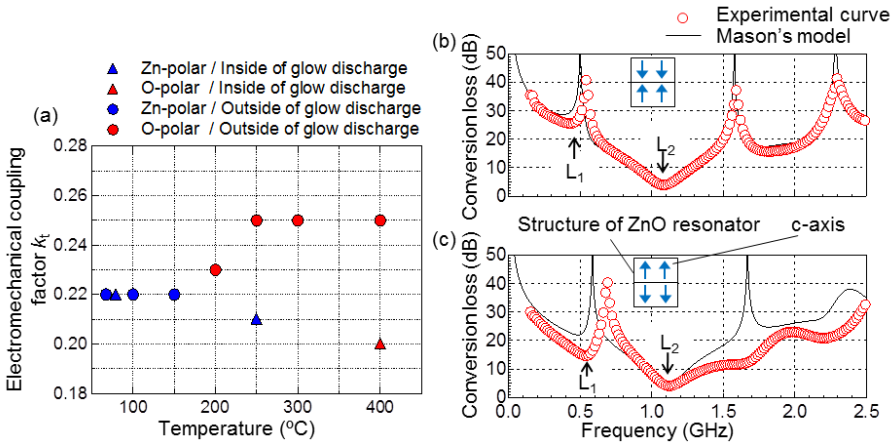

Figure. 1 (a) Polarity and k_t value of ZnO films depending on growth temperature. Frequency response of longitudinal wave conversion loss of (b) O-polar on Zn-polar and (c) Zn-polar on O-polar ZnO inverted polarity resonator.

IUS-SPC-12

08:00 am **Acoustic metamaterial: experimental investigation of the acoustic field scattered by isolated active resonators**

Remi Marchal[1], Bernard Bonello[2], Jinfeng Zhao[1], Olga Boyko[1]; *[1]University Pierre et Marie Curie, France, [2]INSP, CNRS and University Paris 6, France*

Background, Motivation and Objective

Acoustic metamaterials are heterostructures designed to control the propagation of elastic waves. They are generally constituted by local resonators embedded into a homogeneous matrix. Effec-tive mass density and compressibility can be both negative when resonators are excited in vibra-tion(s) which is (are) out-of-phase with respect to the elastic wave that propagates in the matrix.

Isolated silicon pillars and pairs of holes in a silicon plate are potentially "good" candidate to ful-fill this requirement.

Statement of Contribution/Methods

To conduct this study, we used an all-optical experimental technique. Our approach consisted in (i) measuring the eigenfrequencies of the resonators in order to select the one which allows ful-filling the homogenization criteria at the best; (ii) mapping the field associated to an incident Lamb wave scattered by this passive resonator; (iii) finally comparing this "passive" scattered field to the "active" one corresponding to the scattering of the incident Lamb wave by the reso-nator vibrating onto its eigenmode out-of-phase with respect to the incident Lamb wave. Fig. 1 shows the experimental results obtained at step (ii) for silicon pillar 230ìm high and 146ìm in diameter. These structures were elaborated using deep reactive-ion etching technique (DRIE) using Bosch process in a silicon wafer.

Results/Discussion

Along the direction of excitation, at 3MHz, far from the resonance, we see the A0 Lamb mode propagating with a velocity around 2000 m.s-1 and the pillar (at 0 position) vibrating in phase with the wave; the normal displacement on the top was measured to be two times less than the amplitude of the incident wave (Fig. 1a). However, at resonance which takes place at 6MHz, two differences can be observed: first, the displacement on the top of the pillar is seven times more than the one of the incident wave. Secondly, the pillar vibrates out-of-phase for a time much longer than the excitation duration. In addition one can notice the occurrence of re-emitted waves which are out-of-phase with respect to the incident wave (Fig. 1b).

This work is jointly supported by the Agence Nationale de la Recherche and Direction Générale de l'Armement under grant ANR-11-ASTR-01. The samples have been elaborated in MIMENTO facilities at Femto-ST institute in Besançon.

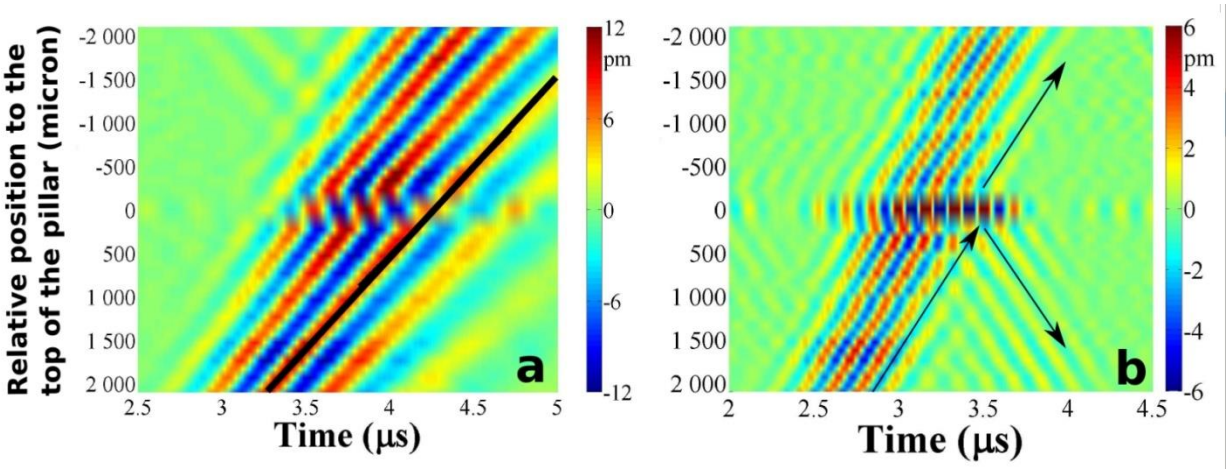

IUS-SPC-13

08:00 am **ScAlN Lamb Wave Resonator in GHz Range Released by XeF_2 Etching**

Akira Konno[1], Shota Sumisaka[2], Akihiko Teshigahara[3], Kazuhiko Kano[3], Ken-ya Hashimoto[2], Hideki Hirano[1], Masayoshi Esashi[1], Shuji Tanaka[1]; *[1]Tohoku University, Sendai, Japan, [2]Chiba University, Chiba, Japan, [3]DENSO CORPORATION, Nisshin, Japan*

Background, Motivation and Objective

40% Sc-doped AlN has about 5 times higher piezoelectric coefficient than AlN just by paying the penalty of doubled dielectric constant. On the other hand, the acoustic velocity of ScAlN decrease with increase in doped Sc, because the elastic stiffness decreases. To obtain both high phase velocity for GHz applications and high electromechanical coupling coefficient (k^2), ScAlN Lamb wave resonators in GHz range were studied.

Statement of Contribution/Methods

The ScAlN Lamb wave resonators were designed based on material constants reported in [1]. The schematic device structure is shown in Figure (a). 1 *f*Êm thick 40% Sc-doped AlN is deposited on a high resistivity Si wafer by co-sputtering Al and Sc targets. On it, an Al interdigital transducer (IDT) and reflectors are fabricated by electron beam lithography and lift-off. The ScAlN film is patterned by BCl_3/Cl_2 reactive ion etching with a photoresist mask to open etching windows for the following release etching. The Lamb wave resonators are finally released by isotropically etching underneath Si with XeF_2.

Results/Discussion

Our simulation suggested that S1 mode had a peak k^2 of 6.5% and a phase velocity of 6700 m/s around a ScAlN thickness of 0.5λ. In this study, the ScAlN thickness and the wavelength λ were set at 1 µm and 2 µm, respectively. S1 resonance frequency is expected to be 3.1 GHz, when the Al IDT thickness is 0.09λ. Figure (b) shows a SEM image of the completed device, where the ScAlN membrane buckled due to a compressive stress of about 1 GPa. Figure (c) shows a typical admittance characteristic near the S1 resonance. A derived equivalent circuit and its frequency response are also shown in Figure (c), showing good agreement with the measured result. The resonance and anti-resonance are clearly seen at 2.63 GHz and 2.72 GHz, respectively, corresponding to k^2 as high as 7.9%. These measured frequencies are somewhat lower than the predicted ones. This discrepancy is probably due to inaccuracy of the used material constants. The quality factors at the resonance and anti-resonance are 136 and 132, respectively, which could be much improved by eliminating parasitic impedances originated from process problems. In conclusion, we first designed, fabricated and tested the ScAlN Lamb wave resonators, and demonstrated the potentiality of high frequency applications.

[1] K. Hashimoto *et al*., IEEE Trans. UFFC, **60**, 3 (2013) in press.

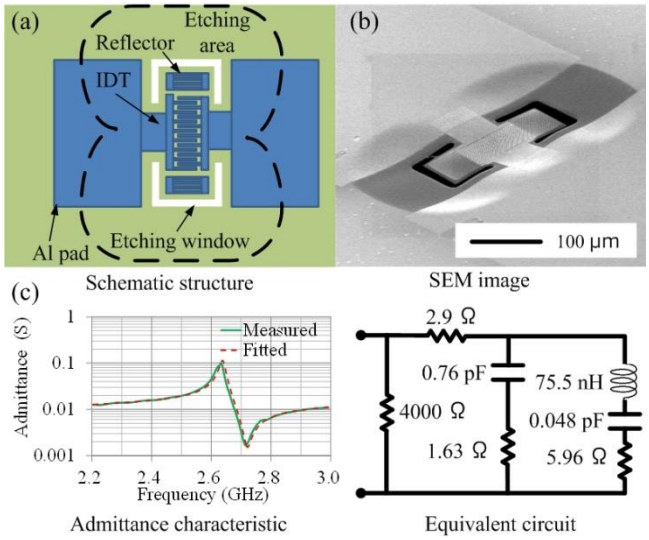

IUS-SPC-14

08:00 am **Advanced 2D Periodic Array and Full Transversal Mode Suppression**

Jiman Yoon[1,2], Markus Mayer[2], Thomas Ebner[2], Karl Wagner[2], Achim Wixforth[1]; *[1]Experimental Physics I, University of Augsburg, Augsburg, Bayern, Germany, [2]Advanced Development Discretes, TDK Corporation, Munich, Bayern, Germany*

Background, Motivation and Objective

Typically, a one-port resonator in SiO_2-covered $LiNbO_3$ displays a series of distinct transversal modes above the resonance frequency. When such resonators are used in filter design without taking any countermeasures, the transversal modes lead to unacceptable passband ripples. In the previous work, "Two dimensional periodic array of reflection centers on electrodes in SAW resonators [Yoon et al, IUS2012]", it has been demonstrated that a 2D periodic array with patches on electrodes can successfully suppress undesired modes within the frequency band of $k_y=[0, \pi/p_T]$, where p_T is the transversal pitch of the periodic array. However, the resonator exhibits strong radiation at the frequency where the periodicity of the transversal pitch of the patches and the wavelength of the transversal mode are equal.

Statement of Contribution/Methods

In this work, we present an improved version of the 2D periodic array from [Yoon et al, IUS2012]. By modification of the patch geometry, $\Delta v/v$ waveguide was optimized and the spurious radiation at $k_y=\pi/p_T$ was suppressed. The required geometry was adjusted on the basis of simulations that employ the well established periodic 2D P-matrix model. In this model, a unit cell is defined with 2 strips, which then is infinitely cascaded taking into account reflection and diffraction. Measured and simulated admittances of resonators are in good agreement.

Results/Discussion

A well-designed periodic array with geometry variations is capable to fully suppress all but the fundamental transversal mode within a certain bandwidth. Besides, the strong peak is removed at the frequency where the periodicity of the transversal pitch coincides with the wavelength of the transversal mode. Therefore the alternative 2D periodic array on the electrodes can be readily employed in designing SAW flters in SiO_2-covered $LiNbO_3$ with excellent performance.

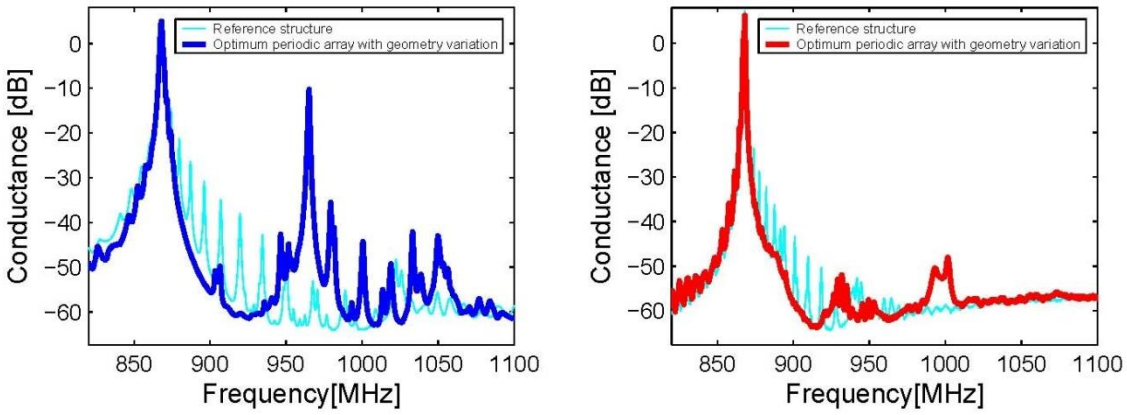

Fig. 1: Comparison of the mode suppression; Reference structure (both-side cyan), a resonator with 2D periodic periodic patches on electrodes (left-side blue) and with geometry variation (right-side red).

IUS-SPC-15

08:00 am **Impact of Surface Periodic Grating on FBAR Structures to Spurious Transverse Resonances**

Jiansong Liu[1], Tatsuya Omori[1], Changjun Ahn[1], Ken-ya Hashimoto[1]; *[1]Graduate School of Engineering, Chiba University, Chiba-shi, Chiba, Japan*

Background, Motivation and Objective

The main resonance of FBAR Structure is caused by the thickness extension vibration. However, the composite structure also acts as a waveguide, and laterally propagating plate modes, namely Lamb modes, cause unwanted spurious resonances. Therefore, their suppression without deteriorating the main resonance is one of the major concerns for designing RF BAW resonators. This study is aimed at discussing applicability of the Bragg reflection in a periodic grating placed on the top electrode of the FBAR structure in order to forbid lateral propagation of the S_1 mode.

Statement of Contribution/Methods

The finite element method (FEM) is employed for the analysis of Lamb wave propagation in the structure. In the analysis, the number of periods is set finite, and both ends are terminated by the absorption mechanism. With this setup, the lateral propagation of eigen modes can be identified from the existence of spurious resonances, while the lateral energy confinement can be evaluated qualitatively by the use of *Q* factor of the main resonance.

Results/Discussion

The investigation is performed for two representative structures, namely, Mo/ZnO/Mo and Ru/AlN/Ru, on which the first-order symmetric Lamb mode exhibits the ″Type-I″ and ″Type-II″ dispersion, respectively. Fig. 1(a) shows, as an example, calculated admittance of the Mo/ZnO/Mo structure without the surface grating in decibels. Series of spurious resonances are seen at frequencies above the main resonance. They are due to lateral propagation of eigen Lamb modes. Fig. 1(b) shows the admittance of the Mo/ZnO/Mo structure with Mo surface grating. It is clear that transverse spurious resonances are completely suppressed by the placement of surface grating. A clean resonance is obtainable provided that the grating period and height are set so that the stop band covers the frequency range where the lateral mode resonances occur.

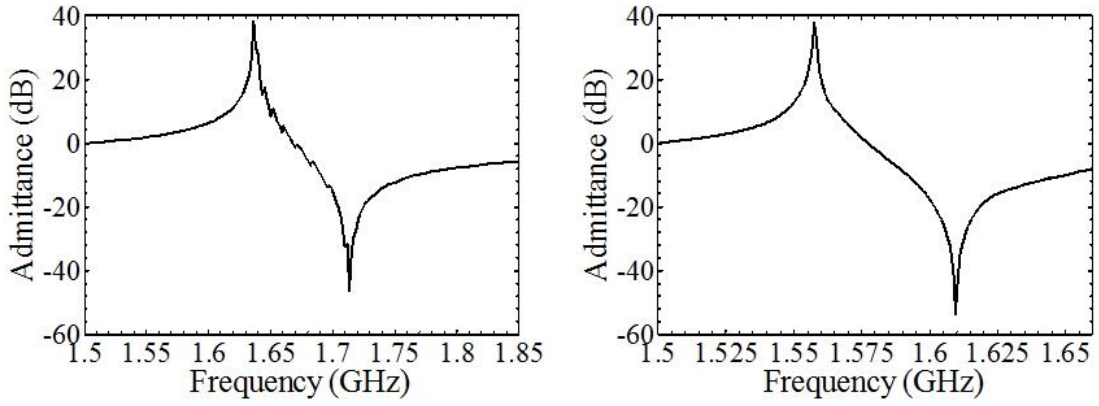

Fig.1(a). Calculated admittance of the Mo/ZnO/Mo structure
Fig.1(b). Calculated admittance of the Mo/ZnO/Mo structure with Mo surface grating

IUS-SPC-16

08:00 am **Multifrequency intravascular ultrasound for assessment of atherosclerotic plaque vulnerability**

Chelsea Munding[1], Emmanuel Cherin[2], Jianhua Yin[2], Hyunggyun Lee[2], David Goertz[2], Brian Courtney[3], Stuart Foster[2]; *[1]Medical Biophysics, University of Toronto, Toronto, Ontario, Canada, [2]Physical Sciences, Sunnybrook Research Institute, Toronto, Ontario, Canada, [3]Schulich Heart Research Program, Sunnybrook Health Sciences Centre, Canada*

Background, Motivation and Objective

Acute coronary syndromes are most often caused by the rupture and thrombosis of an atherosclerotic plaque in the coronary arteries. Plaques that are vulnerable to rupture are characterized by several features, including a thin fibrous cap (<65 μm thick), a large necrotic core, positive remodelling of the vessel wall, inflammation, and angiogenesis of the vasa vasorum. A minimally invasive method of imaging these features would improve our understanding of the natural history of vulnerable plaque and allow the efficacy of possible treatments to be assessed.

Intravascular ultrasound (IVUS) is promising for vulnerable plaque assessment as it is an established clinical tool; however current commercially available devices cannot resolve the fibrous cap or the vasa vasorum. Visualizing the fibrous cap with ultrasound would require the use of high frequencies (>60 MHz) that would not permit the visualization of deeper plaque features. Contrast-specific imaging techniques have been shown to produce signal enhancement in neovascularized plaques; however for this method to be clinically relevant the device should also be capable of high-quality tissue imaging. These requirements lead to a compelling argument for multifrequency IVUS, which would add new capabilities to the existing repertoire.

Statement of Contribution/Methods

We have created a novel prototype to address the goal of multifrequency imaging. It consists of a single stack of two transducers sharing a common ground electrode and backing layer. The signal electrodes are independent. One transducer is tuned to a very high frequency (67 MHz) and one to a more conventional frequency (32 MHz). The 32 MHz element had a -6dB focal beamwidth of 600 μm at 4 mm, and a transmitted pulse length of 30 ns. The 67 MHz side had -6dB beamwidths of 340 μm and 230 μm in the lateral and elevation axes, respectively. The 67 MHz transmitted pulse length was 16 ns.

Results/Discussion

The 32 MHz image (a) shows deeper phantom features, including two hypoechogenic inclusions. The second image is a 32/67 MHz composite (b). The ability of the low-frequency transducer to visualize deeper features is maintained, while the more superficial structures near the centre can be appreciated in much higher resolution. These results demonstrate the potential complimentary, multifrequency imaging of both deep and superficial plaque features.

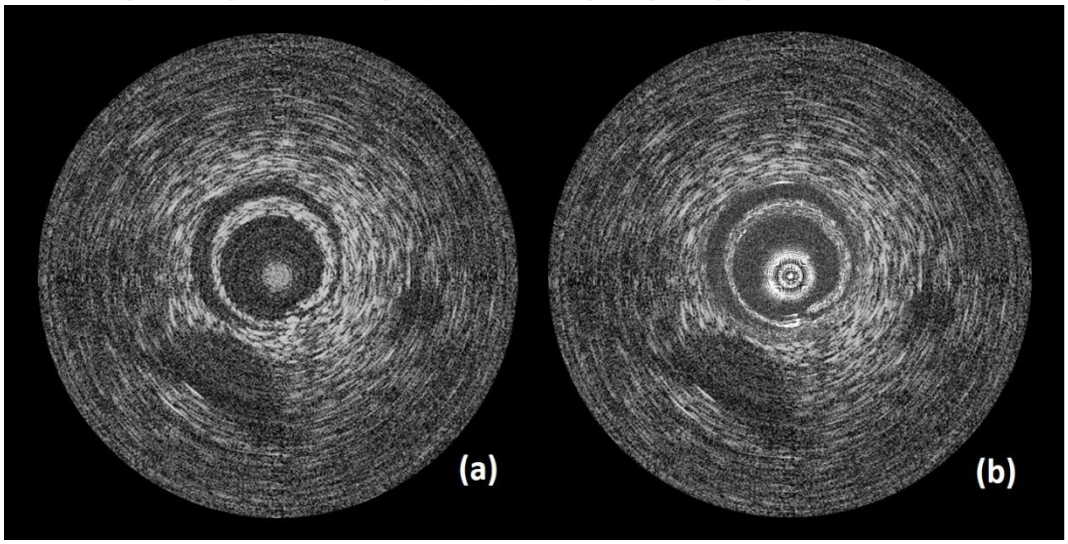

IUS-SPC-17

08:00 am **Performance of a Miniaturized 64-Element High-Frequency Phased Array based on PMN-PT**

Andre Bezanson[1], Robert Adamson[1], Jeremy Brown[1]; [1]*Biomedical Engineering, Dalhousie University, Halifax, Nova Scotia, Canada*

Background, Motivation and Objective

Currently, most fully sampled high frequency (>30 MHz) array transducers are limited to linear/annular arrays where the overall packaging of the transducers remains relatively large. This limits these arrays to topical applications where images must be generated from outside the body. We have previously fabricated a 64-element 42-MHz phased array transducer with 1λ element pitch, which is better suited to internal imaging applications. Using a novel wire bonding technique, we miniaturized the total packaging to a 2.7 mm^2 endoscopic form factor By using an existing grating lobe suppression technique, the beam steers to ±35° without grating lobe artifacts. In this work, we report the full performance characterization of this high-frequency phased array endoscope by generating 3D radiation patterns and beam profiles, images of wire/tissue phantoms, and ex-vivo tissue images.

Statement of Contribution/Methods

The electrical impedance was measured for each element across the array using a precision impedance analyzer and the pulse echo response of each element was measured using a high-frequency pulser-receiver unit. A Visualsonics Vevo 2100 high-frequency linear array ultrasound imaging system was reprogrammed to allow for phased array beamforming with our array specifications. The Visualsonics linear array transducer was replaced with our 64-element phased array endoscope and code was run to steer a focused beam between ±35°. One-way focused radiation patterns were collected using a needle mounted hydrophone at different angles and for B-mode imaging, the individual RF scan lines were exported and offline images were reconstructed.

Results/Discussion

The average electrical impedance magnitude was measured to be 65Ω on resonance with low variance in impedance between elements. Two-way pulse echoes were collected from all 64 elements showing high uniformity. The focused elevation and azimuth beam profiles were found to be in good agreement with the modeled predictions. B-mode images were generated of 25 μm Aluminum wire phantoms spaced by 1 mm steps in a water bath as well as in a tissue phantom (Figure 1) with 60 dB DNR. As our intended application for this miniaturized endoscope is to image the inner ear cochlea, ex-vivo images were generated of cadaveric temporal bones where the intra-cochlear membranes could be clearly seen.

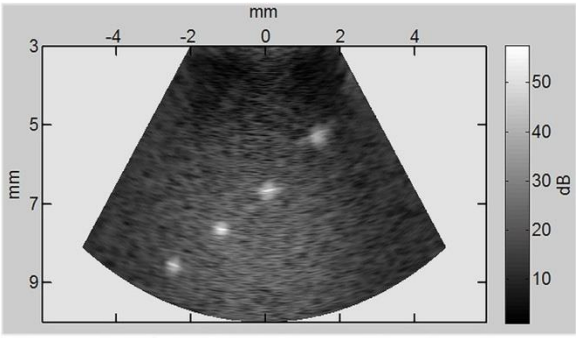

Figure 1: 60 dB DNR Tissue Phantom Image

IUS-SPC-18

08:00 am **Real-time Co-registered IVUS-OCT Catheter for Atherosclerotic Plaque Identification and Stent Deployment Verification**

Teng Ma[1], Jiawen Li[2], Dilbahar Mohar[3], Joseph Jing[2], Matthew Brenner[4], Pranav M. Patel[3], K. Kirk Shung[1], Zhongping Chen[2], Qifa Zhou[1]; *[1]NIH Ultrasonic Transducer Resource Center and Department of Biomedical Engineering, University of Southern California, Los Angeles, California, USA, [2]Beckman Laser Institute & Medical Clinic and Department of Biomedical Engineering, University of California - Irvine, Irvine, California, USA, [3]Division of Cardiology, UC Irvine Medical Center, Irvine, California, USA, [4]Division of Pulmonary and Critical Care, UC Irvine Medical Center, Irvine, California, USA*

Background, Motivation and Objective

Coronary artery disease remains the leading cause of death and disability in the U.S. Intravascular ultrasound (IVUS) is one of the standard medical tests routinely performed to diagnose atherosclerosis by visualizing the structure of affected vessels, identifying the composition of plaques, and providing stent deployment information after angioplasty. Optical coherence tomography (OCT) possesses higher resolution to image vulnerable plaque near the lumen boundary, but with shallow penetration depth. Thus, an integrated IVUS-OCT catheter would potentially capitalize the advantage of sufficient imaging depth of IVUS with the high resolution of OCT while offering improved diagnostic information. Different IVUS-OCT catheter designs have been reported previously by using co-axial, co-planner or sequential configuration, which suffers from either the size of catheter or sub-optimal image co-registration. We report the optimized design of a miniature IVUS-OCT catheter featured by a back-to-back arrangement of a transducer and an OCT probe to enable real-time co-registration of two modalities within one frame.

Statement of Contribution/Methods

The 3D design of the 0.8mm-diameter IVUS-OCT catheter is shown in Fig.1 (a). The OCT fiber connects a 0.35 mm-diameter GRIN lens followed by a micro-prism. The PMN-PT transducer (40MHz, 50% BW) has a rectangular surface of 0.16mm2 and a thickness of 0.3mm. The featured opposite configuration of OCT probe and transducer ensures two modalities co-registered within one frame by simply rotating either of image 180º. The atherosclerotic plaque models are imaged ex vivo to study plaque type identification, and the imaging of stent embed vessels is performed to demonstrate the feasibility of stent deployment verification.

Results/Discussion

The H&E stained histology of rabbit aorta with intima partially thickened is shown in Fig1. (b). Corresponding IVUS image Fig1. (c) is able to provide the full structural image of the vessel with intima and media layer. The irregular lumen surface of the thickened intima indicated by the red arrows is clearly displayed in OCT Fig1. (d) but not with IVUS due to the inferior resolution and near field imaging capability. The sharp surface with strong signal on the surface and high attenuation inside thickened intima demonstrates the characteristic of lipid rich plaque confirmed by histology.

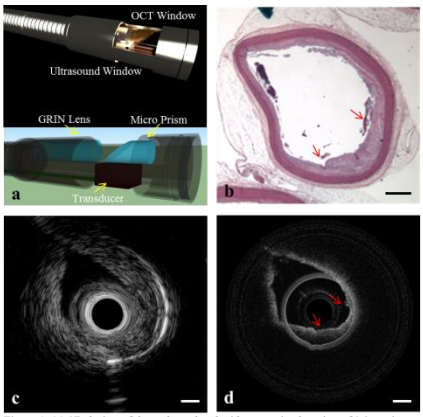

Figure 1. (a) 3D design of the catheter head with protective housing of 0.8mm in diameter. The OCT probe and transducer are arranged in back-to-back configuration to co-register image within one frame. (b) Hematoxylin-Eosin stained histology image of rabbit aorta with intima partially thickened (c) Corresponding IVUS image displays the full structural image of the vessel with measureable vessel thickness information. (d) OCT image shows the strong signal on the irregular lumen surface of the thickened intima indicated by the red arrows in (b). Scale bar: 1mm.

Abdominal elasticity imaging

CONGRESS HALL

Tuesday, July 23 2013, 10:30 am - 12:00 pm

Congress Hallair: **James Greenleaf**
Mayo Clinic College of Medicine

IUS1-D1-1

Corticomedullary Strain Ratio: A Quantitative Marker in Assessment of Renal Allograft Cortical Fibrosis

Jing Gao[1], Robert Min[1], James Hamilton[2], William Weitzel[3], Jonathan Rubin[4]; *[1]Radiology, Weill Cornell Medical College, New York, New York, USA, [2]Epsilon Imaging, Ann Arbor, Michigan, USA, [3]Internal medicine, University of Michigan, Ann Arbor, Michigan, USA, [4]Radiology, University of Michigan, Ann Arbor, Michigan, USA*

Background, Motivation and Objective

In renal transplants, change in corticomedullary ration may be associated with gradually developing renal cortical fibrosis in chronic allograft nephropathy (CAN), the most prevalent cause of chronic allograft dysfunction in the first post-transplant decade and late graft loss. For estimating kidney hardness in CAN, a normalization method is very useful in accurately measuring strain in inhomogeneous and anisotropic tissues, such as kidney. Choosing a soft tissue as a reference for strain normalization is considered challenging. This is specifically true for an adult transplanted kidney that is usually located between pelvic bones laterally and bladder medially, and surrounded by bowel. We prospectively assessed a new quantitative marker - corticomedullary strain ratio to assess the cortical fibrosis in renal transplants.

Statement of Contribution/Methods

We prospectively assessed corticomedullary strain ratio in renal allografts with quasi-static ultrasound elasticity imaging (UEI). Written informed consent was obtained from 33 enrolled patients who underwent renal transplant sonography and biopsy from March 2012 to December 2012. Based on a Banff score criteria for renal cortical fibrosis, 33 renal allografts were divided into 2 groups, Group 1 (n=19) with mild (<25%) renal cortical fibrosis and Group 2 (n=14) with moderate (>26%) renal cortical fibrosis. We used two-dimensional speckle tracking software to perform off-line analysis of strain in the renal cortex and medulla induced by external compression with the ultrasound probe. We used strain in the medulla as reference to normalized renal cortical strain, and then calculated corticomedullary strain ratio (Strain ratio = Strain cortex / Strain medulla). An unpaired two-tailed t-test was used to determine the differences in strain ratio between the two groups. ROC curve analysis was performed to test the best cutoff value of strain ratio to identify moderate renal cortical fibrosis.

Results/Discussion

Strain differed between the cortex and medulla (P<0.01). Strain ratio in group 1 was higher than group 2 (2.06±1.33 vs 0.70±0.20) (p=0.0007). . In ROC analysis, the area under the curve was 0.964. The sensitivity and specificity of using 0.975 as a strain ratio cutoff value to determine a moderate renal cortical fibrosis was 92.9% and 94.7%, respectively. Conclusions – Medullary strain can be used as reference to normalize renal cortical strain. Corticomedullary strain ratio decreases with increasing renal cortical fibrosis. The change of strain ratio on UEI may add a new quantitative marker for monitoring the progression of renal cortical fibrosis following renal transplant.

IUS1-D1-2

In Vivo Measurement of Renal Transplant Viscoelasticity

Matthew Urban[1], Carolina Amador[1], James Greenleaf[1]; *[1]Department of Physiology and Biomedical Engineering, Mayo Clinic College of Medicine, Rochester, MN, USA*

Background, Motivation and Objective

Objective: Common clinical practice is to follow-up a renal transplant with regular protocol biopsies of the transplanted organ to assess presence of inflammation or signs of rejection. The objective of this study was to investigate the viscoelastic material properties of patients with renal transplants. Recent studies using shear wave-based techniques have shown that the elastic mate-rial properties of the kidney increase in presence of inflammation and fibrosis.

Statement of Contribution/Methods

Methods: Under a protocol approved by the Mayo Clinic Institutional Review Board, we studied the transplanted kidneys of 14 patients and the native kidneys of six control subjects, but were unable to measure shear wave speeds in 1 normal subject and 2 transplant patients. We used ultrasound radiation force to generate shear waves in the renal cortex and measured the shear waves using compounded plane wave imaging. For this study we used a Verasonics system equipped with a linear array or curved array transducer (L7-4, C-42, Philips Healthcare, Andover, MA). The frame rate for shear wave detection was 3.33 kHz. We measured the group velocity, c_s, using a time-to-peak algorithm on the displacement data for these subjects, and then the relationship $\mu = \rho c_s^2$ to calculate the elastic shear modulus. We also analyzed the motion using a two-dimensional fast Fourier transform (2D-FFT) method to examine the phase velocity dispersion and fit the data with a Voigt model, where μ_1 is the elastic shear modulus and μ_2 is the shear viscosity. Clinical parameters such as serum creatinine (SCr) and Banff scoring from histology of transplant biopsies were also recorded.

Results/Discussion

Results: We observed a positive trend with SCr and μ in patients with kidney transplants and found a Pearson correlation of R = 0.71 (p = 0.015). The values of the elastic shear modulus (μ) demonstrated an increasing trend with higher Banff score (Fig. 1(a)). An example of the shear wave particle velocity from a transplanted kidney is shown in Fig. 1(b). The Voigt model fit to the shear wave velocity dispersion gave values of $\mu_1 = 7.87$ kPa and $\mu_2 = 2.92$ Pa·s.

Conclusion: We measured the viscoelasticity of renal transplant kidneys. Quantitative shear modulus measurements correlated with clinically significant measurements such as serum tests and biopsy histology. [This study was supported in part by grant DK092255 from NIH.]

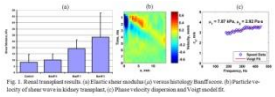

IUS1-D1-3

Shear wave dispersion for fibrosis, steatosis and activity staging. Clinical results on 102 chronic liver disease patients

Thomas Deffieux[1], Jean-Luc Gennisson[2], Laurence Bousquet[3], Dalila Amroun[3], Marion Corouge[3], Vincent Mallet[3], Philippe Sogni[3], Mathias Fink[2], Stanislas Pol[3], Mickael Tanter[2]; *[1]Institut Langevin, ESPCI ParisTech, CNRS UMR 7587, INSERM U979, France, [2]Institut Langevin, ESPCI ParisTech, CNRS UMR 7587, INSERM U979, France, France, [3]Service Hépatologie, Hôpital Cochin, Paris, France*

Background, Motivation and Objective

Quantitative elastography has been established as an efficient tool for chronic liver diseases diagnosis and staging. The local shear modulus is estimated from the shear wave group velocity and then used to assess the fibrosis stage. But shear wave propagation also yields information on the viscosity and other medium properties that could be important for diagnosis. In this study, Shear Wave Spectroscopy is compared with fibrosis/activity scores according to Metavir and steatosis assessed by liver biopsy.

Statement of Contribution/Methods

The shear wave spectroscopy method was implemented and optimized for in vivo studies and applied to a cohort of patients (n=102) with chronic liver diseases(Hepatitis C, Hepatitis B, NASH etc..). Using an ultrafast scanner (Aixplorer, Supersonic Imagine, France) and a 3 MHz curved array (SC 6-1), a plane shear wave is generated inside the liver using acoustic radiation force and is acquired in real time during its propagation using ultrafast imaging. By estimating the phase velocity for each frequency from the k-space, shear wave dispersion curves are computed for each acquisition. Different parameters are estimated such as the dispersion curve slope, shear velocities and Young's moduli for different frequencies as well as the Voigt shear modulus and Voigt viscosity.

Receiver operating characteristic curves are then estimated for the different parameters using the liver biopsy results as the gold standard.

Results/Discussion

Results show that fibrosis and, to a lesser extent, activity can be reliably estimated from the shear wave group velocity as well as from the shear wave dispersion curve by estimating the Young's moduli at 50 Hz and 150 Hz using phase velocities or by the Voigt shear modulus and Voigt viscosity (cf. table 1).

Steatosis is not correlated to any parameters tested in the study including Voigt viscosity or dispersion curve slope.

Those results show that dispersion curves can be used for the determination of the fibrosis stage with good accuracy provided parameters are linked to the medium stiffness.

While the activity level can also be retrieved from those parameters, it is believed that there is a strong correlation between fibrosis and activity levels for most patients. Contrary to preliminary reports and hopes on the issue, steatosis is not found to be correlated to any of the parameters tested here.

	Fibrosis			Activity		Steatosis	
	F>F1	F>F2	F>F3	A>A0	A>A1	S>20 %	S>35%
Young's modulus from group velocity	0.82	0.82	0.87	0.64	0.78	0.58	0.47
Young's modulus @ 50 Hz	0.79	0.83	0.87	0.7	0.8	0.63	0.58
Young's modulus @ 150 Hz	0.81	0.82	0.86	0.67	0.8	0.59	0.43
Voigt Shear modulus	0.75	0.79	0.79	0.67	0.76	0.64	0.6
Voigt viscosity	0.76	0.77	0.82	0.62	0.75	0.62	0.57
Dispersion slope	0.7	0.72	0.8	0.52	0.69	0.55	0.47

***Table 1.** Areas under the curve for the separation of different fibrosis, activity and steatosis stages versus different parameters estimated from shear wave dispersion curves. Grey background denotes area under the curve > 0.8.*

IUS1-D1-4

A Technique for Quantifying Shear Wave Velocity and Attenuation in Tissues and In Vivo Application

Ivan Nenadic[1], Matthew Urban[1], Bo Qiang[1], Shigao Chen[1], James Greenleaf[1]; *[1]Mayo Clinic, USA*

Background, Motivation and Objective

Changes in tissue mechanical properties are associated with various pathological disorders. In order to fully characterize mechanical properties of tissues at a given frequency, knowledge of both shear wave speed and attenuation is necessary. We propose and validate a technique that independently measures shear wave velocity and attenuation. The technique is then applied to measure kidney shear wave velocity and attenuation in patients following kidney transplants.

Statement of Contribution/Methods

A mechanical shaker was used to excite harmonic plane and cylindrical waves in phantoms made of polyvinyl alcohol (PVA) and excised porcine liver in the frequency range 100–500 Hz. In addition, focused ultrasound radiation force from a linear array transducer was used to excite impulsive cylindrical waves 600 μs in length. For all three excitation techniques, pulse-echo ultrasound from the linear array transducer was used to calculate the displacement field. In case of the cylindrical waves, the displacement field was multiplied by square root of the distance vector ($\sqrt{r}$) to correct for the cylindrical diffraction. For all three excitation methods, a two-dimensional fast Fourier transform (2D FFT) of the displacement field was performed in order to obtain the k-space whose coordinates are the frequency (f) and the wave number (k). The shear wave velocity at each frequency was obtained by finding the maximum in the 2D FFT of the given frequency in k-space and dividing the frequency coordinate by the wave number coordinate. The attenuation (α) at a given frequency was calculated using $\alpha = \text{FWHM} \times \pi / \sqrt{3}$, where FWHM is the full width at half maximum of the k-space peak along the given frequency. This method allowed us to measure both shear wave velocity and attenuation at each frequency for the three excitation methods. The velocities and attenuations were measured every 1 mm throughout the thickness of the samples and the values were reported as mean and standard deviations. This method was applied to measure shear wave velocity and attenuation of transplanted kidneys in patients and the measurements were related to the Banff score.

Results/Discussion

The values of shear wave velocity and attenuation at each frequency for the three different excitation methods in both the PVA and excited liver phantom agree within one standard deviation. In addition, the k-space estimates of velocity and attenuation were compared to the values obtained using the traditional methods of phase gradient (for velocity) and amplitude decay (for attenuation) and the results agreed within one standard deviation. The transplanted kidneys with a higher Banff score (more fibrosis and higher risk of transplant rejection) had higher shear wave velocity (from 2.4 m/s to 3.4 m/s) and lower attenuation (from 210 Np/m to 133 Np/m). These results suggest that the proposed method can be used to obtain model-free estimates of tissue shear wave velocity and attenuation.

3D Elasticity Imaging with Acoustic Radiation Force

Kathryn Nightingale[1], Michael Wang[1], Stephen Rosenzweig[1], Ned Rouze[1], Samantha Lipman[1], Kirema Garcia-Reyes[2], Thomas Polascik[3], Mark Palmeri[1]; *[1]Biomedical Engineering, Duke University, Durham, North Carolina, USA, [2]School of Medicine, Duke University Medical Center, Durham, North Carolina, USA, [3]Urology, Duke University Medical Center, Durham, North Carolina, USA*

Background, Motivation and Objective

Acoustic radiation force impulse based elasticity imaging methods have been under development for the past 15 years, and both qualitative on-axis (ARFI) and quantitative shearwave speed (SWEI/SSI) methods have been introduced into the commercial market. ARFI methods employ less processing and provide higher spatial resolution, whereas SWEI methods employ reconstruction algorithms that afford higher contrast. In order to generate robust estimates, simplifying assumptions are widely employed in SWEI methods, and, violation of the underlying assumptions can lead to bias, image artifacts, and difficulty in comparing results obtained with different algorithms.

Statement of Contribution/Methods

We will present results describing sources of bias and artifact in SWEI/ARFI images arising from violation of the common specific assumptions of homogeneity and isotropy, and discuss the development of technologies to address these issues.

Results/Discussion

The advent of extensive parallelism and plane wave imaging has allowed sequence development capable of concurrently acquiring ARFI and SWEI data, and we are developing methods for combining the information from both datasets in order to provide robust, structurally accurate images in heterogeneous and anisotropic materials. We will present results from an ongoing clinical study in which combined 3D ARFI/SWEI datasets are obtained in vivo of the entire prostate gland (Figure 1), and, the results are then correlated with whole mount histology data obtained post radical-prostatectomy. In addition, the advent of real-time volumetric imaging has enabled 3D monitoring of SWS propagation from a single ARFI impulse. Employing a HIFU piston for ARFI excitation integrated with a 2D matrix array and a Siemens SC2000 scanner performing volumetric imaging, SWS propagation is monitored concurrently in three dimensions. In anisotropic materials, such as muscle, we demonstrate the benefits of this 3D SWEI system for determining the principle axes of propagation, and thus accurately accounting for fiber orientation in SWEI measurements (Figure 1).

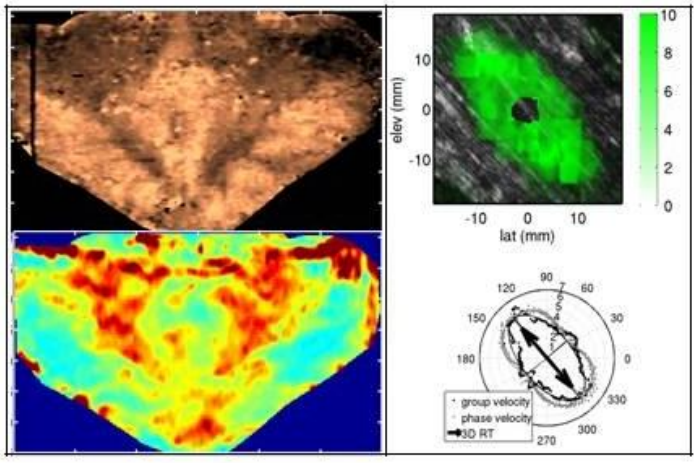

Fig. 1: LEFT: In vivo prostate study: Coronal view of 3D ARFI (top) and SWEI (bottom) images, demonstrating detailed structural information in this lateral/elevational plane;

RIGHT: 3D Ex vivo muscle data: Shear wave displacement 3.7 ms after ARFI push in canine muscle, and the corresponding group and phase velocity and the best fit for the theoretical group and phase velocity curves for a transverse isotropic material. The fiber orientation can be estimated from the angle of the major axes of the fitted curves, and the shear wave speed along and across the fibers can be estimated from the lengths of the major and minor axes, respectively.

Contrast agents and imaging

M4

Tuesday, July 23 2013, 10:30 am - 12:00 pm

Congress Hallair: **Nico de Jong**
Erasmus Medical Centre and University of Twente

IUS1-D2-1

Genetically Encoded Gas Nanostructures as Ultrasonic Molecular Reporters

Mikhail Shapiro[1], Patrick Goodwill[2], Arkosnato Neogy[3], David Schaffer[4], Steven Conolly[2]; *[1]Bioengineering, Miller Institute, UC Berkeley, Berkeley, California, USA, [2]Bioengineering, Electrical Engineering, UC Berkeley, USA, [3]Electrical Engineering, UC Berkeley, USA, [4]Chemical and Biomolecular Engineering, Bioengineering, UC Berkeley, USA*

Background, Motivation and Objective

Ultrasound is currently limited by its lack of suitable nanoscale reporters for molecular imaging. The basic physics of conventional "microbubble" contrast agents, which dictates sizes larger than one micron and half-lives shorter than a few hours, makes them ineffective as labels of specific cells and tissues outside the bloodstream. **Here, we introduce a new class of reporters for ultrasound based on genetically encoded gas nanostructures from buoyant photosynthetic bacteria.** These inherently stable nanoscale reporters overcome some of the main limitations of microbubbles, and raise the possibility of ultrasound contrast engineered and delivered to cells at the genetic level.

Statement of Contribution/Methods

Gas vesicles (GVs) are gas-filled protein-shelled compartments 100-400 nm in size that exclude water and are permeable to gas. They are biosynthesized by photosynthetic cyanobacteria and halobacteria as a means to regulate buoyancy and thereby migrate to optimal aqueous depths for access to light and nutrients. GVs from different species have different shapes and sizes. Like microbubbles, GVs are gas-containing structures, but they exhibit different physics: they are smaller, the gas inside them is at equilibrium with the aqueous environment, they are inherently stable, and their shell is relatively inelastic. Here, we report the first evaluation of GVs as potential ultrasound contrast agents.

Results/Discussion

Our results show that sub-nanomolar concentrations of GVs produce robust ultrasound contrast at frequencies of 5-17 MHz. Contrast mechanisms include linear scattering, attenuation and harmonics, enabling enhanced detection. GV contrast is readily observed *in vitro* and *in vivo* (after subcutaneous injection). Furthermore, differences in genetically-determined critical collapse pressures among GVs from different species enables multiplexed imaging through a serial collapse paradigm. In addition, we show that clustering-dependent contrast enhancement permits the use of GVs as molecular biosensors and reporters of cellular integrity. **These results highlight the potential of this new class of reporters to support unique applications in molecular imaging, and raise the intriguing prospect of genetically engineered and targeted reporters for ultrasound.**

-

Figure: Genetically encoded nanostructures as ultrasound reporters

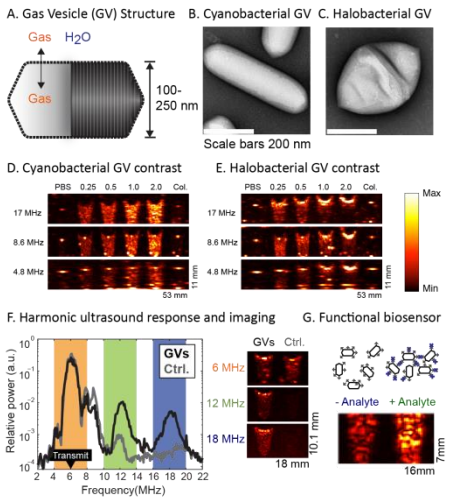

IUS1-D2-2

In vivo imaging of gas vesicles, genetically encoded nano contrast agents

Melissa Yin[1], Emmanuel Cherin[1], F. Stuart Foster[1,2], Mikhail Shapiro[3]; *[1]Sunnybrook Health Sciences Centre, Toronto, ON, Canada, [2]Medical Biophysics, University of Toronto, ON, Canada, [3]Bioengineering, Miller Institute, UC Berkeley, Berkeley, CA, USA*

Background, Motivation and Objective

Current ultrasound contrast agents are limited by confinement to the microcirculation, instability, and limited molecular imaging capability. To address these issues, we have identified a new ultrasound contrast paradigm based on gas vesicles (GVs) – gas-enclosing protein nanostructures of 100-400 nm that regulate buoyancy in halo- and cyanobacteria. Unlike artificial microbubbles, GVs are not pressurized and allow gases to freely exchange with the surrounding medium. This results in a stable nanoscale configuration that is ideal for high frequency ultrasound detection. In addition, GVs are genetically encoded and thereby susceptible to engineering of their properties at the genetic level.

Statement of Contribution/Methods

We have previously established the ability of GVs to produce ultrasound contrast at frequencies of 5-17 MHz, demonstrating linear, harmonic, multiplexed and functional imaging *in vitro* and detection after subcutaneous injection *in vivo* (Shapiro et al, separate abstract). **Here, we report the first imaging study of GVs administered to mice via intravenous injection.** Using a VisualSonics Vevo 2100 high-frequency ultrasound scanner operating at 18MHz, we imaged GVs purified from *Halobacteria NRC-1* (Halo) and *Anabaena flos-aquae* (Ana) in their native form and after surface coating with polyethylene glycol (PEG).

Results/Discussion

Injection of Halo GVs into the tail vein of SCID nude mice resulted in transient nonlinear contrast enhancement in the inferior vena cava (IVC) and prolonged enhancement in the liver (L) and kidney (K) as shown in the figure. The temporal profile of contrast enhancement in these organs suggests that native GVs survive one pass in the microcirculation, and are taken up by the liver, where contrast is persistent. Signal enhancement by Halo GVs was repeatedly observed in 6 difference mice, followed by the disappearance of contrast after collapse with a high-power (> 1MPa) disruption pulse. Chemical modification of Halo GVs with PEG resulted in prolonged recirculation, as evidenced by persistent contrast signal in the IVC (n=2). Ana GVs were also observed in the IVC immediately after injection, but fail to produce persistent non-linear contrast. This study demonstrates the potential of GVs to act as potent ultrasound contrast agents *in vivo* and establishes a path for their future development for specific applications.

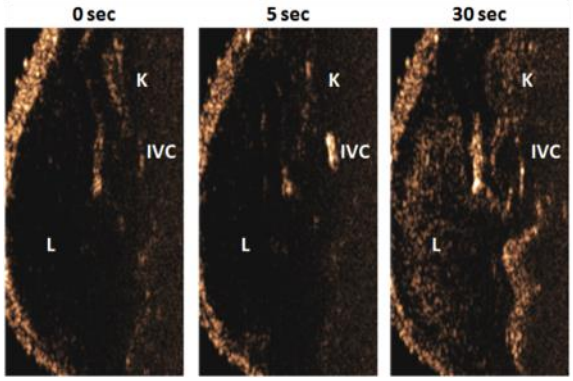

IUS1-D2-3

Ultrasound super-localization (USL) with 3D ultrafast imaging

Yann Desailly[1,2], Olivier Couture[1,2], Mathias Fink[1,2], Mickael Tanter[1,2]; [1]*Institut Langevin, CNRS, Paris, France,* [2]*Institut Langevin, ESPCI, Paris, France*

Background, Motivation and Objective

As in other imaging methods based on waves, the resolution of ultrasound imaging is limited by the wavelength. In optics, this limitation was overcome by super-localizing single events induced by fluorescent excitation (F-PALM). In recent years, our laboratory developed plane-wave ultrasound allowing frame rates up to 20 000 fps. Ultrafast processes such as rapid movement or disruption of ultrasound contrast agents (UCA) can thus be monitored. These rapid events provide us with distinct punctual sources that could be localized beyond the diffraction limit. The aim of this study is to determine the experimental and theoretical limitations of ultrasound super-localization.

Statement of Contribution/Methods

The experimental resolution was determined by observing UCA flowing through microchannels. Ultrafast imaging was performed with a 1.75 MHz (λ = 860 µm) transducer matrix (64 x 8 elements) driven by a SuperSonic Imaging scanner at a frame rate of 1000 kHz. Events lasting less than a thousandth of a second were observed with 3D ultrafast imaging. The punctual echo was backpropagated to find the exact location of the source. The same conditions were used to determine, in simulation, the maximal resolution limit. The timing error of the echo was propagated to find the variation in the super-localization of each bubble.

Results/Discussion

The acquired ultrafast images were differentiated to detect the single events happening within one millisecond. Single ultrasonic echo from microbubbles were observable by 3D ultrafast imaging. As shown in figure 1 , a channel with dimensions of $\lambda/10$ (axial) by $\lambda/5$ (lateral) could be resolved. The theoretical resolution-limit calculated in simulation was around 20 µm.

Ultrasound super-localization can be achieved with 3D ultrafast imaging of ultrasound contrast agent. This method being highly sensitive to motion, a compensation algorithm will be needed. Applying this technique in-vivo could lead to a super-resolve mapping of the vascular network, down to the smallest capillary.

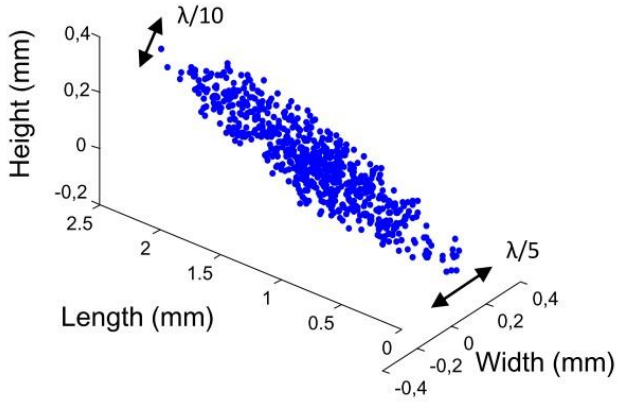

Figure 1 : Super-localized bubbles flowing through a microchannel with dimensions of λ/10 (axial) by λ/5 (lateral)

IUS1-D2-4

Counting bubbles and contrast-to-noise amplification with ultrafast contrast imaging

Olivier Couture[1,2], Yann Desailly[1,2], Mathias Fink[1,2], Mickael Tanter[2,3]; [1]*CNRS, France,* [2]*ESPCI, France,* [3]*INSERM, France*

Background, Motivation and Objective

Perfusion imaging with microbubbles have been impaired by its qualitative nature, which is partly due to the nonlinear relationship between the image intensity and the number of bubbles. We have previously demonstrated that ultrafast contrast imaging can improve contrast-to-tissue ratio both in-vitro and in-vivo (Couture et al. 2009, 2011, 2012). This technique can also be used to isolate punctual events from the passage or disruption of microbubbles, leading to resolution beyond 1/20 of the wavelength (Couture et al. IEEE proc. UFFC 2011). A corollary of this isolation done at ultrafast frame rates is that these punctual events could also be counted one-by-one, providing a method to better quantify the concentration of microbubbles inside a tissue.

Statement of Contribution/Methods

In these experiments, microbubbles were introduced in a wall-less vessel phantom at concentration varying from 1/10,000 to 1/250. Images were obtained on a programmable clinical scanner with a set of line per line focused pulses for conventional contrast imaging (contrast pulse sequence) and with ultrafast plane waves at 10 kHz frame rate. For fair comparison, each type of imaging was performed with the same number of emissions at the same voltage settings (384). The intensity of the ultrafast image was determined by the number of punctual events observed on differential imaging.

Results/Discussion

On differential images, the decorrelation allows single events to be distinguished. The intensity of the channel calculated on the total number of ultrafast events within the plane increases linearly with the concentration (linear fit R squared = 0.94). As expected, the intensity of the channel on the CPS image does not increase linearly with the concentration and reaches a plateau beyond 1/1000 concentration (linear fit R squared = 0.79). Moreover, when the punctual events from fast decorrelation induced by microbubbles are summed, a composite image with a drastic improvement in contrast-to-noise ratio (43 dB) is obtained as compared to conventional bubble-discrimination technique (CPS). This study demonstrates that the observation of microbubbles with ultrafast imaging allow a better assessment of their concentration than conventional contrast imaging techniques. This method could be exploited to better quantify perfusion and molecular targeting with ultrasound.

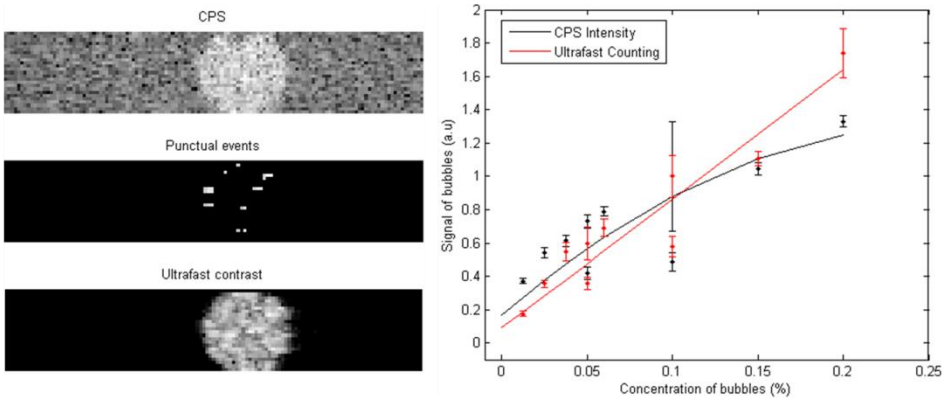

Figure: Imaging of a wall-less vessel phantom with CPS (top), ultrafast contrast imaging (bottom) and differential imaging to observe punctual events (50 dB scale). The intensity on the CPS image saturates at high concentration (right), while the ultrafast event counting technique follows a more linear profile.

IUS1-D2-5

Effect of excitation envelope on volumetric subharmonic vibrations of single contrast agent microbubbles using an acoustical camera

Verya Daeichin[1], Guillaume Renaud[1], Johan G. Bosch[1], Antonius F.W. van der Steen[1,2], Nico de Jong[1,2]; *[1]Thoraxcenter Biomedical Engineering, Erasmus MC, Rotterdam, Netherlands, [2]Interuniversity Cardiology Institute of the Netherlands, Utrecht, Netherlands*

Background, Motivation and Objective

Recently we have shown that a suitable design of the excitation envelope to generate a self-demodulation signal at the subharmonic (SH) frequency can enhance the SH emission of microbubble (MB) contrast agents at 10 MHz [1]. In this study we investigated effects of the excitation envelope on volumetric SH response of individual MB excited in the frequency range of 7-11 MHz with an acoustical set up (acoustical camera [2]) measuring relative volume variations of single MB.

Statement of Contribution/Methods

Using the acoustical camera, we retrieved the radial response of single MicroMarker (VisualSonics Inc.) MB to 1 µs pressure waves (50 kPa to 200 kPa peak to peak) with Gaussian and rectangular envelopes within the frequency range of 7-11 MHz. Each single MB is excited by a sequence of 8 signals with Gaussian and rectangular envelopes and with frequencies of 7, 8, 9 and 11 MHz. The total length of the excitation waves sequence was 24 µs ensuring that the same single MB was excited with all excitation bursts. The vibration responses of the single MB to the 8 excitations are received through the nonlinear coupling with a 50 µs 30 MHz probing wave [2].

Results/Discussion

Amplitudes of relative radial SH vibration of single MB excited with rectangular envelope bursts were up to 3 times larger than when excited with Gaussian envelope bursts. Fig 1 shows an example of retrieved radial response of a single MB to excitations at 50 kPa in time and frequency domain. Amplitude of SH response to a 7 MHz excitation is 1.8% with rectangular envelope corresponding to a pressure of about 2 Pa radiated by a MB with diameter of 3 µm at 2 cm distance. This is 3 times higher than that with Gaussian envelope excitation (0.6% and ~0.7 Pa).

This study suggests that excitation with rectangular envelope enhances the volumetric radial SH response of a single MB up to 3 times compared with excitation with Gaussian envelope at low acoustic pressures (<200 kPa peak to peak). Such an enhanced SH response can be then used for imaging the UCA.

Reference

[1] V. Daeichin et al., Phys. Med. Biol., 2012.

[2] G. Renaud et al., Appl. Phys. Lett., 2012.

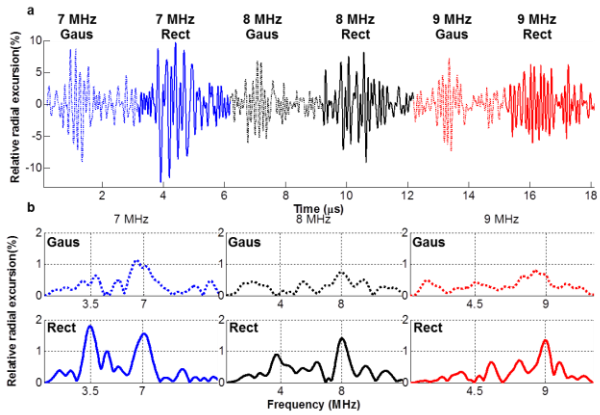

Fig. 1. Relative radial response of a single MicroMarker microbubble to excitations with Gaussian (Gaus) and rectangular (Rect) envelope at 50 kPa and frequency range of 7-9 MHz in time domain (a) and frequency domain (b).

This research was supported by the Center for Translational Molecular Medicine and the Netherlands Heart Foundation (PARISK).

Tuesday, July 23 2013, 10:30 am - 12:00 pm

IUS1-D2-6

Quantitative myocardial perfusion analysis with contrast-enhanced ultrasound bolus tracking – preliminary animal results

Martin Mezl[1,2], Radovan Jirik[1,3], Knut Matre[4], Geir Olav Dahle[4], Ketil Grong[4], Pirjo-Riitta Salminen[4], Mai Tone Lonnebakken[4,5], Torfinn Taxt[6]; *[1]Center of Biomedical Engineering, International Clinical Research Center, St. Anne´s University Hospital Brno, Brno, Czech Republic, [2]Department of Biomedical Engineering, Faculty of Electrical Engineering and Communication, Brno University of Technology, Brno, Czech Republic, [3]Institute of Scientific Instruments of the ASCR, v.v.i., Brno, Czech Republic, [4]Department of Clinical Science, University of Bergen, Norway, [5]Department of Heart Disease, Haukeland University Hospital, Bergen, Norway, [6]Department of Biomedicine, University of Bergen, Norway*

Background, Motivation and Objective

The commonly used perfusion analysis methods, replenishment and bolus tracking, allow only estimation of indices related to the basic perfusion parameters being mean transit time (MTT), blood volume (Vb) and blood flow (Fb). The aim of this study is absolute quantification of the basic perfusion parameters of the myocardium using bolus tracking. This absolute-quantification approach provides independence on variations in patients' vascular-tree and in the bolus application. We extend the absolute quantification bolus tracking method (presented only in two independent papers so far) by evaluation on preclinical data acquired from the pig's heart and compare it with reference blood flow obtained using fluorescent microspheres.

Statement of Contribution/Methods

Open-chest anesthetized male pig was examined by Vivid 7 ultrasound scanner (GE Vingmed Ultrasound, Horten, Norway) with a M4S probe. Three different myocardial blood flow conditions were analyzed (baseline, low and high dose adenosine infusion). For each condition, short-axis and four chamber views of heart were acquired after administration of a bolus (0.2ml) of SonoVue. Reference flow values were obtained using 15 µm fluorescent microspheres. The contrast-agent concentration curves extracted from myocardial regions of interest were fitted to a model formulated as a convolution of the arterial input function (AIF, measured in the left ventricle) and a mono-exponential tissue residual function (TRF). Fb was then estimated as Vb (ratio of the area under the AIF and the contrast-agent concentration curve of the myocardium region of interest) divided by MTT (parameter of the TRF model, obtained by model fitting).

Results/Discussion

Preliminary estimates of myocardial perfusion parameters from 3 to 8 myocardium regions for each perfusion condition are shown in the table as a mean calculated from all regions and their range in brackets. The proposed method underestimated flow compared to the reference values. This might be related to the known effect of increased contrast-imaging signal due to blood flow (as present in the ventricle). However, except for this scaling problem, the trend of the estimated blood flow follows the trend of the reference flow. The study will be extended to include data from more animals to allow a full statistical evaluation.

measurement	baseline	adenosine (low dose)	adenosine (high dose)
short axis view			
Fb (microspheres) [ml/min/g tissue]	1.2	1.2	2.3
Fb (ultrasound) [ml/min/g tissue]	0.7 [0.6 - 0.8]	0.6 [0.5 - 0.6]	1.5 [1.1 - 2.0]
Vb (ultrasound) [ml/g tissue]	0.041 [0.039 - 0.043]	0.073 [0.056 - 0.082]	0.073 [0.055 - 0.082]
MTT (ultrasound) [s]	3.4 [3.1 - 3.9]	7.6 [5.4 - 9.5]	3.0 [2.4 - 3.8]
four chamber view			
Fb (microspheres) [ml/min/g tissue]	1.2	1.3	1.9
Fb (ultrasound) [ml/min/g tissue]	0.6 [0.4 - 0.8]	0.6 [0.5 - 0.8]	1.2 [1.0 - 1.5]
Vb (ultrasound) [ml/g tissue]	0.037 [0.024 - 0.048]	0.028 [0.023 - 0.033]	0.070 [0.053 - 0.090]
MTT (ultrasound) [s]	3.5 [3.2 - 3.9]	2.9 [2.3 - 3.9]	3.7 [3.0 - 4.5]

Novel imaging systems

M5

Tuesday, July 23 2013, 10:30 am - 12:00 pm

Congress Hallair: **Herve Liebgott**
CREATIS

IUS1-D3-1

A 32x32 Integrated CMUT Array for Volumetric Ultrasound Imaging

Anshuman Bhuyan[1], Chienliu Chang[2], Jung Woo Choe[1], Byung Chul Lee[1], Amin Nikoozadeh[1], Omer Oralkan[3], Yagi Takayuki[2], Butrus Khuri-Yakub[1]; *[1]Stanford University, USA, [2]Canon Inc., Japan, [3]North Carolina State University, USA*

Background, Motivation and Objective

Volumetric ultrasound imaging is very important in medicine due to the diagnostic potential it can offer to physicians. Two-dimensional transducer arrays are desirable to capture 3D images. However, large 2D arrays require appropriate interface circuits to reduce the number of backend cables as well as to improve the noise performance. In this paper, we demonstrate volumetric imaging by use of a 32×32 array IC directly integrated with a 32×32 capacitive micromachined ultrasonic transducer (CMUT) array using flip-chip bonding technology.

Statement of Contribution/Methods

The 32×32 CMUT array is designed to operate at a center frequency of 5 MHz with a transducer element pitch of 250 μm. Previous work (Bhuyan et al, ISSCC 2013) shows integration of four 16×16 ICs to a 32×32 CMUT array by use of an interposer. However, the larger 32×32 IC enables direct flip-chip bonding with the CMUT array without the interposer layer, thereby reducing parasitics. It also allows for compact assembly making it possible to build probes with a smaller form factor. Each IC channel has the capability to either transmit or receive. The receive circuitry consists of a transimpedance amplifier and a buffer for signal conditioning of the echo. The transmit circuitry consists of a pulser, shift-registers, and digital logic to enable transmit beamforming. Each element in the array can be excited with a high voltage unipolar pulse of up to 60 V. We packed all the circuitry pertaining to one transducer element within a 250 μm × 250 μm space (i.e., same as the CMUT array element size). For pulse-echo 3D imaging, we use all elements (except diagonals) for transmit and diagonal elements for receive to reduce the number of backend cables without significantly degrading the image quality.

Results/Discussion

The CMUT-IC assembly measure 9.1 mm × 9.1 mm. Each receive channel has a bandwidth of 20 MHz and a transimpedance gain of 200 kΩ. The power per receive channel is 4.5 mW. A circuit board is designed to interface the frontend CMUT-IC assembly to the backend system consisting of an FPGA and a data acquisition system. Wire-phantoms were used in the imaging experiment. We have successfully demonstrated real-time volumetric imaging at a rate of 3 volumes per second and up to a depth of 75 mm. This work is funded by the NIH. Intersil Corporation provided support for fabrication of the ICs.

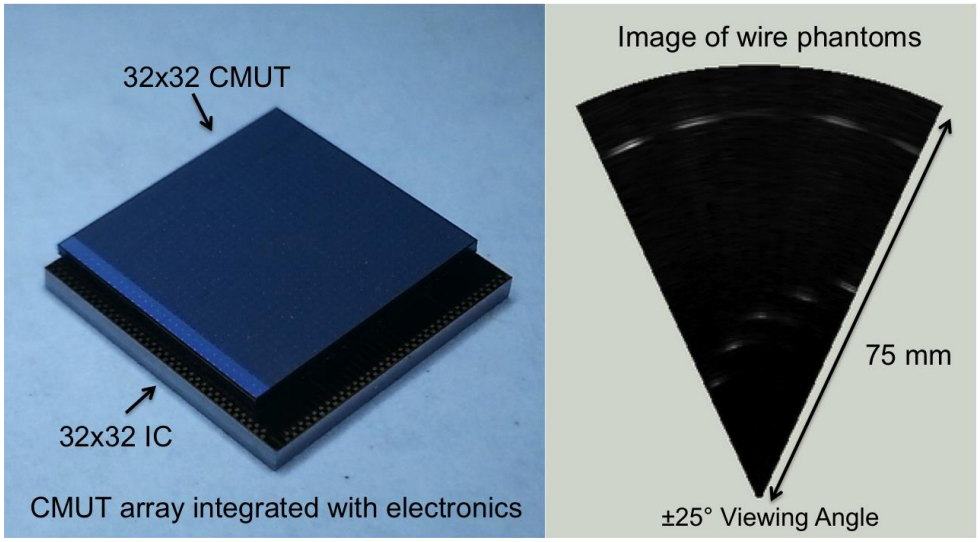

IUS1-D3-2

A Low Cost Open Source High Frame-Rate High-Frequency Imaging System

Jeremy Brown[1], Jeff Leadbetter[1], Michael Leung[2], Andre Bezanson[1], Rob Adamson[1]; *[1]Biomedical Engineering, Dalhousie University, Halifax, NS, Canada, [2]Waterloo University, Canada*

Background, Motivation and Objective

In this paper a low cost open source approach to high-frequency ultrasound imaging is described. This complete imaging system is based around four core components: A 45 MHz imaging transducer, a low cost high accuracy mechanical scanner, a field programmable gate array (FPGA) controlled pulser-receiver unit, and a data acquisition PC running open source interface software.

Statement of Contribution/Methods

The imaging transducer used is a commercially available 45 MHz single-element geometrically focused PZT composite transducer (Daxsonics Inc. Halifax, NS). This transducer is 2.5 mm in diameter and geometrically focused at f/3. The transducer has a bandwidth of 60%, a lateral beamwidth of approximately 110 µm at the focus, and a depth-of-field of 2.4 mm.

The mechanical scanner used to translate the transducer is based on a cantilevered piezoelectric bimorph mechanism. This transducer is attached to the free end of the bimorph using an extension arm, resulting in a bimorph operating frequency of 95 Hz and allowing for up to 190 unique frames per second. The bimorph driving electronics are based on an open source micro-controller, which is programmed to act as a sine wave generator using a direct digital synthesis (DDS) method.

The pulser-receiver uses accurately controlled transmit pulses that correspond to equally spaced image lines in 100 µm intervals as the bimorph transitions from high velocity near the centre of the image to zero velocity at the frame edges. The pulse generation timing is controlled with a low cost commercially available FPGA (Xilinx, Virtex V). Additionally, this FPGA is used to generate timing triggers to synchronize the mechanical scanner, and to generate a reference clock and timing triggers for the data acquisition system.

The data acquisition, processing, and display system consists of PC containing a 500 MHz 16 bit PCIe digitizer (Alazar Technologies Inc., Pointe-Claire, QC) controlled by efficient open source interface software that has been written using the Python programming language. This has allowed for straight forward customization by end users in various applications including M-mode imaging and high-resolution Doppler.

Results/Discussion

Results with the system are extremely promising. B-mode images have been generated for tissue depths between 3.0 and 12.0 mm with an image width of up to 10 mm. Achieved resolution is 50 µm (axial) by 110 µm (lateral) and the tissue signal-to-noise ratio is over 60 dB. During real-time operation, both B and M mode images are displayed at 47.5 fps, and a CUDA based image pro-cessing method is currently being developed in order to display/record the full 190 fps potential.

IUS1-D3-3

MR-compatible ultrasound research platform for motion tracking to reduce motion induced artifacts in MR imaging

Steffen Tretbar[1], Holger Hewener[1], Daniel Speicher[1], Tobias Bartscherer[1], Jürgen Jenne[2,3], André Bongers[4], Matthias Günther[2]; *[1]Fraunhofer IBMT, Germany, [2]Fraunhofer MEVIS, Germany, [3]German Cancer Research Center (dkfz), Germany, [4]mediri GmbH, Germany*

Background, Motivation and Objective

High resolution or time consuming MR-imaging methods suffer from motion artifacts due to breathing (for abdominal organs like liver, kidney or pancreas) or cardiac motion. This has an impact on high resolution morphological images and increasingly on highly sensitive functional MRI. MR-inherent compensation techniques like navigator echoes and other methods, like ECG or respiratory gating can reduce these artifacts. However, these are indirect methods monitoring surrogates, which are not reliably indicating the actual organ positions. To improve MR imaging of moving organs we propose diagnostic ultrasound (US) as additional imaging method for organ motion detection and compensation. The aim of this work was to develop an MR compatible US platform to enable non-invasive hybrid MR-US-imaging and real-time US-motion compensation.

Statement of Contribution/Methods

Motion measurement with an ultrasound system near the MR magnet is challenging regarding the special requirements for setting up the ultrasound system and the ultrasonic transducers. These have to be insensitive to the high electromagnetic fields like we find them outside and inside the tomograph and they may not interfere with the MR-system electro-magnetically. In this work, our US research platform and special ultrasound transducers are presented that meet these requirements. It consists of the beamformer unit, a special LCD display for use close to the MR-magnet, special ultrasound probes (T-shaped 2x64 element phased array transducer) and a sepa-rate PC to be used in the control room of the MRI scanner. The system can use multiple transducers in parallel mode to acquire up to 4 US images simultaneously with up to 50 frames per second. Tracking of moving structures in the ultrasound images is performed by a stochastic tracking algorithm, which fit a contour to the ultrasound data using affine transformations in real-time. Interference of the US system with the MR scanner was measured with standard gradient echo MR sequences, where the excitation pulse amplitude was set to zero.

Results/Discussion

It was possible to make simultaneous measurements (US and MRI) next to and inside the MRT system to reconstruct US motion compensated MR volumes. The interferences in the ultrasound imaging induced by the MRT system can be neglected. The effects of EMC emissions by the US device on the MRT system are measured and characterized with the very sensitive receiver coils of the MR-system as small-bandwidth noise of given frequencies and higher harmonics dominant on the US system (pulse repetition, mid frequency). Data acquisition was done in parallel to the MRI scan of organ movements inside the body. The setup was tested in one 1.5 T and one 3 T MRI system and first ultrasound compensated MR volumes were acquired. In the next steps the system will be combined with a tracking algorithm of automated MR slice correction and we will focus on the non-invasive treatment of moving organs like liver, pancreas or kidney.

IUS1-D3-4

Sonic Millip3De with Dynamic Receive Focusing and Apodization Optimization

Richard Sampson[1], Ming Yang[2], Siyuan Wei[2], Chaitali Chakrabarti[2], Thomas F. Wenisch[1]; *[1]Department of EECS, University of Michigan, USA, [2]School of ECEE, Arizona State University, USA*

Background, Motivation and Objective

3D ultrasound is becoming common for non-invasive medical imaging because of its accuracy, safety, and ease of use. However, high peak bandwidth requirements force strict limits on aperture size, limiting current state-of-the-art designs. Also, the extreme computational requirements (and associated power requirements) of image formation for a large, 3D system has, to date, precluded hand-held 3D-capable devices. Sonic Millip3De is a newly proposed hardware design [1] that leverages modern computer architecture techniques to solve these problems, performing high-resolution ultrasound imaging in a single, low-power chip. This work presents a revised Sonic Millip3De design that incorporates dynamic receive focusing and optimizations to apodization coefficients to achieve high resolution images for a large depth range.

Statement of Contribution/Methods

We outline the recently proposed Sonic Millip3De design, which makes use of 3D die stacking, massive parallelism, and a streaming data flow to perform large-scale 3D synthetic aperture with 1024 channels in a 3-layer stacked system. We build on the iterative delay calculation method of the preliminary design, which enables a 400x storage reduction over naive lookup tables. We introduce a new virtual source firing sequence and dynamic receive focusing scheme that optimizes receive aperture in each depth zone. Together, these optimizations further reduce power requirements while maintaining image quality.

Results/Discussion

We present image quality analysis using Field II simulations of cysts in tissue at varying depths to show that our methods do not degrade CNR over images produced by system without power constraints. Then, using RTL-level design for an industrial 45nm ASIC process, we demonstrate 3D synthetic aperture with 120x88 transducer array with a 16W full-system power budget (400x less than a conventional DSP solution). Using semiconductor technology scaling trends, we project that our design will achieve a sub-5W power budget by the 11nm node.

[1] R. Sampson, M. Yang, S. Wei, C. Chakrabarti, and T. F. Wenisch. “Sonic Millip3De: Massively Parallel 3D-Stacked Accelerator for 3D Ultrasound.” Proc. of the 19th IEEE International Symposium on High Performance Computer Architecture, Feb. 2013.

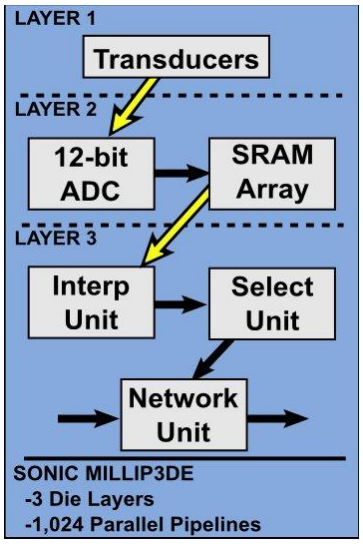

IUS1-D3-5

Lossless Compression with Parallel Decoder for Improving Performance of GPU-based Beamformer

U-Wai Lok[1], Gang-Wei Fan[1], Pai-Chi Li[2]; [1]*National Taiwan University, Taiwan,* [2]*Electrical Engineering, National Taiwan University, Taipei, Taiwan*

Background, Motivation and Objective

The massive data transfer of ultrasound raw data becomes one of the critical limitations for a real time software based beamformer. Lossless compression with sequential decoder can reduce data size of ultrasound raw data but the time-consumed decompression process degrades the performance of data transfer, thus the overall performance is also degraded. Therefore, a fast, parallel decoding scheme is highly desirable. A lossless compression approach associated with parallel decoding on graphics processing units (GPU) is proposed in this study. The hypothesis is that the execution time of transferring compressed data along with decoding is less than transferring the original raw data. Thus, the issue of data transfer is mitigated.

Statement of Contribution/Methods

RF raw data are first demodulated to baseband, and then the baseband data are compressed through our proposed lossless encoder. For the encoder design, baseband data within a channel are grouped into several batches, and the bit length to represent each signal within the same batch is fixed but varied for different batches. The bit length is determined by the sample with the largest absolute value within a batch. In addition, an extra address is utilized to indicate the bit length and the memory location of each batch as shown in figure A. At the decoder side, GPU is only required to compute the bit length and memory position of each sample through address information. Therefore, all samples can be decompressed in parallel in the GPU.

Results/Discussion

The latency to demodulate and compress a frame data in FPGA requires about 4 ms, and the proposed compression ratio reaches 3.5. Hence, the transmission time from front end to the software backend is reduced. At the software backend, the processing time of transferring a compressed frame data from CPU to GPU with the parallel decoder only requires about 5 ms. This is nearly a three-fold improvement. Details of each condition are shown in figure B. The processing time of data transfer from CPU to GPU is reduced by our proposed data compression and parallel decoding process in GPU. Another concomitant benefit of our proposed method is that the data transfer rate between the front end and software backend becomes less demanding.

A

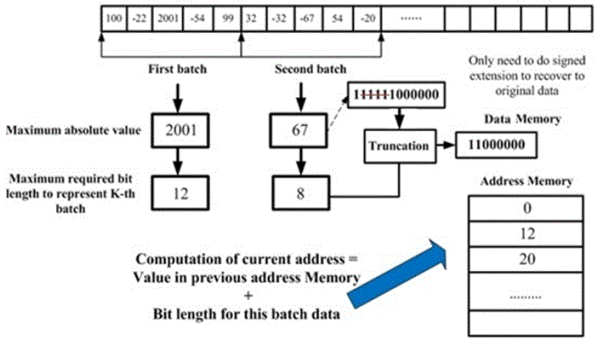

B

Conditions	Time(ms)
Demodulation and encoder in FPGA	3.96
Transmit original RF data from CPU to GPU	16.12
Transmit compressed data from CPU to GPU	3.82
Decoder in GPU	1.21
Transfer compressed data and decoding process	5.04

Figure (A) Illustration diagram of encoder in FPGA and (B) processing time of each condition.

IUS1-D3-6

A Fast Parallelized Eigen-Based Clutter Filter Framework for Ultrasound Color Flow Imaging

Adrian J. Y. Chee[1], Billy Y. S. Yiu[1], Alfred C. H. Yu[1]; [1]*Medical Engineering Program, The University of Hong Kong, Pokfulam, Hong Kong*

Background, Motivation and Objective

Eigen-filters with attenuation response adapted to clutter statistics have emerged as a new class of clutter suppression techniques in color flow imaging (CFI) to achieve high flow detection sensitivity in the presence of tissue motion. There is growing interest to extend this technique beyond laboratory investigations by incorporating it into the CFI processing routine on ultrasound scanners. Nevertheless, bridging such a gap from theory to practice is known to be challenging from a real-time computing perspective because the singular value decomposition (SVD) operation in eigen-filtering is known to pose heavy computational burden. Here we seek to overcome this issue by formulating a new technical framework that enables fast execution of eigen-filtering so as to foster their practical adoption in CFI.

Statement of Contribution/Methods

Our fast eigen-processing framework for CFI was devised by integrating three principles: (1) applying mature eigen-computation algorithms in matrix algebra; (2) leveraging on the single-instruction, multiple-data (SIMD) computing approach that has became prevalent in ultrasound imaging with the advent of graphics processing units (GPU); (3) adopting the single-ensemble-based (Hankel-SVD) eigen-filter paradigm that is algorithmically compatible with SIMD computing. For each CFI pixel, its flow estimates were derived by processing the pixel's slow-time ensemble as follows. First, we computed the SVD of the slow-time ensemble's Hankel matrix using a parallelized algorithm that includes the steps of Householder Transform, QR decomposition, and Givens rotation (implemented through NVidia's CUDA programming tool). After that, the power and frequency of each eigen-component was estimated in parallel using the GPU (via the lag-one autocorrelation method). Adaptive filter order selection was then applied to extract the principal eigen-component corresponding to blood flow. The real-time efficacy of our framework was investigated using a GTX 480 GPU and synthesized CFI datasets with various sizes of pixel counts (P) and slow-time ensemble sizes (N) (5 MHz frequency; 20dB clutter-to-blood signal ratio; 2mm/s max tissue velocity; 38cm/s max flow velocity). Frame processing throughput and the execution time of each computational step were measured and analyzed using CUDA's visual profiler.

Results/Discussion

Using our CFI eigen-processing framework, real-time video-range throughput (24 fps) was achieved for frames with P = 70,000 (128 scanlines, each with 547 depth positions) and N = 10. Flow estimation accuracy was not compromised. Processing time increased exponentially with N: e.g. for P = 10,000, the throughput was >600 fps for N = 4 but was only 23 fps for N = 21. The load only increased linearly with P, implying that our framework is readily scalable for larger frame sizes. To our knowledge, this work is the first demonstration that real-time CFI with eigen-processing can be achieved in practice.

Structural Health Monitoring

NH

Tuesday, July 23 2013, 10:30 am - 12:00 pm

Congress Hallair: **Paul Wilcox**
University of Bristol

IUS2-D-1

Uncertainty Quantification in Ultrasonic Guided Wave Interrogation Using Detection Theory

Michael Todd[1], Eric Flynn[2], Greg Jarmer[1,2], Colin Haynes[1]; [1]*Structural Engineering, University of California San Diego, La Jolla, CA, USA,* [2]*Los Alamos National Laboratory, USA*

Background, Motivation and Objective

Interrogation of structures with ultrasonic waves with either dense or sparse arrays (in the sense of average sensor spacing compared to interrogation wavelengths) is an increasingly popular approach for defect assessment in many applications of structural health monitoring. The ultrasonic scattering properties of defects are exploited in various scattered signal processing schemes that ultimately involve some sort of comparison to a baseline or reference scatter state, as non-damage related features such as boundaries and material changes also induce scatter of ultrasonic energy. Whatever process is used, whether it is used for defect detection ("Is a defect present?"), defect localization ("Given a defect is present, where is it located?"), or defect characterization ("Given that a defect is located, what quantitative information may be determined about it?"), that process will inevitably have uncertainty in it, and that uncertainty is what affects final decision-making based on the analysis. Error sources contributing to uncertainty include environmental nonstationarity, data acquisition/sensor noise, and estimation error in the signal processing itself. The main objective of this paper is to present how the field of detection theory, which has been used heavily in fields such as radar, underwater acoustic signal detection, and communications, may be applied in problems of ultrasonic interrogation in order to obtain defect assessment metrics that are associated with levels of uncertainty.

Statement of Contribution/Methods

Although detection theory is a widely-used approach in some of the above-mentioned fields, of which ultrasonic interrogation shares many of the same objectives (detect or localize something, for example), it has not been used widely in ultrasonic interrogation, or even in structural health monitoring as a whole. Detection theory involves establishing a fundamental hypothesis that clearly states the goal of the interrogation and then uses statistical reasoning to derive a detector, or decision-making condition, based on probabilities of which hypothesis is more likely. When it is important also to consider the consequences of making incorrect decisions (Type I/II errors), a Bayesian formulation is more appropriate. A detector typically involves some sort of weighted likelihood ratio, the specific probabilistic forms of which depend on the objective, the signal processing being used, and the Type I/II error tolerances.

Results/Discussion

This paper will demonstrate elements of applying detection theory to selected experimental problems in ultrasonic interrogation that span objectives (detection vs. localization) and sensing array strategies (sparse vs. dense). In all cases, great improvement in performance (in a ROC sense) is observed when compared to other approaches. The paper will conclude with an extension of this using Bayesian experimental design for optimal (in performance) interrogation.

IUS2-D-2

Computation of Modal Group Delay in the Decomposition of Ultrasonic Waveguide Signals Using the Synchrosqueezed Wavelet Transform

Fabian Bause[1], Boqiang Huang[2], Angela Kunoth[2], Bernd Henning[1]; [1]*Measurement Engineering Group, University of Paderborn, Paderborn, Germany,* [2]*Complex Systems Group, University of Paderborn, Paderborn, Germany*

Background, Motivation and Objective

Due to the modal behavior of geometrically bounded media, ultrasonic guided waves propagate in waveguides as a combination of multiple dispersive wave packets, which can be simulated as a PDE-problem [1]. Given an excitation in time and space, multiple eigen-modes, obtained from solving the PDE, may propagate each with different dispersion characteristics and weight. Considering a broadband pulse exciting from one side of a hollow cylindrical waveguide, the received signal at the other side consists of all propagating eigen-modes that can be considered as narrow band signals approximately.

Statement of Contribution/Methods

To sharpen the time-frequency representation (TFR) of the received waveguide signal, we employ the synchrosqueezed wavelet transform (SWT)[2]. Using a ridge detection algorithm, we successively separate the synchrosqueezed TFR into several narrow band TFRs which can be identified as oscillatory components with time-varying frequency. These separated TFRs are reconstructed as narrow band signals using the inverse SWT. Based on an analytical model of the waveguide, we observe that the decomposed signals resemble the dominant eigen-modes simulated by using the PDE. Moreover, we observe that also the group delay and, therefore, the group velocity of each decomposed signal can be estimated well. This is of high interest when analyzing the characteristics of a given waveguide, such as its acoustic properties, or in non-destructive testing.

Results/Discussion

We apply the proposed method to three received waveguide signals. These were simulated using the analytical waveguide model with a constant geometry but with different materials of increasing damping degree. We also investigate the case with only geometrical dispersion and the one influenced by increasing material dispersion. Finally, we show first results of the signal decomposition and an estimation of the group delay for an experimentally received waveguide signal, and compare it with the ones from simulated signals.

[1] M.J.S. Lowe, Matrix techniques for modeling ultrasound waves in multilayered media, IEEE T UFFC, vol. 42, 1995

[2] I. Daubechies, et.al. Synchrosqueezed wavelet transforms: an empirical mode decomposition-like tool, Appl. Comput. Harmon. Anal., vol. 30, 2011

Fig. 1: Signal decomposition and group delay estimation for a simulated case without damping.

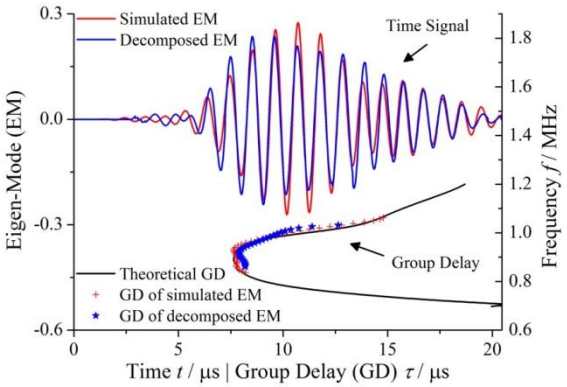

IUS2-D-3

Decomposition of Multipath Lamb Waves with Sparse Wavenumber Analysis for Structural Health Monitoring

Joel B. Harley[1], José M.F. Moura[1]; [1]*Department of Electrical and Computer Engineering, Carnegie Mellon University, Pittsburgh, PA, USA*

Background, Motivation and Objective

Guided waves, such as Lamb waves, are attractive tools for monitoring large civil infrastructures due to their sensitivity to damage. However, distinguishing reflections that originate from damage is often complicated by the multi-modal and dispersive characteristics of guided waves and additional multipath interference from the medium's boundaries. In this paper, we present a method to decompose data into a collection of multipath arrivals, originating from both damage and boundaries, by combining sparse wavenumber analysis with additional L1 minimization techniques.

Statement of Contribution/Methods

Sparse wavenumber analysis is a methodology for accurately recovering the multi-modal and dispersive properties of guided waves, which are usually not precisely known and vary with changes in environmental conditions such as temperature. In previous work, we demonstrated sparse wavenumber analysis with both simulation [1] and experimental data [2] and extended it to predict guided wave signals between two points in a medium [2]. In this submission, we use this predictive power to estimate the number of multipath arrivals in a signal and then to separate them. As we show in this work, sparse wavenumber analysis can separate reflections from damage without the use of a previous baseline. Localization methods can be applied to each decomposed signal to determine the origin of each reflection.

Results/Discussion

We apply our decomposition technique to simulated Lamb wave measurements with five distinct modes and five paths between the transmitter and receiver. The simulated signal has a center frequency of 1.25 MHz and a bandwidth of 100 kHz. Figure 1(a) illustrates the simulated signal and Figure 1(b)-(f) shows its decomposition into five multipath arrivals. When comparing the true multipath arrivals used to construct the simulated data with the five decomposed signals, we find they have correlation coefficients of 0.993, 0.989, 0.989, 0.996, and 0.994. These results show that we can very accurately recover each multipath arrival.

[1] J.B. Harley, A.C. Schmidt, and J.M.F. Moura, "Accurate Sparse Recovery of Guided Wave Characteristics for Structural Health Monitoring", in Proc. of the IEEE Ultrasonics Sym., 2012.

[2] J.B. Harley and J.M.F. Moura, "Sparse recovery of the multimodal and dispersive characteristics of Lamb waves", J. Acoust. Soc. Am., under review.

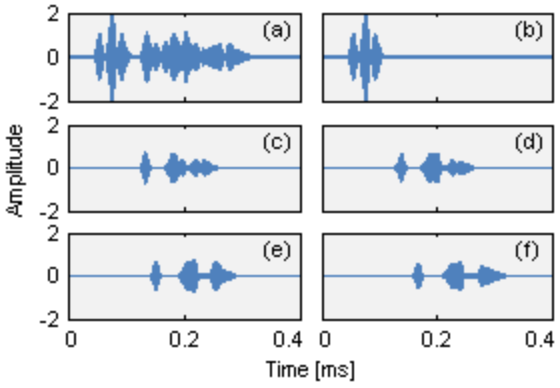

IUS2-D-4

Flexible Ultrasonic Transducers Using Piezoelectric Fiber Composites with Antisymmetric Interdigital Electrodes

Ching-Chung Yin[1], Yu-Chien Wu[2], Shih-Ming Hsu[2]; [1]*Deaprtment of Mechanical Engineering, National Chiao Tung University, Hsinchu, Taiwan,* [2]*National Chiao Tung University, Taiwan*

Background, Motivation and Objective

The piezoelectric fiber composites (PFC) have been utilized as smart materials and structures because of excellent actuating, sensing capabilities and conformability. The conventional PFC devices polarized and actuated by symmetric interdigital electrodes expand or contract simultaneously when a voltage is applied to the electrodes. The

symmetric configuration obstructs PFC from being a fixed-wavelength acoustic transducer. This study presents a PFC acoustic guided wave transducer with new electrode arrangement. It has been shown the flexible transducer has very good performance for structural health monitoring (SHM) applications.

Statement of Contribution/Methods

The PFC device is constructed with unidirectional piezoelectric fibers embedded in epoxy matrix and sandwiched between two flexible polyimide sheets printed with interdigital electrodes. Symmetric electrode layout is adopted for poling process since the electric field intensity is about twice of that yielded by anti-symmetric arrangement. Thereafter, the fabricated ultrasonic transducer is actuated or sensed through the anti-symmetrically aligned electrodes. Extensional vibration will be induced and dominant in the device as the electrodes are exerted by alternating voltage. The transducer adhered to the surfaces of host structures can be used to generate guided waves of desired wavelength. The operating frequency is relevant to the electrode pitch and dispersive characteristics of the host.

Results/Discussion

A parametric study has been conducted to understand the optimal arrangement of electrodes, including width of the electrode, the gap between adjacent electrodes, and so on. An energy-saving design is further considered. The interdigital electrodes are divided into two sets with a space interval of the wavelength multiplied by an integer plus one quarter. A traveling guided wave along the demand direction can be formed by constructive interference of two equal-intensity waves generated by low-voltage orthogonal square wave signals exerting on the electrodes. One megahertz ultrasonic transducers were manufactured and tested. High directivity and very good consistency in both measured and predicted dynamic characteristics have been achieved. The developed flexible ultrasonic transducer can be effectively used to actuate and sense fixed-wavelength guided waves in host structures. Taking advantages of lightweight and conformability, it has a great potential for damage detection in the host structures without unwanted influences of added mass or change in stiffness.

IUS2-D-5

Detection of crack tips in a plate by a pulse laser combined transducer under Lamb wave excitation

Kazuki Nakata[1], Nobuaki Hirose[1], Takaharu Kitamura[1], Mami Matsukawa[1]; [1]*Wave Electronics Research Center, Doshisha Univ., Kyotanabe, Kyoto, Japan*

Background, Motivation and Objective

Evaluation of crack tips remains difficult to be detected because they are often closed. One recent interesting solution to evaluate closed cracks is the nonlinear approach.

For more simple and 2D imaging system to detect crack tips, we suggest a combination technique of two methods. One is a hollow cylindrical PVDF transducer with a pulsed laser to generate and receive ultrasonic pulse waves, making use of the thermoelastic effect. The other is a low frequency longitudinal excitation of the crack. In this study, we tried the detection of crack tip using symmetrical mode Lamb wave excitation. The condition of fluctuating tips was detected as changes of laser induced ultrasonic pulse waves.

Statement of Contribution/Methods

A short laser pulse (1047 nm, 80 μJ, pulse width 5 ns, Spectra Physics) was irradiated to the surface of an acrylic plate sample (35×100×5 mm^3) through the center of a handmade hollow cylindrical PVDF transducer. Ultrasonic pulse waves were generated at the aluminum film on the surface of the sample. The induced ultrasonic wave propagated in the sample, reflected at the reverse side or the inside plane crack, and was received by the PVDF transducer. S_0 Lamb wave at 250 kHz was also excited in the sample using a PZT transducer with water coupling. The frequency was determined by the sample thickness and dispersion relation. The propagation of Lamb wave was confirmed from the distribution of surface displacement (maximum 16 nm) by a laser Doppler vibrometer (Ono sokki). We irradiated the laser pulse to the sample surface at the maximum (expansion) and minimum (contraction) peaks of the Lamb wave, scanning the irradiation position by 0.2 mm as shown in Fig. 1.

Results/Discussion

The effects of fluctuation on the crack tips could be observed as small changes in wave properties. Figure 1 shows the spatial distribution of amplitude spectrum ratio of pulse waves, which propagated at expansion / contraction (E/C) timing. At the frequency of maximum amplitude (5 MHz), the ratio E/C became large at the crack tips. The ratio E/C was from 1.5 to 3.0. In this study, the displacement of Lamb wave fluctuation was very small. The fluctuating effects then seem to be little in the area of large crack and without crack. This technique can only extract the crack tip and do not depend on the surface condition because the difference between expansion and contraction condition was observed.

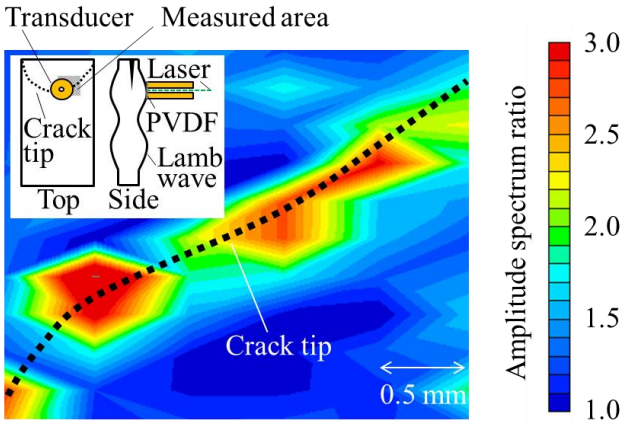

Fig. 1 2D map of the amplitude spectrum ratio near the crack tips.

Saw Design

T1

Tuesday, July 23 2013, 10:30 am - 12:00 pm

Congress Hallair: **Marc Solal**
Triquint Semiconductor

IUS4-D-1

Advanced 2D Periodic Array and Full Transversal Mode Suppression

Jiman Yoon[1,2], Markus Mayer[2], Thomas Ebner[2], Karl Wagner[2], Achim Wixforth[1]; [1]*Experimental Physics I, University of Augsburg, Augsburg, Bayern, Germany,* [2]*Advanced Development Discretes, TDK Corporation, Munich, Bayern, Germany*

Background, Motivation and Objective

Typically, a one-port resonator in SiO_2-covered $LiNbO_3$ displays a series of distinct transversal modes above the resonance frequency. When such resonators are used in filter design without taking any countermeasures, the transversal modes lead to unacceptable passband ripples. In the previous work, "Two dimensional periodic array of reflection centers on electrodes in SAW resonators [Yoon et al, IUS2012]", it has been demonstrated that a 2D periodic array with patches on electrodes can successfully suppress undesired modes within the frequency band of $k_y=[0, \pi/p_T]$, where p_T is the transversal pitch of the periodic array. However, the resonator exhibits strong radiation at the frequency where the periodicity of the transversal pitch of the patches and the wavelength of the transversal mode are equal.

Statement of Contribution/Methods

In this work, we present an improved version of the 2D periodic array from [Yoon et al, IUS2012]. By modification of the patch geometry, $\Delta v/v$ waveguide was optimized and the spurious radiation at $k_y=\pi/p_T$ was suppressed. The required geometry was adjusted on the basis of simulations that employ the well established periodic 2D P-matrix model. In this model, a unit cell is defined with 2 strips, which then is infinitely cascaded taking into account reflection and diffraction. Measured and simulated admittances of resonators are in good agreement.

Results/Discussion

A well-designed periodic array with geometry variations is capable to fully suppress all but the fundamental transversal mode within a certain bandwidth. Besides, the strong peak is removed at the frequency where the periodicity of the transversal pitch coincides with the wavelength of the transversal mode. Therefore the alternative 2D periodic array on the electrodes can be readily employed in designing SAW flters in SiO_2-covered $LiNbO_3$ with excellent performance.

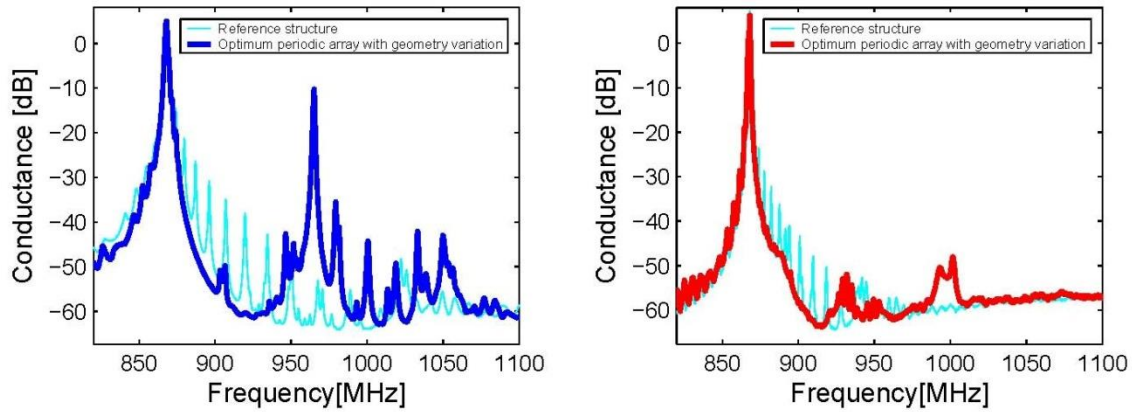

Fig. 1: Comparison of the mode suppression; Reference structure (both-side cyan), a resonator with 2D periodic periodic patches on electrodes (left-side blue) and with geometry variation (right-side red).

IUS4-D-2

Development of High Linearity Duplexers with Low Passive Intermodulation Component

Akira Moriya[1], Makoto Inoue[2], Osamu Kawachi[1]; [1]*TAIYO YUDEN Mobile Technology Co., Ltd, Japan,* [2]*TAIYO YUDEN CO., LTD., Japan*

Background, Motivation and Objective

We have proposed surface acoustic wave (SAW) duplexer to CDMA/LTE markets.Advancements of the communication system are progressing in accordance with the increase of the data user needs.

Technology that uses multi-band and simultaneous communication has been progressing. Effect of mutual interference in the mobile phone increases, deterioration of communication quality is concerned.

Therefore, high frequency devices with lower intermodulation distortion are required.

Statement of Contribution/Methods

In this paper, we found that the IMD value can be improved by optimizing the design of High Linearity duplexer using the non-linear SAW simulator which we developed [1].

Several non-linear terms are considered in this IMD simulation.

Furthermore, in the IMD evaluation system, we used the Low-PIM cables, attenuators, connectors, and new Low-PIM inductors which we developed for matching.

Results/Discussion

As a result of the trial production of duplexer for BC0/B13 system, we obtained about 20dB better than the conventional duplexer IMD value.

In the future, we will promote optimum design considering to the material properties for further miniaturization and Higher-Linearity.

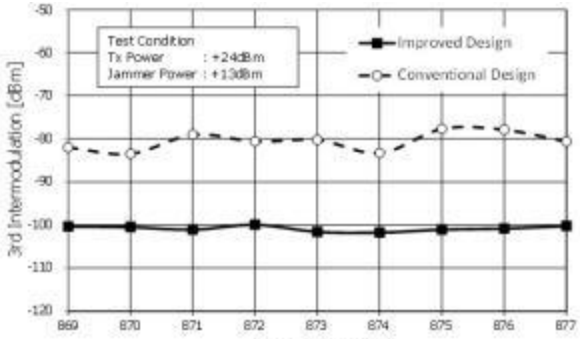

Fig. 3rd Intermodulation for conventional and improved design.

IUS4-D-3

Wide Band Taper SAW Filters with Improved Shape Factor and Phase Response

Rodolfo Chang[1], Svetlana Malocha[1]; [1]*TriQuint Semiconductor, Apopka, Florida, USA*

Background, Motivation and Objective

SAW taper devices used as wideband base station IF filters, have to meet stringent requirements on phase linearity, high selectivity and small device size. The selectivity degradation and phase response distortions in the measured responses not accounted for by simulations was found. The difference between measured and simulated phase responses had parabolic frequency dependence, thus increasing filter contribution in EVM (error vector magnitude) of the system. The steepness of the transition between the passband and rejection band was decreased (compared to the simulated) on the high frequency side. The discrepancy between measured and simulated responses increased as the device operating frequency, bandwidth, and transducer lengths were increased. The wide range of electrode width in the transducers, such as quadrature SPUDT suitable for wide band devices, was a contributing factor as well. The goal of this work was to reduce the discrepancies between simulations and measurements and improve the device performance.

Statement of Contribution/Methods

It was established that the discrepancy between the measurements and simulations was largely caused by the metallization duty factor variation in the fabricated devices both across the aperture of the device and as a function of the electrode width. The duty factor variation was confirmed using SEM measurement of the electrode widths in several locations of the device. The measured electrode widths deviated from the designed by the amount dependent on the position of the measurement site across the aperture and the electrode width. Smaller electrode widths (< 1um) differed significantly more from the designed, compared to the wider electrode widths (> 1.5 um). The reason for this difference was due to fabrication process exacerbated by the drastic difference in electrode widths between the high and low frequency tracks in the taper devices and between electrodes in the same track (1/16 lambda and 3/16 lambda in quadrature SPUDT). In order to correct this fabrication error, a variable bias (additional line width) was applied to transducers¡¦ electrodes. The bias was varied across the aperture, depending on electrode widths. The bias function was constructed based on the above mentioned SEM measurements.

Results/Discussion

A taper device with fractional bandwidth of 17% was designed: one with a fixed bias and another identical design but with a variable bias. The measured response of the device has phase linearity improved by 0.8 degrees and the EVM improved from 2.5% to 1.85%. The rejection on the high frequency side of the passband and the shape factor were also improved from 1.09 to 1.086 due to transition band reduction by 0.232 MHz. An improved agreement between measurement and simulations confirms that the duty factor variation was the cause of the distortions.

IUS4-D-4

Experimental and Theoretical Results of New Unidirectional Interdigital Transducers Using Floating Electrodes

Kazuhiko Yamanouchi[1], **Hiroyuki Odagawa**[2], Ikuya Iwai[2]; [1]*Tohoku University, Sendai, Miyagi, Japan,* [2]*Kumamoto National Colledge of Technology, Japan*

Background, Motivation and Objective

In order to obtain the high performance of Surface Acoustic Wave (SAW) devices, it is very important for the interdigital transducer (IDT) to be made the unidirectional ones (UIDT) together with SAW materials. Especially mobile communication and UWB communication systems require the high efficient unidirectional IDT for phase linear, wide band, low-loss filters at GHz-ranges.

Statement of Contribution/Methods

Many types of unidirectional transducers are proposed. That is (1) UIDT with Multi-phase shifters, (2)Single Phase UIDT, (a) Mass loading and Coupling difference internal reflection type UIDT, (b)Thin film grating type UIDT,(c) Acoustic distribution internal reflection ,(d) Grating strip reflection type UIDT,(e) Natural UDT using anisotropy of substrate and (f) electrode reflection type UIDT, et al. The UDTs of (1) have some demerits of phase shifters and air gap electrodes, meander line with high resistivity, also have some demerits to be used the multi-photolithography techniques.

The UDTs of (2) have some demerits of low transduction and small reflectivity, with many spurious signals and to be used the special substrate and to obtain no back ward directivity (f).

In this paper, the new configuration of the single phase internal reflection type of UIDT with the high transduction efficiency using the excitation electric fields applying between the electrodes and the reflecting floating electrodes are proposed. Also the UIDTs are fabricated using the single-photolithography techniques. Electrode widths are λ/4 and one of gaps are λ/8. Also, the new UDTs with the open and short reflecting electrode with the larger directivity are proposed.

Results/Discussion

The theoretical results showed the good directivity around 6dB and zero insertion loss filters with wide band characteristics. The experimental results using Al and Cu electrodes shows almost the same results of directivity of 8dB using 128° YX $LiNbO_3$ and SiO_2/YX-$LiNbO_3$ with k^2=0.3 and zero Temperature Coefficient of Frequency(TCF). We show the collinear weighting filters with low loss, flat wide band, sharp-cutoff and phase linear.

IUS4-D-5

SAW resonators using electrostrictive effect

Sebastien Alzuaga[1], William Daniau[2], Thomas Baron[1], Gilles Martin[1], Roland Salut[3], Sylvain Ballandras[4], Emmanuel Defay[5]; *[1]Time & Frequency, FEMTO-ST, Besancon, France, [2]Time and Frequency, FEMTO-ST, Besancon, France, [3]Mimento, FEMTO-ST, Besancon, France, [4]FreC'N'Sys, Besancon, France, [5]CEA LETI, Minatec Campus, Grenoble, France*

Background, Motivation and Objective

The use of piezoelectric materials is very well established to generate acoustic waves. In signal processing devices, surface acoustic waves (SAW) and bulk acoustic waves (BAW) are commonly used to manufacture resonators, filters or sensors. The piezoelectric effect is present in certain materials that exhibit non-centrosymetric crystallographic symmetry properties whereas electrostrictive effects exist in all dielectric materials. Electrostriction is a quadratic electromechanical coupling phenomenon that can induce a "pseudo piezoelectric effect" in non piezoelectric media when a static electric field is applied. This effect is studied here to implement a model based on classic piezoelectric theory which will be used to design RF SAW resonators.

Statement of Contribution/Methods

A simplified model and one more complete have been developed in this study to take into account electrostrictive effect in SAW devices allowing FEB/BEM modeling. DC electric field is taken into account to calculate "pseudo-piezoelectric" coefficient at every point of the mesh. Then classic piezoelectric resolution of the problem is achieved to simulate electrostrictive SAW device.

Results/Discussion

Both one and two ports SAW resonators have been manufactured on bulk SrTiO3, exhibiting resonant frequency above 2 GHz and quality factor about 2000 (see fig 1). The influence of DC Bias on resonance frequency has been studied. The tenability of resonant frequency is about 1% for 50V DC voltage. These results demonstrate the interest of electrostriction for SAW resonators as they exhibit relative high Q factor and their resonant frequency can be controlled by DC voltage so that temperature dependence can be compensated in a large range of variation.

Comparison of experimental and simulation results show that higher order coefficients have to be taken into account to predict frequency variation with DC voltage. For SrTiO3, the dependence of elastic constants with electric field is predominant and has to be considered. Further work has to be achieved to measure the coefficients of electric field dependence of elastic constants in order to have a complete model as they are not available in literature

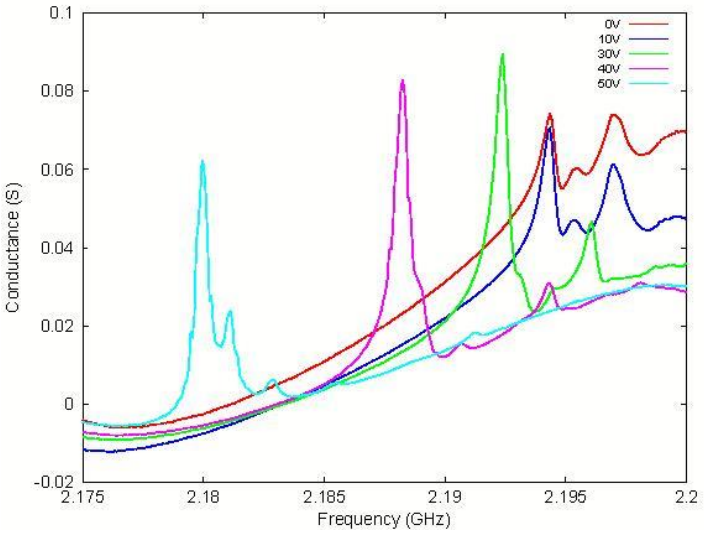

IUS4-D-6

Design of RF IDTs for Efficient Coupling to Wavelength-Scale Structures in Thin Piezoelectric Films

Matt Eichenfield[1], Roy H. Olsson III[2]; *[1]Sandia National Laboraties, Albuquerque, NM, USA, [2]Sandia National Laboratories, USA*

Background, Motivation and Objective

The dimensions of practical radio-frequency (RF) piezoelectric transducers are often constrained by RF impedance- matching requirements. In the gigahertz frequency regime in particular, the capacitance of metal interdigitatal transducers (IDTs) must often be kept large by making the length of the "fingers" much larger than a wavelength.

This constraint on the extent of excitation sources makes it difficult to efficiently excite wavelength-scale structures such as single-mode waveguides and cavities. Figure 1a is a schematic representation of the problem. The wave produced by the sending transducer suffers an insertion loss at the waveguide input of approximately the ratio of the width of the waveguide to the width of the transducer. At the waveguide ouptut, intercepting the wave immediately produces a second, symmetric insertion loss; if the transducer is offset from the waveguide output (as shown), diffraction expands the beam but causes waveguide curvature that will tend to average the received signal to zero as the wavefront curvature increases.

Statement of Contribution/Methods

Using finite element method (FEM) modeling, we show how the fields of complex-source-point Lamb waves (described elsewhere) can be inverted to yield simple IDT shapes that efficiently launch dipole-like beam modes, as shown in Figure 1b. We further show that these dipole-like beam modes are precisely the fields required to efficiently couple to single-mode waveguides and cavities.

Results/Discussion

As a specific example, we demonstrate the design of a pair of focusing IDTs, as shown in Figure 2. Operating at 2 GHz with a maximum width of approximately 60 wavelengths, this transducer can send and receive through a single-wavelength-scale waveguide with a total acoustic insertion loss less than 2 dB.

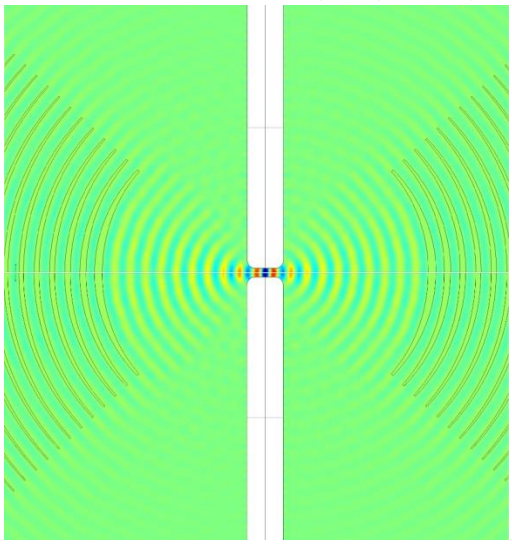

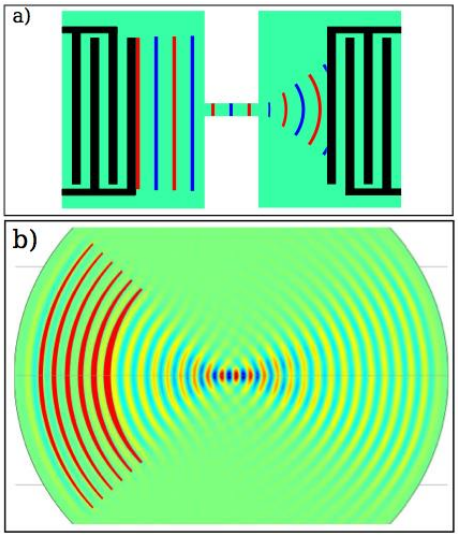

Miniature Devices and IVUS

T2

Tuesday, July 23 2013, 10:30 am - 12:00 pm

Congress Hallair: **Jian Yuan**
Philips Shanghai Apex

IUS5-D-1

Multifrequency intravascular ultrasound for assessment of atherosclerotic plaque vulnerability

Chelsea Munding[1], Emmanuel Cherin[2], Jianhua Yin[2], Hyunggyun Lee[2], David Goertz[2], Brian Courtney[3], Stuart Foster[2]; *[1]Medical Biophysics, University of Toronto, Toronto, Ontario, Canada, [2]Physical Sciences, Sunnybrook Research Institute, Toronto, Ontario, Canada, [3]Schulich Heart Research Program, Sunnybrook Health Sciences Centre, Canada*

Background, Motivation and Objective

Acute coronary syndromes are most often caused by the rupture and thrombosis of an atherosclerotic plaque in the coronary arteries. Plaques that are vulnerable to rupture are characterized by several features, including a thin fibrous cap (<65 µm thick), a large necrotic core, positive remodelling of the vessel wall, inflammation, and angiogenesis of the vasa vasorum. A minimally invasive method of imaging these features would improve our understanding of the natural history of vulnerable plaque and allow the efficacy of possible treatments to be assessed.

Intravascular ultrasound (IVUS) is promising for vulnerable plaque assessment as it is an established clinical tool; however current commercially available devices cannot resolve the fibrous cap or the vasa vasorum. Visualizing the fibrous cap with ultrasound would require the use of high frequencies (>60 MHz) that would not permit the visualization of deeper plaque features. Contrast-specific imaging techniques have been shown to produce signal enhancement in neovascularized plaques; however for this method to be clinically relevant the device should also be capable of high-quality tissue imaging. These requirements lead to a compelling argument for multifrequency IVUS, which would add new capabilities to the existing repertoire.

Statement of Contribution/Methods

We have created a novel prototype to address the goal of multifrequency imaging. It consists of a single stack of two transducers sharing a common ground electrode and backing layer. The signal electrodes are independent. One transducer is tuned to a very high frequency (67 MHz) and one to a more conventional frequency (32 MHz). The 32 MHz element had a -6dB focal beamwidth of 600 µm at 4 mm, and a transmitted pulse length of 30 ns. The 67 MHz side had -6dB beamwidths of 340 µm and 230 µm in the lateral and elevation axes, respectively. The 67 MHz transmitted pulse length was 16 ns.

Results/Discussion

The 32 MHz image (a) shows deeper phantom features, including two hypoechogenic inclusions. The second image is a 32/67 MHz composite (b). The ability of the low-frequency transducer to visualize deeper features is maintained, while the more superficial structures near the centre can be appreciated in much higher resolution. These results demonstrate the potential complimentary, multifrequency imaging of both deep and superficial plaque features.

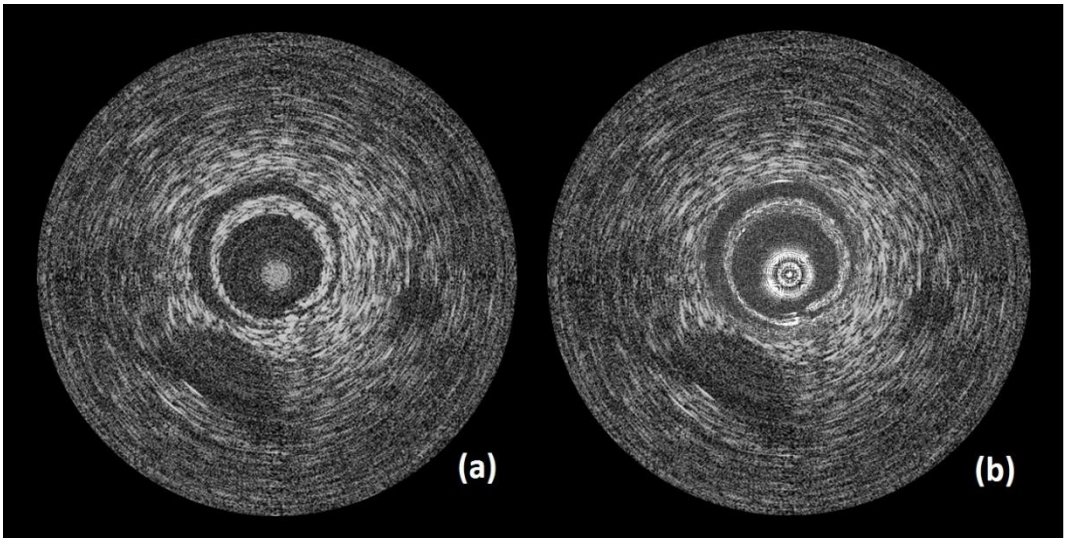

IUS5-D-2

Miniaturized Forward Looking High-Frequency Phased Array Transducer for Intravascular Imaging Applications

Ruimin Chen[1], Nestor Cabrera Munoz[1], Hyung Ham Kim[1], Hsiusheng Hsu[1], Fan Zheng[1], Changgeng Liu[2], Jay Williams[1], Qifa Zhou[1], K. Kirk Shung[1]; *[1]Resource Center for Medical Ultrasonic Transducer Technology, Department of Biomedical Engineering, University of Southern California, USA, [2]Geospace Research, Inc., USA*

Background, Motivation and Objective

Intravascular ultrasound (IVUS) is a medical imaging approach that uses a miniaturized ultrasound transducer attached to the distal end of the catheter to acquire cross-sectional images of blood vessels. Two types of ultrasound transducers are commonly used in the current state-of-art IVUS imaging catheter. One utilizes a rotating side-looking single element transducer. The other is a radial array with multiple elements. A limitation of both types of transducers is that they can only provide side-view image of vessels. This paper presents the design and fabrication of miniaturized high-frequency kerfless and kerfed phased array transducers using high performance piezoelectric materials. Since both

transducers allow sweeping an ultrasound beam to form sector imaging plane in front of the transducer with dynamic focusing depth, they are good candidates for developing forward-looking IVUS catheters.

Statement of Contribution/Methods

Prototypes of kerfless phased arrays have been fabricated. Finite element analysis by PZFlex and sound field simulation by Field II modeling were carried out to validate the array designs. The phased array transducers were fabricated using micromachining technique. Specifically, a 40 μm thick PMN-PT single crystal material was used to fabricate the kerfless phased array transducer. It consists of 32 elements with an element width of 25 μm, a kerf width of 8 μm, and the element length of 1 mm. The kerfed array transducer was also designed to use a 55 μm thick PZT ceramic 2-2 composite to have 32 elements with an element width of 19 μm, a kerf width of 6 μm, and the element length of 1 mm. The total aperture size of both arrays is less than 1 mm^2, which proves the proper dimension to fit in the catheter. Finished acoustic stacks were coated with Parylene C film, which serves as a matching layer as well as a protection layer. The major performance of the array transducers has been characterized. Wire phantom was also imaged to determine axial and lateral resolutions of the array transducers with a high-frequency ultrasonic phased array testing platform.

Results/Discussion

The measured results show that the kerfless array transducer had a center frequency of 40 MHz, a bandwidth of 34%, and an insertion loss of 20 dB. The finite element analysis for the kerfed array with a thicker transducer element exhibited a center frequency of 27 MHz, a bandwidth of 40%, and an insertion loss of 25 dB, which will be verified by ongoing prototype fabrication. These miniaturized array transducers exhibit very high sensitivity and suggest that the potential for IVUS application is promising.

IUS5-D-3

Performance of a Miniaturized 64-Element High-Frequency Phased Array based on PMN-PT

Andre Bezanson[1], Robert Adamson[1], Jeremy Brown[1]; *[1]Biomedical Engineering, Dalhousie University, Halifax, Nova Scotia, Canada*

Background, Motivation and Objective

Currently, most fully sampled high frequency (>30 MHz) array transducers are limited to linear/annular arrays where the overall packaging of the transducers remains relatively large. This limits these arrays to topical applications where images must be generated from outside the body. We have previously fabricated a 64-element 42-MHz phased array transducer with 1λ element pitch, which is better suited to internal imaging applications. Using a novel wire bonding technique, we miniaturized the total packaging to a 2.7 mm^2 endoscopic form factor By using an existing grating lobe suppression technique, the beam steers to ±35° without grating lobe artifacts. In this work, we report the full performance characterization of this high-frequency phased array endoscope by generating 3D radiation patterns and beam profiles, images of wire/tissue phantoms, and ex-vivo tissue images.

Statement of Contribution/Methods

The electrical impedance was measured for each element across the array using a precision impedance analyzer and the pulse echo response of each element was measured using a high-frequency pulser-receiver unit. A Visualsonics Vevo 2100 high-frequency linear array ultrasound imaging system was reprogrammed to allow for phased array beamforming with our array specifications. The Visualsonics linear array transducer was replaced with our 64-element phased array endoscope and code was run to steer a focused beam between ±35°. One-way focused radiation patterns were collected using a needle mounted hydrophone at different angles and for B-mode imaging, the individual RF scan lines were exported and offline images were reconstructed.

Results/Discussion

The average electrical impedance magnitude was measured to be 65Ω on resonance with low variance in impedance between elements. Two-way pulse echoes were collected from all 64 elements showing high uniformity. The focused elevation and azimuth beam profiles were found to be in good agreement with the modeled predictions. B-mode images were generated of 25 μm Aluminum wire phantoms spaced by 1 mm steps in a water bath as well as in a tissue phantom (Figure 1) with 60 dB DNR. As our intended application for this miniaturized endoscope is to image the inner ear cochlea, ex-vivo images were generated of cadaveric temporal bones where the intra-cochlear membranes could be clearly seen.

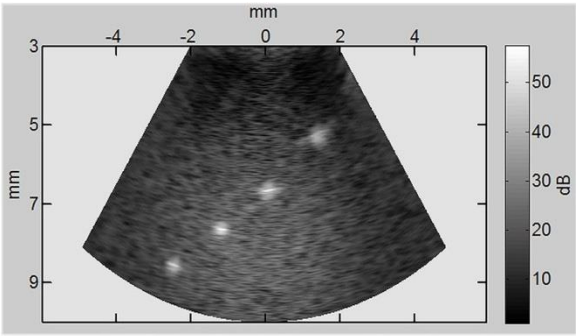

Figure 1: 60 dB DNR Tissue Phantom Image

IUS5-D-4

Small Aperture, Dual Frequency Ultrasound Transducers for Intravascular Contrast Imaging

Jianguo Ma[1], Karl Martin[2], Paul Dayton[2], Xiaoning Jiang[1]; *[1]Department of Mechanical and Aerospace Engineering, North Carolina State University, Raleigh, NC, USA, [2]Joint Department of Biomedical Engineering, University of North Carolina/North Carolina State University, Chapel Hill, NC, USA*

Background, Motivation and Objective

Recent research on vasa vasorum imaging, molecular imaging of thrombus and inflammation, and enhancement of complex clinical situations such as vascular dissections suggests that intravascular contrast imaging may hold great potential in disease assessment. However, nonlinear detection strategies for microbubble contrast agents are most effective near the resonant frequency of microbubble contrast agents, which is typically between 1-10 MHz, much lower than the high frequencies (> 20 MHz) used for intravascular ultrasound (IVUS). A high-frequency imaging strategy utilizing the ultra-broadband response of contrast agents suggests capabilities for very high signal to noise, high resolution imaging at frequencies above 20 MHz. This method has been previously demonstrated with transducers with large apertures, but has not yet been implemented with small aperture high frequency imaging for IVUS. In this project, a new dual-frequency, small aperture ultrasound transducer was designed, fabricated and tested for contrast IVUS applications.

Statement of Contribution/Methods

A 35 MHz receiving transducer with an aperture of 0.6 mm x 0.6 mm was integrated into a 6.5 MHz transmitting transducer with an aperture of 0.6 mm x 3 mm (Figure a & b). The dual-element transducer was fabricated from PMN-PT single crystal and mounted on a 20 gauge needle tip as a model catheter. Testing included field mapping with a hydrophone and pulse excitation on microbubbles flowing through an acoustically transparent micro-tube.

Results/Discussion

The prototyped small aperture, dual frequency transducer showed the ability of transmitting acoustic pressure up to -1.87 MPa and +2.14 MPa at 6.5 MHz, driven by 5-cycle 250 Vpp waveform, which was more than sufficient to induce non-linear oscillation of microbubbles. The 35 MHz receiver showed reasonable -6 dB bandwidth (52.1%) in pulse echo test and loop sensitivity (-38.3 dB) with burst excitation. Data illustrated that detection of broadband energy between 33 and 40 MHz from the contrast agents was readily detectable with the 35 MHz transducer (Figure c). Preliminary results of the transducer showed the capability of transmitting at 6.5 MHz and receiving at 35 MHz for high resolution ultrasound contrast imaging, demonstrating the first example of a prototype transducer for dual-frequency broadband ultrasound imaging for contrast enhanced IVUS.

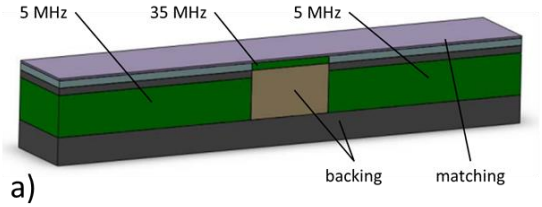

a)

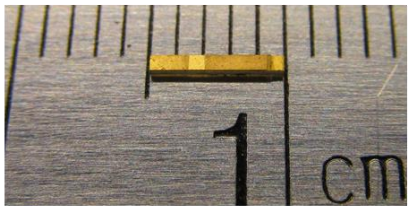

b)

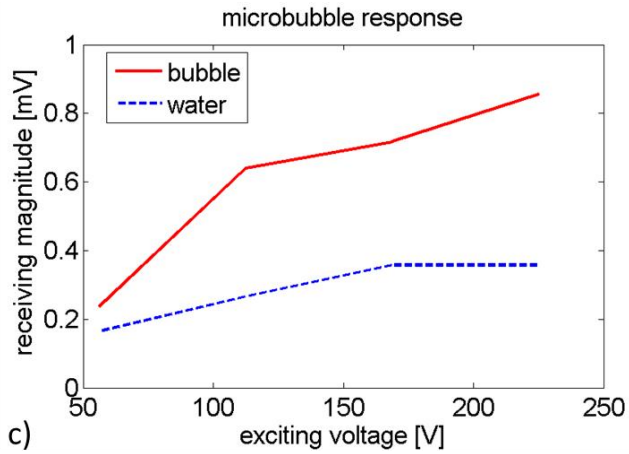

c)

IUS5-D-5

Acoustic Radiation Force Impulse Imaging (ARFI) on an IVUS Circular Array

Vivek Patel[1], **Jeremy Dahl[1]**, David Bradway[1], Joshua Doherty[1], Stephen Smith[1]; [1]*Biomedical Engineering, Duke University, USA*

Background, Motivation and Objective

Our long-term goal is the detection and characterization of vulnerable plaque in the coronary arteries of the heart using IVUS catheters. Vulnerable plaque, characterized by a thin fibrous cap and a soft, lipid-rich, necrotic core is a pre-cursor to heart attack and stroke. Early detection of such plaques may potentially alter the course of treatment of the patient in order to prevent ischemic events. We have previously described the characterization of carotid plaques using linear arrays operating at 9 MHz. In addition, we previously modified circular array IVUS catheters by short circuiting several neighboring elements to produce fixed beam-widths for intra-vascular hyperthermia applications.

Statement of Contribution/Methods

We have modified Volcano Visions 8.2 French, 9 MHz catheters and Volcano Gold 3 French, 20 MHz catheters by short circuiting portions of the array for ARFI applications. The catheters had an effective transmit aperture size of 1.5mm. The catheters were connected to a Verasonics scanner and driven with pushing pulses of 180 Vp-p to acquire ARFI data from a soft gel phantom with a Young's modulus of 2.9 kPa.

Results/Discussion

Figure 1 demonstrates successful ARFI displacement and recovery data from the 9 MHz IVUS catheter. The dynamic response of the tissue-mimicking material demonstrate a typical ARFI response as the gel phantom displaces away and recovers back to its normal position. The excitation response of the tissue-mimicking material showed a peak displacement of 2.3 microns at approximately 4 mm depth. The hardware modifications applied to our IVUS catheters mimick potential beamforming modifications that could be implemented on IVUS scanners. Our results demonstrate that the generation of radiation force from IVUS catheters and the development of intra-vascular ARFI may be feasible.

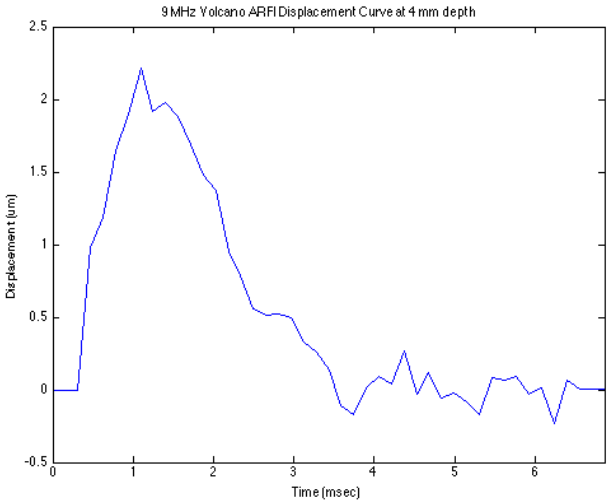

Real-time Co-registered IVUS-OCT Catheter for Atherosclerotic Plaque Identification and Stent Deployment Verification

Teng Ma[1], Jiawen Li[2], Dilbahar Mohar[3], Joseph Jing[2], Matthew Brenner[4], Pranav M. Patel[3], K. Kirk Shung[1], Zhongping Chen[2], Qifa Zhou[1]; *[1]NIH Ultrasonic Transducer Resource Center and Department of Biomedical Engineering, University of Southern California, Los Angeles, California, USA, [2]Beckman Laser Institute & Medical Clinic and Department of Biomedical Engineering, University of California - Irvine, Irvine, California, USA, [3]Division of Cardiology, UC Irvine Medical Center, Irvine, California, USA, [4]Division of Pulmonary and Critical Care, UC Irvine Medical Center, Irvine, California, USA*

Background, Motivation and Objective

Coronary artery disease remains the leading cause of death and disability in the U.S. Intravascular ultrasound (IVUS) is one of the standard medical tests routinely performed to diagnose atherosclerosis by visualizing the structure of affected vessels, identifying the composition of plaques, and providing stent deployment information after angioplasty. Optical coherence tomography (OCT) possesses higher resolution to image vulnerable plaque near the lumen boundary, but with shallow penetration depth. Thus, an integrated IVUS-OCT catheter would potentially capitalize the advantage of sufficient imaging depth of IVUS with the high resolution of OCT while offering improved diagnostic information. Different IVUS-OCT catheter designs have been reported previously by using co-axial, co-planner or sequential configuration, which suffers from either the size of catheter or sub-optimal image co-registration. We report the optimized design of a miniature IVUS-OCT catheter featured by a back-to-back arrangement of a transducer and an OCT probe to enable real-time co-registration of two modalities within one frame.

Statement of Contribution/Methods

The 3D design of the 0.8mm-diameter IVUS-OCT catheter is shown in Fig.1 (a). The OCT fiber connects a 0.35 mm-diameter GRIN lens followed by a micro-prism. The PMN-PT transducer (40MHz, 50% BW) has a rectangular surface of 0.16mm2 and a thickness of 0.3mm. The featured opposite configuration of OCT probe and transducer ensures two modalities co-registered within one frame by simply rotating either of image 180º. The atherosclerotic plaque models are imaged ex vivo to study plaque type identification, and the imaging of stent embed vessels is performed to demonstrate the feasibility of stent deployment verification.

Results/Discussion

The H&E stained histology of rabbit aorta with intima partially thickened is shown in Fig1. (b). Corresponding IVUS image Fig1. (c) is able to provide the full structural image of the vessel with intima and media layer. The irregular lumen surface of the thickened intima indicated by the red arrows is clearly displayed in OCT Fig1. (d) but not with IVUS due to the inferior resolution and near field imaging capability. The sharp surface with strong signal on the surface and high attenuation inside thickened intima demonstrates the characteristic of lipid rich plaque confirmed by histology.

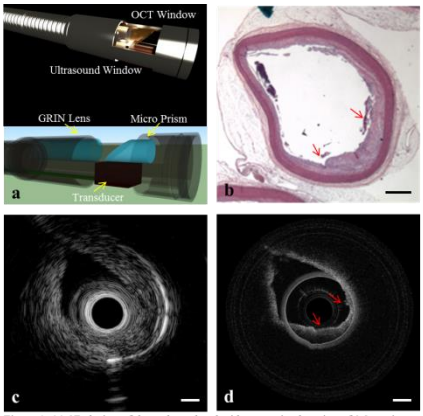

Figure 1. (a) 3D design of the catheter head with protective housing of 0.8mm in diameter. The OCT probe and transducer are arranged in back-to-back configuration to co-register image within one frame. (b) Hematoxylin-Eosin stained histology image of rabbit aorta with intima partially thickened (c) Corresponding IVUS image displays the full structural image of the vessel with measureable vessel thickness information. (d) OCT image shows the strong signal on the irregular lumen surface of the thickened intima indicated by the red arrows in (b). Scale bar: 1mm.

Carotid elastography

CONGRESS HALL

Tuesday, July 23 2013, 02:00 pm - 03:30 pm

Congress Hallair: **Chris de Korte**
Catholic Univ. of Nijmegen

IUS1-E1-1

4D Strain Imaging of Carotid Arteries Using Echo-CT

Renate Boekhoven[1], Marcel Rutten[1], Marc Van Sambeek[2], Frans Van De Vosse[1], Richard Lopata[1]; [1]*University of Technology Eindhoven, Eindhoven, Netherlands,* [2]*Catharina Hospital Eindhoven, Eindhoven, Netherlands*

Background, Motivation and Objective

For the detection and improved diagnosis of vulnerable plaques, fully 3D geometrical, morphological and mechanical characterization of the plaque is essential. 4D (strain) imaging is necessary for this, but the required temporal and spatial resolutions are not available in in vivo imaging methods. In this study, 4D strain imaging is demonstrated in carotid arteries in vitro using an echo-CT approach, i.e., reconstructing the 4D geometry using 2D (+t) images at 36 angles (Boekhoven et al. 2013).

Statement of Contribution/Methods

Four types of vessel segments were subjected to a pulsatile pressure; a straight and eccentric polyvinyl alcohol phantom, a healthy porcine carotid, and a human atherosclerotic carotid . 4D US data were obtained by echo-CT. RF-data were acquired with a MyLab70 scanner (Esaote, NL). Local deformations were estimated using a 2D coarse-to-fine strain algorithm (Lopata et al. 2009). For the concentric phantom and porcine carotid, the SNRe was calculated as a function of the radius r for all angles and over the vessel length, assuming the radial strains to have the same value at equal distances r. Next, the estimated strains were fitted using linear elasticity. A thick-walled (straight phantom) and thin-walled tube (porcine carotid) were used to estimate the Young's modulus (E), assuming plane strain, and incompressibility.

Results/Discussion

Longitudinal cross-sections were reconstructed to a time series of 3D geometries and strains. The now available transverse strain images are shown in Fig. 1A, as well as the 3D strain images (Fig. 1B). Radial strains were normally distributed. Near the lumen, average strains were 15% (phantom) and 12% (porcine) and decayed to 3% near the outer wall. The corresponding SNRe values at end systole were 35 dB ± 8 dB and 25 ± 10 dB, decaying to respectively 17 dB and 10 dB. An estimated E = 40 kPa was found for the phantom and E = 270 kPa for the porcine carotid, both in good agreement with literature (Ribbers et al. 2007; Vychytil et al. 2010). 3D strain imaging in the eccentric phantom and human sample are demonstrated in Fig. 1B.

To our knowledge, this is the first demonstration of 4D echo-CT strain imaging in carotid arteries and phantoms. Strain distributions in the plaque are very complex and cannot be translated into material properties directly. To this end, an inverse finite element modeling approach will be developed.

Figure 1

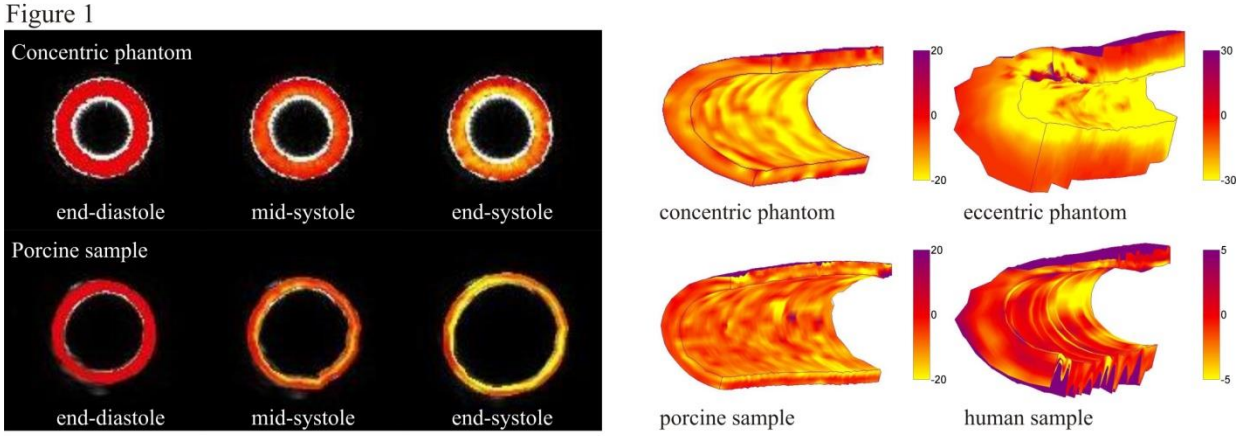

A. B.

IUS1-E1-2

Noninvasive compound carotid elastography: in vivo validation

Hendrik Hansen[1], Gert Jan de Borst[2], Michiel Bots[3], Gerard Pasterkamp[4], Chris de Korte[1]; [1]*Medical UltraSound Imaging Centre, Department of Radiology, Radboud University Nijmegen Medical Centre, Netherlands,* [2]*Department of Vascular Surgery, University Medical Center Utrecht, Netherlands,* [3]*Julius Center of Health Sciences and Primary Care, University Medical Center Utrecht, Netherlands,* [4]*Department of Experimental Cardiology, University Medical Center Utrecht, Netherlands*

Background, Motivation and Objective

Carotid stenosis with plaque rupture is one of the main underlying causes of stroke. Lipid-rich and inflammatory plaques with a thin fibrous cap (vulnerable plaques) have a higher risk at rupture than fibrous plaques (stable plaques). Previously we developed a noninvasive compound elastography method to estimate radial strains in transversal vascular cross sections. The goal of this study is to validate the method in patients and to determine the sensitivity and positive predictive value (PPV) for the detection of histological plaque vulnerability features.

Statement of Contribution/Methods

A Medison Accuvix V10 ultrasound system equipped with an L5-13 linear array transducer was used to acquire ultrasound radiofrequency (RF) data of transversal cross sections of 18 severely stenotic carotid arteries of patients before carotid endarterectomy (CEA; surgical excision of the plaque and inner vessel wall). RF data were acquired at three

different insonification angles (0°, +20 and -20 degrees) at the site of largest stenosis (culprit lesion). Radial strains were estimated from the angular RF data using an iterative cross-correlation based search algorithm followed by compounding. The percentage of plaque area with strains above 1.5% was determined. After CEA, transversal segments of the excised plaque were cut at the culprit lesion site and histologically stained. Based on the staining, the presence of plaque vulnerability features was determined: a thin fibrous cap, a high concentration of lipids, a high concentration of macrophages, and a lack of smooth muscle cells. The sensitivity and PPV of the strain area parameter for the detection of these features were determined.

Results/Discussion

The developed compound elastography method revealed a positive correlation between strain and each of the investigated histology based parameters of vulnerability. The highest sensitivities and PPVs were reached for the detection of thin fibrous caps and superficial macrophages: 80% and 80%, and 100% and 100%, respectively. Furthermore, within individual strain images increased strains were identified at spots that corresponded to regions considered as vulnerable in histology. These results demonstrate the potential of the developed compound elastography method for noninvasive in vivo vulnerable plaque detection.

IUS1-E1-3

Carotid wall elastograhy is superior to intima-media thickness measurements to assess mid-term vascular dysfunction secondary to intrauterine growth restriction (IUGR)

Roch Maurice[1,2], Laurence Vaujois[1], Najat Chibab[1], Anika Maurice[1], Nagib Dahdah[1], Anne-Monique Nuyt[1], Jean-Luc Bigras[1]; *[1]Pediatric Cardiology, Centre de Recherche, Centre Hospitalier Universitaire Sainte-Justine (CRCHUSJ), Montreal, Quebec, Canada, [2]Université de Lyon, CREATIS, Villeurbanne, France*

Background, Motivation and Objective

Background- Several studies have suggested that Intra Uterine Growth Restriction (IUGR) increases the risk of cardiovascular disease and early atherosclerosis. Early detection of arteriopathy is essential for implementing early intervention. Although arterial intima-media thickness (IMT) is known as an index of subclinical atherosclerosis in the adult, its validity in the pediatric age may be limited. We have lately introduced a novel imaging-based biomarker (ImBioMark) to assess intrinsic mechanical features of the arterial wall from B-mode ultrasound data.

Aim- In this work, we evaluated the potential of ImBioMark to investigate, during adolescence, cardiovascular health status of patients born with IUGR. We also compared ImBioMark with automated IMT measurements of the common carotid artery (CCA).

Statement of Contribution/Methods

Methods- The potential sequalae of IUGR on the CCA were examined in a group of adolescents in comparison with healthy controls. IUGR subjects (n = 7) were 13.85 ± 0.46 years old, while the healthy controls (n = 7) were 14.58 ± 0.80 (p = 0.058). Cine-loops of the CCA B-mode data were digitally recorded, and the arterial elastic modulus estimated a posteriori with ImBioMark. IMT of the CCA was automatically calculated using the Philips QLAB software (Philips, Andover, Massachusetts). All the subjects had been formerly evaluated in utero in our fetal echocardiographic laboratory.

Results/Discussion

Results- ImBioMark detected a significant increase of CCA stiffness in IUGR compared to healthy controls, with an elastic modulus of 90.74 ± 11.86 kPa versus 61.30 ± 15.94 kPa, respectively (p = 0.002). There was however no significant difference between IUGR and control subjects in IMT measurement (0.483 ± 0.067 mm versus 0.476 ± 0.051 mm, respectively; p = 0.831).

Conclusion- The impact of IUGR on the CCA vascular wall dynamics was confirmed by ImBioMark. The apparent limitation of IMT measurement in this cohort may be due to the geometrical arterial changes, i.e. the expected thickening, below the detection level at this age. Since early detection of vascular modulation is essential for implementing early intervention in a population at risk, we now intend to extend ImBioMark to investigate larger pathologic cohorts with various degrees of arteriopathy.

IUS1-E1-4

A Feasibility Study of Ultrasound B-Mode and Strain Imaging for Risk Assessment of Carotid Atherosclerotic Plaques Validated by Magnetic Resonance Imaging

Xiaochang Pan[1], Lingyun Huang[2], Shengzhen Tao[1], Manwei Huang[3], Xihai Zhao[1], Le He[1], Chun Yuan[1,4], **Jianwen Luo**[1], Jing Bai[1]; *[1]Tsinghua University, Beijing, China, People's Republic of, [2]Philips Research China, China, People's Republic of, [3]Meitan General Hospital, China, People's Republic of, [4]University of Washington, Seattle, WA, USA*

Background, Motivation and Objective

Conventional B-mode ultrasound images and Doppler/color flow measurements are mostly used to evaluate degree of carotid atherosclerotic stenosis. Alternatively, the correspondence between multi-contrast magnetic resonance (MR) imaging features, plaque composition and histology has been well established (Cai et al, Circulation 2002;Ota et al, Radiology 2010). We proposed to use B-mode echogenecity plus ultrasound strain imaging to quantitatively measure grayscale and mechanical properties of carotid atherosclerotic plaques, and correlate them to multi-contrast MR imaging features known to be associated with high risk plaque histo-pathology.

Statement of Contribution/Methods

Sequences of ultrasound RF data of Philips iU22 system were acquired from 5 human subjects older than 65 years old having carotid plaques with more than 30% stenosis. The inter-frame strain of plaques was estimated to indicate relative stiffness and rupture risk of plaques, using a coarse to fine 2D speckle tracking algorithm based on correlation filtering. The same patients received double blinded MR scans on Philips Achieva 3T TX MR system using multi-contrast protocol. 3D MR images were reconstructed and then slices at the same positions of ultrasound incident angles were registered. Carotid plaques tissue composition was characterized using MR images, while echogenecity and strain (magnitude) in the corresponding ultrasound images were investigated and compared to MR results.

Results/Discussion

11 plaques from these 5 human subjects were analyzed. Plaques with intra-plaque hemorrhage (IPH) or lipid-rich necrotic core (LRNC) are defined as high risk factors while calcification is a stable factor. In ultrasound results, the calcification area of plaques showed high echogenecity and low deformation less than 0.4%, the IPH showed intermediate echogenecity and deformation around 1.5% (Fig. 1), and the LRNC showed the lowest echogenecity and large deformation more than 2%. The locations of ultrasound results are in good agreement with findings on MR results (Fig. 1). Ultrasound quantitative measurements of grayscale and mechanical properties were performed on a small number of human subjects. These preliminary results suggest that it may be feasible to evaluate plaque vulnerability using echogenecity combined with strain values estimated from ultrasound RF data.

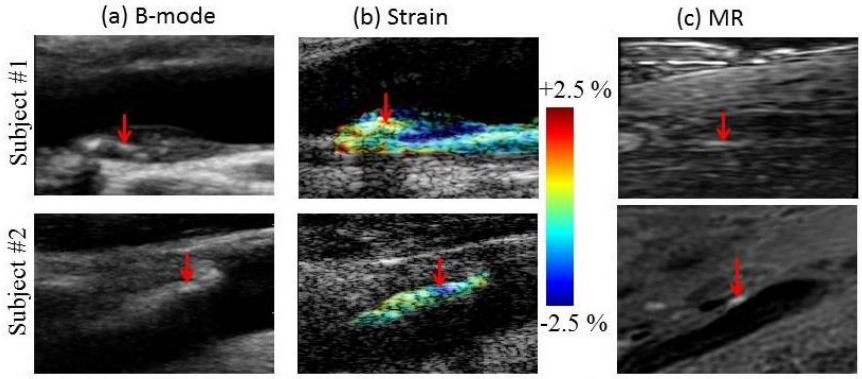

Fig 1. (a) B-mode images, (b) strain images overlaid onto the B-mode images, and (c) MP-RAGE MR image of plaques from 2 human subjects. Arrows indicate IPH. The correspondence between MR and ultrasound images of IPH has not been presented in other literature before. The images of other composition are not displayed due to limited size but will be shown in future presentations.

IUS1-E1-5

Noninvasive arterial pulse pressure mapping using Pulse Wave Ultrasound Manometry (PWUM) in hypertensive aortas and stenotic carotid arteries in vivo

Ronny Li[1], Isaac Jourard[2], Joyce Salomon[2], Prathyush Narayanan[2], Lancelot Walker[3], Cesare Russo[3], Marco Di Tullio[3], Elisa Konofagou[3]; *[1]Biomedical Engineering, Columbia University, New York, NY, USA, [2]Biomedical Engineering, Columbia University, USA, [3]Columbia University, USA*

Background, Motivation and Objective

Elevated arterial pulse pressure (PP), especially in the central arteries, carries high clinical significance as an important risk factor for heart disease. This study compares three noninvasive methods for evaluating PP in hypertensive and stenotic arteries in vivo – brachial sphygmomanometry, applanation tonometry, and Pulse Wave Ultrasound Manometry (PWUM), the latter developed by our group to map the PP waveform across an imaged arterial segment over a single cardiac cycle.

Statement of Contribution/Methods

Using a clinically-validated blood pressure monitor (Omron HEM 705CP), the brachial PP was measured in eleven (N = 11) subjects with systolic hypertension, five (N = 5) subjects with carotid stenosis, and ten (N = 10) normal subjects. RF signals were acquired from the abdominal aortas of the hypertensive subjects and the common carotid arteries of the stenotic subjects using a SonixTouch system (Ultrasonix Medical, Burnaby, Canada) with a 3.3 MHz curvilinear and 10 MHz linear transducer, respectively. A fast, normalized 1D cross correlation-based motion estimation method with a 3.5-mm window size and 95% overlap was used on the RF signals to compute the pulse wave-induced arterial wall displacements. The spatio-temporal variation of the displacements was used to measure the regional pulse wave velocity and incremental distension waveform. The PP waveform at each beam location was derived based on the Laplace Law and the Moens-Korteweg equation, thus 2D mapping the arterial PP in the imaging plane over time. The aortic PP waveform in five (N = 5) of the hypertensive subjects was also recorded using a commercial applanation tonometry system (Sphygmocor CPV, Atcor Medical, USA). The effects of stenosis on the PP waveform obtained using PWUM in stenotic patients was qualitatively evaluated.

Results/Discussion

Figure 1 shows the aortic vs. brachial PP in all hypertensives and normals. For both PWUM and applanation tonometry, there was an overall linear relationship between aortic PP and relatively low (< 80 mmHg) brachial PPs. In all stenotic cases, the PP waveform in the stenosis exhibited greater amplitude and/or deviation in morphology compared to non-stenotic regions, indicating that PWUM may assist in the characterization and detection of stenosis. The feasibility of PWUM and its capability to map pressure differences in pathological arteries was hereby shown.

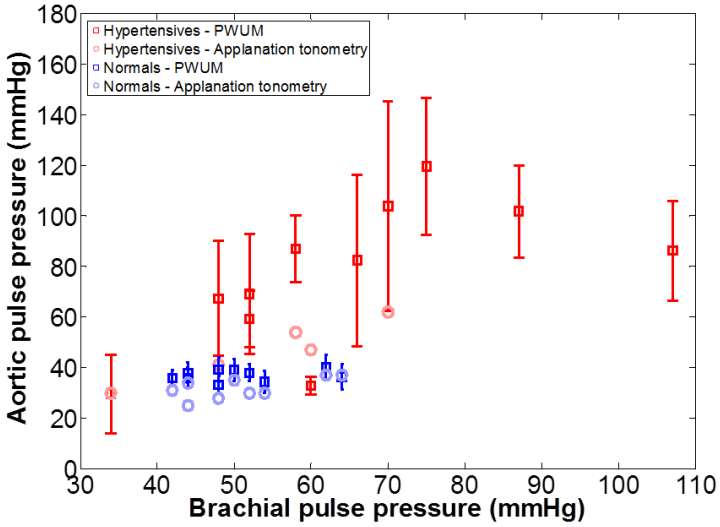

Assessment of longitudinal strain in the Carotid artery wall using ultrasound-based Speckle tracking-validation in a sheep model

Matilda Larsson[1], Peter Verbrugghe[2], Marija Smoljkic[3], Brecht Heyde[4], Nele Famaey[3], Paul Herijgers[2], Jan D'hooge[4]; *[1]Department of Medical Engineering, Royal Institute of Technology - KTH, Sweden, [2]Department of Cardiovascular Sciences, Cardiac Surgery, KU Leuven, Leuven, Belgium, [3]Biomechanics Section, Faculty of Engineering, KU Leuven, Leuven, Belgium, [4]Department of Cardiovascular Sciences, Cardiovascular Imaging and Dynamics, KU Leuven, Leuven, Belgium*

Background, Motivation and Objective

Assessment of strain in the longitudinal direction of the arterial wall has been suggested to improve the evaluation of arterial stiffness and atherosclerosis. However, until recently the longitudinal motion of the artery has been neglected and difficult to assess due to low amplitudes combined with low spatial resolution. Recently, we showed the feasibility of ultrasound-based speckle tracking to assess carotid longitudinal strain in-silico and in-vitro, but validation in the more challenging in-vivo setting is still lacking. Thus, the aim of this study was to validate longitudinal strain assessment in the common carotid artery (CCA) in an animal setup.

Statement of Contribution/Methods

The left CCAs of three sheep were exposed during isofluran anesthesia and two sonomicrometry crystals were sutured onto the artery wall with a longitudinal distance of 5-7mm to obtain reference values of longitudinal strain. The wound was closed and filled with ultrasound gel followed by ultrasound imaging (long-axis images, 45Hz) using a Vivid7 system (GE Healthcare, 12L) at baseline and stress (phenylephrine 0.5mg/ml). Speckle tracking was performed on the envelope-detected data using an in-house algorithm (kernel size: 5λ • ×2λ; normalized cross-correlation; spline-interpolation for subsample motion estimation; 40% window overlap). Longitudinal strain was estimated throughout three cardiac cycles in a region of interest (6mm • ×1mm) positioned in the posterior artery wall. The strain curves were then low-pass filtered by convolution with a normalized rectangular function of 6 samples in length.

Results/Discussion

The estimated strain curves cyclically varied through the cardiac cycle, showing a lengthening of the arterial segment in systole. Good agreement between estimated and reference strain was obtained as illustrated in Fig. 1 and a significant correlation between peak systolic estimated and reference strain was found ($r=0.85$, $p < 0.001$, $N=18$).

The results indicate the feasibility of longitudinal strain assessment in the arterial wall in-vivo using ultrasound-based speckle tracking. However, the surgical exposure may have affected the artery wall properties since lower strain values than previously observed in-vivo were obtained. Moreover, an extension of the study is needed to further establish the feasibility of the method in-vivo.

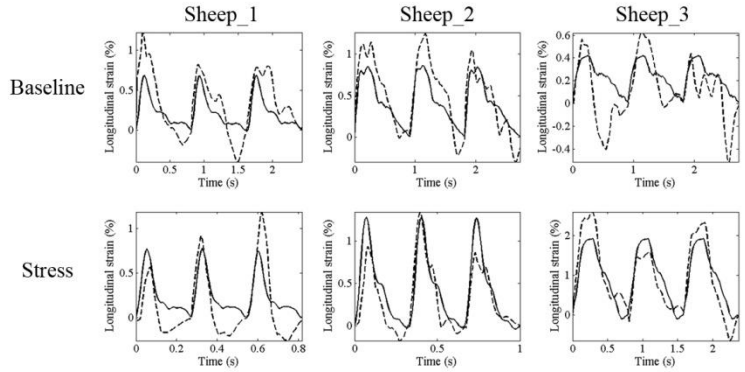

Figure 1 Longitudinal strain curves from the left carotid artery in a sheep model estimated by speckle tracking and SONO at baseline (upper plots) and stress (lower plots). SONO; sonomicrometry.

Beamforming I

M4

Tuesday, July 23 2013, 02:00 pm - 03:30 pm

Congress Hallair: **Pai-Chi Li**
National Taiwan University

IUS1-E2-1

Compensation of the Combined Effects of Absorption and Dispersion in Plane Wave Pulse-Echo Ultrasound Imaging Using Sparse Recovery

Martin Schiffner[1], Georg Schmitz[1]; [1]*Chair of Medical Engineering, Bochum, NRW, Germany*

Background, Motivation and Objective

Conventional strategies for fast image acquisition, e.g. coherent plane wave (PW) compounding or synthetic aperture focusing (SA), are based on physical models that emphasize a lossless medium. However, absorption is a major effect in biological tissues and exhibits a power law dependence on frequency. This dependence is accompanied by a frequency-dependent phase velocity of the ultrasound waves that strongly distorts the shape of broadband pulses (dispersion, cf. (a)).

In this study, we extended our concept for PW pulse-echo ultrasound imaging (UI) based on sparse recovery (SR) [1] to compensate for the combined effects of absorption and dispersion. Our goal was to significantly improve the image quality in fast image acquisition.

Statement of Contribution/Methods

We formulated a linear inverse scattering problem (ISP) to recover spatial fluctuations in compressibility in a specified field of view from measurements of the scattered sound. The governing wave equation contains convolutional loss operators to account for absorption and dispersion based on a time causal model. For excitation, multiple steered broadband PWs were emitted. We adopted a sparse recovery strategy to regularize the ill-posed ISP, i.e. we assumed that there exists a sparse representation of the fluctuations in compressibility in a known basis. We investigated various wavelet bases and block transforms.

For experimental validation, we acquired pulse-echo measurement data from a commercial tissue phantom (A) and a human thyroid (B, *in vivo*). Recovered images were compared to those generated by SA (128 wave emissions), delay-and-sum (DAS; 11 PW emissions), and minimum variance (MV, 11 PW emissions) algorithms.

Results/Discussion

Using only two steered PW emissions and a Daubechies-20 wavelet basis for sparse representation, our concept outperformed SA, DAS, and MV in terms of lateral -6 dB-widths and image contrast (cf. (b) to (f)).

Our SR-based concept in combination with a realistic physical model for wave propagation significantly improved the image quality in comparison to conventional strategies for fast image acquisition. It could thus be beneficial in applications that crucially depend on short acquisition times, e.g. cardiac UI and flow UI.

[1] M.F. Schiffner and G. Schmitz, "Fast Image Acquisition in Pulse-Echo Ultrasound Imaging Using Compressed Sensing", Proc. IEEE IUS, 2012

Financial support by Ziel2.NRW 2007-2013 co-financed by ERDF, grant no. 005-0908-0117.

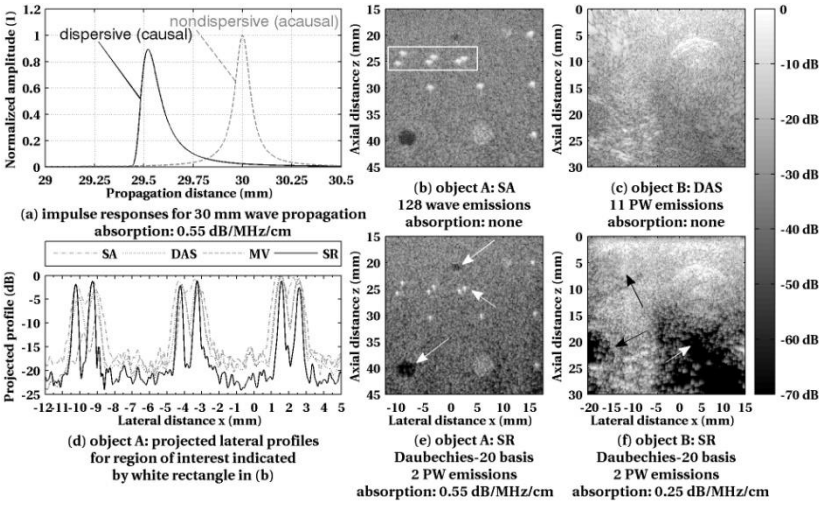

IUS1-E2-2

The Separate Recovery of Spatial Fluctuations in Compressibility and Mass Density in Plane Wave Pulse-Echo Ultrasound Imaging

Martin Schiffner[1], Georg Schmitz[1]; [1]*Chair of Medical Engineering, Ruhr-Universität Bochum, Bochum, NRW, Germany*

Background, Motivation and Objective

The lossless propagation of ultrasound waves in biological tissues is governed by the two mechanical parameters compressibility and mass density. With respect to the scattered sound field in ultrasound imaging (UI), spatial fluctuations in compressibility act as isotropic monopole radiators while spatial fluctuations in mass density act as anisotropic dipole radiators (cf. (a) and (e)). Conventional strategies for beamforming in pulse-echo UI, e.g. delay-and-sum, minimum variance, and synthetic aperture focusing, exclusively account for monopole scattering. This neglect of the inhomogeneous mass density can cause image artifacts.

In this study, we demonstrate that the spatial fluctuations in compressibility and mass density can be recovered separately. Our goals are to obtain space-resolved maps of the two mechanical parameters and to reduce image artifacts.

Statement of Contribution/Methods

We formulated a linear inverse scattering problem (ISP) to recover fluctuations in compressibility and mass density in a specified field of view from measurements of the scattered sound. To distinguish both material parameters by their radiation patterns, we emitted two broadband plane sound waves with different steering angles. The ill-posed ISP was regularized by a substantially modified version of our sparse recovery strategy [1].

We validated our concept using pulse-echo measurement data obtained from simulations and from a human common carotid artery (*in vivo*). The recovered maps were compared to those recovered by neglecting the inhomogeneous mass density.

Results/Discussion

Using simulated data, our concept perfectly distinguished point-like fluctuations in compressibility from those in mass density (cf. (b) to (d)). In (b), the neglect of the inhomogeneous mass density caused image artifacts. For the *in vivo* data, the recovered maps emphasized different details (cf. (f) to (h)). The image quality in terms of resolution and contrast improved in (h). The conventional image (f) contains features of both (g) and (h).

The separate recovery of compressibility and mass density could be beneficial for the classification of biological tissues in plane wave pulse-echo UI, e.g. tumor detection.

[1] M.F. Schiffner and G. Schmitz, "Fast Image Acquisition in Pulse-Echo Ultrasound Imaging Using Compressed Sensing", Proc. IEEE IUS, 2012

Financial support by Ziel2.NRW 2007-2013 co-financed by ERDF, grant no. 005-0908-0117.

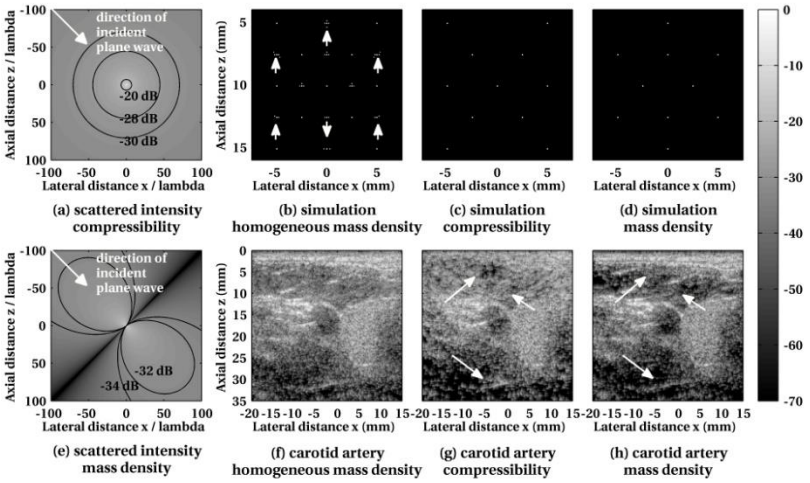

IUS1-E2-3

High Frame Rate Ultrasonic Imaging of the Heart by Placing Virtual Point Sources in Front of Array

Hideyuki Hasegawa[1,2], Yuji Sato[3], Hiroshi Kanai[1,2]; *[1]Graduate School of Biomedical Engineering, Tohoku University, Japan, [2]Graduate School of Engineering, Tohoku University, Japan, [3]Tohoku University, Japan*

Background, Motivation and Objective

We previously developed a method for high frame rate echocardiography [frame rate (FR) > 300 Hz] using a transmit beam, which was spherically diverging from a virtual point source behind the array [Hasegawa and Kanai, J Med Ultrason, 2011. Hasegawa and Kanai, IEEE Trans UFFC, 2012]. Although such diverging beam illuminates a wider area compared with a focused beam or plane wave, sound pressure starts to decrease just after emission. Another type of diverging beam, which is diverging from a focal point of a conventional focused beam, has already been proposed for synthetic aperture imaging [Yagi, et al., 2006 IEEE Ultrason Symp Proc, 2006]. This type of beam can increase sound pressure around the focal point, and it would be useful for applications which require higher sound pressure, such as blood flow imaging. In the present study, the feasibility of high FR echocardiography using conventional focused beams was examined.

Statement of Contribution/Methods

In the present study, multiple focused receiving beams were created using diverging beams in front of focal points of conventional focused transmit beams. Focal distances of 20 and 30 mm and numbers of transmissions N of 7 and 15 were examined. Smaller focal distance achieves a wider diverging angle and the number of transmissions can be reduced. As shown in Fig. (a), wave fronts were assumed to be spherical, and dynamic focusing was used in receive. Since multiple receiving beams were created for each transmission, overlapping receiving beams were averaged in beamformed RF domain.

Results/Discussion

The proposed method was evaluated using an ultrasound imaging phantom (model 54GS, CIRS). Figure (b) shows a B-mode image of the phantom obtained by conventional beamforming (focal distance of transmit beam: 70 mm, dynamic focusing in receive). FR was 39 Hz. Figures (c), (d), and (e) show B-mode images of the phantom obtained by the proposed method at transmit focal distances of 30 mm (N = 15, FR: 316 Hz), 20 mm (N = 15, FR: 316 Hz), and 20 mm (N = 7, FR: 677 Hz), respectively. Spatial resolutions (width at half maximum) of conventional beamforming and parallel beamforming at transmit focal distances of 30 mm (N = 15) and 20 mm (N = 7) were 1.39, 0.98, and 0.92 mm (at 44 mm depth), respectively. As shown in the figures, a B-mode image with a better spatial resolution could be obtained at a very high FR of 677 Hz.

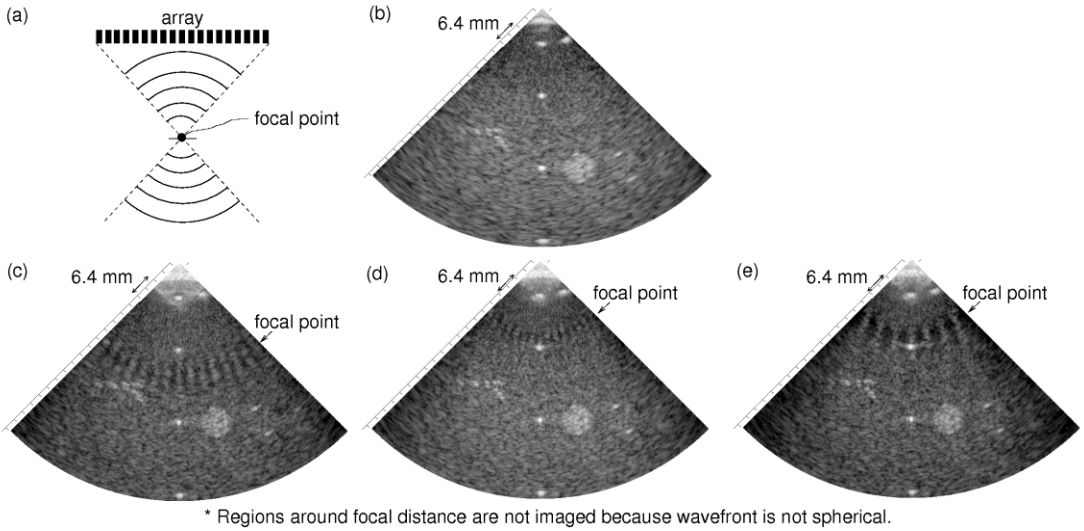

IUS1-E2-4

Real time 3D US-tagging combined with 3D phase-based motion estimation.

Sebastien Salles[1], Hervé Liebgott[1], Damien Garcia[2], Didier Vray[1]; *[1]Université de Lyon, CREATIS ; CNRS UMR5220 ; Inserm U1044 ; INSA-Lyon ; Université Lyon 1, France, [2]CRCHUM, University of Montreal, Departement of radiology, Canada*

Background, Motivation and Objective

By contrast with 2D imaging, quantitative analysis of 3D motion from ultrasound (US) images can provide improved information in several applications, such as arterial mechanical assessment, heart motion and blood flow. Unfortunately, it remains difficult to obtain a high definition of the motion estimate in the lateral and elevation directions (i.e. perpendicular to the beam axis).

To increase the definition in both these directions, a method known as transverse oscillations has been recently extended in 3D by the group of J.A. Jensen. This method enables one to obtain ultrasound fields featuring oscillations along the 3 spatial dimensions using a double 2D tactic. In this approach, two different apodization functions are used for generating elevation and lateral oscillations, respectively.

The aim of this study was to 1) create US-tagged images featuring 3D oscillations using a single apodization function, and 2) evaluate a 3D motion method based on the phases of such images.

Statement of Contribution/Methods

1) The apodization function was designed using the Fraunhoffer approximation. 3D images were generated by transmitting a plane wave and receiving with a specific beamformer defined by a dynamic focalization and the aforementioned apodization function. The link between the acoustic field and the 2D aperture function can be approximated as a Fourier transform. As a result, the 2D apodization function leading to 3D separable modulation must contain 4 distinct peaks.

2) 3D motion vectors were estimated using a phase-based motion estimator exploiting the phase information in the 3D Fourier space. A cubic volume of interest was chosen in the 3D images. The 3 single octants spectra (one for each direction) were used to derive three phase images which are combined to estimate the motion vector between consecutive images.

Results/Discussion

Our US-tagging method was implemented in real time on the Ula-Op research scanner, equipped with a 2D matrix array probe (Vermon, 24×8, element size=0.4×0.4mm, f0=3.9MHz) to obtain pyramidal volumes.

1) The proposed beamforming was validated by imaging an isolated single scatterer providing a 3D PSF showing the expected 3D oscillations (see Fig1.a).

2) Our estimator was then validated on phantom sequences with controlled 3D trajectories The relative axial, lateral and elevation estimate errors in %, were 5 ± 1, 6 ± 2, and 6 ± 3 (see Fig1.b).

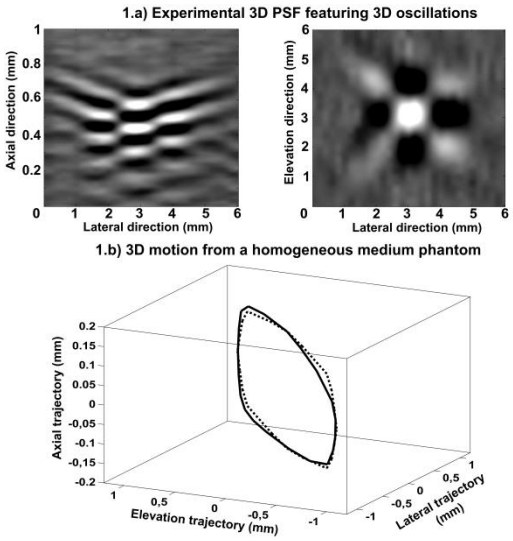

IUS1-E2-5

Towards Establishing a Design Rule for Aperture Parameters in Minimum-Variance Beamforming

Junying Chen[1], Hayden K.-H. So[1], Alfred C. H. Yu[2]; *[1]Dept. of Electrical and Electronic Engineering, The University of Hong Kong, Hong Kong, [2]Medical Engineering Program, The University of Hong Kong, Hong Kong*

Background, Motivation and Objective

In minimum-variance (MV) beamforming, an essential prerequisite for achieving decent performance is a proper choice of its aperture parameters so that the channel-domain correlation matrix needed for adaptive apodization weight derivation can be accurately computed. As a rule of thumb, for a given aperture size with M channels, a sub-aperture size L less than M/2 (i.e. L <= M/2) is known to yield robust (full-ranked) matrix computations, but this is merely a parameter constraint stemming from algebraic considerations. Here, using an inductive approach to analyze the impact of M and L on image quality, we seek to establish a performance-based design rule for how MV beamforming parameters should be defined.

Statement of Contribution/Methods

Raw channel-domain data (127 lines/frame, 1000 pixels/line) was first synthesized using Field II for a variety of imaging views with point targets (single vs. pair-wise; located at focus vs. away from focus) or cysts (diameters considered: 6, 8, 10 mm). Transducer specification corresponded to an Ultrasonix L14-5 array, and the pulsing parameters were: 5 MHz frequency; 2-cycle pulses; 25 mm transmit focus. For these imaging scenarios, MV beamforming (with and without Toeplitz approximation) was applied using a GPU-based real-time MV beamforming core that we developed earlier (as comparison, delay-and-sum (DAS) beamforming with Hanning apodization was also implemented). For different aperture sizes (M = 32, 64, or 128), the quality of beamformed images was analyzed for all possible sub-aperture sizes (L = 1 to M/2) to obtain insight into the impact of aperture parameters in MV beamforming. To facilitate quantitative assessment, lateral resolution (for point-target image views) and contrast (for cyst image views) were determined as indicators of image quality, and their respective gain resulting from the use of MV beamforming (with reference to DAS) was computed as an image quality metric. Results were also correlated against GPU computing time to analyze potential tradeoff between performance gain and computational load.

Results/Discussion

Different combinations of aperture size (M) and sub-aperture size (L) led to significant differences in the performance gain achieved with MV beamforming. For large M (e.g. 128), despite devoting more computing resources (>1s GPU frame time), the image quality gain was limited (for any L, at most 3% contrast increase for a 6 mm cyst located at 50 mm depth: i.e. away from focus), because DAS beamforming already gave decent performance with large apertures. For small L (e.g. less than M/4), although computationally less demanding (<0.1s GPU frame time for M = 32, 64, 128), the image quality gain was also subtle. We found that, to efficiently reap the benefits of MV beamforming, M needs not be overly large, while L should be close to M/4. This may emerge as an MV aperture design rule for achieving significant image quality gains that are commensurate with the devotion of computing resources.

IUS1-E2-6

S-Sequence Encoded Synthetic Aperture B-Scan Ultrasound Imaging

Roger Zemp[1]; *[1]University of Alberta, Edmonton, Alberta, Canada*

Background, Motivation and Objective

A traditional means of acquiring a full synthetic aperture dataset involves transmitting with one element of a linear array and receiving with all elements in parallel, then firing from a different element, receiving in parallel, and repeating until all desired elements have been excited. With this set of echo signals, synthetic aperture focusing can theoretically produce more uniform fo-cusing compared to fixed-focused transmit methods. A disadvantage of this method is poor SNR due to low total emitted energy per transmit event. Temporal coded excitation methods have been previously proposed as a means to partially remedy this. Hadamard aperture coding has also been proposed where elements are weighted with either 1 or -1. These echo data can be trans-formed back into an element-by-element dataset for synthetic aperture focusing, yet with im-proved SNR due to the fact that more than one element is being fired per transmit event. Unfortunately pulse-inversion asymmetry and other nonlinearities lead to non-ideal performance and imaging artifacts.

Statement of Contribution/Methods

Instead of weighting aperture elements with +1 or -1 values, we instead apply 0/1 binary weight-ings selected from S-sequences, which are rows or columns of Hadamard-derived S-matrices of size $N=2^n-1$. The S-matrix has low matrix condition number for stable inversion, and leads low mean-square errors during recovery of effective element-by-element synthetic aperture datasets. Because (N+1)/2 elements are active during a transmit event, up to (N+1)/2 times signal enhancement for an N-element array is possible, compared with traditional element-by-element scanning. Sparse aperture S-sequence encoding with multi-element virtual source excitation can lead to high-SNR fast imaging with minimal distortion. These theoretical advantages are demonstrated with Field II simulations and experiments. A Verasonics array platform was programmed to implement the S-sequence

aperture encoding. Data processing and beamforming was performed offline. Image quality from phantoms and in vivo was compared against traditional synthetic aperture scanning, Hadamard encoding, and more standard imaging schemes.

Results/Discussion

The proposed binary S-sequence scheme offers close to the expected signal-enhancement in ex-periments compared to element-by-element synthetic aperture scanning methods. While it provides less total SNR advantage compared to bipolar Hadamard aperture coding it practically leads to less artifacts as ideal pulse-inversion is not required. The S-sequence aperture coding may prove a practically realizable means of improving SNR in high-resolution and/or fast synthetic aperture imaging systems and could be implementable on many current or emerging commercial systems.

Medical imaging

M5

Tuesday, July 23 2013, 02:00 pm - 03:30 pm

Congress Hallair: **Matthew O'Donnell**
University of Washington

IUS1-E3-1

Spatial coherence and its relationship to human tissue: an analytical description of imaging methods

Gianmarco Pinton[1,2], Gregg Trahey[3], Jeremy Dahl[3]; [1]*Institut d'Alembert, Centre National de la Recherche Scientifique, Paris, France,* [2]*Universite Pierre et Marie Curie, France,* [3]*Biomedical Engineering, Duke University, Durham, NC, USA*

Background, Motivation and Objective

In this paper a theoretical description of spatial coherence in human tissue and its applications to spatial coherence ultrasound imaging are established. In conventional B-mode imaging the image brightness is determined by the amplitude of the backscattered beamformed echoes. The image brightness in spatial coherence imaging is based on the coherence properties of the backscattered signal. Classical spatial coherence theory, which does not take into account tissue structure, doesn't predict the spatial coherence observed in vivo. We aim to answer the questions: what is the relationship between the observed spatial coherence and the structure of the underlying tissue?

Statement of Contribution/Methods

To establish a physical description of coherence imaging we extend the formalism initially developed by Zernike to pulse-echo ultrasound in a model of tissue. This theoretical development is used to used to describe the spatial coherence of an acoustic wave as it propagates through a model of the human abdomen that includes aberration and reverberation clutter. This model is verified with in vivo data from the human abdomen and with simulations of the spatial coherence of the backscattered ultrasound signal in realistic diagnostic imaging conditions. The backscattered field is determined with a finite difference time domain Full-Wave Nonlinear Acoustic (FWNA) simulation that includes multiple scattering and reverberation clutter.

Results/Discussion

The image on the left shows the simulated human abdomen. The image in the center shows the measured and simulated spatial coherence curves demonstrating an empirical agreement. And the image on the right compares the theoretical prediction (clutter + random mirror) with the simulated spatial coherence (total field), which validates the theoretical analysis.

The Fourier acoustics model and simulations demonstrate the physical mechanisms involved in spatial coherence imaging. Reverberation clutter is equivalent to acoustic noise and it decorrelates quickly. The signal backscattered from random scatterers at the focus decorrelates slowly and it depends on the transducer shape and pulse characteristics. Spatial coherence imaging is based on the relative contribution of these two components and is therefore a measure that depends on the wavelength and sub-wavelength scattering environment in the human body.

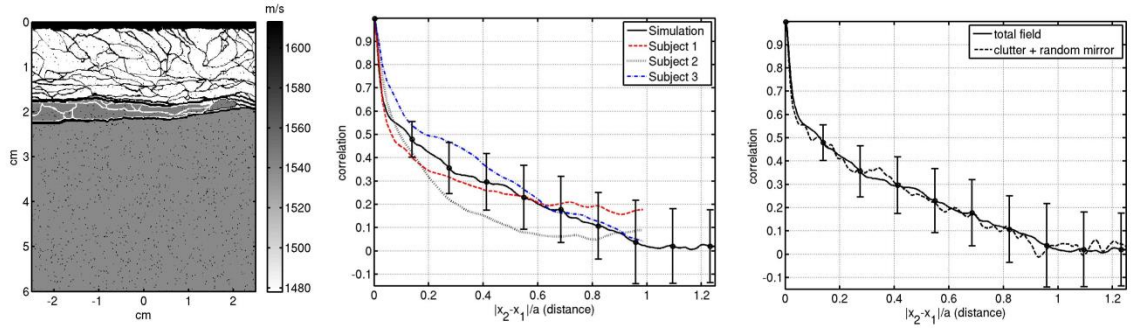

IUS1-E3-2

In vivo performance evaluation of short-lag spatial coherence (SLSC) and harmonic spatial coherence (HSC) imaging in fetal ultrasound

Vaibhav Kakkad[1], Jeremy Dahl[1], Sarah Ellestad[2], Gregg Trahey[1]; [1]*Department of Biomedical Engineering, Duke University, Durham, NC, USA,* [2]*Department of Obstetrics and Gynecology, Duke University Medical Center, Durham, NC, USA*

Background, Motivation and Objective

Fetal scanning is a prevalent application of ultrasound imaging and is widely used to visualize key fetal and maternal structures such as nuchal translucency, cerebral ventricles, placenta, uterine wall, and cervix. However, many fetal ultrasound exams suffer from inadequate visualization of these structures due to ultrasonic clutter. This effect is more pronounced in over-weight and obese patients where approximately 40% of such scans are diagnostically inconclusive. We have previously shown that short-lag spatial coherence (SLSC) imaging and harmonic spatial coherence (HSC) imaging are successful in suppressing clutter, improving contrast and border delineation in simulations, phantoms and *in vivo* liver and cardiac images. In this pilot study, we extend the application of this technique to fetal ultrasound scanning.

Statement of Contribution/Methods

We conducted an IRB approved study to evaluate the performance of SLSC and HSC in 10 first-trimester patients at the Duke University Fetal Diagnostic Clinic. Channel data was collected transabdominally over a 40° field of view using the Siemens S2000 system and the 4C1 probe. This data was used to create matched B-mode, SLSC, Harmonic B-mode, and HSC images. The resulting images were separated into “good” and “poor” quality groups based on the sonographer’s assessment of the B-mode image. Their relative performance was quantified using imaging metrics such as SNR, CNR and contrast.

Results/Discussion

SLSC and HSC images showed significant improvements across all imaging metrics compared to B-mode and harmonic B-mode, respectively. The improvements in clutter suppression and uterine border delineation were greater for "poor" images. The average clutter level in a uniform region of amniotic fluid for a set of 10 "poor" images was found to be -16 dB for B-mode versus -26 dB for SLSC, and -16 dB for harmonic B-mode versus -34 dB for HSC. CNR for the same set of images improved from 1.4 to 2.5 for B-mode versus SLSC and from 1.4 to 3.1 for harmonic B-mode to HSC. In addition to the quantitative improvements, dramatic qualitative improvements were observed in the ability to detect fetal structures such as the choroid plexus, facial features and extremities. We show that SLSC and HSC imaging have the potential to improve fetal feature detection in high noise environments and add diagnostic value to fetal ultrasound imaging.

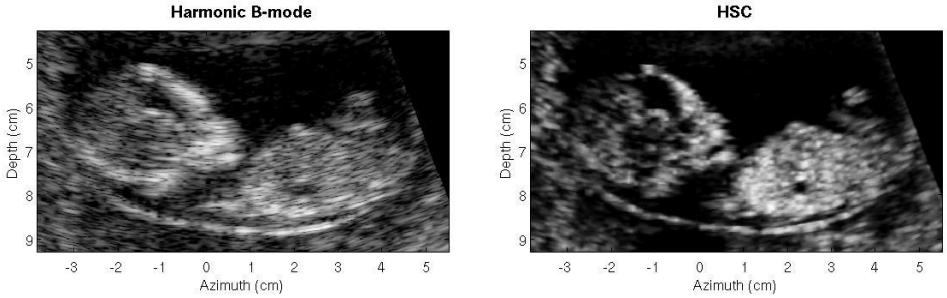

IUS1-E3-3

Ultrafast Acoustoelectric Tomography

Jean Provost[1], Wojciech Kwiecinski[1], Mathias Fink[1], Mickael Tanter[1], Mathieu Pernot[1]; *[1]Institut Langevin, ESPCI ParisTech, CNRS UMR7587, INSERM U797, Paris, France*

Background, Motivation and Objective

Imaging the electrical activity of the body is central to the diagnosis of and treatment planning for some of our most pressing healthcare challenges, including heart and brain diseases. The acoustoelectric effect has recently been shown to provide contrast directly from current densities by measuring ultrasound-modulated electrical impedance in the heart [1]. While promising, these approaches, based on focused emission at low frequency, result in limited signal-to-noise ratios (SNR), and temporal and spatial resolutions. In this study, we developed Ultrafast Acoustoelectric Tomography (UAT), based on plane wave emissions, which provides large SNR and uniformly high spatial and temporal resolutions.

Statement of Contribution/Methods

The acoustoelectric effect is generated when a high frequency variation in pressure perturbs the electrical impedance of a medium undergoing a low frequency current. The difference of potential detected by remote electrodes can be modeled by the convolution over time of the pressure field with the current density. When emitting plane waves at varying angles, this convolution amounts to a Radon transform for which a simulation of the forward problem and a back-projection inversion algorithm were devised. Plane waves between -25 and 25 degrees were emitted using an Aixplorer system (Supersonic Imagine, France) with a 6-MHz linear array probe (MI < 1.9). Electrode potentials were high-passed filtered before entering a differential preamplifier (Lecroy, Chestnut Ridge, NY), an amplifier (Olympus NDT, Waltham, MA), and then averaged and sampled. Currents were applied and imaged in two phantoms containing a 0.9% NaCl solution: 1) a Tygon tube with an inner diameter of 0.87 mm, and 2) a triangular-prism-shaped container (base: 2 mm, height:2.5 cm).

Results/Discussion

Using angles between -25 and 25 degrees, simulations revealed that, contrary to focused approaches, the resolution of UAT is independent of depth with a point-spread function of 0.3 mm by 0.45 mm at 6 MHz. The UAT image of the cross-section of Phantom 1 spanned 1.1 mm by 2.5 mm at -3dB. In Phantom 2, a linear increase with height of current density was found, in accordance with the theoretical current density distribution. Both simulations and phantom experiments demonstrated the capability of UAT to image current density with uniform resolution. Since the acoustoelectric signal originates from the spatial integration of the pressure field at one instant, larger signals are obtained with plane waves when compared against focused emissions. This results in an increased SNR without a trade-off in terms of spatial resolution. Phantom studies also demonstrated the feasibility of UAT at current density levels similar to the ones occurring naturally in vivo and indicate that UAT could become a unique technique to map current density distributions in tissues and image their propagation at very high frame rates.

[1] R. Olafsson et al. IEEE UFFC, 56(3) pp. 565–574, 2009.

IUS1-E3-4

Magnetomotive ultrasound imaging of rat lymph nodes *in situ*: assessment of imaging parameters

Maria Evertsson[1], Magnus Cinthio[1], Sarah Fredriksson[2], Pontus Kjellman[2], Rene in 't Zandt[2], Fredrik Olsson[2], Hans W Persson[1], Tomas Jansson[1]; *[1]Electrical Measurements, Faculty of Engineering, Lund University, Sweden, [2]Genovis AB, Lund, Sweden*

Background, Motivation and Objective

We have developed a frequency and phase gated algorithm to reduce motion artifacts in magnetomotive ultrasound (MMUS) imaging, with promising results in phantom studies (IEEE Trans UFFC 2013, pp 481-491). Here we report results from animal experiments with detection of superparamagnetic iron oxide nanoparticles (SPIO-NP) in lymph nodes *in situ*, a step towards MMUS imaging *in vivo*.

Statement of Contribution/Methods

Seven Wistar rats were injected with 100µL NP solution in one of their hind paws, four with 31nm NPs and three with 67 nm NPs. Further, the injections were given as a low or a high concentration (0.3 and 3 mg iron oxide/mL respectively). Only one animal received the low concentration 67nm NPs. 24 hours post injection the animals were sacrificed and imaged with a high frequency ultrasound scanner (Visualsonics VEVO 2100). Each rat was positioned between the transducer (center frequency 21 MHz) and a solenoid with a cone shaped iron core, imaging the lymph node in the fold of the knee, proximal to the injection site. The solenoid was excited with various voltages (10, 20, 30Vpp) and frequencies (5-15Hz, in steps of 2.5Hz). Displacements were calculated from acquired RF IQ-data. Signal to clutter ratios were given as average displacement in the lymph node divided with that in the fat capsule surrounding the node.

Results/Discussion

Fig. 1 shows: (a) a B-mode image of a rat lymph node after injection of 100µl 0.3mg/mL solution of 31nm NPs; (b) the total magnetomotive displacement at 5Hz 30V coil excitation; (c) the phase distribution at the detected frequency and (d) the frequency and phase-discriminative displacement. The displacement and phase magnitudes can be read from the color bars, note the different scales. The signal to clutter ratio in the case depicted in Fig. 1 (d) was 16.7 dB compared to an average of 6.7dB for all measurements. The displacement tended to decrease with increasing frequency, and to increase with increasing excitation voltage. For example it was approximately twice as large at 5Hz than 15Hz, and three times larger at 30V compared to 10V. There was also a tendency that smaller particles induced a larger magnetomotive displacement. From the phase map 1(c) it can be seen that the magnetomotive displacement of NP-laden tissue induces a counteracting motion with opposite phase in tissue surrounding the lymph node, effectively suppressed by the algorithm, 1(d).

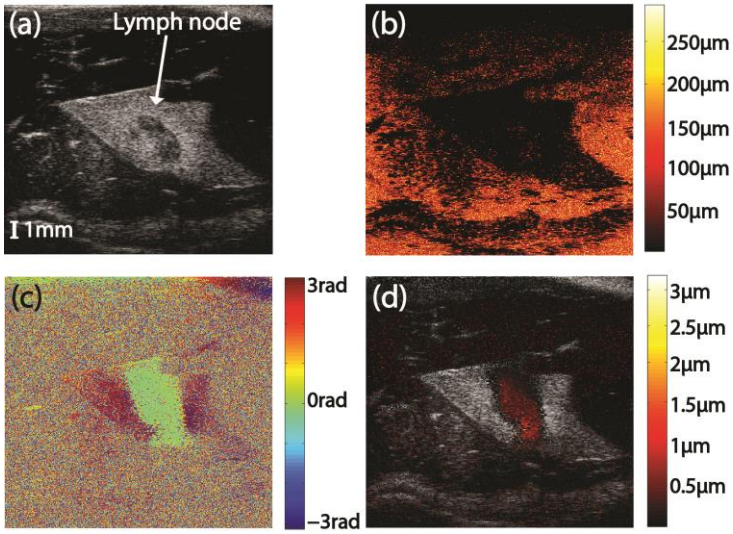

IUS1-E3-5

The Westervelt Equation for Nonlinear Propagation: Numerical Simulations and Experimental Validation of Ultrasonic Fields Produced by Array Transducers

Alexander Doinikov[1], Anthony Novell[1], Pierre Calmon[2], **Ayache Bouakaz[1]**; *[1]INSERM U930, Université François Rabelais, Tours, France, [2]CEA LIST, Saclay, France*

Background, Motivation and Objective

Phased array transducers are used in a variety of ultrasound (US) applications such as medical ultrasonic imaging and therapy and nondestructive evaluation of materials. The development and optimization of imaging modalities and therapeutic strategies require computational methods that accurately predict 3D nonlinear US fields generated by such transducers. The parabolic approximation underlying the KZK equation restricts the domain of validity of this equation, whereas the Westervelt equation is free of such limitations. The aim of our work is to validate the ability of the Westervelt equation to predict the behavior of US beams generated by steered phased array transducers.

Statement of Contribution/Methods

Numerical solutions of the Westervelt equation are carried out and compared with experimental data. The numerical scheme is based on the explicit finite-difference time-domain method on a 3D Cartesian grid. The validation of the developed code is first carried out by using experimental data obtained for two focused circular single-element transducers in the regimes of small-amplitude and finite-amplitude excitations. Afterwards, the comparison of simulated and measured ultrasonic fields is performed for a modified 32-element linear array transducer.

Results/Discussion

The case of linear excitation was tested using a circular transducer with radius a = 23.5 mm and focal length d = 48.6 mm, excited at 1 MHz and an on-source pressure amplitude p0 of 5 kPa. The nonlinear excitation test was made using a circular transducer with a = 13.4 mm and d = 57 mm, excited at 2.25 MHz and p0 = 54 kPa. In this test, the axial and lateral pressure profiles were measured for both fundamental and 2nd harmonic components. Experiments for an array transducer were carried out using a 128-element PZT linear array probe with a pitch of 305 microns and an elevation of 8 mm. A 20-cycle Gaussian pulse centered at 2.5 MHz was generated using Matlab and then transmitted to the fully programmable US system (WaveMaster, M2M, Les Ulis, France) equipped with analog transmitters. In order to validate our theoretical predictions, the probe was adapted to generate grating lobes. Hence, only 1 of 4 elements was connected so the probe functioned as a 32-element linear array transducer. The axial and lateral pressure profiles were measured for the fundamental and 2nd harmonic components at the zero and 20-degree steering angles. Based on the experimental parameters, analogous theoretical profiles were computed. The characteristic computational time was 7 - 10 hours. In all the cases tested, excellent agreement between the simulated and the measured data was observed. Our results show that the developed code is able to correctly capture the effect of grating lobes and to predict accurately the magnitude of the fundamental and 2nd harmonic components at large angles from the main axis.

IUS1-E3-6

Nonlinear Reconstruction of Bulk and Shear Modulus Variations in Isotropic Solids Using the Kazmarcz Method

Leili Salehi[1], Georg Schmitz[2]; *[1]Electrical Engineering and Information Technology, Ruhr-Universität Bochum, Bochum, Germany, [2]Ruhr-Universität Bochum, Germany*

Background, Motivation and Objective

To determine the mechanical properties and morphology of hard tissue like bone, tomographic imaging at relatively low frequencies is a promising option. However, mode conversions between compressional and shear waves require the use of non-linear tomographic methods taking multiple scattering into account. For fluid media, Natterer et al. presented an approach based on the linearization of the forward propagation operator and use of the iterative Kazmarcz method. They derived the adjoint operator for the reconstruction of the material's compressibility. In this paper we consider an isotropic solid material and derive the adjoint operators for the reconstruction of bulk and shear modulus. Based on this, the nonlinear inverse problem was solved for isotropic solids and tested with simulated data.

Statement of Contribution/Methods

Bulk and shear moduli are iteratively reconstructed by the Kazmarcz method. For this, the nonlinear forward wave propagation operator mapping the spatially varying bulk and shear modulus to the measurements on the medium's borders is linearized by its Fréchet derivative. The adjoint operators that map the measurements on the medium's borders to changes of bulk and shear moduli in the medium are derived. For the reconstruction algorithm the forward propagation operator and the backward propagation operator have to be calculated by wave field simulations. A pseudo-spectral time domain (PSTD) simulation is performed for a solution space of 100 mm x 100 mm filled with water with convolutional perfectly matched layers (CPML) on the borders. To evaluate the reconstruction algorithm in line with Natterer's work we used simulated measurement data and a Shepp-Logan phantom. 72 point transducers for transmit and receive are distributed on a circle around the object with varying bulk and shear modulus. The object is insonified with pulse excitation (center frequency 400 KHz, bandwidth 105 KHz) using all transducers in random sequence. Scattered signals are recorded and first used to reconstruct the bulk and shear modulus changes assuming a constant density of 1000 kg/m³.

Results/Discussion

Our results show that the new reconstruction algorithm is able to reconstruct bulk and shear modulus in isotropic solids. Relative errors are below 10%, but more importantly the morphology of the solid inclusion can be imaged geometrically correct. This is a first step towards the reconstruction of hard tissues like bone and cartilage possibly enabling the assessment of the cortical thickness of bones.

Laser Ultrasonics

NH

Tuesday, July 23 2013, 02:00 pm - 03:30 pm

Congress Hallair: **Lawrence Kessler**
Sonoscan Inc.

IUS2-E-1

Laser ultrasonic velocity measurement for Phase transformation investigation in Ti alloy (Ti-6% Al-4% V)

Saeid Zamiri[1,2], Bernhard Reitinger[1], Jürgen Roither[1], Siegfried Bauer[3], Peter Burgholzer[1,2]; [1]*Research Center for Non Destructive Testing GmbH (RECENDT), Linz, Austria,* [2]*Christian Doppler Laboratory for Photoacoustic Imaging and Laser Ultrasonic, Linz, Austria,* [3]*Department of Soft Matter Physics, Johannes Kepler University, Linz, Austria*

Background, Motivation and Objective

Titanium (Ti) alloys sustain highest demands, e.g. in aerospace industries. The mechanical properties of Ti with different percentages of aluminum and vanadium strongly depend on the microstructure and further the change of microstructure with temperature (Phase transformation). Therefore monitoring the phase transformation of Ti is essential and is carried out by using a nondestructive method. We monitor the Phase transformation in a Ti alloy by using a laser ultrasonic (LUS) method based on two wave mixing interferometer which has the key benefits of being fast and contactless with high resolution.

Statement of Contribution/Methods

We will report on monitoring the phase transformation temperature in Ti alloy (Ti-6% Al-4% V) about 1000°C by using a simple contactless LUS method based on two waves mixing in a fast BSO photorefractive crystal. In our LUS laboratory setup, a reference beam and a phase modulated signal beam interfere inside the BSO crystal. Due to the modulated refractive index in the crystal, a grating is formed and the two beams are coupled, and further the reference beam is diffracted in the speckled signal beam direction. The diffracted beams were focused with a lens on a broadband and fast photo-receiver. The experiments were carried out on 1.5 mm thick Ti sheets with 100 mm length. The samples were heated up by applying high current (0-30A) up to a temperature of 1200°C. To generate the ultrasonic bulk waves, picoseconds pulses from a 1064 nm Nd:YAG pulsed laser were focused on the sample backside. The detected bulk waves on the opposite side of the sample (measurement in transmission geometry) with the longitudinal and shear waves are shown in the Figure 1.

Results/Discussion

With the mentioned contactless and fast method it was possible to detect the phase change of Ti-6-4 from α to β phase. From the figure the phase change shows as the temperature increases the ultrasonic wave velocity decreases (time of flight increases) up to 980°C which shows the start of the phase change region in Ti. At 980°C to 1020°C the bulk wave velocity is approximately constant which indicates the process of the phase transformation from α to β phase. Above 1050°C to 1200°C the bulk wave velocity reduces very slowly.

Fig1. Phase change of Ti-6-4 from α to β phase versus Temperature (room to1200°C)

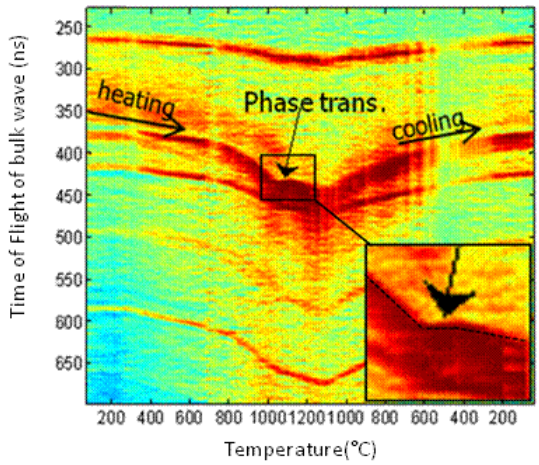

IUS2-E-2

Direct measurement of SAW dispersion relations in the k-ω domains; numerical and experimental studies

Istvan A Veres[1], Clemens Grünsteidl[1], Jürgen Roither[1], Peter Burgholzer[1,2], Todd W. Murray[3], Thomas Berer[1,2]; [1]*Research Center for Non-Destructive Testing GmbH, Linz, Austria,* [2]*Christian Doppler Laboratory for Photoacoustic Imaging and Laser Ultrasonics, Linz, Austria,* [3]*University of Colorado at Boulder, Boulder, USA*

Background, Motivation and Objective

Non-destructive testing and evaluation is gaining increased importance as more and more engineering structures or mechanical components are inspected or monitored regularly. The use of non-contact techniques, such as laser-based ultrasound, has extended the range of possible applications allowing the characterization of micro-scale samples and thin coatings, for example, which can protect materials from corrosion or high temperatures, or provide a reflecting surface. The low optical damage threshold of these submicron layers restricts the use of focused high-power excitation lasers. Recently developed intensity modulated laser-ultrasonics, and its various adaptations such as temporally and spatially modulated laser-ultrasonics, address this problem by significantly reducing the peak power density in the excitation laser source.

Statement of Contribution/Methods

In the presented work, we investigate numerically and experimentally the evaluation of the dispersion relation of SAWs in thin films by temporally and spatially modulated laser-ultrasound. Experimental results are acquired by the combined application of intensity modulated laser-diodes and a spatial light modulator (SLM). Numerical simulations are done by the solution of the coupled heat and wave equations using the finite difference time domain (FDTD) method with a combination of implicit and explicit temporal integration techniques.

Results/Discussion

The developed setup utilizes constructive interference of the SAWs from parallel, equidistant line sources and allows the direct, frequency domain measurement of dispersion relations. Figure (a) shows the surface displacement amplitude measured while varying the modulation frequency and the spatial period of the excitation laser source. Numerical simulations were done in the time domain and the surface displacements were calculated adjacent to the excitation pattern. The amplitude of the interfering SAWs are obtained from the last part of the signal shown in Fig. (b), where the amplitudes at the excitation frequency are steady state. Figure (c) shows the numerical and experimental variation of the amplitudes of the interfering SAWs for different frequencies with a fixed spatial excitation pattern (line spacing). The peak point on this curves gives the corresponding (ω,k) point on the dispersion relation.

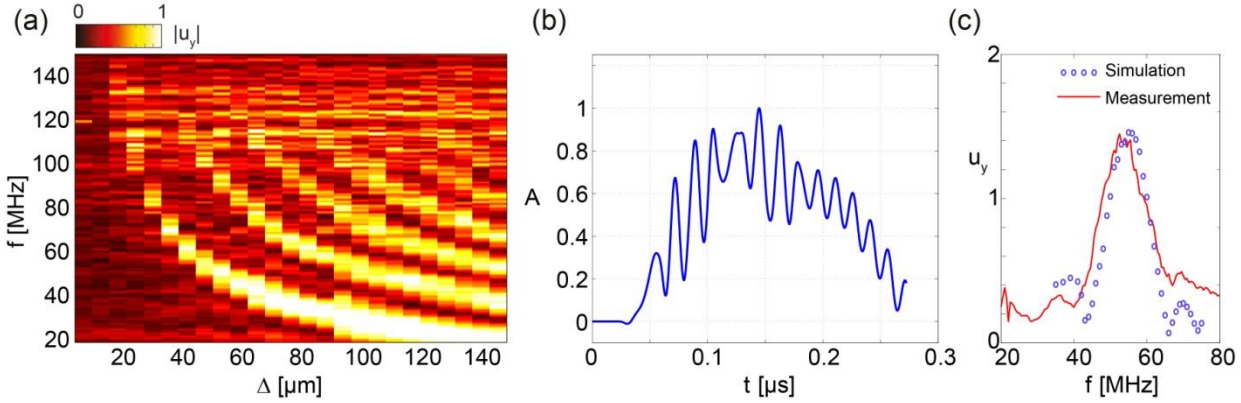

IUS2-E-3

Laser ultrasound detection using a photorefractive balanced detector

Peter Burgholzer[1,2], Saeid Zamiri[1,2], Jürgen Roither[3], Hubert Grün[3], Bernhard Reitinger[3]; *[1]RECENDT, Linz, Oberösterreich, Austria, [2]Christian Doppler Laboratory for Photoacoustic Imaging and Laser Ultrasonics, Linz, Austria, [3]RECENDT, Austria*

Background, Motivation and Objective

Balanced detectors reduce noise and thereby enhance the signal-to-noise–ratio by subtracting an inverted signal from a positive signed signal. If both signals are disturbed by the same noise source this noise is cancelled out.

Statement of Contribution/Methods

We report on a two wave mixing interferometer [1] where the output of two photorefractive crystals (BSO) with opposite polarity of the electrical field is substracted (Fig. 1). We explain how different sources of noise are balanced out, the frequency behavior and bandwidth of this detection scheme, and the resulting noise equivalent surface displacement (NESD). The NESD is also compared for other detection schemes, like a conventional Michelson interferometer.

[1] Ph. Delay, A. Blouin, D. Drolet, J.P. Monchalin, L.A. Montmorillon, G. Roosen, J. Opt. Soc. Am. B 14 1723 (1997)

Results/Discussion

Experimental results are compared to theoretical calculations of the NESD and show that the proposed detection scheme can significantly reduce laser and electrically induced noise. Therefore cheap lasers having a relative high noise and jitter can be used for a low – noise laser ultrasound detection set-up.

Figure 1 Photorefractive balanced detector set-up using two photorefractive crystals with opposite polarity of the electric field and a balanced detector. BS: Beamsplitter; PD1 and PD2: Photodetectors

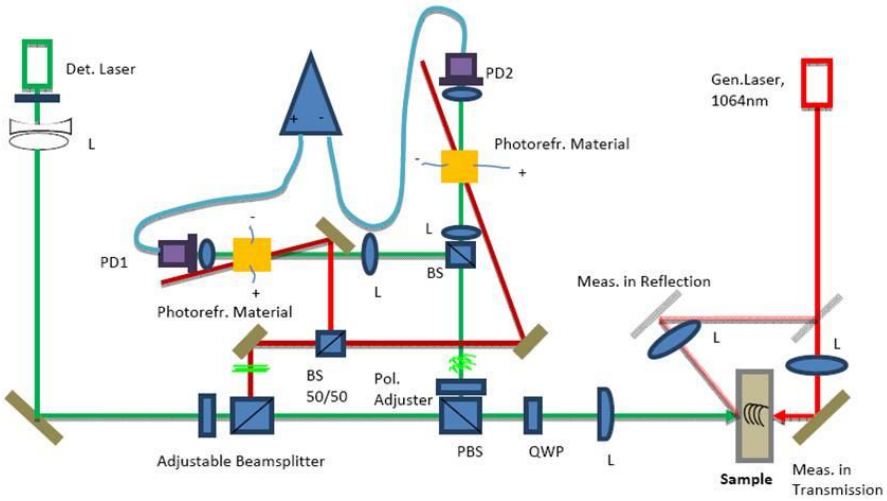

IUS2-E-4

Basic Study of Water Distribution Measurement in Soil Using SLDV -The soil water measurement during plant cultivation-

Tsuneyoshi Sugimoto[1], Yutaka Nakagawa[1], Takashi Shirakawa[1], Motoaki Sano[1], Motoyoshi Ohaba[2], Sakae Shibusawa[2]; *[1]Toin Univ. of Yokohama, Japan, [2]Tokyo Univ. of Agriculture and Technology, Japan*

Background, Motivation and Objective

We propose a method of monitoring and imaging of the water content in the rooting zone using a sound vibration and the Scanning Laser Doppler Vibrometer (SLDV). This time, the soil water measurement during plant cultivation using the sound wave vibration was examined which used negative pressure irrigation.

Statement of Contribution/Methods

To perform the soil water measurement during plant cultivation, a special container was made. Two acoustic holes are installed in the container wall. One is used to irradiate a laser for vibration measurement. A thin polypropylene film was used to prevent the outflow of soil. The other is used to push a sound source (giant magnetostriction vibrator) from the outside. A transparent plastic board was used to cover the hole to prevent transformation by the pressure. Commercial compost purified by a sieve of 2 mm was used as the soil. Japanese mustard spinach was used for a plant, because its growth rate is fast. The burst wave of 1 kHz of sine wave, 5 cycles were used as an output waveform. To compare the propagation velocity of sound, the soil-moisture sensor which measures the water quantity of the soil using the electric permittivity is installed near the rooting zone. Water supply sheet supplies water to the soil from the bottom of the container.

Results/Discussion

From a 10 day measurement result, both the volume water content and the propagation velocity of sound show a big change at the time of water supply and a small change is shown for ON/OFF of the light. And a negative correlation is seen in the propagation velocity of sound and the volume water content.

This time, we can confirm that the water distribution of the plant rooting zone could be estimated by the propagation velocity of sound in the soil.

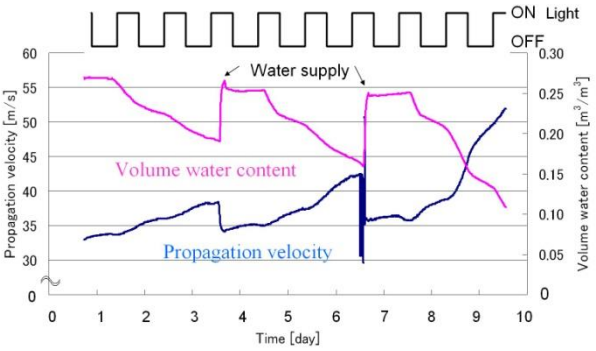

Experimental result. Red line: Volume water contet, Blue line:Propagatin velocity.

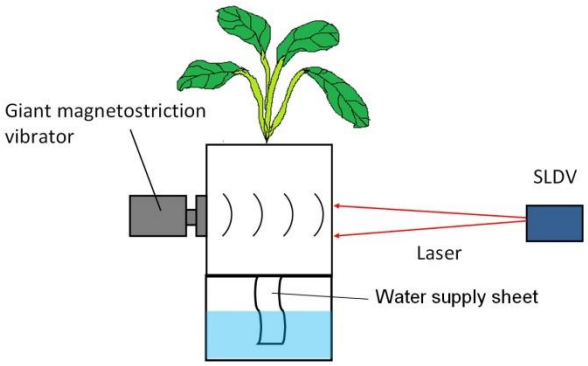

Basic concept of our proposed method.

IUS2-E-5

Detecting defects in adhesion between a metal hemisphere and a polymer base

Ari Salmi[1], Pasi Karppinen[1], Heikki Nieminen[1], Adam Hacking[2], Edward Haeggström[1]; *[1]University of Helsinki, Finland, [2]Harvard School of Medicine, USA*

Background, Motivation and Objective

Detecting localized defects in adhesion is challenging; especially when direct access to the boundary where they reside is not available. Whereas guided ultrasonic waves can characterize such defects, the literature is scarce on such characterization for hemispherical surfaces. We demonstrated capability to quantify the average adhesion between a metal hemisphere and a polymer base [1]. Here we report on progress towards determining: presence of localized defects, their position, size, and strength.

Statement of Contribution/Methods

We describe experiments done on a 5 cm diameter metal hemisphere attached to a UHMWPE (Polyethylene, PE RCH 1000 D150x2000 Etralene) base. Defects in adhesion were generated by drilling holes of different diameter (2 to 20 mm) into the polymer base prior to adhering the hemisphere into it, thus generating known areas with no adhesion. These localized defects were remotely characterized with a guided ultrasonic wave (Lamb quasi-modes) generated by a Nd:YAG (1064 nm, 5 ns pulse duration) pulse from one rim of the cup and detected with a laser Doppler vibrometer, Fig. 1. The sample was attached to a rotation stage and a 360 degree scan (10 degree steps) was done.

Results/Discussion

We determine the feasibility of detecting the presence of defects as well as the feasibility of determining their position. Our results quantify the potential of the method for the proposed task.

[1] A. Salmi et al., IEEE Ultrasonics International, Oct 8-10 2012, Dresden, Germany (in press)

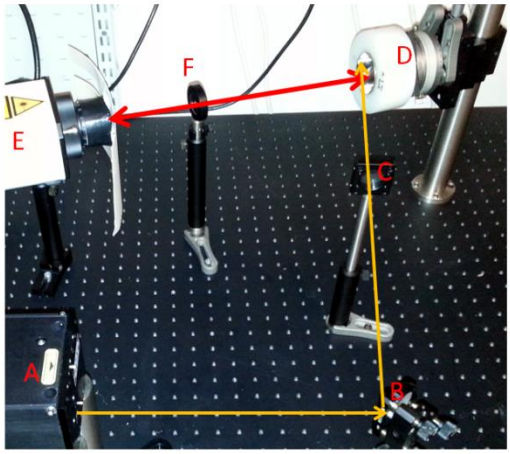

Fig. 1: Measurement setup. The Nd:YAG (A) laser, directed via a mirror (B) is focused (C) onto the sample, which is attached to a rotation stage (D). The excited ultrasonic wave is picked up with a laser Doppler Vibrometer (E), protected by a filter (F).

IUS2-E-6

Surface Acoustic Wave Velocity Mapping of Tissue Sample Using a Scanning Laser Doppler Velocimeter

Yukako Kato[1], Yuji Wada[1], Yosuke Mizuno[1], Kentaro Nakamura[1]; *[1]Tokyo Institute of Technology, Yokohama, Kanagawa, Japan*

Background, Motivation and Objective

Elastography is highlighted in this decade since the hardness of tissue is closely related to the degree of tumor. We have been making a trial to measure the propagation velocity of surface acoustic wave (SAW) to estimate the absolute elastic constant of tissue.

In the previous study, we measured the SAW velocities of different concentration agar and some tissue samples using a swept-source optical coherence tomography since optical method has high spatial resolution. However, it was hard to estimate SAW velocity of sample with high attenuation. In this study, we measured the SAW velocity of tissue sample using a laser Doppler velocimeter (LDV) which can observe smaller displacement.

Statement of Contribution/Methods

We excited SAW on a pork loin sample using a thin aluminum plate of 35 mm in width connected to a moving coil actuator as shown in Fig. 1. We observed a square region of 20 × 18 mm^2 located 10 mm apart from the vibrator when a 3-cycle burst at 1000 Hz was launched. The room temperature was 25 ± 0.5 °C. We scanned 21 points for each of 10 lines along y-axis with 1-mm pitch using the LDV and observed time difference between each two adjacent points. The spacing between the two scanning lines was 2 mm. From the time difference, we figured out the SAW velocity at each point.

Results/Discussion

Figure 2 shows the two dimensional mapping of the SAW velocity on the pork loin. It is clearly observed that the SAW velocity in fat part is faster than that in lean meat part. These results are strongly reflected from the difference in the elastic property of the sample. The dependence of the propagation direction on the results is one of the most interesting subjects to be considered in near future, and it shall provide us more rich information about the tissue characteristics.

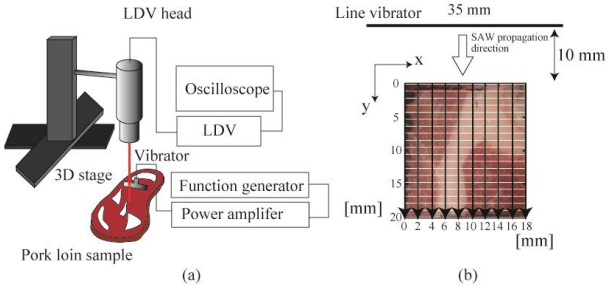

Figure 1. (a) Experimental setup. (b) Scanned area and SAW propagation direction.

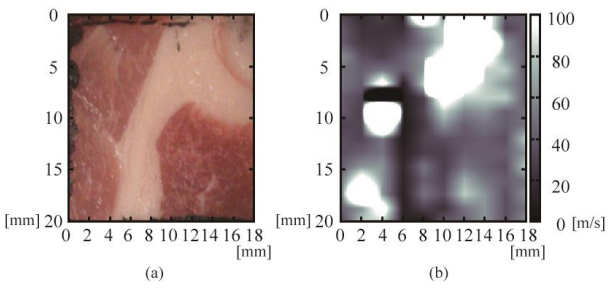

Figure 2. (a) Image of pork loin sample. (b) 2D SAW velocity mapping.

Phononic crystals and metamaterials

T1

Tuesday, July 23 2013, 02:00 pm - 03:30 pm

Congress Hallair: **Tsung-Tsong Wu**
National Taiwan University

IUS3-E-1

Approximate model and experiments on Seismic metamaterials

Sebastien Guenneau[1], Stefan Enoch[1], Emmanuel Javelaud[2], Stéphane Brulé[2]; [1]*Institut Fresnel, Aix-Marseille University, Marseille, France,* [2]*Menard company, France*

Background, Motivation and Objective

Acoustic metamaterials is a fast growing subject which got started using analogies with Pendry's famous electromagnetic paradigms of a flat lens and an invisibility cloak. Concepts of negative refraction whereby light or sound takes the wrong turn are underpinned by negative permittivity/permeability (in optics) and density/compressibility (in acoutics). This talk addresses the question of whether or not acoustic metamaterials can be scaled up in order to control seismic waves.

Statement of Contribution/Methods

We shall describe a preliminary large-scale seismic test held on a soil metamaterial using vibrocompaction probes. The easiest way to interact with surface waves at the air/soil is to modify the global properties of the medium, acting on the soil density and then on the wave velocity. We thus counteract the seismic signal by modifying the distribution of the seismic energy thanks to a metamaterial made of a grid of vertical, cylindrical and empty inclusions bored in the initial soil.

Results/Discussion

Comparison between a simple numerical plate model and experiments are in good agreement, and allow for some deep analogies between ray optics and seismic wave propagation.

IUS3-E-2

Investigation of slow evanescent waves at the surface of immersed micromachined membrane arrays

Shane Lani[1], M. Wasequr Rashid[1], Karim Sabra[1], F. Levent Degertekin[1]; [1]*Georgia Institute of Technology, USA*

Background, Motivation and Objective

Evanescent surface waves can propagate at the surface of immersed periodic membrane arrays, such as of capacitive micromachined ultrasonic transducers (CMUTs). Near the membrane resonance frequency, these evanescent surface waves become strongly dispersive and results in problematic acoustic crosstalk over the array [1]. In contrast, one may exploit these slowly propagating evanescent waves as a means for creating sub-wavelength resolution fields for high-resolution ultrasound imaging and sensing by appropriately tuning the physical characteristics of individual membranes.

Statement of Contribution/Methods

The dispersive behavior of these evanescent surface waves propagating along a micromachined membrane array (CMUT array) was quantified using a computationally efficient linear transient semi-analytic model [2]. Numerical results were validated using FEM and experimental data.

Results/Discussion

The model was compared to an experiment performed on a 16 element 1-D linear CMUT array where each element consists of 4 columns and 45 rows of 45x45µm 2.19µm thick silicon nitride membranes (245µm pitch) immersed in water (Fig. 1a). The first element of the linear array transmitted a pulse while elements 4, 8, 12, and 16 were used as receivers (Fig. 1b). The first arrivals correspond to a wave speed of 1500m/s and contain lower frequencies while higher frequencies around the predicted resonance frequency of 6.5MHz are arriving later. The group velocity of the arrival was determined from a simplified model and was compared to the experiment after time-frequency analysis (Fig. 1c). The results show that the group velocity of the evanescent wave varies from 1500m/s to 400m/s near the membrane resonance as predicted by the model.

A linear semi-analytic model was developed to model the dispersive behavior of evanescent surface waves propagating along periodic micromachined membranes and was verified by experiments on a CMUT array. This numerically efficient approach can be leveraged to efficiently investigate the design space of microengineered surfaces to control the physical characteristics of these slow evanescent surface waves for enhanced sensing and imaging.

[1] P. C. Eccardt, A. Lohfink, and H. G. v. Garssen, in Ultrasonics Symposium, 2005 IEEE, pp. 593-596, 2005.

[2] C. Meynier, F. Teston, and D. Certon, J. Acoust. Soc. Am., vol. 128, pp. 2549-2561, 2010.

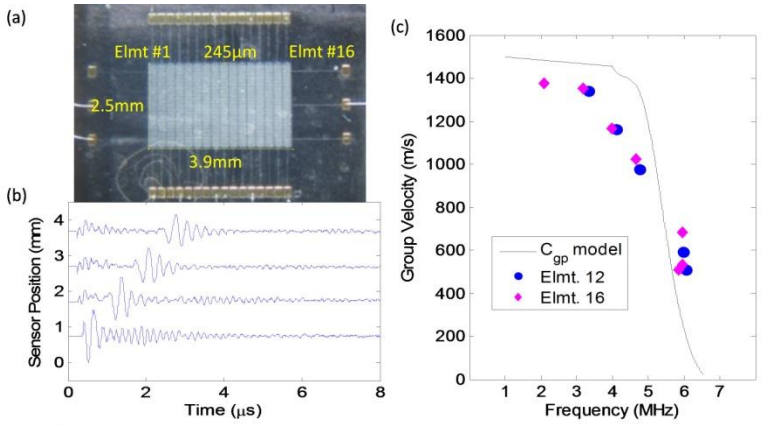

Fig. 1 (a) 1x16 linear CMUT array. Element #1 acts as transmitter. (b) Recorded surface wave arrivals (crosstalk) at Elements 4, 8, 12, and 16. Distances are measured from Element #1. (c) Predicted group velocity of the surface wave (solid line) from the semi-analytical model. Symbols indicate group velocities measured from the dispersive signals received element at Elements 12 and 16 (shown in b).

IUS3-E-3

Acoustic metamaterial: experimental investigation of the acoustic field scattered by isolated active resonators

Remi Marchal[1], Bernard Bonello[2], Jinfeng Zhao[1], Olga Boyko[1]; *[1]University Pierre et Marie Curie, France, [2]INSP, CNRS and University Paris 6, France*

Background, Motivation and Objective

Acoustic metamaterials are heterostructures designed to control the propagation of elastic waves. They are generally constituted by local resonators embedded into a homogeneous matrix. Effec-tive mass density and compressibility can be both negative when resonators are excited in vibra-tion(s) which is (are) out-of-phase with respect to the elastic wave that propagates in the matrix.

Isolated silicon pillars and pairs of holes in a silicon plate are potentially “good” candidate to ful-fill this requirement.

Statement of Contribution/Methods

To conduct this study, we used an all-optical experimental technique. Our approach consisted in (i) measuring the eigenfrequencies of the resonators in order to select the one which allows ful-filling the homogenization criteria at the best; (ii) mapping the field associated to an incident Lamb wave scattered by this passive resonator; (iii) finally comparing this “passive” scattered field to the “active” one corresponding to the scattering of the incident Lamb wave by the reso-nator vibrating onto its eigenmode out-of-phase with respect to the incident Lamb wave. Fig. 1 shows the experimental results obtained at step (ii) for silicon pillar 230ìm high and 146ìm in diameter. These structures were elaborated using deep reactive-ion etching technique (DRIE) using Bosch process in a silicon wafer.

Results/Discussion

Along the direction of excitation, at 3MHz, far from the resonance, we see the A0 Lamb mode propagating with a velocity around 2000 m.s-1 and the pillar (at 0 position) vibrating in phase with the wave; the normal displacement on the top was measured to be two times less than the amplitude of the incident wave (Fig. 1a). However, at resonance which takes place at 6MHz, two differences can be observed: first, the displacement on the top of the pillar is seven times more than the one of the incident wave. Secondly, the pillar vibrates out-of-phase for a time much longer than the excitation duration. In addition one can notice the occurrence of re-emitted waves which are out-of-phase with respect to the incident wave (Fig. 1b).

This work is jointly supported by the Agence Nationale de la Recherche and Direction Générale de l’Armement under grant ANR-11-ASTR-01. The samples have been elaborated in MIMENTO facilities at Femto-ST institute in Besançon.

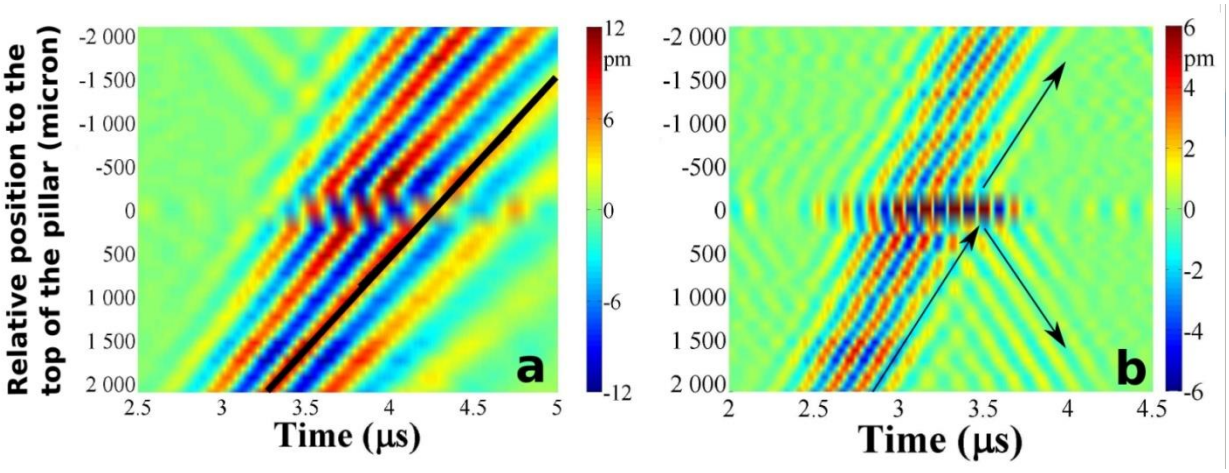

IUS3-E-4

Focusing capability of a phononic crystal based on a hollow metallic structure

Anne-Christine Hladky-Hennion[1], Charles Croënne[2], Jérôme Vasseur[1], Lionel Haumesser[3], Andrew N. Norris[4]; *[1]IEMN (UMR 8520 CNRS), Lille, France, [2]Physics and Materials Science, City University of Hong Kong, Kowloon Tong, Hong Kong, [3]GREMAN (UMR 7347 CNRS), Blois, France, [4]Mechanical and Aerospace Engineering, Rutgers University, Piscataway, USA*

Background, Motivation and Objective

A phononic crystal (PC) made of a network of metallic arms arranged as a regular honeycomb lattice is studied. In the long wavelength limit, the density and bulk modulus of the structure were shown to be equivalent to those of water, and therefore the structure is commonly named metal water structure (MWS). At higher frequency, the metallic structure displays a perfect negative index matching with surrounding water. Thanks to this property, water immersed flat lenses capable of focusing acoustic waves can be realized. The goal of the paper is to present the MWS and to analyse numerically and experimentally the focusing capability of the device.

Statement of Contribution/Methods

Results of the numerical analysis of the MWS spectral properties are first described. Its band structure exhibits an isolated branch, with negative slope and a quasi-longitudinal behaviour, intercepting the water sound line. Index matching is perfect between the MWS and the surrounding external water medium at the frequency corresponding to this intersection point. Moreover, the equifrequency contours are circular indicating isotropy of the phase velocity. Consequently, the MWS is a candidate for negative refraction of acoustic waves. Experimental results unambiguously confirm the focusing capability of the MWS at the operating frequency.

Results/Discussion

The paper presents further analysis of the MWS. First, it is shown that the shape of the interface between MWS and water plays a key role for increasing the energy flux transmitted through the PC. Second, the influences of the location of the source with respect to the lens interface as well as the thickness of the lens are studied. It is shown that these parameters affect the quality of the image. A parametric numerical study is performed with the aim to determine if super-resolution (resolution below half the wavelength) can be achieved with the MWS. Experiments confirm most of the theoretical predictions.

IUS3-E-5

Acoustic metamaterial plate with negative effective mass density

Mourad Oudich[1], Yan Pennec[1], Bahram Djafari-Rouhani[1], Badreddine Assouar[2], Bernard Bonello[3]; *[1]Institut d'Électronique, de Microélectronique et de Nanotechnologie, Université de Lille 1, Villeneuve d'Ascq, France, [2]Institut Jean Lamour, University of Lorraine, Nancy, France, [3]Institut des NanoSciences de Paris, Université Pierre & Marie Curie, Paris, France*

Background, Motivation and Objective

Phononic crystals (PC) are periodic structures designed for acoustic waves manipulation. They can provide band gaps within specific acoustic wavelength ranges, which make them useful for filtering and sensing applications[1]. Recently, new designed PCs called acoustic metamaterials[2] (AMM) attracted more interest as they can provide special behaviors in their effective physical properties like acoustic wave focusing using negative refraction. The new feature of this work is the investigation of an AMM plate with low frequency resonators considered as an effective dispersive medium. We report on a theoretical study of the effective mass density matrix around the resonance frequencies where the gaps are opened.

Statement of Contribution/Methods

The effective medium method[3] is applied to understand the dispersive behavior of a stubbed AMM plate proven to have promising capability for sonic wave shielding and guiding[4]. The AMM is made of soft rubber stubs squarely arranged in a thin aluminum plate. Considering the system as a homogeneous medium for the propagation of elastic waves, the numerically based effective medium model is used to calculate the effective mass density matrix at low frequency range where the wavelengths are large compared to the AMM period. We focused our interest in the stop bands frequencies where divergence of the effective mass density can occur.

Results/Discussion

The calculations results of the effective mass density matrix show that far from the resonant gaps, the diagonal effective mass quantities $\rho 11 = \rho 22$ and $\rho 33$ are close to the average density of the unit cell ρav (see figure 1). However, they become negative in the gaps related to modes with specific polarization: in-plane (blue dots) or out-of-plane displacement field (red dots). Furthermore, we found out that the other matrix density components have zero values except in the vicinity of the resonant frequencies at the gaps edges. Strong anisotropy behavior of the mass density matrix is evidenced for plate waves in the latter frequency ranges.

Acknowledgements. The authors acknowledge the ANR and DGA for their support under the project Metactif, grant ANR-11-ASTR-015.

References

[1] Y. Pennec et al. Surf. Sci. Rep. 65, 229 (2010)

[2] Z. Liu et al. Science 289, 1734 (2000)

[3] R. Zhu et al. Phys. Rev. B 86, 144307 (2012)

[4] M. Oudich et al, New J. Phys. 12, 083049 (2010)

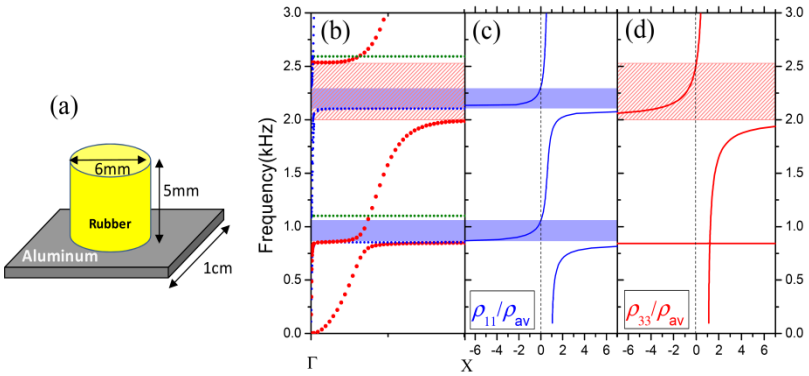

Figure 1. (a) Unit cell of the AMM structure made of cylindrical rubber stubs on aluminum plate of thickness 0.5mm. (b) Band structure where the modes with mainly out of plane displacement components are highlighted in bold red dots and the modes having in-plane dominant displacement plotted with tiny blue dots. Blue and red dashed regions indicate gaps for the modes with dominant in-plane polarization and for those with out-of plane dominant displacement respectively. Dynamic mass densities ρ_{11} (blue solid line) (c) and ρ_{33} (red solid line) (d) are plotted in the frequency range of the band structure. ρ_{av} is the average density of the unit cell calculated by taking into account the rubber and aluminum densities and volumes.

High Frequency Devices and Applications

T2

Tuesday, July 23 2013, 02:00 pm - 03:30 pm

Congress Hallair: **Qifa Zhou**
University of Southern California

IUS5-E-1

A Dual-layer Micromachined PMN-PT 1-3 Composite Transducer for Broadband Ultrasound Imaging

Sibo Li[1], Wenbin Huang[1], Xiaohua Jian[1,2], Yaoyao Cui[2], Xiaoning Jiang[1]; *[1]Mechanical and Aerospace Engineering, North Carolina State University, Raleigh, North Carolina, USA, [2]Medical Imaging Department, Shuzhou Institute of Biomedical Engineering and Technology, Chinese Academy of Sciences, Suzhou, Jiangsu, China, People's Republic of*

Background, Motivation and Objective

Broadband ultrasound imaging including tissue harmonic imaging usually captures acoustic information from the frequency higher than that of transmission waves. It has been widely studied in the imaging of cardiology, bladder and other fluid-filled or cyst structures. Compared to the conventional pulse-echo imaging method, the broadband imaging possesses features in contrast resolution advance and artifacts reduction. However, those benefits require broadband ultrasound transducers (>100%), which are hardly available. Moreover, high sensitivity of transducers is equally important in broadband imaging. On the other hand, PMN-PT 1-3 composite has been increasingly used in medical imaging transducers due to its high piezoelectric coefficients and high electromechanical coupling coefficient (k_t). In this paper, a micromachined PMN-PT 1-3 composite based dual frequency transducer was designed, fabricated and characterized for broadband ultrasound imaging.

Statement of Contribution/Methods

PMN-PT 1-3 composite was fabricated using micromachining technique. Key processes include photolithography, electro-plating, deep reactive ion etching (DRIE), kerf filling and precision lapping. The prepared composite was then characterized by measuring the resonance frequency, dielectric properties and electromechanical coupling coefficient k_t. The dual-layer composite material vibrates in two modes. In the first mode, transmitting at fundamental frequency, both layers are excited at the same time, and in the other mode, only front layer is active serving as a receiver at second harmonic frequency. In this way, the transducer can be used to transmit at 17.5 MHz and receive harmonic echoes at 35 MHz.

Results/Discussion

Micromachined 1-3 composite with kerf size of 5 μm and thickness of 42 μm was fabricated and characterized, showing the resonant frequency of 35MHz and k_t of 0.58. From a KLM model for dual layer configuration, the initial results showed that this dual layer transducer can transmit at 17.5 MHz and receive at 35 MHz. The receiving sensitivity and -6 dB fraction bandwidth are 35 nV/Pa and 81.6%, respectively. The transmitting sensitivity is 60 KPa/V. All above performances hold great potential in broadband ultrasound imaging study. (Figure: Photograph picture of micromachined 1-3 composite and schematic view of the transducer assembly)

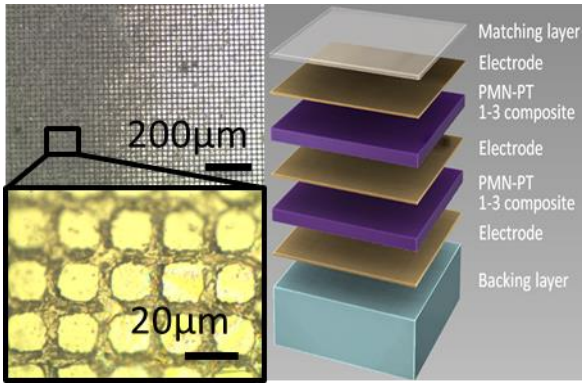

IUS5-E-2

Lead-free high-frequency linear-array transducer (30 MHz) for in vivo skin imaging

Erwan Filoux[1], **Claire Bantignies**[1], Rémi Rouffaud[2], Mai Pham Thi[3], Jean-marc Grégoire[4], Franck Levassort[2]; *[1]R&D, Vermon, Tours, France, [2]GREMAN CNRS7347, Université François-Rabelais de Tours, Tours, France, [3]Research&Technology, Thales, Palaiseau, France, [4]Imagerie&Cerveau INSERM U930, Université François-Rabelais de Tours, Tours, France*

Background, Motivation and Objective

Lead-based piezoceramics and single crystals are extensively used to manufacture high-frequency (HF, >20 MHz) medical transducers with high performances [1, 2]. Due to health and environmental concerns, many countries recently added lead-based compositions to the list of hazardous substances to be substituted by safer materials. For the past ten years, a lot of effort has been put into the development of lead-free piezoelectric materials that provide similar performances and are suitable for industrial manufacturing. Potassium niobate (KN) single crystal was identified as a good candidate because of its high thickness coupling coefficient (up to 65%) and its relatively low mechanical impedance (compared to PZT) that facilitates impedance matching to tissues. This work presents the fabrication of a 30 MHz, linear-array transducer based on a KN, 1-3 piezocomposite. Performances of the transducer were characterized and compared to a PZT-based linear array with similar structure.

Statement of Contribution/Methods

Large polydomain plates, cut at 45° from an as-grown, [001]c-oriented KN crystal, were used to fabricate HF, 1-3 piezo-composites with fine structure. The composites were designed to minimize lateral modes of vibration which can severely degrade imaging performances. Fabrication steps were optimized to achieve a 40 MHz resonant frequency in air with a composite thickness of 69 microns. A single-element transducer was first fabricated to validate the technology and make sure that the performances were suitable for high-resolution skin imaging. A 128-element, linear array was then fabricated with 100 μm pitch and 3 mm elevation aperture. The structure of the transducer (backing, matching

layers, and electric components) was optimized to improve bandwidth and sensitivity. The final probe was integrated in a prototype, real-time, 128-channel scanner [2] to acquire high-resolution images of the human skin in vivo.

Results/Discussion

Results showed that, compared to PZT ceramics, KN single crystals provide low density and high acoustic velocity, both highly desirable for the manufacturing of HF transducers. The central frequency of the linear-array transducer was 30 MHz despite the KN composite being 20% thicker than equivalent PZT-based composites, which makes KN an attractive material to achieve even higher frequencies. The measured thickness coupling factor was over 50 % and the relative bandwidth was about 60%. All 128 elements were active and their sensitivities showed a good homogeneity. A crosstalk between adjacent elements of around 30 dB was measured. High-resolution images of the human skin were acquired and detailed features could be visualized. These promising results should lead to a new generation of "green" transducers that can compete with current state-of-the-art devices.

1. Michau et al., IUS 2004, 898-901
2. Bantignies et al., IUS 2011, 226-229

IUS5-E-3

Micromachined High-Frequency Ultrasound 2-Dimensional Array Transducer

Changgeng Liu[1], Fan Zheng[2], Ruimin Chen[2], Frank Djuth[1], Qifa Zhou[2], Kirk Shung[2]; *[1]Geospace Research, Inc., El Segundo, CA, USA, [2]Biomedical Engineering, University of Southern California, USA*

Background, Motivation and Objective

High frequency two-dimensional array transducers have been studied extensively for applications in real time 3-dimensional ultrasound imaging. In this paper, a miniature, high-frequency, PMNPT composite broadband ultrasonic 2-dimensional array transducer for endoscope or photoacoustic imaging is presented.

Statement of Contribution/Methods

The array has a total 256 elements with the size of 105 μm by 105 μm. The kerf between elements is 5 μm. PMN-PT/Epoxy 1-3 composite was fabricated by photolithography-based micromachining techniques. A PMN-PT single crystal plate was electroplated with Nickel as a hard mask for dry etching. After etching, the etched kerfs were filled with epoxy and the sample was lapped down to the targeted thickness 22 μm. 1500 Å of Cr/Au was sputtered and pattered onto the surface forming 2-D array electrodes. Conductive backing material was then directly applied onto the electrodes and was separated by an insulating material among the elements.

A home-made electric interconnection board and flexible circuits were fabricated for electric interconnection. After alignment under a microscope, the array transducer was assembled with the electric connection board (EIB) and the EIB was bonded to the flexible circuits, which further expand the pitch between electrodes. Finally, the flexible circuits were bonded to PCB boards around the four sides of the transducer. At each side, there was a connector with 64 pins for cable connection to the system.

Results/Discussion

The array transducer was fabricated and was packaged for testing. Pulse-echo response was measured. The central frequency is 50 MHz with the -6 dB bandwidth of 60%. Fig. 1a shows the pictures of an array. Fig. 1b shows the pulse-echo response for a typical array element.

A micromachined high-frequency, PMN-PT composite, ultrasonic 2-dimensional array transducer is presented. Preliminary experimental results are presented. MEMS technology and dry etching technique were demonstrated in fabricating miniaturized complex shape high-frequency ultrasonic array transducers.

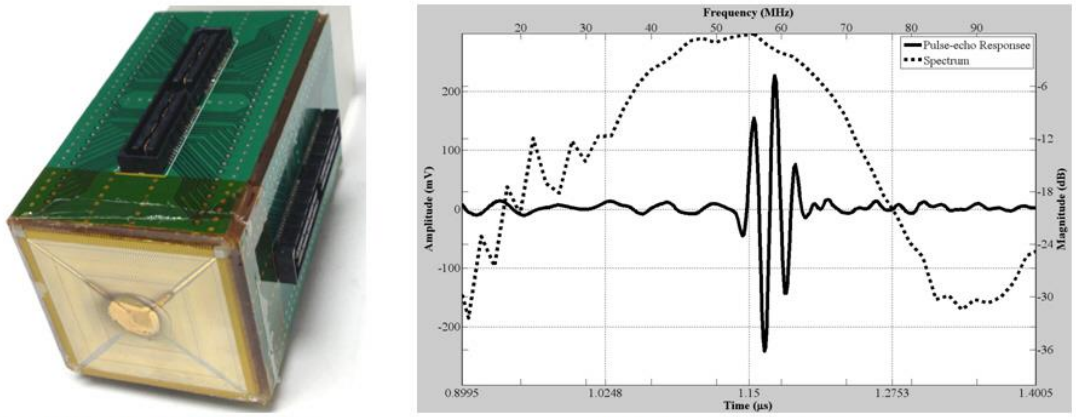

(a) 2-D Array after packaging (b) Pulse echo response

Fig. 1: Picture of the 2-D array transducer and experimental results of pulse-echo response for one element (center frequency is 50 MHz)

IUS5-E-4

Piezoelectric Single Crystal Composite for High Frequency Ultrasound Application

Jian Tian[1], Kevin Meneou[1], Brandon Stone[1], Pengdi Han[1]; *[1]H.C. Materials Corporation, Bolingbrook, Illinois, USA*

Background, Motivation and Objective

Piezoelectric single crystal lead magnesium niobate-lead titanate (PMN-PT) has been successfully commercialized in low frequency medical ultrasound imaging. For high frequency (e.g., >40 MHz) medical ultrasound, application of piezocrystal is delayed largely due to challenges in composite fabrication. As demonstrated in recent research, composite is critical to fully exploit the excellent properties of piezocrystals for high frequency transducers . Optimal design and reliable fabrication of crystal composite will lay the foundation for its application in high frequency ultrasound. In this paper we report design, fabrication and characterization of crystal composite with frequency up to 80 MHz.

Statement of Contribution/Methods

One of the key advantages of piezoelectric composite is the improved electromechanical coupling. To obtain a high coupling factor, crystal pillars in a composite need to have a large aspect ratio. On the other hand, crystal pillars of large aspect ratio present great challenges for subsequent lapping process. We specially designed the composite to optimize coupling while maintaining reasonable machineability. Other factors including pillar geometry, arrangement, crystal orientation, epoxy, and specific transducer requirements were also considered in composite design. Techniques from semiconductor industry such as photolithography and deep reactive ion etching (DRIE) were used to pattern and micro-machine small (<20 um) delicate crystal pillars and narrow kerfs (<5 um). Etched crystal was subsequently filled with epoxy, lapped to final thickness, sputter coated with chromium/gold electrodes and poled. Selected properties of crystal composite were measured on an Agilent 4294A impedance analyzer.

Results/Discussion

Crystal composites with frequency up to 80 MHz were designed and fabricated. Composites with crystal pillars of various aspect ratios were compared. Measurement showed that crystal composite has significantly improved properties over monolithic crystal. In particular, electromechanical coupling factor is up to 0.8 (0.56 for monolithic crystal, 0.5 for PZT ceramics). Higher coupling of crystal composite enables more efficient energy conversion between electrical and acoustic energies. In addition, lower acoustic impedance of crystal composite improves acoustic impedance matching. Such improvements enable broader bandwidth and higher sensitivity for high frequency ultrasound transducers. Initial acoustic test on a 50 MHz crystal composite transducer showed a bandwidth of greater than 80%.

IUS5-E-5

High-Frequency Ultrasonic Transducer for Photoacoustic Application

Qifa Zhou[1], Ruimin Chen[1], Teng Ma[1], Changgeng Liu[2], Joon-Mo Yang[3], Dakang Yao[3], Lihong V. Wang[3], K. Kirk Shung[1]; *[1]Resource Center for Medical Ultrasonic Transducer Technology, Department of Biomedical Engineering, University of Southern California, USA, [2]Geospace Research, Inc., USA, [3]Optical Imaging Laboratory, Department of Biomedical Engineering, Washington University in St. Louis, USA*

Background, Motivation and Objective

Photoacoustic imaging is a novel hybrid imaging technique that combines the virtues of both optics and ultrasound by providing the high contrast of optical imaging, while retaining the high resolution and deep depth imaging capabilities of ultrasonic imaging. Because of these advantages, recently there is much interest in developing novel photoacoustic imaging modalities.

Statement of Contribution/Methods

For photoacoustic imaging, ultrasonic transducer is very critical among all components of photoacoustic imaging system and can determine photoacoustic image quality. Similar to ultrasound imaging, the resolution and imaging depth of photoacoustic imaging is scalable, depending on characteristics of the ultrasonic transducer used, such as center frequency, bandwidth, sensitivity, and shape. However, very few ultrasonic transducers are intentionally designed for photoacoustic application now. In this talk, various high frequency ultrasonic transducers for photoacoustic imaging application will be presented.

Results/Discussion

This talk will discuss high-frequency ultrasonic transducers for three novel photoacoustic imaging approaches: photoacoustic microscopy, photoacoustic endoscopy, and photoacoustic ophthalmoscopy. Piezoelectric single crystal materials with superior performance have been employed in this research. $LiNbO_3$ ring transducer, PMN-PT composite single element transducer and array, PMN-PT needle transducer at 30-60 MHz have been designed and fabricated for each approach. The measured results show that these transducers all had a good bandwidth of over 50 %, and an insertion loss of less than 15 dB. Photoacoustic endoscope imaging systems were developed with these transducers. *Ex vivo* and *in vivo* transesophagus images have been acquired to validate these novel imaging concepts (Nature Medicine, No. 8, 1012). The imaging results strongly supported the enhancements brought by the new transducers and also suggested potential improvements in the future.

Drug and gene delivery

CONGRESS HALL

Tuesday, July 23 2013, 04:30 pm - 06:00 pm

Congress Hallair: **Hairong Zheng**
Institutes of Advanced Technology

IUS1-F1-1

Ultrasound-induced bioorthogonal chemistry in-situ using composite droplets

Marine Bézagu[1], Claudia Errico[1], Victor Chaulot-Talmon[1], Stellios Arseniyadis[1,2], Olivier Couture[1,2], Mickael Tanter[1,3], Janine Cossy[1], Patrick Tabeling[1]; *[1]ESPCI ParisTech, Paris, France, [2]CNRS, France, [3]INSERM, France*

Background, Motivation and Objective

Drug-delivery would undoubtedly become much more powerful if the drug could be prepared at the focus of an ultrasound scanner. In this context, we previously proposed the use of composite droplets comprised of a nanoemulsion of water within a perfluorohexane matrix (4 µm in diameter) for the encapsulation of large payloads, which could be delivered *in-vivo* with an ultrasound scanner (Couture *et al. Medical Physics*, **2011**, 2012). We hypothesized that these droplets could be used to isolate two reactants (**A** and **B**) from one another and deliver them upon vaporization of the perfluorocarbon matrix, thus allowing the *in situ* generation of a new product (**C**) (Figure 1). The steep threshold of release (1.7 MPa PNP at 5 MHz) of these droplets allows the triggering of a chemical reaction with a **high spatial** (mm) and **temporal resolution** (ms).

Statement of Contribution/Methods

The demonstration was achieved by encapsulating a solution of **A** (azidocoumarin) in DMSO into composite droplets of perfluorohexane and releasing the content into the external flow containing **B** (reactive alkyne). Most importantly, the product of the reaction of **A** and **B** is fluorescent (ex: 350 nm, em: 430 nm). The two solutions (**A** encapulsated + **B** in solution) were injected in a microfluidic channel where a 2.25 MHz transducer was focused. A single pulse of 20 cycles was emitted while a camera (10 fps) mounted on a fluorescent microscope (10X, DAPI) recorded the fluorescence induced during the reaction.

Results/Discussion

Within the microfluidic channel, a single acoustic pulse was able to vaporize several droplets, leading to the release of their content in the surrounding medium. As shown below, in the following 100 ms upon release, the fluorescence intensity within the focus zone was multiplied by a factor of 2.9 (**A** + **B**). As the fluorescence is specific to the reaction product, this demonstrates the subsequent formation of the latter after ultrasound release.

In summary, we managed to remotely induce a chemical reaction with ultrasounds by releasing an encapsulated reactant locally into a flow containing its reactive partner. This reaction was limited temporally, following the 10 ms pulse, and spatially, within the focus of the transducer. We expect that such targeted chemistry could lead to the localized release of prodrugs or to the localized production of drugs in-vivo that are either too toxic or unstable to be injected.

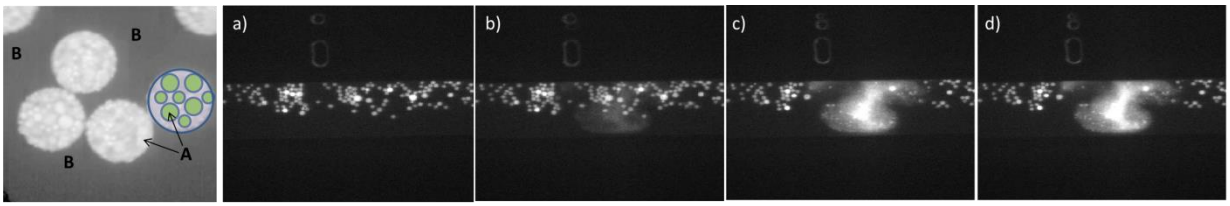

Figure 1. Microscope images of the ultrasound-induced chemical reaction. The release pulse happened between the first and second images (100 ms apart). a) t= −100 ms; b) t= 0, c) t= +100 ms; d) t= +200 ms.

IUS1-F1-2

Targeted Drug Delivery with Focused Ultrasound-Induced Blood-Brain Barrier Opening Using Acoustically-Activated Nanodroplets

Cherry Chen[1], Paul Sheeran[2], Shih-Ying Wu[1], Oluyemi Olumolade[1], Paul Dayton[2], Elisa Konofagou[1,3]; *[1]Biomedical Engineering, Columbia University, New York, New York, USA, [2]Joint Department of Biomedical Engineering, University of North Carolina and North Carolina State University, Chapel Hill, NC, USA, [3]Radiology, Columbia University, New York, NY, USA*

Background, Motivation and Objective

Focused ultrasound (FUS) in the presence of systemically administered microbubbles has been shown to locally, transiently and reversibly increase the permeability of the blood-brain barrier (BBB), thus allowing targeted delivery of therapeutic agents in the brain for the treatment of central nervous system diseases. Currently, microbubbles are the only agents that have been used to facilitate the FUS-induced BBB opening. However, they are constrained within the intravascular space due to their microscale size, limiting the delivery effect at or near the microvessels. In the present study, acoustically-activated nanodroplets were used as a new class of contrast agents to mediate FUS-induced BBB opening in order to study the feasibility of utilizing these nanoscale phase-shift particles for targeted drug delivery in the brain.

Statement of Contribution/Methods

3-kDa dextran was used as the model molecule to confirm BBB opening after FUS was locally applied to target the left hippocampus of C57/BL mice in the presence of both nanodroplets and conventional microbubbles. The acoustic pressure was varied between 0.15 and 0.60 MPa so as to be clinically relevant. The fluorescence intensity increase was quantified to compare the efficiency of FUS-induced delivery dose between these two contrast agents. Passive cavitation detection was used in the attempt to establish a correlation between the amount of dextran delivered in the brain and the acoustic emission recorded during sonication.

Results/Discussion

The BBB opening was consistently achieved using nanodroplets at pressures higher or equal to 0.45 MPa, while the pressure threshold was decreased to 0.30 MPa using microbubbles. The stable cavitation threshold for nanodroplets was found to be 0.48 $kV \cdot s^2$, which was significantly lower than that of microbubbles (2.9 $kV \cdot s^2$). For each acoustic pressure, microbubbles produced greater fluorescence enhancement compared to nanodroplets. The normalized enhancement with pressure followed a linear relationship with

correlation coefficients at 0.76 and 0.94 for nanodroplets and microbubbles, respectively. The dextran delivery achieved using nanodroplets was found to be more homogeneous within the targeted region, and no inertial cavitation was induced even at the highest pressure. Histological evaluation revealed minor damage when the animals were sonicated at 0.60 MPa using microbubbles, corresponding to the onset of inertial cavitation. The present study demonstrated, for the first time, the feasibility of nanodroplet-mediated FUS-induced BBB opening. Our results highlighted the possibility to develop this technology for potential extravascular targeted drug delivery in the brain, extending the delivery region beyond the cerebral vasculature. Future studies are needed to optimize the nanodroplet composition and the acoustic parameters in order to decrease the activation pressure and to achieve higher drug delivery efficiency.

IUS1-F1-3

Enhancements in blood-tumor barrier permeability and delivery of liposomal doxorubicin using focused ultrasound and microbubbles: evaluation during tumor progression in a rat glioma model

Muna Aryal[1,2], Juyoung Park[1], Yong-Zhi Zhang[1], Natalia Vykhodtseva[1], Nathan McDannold[1]; [1]*Radiology, Harvard Medical School, Boston, MA, USA,* [2]*Physics, Boston College, Chestnut Hill, MA, USA*

Background, Motivation and Objective

Due to the heterogeneous permeability of the "blood-tumor barrier" (BTB) along with factors such as increased interstitial pressure, drug efflux pumps and hypoxia, effective drug delivery across the tumor vasculature is often challenging. Focused ultrasound (FUS) combined with microbubbles can enhance the permeability of the BTB in brain tumors, as well as the blood-brain barrier in the surrounding tissue. In this study, dynamic contrast-enhanced MRI (DCE-MRI) was used to characterize the FUS-induced permeability changes of the BTB in a rat glioma model at different times after implantation. These changes were related to the drug concentrations of liposomal doxorubicin (DOX), a chemotherapy agent shown previously to improve survival in animal glioma models.

Statement of Contribution/Methods

9L rat gliosarcoma cells were implanted in the brain in both hemispheres in male Sprague Dawley rats. The rats were randomly divided into three groups, in which one tumor was sonicated at week 1 (n=3), 2 (n=4), or 3 (n=2) weeks after implantation. The non-sonicated tumor served as a control. The sonications were performed at 5-20 locations, depending on the tumor size (0.69 MHz; 0.55-0.81 MPa; 10 ms bursts at 1 Hz for 60s). Each sonication was combined with an IV injection of Definity (10µl/kg) and was preceded by a small dose of DOX (total DOX per animal: 5.67 mg/kg). BTB permeability was assessed before and after FUS using DCE–MRI and pharmacokinetic modeling to estimate the transfer co-efficient (Ktrans) for the MRI contrast agent Magnevist (0.25 mL/kg). The rats were sacrificed one hour after FUS, and DOX concentrations were measured in both tumors via fluorometry.

Results/Discussion

DOX concentrations in the tumors increased by a factor of 1.2 -1.5 in the control tumors as they grew over weeks 1-3. They were enhanced after FUS by a factor of 2.x, 2.x and 2.2 compared to the controls in weeks 1-3, respectively. FUS enhancement of Ktrans by a factor as large as 3 was also observed, but after the first week it was variable, with only minor improvement observed in some cases.

Vascular permeability can increase over time in rapidly growing tumors. While these results are preliminary, they suggest that FUS-induced enhancements in tumor drug delivery are relatively consistent over this time, at least in this tumor model. These results are encouraging, as they suggest that even late-stage tumors can benefit from FUS-induced drug enhancement. Corresponding enhancements in Ktrans were variable after the first week, perhaps reflecting the presence of necrotic areas within the tumor.

IUS1-F1-4

MHz Ultrasonic Drive-In: Localized Drug Delivery for Osteoarthritis Therapy?

Heikki J. Nieminen[1], Alexander Meaney[1], Ari Salmi[1], Ritva Serimaa[1], Edward Hæggström[1]; [1]*Department of Physics, University of Helsinki, Helsinki, Finland*

Background, Motivation and Objective

Of the global population, about 15% suffer from osteoarthritis (OA). To date, there is no therapy that regenerates disrupted articular cartilage (AC). Drug treatments are being developed, however, they are poorly localized [1]. We have shown that 20 kHz ultrasound can deliver particles locally into AC [2]. Here we investigated if MHz focused ultrasound, less prone to cavitation, could enable local delivery of an agent into AC.

Statement of Contribution/Methods

This study is the first to demonstrate that MHz ultrasound can deliver an agent locally into AC.

We prepared one osteochondral plug (dia. = 28 mm) from the femoral condyle of a young cow. The sample was immersed into CT contrast agent (1% w/v, phosphotungstic acid, *i.e.* PTA with 30% v/v ion-exchanged water, 70% v/v ethanol, room temperature) during sonication. Sonication (150 min, f = 1.38 MHz, I_{sptp} = 230 W/cm^2, focus width = 5.9 mm, PRF = 285 Hz, duty cycle = 5.0%, *M.I.* = 2.5) with a custom-made HIFU system (Fig. 1A). The PTA temperature never exceeded 30.0°C. Evaporation was prevented with a polyethene membrane. Following sonication the sample, positioned into a moistened chamber, was imaged with micro-CT (Nanotom 180 NF, GE Sensing & Inspection Technologies, Wunstorf, Germany) (75 kV, 19 µA, voxel size = 38 µm, imaging time = 81 min). PTA delivery was detected based on X-ray attenuation. Adverse structural effects were investigated by light microscopy (angular magnification = 6.5x).

Results/Discussion

At beam focus PTA (2.88 kDa) penetrated 502 ± 14 µm into the cartilage (mean ± *S.E.M.*, n = 5), *i.e.* 45.2% of its thickness (1110 ± 26 µm, n = 5) (Fig. 1B). No PTA delivery was observed outside focus (negative control). Penetration was deeper at the beam center than at the beam perimeter (positive control). Ultrasound did not induce discernible damage to AC. Since at *M.I.* = 2.5 both acoustic streaming and radiation force (tissue vibration) are generated, we propose that the delivery could be caused by these mechanisms.

In conclusion, MHz ultrasound can deliver into AC agents whose passive diffusion speed would otherwise be negligible within the test duration. This technique could allow local and non-destructive delivery of drugs into AC during OA treatment.

[1] S. Abramson, Adv. Drug Deliv. Rev., vol. 58, p. 125–127, 2006.

[2] H. J. Nieminen et al., IEEE Ultrasonics International, Oct 8-10 2012, Dresden, Germany, ID 616.

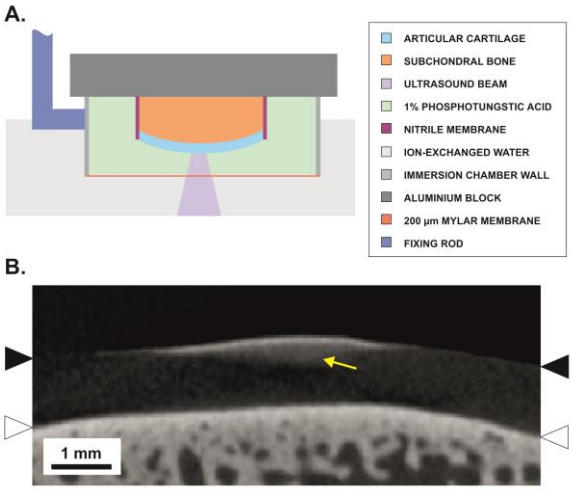

Fig. 1: A. Custom-made MHz setup. B. Contrast-agent was delivered into cartilage only at the sonicated area (yellow arrow). Black and white triangles indicate air-cartilage and cartilage-bone interfaces, respectively.

IUS1-F1-5

Focused ultrasound mediated drug delivery from thermosensitive liposomes

Jean-Michel Escoffre[1], **Anthony Novell[1]**, Mariska de Smet[2], Ayache Bouakaz[1]; *[1]UMR Inserm U930 Imagerie & Cerveau, Université F. Rabelais, France, [2]Eindhoven University of Technology, Netherlands*

Background, Motivation and Objective

Nanomedicine-targeted delivery with non-invasive techniques is required to increase the drug concentration locally and to reduce side effects. Focused ultrasound (FUS) has become a promising strategy for non-invasive local drug delivery by mild hyperthermia. In this study, traditional thermosensitive liposomes (TTSL) encapsulating doxorubicin (DOX) were evaluated for FUS-mediated drug delivery both in vitro and ex vivo.

Statement of Contribution/Methods

U87-MG cell monolayer (in vitro) and spheroids (ex vivo) were incubated to cell medium, free DOX or DOX-loaded TTSL preheated at 37°C and 42°C using FUS at 1 MHz, with a pulse repetition period of 1 ms, 400 cycles per pulse at 1.75 MPa for 10 min. Thermocouple measurements revealed that a volume of 59 mm3 is heated to above 42°C at these applied US settings. Water bath heating was used for comparison. Forty-eight hours later, the DOX uptake and cell viability of U87-MG cell monolayer were assessed by flow cytometry using the native fluorescence of free DOX and MTT test, respectively. The spheroid growth was monitored by microscopy each day after treatment for 11 days.

Results/Discussion

In vitro studies showed quantitative release of the DOX from TTSLs when heated to 42°C with FUS for 10 min, while no release was observed with water bath heating at 37°C. Moreover, we showed that the released DOX from TTSLs by FUS is as efficiently internalized by the glioblastoma cells as the free DOX at 37°C. In vitro therapeutic evaluation showed that the exposure of cell monolayer to FUS-activated TTSLs induced 2.4-fold and 1.7-fold decrease in cell viability compared to control and to TTSLs preheated at 37°C, respectively.

Ex vivo validation showed that after FUS-mediated hyperthermia, preheated TTSLs induced 2-fold decrease in spheroid growth in comparison to the preheated TTSLs at 37°C. In conclusion, our results demonstrate that FUS allows the evaluation of TTSLs and that the FUS stimulation did not modify the properties of the released DOX to be taken up in the cells and spheroids nor its cytotoxicity. This novel therapeutic method has promising features since it can be used to reduce the injected drug dose and to achieve a better therapeutic efficacy. (This work was funded by the European Commission FP7 Program SONODRUGS (NMP4-LA-2008-213706), the ANR project THERANOS - 2010-TECSAN-007 and FEDER PRESAGE 3431 - 35438).

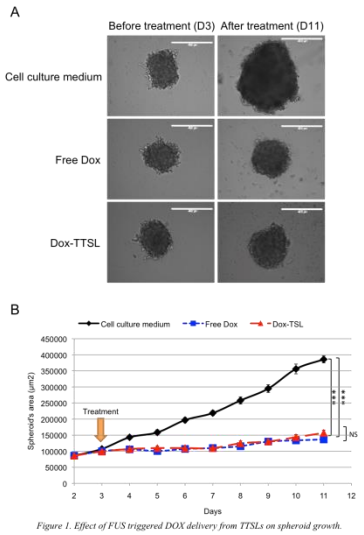

Figure 1. Effect of FUS triggered DOX delivery from TTSLs on spheroid growth.

SPIO-loaded droplets ingested by macrophages for magnetism-assisted drug delivery system

Jia-Jiun Chen[1], Chung-Hsin Wang[1], Chi-Shiun Chiang[1], Chih-Kuang Yeh[1]; [1]*Department of Biomedical Engineering and Environmental Sciences, National Tsing Hua University, Hsinchu, Taiwan*

Background, Motivation and Objective

Ultrasound-triggered acoustic droplet vaporization (ADV) has been confirmed to trigger the perfluorocarbon droplets to liberate encapsulated drugs for tumor therapy. However, the hypoxic regions of tumor impede the drug deposition because of their insufficient vasculatures. Through incorporation of superparamagnetic iron oxide (SPIO) nanoparticles into acoustic droplets, the drug deposition can be further enhanced by magnetism-assisted targeting (MT). Here, we utilized the macrophages that possess homing hypoxia feature to ingest the SPIO-loaded droplets and to investigate the feasibility of using MT to enhance the migration ability.

Statement of Contribution/Methods

The SPIO-loaded droplets were fabricated by sonicating phospholipids with perfluoropentane and aliphatic-terminated SPIO nanoparticles. The SPIO-loaded droplets were incubated with the macrophages for 4 hours, and then, transmembrane cell migration assay was used to assess their migration ability. For performing MT, the culture plate was placed upon a 0.48 T magnet. To assess the SNR enhancement of ADV produced bubbles from the macrophages ingesting SPIO-loaded droplets, B-mode images were acquired by a 7.5 MHz linear array transducer. The vaporization pulses were generated by 2-MHz HIFU with 10-MPa pressure, 3-cycle duration, and PRF of 5 Hz.

Results/Discussion

The macrophages ingested the abundant SPIO-loaded droplets (Fig. a). The macrophages ingesting SPIO-loaded droplets still possessed migration ability (red arrows in Fig. b) and increased 18.74 % migration efficiency after MT. The SNR in B-mode image without and with HIFU insonation were 4.91 dB and 16.66 dB, respectively, showing the SNR enhancement of ADV produced bubbles dramatically increased 11.75 dB (Fig. c).

In this study, the macrophages ingesting SPIO-loaded droplets have been successfully vaporized by HIFU insonation, and their migration ability has also been enhanced through MT. The hypoxia is a major feature of recurrent tumors due to perreceiving an unsuccessful therapy, resulting in the resistance of chemotherapy and radiotherapy. In future, the therapeutic drugs will be encapsulated into SPIO-loaded droplets as a theranostic agent to assess the therapeutic efficiency in recurrent tumors by macrophage-based delivery system in vivo.

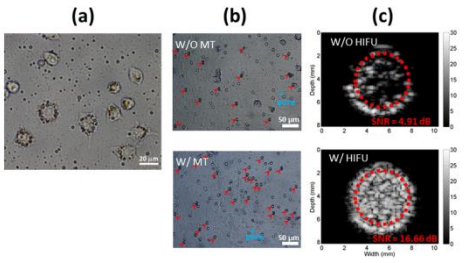

Novel approaches to vector velocity imaging

M4

Tuesday, July 23 2013, 04:30 pm - 06:00 pm

Congress Hallair: **Piero Tortoli**
UniversitàdegliStudi di Firenze

IUS1-F2-1

High Frame Rate Synthetic Aperture Duplex Imaging

Matthias Bo Stuart[1], Borislav Gueorguiev Tomov[1], Michael Johannes Pihl[1], Jørgen Arendt Jensen[1]; *[1]Center for Fast Ultrasound Imaging, Dept. of Elec. Eng., Technical University of Denmark, Kgs. Lyngby, Denmark*

Background, Motivation and Objective

Current implementations of blood velocity imaging use separate acquisition sequences for B-mode and velocity images. This leads to temporal gaps in the acquired data of each type, limits the range of velocities that can be detected, and lowers the achievable frame rates. Using recursive synthetic aperture (RSA) imaging for both B-mode and velocity images allows interleaving the emission events for each imaging modality. This provides continuous data over potentially very long time spans and allows for high frame rate imaging in both modalities. Having continuous data enables detection of a much wider range of velocities than is currently possible. This paper demonstrates duplex imaging using measured data from the research scanner SARUS and offline processing.

Statement of Contribution/Methods

RSA imaging uses a cyclic acquisition sequence. When a given acquisition is made, the low-resolution image contribution produced by the previous instance of this acquistion is replaced by the low-resolution image contribution from the current instance. This produces new images with a frame rate equal to the PRF and can be used for both B-mode and blood velocity imaging. Furthermore, SA imaging allows directional beamforming to be performed. This enables detection of both velocity and angle for blood flow estimation. One emission sequence is defined for each of RSA B-mode and RSA velocity imaging. The emissions from each sequence are interleaved providing continuous data for both modalities at half the actual PRF. A BK Medical 8804 linear array transducer is used with the research scanner SARUS to acquire element data. The B-mode sequence consists of 64 emissions, while the velocity sequence has 8 emissions. The effective PRF of each modality is 5 kHz allowing imaging down to 7.5 cm. Images are made of a recirculating flow rig with laminar flow and a peak velocity of 0.3 m/s. The flow direction is transverse to the ultrasound beam. The cross correlation method is used to estimate both velocity and angle.

Results/Discussion

Ten flow profiles are made covering 80 % of the lumen of the vessel. The mean bias is 0.2 % and the mean relative standard deviation is 4.9 % for the velocity. For the angle, the mean bias is 3.2 degrees and the standard deviation is 1.6 degrees. The strength of the proposed method is that it makes flow data continuously available unlike conventional methods that divide the data acquisition into bigger groups of B-mode emissions and flow emissions. With conventional methods, the operator is required to recognize aliasing and manually adjust the PRF to select the range of velocities to detect. Because data is continuously available with the proposed method, a wide range of velocities can be estimated even at high PRF settings. The method can reduce the operator dependence on flow measurements. Additionally, the proposed method can produce velocity maps at very high frame rates equal to the effective PRF.

IUS1-F2-2

Reconstruction of Flow Velocity inside Vessels by Tracking Single Microbubbles with an MCMC Data Association Algorithm

Dimitri Ackermann[1], Georg Schmitz[1]; *[1]Chair of Medical Engineering, Ruhr-Universität Bochum, Bochum, Germany*

Background, Motivation and Objective

The noninvasive reconstruction of the vascular morphology and the determination of blood velocity are of great importance for the assessment of a tumor therapy. Here, we investigate how to utilize single microbubble tracking from ultrasound B-Mode data for this purpose. In contrast to established PIV (particle image velocimetry) based methods, which are suitable for high particle concentrations developing a speckle pattern, single microbubble tracking aims at determining velocities from low concentrations of floating bubbles. Commonly used tracking algorithms like JPDA (joint probabilistic data association) or MHT (multiple hypothesis tracking) will fail, because of the large number of tracked objects.

Statement of Contribution/Methods

A stochastic approximation of the solution is given by the novel MCMC (markov chain monte carlo) data association algorithm [1], which was implemented and extended by an RTS (Rauch-Tung-Striebel) smoother. The measurements (positions of microbubbles) for target tracking were extracted from B-Mode data by a median filter based background / foreground separation algorithm.

For verification, an experiment with a vessel phantom (1 mm diameter) was set up. A suspension of cyanoacrylate microbubbles (concentration 20/ml) was pumped by a syringe pump (2016, Aitecs, Vilnius, Lithuania) through this vessel. The B-Mode data was acquired with a Vevo 2100 small animal imaging system (Visualsonics, Toronto, Canada) at a frame rate of 255 frames per second.

Results/Discussion

The states (position and velocity) of single microbubbles were estimated by the tracking algorithm. By averaging, a velocity field was calculated from these states (bottom right panel of the figure). The flow direction inside the vessel can be clearly recognized. The histograms of the speed distribution (one count per microbubble and timestep) are shown in the figure (approximate true values: top left panel: 8.8 mm/s; top right panel: 3.5 mm/s; bottom left panel: 1.8 mm/s). The mean values (11.7, 5.56 and 3.5 mm/s) are, up to a bias error (~2 mm/s), in good agreement with the true values.

[1] S. Oh, S. Russell, and S. Sastry, “Markov Chain Monte Carlo Data Association for Multi-Target Tracking,” IEEE Transactions on Automatic Control, vol. 54, no. 3, pp. 481–497, Mar. 2009.

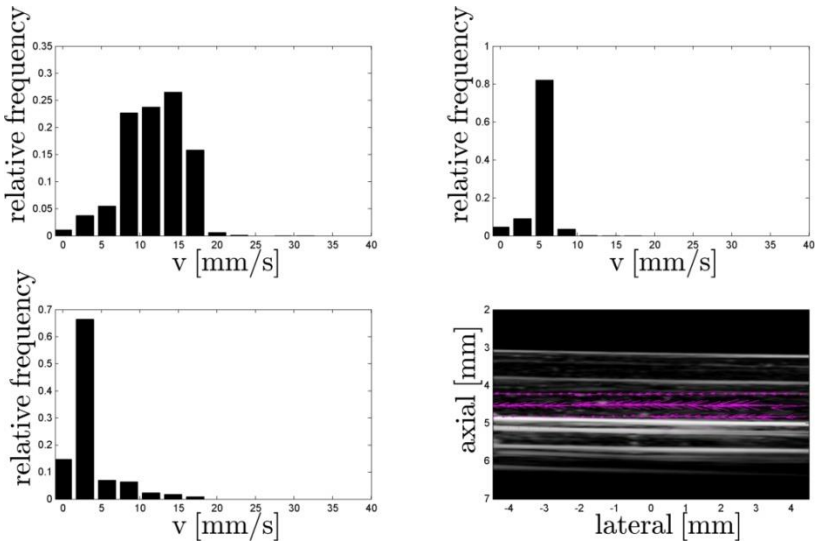

IUS1-F2-3

Spectral velocity estimation in the transverse direction

Jørgen Arendt Jensen[1]; [1]*Center for Fast Ultrasound Imaging, Dept. of Elec. Eng., Technical University of Denmark, Kgs. Lyngby, Denmark*

Background, Motivation and Objective

A method for estimating the velocity spectrum for a fully transverse flow at a beam to flow angle of 90 degrees is described. The approach is based on the transverse oscillation (TO) method, where an oscillation across the ultrasound beam is made during receive processing.

Statement of Contribution/Methods

A fourth order estimator based on the correlation of the received signal is calculated and a Fourier transform of this yields the velocity spectrum. Performing the estimation for short data segments gives the velocity spectrum as a function of time as for ordinary spectrograms, but it also works at a beam-to-flow angle of 90 degrees. The approach is validated using Field II simulations. A 3.4 MHz convex array with lambda pitch is modeled with 64 active elements. The transmit focus is at 200 mm and 2 times 32 elements are used in receive. A dual peak Hamming apodization with a spacing of 96 elements between the peaks is used during receive beamforming for creating the lateral oscillation. Pulsatile flow in a femoral artery placed 40 mm for the transducer is simulated for one cardiac cycle using the Womersly-Evan's flow model.

Results/Discussion

Simulation results are shown in the figure for the new (top) and conventional (bottom) spectrograms. The solid red lines show the true velocity at the vessel center. The bias of the mean estimated frequency is 8.5 % compared to the true velocity and the mean relative std is 12.4 %. This indicates that the new estimation scheme can reliably find the spectrum at 90 degrees, where a traditional estimator yields zero velocity. The estimates degrade, when the angle is different from 90 degrees, but works down to 60-70 degrees. Below this angle the traditional spectrum is best and should be used. The selection between the two spectrograms can be based on the estimated angle at the range gate, which can be obtained using the normal TO estimator without additional beamforming. The conventional approach can automatically be corrected for angles from 0-70 degrees to give a fully quantitative velocity spectrum without user interactions. It should be noted that the velocity range is significantly higher for the new fourth order method compared to traditional estimation, as the lateral wavelength is 2-4 times larger than the axial wavelength. That is beneficial for either keeping the pulse repetition frequency low or for maintaining a high maximum detectable velocity.

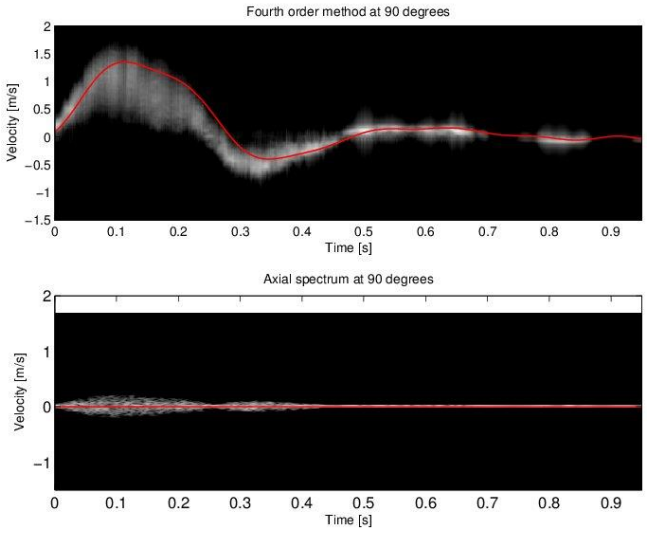

IUS1-F2-4

Real-Time implementation of Vector Velocity Measurement along an M-mode line

Luca Bassi[1], **Stefano Ricci[1]**, Piero Tortoli[1]; [1]*Information Engineering Dept., Università di Firenze, Firenze, Italy*

Background, Motivation and Objective

Standard Doppler ultrasound investigations are limited to detect the axial blood velocity component, as they cannot directly estimate the flow direction. A typical approach for obtaining a 2D velocity vector consists in combining the echoes received from two PW lines investigating the region of interest from different angles. At the Ultrasonics Symposium 2012 we presented a vector Doppler technique that extends the aforementioned method by simultaneously assessing the velocity vectors over 512 points aligned along a line crossing the lumen of the vessel of interest. The method is based on the transmission of plane waves originated from two different sub-arrays of a linear probe and on the directional beamforming of the received echoes along a common line which intersects the vessel. In this work we present the real-time implementation of this vector Doppler method on the research scanner Ula-Op.

.

Statement of Contribution/Methods

Two real-time software modules have been implemented and inserted in the Ula-Op open architecture. One module estimates the mean Doppler frequencies from the 512 beamformed points, while the second module performs the trigonometric combination of the frequencies detected from each sub-apertures to assess the final velocity vectors. The complete sequence of real-time events progresses as follows: 1) Ula-Op fires a steered plane wave from the left sub-aperture and the programmable beamformer focuses along the probe symmetry axis; 2) the module running on the DSP extracts the mean frequencies; 3) points 1-2 are repeated for the right sub-aperture; 4) the latter module on the DSP combines the frequencies and detects the angle and the module for each depth-point; 5) data are communicated to the host PC that shows the results in real-time on a graphical window.

.

Results/Discussion

The US research system Ula-Op was programmed to transmit the plane waves from two 16 mm wide sub-apertures. +12° and -12° steered plane waves were transmitted to produce an overlap region centred at 20 mm depth along the axis of the probe. The real-time vector Doppler modules were activated together with a standard B-mode scanning. A 60 fps on vector Doppler line was achieved simultaneously with 25 fps on the B mode display. Test on in-vitro laminar flows of different rates were carried out in a 8 mm diameter pipe for angles between the pipe and the probe surface in the range 0°~18°. The angle estimation errors were confirmed to be lower than 0.7°, with SD $\leq 2°$. The method, tested on the carotid arteries of volunteers, was able to detect the complex flow configurations present in some part of the cardiac cycle. Movies saved from the real-time display will be presented, that confirm the proposed method suitable to assess in real time the velocity vector profile in large vessels.

.

IUS1-F2-5

Coherent Flow Imaging: A Power Doppler Imaging Technique Based on Backscatter Spatial Coherence

Jeremy Dahl[1], Michael Cook[1]; [1]*Biomedical Engineering, Duke University, USA*

Background, Motivation and Objective

Power Doppler imaging is a commonly used method for the detection of flow in many applications. Although direction of flow is lost with power Doppler, it is valued for its greater sensitivity to slow flow compared to color Doppler imaging. A common problem associated with pulsed Doppler imaging techniques, however, is that the sensitivity to flow is implicitly tied to the wall filter. Pulsed Doppler imaging techniques are degraded when slowly moving tissue or clutter pass through the wall filter and obscure blood flow. We have developed a pulsed Doppler imaging technique similar to power Doppler imaging that is based on the coherence of backscattered blood signal and is less sensitive to clutter-based signals that pass through the wall filter. This technique is an application of short-lag spatial coherence (SLSC) to the detected flow signal in the aperture domain. We have labeled this method coherent flow imaging.

Statement of Contribution/Methods

We acquired individual channel signals from an L12-5 transducer (ATL, Bothell, WA) attached to a Verasonics ultrasound platform (Verasonics, Inc., Redmond, WA) using a conventional pulsed Doppler imaging sequence. Individual channel signals were recorded from a flow phantom at 5 velocities and from *in vivo* carotid arteries. The same channel signals were then used to generate both the power Doppler and coherent flow images.

Results/Discussion

Coherent flow images demonstrated greater sensitivity and smoother flow profiles compared to power Doppler imaging methods. The attached figure compares conventional power Doppler images of the flow phantom to coherent flow images at low and high flow rates. All images are log-compressed and show 20 dB of dynamic range, and the power Doppler images have the thermal noise removed. Like power Doppler imaging, image intensity increased with flow rate in coherent flow imaging. In addition to greater sensitivity, the coherent flow images demonstrated insensitivity to thermal noise, which increases with imaging depth in conventional methods. *In vivo* images of the carotid artery demonstrated similar flow detection improvements as the phantom images. We discuss the implications of this method on current power Doppler imaging applications as well as the impact on wall filters.

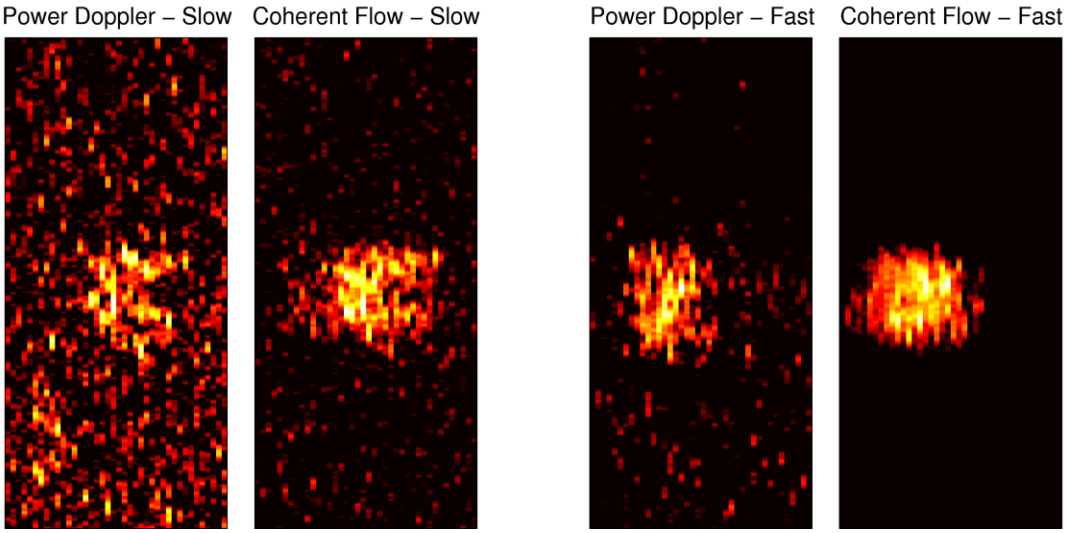

IUS1-F2-6

Frequency-domain high frame-rate 2D vector flow imaging

Matteo Lenge[1,2], Alessandro Ramalli[1], Enrico Boni[1], Hervé Liebgott[2], Christian Cachard[2], Piero Tortoli[1]; *[1]Information Engineering (DINFO), Università degli Studi di Firenze, Firenze, Italy, [2]Université de Lyon, CREATIS ; CNRS UMR5220 ; Inserm U1044 ; INSA-Lyon, Université Lyon 1, France*

Background, Motivation and Objective

Conventional ultrasound flow imaging systems are limited to estimate only the axial component of blood velocity. In this paper, a new method to produce 2D vector Doppler maps is proposed and experimentally tested. Differently from cross-correlation-based methods, local displacements between consecutive high frame rate (HFR) images are estimated in the frequency domain, extending a 1D displacement estimation algorithm so far proposed for elastography applications (doi: 10.1109/TUFFC.2012.2260).

.

Statement of Contribution/Methods

HFR radio frequency images are reconstructed after the transmission of plane waves. Each image is subdivided in partially overlapped matching blocks of about 1.5x1.5 mm^2. After applying an anti-clutter filter, 2D spectra of each block are calculated at a low number (5-10) of frequencies for both axial and lateral directions. Using the DFT shift property, the averaged local displacements in a block are calculated from the spectral phase difference between consecutive frames. Such dis-placements are low-pass filtered in both slow-time and spatial domain and finally converted to 2D velocity vectors. The method has been experimentally tested by using the ULA-OP research system, either in-vitro, in controlled steady laminar flow conditions, and in-vivo, in the carotid arteries and femoral vessels of healthy volunteers.

.

Results/Discussion

2D velocity vectors over extended regions of interest have been obtained in-vitro for different probe-to-flow angles, flow velocities and vessel depths. The errors are calculated on both axial and lateral instantaneous velocity profiles, without averaging over the acquisition, and correspond to a bias below 15% and a standard deviation below 12%. The figure shows the vector map obtained in the common carotid artery and the jugular vein at the systolic peak of the cardiac cycle. Movies will be presented, showing that the HFR approach allows the detection of rapid changes of complex flow, especially close to arterial bifurcations. The algorithm is less computationally expensive than the 2D cross-correlation based method and optimization work is in progress to make it compatible with the requirements of a real-time implementation.

.

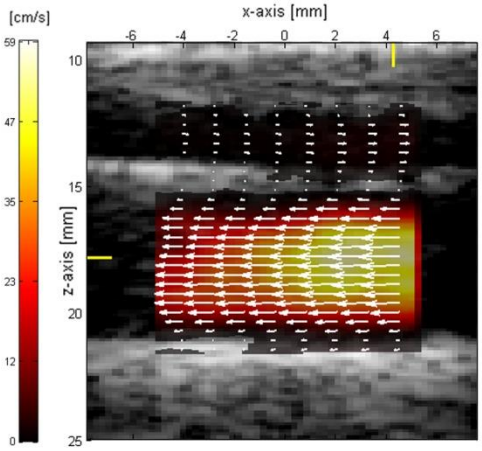

Ultrasound tomography, segmentation, and visualization

M5

Tuesday, July 23 2013, 04:30 pm - 06:00 pm

Congress Hallair: **Hans Bosch**
Erasmus Medical Center

IUS1-F3-1

Evaluation of breast tissue characterization by ultrasound computer tomography using a 2D/3D image registration with mammograms

Torsten Hopp[1], Aurelien Stromboni[1], Neb Duric[2], Nicole V, Ruiter[1]; [1]*Institute for Data Processing and Electronics, Karlsruhe Institute of Technology, Germany,* [2]*Delphinus Medical Technologies, Detroit, USA*

Background, Motivation and Objective

Ultrasound Computer Tomography (USCT) is an upcoming 3D modality for early breast cancer detection. It is expected to provide a quantitative tissue characterization by measuring the sound speed (SOS) and attenuation (ATT) distribution within the breast. For comparison with the standard breast cancer screening method X-ray mammography (XRM), a 2D/3D registration was developed, which serves as basis for the evaluation of the diagnostic value of SOS and ATT. After evaluating the relevance of SOS as quantitative measure in our previous work, now SOS and ATT were combined to classify different types of breast tissue.

Statement of Contribution/Methods

XRMs were segmented into fatty (F) and glandular (G) tissue using semi-automated interactive thresholding. Tumors (T) were annotated manually by an expert using a freehand tool. SOS and ATT volumes were registered to the XRM using our automated 2D/3D registration. Afterwards a maximum intensity projection (MIP) of the registered volume was carried out. For each segmented tissue type in the XRM, the SOS and ATT values at the corresponding region in the MIP were analysed and averaged. A linear support vector machine (SVM) was used to calculate separators between F and G resp. G and T tissue (3 classes) as well as between T and other tissue (2 classes). The diagnostic value of absolute and relative SOS and ATT values to distinguish tissue types was estimated by the training error of the SVMs and compared to earlier results. Semi-transparent overlay images were rendered on mammograms for visualization purposes.

Results/Discussion

Evaluation was carried out with nine datasets. Compared to our previous results using solely SOS, the classification of tissue types, especially of F and G, was considerably improved using a combination of SOS and ATT (3 class error: 7%, Fig. 1, left). In all cases, T could be separated from F and G (2 class error: 0%). The best separation was achieved using the absolute SOS and absolute resp. relative ATT values. Applying the separation to overlay images, F, G and T tissue can be highlighted in the XRMs (Fig. 1, right). To our best knowledge, a quantitative analysis of SOS and ATT in correlation with XRMs has not been carried out before. The method enables comparison of USCT to the standard method XRM. Quantitative information from SOS and ATT can be used in combination with XRM for multimodal diagnosis.

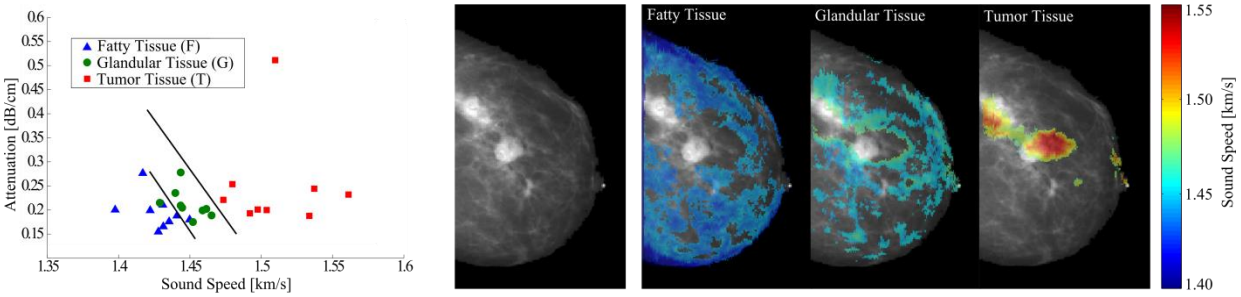

Fig. 1: Scatter plot of average SOS and ATT for fatty, glandular and tumor tissue (left) in the nine datasets. The tissue types were separated using linear support vector machines, indicated by the lines. Semi-transparent overlay of tissue structures separated by SOS and ATT. Within the overlay, the SOS at the particular region is colorcoded.

IUS1-F3-2

First Results of a Clinical Study with 3D Ultrasound Computer Tomography

Nicole Ruiter[1], Michael Zapf[1], Robin Dapp[1], Torsten Hopp[1], Werner Kaiser[2], Hartmut Gemmeke[1]; [1]*Karlsruhe Institute of Technology, Germany,* [2]*Klinikum der FSU Jena, Germany*

Background, Motivation and Objective

A promising candidate for breast cancer imaging is ultrasound computer tomography (USCT). However, current USCT systems are focused in elevation dimension, resulting in a large slice thickness. 3D USCT with a semi-ellipsoidal aperture, emitting and receiving spherical waves, overcomes this limitation by generating full volumes. We designed and built a 3D USCT with a nearly isotropic and spatially invariant 3D point spread function, which is currently tested in clinical study. This work presents first results.

Statement of Contribution/Methods

Ten patients with different lesions were imaged, ranging from benign lesions to malignant tumors. 18 breasts were acquired; for most cases the suspect breast was imaged with 9 Million A-scans (53 GB of raw data) and the contralateral breast with 3.5 Million A-scans (20 GB). A linear frequency coded chirp with a center frequency of 2.4 MHz (50% bandwidth, duration 12.8 µs) was employed.

Transmission and reflection images were derived from the same raw data. Transmission tomography is used to reconstruct speed of sound and attenuation maps. A total variation based numerical minimization algorithm is applied to create (2.7 mm)³ volumes. The reflectivity volumes of the breasts are reconstructed with (0.25 mm)³ resolution using a 3D synthetic aperture focusing technique approach including phase aberration correction based on the speed of sound volumes.

Results/Discussion

The data acquisition could be carried out successfully for all patients with an average imaging time of six minutes per breast. First reconstructions provide promising images. Overlaid volumes of the modalities have qualitative and quantitative information at a glance. In depicted case: tumor which is visible in contrast enhanced MRI can also be clearly seen in USCT images. Further reconstructions and evaluation are currently conducted.

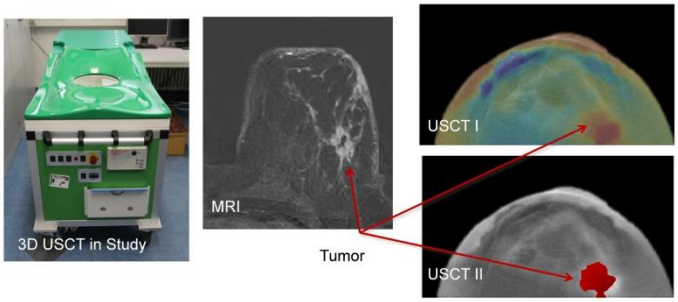

Left: 3D USCT. Center: MRI slice (subtraction image) of a 64 year old patient with large tumor. Right: Overlay of USCT reflectivity and speed of sound (top) and reflectivity overlaid with thresholded combination of attenuation and speed of sound to highlight the tumor (bottom). All transversal slices.

IUS1-F3-3

A new 3D-tomographic ultrasound imaging concept for breast cancer and rheumatoid arthritis diagnostics avoiding water bath techniques

Andreas Koch[1,2], Markus Genser[2], Florian Stiller[2], Reinhard Lerch[2], Helmut Ermert[1,2]; [1]*High Frequency Engineering Research Group, Ruhr-University Bochum, Germany*, [2]*Chair of Sensor Technology, University of Erlangen-Nuremberg, Germany*

Background, Motivation and Objective

Superposition of ultrasound pulse-echo data from multiple aspect angles like 360° around an object (FASC: Full Angle Spatial Compounding) improves image quality, e.g. for breast or finger joint imaging (breast cancer, rheumatoid arthritis). However, FASC systems are mainly realized by linear probes rotating within a coronal plane in a water bath. Drawbacks of this concept are: (1) Increased image quality is confined to 2D; (2) Probe speed in water is limited to avoid object movement caused by water turbulence reducing the number of planes which can be acquired during an appropriate examination time, 3D imaging would be much more time consuming; (3) Water bath technique is critical for clinical environments; (4) Imaging is restricted to body parts immersed in water. For breast imaging this inhibits tumor detection close to the thorax.

Therefore, we present a new approach for 3D-FASC utilizing a mechanical 3D probe combined with a coupling concept which avoids conventional water bath technique.

Statement of Contribution/Methods

An examination couch equipped with a tank and mechanical units for probe movement (Fig. 1) is used as an add-on to a commercial ultrasound scanner (Ultrasonix SonixTouch). Moldings of polyvinyl alcohol (PVA) have been developed for object coupling (female breast, finger joints). For examination, the molding is placed close to the tank surface and the breast/finger is inserted into the molding (Fig. 1). Inside the tank a 3D probe (70° mechanically swept 5 MHz array) is rotated around the molding to acquire rf-data. The probe is tilted by 20° for imaging object areas close to the thorax (breast). Data acquisition is fully automatic including elevational array sweeping, horizontal probe rotation and translation. Data processing steps are: (1) Calibration; (2) Calculation of envelope detected volume datasets; (3) Superposition of all volume datasets.

Results/Discussion

For initial studies the molding located in the water tank with a tissue mimicking breast phantom placed inside was scanned (Fig. 1+2). The 3D-FASC dataset (Fig. 2) shows the great potential of the concept: improved image quality compared to single datasets; successful coupling; phantom parts above the tank can be imaged. Future research will include in-vivo investigation, refraction corrections and development of coupling between probe and molding without any surrounding water.

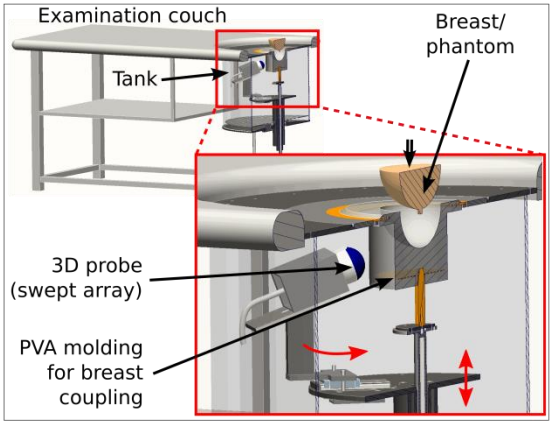

Fig. 1: Cross-section of examination couch equipped with molding for coupling. Breast (tissue mimicking phantom) will be placed into molding. Rf-pulse-echo data aquistion with mechanical 3D probe from 360°.

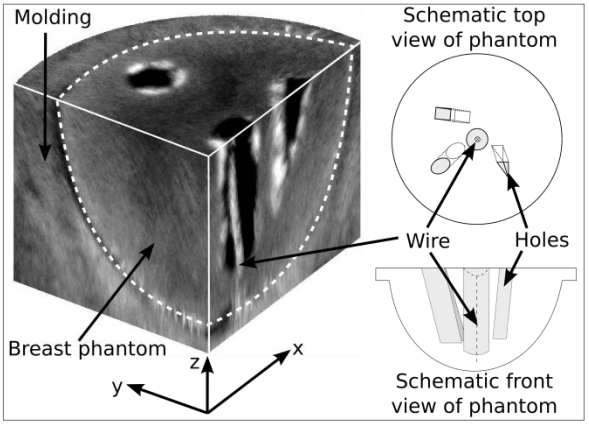

Fig. 2: Three planes (xy, xz, yz) of a 3D-FASC dataset of a tissue mimicking breast phantom are shown. The phantom has 4 holes of different shapes and a tungsten wire was placed into the central hole.

IUS1-F3-4

Simultaneous segmentation of multiple heart cavities in 3D transesophageal echocardiograms

Alexander Haak[1], Gonzalo Vegas-Sanchez-Ferrero[2], Harriet H. Mulder[3], Hortense A. Kirisli[4], Nora Baka[4], Coert Metz[4], Stefan Klein[4], Ben Ren[1], Gerard van Burken[1], Theo van Walsum[4], Antonius F.W. van der Steen[1], Josien P.W. Pluim[3], Johan G. Bosch[1]; *[1]Biomedical Engineering, Erasmus MC, Rotterdam, Netherlands, [2]Image Processing Laboratory, Valladolid University, Valladolid, Spain, [3]ISI, UMC Utrecht, Utrecht, Netherlands, [4]Depts. of Medical Informatics & Radiology, Erasmus MC, Rotterdam, Netherlands*

Background, Motivation and Objective

Three-dimensional transesophageal echocardiography (3D TEE) is an excellent modality for real-time visualization of the heart and monitoring of interventions. However, 3D TEE segmentation is still a challenging task due to the complex anatomy, the limited field of view, and typical ultrasound artifacts. To improve the usability of 3D TEE for monitoring interventions, we propose to segment all cavities within the TEE view with a multi-cavity Active Shape Model (ASM) derived from Computed Tomography Angiography (CTA) in conjunction with a tissue/blood classification based on a Gamma Mixture Model (GMM).

Statement of Contribution/Methods

3D TEE image data of three patients (TEE1, TEE2, and TEE3) were acquired with a Philips X7-2t matrix TEE probe. Tissue probability maps were estimated by a two class (blood/tissue) GMM. A statistical shape model containing left and right ventricle, left and right atrium and aorta (LV, LA, RV, LA, Ao) was derived from CTA scans of 151 patients by Principal Component Analysis. Models from individual cavities (ASM_part: ASM_LV etc.) and of the whole heart (ASM_tot) were generated. First, ASM_tot was aligned with the 3D TEE by indicating 3 anatomical landmarks. Second, pose and shape of ASM_tot were iteratively updated by a weighted update scheme excluding parts outside of the image sector. Third, shape and pose of each ASM_part were initialized based on shape and pose of ASM_tot and iteratively updated in a constrained manner to fit the tissue probability maps.

All 3D TEE sets were manually outlined in multiple short and long axis views by two observers. The mean outline of both observers was compared to the ASM segmentations by calculating average Euclidean point-to-surface distances (P2S).

Results/Discussion

The average inter-observer distance (P2PD) for all 3D TEE is show in the Boxplot. The p2S of the average observer to the initial ASM_tot (Dinit) and to the final ASM_part (Dasm) are shown in the boxplot as well. Dasm of TEE1 and TEE3 are well within the inter-observer range while TEE2 performs worse, which may be due to lower image quality and smaller parts of the cavities within the sector (initial overlap), causing larger uncertainties for the full segmentation. Comparison of the final TEE segmentations to CTA segmentations of the same patients showed good agreement.

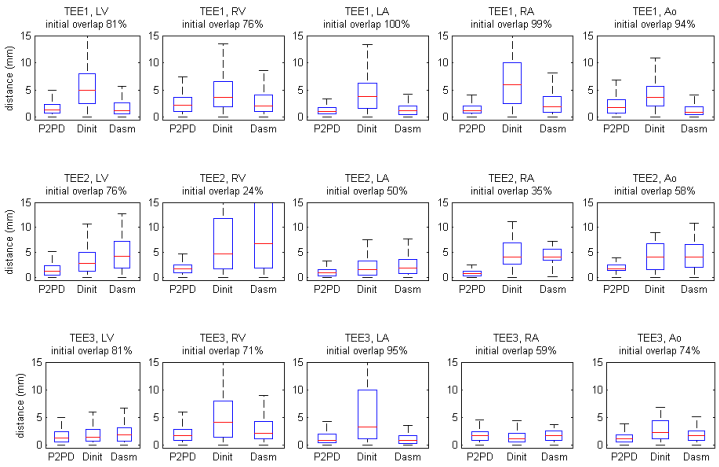

IUS1-F3-5

Hybrid Energy Approach for Real-time B-spline Explicit Active Tracking of Surfaces (heartBEATS)

Daniel Barbosa[1,2], Olivier Bernard[2], Brecht Heyde[1], Thomas Dietenbeck[2], Denis Friboulet[2], Jan D'hooge[1]; *[1]KU Leuven, Leuven, Belgium, [2]CREATIS, INSA Lyon, Lyon, France*

Background, Motivation and Objective

Real-time 3D echocardiography (RT3DE) is now more readily available in daily clinical practice. To date, quantitative analysis of these datasets typically requires significant user interaction, resulting in considerable post-processing times and high intra/inter-observer variability.

The aim of the present study was to develop a fully automatic 3D left ventricle (LV) tracking framework able to deal with the challenging nature of RT3DE data, by combining segmentation and tracking based clues in a hybrid approach, and to assess its performance in the extraction of volumetric functional parameters used in clinical routine.

Statement of Contribution/Methods

To enhance the LV tracking robustness, we couple an affine motion model based on a global optical flow algorithm, estimated on a ROI around the endocardial border, to an existing LV segmentation framework. This is achieved by introducing an energy term that penalizes the deviation to the affine motion. The hybrid nature of this solution can be seen as using the estimated affine motion to enhance the temporal coherency of the segmented surfaces, by enforcing the tracking of consistent patterns, while the underlying segmentation algorithm allows to locally refine the estimated global motion.

24 RT3DE exams were acquired using a Siemens Acuson SC2000 (Siemens Ultrasound, CA). Both end-diastolic and end-systolic volumes were manually contoured by 3 expert sonographers. Their average was taken as reference. The agreement between the automatic tracking results and the reference values was assessed using linear regression and Bland-Altman analysis for end-diastolic, end-systolic and stroke volumes (EDV, ESV and SV), and for ejection fraction values (EF).

Results/Discussion

An overview of the results is given in Table 1. The novel hybrid model improved correlation with the manual references and led to lower bias and tighter limits of agreement. The computation time was around 1s for each 3D frame in a MATLAB implementation.

The hybrid approach showed a significant increase in tracking performance when compared to the underlying pure segmentation solution. Moreover, the proposed algorithm is able to accurately extract relevant cardiac functional indices in a clinical setting, without any user interaction. Finally it opens opportunities to estimate global cardiac strains thanks to underlying affine motion model.

Table 1. LV morphology and global function volumetric assessment using the proposed hybrid algorithm

	heartBEATS		BEATS (pure segmentation)	
	BA (μ ± 1.96σ)	**R**	BA (μ ± 1.96σ)	R
EDV (ml)	**-2.36 ± 23.7**	**0.97**	-3.92 ± 21.6	0.98
ESV (ml)	**-1.06 ± 22.2**	**0.96**	4.97 ± 26.9	0.92
SV (ml)	**-1.30 ± 20.3**	**0.94**	1.05 ± 24.0	0.92
EF (%)	**1.23 ± 12.9**	**0.83**	3.37 ± 15.2	0.78

IUS1-F3-6

In Vivo Needle Visualization in Ultrasound Images Using Tensor-Based Filtering

Bo Zhuang[1], Kris Dickie[1], Laurent Pelissier[1]; [1]*Ultrasonix - Analogic Ultrasound Group, Canada*

Background, Motivation and Objective

Visualizing needles in ultrasound images has always been a challenging task due to their small dimensions and existence of speckle noise inside ultrasound images. Multiple tissue layers above the needle also deflect the sound wave, resulting lower needle signal to noise ratio (SNR). Previously, we have proposed an adaptive spatial compounding method to improve the needle SNR. Phantom studies and in vitro experiments have been conducted. However, one potential problem is multiple tissue layers and other side lobe artifacts have also been enhanced, which creates artifacts.

Statement of Contribution/Methods

In this paper, we propose an improved tensor based filtering method which can enhance the needle visualization while minimizing the tissue layer enhancement. This is achieved through a modified filter structure and Eigen value remapping. Different spatial compounding configurations were also employed to increase the deep angle visualization. In vivo studies were then conducted to verify the performance improvement.

Results/Discussion

The attached two images show the difference between without and with the proposed method in a femoral block. Due to strong layers above the needle, it can not be visualized even it was right inside the ultrasound imaging plane. Through the proposed method, the upper boundary of the needle was enhanced in the right image (shown with an arrow) while other tissue structure remains unchanged. The enhancement of the needle is important since this allows a quick justification on whether a needle is inside the ultrasound imaging plane or not. One interesting issue we found in the enhanced image was the shape of the needle. It was not shown as a straight line even there was no bending involved. This is because of the speed of sound difference in the tissue structure above the needle.

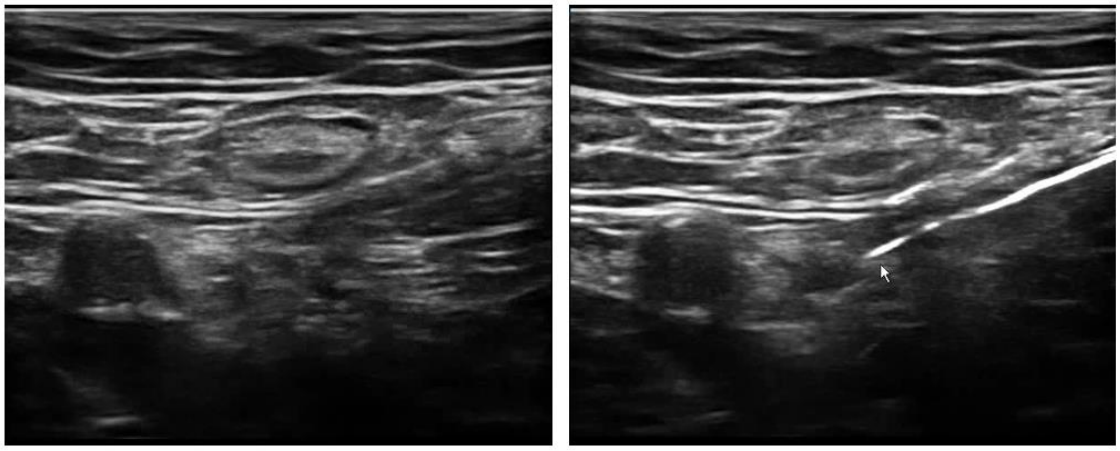

Images without needle enhancement Images with needle enhancement

Ultrasonic Measurements and Characterization

NH

Tuesday, July 23 2013, 04:30 pm - 06:00 pm

Congress Hallair: **Roman Maev**
University of Windsor

IUS2-F-1

GHz Ultrasonics with Arbitrary Code Excitation

Antti I. Meriläinen[1], Ville Kananen[1], Christoffer Fridlund[1], Joona Eskelinen[1], Kay Raum[2], Edward Hæggström[1]; [1]*Department of Physics, University of Helsinki, Helsinki, Finland,* [2]*Julius Wolff Institute, Charité - Universitätsmedizin Berlin, Berlin, Germany*

Background, Motivation and Objective

Coded signals can improve SNR and potentially also imaging in ultrasonic microscopy. Recently we developed a pulse echo module for 200 MHz+ ultrasound microscopy using coded signals (1, 2). I/Q modulation produced high frequency arbitrary signals and RF-switches allowed pulse-echo operation. However, local oscillator crosstalk affected the SNR of the compressed signals. We present an improved design with new RF-components.

Statement of Contribution/Methods

The improved hardware features new components (LTC5598 modulator, AS169-73 switch, MGA-62563 preamplifier) and improved RF shielding. To decrease local oscillator feed-through two up-chirps with different center frequencies were summed into one dual-band chirp without local oscillator frequency component. Arbitrary modulation signals were generated with a programmable function generator (Tektronix TDS3252). Electrical performance was evaluated using a spectrum analyzer (HP8560E) whereas acoustic performance was determined using two different transducers excited with 100-300 MHz and 900-1100 MHz linear chirps (V3989 Panametrics, KSI 525002).

Results/Discussion

Electrical performance: 50 ns switching time from TX to RX, 100-1200 MHz bandwidth, 27 dBm output power to the transducer, and 50 Ohm impedance. Acoustically we achieved 1 GHz+ pulse echo operation (Figure 1 shows a single A-line reflections and spectrum obtained from a sapphire lens). In the 100-200 MHz band we achieved 16 dB SNR increase compared to our earlier results (1). Our most important result is pulse compression in 0.9-1.1 GHz band using arbitrary TX code. This achievement is a first step towards bringing the advantages of coded excitation into GHz ultrasound microscopy.

[1] Meriläinen, A., Fabritius, T., Eskelinen, J., and Hæggström, E., (2013) "Solid state switch for GHz coded signal ultrasound microscopy", Electronics Letter (in press)

[2] Merilainen, A., Fabritius, T., Eskelinen, J., and Hæggström, E., "High frequency broadband arbitrary coded excitation in ultrasound microscopy" IEEE IUS, October 8-10 2012, Dresden, Germany

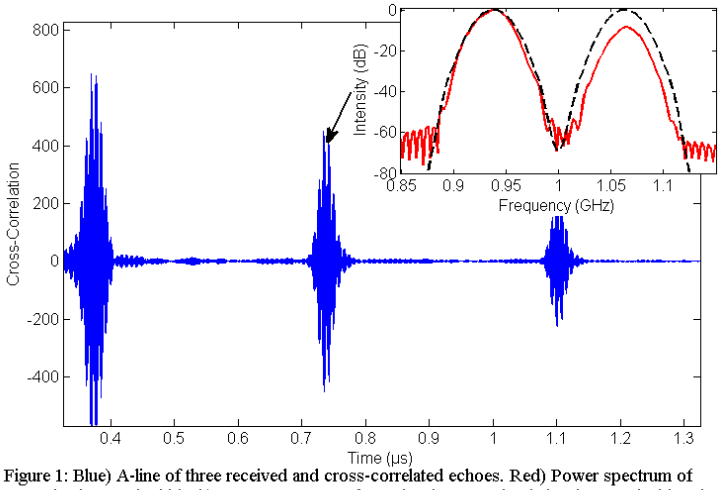

Figure 1: Blue) A-line of three received and cross-correlated echoes. Red) Power spectrum of second echo. Dashed black) Power spectrum of TX signal. Transmitted signal was a dual-band coded chirp (880-995 MHz & 1005-1120 MHz, 450 ns duration.)

IUS2-F-2

Material Microstructure and Ultrasonic Nonlinearity

Aurora Zinck[1], **Sridhar Krishnaswamy**[2]; [1]*Northwestern University, USA,* [2]*Mechanical Engineering, Northwestern University, Evanston, IL, USA*

Background, Motivation and Objective

Ultrasonic nonlinearity measurements have been suggested as an effective tool for the early detection of fatigue damage in metallic structures. However, the correlation between ultrasonic nonlinearity and material damage induced by fatigue or plastic deformation has been observed to be non-monotonic by several researchers including by our group. To clarify the correlation between microstructure and ultrasonic nonlinearity,

the nonlinear ultrasonic behavior of polycrystalline copper is observed at multiple stages of monotonic loading; while under tension, at the loaded peak, while unloading, and after loading. The microstructures corresponding to changes in nonlinearity are examined using hardness testing and transmission electron microscopy. In this system, ultrasonic nonlinearity does not monotonically increase with increased strain and dislocation density. Models that explain drops in nonlinearity are suggested, and destructive testing is used to support findings.

Statement of Contribution/Methods

Several sets of experiments were performed in order to examine nonlinearity through all stages of a sample undergoing uniaxial testing. The first sample was used to observe the nonlinearity parameter β while undergoing loading. Then, a set of 4 samples was used to observe β while relaxing at a constant strain, while unloading, and after unloading. These samples are identified by the maximum strain that they were loaded to: 0.5%, 5%, 12%, and 28%.

The signal used for nonlinearity measurements was generated by a RitecRAM5000 SNAP system. The transducers used to excite transmission of longitudinal waves at a fundamental frequency of 4MHz were 36degree Y-cut lithium niobate crystals mounted in 0.25" high power fingertip transducer casings. In order to ensure repeatable results, a high quality consistent couplant bond was maintained with a sample holder that provided a constant pressure on the transducer, couplant, sample sandwich.

Post-mortem examination of the microstructure was performed using TEM.

Results/Discussion

Based on our set of results, the following conclusions are drawn:

1. Tensile samples under load show a drop in nonlinearity at low strains and an increase in nonlinearity with further increase in strain. This behavior is consistent with what has been recently been observed for edge dislocations in materials with large Poisson's ratios, and is inconsistent with the earlier Hikata model.

2. Acoustic nonlinearity does not monotonically increase with increasing strain or increasing dislocation density in polycrystalline copper

3. In samples that were compared to destructive testing, the lowest nonlinearity is observed at strains where the initiation of low energy dislocation structures occurs. This correlation indicates that β responds to this microstructural change with a drop in value even as the overall dislocation density is monotonically increasing.

IUS2-F-3

Acoustical-Optical Hybrid Microscopy for Characterization of Thin Polymer Films

Hironori Tohmyoh[1], Yuhei Sakamoto[1]; [1]*Department of Nanomechanics, Tohoku University, Sendai, Miyagi, Japan*

Background, Motivation and Objective

This paper describes an acoustical-optical hybrid microscopy which enables us to realize the optical microscope observation of thin polymer film together with the determination of the acoustical properties of the film. Transparent glass plate was first used to observe the acoustic resonant phenomenon at the interface among the water, film and the plate.

Statement of Contribution/Methods

The acoustical properties of polymers have been widely used as a measure to characterize them. Although thin polymer films are difficult to be characterized by the conventional techniques, it is realized by the technique utilizing the acoustic resonant phenomenon[1].

Results/Discussion

The samples were linear low-density polyethylene (LLDPE) films having the thickness (d) of 11.6 and 15.6μm. The LLDPE film was inserted between the water and the glass plate and was vacuum-sealed on the plate. The back-wall echoes of the plate were recorded by the flat-type 100MHz ultrasonic transducer for both cases with and without the films, and their amplitude spectra was obtained (Figure). The ratio of the amplitude spectra in the case with and without the films showed their maximum values at their resonant frequencies. From their characteristics, we determined the acoustic impedance (Z_T), ultrasonic velocity (c_T) and density (ρ_T) of the LLDPE films (Table). Without depending on the film thickness, we were able to accurately determined the acoustic properties of the LLDPE film together with the optical microscope images at the measured area.

The authors would like to acknowledge Prof. M. Saka for his valuable discussions. This work was supported by Grant-in-Aid for Challenging Exploratory Research 24656076 from JSPS.

[1]H. Tohmyoh, T. Imaizumi, M. Saka, Rev. Sci. Instrum., vol. 77, 104901, 2006.

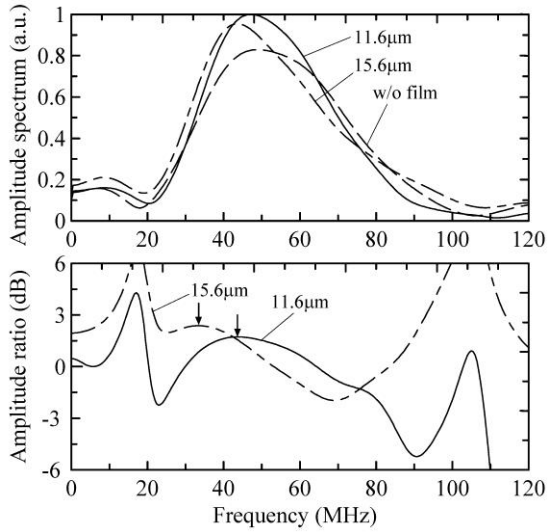

d (μm)	Z_T (MNm^{-3}s)	c_T (×10^3 m/s)	ρ_T (×10^3 kg/m^3)
11.6	1.69 ± 0.01	2.02 ± 0.06	0.84 ± 0.02
15.6	1.77 ± 0.01	2.06 ± 0.03	0.86 ± 0.02

IUS2-F-4

Lorentz Force Hydrophone Prototype Characterization

Pol Grasland-Mongrain[1,2], Jean-Martial Mari[3], Benjamin Roussel[4], Adrien Poizat[2], Jean-Yves Chapelon[2], Bruno Gilles[2], Cyril Lafon[2]; [1]*Université de Lyon, Lyon, France,* [2]*LabTAU, INSERM U1032, Lyon, France,* [3]*University College of London, London, United Kingdom,* [4]*Ecole Normale Supérieure de Lyon, France*

Background, Motivation and Objective

Ultrasound pressure-mapping can be performed with a Lorentz force hydrophone, which is composed of a cylindrical arrangement of magnets around a thin metallic wire. When an ultrasonic wave makes the wire vibrate inside the magnetic field, the Lorentz force induces an electrical current proportional to the integral of ultrasound pressure along the wire. Based on resulting voltages measurements and an hydrodynamic modelling of the phenomenon, 2D pressure field mapping is achieved by performing a tomography through translations and rotations of the wire in the imaging plane. A prototype of such hydrophone has been developed and its characteristics are assessed, with a particular attention put on its resistance to mechanical strain, to determine its potential use in high intensity fields.

Statement of Contribution/Methods

The influence of the wire tension on the signal has been evaluated by increasing its mechanical tension until disruption. Electrical output characteristics were evaluated with an impedance analyser. Ultrasound pressures going from 10 kPa to 10 MPa have been applied on the hydrophone to measure the linearity of signal response. Resistance to cavitation has been evaluated by submitting the wire to a ultrasound-induced cavitation cloud every second during 4800s. Directional response perpendicular to and along the wire direction has been estimated.

Results/Discussion

Results show that the tension of the wire has negligible influence on the signal at ultrasound frequencies which helps validate the hydrodynamic model hypothesis. The impedance has not shown any peak of resonance from 0.15 to 10 MHz with a real impedance between 1 and 60 Ohm and an imaginary between 1 and 4 Ohm. The signal is linear over pressure over the whole tested range and the cavitation had no observable impact on the wire and on the measured signals. The -3dB angular directivity of the response lies between -35° and 35° perpendicularly to the wire and between -20° and 20° along the wire. The directional response can be mainly explained with the Lorentz force expression.

Given these properties, Lorentz Force hydrophones seem particularly suitable for the characterization of high intensity ultrasonic pressure fields.

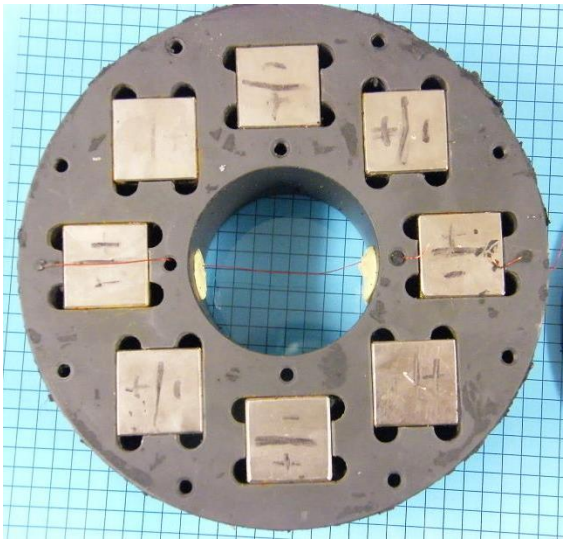

IUS2-F-5

PZT Dust Impact Monitor (DIM) Onboard Rosetta/Philae: Experimental Results and Theoretical Background

Walter Arnold[1,2], Alberto Flandes[3], Attila Hirn[4], Harald Krüger[5], Alexander Loose[5], Matthias Sperl[6], Klaus Jürgen Seidensticker[7], Hans-Herbert Fischer[8]; *[1]Department of Materials, Saarland University, Saarbruecken, Germany, [2]1. Physikalisches Institut, University of Göttingen, Göttingen, Germany, [3]Instituto de Geofisica, Universidad Nacional Autonoma de Mexico, Mexico, [4]MTA Center for Energy Research, Budapest, Hungary, [5]Max-Planck-Institut für Sonnensystemforschung, Katlenburg-Lindau, Germany, [6]DLR, Institut für Materialphysik im Weltraum, Germany, [7]DLR, Institut für Planetenforschung, Berlin, Germany, [8]DLR, Raumflugbetrieb und Astronautentraining, Germany*

Background, Motivation and Objective

The Dust Impact Monitor (DIM) experiment on board the Rosetta spacecraft's lander, Philae, is a cube with three sides covered with piezo-electric sensors (total sensitive area: ~ 70 ccm), aimed at measuring the physical properties of millimetric and sub-millimetric dust particles that move near the surface of comet 67P/Churyumov-Gerasimenko. After being launched in March 2004, the Rosetta spacecraft encounters after a 10.5 years flight the comet 67P in mid 2014 and a landing of Philae is planned for mid-November 2014.

In this work we study the performance of DIM based on impact experiments and compare the measurements with the sensor's expected theoretical behavior as derived from Hertz' theory of elastic impact.

Statement of Contribution/Methods

We present the results of impact experiments performed with spherical particles of different densities and elastic properties. We performed three types of experiment: (a) we analyze the performance of the different sensor sides under identical impacts, (b) we investigate the performance of DIM under impacts of different materials and different impact speeds, and (c) we report on the behavior of the DIM sensor with varying impact angle. We discuss the influence of the microstructure of the PZT sensor on the signal strength and its variation with position of the impacting particles. Our results show that the signal strength and the contact times measured with the DIM PZT sensors can be well approximated by Hertz' contact mechanics.

Results/Discussion

• We present an analysis of the theoretical and experimental performance of the Dust Impact Monitor (DIM) on board the Rosetta lander Philae.

• We show the results of impacts experiments with materials with different elastic properties.

• We derive DIM's dust detection ranges and show that it will cover the bulk of large particles that are expected to follow ballistic trajectories on the surface of comet 67P/Churyumov-Gerasimenko.

IUS2-F-6

MRMR: Multi-Resonance/Multi-Resolution Based Analysis of Ultrasound Waves for High Quality 3D Fingerprint Reconstruction

Aryaz Baradarani[1], Roman Gr. Maev[1], **Fedar Severin[1]**; [1]*University of Windsor, Canada*

Background, Motivation and Objective

Traditional frequency based signal representation intends to decompose signals into superposition of sinusoids. Typically the main assumption in similar approaches is that a given signal is a linear combination of several other base signals. Recently it has been shown that non-stationary signals with oscillations can be well described via a new nonlinear signal decomposition method based on the concept of resonance. The objective of this paper is to introduce the concept of multi-resonance/multi-resolution based technique to analyze acoustic waves in ultrasonic imaging systems. The latter is further investigated to develop an efficient algorithm to construct 3D fingerprint scans.

Statement of Contribution/Methods

In the present work the concept of resonance based signal representation in multi-resolution domain is employed in acoustic image analysis. Since the derivations and implementation are based on the Basis Pursuit theorem, the sparsest possible representation is provided in all subbands of decomposed A-scans obtained through a multi-resonance dual quality-factor representation via a multi-resolution transformation. For the ultrasonic fingerprint scanner proposed technology offers reading of fingerprint patterns along with the sweat porous locations and dermis structure. These additional characteristics, which are unique for any individual, provide outstanding information that can significantly facilitate fingerprint based identification task. Since the mentioned embedded characteristics are located in deeper layers of skin any manipulation on surface of skin cannot cheat the system; thus level of security and identification is guaranteed.

Results/Discussion

The proposed method has been realized in our early prototype of advanced acoustic fingerprint reading system with cylindrical four-lens scanner. Experiments and comparisons with the recent best results in the literature suggest that the proposed multi-resonance/multi-resolution based technique compares favorably to the current amplitude-based practice of acoustic imaging. Furthermore, the effectiveness of the approach is significantly reflected in its capability in detection and extraction of the so-called embedded features, as well as the robust behavior in presence of noise. In view of success of the proposed MRMR method in high quality 3D fingerprint reconstruction it is reasonable to hope for exceptionally high characteristics of disruptive-invariant systems in military applications or biomedical instrumentation.

Memorial Session Ken Lakin

T1

Tuesday, July 23 2013, 04:30 pm - 06:00 pm

Congress Hallair: **Donald Malocha**
University of Central Florida

IUS4-F-1

Kenneth Meade Lakin – A Personal Reminiscence

Robert Addison[1]; [1]*Retired from Rockwell Scientific Company, Thousand Oaks, CA, USA*

Background, Motivation and Objective

Ken was born in Grand Rapids, MI in 1941 and grew up in Portland, MI. After receiving B.S. and M.S. Degrees at the University of Michigan, he arrived at Stanford in the Fall of 1966. My first meeting with him occurred when he was invited to join a group of us who were living in an off-campus apartment in Menlo Park. Most of us were grad students working at Ginzton Lab (the Microwave Lab) on campus.

Statement of Contribution/Methods

Ken's arrival coincided with the start of many new projects in the then new field of surface acoustic waves. His thesis supervisor was John Shaw who assigned him the task of building a surface wave device with amplification. I was working in a different area and was only peripherally aware of the surface wave device problems. Consequently most of my interaction with Ken was via recreational activities and life in the apartment.

Results/Discussion

In this brief reminiscence, I will touch on a few of these activities including backpacking in the Sierras and a memorable sailing trip from Hawaii to California as well as other activities which do not have a direct bearing on his technical achievements. His outstanding technical achievements will be covered in subsequent talks.

_

1967

2010

IUS4-F-2

Memorial: Seminal Papers of Ken Lakin

Rich Ruby[1], Robert Aigner[2]; [1]*Avago Technologies, Menlo Park, CA, USA,* [2]*Triquint, Fl, USA*

Background, Motivation and Objective

Ken Lakin passed away in late 2012. Ken had single mindedly focused on thin film Bulk Wave Devices since the early '80s and continued till his death. His collected papers became the basis of much of today's commercial successes in the area of FBAR and SMR-BAW. This invited paper will highlight some of the most influential works of Ken Lakin. The talk will be broken into two sections; the first part will be a presentation of the early works of Ken that most influenced the FBAR direction, and the second part will cover the later papers of Ken that focused on SMR-BAW.

These works will be placed into context of the times and their value and legacy to FBAR and SMR-BAW production today.

Statement of Contribution/Methods

Results/Discussion

IUS4-F-3

FBAR/BAW in the Context of the Work by Ken Lakin

Rich Ruby[1]; [1]*Avago Technologies, USA*

Background, Motivation and Objective

In the first talk, we reminisced over the life of Ken Lakin, stating with his beginnings in Acoustics. IN the 2nd and 3rd talks we covered seminal papers written by Ken that motivated several companies to start their own programs in FBAR/BAW.

This short 12 minute presentation updates all of us as to where the trail blazed early by Ken has led us today.

The fact is that FBAR/BAW are probably in billions of cell phones and are in almost every country. FBAR/BAW has enabled the wireless industry to create new standards of operating excellence for data rates in Smart phones and tablets. In is in this light that one can truly appreciate the contributions of Ken Lakin.

Statement of Contribution/Methods

Results/Discussion

IUS4-F-4

Complex Peripheral Lamb Modes in FBARs

Jyrki Kaitila[1], John D. Larson III[2]; [1]*Avago Technologies, Germany,* [2]*Avago Technologies, USA*

Background, Motivation and Objective

In FBAR stacks, it is well known that a number of symmetric or anti-symmetric vibration modes, with complex propagation constants, are allowed solutions of the Christoffel equation. Practically, these Lamb wave solutions only use the real part of the allowed propagation constants. However, near some frequencies or cut-off points, the plate wave dispersion relations may require waves with the full complex valued propagation constant to be present in thin film structures.

Statement of Contribution/Methods

Optical interferometry is a tool that has been used for some time to extract the Lamb wave dispersion behavior of piezoelectrically driven thin film resonators (FBARs and SMRs). Typically these measurements are able to only map the real valued dispersion branches. Recently published results have extended the capability also to the evanescent waves (pure imaginary wave number) on the outside area of a plate structure[1].

To the best of our knowledge, these complex wave number modes have not been experimentally detected before. Using the Acoustic Imaging Microscope (AIM) [2], we have recently observed this kind of a wave mode in the active area of a FBAR resonator (dispersion Type II). This mode is located at the periphery of the device, where the active area borders the outside region of the FBAR (see Fig. 1).

Results/Discussion

This paper gives experimental observations of the complex mode, using the AIM and standard S-parameter measurements. Furthermore, a theoretical explanation of the observed behavior, based on the Berlincourt formula for the effective coupling coefficient, is offered. This explanation proposes a laterally "self-confined" mode that arises through the mechanical boundary conditions present at the periphery of the resonator structure.

[1] K. Kokkonen, et. al., "Measurement of Evanescent Wave Properties of a Bulk Acoustic Wave Resonator", IEEE Transactions on Ultrasonics, Ferroelectrics and Frequency Control, vol. 59, p. 557-559, 2012.

[2] K. L. Telschow, et. al., "Full-Field Imaging of Gigahertz FBAR Motion", IEEE Transactions on Ultrasonics, Ferroelectrics, and Frequency Control., vol. 50, p. 1279-1285, Oct. 2003.

Figure 1: Measured displacement amplitude at the edge of the FBAR resonator at 894.5 MHz. Only a small part of the active area of the resonator is shown (from the interior x=0µm, to the edge at x=68µm).

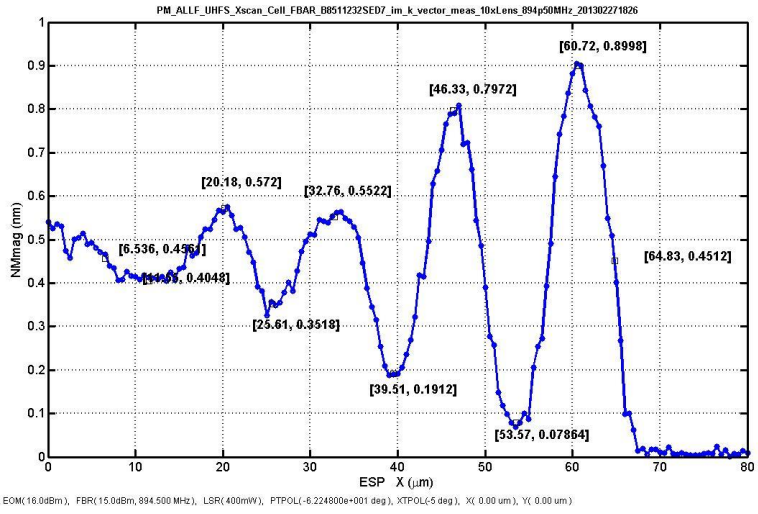

IUS4-F-5

Technology enhancements for high performance BAW duplexer

Alexandre Volatier[1], Gernot Fattinger[1], Fabien Dumont[1], Plamen Stoyanov[1], Robert Aigner[1]; [1]*BAW R&D, TriQuint, Apopka, FL, USA*

Background, Motivation and Objective

These past five years have seen an extremely strong demand of added functionalities on mobile devices materialized by the explosion of the "Smart Phone" market. The growth-rate of RF-BAW technologies has outpaced the growth of the total RF-filter market as a consequence of the fast pace of this market and its hunger for high performance filtering solutions.

Main drivers for technology improvement have been battery lifetime increase (insertion loss reduction), cohabitation of ever increasing number of bands (usually released above 2 GHz or near other band making high selectivity a must-have) as well as reduced available real estate.

Statement of Contribution/Methods

While performance advantages have been the main reason BAW technologies are favored for certain bands such as Band2 (Band25 being undisputed), customers are still expecting improvement from one generation to the next.

In this article we will present the recent improvements in the performance of Solidly Mounted Resonator (SMR) high performance duplexer using Band2 duplexer for illustration purpose.

Results/Discussion

Over the past 4 years insertion loss and rejection steepness were improved dramatically (see table 1). Optimization of resonator intrinsic performance has played obviously a critical role but less expectedly the introduction of new building block (MIM capacitor) capitalizing on SMR technology has proven key for both performances and size reduction. A new design approach based on the selective reduction of the effective coupling coefficient of certain resonators will be presented. We will discuss its impact on slope steepness improvement. The additional flexibility provided by this method enables as well to reduce further the impedance variation presented on the Tx path. This feature is critical to maintain high efficiency and linearity of any Power Amplifier upfront in the transmit chain.

The benefit of this technology enhancement will also be highlighted in term of matching integration and footprint reduction.

Generation year	Max loss (dB) over 1930-1990 MHz bandwidth at room temperature
2009	2.8
2010	2.2
2012	1.9

Table 1: Insertion loss improvement (Band2 Rx) over the past 4 years

Phononic crystals 1

T2

Tuesday, July 23 2013, 04:30 pm - 06:00 pm

Congress Hallair: **Sebastien Guenneau**
Aix-Marseille University

IUS3-F-1

Dispersion Engineering in Aluminum Nitride Phononic Crystal Plates

Bongsang Kim[1], Darren Branch[2], Peggy Clews[2], Janet Nguyen[2], Peter Rakich[3], **Roy Olsson[2]**; *[1]Bosch Research and Technology Center, USA, [2]Sandia National Laboratories, USA, [3]Applied Physics Department, Yale University, USA*

Background, Motivation and Objective

Time domain signal processing circuits including pulse compressors can be realized by engineering dispersion in phononic crystal (PnC) delay lines. We studied the dispersion in PnCs formed from etching circular air holes in a 750 nm thick suspended aluminum nitride (AlN) membrane.

Statement of Contribution/Methods

An image of one of the devices is shown in Fig. 1. Broad band AlN piezoelectric transducers centered at 0.4, 0.8 and 1.2 GHz were placed on either side of a PnC to investigate its dispersive properties. The transducers were spaced 600 µm apart and the length of the phononic crystals were 400 µm. We measured the frequency and time transmission (Fig. 2, 800 MHz shown) and reflection responses of a control device with no PnC (black) and square lattice PnCs with a lattice constant of 5 µm and air inclusion radii of 0.5 (blue), 1.25 (green) and 1.75 (red) µm.

Results/Discussion

Deaf bands in the frequency response were observed, which shifted to lower frequencies as the hole radius was increased. When a broad band pulse was launched from an 800 MHz transducer at time t=0 there was a significant increase in dispersion due to the presence of PnCs. For the control device, the pulse arrives at the receiver 61.5 ns later corresponding to a speed of sound in the AlN plate of 9756 m/s and a wavelength of approximately 12 µm. Enlarging the radius of the air inclusions in the PnC significantly increases the dispersion, increasing both the absolute delay and the received pulse width. We also see an increase in pulse reflectivity for increasing hole radius, indicating that as the material density is reduced, and the dispersion increases, the effective phononic impedance undergoes a significant reduction. This result is a first step in the realization of low Z phononic media and RF time domain signal processing using PnCs.

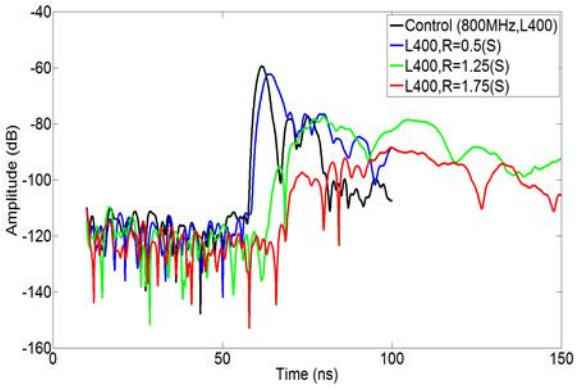

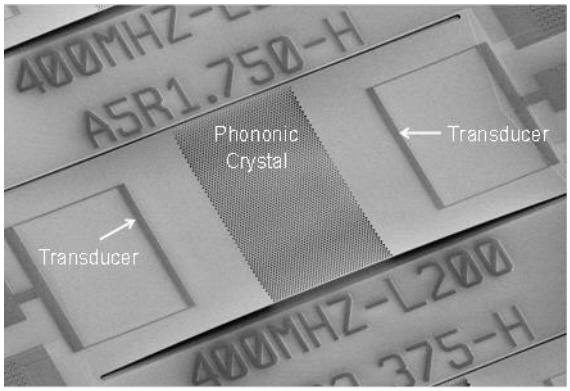

IUS3-F-2

Acousto-Mechanical Tuning of Photonic Crystal Nanocavity Modes

Achim Wixforth[1], Stephan Kapfinger[2], Daniel Fuhrmann[2], Hubert Krenner[2]; *[1]Experimental Physics 1, University of Augsburg, Augsburg, Bavaria, Germany, [2]Experimental Physics 1, Universitaet Augsburg, Augsburg, Bavaria, Germany*

Background, Motivation and Objective

Surface acoustic waves (SAWs) have been proven to be a versatile tool to manipulate charge and spin excitations in low-dimensional semiconductor systems. In particular, in piezoelectric materials such as III-V compound semiconductors the mechanical deformation induced by the SAW is accompanied by larger lateral and vertical electric fields having the same spatio-temporal periodicity. These electric fields strongly interact with mobile charges in the semiconductor whereas the mechanical fields either directly couple to mechanical degrees of freedom or indirectly interact via deformation potential effects.

Statement of Contribution/Methods

In our experiments, the SAW electric fields laterally modulate the confinement potential of a Quantum Well (QW) and spatially separate electrons and holes along the SAW propagation. This is then used to sequentially inject the two carrier species into the confined states of so-called Quantum Dots (QDs) and Quantum Posts (QPs). We show that this acoustic control of the carrier capture provides a novel tuning mechanism for the charge state of QDs and QPs. Moreover, the SAW conveys photogenerated carriers along its propagation direction over macroscopic distances. We employ this charge conveyance effect to inject electrons and holes into individual QDs and QPs remotely located from the excitation laser position, a step towards an acoustically triggered single photon source.

Results/Discussion

The mechanical deformation induced by a SAW can be further employed to deform and break the periodicity in two-dimensional photonic crystal membranes (PCMs). Using finite-difference time-domain (FDTD) simulations we model our experimental SAW-controlled spectral response of the optical mode of a high-Q nanocavity defined in a PCM.

For realistic SAW amplitudes we find a pronounced spectral shift exceeding $\Delta\lambda$=2nm accompanied by only a weak 0.5 times degradation of the Q-factor. In time-integrated experiments, we observe an apparent spectral broadening of the cavity emission consistent with our simulations. In time resolved experiments on such PCMs, however, we in fact observe a mechanically induced periodic modulation of the cavity emission which together with the above mentioned efforts towards a single photon source and employing the Purcell effect will have a large impact on the generation of non-classical light.

IUS3-F-3

Cavity modes and optomechanic interactions in phoxonic crystals

Said El jallal[1], Mourad Oudich[1], **Yan Pennec[1]**, Bahram Djafari-Rouhani[1]; [1]*Institut d'Electronique, de Microélectronique et de Nanotechnologies, Villeneuve d'Ascq, France*

Background, Motivation and Objective

Phoxonic crystals are periodic structures that can exhibit simultaneously phononic and photonic band gaps. When creating defects such as cavities or waveguides inside dual phononic/photonic crystals, it becomes possible to find simultaneously localized phonons and photons in the frequency range of their corresponding band gaps. Then, one can expect an enhancement of the phonon-photon interaction for the purpose of novel optomechanical devices, in particular for the modulation of light by acoustic waves.

Statement of Contribution/Methods

We study the optomechanic interaction in different cavities inserted inside the above crystals, taking account two mechanisms that contribute to the acousto-optic interaction, namely the photoelastic (PE) and moving boundary (MB) effects. The strength of the phonon-photon coupling is evaluated by calculating the modulation of the photonic frequency cavity by the phononic ones. It means that the photonic eigenfrequency is calculated at several selected instants of an acoustic period under the assumption that the acoustic mode strain profile is being frozen at these instants. The strength of the optomechanic coupling is calculated for each phononic and each photonic mode.

Results/Discussion

The results present the contributions of both photoelastic and moving boundaries effects. Indeed, these effects can act differently and their contributions can be in phase and add together or out of phase and partly cancel each other. We present an example of a strip waveguide where phononic and photonic cavity modes can give strong AO coupling. For the modes shown in Figure 1, the total coupling coefficient is evaluated at 2.1 MHz where the MB effect and PE effect contribute additively.

Acknowledgement: This work is supported by the European Commission Seventh Framework Programme (FP7) under the FET-Open project TAILPHOX N° 233833.

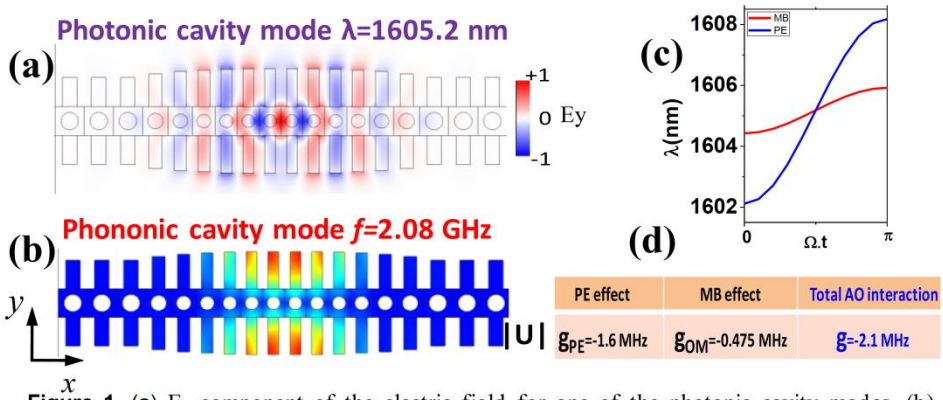

Figure 1. (a) E_y component of the electric field for one of the photonic cavity modes, (b) Amplitude of the displacement field for one of the phononic cavity modes, (c) modulation of the photonic mode by the acoustic cavity mode during half of the acoustic period, (d) the coupling coefficients g_{PE} and g_{MB} for photoelastic (blue solid line) and moving boundaries (red solid line) effects respectively.

IUS3-F-4

Complexity of band structures: Finite element calculation of complex band structures for one and two dimensional phononic crystals

Istvan A Veres[1], Thomas Berer[1,2], Osamu Matsuda[3]; [1]*Research Center for Non-Destructive Testing GmbH, Linz, Austria,* [2]*Christian Doppler Laboratory for Photoacoustic Imaging and Laser Ultrasonics, Linz, Austria,* [3]*Division of Applied Physics, Faculty of Engineering, Hokkaido University, Sapporo, Japan*

Background, Motivation and Objective

Calculations of complex band structures of phononic crystals (PCs) have revealed the presence of complex – evanescent – waves even in complete stop bands. Although, complex dispersion relation of non-periodic systems are well-known, such relations for phononic crystals remained uninvestigated until recently. Evanescent waves describe decaying (spatially varying) fields and are important to fulfill the boundary conditions as transient solutions in non-periodic systems or to predict the spatial-temporal lifetime of elastic waves within complete stop bands in phononic crystals.

Statement of Contribution/Methods

The most popular methods to calculate band structures are probably the plane wave expansion (PWE) technique and the finite element method (FEM). Both methods result in eigenvalue problems, where the unknown frequencies ω are calculated as eigenvalues for a given wave number k. The assumption of a real k in conjunction with Hermitian coefficient matrices leads to real and positive eigenvalues; hence, to real dispersion diagrams. The PWE technique was recently revised to evaluate complex band structures; by solving the governing equation with a given, real frequency ω for the unknown complex wavenumber k. In this work we will apply the finite element method to calculate complex band structures for one and two dimensional PCs.

Results/Discussion

Solution for surface gratings as 1DPCs [Fig.(a)] is discussed with the application of the semi-analytical FEM. The complex band structure is particularly important for such gratings, since the folded surface modes become evanescent beyond the sound cone [Fig.(b)]. This behavior and the complex interconnections between the real propagating modes

are well visible for the presented dispersion relation in Fig.(c). Moreover, an evanescent mode arises within the complete stop band which describes the spatial life time of the elastic waves in the stop band. Calculation of complex band structures with FEM is also extended for 2DPCs with quadratic lattices whereby the different orientations of the wave vector lead to different eigenvalue problems. Orientations parallel to coordinate axes (Γ-X and X-M directions) results in a quadratic eigenvalue problems; the Γ-M direction leads to a quartic eigenvalue problem.

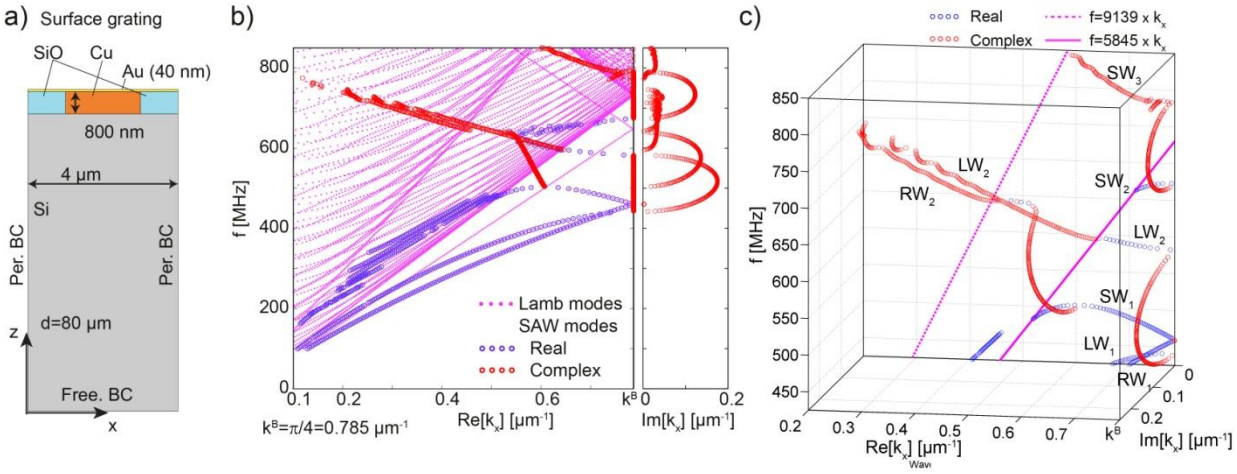

IUS3-F-5

Electric charge band gaps in phononic crystals

Sebastien Degraeve[1], Christian Granger[1], Bertrand Dubus[1], Jerome Vasseur[1], Anne-Christine Hladky-Hennion[1], Mai Pham Thi[2]; *[1]IEMN, Lille, France, [2]THALES Research & Technology France, Palaiseau, France*

Background, Motivation and Objective

Phononic crystals (PCs) present a growing interest in recent years as they can exhibit band gaps where the propagation of elastic waves is forbidden. Bragg band gaps are produced by wave scattering at periodic impedance mismatch zones, while hybridization band gaps are generated by periodic arrangements of resonators. A third kind of band gaps is presented here in the case of a one-dimensional PC exclusively constituted with piezoelectric elements: electric charge band gaps.

Statement of Contribution/Methods

Consider in Fig. 1a a PC made of 14 piezoelectric rods (10 mm length, 5 mm radius) of NCE56 (Noliac) glued and separated by thin brass electrodes. Polarization is alternately oriented along the main axis. Different configurations are studied: electrodes are not connected (Fig. 1a), one out of two electrodes is connected to ground (Fig. 1b), electrodes are alternately connected to ground via an electrical capacitance C1 or C2 (Fig. 1c).

Results/Discussion

Experimental transmissions through the PC presented in Figs. 1a, 1b and 1c are respectively drawn in Figs. 2a, 2b and 2c. These experimental curves are in good agreement with those calculated with the finite element method. Without connections, there is no band gap (Fig. 2a). Although the PC is made of only one material, electrical periodicity exhibits band gaps (Fig. 2b): electric displacement discontinuities induced by the free electric charge contribution occur on the electrodes and electric charge band gaps are produced. Tunability is achieved by using electrical capacitances C1/C2 which set respectively the lower/upper band gap boundary (Fig. 2c). This work is subject to a THALES/CNRS patent and is partially supported by the Agence Nationale de la Recherche with the MIRAGES project ANR-12-BS09-0015 and the region Nord Pas-de-Calais, Fr.

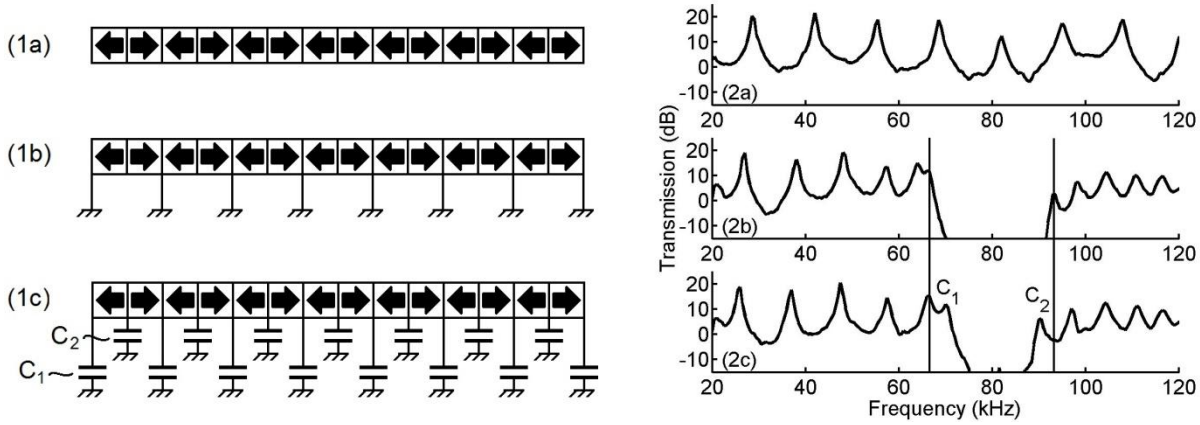

IUS3-F-6

Blazed phononic crystal diffraction gratings with square and hexagonal lattices

Rayisa Moiseyenko[1], JingFei Liu[2], Nico Declercq[2], **Vincent Laude**[1]; *[1]Institut FEMTO-ST, Centre National de la Recherche Scientifique, Besançon, France, [2]UMI Georgia Tech–CNRS, Georgia Institute of Technology, France*

Background, Motivation and Objective

Phononic crystal (PnC) is an artificial 1D, 2D, or 3D periodic structure composed of at least two different materials. Its property of introducing band gaps, i.e., frequency regions for which sound propagation through the structure is forbidden or only evanescent modes are allowed, has attracted much attention for the last 20 years. When the wavelength of an incident plane wave is of the same order as the characteristic obstacle dimensions, the phenomenon of diffraction arises. In general, diffraction in PnC is considered as an undesirable effect and most works consider the low frequency region over which the phononic crystal is non diffracting. Recently, we examined experimentally how the reflected energy distributes among available diffraction orders as a function of frequency [Moiseyenko et al. J. Appl. Phys. 111, 034907, 2012]. It was found that the dispersion of the diffraction orders depends solely on the apparent periodicity of the boundary limiting the PnC, while the diffraction efficiencies depend in a complicated fashion on the phononic properties of the inside of the PnC.

Statement of Contribution/Methods

In this work, we continue the investigation of diffraction by PnC as inspired by blazed optical diffraction gratings. Blazing a grating means shaping the interior of one groove, or periodic unit-cell, so as to maximize diffraction efficiency to a given order. In the context of PnC, blazing can be performed by optimizing the inclusion shape. Furthermore, a problem that exists in acoustics but doesn't for metallic optical diffraction gratings is that transmission never vanishes for natural materials. This problem can be solved for frequencies situated in a phononic band gap, since wave propagation through the crystal can now be prohibited. We have correspondingly fabricated 2D PnC of square-section steel rods in water, for the square and the hexagonal lattices. The design of the PnCs will be discussed, i.e., the choice of lattice parameter and filling fraction so as to obtain maximal diffraction efficiency to a particular order of diffraction.

Results/Discussion

We have experimentally measured the diffraction efficiency as a function of the angle of incidence and of frequency in the MHz range. For each PnC, two versions were considered: one grating with a single line of rods and a PnC grating with 25 layers of rods. An enhanced diffraction efficiency is obtained with the single-line grating, as a result of blazing and acoustic shielding at the fluid-solid interface. It is even observed experimentally that the single layer PnC can yield diffraction efficiencies approaching 100% even away from the strict blazing angle of incidence. When blazing is further combined with a phononic band gap, a maximal experimental efficiency of 98% is achieved at frequencies within the band gap. Results will be shown for the square lattice and for the hexagonal lattice that has the particularity of possessing two different blazing angles.

Beamforming I

Forum Hall

Tuesday, July 23 2013, 01:00 pm - 04:30 pm

Congress Hallair: **Jian-yu Lu**
University of Toledo

IUS1-PB1-1

Clutter Suppression Using Phase Apodization with Cross-correlation in Ultrasound Imaging

Junseob Shin[1], **Jesse Yen[1]**; *[1]Biomedical Engineering, University of Southern California, Los Angeles, CA, USA*

Background, Motivation and Objective

In medical ultrasound imaging with arrays systems, degradation of image quality due to off-axis sidelobes and clutter inherent in conventional delay-and-sum (DAS) beamforming poses a great challenge, particularly in the presence of various levels of phase aberration. In this work, we propose a new beamforming technique called Phase Apodization with Cross-correlation (PAX), similar to Dual Apodization with Cross-correlation (DAX), which utilizes two distinct receive apodizations to introduce grating lobes that help suppress clutter. PAX, however, deliberately introduces and benefits from a parabolic focusing error in the receive delay profiles in clutter suppression. We show in this first study that PAX achieves greater contrast enhancement than does DAX without creating any black artifacts often seen with DAX for strong aberrators.

Statement of Contribution/Methods

Field II simulations of a 3 mm diameter anechoic cyst at a depth of 30 mm were performed. Imaging parameters were chosen to model a 128-element linear array with center frequency of 5MHz, 50% bandwidth, azimuthal element pitch of 308 um. For PAX, a parabolic function with a maximum delay of $3\lambda/4$ a wavelength was used to time-delay individual channel RF data prior to beamforming. The beamformed RF data with parabolic phase apodization were then cross-correlated axially at zero lag with conventional DAS-beamformed RF data. The cross-correlation coefficients were filtered with a median filter of size $2\lambda \times 4\lambda$ to minimize artifacts and then multiplied with DAS-beamformed RF data to suppress sidelobes and clutter. Results were also obtained with DAX for comparison.

Results/Discussion

The beamplots show that effective clutter suppression was achieved with PAX for weak (25ns RMS), medium (35ns RMS) and strong (45ns RMS) aberrators (Figure 1). Particularly, PAX suppressed the high sidelobes that DAX could not by more than 40 dB in all cases. Also, contrast-to-noise ratio (CNR) improvements of 157%, 216%, and 325% were obtained with PAX over DAS for the same three aberrators. In all cases, PAX achieved greater CNR improvements than DAX. In particular, our results suggest that clutter suppression with PAX minimizes black artifacts that DAX suffers from with increased aberrator strength. Experimental work is underway to validate the improvements shown by simulation results.

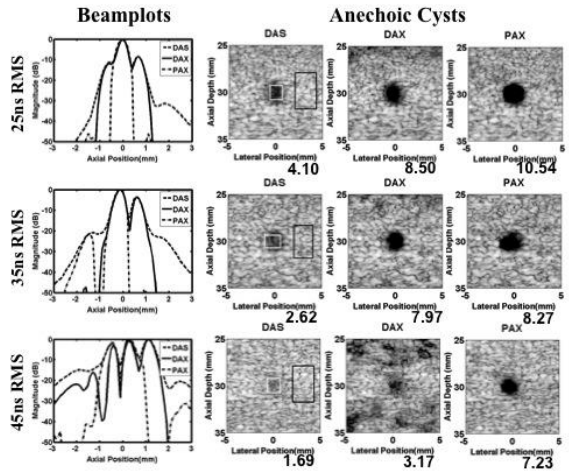

Figure 1: Simulated beamplots and anechoic cysts for different levels of phase aberration. CNR values are shown below each cyst image.

IUS1-PB1-2

Short-Lag Spatial Coherence Combined with Synthetic Aperture Imaging

MooHo Bae[1], Sung-Bae Park[1], Hyun-Woo Jung[1], Mok-Kun Jeong[2], Sung-Jae Kwon[2]; *[1]Hallym Univ., Korea, Republic of, [2]Daejin Univ., Korea, Republic of*

Background, Motivation and Objective

Recently, short-lag spatial coherence (SLSC) imaging has been introduced, which produces images by representing the pixel brightness using the ratio of the coherent sum of signals across an aperture to their incoherent sum, instead of the echo amplitude used in conventional B-mode imaging. This method has great potential for better depicting anechoic cysts thanks to better speckle signal-to-noise ratio (SNR) and contrast-to-noise ratio (CNR). Since SLSC imaging is based on the coherency of received signals, the coherency rapidly decreases as the transmit beam gets wider and thus tends to have poor SNR and CNR outside the focal region, resulting in dark image outside the focal region compared to B-mode imaging and limited depth-of-field. Also, the lateral resolution becomes degraded outside the focal region because the effective receive aperture size of SLSC imaging is small.

Statement of Contribution/Methods

The above problems can be improved directly by placing multiple transmit focal points on a scan line. However, this reduces the frame rate. To prevent this, we propose combining synthetic aperture imaging (SAI) with SLSC. SAI makes it possible to place focal points at virtually all the pixels in an image without reducing the frame rate, thus making the characteristics of SLSC image consistent along the depth.

Results/Discussion

The efficacy of the proposed method is verified through Field II simulation and off-line processing of actual echo signals acquired with an ultrasound scanner from experiments on a tissue mimicking phantom. For simulation, a 5.71 MHz linear probe and a 9 mm x 60 mm phantom were modeled. Figs. 1(a), (b), and (c) are the reconstructed B-mode, SLSC, and combined SLSC-SAI images, respectively. The CNR for cyst B has the same value of 2.95 in both (b) and (c) as it is close to the transmit focal point, whereas that for cyst A is 1.2 in (b) and 1.8 in (c), and that for cyst C is 1.93 in (b) and 2.59 in (c). This clearly demonstrates that (c) is a significant improvement over (b). Also, the point targets in (c) show much more consistent lateral resolution along the depth than in (b). Figs. 1 (d), (e), and (f) are the reconstructed images of an actual test phantom (CIRS model 040), which correspond to (a), (b), and (c), respectively. The same improvement has been achieved as the simulation results. Furthermore, there is no decrease in frame rate because SAI is used.

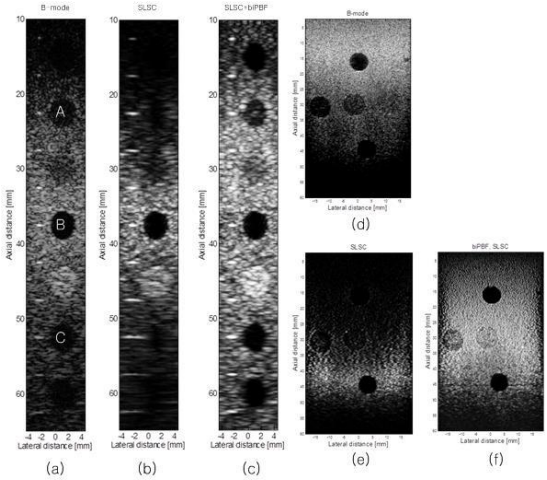

Fig. 1. Comparison of the reconstructed images

IUS1-PB1-3

Clutter Reduction in Plane Wave Synthetic Aperture Imaging

MooHo Bae[1], Sung-Bae Park[1], Hyung-Jun An[1], Deokgon Kim[2], Sung-Jae Kwon[3]; *[1]Hallym Univ., Korea, Republic of, [2]Samsung Medison Co. Ltd., Korea, Republic of, [3]Daejin Univ., Korea, Republic of*

Background, Motivation and Objective

A synthetic aperture imaging (SAI) method which uses a steered plane wave (PW) is advantageous in that the resolution can be improved by covering a wide area with a small number of transmissions, and that the calculation of focusing delay for transmit focus synthesis is relatively simple. Through simulation studies, we found, however, that the clutter level of this method is higher than that of the SAI using virtual sources positioned in the imaging plane (we call this biPBF), and we guess that the main cause is that the area covered by the PW is wider than that of the biPBF so that the scattering occurs over a large area, and the received signal basically has higher clutter levels than the biPBF case. A straightforward solution to this problem would be to use narrower PWs. In this case, however, the number of transmission needs to be increased to cover the same area, resulting in a lowered frame rate.

Statement of Contribution/Methods

In order to maintain the same frame rate while reducing the clutter level, we transmitted simultaneously two PWs that are spatially separated, and furthermore, we used an up-chirp signal for one PW and a down-chirp signal for the other PW, in the same frequency band to minimize the crosstalk between the two PWs, while fully utilizing the probe bandwidth. Despite these measures, we still observed the crosstalk of these signals which resulted in axial direction artifacts of around -50 dB in the reconstructed image as these two chirp signals are not completely orthogonal and there are some leakage waves due to the fringing effect of the transmit aperture. This problem has been solved by applying transmit apodization to reduce the fringing effect of the transmit aperture.

Results/Discussion

The efficacy of the proposed method is verified through simulation using Field II. A 9 MHz linear probe was modeled, and point targets were placed at intervals of 5 mm and 14 mm in the axial and lateral directions, respectively. Figs. 1(a), (b), and (c) show the reconstructed images using the full aperture PW transmission, half aperture PW transmission with up-chirp and down-chirp signals, and transmit-apodized half aperture PW transmission with up-chirp and down-chirp signals, respectively. Fig. 1(c) clearly shows that both the clutter level and axial artifacts are substantially reduced.

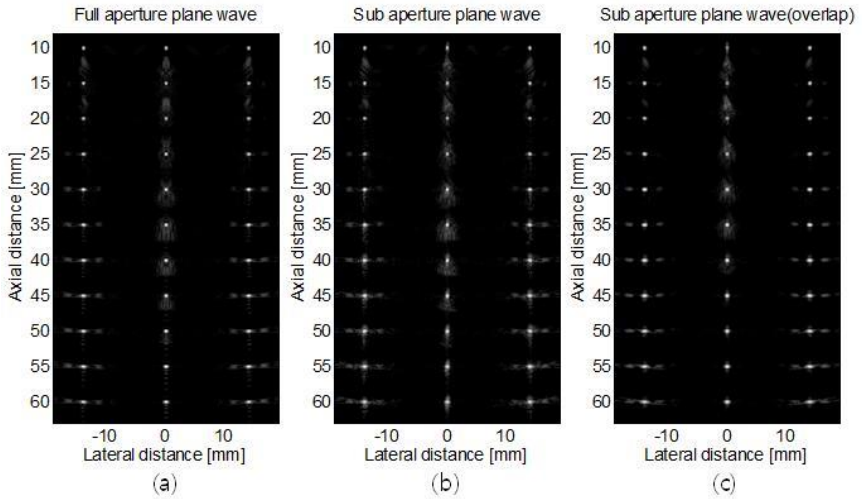

Fig. 1. Comparison of the reconstructed images.

IUS1-PB1-4

Adaptive beamformer with accurate intensity-estimation technique for high-range-resolution vascular ultrasound imaging

Hirofumi Taki[1], Takuya Sakamoto[1], Kousuke Taki[2], Makoto Yamakawa[3], Tsuyoshi Shiina[4], Motoi Kudo[2], Toru Sato[1]; *[1]Graduate School of Informatics, Kyoto University, Kyoto, Kyoto, Japan, [2]Department of Anatomy, Shiga University of Medical Science, Otsu City, Shiga, Japan, [3]Advanced Biomedical Engineering Research Unit, Kyoto University, Japan, [4]Graduate School of Medicine, Kyoto University, Japan*

Background, Motivation and Objective

For the early detection and diagnosis of cardiovascular disease, it is desirable to improve the range resolution of the vascular ultrasound imaging. The employment of frequency domain interferometry (FDI) with the Capon method largely improves the range resolution of ultrasound vascular imaging; however, this methodology often underestimates the echo intensity. In this paper, we propose a compensation method to improve the estimation accuracy in echo intensity acquired by the FDI imaging method with the Capon method.

Statement of Contribution/Methods

Since uniform frequency averaging cannot suppress the correlation between echoes perfectly, the conventional FDI imaging method often underestimates the echo intensity. When the correlation between echoes is suppressed perfectly, the covariance matrix after frequency averaging becomes a Toeplitz matrix. We thus propose a technique that enforces a Toeplitz form on the covariance matrix after frequency averaging. The covariance matrix after the proposed frequency averaging has the identical value in each diagonal line, where the value is calculated by the average in the diagonal direction, as shown in Fig. 1. We call this technique Toeplitz frequency averaging (TFA).

Results/Discussion

The proposed method has the spatial resolution of 0.05 mm with the average estimation intensity error of 0.15 dB, where we employ an ultrasound pulse of 7.5 MHz center frequency. We have applied the proposed method to a swine femoral artery in vitro and a human carotid artery in vivo, as shown in Fig. 2. These results show that our method greatly improves the accuracy in echo intensity estimation. This work indicates the proposed adaptive beamforming technique has high potential to increase the estimation accuracy of echo intensity in ultrasound imaging.

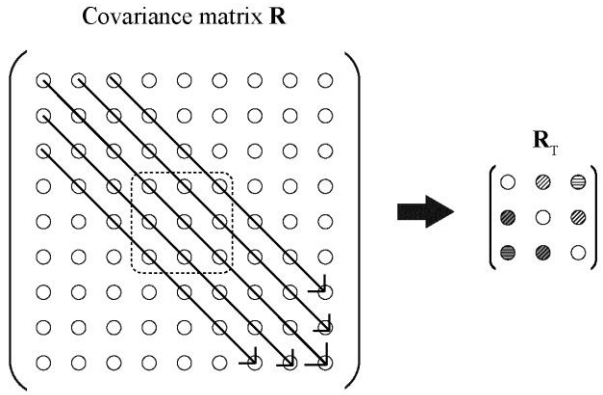

Fig. 1. Covariance matrix after Toeplitz frequency averaging.

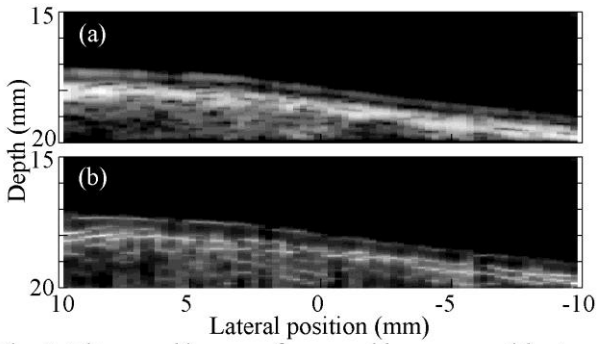

Fig. 2. Ultrasound images of a normal human-carotid-artery in vivo at the posterior wall acquired (a) using a B-mode imaging method and (b) the FDI imaging method with the compensation based on Toeplitz frequency averaging.

IUS1-PB1-5

Theoretical analysis of ultrasound signal coherence in adaptive beamforming

Shougang Wang[1], Sheng-Wen Huang[1], Jean-Luc Robert[1], Sanghamithra Korukonda[1], Francois Vignon[1], Emil Radulescu[1]; *[1]Philips Research North America, Briarcliff Manor, NY, USA*

Background, Motivation and Objective

Adaptive beamforming can help suppress sidelobes and reduce artifacts caused by aberration etc. Thus, the ultrasound image quality can be improved by enhancing the spatial and contrast resolution. This article conducts a theoretical analysis of coherence factor and two-aperture coherence for the purpose of optimum parameters searching.

Statement of Contribution/Methods

A generalized mathematical formulation was derived in an analytic form. The theoretical model was based on the linear description of ultrasound imaging at the transmit and receive focus of the transducer. The speckle spectra for a dot embedded in a homogeneous speckle environment and an anechoic region were modeled with the following assumptions. 1. In the region of interest, there are a large number of random scatterers with their reflection strength following a Rayleigh distribution and the phase following an even-distribution in the range of [-pi, pi]. 2. Each scatterer is independent of any other scatterer. There is no cross-interference between any scatterers.

Results/Discussion

The experimental results with phantom and the theoretical simulation of the coherence factor of a cyst is shown in Fig.1. The two curves agrees with each other. Plots of a dot in a homogeneous speckle environment for different aperture configuration are shown in Fig. 2. Patch refers to the number of elements per group in an Odd/Even periodic manner for a transducer aperture. In conclusion, the established theoretical analysis matches well with the experimental results, within 12% error for homogeneous speckles. The theory can be used for speckle analysis such as dots, homogeneous, hyperechoic and anechoic regions. The analysis gives good illustration of transducer bandwidth effect, with aberration under consideration for further study.

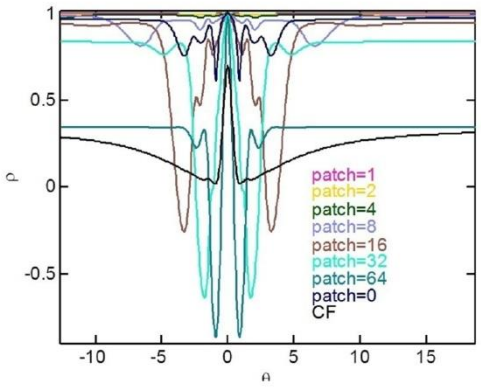

Fig. 2: Plots of Odd/Even Aperture Coherence (OEAC) coefficient of a dot in homogeneous speckle environment for different patch size. Black line is coherence factor (CF) for comparison.

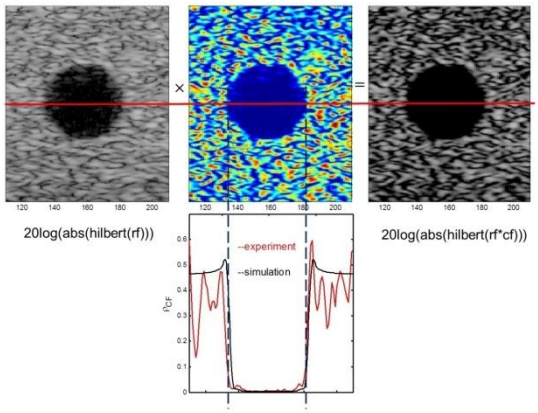

Fig. 1: B mode image (top left), coherence factor map (top middle) and B mode image after apply the coherence factor for adaptive beamforming (top right). Bottom plot shows the comparison of the experimental data and the simulation results at the position of red line.

IUS1-PB1-6

Application of Dual Apodization Cross-correlation to Beamforming by Spatial Matched Filtering for Enhanced Image Contrast

Yuling Chen[1], **Jesse Yen[1]**; *[1]Biomedical Engineering, University of Southern California, Los Angeles, CA, USA*

Background, Motivation and Objective

Through suppressing sidelobe and clutter levels, dual apodization cross-correlation, or DAX, can improve image contrast constructed using delay-and-sum (DAS) beamforming. Artifactual black spots may arise in the regions away from the transmit focus after being DAX processed, because purposely created grating lobes become dominant. Beamforming by spatially matched filtering (SMF) echo signals is a novel method capable of effectively focusing both transmit and receive beams throughout field of view with a single transmit focus. We present our work on applying DAX after SMF beamforming for enhancing image contrast without introducing artifacts at all imaging depths.

Statement of Contribution/Methods

With a single transmit focus at 30 mm depth, channel RF data, experimentally acquired from a 4-board Verasonics data acquisition system with a L7-4 1-D linear array, was beamformed using both DAS and SMF. 4 mm diameter anechoic cysts in a tissue-mimicking phantom located at depths of 20 mm, 30 mm and 40 mm were scanned. Point reflectors at the same depths were used as spatial matched filters. A 6-6 alternating apodization scheme was used to implement DAX. Contrast-to-noise ratio (CNR) was calculated to quantify the improvements of image contrast after being processed by DAX for both beamforming methods.

Results/Discussion

The figure presents cyst images at the depths of 20 mm, 30 mm, and 40 mm before and after DAX was applied. Images were shown along with CNRs, indicating the improvements of image contrast by DAX in all cases. For DAS beamforming, artifacts appeared in DAX-processed images, except for regions near the transmit focal depth of 30 mm. However, no artifacts were seen in the images with SMF beamforming at all three imaging depths.

We successfully applied DAX to SMF beamforming. With a single transmit focus, image contrast was enhanced at all depths without any artifacts being introduced.

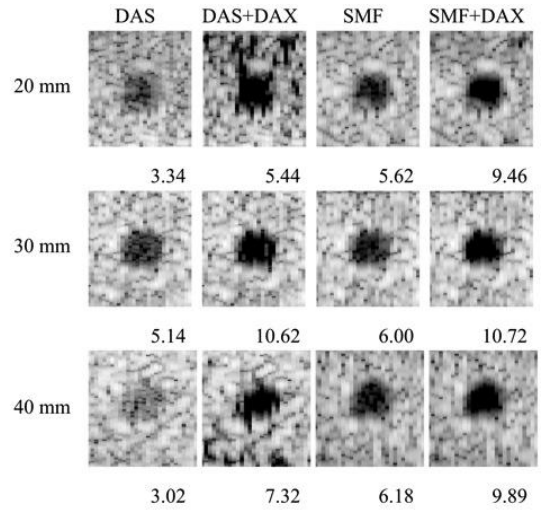

IUS1-PB1-7

Improved Synthetic Aperture Focusing Technique for Heterogeneous Media using an Ultrasonic Speed Map

Carlos Villagómez H. [1], Cecilia Borba[2], Wagner C. A. Pereira[2], Lucía Medina G. [3]; *[1]Biomedical Engineering Lab., Universidad Nacional Autónoma de México, Mexico, DF, Mexico, [2]Biomedical Engineering Program, COPPE/UFRJ, Rio de Janeiro, RJ, Brazil, [3]Faculty of Sciences, Universidad Nacional Autónoma de México, Mexico, DF, Mexico*

Background, Motivation and Objective

The synthetic aperture focusing technique (SAFT) considers that a wave propagates through a homogeneous medium. Therefore, time delay calculation needed to focus a specific region assumes a constant speed. This assumption implies straight lines between each pixel in the imaging space and each measuring point.

In a heterogeneous medium, however, wave speed and direction change at each boundary. Thus, this straight-line behavior is no longer valid, the time-of-flight for the delay calculations are not available. Time-of-flight (TOF) calculations can be overcome by using the Fast Marching Method[1], which is based on the solution of the Eikonal equation.

Statement of Contribution/Methods

Wire phantoms in tissue mimicking materials are used to evaluate lateral resolution improvements (see Figure 1a), whereas contrast phantoms with embedded cylinders of different reflectivity and speed of sound are used to assess the contrast-to-noise ratio and to produce aberrations. Signals coming from phantoms are acquired and the time of flight considering constant velocity and a speed map (see Figure 1b) are computed.

Results/Discussion

The resulting images (e.g. Figure 1c and 1d) are analyzed within the lateral and contrast resolution. Additionally, speckle statistical analyses are applied in two detection tasks of clinical relevance, as treated by Anderson[2]. The first is the detection ability of low contrast lesion, which measure the impact on accurate decision probability as a function of lesion size and contrast levels. The second is target point detection ability, which influences on the correct decision probability as a function of target point reflectivity. As a result, the proposed algorithm generates an increase in resolution and contrast. We evaluate the sensitivity to velocity mismatches and shown that an increase in correct clinical decisions can be achieved.

[1]Sethian, J.A., “A Fast Marching Level Set Method for Monotonically Advancing Fronts”, Proc. Nat. Acad. Sci., 93, 4, pp.1591-1595, 1996.

[2]Anderson, M.E.,"The impact of sound speed errors on medical ultrasound imaging.", Acoust Soc Am, 107, 6, pp. 3540-3548, 2000.

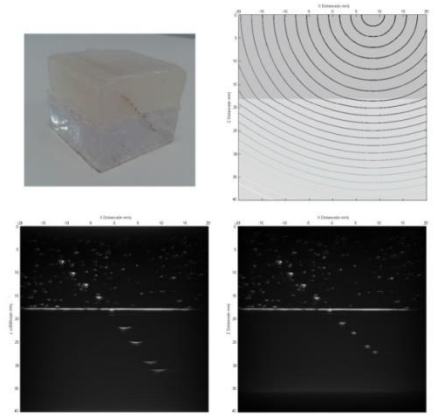

Fig. 1: Experimental results on a two layer phantom with 9 wires. (a) Picture of the phantom, (b) contour plot of the TOF times superimposed on the speed map, (c) image formed with homogenous SAFT, and (d) image formed with improved SAFT algorithm.

Image processing and image guided therapy

Forum Hall

Tuesday, July 23 2013, 01:00 pm - 04:30 pm

Congress Hallair: **Olivier Basset**
Université Lyon I, France

IUS1-PB2-1

4DCT-US image fusion for liver motion monitoring

Remi Blanc[1,2], David Melodelima[1,3], Simon Rit[2], Michel Rivoire[1], David Sarrut[2]; [1]*Leon Berard Cancer Center, Lyon, France,* [2]*CREATIS, Villeurbanne, France,* [3]*LabTAU, LYON Cedex 03, France*

Background, Motivation and Objective

High-intensity focused-ultrasound (HIFU) is a promising technique for treating liver tumors. However, liver motion due to breathing imposes a real-time monitoring of the treatment. To reach this goal and following on previous work, we propose to encase an ultrasound (US) imaging probe into an extracorporeal HIFU device, such that the imaging plane is aligned with the HIFU acoustic axis. Because the tumour itself may not always be visible on US images, we plan to rely on a pre-operative model derived from 4D-Computed Tomography (CT) to infer the tumour location during treatment, using intensity or feature-based registration techniques.

In order to study the feasibility of US guidance according to a pre-operative planning image, we decided to perform US acquisitions, with their consent, on 5 patients undergoing radiotherapy treatment and having a 4D-CT image for planning (Philips Brillance), possibly with injected contrast-agent. A hand-held US probe (Clarity, Elekta) was available, providing 2D images sequences in the coordinate system of the CT scanner thanks to an optical tracking system. No device was available to record a breathing signal during US acquisitions.

Statement of Contribution/Methods

US images were acquired by a radiologist just after the 4DCT, with the request to 1) acquire intercostal sequences of the liver, 2) apply the least possible pressure to avoid deformations 3) target for characteristic structures such as sus-hepatic or portal veins, or the gallbladder and 4) keep the probe fixed with respect to the patient during a normal breathing acquisition.

A breathing signal was estimated for each US sequences using Principal Component Analysis. The obtained phase signals are correlated to the motion of structures in US sequences, and have a frequency coherent with respiration, from 14 to 30 cycles per minute. Inhalation versus exhalation was identified by the user, and the respiratory phase was estimated from the breathing signal using the Hilbert transform.

Results/Discussion

Using this signal and the information from the tracking device, we were able to fuse the modalities spatially and throughout the respiration, displaying a good agreement between both modalities (Fig.1).

In future work, we will develop and compare feature and intensity-based registration methods to compensate for deformation and variability in the breathing patterns.

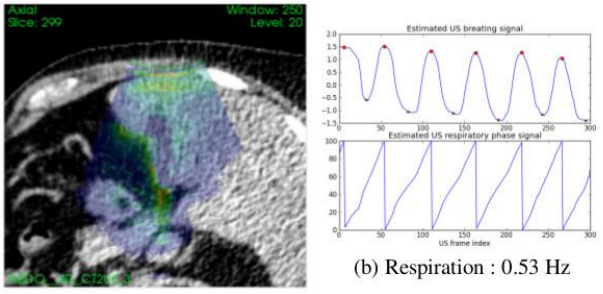

(a) (b) Respiration : 0.53 Hz

Fig. 1: (a) Fusion of a 4DCT and an ultrasound sequence showing the gallblader. The CT volume with a phase corresponding to the current US frame is sliced following the information of the US tracking device. (b) Estimated breathing signal and respiratory phase for the US sequence.

IUS1-PB2-2

Automatic Dynamic Range Optimization for 3D Medical Ultrasound Imaging

Yeonhwa Lee[1], Jinbum Kang[1], Yangmo Yoo[1,2]; [1]*Department of Electronic Engineering, Sogang University, Korea, Republic of,* [2]*Interdisciplinary Program of Integrated Biotechnology, Sogang University, Korea, Republic of*

Background, Motivation and Objective

In 2D medical ultrasound imaging, DR is typically given with a fixed value, and operators have to manually adjust it. However, in 3D ultrasound imaging, it is impossible to adjust DR during 3D data acquisition, leading to low image quality. In this paper, the automatic DR adjustment (ADRA) method was evaluated to optimize the DR value in 3D ultrasound imaging.

Statement of Contribution/Methods

In ADRA, the log average of a reference image is computed and the distance ratio from its log average to each extreme value is obtained. This distance ratio is used for adjusting the DR value of an input image to have similar contrast as the reference image. When the ADRA method is applied to 3D ultrasound imaging, its first frame can be used as a reference image so that consecutive frames during 3D data acquisition can have comparable contrast. To evaluate the performance of the ADRA method, 70 frames of complex baseband *in vivo* abdominal data were acquired with a commercial ultrasound system by moving a 3.5-MHz convex array from the left lobe of liver to kidney of a volunteer. The similarity between the reference frame and the processed ones were assessed by correlation coefficients (CCs) computed from the histogram values.

Results/Discussion

Fig. 1(a) shows the reference image with the dynamic range of 60 dB. The processed images of the 63rd-frame data from the fixed DR (i.e., 60 dB), histogram matching and ADRA methods are shown in Figs. 1(b)-1(d). Figs. 1(e) and (f) are the c-plane of the reconstructed 3D ultrasound images after volume rendering with the fixed DR and ADRA methods. Under visual assessments, compared to the fixed DR and histogram matching methods, the proposed ADRA method shows the similar contrast with the reference in Fig. 1(a). In addition, as shown in Figs. 1(e) and (f), the ADRA provides more uniform contrast in the c-plane image over the fixed DR method that suffers from dark lines indicated as white arrows. The consistent results were obtained with the measured CC values. The proposed ADRA method provided the CC value of 0.9669 ± 0.0199 vs. 0.9611 ± 0.0308 and 0.6768 ± 0.3594, compared to the fixed DR and histogram matching methods, respectively. These results indicate that the proposed ADRA method can automatically adjust DR of the consecutive frames during 3D data acquisition to have uniform contrast, leading to the improvement in image quality of 3D ultrasound imaging.

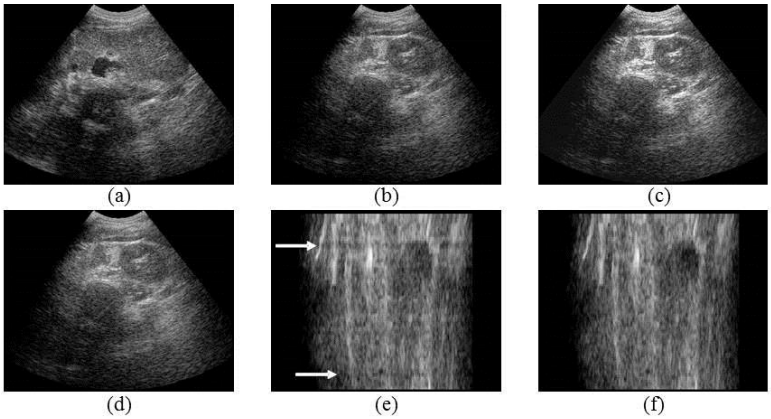

Fig. 1. (a) The reference image (i.e., first frame) of abdominal *in vivo* data using 60 dB DR and the images from the 63rd-frame data when using (b) the fixed DR, (c) histogram matching and (d) ADRA methods. The c-plane of 3D volume data with (e) the fixed DR and (f) ADRA methods.

IUS1-PB2-3

Towards Online Real-Time Strain Estimation: Feasibility Study and Initial Clinical Validation

Daniel Barbosa[1], Olivier Bernard[2], Brecht Heyde[1], Thomas Dietenbeck[2], Denis Friboulet[2], Jan D'hooge[1]; [1]*KU Leuven, Leuven, Belgium,* [2]*CREATIS, INSA Lyon, Lyon, France*

Background, Motivation and Objective

Strain-based functional indices have been shown to provide superior performance in assessing global cardiac function when compared with classical volume-based metrics, such as ejection fraction. Over the past years, 3D speckle tracking has drawn great attention thanks to the benefits of volumetric imaging, which avoids inducing apparent deformation intrinsically linked to 1D/2D methods due to fore-shortening or out-of-plane motion. Nonetheless the 3D strain analysis pipeline remains time consuming, jeopardizing its feasibility in daily clinical routine.

The aim of the present study was therefore to develop a fully automatic 3D left ventricle (LV) tracking framework able to quantify global cardiac deformation near real-time, potentiating its online use during the scanning of the patient.

Statement of Contribution/Methods

We recently proposed a framework allowing fully automatic segmentation of the LV in 3D ultrasound. As in clinical practice global strain is typically used as an index of overall cardiac performance, local tracking algorithms, which are typically computationally intensive, could be substituted by more global approaches. We therefore propose to use a novel tracking framework able to estimate a global affine transformation by defining an anatomical ROI around the initial LV surface and using an optical-flow algorithm to estimate the global cardiac (affine) motion between consecutive frames.

In order to test this approach, 19 RT3DE exams were acquired using a GE VividE9 equipped with a 4V probe (Vingmed Ultrasound, Horten, Norway). Both end-diastolic and end-systolic volumes were manually contoured by 2 experts, from which the global deformation parameters were estimated. Their average was taken as reference. The global area strain (GAS), which combines both longitudinal and circumferential deformation, was chosen as global cardiac function index. The agreement between the automatic tracking results and the reference values was assessed using linear regression and Bland-Altman (BA) analysis.

Results/Discussion

Moderate correlation (r=0.698) was found for the automatic GAS estimation compared with the reference values. BA analysis ([$\mu \pm 1.96\sigma$]=6.0±9.29%) shows that although a significant bias exists, the proposed approach offers competitive limits of agreement when compared with the inter-observer variability range ([$\mu \pm 1.96\sigma$]=0.85±9.52%). The proposed approach takes less than 1 second to perform the tracking between two subsequent frames, in a MATLAB implementation.

These preliminary results point towards the feasibility of online estimation of global deformation parameters without any user intervention and near real-time. Future work will focus on introducing additional tracking data attachment terms (such as monogenic phase conservation) to reduce the estimation bias. The use of the proposed approach for online monitoring of global cardiac function will also be further investigated.

IUS1-PB2-4

Glasses for 3D Ultrasound Computer Tomography

Michael Zapf[1], Nicole Ruiter[1]; [1]*IPE, KIT, Karlsruhe, Germany*

Background, Motivation and Objective

A promising candidate for breast cancer imaging is ultrasound computer tomography (USCT). At KIT a 3D USCT with a semi-ellipsoidal aperture consisting of several hundreds of US transducers was built, called 3DUSCT II. In a measurement spherical waves are sequentially emitted and pressure over time signals are received. SAFT is applied to reconstruct reflectivity images. However, straight forward SAFT imaging leads to blurred images. Typical blur reducing approaches are on signal level: subsets of the signals, time-windowing or heuristic sharpening filters. An image based de-blurring approach is described here and analyzed with simulations and clinical data sets.

Statement of Contribution/Methods

Imaging can be described in the spatial Fourier domain (k-space) as linear process, i.e. as multiplication of the spatial frequencies of the object with function given by the aperture as filter. In literature apertures with significant spatial extend in relation to the object, especially object enclosing apertures, were shown to overestimate low-frequency components. These over-amplified object frequencies are the reason for the blurred characteristic of straight-forward SAFT imaging.

To evaluate this effect a simulation was used. The 3D USCT II aperture was modeled by the spatial position and the frequency characteristic of the ultrasound transducers (CF 2.6MHz and 50% relative BW). As simulated objects perfect point scatterers were chosen and the resolution was calculated using FWHM. An aperture compensation filter was analytical constructed by approximating the 3DUSCT II aperture as a perfect spherical aperture. These 'glasses' were applied on the reconstructed images, correcting the image blur introduced by this specific aperture.

Results/Discussion

21 simulated point scatterers of 0.06mm size were randomly distributed in a 30mm x 30mm ROI centrally placed in the aperture (see Fig. 1 top row). With SAFT imaging eight of the scatterers were not resolved. The mean FWHM of all resolved points was 0.22mm (STD 0.003mm). With aperture compensation only five scatterers were unresolved. The mean FWHM improved to 0.185 mm (STD 0.002mm), an increase in resolution by 15%.

First tests of the aperture compensation on images from a clinical study were encouraging, the blur in the images was significantly reduced and the resolution was enhanced (Fig 1. bottom row).

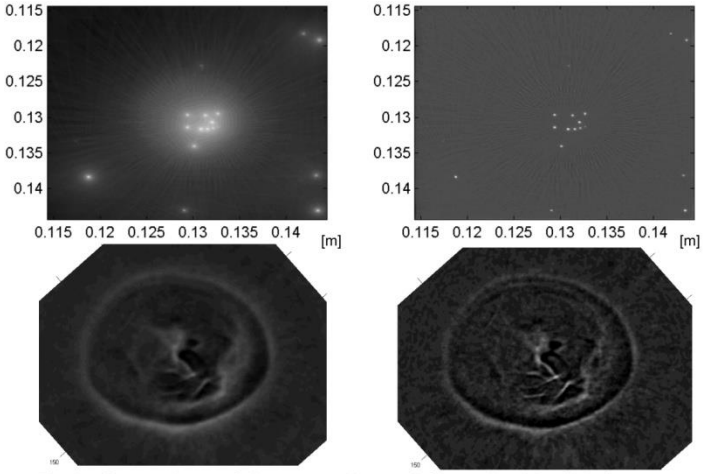

Fig.1: Comparison of images without (left) and with (right) aperture compensation . Top row: simulated point scatters (approx. 3cm x 3cm), bottom row: patient from clinical breast cancer study (approx. 15cm x 15cm).

IUS1-PB2-5

Fusion of 3D echo and cardiac magnetic resonance volumes during live scanning

Gabriel Kiss[1,2], Steven Ford[1,3], Piet Claus[4], Jan D'hooge[1,4], Hans Torp[1]; [1]*MI Lab and Department of Circulation and Medical Imaging, Norwegian University of Science and Technology, Norway,* [2]*St. Olavs Hospital, Trondheim, Norway,* [3]*Høgskolen i Nord-Trøndelag, Steinkjer, Norway,* [4]*Department of Cardiovascular Sciences, K.U.Leuven, Belgium*

Background, Motivation and Objective

The aim of this project was to develop a method for real-time alignment and visualization of 3D echo and CMR volumes during a live 3D echocardiographic scan and to demonstrate its applicability in a typical ultrasound scanning scenario.

Statement of Contribution/Methods

A customized streaming plugin has been implemented in VTK (Kitware Inc.) that has the ability of receiving a live stream of 3D echo data from an ultrasound scanner (GE Vivid E9) using a standard TCP/IP connection. Once received the echo data is scan converted on the GPU and segmented using the RCTL (Real-time Contour Tracking Library) framework. Four anatomic landmarks are computed automatically based on the RCTL tracking results. These are the apex and base of the left ventricle, middle of the outflow tract and the basal attachment point of the right ventricle. The same landmarks are manually identified in the CMR recording, prior to the scanning. Using the two sets of corresponding landmarks a rigid transformation can be computed and the 3D echo data deformed accordingly. The percentage of valid edge detections along the LV surface is also computed and fusion will be carried out only if the fit quality is above a predefined threshold, by this discarding poor quality data. Time synchronization is achieved by considering the frame with the largest volume as end diastole.

Results/Discussion

For testing purposes pre-recorded data of three subjects with myocardial infarction, that underwent 3D echo and CMR short- long-axis cine the same day, has been selected. The alignment process was successful in all cases. Furthermore, the system was also tested on a healthy volunteer during a real-time scanning scenario. It was shown that the alignment was feasible once a good quality 3D recording was available. The streaming, scan conversion, segmentation and alignment of the data can be carried out at a speed of 6 frames per second.

A novel method for fusing and visualizing 3D echo and CMR volumes during an ultrasound scan is presented. The method is useful for teaching (CMR depicts anatomy much better) and for follow-up purposes. Further work will include temporal synchronization based on the ECG signal and the addition of a highly detailed anatomic model of the heart to the 3D scene. Furthermore probe tracking information can be integrated to improve the accuracy of the system and as such the fusion will be less dependent on the image quality.

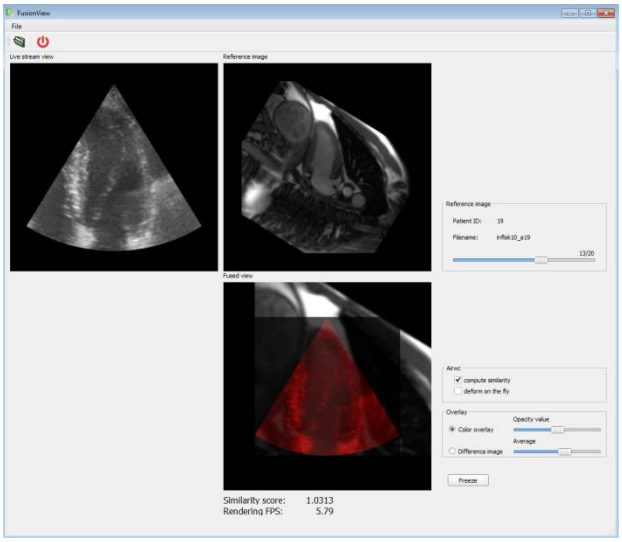

IUS1-PB2-6

Speckle reduction using shearlet thresholding with improved nonlinear anisotropic diffusion

Deep Gupta[1], **R.S. Anand[1]**, Barjeev Tyagi[1]; *[1]Electrical Engineering Department, Indian Institute of Technology Roorkee, Roorkee, Uttarakhand, India*

Background, Motivation and Objective

Currently, the research in medical imaging has produced many different imaging modalities for the clinical purpose. Ultrasound imaging is one of the most important and cheapest instrument of the imaging modalities. The quality of ultrasound imaging is degraded due to different noises and artifacts. Among these noise and artifacts, speckle is a factor which degrades the quality and most importantly texture information. Due to noise, experts may not be able to extract correct and useful information from the images. This paper presents a new hybrid denoising model based on anisotropic diffusion and shearlet transform based thresholding approach.

Shearlet transform is used to provide effective representation of the noisy coefficients because conventional transform such as wavelet is less efficient in representing the sharp transition. In our earlier work, the performance of the shearlet thresholding approach has been evaluated on ultrasound images. Shearlet based thresholding denoising method preserved the edges perfectly. However, these methods also produce the visual distortion and add some fuzzy edges in homogeneous area of the images.

Statement of Contribution/Methods

In existing thresholding methods, coarser approximation coefficients of the image remain unchanged and all finest scale coefficients are processed with thresholding functions. In the present method, a modified anisotropic diffusion technique is applied on the coarser approximation subband of shearlet decomposition. It helps to reduce the fuzzy edges induced by transform based thresholding methods. The anisotropic model proposed by Perona and Malik, is modified by replacing four connected neighboring pixels with eight connected neighboring pixels and adaptive gray level variance with in square window is also incorporate with the gradient to evaluate the diffusivity.

Results/Discussion

To evaluate the performance of the present method, both standard test image and ultrasound images are used. The performance of proposed method is compared with other methods. To evaluate the comparative performance, different parameters are used to analyze its noise suppression, feature and edge preservation capability, separately Table 1 explains the comparative performance analysis of different denoising methods for boat image, degraded with speckle noise of variance 0.2.

Table 1: Comparative performance of proposed method with others

S. no.	Denoising methods	Assessment parameters	
		PSNR	UQI
1	Noisy image	12.73	0.167
2	Median filter	17.87	0.293
3	Lee filter	20.88	0.342
4	Kuan filter	21.05	0.342
5	Anisotropic diffusion	21.27	0.359
6	Fourth order PDE	21.70	0.382
7	SRAD	23.14	0.349
8	Wavelet thresholding	16.41	0.275
9	Wavelet based anisotropic	23.53	0.563
10	Proposed method	23.73	0.618

IUS1-PB2-7

Dynamic Ultrasound Imaging of Cervical Spine Intervertebral Discs

Mingxin Zheng[1,2], Kevin Shiuan[1,2], Aidin Masoudi[2], Daniel Buckland[2,3], Thomas Szabo[1], Brian Snyder[2,4]; *[1]Boston University, Boston, MA, USA, [2]Center for Advanced Orthopaedic Studies, Beth Israel Deaconess Medical Center-Harvard Medical School, Boston, MA, USA, [3]Massachusetts Institute of Technology, Cambridge, MA, USA, [4]Children's Hospital Boston, Boston, MA, USA*

Background, Motivation and Objective

The diagnoses of C-spine injury and degenerative intervertebral disc (IVD) disease are challenging because these conditions are more evident under dynamic loading conditions. Ultrasound (US) imaging can be used to track the movement of vertebrae and IVDs under dynamic conditions noninvasively. The aims of this study were to demonstrate that portable ultrasound can: 1) accurately measure IVD deformation and mechanical compliance *ex-vivo*; 2) provide real-time images of IVDs and dynamic vertebral motion *in-vivo* during simulated tasks.

Statement of Contribution/Methods

The feasibility of the approach was evaluated by tracking the movement of ex-vivo human spines subjected to compressive/distractive loads and dynamic sinusoidal displacement (1 mm @1-8 Hz). A portable diagnostic system with a 7.5 MHz linear array was used to capture a sequence of images during loading. To simulate an in vivo loading condition, five young male volunteers wore US probes and weighted helmets and jumped repetitively from a 1.5 ft. stool. Movement of vertebrae was determined from US image loops by edge detection and related to the movement of vertebrae (*ex-vivo*) and to displacements of the head relative to the torso (*in-vivo*) as measured simultaneously by optical tracking system.

Results/Discussion

Ex-vivo: Dynamic IVD displacements of vertebrae C4-5 & C5-6 measured by US were consistent with optical tracking system data. For motion frequencies <6Hz, US accounted for 60-95% of the true IVD displacements (error: ±0.148 mm). A preliminary dynamic mechanical model of vertebrae linked by IVDs was used to determine compliance parameters.

In-vivo: Amplitude-time curves of IVD deformation measured by US correlated with the vertical displacement of the head relative to torso. Spectral analysis demonstrated that most deformation occurred at frequencies < 6Hz. Wearing a weighted helmet during jumping significantly increased ($p<0.001$) the proportion of inertial head displacement transmitted to vertebrae C4-5. Portable US provides a low cost means of accurately measuring dynamic vertebral motion and C-spine IVD displacement during simulated tasks for frequencies <6 Hz. Preliminary in-vivo data of jumping personnel wearing a weighted helmet demonstrates that portable ultrasound can be used to monitor the effects of transient loading.

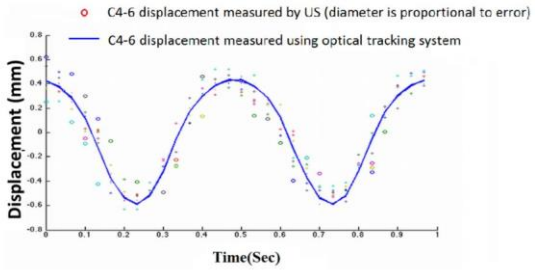

IUS1-PB2-8

3D ultrasound assisted laparoscopic liver surgery by visualization of blood vessels

Satoki Zenbutsu[1,2], Tatsuo Igarashi[2], Ryoichi Nakamura[2], Toshiya Nakaguchi[2], Tadashi Yamaguchi[1]; *[1]Research Center for Frontier Medical Engineering, Chiba University, Japan, [2]Graduate School of Engineering, Chiba University, Japan*

Background, Motivation and Objective

Laparoscopic surgery remains a challenging procedure because visualization of the internal target organ cannot be achieved from the laparoscopic image. We have proposed a laparoscopic surgery support method relying on three-dimensional (3D) images reconstructed using a stereo laparoscope and a 3D ultrasound system. This method can also be used to form two-dimensional (2D) laparoscopic image for the proper visualization of the target organ. The aim of this study is to develop a visualization system providing depth information about blood vessels within the liver. The shape and depth information of blood vessels are then correctly superimposed on a 2D laparoscopic image on the basis following careful registration.

Statement of Contribution/Methods

The distance from the stereo laparoscope to the liver surface is calculated using a stereo matching method. Then, the 3D liver surface shape is reconstructed from the stereo laparoscopic data. In parallel, the ultrasonic volumetric data of the liver is acquired by an ultrasonic diagnostic equipment with a mechanically moved convex probe, then blood vessels and the 3D liver surface shape are obtained using segmentation methods. The coordinates of the laparoscope and the ultrasound are registered by aligning the two 3D liver surface shapes. Finally, the shape and depth information within the liver are calculated, and color-coded blood vessel depth information is superimposed on the original 2D laparoscopic image.

Results/Discussion

The proposed method was evaluated in a phantom experiment (Fig. 1a). The phantom had hypoechoic regions specifically designed to mimic blood vessels whose diameters ranged from 5 mm to 30 mm. The size of each stereo laparoscopic image was 640 * 480 pixels (75 * 55 mm). The 3D ultrasound data was 207 * 224 * 100 pixels (70 mm in depth * 75 mm in lateral * 30 mm in slice) and was acquired with 5.5-MHz center frequency. The registered 3D images with the mean error (ME) of 5.46 mm ± 2.76 mm are shown in Fig. 1b. The 2D laparoscopic image superimposed the color-coded depth of the blood vessels segmented from the 3D ultrasonic data is shown in Fig. 1c. The calculation of depth information had the ME of 7.86 mm ± 3.63 mm.

Our method provides critical information during liver surgery because the depth and shapes of the blood vessels is easily visualized. Future work will focus on improving accuracy prior to clinical transition.

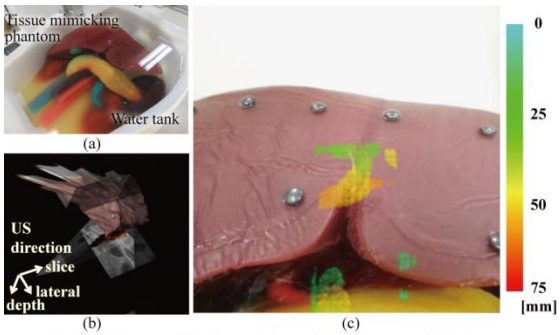

Fig. 1 (a)Phantom, (b)Registered ultrasonic and laparoscopic 3D images, (c)Color-coded depth information superimposed on 2D laparoscopic image

IUS1-PB2-9

A New Automatically Biopsy Needle Tracking Method Using 3D Ultrasound

Yue Zhao[1], Christian Cachard[1], Hervé Liebgott[1]; [1]*CREATIS, CNRS UMR 5220, INSERM U1044, Université Lyon 1, INSA Lyon, France*

Background, Motivation and Objective

Ultrasound (US) guidance of surgery micro-tools has been widely used in clinical practice. One major difficulty in this context is to track accurately and robustly the tool due to the 3D US volume quality. Particularly some anatomical structures can appear very similar to the tool in the images. We present a new biopsy needle tracking method that overcomes these limitations. Our technique is totally automatic and does not need any manual initialization from the user.

Statement of Contribution/Methods

The method uses an automatically region of interest (ROI) choosing strategy and a RANSAC plus Kalman filter procedure (AROI-RK). The main steps of this method are:

Step 1: ROI Initialization. Here the whole US volume must be considered. To enhance the contrast between needle and background a Hessian based line filter is used to calculate the local tubularness in the 3D US volume (Fig. 1b). The RANSAC algorithm runs in the tubularness image and outputs the initial needle position. It initializes also automatically the ROI position.

Step 2: Needle detection. Then the RANSAC algorithm only runs inside the ROI.

Step 3: ROI update and needle tracking. Here Kalman filter is used for two functions: a) update the ROI position; b) optimize the needle position estimation.

The time update equations of Kalman filter use the (k-1)th needle position and the needle tip velocity obtained by a speckle tracking (ST) technique to update the ROI position in the kth volume. Then the RANSAC is run in the kth ROI to get the measurements for Kalman filter and estimate the new position of the needle.

Results/Discussion

To evaluate the performance of our proposed method several series of 3D US volumes with inhomogeneous background and known needle positions are simulated of different contrast ratios between 2 and 4. As less outliers are present in the ROI a clear improvement in tracking thanks to the proposed method has been observed in all situations. An example is given in Fig. 1c. The acceleration of the detection thanks to the use of limited ROI size enables very fast processing and future work will consist in implementing the technique real-time on an Ultrasonix MDP scanner.

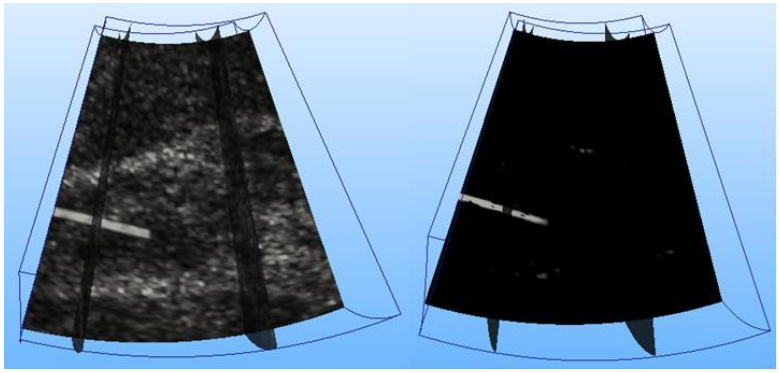

a. The original 3D US volume

b. The tubularness image of the US volume on the left

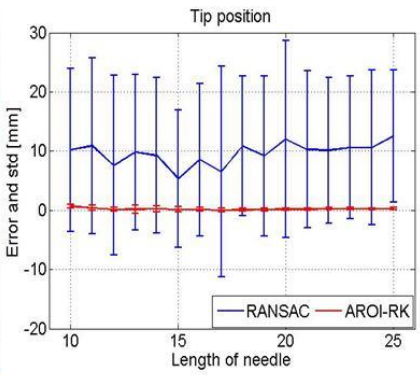

c. The mean error and STD of error of the needle tip position using RANSAC and AROI-RK method

Fig.1 The original 3D US volume, the tubularness image of the volume and the performance of the two methods for tip localization

IUS1-PB2-10

Inter-operator Variability in Defining Uterine Position Using Three-dimensional Ultrasound Imaging

Mariwan Baker[1,2], Joergen Arendt Jensen[3], Claus F. Behrens[1]; [1]*Department of Oncology, University of Copenhagen Herlev Hospital, Herlev, Copenhagen, Denmark,* [2]*Technical University of Denmark, Center for Fast Ultrasound Imaging, Lyngby, Denmark,* [3]*Center for Fast Ultrasound Imaging, Technical University of Denmark, Lyngby, Denmark*

Background, Motivation and Objective

In radiotherapy the treatment outcome of gynecological (GYN) cancer patients is crucially related to reproducibility of the actual uterine position. This study is to evaluate the inter-operator variability in addressing uterine position using a novel 3-D ultrasound (US) system.

Statement of Contribution/Methods

The study is initiated by US-scanning of a uterine phantom (CIRS 404) by six experienced US operators. The phantom represents a female pelvic region, containing a uterus, bladder and rectal landmarks readily definable in the acquired US-scans. The organs are subjected to displacement by applied operator-pressure that mimics an actual GYN patient. The transabdominal scanning was performed using an Elekta Clarity 3D-US system (Clarity® Model 310C00). Clarity consists of a US acquisition-station, workstation, and a 128-element 1D array curved probe. (See figure) The iterated US-scans were performed in three subsequent sessions (totally 18 US-scans) in a period of four weeks, i.e. to investigate the randomness of the inter-operator variability. An additionally optimal US-scan was selected as a reference target volume to the consecutive scans. At first, the phantom was marked with ball bearings for daily laser alignment. In each session the US-scans were acquired by the six operators. The uterus was outlined in each of the US image-sets using Clarity autosegmentation in the workstation. Further, the shifts in the uterine centre of mass relative to the reference were measured for the three orthogonal directions; left (+)-right (LR), anterior (+)-posterior (AP), and inferior (+)-superior (IS), respectively. The same operator delineated the target volumes.

Results/Discussion

The average inter-operator deviation (±1SD) of the daily 6 US scans was (in mm); LR: day 1 (-0.4±0.9), day 2 (-0.3±0.6), day 3 (-1.0±1.2); AP: day 1 (0.0±1.7), day 2 (4.1±0.7), day 3 (3.0±0.9); IS: day 1 (-1.5±2.6), day 2 (0.1±1.8), day 3 (0.1±1.1), respectively. The largest inter-operator discordance was observed to be -5.2 mm in the IS-direction. Previous studies have con-firmed larger inter-fractional uterine positional displacement, in the range of over 10 mm in some cases, which outweighs the magnitude of the current inter-operator variations. Thus, in the current US-phantom-study, the inter-operator variability in addressing uterine position is shown to be insignificant.

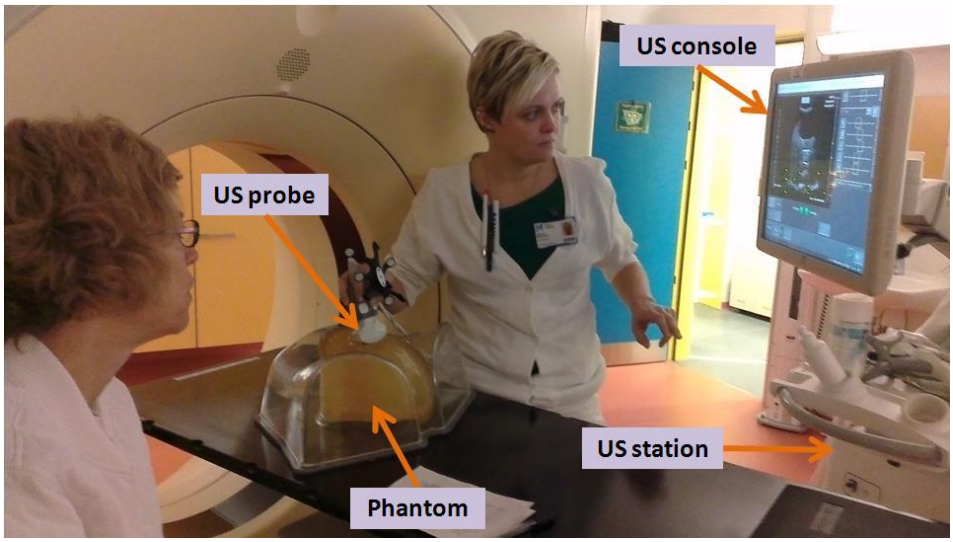

IUS1-PB2-11

Nonlinear Characterization of Tissue and Microbubbles using Nakagami Statistical Model

BAHBAH NARDJESS[1], ANTHONY NOVELL[2], HAKIM DJELOUAH[1], AYACHE BOUAKAZ[2]; [1]*USTHB, Algeria,* [2]*INSERM, France*

Background, Motivation and Objective

The objective of the study is to exploit the statistical signatures of biological tissues and contrast microbubbles in order to develop new strategies for contrast imaging and tissue characterization. For this purpose, the Nakagami statistical model was chosen, because it is more general and simpler to apply than other statistical models, to describe the linear and nonlinear ultrasonic echoes of both contrast microbubbles and tissues.

Statement of Contribution/Methods

Experiments were performed using a commercially available platform with 128 independent channels equipped with analog transmitters. A tissue mimicking phantom containing a 4 mm diameter tube was used to acquire the responses of both tissue and SonoVue microbubbles. Ultrasound images and corresponding RF signals were acquired using transmit signals of 3 and 5 cycles at 2.5 MHz and using different microbubble concentrations (1/10000, 1/5000, 1/2000, 1/1000, 1/500). The applied mechanical index was 0.19.

The statistical analysis was performed on several regions of interest (ROI) located at different positions inside the tissue and contrast regions. The corresponding RF echoes have been analyzed in order to evaluate the Nakagami parameter (m) and the scaling parameter (Ω) according to three filtering procedures: raw data, filtering around the transmitted center frequency (fundamental) and around twice the transmitted frequency (2nd harmonic).

Results/Discussion

Nakagami parameters of the various studied zones present, in most cases a linear increase as a function of microbubble concentration in the studied range.

Moreover Nakagami parameters appeared to be greater when filtering at fundamental frequency in comparison to the other two cases (raw data and 2nd harmonic).

For tissue, the largest values of Nakagami parameters estimated at the fundamental frequency (m=2, Ω=0.2) are smaller than those obtained for the microbubbles which are respectively in the range [5.5-10.5] for Nakagami parameter m and [0.28-0.35] for the scaling parameter Ω. At the 2nd harmonic frequency, for microbubbles, the values are in the range [3.2-6.4] for Nakagami parameter m and [0.22-0.27] for the scaling parameter Ω.

This study shows that the discrimination between microbubbles and biological tissues can be obtained through Nakagami parameters at fundamental and at 2nd harmonic. These results would be useful for improving the image quality and for contrast detection in nonlinear mode.

IUS1-PB2-12

Machine Learning methods for classifying breast masses with ultrasound imaging

Benjamin Levenback[1], Laith Sultan[1], Santosh Venkatesh[2], **Chandra Sehgal**[2]; [1]*Radiology, University of Pennsylvania, USA,* [2]*University of Pennsylvania, USA*

Background, Motivation and Objective

Computer based image analysis of the breast ultrasound images may aid physicians in differentiating benign and malignant masses with higher confidence and help reduce unnecessary biopsies. In this study, we propose to use boosting methods to improve the diagnostic performances of two independent pattern learning methods: logistic regression and naïve Bayes.

Statement of Contribution/Methods

Morphological features were derived from sonographic images by manual tracing of masses in the images. The images were also assessed by radiologists for BI-RADS$_{US}$ features. The two data sets, consisting of traced morphological features and BI-RADS$_{US}$ categories, were used with logistic regression and naïve Bayes to determine probability of malignancy. This generated four separate classifiers. Boosting was performed on two classifiers or all four classifiers at a time in different permutations using a modified ADABoost, where the weightings of each classifier were determined by the square of the differences between the probability of malignancy and actual diagnosis of the previous classifier. The performance of each base classifier and the boosted classifier was evaluated using the area under the curve (AUC) of the receiver operating characteristic (ROC). The algorithms were trained and tested using leave-one-out cross-validation.

Results/Discussion

The base classifiers, when used individually, had AUC values ranging from 0.867 to 0.924. The BI-RADS$_{US}$ features did better than the traced morphological features by a small margin (ΔAUC range 0.019-0.057). When using two base classifiers, the boosted classifiers had AUC values ranging from 0.900 to 0.933. When all four base classifiers were used for boosting, the AUC value averaged 0.940 (range 0.934-0.943). Boosted classifiers with higher-performing base classifiers performed better; the boosted classifiers always outperformed their constituent base classifiers. The order in which individual classifiers were used in boosting did not make a measurable difference in performance.

In conclusion, the results of this study show that pattern learning methods have a high level of performance when used with computer extracted and BI-RADS$_{US}$ features. Although the performance of computer and BI-RADS$_{US}$ features is comparable, the BI-RADS$_{US}$ features in general perform slightly better. Combining BI-RADS$_{US}$ and computer features improved the performance of diagnosis with ROC area approaching 0.950.

Soft tissue characterization II

Forum Hall

Tuesday, July 23 2013, 01:00 pm - 04:30 pm

Congress Hallair: **Michael Kolios**
Ryerson University

IUS1-PB3-1

Basic Study for Characterization of Carotid Plaque Composition Using Ultrasonic Velocity-Change Imaging

Kazune Mano[1], Yu Izukawa[1], Ryosuke Kimura[1], Kenji Wada[1], Toshiyuki Matsunaka[1], Hiromichi Horinaka[1]; *[1]Physics and Electronics, Osaka Prefecture University, Sakai-shi, Osaka-fu, Japan*

Background, Motivation and Objective

The detachment of carotid artery plaque is serious problem because it leads to the brain infarction and the heart infarction. It has been thought that the instability of the vessel plaque relates to the size and the distribution of lipid core. If lipid-rich plaques are found out in early stage, we will be able to protect the plaque rupture by the lifestyle modification, the drug treatment. We have already proposed the ultrasonic velocity-change imaging method to diagnose fatty liver by using the fact that the temperature dependence of ultrasonic velocity is quite different in water and in fat. In this study, we aimed at applying the ultrasonic velocity-change imaging method to the characterization of carotid artery plaque composition.

Statement of Contribution/Methods

Figure 1(a) shows the structure of the blood vessel phantom including the model plaque. It was made of the agar including the graphite powder. A small piece of fat was inserted into the mimic blood vessel. Water, instead of blood, was streamed in the blood vessel phantom by using a tube pump (flow rate:0.5ml/s). The ultrasonic transducer for warming of the phantom is placed near by the 12 MHz ultrasonic linear array transducer. The waveform data of the echo before and after warming for 60 sec. (temperature rise:1~2 deg.C) received by the array transducer connected to the ultrasound equipment were stored in a personal computer. The ultrasonic velocity change corresponding to each scan line was determined from each echo pulse waveform in temperature relaxation process.

Results/Discussion

Figure 1 (b) show the normal B-mode images of the front view and the side view of the phantom, respectively. The phantom structure is observed, but the lipid-rich area is not identified. Figure. 1 (c) shows the ultrasonic velocity-change images of the phantom. The ultrasonic velocity change rate was shown by the gray scale. The dark areas which indicate the minus ultrasonic velocity change rate correspond to lipid-rich area in the phantom.

In conclusion, the lipid-rich area in the blood vessel phantom was clearly shown in the ultrasonic velocity-change image. The ultrasonic velocity-change imaging method has the potential of a useful tool for noninvasive characterization of carotid artery plaque composition.

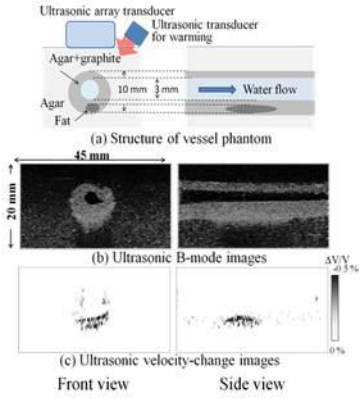

Fig.1 (a) Structure of blood vessel phantom including model plaque, (b) Ultrasonmic B mode images of the phantmn and (c) Ultrasonic velocity-change images.

IUS1-PB3-2

Characterization of Anisotropic Poly(vinyl-alcohol) Gels Prepared Using a Two-zone Controlled Directional Freezing Process

Andrew Dawson[1], Gideon Gouws[2]; *[1]Callaghan Innovation, Lower Hutt, New Zealand, [2]Victoria University of Wellington, New Zealand*

Background, Motivation and Objective

Tissue mimicking phantoms are an important component in medical ultrasound research. They provide a means for developing procedures, calibration of equipment, and repeatability for experiments without the need for real tissue samples. The mechanical properties of conventional PVA phantoms are tailored by applying a number of freezing-thawing cycles to a PVA slurry. Unfortunately these fail to represent the anisotropic microstructure and dimensions of real tissues and hence are limited to low frequency applications. Previously we published a method involving the freeze casting of PVA that produced novel microstructured phantoms suitable for higher frequencies. Characterisation of these revealed good replication of real tissue anisotropy, microstructure dimensions, and mechanical properties such as velocity and attenuation. However, repeatability of these properties and sample solubility were significant issues.

Statement of Contribution/Methods

We will present improvements made in the freeze casting process and characteristics of the samples produced using the new method. A refined two-zone directional freezing process is now used providing greater control over the temperature gradient and freezing rate of the sample. Attention has been paid to ensure the process is simpler and with greater control to achieve better repeatability and minimise operator influence. As a consequence larger phantoms (upto 25mm diameter, 50mm length) can now be fabricated. Impedance, velocity, elasticity, and attenuation properties of the phantoms with variations in PVA slurry concentration, direction of alignment, and freezing rates will be presented over a frequency range of 5-25MHz.

Results/Discussion

Samples fabricated using the improved method exhibit improvements in the repeatability of microstructure and are far less soluble in water. Samples produced are a solid gel that can be immersed for long periods and then removed and still retain their original mechanical stability. If used several times in this way only small amounts of dehydration occur. The samples are highly anisotropic along the direction of freezing and exhibit greater colinearity than samples produced using the original method. Initial characterisation of new samples has been performed along the direction of freezing at 10MHz. Velocities of the samples measured were 1510-1560m/s with acoustic impedances in the range 1.52-1.57MRayl. Attenuation measurements revealed values of 4dB/cm which is in the vicinity of real tissues such as muscle and heart tissue (approximately 5dB/cm at 10MHz). With the improvements in repeatability/solubility and presence of real microstructure the two-zone directional freezing process is an excellent basis to produce anisotropic tissue phantoms for more advanced studies.

IUS1-PB3-3

Polyvinyl Alcohol Cryogel Elastic Artery Phantoms for Ultrasonic Flow and elasticity measurements

Ming Qian[1], Lili Niu[2], Yang Xiao[3], Congzhi Wang[4], Weibao Qiu[3], Hairong Zheng[4]; *[1]Shenzhen Institutes of Advanced Technology, Chinese Academy of Sciences, Shenzhen, Guangzhou, China, People's Republic of, [2]Shenzhen Institutes of Advanced Technology, Chinese Academy of Sciences, Shenzhen, Guangdong, China, People's Republic of, [3]Chinese Academy of Sciecnes, China, People's Republic of, [4]Chinese Academy of Sciences, China, People's Republic of*

Background, Motivation and Objective

Biophysical properties of arteries and blood flow are important in the development of cardiovascular diseases. Increased arterial stiffness causes reduced artery vasomotion and influences local hemodynamics. Correspondingly, blood flow induced pressure and stress can cause endothelium dysfunction and lead to increased arterial stiffness and other cardiovascular events. The fluid-structure interaction in arterial system is complex and needs more studies. Ultrasound-based methods have been broadly applied to flow and elasticity measurements. Designing and fabricating elastic vessel phantoms for use in physiological flow condition can add valuable alternatives to intravital and computational studies. This paper used polyvinyl alcohol(PVA) cryogel to fabricate elastic artery phantoms and performed detailed acoustic and mechanical characterization on the phantoms.

Statement of Contribution/Methods

A PVA solution in water was prepared by mixing and stirring 10wt% PVA powder, 87wt% degassed water, and 3wt% scattering particles at 90¡ãC for about 1 hour to achieve even distribution. The solution was cooled to room temperature and injected into a custom-designed mould, which was then frozen at -20 ¡ãC for 12 h and thawed for 12 h at 20 ¡ãC. The freeze-thaw(f-t) cycle was repeated 1 to 8 times to achieve artery phantoms of desired properties. The phantoms of cylindrical shape were obtained with 6 mm inner diameter, 2mm wall thickness, and 160 mm length. Mechanical and acoustic characterization was performed. Phantom elasticity was measured using a CMT 6104 testing instrument (MTS System Corporation). The Young¡¯s elastic moduli were calculated from the stress-strain curves. The sound speed and the attenuation coefficient of the phantoms were determined using pulse-echo substitution method. Six different transducers were used in this study, operating at 1.0 MHz, 2.25MHz, 3.5 MHz, 5MHz, 7.5MHz, and 10MHz, respectively.

Results/Discussion

A linear increase of Young¡¯s modulus was observed for phantoms from 1 to 8 cycles, from 60.88¡À6.78 kPa to 310.28¡À14.10 kPa. Sound speed was mainly dependent on f-t cycles, but was not reliant on transmit frequency. At fixed transmit frequency, an increase of sound speed can be observed against the number of f-t cycles, from 1535.7 m/s for 1 f-t cycle to 1550.8 m/s for 8 f-t cycles. Sound attenuation coefficient was greatly dependant on the transmit frequency. For a phantom of 1 f-t cycle, the sound attenuation increased from 0.269¡À0.014 dB/cm at 1MHz to 0.958¡À0.019 dB/cm at 10MHz. For a phantom of 8 f-t cycles, it increased from 0.507¡À0.017 at 1MHz to 1.705¡À0.031 dB/cm at 10MHz. The sound attenuation was also dependent on phantom stiffness when the transmit frequency was fixed for different measurements. For example, at 1MHz, the sound attenuation increased from 0.269¡À0.014 for 1 f-t cycle to 0.507¡À0.017 dB/cm for 8 f-t cycles. At 10MHz, from 0.958¡À0.019 for 1 ft cycle to 1.705¡À0.031 dB/cm for 8 f-t cycles.

IUS1-PB3-4

High Sensitivity Estimation of Red Blood Cell Aggregation with Ultrasonic Peak Frequency

Takayuki Sato[1], Yasuaki Watanabe[1]; *[1]Tokyo Metropolitan University, Japan*

Background, Motivation and Objective

Several trials have been conducted on the ultrasonic estimation of the aggregation size of red blood cells (RBCs). Due to the significant changes in size from a single RBC to a large aggregation consisting of hundreds of RBCs, it is impossible to include enough aggregation samples by using an ultrasonic transducer with a small focal zone because the extracted samples might be statistically biased. A technique for detecting the peak frequency of an ultrasonic reflection spectrum was developed that aims at enhancing the sensitivity and statistic accuracy of estimating the aggregation size of RBCs.

Statement of Contribution/Methods

The total loss in the ultrasonic path is reflected in the reflection spectrum and is dominantly characterized with the particle size dependency of the Rayleigh scattering. The reflection coefficient between the RBCs and the serum is very small. However, acquiring the reflection signal from a reflection board placed on the bottom of the container, which accompanies a round trip of the incident wave inside the suspension, can generate an emphasizing effect that is produced by the attenuation characteristics.

The effectiveness of the estimation method described in this study was investigated under the assumption that an aggregation consisting of many RBCs can be substituted by a single large particle with an equivalent diameter.

A 10-MHz transducer with the beam diameter of 6.2 mm, which can include a sufficient number of large aggregations, was immersed in a 2-wt% suspension and a reflection board was placed on the bottom of the container. Peak frequencies for stagnant and running suspensions prepared with monodisperse particles of graphite and acryl (to mimic aggregated RBCs) were acquired at an echo reflection distance of 18 mm.

Results/Discussion

Results showed that the relationships between the particle diameters d and the peak frequencies f_p, which were independent of the material of the particles and flow rate up to 15 cm/sec, were obtained as f_p=-3.14 $\log_{10}$ d+11.0. In experiments with bidisperse particles, the peak frequency was changed proportionally to the mixture ratio of two particle components. Sample suspensions of 2 wt% were prepared with mixture ratios of 1:2, 1:1, and 2:1. The dynamic ranges of the peak frequency were 2.8 MHz between the 6-µm and 46-µm particles and 1.8 MHz between the 5-µm and 10-µm particles.

IUS1-PB3-5

Multiresolution texture features of carotid artery wall and plaque toward identifying vulnerable asymptomatic cases from B-mode ultrasound

Spyretta Golemati[1], Symeon Lehareas[1], Nikolaos Tsiaparas[2], Achilleas Chatziioannou[1], Konstantina Nikita[2], Despina Perrea[1]; *[1]Medical School, National Kapodistrian University of Athens, Athens, Attica, Greece, [2]National Technical University of Athens, Greece*

Background, Motivation and Objective

Efficient management of asymptomatic carotid atherosclerosis remains a crucial issue in clinical practice, because the currently used determinant for deciding surgical or medical treatment, namely the stenosis degree, has proven inadequate. Various features derived from ultrasound image analysis have shown promise for enhancing the effectiveness of decision making. Among these, multiresolution, i.e. wavelet-transform-based, texture analysis has been shown to adequately characterise atheromatous tissue, especially in terms of horizontally oriented texture in longitudinal B-mode sections.

Statement of Contribution/Methods

We sought to investigate the horizontally-oriented multiresolution textural properties of arterial wall and plaque in a carefully selected sample of asymptomatic male subjects. Of the 19 carotid arteries that were interrogated, 7 had low stenosis degrees (50-69%) and 12 had high stenosis degrees (70-100%); the two groups had similar ages. Multiresolution analysis was performed using wavelet packets and the coiflet 1 wavelet, for three levels of decomposition. Seven features were derived from the resulting approximation (A) and horizontal detail (Dh) images, for two segments in each artery, namely plaque and the adjacent intima-media complex (IM).

Results/Discussion

All features were statistically similar between low and high stenosis cases, suggesting that stenosis degree may not be sufficient to characterise the two case types. Differences between IM and plaque were observed for most multiresolution features (Table 1). The differences were more prominent for higher decomposition levels. The feature Dh3A2A1 was different between plaque and IM in the low stenosis cases but was not different in the high stenosis cases. The opposite was observed for Dh2Dh1. Such differences suggest incontinuities in tissue properties and therefore increased vulnerability. In conclusion, multiresolution texture analysis may provide valuable information about normal and atheromatous tissue, because certain tissue properties are revealed at high decomposition levels.

Table 1. Average±std values of multiresolution features for low (LS) and high (HS) stenosis cases. IM: intima-media tissue adjacent to plaque; PLQ: plaque. * indicates statistically significant difference compared to IM (p-value<0.05); ** indicates stronger statistically significant difference compared to IM (p-value<0.01). 1, 2, 3: levels of decomposition. Dh: horizontal detail image; A: approximation image.

	LS		HS	
	IM	PLQ	IM	PLQ
Dh_1	7.18±3.34	6.17±2.18	7.05±.40	6.03±1.97
Dh_2A_1	18.81±7.38	13.99±6.14	18.79±6.35	14.86±4.78
Dh_2Dh_1	11.14±4.86	7.82±.00	10.91±3.52	**7.96±2.84***
$Dh_3A_2A_1$	44.58±15.60	**29.48±10.15***	46.87±16.45	35.96±12.65
$Dh_3Dh_2A_1$	26.66±10.16	15.30±6.10*	25.75±8.78	17.24±6.18*
$Dh_3A_2Dh_1$	9.95±4.64	4.70±1.82*	10.36±4.18	5.46±2.13**
$Dh_3Dh_2Dh_1$	12.14±5.31	6.76±2.33*	11.25±3.30	7.13±2.73**

IUS1-PB3-6

Assessment of median nerve mobility by ultrasound dynamic imaging in carpal tunnel syndrome diagnosis

Tai-Tzung Kuo[1,2], **Ming-Ru Lee**[2], Yin-Yin Liao[2], Wei-Ning Lee[3], Yen-Wei Hsu[4], Jiann-Perng Chen[5], Chih-Kuang Yeh[2]; *[1]Department of Neurosurgery, Hsin-chu Mackay Memorial Hospital, Hsinchu, Taiwan, [2]Department of Biomedical Engineering and Environmental Sciences, National Tsing Hua University, Hsinchu, Taiwan, [3]Department of Electrical and Electronic Engineering, The University of Hong Kong, Hong Kong, [4]Department of Neurology, Hsin-chu Mackay Memorial Hospital, Hsinchu, Taiwan, [5]Department of Physical, Hsin-chu Mackay Memorial Hospital, Hsinchu, Taiwan*

Background, Motivation and Objective

Carpal tunnel syndrome (CTS) is a common entrapment neuropathy resulting from the median nerve dysfunction. Nerve conduction studies (NCS) have been used as a standard for CTS diagnosis. Complementing NCS, ultrasound imaging provides anatomic information on pathologic changes of the median nerve, such as the enlarged median nerve area and the reduced median nerve mobility. However, motion of median nerve is a non-uniform pattern which is dependent on local anatomical, mechanical characteristics, and body movements. The purpose of this study was therefore to measure transverse sliding patterns of the median nerve during finger flexion and extension in ultrasound B-mode images for distinguishing healthy from CTS subjects, and to investigate any correlation between NCS severity and median nerve motion.

Statement of Contribution/Methods

Transverse ultrasound images were acquired from 19 normal, 15 mild, and 10 severe CTS subjects confirmed by NCS and pathologic examination. During each two-second acquisition, their fingers were initially in natural position (t1); the median nerve was then moved toward the ulnar side in finger flexion (t2) and finally the radius side in finger extension (t3) as shown in Fig. (a-c). Greater transverse sliding of median nerve during finger flexion and extension was observed in the normal subjects than in the mild and severe CTS patients. The lateral displacement of the median nerve region was calculated by the multilevel block sum pyramid algorithm and averaged. All the average lateral displacements at different acquisition times were then accumulated to obtain cumulative lateral displacements, which were curve-fitted by polynomial function (Fig. (d)). To differentiate the normal from CTS cases, the R-squared, curvature, and amplitude of the fitted curves were computed, to evaluate the goodness, variation, and maximum value of the fit, respectively.

Results/Discussion

Compared to the CTS patients, the normal subjects had higher R-square, curvature, and amplitude estimates. The three parameters were then inputted to a fuzzy c-means algorithm to classify normal cases and CTS ones. The diagnostic efficiency had an accuracy of 93.2%, a specificity of 100%, and a sensitivity of 88%. Further study includes measuring mechanical strain and stress at different neural sites to provide elasticity of the median nerve.

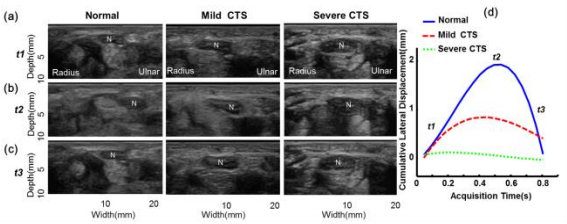

IUS1-PB3-7

Soft-label reinforced rtCAB for guided prostate tissue sampling

Mahdi Tabassian[1], Nicola Testoni[2], Francesca Galluzzo[1], Luca De Marchi[1], Nicolo' Speciale[1], Guido Masetti[1]; *[1]Electrical, Electronic and Information Engineering (DEI), University of Bologna, Bologna, Bologna, Italy, [2]Department of Civil, Environmental and Materials Engineering (DICAM), University of Bologna, Italy*

Background, Motivation and Objective

Prostate cancer (PCa) is second most frequent neoplasy in men, with almost 1 million new cases/year worldwide. Since PCa is not clearly detectable at standard, non-invasive diagnostic methods, Transrectal Ultrasonography (TRUS) guided prostate biopsy (PBx) is mandatory. The procedure consists in a coded tissue sampling by means of a surgical needle. As patient discomfort and adverse event probability grow with each extracted sample, it is desirable to reduce the number of PBx samples without negative impinging on diagnose accuracy. Even if real-time Computer Aided Biopsy (rtCAB) systems can be used to guide tissue sampling to areas with the highest probability of PCa presence, their training is usually affected by ground truth uncertainty due to the unknown tumor distribution.

Statement of Contribution/Methods

The work describes how to reinforce rtCAB systems by considering uncertainty in the labels of the ground truth data. Fast and accurate radio-frequency (RF) signal envelope/phase detectors, maximum likelihood estimators of Nakagami and Von Mises parameters and complex (both nonlinear and linear) classification models will be integrated by an original re-labeling algorithm able to assign soft or crisp class labels to the unlabeled patterns, thus allowing for their inclusion in the training set. By doing so we can avoid collected data wasting and construct a rigorous ensemble learning scheme by merging the decisions of some classifiers, each one trained on a different data representation.

Results/Discussion

The proposed enhanced rtCAB system was implemented making use of CUDA parallel processing capabilities in order to deliver real-time frame rates. Classification model was trained on a specifically build prostate gland adenocarcinoma database (1300+ PBx cores, 26000+ regions of interest). Ground truth for each core was established by an expert physician, providing tissue description and illness percentage for each core. Different types of features are extracted directly from the RF signals and are incorporated in an ensemble learning structure in order to the reduce uncertainties in the learning data. The whole system was optimized to reduce the number of false positives while preserving an acceptable number of false negatives. Comparing to a classical double sextant PBx, the positive prediction value (PPV) of our method is 88% better, with an overall sensitivity of 92%. By providing a real-time feedback to the physician during TRUS, this tool would allow for a reduction by more than 50% in the number of biopsy cores without losing in diagnose accuracy. The optimality of the proposed learning method in dealing with uncertain data was also been tested using subsets of UIUCTex and UCI repository real data sets in which the proposed scheme outperformed the traditional ensemble and evidence-based structures by an improvement in the classification error rate up to 20%.

IUS1-PB3-8

Projection Mode Ultrasonic Microscopy for Cell-size Observation

Agus Indra Gunawan[1], **Naohiro Hozumi**[1], Tomohide Furuhashi[1], Sachiko Yoshida[1], Kazuto Kobayashi[2], Yoshifumi Saijo[3], Seiji Yamamoto[4]; *[1]Electrical and Electronic Information Engineering, Toyohashi University of Technology, Toyohashi, Aichi-ken, Japan, [2]Honda Electronics Co., Ltd, Toyohashi, Japan, [3]Tohoku University, Sendai, Japan, [4]Hamamatsu Univ Sch Med, Hamamatsu, Japan*

Background, Motivation and Objective

Ultrasonic microscope is a powerful tool for biological applications. The authors proposed several modes of cell size observation. In the sound speed mode, the specimen was in contact with water that may bring contaminant from outside. In the acoustic impedance mode, the specimen was separated by the substrate from any contaminant. This study is propose new type of observation for internal structure of biological tissue without introducing contaminants.

Statement of Contribution/Methods

Glioma cells were cultured on a thin polystyrene film. The cultured space was subsequently enclosed between two films, with 15 micrometers in distance. A focused ultrasonic beam, its frequency range being 200 - 400 MHz was transmitted from the rear side of the film (Fig. 1). Two reflections, namely A and B, were observed. A can be interpreted into the acoustic impedance. B represents the projection of the cell structure.

Results/Discussion

Ultrasonic microscopies were obtained by scanning the transducer. The image by reflection A represents the reflection from the interface between cell and film. Weak intensity indicates higher acoustic impedance. The surrounding low intensity region of each cell shows cytoskeleton. Nuclei are supposed to be in the center of cytoskeletons and might show low reflection intensity. Image by reflection B represents the internal attenuation throughout the cell.

This observation mode can be defined as projection mode. Although the image does not precisely indicate the attenuation coefficient of the tissue, internal structure can be observed as a projection. Furthermore in the paper, it will be described that hepatoma was smeared onto a glass substrate and covered with a thin plastic film to observe in the same way. An observation of hepatoma cells was successfully performed (Fig. 2).

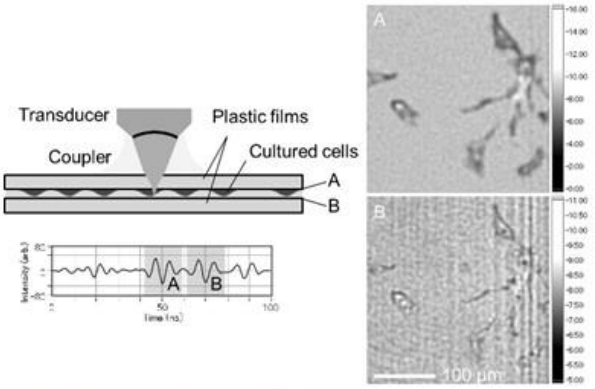

Fig. 1 Ultrasonic alignment and intensity images from two different reflections indicated in arbitrary unit.

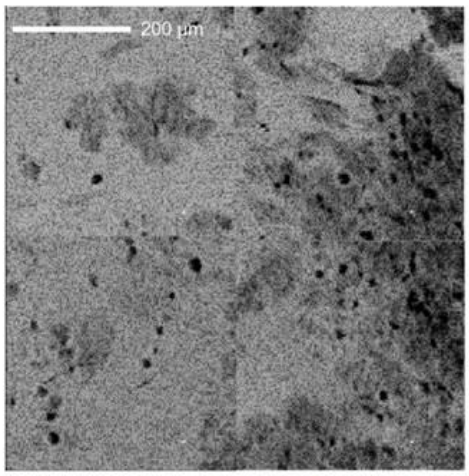

Fig. 2 Reflection intensity image in projection mode of smeared hepatoma, indicated in arbitrary unit.

IUS1-PB3-9

Following-up the regeneration of injured rat muscle through the average pixel intensity of ultrasound biomicroscopic images

Carolina Peixinho[1], Liliam de Oliveira[2], João Machado[1,3]; *[1]Biomedical Engineering Program - COPPE, Federal University of Rio de Janeiro, Brazil, [2]Biosciences and Physical Activity, Federal University of Rio de Janeiro, Brazil, [3]Post-Graduation Program in Surgical Sciences - Department of Surgery, Federal University of Rio de Janeiro, Brazil*

Background, Motivation and Objective

Ultrasound imaging is widely used, in vivo, to detect lesions or morphological changes in a muscle. Regarding studies involving small animals, ultrasound biomicroscopy (UBM) is an adequate scalable tool to image, for example, rat skeletal muscles such as those in the hind limb. In this sense, UBM is useful in studies to establish injury models and to follow-up muscle adaptations, in vivo, enabling investigations regarding different types of treatment, training or rehabilitation programs. This work aims to evaluate changes in image brightness (echo intensity) of a muscle with a laceration injury, and to follow-up these parameter changes during the regeneration process.

Statement of Contribution/Methods

This work contributes with the follow-up of rat muscle regeneration, after laceration injury, based on a UBM image parameter. A 40 MHz UBM system (Vevo 770; VisualSonics, Toronto, Canada) acquired the images of lateral gastrocnemius muscle from both hind legs of 6 Wistar male rats (3-4 months) submitted to a laceration injury protocol on the right hind limb. UBM images from both leg muscles were acquired before and after right leg operation (immediately, 7, 14, 21 and 28 days) and the mean of the image pixel intensity values, for a region-of-interest (2x2mm) over the lesion site, was calculated using ImageJ (National Institute of Health, Maryland, USA). The mean pixel intensity was measured for three image frames from each limb in each condition and API, the average of the three measurements, obtained. Six API values resulted for each leg and each condition. Two-way ANOVA for repeated measures ($p<0.05$) compared the API values between all the conditions and for both limbs.

Results/Discussion

The mean API of the operated leg was significantly lower immediately, 7, 14 and 21 days after injury and significantly higher 28 days after, than the value for the corresponding site before operation. There were no differences between conditions for the non-operated leg, however, a statistical difference between both legs was found for all the conditions after injury. The time course of changes in average API match with the time course of the muscle regeneration process, in which the presence of hypoechoic areas after operation correspond to hemorrhagic cavity caused by the lesion, hematoma, and edema with no observable fibers in the images. As the muscular tissue remodels, then hyperechoic bundles start to appear in the images. Such echogenicity increase is associated with the establishment of scar tissue that provides the wound tissue with the initial strength to withstand the contraction forces applied to it before the repair process completion. The API of UBM images has proven its applicability as a signaling parameter to monitor adaptations of skeletal muscle tissue during regeneration.

Acknowledgments: the authors thank the financial support provided by CAPES, CNPq, and FAPERJ, and the National Center of Bioimaging/UFRJ, which allowed the use of UBM equipment.

IUS1-PB3-10

Characterization of the Colorectal Cancer in a Rabbit Model Using Quantitative High-frequency Endoscopic Ultrasound

Cheng LIU[1], Weibao QIU[2], Yanyan YU[1], Lei SUN[1]; *[1]Interdisciplinary Division of Biomedical Engineering, Faculty of Engineering, The Hong Kong Polytechnic University, Hong Kong SAR, China, People's Republic of, [2]Paul C. Lauterbur Research Center for Biomedical Imaging, Shenzhen Institutes of Advanced Technology, Chinese Academy of Sciences, Shenzhen, China, People's Republic of*

Background, Motivation and Objective

Colorectal cancer (CRC) is the third most common cancer for both men and women in the United States, predicted in 2012 to account for 9% of newly diagnosed malignancies and 9% cancer related deaths. Colorectal cancer at early stage often has no symptoms, which causes delay of timely and successful treatments. Currently, it is difficult to determine early stage CRC by ordinary endoscopy even with dye. Although endoscopic ultrasound (EUS) has been widely used to visualize overall depth-view five-layered structural alteration of colorectal tract for assessing the risk of metastasis and determining the local surgery strategy, its potential to diagnose early CRC has not been confirmed. Recently, high-frequency EUS instrument (20MHz-30MHz) becomes available, but its utility has not been demonstrated on determination of intestinal wall abnormalities such as benign hyperplastic polyp, malignant adenoma and cancer. It is the aim of this research to investigate the potential of quantitative ultrasound (QUS) based on radio frequency (RF) data in diagnosis of early colorectal cancer at high frequency.

Statement of Contribution/Methods

Twelve New Zealand White male rabbits were used, including control rabbits (n=3) and experiment rabbits (n=9) surgically implanted with VX2 tumor cell. A high-frequency EUS system developed by our group was used for data acquisition. Briefly, the EUS system employed a mechanical 30MHz single element side-view endoscopic ultrasound transducer and achieved reconfigurable hardware circuitry, programmable processing algorithms, flexible imaging control and raw RF data acquisition. At 5-, 10-, 15-day intervals

after cancer cell implantation, three rabbits with tumors and one control rabbit were sacrificed. A 10cm segment of colon was rapidly excised and immersed in saline at 25°C. EUS scan was performed into the exercised colon tract to acquire 2D B-mode images and raw RF data. Tumor location, size, margin were determined by B-mode images. Histology was performed afterwards. The acoustic spectra were calibrated, and a linear regression was performed to fit the resulting quasi-linear acoustic spectra. Slope, intercept, correlation coefficient, root mean square deviation and midband fit were obtained and compared between the region-of interests (ROIs) representing colorectal tumors and adjacent normal colon tissue. The results of *ex vivo* ultrasound image, QUS parameters and histology were compared among groups.

Results/Discussion

Significant differences were observed between the parameters from cancerous ROIs and normal colorectal tissue region. The results showed that the complementary information derived from quantitative high-frequency EUS (anatomical versus patho-physiologic) may create better sensitivity and specificity to early colorectal cancer diagnosis.

Medical signal processing

Forum Hall

Tuesday, July 23 2013, 01:00 pm - 04:30 pm

Congress Hallair: **Kendall Waters**
Silicon Valley Medical Instruments

IUS1-PB4-1

Model Based Restoration of the RF Data for High Resolution Vascular Ultrasound Imaging

Ramazan Demirli[1], Chandra Sehgal[2]; [1]*Center for Advanced Communications, Villanova University, USA,* [2]*Department of Radiology, University of Pennslyvania, USA*

Background, Motivation and Objective

The resolution of medical ultrasound images is compromised by the bandlimited ultrasound pulse. Recently, a new class of deconvolution algorithms from the compressive sensing (CS) field has been used in ultrasound imaging for resolution improvement. Compared to the classical deconvolution methods, these CS methods (CSMs) robustly exploit the sparsity of tissue reflectivity (TR) and provide significant resolution gains. However, CSMs assume the ultrasound pulse is invariant throughout the propagation path which is not realistic in tissues due to the frequency dependent absorption and scattering. As such, pulse variance severely compromises the performance of CSMs in estimating the TR with high fidelity. The goal of this study is to develop a new technique that accounts for pulse variance.

Statement of Contribution/Methods

Our method uses Model-Based Estimation Pursuit (MBEP) to restore the RF data in terms of Gaussian Chirplets (GCs) whose delay and amplitude parameters are sensitive to location and strength of scatterers (i.e, TR) and its spectral parameters (center frequency, bandwidth, chirp-rate, phase) are sensitive to dispersion characteristics of the propagation path. MBEP successively extracts GCs from RF data via partitioning, parameter estimation, and removal of estimated echo. First, a partition is obtained based on the most prominent peak in the RF envelope. Then, the parameters of GC are optimized via Maximum a Posteriori Estimation (MAPE) to extract the most likely echo from the partition. MAPE enforces user defined constraints on spectral parameters and controls pulse variance.

MBEP and a CSM (l_1-regulirized Least Squares Deconvolution) were tested on RF data measured from a vessel mimicking phantom consisted of a rubber tube (1/8 inch diameter) with water flow controlled by a peristaltic pump. B-scan and post-beamformed RF data were acquired using the ultrasound scanner, Sonix RP (Ultrasonix, BC, Canada). The RF data were restored using l_1-LSD and MBEP, and log-compressed to obtain B-scan images, which were then compared to B-scan image before restoration qualitatively and quantitatively using the resolution gain (RG). RG is defined as the ratio of the 3dB widths of the average autocorrelation functions of RF lines before and after restoration.

Results/Discussion

MBEP improved the resolution significantly with RG of 9.04. In the MBEP images vessel borders were clearly visible and its fine structures hidden in the B-scans became apparent. The l_1-LSD, on the other hand, due to its inflexibility with varying pulses, failed to delineate vessel's borders and reveal new fine details. Further, the MBEP yielded faster processing (about 10 times) with 20% improvement in RG compared to l_1-LSD.

A novel RF data restoration technique is proposed to improve the resolution of vascular images. The method accounts for pulse variance and can recover the TR with higher fidelity and faster processing time than the state-of-the-art CSMs.

IUS1-PB4-2

Real-Time BAPES Implementation for Fast Spectral Doppler Estimation

Stefano Ricci[1], Riccardo Matera[1], Piero Tortoli[1]; [1]*Information Engineering Dept., Università di Firenze, Firenze, Italy*

Background, Motivation and Objective

The echoes backscattered from blood red cells moving in a vessel are typically elaborated through a spectral analysis to obtain the Doppler frequencies distribution. The conventional processing is based on the Welch estimator implemented through FFT, that is characterized by good spectral resolution only if applied to a large number of samples (e.g. 64-128). Gran et all (doi: 10.1109/TUFFC.2009.1093) proved that the BAPES spectral estimators could produce good spectrograms using down to 16 pulse repetition intervals (PRIs) per frame, thus obtaining better time resolution and/or higher B-mode frame rates when working in Duplex mode. Unfortunately BAPES requires much more calculations than Welch, making a real-time implementation quite challenging.

.

Statement of Contribution/Methods

In this work the implementation of the BAPES method in the Ula-Op Research Ultrasound scanner is reported. In particular the algorithm has been coded for the fixed-point TMS320C6455 Digital Signal Processor (DSP) present on-board. The dynamics of the signal in the critical points of the algorithm has been analyzed to achieve an optimal trade-off between math precision and calculation effort. 16/32 bit and block-floating point math have been used according to the previous study. A carful use of simplifications and approximations have been implemented for reducing the calculations with a limited accuracy loss.

.

Results/Discussion

The presented BAPES implementation, based on 16 overlapped data segment of 16 samples each (31 PRIs per estimate), requires 500k plus 20k clock cycles per frequency point, memory and math operations included. A typical spectral analysis on 128 frequency points is carried out in 3 M cycles, which corresponds to 4.2 ms on the 700 MHz Ula-Op DSP. Thus a high frame rate (e.g. 50 fps) can be easily achieved leaving enough free calculation power for other concurrent operations. The picture reports an example obtained from an in-vitro flow. On the left the sonograms processed by the presented BAPES implementation and the reference calculated by Matlab® are shown. On the right the Doppler spectrum present at 0.2s is compared to the reference (top) and the error (bottom), which corresponds to a -20 dB with respect to the reference, is reported. Spectrograms generated by the real-time implementation will be shown to present no visible difference with respect to the reference.

.

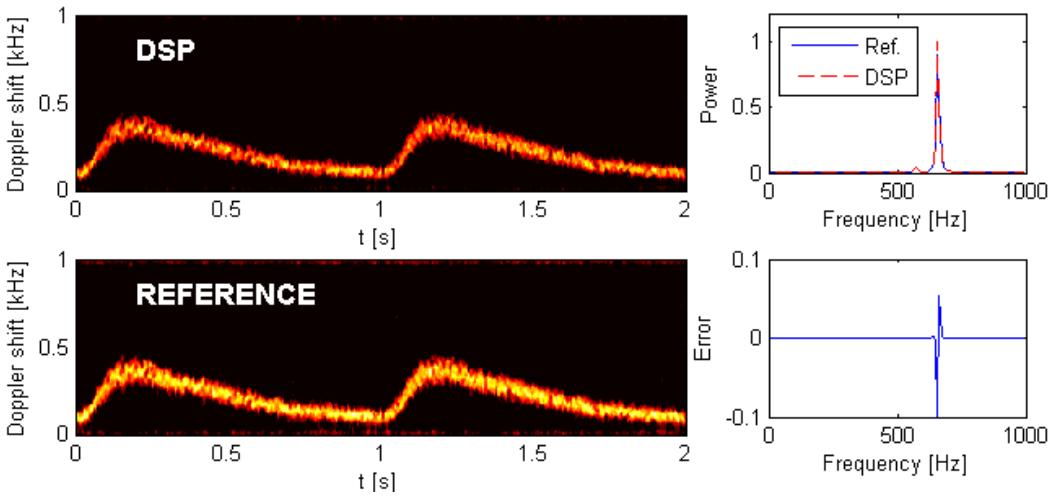

IUS1-PB4-3

Ultrasound Compressed Sensing: Performance Study of Reconstruction on Different Ultrasound Imaging Data

Yen Chuo[1], Tsung-Han Chan[2], Meng-Lin Li[1,3]; [1]*Electrical Engineering, National Tsing Hua University, Taiwan,* [2]*Advanced Digital Sciences Center, Singapore,* [3]*Institute of Photonics Technologies, National Tsing Hua University, Taiwan*

Background, Motivation and Objective

In ultrasound (US) imaging, the imaging frame rate is mainly limited by the speed of sound, imaging depth, and number of measurments (i.e., scanlines). To reduce the data acquisition time and thus to increase the imaging frame rate, the concept of compressed sensing (CS) adapted to US imaging modality emerged in 2010. CS restores signals via sparsifying them with proper domain transformation. It potentially allows an ultrasound image to be reconstructed from relatively few measurements below the Nyquist criterion, thus resulting in reduced data volume or data acquisition time.

Statement of Contribution/Methods

In this work, we investigate performance of reconstruction on different US post-beamformed data when performing US CS with fewer measurements. Three types of post-beamformed data – radio frequency (RF), envelope, and log-converted data are used. Each data type has its own signal distribution, which, given a typical sparse representation, affects sparsifying efficiency during CS reconstruction and hence further determines restored image quality. Field II simulation of a speckle generating phantoms with a hyperechoic cyst is performed. The leftmost panel in the figure is the re-sampled image data used for evaluation of reconstruction performance where there are only 50% of A-lines. Here reconstruction is performed using convex optimization algorithm along the lateral direction and sparse transformation with CDF 5/3 wavelet is typically chosen.

Results/Discussion

The results (the three right panels in the figure) show that for feature recognition, reconstruction on post-beamformed RF and envelope data have close performance, and is better than that on log-converted data. In terms of mean-square-error (MSE), reconstruction on RF data performs best. In addition, under various levels of noises added, the CS-restored US images on different data types maintain the similar characteristics. Based on the signal feature of the post-beamformed RF data along the lateral direction, selecting a better sparse representation of RF data to enable more efficient reconstruction will be our next step.

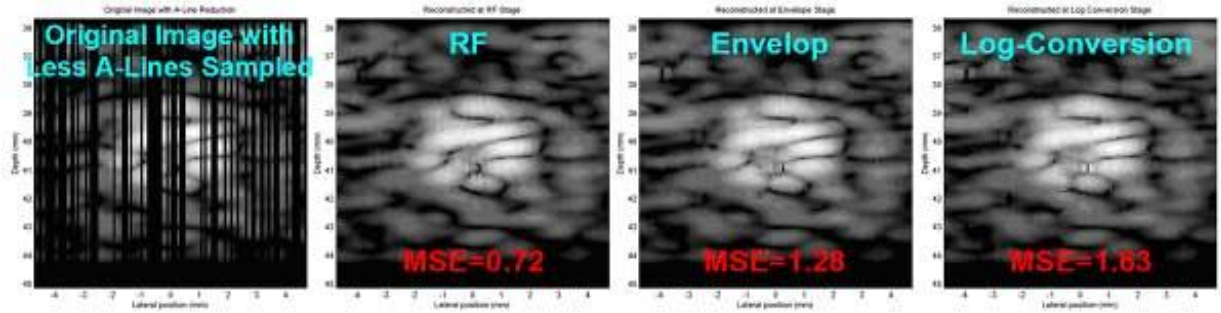

IUS1-PB4-4

Efficient Pulse Compression of Chirp Coded Excitation in Medical Ultrasound Imaging

Changhan Yoon[1], Wooyoul Lee[1], Jin Ho Chang[1,2], Tai-Kyong Song[1], Yangmo Yoo[1]; [1]*Electronic Engineering, Sogang University, Korea, Republic of,* [2]*Interdisciplinary Program of Integrated Biotechnology, Sogang University, Korea, Republic of*

Background, Motivation and Objective

Coded excitation can improve the signal-to-noise ratio in the medical ultrasound imaging. In coded excitation, to preserve axial resolution, pulse compression (PC) is conducted. The PC is commonly performed by applying a matched filter based on the transmitted coded sequence. However, the conventional PC method requires a few hundred filter coefficients when using elongated transmit coded sequences (e.g., chirp), leading to considerably high computational complexity.

Statement of Contribution/Methods

In this paper, an efficient PC method for chirp coded excitation is proposed. In the proposed method, the PC is conducted with the complex baseband in-phase and quadrature (IQ) data after decimation (e.g., L-fold under-sampling) instead of beamformed radio-frequency data. To effectively compress the baseband signal, a complex PC filter is required. However, since both received data and compression filter coefficients are decimated, the computational complexity can be reduced by 4/L2. The performance of the proposed PC method was evaluated with phantom experiments. The beamformed RF data were acquired using a convex array transducer connected to a custom-built ultrasound imaging system that can transmit the weighted chirp waveforms. For the weighted chirp waveform, the center frequency was 2 MHz, and the time duration was 8 us, corresponding to the PC filter of 320 coefficients in the conventional PC method. On the other hand, in the proposed method, the PC filter of only 40 filter coefficients was used.

Results/Discussion

Figure 1 shows the phantom images with the chirp coded excitation method by (a) the conventional and (b) proposed PC methods, respectively. Under visual assessment, the difference between two methods is negligible. For quantitative comparison, the -6-dB axial resolutions were measured for 15 wire targets at the center scanline; those were identical in both methods. The clutter-energy-to-total-energy ratios (CTRs) at a hypo-echoic region (white arrow) were 27.6 dB and 27.4 dB for the conventional and proposed PC methods, respectively. These results indicate that the proposed PC method can reduce the computational complexity by a factor of 16 compared to the conventional PC method while preserving the image quality.

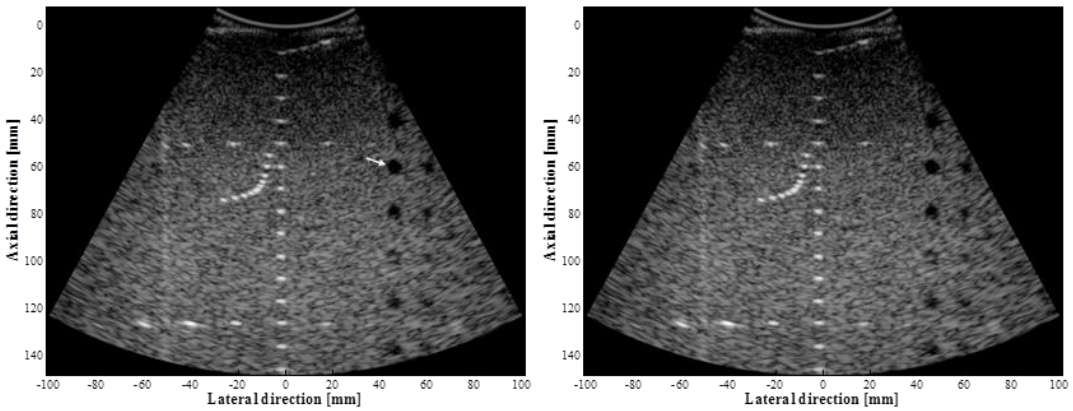

(a) (b)

Fig. 1. The phantom images with chirp coded excitation by (a) the conventional and (b) proposed pulse compression methods, respectively.

IUS1-PB4-5

Effect of a variation of the thickness of cortical bone and soft tissue on the measurement of guided modes propagating in axial transmission

Ludovic Moreau[1], **Jean-Gabriel Minonzio[1]**, Josquin Foiret[1], Maryline Talmant[1], Pascal Laugier[1]; *[1]LIP, UPMC - CNRS, Paris, France*

Background, Motivation and Objective

The potential of ultrasonic guided waves to evaluate indicators of bone fragility has recently been emphasized. The characterization of cortical bone relies on accurate measurements of the guided mode wavenumbers and adequate fitting with a waveguide model. Originally, the approach was validated on homogeneous free bone-mimicking plates of constant thickness. However, the targeted skeletal site (i.e., radius) usually diverges from the ideal free waveguide due to (i) the presence of an overlying soft tissue layer and (ii) the variable thicknesses of both the cortical bone and soft tissue layers. In this work, we aimed at assessing separately the impact of (i) a variable cortical thickness and (ii) of the presence of a soft tissue layer of variable thickness, on the measured guided modes wavenumbers.

Statement of Contribution/Methods

The guided modes wavenumbers of bone-mimicking plates were obtained experimentally using the singular value decomposition-based approach developed for a multi-emitter and multi-receiver probe. They were compared to theoretical values from a free plate model of constant thickness, with transverse isotropic properties.

Measurements were first carried out on plates with a linearly varying thickness. Two angles typical of the inclination encountered in the human radius were considered : 1° and 2°. Then a bone-mickiming plate of constant thickness covered by a 2 mm-thick fat-mimicking layer (bulk compression speed 1430 m.s-1) was tested. The angle between the probe axis and the plate, controlled by a goniometer, was varied from -2° to + 2° with 0.25° increment to mimick the varying thickness of soft tissues at the forearm.

Results/Discussion

The most significant deviations of the experimental wavenumbers from the ones in the plate of constant thickness were:

1/ when the plate thickness increases along the propagation direction, the smallest wavenumber values were not measured. The plate being thinner at the emitter positions, these wavenumbers are not excited and thus cannot be observed. As these values are close to cutoff frequencies, they are particularly important for the waveguide parameter estimation.

2/ a gradient of thickness of the soft tissue along the propagation direction causes an overestimate (underestimate, respectively) of the wavenumbers if the gradient is positive (negative, resp.). This bias is due to the lack of parallelism between the receivers and the bone surface.

Both effects increase with the angle and the mode order. These results expose for the first time several sources of discrepancy between the observed wavenumbers and those of an ideal free plate model. These effects must be taken into account in the future for in vivo measurements.

IUS1-PB4-6

A Study on Ultrasound Speckle Reduction Based on Stochastic Fluctuation of Transmitted Ultrasound Beam

Haruka Suzuki[1], Norio Tagawa[1], Kan Okubo[1]; *[1]Graduate School of System Design, Tokyo Metropolitan University, Hino, Tokyo, Japan*

Background, Motivation and Objective

Many speckle reduction methods have been proposed, and each has shortcomings to be improved respectively. On the other hand, research in engineering application of the mechanism of Sto-chastic Resonance, which can be viewed as a noise-induced enhancement of a weak signal and naturally appears in many neural dynamics, has been advanced variously. In this study, we ex-amine the use of stochastic resonance scheme for speckle reduction.

Statement of Contribution/Methods

Speckle patterns have a spatial randomness, and hence spatial averaging for ultrasound images can suppress speckle patterns. However, it causes blurring of signals to be detected. In this study, by randomly and fractionally vibrating a transducer toward transmit and receive direction, we forcibly vary the sound field of transmitted beam, where imaging targets are supposed to be stat-ic. This makes the temporally random fluctuation of speckle patterns, since a speckle pattern is interference of echoes from many small scatterers. To suppress speckle patterns only and to pre-serve desired signals, averaging of the multiple echoes observed while the vibration should be performed after time-shift processing for the echoes to compensate the change of transducerï¿½fs position caused by the vibration. This averaging is carried out as an RF signal.

Results/Discussion

We confirmed effectiveness of our method through FEM simulations. The pulse containing five carrier signals of 5 MHz was transmitted. The maximum range of the transducerï¿½fs vibration was changed approximately from one pulse width to three pulse width. The 100 echoes observed while the vibration are averaged. SNR defined by the peak value of signal and the mean value of the demodulated speckles improved with 1.9 dB for the one pulse width case, 3.5 dB for the two and 3.4 dB for the three respectively against before processing. It was confirmed that for all cas-es the signals from the tumor have no blurring. On the contrary, simple averaging without the above mentioned time-shift caused heavy signal blurring, although the speckles are reduced easi-ly since it makes use of the spatial randomness of speckles in addition to the temporal one used in our method. Similarly, its SNR was 1.63 dB, 1.15 dB and 0.52 dB for each case, which are much lower than those of our method. In future, we are going to detect the time-shift quantities automatically using echo signals themselves.

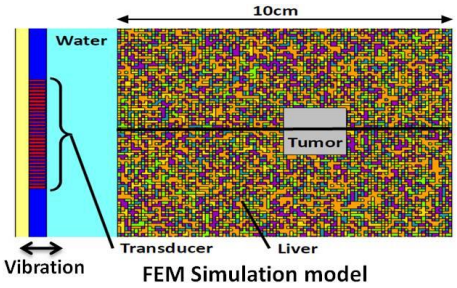

FEM Simulation model

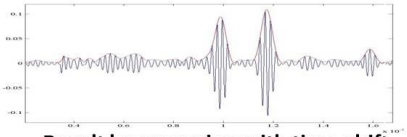
Result by averaging with time-shift for three pulse-widths vibration (proposed vibration method)

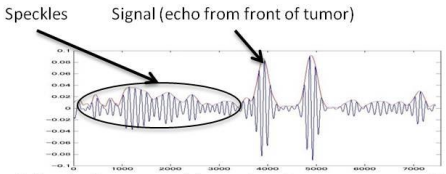

Echo before speckle reduction corresponding to horizontal solid line in simulation model

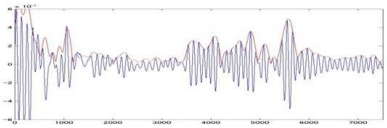
Result by averaging without time-shift for three pulse-widths vibration

IUS1-PB4-7

Recursive Reduction of Frequency Dependent Attenuation for Wide-Band Ultrasound Imaging in a Living Body

Takuya Hiraoka[1], Norio Tagawa[1], Kan Okubo[1], Iwaki Akiyama[2]; *[1]Graduate School of System Design, Tokyo Metropolitan University, Hino, Tokyo, Japan, [2]Depertment of Biomedical Information, Doshisha University, Kyotanabe, Kyoto, Japan*

Background, Motivation and Objective

For high resolution ultrasound imaging of a deep part in a living body, pulse compression with wide-band transmission is suitable, and a wide-band transducer is studied vigorously. However, high-frequency echo is strongly affected by FDA, which makes exact pulse compression impossible and causes image blurring. We already proposed an FDA compensating method in which the transmitted signal echo of which becomes desired FM chirp after distorted by FDA is generated using a referenced echo. For simple tissue model with an FDA coefficient of 1.0/MHz/cm at 1 MHz transmission, we confirmed through simulations that the method performs well, since the coefficient assumed in the method coincides with the setting value of 1.0/MHz/cm. On the other hand, the coefficient of actual tissue is generally regarded as being larger than 1.0/MHz/cm. Since, as expansion of a procedure, the method can estimate the coefficient adaptively and use it for generating the transmitted signal compensating FDA, we examine the effectiveness of the use of an adaptively estimated coefficient.

Statement of Contribution/Methods

We use the simulation model with an FDA coefficient of 1.5/MHz/cm. Our method can be carried out recursively till the echo becomes a desired FM chirp. If FDA depends only on the propagation distance of ultrasound wave and the frequency of it, we can expect that, using the adaptively estimated FDA coefficient, the desired echo can be obtained by one time execution of the method. Conversely, if FDA has more complicated characteristics, even if the adaptively estimated value is used, recursive executions may be required and there is a possibility that the constant use of 1.0/MHz/cm performs better. We compare both schemes to improve our method.

Results/Discussion

On the assumption that a wide-band transducer is developed with a good property, FEM simulations with the transmission bandwidth of 9MHz were conducted. The evaluation results are shown below. We confirmed that the constant use of 1.0/MHz/cm as the coefficient has a superior performance, although the recursive repetition of few times is necessary. On the other hand, when the adaptively estimated coefficient is used, overshooting frequently occurs and several repetitions are required for convergence, the intrinsic cause of which has to be examined. Experimental examinations also have to be done to confirm this phenomenon exactly.

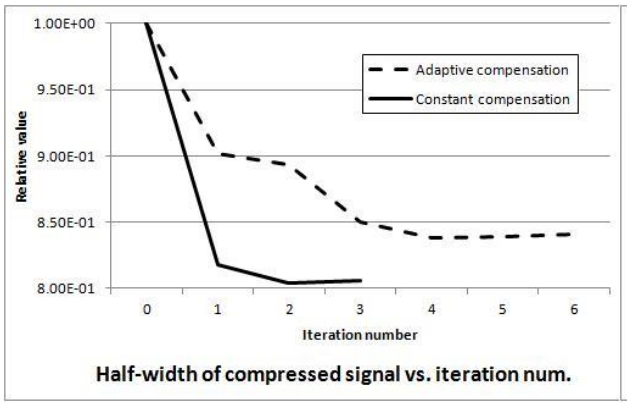

Half-width of compressed signal vs. iteration num.

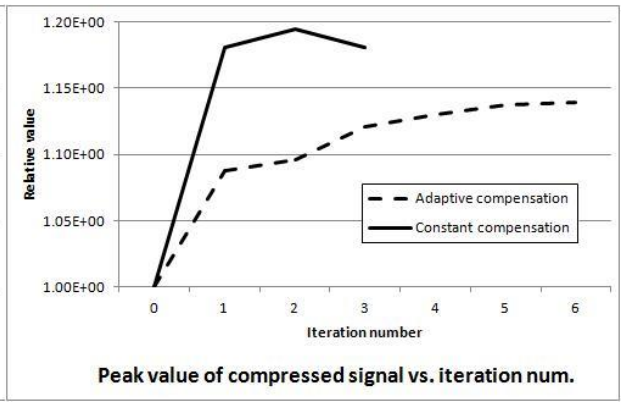

Peak value of compressed signal vs. iteration num.

Therapy I

Forum Hall

Tuesday, July 23 2013, 01:00 pm - 04:30 pm

Congress Hallair: **Zhen Xu**
University of Michigan

IUS1-PB5-1

Fusion modeling for predicting the Impact of in-vivo Liver Motion on HIFU therapies

William Apoutou N'DJIN[1], Jean-Yves CHAPELON[1], David MELODELIMA[1]; [1]*Inserm, U1032, LabTau, Lyon, F-69003, France ; Université de Lyon, Lyon, F-69003, France*

Background, Motivation and Objective

Pre-treatment planning is a key parameter in the development of High Intensity Focused Ultrasound (HIFU) systems. Transducer designs are usually optimized from modeling studies for dedicated applications. However, the development of HIFU strategies for the treatment of localized abdominal tumors is challenged by organ motion during respiration. Motions may influence the safety, efficacy and treatment time or require more complex systems and implementations for motion compensation. Currently, selecting the best approach can be difficult since conventional modeling tools do not provide reliable estimations of in-vivo HIFU ablations in realistic conditions during respiratory activity. And very few quantitative data are available on the effect of real tissues motions on HIFU treatments.

Statement of Contribution/Methods

Here we report in-vivo validation of a fusion modeling method which associates real in-vivo motion data acquired from ultrasound speckle tracking imaging and data from a multi-scale modeling tool. This method aims at estimating the impact of in-vivo liver motion on HIFU treatments by quantifying thermal lesion deformations. A Dice Similarity Coefficient (DSC) was calculated between lesion volumes obtained with and without organ motions. To validate the model predictions, fusion modeling results were compared to in-vivo intraoperative HIFU treatments performed in pig liver during respiration with 2 different ultrasound focusing strategies: (i) a spherical HIFU transducer used to juxtapose 7 × 7 single millimetric cigar-shaped lesions; (ii) a toroidal-shaped HIFU device developed for the treatment of Liver Metastases and used to create one single centimetric lesion.

Results/Discussion

Liver motions were mainly encountered in the cranial-caudal direction with a magnitude ranging 8-12 mm. Fusion modeling indicated that although a millimetric cigar-shaped lesion was stretched drastically and split in the tissues (DSC < 50%), centimetric ablations could be achieved intraoperatively without motion correction after 49 lesion juxtapositions in 8 minutes (DSC > 75%). Without motion correction, the toroidal-shaped HIFU strategy allowed generating large homogeneous lesions more than 10 times faster (6 cm3/min). Although the lesion main diameter was stretched by <15%, liver motion magnitudes observed in this study did not prevent from maintaining acceptable treatment accuracy (DSC: > 75%). Overall, fusion modeling of in-vivo HIFU treatments during respiration were well fitted to the observations made experimentally. The fusion between numerical and in-vivo data provided realistic results which could be useful for optimizing HIFU focusing strategies.

IUS1-PB5-2

Multiobjective optimization technique for treatment planning in HIFU

Mun-Bo Shim[1], Sung-Jin Kim[2]; [1]*Samsung Advanced Institute of Technology, Samsung Electronics, Korea, Republic of,* [2]*Samsung Electronics, Korea, Republic of*

Background, Motivation and Objective

In this study, a multiobjective optimization technique developed by the author is introduced to solve the sequence (or switching) plan of multiple foci, satisfied with the objectives of uniform high dose to the block and fast ablation. High Intensity Focused Ultrasound (HIFU) is a noninvasive medical procedure for localized tissue heating, used mostly in treatment of tumors. The modality of HIFU utilizes focused ultrasound to raise the temperature of the tumor tissue in small localized volumes, resulting in necrosis. To ablate the whole tumor, several of these sonication blocks are need. In case of multiple focusing, the shape and scan time of the single block which is a fundamental factor for planning the positions of the blocks depends on the sequence plan. In the previous study, new HIFU transducer architecture with sparse array (some of total elements), which can generate multiple foci simultaneously was designed and evaluated. Planning the sequence of multiple foci for the block is a time consuming and monotonous task, but requires at the same time expertise and precision. Furthermore, due to the complex characteristics of HIFU treatment, it is difficult to optimize manually. Besides, the objectives of uniform high dose to the block and fast ablation are invariably in conflict, often requiring compromises to be made between them when selecting the best sequence plan for a particular condition.

Statement of Contribution/Methods

In the previous study, a numerical optimization with a 1017-element spherical-section ultrasound phased array transducer operating at a frequency of 1.0MHz with 16 cm radius of curvature was performed for the generation of multiple foci (6, 6, 5, 4, 2, 2 foci in 5 by 5 foci) and sparse array with 507 elements to reduce the number of array elements and RF drive channels. With the acoustic fields of multiple foci and bioheat transfer equation, the multiobjective optimization problem used as the objectives of uniform high dose to the block and fast ablation was formulated in term of the sequence of multiple foci. Pareto-based continuous evolutionary algorithms for multiobjective optimization (MOPCEAs) developed by the author was used to solve the sequence planning. A variety of the sequence ordering methods and two multiobjective problems (2 objectives and 3 objectives) were used to examine the condition satisfied with uniform high dose as well as fast ablation.

Results/Discussion

MOPCEAs allowed us to obtain a diverse Pareto-optimal set of sequence plans that represent the necessary trade-offs between objectives. Unlike the shape of the block produced by single-focus scans, our multi-focus scans could generate various those of the block with uniform high dose in a feasible amount of scanning time. In multiobjective sequence planning, we produced diverse Pareto-optimal solutions, and the treatment planner could navigate through them intuitively.

IUS1-PB5-3

CT based aberration correction for 1 MHz transcranial HIFU therapy: optimization of the speed of sound maps with experimental propagation matrices.

Laurent Marsac[1,2], Mathieu Pernot[1], Mathias Fink[1], Jean-Francois Aubry[1], Mickael Tanter[1]; [1]*Institut Langevin, Paris, France,* [2]*Brain Therapy, SuperSonic imagine, Aix en provence, France*

Background, Motivation and Objective

In transcranial brain HIFU therapy, correction of defocusing effect of the skull must be achieved. Non-invasive correction is currently based on CT scan of the head in order to extract the 3D skull geometry which serves as input data for an acoustic propagation model trough the skull. We previously used a brain therapy system to estimate the accuracy of stereotactically localized heating in human cadaver heads. Here we propose to evaluate different propagation models on real human skulls extracted from these heads using the same system, with a pressure measurement at focus.

Statement of Contribution/Methods

A 512 elements and 1 MHz central frequency spherical probe was used in a water tank and a hydrophone was placed at its geometrical focus. Seven human skulls were mounted on a stereotactic frame and placed between the probe and the hydrophone. Transmitted signal was recorded for each of the emitting elements, for various positions of the hydrophone mounted on stepped motors. A total of 2023 locations in a regular 6x6x12 mm^3 volume around focus with a transverse resolution of 0.375 mm and an axial resolution of 2 mm were scanned with and without skull, leading to experimental propagation matrices. Each skull was then kept on its frame and imaged with a clinical CT scanner. The frame position and skull geometrical model relative to the probe were determined in the probe coordinates. Gold standard focusing was obtained by propagating the time-reversed experimental signal recorded at the probe focus. Non-invasive time-reversal signals were obtained using a 3D finite difference time domain (FDTD) acoustic propagation simulation from probe focus to elements trough the skull model. For each skull, aberration correction was computed for 5 different skull speed of sound distributions in the simulation. Minimum speed of sound (c_{min}) was 1.5 mm/µs and maximum (c_{max}) were respectively to [3, 3.5, 4, 4.5, 5] mm/µs. The different corrections were then used to determine the focusing with the experimental propagation matrices and the 3D maximum amplitude was recorded in each case.

Results/Discussion

Aberration correction has been performed on seven human skulls totalizing 2926 different skull propagation path. The 3D FDTD simulation led to an average amplitude of 83.5 % +/- 3.87 % of the optimal time reversal focusing and took 3 hours to compute. For the seven skulls used, the highest intensity at focus was obtained for c_{max} = 4 mm/µs in six case and for c_{max} = 3.5 mm/us in one case. Transmitting without any aberration correction only allowed to reach 43.3 % +/- 4.54 % of the optimum and led to multiple foci. The use of experimental transfer matrices allowed us to investigate several speed of sound distributions and compare them with the gold standard in the same experimental conditions. In the future, since transfer matrices and corresponding stereotactic CT data are now recorded, other speed of sound models, simulation schemes or signal analysis could be numerically tested and compared.

IUS1-PB5-4

Numerical Estimation of HIFU Focal Error to Breast Cancer Treatment

Ryuta Narumi[1], **Kosuke Matsuki[1]**, Takashi Azuma[1], Kohei Okita[2], Akira Sasaki[1], Kiyoshi Yoshinaka[3], Junichi Shidooka[4], Hidemi Furusawa[4], Shu Takagi[1], Yoichiro Matsumoto[1];
[1]The University of Tokyo, Japan, [2]Nihon University, Japan, [3]National Institute of Advanced Industrial Science and Technology, Japan, [4]Brestopia Namba Hospital, Japan

Background, Motivation and Objective

Acoustic inhomogeneity in the propagation media of HIFU (High Intensity Focused Ultrasound) has a potential risk to cause a focal error. Many research groups reported that the focal error of HIFU beam was critical when propagating media included bones. On the other hand, the focal error due to weakly heterogeneous such as breast tissue was not sufficiently studied. A numerical estimation of focal error after the propagation though breast tissue was described.

Statement of Contribution/Methods

Breast model was constructed from a 3D MRI clinical breast data. All pixel intensity in the volume image was assigned to 4 kinds of typical material; water, connective tissue, fat and glandula mammaria. The respective sound speed of latter three materials were 1465, 1547, and 1615 m/s. HIFU simulator based on a finite-time-domain-method developed in Riken was employed. The simulation grid size was 0.1mm, and was generated through an interpolation from 0.625 mm pitch MRI image data. A 56-channel HIFU transducer with both aperture width and focal length were 100 mm and with a center frequency of 2 MHz was used.

Results/Discussion

Three separated peaks were observed after propagation of breast tissue. The focal shift amount was a few millimeter in both lateral and propagation directions. To confirm the relation between the acoustical inhomogeneous and the focal error, time reversal method in this simulation was employed. A virtual sound source was fixed at the original focal point and a distribution of propagation time on the surface of HIFU transducer was calculated. Based on this value, HIFU beam was transmitted. Figure shows that focal error was successfully suppressed in this case. This result showed that focal error in breast tissue was caused by acoustic inhomogeneous. Finally, to evaluate an effect of skin and that of mixed structure of fat and glandula mammaria independently, two following models were built; the former included a skin and water and the latter included water, fat and glandula mammaria. In these results, focal error was observed only in the model including water, fat and glandula mammaria. This results showed that acoustic inhomogeneity inside of breast was more essential than that of the breast surface.

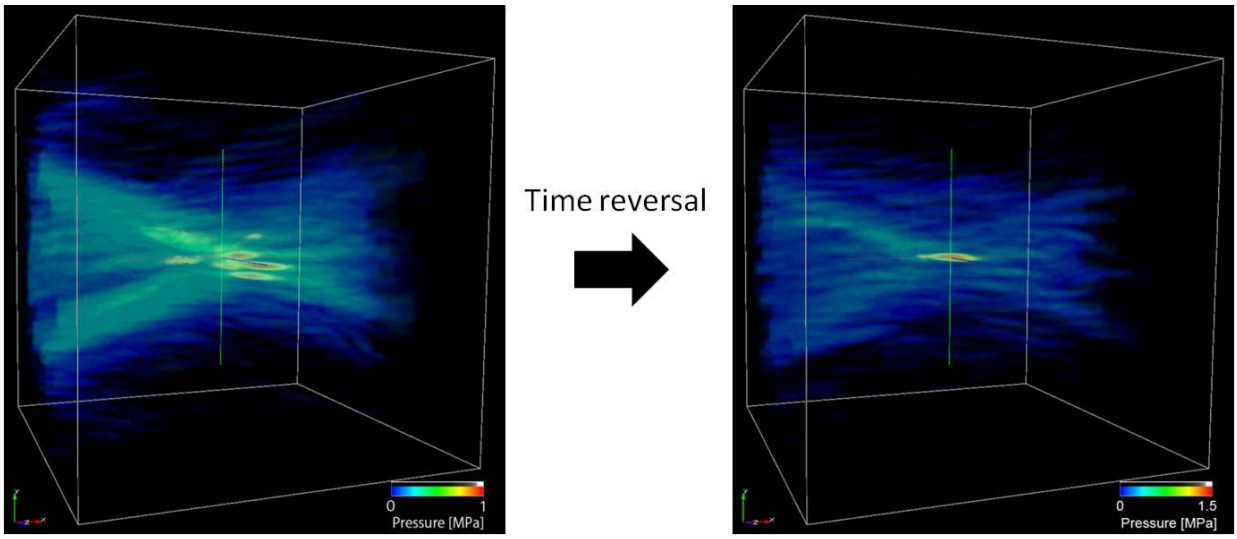

IUS1-PB5-5

Uterine fibroid ablation using a flat phased array: a simulation study of treatment efficiency

Nicholas Ellens[1,2], Kullervo Hynynen[1,2]; [1]*Medical Biophysics, University of Toronto, Canada,* [2]*Physical Sciences Platform, Sunnybrook Research Institute, Canada*

Background, Motivation and Objective

High-intensity focused ultrasound (HIFU) ablation is an effective and desirable means of treating patients with uterine fibroids. Currently, there are several clinically-approved HIFU systems for this application that use spherically-curved transducer arrays to span the fibroid volume with a combination of electrical beam steering and mechanical translation. Previously, we have proposed that it might be possible to complete this task using electronic steering exclusively with a flat array containing a very large number of elements with half-wavelength spacing. This study examines the efficiency and limitations of such a technique.

Statement of Contribution/Methods

Five fibroid patients MR data were segmented to identify tissue boundaries and construct an anatomically correct patient model. Ultrasound (500 kHz) from 6500 piston transducers (spaced 1.5 mm apart, 14 cm aperture) was applied to this multi-layer model and the resultant heating was modelled to assess the bioeffect. Ellipsoidal cells (9 closely-spaced foci, approximately 10 x 20 mm) were ablated sequentially so as to treat the fibroid volume safely and with maximal efficiency. Specifically, peak ablation temperature and inter-cell near-field cooling time were optimized. Finally, efficiency results were compared across different patient anatomies to assess the effects of fat layer thickness and fibroid size and location.

Results/Discussion

Extensive exploration of parameter space indicated that sonication parameter optimization converged on a limit whereby increased treatment efficiency necessitated the accumulation of thermal dose in the near-field, typically at the boundary between the fat and the abdominals. This limit indicates that the conversion of energy to treated volume near the focus is optimized but that further treatment acceleration requires more energy, a fraction of which is necessarily deposited in the near-field. The location of the limit can be shifted favourably by using a larger aperture transducer array. We demonstrate that a peak treatment temperature of 60°C provides the best treatment efficiency to the least near-field heating. Between cell ablations, efficiency and near-field dose were optimized by allowing the near-field to cool to 39.5-40°C. Extrinsic to the array, patient fat layer thickness was the most significant determining factor of efficiency and near-field heating: for each mm of fat, efficiency was found to drop 4±1 mL/hr (r^2=0.82) and near field dose accumulation (in equivalent minutes at 43°C, T_{43}) increased 0.39±0.08 T_{43}/L treated (r^2=0.88). Efficiency decreased and near-field dose increased with increasing fibroid depth, -2.0±0.5 mL/hr (r^2=0.84) and 0.20±0.02 minutes T_{43}/L (r^2=0.96) respectively.

In conclusion, five simulated fibroid patients were treated safely by a flat, large-aperture phased array. Optimized parameters were determined and treatment efficiency was assessed as a function of anatomical variables.

IUS1-PB5-6

Adaptive Displacement Estimation for Optimal Reconstruction of Thermal Strain

Xuan Ding[1,2], Debaditya Dutta[3], Ahmed Mahmoud[3,4], Kang Kim[1,3]; [1]*Department of Bioengineering, University of Pittsburgh, Pittsburgh, PA, USA,* [2]*Medical Scientist Training Program, University of Pittsburgh School of Medicine, Pittsburgh, PA, USA,* [3]*Center for Ultrasound Molecular Imaging and Therapeutics & Heart and Vascular Institute, University of Pittsburgh Medical Center, Pittsburgh, PA, USA,* [4]*Department of Bioengineering, Cairo University, Giza, Egypt*

Background, Motivation and Objective

Ultrasound thermal strain imaging (TSI) utilizes the temperature dependence of the speed of sound to identify lipid and water-bearing tissues. In soft tissue with less than 3°C temperature rise, the apparent displacement induced by sound speed changes can span 1-100 µm with small displacements at the top of the target and larger displacements at the bottom. This gradient results in strains between -0.3-0.6%.

Two-dimensional normalized cross-correlation with zero-phase crossing (2DCC) has been used to estimate displacements created by TSI. 2DCC has been shown to perform better with increasing strains up to 1-2% strain. This might explain the observation that 2DCC performs poorly for small displacement estimates at the top of a target. Phase-shift estimators such as Kasai's autocorrelator have been successfully used to estimate displacements $<\lambda/2$. However, in TSI, displacements $>\lambda/2$ are often present near the bottom of a target. An adaptive displacement estimation algorithm incorporating both 2DCC and Kasai is proposed here to obtain optimal estimates across the entire target.

Statement of Contribution/Methods

A 6 mm diameter cylindrical rubber inclusion embedded in gelatin was simultaneously imaged and heated using VisualSonics MS250 (fc = 21 MHz) with a custom-designed heating transducer that provides a broad heating beam. Displacement was estimated using both 2DCC and Kasai.

If the problem is posed as $Pr(\mu_{true} = \mu_{est} \mid \text{2DCC or Kasai})$, then μ_{est} is a sufficient statistic for this decision and can be compared to a displacement threshold, γ, to determine the most accurate estimate at a given location.

Results/Discussion

From the figure, it can be seen that 2DCC misses the top 0.5 mm of the target whereas Kasai misses the bottom 1 mm. γ was determined empirically from phantom data to be 9.2 µm and a combined estimate was generated which identifies the top and bottom of the target with accuracy to within 0.1 and 0.5 mm respectively as compared to the B-mode image.

We found that phase-shift estimators estimate small displacements better and 2DCC estimates large displacements better. Pinton et al. (2006) also showed that for low SNR and displacement <30 µm, normalized cross-correlation is more biased than Kasai. For displacement >30 µm, they found that Kasai was more biased. We demonstrate that an adaptive displacement estimator more accurately reconstructs TSI.

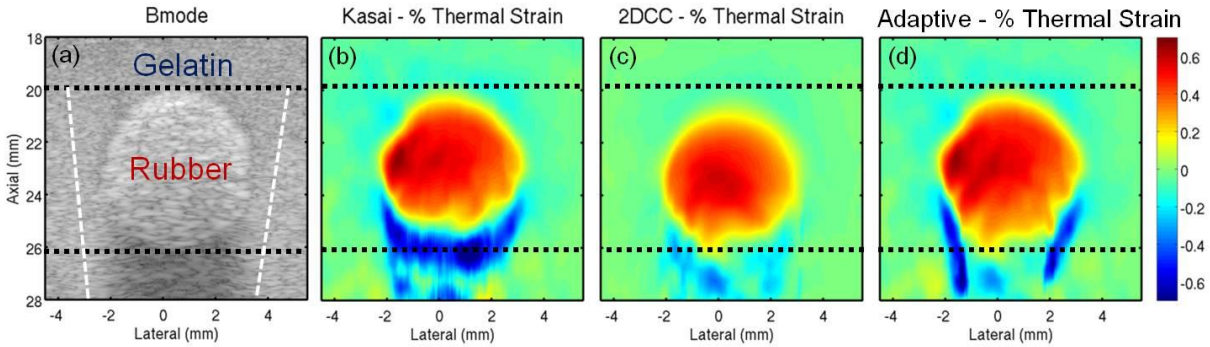

Figure 1: (a) B-mode image of rubber embedded in gelatin. (b) thermal strain image reconstructed using Kasai (c) thermal strain image reconstructed using 2DCC (d) and thermal strain image reconstructed using adaptive algorithm. Colorbars are the same for all thermal strain images and axes are the same for all images. Black dashed lines indicate approximate size of inclusion from B-mode. White dashed lines indicate heating beam.

IUS1-PB5-7

Investigation of the Mechanism of Elastography-based Doppler Feedback of Histotripsy Tissue Fractionation

Ryan Miller[1], Xi Zhang[1], Adam Maxwell[2], J. Brian Fowlkes[1], Charles Cain[1], Zhen Xu[1]; [1]*University of Michigan, USA*, [2]*University of Washington, USA*

Background, Motivation and Objective

Histotripsy controls cavitation to fractionate tissue using high pressure ultrasound pulses. Tissue becomes increasingly fractionated with successive pulses, eventually turning into liquid homogenate. The degree of fractionation can be monitored in real time using color Doppler. Each histotripsy pulse produces and collapses a bubble cloud, leaving persisting residual cavitation nuclei. We hypothesize that these residual nuclei provide enhanced acoustic scattering for appropriately timed color Doppler acquisitions. This allows accurate measurement of the velocity of the treatment tissue resulting from acoustic radiation force imparted by the histotripsy pulses, which correlates to tissue elasticity and level of fractionation.

Statement of Contribution/Methods

An agarose gel tissue phantom was treated with 2-cycle pulses at > 30 MPa over a 5x5x5 grid in a 6 mm cube using a 500 kHz phased array transducer. After all locations had received 50, 100, 250, 500, 1000 and 2000 pulses, a single histotripsy pulse was fired at the center location and monitored for 20 ms with color Doppler acquisitions (6 cycles, 10 kHz PRF) which were post-processed in 10 packet segments to produce the overall velocity profile. To accurately measure the motion of residual cavitation nuclei, simultaneous high-speed optical images were also acquired for particle image velocimetry (PIV) analysis.

Results/Discussion

Optical images clearly showed the push and rebound motion of the residual nuclei following each histotripsy pulse. Average velocity over the focal region from PIV analysis of the residual nuclei matched color Doppler measurements well after 7 ms (Fig 1); with RMS difference between the Doppler and PIV velocities of 0.45 cm/s (with peak velocity ~7 cm/s). With increasing therapy dose, i.e. increased level of tissue fractionation, the rebound time of residual nuclei became substantially longer.

The results support our hypothesis that appropriately timed color Doppler provides an accurate measurement of the velocity of the residual cavitation nuclei in the tissue treated with histotripsy. The difference between the Doppler and PIV analysis was higher within the first 7ms, likely due to the chaotic motion following the bubble cloud collapse. This study provides a better understanding of the elastography-based Doppler feedback of histotripsy tissue fractionation.

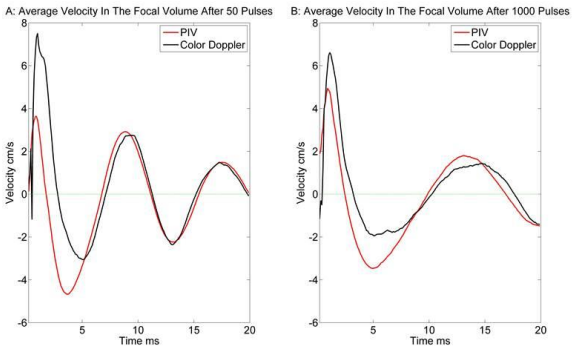

Figure 1: Average velocity profiles in the focal region measured with color Doppler and particle image velocimetry of the optical images of the residual cavitation nuclei after 50 pulses (A), and 1000 pulses (B) showing agreement between the two.

IUS1-PB5-8

Extracorporeal Acute Cardiac Pacing by High Intensity Focused Ultrasound

Amit Livneh[1], Eitan Kimmel[1], Dan Adam[1]; [1]*Department of Biomedical Engineering, Technion-Israel Institute of Technology, Haifa, Israel*

Background, Motivation and Objective

Ultrasound has been shown to produce Premature Ventricular Contractions (PVC's). Clinical interest in this phenomenon arises mainly from observations of arrhythmias occurring during diagnostic ultrasound (US) examinations or lithotripsy. Two clinical applications in which acute cardiac pacing by ultrasound may be valuable are preoperative patient screening in cardiac resynchronization therapy surgery; Emergency cardiac pacing, following an event of cardiac arrest. Yet, previously demonstrated success rate of extra-systole induction by High Intensity Focused Ultrasound (HIFU) in rats is 5-8%. This stands in contrast to previous work in rats using US and contrast agents (UCAs), where success rates of close to 100% were reported.

Statement of Contribution/Methods

Herein, bi-stage temporal HIFU insonnation, using accentuated rarefaction and condensation patterns were applied to anaesthetized rats, for eliciting premature ventricular contractions (PVC's). Insonnation was synchronized to ECG and respiration, using real-time vital-signs monitoring and US imaging. Breath gating was applied to enable pacing at expiration, to mitigate breath related motion. Online US imaging was used for guidance, and its recordings were used for result analysis. This allowed to study the success rate of PVC generation at different timing post ECG R-wave, during the expiration period.

Results/Discussion

Preliminary results demonstrated sequences of successive successful HIFU pacing at the beginning and the end of the diastole. An illustration of such a PVC sequence is provided in the figure below. Intonation triggers are marked by purple circles and red bars. PVCs are characterized by an abnormal QRS complex and a lengthened compensatory period. Fused complexes result from concurrent action potential (AP) propagation form a HIFU induced ventricular ectopic focus and a sinus rhythm AP arriving via the atrioventricular (AV) node. An insonation that was triggered 80 msec after an R-wave did not yield a noticeable response, possibly due to its application during the refractory period. It is suggested that proper spatiotemporal control of insonation is imperative for achieving efficient HIFU cardiac pacing.

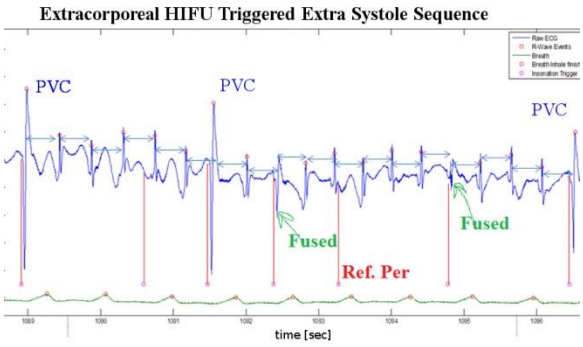

IUS1-PB5-9

Feasibility of thin catheter manipulation in the capillary blood vessel using acoustic radiation force

Takashi Mochizuki[1], Naoto Hosaka[1], Ren Koda[1], Nobuhiko Shigehara[1], Kohji Masuda[1]; *[1]Graduate School of Bio-Application & System Engineering, Tokyo University of Agriculture and Technology, Tokyo, Koganei-Nakacho, Japan*

Background, Motivation and Objective

This objective is to develop a method of direct catheter manipulation using acoustic radiation force without any guide-wire, which allows a thin catheter (less than 0.5mm diameter) to access to the target area such as tumor where nobody has been able to inject it. In the conventional method, a long guide-wire can be manipulated only by the veteran doctors or well-trained technicians to make it access to the target area through the artery. Secondly, a catheter is injected to the target with assist of the guide-wire and the discarded guide-wire is pulled out leaving the catheter. In this manner, since the diameter of the artery or vessel is limited to the additional val-ue of both diameters of the guide-wire and catheter, the current minimal diameter is limited to 2 mm in a case of brain interventional surgery.

Statement of Contribution/Methods

A tube as a catheter is injected into Y shape duct (2 mm diameter) which is simulated the capillary blood vessel. The outer and inner diameters of the catheter are 0.4 and 0.1 mm, respectively. Its material is perfluoroalkylvinylether-tetrafluoroethylene copolymer (PFA).

Results/Discussion

Figure 1 shows experimental results demonstrating catheter manipulation. In Fig.1(a), a catheter is pushed and stops at the central corner of the Y shape duct. And the catheter can go neither channel 1(Ch1) nor channel 2 (Ch2) without ultrasound radiation. On the other hand, the catheter can advance to Ch1 due to the radiation force when ultrasound is emitted from the right side as shown in Fig1. (b). The catheter itself is not visible in the photos, however inner area which is filled up with air and capped with adhesion bond can be observed due to light refraction. The force pushing the catheter was estimated 10 to 100 uN under 500 kPa acoustic pressure and it was observed that bending angle of the catheter was proportional to the acoustic pressure in anther experiment. It becomes clear that manipulation of a thin catheter is possible by using acoustical radiation force in the feasibility experiment. In future, it will be possible to be used for drug delivery with less side-effect.

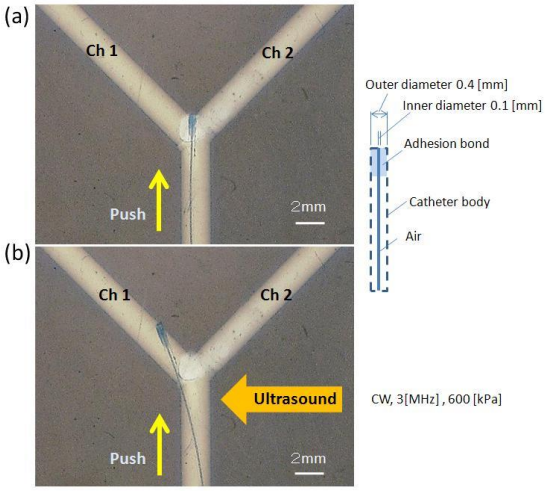

Fig.1.Ultrasound guided catheter experiment

NDE Methods

Forum Hall

Tuesday, July 23 2013, 01:00 pm - 04:30 pm

Congress Hallair: **Mario Kupnik**
Brandenburg University of Technology (BTU)

IUS2-PB1-1

Evaluation of the *Pinus taeda* quality using ultrasound

Ozana M. A. Maia[1], Fabio K. Schneider[2], Joaquim M. Maia[2], Mayara F. G. Souza[2], Marcelo R. Prado[3], Susete R. C. Penteado[4], Wilson R. Filho[4], Edson T. Iede[4]; *[1]CPGEI, Federal University of Technology - Paraná - UTFPR, Curitiba, Paraná, Brazil, [2]CPGEI/DAELN, Federal University of Technology - Paraná - UTFPR, Brazil, [3]DAQBI, Federal University of Technology - Paraná - UTFPR, Brazil, [4]CNPF, Brazilian Agricultural Research Corporation - EMBRAPA, Paraná, Brazil*

Background, Motivation and Objective

The pinus is a type of wood that is widely used as feedstock for the production of softwood pulp and higher quality paper, boards, Medium Density Fiberboard (MDF), Oriented Standard Board (OSB), plywood, veneer, furniture and others. The main problem for the pinus is the attack by the *Sirex noctilio* (wood wasps) that damages the wood due to galleries built by the wasps larvae. The use of non-destructive techniques to assess the quality and to evaluate mechanically the wood has been the focus of many studies and is certainly an essential tool to decrease the production costs.

Statement of Contribution/Methods

This work aimed the use of ultrasound in evaluating the damage of *Pinus taeda* due to the infestation of *Sirex noctilio*. The tests have been done using a 5077PR pulser-receiver (Olympus Corporation), a pair of ultrasound transducers with 50 kHz of central frequencies (models 083-067-038, GE Inspection Technologies), a pair of transducers with 100 kHz central frequencies (models 083-058-769, GE Inspection Technologies), a MSO4104B digital oscilloscope (Tektronix Inc.) and a portable microcomputer for data storage. The pulser-receiver was used to excite the transmitting transducer with negative pulses (-400 V) and to condition the ultrasonic waves that propagated through the pinus samples (seven logs with lengths and diameters in the range of 70 to 94 cm and 9 to 18 cm, respectively) and were received by the receiver transducer. The conditioned signals were acquired by the digital oscilloscope and transferred via USB interface to the computer to be processed using the Matlab (Mathworks Inc.).

The transducers were positioned in the samples to measure the ultrasound propagation velocity and the attenuation in the following modes: axial, radial (lower, middle and upper parts of the logs), orthogonal (middle and upper parts), inclined at 45 degrees (middle and upper parts), orthogonal/transversal (middle and upper parts) and inclined/transversal (middle and upper parts).

Results/Discussion

The initial results of the 960 tests (430 with each pair of transducers) that have been done with the seven pinus samples, six of them damaged by the wood wasps and one without damage, have shown that the infested samples presented a decrease in the propagation velocity and an increase in the attenuation when compared to the control sample results. Just for example, the mean velocity measured in the axial mode (group longitudinal velocities) in one of the infested samples was 2672.7 ± 4.6 m/s and in the control sample it was 3033.5 ± 3.1 m/s. The attenuation was 20.0 ± 2,1 dB. These initial results showed that the ultrasound technique can support the quality evaluation of *Pinus taeda* and detection of infestation of wood wasps. Further tests should be made with a larger number of samples to evaluate the elastic modulus and other ultrasound parameters. The results will be used to define a novel test protocol to be used for material characterization in the agronomical area.

IUS2-PB1-2

Acoustic Imaging of Bump Defects in Flip-Chip devices using Split Spectrum Analysis

Sebastian Tismer[1], Sebastian Brand[1], Sandy Klengel[2], Peter Czurratis[3], Matthias Petzold[1]; *[1]Fraunhofer Institute for Mechanics of Materials IWM, Halle, Germany, [2]Fraunhofer Institute for Mechanics of Materials IWM, Germany, [3]PVA Tepla Analytical Systems GmbH, Westhausen, Germany*

Background, Motivation and Objective

In this paper the performance of multi narrow band spectral analysis was evaluated concerning defect detection in microelectronic components with flip-chip contacts. Today, flip-chip technol-ogies are widely applied for interconnecting silicon dies to a substrate within high-end semicon-ductor packaging technologies. The integrity of the bump solder interconnection is of major con-cern for the reliability in this technology . Non-destructive defect localization and analysis of the flip-chip interconnections operating in a semi-automated mode is strongly desired. Scanning acoustic microscopy combined with subsequent signal analysis has high potential for nondestruc-tive localization of defective flip-chip interconnects.

Statement of Contribution/Methods

Analyzing multiple narrow spectral bands of signals acquired by a scanning acoustic microscope enabled the localization of defective flip-chip interconnects. In the current study a 180 MHz transducer with 8 mm focal length was employed for acoustic data acquisition by SAM. Those data were then analyzed off-line by discrete Fourier transformation, chirp z-transform and cosine transform using custom made MATLAB software.

Results/Discussion

Through multi-narrow band spectral analysis, defective flip-chip interconnects that have not been revealed with standard backscatter integral imaging have been detected successfully. Acoustical-ly found defects have been confirmed by subsequent FIB-cross sectioning and SEM imaging. The high resolution SEM imaging revealed complete delaminations at the interface between the die and the bump.

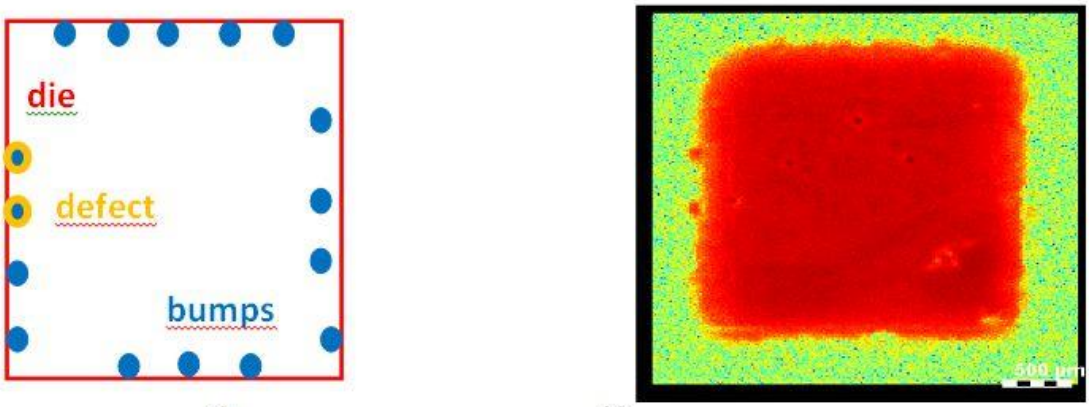

Fig.1: a) schematic b) split spectrum image

IUS2-PB1-3

Optimizing Light Delivery In Scattering Media by Photoacoustic-guided Wavefront Shaping

Thomas Chaigne[1], Ori Katz[1], Emmanuel Bossy[1], Claude Boccara[1], Mathias Fink[1], Sylvain Gigan[1]; *[1]Institut Langevin, ESPCI ParisTech, CNRS UMR 7587, PARIS, France*

Background, Motivation and Objective

Focusing light to the micron scale is the enabling element in many important biomedical applications such as optical microscopy and laser nano-surgery. However, the inherent inhomogeneity of biological tissues results in light scattering, which limits focusing to shallow depths of a few hundred microns. Nevertheless, several groups demonstrated that it is possible to focus light through highly scattering samples by shaping the incident wavefront using Spatial Light Modulators (SLM).

In most of these works, the feedback signal was obtained from a camera placed behind the scattering medium. However, a highly desired goal is to focus light *inside* a scattering sample. To this end, one can no longer position a camera to measure the light intensity at the selected spot. The objective of this work is to study the potential of the photo-acoustic (PA) effect to overcome this limitation.

Statement of Contribution/Methods

We used a PA signal as the feedback signal to enable controlled optical focusing (A): focusing was performed through a scattering medium at an arbitrary position within the focus of a wideband (5 MHz – 70 MHz) single element ultrasound transducer. Two different approaches were developed. The first is based on an iterative algorithm optimizing the PA signal. The second is based on the measurement of a *transmission matrix*, connecting the optical input modes to the acoustical response of the absorbers.

Results/Discussion

Using optimization, we experimentally demonstrate a 20 fold increase in the PA signal generated by an absorber located behind a 1mm thick chicken sample. The signal enhancement was affected by the ultrasound frequency range over which the PA signal was analyzed, as the lateral dimension of the ultrasound focus is determined by the frequency.

We also confirm the validity of the matrix approach, which enables to focus light at will at an arbitrary position of a 1D PA image (B). Focusing inside the scattering medium is currently investigated with these approaches. Contrary to focusing techniques using fluorescent probes, PA offers spatial selectivity based on the resolution of ultrasound imaging.

Within the context of PA imaging, our results show that it is possible to highlight the PA signals from specific regions. This work paves the way towards optical or PA imaging at very high depth, as well as light delivery problems such as laser assisted nano-surgery.

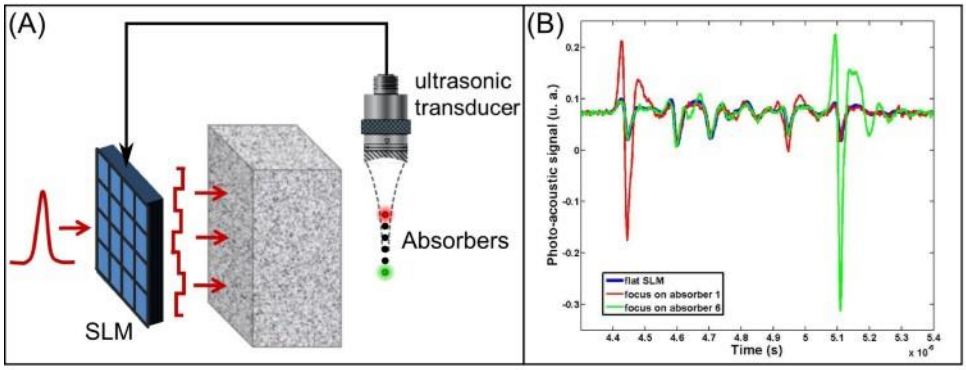

IUS2-PB1-4

Determining the Quality of Space Tether in a Nondestructive manner

Göran Maconi[1], Henri Seppänen[1,2], Timo Rauhala[1], Anni Toppila[1], Sergiy Kiprich[3], Jukka Ukkonen[1], Pekka Janhunen[2], Edward Hæggström[1,4]; *[1]Department of Physics, University of Helsinki, Helsinki, Finland, [2]Finnish Meteorological Institute, Helsinki, Finland, [3]Institute of High Energy Physics and Nuclear Physics, National Science Center Kharkov Institute of Physics and Technology, Kharkov, Ukraine, [4]Helsinki Institute of Physics, Helsinki, Finland*

Background, Motivation and Objective

We propose a nondestructive method to determine the quality of electric solar wind sail (E-sail) tether. The quality of each single wire-to-wire bond of the E-sail tether is defined by four simultaneous non-destructive measurements. The result is verified by a method similar to the standard destructive pull test [1].

The E-sail is a propellantless propulsion method for interplanetary missions. It uses long, thin, centrifugally stretched and positively charged tethers to create thrust from the momentum flux of the solar wind. For micrometeoroid resistivity the multifilament tether is required. Recently we produced a 1 km long multifilament tether utilizing ultrasonic wire-to-wire bonding [2]. To ensure high and consistent quality for space-flying tethers, the bond quality must be measured in a nondestructive manner during the production.

Simulations show that the tethers in a full scale E-sail are stretched by < 50 mN centrifugal force [3]. This sets a limit for minimum tether strength. Previously we have reached more than 100 mN maximum sustainable pull strength in tether bonds [2].

Statement of Contribution/Methods

The setup for the proposed tether quality measurement comprises a custom-built ultrasonic bonding device, a laser doppler vibrometer, an ultrasonic generator, contact resistance measurement electronics and a laser-ultrasonic device. During the bonding process the setup continuously measures voltage and current driving the ultrasonic transducer, the bonding lower wedge displacement, the contact resistance of the bond interface and a laser induced high frequency pulse transmission through the bond interface. All these signals are stored by oscilloscope for post-analysis. The post-analysis results are correlated with the destructive bond pull test results.

Results/Discussion

By non-destructively testing each wire-to-wire bond, we can produce quality-assured tether on the scale required for making a full size E-sail, showing the viability of wire-to-wire bonding in industrial-scale production.

[1] Harman, Cannon: The Microelectronic Wire Bond Pull Test-How to Use It, How to Abuse It, Comp. Hybr. and Man. Tech. IEEE Transactions on, Sep 1978

[2]Rauhala, T. et al. Automatic 4-wire Heytether production for the Electric Solar Wind Sail, IMAPS 2013

[3]Janhunen, P. et al. Electric solar wind sail: Toward test missions. Rev. Sci. Instr. 81, 111301 (2010)

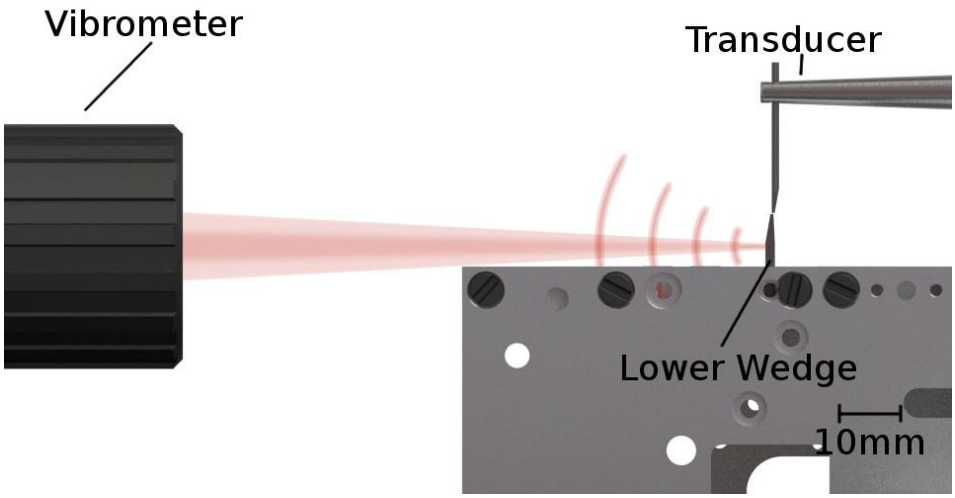

IUS2-PB1-5

Scattering of Fundamental Lamb Wave Modes Obliquely Incident on a Surface Breaking Crack in a Plate

Sridhar Santhanam[1], **Ramazan Demirli[2]**; *[1]Dept. of Mechanical Engineering, Villanova University, USA, [2]Center for Advanced Communications, Villanova University, USA*

Background, Motivation and Objective

The use of guided Lamb waves for non-destructive evaluation of metal and composite plates has been investigated in numerous studies. In order to locate and size defects with Lamb waves, it is important to develop a quantitative understanding of their interaction. When Lamb waves are obliquely incident on a transverse crack in a plate, they are subject to scattering. Part of the energy of the wave is transmitted beyond the crack and part is reflected. A quantitative description of this scattering phenomenon is required. This study develops analytical solutions for the reflection and transmission energy coefficients of the waves scattered by the fundamental symmetric and anti-symmetric Lamb modes incident obliquely on surface breaking cracks.

Statement of Contribution/Methods

In this study, an asymmetric part-through transverse crack, also known as a surface breaking crack, is considered in an isotropic plate. Two different incident Lamb wave modes are considered: the fundamental symmetric S0 and the anti-symmetric A0. The angle of incidence of these waves on the crack plane is varied from 0 to 90 degrees. A single incident fundamental mode can be scattered into multiple reflected and transmitted modes, both in-plane and Shear Horizontal (SH), depending on the propagating frequency. The amplitudes and energy coefficients of the reflected and transmitted modes are determined by enforcing traction free conditions on the crack faces and continuity conditions on the uncracked regions of the crack-plane. A numerical solution is constructed using the method of eigenmode expansion and the principle of reciprocity. Energy coefficients are determined as a function of incident angle and frequency of the Lamb mode, as well as the crack depth to plate thickness ratio.

Furthermore, experiments are conducted with PZT transducers affixed on an aluminum plate to validate the reflection/transmission coefficients of S0 and A0 modes obliquely incident to a machined crack with crack-depth to plate thickness ratios of 0.25, 0.50, and 0.75.

Results/Discussion

At low angles of incidence the in-plane modes are reflected and transmitted with high energy coefficients. As the angle of incidence is increased, the SH wave modes carry away more of the incident energy. The incident symmetric mode S0 produces symmetric as well as asymmetric reflection and transmission modes because of the asymmetric nature of the crack geometry. This is seen with the incident A0 mode as well. These reflections and transmissions obey Snells' law. At higher frequencies, there is a multiplicity of reflected and transmitted modes, making the problem of mode identification and separation difficult.

NDE Imaging and Signal Processing

Forum Hall

Tuesday, July 23 2013, 01:00 pm - 04:30 pm

Congress Hallair: **Erdal Oruklu**
Illinois Institute of Technology

IUS2-PB2-1

Bilinear Time-Frequency Distributions for Ultrasonic Signal Processing and NDE Applications

Jafar Saniie[1], Juan Lu[1], Erdal Orulku[1]; [1]*Electrical and Computer Engineering, Illinois Institute of Technology, USA*

Background, Motivation and Objective

In ultrasonic nondestructive evaluation (NDE) of materials, the frequency-dependent scattering, attenuation, and dispersion make the backscattered signal highly complex and non-stationary. In this study, generalized bilinear time-frequency (GBTF) methods have been applied to the multi-component ultrasonic signals that consist of many overlapping echoes in order to display their signal energy on a joint time-frequency (t-f) plane. The t-f analysis of the ultrasonic target echoes reveal time of arrival and center frequency that is often used in assessment of quality and integrity of materials. However, the GBTF distributions inherently contain artifacts known as cross-terms which obscure the important information regarding target echoes. Therefore, signal processing is essential to recognize the cross-terms and then devise methods to alleviate their adverse impact.

Statement of Contribution/Methods

In this paper, we introduce Singular Value Decomposition (SVD) of Wigner Distribution (WD), a special and widely adapted method of GBTF that improves t-f characterizations of ultrasonic signals. The WD offers the best t-f resolution but grossly suffers because of cross-term artifacts generated due to the inherent bilinear operation of GBTF. This approach has been extended to the SVD of Choi-Williams Distribution (CWD), a well-adapted version of GBTF distributions.

Results/Discussion

Gaussian echoes are used to model the ultrasonic backscattered signals and this model is examined analytically to reveal the pitfalls of WD and CWD. For CWD, the range of the exponential kernel parameter is attained based on the impetus to sustain desirable auto-terms while suppressing the superfluous cross-terms. To broaden the usefulness of this approach, singular value decomposition of WD and CWD are analyzed mathematically and also verified experimentally. The SVD of WD and CWD generates basis functions uniquely corresponding to auto-terms and cross-terms. After identifying and discarding the basis functions corresponding to the cross-terms and noise, the desirable basis functions of auto-terms and their singular values are used to reconstruct the t-f distribution. We have applied SVD to WD and CWD of two overlapping echoes with different arrival times and frequency distributions corrupted with noise. The overlap ranges from 0% to 100% and the SNR from 0 dB - 20 dB. Then, the SVD based, reconstructed t-f is used to estimate the arrival times and center frequencies. This approach resulted in accurate arrival-time and center frequency estimates with less than 4% estimation error with mean values of about 2%. We further used this method to detect flaw echo which is submerged by microstructure scattering noise. The flaw echo in the t-f plane clearly reveals lower frequency distribution at the location of the defect. These numerical results and experimental evaluations confirm that the application of SVD is a desirable approach to improve the accuracy of GBTF.

IUS2-PB2-2

Echo parameter estimation for ultrasonic NDE applications via a two-step compressed sensing

Yufeng Lu[1], **Ramazan Demirli**[2], Jafar Saniie[3]; [1]*Electrical and Computer Engineering, Bradley University, USA,* [2]*Center for Advanced Communications, Villanova University, USA,* [3]*Electrical and Computer Engineering, Illinois Institute of Technology, USA*

Background, Motivation and Objective

In ultrasonic nondestructive evaluation (NDE) applications, the ultrasonic signal often contains many interfering echoes due to the complex physical properties of the propagation path. The pattern of the signal is dependent on irregular boundaries, and the size and random orientation of material microstructures. Furthermore, a large volume of data collection is required in the assessment of outsized structures. The ultrasonic NDE process, including data collection and feature extraction, becomes computationally expensive for in-situ NDE characterization. Recently, compressed sensing (CS) has been successfully applied to data intensive imaging applications providing significant reductions in sampling rate with minimal loss in image quality. Through CS, a signal can be sparsely represented in a certain domain, where most of the coefficients are null or close to zero. The aim of this study is to design a compressed sampling scheme for ultrasound NDE signals and explore the feasibility of echo parameter estimation based on this sampling method.

Statement of Contribution/Methods

Gaussian Chirplet (GC) is a common model to represent a broad range of ultrasonic signals, narrowband or wideband; symmetric or skewed; nondispersive or dispersive. In this investigation, a model-based CS is studied to combine lower rate sampling schemes with GC-based signal decomposition and parameter estimation. Using the CS framework, innovation rate sampling and annihilating filter are used to acquire ultrasonic data and estimate the time-of-arrivals (TOAs) and amplitudes of GCs. While TOA estimation is satisfactory, it is observed that amplitude estimation is sensitive to the sparseness of sampling rate and noise. For accurate amplitude estimation, we propose a second iteration in data acquisition with sparse sampling utilizing the estimated TOA to acquire the actual echo amplitude. With the estimated TOAs from the two-step CS and the prior information of the transducer bandwidth, a repeat data acquisition with a windowing approach is used to isolate and acquire dominant chirplets for analysis.

Results/Discussion

It is shown that the two-step CS can estimate the TOAs of ultrasonic echoes with high accuracy in the presence of noise with SNR as low as -5 dB. Furthermore, the estimation is robust to the inaccurate knowledge of the transducer bandwidth. The two-step CS approach is successfully applied for signal decomposition and parameter estimation for a typical NDE signal obtained from a steel block rich of diffuse and specular scatterers. CS offers very efficient data acquisition for ultrasonic sensing systems. In this study, the CS framework is incorporated to conventional ultrasonic signal processing for NDE applications. The two-step CS enables signal decomposition and parameter estimation with a minimal effort in data collection. The study has broad applications in imaging, material characterization, target detection and pattern recognition.

IUS2-PB2-3

Relation between Sampling Frequency and Truncation index inTruncated Singular Value Decomposition for UT probe Array

Yoshiiro Nishimura[1], Takayuki Suzuki[2], Katsumi Fukuda[3], Mugito Ishii[3], Masatoshi Fukuta[4]; *[1]National Institute of Advanced Science and Tecnology, Japan, [2]National Institute of Advanced Science and Technology, Japan, [3]Tokyo National College of Technology, Japan, [4]National Institute of Advanced Science and Tecnology*

Background, Motivation and Objective

UT probe array is a convenient NDT method that can detect internal defects within a inspected object more quickly than UT point focus probe. Inverse problem solving is a method to produce images of internal defects as well as Aperture Synthesis Technology but response functions used by inverse problems are often singular due to poor precisions of numerical calculation. Internal images of inspected objects are unable to be solved particularly if high resolution images are required. If objects whose acoustic velocities are very high are inspected, their wave lengths are long and the quality of the image reconstructed y aperture synthesis become worse. The methods to derive better defect image are required.

Statement of Contribution/Methods

Acoustic velocities of Silicon Nitride (SN) is about 12000m/s, that is six times that of water. Submerged Inspecting a defect 100mm deep within SN samples corresponds to inspecting an object 600 to 800 mm away in water. A large UT probe array operating at 5MHz and 3D scanning system was developed for inspecting it. Two kinds of image reconstruction programs, aperture synthesis and Truncated Singular Value Decomposition (TSVD), were developed and the results derived by them were compared. Relation between sampling frequency and truncation index was examined as well.

Results/Discussion

We calculated images (128x512) of internal defects from time series of wave data measured by a UT probe array with 32 elements. Figure presents an image of numerical model of SN sample with two slit defects 100mm deep and 32 elements UT probe array, an image reconstructed by synthesis aperture and those calculated using TSVD with different truncation index k=128, 256,512,1024. Two slit defects in images reconstructed using TSVD can be identified but those in that using aperture synthesis cannot. TSVD was proved to be effective to solve inverse problem and to produce better image of internal defect 100mm deep than aperture synthesis. An effect of truncation index was presented as well.

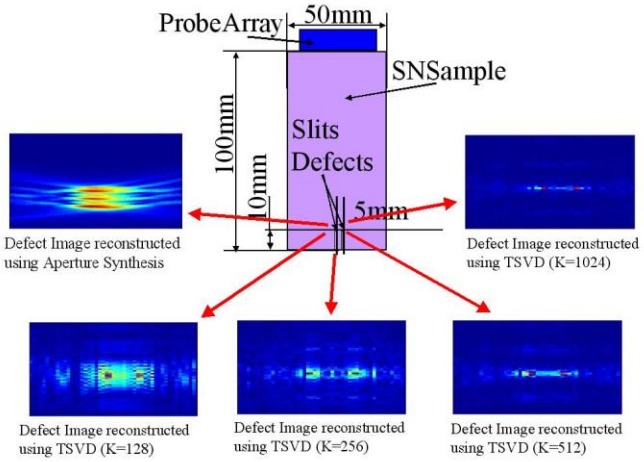

IUS2-PB2-4

The use of instantaneous phase for improving sparse arrays images

Vander Prado[1], Ricardo Tokio Higuti[1], Cláudio Kitano[1], Óscar Martínez-Graullera[2]; *[1]Electrical Engineering, UNESP - Universidade Estadual Paulista - Faculdade de Engenharia de Ilha Solteira, Ilha Solteira, SP, Brazil, [2]Centro de Acústica Aplicada y Evaluación No destructiva, CSIC - Consejo Superior de Investigaciones Científicas, Madri, Spain*

Background, Motivation and Objective

Sparse arrays have pitch larger than half wavelength (λ/2) and there is a reduced number of elements in comparison with a full-populated array. Consequently, there is a reduction in cost, data acquisition and processing. However, conventional beamforming techniques result in large side and grating lobes, and consequently in artifacts in the image. In this work the instantaneous phase (IP) of the signals is used in a beamforming technique to improve images obtained from sparse arrays configurations.

Statement of Contribution/Methods

The IP image is obtained in a similar way as the Total Focusing Method (TFM), but instead of summing the instantaneous amplitudes at determined instants, the IP is used. After this, a threshold based on a statistical analysis and the number of signals used in beamforming is applied to each pixel, in order to determine if that pixel is related to a defect or no. If it is not considered a defect, the pixel value is attenuated to improve contrast and reduce image artifacts. Three sets of data are used to evaluate the technique, considering medical and non-destructive testing: a simulated point reflector (PSF - point spread function) using a 32 elements array, 2λ-pitch at 5 MHz and propagation velocity (c) of 1540 m/s; a medical phantom (CIRS model 040GSE) using a 7λ-pitch 32 elements array at 10 MHz and c = 1540 m/s; and an aluminum plate with artificial defects and an 8 elements array, pitch of λ at 330 kHz coupling the low dispersive S0 Lamb wave mode with c = 5240 m/s. Then the IP images are compared to the conventional amplitude TFM images.

Results/Discussion

In the PSFs (see figure) it is possible to observe the grating lobes effects with large amount of image artifacts in the TFM image and the improvement obtained by the use of the IP. The phantom presents reflectors with different contrasts and noisy background. The use of the IP improves the contrast significantly, giving a good idea of the reflectors. For the non-destructive testing using Lamb waves, although there are few elements in the sparse array, in the IP image most defects are detected and there are some artifacts. However, the result is much better when compared to the TFM image, because there is a lower intensity dead zone and higher contrast. The use of the IP information with sparse arrays reduces side and grating lobes effects and is a good alternative to reduce system complexity while maintaining image quality.

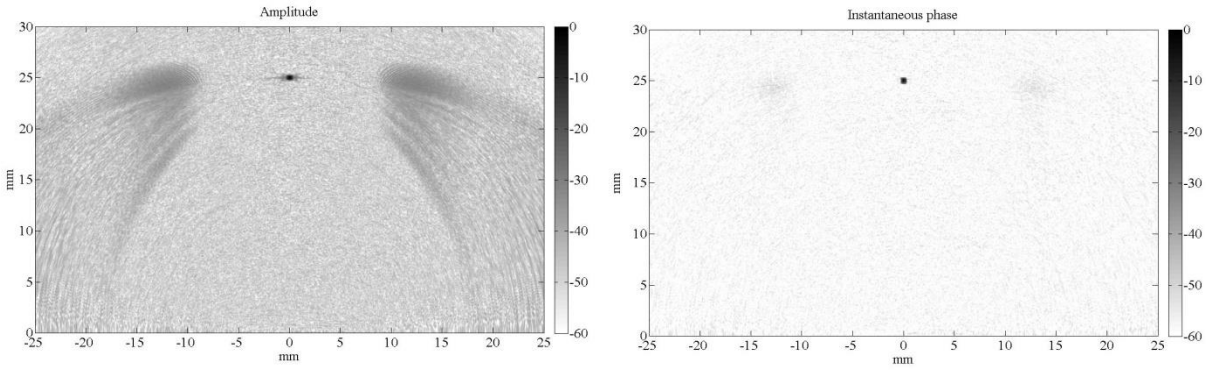

IUS2-PB2-5

An enhanced Ultrasound technique for 3D Palmprint Recognition

Antonio Iula[1], Enrico Boni[2], Alessandro Ramalli[2]; *[1]University of Basilicata, Potenza, ITALY, Italy, [2]University of Firenze, Italy*

Background, Motivation and Objective

Biometrics is being increasingly used to establish person recognition in a large number of civilian applications.

Among the other biometric characteristics, palmprint has proved to be one of the most unique and stable biometric characteristics. Almost all the current palmprint recognition techniques are optical based and capture the 2-D image of the palm surface but, recently, palmprint recognition techniques using 3-D information of the palm surface have been proposed.

Ultrasounds have been exploited in biometric applications mainly for fingerprint recognition. Their main advantages over the other methods are the intrinsic capability of providing 3D information and of detecting life (Doppler mode). Furthermore, they are not sensitive to the surface contaminations, such as stain, dirt, oil, ink.

One of the authors has recently experimented the use of ultrasounds for palmprint and vein pattern recognition by using an ultrasonic linear array transducer that moves in a direction perpendicular to the electronic scanning plane. First results, although very promising, have shown a number of limitations due to the fact that both the commercial ultrasound system and the positioning system employed were not designed for the specific application.

Statement of Contribution/Methods

In the present work, a new system for the acquisition of the ultrasound images is proposed; it is based on the open ultrasound platform ULA OP, which allows nonstandard and dedicated transmit/receive strategies and is able of providing a very quick acquisition. A commercial ultrasound probe (LA435 by Esaote) is mechanically shifted along the elevation direction, to cover the region of interest of the human palm hand. An improved automated system guarantees stable and repeatable measurements. At each step a B-Scan is acquired and stored. These data are then acquired and elaborated in MATLAB environment to provide several renderings of the 3D palmprint.

Results/Discussion

The hands of several users were scanned and the corresponding 3D palmprints were extracted. The potential distinctiveness of the proposed biometric characteristic can be appreciated by a visual comparison of the palmprints of different users and, on the other hand, of palmprints of the same person acquired at different times. 2D renderings of some samples are compared with those acquired with conventional techniques as well.

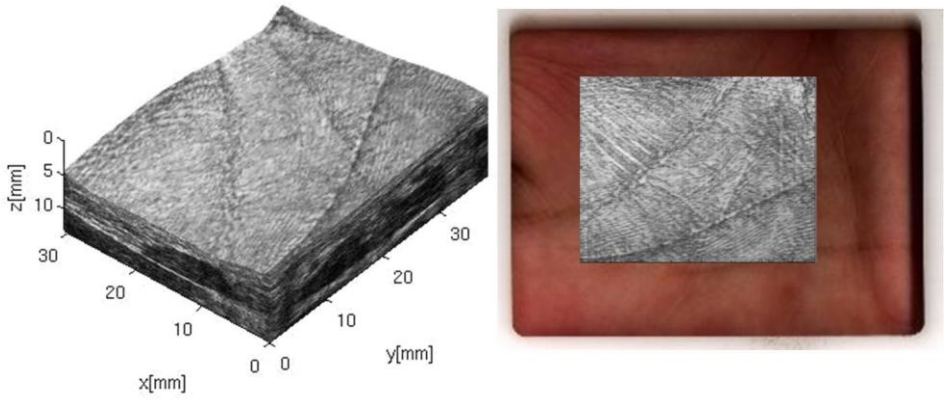

IUS2-PB2-6

The quality control of the spot welds using enhanced total focusing method

Vykintas Samaitis[1], Elena Jasiuniene[1], Liudas Mazeika[1], Ruth Sanderson[2]; *[1]Prof. K.Barsauskas Ultrasound Research Institute, Kaunas University of Technology, Kaunas, Lithuania, [2]TWI Ltd, United Kingdom*

Background, Motivation and Objective

Spot welds are widely used in automotive industry to join various parts made out of metal sheets. Conventional cars usually have more than 3000 welds, which play a critical role ensuring the required strength of the car body and the safety for the humans. Therefore the quality of the welded joints should be evaluated by means of destructive or non-destructive methods. The most common non-destructive method for the quality assessment of the welded joints is based on measurements of the A-scans using a single crystal probes. However in such approach the probe must be selected according to the diameter of the weld and the accurate location of the probe in the center of the weld is required. The application of the phased arrays for the spot weld testing enables to overcome these problems. Using this approach the accurate positioning of the phased array is not required and one array for all diameters of welds could be used. However in this case in order to extract the information about the dimensions and the quality of the weld, advanced signal processing techniques are required. The objective of this work was to develop the imaging technique for inspection of spot welds, which would enable accurate determination of the dimensions and the geometry of the welded area and would visualize the defects in the weld.

Statement of Contribution/Methods

As the most promising technique, the enhanced total focusing method was proposed to post-process the signals acquired using 2D ultrasonic matrix array. Such approach in general enables to reconstruct the 3D image of the spot weld. In order to reduce the background noise and to obtain uniform sensitivity at different depths the conventional total focusing method was enhanced to take into account the directivity patterns of the phased array elements and the divergence of the ultrasonic beam due to the propagation distance. The enhanced total focusing method was verified using the finite element model of the good weld, the undersized weld and the weld with the pore. Simulations were carried out using quarter of 16 by 16 matrix array placed on the two 1.5mm welded steel sheets. The excitation was applied to each element of the array in the sequence and the signals were recorded from all of them to simulate full matrix capture data acquisition.

Results/Discussion

The post processing of the signals obtained from the finite element simulations demonstrated that the enhanced total focusing method enables to reconstruct the 3D structure of the weld, to determine the size and the shape of the welded area and to indicate the non-homogeneities. It was shown that any cross-section of the weld can be reconstructed from the 3D data which enables to analyze the weld and to estimate the depth and the area of any non-uniformity. The small reflectors such as pores can be clearly detected and their positions as well as dimensions can be estimated.

IUS2-PB2-7

Generating a pencil beam from a focused transducer using Stolt migration

Mariana Melo Mota[1], **Paul van Neer[2]**, Arno Volker[2]; *[1]TNO, Portugal, [2]TNO, Netherlands*

Background, Motivation and Objective

Scanning using a focused transducer gives a narrow focus depth, although locally there is a high resolution. Because the focal point can be considered as a second source, the wavefield can be split in its causal and anticausal parts. Imaging can be performed efficiently with a mapping algorithm in the wavenumber domain (f-k or Stolt migration), achieving a pencil beam.

This work investigates the potential of this mapping algorithm on simulated and experimentally obtained data.

Statement of Contribution/Methods

The target geometry consisted of a line of point deflectors (pins) mounted in a water tank. The experimental dataset was obtained by scanning along the line of deflectors using an xyz-system. A 1 MHz transducer was used with diameter 1.5'' and focal distance 3''. The simulated dataset was created using an in-house implementation of a wavefield extrapolation algorithm. Imaging of the simulated and experimental datasets was performed using a custom implementation of the Stolt mapping algorithm.

Results/Discussion

The aforementioned concept is illustrated on simulated data, where the -6dB lateral point spread functions (PSF) were improved by 91.3%, 0% and 90.5% in the near-field (2.5cm), focus (7.4cm) and far-field (13.5cm), respectively. Measurements confirm this pattern, and showed improvements in the PSFs by 86.8%, 0% and 60.0% at the same distances.

The enhancement of the resolution using the mapping algorithm effectively creates a pencil beam from the focused beam of the transducer in both the simulations and the experiments.

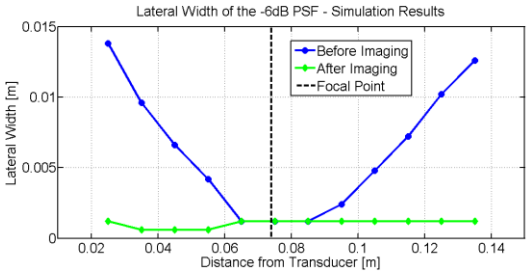

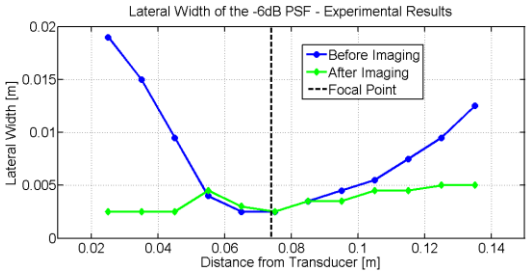

Sensor Applications

Forum Hall

Tuesday, July 23 2013, 01:00 pm - 04:30 pm

Congress Hallair: **Pierre Khuri-Yakub**
Stanford University

IUS2-PB3-1

A Pulse-to-Pulse Incoherent Flow Measurement with Frequency-Coded Signals

Manuel Haide[1]; [1]*Institute for Applied Research, University of Applied Sciences Ulm, Ulm, Baden Württemberg, Germany*

Background, Motivation and Objective

Ultrasonic flow measurement sensors for calculating the discharge of open channels are becoming more and more important in monitoring environmental phenomena as well as in intelligent water management. Especially, for multi-phased fluids the application of reflection based method is nowadays indispensable. This method extracts the velocity from a bunch of slip-free moving particles in the stream by analyzing the time-, phase- or frequency shift of their echoes.

Statement of Contribution/Methods

This article describes a pulsed method, whereby receiving and transmitting takes place intermittently with the same radiator. Similar to the pulse-to-pulse coherent method, in which the velocity and range unambiguousness is limited by the Nyquist-criterion and the pulse repetition frequency, the pulse-to-pulse incoherent method is also subject to restrictions. The boundary conditions for both methods are demonstrated in this article. With greater penetration depth, it becomes more and more difficult to ensure the unambiguousness. Signal-coding is required. For different reasons phase coding is not adequate.

Results/Discussion

Therefore one approach is, even for relatively narrow-band ultrasonic transducers, a frequency coding concept for a pulse-to-pulse incoherent method. The features of those encoded signals are given by a nearly orthogonal relation to each other and optimal autocorrelation properties. Beyond that, a filter bank is presented to separate the respective signal codes from the received signal and to determine the runtime of the echo. This concept has been verified by measurements from a stream of a filled pipe. By knowing the pulse repetition frequency and the time difference of the echo runtime, the speed of particles, respectively the flow rate could be analyzed statistically. It could be demonstrated, that the velocity distribution of the measurement has a high correlation to the actual flow rate of the pipe and corresponds to the Doppler-spectrum of a continuous wave (CW) sensor. Due to the excellent characteristics of the coded signals, as well as, their measurement results, this approach stays in a direct competition to classical methods. However, it allows new perspectives for a wide range of signal processing algorithms.

IUS2-PB3-2

Study about the propagation of airborne ultrasonic wave through a heel for bone-density estimation

Shinnosuke Hirata[1], Katsuyuki Kiso[2], Kotaro Hoshiba[1], Hiroyuki Hachiya[1], Nobuo Niimi[3]; [1]*Dept. of Mechanical and Control Engineering, Tokyo Institute of Technology, Meguro-ku, Tokyo, Japan,* [2]*Dept. of Control and Systems Engineering, Tokyo Institute of Technology, Meguro-ku, Tokyo, Japan,* [3]*NIPPON SIGMAX CO.,LTD., Shinjuku-ku, Tokyo, Japan*

Background, Motivation and Objective

Bone density and elasticity can be measured from acoustic propagation parameters in a cancellous bone. In typical Ultrasound Bone Densitometers, ultrasonic waves of several MHz are used to obtain the efficient resolution. However, the propagation path of ultrasonic waves must be filled with mediums, whose acoustic properties are similar to water, to reduce attenuation or reflection from a boundary. Therefore, bone-density estimation using airborne ultrasonic waves has been proposed. In the proposed method, bone density can be estimated by non-contact inspection.

Statement of Contribution/Methods

In this paper, Ultrasound Bone Densitometers for a calcaneus, which is a cancellous bone in a heel, is discussed. In case airborne ultrasonic waves pass through a heel, their waves attenuate more than 65 dB, which is simply estimated from acoustic impedance of air, tissue, and bone. Therefore, pulse compression using M-sequence is employed to improve the S/N of received signal. In case the transmitted signal is n-order of M-sequence modulated signal, the S/N of received signal is improved 3n dB by cross correlation of the received signal and the reference signal, which is corresponding to the transmitted signal.

Results/Discussion

Airborne ultrasonic waves, which passed through a heel, can be observed by using 18th-order M-sequence modulated signal. The reserved signals after cross correlation are illustrated in the figure. In the case of no object between transducers, the amplitude of received ultrasonic wave was approximately 190 mV. In the case of the heel between transducers, the amplitude of passed ultrasonic wave was approximately 0.0018 mV. Therefore, attenuation of airborne ultrasonic wave through a heel was approximately 100 dB. The propagation velocity of passed ultrasonic wave should be measured to estimate bone density.

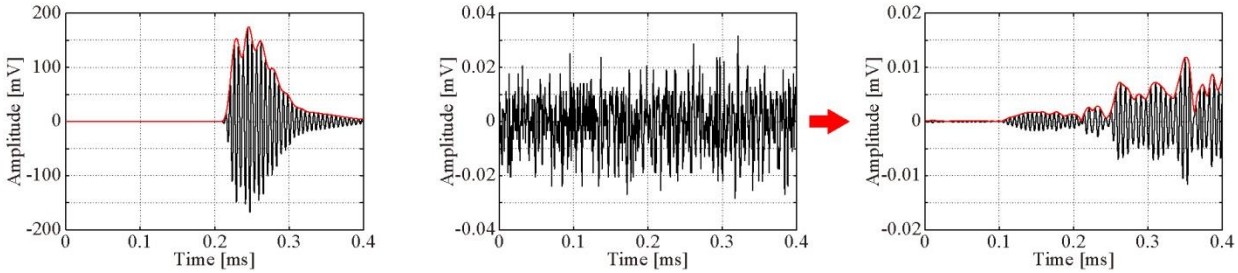

IUS2-PB3-3

Discriminating samples of drinkable water by their ultrasound time-of-flight (TOF)

He Yin[1], Ahmad Afaneh[2], Alexander Kalashnikov[1]; *[1]Electrical Electronic Engineering, Nottingham University, Nottingham, NOTTS, United Kingdom, [2]Computer Systems Engineering, Birzeit University, Birzeit, Jordan*

Background, Motivation and Objective

Water is the most important liquid for human existence. The recommended daily intake of water for humans varies according to different sources, but is about 2 L per day. However, distilled and even low mineral content (less than 50 ppm of solids) water is tasteless and does not quench thirst well. On the other hand, if the mineral content rises to 500 ppm and above, water generally becomes too salty for drinking. Water (and liquid foodstuffs like juices, milk, etc.) can be destructively analyzed for freshness, quality, and absence of contaminants at dedicated chemical laboratories, but such off site tests lead to considerable expenses and time delays. This study aimed to establish whether ultrasound propagation parameters, particularly ultrasound time-of-flight (TOF), could be used to differentiate among water samples online, onsite and at low cost.

Statement of Contribution/Methods

It has been shown that ultrasound TOF could be sensitive to changes in chemical composition on the order of tens to hundreds parts per million in the course of certain chemical reactions [1]. It was also found that the resolution of the ultrasonic instrument used was insufficient for accurate measurement, and the influence of temperature variations could dominate the measurement results. The first issue was addressed by the development of high accuracy data acquisition architecture, which was coupled with embedded processing of the received waveforms; the temperature reference was obtained by using a cavity filled with deionized water [2]. This instrumentation was applied to measurements of the water samples reported here.

Results/Discussion

The experimental records of the ultrasound TOF across the range of temperatures referenced by the TOF showed a clear distinction between:

- drinkable water and water contaminated by bacteria samples;
- water sourced in different countries (UK, France, China);
- sparkling and still bottled water;
- oceanic and bottled water.

The experimental results obtained to date show the feasibility of applying ultrasound TOF as a discriminating factor among various samples of drinkable bottled water provided that the instrument operates at high temporal resolution (1 GHz sampling frequency) and an accurate temperature reference is available (TOF in deionized water held at the same temperature as the sample was used). This makes it potentially possible to develop onsite, online and low cost instrumentation for quality control of liquid foodstuffs.

[1] A.N.Kalashnikov, K.L.Shafran, V.G.Ivchenko et al, "In situ ultrasonic monitoring of aluminum ion hydrolysis in aqueous solutions: instrumentation, techniques and comparisons to pH-metry ", *IEEE Trans Instrum Measur*, 56(4), 1329-1339.

[2] A.Afaneh and A.N.Kalashnikov, "Embedded processing of acquired ultrasonic waveforms for online monitoring of fast chemical reactions in aqueous solutions", in *Advanced distributed measuring systems – exhibits of application*, 2012, 67-93.

IUS2-PB3-4

Analysis of Change in Motional Capacitance of Quartz-Crystal Tuning-Fork Tactile Sensor Induced by Viscoelastic Materials in Contact with Its Base

Hideaki Itoh[1], Naoki Hakakeyama[2]; *[1]Faculty of Engineering, Shinshu University, Nagano, Nagano, Japan, [2]Shinshu University, Japan*

Background, Motivation and Objective

If we want to measure both Young modulus and viscosity coefficient of materials using a conventional instrument, an adequate instrument to fit the hardness type of samples must be chosen. For example, a tension test is used for measuring Young modulus of hard materials such as plastics or metals. On the other hand, rotary viscometer and dynamic mechanical analysis system (DMA) are also used for measuring Young modulus and viscosity coefficient of soft materials such as rubbers. However, these instruments have some drawbacks: the price of hardware is more expensive; the shape of test piece is officially fixed for measurement.

To date, the vibrating tactile sensors using the change in frequency and resistance has been studied. As far as we know, our vibrating tactile sensor using the change in motional capacitance [1],[2] is the first one.

Statement of Contribution/Methods

We already showed that the change in the reciprocal of its motional capacitance difference (delta) (1/Ca) before and after the base of sensor getting into contact with materials changed with the Young modulus of materials.[2] As for the plastics, the calculated and measured values of delta (1/Ca) were found to be almost equal. However, as for the silicone rubbers, the measured value of delta (1/Ca) was found to be considerably larger than the calculated value of delta (1/Ca) using Young modulus of them. This fact suggests

that the viscoelasticity of materials in contact with the base affects directly the motional capacitance of quartz-crystal tuning fork tactile sensor. There are no reports to explain theoretically the experimental results of capacitance changes of a vibrating tactile sensor induced by the viscoelastic materials in contact with its base.

Results/Discussion

Figure 1 shows the change in the reciprocal measured motional capacitance delta (1/Ca) for neoprene rubbers and plastics against the Young moduli of materials. In this study, we investigate theoretically and experimentally that the change in the motional capacitance of quartz-crystal tuning-fork tactile sensor varies with both the dynamic Young modulus and viscosity of amorphous polymers such as neoprene rubbers.

This work was partly supported by Grant-in-Aid for Scientific Research (c) in Japan.

[1] H. Itoh and N. Hatakeyama, Jpn. J. Appl. Phys., vol.49, 07HC03, 2010.
[2] H. Itoh and N. Hatakeyama, Jpn. J. Appl. Phys., vol.49, 126702, 2010.

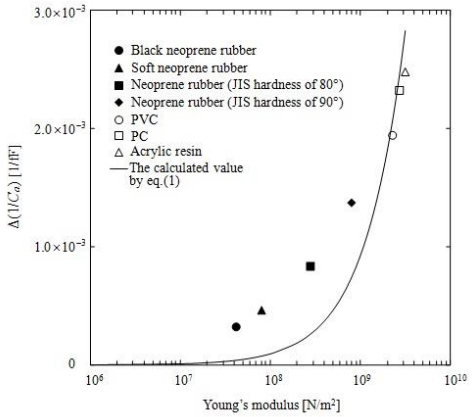

Fig.1 Measured $\Delta(1/C_a)$ vs Young's moduli of materials for neoprene rubbers and plastics. The solid line is the calculated value of $\Delta(1/C_a)$.

IUS2-PB3-5

Determination method of liquid concentration using SH-SAW sensor without reference liquid

Jun Kondoh[1], Saburo Endo[2], Takuya Nozawa[2]; [1]*Graduate School of Science and Technology, Shizuoka University, Hamamatsu-shi, Shizuoka, Japan,* [2]*Graduate School of Engineering, Shizuoka University, Hamamatsu-shi, Shizuoka, Japan*

Background, Motivation and Objective

A liquid phase sensor is realized by using a shear horizontal surface acoustic wave (SH-SAW). The SH-SAW sensor needs reference liquid for the sensor calibration. If the sensor is applied to concentration monitor in a liquid flow system, the sensor must be detached from the line for calibration before measurements. This is one of obstacles for commercialization of the SAW sensor. It is important to develop liquid concentration measurement method without reference liquid.

In this paper, we focus a methanol (MeOH) sensor for a direct methanol fuel cell (DMFC). MeOH sensors have been commercialized. However, those sensors need calibration before each measurement using water. Therefore, development of SH-SAW methanol sensor which does not need reference liquid at each measurement is very significant.

Statement of Contribution/Methods

The SH-SAW sensor fabricated on 36YX-LiTaO3 was used to determine the MeOH concentration. Detection mechanism of the permittivity is the electrical perturbation. The approximate equation for the electrical perturbation was derived. The equation involves not only liquid parameters, but also an electromechanical coupling coefficient of the substrate. As operating temperature of the DMFC is varied, temperature dependencies in those properties must be considered. A liquid parameters as a function of temperature is obtained from literature. The coupling coefficient is calculated using the numerical method under considering temperature dependencies of the material constants. The equation considering temperature was compared with the experimental results. Temperature was varied from 10 to 80 °C. Then the determination method of MeOH concentration is proposed on the bases of the equation.

Results/Discussion

The SH-SAW sensor was inserted into a liquid-flow system with a pump. Sample was 3 wt% MeOH. The liquid vessel was kept in a temperature-controlled chamber and varied from 10 to 80 °C. Temperature was measured using a thermometer. As the measured and calculated phases agree well, we consider determination method of MeOH concentration based on the equation. Using the equation, phase for the water is calculated as a function of temperature and memorized (DATA1). The relationship between phase shift based on water and concentration was also memorized (DATA2). From the actual measurements, phase (PHA) and temperature are obtained. Using temperature information, phase of water (PHW) is taken from the DATA1. Phase shift, PHA-PHW, was calculated. Comparing the phase shift with the DATA, concentration of MeOH solution is decided. Validity of the proposed method was confirmed through experiments.

In this paper, we discuss the MeOH concentration detection method without reference liquid. The method will be used for other liquid. Therefore, on-line monitoring of liquid in the liquid flow system is possible using the SH-SAW sensor.

IUS2-PB3-6

Gas Sensor for Sensor Network Using Resonators with Double-Reflection SAWs to Achieve Large Interaction Areas within Small Chip

Mitsutaka Hikita[1], Hosaka Jun[1]; [1]*Kogakuin University, Japan*

Background, Motivation and Objective

Recently proposed sensor network will be a very promising system combined with HEMS (Home Energy Management Systems) and other sensing installations. To detect CO, environmental gas and hydrogen leakage from future fuel cars, we published the novel SAW sensor with self-temperature-compensated characteristics on the assumption of garage use at -40 to 80 degree C (Ref. 1). However, the sensor nodes require not only extreme low-power consumption but also very small-sized devices. In the conventional SAW delay-line sensor, long interaction length requires increase of the chip size. In order to achieve compatibility of small chip size and low insertion loss, we investigate resonators with double-reflection SAWs.

Statement of Contribution/Methods

A low-loss sensor constructed with three lattice-circuit resonator delay lines (Fig.1) was previously invented. LC-2 and LC-3 provide standard phases with pi/2 difference, while LC-1 is used for sensing, which provides self-temperature-compensation because of unchanged relative phase relations between output signals for temperature. We developed single-reflection SAW resonators with large spaces, P = 50 wavelengths and P + wavelength/4 respectively, between IDTs and reflectors for reactive films (Fig.2). In order to increase the effective interaction areas, we have investigated double-reflection resonators with spaces, P = 50 wavelengths and P + wavelength/8 respectively. Each resonator consists of upper and lower reflectors, which are mutually shifted by wavelength/4 respectively (Fig.3).

Results/Discussion

Experimental results in Fig.2 for the lattice-circuit delay line with single-reflection resonators have 4dB loss and about 1 micro-sec, i.e. about 160 wavelengths. Simulation results in Fig.3 with double-reflection resonators show about 1.8 micro-sec, i.e. about 290 wavelengths, and similar loss characteristics using same chip size. In this structure, SAWs reflected once from the reflectors are cancelled mutually, while those reflected twice between the reflectors are added in phase. These results show possibility for achieving both low-loss and long-propagation characteristics without increasing chip size. Other delay lines in Fig.1 can be constructed by introducing wavelength/16-space differences between IDTs and reflectors. 1. M. Hikita and J. Hosaka. in IEEE Ultrason. Symp. Proc., 2012.

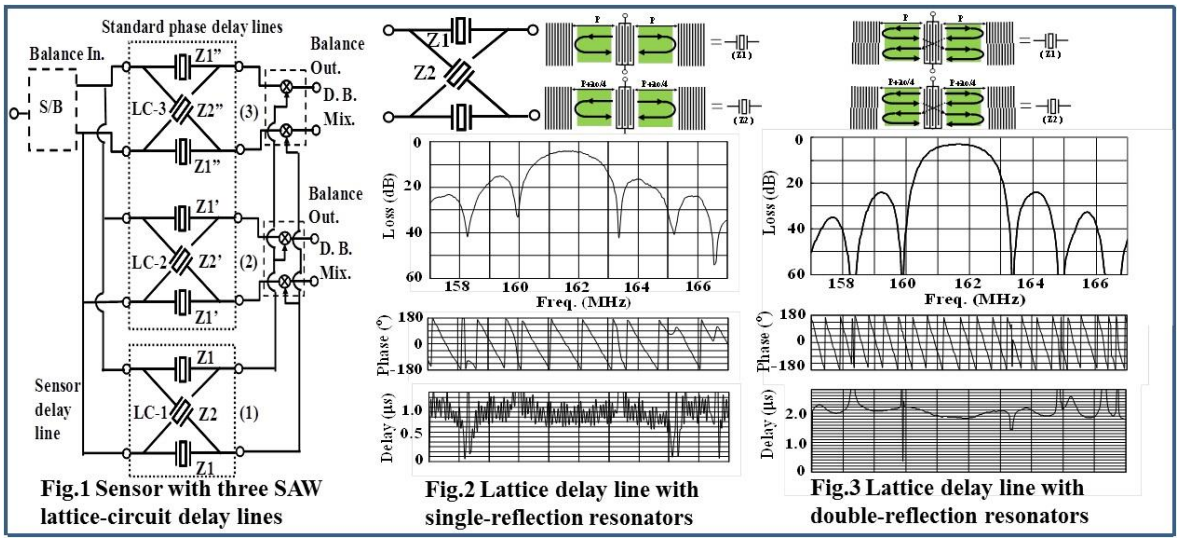

Fig.1 Sensor with three SAW lattice-circuit delay lines

Fig.2 Lattice delay line with single-reflection resonators

Fig.3 Lattice delay line with double-reflection resonators

IUS2-PB3-7

Accurate Round Trip Delay Time Estimator for Simultaneous Identification of Multiple SAW ID Tags

Maria Klaffenboeck[1], Stefan Schuster[1], Stefan Scheiblhofer[2], Andreas Stelzer[1]; *[1]Institute for Communications Engineering and RF-Systems, Johannes Kepler University, Linz, Austria, [2]Hainzl Industriesysteme, Linz, Austria*

Background, Motivation and Objective

The simultaneous identification of multiple surface acoustic wave identification (SAW ID) tags of delay line type using a frequency-stepped continuous-wave radar requires an accurate unbiased estimation of the reflector delays (round trip delay times – RTDTs). In this case multiple cisoids interfere due to the superposition of the tags' impulse responses. Usage of standard estimators like the fast Fourier transform (FFT) and occurring distortions due to nonlinear transfer functions of the components lead to biased RTDT estimates, with higher risk of erroneous tag detection in this case. Taking amplitude distortions (AD) and phase distortions (PD) into account within the signal model and estimating the parameters of the single cisoids iteratively, we obtain more accurate RTDT estimates. Hence, the spatial density of the encoded data on the tags can be higher, thus more information can be placed on a tag. Additionally, the probability of correct tag detection increases at low signal-to-noise ratios.

Statement of Contribution/Methods

In a first step, the AD and PD are calculated using measurements of specially designed calibration tags. The resulting model of the distortions is used to compute accurate signal models of the SAW tags, cf. Fig. below, which is the key for high resolution RTDT estimates. The unknown parameters of each possibly superposed cisoid are estimated within an iteration process. Starting with the most powerful cisoid, the signal model is iteratively refined by including additional tones and re-estimating cisoids until a predefined abort criterion is reached. The accuracy of the RTDT estimates can be increased in each iteration step, if this procedure is performed several times, which is presented within the final paper.

Results/Discussion

Although the presented method is computationally more extensive than commonly used estimators (e.g. FFT), the accuracy of the RTDT estimates is greatly improved. Even multiple reflections on a single SAW tag and interferences from other tags can be handled correctly. Identifying multiple tags with mutually interfering impulse response patterns strongly requires high-resolution RTDT estimators, since the results are biased using common FFT based estimators. Interfering signals can be suppressed up to 30 dB. The performance of this algorithm is validated in various Monte Carlo simulations and measurements.

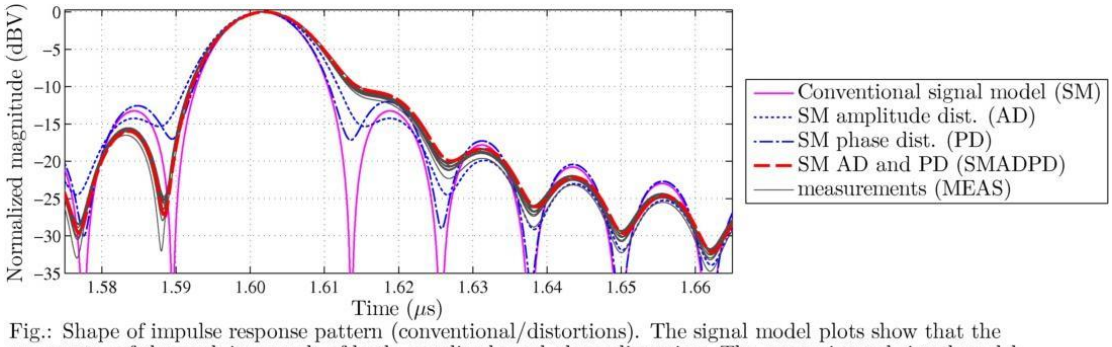

Fig.: Shape of impulse response pattern (conventional/distortions). The signal model plots show that the asymmetry of the peak is a result of both, amplitude and phase distortion. The approximated signal model (SMADPD) is in good match with the measurements (MEAS).

IUS2-PB3-8

Thin Films and Techniques for SAW Sensor Operation Above 1000°C

Roby Behanan[1], Scott Moulzolf[1], Mike Call[1], David Frankel[1], George Bernhardt[1], Robert Lad[1], **Mauricio Pereira da Cunha[1]**; *[1]University of Maine, Orono, Maine, USA*

Background, Motivation and Objective

High temperature (300°C to 1800°C) wireless sensors have applications in energy exploration and generation, harsh environment industrial processing, and aerospace engineering. Existing surface acoustic wave (SAW) technology developed at the University of Maine allows the fabrication of sensors that can deliver long-term stable operation up to 850°C. Since piezoelectric langasite (LGS) substrates can perform up to their melting point of ~1400°C, it is desirable to extend the SAW sensor temperature range of operation. In addition, it is desirable to increase the wireless SAW operating frequency towards the GHz range, thus diminishing the dimensions of the interdigital transducers (IDTs) electrodes. Exposure of co-deposited Pt-Rh/ZrO_2 IDT electrodes with line widths ~2µm to temperatures above 1000°C creates Pt-rich nano-whiskers (figure inset) that are long enough to short the SAW interdigital transducers (IDTs), thereby making the devices unusable.

Statement of Contribution/Methods

In this work, SAW sensors have been fabricated using several types of electrode film materials and techniques in order to extend both the temperature and frequency of operation. In addition to the Pt-Rh/ZrO_2 co-deposited and nanolaminate electrodes, new electrode materials such as Pt-Al and PtAl_2O_3 were explored. To mitigate the growth of nano-whiskers, two techniques proved effective: the use of a protective Al_2O_3 capping layer deposited over the entire SAW sensor surface using atomic layer deposition (ALD); and the use of multi-layered Pt-Rh/ZrO_2 nanolaminate electrode architectures.

Results/Discussion

Multilayer Pt-Rh/ZrO_2 electrodes, comprised of four layers of Pt-Rh (20nm) interleaved with four layers of ZrO_2 (7.5nm), and capped by an ALD Al_2O_3 layer successfully inhibited nanowhisker formation. Results from SAW devices using Pt/Al and Pt/Al_2O_3 films revealed operation above 1000°C. The figure plot shows the measured $|S_{11}|$ response from an ALD Al_2O_3 capped SAW resonator sensor after heating at three different temperatures: 850°C for 4 hours (solid curve); 1000°C for 3 hours (dashed curve); 1050°C for 3 hours (dotted-line curve). The results show successful device operation beyond 1000°C. These achievements open the possibility for harsh environment SAW wireless sensor application beyond the 1000°C mark.

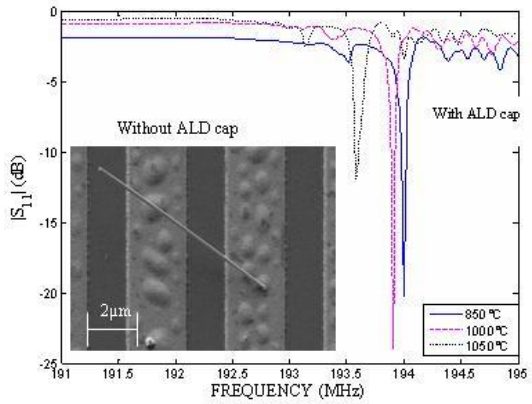

Modeling in physical acoustics

Forum Hall

Tuesday, July 23 2013, 01:00 pm - 04:30 pm

Congress Hallair: **Koen van Dongen**
Delft University of Technology

IUS3-PB-1

SH-SAWs in Piezoelectric Structure with an Imperfectly Bonded Viscoelastic Layer

Jing Cui[1], **Jianke Du[1]**, Ji Wang[1]; *[1]Ningbo University, China, People's Republic of*

Background, Motivation and Objective

It is well known that numerous investigations have been undertaken for the analysis of shear-horizontal surface acoustic waves(SH-SAWs) in piezoelectric structures. SH-SAWs have wide applications in biosensing and chemical sensing fields, where the cells or DNA molecules are often modeled as viscoelastic layer loaded on the piezoelectric substrate. The mass layers in most of the existing theoretical results on acoustic wave sensors are perfectly or rigidly bonded to the piezoelectric structures in the sense that the mass layers have the same displacement as the substrate surfaces. In practice the mass layer in chemical and biological sensor applications may not follow the substrate surfaces perfectly, i.e., the interface between viscoelastic layer and piezoelectric substrate isn¡¯t always perfect. These all call for further study of the effects of imperfectly bonded viscoelastic mass layers.

Statement of Contribution/Methods

In this paper, we want to examine the effects of the viscosity of mass layer and the imperfect interface bonding on the dispersion relations of the waves. An analytical approach is taken to investigate SH-SAW propagating in layered piezoelectric structures where a thin viscoelastic layer imperfectly bonded to a semi-infinite piezoelectric substrate. The governing equations of the SH waves are obtained on the basis of the linearly electro-elastic theory. The shear-lag model is used to analyze the effect of an imperfectly bonded viscoelastic layer.

The analytical solution of dispersion relations are obtained for mechanical and electrical boundary conditions for the viscoelastic mass layer with perfect or imperfect interface. The phase velocity is calculated and figured. The distributions of the displacements and the shear stresses are also investigated and figured. The effects of the viscoelasticity and imperfect interface on the properties of the SH-SAWs are discussed in detail.

Results/Discussion

The results show that the viscosity of the layer and imperfect interface bonding have significant effects on the phase velocity, displacements and shear stress of SH-SAWs. We can find that the phase velocity decreases with the increase of the viscosity coefficient. When the interface bonding is imperfect, the phase velocity decreases significantly with the wavenumber in either electrically shorted or open case. The attenuation decreases with the increase of the interface stiffness coefficient. The results can be helpful for the design of the piezoelectric acoustic wave sensors or resonators.

IUS3-PB-2

An Analysis of the Frequency-temperature Relations of SC-cut Quartz Crystal Plates with the Lee Plate Theory

Tingfeng Ma[1], Wejun Wang[1], Jianke Du[1], Dejin Huang[1], **Ji Wang[1,2]**; *[1]Ningbo University, Ningbo, Zhejiang, China, People's Republic of, [2]Haifeng Electronics Co., Ltd., China, People's Republic of*

Background, Motivation and Objective

The analysis of high frequency vibrations of piezoelectric crystal plates at the thickness-shear modes are of great importance in resonator design. In addition to fundamental issues like the vibration frequency, practical needs on the effects of complication factors such as the electrodes and temperature fluctuation are also required to be available for the optimal selection of structural parameters. The plate theories by Mindlin and Lee have been widely used for this purpose, and further improvements of techniques handling complications have been sought.

Statement of Contribution/Methods

The incremental thermal field theory for the consideration of temperature effect on the frequency stability of quartz crystal resonators by Lee and Yong has been making good prediction within the framework of the Mindlin plate equations (Lee and Yong, Journal of Applied Physics, 60, 2327-2341, 1986). Lately, Lee has made improvements for better predictions on the thickness-shear vibrations and couplings of spurious modes. In addition, Lee and collaborators have considered the piezoelectric effects and the driving voltage as part of the extended studies on quartz crystal resonators (Lee and Lin, J. Appl. Phys., 83, 7822-7833, 1998). Since the results are consistent with earlier studies, the advantage of Lee plate equations can be better taken by including thermal effect analysis also. It is found that changes on the equations are minimal, and the equations are ready to use for the complete analysis of resonators with the Lee plate theory.

Results/Discussion

With the modified Lee plate equations and thermal field considered, we are ready to use the new equations for the frequency-temperature relations which are essential in the quartz crystal resonator development. As we have found, the frequency change curve in the operating range of a quartz crystal resonator is consistent with the predictions of Mindlin plate theory. Equations for the analysis of thermal effect on the quartz crystal resonators of SC-cut with the modified Lee plate equations have been obtained, and the solution procedure are proven to be the same with earlier equations based on the Mindlin plate equations. We now are able to design resonators with the choice of Mindlin or Lee plate equations based on individual choices.

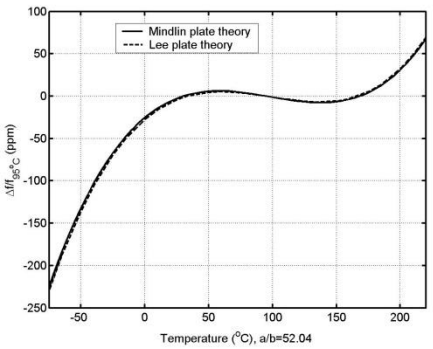

IUS3-PB-3

An Analytic Method of Solving the Problems of Reflection and Refraction of Waves in Piezoelastic Media

Sadriten Tleukenov[1], Nurkhat Zhakiyev[1]; [1]*Department Technical Physics, L.Gumilyov Eurasian National University, Astana, Kazakhstan*

Background, Motivation and Objective

We report analytical solution of reflection and refraction problems at the boundary of the aniso-tropic piezoelectric media. Anisotropic piezoelectric medium with orthorhombic syngony of class 222 and hexagonal syngony of class 622 are considered. The solution is obtained by matriciant method[1]. Usually such tasks for a full Maxwell's system equations are solved by quasistatic approximation[2] and mainly considered the anisotropy of high symmetry.

Statement of Contribution/Methods

We have described the Interaction between elastic and electromagnetic waves is considered as a joint equation set of elastic medium motion and full Maxwell's equations(1). The solution of Eqs.(1) is written in the form $f(x,y,z,t)=f(z)exp(i\omega t-imx-iny)$ that reduces this equation set to a system of ordinary differential equations of the first order with variable coefficients(2).In general, the matrix of B has the order (10x10). In particular, when considering waves in orthorhombic media of class 222 and hexagonal syngony of class 622 along the plane (xz), where the component of the wave vector ky=n=0 the matrix is divided into two (6x6) and (4x4) matrices. The matrix (4x4) describes propogation of coupled elastic transverse wave with Y-polarization and TM electromagnetic waves. The structure of B in(5),it contains all piezoelastic parameters of the medium.

Previously, for such systems matriciant was constructed in analytical form[3,4](3).

Results/Discussion

Using Eq.(3) problem of reflection and refraction of coupled elastic and electromagnetic waves is formulated with boundary conditions(4), where **W** are fields of the incident, reflected and refracted waves. Conditions(4) include continuity of the fields on the plane boundary and take into account effect of media on propagation of waves. From the representation of the solution in the form Eq.(3) the reflection and refraction matrices are obtained(5).

Accounting matrix **R** (Eq.5) in boundary conditions Eq.(4) gives the solution for the reflection and refraction matrices in the explicit form (6).

References

[1] Tleukenov S.K., Matriciant method.-Pavlodar:PSU after S.Toraigyrov,148 p.2004.

[2] X.Yuan, Z.H.Zhu: Reflection and refraction of plane waves at interface between two piezoelectric media. Acta Mech 223, 2509–2521 (2012)

[3] Tleukenov S.K., Zhakiyev N.K., Yeltinova L.A. Propagation of coupled waves of different nature in anisotropic continuous media: universal method for theoretical description, General Meeting of Asian Consortium on Computational Materials Science (ACCMS), Sendai, Japan, 2012.

[4] Tleukenov S.K., Wave processes and method matriciant. Scientific journal Bulletin L.N.Gumilyov Eurasian National University, Vol.4, 68-74, 2011.

$$\frac{\partial \sigma_{ij}}{\partial x_j}=\rho\frac{\partial^2 u_i}{\partial t^2};\ rot\,\vec{E}=-\frac{\partial \vec{B}}{\partial t};\ rot\,\vec{H}=\frac{\partial \vec{D}}{\partial t};\ \begin{cases}\sigma_{ij}=c_{ijkl}\varepsilon_{kl}-e_{ijk}E_k\\ D_i=\vartheta_{ik}E_k+e_{ikl}\varepsilon_{kl}\end{cases}(1)$$

$$\frac{d\vec{W}}{dz}=\hat{B}\vec{W};\ \vec{W}=(u_y,\sigma_{yz},H_y,E_x)^t;\ \vec{W}(z)=T\vec{W}_0 \qquad (2)$$

$$T_{aver}=\frac{P-\tilde{p}_2E}{\tilde{p}_1-\tilde{p}_2}\left[E\cos(\tilde{k}z)+\frac{\langle B\rangle}{\tilde{k}}\sin(\tilde{k}z)\right]-\frac{P-\tilde{p}_1E}{\tilde{p}_2-\tilde{p}_1}\left[E\cos(\tilde{\chi}z)+\frac{\langle B\rangle}{\tilde{\chi}}\sin(\tilde{\chi}z)\right](3)$$

where $\hat{P}=E+\frac{\hat{B}^2h^2}{2}$, $\tilde{p}_i$ are the roots of the characteristic equation of matrix $\det(\hat{P}-\lambda E)=0$, $\tilde{p}_1=1-\frac{k^2h^2}{2}$; $\tilde{p}_2=1-\frac{\chi^2h^2}{2}$.

$$\left(\frac{1}{2}E-R\right)\vec{W}_0+\left(\frac{1}{2}E+R\right)\vec{W}_R=\left(\frac{1}{2}E-R_1\right)\vec{W}_t,\ \vec{W}_0+\vec{W}_R=\vec{W}_t \quad (4)$$

$$R=-\frac{B+k\,\chi\,B^{-1}}{2\,i\,(k+\chi)},\qquad B=\begin{pmatrix}0 & b_{12} & b_{13} & 0\\ b_{21} & 0 & 0 & b_{24}\\ -i\omega b_{24} & 0 & 0 & b_{34}\\ 0 & -i\omega b_{13} & b_{43} & 0\end{pmatrix} \qquad (5)$$

$$\vec{W}_R=(R+R_1)^{-1}(R-R_1)\vec{W}_0=Q\vec{W}_0;\quad \vec{W}_t=(\hat{E}+Q)\vec{W}_0 \qquad (6)$$

IUS3-PB-4

A new analytical expression for fast calculation of the transient far field of a rectangular baffled piston

Alejandra Ortega[1], Ling Tong[1], Jan D'hooge[1]; [1]*Cardiovascular imaging & dynamics, Katholieke Universiteit Leuven, Leuven, Belgium*

Background, Motivation and Objective

3D ultrasound imaging has gained clinical importance. For which 2D matrix array transducers and the associated (two-stage) beam forming are essential. Given the large number of degrees of freedom and the complexity of this problem, simulation tools play an important role. Hereto, the spatial impulse response (IR) method (as implemented in e.g. FieldII) is commonly used. Unfortunately, given the large element count of 2D array transducers and the inefficient analytical expression of the IR of an individual element, simulation times can become a bottle neck. The aim of this study was therefore to derive a new analytical expression to speed up the calculation process.

Statement of Contribution/Methods

The IR of an arbitrary point of observation (POO) is calculated as the arc-length of intersection of a sphere (of growing radius with time) with the transducer's surface. The classical method provides (amongst other geometries) an analytic expression for a POO above the corner of a rectangular transducer. And the response in an arbitrary POO is calculated as the sum/subtraction of such rectangles. Thus, most of the IR estimations for a POO outside the transducer area are redundant as given contributions are calculated to be subsequently recalculated and subtracted. The proposed analytical expression directly calculates the arc-length of any POO therefore avoiding unnecessary calculations.

The classical and proposed expressions were implemented in MATLAB and the IR was calculated at different POO along the diagonal of a rectangular single element transducer (9.28x9.28mm), and of a 2D array transducer(same size; 32x32 elements). The resulting IR's were compared and the time required for their calculation was recorded.

Results/Discussion

For all POO, the IR's calculated with both expressions were identical. For the single element, the mean calculation time reduced from 64.72ms per POO for the classical expression to 2.39ms for the proposed one, resulting in a total speed up of 26.96±0.7 times. The figure shows the time difference between the two methods as a function of the POO position. For the 2D array, the total speed up was 10 times.

The proposed expression significantly speeds up the calculation time of the IR while remaining equally accurate. This new expression will be particularly relevant for 2D matrix transducer design where computation times remain high.

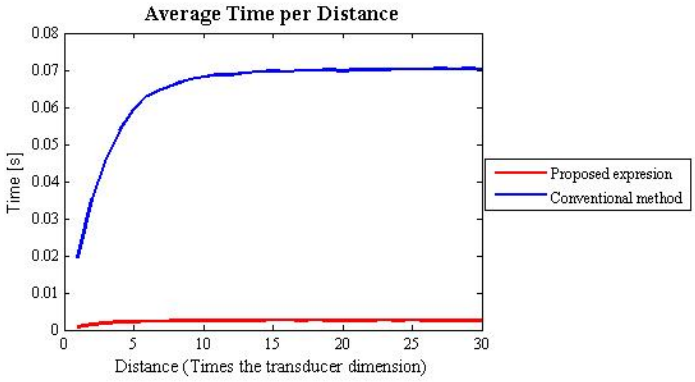

Figure. Average time per distance expended to calculate the impulse response of a 1D array of a point in the pressure field fixed in depth at 4cm, and moving away from in a diagonal from the element's center from 1 to 30 times the size of the transducer elevation and azimuth directions. Blue, conventional method. Red, proposed expression

IUS3-PB-5

Nonlinear acoustic propagation simulation tools: Comparison of BBGASM and INCS up to the fifth harmonic components

François Varray[1], Libertario Demi[2], Koen W.A. van Dongen[3], Olivier Basset[1], Christian Cachard[1], Martin D. Verweij[3]; *[1]Creatis, Université de Lyon ; CNRS UMR5220 ; Inserm U1044 ; INSA-Lyon ; Université Lyon 1, Villeurbanne, Rhone Alpes, France, [2]Lab. of Biomedical Diagnostics, Eindhoven University of Technology, Eindhoven, Netherlands, [3]Lab. of Acoustical Wavefield Imaging, Fac. of Applied Sciences, Delft Univ. of Technology, Delft, Netherlands*

Background, Motivation and Objective

Acoustic propagation is inherently nonlinear, and the generated higher harmonics can be used in diagnostic and therapeutic applications. A few nonlinear simulation tools are described in the literature. The Iterative Nonlinear Contrast Source (INCS) method uses a contrast source in a linear background medium to capture the nonlinear behavior. This leads to an integral equation, which is solved in an iterative way. The resulting full-wave method is very accurate, at the cost of a repeated evaluation of convolutions over the entire 3D spatial and 1D temporal computational domain. The Broad-Band Generalized Angular Spectrum Method (BBGASM) is a forward-stepping method that involves a finite difference scheme in the Fourier domain to handle the axial propagation of the nonlinear wave. This method is not limited in the number of harmonics and their possible nonlinear interaction. The method is very fast because it is not iterative and it avoids the convolution with respect to the axial coordinate. Both methods provide the nonlinear acoustic field evolution in inhomogeneous nonlinear media such as contrast agents or pathological tissues. The objective of the paper is to evaluate the performance of both tools to express the non linearity in terms of accuracy, computation speed and potential applications.

Statement of Contribution/Methods

Theoretical mathematical frameworks of both methods are first presented using or not inhomogeneous coefficient of nonlinearity. Next, nonlinear wave propagation in two different nonlinear media is simulated with BBGASM and INCS. The first medium is homogeneous and is used to validate the accuracy of both methods considering up to the 5th harmonic components. The second medium is used to compare the simulated acoustic fields in the specific case of inhomogeneity in the nonlinear parameter.

Results/Discussion

The two methods are used to model the pressure wave field generated by a 64 element linear array. Each element is excited with a Gaussian pulse with a center frequency equal to 1 MHz, resulting in a 1 MPa pressure at the transducer surface. The profiles of the total nonlinear wavefields are very close in both nonlinear cases. To further validate the resulting fields, the maximum pressure of each harmonic has been computed. With the homogeneous phantom, the relative deviation of BBGASM as compared to INCS for the fundamental and its harmonics is 1.05%, 1.9%, 8.7%, 7.8% and 9.1%. In the inhomogeneous case, similar deviations are obtained. On the other hand, for both cases the computation time for INCS is in the order of 2 hours on 40 parallel cores, while for BBGASM it is only 1 minute on a standard laptop. In conclusion, both tools present particular advantages and disadvantages and can be used according to the application. For fast simulation and quick estimation, BBGASM performs well. For accurate pressure field evaluation, INCS is preferred. Moreover, INCS can also handle non homogeneous wave velocities and medium attenuation.

IUS3-PB-6

A computationally efficient elastic wave model with power-law absorption

Bradley Treeby[1], Ben Cox[1]; *[1]Department of Medical Physics and Bioengineering, University College London, London, United Kingdom*

Background, Motivation and Objective

The simulation of elastic wave propagation has a large number of applications in ultrasonics, including the classification of bone diseases, non-destructive testing, and the design of SAW devices. In biomedical ultrasound in particular, elastic wave models have been used to investigate the propagation of ultrasound waves in the skull and brain, to optimise the delivery of therapeutic ultrasound through the thoracic cage, and to study the destruction of calculi inside the human body. However, most existing elastic wave models are based on low-order finite-difference schemes and thus require large numbers of grid points per wavelength to avoid numerical dispersion. Moreover, they do not account for the power-law acoustic absorption experimentally observed in human tissue, which is critical for model-based dosimetry and treatment planning. The objective of this work was to derive and implement a computationally efficient 3D elastic wave model for isotropic media with power-law acoustic absorption.

Statement of Contribution/Methods

The model is based on two coupled equations describing the stress and particle velocity within the medium. These are discretised using a time-stepping pseudospectral scheme, where spatial derivatives are computed using the Fourier collocation spectral method and temporal derivatives are computed using finite-differences. At each timestep, the particle velocity is split into compressional and shear components using a dyadic wavenumber tensor. This allows the use of a k-space correction to the time stepping scheme that minimises numerical dispersion. It also allows the inclusion of power law absorption term without memory penalties. The absorption term is derived from a fractional Kelvin-Voigt model where the temporal derivative of the strain is replaced with a fractional derivative. The use of the splitting step allows this to be converted to a fractional Laplacian via the lossless dispersion relation using the appropriate compressional or shear wave speed. This can then be computed efficiently using Fourier spectral methods (the fractional Laplacian is non-local in space rather than time). The model allows the medium properties to be heterogeneous, in addition to including different power-law absorption behaviour for the shear and compressional waves.

Results/Discussion

The accuracy of the model is validated against several canonical examples, including reflection and transmission by a homogeneous half-space, scattering by a spherical inclusion, and the absorption of a plane-wave. For accurate reflection coefficients, the model requires only three grid points per acoustic wavelength. This represents a considerable saving compared to finite-difference methods, which require at least 15-20. The low numerical dispersion introduced by the model is also compared against existing time domain codes. The model will be released as part of the open source k-Wave Toolbox, and has a large number of potential uses.

IUS3-PB-7

Time-domain Simulations of the Acoustic Streaming Produced by a Propagating Wave Radiated by a Circular Piston

Arturo Santillan[1]*; [1]Department of Technology and Innovation, University of Southern Denmark, Odense M, Fynn, Denmark*

Background, Motivation and Objective

During the last decades the investigation on the use of high-intensity ultrasound for practical applications has been widely increased. As a consequence, there has been a renew interest in the study of acoustic streaming. A significant part of the investigation on acoustic streaming has considered acoustic waves in cavities and the interaction of the waves with boundaries. In this paper a different kind of acoustic streaming is studied, the strong jet-like wind generated by a beam of sound radiated by a powerful ultrasonic source. Nonlinear effects produced by an acoustic wave radiated by a circular piston will be presented. The main motivation has been a further understanding of the nonlinear effects associated with a propagating wave.

The general objective of the work described in this paper has been to simulate the radiation of sound in air by a circular piston and to understand the physical mechanisms involved. The implementation of the complete nonlinear terms of the fundamental equations of acoustics and the simulation of the temporal evolution of the sound field have been the aim of the investigation. In this way, a complete description of the sound field should be achieved.

Statement of Contribution/Methods

The work contributes to further understand the nonlinear effects produced by a propagating wave of high intensity and the associated physical mechanisms.

The numerical simulations are implemented by using the classical finite-difference time-domain (FDTD) algorithm. For the simulations, the sound wave is considered to be radiated by a circular piston, and air is assumed as the medium of propagation. The numerical method is formulated in cylindrical coordinates for axial symmetry configurations. To simplify the problem, temperature effects and heat conduction are not taken into account.

Results/Discussion

It is shown that the FDTD method can be used to simulate both the evolution in time of a high-amplitude propagating wave and the associated nonlinear effects. The obtained values of the sound pressure and particle velocity include also the time-independent quantities. Particularly, the time average of the calculated sound pressure gives the mean Eulerian excess pressure, and the time average of the particle velocity gives the acoustic streaming. Therefore, mean excess pressure and acoustic streaming are not calculated as a function of first-order approximations of the steady-state values of the acoustic variables. In addition, the spatial distribution of the net flow of mass is calculated and analysed.

Obtained numerical results are in good agreement with known solutions, even in the cases in which quite high amplitudes of the sound waves are considered.

IUS3-PB-8

Modeling of sound propagation in media with continuously changing properties towards a locally resolved measurement of sound velocity

Mario Wolf[1], Elfgard Kühnicke[1], Michael Lenz[1], Martin Bock[1]*; [1]Solid-State Electronics Laboratory, Tu Dresden, Dresden, Saxony, Germany*

Background, Motivation and Objective

As sound velocity depends on the mechanical properties of the propagation medium, it can be used as a measure for these properties. A locally resolved measurement of sound velocity allows studying and optimizing many processes. Examples are mixing processes or chemical reactions in industry, and monitoring of hyperthermia cancer therapy in medicine.

A novel technique has already been developed to measure sound velocity and distance simultaneously with only one transducer by determining the focal point of the transducer from the echoes of moving scattering particles. High accuracy could be reached for media with constant sound velocity, and the method is supposed to be extended to measure e.g. a temperature gradient. For this problem, the focus point has to be predicted by simulation. If the material properties are continuous functions of location, additional terms appear in the wave equation. For that reason, sound velocity depends not only on the material parameters but also on their derivative with respect to position.

Statement of Contribution/Methods

The focal position, which depends on sound velocity, can be used as an additional piece of information besides the time of flight. Averaging over a sufficient number of echo signal amplitudes allows considering a uniform distribution of scattering particles. Thus, the maximum position of the average echo amplitude is correlated to the focal position. Via calculated calibration curves, the measuring position and the sound velocity at this point can be determined from the position of the maximum of average echo amplitude.

An annular array, whose elements are driven with different time lags, is used to move the focal point along the acoustic axis of the transducer. This allows measuring sound velocity locally resolved and noninvasively.

The modified wave equation is solved for cylindrical problems in the frequency domain, and new GREEN's functions are developed. The results are used to calculate sound fields of extended sources. Thus, the simulations can be compared with the measurements, where a temperature gradient was generated in water.

Results/Discussion

A novel model of sound propagation in media with a continuously varying sound velocity is presented. The results are applied to extend half-analytical simulation methods, and the sound fields of extended sources are calculated. The results show good agreement with the measurements.

IUS3-PB-9

Compressional acoustic waves in structure "Piezocylinder – viscoelatic layer – liquid"

Andrei Teplykh[1], Boris Zaitsev[2], Iren Kuznetsova[3]; [1]*Laboratory of physical acoustics, Institure of Radioengineering and Electronics, Saratov Branch, Saratov, Saratov, Russian Federation,* [2]*Institute of Radioengineering and Electronics, Saratov Branch, Russian Federation,* [3]*Institute of Radioengineering and Electronics, Russian Federation*

Background, Motivation and Objective

In the paper the characteristics (phase velocity and attenuation coefficient) of compressional acoustic waves propagated in piezoelectric cylinder covered by viscoelastic polymeric layer and immersed into viscous fluid are investigated. At the present time it is known a large number of works devoted to the investigation of the influence of the liquid on the characteristics of the different types of acoustic waves (such as surface, leaky, plate and cylinder acoustic waves). It is well known that propagation of such waves can be accompanied by radiation of bulk acoustic wave into liquid contacting with the waveguide. This happens in the case if the phase velocity of the wave in the corresponding structure exceeds the speed of sound in the liquid. Due to this, the attenuation of corresponding waves caused by two reasons: it is the viscosity of the liquid and radiation losses. Our calculations allow us to estimate the contribution of each of these mechanisms into the overall attenuation.

Statement of Contribution/Methods

Previous research has shown that nanocomposite polymeric materials based on matrices of high-pressure polyethylene with embedded metallic nanoparticles are characterized by acoustic impedance much lower than acoustic impedance of piezoelectric crystals. Therefore, it can be assumed that use of these materials as matching layers between piezocylinder and liquid will increase the efficiency of radiation of bulk acoustic waves into liquid caused by compressional waves. Our calculations have shown that it is really happens and the attenuation coefficient of compressional waves depends on the thickness of the matching layer nonlinearly. The regions of clearly noticeable maxima of attenuation are observed. This phenomenon can be explained by the fact that nanocomposite matching layer mechanically free from the side of liquid, and mechanically clamped from the side of piezocylinder because of differences of acoustic impedances between nanocomposite, piezocrystal and liquid. The matching layer resonates in the case of its thickness $d=n\lambda/4$, where λ – length of wave propagated in the structure, n is a positive odd number.

Results/Discussion

The authors believe that the considered structures can be used in the development of effective hydro-acoustic emitters.

IUS3-PB-10

Shear horizontal waves in piezoelectric plates with polarization gradient

Bernard Collet[1]; [1]*Institut Jean le Rond d'Alembert, CNRS UMR 7190, Université Pierre et Marie Curie, T65, Case 162, 75252 Paris Cedex 05, France*

Background, Motivation and Objective

In general, piezoelectrics modelling needs the consideration of an additional state variable to the strain, which usually is taken to be the electric field vector. Its energetically conjugate quantity is the electric displacement. An other possibility is to choose the (diplole) polarization vector as independent variable, in this case the conjugate variable is a local electric field. A standard extension to the direction the weak nonlocality concists in the inclusion in the stored energy density of the first polarization gradient. In this case, the conjugate to the polarization gradient quantity is a second order tensor which represents the shell-shell interactions

Statement of Contribution/Methods

The motivation of this work is to explore the effects of the polarization gradient into the constitutive laws for piezoelectric crystals by analyzing the propagation of shear–horizontal waves in plates. Specifically, the piezoelectric materials possess 6mm symmetry and the faces are orthogonal at basal plane. The dispersion relations are obtained explicitly not only for completely electroded faces and unelectroded faces but also but also for electroded face on a one side.

Results/Discussion

The generalized slowness curves, the real, imaginary and complex dispersion branches for selected ferroelectric crystals as well as modes spatial distribution in plates are obtained and discussed.

The obtained results show that exists as for others gradient theories a characteristics length which may have significant size effects for SH-devices operating at very high-frequency and short wavelength.

SAW Transducers & Propagation

Forum Hall

Tuesday, July 23 2013, 01:00 pm - 04:30 pm

Congress Hallair: **Masanori Ueda**
Taiyo Yuden

IUS4-PB1-1

Analysis of a SAW Transducer Having Aperiodic Multi-Electrode Cells Using a Coupled FEM/BIE Numerical Model

Pascal Ventura[1], **Pierre Dufilié[2]**, Frédéric Hecht[3]; *[1]laboratoire LEM3, Metz, France, [2]Phonon Corporation, Simsbury, Connecticut, USA, [3]Laboratoire Jacques Louis Lions, Paris, France*

Background, Motivation and Objective

Low loss SAW filters sometimes require a structure with a complex geometry in order to improve the electroacoustical response (coupling coefficient, reflection coefficient, static capacitance).

Most of the coupling of mode models and P matrix models use parameters obtained from a single electrode periodic transducer analysis.

In the case of complex electro acoustical cells (like Hanma-Hunsinger cells), it is sometimes necessary to obtain the COM parameters from the analysis of the entire electro acoustical cell, which means assuming that the filter contains an infinite array of identical electroacoustical cells the elementary cell of which is made of several electrodes.

Statement of Contribution/Methods

At the 2011 IEEE Ultrasonics Symposium, an original coupled Finite Element Model / Boundary Integral Equation (FEM/BIE) was presented in order to simulate an infinite array of single metallic electrodes.

In this paper, a generalization of this model to elementary cells more complex than one electrode will be presented. Like in the 2011 publication [1], the Finite Element Method is used for the finite part of geometry (the electrodes, part of the dielectric, and part of the piezoelectric substrate), while the semi infinite part of the geometry (piezoelectric part, and dielectric part) are taken into account using a Boundary Integral Equation.

Results/Discussion

The theoretical and the numerical parts of the model will be presented, as well as Coupling of Modes or P matrix parameters determination for Hanma-Hunsinger low loss cells with various substrate materials and orientations.

Using the results of the FEM/BIE analysis, a simulation of a filter containing modified Hanma-Hunsinger electroacoustical cells is made and is compared with measurements.

[1] P. Ventura, P. Dufilié, and F. Hecht, "Optimized STW Devices with Buried Electrodes Based on a Mixed FEM/BEM Numerical Model", 2011 IEEE Ultrasonics Symposium, pp. 563-567

IUS4-PB1-2

Acoustic loss mechanism in Silicon Dioxide Films for Temperature Compensated Surface Acoustic Wave Devices

Satoru Matsuda[1], Michio Miura[1], Takashi Matsuda[1], Masanori Ueda[1], Yoshio Satoh[1], Ken-ya Hashimoto[2]; *[1]TAIYO YUDEN CO.,LTD., Japan, [2]Graduate School of Engineering, Chiba University, Japan*

Background, Motivation and Objective

Recently, temperature compensation of surface and bulk acoustic wave (SAW/BAW) technologies has been paid much attention due to strong demand on radio frequency (RF) wideband filters with excellent temperature stability. For the purpose, use of the SiO2 overlay has been extensively studied. In temperature compensated SAW devices, it is very important to understand the attenuation mechanism in SiO2 films. We discussed the correlation between the SAW attenuation and the optical properties of the SiO2 and SiOF film [1,2]. In the case of the SiO2 film, the Q factors of SAW devices degraded with a decrease in the deposition temperature T, and the optical characterization indicated that the excess increase is mainly due to the Rayleigh scattering in SiO2 film. This paper reports the result when T is further increased.

Statement of Contribution/Methods

We fabricated a series of SAW devices using the SiO2/Cu/LiNbO3 structure, and measured their device performances. The SiO2 films were deposited by the chemical vapor deposition (CVD) method. Except T, the other deposition conditions, i.e., deposited pressure, RF power and gas flow rate, were unchanged with those used form the results given in [2]. The SiO2 films were also deposited on the Si wafer with same conditions and optical properties were measured with FT-IR, Raman spectroscopy and spectrometer.

Results/Discussion

SAW devices showed higher Q factor with higher T. Anti-resonance Q factor of SAW devices increased to 702 at 325^{o}C. However, improvement was not obvious when T was higher than 275^{o}C. TCF of the devices was almost unchanged with T. Optical characterization was applied to the SiO2 films. The result shows that optical characteristics scarcely changes with T when T is higher than 275^{o}C. This means that the Rayleigh scattering is a major contributor of the Q degradation when the acoustic loss in SiO2 films is small.

[1] S. Matsuda et al., Proc. IEEE Ultrason. Symp. (2012) [to be published]

[2] S. Matsuda et al., IEEE Trans. Ultrasonic., Ferroelec., and Freq. Contr. (2013) [to be published]

IUS4-PB1-3

Direct Calculation of First and Second Order Temperature Coefficients of Delay for Surface Acoustic Waves on Anisotropic Substrates

Valery Grigorievsky[1], Victor Plessky[2]; [1]*IRE RAS, Russian Federation,* [2]*GVR Trade SA, Switzerland*

Background, Motivation and Objective

Temperature coefficient of delay (TCD) is an important parameter that very often included in specifications of SAW components. For SAW resonators and resonator filters this parameter is also referred to as temperature coefficient of frequency (TCF) and determines deviations of resonant frequencies under variations of ambient temperature. Temperature behavior of a SAW component is usually estimated by calculation of delay time or resonant frequency as a function of temperature taking into account temperature coefficients of material constants for substrate and layers, and then fitting the resulting curve by a polynomial. The coefficients of the polynomial represent temperature coefficient of the first order (TCF1), second order (TCF2), and so on. To avoid multiple calculation and fitting processes in the present report it is proposed to use an extension of the Laguerre polynomial approach [1] to calculate directly the first and second order temperature coefficients of delay for surface acoustic waves on anisotropic substrates. An initial objective of this work was to implement the global search for temperature stable propagation directions in materials with known temperature coefficients of material constants up to the second order, such as quartz and langasite.

Statement of Contribution/Methods

The problem of SAW propagation on an anisotropic substrate by expansion of all wave fields in series of Laguerre polynomials can be formulated as an eigenvalue problem. The minimum eigenvalue of this problem is the SAW velocity squared [2]. The temperature coefficients of material constants can be arranged as a matrix of perturbation to the main matrix of the problem, and the formulas of perturbation theory can be used directly to calculate corrections to the unperturbed eigenvalues. Using the data of thermal expansion coefficients the TCD or TCF can be calculated. To compute TCF1 only the first order temperature coefficients of material constants and all unperturbed eigenvalues are included in calculations, whereas to compute TCF2 the second order temperature coefficients of material constants and unperturbed eigenvectors must be involved in calculations additionally.

Results/Discussion

The global search for temperature stable propagation directions for SAW in quartz and langasite has shown that TCF2 is negative near the propagation directions with TCF1 close to zero. Calculated TCF for various cuts of quartz and langasite will be reported.

[1] S.Datta and B.J.Hunsinger, "Analysis of surface waves using orthogonal functions," J. Appl. Phys. Vol. 49 , No. 2, pp. 475-479, 1978.

[1] Y.Kim and W.D.Hunt "A Laguerre Polynomial Approach to Surface Acoustic Wave Propagation in Multilayered Structures," 1990 IEEE Ultrasonics Symposium Proceedings pp. 179-183.

IUS4-PB1-4

High Temperature Stable Leaky Surface Wave Propagation Properties of SiO_2/Electrodes/Rotated Y-X $LiTaO_3$ Structure with Super High Coupling

Kazuhiko Yamanouchi[1]; [1]*Tohoku University, Sendai, Miyagi, Japan*

Background, Motivation and Objective

The success of practical SAW devices in the field of filters, signal process and others depend upon the choice of substrate materials. The properties for SAW devices would be the electromechanical coupling coefficient k^2 (should be as high as possible) the temperature coefficient of frequency, TCF (should be as small as possible) and small spurious response. The leaky SAW substrate of $LiTaO_3$ have large k^2 and comparable small TCF. However leaky SAW has a small propagation loss by the short or open surface conditions.

Statement of Contribution/Methods

Rotated Y-X $LiTaO_3$ and SiO_2/ Y-X $LiTaO_3$ of Leaky surface waves are theoretically and experimentally analyzed by K.Yamanouchi etal [1]. However, in this paper, the mass loading effect of electrode thickness of IDT did not take into account. Therefore, almost the zero propagating cut angles are the same at the short and open surface conditions.

In this paper, electrode (Al, Cu)/Rotated Y-X $LiTaO_3$ and SiO_2/electrode (Al, Cu)/ Y-X $LiTaO_3$ of Leaky surface waves are analyzed using the mass loading effects of electrodes and dielectric layers. Also, the second order of TCF of leaky surface waves are analyzed and zero TCF results obtained.

Results/Discussion

(Al, Cu)/Rotated Y-X $LiTaO_3$ results show the very low propagation loss and high coupling substrates of new cut angles with the TCF of 20ppm/C at short surface.

SiO_2/electrode (Al, Cu)/ Y-X $LiTaO_3$ results of Leaky surface wave show the very low propagation loss and high coupling substrates of new cut angles with the TCF of 0 ppm/C at SiO_2 thickness of $H/\lambda=0.1$ in short surface. We show new cuts of the higher k^2 and zero propagation loss of $LiTaO_3$ Substrates with zero TCF. Also we show the experimental results.

Ref. [1] K.Yamanouchi, etal, Wave Electronics, 3(1979),pp.319-333, Elsevier Scientific Publishing Company.

IUS4-PB1-5

SAW resonance transmission through strip acoustic waveguides

Alexander Darinskii[1], Manfred Weihnacht[2,3], Hagen Schmidt[2]; [1]*Institute of Crystallography RAS, Russian Federation,* [2]*IFW Dresden, Germany,* [3]*InnoXacs, Dippoldiswalde, Germany*

Background, Motivation and Objective

When scattered from a strip deposited on the substrate, an incident SAW converts into reflected and a transmitted SAWs as well as into bulk waves. Usually the conversion coefficients depend fairly smoothly on the parameters, such as the frequency or the angle of incidence. This paper demonstrates that the conversion coefficients can change strongly and abruptly if the strip-substrate contact supports an acoustic leaky mode whose phase velocity is greater than the SAW phase velocity on the free surface of the substrate.

Statement of Contribution/Methods

Let a harmonic SAW be incident onto the strip under an angle θ. The wave number is k. The scattered acoustoelectric fields are found by FEM. The strip is supposed to be of finite width along the x-axis but of infinite length along the y-axis. Therefore all fields will vary with y-coordinate as $\exp[ik\sin(\theta)y]$ so that it is sufficient to use 2D FEM simulations in the xz-plane. The substrate is half-infinite. Accordingly, the computational domain is truncated by a perfectly matched layer (PML) from the bottom as well as from the right-hand and the left-hand sides. PML also truncates the space above the substrate. This space is included in the computational domain, since the substrate is piezoelectric. The amplitudes of the reflected and the transmitted SAWs are obtained by applying the discrete Fourier transform to the displacements on the surface of the substrate.

Results/Discussion

The computations are performed for the z-cut of an AlN substrate pertaining to the symmetry group 6mm. In this case, the surface of the cut (xy-plane) is the plane of transverse isotropy. The strip is made of Pt or Al. The incident SAW is sagittally polarized. Waveguide modes appear at the strip-substrate contact because of the localization of the SH BAW propagating in the xy-plane. This SH BAW belongs to the branch of fast transverse BAWs. Depending on the phase velocity, some of these waveguide modes can be leaky due to the irradiation of SAW and of slow transverse BAWs. The excitation of a leaky mode by SAW leads to a singular behavior of the reflection and the transmission coefficients. The dependences of the magnitude and the phase of these coefficients on various parameters, such as the angle of incidence, the frequency, the width and the thickness of the strip, are studied. It is found that the magnitude of the reflection and the transmission coefficients abruptly almost vanish and abruptly increase almost to unity within a narrow resonance interval of angles of incidence. The influence of the BAW irradiation inwards the substrate on the sharpness of the resonance is also investigated. In particular, it follows from our simulations that the resonance reflection – transmission at a strip can be useful for controlling the SAW propagation on certain substrates. Such a method is applicable provided that the strip gives rise to waveguide modes propagating faster than SAW.

IUS4-PB1-6

Balanced Low-Loss Narrowband 3-IDT Double Mode SAW Filters with Improved Selectivity

Sergei Doberstein[1]; [1]*ONIIP, Russian Federation*

Background, Motivation and Objective

The wideband balanced double-mode SAW (DMS) filters with a fractional bandwidth of 2-6% became major as the RF filters for the telecommunication equipment[1]. However there are many applications and nowadays market demands for the narrowband SAW filters with a fractional bandwidth of less than 1% having low loss and high selectivity.

Statement of Contribution/Methods

This paper presents the new balanced low-loss narrowband DMS filters with improved selectivity on 42°YX $LiTaO_3$. The filters are realized as 3-IDT scheme on the longitudinal first and third resonance modes. A narrow passband of the filters is formed by means of decrease in frequency difference between these modes with choosing a definite distance between the central IDT and side IDTs eliminating their contact[2]. Also the frequency responses of the central weighted IDT and reflectors involve in forming narrow passband of the filters. In this case the both long central IDT and reflectors are used. Moreover, passband width of the filters depends on a reflection coefficient of the reflector electrodes. This coefficient is determined by the electrode thickness and metallization ratio. It is possible to obtain a reduction in the fractional bandwidth of the filters in choosing electrode thickness and metallization ratio slightly below the values for a condition of the minimum insertion loss. A shape of the frequency response of the filters is determinated by the weighting function of the central IDT, length of the reflectors, relationship between the electrode periods of the central IDT, side IDTs and reflectors. An optimization of the mentioned parameters allows to obtain a specified selectivity of the filters with a fractional bandwidth of less than 1% on retention of the low loss and in the absence of the matching elements. In this case the weighted central IDTs become the lesser long and selfmatching of them is improved in contrast to known methods[3]. The balanced operation of the filters is made by symmetrical connection of the central IDT and side IDTs to the loads. To increase the selectivity of the filters the cascaded connection and phase weighting are employed. The constructional and topological optimization of the SAW filters is provided with a computer simulation using an equivalent circuit model.

Results/Discussion

The 300-342 MHz samples of the balanced SAW filters have shown the insertion loss of 3 dB, 2-dB bandwidth of 2.9-3.3 MHz, stopband attenuation of 60 dB at ±11.25 - ±12.8 MHz offsets from a center frequency in a 50-Ω balanced/unbalanced system. The filters are not require the matching elements and housed in the 5x5x1.35 mm SMD packages. Our new balanced low-loss narrowband DMS filters with improved selectivity will find wide use as IF filters in the telecommunications equipment. [1] O. Kawachi et al., IEEE Trans. on UFFC, vol. 54, N^0 10, pp. 2159-2164, 2007. [2] T. Morita et al., Proc. IEEE Ultrason. Symp., pp. 95-104, 1992. [3] M. Hikita et al., Electron. Lett., vol.19, N^0 22, p.944-945, 1983.

IUS4-PB1-7

Resonance Properties of APTUDT on SAW vs. Electrode Track Apertures

Sergey Biryukov[1], Hagen Schmidt[1], Manfred Weihnacht[1]; [1]*IFW Dresden, Dresden, Germany*

Background, Motivation and Objective

Recently [1] a novel single-phase unidirectional transducer (SPUDT) cell type on SAW with two quarter-wavelength electrodes per one-wavelength period P was proposed for the multi-track solution consisting of alternating active IDT tracks and passive reflector tracks. Such 2D-periodic structure is called active-passive-track unidirectional transducer or APTUDT. It permits to implement SPUDTs for 2.45 GHz (ISM frequency band) in spite of the existing standard lithography limitations. By shifting adjacent tracks with equal apertures relative to each other the non-reflective IDT also can be created for high frequency range [2] in contrast to well-known IDT using split electrodes with width P/8 only. So, the properties of new promising structure should be investigated in details. The objective of this work is to investigate the influence of active and passive track apertures on the resonance properties of APTUDT.

Statement of Contribution/Methods

2D-periodic electrode structure can support a few modes of SAW. The shapes of such modes and the conditions for their existence depend on both the shift of active and passive tracks with respect to each other and the ratio of their apertures. As a consequence, by changing these geometrical parameters the efficiency of SAW generation can be controlled as well as the frequencies of resonances. Note that such geometrical parameters are absent in the standard one track IDT.

Results/Discussion

The electrical admittance Y of the APTUDT cell with aluminum electrodes placed on 128 YX LiNbO3 has been simulated by 3D FEM in vicinity of 2.45 GHz for different apertures of active and passive tracks and a set of shifts between adjacent tracks. The period of the structure along the direction of SAW propagation equal to P=1.6 micrometers and electrode thickness ratio h/P=0.06 have been fixed. The apertures of tracks and shift between tracks are varied over the range 0.5P-2P and the range 0-0.145P, respectively. It has been found that by altering these geometrical parameters remarkable shifts of resonance frequencies either in the same direction or in opposite directions, as well as a strong increase or decrease of the electrical admittance amplitude at the resonance frequencies can be achieved. APTUDT structure has maximal possible dimensions of its elements for a cell period equal to one wavelength. It permits to implement multifunctional SAW devices for 2.45 GHz in spite of the existing technological limitations.

[1] S. V. Biryukov, G. Martin, H. Schmidt, and B. Wall, “Low-loss unidirectional transducer for high frequency surface acoustic wave devices,” JAP, 110, 076103, 2011.

[2] S. V. Biryukov, G. Martin, H. Schmidt, and M. Weihnacht, “Non-Reflective Electrode Cell for SAW with Quarter-Wavelength Electrodes,” in Proc. 2012 IEEE International Ultrasonics Symposium.

Harsh Environment & High Power

Forum Hall

Tuesday, July 23 2013, 01:00 pm - 04:30 pm

Congress Hallair: **Mauricio Pereira da Cunha**
Univ. of Maine

IUS4-PB2-1

Thermally Stable SiO_2/AlN Lamb Wave Resonators Utilizing Lowest-Order Quasi-Symmetric Mode at High Temperatures

Jie Zou[1], Chih-Ming Lin[1], Albert P. Pisano[1]; [1]*Department of Mechanical Engineering, University of California at Berkeley, Berkeley, California, USA*

Background, Motivation and Objective

Piezoelectric microacoustic devices operating in high temperature environments have attracted great interest in various industries, including automotive, aerospace, gas and petroleum exploration, and power electronics. Intrinsically temperature-compensated Lamb wave resonators using an AlN/SiO_2 composite structure have achieved zero first-order TCF at high temperatures, but suffer from a lower quality factor (Q) due to the excessive stress at the interface and a smaller electromechanical coupling coefficient (k^2) due to the additional SiO_2 layer.

Statement of Contribution/Methods

In conventional AlN Lamb wave resonators, the counter-electrode is used to introduce a uniform vertical electric field in the piezoelectric layer and accordingly a higher k^2. However, the interface strain between the counter-electrode and piezoelectric layer degrades the Q. It is interesting to investigate the SiO_2/AlN layered structure associated with a high coupling coefficient when the AlN layer is relatively thick and the interdigital transducer (IDT) is placed at the interface. This new SiO_2/AlN structure utilizing a thick AlN membrane simultaneously offers superior temperature stability, high Q, and large k^2 at high temperatures.

Results/Discussion

Figure 1(a) shows the electromechanical coupling coefficient k^2 for the lowest-order quasi-symmetric (QS_0) mode as a function of the AlN thickness normalized to the wavelength (h_{AlN}/λ). In configurations B and D, when the IDT is placed at the interface, the Lamb wave stress field tends to be involved in the piezoelectric layer most for h_{AlN}/λ equal to 0.5, and thus the electromechanical coupling coefficient becomes strongest. The difference between the two configurations is negligible since the vertical electric field induced by the counter-electrode in configuration B is weak and non-uniform for a thick AlN plate. As is shown in Figure 1(b), by designing the SiO_2/AlN thickness ratio to obtain a positive TCF at room temperature, the configuration D resonator can exhibit its turnover temperature at high temperatures. In other words, the temperature-compensated SiO_2/AlN resonators utilizing the QS_0 mode simultaneously achieve good temperature stability, high Q, and large k^2 at high temperatures. These simulation results lay the foundation for temperature-compensated SiO_2/AlN Lamb wave resonators for high temperature applications. The Lamb wave devices are under fabrication and will be presented in the full paper.

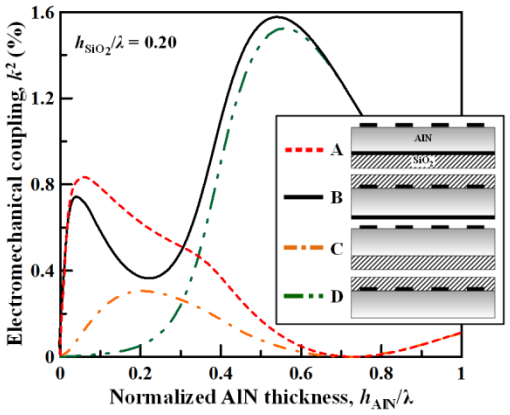

Figure 1(a). Simulated electromechanical coupling strength of four Lamb wave resonator configurations utilizing the QS_0 mode.

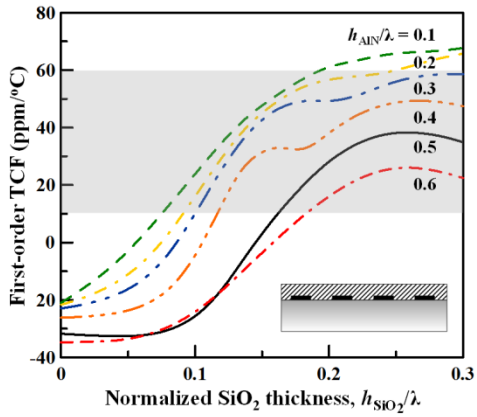

Figure 1(b). Simulated first-order TCFs of the configuration D resonator utilizing the QS_0 mode with various normalized AlN thicknesses, h_{AlN}/λ.

IUS4-PB2-2

Platinum/AlN/Sapphire SAW resonator operating in GHz range for High temperature Wireless SAW sensor

Eloi Blampain[1], **omar Elmazria**[1], Ouarda Legrani[1], Stefan Mc Murtry[1], Chen Fu[2], Kee-Keun Lee[2], Sang Sik Yang[2]; [1]*Institut Jean Lamour, UMR 7198, Université de Lorraine - CNRS, Vandoeuvre les Nancy, France,* [2]*Ajou University, Suwon, Korea, Republic of*

Background, Motivation and Objective

Our previous works have shown that AlN/Sapphire is a promising solution as piezoelectric structure for high-temperature SAW applications. In low-oxygen environments, it even shows far better performance than langasite as the latter undergoes strong O and Ga losses in such conditions [1]. However, the investigations were performed at relatively low frequency (400 MHz). Therefore, the aim of this work is to investigate, versus temperature in the range 20-600°C, a Pt/AlN/Sapphire SAW resonators operating in GHz range.

Statement of Contribution/Methods

Synchronous SAW resonators operating at 2.45 GHz ISM band were designed using layered FEM/BEM modeling. The structure is consisted of 1 µm-thick (002) AlN films, grown on c-plane sapphire substrate. The IDT and reflectors were realized using 100 nm thick platinum film. Wavelength was fixed to 1.7µm leading to obtain the targeted

frequency but also the optimal electromechanical coupling coefficient (K^2). The device was then realized using an e-beam lithography and Ion beam Etching. S_{11} parameters of the resonator were measured up to 500 °C, using a network Analyzer and a specific station probe.

Results/Discussion

As expected by simulation the center frequency of the first mode is measured at 2.45 GHz at room temperature (RT). In addition to the peak at 2.45 GHz, two others peaks appear: one at 4.43 GHz corresponding to a second mode and one at 6.9 GHz corresponding to the harmonic of the first mode (Figure 1).

The variation of the center frequency with temperature shows a very good linearity between RT and 500°C. The measured TCF for the first and second modes are respectively -34 ppm/°C and -39ppm/°C. The electromechanical coupling coefficient as well as the quality factor (Q) were also measured versus temperature for both modes. Results show that K2 is enhanced with temperature increasing from 1.85% (1.9 % calculated) at RT to 2.25% at 500°C for the first mode and from 0.92% to 1.15% for the second mode. However the quality factor decreases with temperature by around 22% between RT and 500 °C for both modes. The experimental results are consistent with theoretical predictions at low temperature and provide new data at high temperature. Effort in the design of platinum electrodes is underway to improve the Q of the resonator.

[1] T. Aubert, O. Elmazria, et al. Proc. of 2011 IEEE Inter. Ultras. Sympos.; pp 2082.

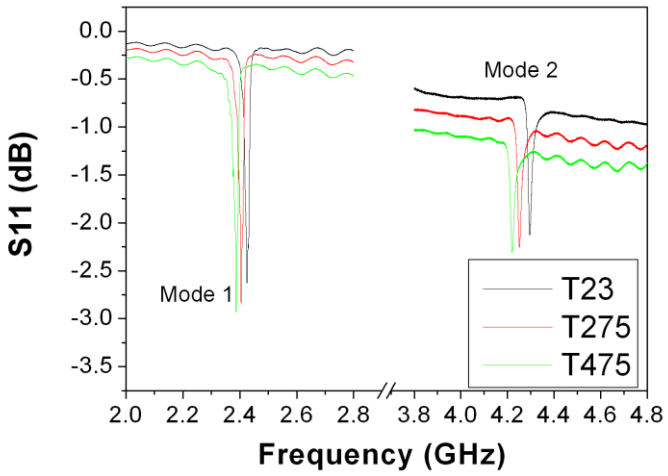

IUS4-PB2-3

Investigation of the CTGS Single Crystals Potential for High Temperature SAW Devices

Sergey Sakharov[1], Alexei Zabelin[1], Andrey Medvedev[1], Svetlana Bazalevskaya[1], Oleg Buzanov[1], Dmitrii Roshchupkin[2], Serguei Kondratiev[1], Alexander Shvetsov[3], Sergei Zhgoon[3]; *[1]JCS Fomos-Materials, Russian Federation, [2]Institute of Microelectronics Technology and High-Purity Materials Russian Academy of Sciences, Russian Federation, [3]National Research University "Moscow Power Engineering Institute", Moscow, Russian Federation*

Background, Motivation and Objective

High temperature operation is becoming increasingly attractive for SAW devices intended for high temperature wireless sensors. Beside already established materials such as LGS, LGT and LGN, new materials such as CTGS show new promising and useful features.

Statement of Contribution/Methods

SAW resonators were patterned on CTGS wafers with different orientations at different propagation angles. Ir was used as a metal without additional adhesion layers. Resonator responses were acquired with a network analyzer. Resonance frequencies of the responses were measured and processed to obtain temperature behavior.

Results/Discussion

For the cut with Euler angles (0, 90°, 0) almost linear behavior was observed with TCF close to –35 ppm/°C. The turnover point of the fitted parabolic curve gradually changed with propagation angle ψ (0, 90°, ψ) from negative temperatures up to about +550°C at (0, 90°, 90°). This also means that this material gives orientations (close to (0, 90°, 40°)) with the turnover point near the room temperature. Surrounding orientations should probably be same useful (the turnover point change is about 0.5°C with ψ angle change by 1′ for these orientations). The coefficient at the quadratic term (with Ir metal) has a low value of about -30 ppb/°C^2. This value is several times lower than that of most langasite cuts and is close to that of ST-quartz. The material seems to be chemically stable at high temperatures.

CTGS shows great potential and useful properties for devices operating in a wide temperature range. Similar to ST-quartz, CTGS can serve for temperature compensated resonators and filters at room temperature. It can also work in devices operating at temperatures up to several hundred degrees C.

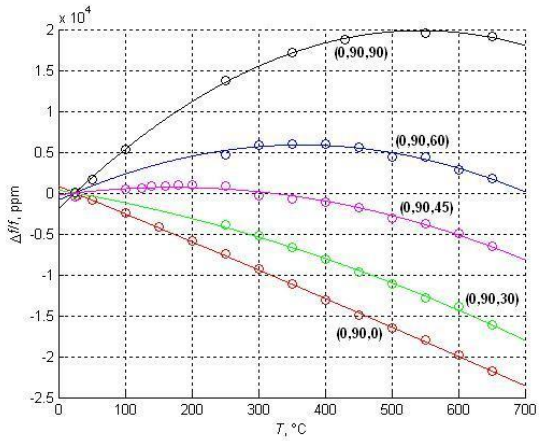

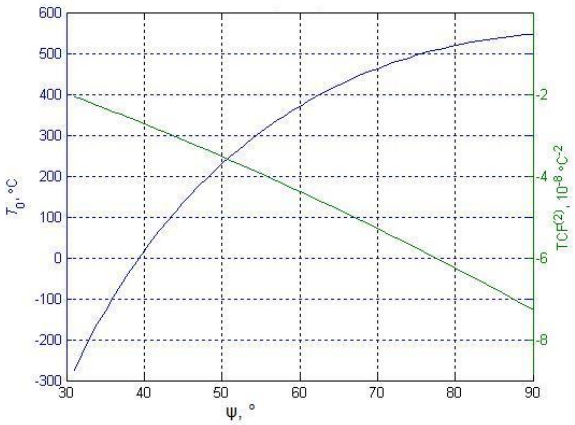

IUS4-PB2-4

Thermal Characterization of Surface Acoustic Wave Devices

Christian Huck[1,2], Herbert Zidek[2], Thomas Ebner[2], Karl Wagner[2], Achim Wixforth[1]; *[1]Institute of Physics, University of Augsburg, Augsburg, Germany, [2]TDK Corporation, Munich, Germany*

Background, Motivation and Objective

Surface Acoustic Wave (SAW) technology has proven to be a powerful tool for the high demands made on RF filter applications in modern telecommunication systems. As mobile implementations require continuous reduction in component size, heat evolution at high electrical power levels due to dissipation becomes more and more important. Therefore, investigating the thermal behavior of SAW resonators is an important task to optimize the filter design.

Statement of Contribution/Methods

A common method for temperature determination of SAW filters uses the frequency shift of the transfer function in order to determine the chip temperature indirectly. Variation of the ambient temperature results in the Temperature Coefficient of Frequency (TCF) which serves as a figure of merit to map the frequency shift of the loaded component to an accurate value of the temperature change. An alternative approach for thermal characterization evaluates the unitarity violation which quantifies the entire power loss in the device assuming its total conversion into heat.

However, these electrically determined temperatures are attributed homogeneously to the entire chip without taking local inhomogeneities into account. Furthermore, these indirect methods create problems as soon as additional effects also causing a frequency shift play a role. Hence, the study of temperature dependent effects requires a direct nondestructive measurement method to precisely ascertain the spatial distribution of the device temperature.

In this context, we present two optical measurement techniques for the thermal mapping of coated SAW devices: the contacting Liquid Crystal Thermography (LCT) and the noncontacting Infrared Thermography (IRT). LCT is based on Thermochromic Liquid Crystals (TLCs) which exhibit temperature-dependent color changes by selectively reflecting incident white light. IRT relies on the temperature-dependent emitted radiant energy of the device under investigation.

Results/Discussion

In this work, the thermal behavior of SAW resonators is investigated using LCT and IRT to complement earlier results determined by conventionally evaluating frequency shifts and unitarity violation. Apart from mean temperatures obtained indirectly by such conventional electrical methods, LCT and IRT provide spatially resolved measurements of the temperature distribution on the component. Moreover, these optical techniques eliminate measurement uncertainties caused by other effects resulting in a frequency shift or power loss in the device. In this regard, they serve as independent and direct measurement schemes unlike evaluations based on TCF or unitarity violation. Results of all measurement methods are compared with FEM simulations and deviations between them are discussed.

IUS4-PB2-5

Acoustic Characteristics of the Third-Order Quasi-Symmetric Lamb Wave Mode in an AlN/3C-SiC Plate

Chih-Ming Lin[1], Yung-Yu Chen[2], Valery V. Felmetsger[3], Debbie G. Senesky[4], Albert P. Pisano[1]; *[1]Mechanical Engineering, University of California at Berkeley, Berkeley, CA, USA, [2]Mechanical Engineering, Tatung University, Taipei, Taiwan, [3]PVD Product Group, OEM Group Incorporated, Gilbert, AZ, USA, [4]Aeronautics and Astronautics, Stanford University, Stanford, CA, USA*

Background, Motivation and Objective

The quality factor (*Q*) of the aluminum nitride (AlN) Lamb wave resonator utilizing the lowest-order symmetric (S_0) mode is degraded significantly while the interdigital transducer (IDT) finger width decreases to nanometer scales for operation at high resonance frequencies. Recently, the high-order Lamb wave mode propagating in an AlN/3C-SiC composite plate has been demonstrated to show the remarkable capability to enable a micromechanical resonator with high resonance frequency, high *Q*, and low motional impedance simultaneously.

Statement of Contribution/Methods

In this work, a comprehensive study of the acoustic characteristics of the third-order quasi-symmetric (QS_3) Lamb wave mode propagating in the AlN/3C-SiC composite plate was performed theoretically and experimentally. The effective permittivity and Green's function methods are employed to compute the phase velocities and electromechanical coupling coefficients of the QS_3 Lamb wave mode. A two-port delay line configuration utilizing the QS_3 Lamb wave mode were designed and fabricated on the AlN/3C-SiC composite plate. The experimental results show that the QS_3 Lamb mode is preferred to enable a low-loss narrowband filter with a 3dB bandwidth of 0.1% at 2.95 GHz.

Results/Discussion

Figures 1 (a) and (b) show the calculated phase velocity and electromechanical coupling dispersion of the QS_3 Lamb wave mode propagating in an AlN/3C-SiC composite layer while the 3C-SiC and AlN thicknesses are 2.6 μm and 2.5 μm, respectively, which corresponds to a wavelength of 12 μm. It should be noted that the QS_3 mode in the 3C-SiC composite layer offers high phase velocities above 30000 m/s and less dispersion in comparison to Lamb waves propagating in a single AlN layer. The electromechanical coupling

coefficient of the QS_3 mode is also enhanced by the introduction of the 3C-SiC layer. The Lamb wave devices presented in this work were tested at room temperature in air and the S_{21} parameters were measured with 50 ohm terminations using a network analyzer. Figure 2 depicts the measured transmission frequency spectrum of the AlN/3C-SiC delay line structure utilizing the QS_3 Lamb wave mode which exhibits an insertion loss of -17 dB and a narrow 3dB bandwidth of 0.1% at approximately 2955 MHz and shows the potential applicability for the narrowband filter bank transmission architecture.

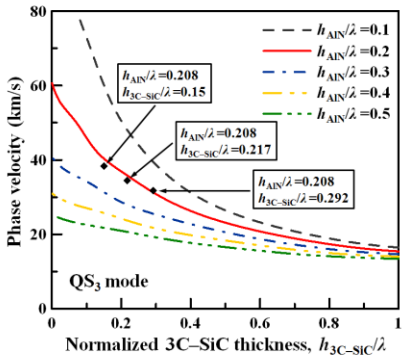

Figure 1(a). Simulated phase velocity dispersion of the QS_3 mode in an AlN/3C-SiC layer.

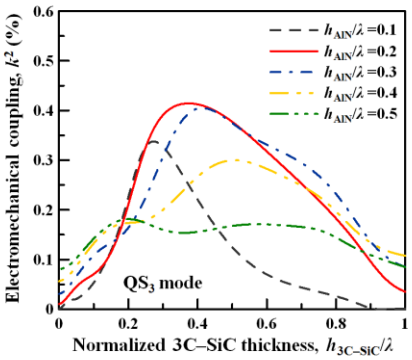

Figure 1(b). Simulated electromechanical coupling dispersion of the QS_3 mode in an AlN/3C-SiC layer.

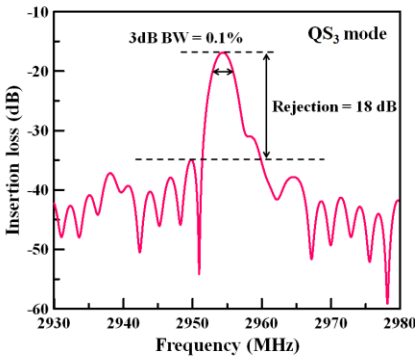

Figure 2. Measured transmission frequency spectrum of the Lamb wave delay line utilizing the QS_3 mode.

Ultrasonic Transducers and Materials

Forum Hall

Tuesday, July 23 2013, 01:00 pm - 04:30 pm

Congress Hallair: **Wei Ren**
Xi'an Jiaotong University

IUS5-PB-1

Validation of an approximation formula of the effective $d_{33,eff}$ of periodic and non-periodic 1-3 composites

Sabine Kern[1], Christoph Pientschke[1], Hartmut S. Leipner[1]; [1]*Interdisciplinary Center of Materials Science (CMAT), Martin-Luther-University, Halle (Saale), Germany*

Background, Motivation and Objective

1-3 composites consisting of piezoelectric rods embedded in a polymer matrix are used for ultrasonic applications. For these materials the effective piezoelectric coefficient $d_{33,eff}$ was measured. The $d_{33,eff}$ can be also calculated with an approximation formula by using the elastic properties of the constituents, their volume fraction and the d_{33} of the piezoelectric rods. A highly sensitive method for measuring the d_{33} of thin rods was used to validate the approximation formula.

Statement of Contribution/Methods

In this work, periodic dice-and-fill composites and non-periodic 1-3 fiber composites were investigated, both consisting of the same PZT material. Composites of different thicknesses (1.5mm and 3mm) and volume fractions (35% and 65%) were characterized regarding their effective piezoelectric coefficients $d_{33,eff}$. Additionally, the d_{33} of the bare ceramic were determined. For that purpose the d_{33} bulk value of the PZT material and the d_{33} of the single fibers were directly measured. For determining the small-signal piezoelectric coefficient, the longitudinal piezoelectric displacement was measured by a capacitive displacement sensor.

Results/Discussion

The experiments show that the $d_{33,eff}$ of fiber composites is about 30% lower than the $d_{33,eff}$ of the dice-and-fill composites. This could be attributed to the d_{33} of the ceramic rods and fibers contained in the composites which differ by the same amount. With these values, the effective $d_{33,eff}$ of the composites were calculated by the approximation formula. For fiber composites with a high fiber volume fraction (65%), the calculated and the measured $d_{33,eff}$ are in agreement independent of their thickness. For dice-and-fill composites with a higher thickness (3mm), the calculated piezoelectric coefficient is consistent with the measured one. However, there are deviations for fiber composites with a low volume fraction of fibers (35%) and for dice-and-fill composites with a small thickness (1.5mm). Deviations are to be expected because the approximation formula neglects all geometric properties of the composite except the volume fraction. The smaller the aspect ratio of the lateral dimension of the rods or fibers to the thickness of the composite is, the higher is the difference between the calculated $d_{33,eff}$ and the actual one. This is in accordance with results of finite-element-calculations. Additionally, a locally varied fiber volume fraction in non-periodic composites causes variations in the locally measured $d_{33,eff}$ which leads to a deviation in the calculated $d_{33,eff}$. This effect is more distinct for lower fiber volume fractions.

The approximation formula for the calculation of the effective piezoelectric coefficient by using the measured piezoelectric coefficient of the ceramic constituent has been validated for periodic and non-periodic 1-3 composites. Remaining differences may be explained by considering influences of the aspect ratio and the volume fraction.

IUS5-PB-2

08:31 am **Fabrication and Characterization of Thick Film Piezoelectric Lead Zirconate Titanate (PZT) By Tape Casting Processing**

Yingying Sun[1], Lifeng Qin[2], **Qing-Ming Wang**[3]; [1]*University of Pittsburgh, USA,* [2]*Xiamen University, Xiamen, Fujiian, China, People's Republic of,* [3]*Department of Mechanical Engineering and Materials Science, University of Pittsburgh, Pittsburgh, PA, USA*

Background, Motivation and Objective

In many transducer applications, particularly for high frequency ultrasonic transducers, PZT thick films are needed with thickness from 10 μm to 100 μm. However, fabrication of high quality PZT thick film has been a challenge by traditional ceramic processing, sol-gel spin-on coating, and ceramic slurry screen printing. The goal of this work is to fabricate high quality PZT thick films by tape casting processing and to characterize the electromechanical properties of PZT thick films

Statement of Contribution/Methods

For the property characterization, a normalized electrical impedance spectrum method developed recently was used to determine the complex piezoelectric, elastic, dielectric coefficients, and electromechanical coefficient from the electrical impedance measurement of thick film resonators using an impedance analyzer. Microstructures of PZT thick films were also studied by SEM.

Results/Discussion

A piezoelectric constant d_{31} of about -181pm/V was derived from the measurement of a unimorph actuator (23μm PZT/110μm stainless steel foil), which was very close to the measurement results of thicker films. PZT thick films with different compositions were fabricated and characterized. It was found the relative permittivity ($\varepsilon^T_{33}/\varepsilon^0$) measured is in the range of 1532~4829, piezoelectric stress constant (e_{33}) in the range of 15 C/m^2-26 C/m^2, piezoelectric strain constant (d_{31}) in the range of -169×10^{-12} C/N to -314×10^{-12} C/N, electromechanical coupling coefficient (K_t) in the range of 0.48-0.53 and K_{31} in the range of 0.35-0.38.

The results shows tape-casting processing can be used to fabricate high quality PZT thick film resonators, and the extracted material constants can be used for device design and application.

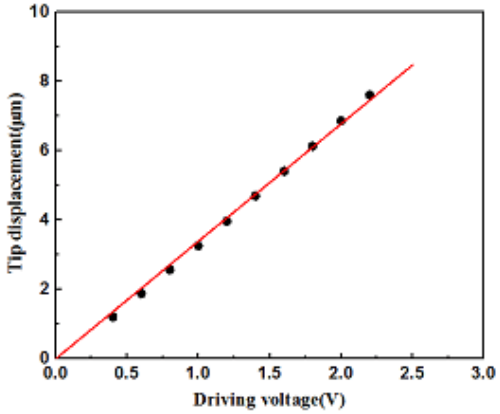

Fig. 2 Applied voltage and tip displacement relationship for a PZT thick film/stainless steel unimorph actuator.

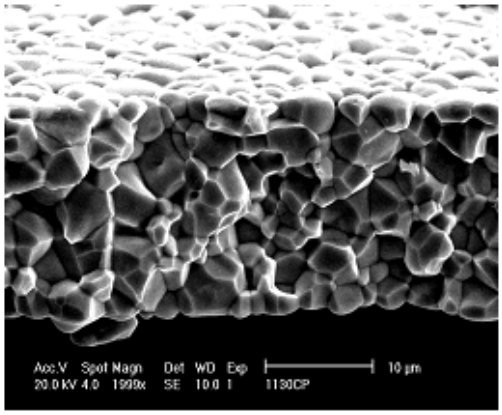

Fig.1 SEM microstructure of dense PZT thick film fabricated by tape-casting processing

IUS5-PB-3

08:32 am **Modification of the Ultrasonic Properties of Elastomers Loaded with Magnetic Particles by Applying Magnetic Fields During Vulcanization.**

Iker Agirre Olavide[1], Maria Dolores Fariñas[2], Mounir Bouali Sidi[1], Maria Jesus Elejabarrieta[1], Tomas Gomez Alvarez-Arenas[2]; *[1]Universidad de Mondragón, Mondragon, Guipuzcua, Spain, [2]Spanish National Scientific Research Council (CSIC), Madrid, Madrid, Spain*

Background, Motivation and Objective

Particle loaded polymers have been largely used as backing materials and matching layers because their properties can be easily engineered by changing the filler concentration. Use of magnetic particles has recently been theoretically proposed as fillers to produce active matching layers whose response can be modified upon the application of magnetic fields. In this paper, we propose to engineer anisotropic composite properties by loading elastomers with magnetic particles and by applying magnetic fields during vulcanization to establish well defined patterns in the particles spatial distribution that induce an anisotropy that effectively modifies the ultrasonic properties.

Statement of Contribution/Methods

Silicone rubber plates (1±0.02 mm thick)loaded with 1.25±0.55 μm carbonly-iron particles, with particle volume concentration from 0 to 30% in steps of 5% were produced with and without the presence of a magnetic field applied normal to the plate surface during vulcanization. Samples were studied using SEM to verify the proper effect of the magnetic field on the distribution of the particles (see Figure). Ultrasonic properties of the samples were then measured using different techniques. 1. Air-coupled wide-band through transmission at normal and oblique incidence (0-45 degres) in the frequency range 0.1-1.5 MHz. These measurements were also used to study material anisotropy. 2. Through transmission, direct contact and wide band to measure time of flight and insertion losses (3-6 MHz).

Results/Discussion

From measured longitudinal and shear wave velocities and attenuation coefficients the elastic constant were worked out. For the unloaded elastomer we obtained 1020 and 220 m/s (Poisson's ratio = 0.47) and 20 Np/m at 0.5 MHz, respectively. Variation of the elastic constants with the filler volume fraction follows the Hashin-Strikmann lower bound. The effect of the application of a magnetic field during vulcanization exhibit a major impact on the attenuation coefficient and its variation with the frequency in the 3-6 MHz frequency range, increments of the Insertion losses up to 15 dB were observed for certain frequency bands. Significant effects of the orientation of the particles were also found on the propagation of shear waves polarized in the direction of the magnetic field. Potential and novel applications of this technology are also discussed.

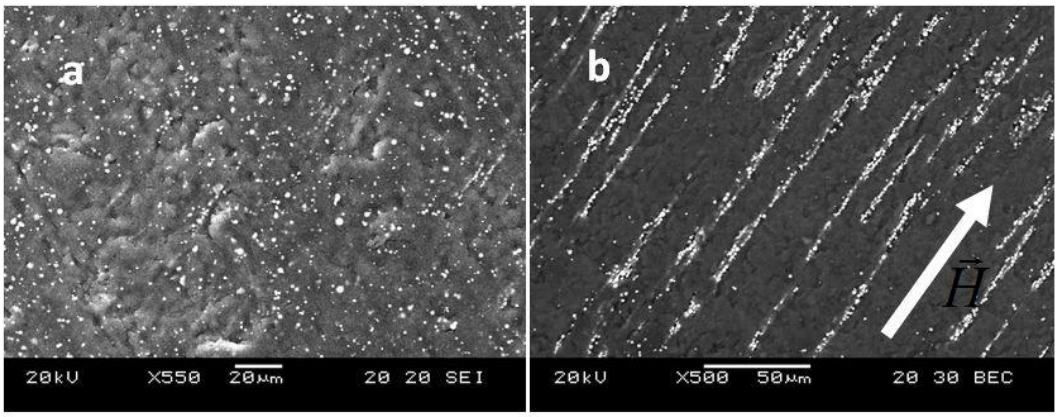

SEM images of the cross-section of the samples a)Vulcanized without magnetic field, isotropic MRE and b) Vulcanized under the magnetic field, anisotropic MRE. White arrow indicates magnetic field direction.

IUS5-PB-4

08:33 am **Development of a HighlyAttenuativeBacking for Ultrasonic Transducers with PeriodicArrangement of PolymericRods inside the Backing**

Byungkuk Bae[1], Hyungkeun Lee[1], Wonseok Lee[2], Susung Lee[1], Yongrae Roh[2]; *[1]Probe Acoustic/Alpinion Medical System, Seoul, Korea, Republic of, [2]School of Mechanical Engineering/Kyungpook National University, Daegu, Korea, Republic of*

Background, Motivation and Objective

The competency we normally expect from a good backing for ultrasonic transducers is high attenuation and good acoustic impedance matching with a piezoelectric element. The backings are generally made of composites of metal or metal oxide power and epoxy resin or rubber. Attenuation of acoustic waves is generally achieved by viscous absorption of acoustic energy by the polymer and wave scattering by the metal particles. The attenuation of a backing always needs to be as high as possible since the thickness of the backing layer can then be reduced, which allows miniaturization of the transducer. However, improving the attenuation by the conventional two phase mixture has certain limitation.

Statement of Contribution/Methods

In this work, a new highly attenuative backing has been developed by installing cylindrical silicone robber rods periodically inside the two phase mixture. The scattering of ultrasonic waves is dramatically increased by the polymeric rods, which results in big improvement of the attenuation. The silicone rubber rods aremolded first, and aredisposed periodically on a plane. Then a mixture of epoxy and metallic powderis castedaround the rods, and is curednot to have any vacancies.Figure 1 shows the silicone rubber rods that have the diameter of 1.0mm and are disposed with the interval of 0.5mm. A mixture of tungsten powder and epoxy (3M DP460) was prepared with the ratio of 35:65, and cast onto the rods. Configuration of the rod and the mixture was determined to have these values through optimization with PZFlex. Another backing plate was fabricated as well with the same mixture but without the silicone rods.

Results/Discussion

The backing plates were characterized through ultrasonic pulse-echo tests. The backing plate without the silicone rods was measured to have acoustic impedance of 3.1 Mrayl and attenuation of 11.0dB/mm. The backing plate including the silicone rods was measured to have acoustic impedance of 2.9 Mrayl and attenuation of 19.3 dB/mm. Significant improvement of the attenuation has been confirmed through the experiments. Acoustic impedance of the backing can be increased if needed by controlling the volume percent of tungsten powder without causing much variation of the attenuation. This highly attenuative backing isapplicable to various size-constrainedultrasound probes like TEE and mechanical 3D transducers.

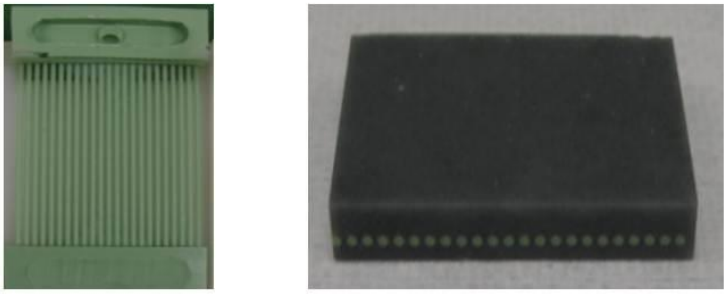

(a) silicone rubber rods (b) cured backing

Fig. 1. Photographs of the highly attenuative backing.

IUS5-PB-5

08:34 am **Measurement of Temperature Dependence in Material Coefficients of PZT Ceramics for Acoustic Emission Sensors**

Jiri Fialka[1], Petr Benes[2], Stanislav Klusacek[1]; *[1]Central European Institute of Technology (CEITEC), Brno University of Technology (BUT), Brno, Czech Republic, [2]Department of Control and Instrumentation (DCI), Brno University of Technology (BUT), Brno, Czech Republic*

Background, Motivation and Objective

The behaviour of material coefficients of PZT ceramics at temperatures approaching the Curie point is a problem hitherto not examined in detail. However, this field offers several interesting perspectives such as the possibility of controlled depolarization of the piezoceramic material in the volume of a sample. The development and calibration of piezoelectric acoustic emission sensors are among traditional scientific activities pursued by our research laboratory; therefore, the experiments described in this paper were set up to verify whether electrical parameters of a sensor could be changed via applying a temperature gradient to perform partial depolarization of the piezoelectric element of the sensor. In general terms, the described change will subsequently reflect in frequency characteristics of acoustic emission sensors, where PZT ceramics are used as an active measuring element. Significantly, the measurement of temperature dependences in piezoelectric materials used for the sensors also enables us to determine the degree of stability that characterizes the sensitivity and accuracy of the sensor and allows us to establish the maximum temperature ranges for regular operation.

Statement of Contribution/Methods

In the experiment, we applied two temperature ranges according to the parameters of the calibration furnaces. While the first range spanned between -40°C and 140 °C, the second one was defined by the boundary temperatures of 25°C and 330°C, where the latter value (330°C) corresponds to the Curie point of the applied NCE 51 piezoelectric ceramics. The samples were cycled at gradually increasing maximum temperatures, and changes of the material constants were observed. The presented paper contains a detailed description of several processes, namely the measurement procedure, the calculation of the material coefficient matrix via the frequency method, and the procedure of fabricating the individual samples to be measured. We performed the measurement of the samples for radial, thickness, transverse longitudinal, longitudinal, and transverse shear oscillations. In samples of PZT ceramics, the measurement of temperature dependences up to the Curie temperature places high priority on the characteristics of the applied measuring devices. Thus, the authors of the paper have included a detailed discussion of suitable apparatuses related to each measurement procedure.

Results/Discussion

The central result acquired from the performed research activities consists in both the measured temperature dependences and the sum of recommendations concerning the correct procedure to be adopted in PZT ceramics measurement realized at a wide range of temperatures and with minimum error.

IUS5-PB-6

08:35 am **Droplets, vapours and clouds – a new approach to capacitive transducer manufacture**

Richard O'Leary[1], Gerald Harvey[2]; [1]*University of Strathclyde, Glasgow, United Kingdom,* [2]*Weidlinger Associates, Glasgow, United Kingdom*

Background, Motivation and Objective

Capacitive ultrasonic transducers comprise a substrate patterned with a regular array of uniformly dimensioned cavities above which a membrane is positioned. Transmission and reception of ultrasound is effected via controlled electrical or mechanical stimulus of the membrane, respectively. This paper decribes a new facile process for the manufacture of capacitive devices employing micropatterning of polymer substrates.

Statement of Contribution/Methods

A positive mask of the desired cavity microstructure is deposited onto a polystyrene substrate as droplets of ethylene glycol solution, 50% v/v in water. Droplet deposition is undertaken using either a 2-d positioning system equipped with a piezoelectric droplet generator or an air-pressured atomiser. The substrate is then exposed, 3-30 minutes, to a saturated toluene vapour which is absorbed by the polystyrene causing swelling of the surface except in the areas where the droplets are situated. The substrate is then air-dried at 20 Celsius. The resultant cavities are characterised using a Veeco white light interferometer, the figure details example cavities where the radius is 500µm and depth 3µm.

Results/Discussion

Cavity diameter is controlled by the diameter of the deposited droplets. The atomiser method results in randomly distributed cavities, 50-250µm diameter. The piezoelectric droplet method gives more uniform spatial distribution, multiple droplets are deposited to vary the diameter cavities - 100-700µm being typical. Cavity depth, 200nm-10µm, is directly proportional to the time the sample is exposed to the toluene vapour. Importantly, diameter and depth can be controlled independently.

The PZFlex finite element (FE) software, deployed on custom cloud computing architecture allowing for 100's of simultaneous parallel simulations, has been employed to explore the potential for the use of the micropatterned substrates in the manufacture of capacitive ultrasonic transducers. This new cloud approach has facilitated reducing months of intensive FE modelling to a few days. The results have been employed to guide the optimisation of the patterning process in order to manufacture devices suited to air-coupled non-destructive testing. The paper describes the results of the finite element modelling, the optimisation of the manufacturing route and the characterisation of the resultant devices.

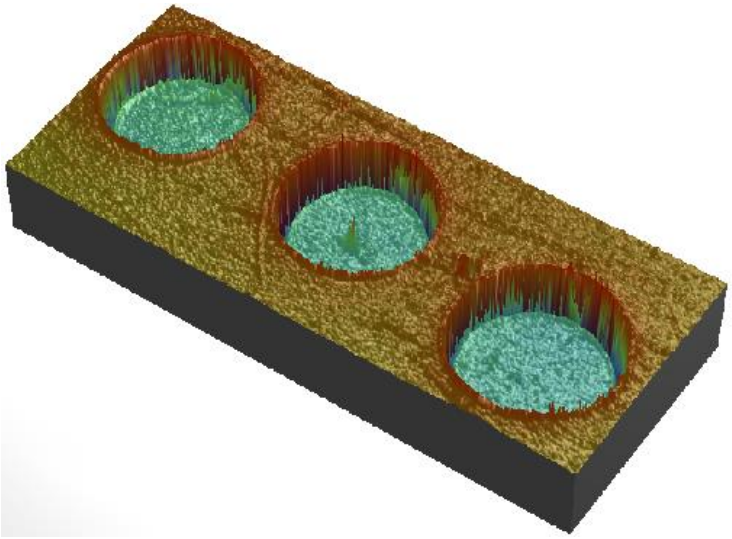

IUS5-PB-7

08:36 am **Micromachined structures for non-linear ultrasonic transduction**

Omololu Akanji[1], David Hutchins[1], Simon Leigh[1]; [1]*School of Engineering, University of Warwick, Coventry, Warwickshire, United Kingdom*

Background, Motivation and Objective

Recent studies have shown that ultrasonic propagation along chain-like structures (such as a line of spherical particles) can give very interesting properties. It is now known that non-linear propagation can take place along these chains, and this leads to some fascinating possibilities. This is because propagation is in the form of solitary waves. These have much different properties to standard propagation along a wire for example, because the propagation is non-liner, i.e. it is a function of driving amplitude. It is also a function of applied external stress. There is thus the possibility, when a material containing these structures is used as a front plate to a standard ultrasonic piezoelectric device, that a transducer could give outputs not possible under linear behaviour. One of these is the so-called "sound bullet".

Such materials have not been studied previously at ultrasonic frequencies of 1 MHz and above, and yet they could provide a new approach to transducer design.

Statement of Contribution/Methods

At ultrasonic frequencies, these chain-like structures would need to be created using novel fabrication (micromachining) techniques. This is because of their size - such chains would need columns of spheres (or other shapes) with diameters of 1 mm or less. In addition, there is a need to model this propagation, so as to understand the nature of propagation, and the type of behaviour that would result.

Results/Discussion

A study is being performed into these materials, and the properties that they would exhibit within an ultrasonic transduction system. Numerical modelling has been performed, to predict the performance as a function of geometry and material from which the chains are made. An example of a prototype material is shown in the figure. This is an array of 1

mm diameter spheres, created using 3D printing, in this case as a 2D array. Propagation along such structures has been studied, both experimentally and by modelling, and the results will be presented. It will be demonstrated that such an approach has the potential of enhancing ultrasonic measurements of various types, including medical imaging.

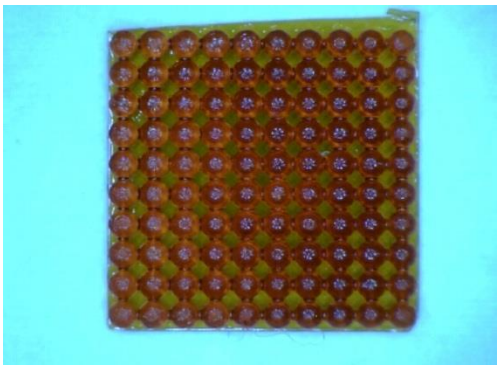

IUS5-PB-8

08:37 am **Characterization of Hydrophone with Hydrothermal PZT Thick Film Vibrator and Ti Front Layer for Measurement in High Intensity Therapeutic Ultrasound**

Nagaya Okada[1], Yoshiyuki Asakura[1], Michihisa Shiiba[2], Takeyoshi Uchida[3], Masahiro Yoshioka[3], Tsuneo Kikuchi[3], Minoru K. Kurosawa[4], Shinichi Takeuchi[2]; *[1]Research and Development Div., HONDA ELECTRONICS CO., LTD., Japan, [2]Department of Clinical Engineering, Faculty of Biomedical Engineering, Toin University of Yokohama, Japan, [3]National Metrology Institute of Japan (NMIJ), National Institute of Advanced Industrial Science and Technology (AIST), Japan, [4]Interdisciplinary Graduate School of Science and Engineering, Tokyo Institute of Technology, Japan*

Background, Motivation and Objective

Recently, ultrasound treatment methods, such as high intensity therapeutic ultrasound (HITU) are increasingly used in medical applications such as tumor therapy. The determination of the acoustic output of ultrasound equipment is important as regards aspects of quality assurance and safety of the patients. However, hydrophone measurements are difficult in the case of HITU fields at high clinical power levels since these sensors may easily be damaged when scanning the focus region.

Statement of Contribution/Methods

We have developed small aperture sensor with longer lifetime by the deposition of a hydrothermally synthesized lead zirconate titanate (PZT) thick film on the reverse surface of Ti plate. The deposited film is protected from acoustic cavitation by the Ti plate.

In this study, we fabricated hydrophones that had backing material with specific acoustic impedance from 20 to 30 MRayls to improve the frequency characteristics of receiving sensitivity (Fig. 1).

Results/Discussion

The spatial intensity distribution profile of a 1MHz HITU transducer (diameter : 80 mm, geometric focal length : 50 mm) was measured at a focus region without destruction due to cavitation. The hydrophone sensitivity responding to continuous wave power level up to 50 W was measured (Fig. 2). The sensitivity was responded linearly up to about 8 MPa. This value was estimated on comparing with the standard hydrophone at 1 W. However, sensitivity of this hydrophone should be calibrated with higher acoustic pressure for higher acoustic power measurements.

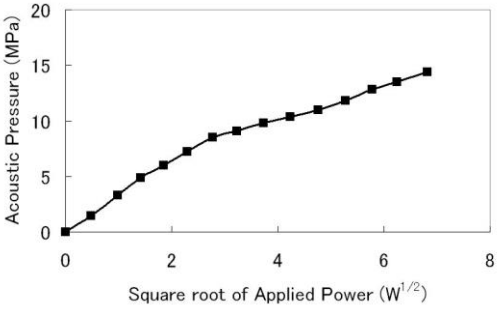

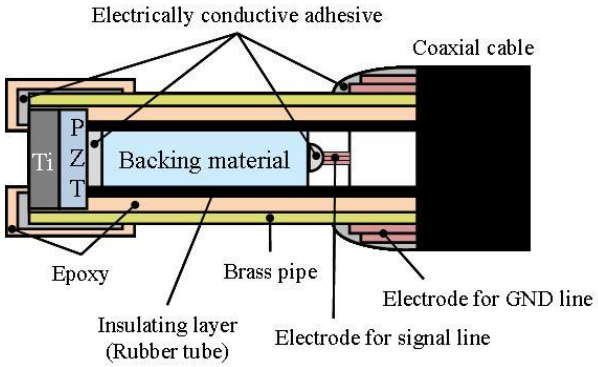

IUS5-PB-9

08:38 am **Dual frequency transducer for Images using thick film**

Sergio N. Gwirc[1], Juan Carlos Gómez[1], Federico Dos Reis Copello[1], **Nestor Marino**[1]; *[1]Electrónica e Informática, Instituto Nacional de Tecnología Industrial, San Martín, Buenos Aires, Argentina*

Background, Motivation and Objective

The double layer is an intrinsic characteristic of thick film technology when using screen printing to deposit PZT film. In previous work we have shown the good emission and high sensitivity characteristics of this type of transducers, in low impedance medium. This paper explores the possibility of using the emission capability in two simultaneous frequencies for the acquisition and analysis of medical images.

Statement of Contribution/Methods

The basic transducer element comprises a PZT film (included 3% glass) of about 160 microns thick, deposited on an alumina substrate to form a two layers structure. The film disk geometry and diameter of 6 mm, adheres to the lower electrode of Pd / Ag which is on the alumina and then the upper electrode paste is applied to the PZT sintered at 850°C. The film is polarized with an electric field of 3 kV / mm at 120°C. The transducer is used without backing neither matching with the medium.

The transducer emits pulses containing frequencies at 2.8 and 6.4 MHz, with respective bandwidth of 0.7 and 0.8 MHz approximately. The difference in amplitude for the frequencies is between 4 and 40 dB, depending on the type of electrical excitation used, matching to the electric generator and also the acoustic matching in the rear face of the transducer. This study looking for optimizes the use of the signals of these two frequencies to obtain individual images for each one with the same transducer, or a combination of both to improve imaging for diagnostic.

Results/Discussion

The transducer was used in mode M scan, in steps of 0.25 mm, to compose an image of a phantom made of agar, and containing a PDMS prismatic shape inclusion, whose section was 2.8x4.8 mm. Each scan was recorded and processed using band pass filters centered at each of the transmission frequencies. It is clear in the figure the two walls at both frequencies with lower emission intensity in the high frequency due to the smaller amplitude of that component.

Fig. 1: Scan B phantom image. Filtered at 6.4 MHz (top) and at 2.4 MHz (below), excited each one at the corresponding frequency.

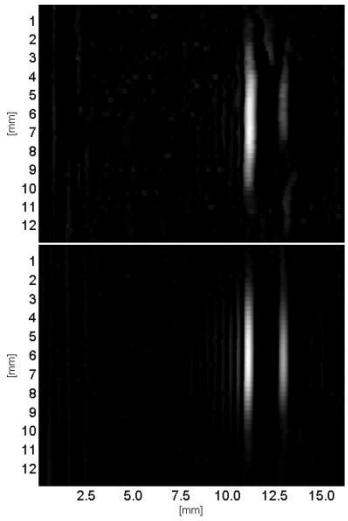

IUS5-PB-10

08:39 am **Lesion expansion by using dual-concentric-sectored HIFU transducer with phase-shifted ultrasound**

Jong Seob Jeong[1]; [1]*Department of Medical Biotechnology, Dongguk University, Seoul, Korea, Republic of*

Background, Motivation and Objective

A split-focus scheme capable of simultaneously generating multiple foci can increase the necrotic volume and thus results in reduced treatment time in HIFU (High-Intensity Focused Ultrasound) surgery. Because most split-focus techniques generate multiple foci in the lateral direction, the lesion expansion in the axial direction is relatively smaller than that in other directions. In this study, a dual-concentric-sectored HIFU transducer with phase-shifted ultrasound scheme is presented to generate multiple foci in the lateral and axial direction resulting in the extended-necrotic lesion in both directions. The performance of the proposed method was demonstrated through Field-II and bioheat transfer simulations.

Statement of Contribution/Methods

A simulated transducer is composed of a disc- and an annular-type element with a confocal point, and both elements are divided into two parts in lateral direction. Each part in the transducer is connected to four signals with 0° and 180° phases alternately, and all parts are activated simultaneously. The center frequencies of all elements are 4 MHz and the f-number (focal depth/aperture size) increases from 0.8 to 1.4 by changing the focal depth with the fixed aperture size (20 mm).

Results/Discussion

The simulation results showed that four focal zones were simultaneously generated in the lateral and axial direction (Figure 1). The -6 dB lateral beamwidth for each lobe was 0.46 mm and thus total lateral beamwidth was 0.92 mm, which was 74% broader than the single element transducer with identical dimension. The -6 dB axial beamwidths of the near-field and the far-field lobes were 2.98 mm and 3.46 mm, respectively. Thus, the total axial beamwidth (= 6.34 mm) was 83 % longer than the single element transducer. In the case of the bio-heat transfer and thermal dose simulation, the maximal peak temperatures for the near- and far-field lobes were 92°C and 69°C, respectively. The necrotic length and the width of the proposed method were about 70% longer and 80% broader than those of the single element transducer.

Our preliminary simulation results show that the lesion size in the axial direction can be increased by using a dual-concentric-sectored transducer with phase-shifted ultrasound. Thus, the proposed method can be useful for treating a deep seated target and for reducing the overall treatment time during HIFU surgery.

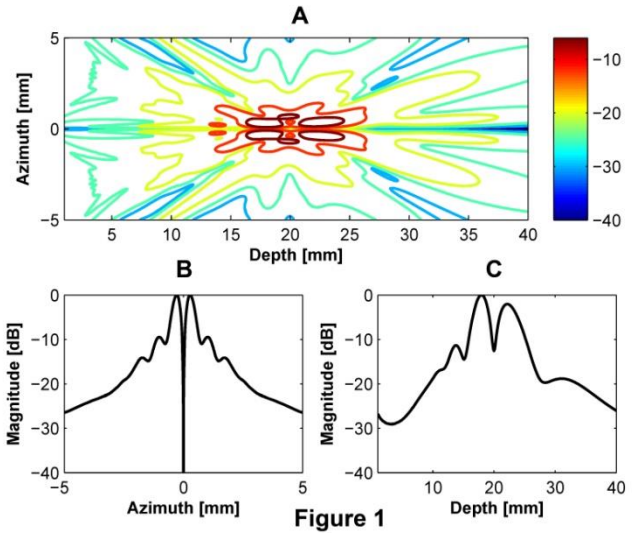

Figure 1

IUS5-PB-11

08:40 am **HIFU Transducer with Controllable Curvature**

Jungsoon Kim[1], **Moojoon Kim[2]**, Kanglyeol Ha[2], Seonae Hwangbo[3], Mincheol Chu[3]; *[1]Tongmyong University, Korea, Republic of, [2]Pukyong National University, Korea, Republic of, [3]Korea Research Institute of Standards and Science, Korea, Republic of*

Background, Motivation and Objective

It is not easy to change the focal length of a HIFU transducer. In this study, we suggest a focal length controllable concave-type ultrasonic transducer by changing curvature of the concave surface. This transducer can change the focal depth, and it enables to choose targets in wide range.

Statement of Contribution/Methods

To change the curvature, we make a pressure difference between both surfaces of the concave, on which piezoelectric elements are arrayed as shown in Fig. 1. The resonant frequency of the each piezoelectric element was 2 MHz, and the 37 elements were arrayed hexagonally on the silicon rubber surface. The acoustic fields were measured with different curvature to investigate the driving performance of the array transducer.

Results/Discussion

As an example, when the radius of curvature was 105 mm, the acoustic field was measured as shown in Fig. 2(a). The acoustic field was also calculated as shown in Fig. 2(b). These results show a tendency similar to that of measured ones even though there are many speckles due to noise. We confirmed that the focal point of the transducer could be easily controlled without the electric phase control of the each element.

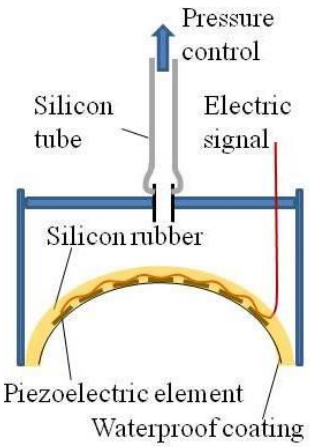

Fig. 1

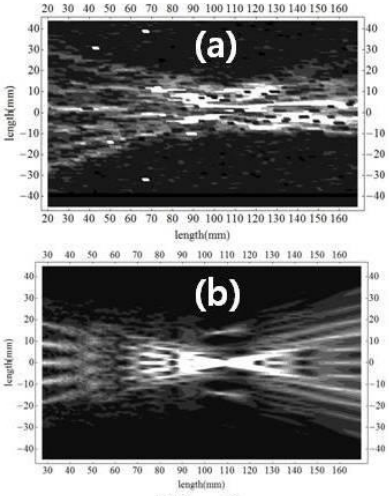

Fig. 2

Tuesday, July 23 2013, 01:00 pm - 04:30 pm

IUS5-PB-12

08:41 am **Development of wearable and flexible ultrasonic sensor for skeletal muscle monitoring**

Ibrahim AlMohimeed[1,2], Hisham Turkistani[1,3], **Yuu Ono[1]**; *[1]Carleton University, Canada, [2]Majmaah University, Saudi Arabia, [3]Saudi Food and Drug Authority, Saudi Arabia*

Background, Motivation and Objective

Monitoring of skeletal muscle activities is useful not only for diagnosing neuromuscular disorders but also for understanding musculoskeletal dynamics and for evaluating the effectiveness of physical training and rehabilitation. Ultrasonic techniques provide promising methods that allow detailed noninvasive study of muscles. However, one of the challenges for accurately monitoring muscle contraction is the motion artifacts due to inconsistent movement of the ultrasonic probe employed. In addition, the probe pressed against a body surface may limit underlying muscle activities. Therefore, an objective of this research is to develop a lightweight, wearable ultrasonic sensor that does not affect or restrict the movements of muscle and the other tissues during monitoring.

Statement of Contribution/Methods

A 110-μm thick polyvinylidene fluoride (PVDF) film was chosen as a piezoelectric material because of its lightweight, flexibility and good acoustic impedance matching to biological soft tissues. The top and bottom electrodes were made of silver ink with the area of 15 mm by 15 mm. Electrical wires were attached to the electrodes, and then the top and bottom sides of the entire structure were covered by a polyimide film with a silicone adhesive for protection and electrical insulation. No matching layer or backing material was constructed so that the sensor was flexible and lightweight. The total weight and thickness of the sensor developed were less than 1 g and 0.2 mm, respectively. In order to investigate its ultrasonic characteristics such as center frequency, bandwidth and conversion loss, numerical simulations were conducted for this multilayer structure using the Mason's equivalent circuit model including the dielectric and mechanical losses of the PVDF film.

Results/Discussion

First, the ultrasonic performance of the developed sensor was evaluated. The sensor was attached onto the top surface of a 12.5-mm thick Plexiglas plate and the ultrasonic signal reflected from the bottom surface was examined. The peak frequency and bandwidth of the signal were 1.7 MHz and 1.6 MHz (94%), respectively, which are suitable for medical applications. The numerical simulations showed that the peak frequency and bandwidth of the sensor were greatly affected by the silicone adhesive layer thickness of the protection film with the presented configuration. Next, an in-vivo experiment to monitor muscle contraction was conducted. The sensor was fixed onto a forearm near the wrist using adhesive tape. The ultrasonic signals reflected from the muscle/bone (radius) interface were acquired in M-mode for 10 s while the muscle beneath the sensor contracted voluntarily by bending the wrist backward every 2 s. The tissue thickness between the sensor and bone was calculated using the time-of-flight of the acquired signals. It was successfully monitored that the tissue thickness varied up to about 400 μm (5%) in accordance with the muscle contraction performed.

Microbubbles and therapy

CONGRESS HALL

Wednesday, July 24 2013, 10:30 am - 12:00 pm

Congress Hallair: **Ayache Bouakaz**
INSERM

IUS1-G1-1

Intravascular Ultrasound-Based Imaging and Drug Delivery

Ali Dhanaliwala[1], Johnny Chen[1], Joseph Kilroy[1], Linsey Phillips[2], Adam Dixon[1], Brian Wamhoff[1], Alexander Klibanov[1], **John Hossack[1]**; *[1]University of Virginia, USA, [2]University of North Carolina, USA*

Background, Motivation and Objective

Current methods for delivery of an anti-restenosis drug to an arterial vessel wall post-percutaneous transluminal angioplasty and stent placement are limited in terms of drug choice, dosing level, and ability to assure drug coverage between the struts of a drug eluting stent. An ideal solution for the diagnosis and treatment of vascular disease must involve high-resolution imaging and quantitative characterization of an atherosclerotic lesion and the means to provide a comprehensive and versatile therapy that can be completed within a single catheterization procedure. Intravascular ultrasound (IVUS) provides real-time, radiation-free, imaging and assessment of atherosclerotic disease in terms of anatomical, functional and molecular information.

Statement of Contribution/Methods

The design of a dual imaging and therapy IVUS catheter is described and initial results documenting gene and drug delivery reported. Microbubbles and drug / gene (associated or co-injected) are dispensed from the catheter tip. Using this approach, it becomes possible to address the need for complete vessel wall coverage and achieve delivery in regions poorly addressed using conventional stent-based approaches (e.g. near bifurcations). Additionally, we propose to integrate microfluidic devices directly within the catheter to enable real-time production of microbubbles. Using a flexible substrate and a flooded lumen enables the microfluidic device to be compatible with the challenging dimensions of a catheter. By placing the microfluidic device in the catheter, the need for long-term microbubble stability is mitigated. This tolerance for limited stability facilitates the rapid production of microbubbles i.e. > 500,000 microbubbles/s. Rapid downstream microbubble disintegration may allow the use of larger microbubbles with increased therapeutic potential and minimal risk of embolism

Results/Discussion

We have established that: 1) using in situ microfluidic-based production of microbubbles directly upstream of smooth muscle cells significantly enhanced drug delivery (up to 80% delivery), 2) in an ex vivo porcine artery, model drug (DiI) delivery increased six fold within the -6dB beamwidth of the transducer, and 3) using transcutaneous ultrasound and rapamycin microbubbles on an injured rat carotid resulted in a 34.9% reduction in neointima formation.

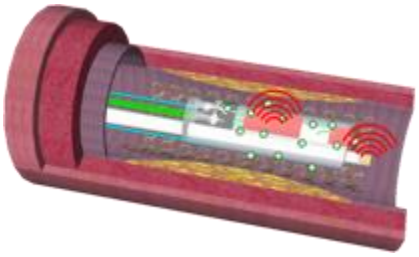

IUS1-G1-2

Investigating the interaction between individual microbubbles and fibrin clots exposed to ultrasound

Christopher Acconcia[1,2], Ben Leung[2], Kullervo Hynynen[1,2], David Goertz[1,2]; *[1]Medical Biophysics, University of Toronto, Toronto, Ontario, Canada, [2]Sunnybrook Research Institute, Toronto, Ontario, Canada*

Background, Motivation and Objective

Despite the considerable body of work indicating the potential of ultrasound (US) stimulated microbubbles (MBs) to enhance thrombolysis, with and without lytic agents, the mechanisms involved remain largely speculative. We previously demonstrated, using dilute suspensions of Definity, that MBs were capable of penetrating and damaging fibrin clot networks. Fibrin networks are the primary constituent of blood clots responsible for their mechanical integrity, and are widely used in the assessment of thrombolytic agents. The objective of this work was to investigate the effect of MB size and US exposure conditions on the ability of individual MBs to penetrate and disrupt fibrin clots.

Statement of Contribution/Methods

An apparatus was developed to optically tweeze MBs adjacent to the fibrin clot boundary. Clots were observed with fluorescent and white light fast frame (~10kHz) imaging. Definity MBs (n=142, diameters 2-8 µm) were exposed to 1 MHz US with pressures from 0.1-0.6 MPa and pulse lengths of either 0.015 or 1 ms (duty cycle 15%). 200nm fluorescent beads were used to delineate the fluid/clot boundary and provided a marker of fluid uptake into the clots. 3D two-photon microscopy was employed to assess damage to the fluorescently tagged fibrin network. Both 'coarse' and 'fine' fibrin clots were examined.

Results/Discussion

MBs were observed to penetrate clots to depths proportional to the number of pulses applied. Penetration was frequently associated with locally disrupted fibers along the MB path and accompanied by the uptake of nanobeads (Figure). In fine clots the penetration threshold for the 1 and 0.015ms pulses was 0.4 and 0.6 MPa, respectively. For 1ms pulses at 0.4 MPa, MBs with diameters of 3.25-3.75µm had the highest probability of penetrating (100%, n=9). In coarse clots the penetration threshold was 0.2 MPa with no clear size dependent penetration observed, likely due to their large pore sizes relative to the MBs. Under similar conditions (e.g. MB size: 4.1 µm, 0.4 MPa, 1ms pulse) penetration velocities reached up to 0.06 and 0.22 m/s in fine and coarse clots, respectively.

These results provide direct evidence that individual MBs can penetrate and disrupt fibrin networks, suggesting one mechanism by which US stimulated MBs potentiate thrombolysis. The method employed has relevance to the design of improved pulsing schemes and MB agents for sonothrombolysis.

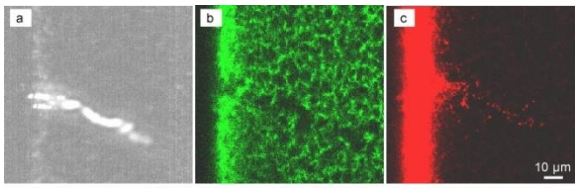

Figure : An example of fast frame (*a*) and two-photon fluorescence imaging (*b,c*) results from the sonication of an individual Definity microbubble placed initially adjacent to the boundary of a fine fibrin clot. Panel *a* is a standard deviation projection over time of the fast frame images acquired during a penetration event. Panel *b* and *c* are fluorescence images of the bubble induced fibrin network disruption (*b*) and transport of beads into the clot (*c*).
Sonication conditions: 0.4 MPa, 1 ms pulse, 20 pulses. MB size: 4.1 µm.

IUS1-G1-3

Experimental and numerical investigation of microbubble-loaded stemcell dynamics during ultrasound exposure

Tom Kokhuis[1,2], Benno Naaijkens[2,3], Lynda Juffermans[2,4], Otto Kamp[2,5], Antonius van der Steen[1,2], Michel Versluis[6,7], Nico de Jong[1,2]; *[1]Biomedical Engineering, Erasmus MC, Rotterdam, Netherlands, [2]Interuniversity Cardiology Institute of the Netherlands, Utrecht, Netherlands, [3]Pathology, VU Medical Center, Amsterdam, Netherlands, [4]Physiology, VU Medical Center, Amsterdam, Netherlands, [5]Cardiology, VU Medical Center, Amsterdam, Netherlands, [6]Physics of Fluids Group, University of Twente, Enschede, Netherlands, [7]MIRA Institute of Biomedical Technology and Technical Medicine, Enschede, Netherlands*

Background, Motivation and Objective

The use of stem cells in clinical therapy is hampered by the lack of persistence of high numbers of stem cells at the site of injury [1]. We have proposed a new technique, in which targeted microbubbles are conjugated to stem cells, creating echogenic complexes dubbed StemBells, which can be targeted to the injured tissue. Moreover, the conjugation of the microbubbles makes the stem cells more susceptible to acoustic radiation force and facilitates ultrasound (US)-mediated stem cell tracking. The objective of this study was to investigate the dynamics of these StemBells in an US field. A modified Rayleigh-Plesset model was developed to corroborate our experimental findings.

Statement of Contribution/Methods

StemBells were created by fully decorating adipose-derived stem cells (mean size 16 µm) with CD90-targeted microbubbles (mean size 3.5 µm) under continuous rotation. The StemBells were insonified at frequencies between 0.4 and 3 MHz at various pressures (50-200 kPa). Dynamics were imaged with the ultra-fast Brandaris128 camera [2]. To investigate the dynamics of the StemBells numerically, a modified Rayleigh-Plesset equation was derived. A StemBell was modeled as a liquid globule surrounded by a thin gas shell, mimicking respectively the stem cell and the layer of microbubbles around. The gas shell was assumed to have an effective shell elasticity χ and effective shell viscosity κ_s.

Results/Discussion

StemBells were found to be very stable during repetitive US insonifications. Interestingly, StemBells appeared to be pulsating like one big bubble. The close packing of targeted bubbles was found to lower the frequency of maximum response (f_{MR}) of the individual bubbles (normally 1.5 - 2 MHz) drastically, causing an apparent shift in the f_{MR} of the StemBells to lower frequencies. The figure shows the resonance curves of two StemBells insonified between 1 and 3 MHz (panel A) and between 0.4 and 0.8 MHz (panel B). Between 1 and 3 MHz, the frequency response of a StemBell falls off with increasing frequency, implying $f_{MR} < 1$ MHz. Insonification between 0.4 and 0.8 MHz revealed a f_{MR} around 0.6 MHz. The corresponding brightfield, cell (green) and microbubble (red) fluorescence images are shown below each panel. The experimental resonance curves of the StemBells were predicted by our model including values of κ_s of the order 10^{-7} kg/s and χ of 3.5 N/m.

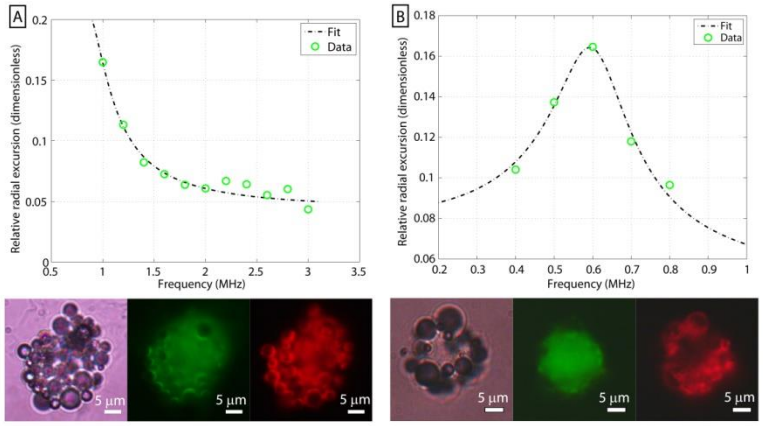

[1] Lee et al. *Stem Cells* 25:712 (2007)
[2] Gelderblom et al. *Rev Sci Instrum* 83:103706 (2012)

This work was supported by the Dutch Technology Foundation STW

IUS1-G1-4

Synthesis of Albumin Microbubbles using a Microfluidic Device for Real-Time Imaging and Therapeutics

Johnny Chen[1], Ali Dhanaliwala[1,2], Adam Dixon[1], Shiying Wang[1], Alexander Klibanov[2,3], John Hossack[1,2]; *[1]Biomedical Engineering, University of Virginia, Charlottesville, Virginia, USA, [2]Robert M. Berne Cardiovascular Research Center, Charlottesville, Virginia, USA, [3]School of Medicine-Cardiovascular Division, University of Virginia, Charlottesville, Virginia, USA*

Background, Motivation and Objective

Microbubbles (MBs) are ultrasound theranostic agents with a shell stabilized gas core. Albumin is an ideal shell material as it can form a stable shell and is a naturally occurring protein giving it an excellent safety profile. Albumin MBs synthesized using sonication are polydisperse, and when administered systemically, result in MB loss via filtration and

clearance. We propose to use a flow-focusing microfluidic device (FFMD) to generate albumin MBs directly at the point of use in order to facilitate production of monodisperse MBs and minimize MB loss. Using albumin is also a step towards fabricating a biological MB from endogenous materials (i.e. blood and air/nitrogen).

Statement of Contribution/Methods

MB production from a FFMD utilizing bovine serum albumin (BSA) and nitrogen gas was characterized for diameter and production rate. MB stability was calculated by measuring the decrease in b-mode image intensity over time from a solution of MBs. To determine therapeutic potential, MBs were produced upstream of smooth muscle cells (SMCs) under flow and delivery of a model drug was measured following insonation.

Results/Discussion

For a constant gas pressure, MB diameter and production rate were linearly related to the liquid flow-rate (R^2>0.99 and >0.70, respectively). MBs produced with BSA coalesced downstream (Fig. 1a). Adding dextrose (10% w/v) eliminated coalescence (Fig. 1b). B-mode image intensity of 13 µm diameter MBs required 30s to return to baseline from peak intensity. MBs produced by a FFMD insonated at a peak negative pressure of 200 kPa successfully enhanced delivery of calcein, a membrane impermeable fluorophore to SMCs, with 58.0% cells retaining calcein, compared with 0.36% for the case with no ultrasound ($p < 0.0001$). FFMDs enabled real-time *in situ* production of monodisperse MBs with large diameters and low stability. This method reduces the chance of gas entrapment while maintaining the therapeutic benefit of large MBs and uniform acoustic response of monodisperse MB. Our microfluidic method enables miniaturization, allowing intravascular production, imaging, and delivery of transiently stable MBs via a catheter [1].

[1] A. Dhanaliwala et al., "Liquid flooded flow-focusing microfluidic device for in situ generation of monodisperse microbubbles," Microfluidics and Nanofluidics, pp. 1–11, 2012.

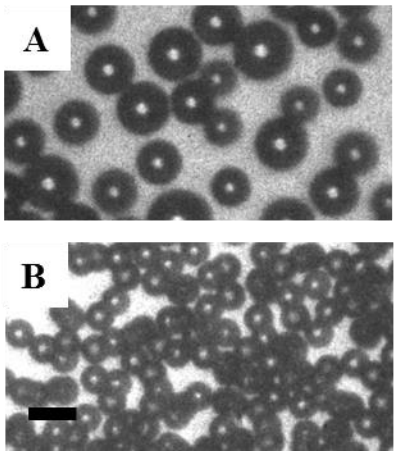

Fig. 1: Images of microbubbles fabricated with a FFMD. (A) A solution of plain BSA produces microbubbles that coalesce. (B) Adding 10% dextrose eliminates microbubble coalescence and maintains monodispersity. Scale bar = 20 µm.

IUS1-G1-5

Automatic respiratory gating for perfusion quantification of DCEUS

Damianos Christofides[1], Edward Leen[2], Michalakis Averkiou[1]; [1]*Department of Mechanical and Manufacturing Engineering, University of Cyprus, Nicosia, Cyprus,* [2]*Imaging Department, Hammersmith Hospital, London, United Kingdom*

Background, Motivation and Objective

Respiratory motion causes significant problems in the quantification of dynamic contrast enhanced ultrasound (DCEUS). A solution to this problem, currently used in clinic, is for patients to perform breath holds. This solution is not ideal, as many patients are unable to perform breath holds that last the duration of a DCEUS examination and also breath holds can affect hemodynamics.

Many post-processing solutions have been proposed in the literature to address the problem of respiratory motion either by manual intervention by the user (Averkiou et al. 2010) or by automated techniques (Mulé et al. 2011; Rognin et al. 2006). In the present study a novel technique is presented by which automatic respiratory gating (ARG) is performed on dual contrast display mode (contrast/tissue) loops.

Statement of Contribution/Methods

The proposed ARG algorithm was applied on the B-mode (tissue) side of the dual display acquisition. The algorithm was based on frame subtraction from the average of all the frames to detect the amount of motion associated with each pixel coordinate of the B-mode loop. Then, frequency domain analysis was used to identify the contribution of respiration to the motion. Regions where motion was detected were ranked according to the frequency and motion analyses; the respiratory kinetics curve was extracted from the highest ranked region.

Fourteen clinical cases of liver metastases from colorectal cancer were used to test the effectiveness of the ARG algorithm, in removing respiratory motion from DCEUS time intensity curves extracted from lesions. Both the ARG-processed data and the non-ARG-processed data were fitted to a lognormal indicator dilution model. The goodness of fit of all data sets to the model was established using the coefficient of determination (R^2) and the root mean square error (*RMSE*).

Results/Discussion

Statistical analysis was performed on the results indicating statistically significant benefits of using the ARG algorithm (Fig. 1). The R^2 value of the ARG-processed data was significantly greater while the *RMSE* was lower. The algorithm was able to process 100 frames at 0.9±0.1 seconds (Intel E8400 CPU at 3GHz with 2GB RAM).

The ARG algorithm presented is fast, easy to use, fully automated, straightforward to implement -since it uses data already available from any dual display acquisition- and effective in removing respiratory motion.

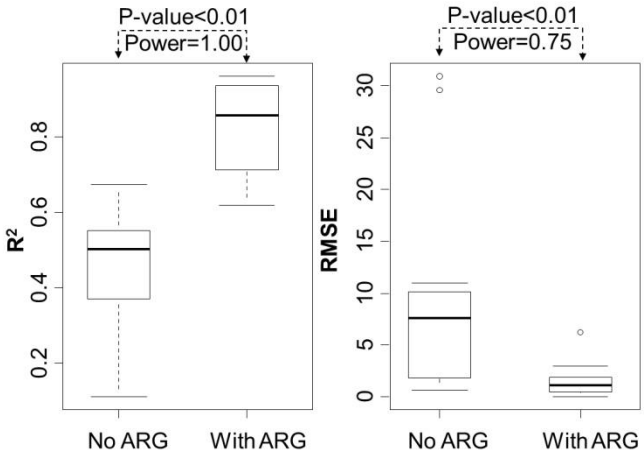

Fig. 1. Boxplots of R^2 and *RMSE* values with and without ARG, along with t-test p-values and power.

New elasticity imaging methods and applications

M4

Wednesday, July 24 2013, 10:30 am - 12:00 pm

Congress Hallair: **Brett Byram**
Duke University

IUS1-G2-1

Imaging of Shear Waves Induced by Lorentz Force

Pol Grasland-Mongrain[1,2], Stefan Catheline[2], Sandra Montalescot[3], Cyril Lafon[2]; *[1]Université de Lyon, Lyon, France, [2]LabTAU, INSERM U1032, Lyon, France, [3]Ecole Normale Supérieure de Cachan, France*

Background, Motivation and Objective

One of the main challenge in shear wave elastography is the inital movement creation. Most of nowadays techniques are using manual compression or acoustic radiation force.

On another hand, by applying an electrical current in a conductor submitted to a magnetic field, a movement is induced by Lorentz force. This movement is propagating as a combination of compressional and shear waves. In this study, we observed for the first time in a tissue-mimicking phantom shear waves induced by Lorentz force.

Statement of Contribution/Methods

In our experiment, a 50 V, 8 ms electrical burst has been applied by two electrodes in a gelatin phantom placed in a 300 mT magnetic field. The phantom has an electrical conductivity of about 1 S/m due to the presence of salt and presented a strong ultrasonic speckle due to the adding of small particles of graphite. A 8 MHz monoelement ultrasonic transducer was emitting and receiving echoes over a line. Speckle tracking algorithm allowed to follow small movements over a line in the phantom. The transducer was then moved vertically to create line by line an image. Experiment was repeated without magnetic field, without current or with insulating phantom to objectivize the phenomenon.

Results/Discussion

Results showed an initial movement due to Lorentz force and arisen propagation of a shear wave through the phantom. Its velocity is around 5 m/s, which is a typical shear wave velocity for soft material. The presence of magnetic field, electrical current and conductive phantom are necessary to see the wave. These results could lead to a shear wave elastography technique based on the combination of electrical current and magnetic field.

IUS1-G2-2

Optoacoustic Elastography for Tissue Biomechanical Property Characterization Using a Ring Transducer

Teng Ma[1], Rui Li[2], Wenjuan Qi[2], Qifa Zhou[1], Zhongping Chen[2], K. Kirk Shung[1]; *[1]Department of Biomedical Engineering, University of Southern California, Los Angeles, California, USA, [2]Beckman Laser Institute & Medical Clinic, University of California, Irvine, Irvine, California, USA*

Background, Motivation and Objective

Elastography, capable of quantitatively providing the biomechanical properties information of tissue, plays a key role in the clinical diagnosis, such as cancerous tumor detection and atherosclerotic plaque characterization. Phase-resolved optical coherence elastography (PR-OCE) possesses superior resolution, high imaging speed with the capability of providing point-by-point elastogram mapping. Acoustic radiation force (ARF) generated by high-intensity ultrasound bursts, offers the dynamic excitations with the benefits of directly and remotely inducing the localized displacement of tissue within the region of interest. Different methods of beam forming are capable of producing ARF such as AM beam geometry and confocal dual beam geometry. In this work, we successfully differentiate the biological tissues with different biomechanical properties utilizing a ring transducer with AM beam geometry in PR-OCE system, which demonstrates the feasibility and superiority to move this imaging system into clinical application.

Statement of Contribution/Methods

The PR-OCE vibration detection system is similar to a previous publication using an 890 nm spectral domain OCT system with the minimum phase being detected of 1.5mrad. The sample is excited by a 4MHz focused ring transducer driven by a 500 Hz AM modulated square wave. The transducer has a focal width of 1.2 mm and length of 1.5 mm at a working distance of 49mm. This featured confocal configuration enables the 2D scanning within the insonation field, in which we assume the ARF induced particle displacements are evenly distributed. The instantaneous axial velocity of vibration can be extracted from the phase shift information measured PR-OCE system to characterize the biomechanical properties. We imaged the cancerous kidney tissue, and the results are confirmed by the histology.

Results/Discussion

The 3D OCT intensity image in Fig.1 (a) provides a general morphological view of the sample. However, in Fig1 (b), the OCE image displays regions with different vibration phase contrast, where the red area indicates the stiffer cancerous tumor tissue, and the green area indicate the softer fat tissue. The fused OCT and OCE image is shown in Fig1(c). The 2D OCE image Fig1 (d) clearly agrees with the histology image Fig.1 (e) in its capability of distinguishing the cancerous tumor tissue on both sides with the middle soft tissue.

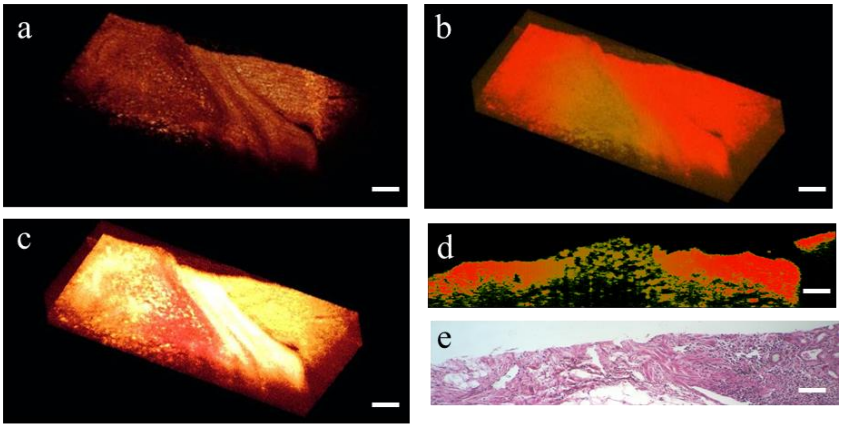

Figure.1 (a) 3D OCT intensity structural image of kidney tissue. (b) 3D OCE phase image under ARF excitation. (c) Fused OCT and OCE image. (d) 2D B-scan OCE image corresponding to the across blue line in (b). (d) Histology image Scale bars:100um.

IUS1-G2-3

Assessing Cross-sectional Elasticity Map by Dynamic Imaging Acoustic Waves with Phase Sensitive Optical Coherence Tomography

Shaozhen Song[1,2], Zhihong Huang[2], Ruikang Wang[1]; *[1]Department of Bioengineering, University of Washington, Seattle, WA, USA, [2]School of Engineering, Physics and Mathematics, University of Dundee, Dundee, Scotland, United Kingdom*

Background, Motivation and Objective

Elastography is an ideal method to reveal local stiffness inside soft tissue for providing additional information for clinical diagnose. In order to achieve a high resolution to determine the microstructures of biological tissues, optical methods are gaining more interests to detect mechanical response of tissue. Here we proposed the combined acoustical and optical method for imaging the propagating shear waves and mapping the shear modulus with a high resolution that could not be achieved by traditional competing elastography modalities.

Statement of Contribution/Methods

To achieve fast dynamic imaging of 2-D cross-sectional acoustic waves in 5 KHz range, we used the phase sensitive optical coherence tomography (PhS-OCT) system to remotely record the full domain sub-micron amplitude mechanical wave propagation in the imaging plane, with high equivalent frame rate (~47KHz) and high spatial resolution. The acoustic waves are generated by a stack piezoelectric transducer, which is synchronized with OCT system, operated in M-B mode. The 2-D elastography image is retrieved from measuring the dynamic temporal-spatial shear wave propagation in the imaging region and thus calculating localized shear wave velocity. Then the quantitative accuracy of this method was examined by validating experiments on agar phantoms.

Results/Discussion

We imaged the wave propagation in a series of agar phantoms, with concentrations from 0.5% to 2.0%, the shear wave velocity by time-of-flight calculation are from 1.79 m/s to 7.05 m/s, which reached a good agreement with literature values. A quantitative shear modulus map for a phantom with a stiff inclusion is also reconstructed. The shear modulus map is overlaid on the tomographic image, with an imaging depth of ~1.2mm and 25 um/10 um lateral/axial resolution. The position and shape is clearly visualized on this elasticity map, the boundary of the stiff inclusion matches well with its expected position.

The shear wave imaging method shows a remarkably good ability to obtain the accurate elastic modulus results and high-resolution elasticity map. This technique opens up the opportunities for future studies of mechanical property measurements of tissue microstructures, especially for clinical applications in ophthalmology and dermatology.

IUS1-G2-4

Passive shear wave imaging using low frame rate scanners

stefan catheline[1], Rémi Souchon[2], Matthieu Ruppin[3], Javier Brum[4], Au Hoang Dinh[5], Jean-Yves Chappelon[5]; *[1]LabTAU, University of Lyon, INSERM U1032, LYON, France, France, [2]labtau, University of Lyon, INSERM U1032, France, [3]ISTerre, University of Grenoble, France, [4]Institute of Physics, University of Montevideo, Uruguay, [5]University of Lyon, INSERM U1032, France*

Background, Motivation and Objective

The main drawback of static elastography holds in the lack of knowledge of the stress field. It results in a strain imaging technique not systematically related to the medium elasticity. But one of its crucial advantages resides in its simple implementation on commercial ultrasonic scanners. On the other hand, shear wave imaging or transient elastography has proved its ability to quantitatively retrieve the local elasticity of soft tissues. But it relies on special electronics called ultrafast scanners. We propose in this paper a solution to conduct shear wave imaging while keeping a standard frame rate imaging (25Hz).

Statement of Contribution/Methods

The idea is to use a diffuse shear wave field and time reversal. This new approach is based on spatiotemporal correlation of combinations of the field, its gradient and its time derivative. The physics principles are first described and tested on numerical finite difference simulations of a diffuse field. Computations and approximations clearly stated shows how mechanical properties of the propagative medium are extracted from an ideal lossless diffuse field.

Results/Discussion

This approach is then tested in experiments. A first experiment in a CIRS® phantom containing four inclusions, 5 mm diameter with shear elasticity ranging from 8 to 70 kPa, was performed. The experiment is the following: in a first step, a diffuse wave field is created inside the sample by random finger impacts given from the surface during 20 seconds. The 2D displacement field is then measured inside the soft solid using speckle tracking algorithms developed in elastography. It involves a Hoak system (Brujel and Kjaer) 192 channels array working at 12MHz with a repetition frequency of 25Hz. In a second step, the displacement at one point chosen as a virtual source is correlated to the other points of

the image in order to compute a time reversal field in the computer. The undersampling of displacements in time does not alter the spatial coherence. Quantitative elasticity images are retrieved in spherical calibrated inclusions. Beside a first in vivo test on the thyroid of a healthy volunteer is discussed.

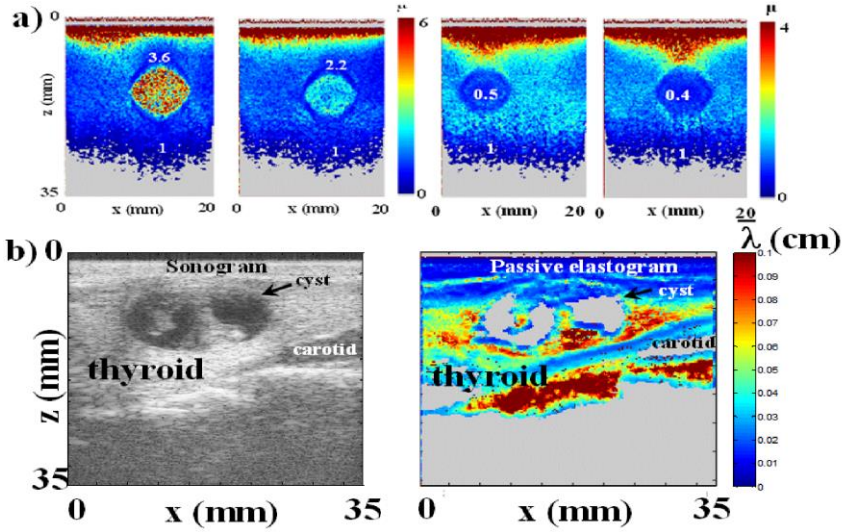

IUS1-G2-5

In Vivo Achilles Tendon Elasticity Assessment using Supersonic Shear Imaging: a feasibility study

Javier Brum[1], Jean Luc Gennisson[1], Mathias Fink[1], Mickael Tanter[1]; *[1]Institut Langevin - Ondes et Images, ESPCI ParisTech, CNRS UMR 7587, Inserm ERL U979, Paris, France*

Background, Motivation and Objective

Common tendon disorders (e.g. Achilles tendon rupture or flexor tendon injury) are responsible for substantial morbidity in sports and work. Repetitive tendon overload result in a degenerative condition called tendinopathy. Successful treatment of tendinopathy seeks to restore the tendon mechanical functions. However, unsatisfactory results are common and the mechanical properties of the injured tendon are hard to assess quantitatively during the recovery process. As a consequence, a non-invasive tool capable of quantifying tendon stiffness is of great need clinically. In this work, the Supersonic Shear Imaging (SSI) technique was adapted to map the Young's modulus of extremely stiff and geometrically complex media as tendons.

Statement of Contribution/Methods

To test the SSI performance, an *in vivo* experiment was carried out in the Achilles tendon of eight healthy volunteers. The 8 MHz ultrasonic probe was placed over the Achilles tendon parallel to the fiber orientation. Two situations were considered: a contracted position corresponding to a 90° angle between the foot and the tibia bone, and a relaxed position corresponding to a plantar flexion of 135°. The SSI technique consists basically of three steps: first, the tissue is locally stressed using the radiation force of a focused ultrasound beam, resulting in a broadband shear wave generation (300 – 1600 Hz). Second, the system is switched into an ultrafast imaging mode to track the shear wave propagation. Since tendons are very stiff, shear waves will propagate very fast requiring a very high frame rate, which is not feasible with current imaging techniques. In this work the imaging frame rate was increased up to 20 kHz. Finally, the tissue stiffness is retrieved by extracting the shear wave speed dispersion curve (i.e. relation between shear wave speed and frequency) by performing a 2D Fourier transform to the measured displacement field inside the tendon.

Results/Discussion

For each subject, a significantly increase in the shear wave speed dispersion curve was observed for the contracted position (relaxed position considered as reference), indicating tendon stiffening. Assuming that the tendon acts as a transverse anisotropic cylindrical wave guide, the measured dispersion curve corresponds to the lowest flexural mode. For this mode, at high frequencies, the phase velocity approaches the Rayleigh velocity, which is linked to the tendon Young's modulus. At 1600 Hz, phase velocities of 11.2 ± 3.1 m/s and 27.8 ± 8.2 m/s were measured for the relaxed and the contracted position respectively (mean value ± standard deviation). From these values a Young's modulus of 0.42 ± 0.26 MPa and 2.58 ± 1.74 MPa is respectively retrieved, in good agreement with reported results. These results confirm the potential of the SSI technique for the *in vivo* Achilles tendon elasticity assessment and demonstrate that dispersion should be taken into account in order to solve the inverse problem in the low frequency range.

IUS1-G2-6

Ultrasound strain imaging in peripheral neuropathy: a preliminary in vivo study

Yin-Yin Liao[1], Wei-Ning Lee[2], Ming-Ju Lee[1], Chih-Kuang Yeh[1]; *[1]Department of Biomedical Engineering and Environmental Sciences, National Tsing Hua University, Taiwan, [2]Department of Electrical and Electronic Engineering, The University of Hong Kong, Hong Kong*

Background, Motivation and Objective

Peripheral compression neuropathy is caused by localized interference of structural changes in the nerve or adjacent tissues. The mechanism of nerve movement during limb motion is a key to understanding entrapment neuropathy, which has been diagnosed in a qualitative way by ultrasound imaging. To our knowledge, there is no study on the quantitative assessment of motion and concomitant strain of the nerve. The objective of this study was therefore to employ a two-dimensional (2D) ultrasound strain imaging method to quantify the mechanical behavior of the median nerve (MN) and the transverse carpal ligament (TCL) for the diagnosis of nerve compression syndrome.

Statement of Contribution/Methods

The wrists of both healthy volunteers (n=10) and patients (n=16) confirmed by nerve conduction tests were studied. Radio-frequency (RF) ultrasound data of the transverse wrist were acquired, during which the subjects were asked to perform one cycle of the finger motion, namely from an open palm to a clenched fist, and then to an open palm. The 2D displacements between consecutive RF frames were firstly estimated through normalized cross-correlation and a recorrelation strategy. The 2D strain tensor was then obtained from the estimated 2D displacements using a least-squares strain estimator. To differentiate normal (Fig. (a)) from abnormal (Fig. (b)) cases, the MN (solid line) and TCL (dashed line) zones were characterized by the incremental axial and shear strains, respectively. The positive and negative axial strains respectively indicated axial extension or compression of the MN, while the shear strain was used to depict lateral sliding between the MN and TCL. The absolute cumulative axial/shear strain during one cycle of the finger motion in the MN/TCL zone is shown in Fig. (c).

Results/Discussion

The slopes of shear strains in the TCL for the normal and abnormal cases were 0.33±0.03 (mean±standard error) and 0.11±0.01 ($p<0.01$), respectively; the slopes of axial strains in the MN in both cases were 0.19±0.02 and 0.08±0.01 ($p<0.05$), respectively. Reduced shear and axial strains in the patients stemmed from the restricted movement of the MN due to the increased carpal tunnel pressure during finger motion. The results show that ultrasound strain imaging that depicted the mechanics within the carpal tunnel might serve as a potential diagnostic tool for nerve compression syndrome.

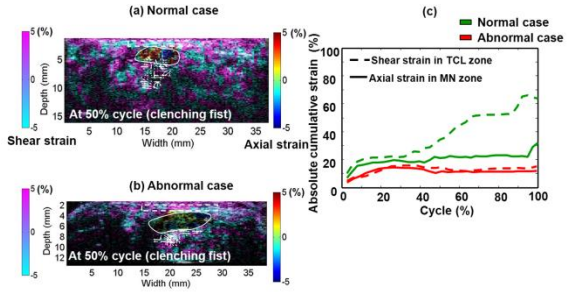

New medical devices

M5

Wednesday, July 24 2013, 10:30 am - 12:00 pm

Congress Hallair: **Stuart Foster**
University of Toronto

IUS1-G3-1

Breast imaging using ultrasound tomography: From clinical requirements to system design

Olivier Roy[1,2], Steven Schmidt[1,2], Cuiping Li[1,2], Veerendra Allada[1,3], Erik West[1], David Kunz[1], Neb Duric[1,2]; *[1]Delphinus Medical Technologies, USA, [2]Karmanos Cancer Institute, USA, [3]Iowa State University, USA*

Background, Motivation and Objective

Ultrasound tomography (UST) is a breast imaging modality that is radiation free, operator independent, and does not involve breast compression. In a UST scan, the breast is surrounded by a transducer ring that moves along the coronal axis from the chest wall to the nipple region. The deployment of UST in a clinical setting is technically challenging from three major standpoints: acquisition speed, storage capability, and computational requirements. Data acquisition must be fast to maximize patient throughput and minimize image registration artifacts. Unlike traditional ultrasound, hundreds of gigabytes of data must be acquired, buffered, and processed to image various characteristics of breast tissues such as sound speed, attenuation, and reflectivity. The tomographic image reconstruction methods are non-linear, iterative algorithms with significant computational complexity. Moreover, the scanner hosting the acquisition and reconstruction components must satisfy stringent cost, power, and size requirements. For decades, the above constraints have hindered the practicality of UST in a clinical scenario. Our objective was to design a UST system that addresses the above requirements.

Statement of Contribution/Methods

Our group has designed, implemented, and deployed a fully operational UST system named SoftVue. Acquisition, buffering, and processing of data are running on a blade server architecture. We have developed custom data reduction techniques, a high speed communication architecture, and state-of-the-art image reconstruction algorithms running on both CPUs and GPUs. SoftVue processing core is robust, scalable, and versatile. Our main contribution is the demonstration that UST technology is now a viable paradigm for medical imaging.

Results/Discussion

We present a complete system design of SoftVue processing engine. The key design choices are reviewed, and the system performance is analyzed. SoftVue sustains an average scan rate of a slice every 2.5 seconds and can buffer up to 350 slices of data depending on the chosen data reduction scheme. For an average size breast, a bilateral scan with a 3 millimeter inter-slice spacing can be achieved in a couple of minutes, and images are ready for review by the radiologist in less than 15 minutes. We outline the strengths and limitations of the current system and discuss possible improvements.

IUS1-G3-2

An Integrated Ring CMUT Array for Endoscopic Ultrasound and Photoacoustic Imaging

Amin Nikoozadeh[1], Chienliu Chang[2], Jung Woo Choe[1], Anshuman Bhuyan[1], Byung Chul Lee[1], Azadeh Moini[1], yagi takayuki[2], Pierre T. Khuri-Yakub[1]; *[1]Stanford University, USA, [2]Canon Inc., Japan*

Background, Motivation and Objective

Ring arrays have many advantages in catheter-based and endoscopic ultrasound imaging applications where real-time volumetric imaging is desired. The sparse nature of a Ring 2D array implies fewer elements than a fully populated 2D array of the same extent. The ring geometry provides a central lumen that can be utilized for a variety of applications, such as introducing optical fibers for photoacoustic imaging.

Statement of Contribution/Methods

We designed and fabricated a 512-element Ring CMUT array using our polysilicon sacrificial layer process with through-wafer via interconnects. The transducer array elements are arranged into four concentric rings #1-4 each consisting of 128 elements. They are placed on concentric circles with diameters of 6.0, 7.2, 8.5, and 9.7 mm for rings #1-4, respectively. All 128 transducer array elements within each ring are the same; however, they differ among the four rings in size and center frequency. The center frequencies are 10, 7, 5, and 4 MHz for rings #1-4, respectively. The different center frequencies are chosen such that the lateral resolution for all the ring apertures remains the same at a given depth.

This Ring CMUT array was integrated with custom integrated circuits (ICs) in a pin-grid-array (PGA) package for bench-top testing. The ICs mainly provide low-noise amplifiers for each transducer array element and their architecture enables seamless connection to any commercial imaging system. The CMUT array is flip-chip bonded to a custom quartz fan-out board that provides the connections between the CMUT and the ICs. Due to the large number of elements in the array, each assembly is wire-bonded in such way to enable imaging with one full ring at a time (i.e., 128 elements).

For real-time imaging, we use a PC-based platform from Verasonics that provides 128 channels. Our in-house imaging software for a ring array uses synthetic phased-array imaging method with Hadamard coding and also employs Norton's weightings and cosine apodization.

Results/Discussion

Our first PGA assembly provides connections to ring #3 of a Ring CMUT array. We have successfully demonstrated real-time imaging with this assembly using metal spring and fluorocarbon wire phantoms and photoacoustic imaging experiments are imminent. Additional assemblies will be prepared to experiment with the other three rings in the CMUT Array.

This work was supported by Canon Inc.

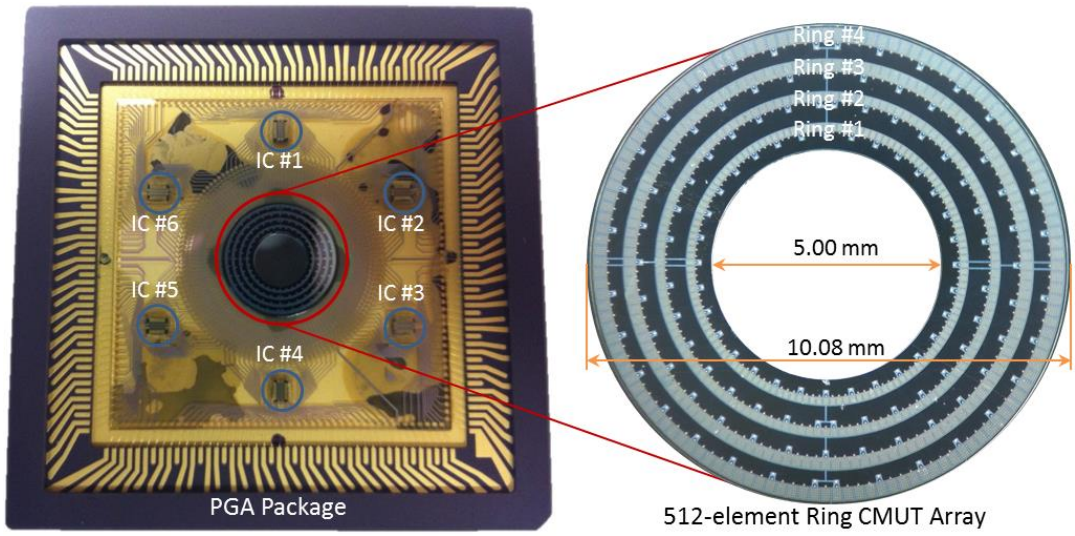

IUS1-G3-3

Microstructure Design for Detection of Implantable Device Using Ultrasound

I-Chin Wu[1], Pai-Chi Li[2]; [1]*BEBI, National Taiwan University, Taiwan,* [2]*Electrical Engineering, National Taiwan University, Taiwan*

Background, Motivation and Objective

Implantable medical devices have been developed for disease monitoring and treatment. One example is the wireless neural stimulator. In our previous study, wireless power and communication using ultrasound was proposed and demonstrated on animals. It is shown that the focusing capability at depth of ultrasound has advantages over electromagnetic waves in such applications. Another issue in this context is the detection of the implanted device. This is critical as the acoustic energy is tightly focused. Our hypothesis is that by properly designing microstructures of the housing of the implantable device, specific spectral characteristics can be achieved and utilized for effective detection.

Statement of Contribution/Methods

The proposed design of the microstructure is analogous to the steps of a Maya pyramid. The Maya pyramid has a stair-shaped structure that causes the echo sounds like a chirp when one claps hands in front of it. Such a sound effect is believed to be resulted from the path length difference among stairs from the sound source. Similarly, a stair-shaped microstructure can be designed and the implantable device can be detected by analyzing the spectral characteristics of the returning echo. The design is evaluated by using both simulations and experiments using a setup illustrated in figure A. A 3D printer is used to produce a prototype with the desired microstructure. Because path length difference increases as echoes from outer portion of the device are received, a decrease in instantaneous frequency is expected.

Results/Discussion

The time-frequency analysis results are shown in figure B (measurements vs. two simulations). The experimental results show that the instantaneous frequency decreases from around 6.8 MHz to 6 MHz within the duration of the echo (around 0.45 micro second). The results are in good agreement with the simulations by assuming 4 steps in the microstructure. Several parameters can be evaluated to further improve performance of the proposed method. For example, a narrower focal spot is expected to produce a more predictable change in the instantaneous frequency. Nevertheless, it is clearly demonstrated that the stair-shaped microstructure can be used for detection the implanted device using ultrasound. Such a method can also be applied to detection of the needle during biopsy.

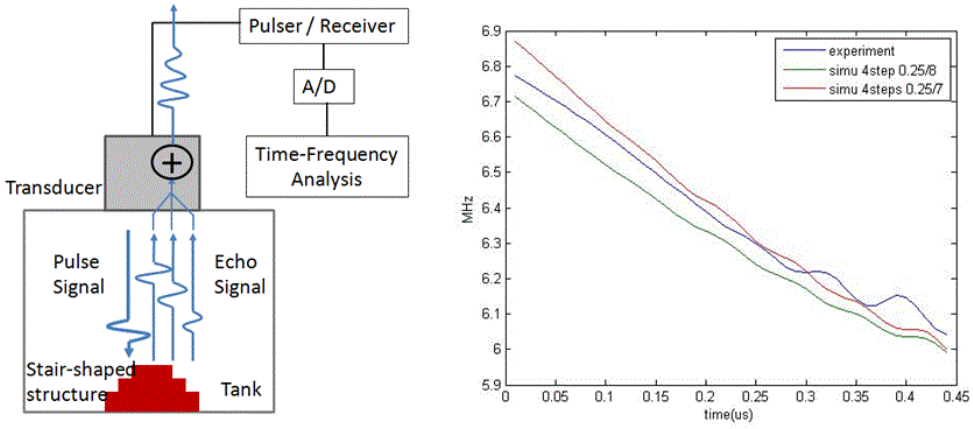

A **B**

A. Experimental setup. B. Time-frequency analysis results of experiments and simulations.

IUS1-G3-4

In-plane needle-tip localization with sub-millimeter precision using an ultrasonic optical fiber hydrophone

Jean Martial Mari[1], Simeon West[2], Ben Cox[1], Paul Beard[1], Adrien Desjardins[1]; [1]*Medical Physics and Bioengineering, University College London, London, United Kingdom,* [2]*Anaesthetics, University College Hospital, London, United Kingdom*

Background, Motivation and Objective

Accurately and efficiently guiding a medical device (e.g. a needle or catheter) to a target in the human body is of critical importance in a wide range of minimally invasive procedures, such as peripheral nerve blocks, central venous catheterizations, biopsies, and electrodes insertions. B-mode ultrasound is commonly used for guidance, but determining the position of the medical device tip remains challenging even for experienced physicians. Ultrasound reflections can arise from many locations on the medical device, so it is often unclear whether the part of the device that is visible on the image corresponds to the actual location of the device tip. If the needle tip is not visible, it can enter a critical structure and cause life-threatening complications such as pneumothorax, nerve damage, and toxicity from intravascular injections. Several methods for improving medical device guidance have been proposed, including mechanical needle guides, electromagnetic tracking, echogenic needles, and 3D ultrasound imaging [1,2], but challenges with identifying the device tip remain.

Statement of Contribution/Methods

In this study, we present a new method for identifying and tracking medical devices within the ultrasound imaging plane. With this method, ultrasound pulses from an ultrasound imaging probe are received with a fiber optic hydrophone [3] that is positioned within the medical device. This method was implemented with an Ultrasonix RP 500 system and a linear transducer array. The hydrophone and ultrasound signals were acquired with a custom Labview program, and the derived position was displayed with a color overlay (Fig. 1).

Results/Discussion

Using a tissue mimicking phantom, ultrasound pulses could be clearly resolved in the processed hydrophone signals. The measured lateral resolution was 0.39 ± 0.28 mm, and the depth resolution was 0.25 ± 0.11 mm. The method presented in this study has strong potential to increase procedural efficiency and safety in a manner that is compatible with current clinical practice.

1 Harmat et al. Needle tip localization using stylet vibration. UMB 2006.

2 Mari et al. Ultrasonic scanning of straight micro tools in soft biological tissues: methodology and implementation. Ultrasonics 2011.

3 Morrisa et al. A Fabry–Pérot fiber-optic ultrasonic hydrophone for the simultaneous measurement of temperature and acoustic pressure. JASA 2009.

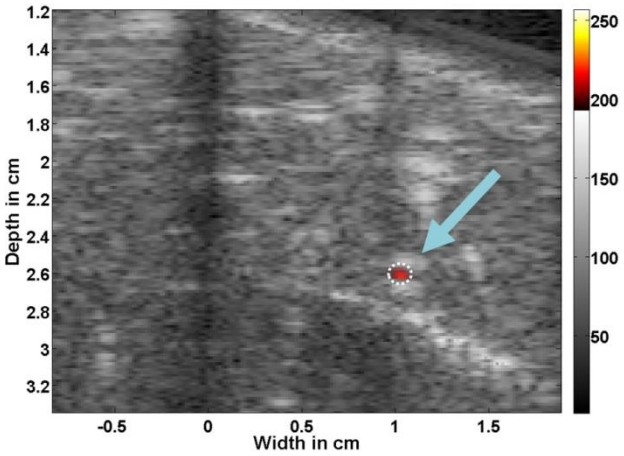

Fig. 1. Determined position of a needle tip in a tissue mimicking phantom, as shown with an overlay (red dot) and an arrow.

IUS1-G3-5

Magnetic Linear Actuator for Vascular Access Surveillance

Grant Kruger[1,2], John Pitre Jr. [3], Alan Vollmer[4], Leo Koziol[2,4], Joseph Bull[3], William Weitzel[2,4]; [1]*Department of Mechanical Engineering, University of Michigan, Ann Arbor, Michigan, USA,* [2]*VA Medical Center, Ann Arbor, Michigan, USA,* [3]*Biomedical Engineering, University of Michigan, Ann Arbor, Michigan, USA,* [4]*Internal Medicine, University of Michigan, Ann Arbor, Michigan, USA*

Background, Motivation and Objective

Vascular access (VA) maintenance is essential for dialysis care. However, the non-linear, patient specific formation of stenoses reduce treatment efficiency. Various methods are used to monitor VA blood flow and/or pressure. However, these are surrogates for stenosis rather than direct measurements. Also, there is no reimbursement for VA surveillance and measurements consume clinical time, making more than biweekly measurements difficult to schedule. Biological variability of hemodynamics and stenosis formation increases the chance of infrequent observations missing stenosis formation.

We are currently developing an ultrasound (US) system and probe (Fig. 1a) intended to slide between the dialysis needles and enable operator independent VA geometry and flow measurement during dialysis treatments.

Statement of Contribution/Methods

Dual opposing NdFeB magnets generate a high density flux and a scan head with a coil on a low friction slide is actuated according to the Lorentz Law. A single 8 MHz 5 mm dia. (20 mm focus) US transducer is fixed to the scan head. Feedback from an optical encoder allows Doppler or image registration as well as accurate control of scan head kinematics (max. resolution of 85 µm.). Overall dimensions of the probe are 40 x 30 x 5 mm, with a travel of 20 mm. A Polymethylpentene window with a Phenylmethyl Siloxane fluid (Dow Corning 710) provides an acoustic coupling medium (ACM) between the transducer and exterior.

Results/Discussion

Figure 1b provides the magnetic circuit simulation result, showing an average flux density of 0.028 T intersecting the coil. Along with the coil geometry and current this results in a max. force of 66 mN. Experiments reveled the actual force is 40 mN, suggesting 26 mN is lost to friction. In air the transit time is 31 ms. However, when placed in the ACM the

mean acceleration drops from 26 to 0.07 $m.s^{-2}$ and transmit time increases from 31 to 656 ms. This suggests the ACM reduces the force from 40 to 0.1 mN due to the ACM viscosity.

Even though significant ACM resistance is incurred, the probe can perform automated 2D Doppler scans of the VA geometry or positioning of the transducer over the center of the VA so a Doppler gate can be scanned axially. We are currently investigating alternate materials to minimize ACM resistance for higher speed imaging.

This work was supported in part by a Coulter Foundation grant and NIH grant 1R41HL110430.

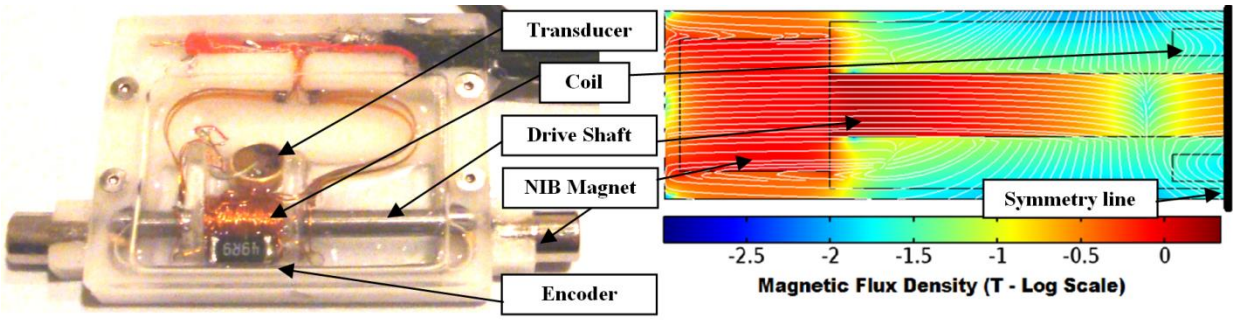

Fig. 1: VA Scanner prototype; a) Low-profile probe, b) Computational simulation of magnetic design.

IUS1-G3-6

Pocket-Sized Ultrasonic Nebulizer For Inhalation Drug Delivery*

Chen Tsai[1,2], R. W. Mao[1], S. K. Lin[1], Y. Zhu[1], S. C. Tsai[3]; *[1]Electrical Engineering and Computer Science, University of California, Irvine, Irvine, CA, USA, [2]Institute of Optoelectronics and Photonics, National Taiwan University, Taipei, Taiwan, [3]Chemical Engineering and Materials Science, University of California, Irvine, Irvine, CA, USA*

Background, Motivation and Objective

Droplet generation has continued to be an area of broad interest with many applications among which is inhalation (pulmonary) drug delivery. Inhalation is a vitally important route for non-invasive drug delivery for both systemic and local applications. Control of aerosol (particles or droplets in air) size to the optimum range (2 to 5μm) and throughput plays a critical role in the efficient and effective delivery of inhaled medications to the lung. Current commercial devices are metered dosed inhalers (MDI), dry powder inhalers (DPI), and wet nebulizers. All these devices suffer from broad particle size (polydisperse) distributions (with large geometrical standard deviation GSD >1.5) and low throughput (0.16 to 0.42 ml/min), mak-ing it difficult to deliver often expensive drug of desirable particle sizes and sufficient amount to targeted sites precisely and rapidly. The silicon-based MHz multiple-Fourier horn ultrasonic nozzle we reported recently [1-3] has demonstrated capability of producing high-throughput mi-crometer-sized monodisperse droplets at low drive power and, thus, fulfilling the unmet needs, e.g., detoxification of cyanide poisoning [4]. Here we report realization of the first pocket-sized ultrasonic nebulizer for inhalation drug delivery using such nozzles.

Statement of Contribution/Methods

Drug solutions were transported to the end face of the 1-2 MHz 3-Fourier horn nozzle externally for nebulization. Resonance among the multiple Fourier horns resulted in greatly enhanced lon-gitudinal displacement on the nozzle end face that readily facilitated temporal instability of the Faraday waves on the drug solution and, thus, ejection of micrometer-sized monodisperse drug aerosols. The centimeter-size MEMS-based nozzles together with low electrical drive power re-quirement enabled realization of pocket-sized ultrasonic nebulizers.

Results/Discussion

Monodisperse medicinal aerosols of diameter range 2.2 to 4.6 μm have been produced at throughput as high as 500μl/min and electrical drive power as low as 0.3 watt. The centimeter-sized nozzles together with low power requirement enabled most recent realization of the first pocket-sized ultrasonic nebulizer (8.6 x 5.6 x 1.5 cm^3) that contains nozzle, IC electronic driver, cell-phone battery, micro pump, drug reservoir, and liquid feed. A variety of common drugs for asthma, chronic obstructive pulmonary disease (COPD), diabetics, hypertension, cystic fibrosis, etc. such as albuterol (isoproterenol), Humulin U-100, cobinamide, and interferon-γ have been nebulized with desirable aerosol size and high throughput. Other applications include delivery of genes and lipid-based micro-encapsulated biological entities or therapies.

[1] IEEE Trans. on UFFC, 56 (9), 1968-1979, 2009. [2] Lab Chip, 10, 2733-2740, 2010. [3] PRL, 108, 154501-1 to 5, 2012. [4] Presented at 2012 IUS, Oct 7-10, Dresden, Germany.

* Supported by the National Institute of Health (NIH), USA.

NDE - Ultrasonic Applications

NH

Wednesday, July 24 2013, 10:30 am - 12:00 pm

Congress Hallair: **Donald Yuhas**
Industrial Measurement Systems

IUS2-G-1

Prototyping and evaluation of ultrasonic particle filter considering water flux and sound propagation direction

Takuya Kambayashi[1], Tomonori Saeki[1], Kentaro Nakamura[2]; *[1]Yokohama Research Laboratory, Hitachi,Ltd., Yokohama, Japan, [2]Tokyo Institute of Technology, Yokohama, Japan*

Background, Motivation and Objective

Water supply market is growing rapidly over the world, and water recycle technology is becoming the most important issue. Coagulation and filtering methods have been common for recycling waste water. In both methods, however, we need to supply consumables such as co-agulants and filters, periodically. To realize a sustainable water system for protecting environment, it is highly required to reduce such consumables. Filtering using acoustic radiation force (ARF) is a promising candidate method which works without those consumables.

Statement of Contribution/Methods

We propose, in this report, a novel design for water filtering device by means of ARF. Ultrasonic transducer is located so that the direction of the ultrasound propagation is parallel to the flow as shown in Figure 1. In the device, since suspended particles have more chances to encounter generated nodes in the standing wave ultrasonic field, trapping capability is improved.

Results/Discussion

Figure 2 shows turbidity and reduction efficiency after filtration with the proposed device working at 2.26MHz as functions of the initial turbidity. The reduction ratio of turbidity is also calculated and plotted in the figure. The reduction ratio was successfully reached to 80% or more. This means that, for example, water with the turbidity of 16.8 degrees is purified to that of 2.1 degrees.

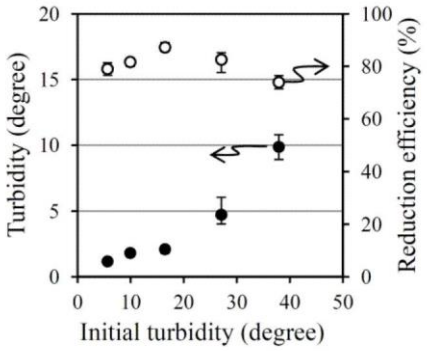

Figure 2 Turbidity after filtration vs. initial turbidity

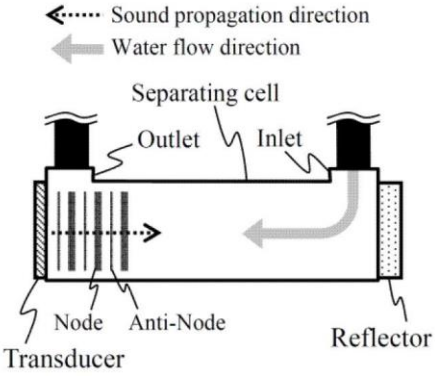

Figure 1 Schematic diagram of separating cell

IUS2-G-2

Study on Non Contact Acoustic Imaging Method for Concrete Structures - Improvement of Signal-to-noise Ratio by using Tone Burst Wave Method -

Ryo Akamatsu[1], Tsuneyoshi Sugimoto[1], Noriyuki Utagawa[2], Kageyoshi Katakura[3]; *[1]Graduate School of Engineering, Toin University of Yokohama, Japan, [2]Sato Kogyo Co., Ltd., Japan, [3]Meitoku Engineering Laboratory, Japan*

Background, Motivation and Objective

Now, hammering test is widely used for non-destructive inspection for concrete structures. However, this method has a disadvantage that it is difficult to inspect the places where people cannot reach such as a bridge girder, a tunnel roof. Therefore, we propose a Non Contact Acoustic Imaging method(NCAI). In this method, a sound wave which has wide frequency range is emitted to concrete surface, and then a defective part on the concrete surface is resonated. The vibration velocities on the concrete surface is measured two-dimensionally by a Scanning Laser Doppler Vibrometer(SLDV).

In our past study, using a Long Range Acoustic Device(LRAD) as a high-power directional sound source, it was demonstrated that remote measurement can be fulfilled at a distance of 10 m or more from the measurement target.

Statement of Contribution/Methods

In our proposed method, although a high sound pressure of approximately 100 dB is needed near the concrete surface, the high sound pressure has a bad effect for the signal to noise ratio of the measurement result. Thus, we propose a new driving method using tone burst wave. Tone bursts composed of a silence time and a short pulse obtained by dividing a wide frequency band are used. By using the tone bursts, the time when the measurement instrument is vibrated by the sound wave can be separated. To confirm an effectiveness of our proposed method, we conducted an experiment using a concrete test piece which has artificial defects.

Results/Discussion

Fig. 2 shows the vibration velocity spectrum of the defective part. If the chirp is used, a deep defect detection is difficult. However, the peak of defect can be observed when using the tone burst, since the noise level is significantly reduced. As a result, the signal to noise ratio of 15 dB was improved than using the chirp.

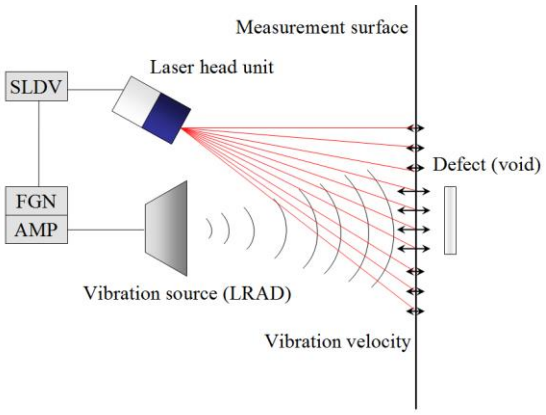

Fig.1 Fundamental concept

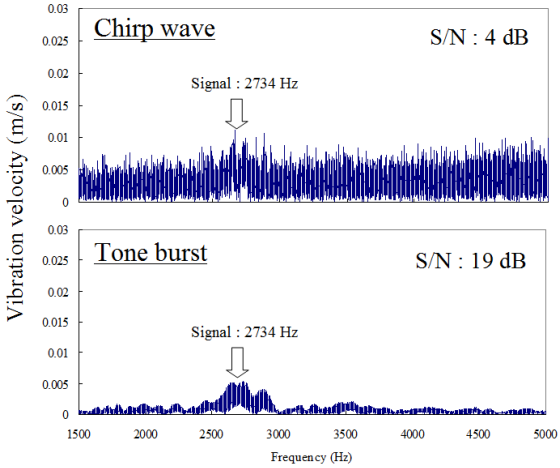

Fig.2 Vibration spectra on the defective part.
The size of the defect is 30 × 30 cm^2, and the depth is 7.5 cm

IUS2-G-3

Multi-mode Tandem Ultrasonic Technique for Tube Inspection

Shivaprasad S[1], Kannan C[2], Sova Bhattacharya[2], S P Singh[2], Krishnan Balasubramaniam[1]; *[1]Department of Mechanical Engineering, Indian Institute of Technology Madras, Chennai, Tamil Nadu, India, [2]R&D Center, Indian Oil Corporation Limited, Faridabad, Haryana, India*

Background, Motivation and Objective

Many tubes used in petrochemical industries for fluid transport are subjected to high temperature and stress levels. Over a period of time, these tubes are expected to degrade owing to different creep mechanisms, sometimes leading to catastrophic failure. The damages ranging from formation of isolated cavities to presence of micro cracks are expected as result of creep mechanism. The existing method of ultrasonic inspection involves the generation of a longitudinal wave at appropriate angle of incident in order for the mode to travel across the chord of the tube and then received using an identical transducer. This technique has been shown to be un-reliable due to the variations in the type and orientation of the cracks.

Statement of Contribution/Methods

Here, a new multi mode tandem configuration ultrasonic technique, that utilizes the two bulk wave modes in a tandem configuration, i.e. both Longitudinal and Transverse modes propagating along the chord of the tube, has been employed in order to improve the reliability of inspection. The transverse waves were found to be more sensitive to flaw orientations that were more circumferential. Eight different configuration of inspection were carried out using the multi mode inspection technique.

Results/Discussion

Inspection configuration for longitudinal wave modes are shown in Fig (1a), where A-B refers to transducer “A” acting as transmitter and “B” acting as receiver. Similarly another set of four configurations were carried out for shear wave mode generated at different angle of inclination of the wedge. A-scans obtained using this technique for A-B configuration of Shear and longitudinal wave modes are shown in Fig (1b).In addition, the Shear wave mode were found to be less mode converted and sensitive towards the defects.Snap shot of Finite element simulation performed using ABAQUS® are shown in Fig (2a) & (2b). Both the FEM model and the experiments validate the improved sensitivity and consequently the reliability of the tandem approach.

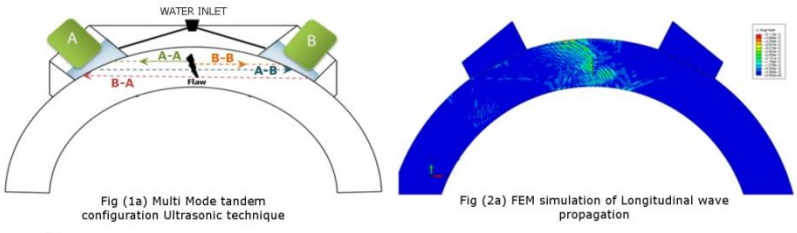

Fig (1a) Multi Mode tandem configuration Ultrasonic technique

Fig (2a) FEM simulation of Longitudinal wave propagation

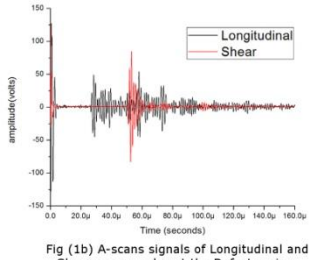

Fig (1b) A-scans signals of Longitudinal and Shear wave modes at the Defect region

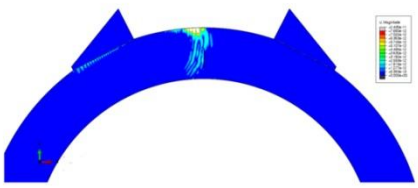

Fig (2b) FEM simulation of Shear wave propagation

IUS2-G-4

Ultrasonic dynamic air-gap monitoring system for large hydro-generators

Julio Cezar Adamowski[1], Alan Souza[1], Allan Lima[2], Paulo Oda[2], Hamiltin Tiba[2]; *[1]Mechatronics, Universidade de Sao Paulo, Sao Paulo, SP, Brazil, [2]Engenharia, Companha Energetica de Sao Paulo - CESP, Sao Paulo, SP, Brazil*

Background, Motivation and Objective

The dynamic air-gap monitoring of hydro-generators consists of the distance measurement between rotor poles and stator while it is in operation. A commercially available capacitive sensor has been used in the air-gap monitoring of hydro-generators in the last two decades. The capacitive sensor is installed inside the stator of the generator within the air gap between rotor and stator requiring removal of the rotor for its installation. In the case of a generator already in operation, its installation represents a high cost. This work presents a new approach for the air-gap measurement performed by measuring the time of flight of an ultrasonic wave traveling between the stator and the rotor. The air-gap sensors are installed in the ventilation ducts of the stator, from its outer surface to its inner surface.

Statement of Contribution/Methods

The measuring system consists of two pairs of small-size rectangular (4.5 x 8.0 mm) piezocomposite ultrasonic transducers (400 kHz), operating in pitch-catch scheme, which were designed for allowing their installation in ventilation ducts from outside the hydro-generator stator. The correlation between the time of flight of the ultrasonic wave and the air gap depends on the air temperature which can reach 80°C and the flow of the air being moved by the rotor between the emitter and receiver of the pitch-catch transducer. The tangential velocity of rotor is 53.8 m/s at nominal speed of the hydro-generator. Two ultrasonic transducers are mounted at the ends of two printed circuit board strips containing a low noise preamplifier and a temperature sensor comprising a pitch-catch transducer set. Two sets of pitch-catch transducers form an air-gap measuring unit, which is interconnected to a remote control and processing hardware via two coaxial cables. The correction of the ultrasonic propagation velocity is based on the air temperature measured close to the ultrasonic transducer. The effect of the air flow velocity in the air-gap region is compensated by calculating the average of the times of flight in the air flow direction and in the opposite direction to the flow. The control and processing hardware delivers the air-gap length with a resolution of 0.04 mm. The air gap is measured at a rate of 2 kHz.

Results/Discussion

The ultrasonic air-gap monitoring sensor was installed in the hydro-generator number 5 (UG05 – 170MW) of the hydroelectric power plant of CESP, Ilha Solteira, Brazil. This generator has 84 poles and the average of statically measured air gap is about 16.0 mm. The air-gap sensors are installed in the ventilation ducts of the stator, from its outer surface to its inner surface. The air-gap sensor was tested on several conditions of machine operation, showing a repeatability of 0.1 mm in the dynamic measurement of the air gap.

IUS2-G-5

On-chip spatially controlled sonoporation of single cell with microbubble cluster cavitation by surface acoustic waves

Long Meng[1], Peng Jiang[1], Feiyan Cai[1], Lili Niu[1], Hairong Zheng[1]; *[1]Shenzhen Institutes of Advanced Technology, Chinese Academy of Sciences, China, People's Republic of*

Background, Motivation and Objective

Spatial manipulation of bubble cavitation has drawn increasing interest in recent years, not only for better understanding of the complex mechanisms of the sonoporation, but also the potential applications in drug development. Several methods have been adopted to spatially control the bubble cavitation, such as optical tweezers, chemical bonding and high intensity focused ultrasound. However, it is still challenging to integrate the bubble manipulation with cavitation into a lab-on-a-chip system. In this paper, we present a novel microfluidic device that combines precise manipulation with cavitation for regulating the single cell permeability by surface acoustic waves (SAW).

Statement of Contribution/Methods

Two pairs of perpendicular interdigital transducers (IDTs), having a pitch of 160 µm, was deposited on a 128 Y-X LiNbO3 substrate. Then, a PDMS microchannel was bonded to the substrate using oxygen plasma treatment. The microbubbles were fabricated in-house and the size distribution of microbubbles ranges from 0.5µm to 10µm. To precisely transport the microbubbles to the specific localized regions, the phases-shift method was utilized. By modulating the relative phase of IDTs, the position of pressure nodes of the standing wave changes correspondingly resulting in the transportation of the microbubbles. Cell viability and membrane integrity was assessed by FDA and PI uptake.

Results/Discussion

When applied continuous sinusoidal signal to four IDTs, the microbubbles began to aggregate into cluster. Then, a high energy pulse was excited to one IDTs, the microbubble cluster produced a violent vibration, and collapse ultimately (Fig. 1a). Fig. 1b shows the microbubble cluster is driven to cell A and the location where cluster collapse is close to cell A. The cell A emits red fluorescence, indicating the pores of membrane are generated. Meanwhile, the cell B was only subjected to the SAW and the cellular membrane is intact. Moreover, after about 20min, the green fluorescence Intensity between A and B was almost same, which verify the pores are reversible. Thus, this method has high selectivity and enables to realize specific localized sonoporation on a chip.

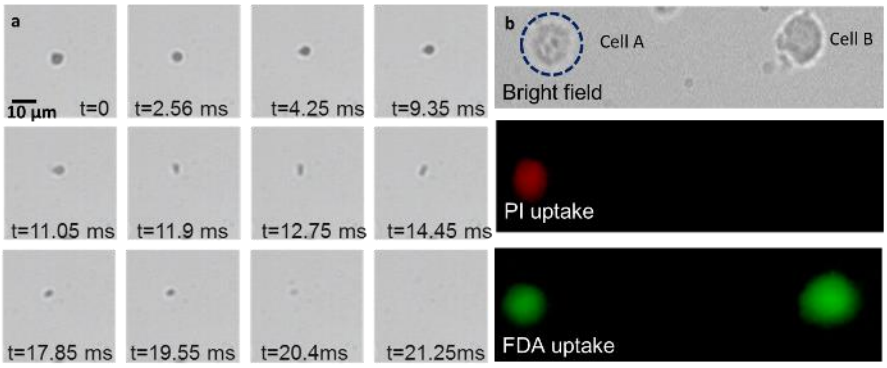

IUS2-G-6

Acoustic Radiation Forces in Monitoring of Nanoparticles in Biological Fluids

Aba Priev[1], Victor Ponomarev[1], Yechezkel Barenholz[1]; *[1]Biochemistry, Hebrew University, Jerusalem, Israel*

Background, Motivation and Objective

The high sensitivity of ultrasonic velocity and attenuation to composition and state of biomedical formulations and biological fluids containing nanoparticles is now well established. Unfortunately, existing devices include measurements of the acoustic properties of fluids at different temperatures and therefore require waiting for temperature equilibration of the fluid sample when the sample is heated or cooled and cannot be used for real-time monitoring.

Statement of Contribution/Methods

In this paper an innovative technology for particle monitoring based on ultrasonic standing waves has been described. A proprietary unique feature of the developed ultrasonic technology is that it employs a combined mode of operation using high-intensity standing waves for separation of the nanoparticles of fat, protein, liposome formulations, and bacteria, and low-intensity standing waves for compositional analysis.

Results/Discussion

High accuracy for ultrasound velocity measurements (up to 0.0002%) and ultrasound attenuation (of about 0.2%) have been achieved. Testing of the ultrasonic system was carried out on different protein and liposome formulations. Comparative analyses of the ultrasonic method with standard reference techniques have produced linear calibration curves for major components, with correlation coefficients higher than 0.98. It is thus possible to monitor content of protein, fat, liposome and bacteria in biological fluids.

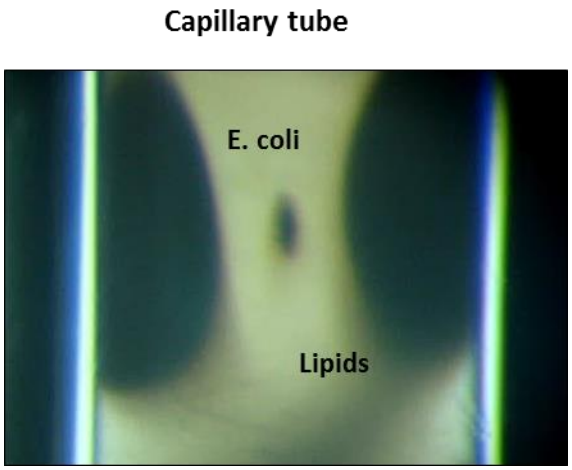

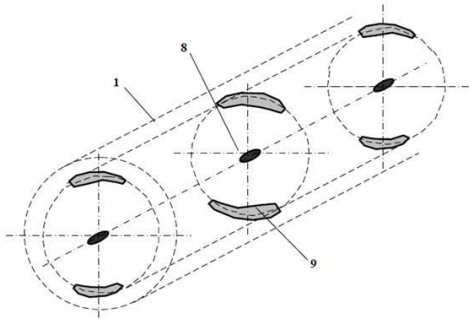

CMUTs and Airborne Applications

T1

Wednesday, July 24 2013, 10:30 am - 12:00 pm

Congress Hallair: **Yongrae Roh**
Kyungpook National University

IUS5-G-1

Air-coupled CMUTs operating at ambient pressures ranging from 1 to 20 atm

Min-Chieh Ho[1], **Kwan Kyu Park[1]**, Kristian Eckhoff[2], Mario Kupnik[3], Butrus T. Khuri-Yakub[1]; *[1]Edward L. Ginzton Laboratory, Stanford University, Stanford, CA - California, USA, [2]Fluenta AS, Bergen, Norway, [3]Brandenburg University of Technology, Cottbus, Germany*

Background, Motivation and Objective

We present FEA results and validation measurements of capacitive micromachined ultrasonic transducers (CMUTs) in permanent contact mode over a wide pressure range (1-20 atm). The CMUTs are designed so that their plates are already in contact with the bottom of the cavities during operation over the entire pressure range. This design has been proven to offer an operating frequency and coupling efficiency which are less sensitive to the change of ambient pressure (Ho et. al., IUS 2010). In this work, we present an improved design, including fabrication process details that allowed us to extend the pressure range by 285%.

Statement of Contribution/Methods

Previously we presented pitch-catch measurement results for a pair of CMUTs up to 7 atm. To improve the mechanical strength of the devices to withstand even higher pressures, several changes were made in this iteration. The fabrication still is based on a thick buried oxide layer process (Kupnik, et. al., IUS 2010). With the goal to reach an improved mechanical strength, the silicon plate thickness was increased from 40 – 60 μm to 55 – 70 μm to provide smaller deflection-to-thickness ratios and a larger bonding area (315% - 802% of the previous design) was used. This time the gap was wet etched by tetramethylammonium hydroxide (TMAH), instead of deep reactive ion etching (DRIE), for better cross-wafer uniformity. We performed both electrical input impedance and acoustical pitch-catch measurements in a pressure chamber. The received signals were amplified by a low-noise amplifier with a gain of ~26 dB.

Results/Discussion

All designs with 2000 μm radii, 65-μm-thick plates, 7.7 μm gap heights and with 300, 500, and 700 μm wide bonding area overlap for the plate, performed from 1 - 20 atm without a single failure. The devices were biased at 200 – 275 V. The short circuit resonance frequencies increased monotonically from 127 kHz at 1 atm to 525 kHz at 20 atm, which is in excellent agreement to our model (< 4.5%). Pitch-catch measurements with burst excitation were performed with a pair of CMUTs with 700 μm bonding length biased at 250 V dc. After compensating for the amplifier frequency response and diffraction loss, the calculated insertion loss is -15 dB and -33 dB at 3 atm and 20 atm, respectively. The received signal had good SNR over the entire pressure range. The bandwidth increased from 8 kHz at 1 atm to 35 kHz at 20 atm, while the fractional bandwidth stayed at 7% from 1 to 20 atm.

Our results prove that the CMUTs in permanent contact mode are reliable and efficient over a wide pressure range and their response is consistent with our FEA predictions. In addition, these transducers are a good solution for chemical sensing in process industry or range finding applications in harsh environments.

This research is supported by Fluenta AS, Norway.

IUS5-G-2

Designing Lossless Wide Bandwidth CMUTs for Airborne Applications Using Nonlinear Effects

Asli Unlugedik[1], Abdullah Atalar[1], H. Kagan Oguz[1], Hayrettin Koymen[1]; *[1]Electrical and Electronics, Bilkent University, Ankara, Ankara, Turkey*

Background, Motivation and Objective

Airborne CMUTs designed with conventional methods do not yield a wide bandwidth operation because of the low acoustic impedance of air. In this paper, we propose a new approach for a wider bandwidth without sacrificing the sensitivity.

Statement of Contribution/Methods

A low quality factor can be achieved by either increasing the radius-to-thickness ratio, a/t_m, or reducing the material density-to-medium density ratio. Even with a relatively low density of silicon (2330 kg/m^3), the density ratio remains at about 2000. When a/t_m is increased, the resonance frequency becomes lower and atmospheric pressure strains the membrane by deflecting it. The stiffness [1] of the membrane increases and an upward shift in resonance frequency occurs. A relatively thin membrane with a low mass can act like high stiffness material when it is deflected beyond its linear operation limits. By this approach, the mechanical impedance of the membrane is lowered, resulting in a wider bandwidth operation. Crystalline silicon is a remarkably flexible material and its fracture stress is around 7000-9000 MPa [2]. These properties make it suitable to be used as a membrane material where the membrane is stiffened by static deflection. The ratio of center deflection to membrane thickness of the circular CMUTs is usually selected to be less than 0.2 to keep it in the linear region. In this operation mode, there is no stiffening effect. The lowest quality factor is achieved by the highest a/t_m ratio, which is limited by the gap height. In the linear operation mode, a quality factor of about 140 is achievable with silicon membranes. If the center deflection-to-thickness ratio is allowed to exceed 0.2, the stiffening effect comes into play, and lower quality factors are obtained. Higher a/t_m ratios, hence lighter membranes are possible for the same resonance frequency. Designs in this range must consider and control of the induced stress in the membrane. The stress induced by deflection due to atmospheric pressure and DC bias is the maximum at the periphery of the clamped membrane. To avoid any fracture in silicon, this stress must be kept below a safe level. We developed a design procedure in which a significantly lower quality factor is obtained with the minimum gap height at a given frequency.

Results/Discussion

We obtain very good agreement with the finite element analysis. As an example, we consider a membrane with a/t_m ratio larger than 100. The maximum induced stress, due to depression by atmospheric pressure and DC bias voltage, is kept at 1000 MPa. In this case, the mechanical quality factor can be made less than 50 at the 30 kHz resonance frequency.

[1] M. Kupnik, et.al., "F.E.A. of Stress Stiffening Eff. in CMUTS", ULTSYM, p. 487-490, 2008.

[2] Kurt E. Petersen, "Silicon as a Mechanical Material", Proceedings of the IEEE, vol. 70, NO. 5, 1982.

IUS5-G-3

CMOS-based Capacitive Micromachined Ultrasonic Transducers Operating without External DC Bias

Fang-Yu Lin[1], Wei-Cheng Tien[1], Pai-Chi Li[2]; *[1]BEBI, National Taiwan University, Taiwan, [2]Electrical Engineering, National Taiwan University, Taipei, Taiwan*

Background, Motivation and Objective

In this study, a zero-bias CMOS-based CMUT is proposed. Traditionally, a CMUT device has to be biased at approximately 80%~95% of the collapse voltage. The requirement of an external DC bias increases complexity of the front-end electronics. Furthermore, reliability issues and safety concerns are present and need to be considered. Recently, zero-bias CMUTs have been proposed and developed by pre-charging through direct wafer-bonding. In this study, we adopt such a design so that it is fully CMOS compatible and thus can be monolithically integrated with other interface circuits.

Statement of Contribution/Methods

The zero-bias CMOS-based CMUT is implemented based on TSMC 0.35μm CMOS-MEMS process. The collapse voltage is lowered down to 150V by scarifying the thinnest layer (polysilicon) as the gap and sealing the device by depositing a thin film of parylene C as shown in figure A. The charge traps are formed in membranes, insulating layers and also the interface between those layers. We use a pulser for excitation and thus there is no DC bias applied. During each pulse excitation, extra charges are injected into the charge traps in the device and retain there for several seconds. Consequently, these charges create an inter-electric field to increase the receiving sensitivity.

Results/Discussion

Figure B shows a C-scan image of a coin obtained by the proposed device. No drift and no decay were observed after long operating time. Compared with conventional CMUTs, zero-bias CMOS-based CMUTs show comparable bandwidth and sensitivity performance as demonstrated in the spectra shown in figure C (solid: zero bias, dotted: 20V). Performance of the proposed zero-bias CMUT is comparable with the conventional design where a DC bias is required. We believe that this is the first time that a zero-bias CMOS-based CMUT is demonstrated in the literature.

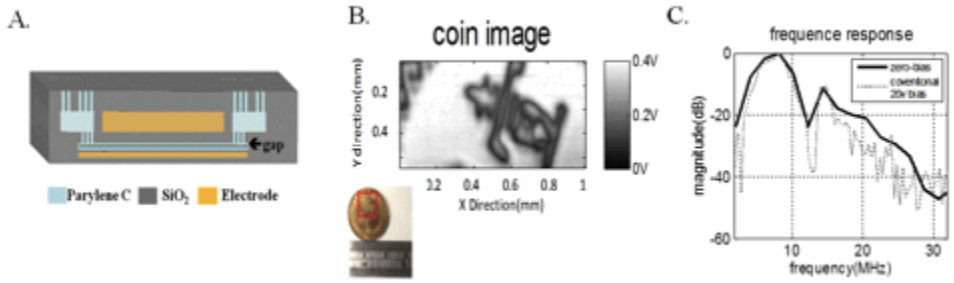

Figure (A)Cross sectional view (B)Image made from the proposed device(C) zero bias (solid) and 20V (dotted)

IUS5-G-4

Phase shift micro-beamforming of CMUT arrays using the spring-softening effect

Alessandro Stuart Savoia[1], Giulia Matrone[2], Giovanni Magenes[2], Nicola Lamberti[3], Giosuè Caliano[1]; *[1]Dipartimento di Ingegneria, Università degli Studi Roma Tre, Roma, Italy, [2]Dipartimento di Ingegneria Industriale e dell'Informazione, Università degli Studi di Pavia, Pavia, Italy, [3]Dipartimanto di Ingegneria Industriale, Università degli Studi di Salerno, Fisciano, Italy*

Background, Motivation and Objective

In phased array systems, a partial beamforming can be carried out inside the probe to reduce the channel count from the transducers to the main imaging system. Such technique, known as micro-beamforming, involves the application of a delay-and-sum beamforming to small groups of adjacent array elements using dedicated electronics.

In Capacitive Micromachined Ultrasonic Transducers (CMUTs), it is possible to control the dynamic behavior by exploiting the spring-softening effect due to the electrostatic force non-linearity. In particular, the phase of the transmission and reception frequency responses can be varied by adjusting the bias voltage applied to the CMUT.

In this paper we propose a phase shift micro-beamforming method based on the spring-softening effect in CMUTs. We analyze the performance obtainable from the application of this method to a typical phased array configuration for medical imaging.

Statement of Contribution/Methods

By using a lumped parameter model, we analyze how the extent of the phase variation in response to a bias voltage change depends on the quality factor of the CMUT cells. We show that, using a relatively high quality factor CMUT although yet allowing broadband immersion operation, it is possible to obtain up to 90° phase shifts at the center frequency, by varying the bias voltage. By inverting the sign of the bias voltage, an additional 180° phase shift is achievable.

Using Field II software, we model a 16-element phased with a pitch of 2λ. Each array element is divided into 4 sub-elements, spaced λ/2, to each of which different impulse responses, computed at the bias voltages corresponding to the desired phase shifts at the center frequency, are assigned.

We perform simulations using narrowband (continuous wave) and broadband (1- to 4-cycle sinusoidal bursts) excitation signals. Transmission and two-way beampatterns, and point spread functions are computed for different steering angles.

Results/Discussion

We show that, with a 50% -6 dB two-way fractional bandwidth CMUT, the grating lobe level of the transmission and the two-way radiation patterns may be kept below respectively -23 dB and -46 dB using broadband excitation signals for maximum steering angles of ±45°.

We finally discuss the benefits of the application of this method to 2D phased array systems.

It is worth highlighting that the proposed micro-beamforming method, unlike the other approaches previously presented, can be used both in transmission and reception operation. It also allows to control all the micro-beamformers in parallel, thus reducing significantly the number of required driving signals.

IUS5-G-5

An experimental study on coded excitation in CMUT arrays to utilize simultaneous transmission multiple-zone focusing method with frequency divided sub-band chirps

Bae-Hyung Kim[1], Seungheun Lee[1], Youngil Kim[1], Kyungil Cho[1], Taeho Jeon[1], Jongkeun Song[1]; [1]*Samsung Advanced Institute of Technology, Samsung Electronics Co., Yongin-si, Gyeonggi-do, Korea, Republic of*

Background, Motivation and Objective

CMUT-on-ASIC integration techniques are promising for the development of lower cost smaller volume scanners with higher performance in terms of features and image qualities because it minimizes parasitic capacitances and ultimately improves signal-to-noise ratio (SNR). Moreover, a frequency bandwidth of CMUT array is known as relatively broader than that of other ultrasonic transducer arrays. To utilize the wide bandwidth characteristic of the CMUT arrays, in this paper, we investigate a FDMA (frequency division multiple access) based ultrasound imaging technique by simultaneously firing orthogonally band-divided chirp signals with CMUT arrays to provide dynamic transmit focused imaging.

Statement of Contribution/Methods

In this work, the frequency divided sub-band chirps with orthogonal property are simultaneously fired on multiple ranges, in which each signal is focused at a different range, in one transmission event. This paper also presents an ultrasound image-formation method and a modulation and demodulation process of orthogonal sub-band coded signals designed within the frequency bandwidth of the CMUT arrays. The presented method is verified by computer simulations and experiments. The -6dB bandwidth of CMUT arrays that we developed is about 120% of 4.6 MHz center frequency, which is more than twice that of the conventional transducer arrays. In this work, two-way point-spread-functions (PSFs) of the pulsed-wave (PW) system to compare the presented FDMA based multi-zone focusing method with the conventional single frequency (SF) focusing method using a short pulse are simulated using Field II. In the experiment, two sub-band chirp signals with -6dB BW of 2MHz~4.2MHz and 7.3MHz~5.1MHz, respectively, are simultaneously fired with CMUT arrays to focus at different range. The chirp signal made by AWE (arbitrary waveform editor) in PC is down-loaded to AWG (arbitrary waveform generator) through GPIB board which connects PC and AWG (arbitrary waveform generator).

Results/Discussion

The simulation results using a computer generated tissue mimicking phantom show that the presented method can be achieved with both increased image quality and frame rate. The experimental results also verify that the simultaneously transmitted sub-band chirp signals for the presented FDMA based multi-zone focusing method are successfully separated into two compressed signals from a received RF-echo data. By using the captured RF-echo data, the pulse compression and separation with correlators are performed in PC. The presented method using orthogonal sub-band chirp signals is feasible for an ultrasound imaging technique using wide bandwidth CMUT arrays with higher performance in terms of features and image qualities. Currently, we are extending the presented approach to volumetric ultrasound imaging scanners using 2-D CMUT-on-ASIC arrays.

IUS5-G-6

Optimized airborne ultrasonic ferroelectret transducer by adjustment of transducer foam structure, elastic properties and charging degree

Martynas Sborikas[1,2], Michael Wegener[1,2]; [1]*Functional Materials and Devices, Fraunhofer Institute for Applied Polymer Research, Potsdam, Germany,* [2]*Institute of Physics and Astronomy, University of Potsdam, Potsdam, Germany*

Background, Motivation and Objective

Piezoelectric materials are widely used as sensor and actuator materials, while research in material development is focused on dipolar orientation processes, space-charge trapping mechanisms and electrical-mechanical interactions. Ferroelectrets, electrically charged cellular space-charge electrets, present the recent addition to the field of piezoelectric materials. Depending on the preparation, ferroelectrets show high piezoelectric activities, adjustable resonance frequencies, and very low acoustic impedances, they are light and flexible and usable in different acoustic transducer arrangements. For example, ferroelectrets are recently embedded as transducer materials into airborne sensor systems, phased arrays or vortex generators.

Statement of Contribution/Methods

Ferroelectrets are usually prepared by a gas-diffusion expansion of cellular polymer films, accompanied by a heat treatment. In order to render the cellular films piezoelectric, they are electrically charged either in a corona discharge or by applying an electric field in direct contact. The piezoelectric properties are determined by a mechanical excitation of a transducer film and in-situ measuring of the electrical output or by analysing the piezoelectric resonances with the impedance spectroscopy.

Results/Discussion

Here, we present processing and preparation methods for classical ferroelectrets which allow to adjust their coupling factor, acoustical impedance, resonance frequency, as well as their Figure of Merit (FOM). In detail, the correlation of geometric, elastic and charge-trapping properties of cellular samples to the determined ultrasonic transducer-related properties are discussed. Examples are: (i) Different processing routes of the foam structure of cellular films with an initial thickness of 40 µm allow e.g. the adjustment of the FOM in the range of 0.2 to 1.8 or from 0.1 to 1100 for ferroelectrets polarized either with low or with high electric fields. (ii) The film-thickness reduction of expanded cellular films results in slight or double increase of the electro-mechanical coupling coefficient, depending on the type of initial foam. (iii) In addition, an adjustment of the width of the transducer thickness-extension resonance is reported, e.g. an increase of width by a factor of about two compared with a non-treated sample. In general, preparation steps are discussed which lead to optimised air-borne ultrasonic transducer properties.

Materials and Processes for Microacoustics

T2

Wednesday, July 24 2013, 10:30 am - 12:00 pm

Congress Hallair: **Robert Aigner**
Triquint Semiconductor

IUS4-G-1

Electromechanical coupling k_t and GHz longitudinal wave velocity in ScAlN films near phase boundary

Masashi Suzuki[1], Takahiko Yanagitani[1]; [1]*Nagoya Institute of Technology, Nagoya, Japan*

Background, Motivation and Objective

Enhancement of piezoelectricity was recently found in Sc doped AlN film. Low electromechanical coupling k_t value in AlN films is a problem in BAW and SAW resonators, although they have high Q factor. In last year, we reported the increase of the kt value in $Sc_xAl_{1-x}N$ film ($0 \leq x \leq 0.35$). It is expected that the k value of ScAlN films reaches maximum near the phase boundary which should appear near x=0.5. However, the piezoelectric and elastic properties in the GHz range near the phase boundary have not been reported.

In this study, we investigate the effect of Sc concentration on k_t and GHz longitudinal wave velocity in ScAlN films near the phase boundary.

Statement of Contribution/Methods

HBAR (High-overtone bulk acoustic resonator) structure consisting of highly c-axis oriented $Sc_xAl_{1-x}N$ ($0 \leq x \leq 0.62$) film / Ti electrode film / silica glass substrate were fabricated by using Sc ingot sputtering. k_t value and longitudinal wave velocity were estimated from a conversion loss of HBARs.

Results/Discussion

As shown in Fig.1, the c-axis lattice constant estimated from XRD peak increased with increasing Sc from x=0 to 0.35, and started to decrease at x=0.35. Rocking curve FWHM are almost constant between x=0 and 0.39.

As shown in Fig.2, the k_t^2 value increased with increasing Sc from x=0 to 0.41. Significant decrease of the k_t^2 value was observed for x > 0.47. This decrease may be due to the phase transition from a piezoelectric wurtzite to a non-piezoelectric cubic. The longitudinal wave velocity decreased with the increase of Sc from x=0 to 0.41. The k_t^2 value and the velocity of $Sc_{0.41}Al_{0.59}N$ film near the phase boundary was 135% and 76% of that of pure AlN single crystal, respectively. Characteristic of the increase of k_t value and the decrease of the elasticity near the phase boundary are similar to well-known MPB in PZT.

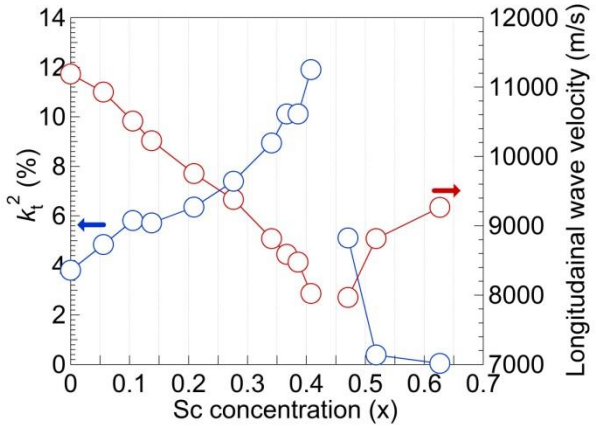

Fig.2 Electromechanical coupling k_t and longitudinal wave velocity of $Sc_xAl_{1-x}N$ films (x=0-0.62)

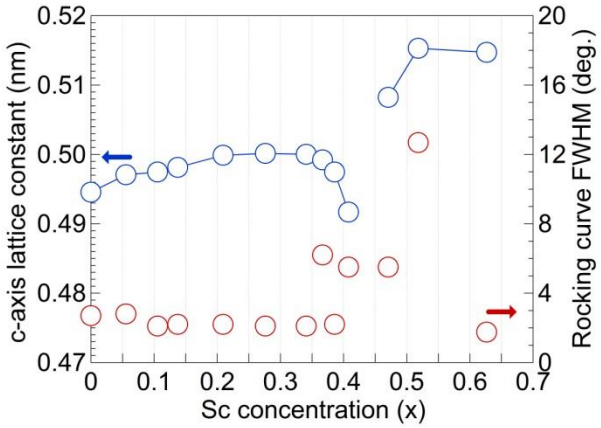

Fig.1 c-axis lattice constant and rocking curve FWHM of $Sc_xAl_{1-x}N$ films (x=0-0.62)

IUS4-G-2

Highly oriented (00.2) aluminum nitride close to single crystal using (111) Titanium Nitride buffer layer for microwave high power electro-acoustic devices

Ali Soltani[1], Abdelkrim Talbi[2], Vincent Mortet[3], Abdallah Bassam[4], Jean-Claude Gerbedoen[2], Gilles Patriarche[5], Jean-Claude Dejaeger[1], Phillipe Pernod[2]; [1]*IEMN-UMR CNRS 8520, PRES Université Lille Nord de France, France, France, Metropolitan,* [2]*LIA LICS-IEMN UMR CNRS 8520, ECLille, PRES Université Lille Nord de France, France, France, Metropolitan,* [3]*CNRS - LAAS; 7 Avenue du Colonel Roche, F-31077 Toulouse, France., France, Metropolitan,* [4]*Atomic Energy Commission Syrian, BP 6091, Damascus, Syrian Arab Republic, Syrian Arab Republic,* [5]*LPN-CNRS, UPR20, Route de Nozay, 91460 Marcoussis, France, France, Metropolitan*

Background, Motivation and Objective

During the last decade, a great interest was carried on the development of high power devices operating in super high frequency range involving wide band gap materials, mainly based on AlN, GaN and their alloys. Published works dedicated to the synthesis of crystallized AlN thin films report on MBE and CVD deposition techniques where high substrate temperature is required. Currently, the crystalline quality of AlN thin films deposited directly on silicon by low temperature Physical Vapor Deposition growth technique is generally considered as satisfactory. In most designs of piezoelectric MEMS/NEMS devices, we need to integrate a conductor electrode between the piezoelectric layer and the substrate. High power devices operating in microwave range requires the growth of a piezoelectric thin film highly-oriented along the total thickness on metallic buffer layer. The goal of this study is to synthesize a metallic buffer layer prior to AlN thin film deposition in agreement with these requirements.

Statement of Contribution/Methods

Titanium Nitride (TiN) thin film was chosen as a buffer layer because of its low electrical resistivity and low lattice mismatch between AlN(00.2) and (111) oriented cubic TiN. First, highly stress TiN thin films are deposited on (100) silicon substrate by sputtering at low temperature followed by a annealing under vacuum. This permits to reduce drastically the intrinsic stress and to improve the TiN crystal orientation and favors (111) planes. In the second time, highly oriented AlN thin films are successfully obtained by sputtering at low temperature on different TiN buffer layers (TiN/Si and TiN/Nanocrystalline diamond(NCD)/Si).

Results/Discussion

Figure 1 shows transmission responses of different acoustic wave devices. Sample 1 (S1) was performed on commercial AlN (MBE) on sapphire substrate used as reference. Sample 2 (S2) was performed on sputtered AlN/TiN/NCD on silicon substrate. Sample 3 (S3a) and (S3b) was performed on AlN/TiN/Si and free AlN/TiN membrane, respectively. Side lobe rejection of devices made on AlN including TiN buffer layer are similar to those obtained on epitaxial layer (S1). The integration of high quality AlN thin films on TiN/NCD membrane was also successfully achieved. The obtained performances are very promising to achieve high power electro-acoustic devices.

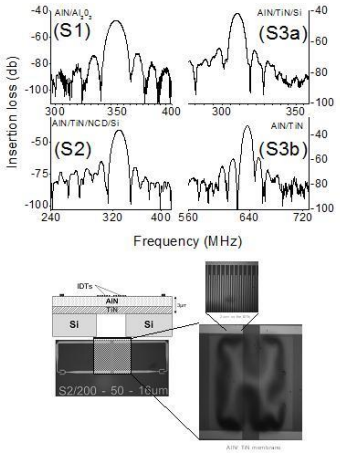

Fig.1: top view- Insertion loss of SAW devices made on AlN epitaxy on Al_2O_3 (S1), sputtered AlN (Sp) on Si(100) (S2), AlN(Sp)/TiN/NCD/Si(100) (S3a) and an AlN(Sp)/TiN membrane (S3b); bottom view- Schematic view of the composite membrane.

IUS4-G-3

ScAlN Lamb Wave Resonator in GHz Range Released by XeF_2 Etching

Akira Konno[1], Shota Sumisaka[2], Akihiko Teshigahara[3], Kazuhiko Kano[3], Ken-ya Hashimoto[2], Hideki Hirano[1], Masayoshi Esashi[1], Shuji Tanaka[1]; *[1]Tohoku University, Sendai, Japan, [2]Chiba University, Chiba, Japan, [3]DENSO CORPORATION, Nisshin, Japan*

Background, Motivation and Objective

40% Sc-doped AlN has about 5 times higher piezoelectric coefficient than AlN just by paying the penalty of doubled dielectric constant. On the other hand, the acoustic velocity of ScAlN decrease with increase in doped Sc, because the elastic stiffness decreases. To obtain both high phase velocity for GHz applications and high electromechanical coupling coefficient (k^2), ScAlN Lamb wave resonators in GHz range were studied.

Statement of Contribution/Methods

The ScAlN Lamb wave resonators were designed based on material constants reported in [1]. The schematic device structure is shown in Figure (a). 1 fÊm thick 40% Sc-doped AlN is deposited on a high resistivity Si wafer by co-sputtering Al and Sc targets. On it, an Al interdigital transducer (IDT) and reflectors are fabricated by electron beam lithography and lift-off. The ScAlN film is patterned by BCl_3/Cl_2 reactive ion etching with a photoresist mask to open etching windows for the following release etching. The Lamb wave resonators are finally released by isotropically etching underneath Si with XeF_2.

Results/Discussion

Our simulation suggested that S1 mode had a peak k^2 of 6.5% and a phase velocity of 6700 m/s around a ScAlN thickness of 0.5λ. In this study, the ScAlN thickness and the wavelength λ were set at 1 μm and 2 μm, respectively. S1 resonance frequency is expected to be 3.1 GHz, when the Al IDT thickness is 0.09λ. Figure (b) shows a SEM image of the completed device, where the ScAlN membrane buckled due to a compressive stress of about 1 GPa. Figure (c) shows a typical admittance characteristic near the S1 resonance. A derived equivalent circuit and its frequency response are also shown in Figure (c), showing good agreement with the measured result. The resonance and anti-resonance are clearly seen at 2.63 GHz and 2.72 GHz, respectively, corresponding to k^2 as high as 7.9%. These measured frequencies are somewhat lower than the predicted ones. This discrepancy is probably due to inaccuracy of the used material constants. The quality factors at the resonance and anti-resonance are 136 and 132, respectively, which could be much improved by eliminating parasitic impedances originated from process problems. In conclusion, we first designed, fabricated and tested the ScAlN Lamb wave resonators, and demonstrated the potentiality of high frequency applications.

[1] K. Hashimoto *et al*., IEEE Trans. UFFC, **60**, 3 (2013) in press.

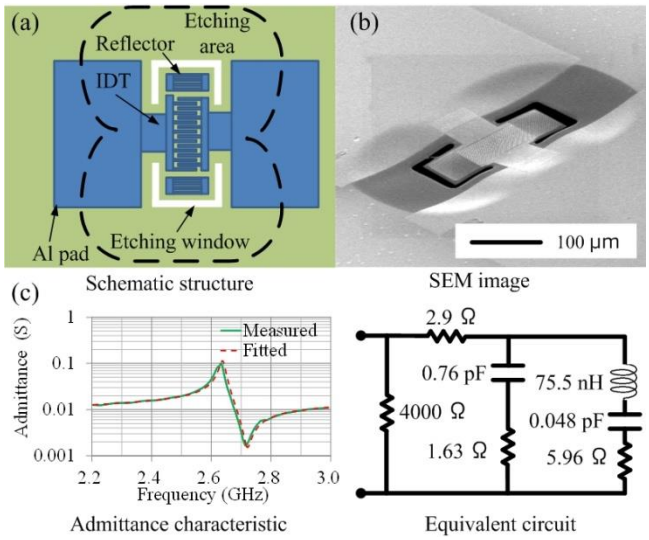

IUS4-G-4

Highly piezoelectric co-doped AlN thin films for bulk acoustic wave resonators

Tsuyoshi Yokoyama[1], Yoshiki Iwazaki[1], Yousuke Onda[1], Tokihiro Nishihara[1], Masanori Ueda[1]; [1]*TAIYO YUDEN CO., LTD., Japan*

Background, Motivation and Objective

Aluminum nitride (AlN) thin films have become a standard material for RF bulk acoustic wave (BAW) filters and duplexers in mobile communication systems. Recently, it has been reported that Al substitution by scandium (Sc) allows for an anomalous increase of piezoelectric response. Furthermore, a few research groups have confirmed large electromechanical coupling coefficients in Sc-doped AlN based BAW resonators. Therefore, doped AlN thin films have attracted significant interest due to improve in the resonance characteristics.

In this study, we investigated doping elements which improve piezoelectric properties of AlN by using computational material design method based on first-principle calculation and experiments.

Statement of Contribution/Methods

We have carried out first-principle calculation in order to investigate the effect of the doping element into AlN exerted on crystal structure and piezoelectric constants of doped AlN. Furthermore, we deposited the doped AlN thin films using reactive sputtering system and measured their lattice constants and piezoelectric constants.

Results/Discussion

We verified a significant increase of the piezoelectric constants of AlN with co-doping of magnesium (Mg) and zirconium (Zr) by first-principle calculation. Fig. 1 shows the dependence of the normalized piezoelectric constants of Mg and Zr co-doped AlN as a function of total concentrations of Mg and Zr. Here, the normalized piezoelectric constant indicates a piezoelectric constant normalized by the piezoelectric constant of pure AlN. The piezoelectric constant of Mg and Zr co-doped AlN was shown to gradually increase with increasing the total concentrations of Mg and Zr. When the total concentration of Mg and Zr was 35atomic %, the piezoelectric constant of Mg and Zr co-doped AlN exhibited about three times larger than that of pure AlN.

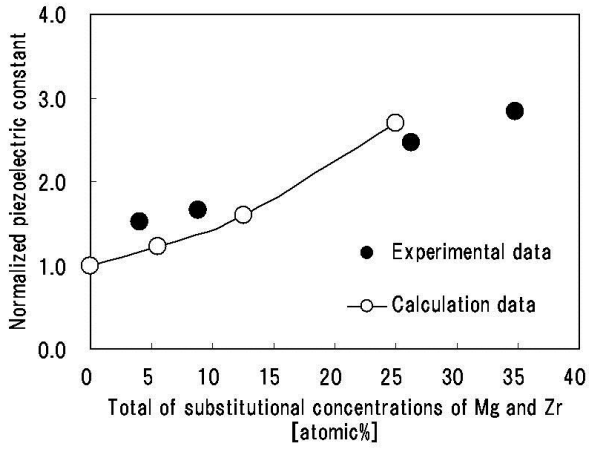

IUS4-G-5

Development of Stealth Dicing Technology for RF IC

Naoki Uchiyama[1], **Joji Sakakiyama[1]**; *[1]Electron Tube Division, Hamamatsu Photonics K.K., Iwata, Shizuoka, Japan*

Background, Motivation and Objective

Recently, portable devices such as Smart Phone or Tablet PC are required to deal larger communication capacity and faster connection speed, and Micro-acoustics (SAW, FBAR, MEMS and Transducers devices) as a key device for those requirements are evolving remarkably. As the market requiring RF devices grows, the demands for mass-productivity and cost reduction has been increasing. Processing LiTaO3 or LiNbO3 used as wafer substrate of those devices by conventional blade dicing has some issues like crack, chipping and slow process speed due to its fragile structure. Furthermore, improving chip acquisition rate by reducing process losses reached the ceiling.

Statement of Contribution/Methods

To popularize RF elements, breakthrough technology against these issues are essential. We support innovation in RFIC manufacturing by developing internal laser process (Stealth Dicing) technology to achieve high-speed and high-quality dicing process for RFIC devices.

Results/Discussion

Instead of conventional method, we originally developed the Stealth Dicing. By condensing permeable pulse laser inside wafer and high speed scanning, the stealth dicing provides high speed and high quality process without damage and debris on surface.

Now hundreds of SD engines have been already making a large contribution to reducing costs in semi-conductor manufacturing factories all over the world, especially Si-wafer such as MEMS or memory.

The attached picture shows cutting qualities of LT processed by the SD engine for LT/LN. Substantially there is no process loss, therefore SD engine enables to reduce dicing width to 10um minimum at design phase, and then acquisition rate per wafer becomes 11% higher (0.5mm square chip from 4inch wafer).

Processed Black-LiTaO3 t250 um : Surface (Left), Cutting Edge (Center), Cross-section Edge (Right)

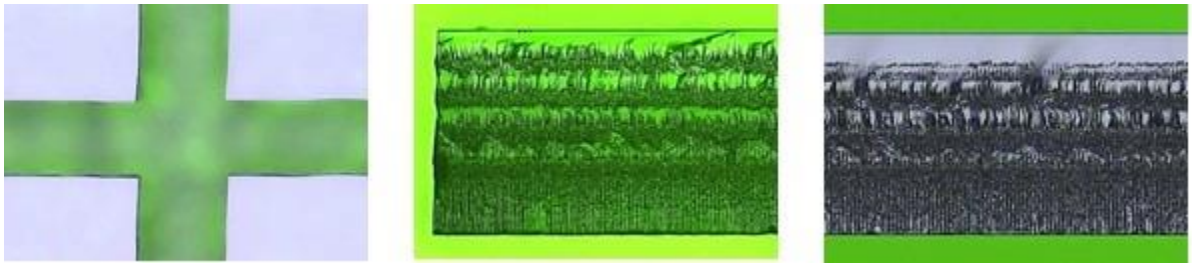

Photoacoustic imaging and microscopy

CONGRESS HALL

Wednesday, July 24 2013, 02:00 pm - 03:30 pm

Congress Hallair: **Stanislav Emelianov**
University of Texas at Austin

IUS1-H1-1

Studying Biological Systems with Multi-Spectral Optoacoustic Tomography

Vasilis Ntziachristos[1]*; [1]Institute for Biological and Medical Imaging, Helmholtz Zentrum München & Technische Universität München, Neuherberg, Bavaria, Germany*

Background, Motivation and Objective

Optical imaging is unequivocally the most versatile and widely used visualization modality in the life sciences. Yet it is significantly limited by photon scattering, which complicates imaging beyond a few hundred microns. For the past few years however there has been an emergence of powerful new optical imaging methods that can offer high resolution imaging beyond the penetration limits of microscopic methods. These methods can prove essential in cancer research.

Statement of Contribution/Methods

Of particular importance is the development of multi-spectral opto-acoustic tomography (MSOT) that brings unprecedented optical imaging performance in visualizing anatomical, physiological and molecular imaging biomarkers. One of the attractive features of the method is the ability to offer 10-100 microns resolution through several millimetres to centimetres of tissue and real-time imaging. In parallel we have now achieved the clinical translation of targeted fluorescent probes, which opens new ways in the interventional detection of cancer in surgical and endoscopy optical molecular imaging.

Results/Discussion

This talk describes current progress with methods and applications for in-vivo optical and opto-acoustic imaging in cancer and outline how new opto-acoustic and fluorescence imaging concepts are necessary for accurate and quantitative molecular investigations in tissues.

IUS1-H1-2

Coherence-weighted beamforming and automated vessel segmentation for improving photoacoustic imaging of embryonic vasculature using annular arrays

Parag V. Chitnis[1], Orlando Aristizabal[2], Ashwin Sampathkumar[1], Erwan Filoux[1], Jonathan Mamou[1], Jeffrey A. Ketterling[1]*; [1]F. L. Lizzi Center for Biomedical Engineering, Riverside Research, USA, [2]Skirball Institute of Biomolecular Medicine, New York University School of Medicine, USA*

Background, Motivation and Objective

In vivo imaging of embryonic vasculature is crucial to the study of developing physiology and congenital diseases. Mouse embryos are the preferred animal models for such studies, but require an imaging depth of several mm while maintaining sub-mm resolution. Photoacoustic (PA) imaging using high-frequency ultrasonic (HFU) transducers is a viable technique for depicting micro-vasculature. This work applies adaptive delay-and-sum (DAS) beamforming and automated vessel-segmentation algorithms to 3D PA data acquired from an in vivo mouse embryo using a HFU annular array for enhanced depiction of embryonic vasculature.

Statement of Contribution/Methods

A 5-element, 40-MHz annular array was modified to accommodate a co-axial, 532-nm laser beam and was raster scanned to acquire 3D PA-image data. At each scan location, one laser pulse was fired and the resulting PA signals were simultaneously digitized on all channels and recorded. The 5-channel PA data were processed using a conventional DAS algorithm and a coherence factor (CF), defined as the ratio of coherent energy to the total energy, was computed at all depths. The DAS-processed A-line at each scan location was weighted with the corresponding CF line. The performance of the conventional DAS and CF-weighted DAS were quantitatively compared using log-compressed B-mode images of an 80-µm diameter hair. 3D PA data were then obtained from a 12-day-old mouse embryo in an externalized, intact uterus. The 3D data were processed with CF-weighted DAS followed by an automated vessel-segmentation algorithm involving multi-scale Gaussian diffusion and 2nd order spatial derivatives.

Results/Discussion

The CF-based DAS scheme applied to the hair phantom improved SNR by more than 10 dB in comparison to conventional DAS. B-mode images of the hair with a 20-dB dynamic range obtained from CF-based DAS of PA data resulted in a lateral dimension of less than 200 µm at depths ranging from 8-20 mm, whereas the conventional DAS resulted in lateral dimension exceeding 1 mm at locations away from the geometric focus. A similar improvement in SNR was observed for the processed embryonic data as was a qualitative improvement in sharpness of vasculature. In addition, the vessel-segmentation algorithm suppressed speckle and connected vascular structures together, which enhanced depiction of major blood vessels in the mouse embryo.

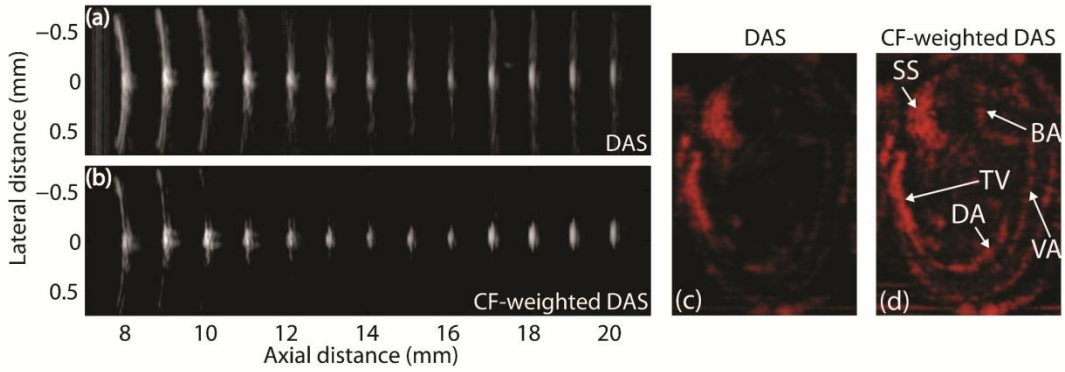

B-mode image of an 80-μm hair with (a) DAS and (b) CF-weighted DAS. Mid-sagittal section of a 12-day old embryo with (c) DAS and (d) CF-weighted DAS. SS: sagittal sinus, BA: basilar artery, TV: tail vein, DA: descending aorta, VA: vertebral artery.

IUS1-H1-3

3D Photoacoustic Imaging with Aperture-Encoded Top Othogonal to Bottom Electrode (TOBE) 2D CMUT Arrays

Roger Zemp[1], Alexander Sampaleanu[2]; [1]*University of Alberta, Edmonton, Alberta, Canada,* [2]*University of Alberta, Canada*

Background, Motivation and Objective

Photoacoustic imaging with 2D arrays may lead to high-resolution 3D imaging of optically absorbing chromophores for functional and molecular imaging. Technical challenges include unrealistic channel counts for directly wired large 2D arrays, non-trivial interconnects, and shrinking per-channel signal with decreasing element size. Capacitive micromachined ultrasound transducers (CMUTs) offer significant promise for dense 2D arrays, however, the afforementioned SNR challenges are compounded when active capacitance of small elements may be dwarfed by parasitic capacitance of interconnects and cables, and system complexity can be un-realistically high with large 2D arrays. Recently we introduced a unique top-orthogonal-to-bottom electrode (TOBE) 2D capacitive micromachined ultrasound transducer (CMUT) architecture capable of 3D ultrasound imaging with only N transmit/receive channels and N bias channels for addressing an NxN array.

Statement of Contribution/Methods

Here we apply TOBE CMUT arrays to photoacosutic imaging. By biasing only one column at a time and routing receive signals along rows, all the elements in the column may receive photoacoustic signals in parallel. Dynamic receive focusing is then applied to form a laterally-focused but elevationally unfocused RF B-scan for each laser pulse. Then another single column is biased to effectively scan the active columnar linear array from column to adjacent column. Synthetic aperture methods are then applied to retrospectively focus the set of RF data along the elevation direction to form a focused 3D image. This approach has the principal disadvantages that only a single column is effectively active and there is no active (but rather retrospective) elevational transmit focusing, leading to poor signal-to-noise ratio. To address this difficulty we propose a novel coded aperture pulse sequence that has the potential to significantly improve signal-to-noise without requiring additional pulses to form an image. Each laterally-focused B-scan is acquired with columns biased in an on/off binary pattern chosen from S-sequences which are rows of an NxN Hadamard S-Matrix in a way similar to encoding methods previously used to improve signal-to-noise in optical spectroscopy. While each pulse-echo measurement is due to the contributions of a number of binary-encoded columns, the signal due to each respective row can be decoupled by applying the inverse of the S-matrix to the measured data, followed by synthetic aperture retrospective focusing.

Results/Discussion

Analytical constructions, Field II simulations and experimental measurements validate the proposed technique. Because for each S-sequence, there are (N+1)/2 columns biased at a time, this scheme offers (N+1)/2 times the amount of receive signal over N bias sequences for an NxN array. The feasibility of the proposed technique is demonstrated in small 30x30 CMUT arrays interfaced to a Verasonics imaging system.

IUS1-H1-4

Multi-focus Optical Resolution Photoacoustic Microscopy

Parsin Hajireza[1], Alexander Forbrich[1], Roger Zemp[1]; [1]*ECE, University of Alberta, Edmonton, AB, Canada*

Background, Motivation and Objective

Optical-resolution photoacoustic microscopy (OR-PAM) uses optical absorption contrast to visualize superficial capillary networks and quantify morphological and functional parameters such as oxygen saturation and consumption; however, due to optical scattering in tissue high-resolution imaging is limited to within one transport mean free path (< 1mm).

There is a tradeoff between depth of focus and lateral resolution in OR-PAM, hence for high-ly focused high-resolution systems, only a small depth range is in focus. Therefore achieving a uniform energy distribution over the entire field-of-view with high resolution is very challenging

Statement of Contribution/Methods

In this paper for the first time we propose a multi-focused OR-PAM system taking advantage of stimulate Raman scattering (SRS) and chromatic aberration. A yterrbium-doped fiber laser is used to generate the SRS peaks in a 3.5m polarization-maintaining single mode fiber with wave-length peaks at 543, 560, 570, 580, 590, and 600nm and pulse energies between 300 and 400nJ. The divergent multi-wavelength light at the output of fiber is collimated using a collimator lens, scanned by 2D galvanometer scanning mirrors, and focused tightly using an objective lens. The collimator lens and objective lens are chosen to take advantage of chromatic aberration so that different wavelength bands focus at slightly different depths. The maximum amplitude of photo-acoustic signals is mapped to form C-scan images.

Results/Discussion

This technique dramatically improves the depth of focus of OR-PAM from ~30µm to ~400µm and provides a uniform resolution and energy distribution for the entire field of view of 3D blood vessel networks. The effective signal-to-noise ratio of C-scan Maximum amplitude projection images is improved by ~50% due to improved visualization of vessels at different depths. Figure 1 shows carbon fiber network images using (a) 532nm, (b) 560nm and (C) the combination of 532,543 and 560nm wavelengths. The result shows that the combination of all wavelengths with bigger depth of field provides more structural details at different depths. The improved depth of focus could be valuable for structural imaging of microvascular morphology without the need for mechanical scanning in the depth direction.

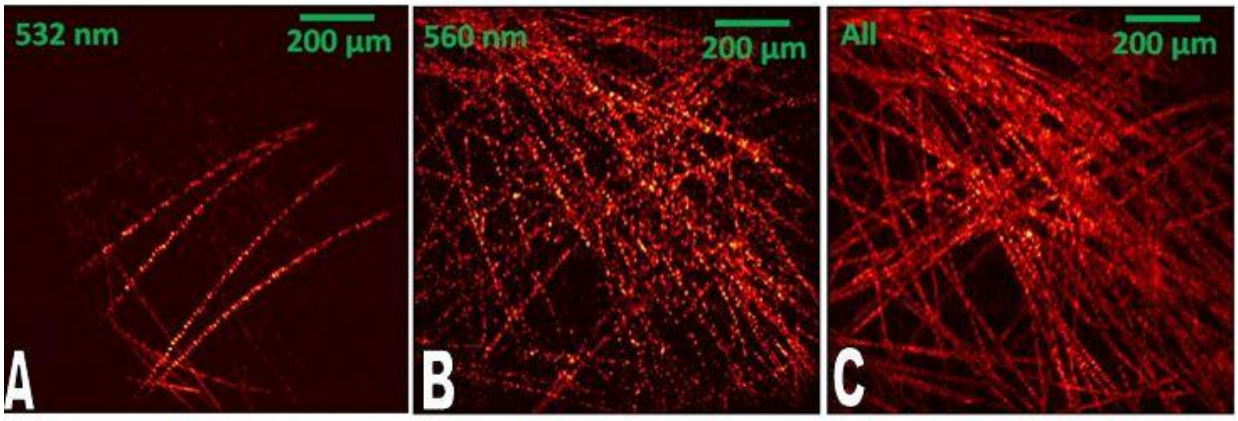

IUS1-H1-5

Feasibility of optical-resolution photoacoustic microscopy through a multi-mode optical fiber

Olivier Simandoux[1], Ioannis N. Papadopoulos[2], Salma Farahi[2], Jean-Pierre Huignard[3], Christophe Moser[2], Psaltis Demetri[2], Emmanuel Bossy[1]; *[1]Institut Langevin, ESPCI ParisTech, CNRS, INSERM ERL U979, Paris, France, [2]School of Engineering, Ecole Polytechnique Fédérale de Lausanne (EPFL), Lausanne, Switzerland, [3]Jphopto-consultant, Paris, France*

Background, Motivation and Objective

Optical resolution photoacoustic microscopy (OR-PAM) is a recent and rapidly developing imaging technique that has the ability to provide label-free images of tissue based on optical absorption with micron scale resolution close to the tissue surface. Previously reported OR-PAM setups are based on a conventional focusing and scanning system that usually comprises of lenses and mechanical actuators, limited to external tissue surface. In this work, both focusing and scanning are done through a multimode fiber using digital phase conjugation (DPC) in a lensless setup without mechanical actuators. The main objective of this work is to demonstrate the feasibility of OR-PAM using DPC through a multimode fiber.

Statement of Contribution/Methods

The imaging setup is in a transmission configuration. The imaged samples consisted of ≈20 µm diameter nylon wires immersed in a water tank. The wires were illuminated through a 200 µm diameter multimode fiber by 5 ns laser pulses at a wavelength of 532 nm. A diffraction limited focus spot was scanned through the fiber using a phase-only SLM (Papadopoulos et al, Optics Express 20(10), 2012). A spherically focused PVDF transducer with a central frequency of 20 MHz and transverse focal dimension of approximately 200 µm was used to detect the photoacoustic signals.

Results/Discussion

Fig. 1(b) shows a photoacoustic image of the wires, corresponding to the bright-field optical image shown in Fig. 1(a). The image is taken 250 µm away from the fiber tip within the fixed focal plane of the transducer. Fig. 1(b) clearly shows a micron scale resolution, defined by the focus spot size at the output of the fiber using DPC. Our results demonstrate the feasibility of OR-PAM at the distal tip of a multimode optical fiber, thus opening a wide range of applications, especially in minimally invasive endoscopic OR-PAM.

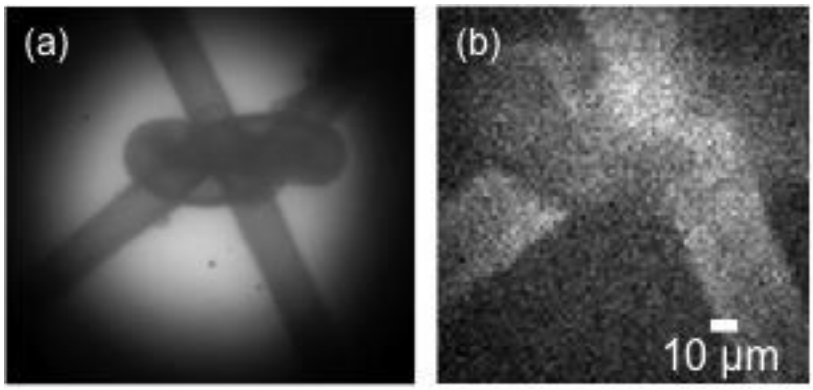

Blood brain barrier opening

M4

Wednesday, July 24 2013, 02:00 pm - 03:30 pm

Congress Hallair: **Kullervo Hynynen**
University of Toronto

IUS1-H2-1

A Preclinical Toxicological Study for Repeated Opening of the Blood-Brain Barrier with an Implantable Ultrasound Device

Catherine Horodyckid[1,2], Michael Canney[3,4], Alejandra Uzcategui Pedroza[4], Alexandre Vignot[1], Cyril Lafon[4], Jean-Yves Chapelon[4], Alexandre Carpentier[2,5]; *[1]CarThera Research Team, Brain and Spine Institute, Paris, F-75013, France, [2]Pitié Salpêtrière hospital, Neurosurgery Department, Assistance Publique Hôpitaux de Paris, Paris, F-75013, France, [3]CarThera Research Team, Brain and Spine Institute, Paris F-75013, France, [4]Inserm, U1032, LabTau, Lyon, F-69003, France, [5]Sorbonne University, Paris 6 school of Medicine, Paris, F-75013, France*

Background, Motivation and Objective

The main limitation to the efficacy of chemotherapy in the brain is the blood-brain barrier (BBB). It has been shown that delivery of pulsed ultrasound in combination with echogenic microbubbles can temporarily disrupt the BBB to deliver drugs that normally cannot reach interstitial brain tissue. We have developed an implantable ultrasound device for inducing broad and temporary opening of the BBB that can be easily used in routine practice during repeated chemotherapy sessions. Our previous studies on rabbits have shown that the BBB can be opened over a broad region within the brain and allow for uptake of chemotherapy agents with no acute effects for acoustic pressures of less than 0.7 MPa using a 1 MHz transducer.

The purpose of this study was to determine if BBB opening can be reproduced in an animal model with a cerebral volume closer to the size of humans. In addition, toxicity of repeated BBB opening by unfocused ultrasound was analysed using magnetic resonance (MR) and positron emission tomography (PET) imaging, electroencephalography (EEG), behavioural scales, and histopathologic analysis.

Statement of Contribution/Methods

Four beagle dogs and three primates were included in the study. The dogs were used for short-term toxicity experiments and a non-implantable 1 MHz ultrasound source was used for BBB opening with a followup period from 1 day to 1 week. Primates were used for long-term toxicity studies and received 7 ultrasound sonications every 2 weeks during the course of 3.5 months using an implantable ultrasound device. Toxicological analysis was performed using MRI, PET imaging, electrophysiological, behavioural, and histological analysis. The transducer was operated in pulse mode with a burst length of 25 ms and a pulse repetition frequency of 1 Hz for 120 seconds. Peak acoustic pressure levels from 0.6 MPa to 0.8 MPa were used and a microbubble contrast agent (Sonovue, Bracco Imaging, France) was intravenously injected (0.1 cc/kg) during sonications.

Results/Discussion

MRI images acquired after sonication showed a T1-contrast enhancement area underneath the transducer persisting for more than 4 hours that indicated a region of BBB opening that was 5 cm in depth and 1 cm in diameter. MRI control at day 1, 2, 7 and 15 showed normal healthy brain with a closed BBB. PET images with [18F]FDG and [18F]DPA-714 did not show any change in cerebral metabolsim of glucose or any signs of inflammation. No epileptic signs or non-pathologic cinduction were observed in EEG. Behavior in all animals appeared to be normal. Histological analysis showed no haemorrhagic processes, no petechia and only few red cell extravasations were observed.

The studies performed on each group confirmed that unfocused ultrasound emission can widely open the BBB with efficacy at an acoustic pressure from 0.6 MPa to 0.8 MPa without any acute, sub-acute or chronic lesions. Work supported by CarThéra SAS.

IUS1-H2-2

Investigating enhanced permeability of blood-brain barrier disruption (BBBD) using dorsal-based ultrasound exposure and two-photon imaging in an animal model

Tam Nhan[1,2], Alison Burgess[1], Kullervo Hynynen[1,2]; *[1]Physical Sciences, Sunnybrook Research Institute, Toronto, Ontario, Canada, [2]Medical Biophysics, University of Toronto, Toronto, Ontario, Canada*

Background, Motivation and Objective

Two-photon microscopy (2PM) allows real-time monitoring of focused ultrasound (FUS) and microbubble (MB)-assisted blood-brain barrier (BBB) disruption of intact cerebral vasculature. From this study, the enhanced permeability of the BBB can be qualitatively evaluated for substances of various sizes (10-70kDa dextrans-conjugated to Texas Red) at different acoustic pressures (0.2-0.8MPa).

Statement of Contribution/Methods

A thin cylindrical transducer was attached to the dorsal surface, covering a cranial window in the rat skull (Fig. 1a-b) and the transducer was driven in thickness mode (f=1.1MHz). The ultrasound focal zone was colocalized with the 2PM imaging field of view. Intravenously (IV) injected Texas Red (TR)-conjugated dextrans allowed visualization of the vasculature and served as a test substance to be delivered across the BBB. 2PM imaging was continuous over the course of the experiment; from the IV injection of MBs through the 120s sonication and ensuing leakage of TR from intra- to extra-vascular space (Fig.1c). Vessel segmentation of 3D microscopic data was performed to track averaged signal intensities of the two compartments over time (Fig. 1d). The apparent permeability constant was determined using an approach introduced by Dreher et al (M. R. Dreher et al, "Tumor Vascular Permeability, Accumulation, and Penetration of Macromolecular Drug Carriers", J. Nat. Can. Ins, vol. 98, p. 335-344, 2006).

Results/Discussion

The measured values for 10kDa and 70kDa range from 9.85e-4 to 1.09e-1 min-1 and 9.56e-4 to 5.33e-2 min-1, respectively. Fig. 1e summarizes the average permeability constants for both 10kDa and 70kDa TR-dextran at four pressure levels (n=5 per group). Statistical analysis shows a significant difference in the permeability constants between 10kDa and 70kDa at 0.6MPa and 0.8MPa. Overall, the linear increase of the permeability at increasing pressures agrees with MRI-guided FUS observations on signal enhancement of Gadolinium contrast agent (N. McDannold et al, "Use of Ultrasound Pulses Combined with Definity for Targeted Blood-Brain Barrier Disrup-tion: A Feasibility Study", Ultrasound in Med. & Biol., vol. 33, p. 584-590, 2007).

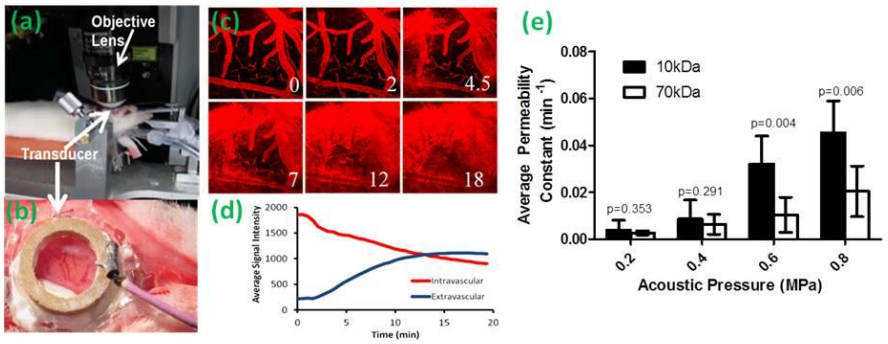

Fig. 1: (a) Experimental setup for dorsal-based BBBD with FUS+MB and 2PM monitoring. (b) Zoom-in of the cylindrical transducer. (c) An example of cerebral vasculature undergoing BBBD manifested as 10kDa TR extravasation. (d) Quantitative signal intensity changes in intra- and extra-vascular compartments over time of data shown in (c). (e) A comparison of permeability constant measured for 10kDa and 70kDa at acoustic pressure range of 0.2-0.8MPa.

IUS1-H2-3

Transcranial mapping of microbubble oscillations during focused ultrasound blood brain barrier disruption: modeling and experimental validation in macaques

Costas Arvanitis[1], Greg Clement[1], Margaret Livingstone[2], Nathan McDannold[1]; *[1]Radiology, BWH, Harvard Medical School, Boston, Massachusetts, USA, [2]Neurobiology, Harvard Medical School, USA*

Background, Motivation and Objective

Several emerging therapies with potential for use in the brain harness interactions between ultrasound and microbubbles generated during sonication or introduced into the vasculature, but methods to monitor them in real-time are in their infancy. Here, we investigated the ability of passive imaging to localize and characterize acoustic cavitation transcranially during focused ultrasound-induced blood brain barrier disruption (FUS-BBBD). This ability was evaluated numerically and experimentally in macaques.

Statement of Contribution/Methods

We developed a 3D FDTD simulation that takes into account the density, speed of sound and absorption of the brain and bone segmented from CT scans, and numerically modeled the propagation of acoustic emissions emitted from oscillating microbubbles towards a US imaging array. We then used passive cavitation mapping to evaluate the apparent location of the cavitation activity after transcranial transmission. The simulations were compared to data obtained during FUS-BBBD experiments performed in macaques under MRI guidance using a clinical FUS system developed for transcranial sonication (ExAblate, InSightec). US images were obtained with a 64-element 3.21 MHz linear array and a research driving system (Verasonics). The US imaging plane was registered to the MRI using fiducial markers visible in both modalities; CT and MRI were aligned using rigid body registration. The location of the cavitation activity in the passive US imaging was compared to that of MRI-evident BBBD. The simulations allowed us to determine whether the macaque skull shifted the apparent location of the cavitation activity and to investigate the effect of activity outside of the US imaging plane. In total, we sonicated 4 locations in the cingulate cortex in 3 animals (10 ms bursts applied at 1 Hz for 1.5 min, 0.02ml/kg Definity). A total of 240 cavitation maps were obtained.

Results/Discussion

The simulations showed minor differences between the apparent and true location of the cavitation activity, suggesting that the macaque skull produced only limited aberration. Simulated out-of-plane cavitation sources (up to 10 mm) had only a minor impact (< ~1mm) on the localization accuracy. Overall, good agreement between the simulated and experimentally formed cavitation maps during FUS-BBBD was observed. The median distance between the cavitation activity and the resulting BBBD (0.0±7.5 and 0.3±1.0 mm in the axial and transverse directions of the US imaging) was close to the expected resolution, when passive imaging was performed using the speed of sound extracted from the simulations.

These results demonstrate that passive imaging can be used to localize cavitation activity transcranially during FUS-BBBD. They also suggest that hybrid US/MR imaging combined with CT images and numerical simulations can provide comprehensive planning and online guidance for FUS-BBBD and other emerging cavitation-based therapies.

IUS1-H2-4

Safety and efficacy of blood-brain barrier disruption with focused ultrasound in a mouse model of Alzheimer's disease

Alison Burgess[1], Sonam Dubey[2,3], Isabelle Aubert[3,4], Kullervo Hynynen[2,5]; *[1]Physical Sciences, Sunnybrook Research Institute, Canada, [2]Sunnybrook Research Institute, Canada, [3]Laboratory Medicine and Pathobiology, University of Toronto, Canada, [4]Biological Sciences, Sunnybrook Research Institute, Canada, [5]Medical Biophysics, University of Toronto, Canada*

Background, Motivation and Objective

Focused ultrasound (FUS) has been shown to effectively disrupt the blood-brain barrier (BBB) leading to a reduction of amyloid plaque load in a mouse model of Alzheimer's disease (AD). However, in the majority of AD patients, amyloid is also found deposited in the walls of vessels, disrupting cerebrovascular regulation and increasing the susceptibility of the vessels to breakage. Therefore, further investigation into the safety and efficacy of FUS-mediated BBB disruption in the presence of amyloid pathology is required.

Statement of Contribution/Methods

In this study, we used a transgenic (Tg) mouse model of AD and their non-transgenic littermates at 8 months of age. The 8 month old mice were chosen to represent late-stage AD since this is when the vessels will be the most compromised. The mice received weekly MRI-guided FUS treatments (1.68MHz, 10ms pulses, 1Hz PRF, 120s duration) to disrupt the BBB in the hippocampus and were assessed using several cognitive tests.

We also used two-photon microscopy for real time visualization of BBB disruption in the presence of vascular amyloid deposits. Image analysis was used to compare the temporal dynamics of BBB permeability in the Tg and non-Tg mice.

Results/Discussion

Following repeated FUS treatments to disrupt the BBB, the mice were subjected to tests of learning and memory. There was no difference between the performance of FUS-treated and control groups indicating the repeated FUS treatments did not result in cognitive deficits in Tg or non-Tg mice. Additionally, in some tests, FUS-treated Tg mice performed significantly better than their untreated Tg controls. These data suggest that repeated FUS treatments are safe and may even improve cognitive function in Tg mice.

Using two photon microscopy, we determined that BBB disruption occurs at similar pressures and in vessels of similar size in both Tg and non-Tg mice. However, the time required for the BBB to close following FUS is longer in the Tg mice.

Together this data suggests that FUS-mediated BBB disruption is both safe and effective for delivery of drugs to the brain in the presence of AD pathology.

IUS1-H2-5

Monitoring of FUS-induced BBB opening in non-human primates using transcranial cavitation detection in vivo and the human skull effect

Shih-Ying Wu[1], Fabrice Marquet[1], Yao-Sheng Tung[1], Tobias Teichert[2], Matthew Downs[1,2], Cherry Chen[1], Vincent Ferrera[2], Elisa Konofagou[1]; *[1]Biomedical Engineering, Columbia University, USA, [2]Neuroscience, Columbia University, USA*

Background, Motivation and Objective

Focused ultrasound (FUS) with microbubbles (MB) has shown great promise in assisting brain drug delivery by noninvasively and transiently opening the blood-brain barrier (BBB). For the treatment to be safe and effective toward clinics, real-time monitoring with transcranial passive cavitation detection (PCD) is critical without requiring on-line MRI. The objective of this study was thus to determine the PCD detection threshold through a human skull in vitro, and the feasibility of guidance of the BBB opening using PCD in non-human primates (NHP) in vivo for creating a uniform disruption spot with reproducibility at the pressures of safety.

Statement of Contribution/Methods

In the in vitro experiments, the in-house lipid-shelled, monodisperse MB (median diameter: 4-5 μm) were injected into a 4-mm channel in the phantom below a degassed human skull (cleaned and degreased parietal bone) to mimic a set of brain capillaries within FUS focal spot. During sonication (FUS frequency: 0.5 MHz, PNP in situ: 50-450 kPa, pulse length: 100 cycles, PRF: 10 Hz, duration: 2 s), a hydrophone confocal with the FUS transducer served as the PCD. The harmonic, ultraharmonic, and broadband signal amplitudes within 1-5 MHz of the PCD signals with and without the skull in place were separated using comb filters for quantifying the stable cavitation dose (SCD) and the inertial cavitation dose (ICD). In the in vivo experiments, the MB were injected intravenously in two rhesus macaques at the beginning of sonication (PNP in situ: 200-275 kPa, pulse length: 5000 cycles, PRF: 2 Hz, duration: 120 s), with a total of 23 sonications in caudate/putamen while monitoring the SCD and ICD in real time. Both T1-weighted and T2-weighted MRI were performed after sonication to confirm the opening and lack of edema, respectively.

Results/Discussion

The SCD using harmonic signals and ICD were calculated within the range of 1-5 MHz through the human skull and used to monitor the bubble activity during BBB opening in NHP in vivo with real-time feedback. BBB opening in primates was achieved with null ICD and found to be 96% successful and reproducible within millimeters without MR targeting or monitoring while maintaining the required safety.

In the in vitro experiments, the transcranial PCD attenuation was found to be 24-25 dB through the human skull, which was comparable to that of the monkey skull (23-25 dB). In the in vivo experiments involving 23 sonications in two monkeys, there was a 96% (22/23) success in opening the BBB. The BBB opening at 250-275 kPa showed a null ICD while the SCD reached a plateau at 20 dB in 10 s after the MB injection. The MR images confirmed high repeatability of the opening patterns over multiple trials with a mean lateral focal shift of 1 mm. No significant difference was observed in terms of PCD monitoring and BBB disruption between the caudate and putamen. No edema, behavioral or physiological changes were detected after treatment in any of the animals in this study.

IUS1-H2-6

Localized Delivery of the Neurturin (NTN) neurotrophic factor through Focused Ultrasound - mediated Blood-Brain Barrier Opening

Gesthimani Samiotaki[1], Oluyemi Olumolade[2], Shutao Wang[2], Elisa Konofagou[3]; *[1]Biomedical Engineering, Columbia University, USA, [2]Columbia University, New York, New York, USA, [3]Biomedical Engineering, Columbia University, New York, New York, USA*

Background, Motivation and Objective

The blood-brain barrier (BBB) constitutes the major obstacle in drug delivery to the brain, serving as a physical and metabolic barrier which excludes all hydrophilic molecules with molecular weight (MW) of above 400 Da. Focused ultrasound in conjunction with microbubbles has been shown to open the BBB non-invasively, locally and transiently to allow the delivery of molecules to the tissue parenchyma. Neurturin (NTN), a member of the glial cell-line derived neurotrophic factor family, has been demonstrated to have neuroprotective and regenerative effects on dopaminergic neurons, suggesting its therapeutic potential for Parkinson's disease (PD). The caudate putamen (CP) and substantia nigra (SN) are the brain structures mostly affected in PD animal models, and were selected as the target areas in this study.

Statement of Contribution/Methods

First, fluorescently tagged dextrans with MW of 40 kDa, on the same order of magnitude as the size of NTN (23.6 kDa), were used for the optimization of the acoustic parameters for drug delivery in both CP and SN. The FUS parameters were selected as follows: 1.5 MHz (center frequency), 0.45 MPa peak-negative acoustic pressure, 10 Hz PRF, 10000 cycles (6.6 ms), 1 min duration on each targeted location. Polydisperse manufactured in-house lipid-coated microbubbles (8×10^5 #/g) were injected prior to sonication. T1-weighted FLASH MR images (1 T , ICON, Bruker, Billerica, MA, USA) were used to detect and quantify the volume of the BBB-opening. NTN (20 mg/ kg, Invitrogen, CA, USA) diluted in saline was injected to CB57/bl wild type mice (25 g), and the diffusion was detected using fluorescent microscopy.

Results/Discussion

Opening volume in both CP and SN was measured 30.0 ± 1.8 mm ^{3} in T1-w MR images. Successful delivery of NTN was confirmed by fluorescent microscopy (Figure 1). The diffusion area was less than Dextrans, possibly due to NTN's low circulation half life. ELISA was performed to quantify the amount of NTN in the sonicated regions and was measured to be 210.58 ng, i.e., 0.04% of the 500 μg injected intravenously, which is comparable to the therapeutic dosages, delivered via convection enhanced delivery. These findings confirm the successful delivery of NTN to the brain parenchyma which could serve as a good therapeutic candidate for reversing the degenerative phenotype in PD animal models.

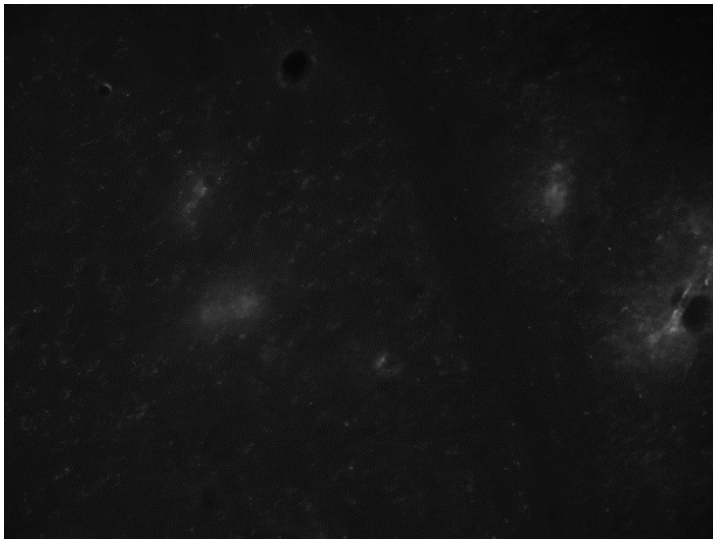

Soft tissue characterization II

M5

Wednesday, July 24 2013, 02:00 pm - 03:30 pm

Congress Hallair: **William O'Brien**
University of Illinois

IUS1-H3-1

Towards Backscattering Tensor Imaging (BTI): Analysis of the Spatial coherence of ultrasonic speckle in anisotropic soft tissues

Clément Papadacci[1], Mathieu Pernot[1], Mickael Tanter[1], Mathias Fink[1]; [1]*Institut Langevin, CNRS, ESPCI, Paris, France*

Background, Motivation and Objective

The assessment of fiber architecture is of major interest in the progression of myocardial disease. Recent techniques such as MR Diffusion Tensor Imaging or Ultrasound Elastic Tensor Imaging (ETI) can derive the fiber directions by measuring the anisotropy of water diffusion or tissue elasticity, but these techniques present severe limitations in clinical setting. We propose to investigate the anisotropy of the backscattered ultrasound field. The spatial coherence of the backscattered field was previously shown to vary with the fibers direction in composite solid materials. In this study, we measure the spatial coherence of ultrasonic speckle in skeletal muscles and myocardial tissues, determine the fibers directions and compare it to ETI.

Statement of Contribution/Methods

Acquisitions were performed using a linear transducer array (6MHz, 128 elements, 0.2mm pitch, Vermon) connected to an ultrasonic scanner (SuperSonic Imagine) mounted on a rotation device with angles from 0° to 355° by 5° increments to image ex vivo bovine skeletal muscle and porcine LV myocardial samples. At each angle, a focused ultrasonic pulse was transmitted and the backscattered echoes recorded. After backpropagation, the autocorrelation of the signals received on the transducers was performed by pairs to compute the spatial correlation function. The coherence factor was measured as the integral of the correlation function over 40 elements. Shear Wave Imaging was performed at each angle by imaging at 8,000 frames per second the propagation of a shear wave induced by the acoustic radiation force of a focused ultrasound burst (300µs).

Results/Discussion

The coherence varied by a factor of 3 with the probe angle in skeletal muscle and myocardium. In skeletal muscle, maximal/minimal coherence was found for the probe parallel/perpendicular to the fibers. In myocardium, the coherence was assessed across the entire myocardial thickness, and the position of maxima and minima varied transmurally due to the complex fibers distribution. The shear wave speed (3.9 m/s across the fibers to 5.9 m/s along the fibers) variation with the probe angle was found to follow the coherence variation. Spatial correlation can thus reveal the anisotropy of the ultrasonic speckle in skeletal muscle and myocardium. BTI could be used on any type of ultrasonic scanner for non invasive evaluation of myocardial fibers.

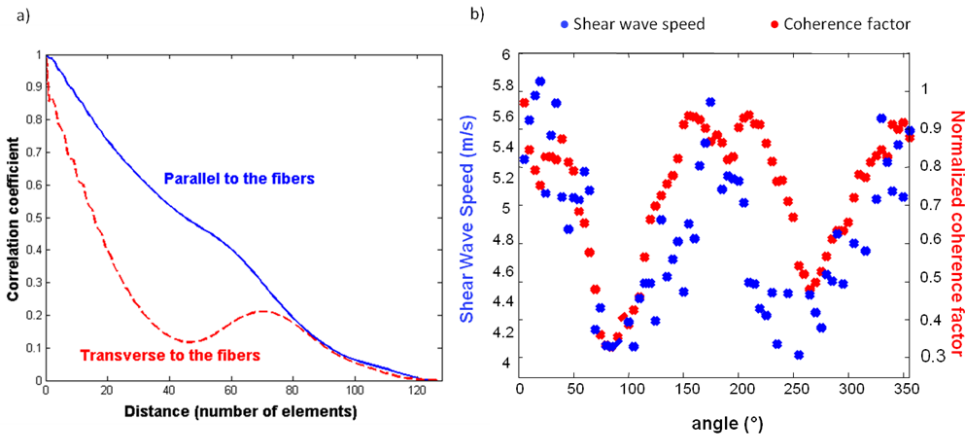

Figure: a) spatial correlation functions when the probe is set parallel and transverse to the fibers. b) Variation of the coherence factor and shear wave speed with the probe angle.

IUS1-H3-2

Sound Field Analysis for Biological Acoustic Impedance Microscope for Its Precise Calibration

Naohiro Hozumi[1], **Agus Indra Gunawan**[1], Shota Kajima[1], Sachiko Yoshida[1], Kazuto Kobayashi[2], Yoshifumi Saijo[3], Seiji Yamamoto[4]; [1]*Electrical and Electronic Information Engineering, Toyohashi University of Technology, Toyohashi, Aichi-ken, Japan,* [2]*Honda Electronics Co., Ltd, Toyohashi, Japan,* [3]*Tohoku University, Sendai, Japan,* [4]*Hamamatsu Univ Sch Med, Hamamatsu, Japan*

Background, Motivation and Objective

The authors proposed the acoustic impedance microscopy. A target is placed on a plastic substrate. Ultrasonic beam, which is focused on the target is transmitted and the reflection is received by the same transducer. The reflection is normalized by using pure water, and interpreted into acoustic impedance. As the beam is focused, oblique incident analysis is required to acquire a precise interpretation.

Statement of Contribution/Methods

Sound potential is calculated at a particular plane, and decomposed into plane wave components with different wave numbers using Fourier Transform. Both pressure and shear waves are generated and taken into account, when oblique incident impinging the substrate. If the propagating signals are shaped as pulse, pressure and shear waves can be separated in time domain. Reflection signal is calculated for each plane wave component, and the integral through the k-space represents the received signal.

Results/Discussion

As the substrate has higher acoustic impedance than target, the normalized reflection intensity reduces with the increase in acoustic impedance of the target. The experimental plots were acquired by using different contents of saline solutions do not agree with the curve calculated by assuming vertical incidence. However they agree with the calculation results by sound field analysis. Frequency dependence is negligible in the region of 30 - 100 MHz (Fig. 1).

By scanning the transducer, an acoustic impedance microimage was acquired and calibrated base on the above analysis, as shown in Fig. 2. Molecular, Purkinje, granular layers and white matters of cerebellar tissue of rat are clearly identified. As a conclusion, sound field analysis made it possible to precisely calibrate the response to a focused beam into characteristic acoustic impedance.

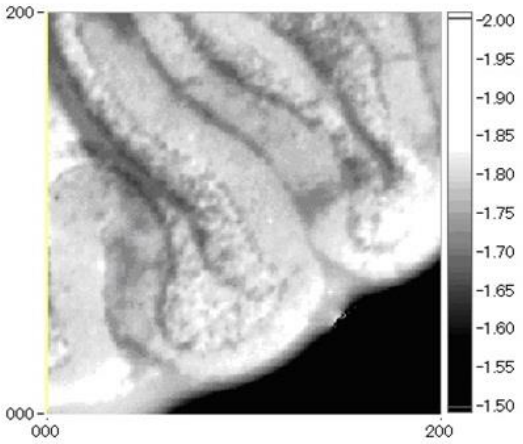

Figure 2. Acoustic impedance micro-image of cerebellar tissue of rat (2mm x 2mm, indicated in MNs/m^3).

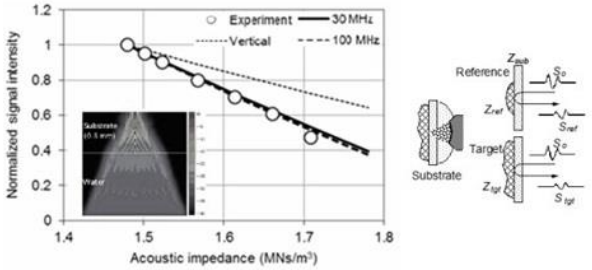

Figure 1. Signal intensity as a function acoustic impedance of the target. Normalized by the intensity when water is the target. Substrate: polystyrene. Vertical: assuming vertical incidence.

IUS1-H3-3

Spatial-resolution optimization of 3D high-frequency quantitative ultrasound methods to detect metastatic regions in human lymph nodes

Jonathan Mamou[1], Emi Saegusa-Beecroft[2], Alain Coron[3], Michael L. Oelze[4], Tadashi Yamaguchi[5], Masaki Hata[2], Eugene Yanagihara[2], Junji Machi[2], Pascal Laugier[3], Ernest J. Feleppa[1]; *[1]F. L. Lizzi Center for Biomedical Engineering, Riverside Research, USA, [2]University of Hawaii and Kuakini Medical Center, Honolulu, HI, USA, [3]Université Pierre et Marie Curie and CNRS, Paris, France, [4]University of Illinois at Urbana-Champaign, Urbana, IL, USA, [5]Chiba University, Chiba, Japan*

Background, Motivation and Objective

Proper staging and treatment of cancer require accurate detection of lymph-node metastases, but current histological methods fail to detect small, but clinically significant metastases. We used novel 3D quantitative ultrasound (QUS) methods to identify metastatic regions in freshly excised lymph nodes from cancer patients.

Statement of Contribution/Methods

Individual lymph nodes were scanned in 3D using a 26-MHz, single-element, F2 transducer with a 12-mm focal length. QUS methods quantified the backscatter coefficient to yield four estimates derived from RF signals in cylindrical regions of interest (ROIs) having equal lengths and diameters ranging from 0.4 to 1 mm. Step-section histology was performed at 50-µm intervals to assure that no clinically significant cancer would be missed. To optimize the tradeoff between QUS-estimate quality and the spatial resolution of the estimates, the effect of ROI size on estimate bias and variance was investigated using a database of 102 lymph nodes of colorectal cancer patients. Estimates were combined using linear discriminant approaches and ROC curves were computed to assess classification performance. A Bayesian approach was used to convert the discriminant scores to 3D cancer-probability estimates throughout each lymph node.

Results/Discussion

Figure 1 displays color-coded cancer probability for four ROI sizes; it shows that more voxels become ambiguous (orange) or positive (red) as ROI size decreases. Analysis indicated that ROIs with a 0.8-mm length and diameter improved spatial resolution and minimally degraded estimate quality with an average variance increase of <20% for each estimate. ROIs having 0.7-mm length and diameter improved resolution further, but variance increased by 30%. Smaller ROIs degraded estimate quality excessively. Finally, classification performance was not affected by ROI size when average QUS estimates throughout each lymph node were used to train classifiers. The area under the ROC curve remained greater than 0.95 for all ROI sizes.

Our QUS methods potentially can reduce the rate of false-negative determinations drastically by efficiently guiding pathologists to suspicious regions in lymph nodes, and having the best possible spatial resolution while retaining adequate estimate quality is critical. This study provides our first experimental basis for optimizing ROI size.

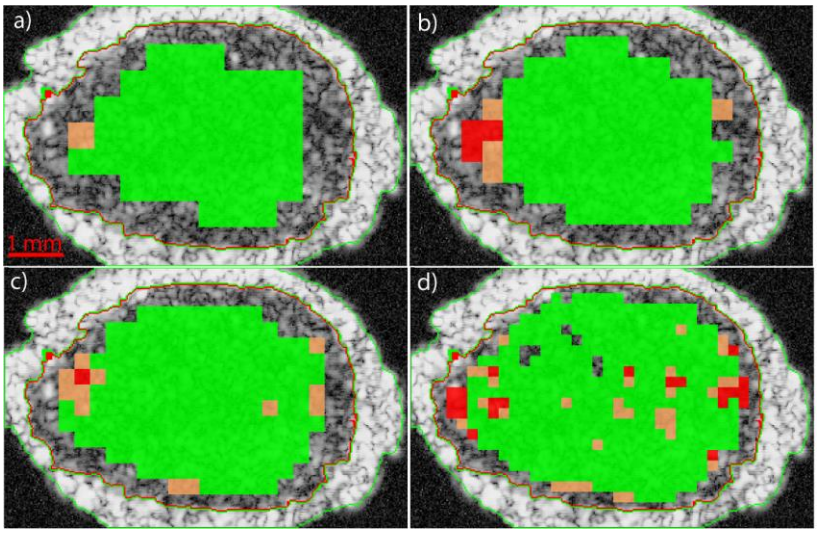

Fig. 1: Illustrative cancer probability QUS images of a non-cancerous lymph node as a function of ROI size: a) 1-mm length and diameter, b) 0.8-mm length and diameter, c) 0.6-mm length and diameter, and d) 0.4-mm length and diameter; "holes" indicate ROIs where the SNR was insufficient to obtain QUS estimates.

IUS1-H3-4

On the use of the Structure Factor Model to understand the measured backscatter coefficient from concentrated cell pellet biophantoms

Emilie Franceschini[1], Régine Guillermin[1], Franck Tourniaire[1], Edouard Lamy[2], Jean-François Landrier[3]; *[1]Laboratoire de Mécanique et d'Acoustique LMA-CNRS UPR 7051, Université d'Aix-Marseille, Marseille, France, [2]Laboratoire de Biochimie, Faculté de Pharmacie, Université d'Aix-Marseille, Marseille, France, [3]Nutrition, Obésité et Risque Thrombotique, UMR INSERM 1062/INRA 1260, Université d'Aix-Marseille, Marseille, France*

Background, Motivation and Objective

Quantitative ultrasound technique utilizes the amplitude and frequency dependence of the backscatter coefficient (BSC) to estimate the size and concentration of scatterers. QUS techniques rely on theoretical scattering models to fit the BSC from biological tissues to an estimated BSC using an appropriate model. Franceschini and Guillermin (J. Acoust. Soc. Am. 132(6) 3735-7347 2012) recently showed that the Structure Factor Model (SFM) was the more suitable theoretical scattering model for dealing with concentrated medium, such as densely packed cells in tumors. The aim of the present study is to use the SFM to understand and identify the scattering sites in concentrated cell pellet biophantoms.

Statement of Contribution/Methods

The biophantoms consisted of a suspension of human erythromyeloblastoid leukemia (K562) cells trapped in a mixture of plasma and thrombin. The biophantoms had identical cells (cell radius a_c around 7.64 µm) but have different cell volume fractions φ_c of 0.01, 0.05, 0.1 and 0.3. Ultrasonic backscatter measurements were made from frequencies from 10 MHz to 42 MHz using an ultrasound scanner (Vevo 770, Visualsonics, Toronto, Canada) equipped with the RMV 710 and 703 probes.

Results/Discussion

Figure 1 shows the measured BSC for four studied cell volume fractions: 0.01, 0.05, 0.1 and 0.3. In order to understand these four measured BSC behaviors, one cell (composed of a nucleus and of a cytoplasm) was assumed to scatter as an effective and single fluid sphere. An optimization procedure was then performed to minimize a cost function, which is the average over frequency of the difference between the sum of four measured BSC and the sum of four estimated BSC using the SFM. Two parameters were estimated: the effective scatterer radius a_{eff}=6.23 µm and the corresponding effective impedance contrast γ_z=0.0603. Note that the corresponding effective volume fraction was computed as $\varphi_{eff}=(a_{eff}/a_c)^3\varphi_c$, during the minimization procedure, assuming that the cell radius a_c and the cell volume fraction φ_c are known a priori.

Considering one cell as an effective and single fluid sphere, the SFM explains the amplitude and frequency dependence of BSCs from the four studied biophantoms. Future works are to extend the study to various cell volume concentrations and various cell lines.

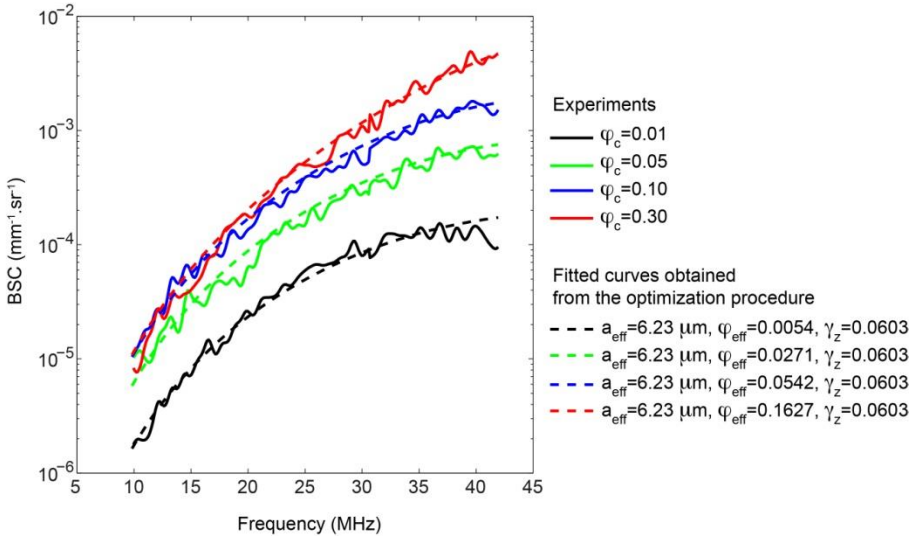

IUS1-H3-5

A Summary Measure of Backscatter Anisotropy in the Non-Pregnant Cervix

Timothy J. Hall[1], Lindsey C. Carlson[1], Quinton Guerrero[1], Helen Feltovich[1,2]; *[1]Medical Physics, University of Wisconsin, Madison, WI, USA, [2]Maternal Fetal Medicine, Intermountain Healthcare, Park City, UT, USA*

Background, Motivation and Objective

The uterine cervix is composed of pseudo-aligned and cross linked collagen. As the cervix softens, as it does during pregnancy in preparation for childbirth, the collagen cross links break down and the collagen fibers become disordered. Previous studies of acoustic backscatter with steered beams demonstrate excess loss in backscattered power (beyond that observed for spherical scatterers) indicative of the presence of aligned scattering structures. Surface plots of the excess backscattered power loss (eBSPL; see figure below) as a function of beam steering angle and depth into the cervix tissue demonstrate a great deal of difference between the degree of organization within these surface plots for the cervix of women who have never given birth (nulliparous) and women who have given multiple births (multiparous). Our intent is to develop a summary measure of the symmetry within these surface plots as a surrogate measure for the degree of organization of the collagen microstructure of the cervix. That summary measure could be an early indicator of collagen remodeling in pregnancy and a risk factor for preterm birth.

Statement of Contribution/Methods

Hysterectomy specimens were obtained from 36 subjects, 7 of whom received a prostaglandin agent (misoprostol) the night prior to surgery to ripen/soften the cervix. Specimens were bivalved, placed in saline solution, and scanned with a Siemens Acuson S2000 system using a prototype catheter linear array transducer aligned parallel to endocervical canal. Radiofrequency echo signals were obtained at five positions along the canal (10-30mm from the external os) with acoustic beams steered from -40^o to 40^o in steps of 4^o at each location. Similar measurements with the same system settings were acquired from a phantom to compute the eBSPL at each position along the cervical canal. A summary measure of the eBSPL surface plots incorporates their symmetry and the total eBSPL.

Results/Discussion

Multivariate analysis of the symmetry in the eBSPL surface plots, the total eBSPL and the summary measure demonstrates a significant difference in these surface plots between unripened and ripened hysterectomy specimens ($p < 0.001$ in all cases). This increased backscatter anisotropy suggests a significant difference in the collagen microstructure caused by the prostaglandins.

This work was supported by NIH grant R21HD063031.

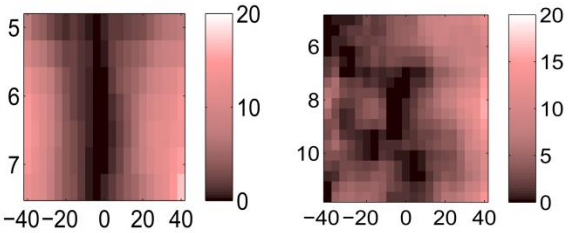

Surface plots of the excess backscatterer power loss as a function of beam steering angle and depth for a nulliparous cervix (left) and a ripened multiparous cervix (right). The summary measure of anisotropy are 11.6 and 3.49, respectively.

IUS1-H3-6

High-frequency backscatter analysis of human articular cartilage

Nils Männicke[1], Martin Schöne[1], Matthias Gottwald[2], Felix Göbel[3], Michael Oelze[4], Kay Raum[1]; *[1]Julius-Wolff Institute, Charité Universitätsmedizin Berlin, Berlin, Germany, [2]Department of Surgery, Hospital Köln-Holweide, Cologne, Germany, [3]Department of Orthopaedics and Traumatology, Carl-von-Basedow-Klinikum, Merseburg, Germany, [4]Department of Electrical Engineering, University of Illinois at Urbana-Champaign, Urbana, IL, USA*

Background, Motivation and Objective

Only a few studies have investigated acoustic backscatter originating from the cartilage matrix and so far only integrated spectral amplitudes have been considered in the analyses. More thorough spectral and envelope statistics analysis techniques may more accurately describe tissue alterations in the course of osteoarthrosis. Furthermore, ultrasound backscatter signals extend the diagnostic range from cartilage surface and subchondral bone parameters to the tissue matrix.

Statement of Contribution/Methods

52 punch biopsies of human cartilage were collected and scanned in time-resolved C-scan mode using a scanning acoustic microscope with a single-element 40-MHz transducer. From these data, spectra were estimated from short time gates at regions with low inclination and averaged with respect to their time delay to the tissue surface to account for the curved shape of articular cartilage. The depth-dependent spectral slope and amplitude profiles were used to estimate the maximum values within the first 300 µm. The surface reflection was excluded from analysis. In addition, the homodyned k distribution was used to model the signal amplitude of the envelope at tissue depths between 200 and 600 µm. The k (is ratio of coherent to incoherent signal energy) and µ (~ related to the scatterer number density) parameters were estimated from the envelope data. ANOVA was carried out for the acoustic parameters with respect to a subscore of the Mankin grading system that is related to cellular abnormalities of the cartilage matrix. The grading was performed on 2D histological cross sections by two trained clinicians. Additionally the cell number density was assessed.

Results/Discussion

Moderate positive correlations between cell number and backscatter amplitude (R^2=0.43) and μ (R^2=0.22), respectively, were observed. The backscatter amplitude parameters as well as k were not statistically significantly different with respect to cellular abnormalities, whereas μ was significantly lower for advanced stages of degeneration (F=3.6). The decrease and the extrapolation to the surface of the spectral slope were significantly higher for samples without signs of degeneration (F=3.5 and F=7.7, respectively). The highest significance levels and F-ratios were obtained for the maximum spectral slope value within the superficial zone of cartilage (F=21.4).

The results suggest that amplitude based parameters alone are insufficient to discriminate different stages of spontaneous degeneration and that in contrast, relational differences of frequency contributions as well as envelope statistics are sensitive to osteoarthritic changes. Due to the correlation of backscatter amplitude and cell number, differences of the spectral slopes are likely due to cellular degenerations. Future investigations will focus on elucidating scattering sources in order to improve the diagnostic potential of ultrasound for cartilage assessment.

Liquid and Flow

NH

Wednesday, July 24 2013, 02:00 pm - 03:30 pm

Congress Hallair: **Mario Kupnik**
Brandenburg University of Technology (BTU)

IUS2-H-1

Volumetric characterization of ultrasonic transducers for gas flow metering

Maik Hoffmann[1], Alexander Unger[1], Min-Chieh Ho[2], Kwan-Kyu Park[2], Butrus T. Khuri-Yakub[2], Mario Kupnik[1]; *[1]Brandenburg University of Technology (BTU), Cottbus, Germany, [2]Stanford University, Stanford, USA*

Background, Motivation and Objective

The optimum design of ultrasonic gas flow meters requires exact knowledge of transducer performance in terms of acoustic beam characteristics. In particular for commercially available air-coupled ultrasonic transducers, the information revealed in datasheets concerning beam profile shapes, often times is oversimplified. Another need is the characterization of efficient air-coupled capacitive micromachined ultrasonic transducers (CMUTs), in particular devices featuring new operation modes [Ho et. al., IUS 2010]. These devices are currently entering the large-pipe-diameter flow meter arena. Thus, we present an efficient transducer characterization system, capable to measure the complete volumetric sound pressure field with high spatial resolution. Further, we focus on details concerning data processing and how to visualize the results in such a way, that conclusions for designing ultrasonic gas flow meters can be drawn.

Statement of Contribution/Methods

First, by using a large PC-controlled 3D stage, we automatically position a calibrated 1/8″-microphone (B&K 4138-A-015, 6 Hz to 140 kHz) in a volumetric fashion in front of the transmitting transducer. During this first step, however, the center axis of the circular microphone is kept orthogonal to the transducer front face, which ensures efficient measurements, but requires a second step depending on the wavelength-to-aperture ratio of the microphone. Thus, in this second step the system allows a single angular response measurement to obtain a correction curve that is then used for all grid locations. For data acquisition an oscilloscope (Yokogawa ScopeCorder DL750) with a resolution of 16 Bit and a sampling rate of 1 MS/s is used. After gathering the data without any averaging, the system performs all required post processing for optional interpolation and visualization. Then all key parameters, such as sound pressure levels, beam profiles in 3D (symmetry and directivity), diffraction loss curves in arbitrary directions, and time of flight data (ideal for flow meter design), are extracted.

Results/Discussion

To demonstrate the capability of the system, we performed several characterization runs of single-cell CMUTs with a plate diameter of 4 mm. Based on a complete volumetric measurement, consisting of 29889 (27 x 27 x 41) locations over a total volume of 0.95 m^3, we compare the results side-by-side (3D-isosurfaces and 2D-slices in various directions) for two different CMUT biasing conditions (conventional and beyond pull-in point). These two biasing conditions produce two different plate mode shapes at two different frequencies (55.5 and 82.3 kHz).

The system allows us to design an ultrasonic gas flowmeter and to explore different transducer operation modes and flow cell arrangements. In addition, the system is also useful as a model validation platform for other applications, such as range finding, gesture sensing, anemometers, and ultrasonic communication, to name a few.

IUS2-H-2

A pMUT based flowmeter: a feasibility study

Paul van Neer[1], Tristan Robers[1], Arno Volker[1]; *[1]TNO, Netherlands*

Background, Motivation and Objective

About 15 years ago the first articles appeared in literature on the use of piezoelectric micromachined ultrasound transducers (pMUTs) to generate and receive sound. These pMUTs are efficient ultrasound sources and receivers in gasses, and are cheap to produce due to their lithographic production process. Making use of their 1st resonance frequency, a good signal to noise ratio (SNR) can be obtained with very limited power. This is of interest for low cost-low power gas flow meters.

However, using pMUTs in this application also poses challenges; 1) pMUTs are almost omnidirectional and 2) pMUTs are very narrow-banded. A pMUT's resonance frequency mainly depends on the membrane radius, which varies due to production. In the current work the suitability of pMUTs for a flowmeter is investigated.

Statement of Contribution/Methods

To match the resonance frequencies of the transmitting and receiving pMUTs, a DC bias voltage (from -4V to +4V) was applied to the transmitting pMUT.

The flow setup consisted of two pMUTs (radius 0.2 mm, resonance frequency 510 kHz) mounted on the same side of a pipe (cross-section 2 cm) with an inter-pMUT distance of 1 cm. The transmitting pMUT was excited using 5 V Gaussian apodized sine bursts with a bandwidth of 2 kHz at the pMUT's resonance frequency. The signals produced by the receiving pMUT were amplified by a custom made pre-amplifier. Pressurized air was used to create a gas flow past the pMUTs. The gas flow speed was calculated using a specially developed algorithm to extract accurate arrival times for narrow band signals.

Results/Discussion

By varying the DC bias voltage the pMUTs resonance frequency could be shifted by ~5 kHz (see figure), which was sufficient to match the resonance frequencies of both pMUTs. The application of a bias Voltage increased the intensity of the emitted sound by 8 dB. The SNR of the received signal was ~40 dB.

The direct sound path between the pMUTs provided a good estimate of the flow velocity. The first arrival in the time signal (at 30 µs) was the direct path between both pMUTs. 92 µs later the echo bouncing off the opposite wall of the rectangular pipe arrived. For flow velocities of a few m/s, time shifts of a few tenth of a wavelength are measured. With the current SNR this can be done with good accuracy.

An initial investigation of the suitability of pMUTs for gas flow measurements was conducted. Encouraging initial results were presented.

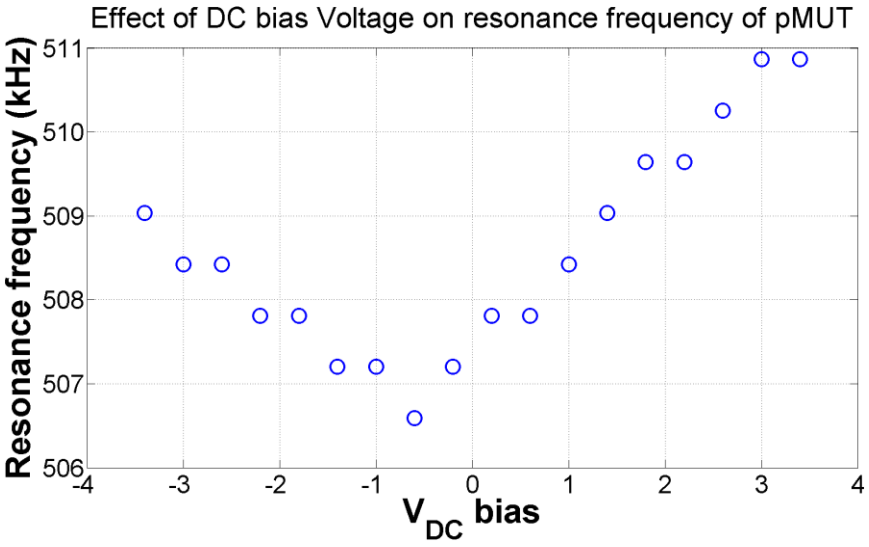

IUS2-H-3

A Robust Doppler Imaging Method Using Log-step Multicarrier Ultrasonic Signals

Yasushige Maeda[1], Masanori Sugimoto[2], Hiromichi Hashizume[3]; *[1]Department of Informatics, The Graduate University for Advanced Studies, Tokyo, Japan, [2]Department of Computer Science, Hokkaido University, Sapporo, Japan, [3]Information Systems Architecture Science Research Division, National Institute of Informatics, Tokyo, Japan*

Background, Motivation and Objective

The authors have reported the effectiveness of log-step multicarrier imaging which achieved an around 20 times improvement in ultrasonic Doppler velocity estimation than the traditional method. In this method we employed an ordered phase log-step multicarrier signal which consists of 54 different carriers with exponential frequency separations. This waveform, which does not change the mutual frequency ratios of the component carriers of the Doppler-affected signals, plays a central role for the high precision Doppler imaging. In this paper we describe an im-provement of our Doppler imaging methodology which shows the same precision level of veloci-ty estimation even under an SNR -10dB.

Statement of Contribution/Methods

Like other wide-band signals (e.g. frequency chirp signal), the cross-correlation of an ordered phase log-step multicarrier signal makes a temporal (range-detection) shift of a moving object. The amount of the temporal shift is given in the formula $\tau=T_1\ (1-(1/\rho))$ by theoretical calculation, where T_1 is one of the parameters to determine a log-step multicarrier signal, and ρ the amount of Doppler shift or the multiplicative factor to the frequency of the signal.

Two kinds of signals with different inclinations of temporal shift are obtained by specifying $T_1>0$ (up) and $T_1<0$ (down). We transmit a concatenation of up and down log-step multicarrier signals. As they provide the opposite temporal shifts of a detected moving object, we can estimate the velocity of the object by measuring the span between the temporal shifts. Hence by measuring the span, we calculate the amount of the Doppler shift ρ according to the formula.

Results/Discussion

We use this algorithm to estimate the amount of Doppler shift abstractly, and apply the previously proposed algorithm for a precise estimation. The resulting hybrid algorithm yields both high SNR tolerance and high accuracy for a wide estimation range.

A computer simulation showed a high availability of the hybrid algorithm (Fig. 1), which extends the estimation range $0.95<\rho<1.05$, and the SNR tolerance under -10dB.

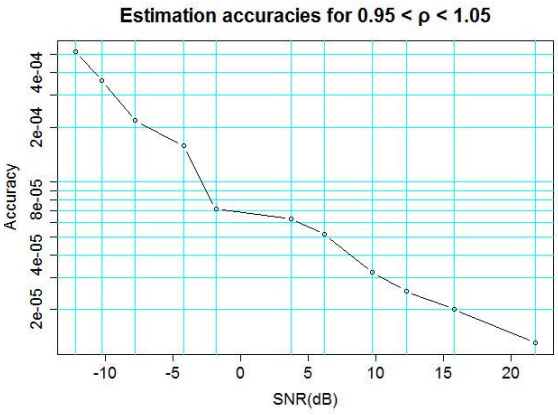

IUS2-H-4

Reflections and standing waves for particle concentration in microfluidic channels

Erin Dauson[1], Irving Oppenheim[1], Kelvin B. Gregory[1], David W, Greve[2]; *[1]Civil and Environmental Engineering, Carnegie Mellon University, Pittsburgh, PA, USA, [2]Electrical and Computer Engineering, Carnegie Mellon University, Pittsburgh, PA, USA*

Background, Motivation and Objective

There is considerable interest in the development of technology for separation and concentration of particles or bacteria in microfluidic channels using standing acoustic waves. For larger channels the wave periodicity is of the order of the wafer thickness; consequently the creation and interference of acoustic waves becomes complex. We have studied the concentration of particles in a channel 500 µm wide experimentally and by simulation.

Statement of Contribution/Methods

We fabricated interdigitated transducers with a periodicity of 200 micrometers in pairs on a 128° Y-cut $LiNbO_3$ substrate 0.5 mm thick. A PDMS microfluidic channel wide was adhered to the substrate between the two transducers. When driving a single transducer at frequencies near 20 MHz, 10 µm polystyrene spheres in water aligned at equilibrium positions spaced about 100 µm. The equilibrium positions shifted as the driving frequency was changed.

Impedance measurements were performed on the transducers before and after mounting the PDMS channel. Prior to mounting the channel, peaks in the real component of the impedance were observed with frequency spacing consistent with reflections from both the undriven transducer and the far edge. After mounting the channel peaks were reduced in magnitude and broadened and peak positions spread, with spacing consistent with reflection from the PDMS channel or the near edge. Peak broadening is expected because of acoustic damping in PDMS.

Simulations of the full length of the propagation path, including both transducers were performed using COMSOL 4.3a. Wave displacements were apparent through the full thickness of the substrate, possibly due to plate waves or interfering bulk waves. Complex behavior is not unexpected as surface waves undergo both reflection and mode conversion at discontinuities.

Results/Discussion

Standing waves for the localization and manipulation of particles can be created with a single driven transducer by taking advantage of reflections at discontinuities and edges. The prediction and control of equilibrium positions depends in a complex way on the transducer, substrate and channel dimensions. Fabrication of channels with low-loss material may be advantageous in enhancing standing wave amplitude.

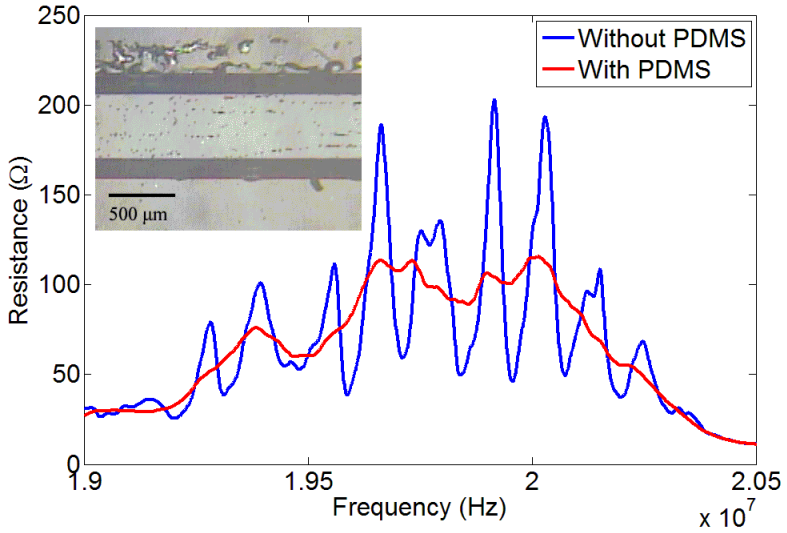

IUS2-H-5

Ultrasound Standing-wave Bio-Reactor design and testing on aerobic activated sludge

karel keesman[1], niels de beus[1], jan klok[1], hans cappon[2]; [1]*wageningen university, Netherlands,* [2]*HZ University of Applied Science, Netherlands*

Background, Motivation and Objective

In most wastewater treatment processes, solid-liquid separation is an expensive step. Usually, either a large basin for settling or membranes, which are prone to fouling and thus high operational costs, for filtration are implemented. In the, recently patented, Ultrasound Standing-wave Bio-Reactor (USBR), the settler or membrane unit is replaced by an ultrasonic separation device, using ultrasound standing wave technology (see e.g. Benes et al, 1997) at frequencies in the range of MHz, see Figure 1.

Figure 1. Photograph of the experimental set-up.

The main objective of this study is to experimentally investigate the ultrasonic separation efficiency of water-activated sludge suspensions, which is in line with our previous work on modelling and control in acoustic separation of suspensions using a numerical-experimental approach (Cappon and Keesman, 2012a,b; 2013).

Statement of Contribution/Methods

Two sets of experiments were performed. In the first set, the inflow and outflow were changed such that a setting for optimal separation efficiency could be derived.

The second set of experiments aimed at obtaining insight into the changes in biological activity of the activated sludge as a result of ultrasound exposure via activity tests.

Results/Discussion

Experiments on the activated sludge showed that a separation efficiency of approximately 95% was obtained at a filtrate flow rate of 0.4 L/h and a concentrate flow rate of 2 L/h.

Biological activity tests showed that the activated sludge remained viable when exposed to ultrasound.

In conclusion, ultrasound separation provides a promising technique that could have industrial application for activated sludge separation in the future.

References

Benes E, et al (2001) IEEE Ultrasonics Symposium, 7 - 10 Oct 2001, Atlanta, GA. USA 649 - 659.

Cappon HJ and Keesman KJ (2012), IEEE Trans. UFFC, vol. 59, no. 5, pp. 1023–1032.

Cappon HJ and Keesman KJ (2013) IEEE Trans. UFFC, vol. 60.

Cappon HJ, Stefanova LA and Keesman KJ (2013) Separation Purification Technology 103, 321–327

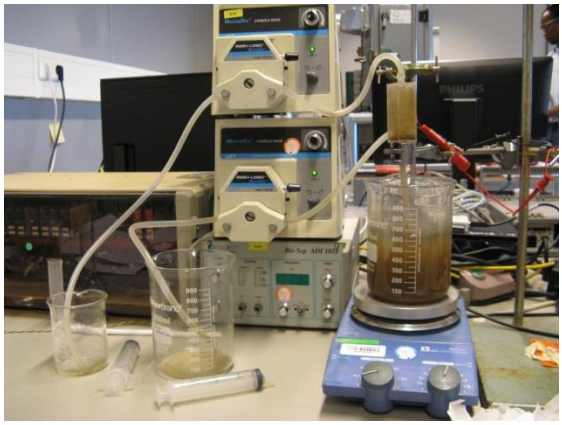

IUS2-H-6

Analysis of ultrasonic reflection coefficient: application to adhesion measurement at solid/fluid or solid/solid interfaces

Nicolas Collier[1,2], Dorothée Callens-Debavelaere[2], Pierre Campistron[2], julien Carlier[2], Bertrand Nongaillard[2], Guillaume Delaplace[1]; *[1]INRA, Villeneuve d'Ascq, France, [2]IEMN, Valenciennes, France*

Background, Motivation and Objective

The characterisation of adhesion between solid/fluid and solid/solid is an important issue for several disciplines (microfluidics, cell adhesion...). Only few methods allow both non-invasive and online adhesion measurements. We therefore propose in this work, an ultrasonic device developed to partially fill this gap.

Statement of Contribution/Methods

Our method is based on the study of the shear wave's reflection at the interface between two layers. Shear waves are generated by a 25MHz ultrasonic transducer. A model has also been developed in order to describe the quality of adhesion between these two layers. Each layer is described by its acoustic impedance and the reflection coefficient at the interface between them is deduced and processed to obtain a normalised adhesion parameter.

On one hand, solid/fluid adhesion has been tested with various viscous fluids (glucose syrup) and different solid surfaces (glass and stainless steel) to find out the values of adhesion. Values of ultrasonic reflection coefficients allow classifying the fluids in function of adhesion.

On the other hand, our ultrasonic technique has been employed for characterise the adhesion solid/solid. Particularly, we have studied the adhesion between glass and Polydimethylsiloxane (PDMS). The knowledge of adhesion characteristics between them is crucial in many fields. The bonding strength between glass and PDMS was evaluated quantitatively by a pulling force technique. Several adhesion levels were obtained by oxygen plasma treatment.

Results/Discussion

Classification of Solid/fluid adhesion is in agreement with results obtained by comparing viscosity values or axial forces required to separate solid/fluid interface.

For solid/solid adhesion cases, ultrasonic measurements are in good agreement with pulling-force measurements.

Such technique for characterizing the adhesion is interesting for many applications in various fields like food industry, especially for adhesion quantification of deposits (organic or bacterial) in heat exchangers.

High Power Ultrasound Applications

T1

Wednesday, July 24 2013, 02:00 pm - 03:30 pm

Congress Hallair: **Sorah Rhee**
Ethicon Endo-Surgery

IUS5-H-1

Prototype therapeutic array transducer element using coresonance between hemispherical piezoceramic shell and water

Shin-ichiro Umemura[1], Kenji Otsu[2], Shin Yoshizawa[2]; *[1]Tohoku University, Sendai, Japan, [2]Tohoku University, Japan*

Background, Motivation and Objective

A typical array transducer for high-intensity focused ultrasound (HIFU) treatment uses 1-3 composite. Since it uses the thickness mode, a high voltage in the order of a few hundred volts is required to generate ultrasonic power needed for the treatment. To reduce the voltage level, we have been developing hemispherical transducer elements using the breathing mode. Good acoustical matching has been expected by utilizing the corresonance between the hemispherical piezoceramic shell and the half enclosed water sphere, without any matching layers. The objective of this study is to test the real performance of the new transducer concept by fabricating a prototype element.

Statement of Contribution/Methods

To reduce the difficulty of prototype fabrication, the resonant frequency was chosen to be 0.25 MHz, although 0.5-1 MHz may be optimum for the treatment. The air-backed concave spherical PZT element has an inner diameter of 8 mm and a thickness of 0.7 mm. Both amplitude and phase of the two-dimensional acoustic field transmitted by the prototype transducer element were measured. Then, the acoustic fields produced by an array transducer consisting of the prototype array elements were numerically simulated in the manner of acoustic holography.

Results/Discussion

Figure.1 shows an example of the acoustic fields produced by a 696 channel focused array transducer consisting of the prototype transducer elements at 0.25 MHz. Here, the focus was steered 60 mm away from the geometric focus of the array transducer with a spherical curvature of 300 mm. The array was carefully configured so that it does not have particular spatial frequency components causing grating lobes. The prototype element has an impedance of 170 Ω at the resonant frequency. From this, it is estimated that only 40 Vpp is needed to generate an acoustic power of 1 W per channel. Although the prototype was scaled 2-4 times larger than the optimum size for typical HIFU treatment, it was demonstrated that the prototype transducer element of the new concept had the performance to generate focal ultrasound for HIFU treatment at a relatively low drive voltage level.

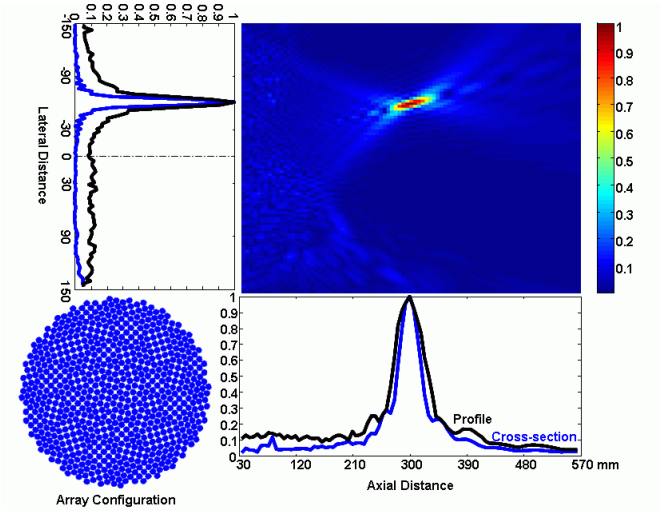

Fig. 1 Acoustic pressure field generated by 696ch array transducer at 0.25 MHz.

IUS5-H-2

High Intensity Ultrasound Transducer with a Multi-lens Structure

Kyle P. Morrison[1], George W. Keilman[1], Misty L. Noble[2], Carol H. Miao[2,3]; *[1]Sonic Concepts, Inc., Bothell, WA, USA, [2]Seattle Children's Research Institute, Seattle, WA, USA, [3]University of Washington, Seattle, WA, USA*

Background, Motivation and Objective

The delivery of uniform high intensity ultrasound (HIU) over a large aperture area has proven to enhance gene transfection in large tissue volumes using planar transducers. One must consider a transducer's geometry, frequency and sound speed of the tissue medium to determine its near field distance and the lateral focal full-width half maximum (FWHM). The underlying H-185 transducer uses unique geometric concepts to increase gene transfection rates compared with planar transducers.

Statement of Contribution/Methods

Mechanical constraints allowed for a flat 1.1 MHz transducer with a Ø50 mm aperture. The desired acoustic parameters were written to:

a) Disrupt the diffraction field within 1 cm from the transducer to eliminate near field effects

b) Develop a pressure focal gain of 2 within 1 cm from the transducer's surface

c) Sustain 2 to 2.8 focal gain throughout the treatment volume up to 5 cm from the transducer

d) Sustain >65% conversion efficiency from 0.9 to 1.3 MHz

e) Achieve a peak negative pressure of 3.3 MPa at the radiating surface

The natural focus for a Ø50 mm planar device is estimated to reach its peak pressure gain of 2 at 46 cm from the transducer's surface. Standard multi-channel electronics and array transducers would require equipment outside the budget of this project. Therefore, point spread function simulations were used to assist in developing a design by superimposing multiple slightly focused elements using one channel.

Results/Discussion

The H-185 configuration has been designed to meet all of the criteria outlined above and uses one RF channel, one piezoceramic element and a faceplate comprised of multiple plano-concave lenses. The faceplate material uses a proprietary conductive composition to acoustically match between the piezoceramic and tissue, and to yield a maximum allowable efficiency over a large operating band. Two different faceplate geometries were developed:

1) H-185A uses multiple spherical lenses to achieve slight focusing along the focal axis

2) H-185B uses multiple cylindrical lenses to achieve slight focusing along the focal plane

The concave lenses were designed specific to the faceplate material in both cases.

Experimental measurements of the H-185 validated the acoustic parameters outlined above and has proven to increase gene transfection compared to a planar transducer in large animals.

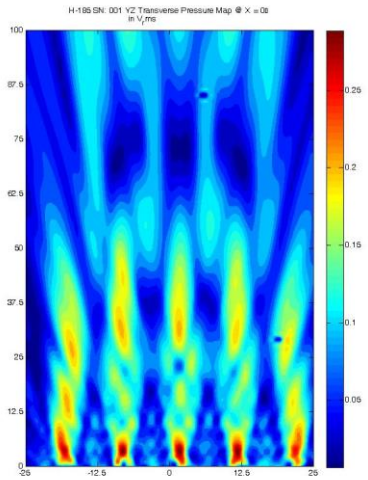

IUS5-H-3

Effects of Soft Tissue Load and Power Level on Ultrasonic Cutting Tool Driven by PMN-PT d31 Plates

Yang Kuang[1], Muhammad Sadiq[1], Sandy Cochran[1], Zhihong Huang[1]; [1]*University of Dundee, United Kingdom*

Background, Motivation and Objective

The performance of a d31-mode planar configuration ultrasound cutting tool, as reported previously [M.Sadiq, IUS 2011], provides many advantages over the conventional sandwich transducer configuration used in ultrasound scalpels but it is more susceptible to operating conditions. During soft tissue cutting, the tissue acts as significant physical load on the tool while the high driving power introduces nonlinearity. Both affect the working characteristics of the cutting tool, including resonant frequency and electric impedance values, leading to a significant reduction in performance. This paper aims to report the effects of both the soft tissue load and power level to improve understanding of the ultrasonic cutting process.

Statement of Contribution/Methods

In this study, ex-vivo animal tissue (poultry breast) was used, cut into 20 x 20 mm2 specimens. The planar ultra-sound cutting tool was clamped onto a commercial material testing system which provides downward load and displacement control. The tip of the ultrasonic tool was introduced into the tissue to depths of 1, 5, 7 and 10 mm. At each depth, firstly, a frequency sweep around resonance was conducted at different current levels (0.03, 0.05, 0.07 and 0.09A zero-to-peak). Secondly, the ultrasound cutting tool was driven continuously by a bespoke resonance tracking and vibration stabilization system until its characteristics reached a steady state. During all the experiments, an infrared camera was used to monitor the temperature of the piezocrystal PMN-PT d31 plates used in the device.

Results/Discussion

The resonant frequency of the cutting tool shifts to lower values with increasing power level (shifting by 300 Hz at 0.09A). When driven continuously, the temperature of the PMN-PT plates increases quickly and finally stays at values (50°C at 0.09A)dependent on the power level and independent of coupling depth. This temperature causes a further frequency shift (1.2 kHz at 0.09A). Increased mechanical loss was also observed with increased power levels. The radiation impedance, which is dependent on the coupling to the soft tissue, increases linearly with the square of cutting depth as expected. However, it decreases with the power level, shown in Fig. 1. This implies that with higher vibration amplitude, the contact between the ultrasonic cutting device and the tissue is reduced.

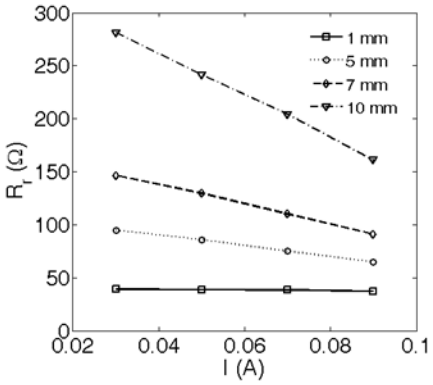

Fig. 1: The radiation impedance increases with cutting depth and decreases with power level

IUS5-H-4

Reduced Penetration Force through Ultrasound Activation of a Standard Needle - An Experimental and Numerical Study

Muhammad Sadiq[1], **Xiaochun Liao[1]**, George Corner[2], Sandy Cochran[3], Zhihong Huang[1]; *[1]Bioengineering Research Centre, University of Dundee, Dundee, Scotland, United Kingdom, [2]Department of Medical Physics, Ninewells Hospital and Medical School, Dundee, Scotland, United Kingdom, [3]Institute for Medical Science and Technology, University of Dundee, Dundee, Scotland, United Kingdom*

Background, Motivation and Objective

Needle insertion in soft tissue has attracted considerable attention in recent years because of its applications in minimally invasive percutaneous procedures such as cancer biopsy and regional anaesthesia. In such procedures, accurate needle placement is essential for effective treatment and to minimize complications. However, clinical studies have shown that tissue deformation and needle deflection contingent on needle penetration force are common reasons behind needle placement errors, leading to missampling of tissues in biopsy, incomplete anaesthesia and possible post-operative morbidity. Reducing the needle penetration force is therefore one method to improve needle-based interventional procedures. Here, we report an ultrasound device capable of significantly reducing this force through action similar to the ultrasound cutting used in ultrasound assisted surgeries, along with numerical simulations of the device operation to elucidate tissue behaviour during interventional procedures.

Statement of Contribution/Methods

The device is based on a piezoelectric transducer with a conventional sandwich structure modified to match the requirements of a range of needle-based procedures. It has also been designed to meet the practical needs of the end users, in this case experienced clinicians, and thus allows gripping of standard needles with gauge $\geq$ 20 and length $\geq$ 10 cm. The device is able to activate needles with displacement amplitude $\geq$ 6 µm when driven with Vp-p = 50 V (power P = 6 W) signal at its resonant frequency, f = 21.7 kHz.

To assess the viability of the device and to prove the design concept, pre-clinical trials were carried out on a variety of specimens including tissue mimics and ex-vivo animal tissue. The simulations were performed using the finite element analysis package, ABAQUS (Dassault Systems, France, 6.8-2008). For accurate analyses, material properties for the specimens were obtained through in-house mechanical testing of each specimen using a commercial material testing machine (H5KS, Tinius Olsen Inc., Horsham, USA).

Results/Discussion

Pre-clinical trials on ex-vivo tissue and tissue mimicking phantom have shown that the device is able to activate needles to reduce penetration forces by up to 40 % and needle deflection by 20%. This has two practical clinical benefits: sampling accuracy and reduction in pain as the needle is inserted into the tissue. In addition to confirming the benefit of the activated needle in reducing the penetration force, the simulation work has also contributed to knowledge of the stress distribution in tissue during needle insertion. This allows us to understand better the needle-tissue interaction in a range of needle based interventional procedures.

IUS5-H-5

Smart cymbal transducers with Nitinol end-caps for power ultrasonics applications

Margaret Lucas[1], Andrew Feeney[1]; *[1]University of Glasgow, Glasgow, United Kingdom*

Background, Motivation and Objective

A Class V cymbal flextensional transducer is composed of a piezoceramic disc or ring sandwiched between two cymbal-shaped shell end-caps. The cymbal transducer was developed in the early 1990s and has primarily been used in sensing and actuation. It has only very recently been studied for high amplitude and high power applications, and consequently implementation in this application space remains undeveloped. Shape memory alloys (SMAs) are a unique class of metals that have been adopted in a wide range of applications as a result of exhibiting two interesting properties. The first is the shape memory effect (SME), where the material is able to recover to a set configuration under the influence of a phase transformation induced by heating. The second is the superelastic effect, which occurs isothermally when the material is stressed at a temperature above its austenitic transformation temperature. The material undergoes a change in which the austenitic microstructure is reoriented to martensite. One type of SMA which has received much attention in recent years is Nitinol, which has been particularly popular due to its excellent strain recovery, durability, fatigue strength and corrosion resistance. However, research aiming to exploit the properties of SMAs in high power ultrasonic applications is limited.

Statement of Contribution/Methods

This paper investigates the effects of both of these properties of SMAs on the dynamic performance of a cymbal transducer, through experimental characterisation employing electrical impedance measurements, vibration response measurements and experimental modal analysis.

Results/Discussion

The results demonstrate that the superelastic effect is exhibited as a nonlinearity in the response of the transducer at raised voltage levels, resulting from the local emergence of martensite phase behaviour of the material. This leads to the design and fabrication of a power ultrasonic device with an active tunable resonance frequency, through a phase shift of the SMA. The understanding of the observed transducer response is enabling the development of tunable ultrasonic transducers, particularly for incorporating in ultrasonic cutting devices which are required to penetrate more than one material.

Thin films

T2

Wednesday, July 24 2013, 02:00 pm - 03:30 pm

Congress Hallair: **emmanuel defay**
CEA LETI Minatec

IUS3-H-1

ELECTRICAL TUNABILITY OF ALN ELASTIC CONSTANTS: DIRECT MEASUREMENT BY ULTRAFAST ACOUSTICS

Arnaud Devos[1], Patrick Emery[1], Emmanuel Defaÿ[2]; *[1]IEMN, Lille, France, [2]CEA-LETI, Grenoble, France*

Background, Motivation and Objective

The elastic properties of materials currently used by the microelectronic industry are poorly known. More and more applications require the knowledge of Young modulus or mass density of such materials especially in thin-films (MEMS, BAW resonators, strained MOS transistors…). So there is a need for a better understanding of mechanical properties at sub-micron scale.

The materials these nano/microstructures are made of may strongly depend on the deposition/fabrication process. For example, due to the use of fast elaboration processes at moderate temperatures, thin film materials are often in metastable states, with no equivalent bulk structures. Most of the thin films are polycrystalline materials and their elastic properties are averaged over all the grains.

If such a dependence of elasticity on material growth process can be seen as a problem, it can also be very useful for tuning the elastic properties of thin-film for some specific applications. For that one needs some dedicated characterization techniques able to reach accurately elastic properties at nanoscale.

Statement of Contribution/Methods

We present a technique based on ultrafast acoustics which permits us to measure the electrical dependence of the elastic properties of a thin piezoelectric layer. Ultrafast acoustics offers a unique way of measuring elastic properties of thin-layer in a non-destructive way using ultrashort optical pulses.[1] We apply this technique to a thin layer to which a dc voltage is simultaneously applied.

The electric field affects simultaneously the sound velocity and the film thickness. Indeed, the electric field changes the C33 elastic constant through the elastoelectric effect and thus the longitudinal sound velocity. It also modifies the film thickness through the inverse piezoelectric effect. The two effects can be separated by use of a semi-transparent top electrode.[2]

[1]. A. Devos, R. Cote, G. Caruyer, and A. Lefevre, Appl. Phys. Lett. 86, 211903 (2005).

[2]. A. Devos, P. Emery, E. Defay, N. Ben Hassine, and G. Parat, Rev. Scientific Instruments 84, 015007 (2013)

Results/Discussion

A demonstration is presented on a thin AlN film. From that the d33 piezoelectric coefficient and the stiffness variation induced by the bias in AlN are measured. The linear elastoelectric effect is found to dominate significantly the piezoelectric effect in AlN which is consistent to what has been proposed by Lanz from electrical measurements.[3]

[3]. R. Lanz, Ph.D. dissertation, Ecole Polytechnique Fédérale de Lausanne, 2004.

IUS3-H-2

Young modulus and Poisson ratio of polycrystalline and single crystal PZT thin-film measured by picosecond ultrasonics

Fabrice Casset[1], Arnaud Devos[2], Julie Abergel[1], Gwenael Le Rhun[1], Bertrand Vilquin[3], Guillaume Saint-Girons[3], Romain Bachelet[3], Patrick Emery[4], Pascal Ancey[5], Stéphane Fanget[1], Emmanuel Defay[1]; *[1]CEA, LETI, MINATEC Campus, France, [2]IEMN-ISEN, France, [3]INL, France, [4]MENAPIC, France, [5]STMicroelectronics, France*

Background, Motivation and Objective

Pb(Zr0.52, Ti0.48)O3 (PZT) thin-films are well suited to actuators applications thanks to its high piezoelectric coefficients [1]. Although polycrystalline films are overwhelming, their single crystal counterparts could allow a significant improvement of these films' properties [2]. Besides, for sake of predictive MEMS design, the accurate knowledge of the mechanical properties of the materials is required especially because thin films behavior can exhibit significant changes with respect to bulk. In this paper we show Picosecond Ultrasonics (PU) measurements performed on single and polycrystal sol-gel PZT thin-film on Si wafers, leading to obtain their Young modulus (E) and Poisson ratio.

Statement of Contribution/Methods

PU uses a femtosecond laser to excite and detect acoustic waves in the hundreds of GHz range (cf Fig. 1). Such an optical setup offers the opportunity to implement a sonar at the nano-scale. For transparent material such as PZT deposited on a metallic layer, the pump pulse generates a thermal strain at the metal/PZT interface and then induces a longitudinal acoustic pulse propagation normally to the surface (Fig. 1-a). Acoustic pulses propagation and interferences allow using all the detection mechanisms relative to colored PU (Brillouin, echoes…). Thanks to a nanostructured metallic layer deposited on the sample surface (Fig. 1-b), we can also extract the transverse acoustic velocity from the in-plane Rayleigh velocity using the same optical technique [3]. With the isotropic material approximation, we can extract E and Poisson from longitudinal and transverse velocities using the theory of elasticity.

Results/Discussion

From the Brillouin oscillation period, we accurately measured the longitudinal acoustic velocity, namely 4.73nm/ps for poly-PZT. Using Pt nanostructured cubes, we extracted the transverse acoustic velocity (1.95nm/ps) from the in-plane Rayleigh velocity (1.84nm/ps). It leads to EpolyPZT=82 GPa and Poisson=0.39 for polycrystalline PZT [4]. The longitudinal velocity of single crystal PZT is 13% higher than poly-PZT, namely 5.45nm/ps. Consequently, we extracted PZT single crystal Young modulus, namely EmonoPZT=112 GPa. Finally, we plan to perform the complete single crystal PZT characterization in close future, through transverse velocity measurement using the same surface nanostructuration

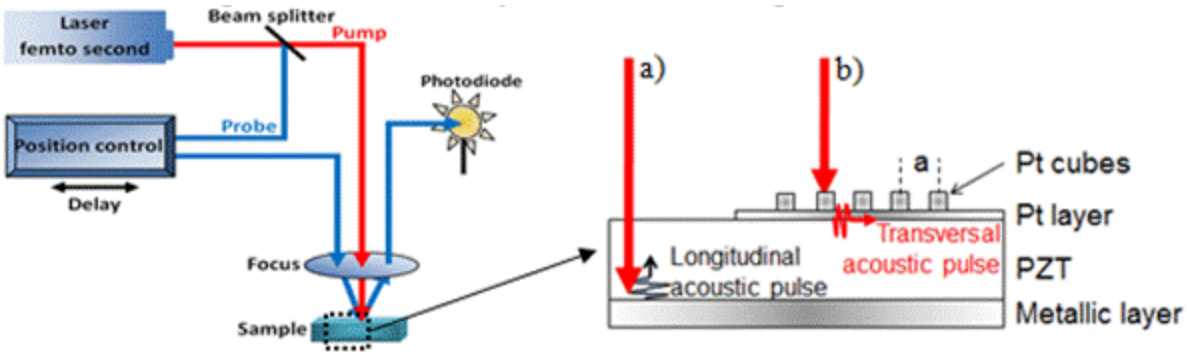

IUS3-H-3

Sputter deposition of stress controlled piezoelectric AlN and AlScN films for ultrasonic and energy harvesting applications

Stephan Barth[1,2], Hagen Bartzsch[1], Daniel Glöß[1], Peter Frach[1], Thomas Herzog[3], Susan Walter[3], Henning Heuer[3]; *[1]Fraunhofer Institute for Electron Beam and Plasma Technology (FEP), Germany, [2]Institute for Solid State Electronics, Dresden University of Technology, Dresden, Germany, [3]Fraunhofer Institute for Nondestructive Testing, Dresden Branch (IZFP-D), Germany*

Background, Motivation and Objective

The paper will report on the deposition and characterization of piezoelectric AlN and AlScN films. Potential applications of the films are in ultrasonic microscopy, energy harvesting and SAW/ BAW filters. To demonstrate the potential in ultrasonic applications, the pulse echo method was used.

Statement of Contribution/Methods

The depositions were done by reactive pulse magnetron sputtering using the Double Ring Magnetron DRM400 sputter source. This type of magnetron combines two concentric discharges from metallic targets in order to deposit uniform films on substrates with a diameter of up to 200mm. In the case of AlN depositions, pure Al targets were used. AlScN was deposited by reactive co-sputtering of an Al and Sc target. Argon and Nitrogen were used as inert and reactive gas, respectively. Using the DRM 400, the pulse mode of the pulse magnetron sputtering process can be changed between unipolar and bipolar, resulting in different plasma properties. In the unipolar pulse mode, a pulsed dc is applied between each of the two targets and the separate hidden anode. In the bipolar pulse mode, a voltage with alternating polarity is applied between the two targets. Using suitable powering and reactive gas control, a deposition rate of up to 200nm/min was achieved by stationary coating. This very high deposition rate allowed the deposition of very thick films with up to 50µm thickness.

Results/Discussion

The films were characterized regarding piezoelectric coefficient d_{33}, film stress, structure and morphology. The piezoelectric coefficient d_{33} of AlN films was up to 9pm/V on silicon substrates. X-ray diffraction (XRD) revealed highly textured AlN films with no visible peaks besides those of the (001) orientation. XRD rocking curves show very good alignment of the c-axis perpendicular to the surface and a FWHM of between 2° and 4°. Film stress of AlN ranges from -2GPa to +0,2GPa and strongly depends on film thickness, deposition pressure and pulse mode. Adaptation of film stress was required to achieve very thick films without film delamination while still exhibiting good piezoelectric responses. The measured stress for deposited 50µm thick AlN films was between -230MPa (compressive) and 130MPa (tensile). The d_{33} stayed well above 6pm/V for those samples.

By scandium doping of the film, d_{33} could be raised up to 29pm/V. The measured stress values were similar to those of pure AlN films.

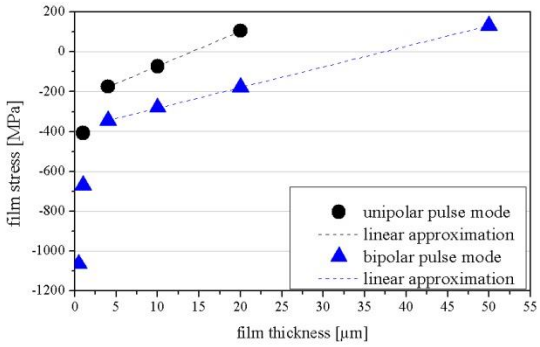

Fig. 1: Film stress versus film thickness for both puls modes

IUS3-H-4

Low temperature sputtered nearly-epitaxial AlN films on sapphire substrates

Aude Lefevre[1], Ewen Henaff[1], **Alexandre Reinhardt**[1], Pierre Patrick Lassagne[1], Christophe Billard[1]; *[1]CEA, Leti, Grenoble Cedex, France, Metropolitan*

Background, Motivation and Objective

The deposition of Aluminum Nitride (AlN) on sapphire has received a large interest for high velocity Surface Acoustic Waves (SAW) applications. Additionally, High Overtone Bulk Acoustic Resonators (HBAR) using AlN on Sapphire substrates exhibit extremely high quality factors in the GHz range. For SAW applications, AlN films are usually epitaxially grown on sapphire substrates using high temperature processes, while for HBAR applications sputtered films are more conventionally used, since a bottom metal electrode is required. In this paper, we investigate the sputtering of AlN on sapphire substrates, to analyze the influence of the substrate on growth conditions and orientation.

Statement of Contribution/Methods

1 µm-thick AlN films were deposited using magnetron DC pulsed reactive sputtering at a temperature between 300 and 400°C, on four sapphire crystal cuts: A, C, R and M. Deposition was performed either directly on the sapphire substrates, or on 200 nm thick molybdenum films deposited in the same equipment on a thin AlN seed. Reference samples were grown with an additional amorphous SiO_2 film located on top of the substrate. X-Ray diffraction patterns were measured for all samples to determine the crystalline orientation of the deposited films. φ-scans were also performed to determine the in-plane orientation of the films.

Results/Discussion

As expected, films grown on sapphire substrates covered by a thin amorphous SiO_2 layers exhibit a preferential (001) orientation for AlN and (110) for Mo, with no preferential in-plane orientation, whatever the wafer cut. When AlN and/or Mo films are deposited directly on sapphire, the orientation of sapphire clearly has an impact on the film growth. Mixed AlN orientations were found on M substrates; A and C substrates promote the growth of (001) AlN films while the R-axis substrate generates (110) orientation. Interestingly, epitaxial relations were found between sapphire and AlN. When AlN is grown on Mo electrodes, only A and C sapphire keep the same orientation and epitaxial relations. This is attributed to a local epitaxial growth of the AlN seed on Sapphire, then Mo on AlN, and finally AlN on Mo, despite the low temperature deposition process. As shown below, electrical measurements of HBAR resonators reveal quality factors reaching 27,000 at 2.5 GHz, promoted by the substrate, but also revealing excellent AlN film quality.

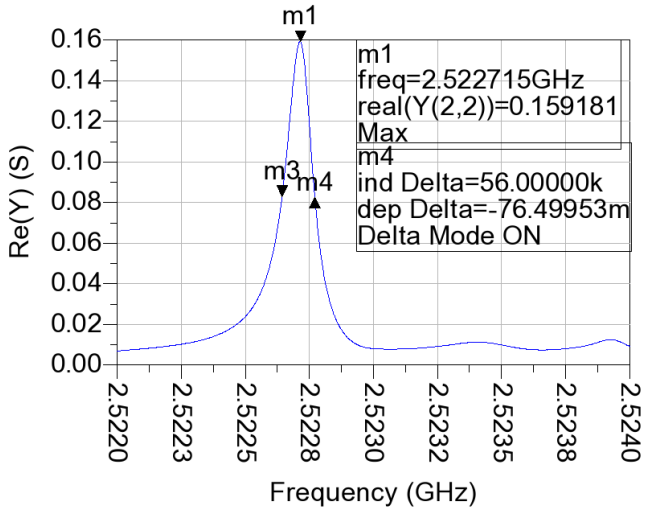

IUS3-H-5

Enhancement of electromechanical coupling k_t in rare earth doped c-axis oriented GaN films

Masashi Suzuki[1], Takahiko Yanagitani[1]; [1]*Nagoya Institute of Technology, Nagoya, Japan*

Background, Motivation and Objective

GaN film BAW and SAW resonators are promising for monolithic integration with other GaN semiconductor devices and circuits on the same chip. However, low electromechanical coupling k_t of GaN films is a serious problem for resonators. High piezoelectricity in rare earth doped GaN was recently predicted by ab initio calculation [1], but piezoelectric properties have not been reported experimentally.

In this study, rare earth doped c-axis oriented GaN films was grown and the k_t of films were investigated.

Statement of Contribution/Methods

Rare earth doped (0001) GaN film was grown on Ti electrode film / silica glass substrate by using RF magnetron sputtering. Rare earth metal ingots were put on vacuum-nitrided Ga liquid metal target. RF bias (2-5 W, 60MHz) was applied to the substrate during deposition to enhance possitive ion irradiation to the substrate, which induces the nitridation of the films. Conductive metallized Ga film was grown in the case that RF bias was not applied. Crystalline orientation of films were determined by XRD pattern and rocking curve (R. C.) FWHM value. HBARs (High-overtone bulk acoustic resonator) were prepared, and the k_t value of films were determined from a longitudinal wave conversion loss of HBARs [2].

Results/Discussion

As shown in Table I, the k_t^2 value in YGaN or DyGaN films seems to be slightly higher than that of pure GaN film. In contrast, significant increase of the k_t^2 value was observed in YbGaN film. Enhancement of piezoelectricity was found only in YbGaN fllm.

Fig. 1 shows k_t^2 value of $Yb_xGa_{1-x}N$ films ($0 \leq x \leq 0.48$). The k_t^2 value increased with increasing Yb from x=0 to 0.33, which is not only due to the decrease of R. C. FWHM value. The k_t^2 value reached maximum of k_t^2=3.1 % at x=0.3, and this value is approximately 170% of that of pure GaN MOCVD film [3]. Significant decrease of the k_t^2 value was observed for x > 0.35. This decrease may be caused by the phase transition from a piezoelectric wurtzite phase to a non-piezoelectric crystal phase.

[1] A. Alsaad, et al., Eur.Phys. J. B, 54 (2006) 151.

[2] T. Yanagitani and M. Kiuchi, J. Appl. Phys. 102, 044115 (2007).

[3] D. Neculoiu, et al., IEEE MTT-S Inter. Microwave Symp. Digest, 1 (2007) 877.

Table I Properties of rare earth doped GaN films

	Ingots (g)	Atomic ratio (%)	XRD peak	R. C. FWHM (deg.)	k_t^2 (%)
GaN	0	0	Yes	6.5	0.45
ScGaN	1.0	13	Yes	14.8	—
YGaN	1.0	10	Yes	7.0	0.59
LaGaN	1.0	8	No	—	—
PrGaN	1.0	14	No	—	—
NdGaN	1.0	10	No	—	—
SmGaN	1.0	24	No	—	—
GdGaN	1.0	8	Yes	14.5	0.03
DyGaN	1.0	14	Yes	7.3	0.81
HoGaN	1.0	6	No	—	—
TmGaN	1.0	9	Yes	7.4	—
YbGaN	1.0	17	Yes	5.5	2.0

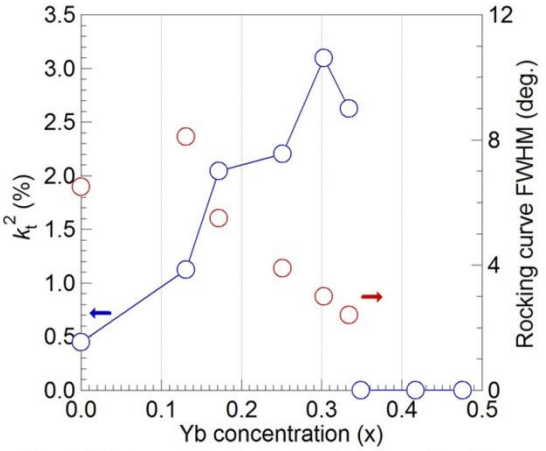

Fig. 1 Electromechanical coupling k_t and rocking curve FWHM of $Yb_xGa_{1-x}N$ films (x=0-0.48)

IUS3-H-6

Polarity control of c-axis oriented ZnO films and application to polarity-inverted ZnO multilayer resonators

Ryosuke Hashimoto[1], Takahiko Yanagitani[2], Ryo Ikoma[1], Shinji Takayanagi[1], Masashi Suzuki[2], Hiroyuki Odagawa[3], Mami Matsukawa[1]; *[1]Doshisha University, Japan, [2]Nagoya Institute of Technology, Japan, [3]Kumamoto National College of Technology, Japan*

Background, Motivation and Objective

Physical constants, such as nonlinear optical coefficient and piezoelectric constant, are reversed in sign between Zn- and O-polar ZnO. Polarity control of ZnO is therefore important for optical and piezoelectric devices. Generally, the polarity of ZnO is controlled by using an epitaxial technique. In this study, we report a method for controlling polarity of ZnO by adjusting the amount of ion bombardment and substrate temperature during sputtering deposition.

Statement of Contribution/Methods

ZnO films were grown on the Al/Ti/SiO_2 substrates by an RF magnetron sputtering technique. The amount of ion bombardment inside the glow discharge is larger than that of the outside [1]. We set the substrate inside or outside the glow discharge to induce or reduce the ion bombardment. The substrate temperatures were adjusted from 70 to 400 ºC. Au top electrode was evaporated on each ZnO film to fabricate a HBAR (high overtone bulk acoustic resonator) structure. Sign of the polarities of the ZnO films were determined by sign of the piezoelectric response when compression stress is applied to the sample. k_t values were estimated by a conversion loss of the HBAR. Finally, we fabricated two types of polarity-inverted ZnO multilayer resonators consisting of O-polar on Zn-polar or Zn-polar on O-polar ZnO structure. Zn-polar and O-polar ZnO films in this structure were grown outside the glow discharge at 150°C and 400°C, respectively.

Results/Discussion

Fig. 1 (a) shows polarities and k_t values of ZnO films grown at different substrate temperatures. Zn-polar ZnO films were grown below 150°C, whereas O-polar ZnO films were grown above 300°C. Around 250°C, the polarity of ZnO films might be determined by the amount of ion bombardment to the substrate. Fig. 1 (b) and (c) show conversion losses of polarity-inverted ZnO multilayer resonators consisting of (b) O-polar on Zn-polar and (c) Zn-polar on O-polar ZnO structure. Fundamental thickness extensional modes (L_1) resonances were suppressed and second-overtone modes (L_2) resonances were strongly excited. These results indicate that two layered ZnO resonators have O-polar on Zn-polar or Zn-polar on O-polar ZnO inverted polarity structure as expected. We demonstrated that this method could control polarity of ZnO without epitaxial technique.

[1]S. Takayanagi, et al., *Appl. Phys. Lett*., 101(2012) 232902.

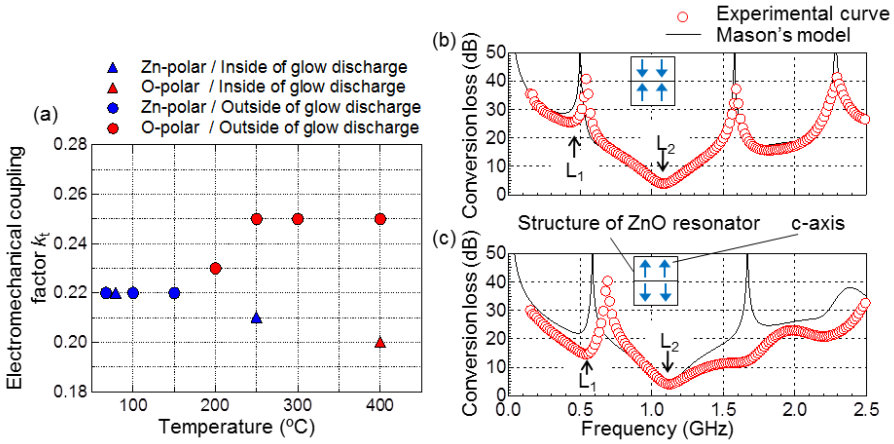

Figure. 1 (a) Polarity and k_t value of ZnO films depending on growth temperature. Frequency response of longitudinal wave conversion loss of (b) O-polar on Zn-polar and (c) Zn-polar on O-polar ZnO inverted polarity resonator.

Cardiovascular imaging

CONGRESS HALL

Wednesday, July 24 2013, 04:30 pm - 06:00 pm

Congress Hallair: **Jeremy Dahl**
Duke University

IUS1-I1-1

Improvement of Axial Spatial Resolution of Ultrasound Image Using Wiener Filter for Measurement of Intima-Media Thickness of Carotid Artery

Hideyuki Hasegawa[1,2], Sho Kageyama[1], Hiroshi Kanai[1,2]; *[1]Graduate School of Biomedical Engineering, Tohoku University, Japan, [2]Graduate School of Engineering, Tohoku University, Japan*

Background, Motivation and Objective

Measurement of intima-media thickness (IMT) of the carotid artery by ultrasonography is widely used for diagnosis of atherosclerosis. For accurate measurement of IMT, in the present study, a method based on the Wiener filter was developed for improvement of image spatial resolution.

Statement of Contribution/Methods

There are many studies on improvement of spatial resolution by trying to remove the point spread function (PSF) of an ultrasound system using a deconvolution filter. In most of developed methods, PSF is separately measured using a target, such as a fine wire in water, prior to the actual in vivo measurement. However, it is difficult to predict the subject-dependent change in PSF due to frequency-dependent attenuation by tissue. Therefore, conventional deconvolution filters do not work effectively. PSF is determined by the transfer function H(f) (including transfer function of ultrasonic probe and tissue attenuation property). In the present study, the magnitude |H(f)| was estimated by averaging power spectra of RF echoes in all scan lines obtained from the actual in vivo measurement to consider frequency-dependent attenuation. Although there are many dips in the respective power spectra due to interference of echoes from many scatterers, such dips can be suppressed by averaging power spectra because locations of dips are different line by line owing to randomness of scatterer distribution. On the other hand, the phase of H(f) was estimated beforehand from the phase of frequency spectrum Y(f) of the transmitted ultrasound signal received by a hydrophone placed in water because attenuation by tissue does not affect the phase of the transfer function. The phase of squared Y(f) was used as the phase of H(f) by considering a pulse-echo measurement. From the estimated H(f), a deconvolution filter was designed using the Wiener filter.

Results/Discussion

Improvement of axial resolution was evaluated by measuring an echo from a fine wire placed in water. Axial resolution defined by the width at half maximum was improved from 0.2 mm to 0.12 mm. Furthermore, the proposed method was applied to RF echoes obtained from a carotid artery. As shown in the bottom of the figure, axial resolution was significantly improved compared with conventional B-mode image in the top of the figure.

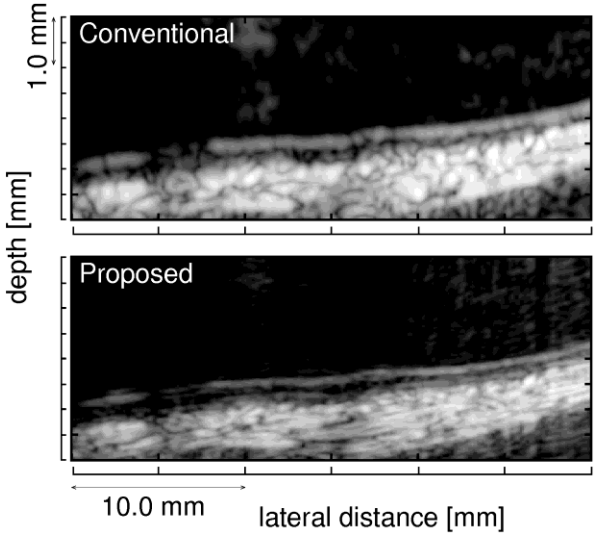

IUS1-I1-2

New Quantification Methods for Carotid Intraplaque Neovascularization in Contrast Enhanced Ultrasound (CEUS)

Zeynettin Akkus[1], Gonzalo Vegas Sanchez-Ferrero[2], Guillaume Renaud[1], Stijn C.H. van den Oord[3], Arend F.L. Schinkel[3], Nico de Jong[1], Antonius F.W. van der Steen[1]; *[1]Biomedical Engineering-Thoraxcenter, Erasmus MC, Netherlands, [2]Image Processing Laboratory, University of Valladolid, Spain, [3]Department of Cardiology, Thoraxcenter, Erasmus MC, Netherlands*

Background, Motivation and Objective

Carotid intraplaque neovascularization (IPN) has been associated with progressive atherosclerotic disease and plaque vulnerability. Therefore, its accurate quantification might allow early detection of plaque vulnerability. CEUS can detect these small microvessels. To quantify IPN, we developed quantitative methods which are perfusion analyses based on time intensity curve (TIC) and maximum intensity projection (MIP), vascular structure analysis (VSA), and statistical segmentation (SS).

Statement of Contribution/Methods

Plaque region of interest (ROI) is manually drawn and motion compensation is applied before each analysis. In TIC and MIP, we examine perfusion dynamics and regions within plaques. In VSA, we detect and track contrast spots to examine microvessels network. In SS, we classify plaque intensities into different components for quantification of IPN. Through an iterative expectation-maximization algorithm, plaque pixels are initially labeled into artifacts, contrast, intermediate and background class. Next, spatiotemporal and neighborhood information is used to relabel intermediate class pixels, remove artifacts and correct false-contrast. From the applied analyses, we derived several parameters – MIP based IPN surface area (MIPNSA), MIP based IPN surface ratio (MIPNSR), SS based IPN surface area (SSIPNSA), plaque mean intensity, mean plaque contrast percentage, and number of microvessels (MVN) – and compared them to visual grading of IPN by two independent physicians. We analyzed 45 carotid arteries with stenosis. To verify if SSIPNSA improves the suppression of artifacts, we analyzed 8 plaques twice, with saturation artifacts included and excluded from the ROI.

Results/Discussion

MIPNSA (r=0.719), SSIPNSA (r=0.698), MIPNSR (r=0.484) and MVN (r=0.538) were found to be significantly correlated to visual scoring ($p<0.01$). The MIPNSA & SSIPNSA parameters gave the best distinction between visual scores. SSIPNSA (3.9±3.2 mm2 with vs. 3.8±3.2 without artifact) gave slightly higher areas but proved less sensitive for artifacts than MIPNSA (9±3.3 with vs. 3.2±2.9 without). If there are artifacts within plaque ROI, SSIPNSA will suppress artifacts and gives more reliable results than MIPNSA (fig. 1). MIPNSA, SSIPNSA, MIPNSR and MVN may thus have the potential to replace qualitative visual scoring and to measure the degree of carotid IPN.

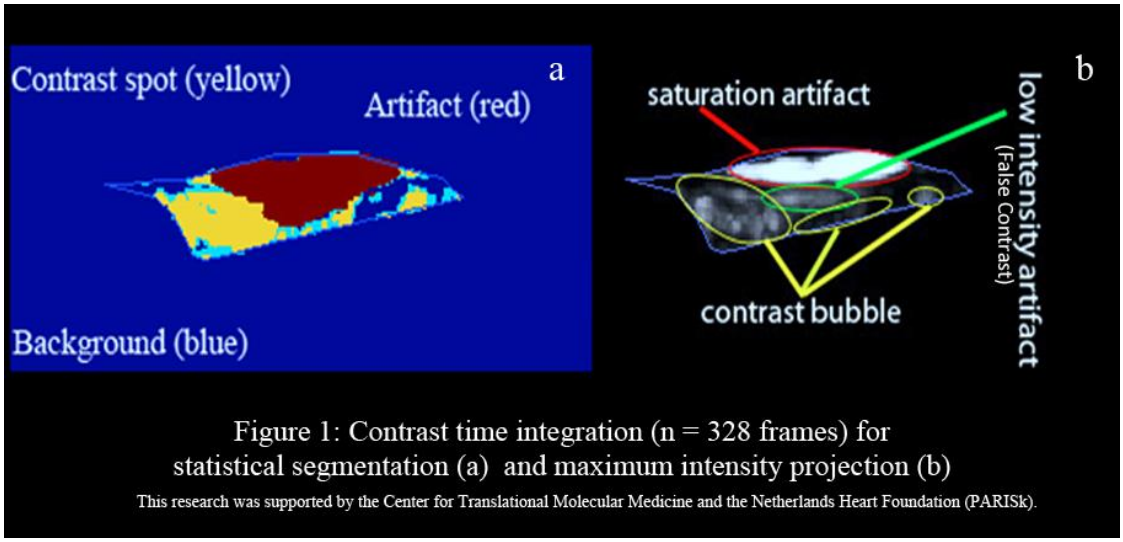

Figure 1: Contrast time integration (n = 328 frames) for statistical segmentation (a) and maximum intensity projection (b)

This research was supported by the Center for Translational Molecular Medicine and the Netherlands Heart Foundation (PARISk).

IUS1-I1-3

Monitoring the Formation of Aneurysms and Ruptures in Murine Aortas with Pulse Wave Imaging (PWI)

Sacha Nandlall[1], Monica Goldklang[1], Jeanine d'Armiento[1], Elisa Konofagou[1]; [1]*Columbia University, New York, NY, USA*

Background, Motivation and Objective

Aortic Aneurysms (AAs) are a common vascular disease. The leading cause of AA-induced death is rapid internal bleeding following a sudden rupture of the vessel wall, typically within the sac of the aneurysm. This study aims at assessing the capability of Pulse Wave Imaging (PWI) to differentiate normal murine aortas from AAs and ruptures, even when these abnormalities are not visible or easily detectable on a standard B-mode. PWI is a non-invasive technique for tracking the propagation of pulse waves along the wall of the aorta at high spatial and temporal resolutions. The velocity of these waves is a well-established marker of wall stiffness, which is closely related to the likelihood of rupture.

Statement of Contribution/Methods

An AA model was generated by infusing thirteen (n = 13) ApoE/TIMP-1 knockout mice with angiotensin-II, delivered at a constant flow rate via subcutaneously implanted osmotic pumps. The suprarenal sections of the abdominal aortas were scanned every 2-3 days after implantation using a Visualsonics Vevo 770 imager with axial and lateral resolutions of 62 and 115 µm, respectively. Pulse wave propagation was tracked at an effective frame rate of 8 kHz by using retrospective ECG gating. The displacements induced by the pulse waves were estimated by performing 1-D cross-correlation on the radiofrequency echo signals.

Results/Discussion

In normal aortas, the pulse waves propagated at constant velocities ($r^2 \geq 0.9$) between 2-4 m/s, indicating that the composition of these vessels was relatively homogeneous. In the nine (n = 9) mice that developed abdominal AAs where the vessel diameter had increased by at least 50%, the wave speeds exhibited higher variances along the wall ($r^2 < 0.9$). Moreover, the wall displacements induced by the pulse waves were at least 80% lower within the aneurysm sacs, indicating that the AAs had a higher relative stiffness. Finally, in the five (n = 5) mice that developed ruptures at the sites of their AA, higher displacements directed outwards from the lumen were observed throughout the cardiac cycle, and axial blood flow measurements obtained with pulse wave Doppler imaging indicated outward flow at rates of up to 40 cm/s. These findings show that PWI can be used to distinguish normal murine aortas from AAs and ruptures. Hence, PWI could potentially be used to monitor human aneurysms by providing information complementary to standard B-modes.

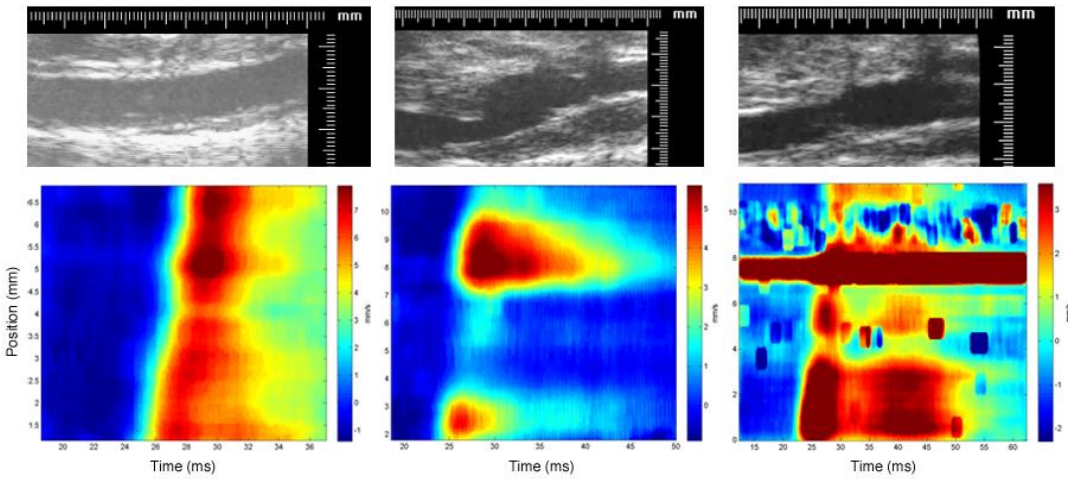

Example B-mode images (top) and spatiotemporal pulse wave propagation plots (bottom) for normal (left), aneurysmal (middle) and ruptured (right) aortas.

IUS1-I1-4

Volumetric SLSC imaging of vasculature on a clinical matrix array

Marko Jakovljevic[1], Brett Byram[1], Jeremy Dahl[1], Gregg Trahey[1,2]; [1]*Biomedical Engineering, Duke University, Durham, North Carolina, USA,* [2]*Radiology, Duke University, Durham, North Carolina, USA*

Background, Motivation and Objective

Vessel images created with conventional high-speed volumetric ultrasound systems are often plagued with noise due to complex beamforming electronics and the use of broad transmit beams. We implement the short lag spatial coherence (SLSC) imaging on a clinical matrix array and 3-D ultrasound scanner in an attempt to improve image quality in flow phantoms and *in vivo* liver vasculature. We use color Doppler as a gold standard to compare visibility of vessels between the resulting SLSC volumes and the corresponding B-mode volumes.

Statement of Contribution/Methods

The individual-channel signals needed to reconstruct complete B-mode and SLSC volumes of the flow phantom and *in vivo* liver vasculature were recorded of a Siemens 4z1c matrix array on a Siemens SC2000 ultrasound scanner at the rate of 4 volumes per second using custom acquisition sequences. Color Doppler volumes were acquired concurrently with the channel data using default sequences on the scanner. Contrast and CNR of the vessels of interest were then computed for the complete matching B-mode and SLSC volumes using thresholded Doppler signal as a mask to select the regions inside the vessels.

Results/Discussion

Phantom and *in vivo* results indicate that the volumetric SLSC imaging reduces acoustic noise and improves visualization of the vessels when compared to conventional 3-D B-mode imaging. For the flow-phantom acquisition, contrast and CNR of the vessel are 8.17 dB and 2.18 for the SLSC volume and 4.89 dB and 0.68 for the B-mode volume. Improvements in contrast and CNR for the *in vivo* SLSC volumes depend on the quality of B-mode volumes and become more prominent as the acoustic noise in the B-mode volumes increases. 3-D views of matching B-mode, SLSC, and color Doppler volumes created from a sample *in vivo* acquisition are shown below; selected 2-D slices of these volumes are displayed as well. While both B-mode and SLSC images are of good quality, 2-D and 3-D SLSC images show suppressed clutter inside the vessels lumen and smoother surrounding tissue. Doppler images show full extent of the long vessel spanning axially down the field of view. Using Doppler signal to select a region inside of this vessel (highlighted in red in 3-D Doppler image), contrast and CNR are computed to be 10 dB and 2.3 for the complete SLSC volume and 14 dB and 1.6 for the complete B-mode volume.

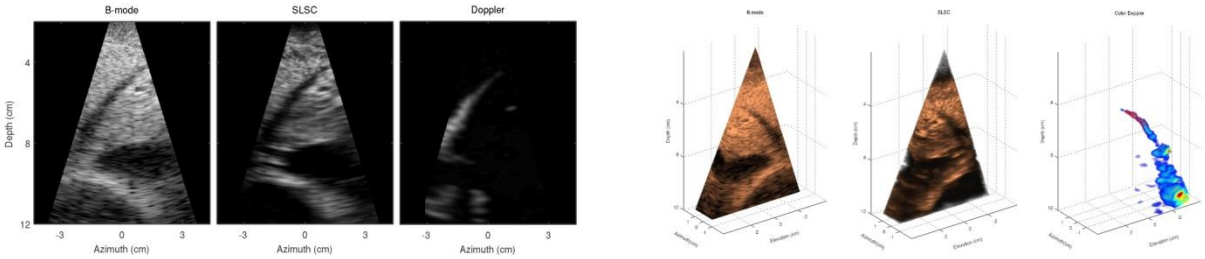

IUS1-I1-5

Reducing Clutter Noise in Fast Ultrasound Imaging with Transverse High-Pass Filtering

Jian-yu Lu[1]; [1]*Bioengineering, The University of Toledo, Toledo, Ohio, USA*

Background, Motivation and Objective

Fast ultrasound imaging such as plane wave imaging and imaging with waves of small divergences is gaining a renewed interest in recent years due to the need of high image frame rate for elasticity imaging of moving objects, blood flow velocity vector imaging, and fast cardiac imaging. However, due to a relative flat wave front of the plane wave or waves that have small divergence angles, it is observed that there is clutter noise that appears as strips that are generally in parallel with the surface of the transducer. The clutter

noise is produced by imperfect receiver electronics, multiple reflections among parallel objects, and multiple reflections between the objects and the transducer surface. The clutter noise is most obvious in anechoic areas, at deeper depths where receiver gain is high and echo signals are weak, and the steering angle is small.

Statement of Contribution/Methods

In this study, a high-pass filter of -3-dB cut-off frequency of about 0.178 mm^{-1} was applied along the axis that is in parallel with the transducer surface in the Fourier domain of two-dimensional (2D) images before envelope detection to reduce clutter noise. Images of an ATS 539 tissue mimicking phantom were produced experimentally with plane waves and waves of small divergence angles in transmissions using a home-made HFR imaging system, and were reconstructed with the HFR imaging method developed previously based on Fourier transformations. In the experiment, a 128-element, 19.2-mm aperture, and 2.5-MHz linear array transducer of about 58% -6-dB pulse-echo fractional bandwidth was used. 11 transmissions of steered plane wave (SPW) and steered diverging beams (SDB) of 6 and 9-degrees of divergence angles were used to obtain images that have a field of view larger than 90 degrees and a depth of 165 mm.

Results/Discussion

Images produced with and without the clutter reduction are shown in the first and second rows respectively in the figure. Images in the first, second, and third column are produced with the SPW, 3-degree SDB, and 9-degree SDB, respectively. It is clear that images with the clutter reduction have much less clutter noise in the projection area (the vertical strip) under the transducer that is at the center top of the images. The clutter reduction is especially noticeable at deeper depths where the signals are weak. The overall quality of images is improved after the clutter reduction.

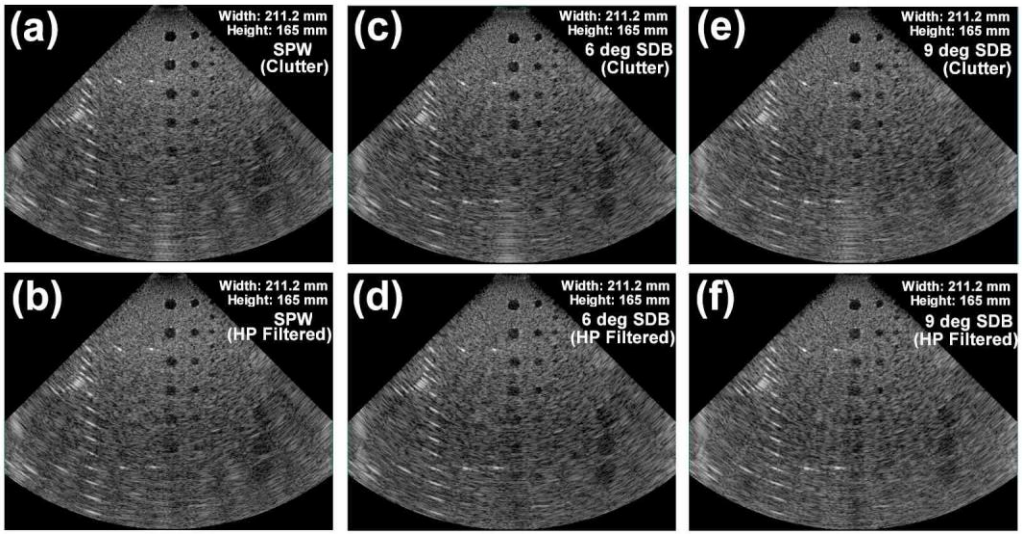

IUS1-I1-6

An automated pipeline for regional strain estimation from volumetric ultrasound data

Brecht Heyde[1], Daniel Barbosa[1], Ana-Maria Daraban[1], Ruta Jasaityte[1], Piet Claus[1], Frederik Maes[2], Jan D'hooge[1,3]; *[1]Cardiovascular Imaging and Dynamics, University of Leuven, Leuven, Belgium, [2]ESAT/PSI - Medical Image Computing, University of Leuven, Leuven, Belgium, [3]Medical Imaging Lab, Norwegian Institute for Science & Technology, Trondheim, Norway*

Background, Motivation and Objective

Strain estimation techniques can provide valuable insights into regional (dys)function. However, a manual delineation of the left ventricle (LV) is required, intrinsically leading to a time consuming analysis with significant observer variability. In this study we therefore propose a fully automated strain estimation strategy with a minimal user input, and illustrate its applicability in a realistic clinical setting.

Statement of Contribution/Methods

First, a previously developed fully automatic segmentation method using B-spline active surfaces (BEAS) with a geometrical regularizer was used to identify the LV axis and to delineate the endocardium. The epicardium was identified by growing the detected endocardial surface along its normal direction until an intensity interface similar to the endocardium was found. As such, a region-of-interest (ROI) for strain estimation was created.

Next, tracking was performed using a previously developed 3D elastic registration technique based on a B-spline free-form deformation model adapted to the subject-specific LV anatomy to improve regularization. As such, an attractive automated pipeline for regional strain estimation was created requiring only two user-inputs: indicating the right-ventricular insertion point to orient the tracked ROI and selecting end-systole (ES) for timing.

To test the proposed approach, volumetric data (32±3 Hz) was recorded in 3 healthy volunteers and 3 patients with acute myocardial infarction, using a GE VividE9 equipped with a 4V probe (1.7/3.3 MHz).

Results/Discussion

User interaction time was considerably shorter than manual contouring (19±3s vs 390±90s) and eliminated observer variability. Fig 1 illustrates that healthy volunteers had a normal homogeneous ES strain pattern using the automated approach, while dysfunctional regions in patients could be identified. Compared to the remote regions, ES strain was reduced by 13.7%, 3.8% and 8.5% for the automated method, and by 12.3%, 5.0% and 9.0% if manually contoured, in the radial, longitudinal and circumferential direction respectively.

We developed a fully automated strain estimation pipeline, showing reliable strain estimates which were in agreement with outcomes if the ROI was manually delineated, but with a considerable lower user-interaction time. The proposed approach is an attractive solution for clinical practice.

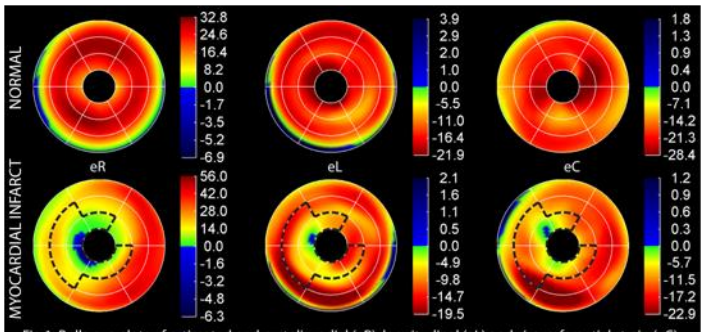

Fig.1. Bulls-eye plots of estimated end-systolic radial (eR), longitudinal (eL) and circumferential strain (eC) using the automated method for (top) healthy subject and (bottom) patient with an acute myocardial infarct. The dysfunctional area as identified by wall motion scoring is highlighted.

Improved elasticity imaging methods

M4

Wednesday, July 24 2013, 04:30 pm - 06:00 pm

Congress Hallair: **Mickael Tanter**
Institut Langevin, ESPCI

IUS1-I2-1

Assessment of the Depth-Dependence of the Mechanical Parameters of a Layered Medium Using Surface Excitation and Motion Measurements on the Surface

Salavat Aglyamov[1], Shang Wang[2], Andrei Karpiouk[1], Jiasong Li[2], Michael Twa[3], Stanislav Emelianov[1], Kirill Larin[2]; *[1]Biomedical Engineering, University of Texas at Austin, Austin, TX, USA, [2]Biomedical Engineering, University of Houston, Houston, TX, USA, [3]College of Optometry, University of Houston, Houston, TX, USA*

Background, Motivation and Objective

Acoustic radiation force can be used to remotely palpate soft tissues. When acoustic radiation force is applied to the surface of the object and displacements are available only on the surface, it is challenging to provide the viscoelastic properties of tissues with layered structures. For example, in ophthalmological applications (crystalline lens or cornea) often only surface measurements are possible. The goal of the current study is to develop a reconstruction method to estimate depth dependence of the mechanical properties of a medium based on motion measurements on the surface.

Statement of Contribution/Methods

The forward problem was solved analytically in the frequency domain using a Hankel transform. An acoustic impulse was considered as an axisymmetric force generated on the upper surface of the layer. The experiments were performed using gelatin-based phantoms with a different shear elastic modulus in each layer, adjusted by gelatin concentration. A 3.7 MHz single-element focused transducer and a phase-sensitive OCT system were used to apply the radiation force and to measure displacements on the surface, respectively.

Results/Discussion

The results of this study demonstrated good agreement between theoretical predictions and experimental measurements. Figure 1 presents an example of comparison between displacements measured on the surface of a homogeneous gelatin phantom with different durations of acoustic pulse and theoretical predictions. The Young's modulus of the phantom was independently measured using a uniaxial test (5.8 kPa). While low-frequency vibrations were sensitive to deep layers, high-frequency vibrations attenuated rapidly with depth and only superficial layers were involved in the high-frequency medium response. Therefore, the depth-dependence of the mechanical parameters can be resolved by relying on the spectral analysis concept.

The results of theoretical analyses and experimental studies suggest that the developed theoretical model accurately describes the motion of the layered medium in response to the acoustic pulse and the model can be used to evaluate viscoelastic properties of a medium.

This study was supported by NIH grants EY022362 and EY018081.

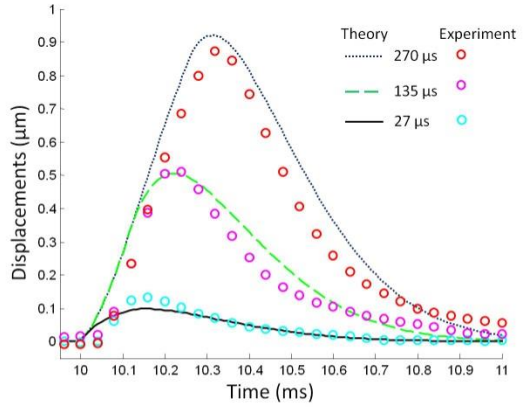

Fig.1: Comparison of theoretically predicted and experimentally measured displacements on the surface of gelatin phantom for different excitation times.

IUS1-I2-2

Two-dimensional Shear Elasticity Imaging Using Multiple Mechanical Vibration Sources and Directional Filtering

Heng Zhao[1], Pengfei Song[1], Armando Manduca[1], Matthew Urban[1], Stefan Catheline[2], James Greenleaf[1], **Shigao Chen**[1]; *[1]Mayo Clinic College of Medicine, USA, [2]University of Lyon, France*

Background, Motivation and Objective

Compared to ultrasound radiation force, mechanical vibration is capable of: A) delivering sufficient motion into deep tissues; B) producing shear waves from multiple directions for compounding images if multiple sources are used. However, the propagation direction of the shear waves generated by such method can be complicated and unpredictable,

which make it difficult to measure shear wave speed (c_s). In this study, we propose using multiple vibration sources to produce a multi-direction shear wave field, and creating a 2D c_s map after applying directional filtering to the field.

Statement of Contribution/Methods

As shown in Fig. 1(a), 10 electromagnetic vibrators controlled by a function generator were randomly attached to the surface of an elasticity QA phantom (Model 049, CIRS Inc., Norfolk, VA). The function generator sent out 20 pulses (randomly distributed over 500 ms with pulse widths each of 4 ms) to drive the vibrators. The excitation was triggered by a Verasonics ultrasound system (Verasonics, Inc., Redmond, WA) which subsequently monitored the motion in the 2D image plane using a 5 MHz L7-4 transducer (Philips Healthcare, Andover, MA) operating in flash imaging mode (frame rate = 2 kHz, detection duration = 0.6 second). The shear wave field was filtered by eight directional filters at 45 degree increments, resulting in 8 sets of shear wave data. Longitudinal waves were suppressed by a spatial filter that cuts off waves with low wave numbers. Eight 2D c_s maps were produced from the filtered signals using a time-of-flight method based on local cross-correlation. The final 2D c_s map was reconstructed by correlation coefficient weighted summation of the speed maps in 8 directions.

Results/Discussion

Fig. 1(b) shows the final c_s map of the inclusion phantom using the proposed method. The calculated Young's modulus was 66.8 ± 8.0 kPa and 31.9 ± 5.4 kPa for the inclusion and the background, respectively, as compared to nominal values of 80 ± 8 kPa and 25 ± 4 kPa, respectively. The method has good penetration and boundary delineation. Overestimation in the background is due to out-of-plane shear waves. Underestimation in the inclusion may be caused by the spatial filtering which removes high speed waves. For softer inclusions, the bias due to spatial filtering may be less.

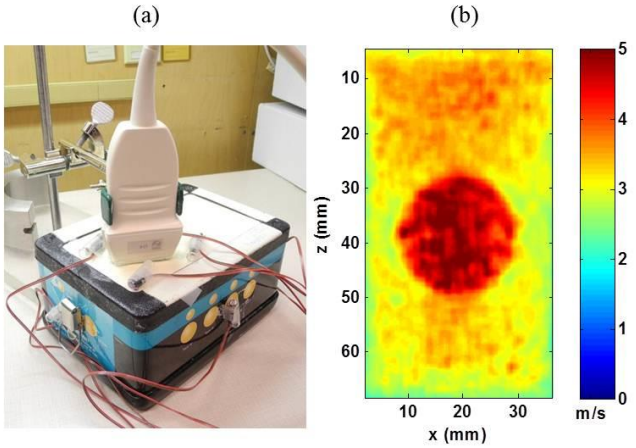

Figure 1 (a) Experimental setup for the proposed method. (b) Reconstructed 2D c_s map.

IUS1-I2-3

Bayesian Shear Wave Speed Estimation for In Vivo 3D Imaging of the Prostate

Stephen Rosenzweig[1], Ned Rouze[1], Brett Byram[1], Mark Palmeri[1], Thomas Polascik[2], Kathryn Nightingale[1]; [1]*Biomedical Engineering, Duke University, Durham, NC, USA,* [2]*Department of Urology, Duke University, Durham, NC, USA*

Background, Motivation and Objective

SWEI is a quantitative ultrasound elasticity imaging technique that has shown promise for visualizing structure and pathology within the prostate[1]. To estimate the shear wave speed, time of flight based reconstruction algorithms are widely used, assuming a known direction of wave propagation and homogeneous, isotropic tissue within the reconstruction kernel. Violation of these assumptions can lead to image artifacts generated by reflected waves at structural boundaries[2,3]. In this work, a maximum a posteriori estimator (MAPE) for shear wave speed is investigated to reduce the noise and image artifacts in the presence of tissue heterogeneity.

Statement of Contribution/Methods

The wave arrival time is assumed to be Gaussian distributed; thus, the maximum likelihood estimator (MLE) estimate is the least squares linear regression of the wave arrival times versus lateral position. In contrast, MAPE utilizes the same likelihood function combined with a generalized Gaussian prior distribution[4]. FEM simulations of a uni-directional shear wave with ultrasonic tracking[2] are performed to compare the MLE with the MAPE estimates using standard, narrow generalized, and wide generalized Gaussian prior distributions. In addition, volumetric in vivo SWEI prostate data are analyzed to compare performance of the estimators with the concurrently acquired ARFI data.

Results/Discussion

Shown below are example MAPE and median filtered MLE reconstructed SWEI images of the simulated data with a 10mm, 20kPa Young's modulus sphere in a 5kPa background. Averaged over ten speckle realizations, inside the sphere, the MLE estimate had a bias of -0.31 m/s and variance of 0.153 m/s and the MAPE estimates had biases of -0.44, -0.37, and -0.21 m/s and variances of 0.035, 0.054, and 0.245 m/s for the standard, narrow generalized and wide generalized Gaussian prior distributions, respectively. We have demonstrated the utility of the MAPE to reduce the variance or bias in shear wave speed estimates in validated simulations. We will present the optimal tradeoff achieved with the narrow generalized Gaussian prior distribution as applied to in vivo data.

[1] Barr, R et al. Ultrasound Quarterly, 2012. 28(1): p. 13-20.

[2] Rouze, N et al. IEEE UFFC, 2012. 59(8): p. 1729-1740.

[3] Deffieux, T et al. IEEE UFFC, 2011. 58(10): p. 2032-2035.

[4] Bouman, C et al. IEEE Image Processing, 1993, 2, (3), pp. 296-310

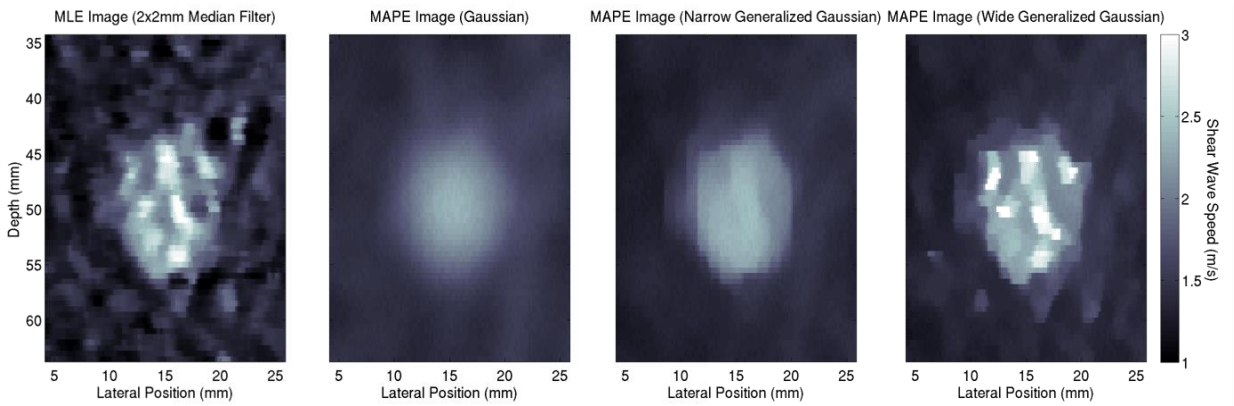

IUS1-I2-4

Fast Shear Compounding Using Directional Filtering and Two-dimensional Shear Wave Speed Calculation

Pengfei Song[1], Armando Manduca[1], Matthew W. Urban[1], Heng Zhao[1], James F. Greenleaf[1], Shigao Chen[1]; *[1]Physiology and Biomedical Engineering, Mayo Clinic College of Medicine, Rochester, MN, USA*

Background, Motivation and Objective

Shear compounding illuminates the imaging field with different angled shear waves from which elasticity maps can be reconstructed and compounded to increase signal-to-noise-ratio (SNR) and contrast of the image (Bercoff, UFFC 2004). However, the shear imaging frame rate may be reduced by the multiple separate generations and detections of different angled shear waves. To preserve frame rate and increase efficiency of shear compounding, this study proposes a fast shear compounding method by producing multiple shear waves with different angles at different spatial locations *simultaneously* to obtain a full field-of-view (FOV) 2D compounded shear elasticity map with only one cycle of shear wave generation and detection.

Statement of Contribution/Methods

A curved array C4-2 was used to transmit 5 unfocused push beams simultaneously into an elasticity QA phantom (Model 049, CIRS Inc.) with multiple inclusions, which produced shear waves with 8 propagation directions within the FOV so that each inclusion would experience multiple shear waves with different angles (Fig. 1a). A Verasonics ultrasound system immediately switched to flash imaging mode (PRF = 2.78 kHz) after push and detected the multiple shear waves. Eight spatial-temporal directional filters were designed for 8 propagation directions of the shear wave, forming 8 sets of shear wave data. A 2D shear wave speed calculation method was developed to estimate shear wave speed along both lateral and axial directions so that a true speed can be obtained geometrically, using a robust estimation process (Anderssen-Hegland, AMS 1999) to improve the smoothness of local shear wave speed estimation while preserving the spatial resolution. Shear compounding was then done by weighted summing (by correlation coefficients) of the shear wave speed maps from all 8 directions.

Results/Discussion

Fig. 1b shows a smooth full FOV 2D compounded shear wave speed map of the phantom from one push-detect acquisition (<25 ms). Three types of inclusions with sharp boundaries and good contrast to background can be clearly resolved. Results from Fig. 1c show good agreement between the elasticity measurement and nominal values. These results indicate that the proposed shear compounding method is effective in providing smooth shear elasticity maps with a large FOV and good contrast while preserving high imaging frame rate.

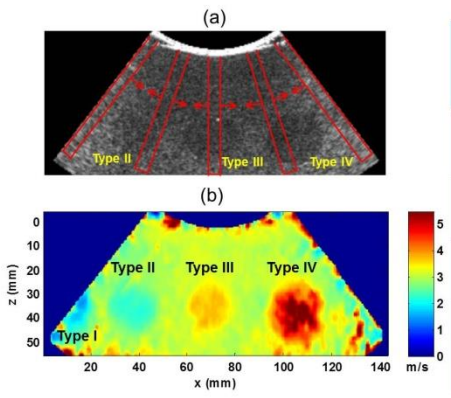

(c)

	Measured values (kPa)	Nominal Values (kPa)
Type II	16.9 ± 1.33	14 ± 4
Type III	41.0 ± 1.84	45 ± 5
Type IV	72.3 ± 11.8	80 ± 8
Back-ground	28.0 ± 2.16	25 ± 4

Figure 1. (a) B-mode image of the phantom. The red rectangles indicate the unfocused push beams; the red arrows indicate the shear wave propagation directions. (b) 2D shear wave speed map of the phantom. Type I inclusion can not be resolved in (a) but can be partially resolved in (b). No spatial smoothing filters were applied to this map. (c) Comparisons between the Young's modulus measurements from the compounded map (b) and the nominal values. The Young's modulus is given by $3\rho c^2$ (ρ is density; c is shear wave speed).

IUS1-I2-5

Temporal guided search for elastography motion tracking

Matthew Bayer[1], Timothy Hall[1]; *[1]Medical Physics, University of Wisconsin-Madison, Madison, Wisconsin, USA*

Background, Motivation and Objective

Guided search, where displacement estimates at selected locations in an image are used to predict the displacement of neighboring locations, has proven successful in elastography by improving accuracy and reducing computation time. Nearly all guided-search algorithms in the literature obtain guidance from estimates that are nearby *in space*; but it is also possible that effective guidance could be obtained from estimates nearby *in time*. Such a strategy would be useful for tracking sequences of ultrasound images, as in multicompression techniques. It is especially relevant for the reconstruction of the elastic nonlinearity of tissue, which requires large deformations and therefore long image sequences.

One source of temporal guidance is the past displacement history of a region of tissue, which may have predictive power for its future motion. A second source of guidance is the necessary consistency among displacement estimates of different step sizes. Given a sequence of three image frames, for example, accumulating the displacements between each consecutive pair must be consistent with tracking directly between the first and third image frames. Both past displacement history and consistency between step sizes could be exploited by tracking algorithms.

Statement of Contribution/Methods

Three algorithms that use temporal guidance are proposed. The first method uses the Viterbi algorithm to dynamically regularize the discontinuity of displacement estimates in time. This method is directly analogous to previously proposed algorithms that have used the Viterbi algorithm over spatially neighboring estimates. In the second algorithm, displacement estimates over small increments of motion are accumulated and used as guidance for estimates over larger increments. The third method combines these two approaches, so that larger-strain estimates are incorporated as extra data into the Viterbi process. Algorithm effectiveness was measured by the frequency of peak-hop errors in a sequence of freehand images of an elastography phantom. The sequence contained 13 images taken at a low strain rate, so that the total compressive strain in the last frame was about 1%. Peak hops were located by comparing with the results of a spatial guided-search algorithm, which was judged by manual inspection to have eliminated all peak hops.

Results/Discussion

When compared to simple block-matching between the first and last image in the sequence, the proposed algorithms reduced peak-hop errors by 97%, 74%, and 96% respectively. While these results do not quite equal the performance of the spatial guided-search algorithm, they nonetheless show that temporal information can successfully guide motion tracking. In tissue, where spatial continuity is less reliable than in phantoms, temporal guidance may be a valuable complement to spatial guidance.

The authors gratefully acknowledge support from NIH grants T32CA0009206 and R01CA140271.

IUS1-I2-6

Iterative autocorrelation motion estimation with application to elastography imaging

Svetoslav Nikolov[1]; [1]*BK Medical Aps, Farum, Nordsjæland, Denmark*

Background, Motivation and Objective

Precise, robust and efficient motion estimation is needed in elasticity imaging. Two are the main estimation techniques: spatial shift estimation using block matching (speckle tracking), and phase-shift estimation. The phase-shift estimators are robust and easy to parallelize as they don't do searching. The down-side is that large displacements result in phase aliasing and larger variance of the estimates.

Statement of Contribution/Methods

This paper presents a method that uses two iterations of phase estimation to achieve high precision, and an algorithm that unwraps the phase and removes glitches from the estimation process.

First, the phase-shift at every pixel is found via lag-zero cross correlation between two frames. Then the phase is unwrapped and converted to displacement, which is quantized to the nearest sample. These are used as correlation lags for the cross-correlation in the second iteration. Only cross-correlation at non-zero lags is calculated. The variance is low, but glitches are present at the transitions from lag to lag. The last step involves a specially designed algorithm that detects the transitions, and estimates and removes the glitches.

Results/Discussion

The algorithm was implemented in OpenCL and runs in real time at 60 frames/second producing 192 lines and 1600 estimates per line on ATI Radeon HD 5870. Data is streamed from a BK UltraView ProFocus scanner.

The improvement of the approach is assessed from the signal-to-noise ratio (SNR) of the displacement estimates at non-zero lags. Fig. 1a shows the SNR of a free-hand acquisition of 110 frames using a 6-MHz, 192-element linear array with 300 um pitch. The scanned target is a breast elastography phantom, model 059, by CIRS.

The scan depth is 5 cm, and the sampling frequency of the complex base band signal (IQ) is 20 MHz. The average improvement of the SNR is 6.2 dB. Fig. 1b shows that the lags found at iteration 1 for frame 62 vary from 0 to -4.

Fig. 1c and 1d illustrate that the variance of estimates from a standard lag-0 phase shift estimator increases with displacement magnitude, while the approach described in this paper maintains the same variance in the whole image.

In conclusion, the presented method decreases the variance of motion estimates at large displacements and increases the effective range of elasticity imaging. It is also suitable for real-time implementation.

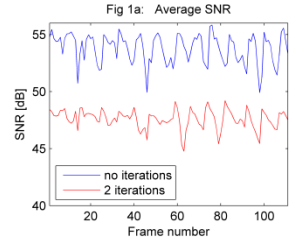
Fig 1a: Average SNR
SNR [dB]
Frame number
no iterations
2 iterations

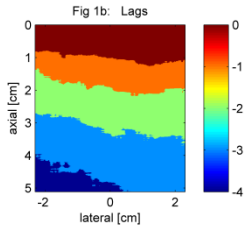
Fig 1b: Lags
axial [cm]
lateral [cm]

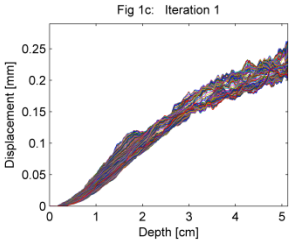
Fig 1c: Iteration 1
Displacement [mm]
Depth [cm]

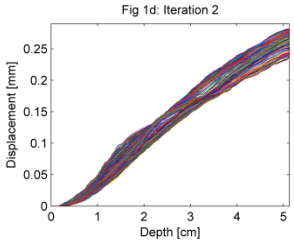
Fig 1d: Iteration 2
Displacement [mm]
Depth [cm]

Beamforming II

M5

Wednesday, July 24 2013, 04:30 pm - 06:00 pm

Congress Hallair: **John Hossack**
University of Virginia

IUS1-I3-1

Apodization Schemes for SLSC Imaging: Simulation, Phantom and in vivo Demonstrations of Image Quality

Nick Bottenus[1], Jeremy Dahl[1], Gregg Trahey[1,2]; [1]*Biomedical Engineering, Duke University, Durham, North Carolina, USA,* [2]*Department of Radiology, Duke University, Durham, North Carolina, USA*

Background, Motivation and Objective

In conventional B-mode ultrasound, apodization is often used to reduce sidelobes at the expense of main lobe width, reducing resolution but improving overall target visibility. In short-lag spatial coherence (SLSC) imaging, images are produced using the correlation between echo signals received across the aperture domain rather than coherently summing the signals. SLSC imaging is unique in that the contrast in the resulting image is dependent on the local coherence, which itself is a product of the lateral pressure profile in the field. When the transmit aperture is apodized using conventional windows, the coherence curve is distorted and the resulting image quality is degraded. Using unconventional windows, we demonstrate that it is possible to develop an apodization scheme to improve detectability in the SLSC image.

Statement of Contribution/Methods

Using a single transmit element and all receive elements on an array, we acquire full channel data in real time and store the resulting data sets for offline processing. Using the virtual source concept, we can then construct synthetic channel data sets with arbitrary transmit and receive apodizations. This synthetic aperture tool allows us to evaluate families of apodization functions with matched target and noise conditions, isolating the effects of the apodization.

Results/Discussion

We compare the effects of conventional windows such as the Tukey family, the Hamming window and the raised cosine to inversions of these windows with various levels of modulation (the window subtracted from a constant). The attached figure shows sample apodizations, demonstrating a boxcar apodization, a Tukey window and an inversion of the Tukey window for B-mode and SLSC images of a -12 dB simulated lesion. The contrast-to-noise ratio (CNR) is shown in each case, demonstrating improved visibility in the inverse Tukey SLSC case. We discuss the effects of apodization in SLSC using Field II simulations, phantom studies and in vivo images.

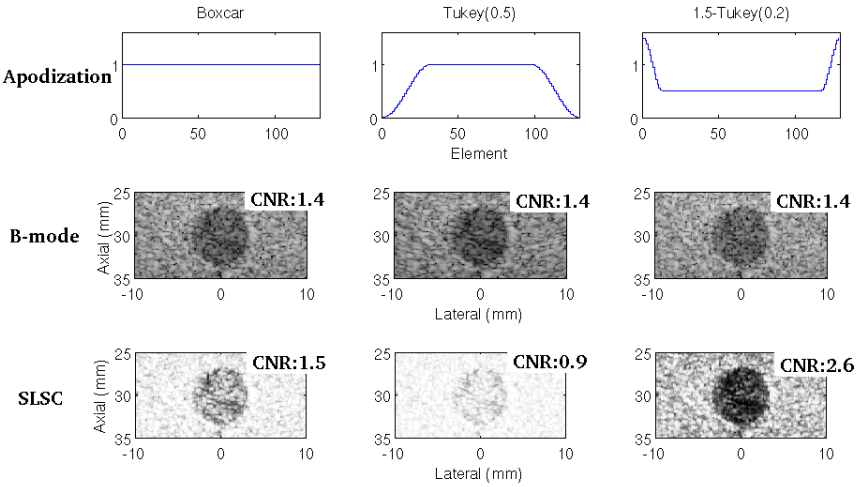

IUS1-I3-2

In vivo demonstration of a real-time simultaneous B-mode/spatial coherence GPU-based beamformer

Dongwoon Hyun[1], Gregg Trahey[1], Jeremy Dahl[1]; [1]*Duke University, Durham, NC, USA*

Background, Motivation and Objective

Short-lag spatial coherence (SLSC) imaging is an advanced beamforming technique that displays the level of spatial coherence in ultrasonic backscatter, unlike traditional delay-and-sum (B-mode) beamforming, which displays echo magnitude. SLSC images have demonstrated greater resistance to clutter than B-mode images formed using the same data in simulations, phantoms, and *in vivo* experiments, and have shown further improvements when combined with harmonic imaging. However, implementing SLSC imaging in real-time is challenging because the SLSC algorithm is computationally expensive and requires access to the raw channel signals. By using a GPU-based software beamformer, we have developed a real-time SLSC imaging system capable of up to 6 frames per second.

Statement of Contribution/Methods

The Verasonics (Verasonics Inc., Redmond, WA) platform was used to acquire raw channel data in real-time using the ATL L12-5 and P4-2 transducers, transmitting at 7.5 MHz and 2.5 MHz, respectively. Pulse-inversion harmonic imaging was implemented as well. A GPU-based software beamformer dynamically focused the raw signals, computed both

the B-mode and SLSC images, and displayed them in real-time. The system was used to image lesion phantoms and *in vivo* thyroids and livers. Imaging performance was quantified using the contrast-to-noise ratio (CNR) metric.

Results/Discussion

SLSC images generated using the real-time system were consistent with those observed in previous studies, and showed similar clutter reduction and CNR improvements over B-mode. A sample screenshot of the on-screen display from an *in vivo* liver scan is provided in Figure 1. Note the enhanced contrast and definition of the vasculature in the SLSC image (right). The CNR of the phantom lesion increased from 1.5 to 1.7, the CNR of vasculature in the thyroid increased from 1.8 to 3.6, and the CNR of the gallbladder increased from 1.1 to 2.6. Using the GPU, computational throughput was increased 60-fold over previous CPU implementations. The framerates of the SLSC imaging system were dependent on the imaging parameters (e.g. number of beams), and ranged from 1 to 6 fps under realistic imaging conditions. We demonstrate videos of this system showing *in vivo* imaging of liver and thyroid at these frame rates.

This research was supported by NIBIB grant R01-EB013661.

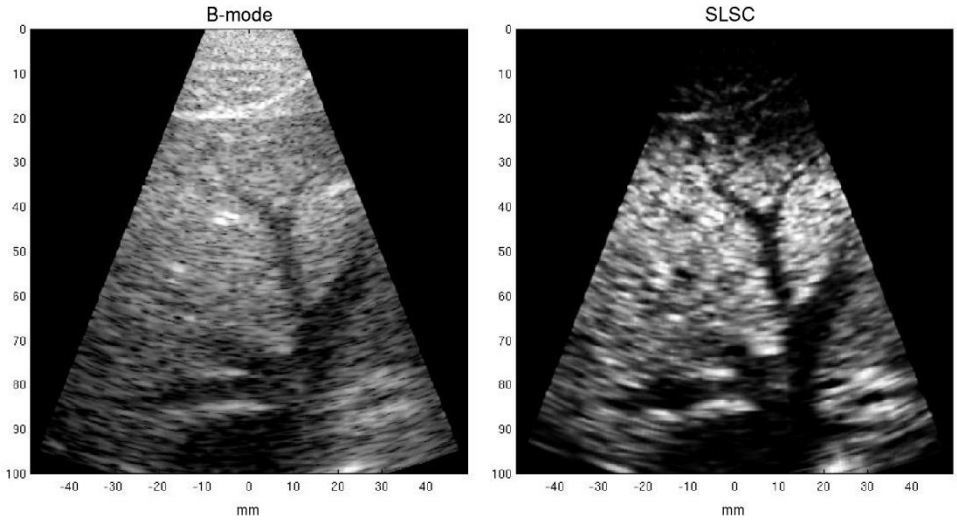

IUS1-I3-3

Transcranial Image Quality Improvement with a Multi-Step approach

Francois Vignon[1], William Shi[1], Vijay Shamdasani[2], Paul Kalman[2], Douglas Maxwell[2], Jeffry Powers[2]; *[1]Philips Research North America, USA, [2]Philips Healthcare, USA*

Background, Motivation and Objective

Transcranial ultrasound image quality suffers from the presence of the skull bone in the acoustic path, leading to beam defocusing and loss of spatial and contrast resolution. Besides the requirement of an adequate transtemporal acoustic window, phase aberration correction and adaptive beamforming through the application of spatially-dependent weights (e.g. Wiener Factor (WF)) have been proposed to refocus wavefronts and mitigate the effects of sidelobes. The objective of this study was to test the effectiveness of a combination of techniques to enhance transcranial image quality.

Statement of Contribution/Methods

The concept of a large array reconfigurable to the acoustic window size is demonstrated by using a large footprint (~4cmx2cm) matrix array (Philips X6-1). The array is placed on the skull and only the (2cmx1cm) sub-aperture that receives most energy from the region of interest is used for receive beamforming, ensuring consistent and robust use of the best acoustic window. 2D receive-only aberration correction is then performed on fundamental and harmonic B-mode per-channel data. Receive-only correction is easier to implement than two-way correction and is expected to yield almost as much benefit. Harmonic data is preferred because the harmonic transmit beam is naturally better focused than the fundamental one. WF weighting is finally applied in the channel domain. Five volunteers were scanned transtemporally in the brain stem plane and image quality improvements were assessed by a professional sonographer.

Results/Discussion

In all 5 cases, the image quality improvements from combined receive aperture optimization, aberration correction and WF weighting were judged clinically significant. The figure shows the harmonic image on one subject when (a) using the full aperture for receive beamforming, (b) using a receive aperture matched to the measured acoustic window size and position, (c) adding receive aberration correction, and (d) further adding WF weighting. Optimal window selection had the greatest effect on image quality, significantly improving image SNR. Aberration correction provided marginal resolution improvement in a small sector of the image (the isoplanatic patch); the improvements from aberration correction only were deemed clinically insignificant. WF weighting further increased the apparent SNR.

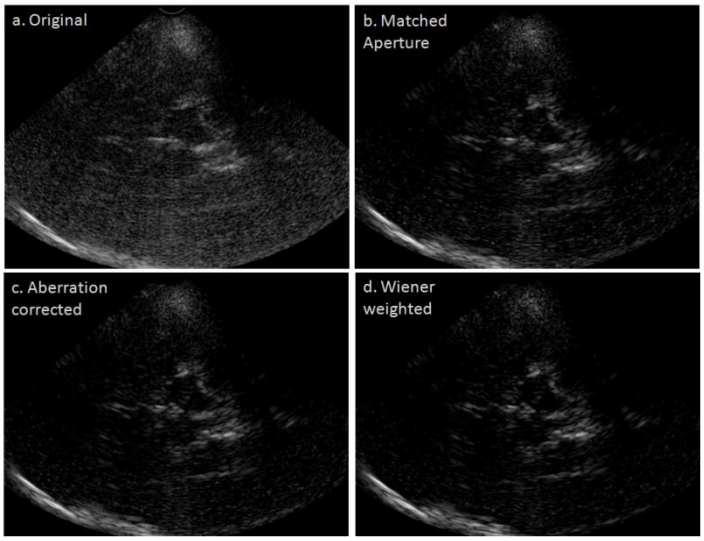

IUS1-I3-4

Clutter, multiple reverberation and aberration in brain imaging

Gianmarco Pinton[1,2]; [1]*Institut d'Alembert, Centre National de la Recherche Scientifique, Paris, France,* [2]*Universite Pierre et Marie Curie, France*

Background, Motivation and Objective

Current research on ultrasound propagation in the head has been directed towards therapeutic applications and to a lesser extent towards brain imaging. The skull is a strong phase aberrator that degrades the image quality and several methods have been developed to correct this aberration. However reverberation, between the skull and the transducer or within the skull, also has an impact on image quality. Yet it has not previously been characterized. The objective of this paper is therefore to determine the impact of reverberation clutter on brain imaging and to compare its significance to aberration.

Statement of Contribution/Methods

Two previously established techniques are combined in this paper. First to quantify aberration and reverberation clutter a three dimensional full-wave nonlinear acoustic simulation is used to propagate ultrasound through the temporal acoustic window of the human skull measured with computed tomography. The phase aberration is calculated by transmitting an outward propagating pulse from a point target to a large 2D 5 x 5 cm transducer. Then the corrected wave is retransmitted from the transducer to the point target. These techniques have been previously established and validated in the context of brain therapy. Second, techniques that have been used to characterize reverberation clutter in conventional ultrasound imaging are applied. The resulting phase aberration maps and point spread functions (PSF) quantify the contribution of aberration and reverberation to the degradation of the 3D PSF.

Results/Discussion

The left figure illustrates the transmitted imaging pulse after aberration correction. On the middle a reference transmit-receive point spread in a homogeneous medium (i.e. with no skull). On the middle right a transmit-receive PSF for transmission through the skull with phase corrected (note the mirror PSF at the bottom of the image, demonstrating one of the consequences of reverberation). On the far right the phase map across the transducer face.

In conclusion we demonstrate that reverberation clutter significantly degrades ultrasound imaging in the brain and that this effect increases with frequency. This suggests that clutter reduction methods, such as harmonic imaging, or spatial coherence imaging, may contribute significantly to image quality improvements for large 2D arrays in brain imaging.

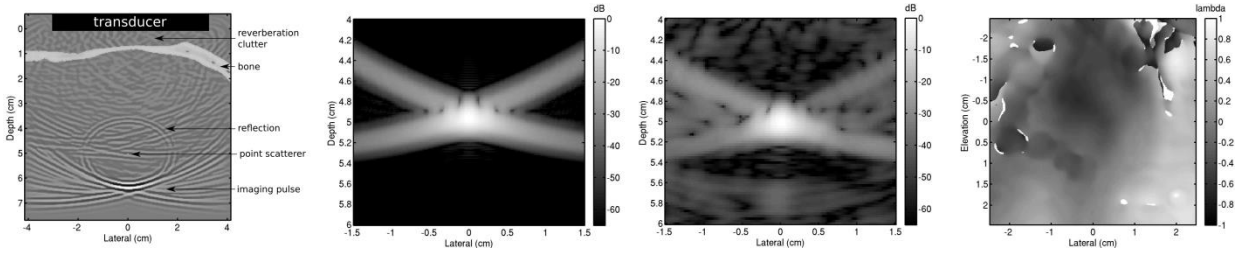

IUS1-I3-5

A model based beamformer utilizing spatial chirps to suppress off-axis and near-field clutter

Brett Byram[1]; [1]*Biomedical Engineering, Duke University, USA*

Background, Motivation and Objective

Traditional beamforming effectively attenuates signals received from scatterers located off-axis from the main beam but fails to adequately suppress signals originating in the near-field from reverberation. Reverberation has recently been reintroduced as a dominant clutter source in many clinical scenarios. Aperture domain coherence methods have been shown to reduce all clutter mechanisms, but coherence images are fundamentally different from B-mode and the radio frequency (RF) signal is lost. In order to preserve the B-mode image and RF signal, a new model based beamformer is proposed.

Statement of Contribution/Methods

The new beamforming model is derived from the Fresnel approximation and accounts for backscatter originating in the near-field and off-axis. The model is the summation of linear frequency modulated (chirp) sinusoids sampled across the array. Each sinusoid's chirp-rate encodes the returning wave's depth of origin, while frequency encodes arrival angle relative to the beam axis. The model can be used to decompose the signal sampled spatially across the array into the origins of the waves arriving at the transducer concurrently. Waves originating from the region of interest can be reconstructed into RF signals. The chirp beamforming algorithm is applied to channel data from 5 patients using the Siemens S2000 and C4-1 curvilinear array (Siemens Healthcare, Mountain View, CA). Data were acquired at 2 MHz center frequency across 64 channels centered about each beam axis. Matched simulations have also been performed.

Results/Discussion

The results demonstrate feasibility and significance. Simulations demonstrate that the two-sided -20dB beamwidth for a point displaced laterally was 2.1mm, while the one-sided -20dB width for an axially displaced point was 9.3mm indicating increased susceptibility to reverberation clutter. In vivo quality with and without the new beamformer was assessed with contrast and contrast-to-noise ratio (CNR) using manually selected regions on normal images. Across five patients contrast improved 5.51±1.2dB. The CNR change was -1.1±3.9dB. The CNR change links to decreased speckle SNR in decluttered images suggesting regions of perceived pure speckle may have structure hidden by clutter. Example images are shown from the same data, beamformed with normal and chirp based methods both displayed with 65dB dynamic range.

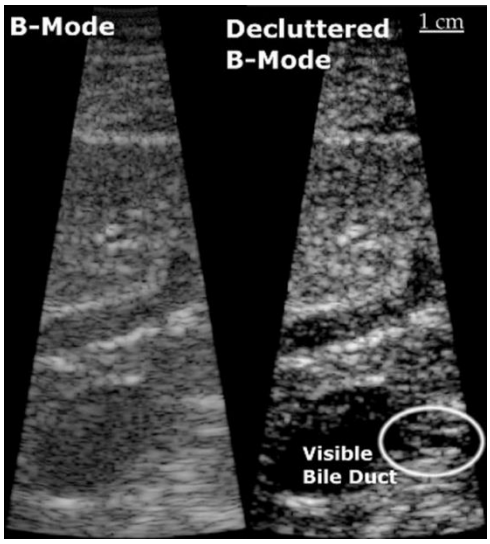

IUS1-I3-6

Identification and Impact of Blocked Elements in 1-D and 2-D Arrays

Marko Jakovljevic[1], Jeremy Dahl[1], Gregg Trahey[1,2]; *[1]Biomedical Engineering, Duke University, Durham, North Carolina, USA, [2]Radiology, Duke University, Durham, North Carolina, USA*

Background, Motivation and Objective

While methods have been developed to alleviate image degradation in the presence of blocked elements, characteristics of their signals as well as the extent to which they degrade the image quality are not fully understood. Using a newly developed tool for rapid single-channel acquisition on a matrix array, we systematically address these aspects of the problem on *in vivo* channel data from a fully sampled 2-D array and extend our results to 1-D arrays with partially blocked elements.

Statement of Contribution/Methods

We acquired individual-channel signals on the human liver intercostally, using a Siemens 4z1c matrix array on a Siemens SC2000 ultrasound scanner. Amplitude and the nearest-neighbor normalized cross-correlation of these signals were computed to identify the blocked elements in the 2-D aperture. The channel-signals were summed coherently in the elevation dimension to create a synthetic 1-D aperture data-set. Image degradation due to partially blocked elements was measured by creating a series of (2-D) B-mode images for a growing synthetic 1-D aperture and calculating contrast and CNR of the liver vasculature for each image.

Results/Discussion

Sample images in the left figure display normalized amplitude and nearest-neighbor cross-correlation of the individual-channel signals of the matrix array from a single transmit event and averaged over 4 cm of depth. The region of dark pixels located on the left side of both images is caused by the ribs blocking the left part of the aperture; signals from the blocked channels have 8.4 dB lower average amplitude than the signals recorded on the remainder of the aperture. The right figure shows similar amplitude and correlation information as the left figure, but for a single row of elements over the range of transmit-beam steering angles. As the transmit beams are steered away from the ribs, the number of blocked elements in the row decreases. For the synthetic 1-D aperture, contrast and CNR increase with increasing aperture size until the signals from the partially blocked elements are included. Contrast and CNR reach maxima of 9.2 dB and 1.3, respectively, for the 21-element synthetic aperture and then gradually decrease to 7.1 dB and 1.03 for the full aperture. Control measurements show a constant increase in contrast and CNR in the absence of blocked elements with maxima of 10.8 dB and 1.5 reached at full aperture.

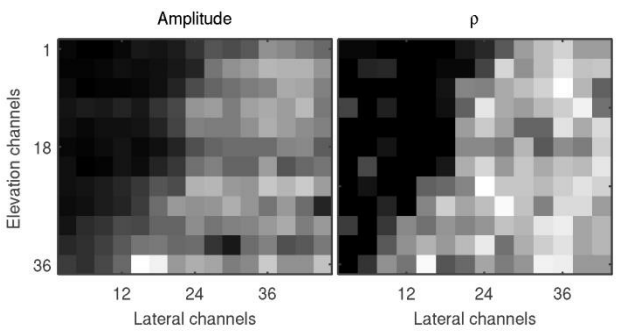
Amplitude
ρ
Elevation channels
1
18
36
12
24
36
Lateral channels
12
24
36
Lateral channels

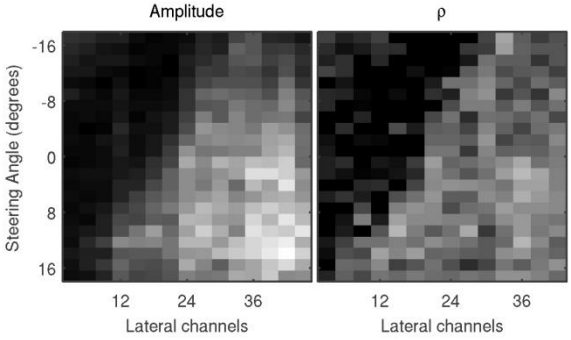
Amplitude
ρ
Steering Angle (degrees)
-16
-8
0
8
16
12
24
36
Lateral channels
12
24
36
Lateral channels

SAW Sensor Applications

NH

Wednesday, July 24 2013, 04:30 pm - 06:00 pm

Congress Hallair: **David Greve**
Carnegie Mellon University

IUS2-I-1

Response of quartz ball surface acoustic wave (SAW) sensor to trace moisture

Kazushi Yamanaka[1], Satoshi Hagihara[1], Tomohiro Saito[1], Oizumi Oizumi[1], Nobuo Takeda[1], Shigo Akao[1,2], Kosuke Takayanagi[2], Takayuki Yanagisawa[2], Noritaka Nakaso[2], Yusuke Tsukahara[2], Toshihiro Tsuji[1]; [1]*Tohoku University, Japan,* [2]*TOPPAN PRINTING CO. LTD., Japan*

Background, Motivation and Objective

Trace moisture measurement less than 1 ppm is necessary to evaluate highly pure gases for EL displays and semiconductor processes. A capacitive hygrometer needs more than 7 minutes which is not fast enough. In this situation, quartz ball surface acoustic wave (SAW) sensor [2] without sensitive film enabled to measure 1 ppm moisture in only 15 seconds [3], though response mechanism is not clear. On the other hand, it is reported that damaged layer of quartz caused by friction against another quartz reacted with water at room temperature [4]. Since the quartz ball SAW sensor was lapped by colloidal silica, there is a possibility that similar phenomenon might take place. Therefore, we evaluate damaged layer in the quartz ball SAW sensor to reveal the response mechanism.

Statement of Contribution/Methods

The delay time responses of sensor A and B to trace moisture are shown in Fig 1(a). Significant response appeared in sensor A, where the velocity of quartz was increased by water vapor due to negative delay time change. The response was not appeared in sensor B. In the subtracted signal, Fig 1(b), thermal drift was canceled by these differences and the concentration of 0.1 ppm was detected with sufficient S/N ratio. The evaluation of damaged layer was performed by composition analysis by EDX and SIMS, as well as by crystallinity evaluation based on etching by buffered hydrofluoric acid (BHF) and topography obser-vation by laser scanning microscope (LSM).

Results/Discussion

The LSM image in Fig 2(a) after etching showed that sensor A had many grooves, pits and irregular profile indicating low crystallinity and amorphous silica. But, sensor B had a flat surface in Fig 2(b). Though a few pits were observed they had linear profile suggesting crystal facets, indicating absence of amorphous silica. These results suggest that the response of the quartz ball SAW sensor is originated from hydration of damaged layer introduced by the lapping process of ball with the strained Si-O-Si bridges. Since the damaged layer extends to subsurface of tens of nm, it can explain the robustness of the present sensor for more than one year, which recovers by clean nitrogen flow even after contaminated by manipulation.

References:

1 Funke, et al; Rev. Sci. Instrum.74 (2003) 3909. 2 Yamanaka et al, IEEE Trans. UFFC. 53 (2006) 793. 3 Takeda et al, Int. J. Thermophys. 33 (2012) 4 Nakamura et al, Geophys. Res. Lett. 39 (2012) L21303.

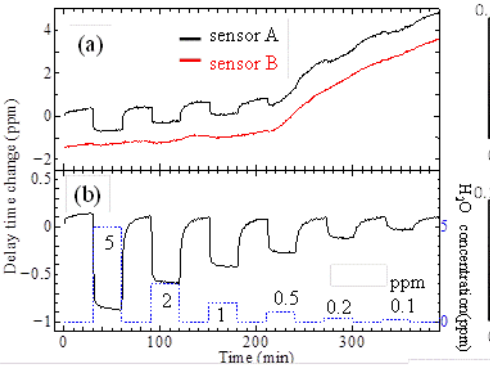

Fig. 1 (a) Delay time response to trace moisture (b) Difference of sensor A and B

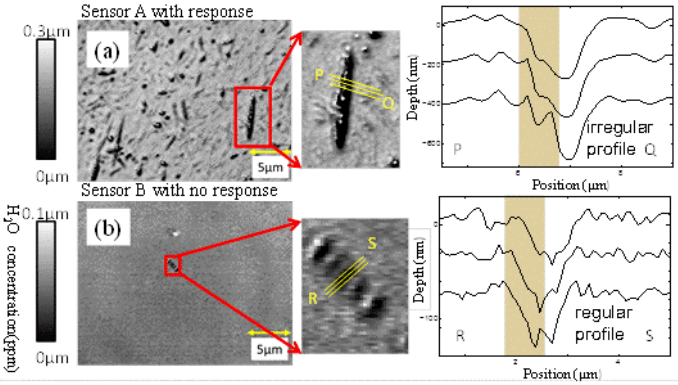

Fig. 2 (a) LSM image and profile of etched sensor A showing irregular grooves (b) Image of sensor B with flat surface and profile of a pit with crystal facets

IUS2-I-2

Characterization of liquids using leaky surface acoustic waves in YX-$LiTaO_3$

Daumantas Ciplys[1], Romualdas Rimeika[1]; [1]*Department of Radiophysics, Vilnius University, Vilnius, Lithuania*

Background, Motivation and Objective

Surface acoustic waves (SAW), being very sensitive to properties of media adjacent to the propagation surface, present an excellent tool for characterization of liquids. Several types of sensors for liquids based on Love, leaky waves and acoustic plate modes were proposed [1], but necessity of transducer isolation from liquid or use of thin, hence mechanically fragile, substrates and multi-mode operation remained of additional concern. Recently, we have demonstrated the efficiency of strongly radiating leaky SAWs in YX-lithium tantalate for sensing purposes [2]. It was objective of the present work to develop on this basis a method for liquid characterization that would be free of above mentioned drawbacks.

Statement of Contribution/Methods

We report on the strong response of leaky SAWs in YX-$LiTaO_3$ to the changes in liquid conductivity and apply this effect for liquid characterization. The experimental configuration shown in the inset of Figure comprises a lithium tantalate substrate (1) with two interdigital transducers (IDTs). The leaky surface acoustic wave (LSAW) excited by the input IDT (2) radiates energy into the crystal bulk in the form of well-defined obliquely propagating beam. Upon reflection from the opposite substrate face, this beam excites a leaky surface wave, which re-radiates the bulk beam that is received by the output IDT (3). The drop of liquid under test (4) was deposited on the acoustic beam reflection region, and the transmission loss and phase shift between the two IDTs were measured using a radio-frequency network analyzer. The potassium nitrate (KNO_3) solution in distilled water of different concentrations was used as a test liquid of varying conductivity.

Results/Discussion

The measured variations in amplitude and phase of transmitted acoustic signal with solution conductivity are shown in Figure. The observed dependencies are explained by the acoustoelectric interaction of the leaky wave at the crystal-liquid interface, and a reasonable agreement between the experimental measurements and theoretical calculations is obtained. A unique combination of amplitude and phase changes at given conductivity can be used as a characteristic signature of a liquid for its identification. We have demonstrated such a possibility using several commercial brands of mineral water with different ionic composition.

1. C. R. Evans et al, "Lithium tantalate layer guided plate mode sensors", Sens. Actuators A., vol. 132, p. 241-244, 2006.

2. R. Rimeika et al, "Acoustoelectric effects in reflection of leaky acoustic waves from LiTaO3 crystal surface coated with metal film", Appl. Phys. Lett., vol. 98, 052909 (1-3), 2011.

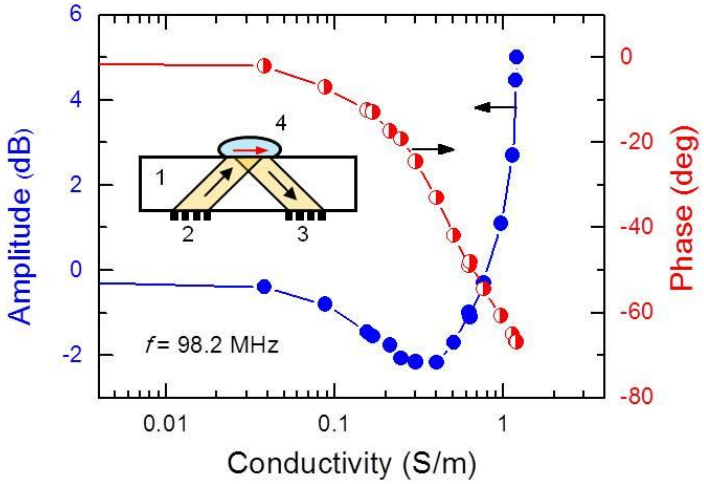

IUS2-I-3

Wireless Sensing in Hostile Environments

Mauricio Pereira da Cunha[1]; [1]*Department of Electrical and Computer Engineering, University of Maine, Orono, ME, USA*

Background, Motivation and Objective

Microwave acoustic devices have long been shown to provide sensitive platforms for physical and gas sensors. Several acoustic modes, including bulk, surface, pseudo-surface, plate, and interfacial waves, have been explored to sense variations in measurands such as temperature, pressure, stress, chemical etch rate, and liquid or gas concentration. Piezoelectric substrates introduced over the past two decades, such as the langasite (LGS) family of crystals, gallium orthophosphate, and aluminum nitride have enabled the exploration of microwave acoustics sensing at temperatures above 500°C. However the ability of the substrate to withstand high temperatures is only one of the requirements for sensor operation in harsh environments. Other prerequisites are: the development of stable high-temperature device electrodes; appropriate packaging; and resilience to thermal shock and thermal cycling of the entire system. Acoustic wave sensors capable of meeting these requirements have been developed. These sensors offer additional attractive features such as wireless battery-free operation and the capability of interrogating multiple devices.

Statement of Contribution/Methods

In this paper, the wireless operation of microwave acoustic wave sensors in harsh environments will be reviewed, and the most recent achievements highlighted, focusing in particular on surface acoustic wave (SAW) sensor technology. Wireless harsh environment SAW sensors have been interrogated in time, frequency, or code domain, with each of these techniques allowing multiple devices to be addressed by the same interrogator. Harsh environment LGS sensors have been designed and fabricated for use on static and rotating parts, and for temperatures up to 1000°C. In tests on rotating parts, such sensors endured multiple acceleration/deceleration cycles with centrifugal loads up to 53,000 g's. The sensors have also survived thermal shock tests and long term operation at high temperature. Harsh environment pressure sensors have been tested up to 225 psia and 500°C. Recent work targets sensor operation beyond 1000°C, and include advances in electrode development, electrical connections, and packaging.

Results/Discussion

Wireless hostile environment microwave acoustic sensors capable of operation up to 1000°C have transitioned from laboratory proof-of-concept to commercial devices and systems during the last decade. Significant advances, discussed in this paper, were required regarding thin film electrode research; device design; and packaging to achieve sensor operation and reliable performance up to these temperatures. Recent accomplishments in thin film technology and packaging are extending the technology to even higher temperatures, beyond 1000°C. These technological advances have enabled wireless microwave acoustic sensor applications in hostile environments such as power plants, turbine engines, refineries, and harsh industrial processes.

IUS2-I-4

Ultrasonic Measurement of Heat Flux

Donald Yuhas[1], Keith Karasek[1], Joseph Lloyd[1], Tom Klosowiak[1]; [1]*Industrial Measurement Systems, Aurora, IL, USA*

Background, Motivation and Objective

Accurate heat flux values are needed in the field of fluid mechanics and heat transfer. Maximizing or minimizing the thermal energy transfer in many systems is crucial to their optimum performance. Existing heat flux sensors include thermopiles and calorimeters, which measure spatial gradients or temporal temperature variations in such a way as to derive the heat flux. These intrusive devices disturb the phenomena being measured, require tedious calibration, and have bandwidth limitations. The present work describes the development and validation of ultrasonic-based techniques to measure heat flux.

Statement of Contribution/Methods

Ultrasonic-based heat flux measurements represent a significant departure from conventional techniques. In this study, we show that heat flux measurements can be made using precise measurements of time-of-flight (ToF) variations of ultrasonic echoes obtained from a heated surface. Several experiments have been carried out on 80 mm long rods, heated at one end with an IR source. Ultrasonic sensors attached to the non-heated end of the rod are used in pulse-echo mode to record echoes from the heated surface. In these experiments, 10 MHz echo data is recorded at repetition rates as high as 5000 Hz. Even though the piezoelectric sensor is 80 mm from the heated surface, the ToF response to the heating event is immediate, rising rapidly when the IR source is turned on and reaching a maximum value as the heating source is switched off.

Results/Discussion

Experiments were carried out on three different rod materials; copper, aluminum, and titanium. In a separate series of experiments, the velocity temperature coefficients, which are necessary for heat flux determinations, were measured for each rod material. These results are combined with analytical models to produce ultrasonic-based estimates of heat flux. The models show that the heat flux is directly proportional to the time derivative of the ToF variation. To validate the ultrasonic-based heat flux estimates, thermal models are used to calculate the heat flux. Transient thermal models have been developed using COMSOL and have been calibrated in a separate series of heating trials where multiple thermocouples are used to measure the temperature profile. The thermal models not only to produce independent heat flux estimates but also to enable simulation the ToF data. The characteristics of the time history of the measured ToF variations is in excellent agreement with the simulated results. For the three materials and test conditions used in this study, ultrasonic-based heat flux values of 2.75 +/-.25 x 10^5 W/m^2 were measured. This compares favorably to the thermal model-based estimates of 2.5 x 10^5 W/m^2. The ultrasonic-based measurement has excellent temporal response and the operating temperature is limited only by the melting point of the probe material. Reliable and robust operation is possible because the active portion of the sensor is remote from the heated surface.

IUS2-I-5

Comparison of Newtonian and non-Newtonian fluid dynamics on removal efficiency of non-specifically bound proteins in SAW biosensors

Kamlesh Suthar[1], Mandek Richardson[2], Subramanian Sankaranarayanan[1], **Venkat Bhethanabotla[2]**; *[1]Center for Nanoscale Materials, Argonne National Lab, Argonne, IL, USA, [2]Chemical Engineering, University of South Florida, Tampa, FL, USA*

Background, Motivation and Objective

Surface acoustic wave (SAW) devices are ideally suited for biosensing applications because they are cheap, compact, and detect biomarkers at clinically relevant concentrations. In a real application, samples will include serum or blood where Non-Newtonian behavior exists. In addition, when sensing in blood non-specifically bound proteins accumulate on the sensor surface producing a spurious response. We have recently shown that SAW induced acoustic streaming can be used for the removal of non-specifically bound (NSB) proteins . The motivation of this work is to determine if efficient removal of NSBs can be achieved within a Non-Newtonian fluid.

Statement of Contribution/Methods

Using a computational fluid-structure interaction finite element model, we compare the influence of Newtonian and non-Newtonian fluid dynamics on the acoustic streaming and fluid velocity profiles induced by SAWs. Several different substrates were evaluated in this study: YZ LiNbO3, ST-Quartz, and ZnO/ST-Quartz with an aim to realize a device that can simultaneously detect biomarker(s) and perform removal.

Results/Discussion

Depending on the nature of the substrate and fluid properties, the removal efficiencies can be significantly different. For example, a transient analysis of the fluid flow profiles generated by SAWs in YZ LiNbO3 showed significant differences in fluid velocity patterns, magnitudes of fluid velocities, and wall shear stresses for a Non-Newtonian fluid compared to a Newtonian. Our results indicate peak fluid velocities decreased for non-Newtonian fluid loading suggesting a significant viscous dissipation of energy compared to a Newtonian fluid (Fig 1). The extent of induced shear stresses at the piezoelectric device-fluid interface is nearly two orders of magnitude higher for Non-Newtonian fluids. These results indicate that removal efficiencies are likely to be lower for Non-Newtonian fluids compared to Newtonian. Our computational work focuses on identifying optimal device design (transducer and delay path modification), type of substrate (mutilayered), fluid properties and optimal operating conditions (voltage, device frequency, waveguide) to maximize removal efficiencies in devices interacting with Non-Newtonian fluids. Experimental tests involving each of the substrates mentioned will be performed to corroborate findings from simulations.

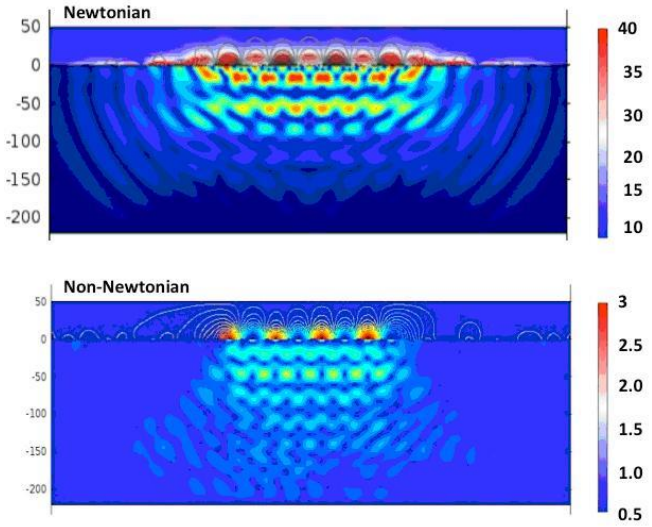

Memorial Session Clinton Hartmann

T1

Wednesday, July 24 2013, 04:30 pm - 06:00 pm

Congress Hallair: **Ben Abbott**
Triquint Semiconductor

IUS4-I-1

Clinton Sylvester Hartmann: His Achievements and Our Unwritten Stories

Ken-ya Hashimoto[1]; [1]*Graduate School of Engineering, Chiba University, Chiba, Japan*

Background, Motivation and Objective

A brilliant super-star in the SAW community, Clinton Sylvester Hartmann passed away in Dallas, TX, on February 4, 2013, at the age of 68. Clinton is internationally recognized as one of the pioneers in SAW technology. He devoted his 40+ years career developing a wide variety of SAW related technologies from wave phenomena to systems applications. His inventions and developed technologies are indispensable for current SAW devices.

Clinton was also an excellent mentor. "Guru" might be appropriate. A lot of major players in the SAW community have enhanced their capabilities through collaborative work with him. I am one of them, and his impact to my life is enormous in various aspects. I feel so sorry for the younger generations who did not have the chance to see him and receive his guidance.

Statement of Contribution/Methods

In this talk, Clinton • fs professional career and achievements are reviewed at first, and then a few stories between Clinton and me are introduced. The stories tell how deeply Clinton contributed to my career up and early, including achievements such as FEM/SDA and 42-LT. They also show how Clinton motivated, trained and directed one young engineer. I trust such mentoring should be imitated by everyone who would lead young talents. In fact, this is the way that I intend to do when I interact with young bright engineers as well as talented students.

Results/Discussion

Clinton was already a super star when I started to work on SAW devices as my undergraduate work in 1977, and I wonder whether I am the right person to give a tribute talk for Clinton. But I was drafted by his followers because I am in the academia and thus relatively free to talk about secret stories.

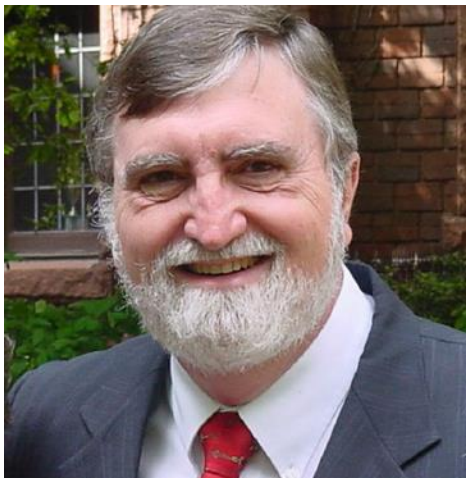

IUS4-I-2

A Simple Design Procedure for Triple Transit Suppression in an Apodized – Withdrawal Weighted Transducer Filter Structure

Pierre Dufilie[1], Clement Valerio[1]; [1]*Phonon Corporation, Simsbury, CT, USA*

Background, Motivation and Objective

High performance SAW filters are characterized by their linear phase, small shape factor, small passband ripple, and high rejection. Classical filter design structures can achieve these performances, however the triple transit time spurious for these structures is typically twice the insertion loss. The triple transit level can be reduced by adding low loss cell structures (such as Hanma-Hunsinger, EWC) to the transducers, however the filter analysis becomes inaccurate with the introduction of mechanical reflections (problems analyzing diffraction effects).

The objective of this work is to develop a synthesis technique for high performance SAW filters with triple transit suppression.

Statement of Contribution/Methods

A synthesis technique has been developed for inline filters on quartz using an apodized transducer and withdrawal weighted transducer (WWT) with split fingers. The first step of the synthesis is to design the apodized and WWT using a classical analysis which includes secondary effects including complete diffraction analysis and distributed bus bar parasitics. Next, an analysis of a WWT-WWT structure is made using identical WWTs with the classical analysis. Then a low loss synthesis is made with a pair of withdrawal weighted DART transducers (WWDT) obtained by replacing some of the split finger cells with modified Hanma-Hunsinger (HH) cells. The synthesis optimizes the triple transit

(TT) for the WWDT-WWDT structure while keeping S21 tne same as for the WWT-WWT classical analysis (TT gated). The final filter design is an inline filter with an apodized and a withdrawal weighted DART transducer.

Results/Discussion

The synthesis technique was used to design a 23dB loss quartz filter 180MHz with 0.5dB bandwidth of 2.57MHz and a 50dB bandwidth of 6.11MHz. Devices were manufactured with both the classical WWT design and the version with HH-cells. Measured data is presented for both versions. The classical design achieved 51dB TT while the version with HH-cells achieved better than 62dB.

The developed synthesis technique for improving triple transit in high performance SAW filters suppresses the triple transit level by more than 10dB while retaining other classical filter performances.

IUS4-I-3

A Compact High-Performance EWC/SPUDT SAW Channelizer

Clinton S. Hartmann[1], **Shen Jen[2]**, Tom A. Martin[3]; *[1]RF SAW, Inc., Dallas, Texas, USA, [2]Crystal Photonics, Inc., Sanford, Florida, USA, [3]Phonon Corporation, Simsbury, Connecticut, USA*

Background, Motivation and Objective

A family of Electrode-Width-Controlled (EWC) SPUDT filters for a high performance miniature SAW channelizer was reported in the 1993 Ultrasonics Symposium [1]. Because of time and space constraints, some of the technical details were omitted from the paper.

To commemorate the passing of Clinton S. Hartmann, we will present several previously unpublished techniques in three areas of interest that contributed 3 years later to the successful development of a field-deployed SAW channelizer module.

Statement of Contribution/Methods

The first area concerns the implementation of the transduction and reflection tap weights of the SPUDT design. Here a highly accurate yet practical scheme was devised. This involves a modified EWC structure with three equal-width electrodes. The desired reflectivity is achieved in part by varying the separation between the two transduction electrodes, whereas the distance from the centerline of these two to the center of the nominally "wide" reflecting electrode remains λ/2. This enables a fabrication insensitive electrode pattern, yet makes available a wide range of net reflectivity.

The second area concerns the design of a frequency selective multi-strip coupler (MSC) that is needed for double apodized design to assure high out-of-band rejection. The MSC was conceived and analyzed from the perspective of basic short transducer sections with λ/8 electrodes placed on λ/4 centers. Each transducer section is odd multiple of λ/4 long. The sections are electrically interconnected. The new MSC effectively suppresses the strong second harmonic response of the EWC/SPUDT without incurring excessive coupler loss.

The third area concerns various techniques for spurious signal reduction in both time and frequency domains. These are by way of judicious SAW die layout, wire bonding scheme, and processing of both the top and bottom surfaces of the SAW chip.

Results/Discussion

The compact SAW channelizer has 7 unshielded SAW dies in a single multi-chip module with no electrical matching for SAW transducers. The channels are centered at 267.5, 287.5, .., 387.5 MHz. Representative results of the channelizer performance, summarized briefly below, will be presented to illustrate the success of the techniques discussed.

- Near-in (35 to 45 MHz from center Fc) frequency sidelobe suppression > 55 dB
- Far-out (0 to 1000 MHz except Fc±45 MHz) frequency sidelobe suppression > 60 dB
- Near-in (< 300 ns from peak) time sidelobe > 35 dB below peak
- All other time spurious (including RF feed through) > 65 dB below peak

[1] "Synthesis and Performance of Medium Bandwidth, Low Time-Spurious, High Out-of-Band Rejection SPUDT Filters", S. Jen and C. S. Hartmann, 1993 IEEE Ultras. Symp. Proc., p.9.

IUS4-I-4

A Reduced Model for Fast and Accurate Simulation of Surface Acoustic Wave Devices

Ken-ya Hashimoto[1]; *[1]Graduate School of Engineering, Chiba University, Chiba, Japan*

Background, Motivation and Objective

Speed up and accuracy improvement are always demanded to simulation tools for surface acoustic wave (SAW) devices. Although behavior models such as the coupling-of-modes (COM) are quite speedy, their accuracy is sometimes insufficient, for example when influence of bulk acoustic waves (BAWs) is not negligible. On the other hand, full wave analyses such as FEM/BEM analysis offer good accuracy, however their calculation speed is not applicable for iterative optimization of the device design.

Statement of Contribution/Methods

This paper describes a reduced 1D model for the full wave simulation of SAW devices in high speed with reasonable accuracy.

Simplifications underlying the COM model are introduced to the full wave analysis of the SAW device structure supporting the Bleustein-Gulyaev-Shimizu wave. Namely, all the field quantities are assumed to vary almost periodically in space, only their fundamental spectral components are considered in the analysis, and the surface stress is assumed to be proportional to the surface displacement. Then we obtain a 1D integral equation with respect to the surface charge to be solved. Parameters to be determined in advance are, 1) the SAW velocities on free and short surfaces, 2) the bulk wave velocity, and 3) two parameters equivalent to those defined by Plessky[1]. This means we can readily adopt all the parameters determined for the COM analysis based on Plessky's model for this analysis. It is also shown that frequency dispersion of the reflection, propagation, and excitation properties as well as the SAW attenuation can be included in these parameters.

Results/Discussion

First, the synchronous IDT structure is analyzed. In the case, the input admittance is given in a closed form, and it can be reduced into a form given by Koskela, et al[2] when further approximations are applied. It should be noted that the author indicated in [3] that Koskela's form offers good accuracy for the simulation of SH-type SAW characteristics including significant SAW-BAW interaction in the synchronous IDT structure.

This model can be applied also to the analysis of general structures with finite device length. For example, application of the moment method enables us to reduce the 1D integral equation to simultaneous linear equations. Since only macroscopic charge distribution is necessary in this analysis, coarse discretization is acceptable, and this allows us to shorten the calculation time.

[1] V.P.Plessky, "A two-parameter coupling-of-modes model for shear horizontal type SAW propagation in periodic gratings," Proc. IEEE Ultrason. Symp. (1992) pp. 195-200.

[2] J.Koskela, V.P.Plessky and M.M.Salomaa, "Analytic model for STW/BGW/LSAW resonators," Proc. IEEE Ultrason. Symp. (1992) pp. 135-138.

[3] K.Hashimoto, T.Omori and M.Yamaguchi, "Modelling of Shear-Horizontal-Type Surface Acoustic Waves and Its Application to COM-Based Device Simulation," Proc. IEEE Ultrason. Symp. (2001) pp. 127-132.

IUS4-I-5

Triple Transit Suppression in Electrically Long Dispersive Transducers

Pierre Dufilie[1], Clement Valerio[1]; [1]*Phonon Corporation, Simsbury, CT, USA*

Background, Motivation and Objective

Pulse compression radar systems with large dynamic range require more than 75dBc of time spurious suppression. The dynamic range is also affected by the insertion loss of the SAW device and the noise figure of the receiver chain. The noise figure and other system parameters are improved by having good input and output return losses for the SAW compressor.

Typically a good return loss for a wide band filter is obtained by using 2-pole electrical matching networks. This can result in better than 13dB return loss over the compressor bandwidth, however these matching networks present a frequency-dependent complex electrical load to the SAW transducer. The transmission line effects of electrically long dispersive transducers modify the frequency-dependent electrical loading.

The objective is to cancel the acoustic reflections generated by the electrical loading with mechanical reflection cells without modifying the electroacoustic amplitude and phase of the original cells. The mechanical reflection magnitude and phase must be adjustable.

Statement of Contribution/Methods

Cell structures such as Hanma-Hunsinger cells and EWC cells have fixed reflection phase and hence cannot be used to substantially improve the triple transit level.

A cell structure has been developed which has independent control over electoacoustic coupling, mechanical acoustic reflection magnitude, and mechanical acoustic reflection phase. This property allows the SAW compressor to be optimized without regard to the triple transit level, and then to separately minimize the triple transit by adjusting the mechanical reflections. Details of this new cell structure are presented.

Results/Discussion

The triple transit suppression technique was used in the design of an unweighted in-line dispersive filter at 150MHz having a 10% bandwidth and 3.7us dispersion. Using a split finger design the filter achieved a 28dB midband insertion loss. When tuned with simple 2-element tuning networks the achievable triple transit is 60dB but with return loss of 6dB. When tuned with a two-pole matching network the achieved return loss is better than 15dB over the entire bandwidth but with a degraded triple transit level of 50dB.

The filter was redesigned using the new cell structure. This new design achieved 28dB midband insertion loss, better than 15dB return loss over the bandwidth, and better than 80dB triple transit. These performance improvements were not possible to achieve using cell structures such as Hanma-Hunsinger and EWC.

IUS4-I-6

Feasibility of SAW Tags in the 6 GHz Frequency Band

Sergey Suchkov[1], **Boris Sveshnikov**[1], Sergey Yankin[1], Sergey Nikitov[2], Dmitry Suchkov[1], Victor Plessky[3]; [1]*Saratov State University, Russian Federation,* [2]*Institute of Radio-engineering and Electronics of RAS, Russian Federation,* [3]*GVR Trade SA, Switzerland*

Background, Motivation and Objective

The unlicensed 5.65-6.425 GHz industrial frequency band is available in Russia for radio applications. In application to RFID systems this frequency range has several obvious advantages: it's band greatly overcomes the widely used 2.45 GHz ISM band (B=775 MHz vs. 82.5 MHz) and thus allows us to reduce the chip and antenna sizes and to increase antenna gain. Besides, rather high levels (up to 1W) of the interrogation signals are permitted. Although the SAW propagation loss strongly increases at these frequencies, some reduction of the reflection response losses can be achieved due to significantly shorter duration of coding pulses and shorter distance between them. The objective of this work is to study feasibility of SAW-tags at this frequency range.

Statement of Contribution/Methods

The device performance has been simulated using both our FEM/BEM software and the COM-analysis technique based on the COM-parameters found by means of "COMSOL Multiphysics" tools. The reflection coefficient magnitude $r(n, wn)$ for the plane SAW per reflector's pitch (p) and the dissipation coefficient $\zeta(n, wn)$, coupled with scattering of SAW beams into bulk acoustic wave modes, were calculated for different n-values and normalized width $wn=w/\lambda$ of electrodes under chosen normalized metal height $hn=h/\lambda$. Then the polynomial approximations of these coefficients - as functions of n and wn - were evaluated. Within an interval $[r_{min};r_{max}]$, where a function $r(n, wn)$ is varying monotonically for a given hn-value, one can approximate the inverse function $wn(n, r)$ by polynomials too. This information is used to form a table showing the required width and number of strips in each synthesized reflector.

Results/Discussion

An example, the in-line SAW tag designed for a 6-GHz frequency range has been simulated. It consists of an IDT and 7 weighted reflectors formed by the short-circuited *Al* strips on a 128-$LiNbO_3$ substrate. As expected, the reflected pulses duration is about Δt=1.3 ns and the tag's insertion loss (dependent on the initial delay) reaches an acceptable level of 50dB – to 55dB. Fig.1 below illustrates the FEM/BEM simulation results for the pulse response of the tag containing standard IDT with N_{pairs}=7 under p=331.3 nm and *Al* thickness h=40 nm. It agrees well with the response found by means of the abovementioned COM-analysis. These results encourage us to manufacture such device in the nearest future.

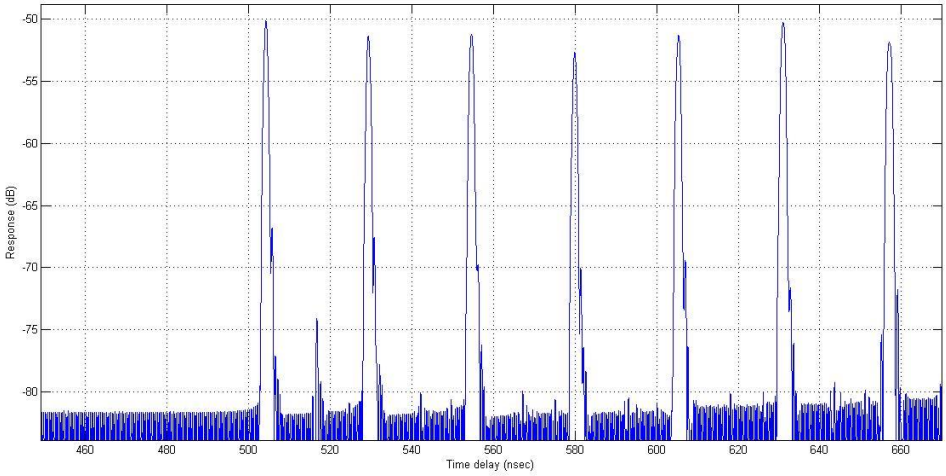
-50
-55
-60
-65
-70
-75
-80
Response (dB)
460
480
500
520
540
560
580
600
620
640
660
Time delay (nsec)

Physical acoustics 1

T2

Wednesday, July 24 2013, 04:30 pm - 06:00 pm

Congress Hallair: **Andreas Mayer**
Hochschule Offenburg

IUS3-I-1

Recent developments in the theory and applications of 'acoustic black holes'

Victor Krylov[1]; [1]*Aeronautical and Automotive Engineering, Loughborough University, Loughborough, Leicestershire, United Kingdom*

Background, Motivation and Objective

'Acoustic black holes' are relatively new physical objects that have been introduced and investigated mainly during the last decade (see e.g. Krylov, 2004). They can absorb almost 100% of the incident wave energy, which makes them attractive for such traditional engineering applications as vibration damping and sound absorption. They could be useful also for some ultrasonic devices using Lamb waves to provide anechoic termination. The main principle of the 'acoustic black hole effect' is based on a gradual power-law-type decrease in velocity of the incident wave with propagation distance, linear or faster, to almost zero, which should be accompanied by efficient energy absorption using the attached highly absorbing materials, e.g. polymeric films. So far, this effect has been investigated mainly for flexural waves in thin plates for which the required gradual reduction in wave velocity with distance can be easily achieved by changing the plate local thickness according to a power law, with the power-law exponent being equal or larger than two.

Statement of Contribution/Methods

The present paper provides a brief review of the theory of acoustic black holes, including their comparison with 'optic black holes' introduced about three years ago. Review is also given of the recent experimental work carried out at Loughborough University on damping structural vibrations using the acoustic black hole effect. This is followed by the discussion on potential applications of the acoustic black hole effect for sound absorption in air.

Experimental investigations have been carried out on a variety of plate-like and beam-like structures. Such structures included plates or beams bounded by the attached power-law wedges, with the addition of small amounts of absorbing materials at the sharp edges. The above-mentioned wedge-like structures at the edges materialise one-dimensional acoustic black holes. Other structures that have been investigated were plates with tapered indentations (pits) of power-law profile. In the case of quadratic or higher-order profiles, such pits materialise two-dimensional acoustic black holes for flexural waves. To increase the efficiency of damping, ensembles of several black holes have been used.

Results/Discussion

The results of the experimental investigations demonstrated that in all of the above-mentioned cases the efficiency of vibration damping based on the acoustic black hole effect is substantially higher than that achieved by traditional methods. The key advantage of using the acoustic black hole effect for damping structural vibrations is that it requires very small amounts of added damping materials, which is especially important for vibration damping in light-weight structures used in aeronautical and automotive applications.

References:

Krylov, V.V., New type of vibration dampers utilising the effect of acoustic 'black holes', Acustica-Acta Acustica, 90(5), 830-837 (2004).

IUS3-I-2

Leaky Wedge Acoustic Waves in Single-Crystal Silicon

Alexey Lomonosov[1,2], **Pavel Pupyrev**[1,3], Peter Hess[2], Andreas Mayer[3]; [1]*General Physics Institute, RAS, Moscow, Russian Federation,* [2]*Institute of Physical Chemistry, University of Heidelberg, Germany,* [3]*HS Offenburg - University of Applied Sciences, Gengenbach, Germany*

Background, Motivation and Objective

Wedge acoustic waves are guided by the apex of an edge formed by two intersecting planar surfaces of a solid elastic medium. In ideal wedges, these waves are non-dispersive like surface acoustic waves in homogeneous halfspaces. In isotropic media, their speed is lower than the Rayleigh wave velocity. Potential applications include NDE, sensors, and actuators.

In anisotropic media, the existence of leaky surface acoustic waves is a well-known phenomenon widely used in signal-processing devices. Very recently, their analogs at the apex of an elastic silicon wedge have been found in experiments using laser-ultrasonics [1].

Statement of Contribution/Methods

With a laser-operated mode-selective transducer developed for these purposes, surface acoustic wave (SAW) pulses and acoustic pulses localized at the apex of the wedge were excited. In addition to a wedge-wave pulse (WW) with low speed, a pseudo-wedge wave pulse (p-WW) was found with a velocity higher than the velocity of shear bulk waves, propagating in the same direction. (An example is shown in the figure below.) Several geometries in the highly anisotropic silicon crystals were investigated with wedge angles of 90° and 70.5°.

With a probe-beam deflection technique, the propagation of the WW pulses was monitored on one of the surfaces of the wedge at variable distance from the apex. In this way, their depth structure and the leakage of the p-WW could be visualized directly.

Calculations were carried out using FEM and a method based on a representation of the displacement field in Laguerre functions. Based on the latter, an "apex-projected density of states" was calculated, where the p-WW emerge as sharp peaks.

Results/Discussion

The speeds of the wedge wave and p-WW pulses were confirmed in the calculations. A detailed analysis of the strain distribution of the wedge and pseudo-wedge pulses on the surfaces of the wedge is given. Especially, the interaction of p-WW pulses with the surface and bulk waves is demonstrated.

This work is supported by Deutsche Forschungsgemeinschaft (Grant No. Ma 1074/11).

[1] A. M. Lomonosov, P. Hess and A. P. Mayer, Appl. Phys. Lett. 101, 031904 (2012).

Figure: Retarded time as function of propagation distance.

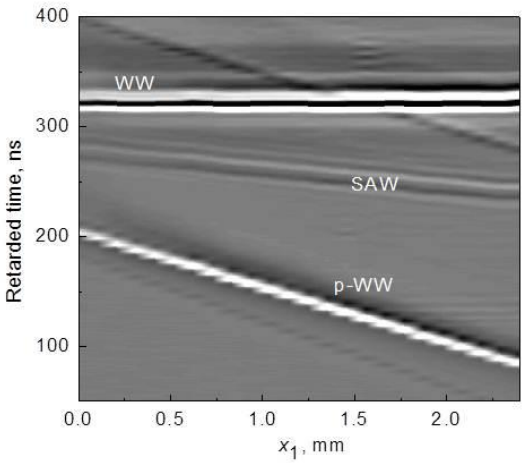

IUS3-I-3

The Influence of Support-Configurations on the Acceleration Effects of Doubly Rotated Quartz Resonators at High Temperatures

Mihir Patel[1], Bikash Sinha[1]; [1]*Mathematics and Modeling, Schlumberger-Doll Research, Cambridge, MA, USA*

Background, Motivation and Objective

Acceleration sensitivity of quartz based resonator has been one of the challenges that have been addressed to achieve extremely stable frequency source. However, many applications of stable frequency source require good frequency stability in environments with high acceleration fields at high temperature. Previous studies of acceleration effects on a quartz resonator on simple mounts have generally been limited at room temperature. The effect of thermal stresses and strains due to mounting supports at high temperatures on the acceleration sensitivity of quartz resonator has not been studied. It is therefore, of fundamental importance to study the influence of various design parameters on the acceleration sensitivity of quartz resonators at high temperatures. The objective of this paper is to investigate the influence of different mounting support configurations on the acceleration effect for different doubly rotated quartz cuts for temperature up to 210 degC.

Statement of Contribution/Methods

Three-dimensional (3-D) piezoelectric equations of finite elasticity in Lagrangian formulation, including nonlinear anisotropic stress-strain relations are employed as the governing equations of motion in the absence and presence of a given acceleration loading. 3-D equations for small vibrations superposed on a statically loaded resonator are obtained from the difference between the field equations corresponding to the absence and presence of acceleration loading. These equations are employed in a 3-D finite-element model (FEM) to study the acceleration effects on the thickness vibrations of doubly rotated quartz based circular resonators. Computational results using this model have been obtained for the acceleration effect on a 90 um thick circular resonator for the slow and fast thickness-shear modes for the SC-cut, SBTC-cut, and rotated X-cut for temperature up to 210 degC.

Results/Discussion

We report the calculated total acceleration sensitivity (Γ x 10^{-10}/g) as a function of the azimuthal angle, which is the angle between the crystalline axis of a resonator plate, and the direction of the body force introduced by an acceleration applied to the resonator. The C-mode for the SC-cut resonator exhibits total Γ of 2.93 and 2.09, respectively, at 25 and 210 degC. Good agreement has been obtained between the results obtained from the FEM method and some of the published measured data. The influence of mounting configurations on the stress compensated slow and fast thickness-shear mode for doubly rotated quartz is obtained up to 210 degC. Calculated results show that the mounting supports influence the acceleration sensitivity for doubly rotated quartz based resonator at high temperatures. The mounting thermal stresses are compensated by selecting the optimal mounting support configuration for different doubly rotated quartz resonators to achieve a stable frequency source operating at temperatures as high as 210 degC.

IUS3-I-4

Thermoelastic Logging for Rock Thermal Properties

Bikash Sinha[1], Andrew Norris[2]; [1]*Mathematics and Modeling, Schlumberger Doll Research, Cambridge, MA, USA,* [2]*Mechanical Engineering, Rutgers University, Piscataway, NJ, USA*

Background, Motivation and Objective

Thermal properties of rocks play an important role in the design of stimulation programs for improved productivity of heavy oil, tar sands and shale oil. Steam injection is routinely used in enhanced oil recovery projects to reduce the heavy oil viscosity and increase its mobility. Measurements of thermal properties on thousands of rock samples have shown a strong presence of heterogeneity and anisotropy in rock thermal properties over spatial scales ranging from centimeters to tens of meters. Optimal reservoir stimulations require a better understanding of this variability instead of using average values of thermal properties based on point measurements on a few cores to characterize the entire reservoir. In addition, estimation of the formation temperature from the dispersion characteristics of elastic wave propagation in a fluid-filled borehole can help to identify cooler layers containing fluid-filled fractures from the warmer unfractured formations.

Statement of Contribution/Methods

Thermoelastic logging can detect differences between the borehole fluid (mud) and the far-field formation temperatures. Radial temperature distributions caused by such temperature differences introduce thermal stresses in the near-wellbore region that perturb the borehole Stoneley and flexural dispersions. Thermal stresses are determined in terms of the rock elastic moduli and thermal expansion coefficients for a given temperature difference between the borehole fluid and far-field formation temperature. When the borehole fluid is at a lower temperature than the formation temperature obtained from the geothermal gradient, this difference introduces tensile stresses in the near-wellbore annulus. This paper describes a volume integral formulation that computes changes in the borehole Stoneley and flexural dispersions caused by the presence of radially varying thermal stresses away from the borehole surface. Differences between the borehole dispersions in the presence and absence of such thermal stresses can be used to estimate the rock thermoelastic constant. Rock thermal properties are estimated within the radial depth of investigation of sonic tools when the borehole fluid temperature and radial variation of rock temperature away from the borehole surface are known.

Results/Discussion

Characteristic changes in the Stoneley and flexural dispersion signatures provide evidence of either increasing or decreasing temperatures away from the borehole surface. These signatures can be used to estimate the magnitude of tensile or compressive thermal stresses at the borehole surface together with the radial boundary of the temperature variation where the steady-state far-field temperature is attained.

IUS3-I-5

Full-wave nonlinear ultrasound simulation in an axisymmetric coordinate system using the discrete sine and cosine transforms

Elliott Wise[1], Bradley Treeby[2]; [1]*Research School of Engineering, Australian National University, Canberra, Australia,* [2]*Department of Medical Physics and Bioengineering, University College London, London, United Kingdom*

Background, Motivation and Objective

The simulation of nonlinear ultrasound propagation is a computationally intensive task, as high-resolution grids are needed to represent the small acoustic wavelengths present. Under some circumstances, 3D simulations can be approximated by axisymmetric systems in cylindrical coordinates, which are effectively 2D and hence less computationally expensive. This is particularly relevant to high intensity focussed ultrasound where focussed cylindrical transducers are often used. Axisymmetric ultrasound simulations have previously been performed using the KZK equation, however, such models are inaccurate near the transducer or far from the axis, and typically only account for one-way wave propagation. The objective of this work was to develop an accurate and efficient full-wave axisymmetric model to overcome these limitations.

Statement of Contribution/Methods

The model is based on the first-order form of a generalised Westervelt equation that includes the effects of tissue heterogeneities (sound speed, density, and nonlinearity) and thermoviscous absorption. A novel spectral method based on the discrete cosine and sine transforms is used to calculate spatial derivatives, while a leapfrog scheme is used for time integration. The cosine and sine transforms assume symmetric and antisymmetric extensions to the wavefield and allow the imposition of Neumann and Dirichlet boundary conditions along the domain boundaries. The approach is computationally efficient (the discrete transforms can be computed via the FFT), and requires only 2 grid points per minimum wavelength.

Results/Discussion

The axisymmetric model was validated using analytical solutions to several canonical problems. Nonlinear propagation and thermoviscous absorption were validated using a solution to Burgers' equation for a progressive plane wave. The simulated wave-field for piston source was also compared with solutions to the KZK equation and the Rayleigh integral (see figure). The propagation of waves through a heterogeneous interface was validated by comparing the reflection and transmission coefficients to analytical values. These comparisons demonstrate the model's accuracy, highlight the computational efficiency of the pseudospectral method, and demonstrate the benefits of the model over those based on the KZK equation.

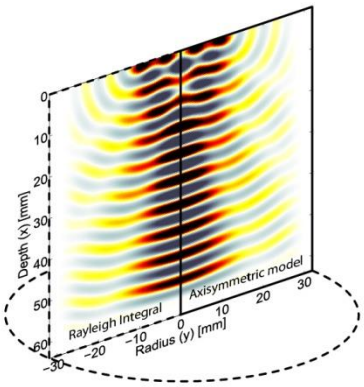

Beamforming II

Forum Hall

Wednesday, July 24 2013, 01:00 pm - 04:30 pm

Congress Hallair: **Kai Thomenius**
General Electric's Corporate R&D

IUS1-PC1-1

Evaluation of a Nonlinear, Simultaneous Compressibility and Mass Density Reconstruction Algorithm in Contrast to Established, Linear Ultrasound Imaging Approaches

Markus Hesse[1], Georg Schmitz[1]; [1]*Institute of Medical Engineering, Ruhr-University Bochum, Bochum, Germany*

Background, Motivation and Objective

While established linear pulse-echo imaging methods like B-mode, synthetic aperture (SA) focusing, and delay-and-sum (DAS) beamforming solely image tissue boundaries (high spatial frequencies) under single scattering, several nonlinear reconstruction methods have been proposed to compute quantitative, separated maps (containing low and high spatial frequencies) of the tissue's compressibility and mass density under multiple scattering, e.g. [1]. In our study, we pick up the approach in [1] and evaluate the image quality in contrast to SA and DAS numerically for identical raw data sets from a fixed, linear array.

Statement of Contribution/Methods

Using a standard Shepp-Logan phantom with realistic soft tissue compressibility and mass density values, we apply a FDTD-code to simulate two pulse-echo raw data sets (0.1 and 0.2 MHz center frequency). We utilize the nonlinear approach to reconstruct the phantom's compressibility and mass density simultaneously. Thus, the 0.1 MHz data set is used to image homogeneous tissue regions (low spatial frequencies), whereas the 0.2 MHz data set is applied to reconstruct sharp boundaries (high spatial frequencies). The approach solves an inverse scattering problem using the Kaczmarz method iteratively; therefore, a numerical forward wave propagation and a residual backpropagation is used for reconstruction. Applying the 0.2 MHz data set, we compute SA and DAS reconstructions using both predefined and adapted apodization weights (calculated by a minimum variance beamformer). Moreover, we simulate raw data sets from a numerical wire phantom to evaluate axial and lateral resolutions of all methods.

Results/Discussion

Results are shown in Figure 1. Nonlinear reconstruction provides high-resolution images (a), (b) with a mean magnitude of relative error of about 4.27 % and 3.18 % within a diagnostically significant region in both images. SA and DAS yield artifact-affected, less detailed images mainly showing tissue boundaries (c)-(f). The nonlinear approach reaches similar -6dB lateral resolutions to SA and yields smaller axial -6dB widths in contrast to SA and DAS. Due to the study's results, the nonlinear approach has the potential to reconstruct high resolution quantitative images.

[1] L. Salehi and G. Schmitz, Nonlinear Reconstruction of Compressibility and Density Variations using the Kaczmarz Method, Proc 2012 IEEE IUS

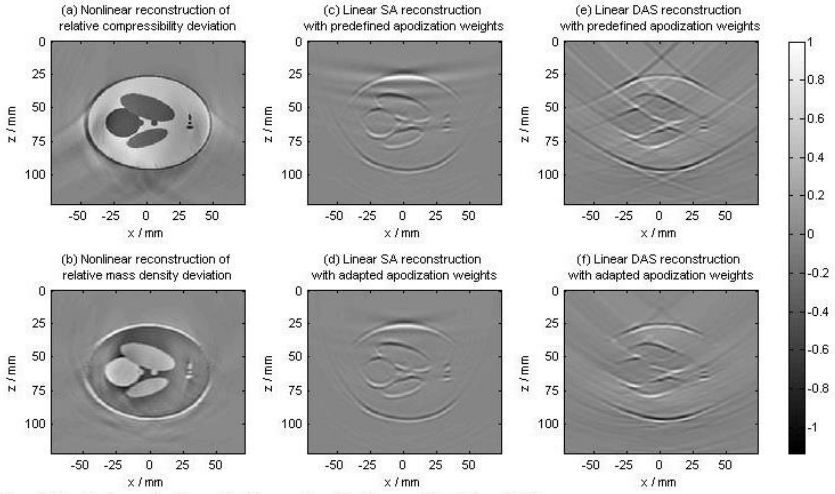

Figure 1: Normalized reconstruction results. All approaches utilize the same data sets for calculation.

IUS1-PC1-2

Beamforming and imageforming for 3D ultrasound imaging system using 2-D CMUT-on-ASIC arrays

Bae-Hyung Kim[1], Suhyun Park[1], Seungheun Lee[1], Youngil Kim[1], Kyungil Cho[1], Taeho Jeon[1], Jongkeun Song[1]; [1]*Samsung Advanced Institute of Technology, Samsung Electronics Co., Yongin-si, Gyeonggi-do, Korea, Republic of*

Background, Motivation and Objective

Recently, we have introduced a scalable 2-D CMUT arrays integrated with reconfigurable front-end (FE) ASICs. For real-time 3-D ultrasound imaging, manipulating massive ultrasound data acquired from a large number of system channels is a challenge as is fabricating and interconnecting hundreds or thousands of elements of 2-D array with the imaging system's FE electronics. The objectives of this work are to design 2D array configurations for the scalable 2-D CMUT-on-ASIC arrays, and to explore optimal volume beamforming and imageforming methods for real-time 3-D volumetric ultrasound imaging scanners using the 2-D CMUT-on-ASIC arrays.

Statement of Contribution/Methods

The volumetric phased array ultrasound imaging system using a 2-D M x N transducer array scans the pyramidal volume in a sequence of azimuth and elevational dimensions to provide a few illustrative scan lines. In the presented volume scanning method, either defocused or focused beams are fired from the selected transmit channels and only one set of row elements in transverse direction are received. And then, next set of row elements in transverse direction are received sequentially. This volume scan method can produce a volume image with synthetic transmit focused and receive dynamic focused beams in longitudinal direction and conventional receive dynamic focused beams in transverse direction. This method is nicknamed '2-D Electric-Wobbling'. This volume scan method can produce a volume image with synthetic transmit focusing using defocused transmit beams and receive dynamic focused beams in longitudinal direction, and conventional receive dynamic focused beams in transverse direction. In the proposed method, 2-D defocusing can also be applied to employ the synthetic transmit focusing technique using virtual sources for better image quality, and the cross array imaging technique for better scanning speed.

Results/Discussion

Computer simulation and experimental results to verify the performance of the proposed methods have been performed. The off-line imaging test for wire phantoms is performed to evaluate the designed array configurations and methods. After firing non-focused beams from 8k channels of CMUT-on-ASIC arrays, RF-echo data samples from 8k receive channels are captured and the off-line B-mode volume rendered images are reconstructed. In this paper, efficient 2-D array designs, and volume beamforming and imageforming methods for real-time 3-D ultrasound imaging systems are reported to provide the best image quality given the hardware configurations.

IUS1-PC1-3

Thomson's multitaper high frame rate compounding for speckle reduction

Matthieu Toulemonde[1,2], Olivier Basset[1], Piero Tortoli[2], Christian Cachard[1]; *[1]Université de Lyon, CREATIS ; CNRS UMR 5220 ; Inserm U1044 ; INSA, Villeurbanne, France, [2]Microelectronic Systems Design Laboratory, Università di Firenze, Firenze, Italy*

Background, Motivation and Objective

In ultrasound imaging, speckle can be considered either as information or noise. Thomson's multitaper (TM) method [Jensen et al., IEEE UFFC, 2012] was proposed to reduce speckle noise in B-mode images. The drawback of this technique is the resolution decrease. Spatial and frequency compounding or multi-focus (MF) imaging can improve TM approach but consequently increase the acquisition time and consequently the sensitivity to movement. To counterbalance this problem, the paper proposes to combine the TM with a high frame rate (HFR) acquisition to perform the compounding. This multitaper high frame rate (MHFR) approach allows to preserve a standard imaging rate with an image quality with reduced speckle.

Statement of Contribution/Methods

HFR transmission uses steered plane waves which are transmitted successively in the media. The final image is obtained by a combination of the received signal after reconstruction. MHFR method consists to apply several orthogonal tapers during image reconstruction in order to obtain different radio frequency (RF) images for each transmission angle. For one taper, different RF images obtained from different steering angles are averaged and then, considering the different tapers, the B-mode images are averaged to obtain final MHFR image.

Results/Discussion

FIELD II simulator and Ula-op scanner were used for simulations and experimental acquisitions with phantom including wires and cyst (Fig). MHFR approach is compared to MF images and standard images obtained with a single focalization depth. MHFR is computed with 61 steering angles from -15° to 15°, MF considers seven focal depths, from 12.5 mm to 42.5 mm and standard images uses a focalization at 20 mm. With these parameters, the acquisition time for MHFR, standard images and MF is, 3.6 ms, 3.7 ms and 26.2 ms, respectively. The techniques are evaluated from their SNR, CTR and axial and lateral resolutions.

Either in simulation or experimentally, SNR, CTR and resolutions of MHFR and MF are close for ROI at different depths. The standard image, as expected, has same values than other approaches only at his focal depth. It is shown that a similar image quality is obtained with only 8 steering angles.

This study shows that MHFR technique allows to reduce the speckle noise, to obtain a resolution comparable to MF technique and has a low acquisition time permitting to be less sensitive to movement.

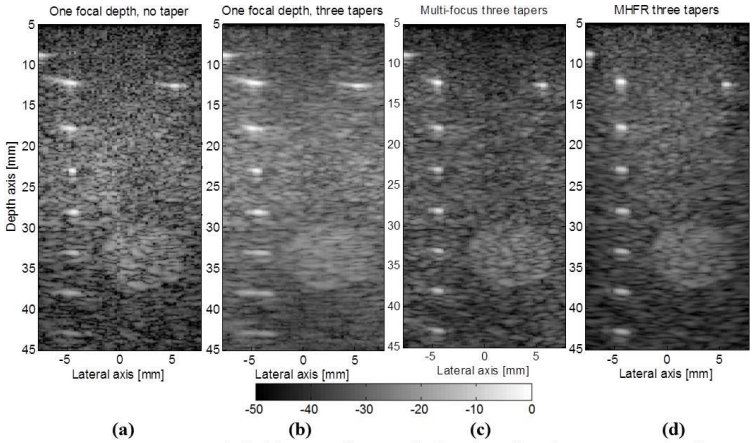

Figure : Log compressed (dB) images of cyst and wires from the UlaOp scanner, (a - b) one focal depth at 22.5 mm without and with three tapers apodization in reception, (c) MF with three tapers apodization in reception and (d) MHFR with three tapers apodization in reception and 61 transmitted angles.

IUS1-PC1-4

Fast Three-Dimensional Ultrasound Cardiac Imaging using Multi-Transmit Beam Forming: A Simulation Study

Ling Tong[1], Alejandra Ortega[1], Hang Gao[1], Jan D'hooge[1]; *[1]Department of Cardiovascular Sciences, KU Leuven, Leuven, Belgium*

Background, Motivation and Objective

Current volumetric cardiac ultrasound systems suffer from relatively low spatiotemporal resolution limiting their applicability in clinical practice. We have previously demonstrated in 2D that a proper implementation of a 4 multi-line transmit (4MLT, i.e 4 simultaneous transmits) system can increase frame rate without compromising spatial resolution or SNR significantly. The aim of the current study was to verify whether our 2D findings could be extrapolated to 3D in order to set up a system that would allow for fast volumetric imaging based on MLT beam forming.

Statement of Contribution/Methods

A 64x48-element 2D phased array (2.5MHz; 50% bandwidth) transmitting 16 MLT beams was simulated using a GPU-based implementation of the impulse response method (cf. Field II). The 16MLT beams were positioned in 4 planes in the elevation direction with an inter-plane opening angle of 22.5°. In each of these planes, 4 MLT beams were equally spread with an inter-beam opening angle of 22.5°. To suppress crosstalk, the 4 planes were rotated 45° to be close to the diagonal of the transducer aperture as previously proposed for a 5MLT system. In addition, the MLT beams in neighboring planes were staggered 11.25° to suppress crosstalk further. Finally, based on our findings in 2D, the effect of a (2D) Tukey (α=0.5) windowing function was tested on transmit and receive. For every MLT beam, one receive beam was formed using dynamic focusing.

Results/Discussion

Two-way beam profiles of the 16MLT system in a C-plane at a depth of 50mm are given in the Figure. As expected, rotating the 4 planes to be close to the diagonal of the aperture resulted in a reduction of crosstalk under about -40dB level. Staggering the MLT beams in neighboring planes suppressed the crosstalk further down to -50dB (Fig b). Similar to our findings in 2D, additional Tukey apodization could also further suppress crosstalk down to -50dB (cf. Fig c, d). These findings show that the proposed 16MLT system could effectively generate good volumetric images at 16-fold volume rates without significantly compromising spatial resolution or SNR. In addition, given sufficient parallel beam forming capacity of the system, the proposed 16MLT could be combined with 4 parallel receive lines (4MLA) to increase frame rate by a factor of 64 allowing for dense 90x90 degree volumetric imaging at 30Hz.

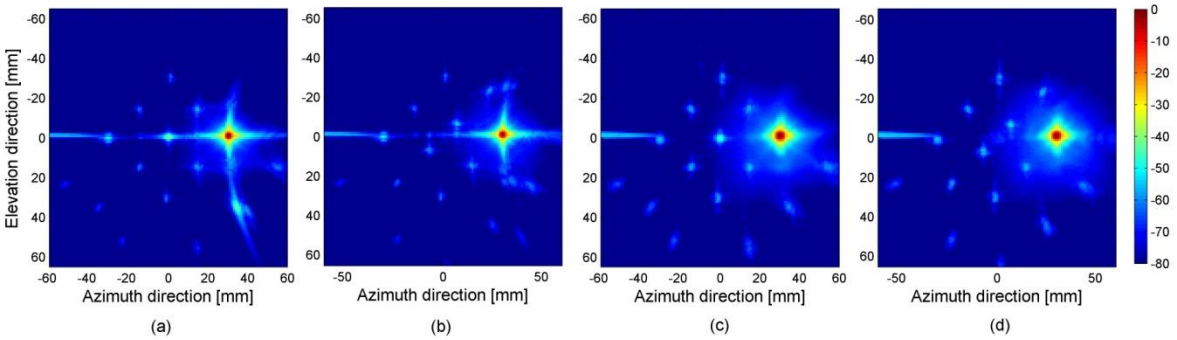

Figure. Two-way beam profiles of different 16MLT systems in C-plane at a depth of 50mm. (a) and (c) The 4 planes were rotated 45° to be close to the diagonal of the aperture; (b) and (d) the MLT beams in neighboring planes were staggered by 11.25°; (c) and (d) a 2D Tukey windowing function was employed on transmit and receive for the two different 16MLT transmit patterns. Please note that a dynamic range of 60dB is typically used in ultrasound imaging. A dynamic range of 80dB was used here however to better appreciate the presence of crosstalk.

IUS1-PC1-5

3D Ultrasound Imaging Performance of a Row-Column Addressed 2D Array Transducer: A Measurement Study

Morten Fischer Rasmussen[1], Jørgen Arendt Jensen[1]; [1]*Center for Fast Ultrasound Imaging, Dept. of Elec. Eng., Technical University of Denmark, Kgs. Lyngby, Denmark*

Background, Motivation and Objective

For ultrasonic 3D imaging, 2D array transducers are required to achieve real–time scanning of a volume. The number of elements in a fully addressed 2D array scales with the square of the number of elements in each dimension. To control the individual elements in the array, a connection is necessary to each element. However, addressing each element individually results in a vast amount of interconnections and posses a great challenge in acquiring and processing the large amount of data. An NxN element array can be operated using just 2N connections when row-column addressing is used. This is opposed to the NxN connections needed when conventionally addressing the elements. An earlier publication by the authors investigated the 3D imaging performance of row-column addressed arrays via simulations. The simulations showed that a good imaging performance is achievable when apodizing the sub-elements within each row and column element, thereby suppressing ghost echoes. In this paper, the imaging performance of a 32+32 element row-column addressed array and the effect of applying sub-element apodization is investigated via measurements carried out using the experimental ultrasound scanner SARUS and a 32x32 element transducer made by Vermon, Tours, France.

Statement of Contribution/Methods

A 2D row-column addressed array with 32+32 elements is emulated by the 32x32 fully addressed array with 0.3mm pitch and a center frequency of 3.5MHz. In transmit all elements in the same row emit the same signal. When receiving, the signals measured from the same column are summed to one signal, before being fed to the beamformer. The elevation direction can thereby be focused in transmit and the lateral direction in receive. The imaging quality is investigated by 3D measurements of a wire phantom at 12mm depth. The 3D volume is sliced across the direction of the wire, into a 2D B-mode image.

Results/Discussion

In the right figure, apodization is applied to the sub-elements, whereas it is not applied in the figure to the left. The sub-element apodization is seen to suppress the ghost, which is marked by the gray box, by around 10dB. The main lobe shape is not influenced by application of the sub-element apodization. The FWHM is in both cases approx. 1.4mm which is the same as predicted by Field II simulations. It was demonstrated that full 3D ultrasound imaging can be achieved using only 32 channels at a time.

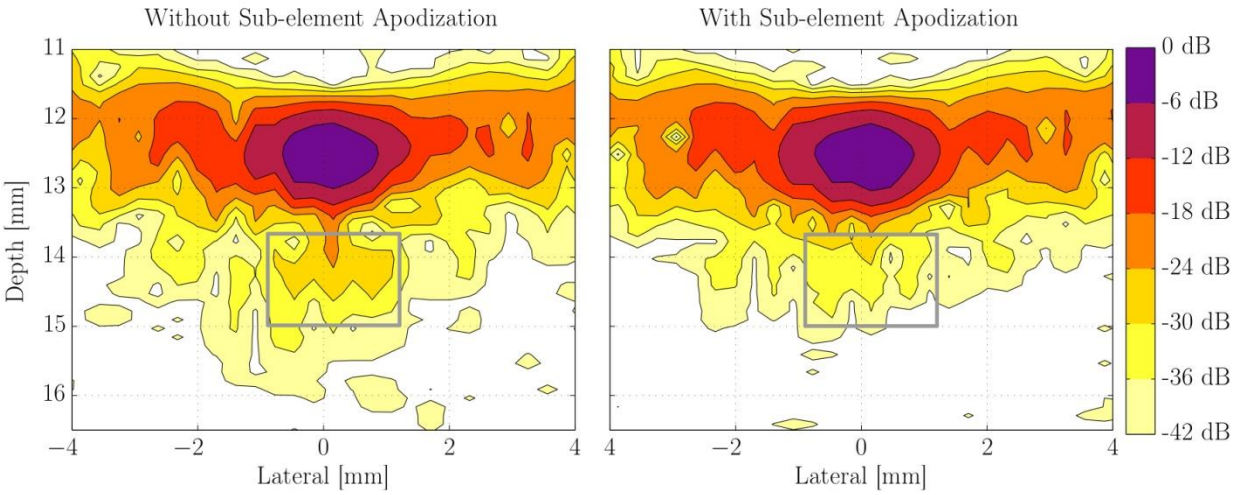

IUS1-PC1-6

Ultrasound Image Quality Optimization with Adaptive Global Sound Speed Correction

Yu-Ming Wei[1], Pai-Chi Li[2]; [1]*National Taiwan University, Taiwan,* [2]*Electrical Engineering, National Taiwan University, Taipei, Taiwan*

Background, Motivation and Objective

Imaging with correct sound speed is an important factor to ensure beamforming accuracy and thus final image quality in diagnostic ultrasound. In most clinical imaging systems, however, a predetermined constant sound speed is used, so the mismatch between the presumed value and the actual sound speed distribution is likely to result in degradation in both spatial and contrast resolution. In this study, a global sound speed estimation method is proposed to optimize beamform-ing quality in a phased array system.

Statement of Contribution/Methods

Previous approaches of global sound speed estimation typically apply the minimum average phase covariance method or the speckle auto-covariance function method to estimate the optimal sound speed in an iterative fashion. It was found that that large errors may still be present on actual clinical data. The method proposed in this study utilizes the sub-aperture imaging technique to form two images, and the mean error between them is calculated with various sound speed values. Finally, the sound speed with the minimum mean error is chosen as the optimal value. This can be implemented with a parallel architecture as shown in figure A.

Results/Discussion

The optimal speed from the proposed method provides better CNR on all our experimental data from standard tissue mim-icking phantoms, aberration phantoms as well as clinical breast data. With our proposed method, the sound speed estima-tion error is about ±0.7% (±10m/s), which is better than ±2.1%(±30m/s) with the auto-covariance method and ±2.7%(±40m/s) with the minimum average phase covariance method. The proposed method has better performance in automatic global sound speed estimation than the conventional methods. In addition, it can be efficiently implemented in software. On a GPU platform with CUDA, the computations can be fin-ished within 1 sec.

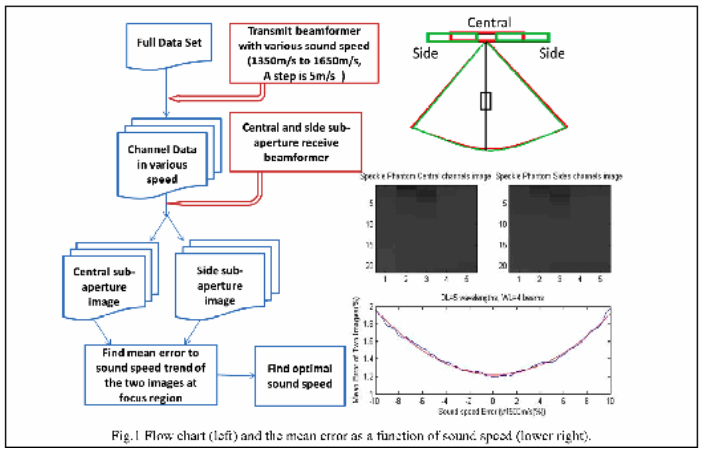

Fig.1 Flow chart (left) and the mean error as a function of sound speed (lower right).

IUS1-PC1-7

Parallel Transmit Beamforming by means of Orthogonal Frequency Division Multiplexing: Implementation on an open research platform

Jacopo Viti[1,2], Libertario Demi[3], Lieneke Kusters[3], Francesco Guidi[1], Massimo Mischi[3], Piero Tortoli[1]; [1]*Information Engineering (DINFO), Universita' degli Studi di Firenze, Firenze, FI, Italy,* [2]*Biomedical Engineering - Thoraxcenter, Erasmus MC, Rotterdam, Netherlands,* [3]*Lab. of Biomedical Diagnostics, Eindhoven University of Technology, Eindhoven, Netherlands*

Background, Motivation and Objective

Transmit or receive parallel beamforming techniques are used in ultrasound (US) imaging systems to improve the achievable data acquisition rate. In particular, transmitting parallel focused beams grants a higher peak pressure, but interbeam interference is an issue. To overcome these shortcomings, a new approach has been recently presented which relies on orthogonal frequency division multiplexing (OFDM) to perform parallel beamforming in transmission. With this technique multiple beams are transmitted by allocating each beam in a different portion of the system bandwidth. Numerical studies showed that this method can be preferable over parallel beamforming in reception when performing second harmonic imaging . In this work, this method has been implemented on an advanced open platform for ultrasound research (ULA-OP) and the achievable resolution and interbeam interference have been investigated.

.

Statement of Contribution/Methods

The Esaote (Firenze, Italy) LA533 linear array probe has been connected to the ULA-OP system . An active aperture of 64 elements is used to transmit and receive US bursts at three different frequencies; all bursts are windowed with a Gaussian envelope and have an identical time length. The bursts are non-overlapping in time within the same pulse repetition interval. The acoustic beams are focused at 40 mm; no beam steering is applied. All measurements are performed in a water tank, with 0.1 mm diameter nylon wires placed at the acoustic focus. Raw RF data is downloaded from ULA-OP to a PC to perform off-line parallel beamforming. The images are then processed to measure axial and lateral resolution and the intensity of residual artifacts due to interbeam interference. Fundamental and second harmonic imaging performance has been investigated for different combinations of modulation frequency (from 4.3 MHz to 6.7 MHz), pulse length (from 2 ìs to 8 ìs), and cutoff frequency of the lowpass filter used after demodulation (from 0.05 MHz to 1.2 MHz).

.

Results/Discussion

Implementing the OFDM method requires a tradeoff between axial resolution, interbeam interference and the number of beams. With the proposed set-up, up to five lines may be acquired in parallel while retaining an axial resolution in the order of 2 mm and 1 mm with interbeam interference in the order of -15 dB and -20 dB for fundamental or second harmonic imaging, respectively.

.

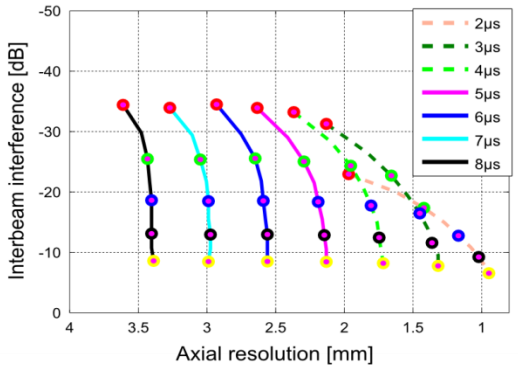

OFDM tradeoff for fundamental imaging using 5.5 MHz pulses with 2-8 us duration, and 1 MHz channel separation.

IUS1-PC1-8

Multiple Zone Beamforming in FOCUS

Yi Zhu[1], Thomas Szabo[2], **Robert McGough[1]**, *[1]Electrical and Computer Engineering, Michigan State University, East Lansing, MI, USA, [2]Biomedical Engineering, Boston University, USA*

Background, Motivation and Objective

Software tools for diagnostic ultrasound simulations are under continuous development in FOCUS (http://www.egr.msu.edu/~fultras-web). Previously, the accuracy and memory efficiency of the FOCUS software were demonstrated [Zhu et al, IUS 2012] and compared to Field II, which is an accepted reference for simulations of diagnostic ultrasound. These initial evaluations used single zone beamformers for the transmit and receive apertures. To leverage the fast, accurate, and memory efficient algorithms in FOCUS for ultrasound imaging simulations, multiple zone beamformers and other new features are needed.

Statement of Contribution/Methods

An efficient approach for simulating multiple zone beamforming is demonstrated in FOCUS. After decomposing the input pulse, intermediate transient signals are computed for the transmit and receive apertures with the fast nearfield method combined with time-space decomposition. These intermediate signals are stored and then repeatedly reused, which greatly improves the computational efficiency of the beamformer. The contributions from each decomposed signal are superposed, and the results are then convolved for each combination of transmit and receive zones.

Results/Discussion

B-mode images are simulated in FOCUS and in Field II using 5 transmit and receive zones. The temporal sampling frequency for the FOCUS simulations is 40MHz, and the temporal sampling for the Field II simulations is 200MHz. For each simulation, A-lines are computed and B-mode images are formed for a linear arrangement of 20 point scatterers. The results, which are shown below, demonstrate that the images and A-lines obtained with these two programs are in excellent agreement. [This work was supported in part by NIH grant R01 EB012079].

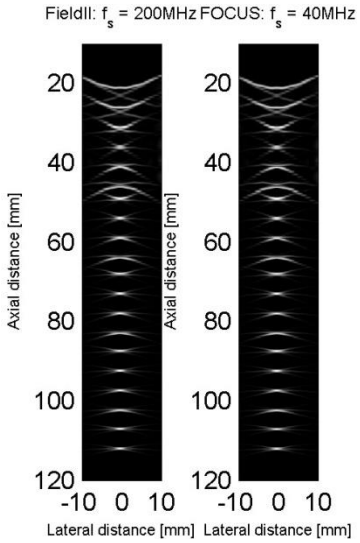

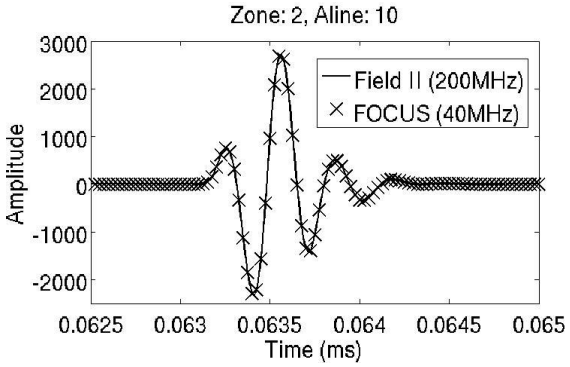

IUS1-PC1-9

Fast Coronary Doppler Vibrometry to Detect Myocardial Vibration Associated with Coronary Artery Stenosis Using Flash Imaging

Jongin Park[1], Jeesu Kim[1], Seok-Min Wi[1], Kwangju Kim[1], Daehyun Lee[1], Sungjoo Yoo[1], Jong-Seon Park[2], Ung Kim[2], Wonjong Park[2], Jin S. Lee[1,3]; *[1]Department of Electrical Engineering, Pohang University of Science and Technology, Korea, Republic of, [2]Division of Cardiology, Yeungnam University Medical Center, Korea, Republic of, [3]Department of Creative IT Excellence Engineering, Pohang University of Science and Technology, Korea, Republic of*

Background, Motivation and Objective

Recently, a new noninvasive ultrasonic technique called coronary Doppler vibrometry (CDV) was developed to detect audio-frequency vibrations in the vessel wall and surrounding tissues, which are generated by the turbulence flow associated with the stenosed coronary artery. Inspiring clinical results were derived from previous studies, but CDV suffers from long data acquisition time because we must obtain myocardial tissue Doppler data from multiple locations adjacent to coronary arteries in each echocardiography view. To obtain the data quickly, we propose to use unfocused transmit beam method called flash imaging. We can interrogate all segments associated with coronary arteries by using only one unfocused beam in each echocardiography view, and we need less data acquisitions. We confirmed the feasibility of the proposed approach through the clinical study.

Statement of Contribution/Methods

We recruited 50 subjects with known or suspected coronary artery stenosis from the hospital. To configure flash imaging technique, we used a 128-transmit/64-receive channel Verasonics ultrasound system with a 2-4 MHz phased-array transducer. From the acquired data, the myocardial tissue velocity was derived manually at each sample location. To characterize the vibrations, we generated the tissue velocity spectrum, and then estimated the vibration power by integrating the spectrogram values between 400-800 Hz during the early diastole period. A vibration index (VI) was introduced as a measure of vibrations in each subject. Fig. 1 shows how to do an analysis.

Results/Discussion

We were able to collect the data in a short time (5-7 min per subject). The proposed method has the potential advantage over the previous method in that it significantly reduces the data acquisition time. We also successfully identified normal and abnormal subjects with high sensitivity and specificity. In the right coronary artery (RCA) cases, we obtained a sensitivity of 88% and a specificity of 83%, and noticed significant difference between normal and abnormal subjects ($p=0.002<0.05$, one-tailed t-test). There are still several limitations such as side-lobe effect, lower SNR, and the system quality but we believe that CDV with flash imaging technique is feasible and promising.

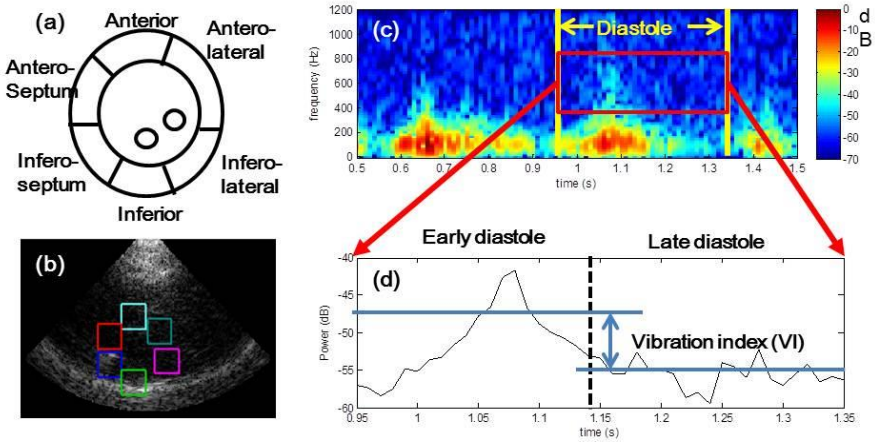

Fig.1. Myocardial tissue vibration analysis. (a) Schematic view at the basal level in parasternal echocardiography view. (b) Image of flash imaging with range gates. (c) Myocardial tissue velocity spectrum obtained from infero-septum. (d) A vibration index (VI) calculation. VI is introduced as a measure of vibrations computing the difference between the estimated powers of early diastole and late diastole.

Blood velocity estimation and applications

Forum Hall

Wednesday, July 24 2013, 01:00 pm - 04:30 pm

Congress Hallair: **Damien Garcia**
CRCHUM - Research Centre, University of Montreal

IUS1-PC2-1

Transcranial Doppler ultrasound using adaptive beamforming technique for the suppression of high-intensity interferences

Shigeaki Okumura[1], Aya Kita[2], Hirofumi Taki[1], Toru Sato[1]; *[1]Department of Communications and Computer Engineering, Kyoto University, Kyoto, Kyoto, Japan, [2]Sakai Rumi Clinic, Kobe, Hyogo, Japan*

Background, Motivation and Objective

The control of vasospasm is important in the postoperative management after the occurrence of subarachnoid hemorrhage. Transcranial Doppler ultrasound (TCD) is a non-invasive and repeatable test that measures the blood flow in the cranium; however, TCD has low reliability because of the high-intensity clutter returned from the cranium. In this study, we propose a method that suppresses the high-intensity interferences with adaptive beamforming technique.

Statement of Contribution/Methods

Since the interference from the cranium has high echo-intensity, its time-varying component should not be negligible. We thus employ a moving target indicator (MTI) and spatial domain interferometry (SDI) with the Capon method. First, we apply a MTI filter to the received data at each element individually. Next, we apply SDI with the Capon method to the data after MTI filtering for the suppression of the time-varying components of interferences. We average the covariance matrix at the adaptive beamforming in the range direction, where this process prevents the deterioration of the temporal resolution.

Results/Discussion

In the simulation study, we assume that the received signal consists of the echo from red blood cells (RBCs), an interference from the cranium and interferences from the surrounding tissues, where the blood flow velocity is 0.5 m/s. Tissue scatterers were situated with a scattering intensity 30 dB higher than RBCs. The intensity of time-varying component of each interference is 40 dB lower than that of the interference. Fig. 1 shows the blood flow velocities estimated by a conventional method with a MTI filter and the proposed method using a MTI filter and SDI with the Capon method. When the cranium echo intensity normalized by the blood signal intensity is more than 40 dB, the performance of the conventional method deteriorates severely. In contrast, the proposed method succeeded to estimate the blood flow velocity of 0.5 m/s with the root mean square error (RMSE) of less than 0.2 m/s under the condition that the normalized cranium echo intensity is 60 dB and less. These results show the potential of the proposed method to improve the accuracy in estimating blood flow velocity under the condition that a high-intensity interference exists. We believe that the proposed method is suitable for TCD.

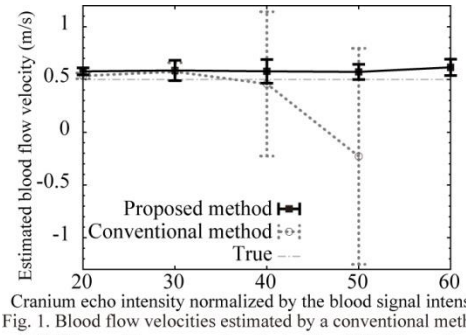

Fig. 1. Blood flow velocities estimated by a conventional method with a MTI filter and the proposed method with a MTI filter and spatial domain interferometry. True blood blow velocity is 0.5 m/s.

IUS1-PC2-2

New Adaptive Clutter Rejection based on Spectral Decomposition and Tissue Acceleration for Ultrasound Color Doppler Imaging

Geunyong Park[1], Youngtae Kim[2], HWAN SHIM[2], HYUN-WOO KOH[2], JaeJin Lee[1], Sunmi Yeo[1], Yangmo Yoo[1]; *[1]Department of Electronic Engineering, Sogang University, Seoul, Korea, Republic of, [2]Digital Media & Communication R&D Center, Samsung Electronics Co., Ltd., Suwon, Korea, Republic of*

Background, Motivation and Objective

In ultrasound color Doppler imaging, effective clutter rejection is essential for estimating flow velocity and power. Since the clutter has time-varying characteristics, it is challenging to suppress it with a static clutter filter. Previously, we proposed an adaptive clutter filtering method where accelerating tissue velocities are utilized for determining an optimal filter. However, it suffers from excessive rejection of flow signals close to the clutter.

Statement of Contribution/Methods

In this paper, a new adaptive clutter rejection (ACR) based on spectral decomposition and tissue acceleration is proposed. In the proposed method, to determine an appropriate clutter filter, tissue and flow characteristics are analyzed by singular value decomposition and tissue acceleration of backscattered Doppler signals (i.e., clutter mean velocity and power, flow mean velocity and tissue acceleration factor). To evaluate the ACR method, phantom and in vivo experiments were conducted. For the phantom experiments, 20 frames of complex baseband data were acquired with a commercial ultrasound system (V10, Samsung Medison, Seoul, Korea) using a 3.5-MHz convex array probe by tapping over the flow phantom (Gammex 1425A LE, Gammex, Middleton, WI, USA) surface to mimic tissue movements. Similarly, 20 frames of in vivo liver data were also acquired.

Results/Discussion

The performance of the proposed ACR method was compared with conventional clutter rejection methods, i.e., static (ST) and down-mixing (DM), using a commonly-used flow signal-to-clutter ratio (SCR). From the phantom experiments, the ACR method provided 4.0 dB and 3.4 dB improvements in SCR over the ST and DM methods where the 3rd-order IIR filter with projection initialization is used. The consistent results were obtained with the in vivo experiments as shown in Fig. 1 where the color Doppler images with frequency estimates without power thresholding obtained from three methods are visualized. In ACR, as shown in Fig. 1(d), six clutter filters were dynamically selected depending on the varying clutter characteristics. The improvement in SCR from the ACR method is 4.5 dB and 3.3 dB, compared to the ST and DM methods. These results indicate that the proposed ACR based on spectral decomposition and tissue acceleration can improve image quality in ultrasound color Doppler imaging by effectively removing the clutter.

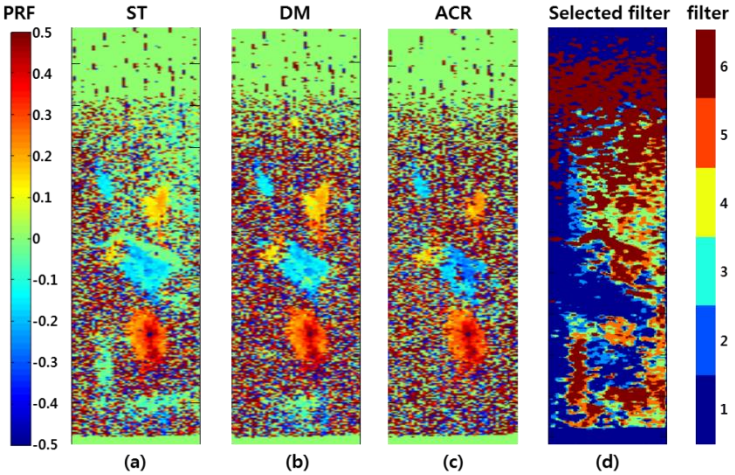

Figure1. Color Doppler image with velocity estimates form the (a) ST, (b) DM and (c) ACR methods and (d) selected clutter filter for ACR

IUS1-PC2-3

Anthropomorphic Flow Phantom Design Using Stereolithography: A Novel Approach Based on Direct Fabrication of Thin-Walled Compliant Vessels

Simon S. M. Lai[1], Billy Y. S. Yiu[1], Alexander K. K. Poon[1], **Alfred C. H. Yu[1]**; *[1]Medical Engineering Program, The University of Hong Kong, Hong Kong*

Background, Motivation and Objective

Anatomically realistic flow phantoms are essential tools for vascular ultrasound investigations. They are conventionally developed using investment casting; however, this technique is known to require skilled craftsmanship, and it is difficult to incorporate multiple pathological features into the phantom's vessel geometry. In this work, we seek to devise a new phantom design framework that can efficiently produce complex vessel models resembling diseased arteries. Stereolithography is proposed here as a direct way of fabricating thin-walled compliant vessels.

Statement of Contribution/Methods

Anthropomorphic vessel geometries were first drafted in SolidWorks. Carotid bifurcation models were developed for demonstration; we designed thin-walled (0.8 mm thick) vessels that concurrently possessed two diseased vascular conditions: 1) eccentric stenosis (50%), and 2) plaque ulceration (Types I/III). Vessel tubes were fabricated using a stereolithography machine with build resolutions of 16 um and 42 um respectively for layer thickness and along each layer plane. To produce elastic vessels, a compliant photopolymer was used. Each thin-walled vessel was coupled to an agar tissue mimicking material, and it was connected to a Shelley gear pump. To analyze their operational performance, Doppler ultrasound and color flow imaging were performed using a SonixTouch scanner (scan freq: 5 MHz). Material characterization was also performed via uniaxial load testing (for elastic modulus estimation) and insertion-loss pulse transmission measurements (for acoustic speed and attenuation).

Results/Discussion

Our phantoms were found to yield Doppler spectrograms with significant spectral broadening and color flow images with mosaic patterns (typical of disturbed flow in stenosed and ulcerated vessels). The vessel wall's elastic modulus (391 kPa) was within the nominal range for human arteries. The vessel material's acoustic speed was 1801 m/s, and its attenuation coefficient was 1.58 dB/mm/MHz^n with a power coefficient of 0.97. These findings suggest that phantoms produced from our framework have potential to serve as ultrasound-compatible testbeds that can simulate complex flow dynamics similar to those observed in real vasculature. We will be using them to validate the feasibility of new flow imaging methods in cases with significant flow disturbance.

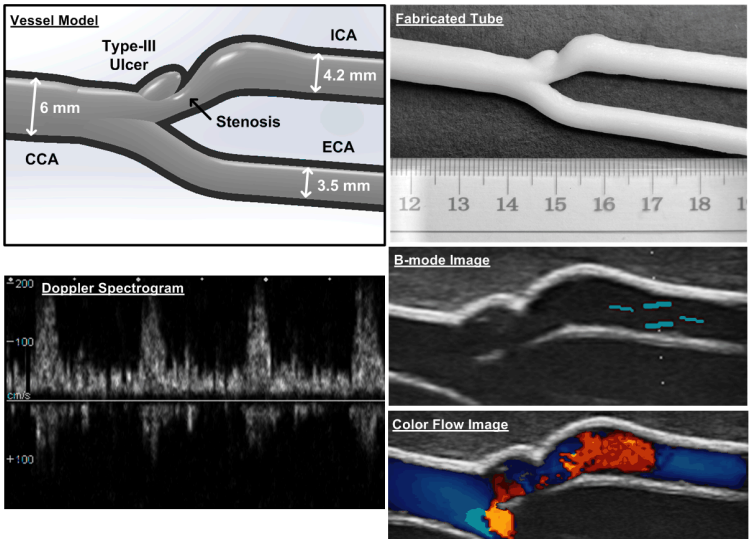

IUS1-PC2-4

Slow-time Golay Decoding for Doppler Detection of High-velocity Blood Flow

Che-Chou Shen[1], **Pin-Hsian Liu[1]**, Jyun-Gong Yu[1]; *[1]National Taiwan University of Science and Technology, Taipei, Taiwan*

Background, Motivation and Objective

Conventionally, Golay excitation is decoded by two complementary transmit waveforms (i.e., A and B transmit) whose autocorrelation is summed for range side lobe cancellation. When the imaged object moves between the two transmit, however, Golay decoding degrades due to the occurrence of residual side lobe. Consequently, Doppler application of Golay code is generally limited to quasi-stationary tissue or low-velocity blood flow. In this study, it is proposed that a simple filtering can be utilized in the Golay-encoded Doppler system for high-velocity blood flow.

Statement of Contribution/Methods

In the proposed method, the blood flow is imaged by a sequence of alternating A and B transmit waveforms. The received echo is first processed by respective matched filter in the fast time and then stored in the memory for Doppler estimation. Since Golay excitation produces in-phase mainlobe component between A and B transmit, the corresponding Doppler spectrum is located around the DC region. On the contrary, the sidelobe component has its phase reversed every time the transmit waveform alters between A and B. Therefore, the Doppler frequency of sidelobe is at about half of the pulse-repetition-frequency (PRF). To extract the mainlobe without any sidelobe interference, low-pass filtering with cut-off frequency of PRF/4 can be performed in the slow time. The low-pass filter can be readily integrated with the existing clutter filter to provide a sidelobe-free detection with Doppler frequency up to PRF/4.

Results/Discussion

Color Doppler images of blood flow phantom were constructed to verify the proposed method. Compared to conventional method, the filtering method effectively suppresses range sidelobe level (RSLL) of Golay decoding. Fig(A) shows that, at a Doppler frequency of about PRF/10, the RSLL reduces by 10-15 dB for different bit lengths. Corresponding color Doppler images in Fig.(B) also illustrates that the conventional method suffers from severe sidelobe interference so that false blood flow appears. On the other hand, the filtering method can remove the artifacts to restore the correct flow information.

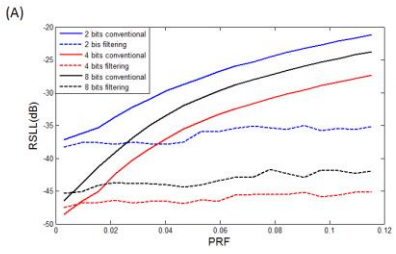

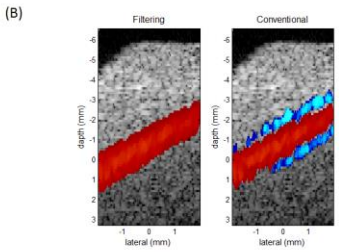

IUS1-PC2-5

High Sensitivity Blood Color Flow

Lei Li[1]; [1]*ultrasound imaging division, SHENZHEN MINDRAY BIO-MEDICAL ELECTRONICS CO.,LTD, China, People's Republic of*

Background, Motivation and Objective

Blood Color flow (CF) imaging is useful to locate flow in a region of interest(ROI), the sensitivity is limited by the transmit voltage which is adaptied to avoid violation of current limitations such as mechanical index(MI) or skin surface temperature defined by FDA. A new method to increase CF imaging sensitivity is proposed in the pater.

Statement of Contribution/Methods

CF imaging is always shown with the B Mode imaging. B Mode imaging is limited by MI with high transmit voltage and short pulse, CF imaging is always limited by skin surface temperature with low voltage and long pulse, which means the temperature can't exceed 43ºC in half of an hour.

High sensitivity CF imaging mode is defined like this, B Mode imaging transmit voltage is decreased to weaken the influence to MI, and CF imaging transmit voltage is enhanced with the limitation of MI to increase the sensitivity. At this time, the temperature will be increased faster than normal mode. System will auto change the operating state from high sensitivity mode to normal mode, temperature will be reduced, and skin surface temperature can't exceed 43ºC.

Results/Discussion

Figure1 compares the temperature change between high sensitivity and normal mode. It shows the temperature will never exceed 43ºC. CF imaging transmit power can be raised about 4dB~6dB at high sensitivity mode, increase of SNR is achieved. Figure 2 shows the improvement of CF imaging sensitivity obviously.

This work has improved CF imaging sensitivity or penetration. These features are especially desirable for tiny flow or difficult-to-image patients, where body habitus makes satisfactory image quality problematic.

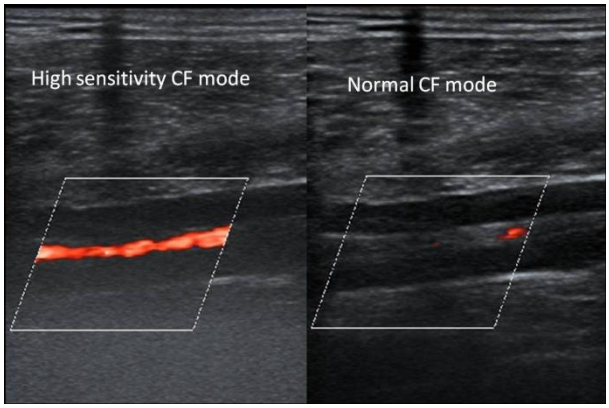

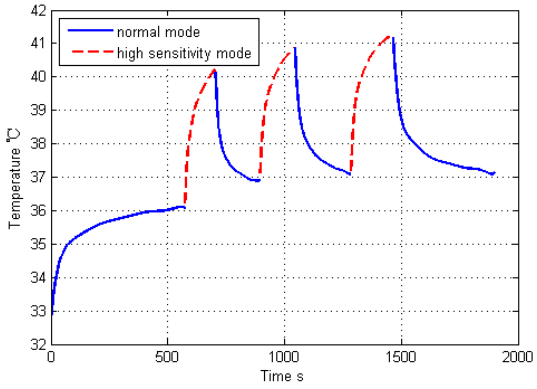

IUS1-PC2-6

The multigate Doppler approach for assessing hemodynamics in a forearm vascular access for hemodialysis purposes

Abigail Swillens[1], Stefano Ricci[2], Piero Tortoli[2], Patrick Segers[1]; [1]*IBiTech-bioMMeda, Ghent University, Belgium,* [2]*Electronics & Telecommunications Dept, University of Florence, Italy*

Background, Motivation and Objective

To create an accessible high blood flow vessel for hemodialysis purposes, patients with end-stage renal disease typically get a surgical connection of a vein with the radial artery (arterio-venous fistula=AVF). The AVF ideally matures, but non-maturation frequently occurs, with post-operative volume flow and wall shear stress important markers to assess AVF remodeling. In this complex flow setting, we investigated the accuracy of the multigate Doppler approach to quantify these hemodynamical parameters, since this technique has the obvious advantage of capturing the spatial velocity profile.

Statement of Contribution/Methods

Multiphysics simulations directly coupling computational fluid dynamics (CFD) & Field II were performed to assess: (i) volume flow and (ii) shear rate, from the multigate Doppler spectra. The CFD-model was based on patient-specific MR-scans of the arm vasculature *pre* and *post* surgery. A linear array probe (LA523, Esaote) was simulated, firing pulses with PRF=12/24 kHz (*preop/postop*) and f0=8MHz. Volume flow was obtained via: (i) integration of the velocity profile; (ii) the centerline velocity (assuming parabolic flow). Shear rate was defined as the 1D-derivative of the angle-corrected velocity (ϑ=60°/78° for *preop/postop*).

Results/Discussion

Fig.1A demonstrates velocity profiles in the radial artery at peak systole (timing indicated in fig.1C), as derived from the multigate Doppler spectrum (pink) compared to CFD-data (blue), for both the *preop* and *postop* case. Fig.1B shows the corresponding shear rate data, with a clear underestimation of peak shear rate by US, especially for the *postop* case. Fig.1C shows the volume flow throughout the cardiac cycle compared to the CFD-reference. Both the integration and centerline data perform well for the *preop* case (19% and 15% bias in mean flow respec-tively). For the *postop* case, the integration method outperforms the centerline technique, with a bias of -21% and -50% in mean flow respectively.

Conclusion: The extreme *postop* flow conditions (high velocity magnitudes and complex flow profiles) hamper accurate assessment of both wall shear rate and volume flow, while reasonable estimates are obtained *preop* (lower velocity magnitudes and laminar flow). However, we should mention the imaging setup for the shear rate detection should be optimized in future work.

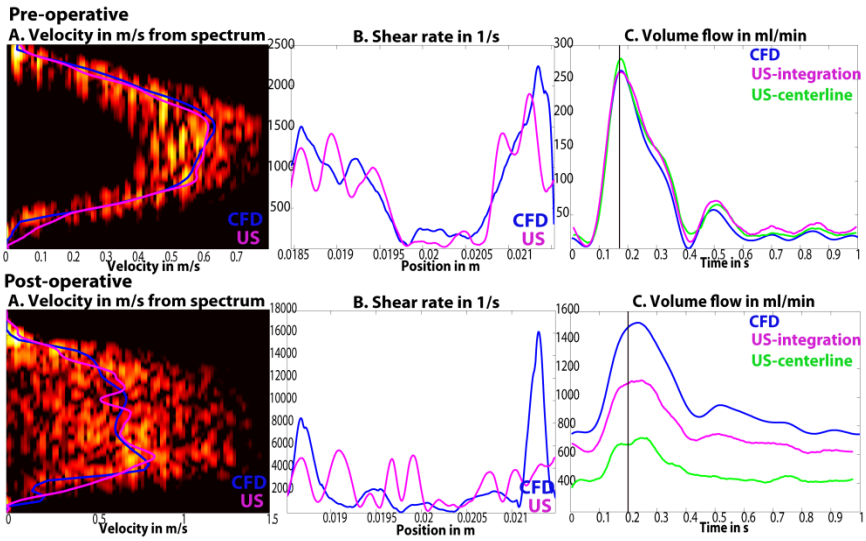

IUS1-PC2-7

Numerical modeling of the dynamic of ultrasound contrast agents in vascular network: Validation Study

Laure Boyer[1], Pauline Le Notre[1], Stephen Randall Thomas[1], Ingrid Leguerney[1,2], Nathalie Lassau[1,2], Stephanie Pitre-Champagnat[1]; *[1]IR4M-UMR 8081, Univ Paris Sud - CNRS, Villejuif, France, [2]IRCIV, Institut Gustave Roussy, Villejuif, France*

Background, Motivation and Objective

Dynamic Contrast-Enhanced Ultrasonography (DCE-US) is a particularly attractive method to assess the tumor microvasculature from the concentration quantification of ultrasound contrast agents (CA) within lesion. This method does not yet benefit methodological tools imported from physics to characterize the ability of the quantification methods to evaluate the tumor microcirculation. In this context, we developed the first numerical modeling (NM) based on Computational Fluid Dynamics software for studying the quantification methods to describe the tumoral perfusion in a complex vascular network and to apprehend their variations according to the tumor growth, configurations of hemodynamic and CA injections. The aim of this study is to validate this approach in comparison with DCE-US experimentations on simple geometrical configuration composed of 1 bifurcation of fluids.

Statement of Contribution/Methods

NM was performed with Fluent software (ANSYS, France), which modeled blood and CA flows in vascular network with laminar flow described by Poiseuille's law. Geometry of the numerical and experimental phantom was a 31cm length tube and 2mm in diameter with 1 bifurcation with 2 parallel tubes located at 23cm of the input phantom. Volume of injected CA was 0.1mL with 26, 34, 41 and 56mL/min of blood flows. Realistic injection of CA by bolus was implemented in NM. DCE-US experimentations were performed with an Aplio scanner (Toshiba Medical Systems, Japan) and a 12MHz probe with SonoVue® (Bracco, Italy) as CA. Comparison of area under the curve (AUC) from the time-concentration of CA curves was performed between experimental data and NM.

Results/Discussion

The numerical time-concentration of CA curves were similar to those obtained experimentally and showed the same variations of AUC values according to the different blood flows with a maximum difference of 11%.

In conclusion, NM with the Fluent software was validated for studying the blood and CA dynamics in a simple geometry. Results obtained with a vascular network more realistic composed of 30 vessels will be presented.

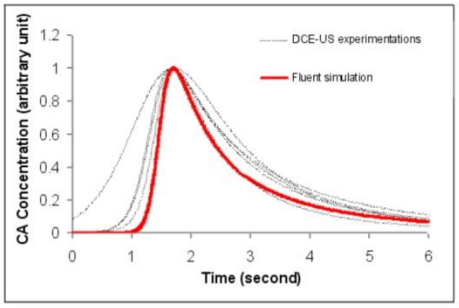

Figure 1: Time-concentration of CA curves obtained by numerical simulation and experimentations with a blood flow of 41mL/min. CA Concentrations were normalized.

Contrast agents and drug delivery

Forum Hall

Wednesday, July 24 2013, 01:00 pm - 04:30 pm

Congress Hallair: **Nobuki Kudo**
Hokkaido University

IUS1-PC3-1

Model drug delivery by transiently stable microbubbles produced by a microfluidic device

Adam Dixon[1], Ali Dhanaliwala[1], Johnny Chen[1], **John Hossack[1]**; [1]*University of Virginia, USA*

Background, Motivation and Objective

Focal drug delivery to the vessel wall facilitated by intravascular ultrasound and microbubbles holds promise as a therapy for atherosclerosis. We evaluated whether drug delivery could be achieved using microbubbles produced in real-time by a microfluidic device, with the ultimate goal of real-time microbubble production at the tip of an IVUS catheter. By generating microbubbles in close proximity to the therapeutic site, microbubble stability is no longer a concern. As a result, transiently stable microbubbles can be utilized. We validate that this microbubble production strategy enables effective drug uptake in vitro across a range of ultrasound, microbubble, and fluid flow parameters.

Statement of Contribution/Methods

Smooth muscle cells were plated on a Thermanox membrane and placed in a flow chamber. A flow-focusing microfluidic device (FFMD) producing 8 µm diameter monodisperse microbubbles was placed within the flow chamber and ultrasound was applied to enhance uptake of calcein. Acoustic pressures up to 300 kPa and flow rates up to 18 mL/s were investigated. FFMD produced microbubbles were stabilized with a PEG40 stearate shell and had either a perfluorobutane (PFB) or nitrogen gas core. Calcein delivery efficiency was quantified by counting the fraction of cells that internalized calcein.

Results/Discussion

Microbubble size distribution and stability upon ejection from the FFMD into an air saturated medium depended on the composition of the gas core. PFB microbubbles initially grew and then shrank over time (half-life = 40.7s). Nitrogen microbubbles did not expand and exhibited a shorter half-life of 18.2s (Fig 1A).

Calcein delivery was observed at all flow rates, with maximal delivery at 9 ml/s and maximal cell death at 2 ml/s (PNP = 300 kPa). PFB-core microbubbles required higher acoustic pressures (>200 kPa) than nitrogen-core microbubbles (>100 kPa) to achieve calcein delivery (Fig 1B,C).

This is the first demonstration of in vitro ultrasound-mediated drug delivery using microbubbles produced by a microfluidic device in real-time. We showed that microbubbles with short half-lives are still effective as drug delivery agents (>70% of cells internalized calcein) and that ultrasound pressure, flow rate, and microbubble composition all affected drug delivery.

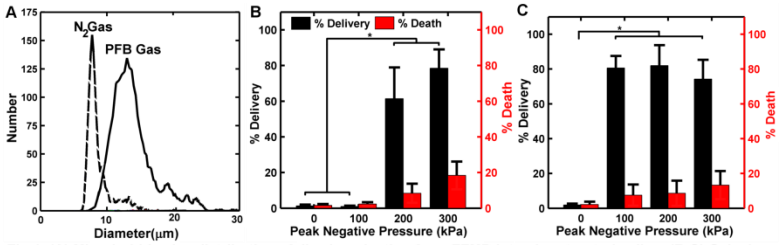

Fig 1. (A) Microbubble size distributions following ejection from FFMD into air-saturated saline. (B,C) Calcein delivery and cell death for PFB and nitrogen gas microbubbles, respectively, at 300 kPa PNP and 9 ml/s flow.

IUS1-PC3-2

High-Frequency Subharmonic Imaging of Liposome-Loaded Microbubbles

James McLaughlan[1], Nicola Ingram[2], Radwa Abou-Saleh[3], Sevan Harput[1], Tony Evans[4], Stephen Evans[3], Louise Coletta[2], Steven Freear[1]; [1]*Electronic and Electrical Engineering, University of Leeds, Leeds, United Kingdom,* [2]*Leeds Institute of Molecular Medicine, University of Leeds, Leeds, United Kingdom,* [3]*School of Physics and Astronomy, University of Leeds, Leeds, United Kingdom,* [4]*Leeds Institute of Genetics, Health and Therapeutics, University of Leeds, Leeds, United Kingdom*

Background, Motivation and Objective

Phospholipid microbubbles are commonly used as contrast agents in the high-frequency ultrasound imaging of mice and their ability to generate subharmonic emissions allows them to be distinguished from tissue. The attachment of fluorescent marker filled liposomes to microbubbles has been shown to reduce their subharmonic threshold, which could provide a significant advantage for the use of these therapeutic agents for molecular imaging in-vivo. The aim of this study is to compare the subharmonic response of microfluidic manufactured microbubbles that have been loaded with drug-filled liposomes, when imaged using a preclinical ultrasound scanner in-vitro and in-vivo.

Statement of Contribution/Methods

The VisualSonics Vevo770 ultrasound system was used to perform fundamental (40MHz) or subharmonic (15MHz) imaging on either a tissue-mimicking flow phantom or nude mice. A solution of microfluidic manufactured microbubbles ($2x10^7$ microbubbles/ml), with or without liposomes attached was dispensed into a flow phantom with a syringe driver. The transmit power was set to 50%, with fixed 10 and 22dB gain settings for fundamental and subharmonic imaging, respectively. A total of 550 frames were acquired at a rate of 30Hz, which was repeated four times for both types of microbubble populations. These frames were exported from the VisualSonics software and loaded into Matlab, where the image intensity was calculated for the region containing microbubbles on each frame.

Results/Discussion

The figure (a-c) shows B-mode frames acquired from both fundamental and subharmonic imaging modes. (a) is a frame acquired in the absence of microbubbles, (b) is acquired during fundamental imaging of liposome-loaded microbubbles flowing through the channel, and (c) is the corresponding subharmonic image. Panels (d-e) show the averaged image intensity within the channel for fundamental and subharmonic imaging modes for de-ionised water, microbubbles only and liposome-loaded microbubbles. (e) demonstrates

that liposome-loaded microbubbles generated more subharmonic response and showed greater image intensity compared with equivalent unloaded microbubbles for subharmonic imaging. These results suggest that molecular imaging could be enhanced through the use of liposome-loaded microbubbles and subharmonic imaging. In-vivo imaging results will be presented.

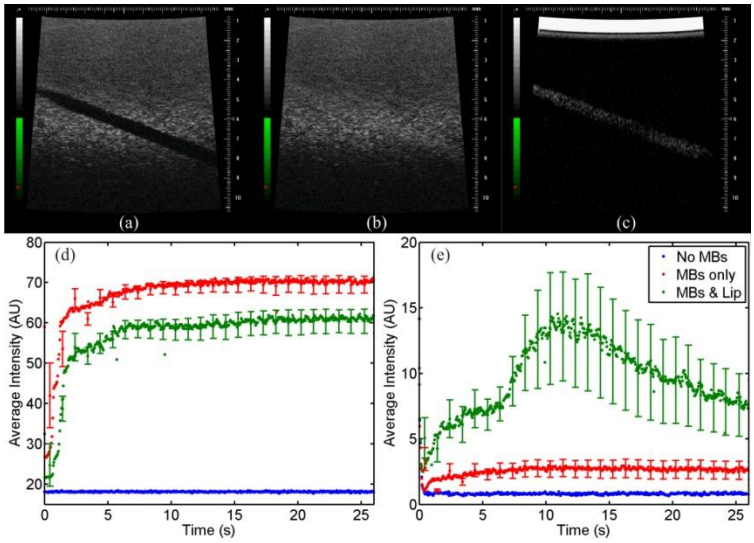

IUS1-PC3-3

Improving Tumor Accumulation with SPIO-Loaded Acoustic Nanodroplets and Magnetic Targeting

Yi-Ju Ho[1], Jia-Jiun Chen[1], Chih-Kuang Yeh[1]; *[1]National Tsing Hua University, Taiwan*

Background, Motivation and Objective

Acoustic droplet vaporization (ADV) has shown the potential as a mechanical and chemical theranostic strategy for tumor treatments. Nanodroplets (NDs) have been reported tending to accumulate in tumor tissue by means of passive targeting and tumor enhanced permeability and retention (EPR) effect. However, solid tumors have a raised interstitial fluid pressure to obstacle the efficiency of NDs accumulation within the tumor. Therefore, NDs encapsulation of superparamagnetic nanoparticles (SPIO-NDs) shows a promising solution to achieve magnetism-assisted active targeting (MT) process. Moreover, SPIO-NDs can also provide the functionality for MR-guided and ultrasound-triggered vaporization.

Statement of Contribution/Methods

The SPIO-NDs were fabricated by intensely sonicating lipids with perfluorocarbon and aliphatic-terminated SPIO. Dorsal skinfold window chamber mice (n=6) implanted prostate tumor cells were used to observe EPR effect by acousto-optical integrated imaging system. The fraction areas of SPIO-NDs leaking into the tumors were measured under the cases of with/ without a 0.48-T MT for 7 hours. In-vitro phantom experiments were adopted to verify ADV process. The SNRs of B-mode images of diluted SPIO-nanodroplets after ADV were calculated under the ultrasound (US) exposures (2 MHz, 10 MPa, 5 Hz PRF and 3 cycles) for 10 second.

Results/Discussion

In Fig. a, the tumor EPR effect (yellow arrows) were observed through the SPIO-NDs (with mean sizes of 404±140 nm) extravasated tumor vessels (black arrows) and deposited in tumor tissue (green). The fraction areas (Fig. b) by with and without MT were 36.6±13.9% and 87.6±13.1% ($p<0.05$), respectively. The B-mode images (Fig. c) after ADV showed that SNRs of contrast-enhanced images increased with SPIO-NDs concentration increasing. The in-vivo results revealed that improving the tumor accumulation of SPIO-NDs with MT is feasible. The animal WC tumor model was convenient to real-time observe by acousto/ optical methods simultaneously. Future work includes conjugating with specific targeting antibodies on SPIO-NDs surface to increase intracellular drug accumulation.

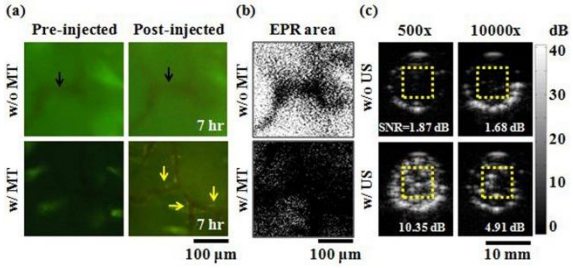

IUS1-PC3-4

Theoretical Model for Acoustic Streaming Generated by a Bubble Near a Wall

Alexander Doinikov[1], **Ayache Bouakaz**[1]; *[1]INSERM U930, Université François Rabelais, Tours, France*

Background, Motivation and Objective

The ability of an acoustically driven bubble to generate a stationary vortical flow in the surrounding liquid is of interest for many technical and medical applications. This effect, known as acoustic streaming, leads to the effective mixing of the liquid and induces stresses on adjacent objects such as cells and tissue surfaces. The existing theory is restricted to the case of a bubble in an infinite liquid. The aim of our work is to develop a theory that describes the generation of acoustic microstreaming in the case of a bubble beside a wall.

Statement of Contribution/Methods

The main contribution to acoustic streaming normally comes from the radial and translational modes of the bubble oscillation. In an infinite liquid, the bubble translation is caused by the incident wave alone. Near a wall, the bubble translation is also caused by the wave scattered by the bubble and then reflected from the wall. If the bubble is driven near resonance, the translation caused by the reflected wave is much stronger than that due to the primary incident wave. As a result, the acoustic streaming generated by the bubble should increase considerably. We developed a theory that allows for the effect of a wall on acoustic streaming under the following assumptions. A spherical gas bubble is suspended in a viscous incompressible liquid and undergoes linear radial and translational motions in response to ultrasonic insonation. The bubble-wall distance is relatively large compared to the bubble radius. The normal liquid velocity tends to zero at the wall. The bubble is driven near resonance, taking into account that the presence of the wall changes the resonance frequency of the bubble.

Results/Discussion

Equations have been derived that describe the velocity and stress fields of the acoustic streaming generated around the bubble and within the viscous boundary layer at the wall. The equations were then used in numerical simulations in order to study how the presence of the wall changes the acoustic streaming around the bubble as compared to that in an infinite liquid. It was found that if the bubble is driven near resonance, the presence of the wall does increase considerably the intensity of the acoustic streaming. As an example, calculations were made for a bubble with diameter 5 microns, located at 5 bubble radii from the wall, and driven at 1.5 MHz (the bubble resonance frequency at this distance). It was found that the peak tangential velocity of the acoustic streaming at a distance of 2δ from the bubble surface (δ is the viscous penetration depth) is 60 times as large as that in an infinite liquid, and the peak tangential stress is nearly 70 times as large as that in an infinite liquid.

In conclusion, our model is able to predict the microstreaming generated by a bubble next to a wall. These findings are of importance to elucidate mechanisms behind sonoporation. Experiments to validate these findings are underway.

IUS1-PC3-5

Differentiation of vascular distribution and flow patterns in tumors with Dynamic Contrast-Enhanced Ultrasound (DCE-US) perfusion maps

Alexandre Dizeux[1,2], Guillaume Barrois[1,2], Thomas Payen[1,2], Alain Coron[1,2], Olivier Lucidarme[2,3], Delphine Le Guillou-Buffello[1,2], S. Lori Bridal[1,2]; *[1]Université Pierre et Marie Curie, Paris, France, [2]CNRS, UMR 7623, Laboratoire d'Imagerie Paramétrique, Paris, France, [3]Functional Imaging Laboratory, INSERM 678, Department of Radiology, GH Pitié-Salpêtrière,Assistance Publique-Hôpitaux de Paris, Paris, France*

Background, Motivation and Objective

DCE-US has demonstrated potential to detect functional tumor modifications during therapy. Microvascular flow parameters are obtained by fitting echo-power vs. time from a region of interest (ROI) contrast-tracer models. ROIs generally include large portions of the tumor but spatial information on the microvascular flow is lost. In this work, comparison of two ectotopic tumor models, with different vascular patterns, colorectal (CT26, N = 4) and lewis lung carcinoma (3LL, N = 6), reveals the necessity to consider spatial information. A more sensitive and robust mapping of tumor perfusion is proposed and demonstrates capacity to discriminate and quantify local differences in flow patterns which would not be identified with full-tumor ROIs.

Statement of Contribution/Methods

Data were acquired with a clinical ultrasound system (Aplio 512; Toshiba, 7-14MHz) in contrast pulse sequence mode. SonoVue contrast agent (50 µl) was injected via the caudal vein with a controlled injection system [1]. For day 19, one pair of tumors matched in size (± 15%) and overall perfusion was identified to demonstrate the technique. Parametric maps were made using in-house software applies a novel estimation method based on more realistic hypotheses for the statistical nature of contrast-ultrasound signals (Pixels, 265 µm by 265 µm) [2].

Results/Discussion

Figure 1.a presents echo-power curves, Peak Enhancement (PE) and Time To Peak (TTP) from a ROI including whole tumor for CT26 and 3LL, respectively. Curves and parameters are not different within the variability of the measurement [1]. The TTP parameters as mapped in Figure 1.b, shows the lack of contrast uptake in the center of the CT26 tumor. The histogram displays the percentage of pixels throughout the entire tumor volume with each TTP. Thirty-five % of voxels in the CT26 tumor present no significant contrast uptake as compared with 1% in 3LL. The time-delay (s) to the mode of the TTP (histogram maximum) is greater for the CT26 than the 3LL tumors, indicating overall slower filling.

Quantitative perfusion maps demonstrated clear differences in the TTP distribution where the average TTP and PE from entire-tumor ROIs did not. Analysis of the relative distribution of pixels in the perfusion maps can characterize relative flow between tumors within the vascularized regions.

[1] Dizeux et al IEEE Ultrasonics Proc. 2012

[2] Barrois et al ISBI 2013

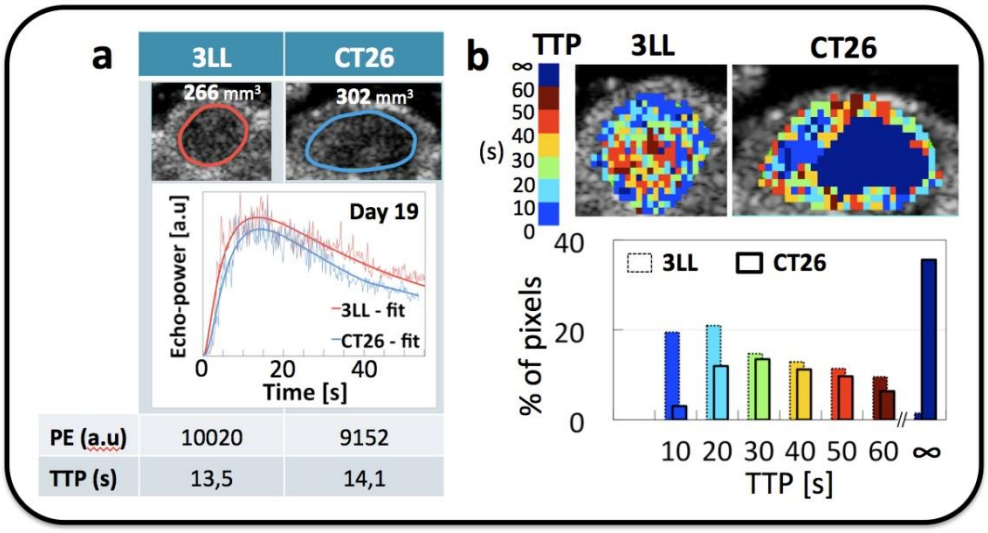

IUS1-PC3-6

Rapid Accumulation of Doxorubicin via Ultrasound Triggered Drug Delivery to Overcome Drug Resistance of MCF-7/ADR Cells and Its Mechanism

Zhiting Deng[1], Fei Yan[1], Qiaofeng Jin[1], Hairong Zheng[1]; [1]*Paul C. Lauterbur Research Center for Biomedical Imaging, Shenzhen Institutes of Advanced Technology, Chinese Academy of Sciences, China, People's Republic of*

Background, Motivation and Objective

Liposome-microbubble complexes (LMC) in combination with therapeutic ultrasound have become a promising strategy for drug delivery. Doxorubicin is an anthracycline antibiotic with antineoplastic activity through preventing DNA replication and inhibiting topoisomerase II. However, its antitumor effects are greatly impaired by multidrug resistance (MDR), which is one of the critical reasons leading to unsuccessful chemotherapy. The aim of this work was to evaluate the feasibility of reversing MDR by using doxorubicin-liposome-microbubble complex (DLMC) combined with ultrasound.

Statement of Contribution/Methods

DLMC were obtained by conjugating doxorubicin-loaded liposomes with perfluoropropane-containing lipid shelled microbubbles by avindin-biotin system. Intracellular uptake, accumulation and retension of DOX in drug resistant MCF-7/ADR cells were detected post treatment with DLMC plus ultrasound. Generation of reactive oxygen species (ROS) post treatment were detected by DCF fluorescence distribution at the wavelength of 535 nm by a multimode plate reader. And γ-H2AX foci staining was utilized to detect DNA double-stranded breaks in MCF-7/ADR cells that had been subjected to DLMC plus ultrasound.

Results/Discussion

We observed rapid intracellular uptake and nuclear accumulation of DOX in resistant MCF-7/ADR cells, and less efflux of drug after treatment with DLMC plus ultrasound by using confocal microscopy. DLMC with ultrasound caused 70.17% increase in reactive oxygen species (ROS) production, compared to 29.82% increase post treatment with DOX-liposomes and ultrasound in MCF-7/ADR cells. In addition, more severe DNA damage indicated by γH2AX+ immunofluorescence staining were detected in DLMC plus ultrasound treated cells. In conclusion, the study indicated that the DLMC plus ultrasound significantly enhanced the DNA damage to drug resistant cells, and could be used as a potential approach to overcome MDR in cancer cells.

IUS1-PC3-7

Dynamic and Structural behavior of Magnetized PVA-shelled Microbubbles: Acoustic Characterization

Satya VVN Kothapalli[1], Gio Paradossi[2], Lars-Åke Brodin[1], Dmitry Grishenkov[1]; [1]*Division of Medical Engineering, School of Technology and Helath, Royal Institute of Technology, KTH, Huddinge, Stockholm, Sweden,* [2]*Dipartimento di Chimica, Università di Roma Tor Vergata, Rome, Rome, Italy*

Background, Motivation and Objective

The combination of iron oxide superparamagnetic nanoparticles (SPOINs) and micro sized gas bubbles encapsulated into poly vinyl alcohol (PVA) shell is manufactured as a bimodal contrast agent for ultrasound and MRI imaging modalities. The structural properties of shell influences the radial oscillations of bubbles upon insonation hence altering acoustic and echogenic characteristic of proposed contrast agent.

Statement of Contribution/Methods

In this work, we examine the acoustic properties of two types of magnetic PVA-shelled MBs. These are manufactured by two following strategies: (1) SPIONs were chemically conjugated on the surface of plain PVA-shelled MBs (Type A) and (2) SPIONs were physically entrapped in the shell during the formation of polymer MBs (Type B). Experimental evaluation of acoustic attenuation coefficient and phase velocity at room temperature (24 °C) were probed at an incidental pressure is equal to 25 kPa, and within the frequency range between 3 and 14 MHz. A linearized version of modified Church model is utilized to recalculate frequency dependent viscoelastic properties of the MBs shell, i.e. storage, G'(ω), and loss, G"(ω), modulus, from simultaneous fit of attenuation and phase velocity curves. In this model, the SPOINs interaction with PVA shell is neglected. Theoretically calculated attenuation and phase velocity spectrum were compared with the experimental data at a modest concentration. Two statistical quantities, mean square error (MSE) and correlation coefficient (R) were introduced to estimate the quality of fit. In addition, an ordinal ranking system was implemented to automatically identify the best fit.

Results/Discussion

The mathematical model predicts higher values of storage and loss modulus, undamped resonance frequency, f0, and damping ratio,ζ, for MB Type B. The ζ value greater than 1 that was estimated for MB Type B represents overdamped harmonic oscillator, whereas for MBs Type A the transition between underdamped (<1) and criticaldamped (=1) oscillator were observed. The predicted f0 are 13.4 MHz ± 2.2 MHz and 27.65 MHz ± 5.99 MHz for MB Type A and B, respectively. The values of pressure threshold Pthr at which MB shell fractures are in accordance with the values of storage modulus reported for each MBs type. The storage modulus for MB type B is much higher than for MB Type A (34.45 MPa and 11.23 MPa respectively) and thereby, a higher peak negative pressure is needed to fracture MB Type B compare to MBs Type A (1.25 MPa and 1.05 MPa respectively). In a conclusion, having the resonance frequency within the limit of clinical medical ultrasound, i.e. 15 MHz, MB Type A can be utilized as a conventional ultrasound contrast agent. On the contrary, custom designed imaging sequence based on primary or secondary radiation force is needed in order to visualize more rigid MBs Type B.

IUS1-PC3-8

Production approaches for microbubbles loaded with nanoparticles

Marianne Gauthier[1], Qian Yin[2], William D. O'Brien, Jr[1]; [1]*Bioacoustics Research Laboratory, Electrical and Computer Engineering, University of Illinois at Urbana-Champaign, Urbana, Illinois, USA,* [2]*Department of Materials Science and Engineering, University of Illinois at Urbana-Champaign, Urbana, IL, USA*

Background, Motivation and Objective

We evaluated and compared two different approaches to make microbubbles (MBs) loaded with Cy5-PLA50 nanoparticles (NPs) for further drug delivery studies.

Statement of Contribution/Methods

MBs were produced by sonicating bovine serum albumin (BSA) and dextrose solution according to Borrelli et al (Ultrasonics Sonochemistry, 2012 Jan;19(1):198-208). NPs consisted in Cy5-PLA50 conjugate. Protocol 1 involved incorporating the NPs into the BSA-dextrose solution before the sonication step. Protocol 2 involved mixing MBs and functionalized NPs (f-NPs), resulting from mixing the initial Cy5-PLA50 and PLA-PEG-COOH conjugates. For each protocol, unloaded MBs were produced as a reference. Two parameters were quantitatively analyzed using both analysis of variance (ANOVA) and t-tests: diameter was evaluated using a circle detection routine based on the Hough transform while the number density was determined using a hemocytometer. Both parameters were evaluated for the MBs-NPs and unloaded MBs at 5 time points (see Fig. 1). Qualitative evaluation of fluorescence for MBs+NPs was also performed.

Results/Discussion

Protocols 1 and 2 lead to significantly different MBs+NPs (see Fig. 1). Fluorescence images were acquired from H2 to D2. For protocol 1, no fluorescence remained after D1 for MBs-NPs. For Protocol 2, MBs-NPs exhibited fluorescence stability after H6.

To our knowledge, this is the first time protocol 1 has been tested to load albumin MBs with Cy5-PLA50 NPs. Inefficiency of protocol 1 to provide stable MBs+NPs justifies the more common use of f-NPs to target MBs for drug delivery purposes. [Supported by NIH R37EB002641].

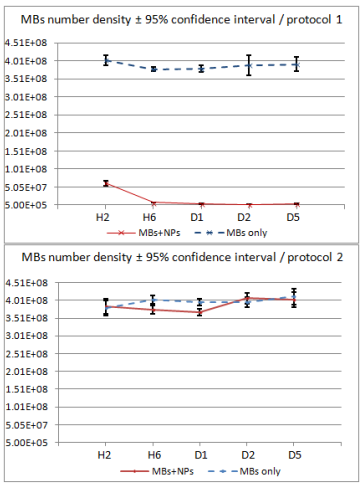

Fig. 1: Number density (number of MBs/mL) as a function of the elapsed time from making MBs and MBs-NPs (H: hour, D: day)

Photoacoustic imaging

Forum Hall

Wednesday, July 24 2013, 01:00 pm - 04:30 pm

Congress Hallair: **Roger Zemp**
University of Alberta

IUS1-PC4-1

Nanoparticle-mediated photothermal tumor therapy monitored with photoacoustic and magnetic resonance thermometry

Richard Bouchard[1], Trevor Mitcham[1], Yang Lui[1], Hannah Lee[1], Jason Stafford[1], Marites Melancon[1]; *[1]MD Anderson Cancer Center, Houston, Texas, USA*

Background, Motivation and Objective

Nanoparticle-mediated photothermal therapy permits highly conformal ablation of malignant tumors. Real-time image guidance that provides both visualization of particles and estimation of local temperature is necessary to facilitate adaptive photothermal therapy techniques. To permit intraoperative as well as bedside monitoring (i.e., for a point-of-care implementation) of photothermal therapy, a dual-modality nanoparticle that allows for both magnetic resonance(MR)- and photoacoustic(PA)-based thermometry is needed. The objective of this study is to demonstrate the feasibility of using nanoparticles composed of superparamagnetic iron oxide coated with a gold nanoshell (SPIO@AuNS) to mediate photothermal therapy of a tumor under either MR or PA guidance.

Statement of Contribution/Methods

SPIO@AuNS particles (broadband absorption in NIR) were fabricated to have an average diameter of 80 nm and an average Au shell thickness of 8 nm. MR phantom studies (particles embedded in 1.5% agar) were conducted with a 1.5-T GE Signa Excite HDxt MR system, while PA phantom (particles imaged in a polyethylene tube immersed in water) and in vivo studies were conducted with a VisualSonics Vevo LAZR PA-ultrasound (PAUS) small-animal imaging system (808 nm; 21 MHz). In vivo imaging was achieved after intratumoral injection of 50 uL of SPIO@AuNS particles (OD @ 808 nm=1, 6.7 x 10e10 particles/mL) in mice bearing 4T1 breast tumors. Local heating was induced in all phantom and in vivo studies with a 6W CW (808 nm) laser. Temperature phantom estimates were cross-validated between MR and PA studies with independent fluoroptic thermometer measurements.

Results/Discussion

Good agreement (within 3 degrees) was achieved between phantom temperature estimates obtained with MR-based (A) and PA-based thermometry through a 40-degree temperature increase. 3D PAUS imaging (B) shows clear delineation of the injected SPIO@AuNS particles within a subcutaneous breast tumor. Parametric analysis (D) of local heating monitored with PA imaging at the treatment site (violet ROI in C) demonstrated a sustained 18-degree temperature increase for 120 seconds of treatment (D; red & blue lines indicating irradiation start & stop). This study demonstrates the potential for using SPIO@AuNS particles for PA- or MR-guided photothermal therapy for accessible tumors in the breast, prostate, or neck.

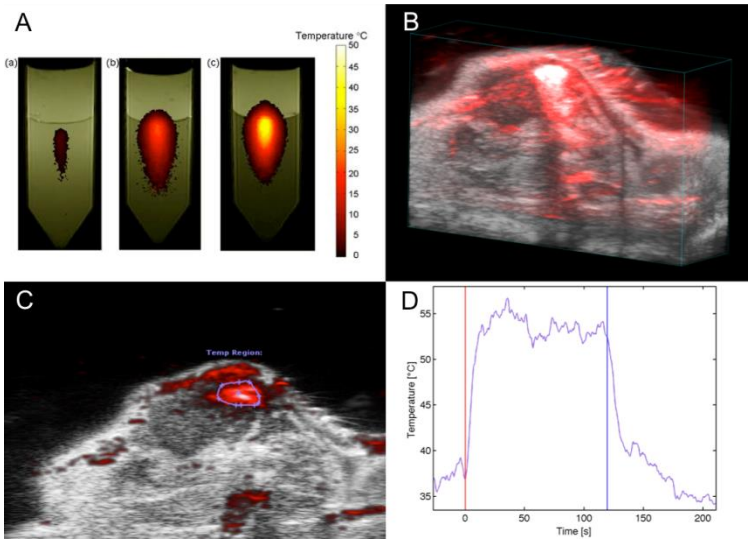

IUS1-PC4-2

Feasibility Study of Identification of Microcalcifications Associated with Benign and Malignant Breast Cancer using Array-based Photoacoustic Spectroscopy

De-Yi Chiou[1], Shi-Bing Luo[1], Wang-Ting Tieng[1], Meng-Lin Lee[2], Shin-Cheh Chen[3]; *[1]ITRI, Taiwan, [2]NTHU, Taiwan, [3]CGMH, Taiwan*

Background, Motivation and Objective

Breast microcalcification is one of the important indicators for early breast cancer detection. Micro-calcification is clinically observed in 85% of invasive DCIS (ductal carcinoma in situ) patients. Generally, two types of microcalcifications can be found in breast tissue. Type-I is composed of Calcium Oxalate Dihydrate (COD) and type-II is composed of Calcium Phosphate (Hydroxyapatite, HA). Previous studies have indicated that both types can be correlated with benign and malignant diseases. Currently, Radiog-raphy (X-ray) and ultrasound (US) are most widely used diagnostic imaging methods. However, they possess some limitations in micro-calcification screening. Furthermore, there is no reliable way to non-invasively distinguish between type-I and type-II micro-calcifications.

Statement of Contribution/Methods

In this study, an array-based photo-acoustic imaging (PAI) system is established for visualization and spectroscopy of microcalcifications. The system components include: Nd-YAG pulsed laser, linear-arrayed US transducer for PA signal detection, and US imaging engine. Artificial HA and COD particles with sub-mm dimensions are prepared and embedded in verified phantoms whose optical properties are similar to those of human breast. First, we have successfully demonstrated that 0.3~0.5mm HA are clearly observed in the phantom with deep penetration of 3~3.5cm, which is adequate for clinical requirements. Second, we also tried to distinguish HA and COD micro-calcifications in the PA image by adjusting the incident laser wavelength.

Results/Discussion

Figure 1 shows normalized PA signal amplitudes of HA and COD particles as a function of wavelength. It was found that PA signal amplitude increased as the excitation wavelength was decreased according to spectroscopic fingerprint. The corresponding linear fitting curves based on the least-square approach were also shown in Fig. 1. It was found that the slope of HA is relatively larger than that of COD. With support of the proposed approach, non-invasive prior detection of the presence of micro-calcification, even its type, would be a useful information for physicians for diagnosing the occurring possibility of benign and malignant diseases. Moreover, high compatibility with US makes PAI a suitable add-on tool for supporting image-guided breast biopsy for pathology.

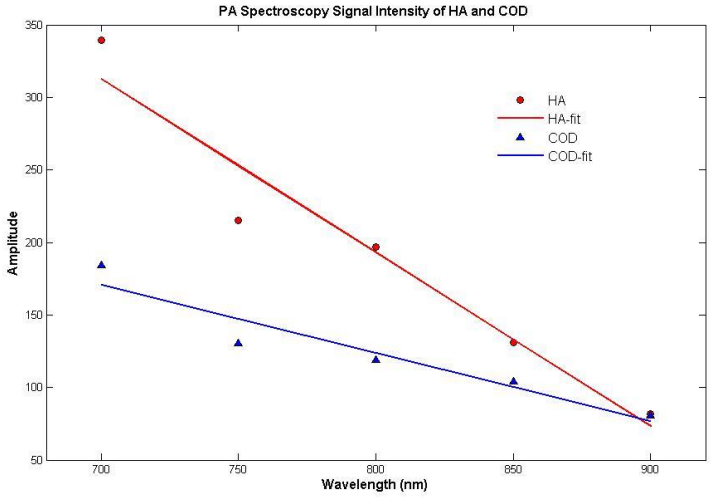

IUS1-PC4-3

Enhanced Photoacoustic Detection of Calcifications with Molecular Targeting: Feasibility Study

Tsai-Chu Hsiao[1], Ren-Jei Chung[2], Meng-Lin Li[1,3]; *[1]Institute of Photonics Technologies, National Tsing Hua University, Taiwan, [2]Graduate Institute of Biotechnology, National Taipei University of Technology, Taiwan, [3]Electrical Engineering, National Tsing Hua University, Taiwan*

Background, Motivation and Objective

Calcification is one of the important indicators for breast cancer diagnosis. Albiet the current gold standard for micro-calcification identification, X-ray mammography is inevitably with ionizing radiation and carcinogenic risk. Because of speckle noises, ultrasound (US) imaging owns low contrast between breast tissues and micro-calcifications and thus low detectability. Recently, our study has demonstrated the feasibility of photoacoustic (PA) imaging as an alternative imaging modality of micro-calcifications, presenting high optical contrast and up-to-3-cm imaging depth of micro-calcifications in a chicken breast phantom. However, the penetration depth need to be further improved in order to cover full-figured patients and other clinical applications.

Statement of Contribution/Methods

In this study, we intend to verify the feasibility of enhanced PA detection of calcifications via molecular targeting and thus the potential in improvement of the imaging depth of micro-calcifications. An IR-Dye with bisphosphonate ligand offering specific binding to hydroxyapatite (HA), the major composition of breast calcification, was used as a molecular probe and a PA contrast agent as well. The HA particles, HA powders and calcium oxalate (COM, another composition of breast calcification) powder were incubated with various concentration of IR-Dye in 1X PBS solution. A fluorescent scan was made to confirm the binding after PBS flushing out. Then the photoacoustic signals of IR-Dye incubated HA particles were measured from 680 to 830 nm using a custom-made 5-MHz photoacoustic imaging system.

Results/Discussion

Three groups of 1-mm HA particles incubated with 1.0 uM, 0.5 uM IR-Dye and PBS solution, respectively, were all imbedded in a gelatin phantom for the measurement. The PA signals (the case with 1.0 uM IR-Dye incubation) increased toward 680 nm – the peak-absorption wavelength of the IR-Dye (see the figure). At 680 nm, the PA signal enhancement via molecular targeting was more than ~12 dB which can contribute to 1-cm improvement in penetration depth in human breast tissue. Overall, it is shown that targeting IR-Dye is promising for the improvement of PA imaging depth of micro-calcifications and also for differentiation of calcification types, e.g., HA and COM. Our preliminary results on real human calcifications will also be presented.

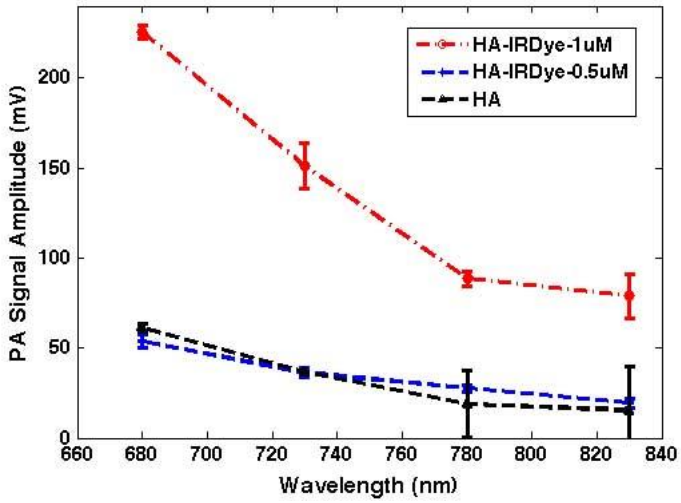

IUS1-PC4-4

Image Quality Improvement based on Inter-frame Motion Compensation for Photoacoustic Imaging: Preliminary Study

Minjae Kim[1], Jeeun Kang[1], Jin Ho Chang[2], Yangmo Yoo[1]; *[1]Department of Electronic Engineering, Sogang University, Seoul, Korea, Republic of, [2]Interdisciplinary Program of Integrated Biotechnology, Sogang University, Seoul, Korea, Republic of*

Background, Motivation and Objective

Photoacoustic imaging (PAI) is capable of providing real-time anatomical and functional information of pathological changes. In PAI, the frame averaging (FA) technique is commonly used for enhancing signal-to-noise ratio (SNR) instead of increasing the power of a pulsed laser to avoid adverse effects. However, the FA technique suffers from motion artifacts due to the limited pulse repetition frequencies (PRFs) (e.g., 10-20 Hz) of a commonly-used Nd:Yag laser. In this paper, to improve image quality of PAI, a new FA technique combined with inter-frame motion compensation (i.e., FA-IFMC) is proposed.

Statement of Contribution/Methods

To evaluate the proposed FA-IFMC method, radio-frequency (RF) data of each frame were acquired while introducing motions by moving an ultrasound transducer to right and lower directions eight times by steps of 0.2 mm with a mechanical arm (Sigma Koki Inc., Tokyo, Japan). At each position, RF data of four frames were averaged, and then envelop detection and scan-conversion were performed to generate a PA image. From the 16 PA images, motion vectors between two adjacent PA images were determined by employing a three-step search block matching (TSS-BM) method. In FA-IFMC, the estimated motion vectors were used for reconstructing motion-free PA images, and these images were averaged to increase SNR. The RF data acquisition was conducted with a commercial ultrasound imaging system (Ultrasonix, Inc., Canada) for the 0.9-mm diameter graphite lead-injected chicken breast. For the laser excitation, a Surelite Nd:YAG OPO system (Continuum Inc., USA) was used at the rate of 10 Hz and at the wavelength of 700nm with a bifurcated fiber bundle.

Results/Discussion

Figure 1(a) shows the reference image reconstructed by averaging 64 PA frame RF data without any motions. As shown in Figs. 1(b) and 1(c), the proposed FA-IFMC method substantially reduces the blurring artifacts caused by motions compared to the FA method. The FA-IFMC method shows 4.2 dB and 0.83 mm improvement in peak signal-to-noise ratio (PSNR) (i.e., 23.4 dB vs. 27.6 dB) and 3-dB axial resolution (i.e., 1.49 mm vs. 0.66 mm), respectively, compared to the FA method. These results indicate that the proposed FA-IFMC method can enhance image quality of PAI by reducing blurring artifacts from motions.

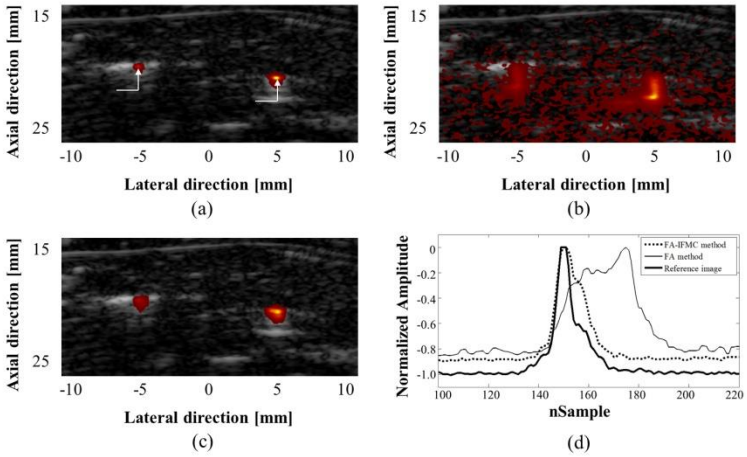

Figure 1. (a) Reference PAUS image reconstructed by 64 PA frame RF data without any motions (white arrows indicate the direction of introduced motions) and PAUS images reconstructed by (b) the FA method and (c) the proposed FA-IFMC method, respectively. (d) Axial beam profile of respective methods.

IUS1-PC4-5

Three-dimensional Imaging of the Vasculature in Chicken Embryo by Combination of Ultrasonic and Photoacoustic Imaging

Mika Sato[1], Takuya Izumi[1], Yuji Watanabe[2], Harukazu Nakamura[2], **Yoshifumi Saijo[1]**; [1]*Graduate School of Biomedical Engineering, Tohoku University, Sendai, Miyagi, Japan*, [2]*Institute of Development, Aging and Cancer, Tohoku University, Sendai, Miyagi, Japan*

Background, Motivation and Objective

Because numbers of photoacoustic (PA) imaging techniques have been developed, it becomes more important to obtain different information from ultrasound (US) imaging. Vascular network is a good target for PA imaging with conventional 532 nm laser because the extinction coefficient is of red blood cell is high between 500 and 600 nm. Different from the US Doppler technique, PA imaging can visualize the low speed blood flow in small vessels.

The objective of the present study is to visualize the vasculature of living chicken embryo by combination of the high frequency US and diode-laser based PA imaging.

Statement of Contribution/Methods

Laser pulses were generated by a semiconductor diode laser (L11038-02Y, Hamamatsu Photonics, Japan) with the wavelength of 532 nm, the pulse width of 3.4 ns, the output power of 430 μJ and the repetition rate of 100 Hz. PA signal was received by a 50 MHz concave ultrasound transducer with a 1 mm hole in the central part to get through an optical fiber in order to concentrically align the light illumination and signal reception. Mechanical scanning of the transducer was realized by using an x-axis stage (SGSP20-20, Sigma-koki) and a stage-driver (Mark-202, Sigma-koki). A digitizer card (DP1400, Acqiris, Inc.) installed in the PC was used to acquire the PA signal with the sampling rate up to 1 GSample/s. Lab-VIEW program was used to control the stage-driver and the function generator (MF1944B, NF, Inc.) which sent a trigger to a semiconductor laser. Three-dimensional images were reconstructed from serial US and PA images.

Fertile chicken eggs from a local farm were incubated at 38 °C in a humidified atmosphere for 3 days. They were placed in a shallow dish after 3 days of incubation for easy observation with US and PA imaging. This procedure was done by simply cracking the underside of the egg and gently dropping the content into the sterilized dish. Phosphate-buffered saline was filled in the dish for US coupler.

Results/Discussion

Figure shows the US imaging (left) and US-PA merged imaging (right) of chicken embryo. US imaging visualized overview of the whole body, especially, the vertebral column was clearly displayed. PA imaging visualized the heart and great vessels including aortic arch. This study showed the feasibility of US-PA combined imaging for observation of *ex ovo* chicken embryo. This study also showed the feasibility of US-PA combined imaging for developmental biology.

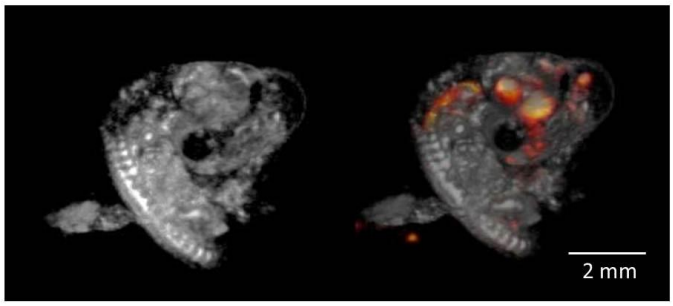

IUS1-PC4-6

Investigation of Photoacoustic Signal Strength as a Function of Scan-Speed and Laser-Repetition-Rate

Wei Shi[1], Peng Shao[1], Roger Zemp[1]; [1]*Electrical & Computer Engineering, University of Alberta, Edmonton, Alberta, Canada*

Background, Motivation and Objective

Optical-resolution photoacoustic microscopy (OR-PAM) can produce micron-scale, high-resolution images of optically-absorbing chromophores. The pressure rise of photoacoustic (PA) signals is proportional to the Greneisen parameter, which is temperature dependent. High laser repetition-rates may cause overlapping of adjacent laser pulses on targets in laser-scanning OR-PAM. When laser-pulse-repetition intervals are shorter than thermal relaxation times, the zone of laser-spot overlap between pulses can generate higher PA signal than cases where beam-spots do not overlap or in cases where laser pulse-intervals are longer than the thermal relaxation time. This is because subsequent laser pulses experience higher Gruneisen parameters than previous pulses due to temperature rises induced by the previous pulses. The purpose of this investigation is to better understand PA signal strength as a function of scan-speed & laser-repetition-rates, & to study the implications of this for image quality & novel imaging schemes leveraging this nonlinearity.

Statement of Contribution/Methods

In our OR-PAM system, the laser pulses were generated by a 532 nm diode-pumped nanosecond-pulsed Ytterbium fiber laser with 20-600 kHz repetition rates. Raster scanning is realized by using a 2D galvanometer scanning mirror system, while the scanning speed of each mirror can reach up to ~kHz depending on the scanning angles required. The maximum scanning angle determines the field of view (FOV) in the image. In our studies, the laser pulse energy was adjusted to 100nJ & the FOV was set to 250 × 250 μm. To realize non-overlapping laser pulses during imaging, the laser repetition-rate was set to 32 kHz. The slow & fast scanning speed was set to 40 & 800 Hz, respectively. The average interval between pixels was 12.5 μm, about twice as large as the focused optical spot size (~6 μm) & hence laser pulses did not overlap. To realize overlapping laser pulses, the laser PRR was set to 320 kHz & the slow & fast scanning speed was set to 1 & 400 Hz, respectively. With these settings average interval between pixels was 2.5 μm, less than half of the focused optical spot size. Therefore, laser pulses overlapped with ~3 μs intervals which are much less than the thermal relaxation time of targets used in our experiments.

Results/Discussion

Rapidly overlapping PA signals showed > 50% increase compared to non-overlapping signals in our phantom studies with rat blood, & the increase was more than 40% & 20% for our studies with black tape & hair, respectively. The results are consistent with theoretical predictions of PA signal enhancement due to ~10 degrees of temperature rise. In vivo

microvasculature imaging of rat ears was performed with & without fast-repetition overlapping pulses. Image quality metrics including contrast-to-noise is reported. Implications of these thermal nonlinearities are discussed for application to optimize image quality & to design future super-resolution imaging systems.

Clinical applications of strain imaging

Forum Hall

Wednesday, July 24 2013, 01:00 pm - 04:30 pm

Congress Hallair: **Caterina Gallippi**
UNC Chapel Hill and NC State University

IUS1-PC5-1

Displacement Estimation of Arterial Wall from Multiple Directions by Utilizing Diverging Transmit Beam for Synthetic Aperture Ultrasound Imaging

Hideyuki Hasegawa[1,2], Hiroshi Kanai[1,2]; *[1]Graduate School of Biomedical Engineering, Tohoku University, Japan, [2]Graduate School of Engineering, Tohoku University, Japan*

Background, Motivation and Objective

Measurement of elasticity of the arterial wall is useful for diagnosis of atherosclerosis. We developed an axial displacement estimator for measurement of regional motion and deformation of the arterial wall in the arterial longitudinal section. However, this method cannot be applied to the arterial cross section because the direction of motion due to an increment of blood pressure coincides with the axial direction only at the ultrasonic beam which passes through center of the artery. In the present study, a method using spherically diverging beams (DBs) from virtual point sources behind an array was examined for synthetic aperture (SA) imaging and displacement vector estimation.

Statement of Contribution/Methods

As shown in Fig. 1(a), DBs were produced by sequentially activating array elements from center to edge of an aperture (composed of 96 elements). For each transmission, 61 receiving beams (RBs) were created at angular intervals of 1 degree. The transmit aperture was stepped in the lateral direction at a pitch of 0.2 mm to perform 96 transmissions sequentially. For SA imaging, all RBs were used (overlapped beams were compounded), and RBs from -25 to 25 degrees at intervals of 5 degrees were used to estimate the displacement at a point of interest from multiple directions.

Results/Discussion

Figures 1(b) and 1(c) show B-mode images of a urethane phantom obtained by conventional beamforming and SA imaging using DBs. Echoes from interfaces are imaged in a wider region by SA imaging. Fig. 1(d) shows a single-angle image obtained from RBs at a steering angle of 20 degrees. There are many undesirable echoes from grating and side lobes. Echoes from main lobe were enhanced by evaluating the coherence factor (CF) among echo signals received by transducer elements as shown in Fig. 1(e). Fig. 1(f) shows the displacement at a red point in Fig. 1(c) estimated from multiple directions. The estimated displacements should follow cosine law with respect to the steering angle. Less least-square difference between the estimated displacements and cosine curve of 0.52% was obtained without CF compared with 0.75% obtained with CF. RBs without CF was superior for displacement estimation even though undesirable echoes were present. Synthetic aperture imaging and estimation of the displacement from multiple directions was possible using diverging transmit beam from virtual point sources.

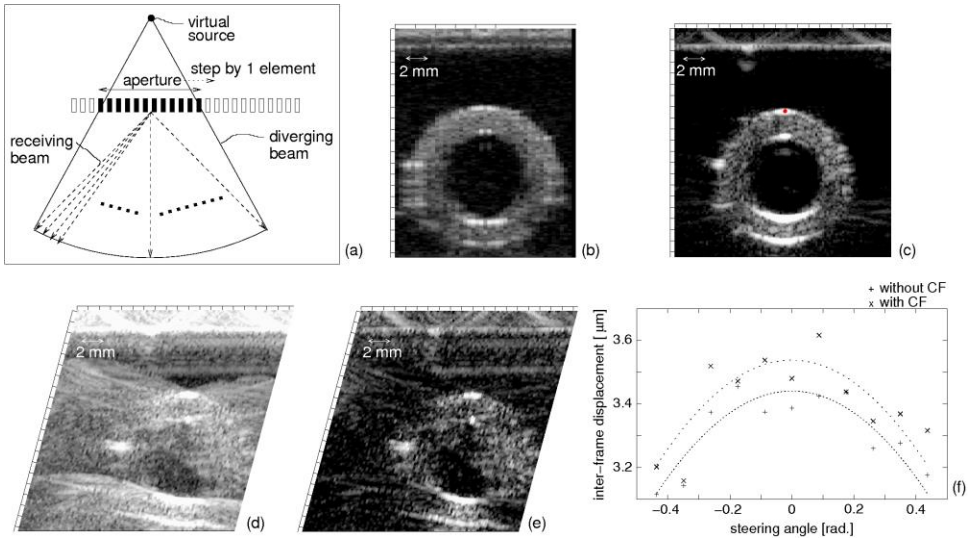

IUS1-PC5-2

Cardiac motion assessment from echocardiographic image sequences by means of the structure multivector

Martino Alessandrini[1], Adrian Basarab[2], Hervé Liebgott[1], Olivier Bernard[1]; *[1]Université de Lyon; CREATIS; CNRS UMR5220; Inserm U1044; INSA-Lyon; Université Lyon 1; Lyon 69622, F, France, [2]Université de Toulouse; IRIT; CNRS UMR5505; 118 Route de Narbonne, F-31062 Toulouse cedex 9, France, France*

Background, Motivation and Objective

Cardiac motion analysis in echocardiography is an active field of research. In this context we contributed a motion estimation algorithm [Alessandrini et al., TIP 2013] where the standard brightness constancy assumption is replaced by the conservation of the image phase, computed by means of the *monogenic signal*. Image phase is independent on the image intensity and hence insensitive to the temporal variations in local contrast commonly encountered in cardiac ultrasound. This property allowed outperforming state-of-the-art intensity-based algorithms.

Monogenic phase is computed by locally approximating the image as a 1D wave. Nevertheless, the 1D model is not ideal in the case of ultrasound images. Indeed the typical granular texture determined by the speckle noise rather requires modeling structures whose size is limited in both dimensions. In this context we present a novel motion estimation algorithm based on a more complex image model better suited for ultrasound images.

Statement of Contribution/Methods

Monogenic signal is replaced by a more advanced image analysis tool: the *structure multivector*. In this new formalism the image is locally modeled as the superposition of two perpendicular waves. Their local amplitude, orientation and phase are automatically computed from the responses to five spherical quadrature filters. The two wavelengths are directly related the speckle size in the two perpendicular directions.

The displacement is computed by solving the optical flow equation jointly for the two image phases. A local affine model accounts for typical cardiac motions as contraction/expansion and shearing; a *coarse-to-fine* B-spline scheme allows for a robust and effective computation of the model parameters and a pyramidal refinement scheme helps deal with large motions.

Results/Discussion

We assessed the performance on *ultra-realistic* simulations of one short axis and one apical 4 chambers sequence (46+53 frames) [Alessandrini et al., ICIP 2012] embedding a known motion field. Endpoint-error was used as accuracy metric. We compared against our monogenic-based algorithm and block matching (BM, interpolation factor 10 along x and y), which is still the reference for motion estimation in ultrasound. We achieved error reductions of 13% and 30% respectively (cf. Fig). The speedup w.r.t. BM was x50. These results encourage an evaluation on clinical data.

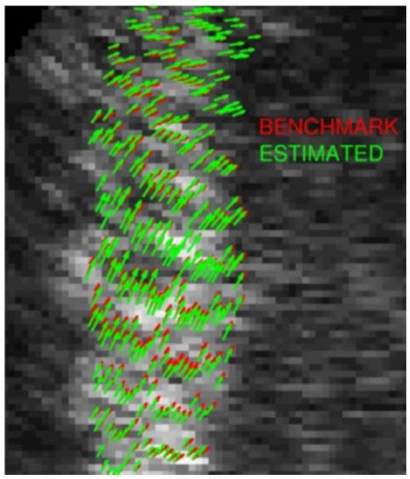

A4C sequence. Zoom on ventricular septum during systolic contraction. EE = 0.21.

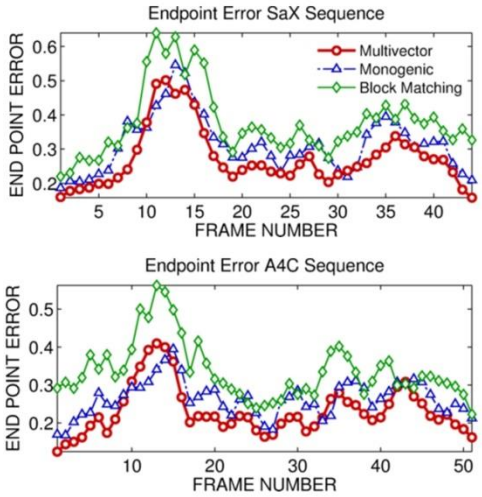

IUS1-PC5-3

A Feasibility Study of Developing an Acoustic Radiation Force Impulse Imaging for Intravascular Ultrasound

Cho-Chiang Shih[1,2], Pay-Yu Chen[2], Chih-Chung Huang[2]; *[1]Graduate Institute of Applied Science and Engineering, Fu Jen Catholic University, Taiwan, [2]Department of Electrical Engineering, Fu Jen Catholic University, Taiwan*

Background, Motivation and Objective

Determination of the elastic properties of plaque and vessel has a great significance in clinical diagnosis. Currently, intravascular ultrasound (IVUS) has been used for visualizing the epicardial vessels, and the location of plaque can be determined in real time. However, it is still difficult to estimate the elastic properties of different plaques and vessels using conventional IVUS image. In order to assess the elastic properties of soft tissue, several kinds of elastography have been proposed for noninvasive examination, such as acoustic radiation force impulse imaging (ARFI) and shear wave imaging. However, most of these elastographs are not suitable for visualizing the plaque and epicardial vessels due to imaging resolution. In order to overcome this problem, an idea of combining the IVUS and high frequency AFRI was proposed in present study.

Statement of Contribution/Methods

In this preliminary study, a confocal ultrasonic transducer was fabricated for high resolution ARFI imaging. The outer element with a frequency of 11 MHz was used to generate acoustic radiation force for creating the tissue displacement, and the displacements can be detected by 48 MHz inner element using echo-tracking algorithm. Since the size of this transducer is still larger, the experiments were carried out using an artificial vessel phantom with an authentic porcine plaque (artificial-induced). A linear scan was used to replace a rotating scan for verifying the feasibility of this novel idea, as shown in Fig 1(a).

Results/Discussion

Figure 1(b) shows the conventional echogenic image and its corresponding high resolution ARFI image from phantom, respectively. The location and dimension of plaque were observed obviously in echogenic image, and the distribution of stiffness was also obtained clearly using AFRI. The experimental results demonstrated the feasibility of using AFRI for IVUS. Figure 1(c) shows the concept of IVUS transducer design which both elements will be fabricated on the side of IVUS catheter. The intravascular elastography will be obtained by rotating the IVUS transducer. The next works will focus on transducer fabrication.

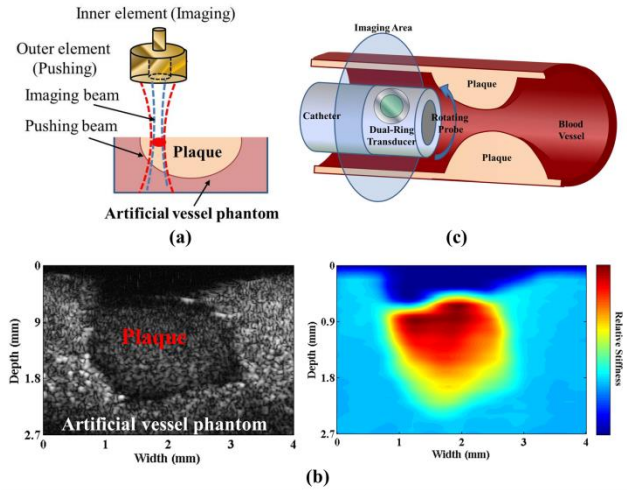

IUS1-PC5-4

Supersonic Shear Wave Imaging to Assess Arterial Anisotropy: Ex-vivo Testing of the Horse Aorta

Darya Shcherbakova[1], Clément Papadacci[2], Abigail Swillens[1], Annette Caenen[1], Veronique Saey[3], Sander De Bock[1], Koen Chiers[3], Mickaël Tanter[2], Mathieu Pernot[2], Patrick Segers[1]; *[1]IBiTech-BioMMeda, Ghent University, Ghent, Belgium, [2]Institut Langevin, Paris, France, [3]Faculty of Veterinary Medicine, Laboratory of Veterinary Pathology, Ghent University, Merelbeke, Belgium*

Background, Motivation and Objective

Data indicate that supersonic shear wave imaging (SSI) allows for a direct non-invasive quantification of the stiffness and fiber architecture of fibrous tissues such as the myocardium. Arteries also exhibit a complex layered, anisotropic and fibrous nature, leading to a pressure(stretch)-induced stiffening. The aim of this study was to assess the sensitivity of SSI to (a) stretch-induced arterial stiffening, and (b) arterial anisotropic behavior.

Statement of Contribution/Methods

Tests were performed on freshly excised horse aortas (N=2). First, a cylinder with height 6-8 cm was dissected from the proximal descending aorta, and opened to obtain a rectangular test specimen with width 6-8 cm and of sufficient length (about 8-10 cm). Thickness was in the order of 4-6 mm. The tissue was subsequently mounted in a uniaxial tensile test bench for mechanical loading under both quasi-static and dynamic (stretch rate 7.7 %/s) loading conditions. Stretch was applied in the vessel's circumferential direction and varied between 10% (pre-stretch) and 35%. Mechanical tests provided stress-strain data and reference values for the mechanical tissue parameters. At the same time, SSI was performed with the probe positioned over a range of angles of 0° (along circumferential direction) to 180°. The set-up is displayed in Fig. 1A.

Results/Discussion

Fig 1B shows a typical dynamic loading curve, with a clear non-linear behavior indicating the anticipated stretch-induced stiffening of the artery (due to the progressive recruitment of collagen fibers). Assuming bi-linear behavior, the Young elasticity modulus increases by 130 %. SSI at 0° clearly mirrored the cyclic stretch loading, with shear wave velocities ranging between 6.6 m/s (10% stretch) and 10.2 m/s (35% stretch), as shown in Figure 1C. Shear wave velocity progressively lowered in amplitude and cyclic variation, with values varying from 4.9 to 6.1 m/s for 30° and from 3.1 to 3.8 m/s for 90°.

We demonstrated the feasibility of simultaneous dynamic loading of excised horse aorta and SSI measurements. In this uniaxial loading set-up, SSI was most sensitive in detecting stretch-induced stiffening in the circumferential direction. Shear wave velocities were markedly lower in the other direction, most likely a consequence of arterial anisotropy or due to uniaxial stretching.

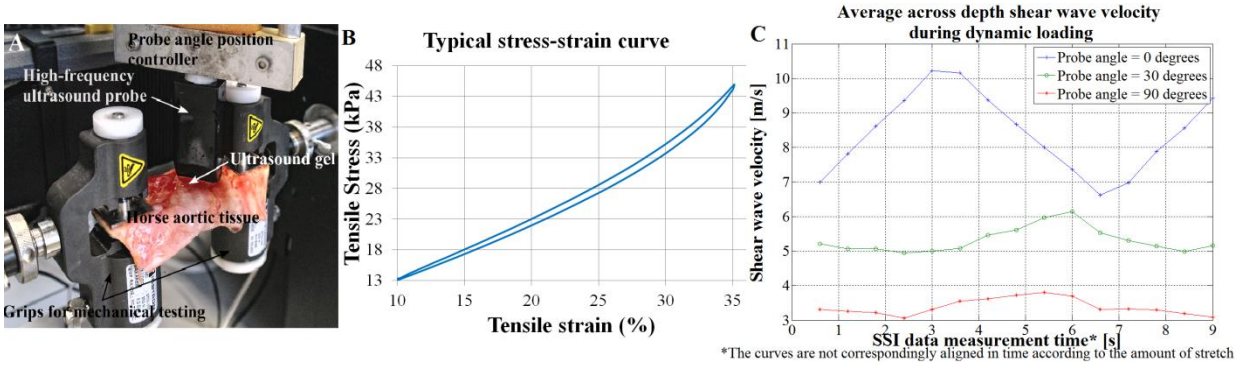

IUS1-PC5-5

Shear wave elasticity measurements from natural pulsatility of human carotid artery: a preliminary *ex vivo* study.

Redouane Ternifi[1], Jean-Pierre Remenieras[1], Emmanuel Nicolas[1], Emmanuel Simon[1], Samuel Callé[1]; *[1]UMRS INSERM U930, Université François Rabelais de Tours, France*

Background, Motivation and Objective

In order to study mechanical properties of tissues by tracking the natural movement such as brain pulsatility or artery wall motion, ultrafast passive elastography processing is used to estimate tissue elasticity. Indeed, determination of local tissue elasticity is becoming increasingly important in the diagnosis of tissue disease. In this work, we studied the Shear Wave Velocity (SWV) propagation due to natural artery wall movement and the aim was to test the feasibility of measuring SWV using an ultrafast ultrasound imaging system.

Statement of Contribution/Methods

These initial investigations have been realized using an *ex vivo* human carotid placed in a calibrated viscoelastic phantom (E=30 kPa, Young's modulus). The wall pulsation of the carotid, induced by a flow pump, was used as an internal source of mechanical stress. For the purpose of measuring SWV, IQ complex data are acquired with the Aixplorer Ultrafast Scanner (SuperSonic Imagine) using 256 elements linear probe, centered at 7.5MHz. The ultrafast acquisition allowed 2s signals, at a PRF of 500Hz. Two methods for measuring the SWV are tested: cross-correlation techniques (coupled with a parabolic interpolation) in the time domain, and monitoring phase shifts in the frequency domain. Both methods estimate the time delay (τ) between consecutive velocity curves, for several depths. The τ; values were plotted over depth to generate spatio–temporal profiles of tissue motion. From these profiles, the SWV was estimated through linear regression assuming homogeneous elasticity in the phantom.

Results/Discussion

Figure 1-(a) shows an example of velocity curves estimated at different depth as indicated in the Bmode image of the *ex vivo* carotid surrounded with a phantom (b). We track τ; between velocity curves from the carotid wall to 2cm depth with a step of 0.2 cm. We obtained an average value of SWV=3.1 m/s (E=26 kPa) with the cross-correlation and SWV=3.2 m/s (E=27.8 kPa) with FFT. These results are close to the phantom elasticity, which shows the good performance of the two techniques. The monitoring of attenuation allows us to determine the viscous parameters.

Potential applications of this approach include local measurements of SWV, tissue characterization, and the development of noninvasive methods for studying the relationship between blood-flow dynamics and tissue elasticity in clinical research.

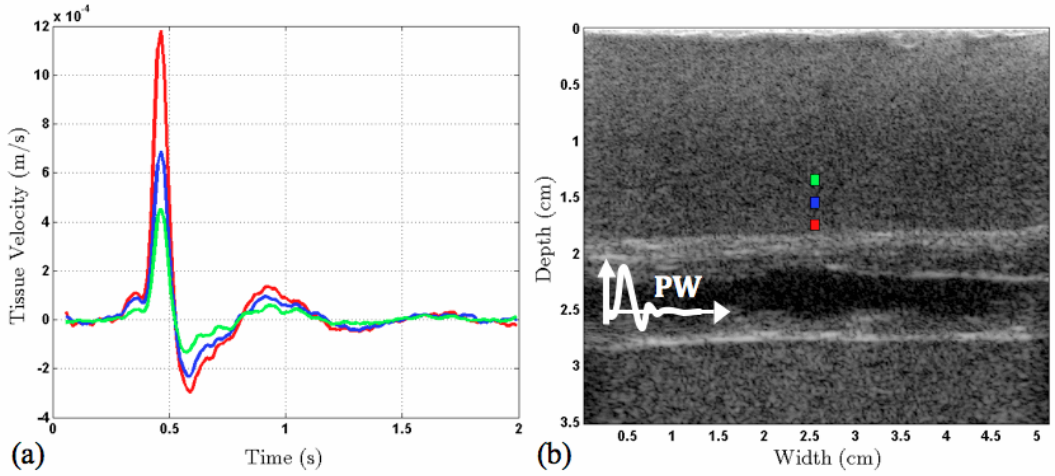

Figure 1: (a) - Curves of velocity at different depths and (b)-Bmode image of carotid surrounded by phantom.

IUS1-PC5-6

A Phase-based Motion Estimation Technique for Mouse Cardiac Function Using the Monogenic Signal and High Resolution Ultrasound

Dan Lin[1], Brent A. French[1], John A. Hossack[1]; [1]*University of Virginia, USA*

Background, Motivation and Objective

Regional tissue motion estimation using medical ultrasound images is an important first step in solving many problems with significant applications that include non-invasive detection of a tumor via tissue elastography or myocardial infarction assessment in echocardiography. Many existing techniques for estimating motion are based on block-matching using B-mode image intensity, and phase information is often neglected. In image processing, it is widely accepted that the information carried in the image phase is more important than information carried by its amplitude. In this work, we showed a phase-based motion estimation technique that is both accurate and fast.

Statement of Contribution/Methods

Displacement between two consecutive frames is estimated based on the difference in phase, which is obtained from the monogenic signal using a spherical quadrature filter and the Riesz transform. This approach in displacement estimation was compared with a minimum sum of absolute differences (MSAD) block-matching algorithm. Both tracking algorithms were applied to moving phantom data, where ground truth displacement is known, and in vivo mouse heart data. Both data sets were acquired with a transducer operating at 30MHz. Motion estimation using block-matching was implemented with 0.2mm x 0.2mm pixel blocks. For phase-based motion estimation technique, the monogenic signal was computed for each frame, and the difference in phase between two consecutive frames was also computed for displacement estimation.

Results/Discussion

For the phantom data, tracking errors were 2.4±0.2% and 2.5±0.2% for phase-based and block-matching techniques, respectively. Tracking error for in vivo mouse heart data is calculated based on the ratio of the length of final displacement vector to the length of the trajectory, and were 5.3±1.6% and 7.1±2.1% for phase-based and block-matching techniques, respectively. In conclusion, phase-based motion estimation is an improved alternative to block-matching as it utilizes important phase information. Tracking resolution for phase-based tracking is theoretically limited only to image pixel resolution, meaning every pixel can be tracked without sacrificing tracking accuracy. While it is also possible to track every pixel using block-matching, accuracy and computation cost would require optimization of kernel and search block sizes.

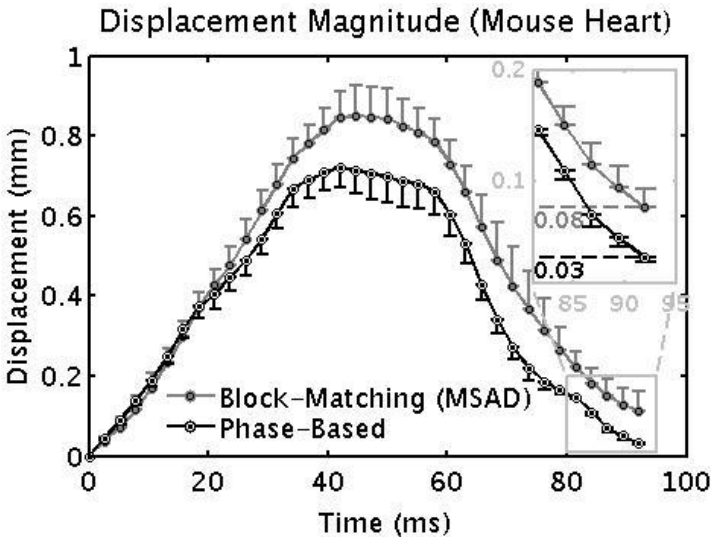

IUS1-PC5-7

Comb-push ultrasound shear elastography (CUSE) for detection and classification of breast lesions: preliminary in vivo study

Mohammad Mehrmohammadi[1], Pengfei Song[1], Shigao Chen[1], James F. Greenleaf[1], Mostafa Fatemi[1], Azra Alizad[1]; [1]*Physiology and Biomedical Engineering, Mayo Clinic, Rochester, MN, USA*

Background, Motivation and Objective

Breast cancer is the second most common cancer among American women. According to the American Cancer Society, bout 12% of women in the US will develop invasive breast cancer during their lifetime. Currently, breast biopsy is the gold standard method used to distinguish between benign and malignant lesions in breast. However, reports indicate that about 80% of biopsies turn out to be negative. Unnecessary biopsies of benign masses result in significant emotional, physical, and financial consequences.

Statement of Contribution/Methods

It is generally known that mechanical (i.e. viscoelastic) properties of breast lesions are important markers of malignancy. Therefore, quantitative assessment of the viscoelastic properties of breast tissues can lead to development of a noninvasive assessment tool with high sensitivity and specificity. In this study, we present preliminary results of a novel 2-D shearwave elasticity imaging technique (CUSE) in detection and classification of lesions in patients with breast abnormalities. Our imaging system is developed on the platform of a fully programmable digital ultrasound system (Verasonics, Inc. Redmond, WA, USA). This system is capable of producing multiple acoustic radiation force beams, including focused and unfocused beams, at multiple locations within the breast to remotely vibrate tissues and thus generate shear waves. Upon generation of shear waves, the system acquires pulse-echo ultrasound data within a B-scan plane. The pulse-echo data is then utilized to detect shear waves and calculate their speed in a 2-D space. The shear wave speed information is used to reconstruct a map of Young's modulus of the breast tissue.

Results/Discussion

The performance of the system was initially evaluated by testing using a set of tissue mimicking phantoms. Following the initial assessment of the system, preliminary human studies were performed under a protocol approved by the institutional review board (IRB). The human studies were performed on a group of patients with suspicious breast masses who were scheduled for breast biopsy. The study was conducted prior to biopsy. The results of our phantom study (standard elasticity phantom, CIRS, Model 049) indicate the accuracy of the proposed technique in identifying inclusions with larger stiffness and also in quantifying the mechanical properties of the background and inclusions (Fig 1.a). The quantitative values measured by our technique (Fig 1.b) shows a close agreement with the nominal Young's modulus values of the elasticity phantom. Furthermore, our in vivo results demonstrate the feasibility of the method in humans. For example, in normal breast tissue, the average shear wave speed was measured less than 2 m/s which is significantly less than the shear wave speeds reported for malignant lesions (above 6 m/s). Further research is needed to fully evaluate the utility of the proposed method in the clinical applications.

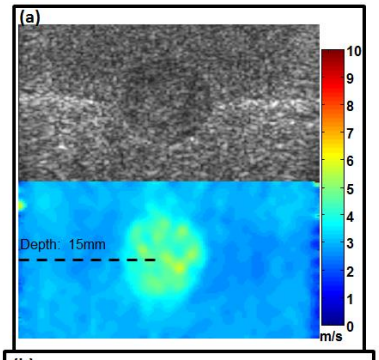

(b)

Material type	Nominal Young's modulus (mean - kPa)	CUSE measurements (mean - kPa)
Background	25	23.5
Inclusion type 1	45	36
Inclusion type 2	80	76

Advanced front-ends for medical imaging

Forum Hall

Wednesday, July 24 2013, 01:00 pm - 04:30 pm

Congress Hallair: **David Vilkommerson**
DVX, Inc.

IUS1-PC6-1

Ultrasound Analog Front End Integrated Circuit with Digital Heterodyning for Data and Computation Rate Reduction

Ashraf Saad[1], **Gina Kelso[1]**, Corey Petersen[1], Joshua Nekl[1], Daniel Rey-Losada[1]; *[1]Analog Devices Inc., USA*

Background, Motivation and Objective

Diagnostic ultrasound image quality is a primary technology driver in the field. Better resolution images require higher frequency probes, while better harmonic images require higher dynamic range. These factors triggered the adoption of Analog-to-Digital converters (ADCs) with higher sampling rates and resolution.

As a consequence, the data bandwidth between the ADCs and the beamformer is drastically increasing, putting more memory burden on the beamforming hardware and posing routing challenges due to increased number of I/O lanes. In addition, the computational complexity of the beamformer scales up with the input data bandwidth. One additional factor that exacerbates the computational challenge is the support of high count parallel receive beamforming, which is a key enabler for high volume rate 3D ultrasound imaging. As an example, the data bandwidth of a 128 channel system with 14-bit 40-MHz ADCs is 71.7 Gbps.

We will discuss an efficient hardware implementation of an octal ultrasound analog front end (AFE) chip that integrates a per RF channel digital heterodyning block as a way of reducing the data bandwidth and I/O lanes between the ADCs and the beamformer.

Statement of Contribution/Methods

Nowadays, available octal ultrasound AFE integrated circuits enable circuit board area reduction that facilitates lower form factor ultrasound systems. However the raw RF data rate is increasing with increased ADC sampling rate and resolution. By integrating a per channel digital heterodyning block with the AFE, the output can be a much lower rate baseband I&Q signal compared to the raw RF signal while maintaining the signal bandwidth. The heterodyning block implements a per channel digital quadrature demodulator and decimator.

The quadrature demodulator incorporates a numerically controlled oscillator to generate the baseband I&Q signals. The demodulator is followed by a programmable poly-phase FIR decimating filter. The octal AFE with digital functionality still consumes low per channel power (<150 mW), making it suitable for small form factor systems. The chip also implements the new JESD204B serial digital output that allows packing the heterodyned data of all 8 channels on one high speed lane (up to 5 GBPS), which greatly simplifies the I/O routing.

Results/Discussion

The designed AFE chip represents a new milestone in the vertical integration of the analog and digital processing in ultrasound systems. Data rates can be reduced by more than 50%, especially for high frequency probes. The newly designed AFE chip will enable demodulation-based beamforming techniques. The chip will also facilitate per channel data migration to a general purpose processor or a DSP to enable more advanced imaging applications, such as shear wave Elastography. In addition, this technology will simplify the realization of 3D systems by reducing the computational rates for high count parallel receive beamforming algorithms via reducing the input data bandwidth.

IUS1-PC6-2

Single-chip Ultra High Slew-rate Pulse Generator for Ultrasound Scanner Applications

Chin Hsia[1], Yen-Chung Huang[2], Chih-Wen Lu[3]; *[1]Industrial Technology Research Institute, Hsinchu, Taiwan, [2]National Chi Nan University, Nantou, Taiwan, [3]National Tsing Hua University, Hsinchu, Taiwan*

Background, Motivation and Objective

Low power, high speed pulse generator is one of the most critical components for multichannel, portable and compact ultrasound scanners. Conventional off-the-shelf pulse generator generally operates within 20~30 MHz frequency range and the switching speed is limited to drive diverse transducers. In this paper, we propose a single-chip architecture of ultra high slew-rate pulse generator to support ultrasound scanners for a wide range of frequency operation.

Statement of Contribution/Methods

The ultra high slew-rate two-stage pulse generator is shown in Fig. 1. The digital circuit in the first stage, which synthesizes two driving signals from the input and one is half-period delay from the other, is designed to drive the second stage, MP1 and MN1, a pair of high voltage power inverter. The high speed level shifters, which are composed of low breakdown CMOS devices, are designed at high side and low side, respectively, to boost voltage levels between the input and the power inverter. To avoid shoot-through current flowing through MP1 and MN1, a high speed dead-time control circuit generates non-overlap switching signals to drive the power inverter. A digital clamp signal, which passes through a second lower level shifter, is used to turn on the active damper, MP2 and MN2, to achieve fast zero return voltage and reduce output ringing while switching off the power inverter. Two always-on transistors, MD1 and MD2, are inserted between the out put node and the damper to prevent unexpected turn-on of MP2 and MN2 during the high voltage switching at the output.

Results/Discussion

The circuit is implemented using VIS 0.25um BCD 1P5M process. The chip is taped out and fabricated for validation. The simulated performance is shown in Fig. 2. Maximum slew-rate of the pulse generator can achieve more than 30KV/usec, which corresponds to 80V dynamic voltage swing with more than 65 MHz frequency bandwidth. The time constant of zero return voltage is significantly improved by using the damper. The second harmonic distortion at the output of pulse generator is lower than -55 dBc. The results indicate that the potential and applicability of the proposed pulse generator for transducer drivers where ultrasound scanners with a wide frequency operation capability are desired.

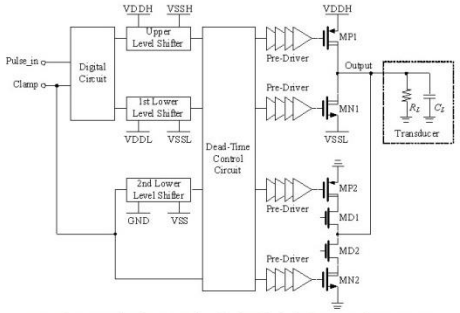

Fig. 1 The proposed architecture of single-chip ultra high slew-rate pulse generator

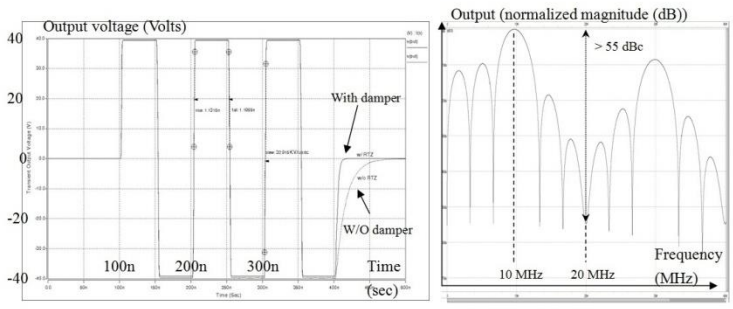

Fig. 2 The simulated performance of single-chip ultra high slew-rate pulse generator

IUS1-PC6-3

Wideband Portable Power Amplifier Design for Very High Frequency Ultrasonic Transducers Applications

Hayong Jung[1], Hojong Choi[2], K. Kirk Shung[2]; *[1]NIH Transducer Resource Center and Department of Biomedical Engineering, University of Southern California, Los Angeles, California, USA, [2]NIH Transducer Resource Center and Department of Biomedical Engineering, University of Southern California, LA, CA, USA*

Background, Motivation and Objective

The power amplifier (PA) is used to drive the ultrasonic transducers. As the operating frequency of the transducer increases, the PA design would be more challenging due to higher demanding specification such as sensitive noise level and wide bandwidth of the ultrasound system. Another issue is that the commercial equipment is quite bulky so the long coaxial cables need to be used to integrate other ultrasound system parts, which the cable loading generate dramatic effect for the high frequency transducer's performances. Therefore, a low-noise and wideband portable power amplifier is proposed.

Statement of Contribution/Methods

A wide-band Class A PA was designed using LDMOS (PD57006). The topology of the PA is a 1-stage common-source amplifier with inductor-capacitor matching circuits. In order to estimate the performance of the power amplifier, the PA was tested with a function generator and displayed the waveforms on the oscilloscope and spectrum analyzer. To evaluate the performances of the PA, the pulse-echo measurement with a transducer with a 40 dB preamplifier was also performed.

Results/Discussion

The measurement results show that PA has a gain of 15.8~17.8 dB in the range of 100 to 250 MHz and its current consumption of 0.3~0.4A. The measured 1-dB compression point was as a 26.3Bm. The 3rd order input and output inter-modulation point (IIP3 and OIP3) were 12.25 dBm and 27.25 dBm, respectively. And, the measured noise figure is 2.14~2.98 dB in the range of 80~120MHz. With a 150 MHz LiNbO3 transducer excited by the PA, the peak-to-peak voltage and -6dB bandwidth of the echo signal was 64 mV and 52.3 %. These results show that this low-cost wideband portable power amplifier would be useful for very high frequency imaging or acoustic tweezer applications.

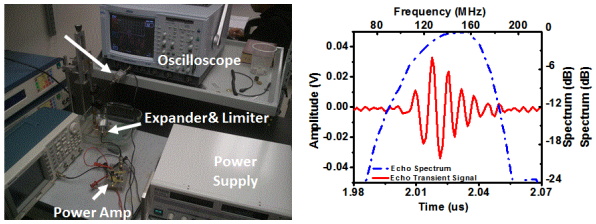

Fig 2.(a) Test Bench(left) and (b) The pulse-echo measurement data with 150 MHz z $LiNbO_3$ transducer using designed power amplifier and 40 dB reamplifier(right).

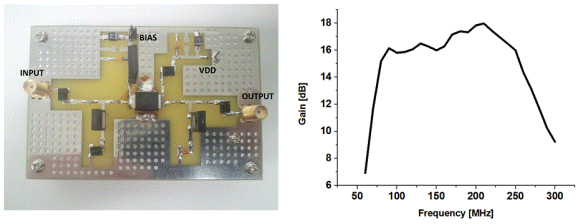

Fig. 1. (a) Designed power amplifier (left, Dimension : 96.52×63.5 mm²) and (b) measured gain(right)

IUS1-PC6-4

Linearizer Circuit of the Power Amplifier for Very High Frequency Ultrasonic Transducers Applications

Hojong Choi[1], Hayong Jung[1], K. Kirk Shung[1]; *[1]NIH Transducer Resource Center and Department of Biomedical Engineering, University of Southern California, Los Angeles, CA, USA*

Background, Motivation and Objective

Power amplifiers are used to excite the ultrasonic transducers. Since the dynamic range of the high voltage signals transmitted from the power amplifier is related to the imaging resolution of the ultrasound system. A linear power amplifier is desirable because of its higher dynamic range. The novel linearizer circuit using a resistor-capacitor-inductor circuit and MOSFET was designed to enhance the linearity, which is the ability to amplify a signal without distortion, of the power amplifier by lowering non-linear harmonic distortion. In order to use the array imaging system, this linearizer circuit was also simplified without systematical approach such as algorithm optimization.

Statement of Contribution/Methods

A linearizer circuit and 16-dB Class A power amplifier were designed and implemented in a printed circuit board. To evaluate the performances of the power amplifier with and without the linearizer circuit, the 2nd and 3rd harmonic distortions (HD2 and HD3) were measured using spectrum analyzer. The pulse-echo measurement was also performed to estimate the harmonic performances of the linearizer and power amplifier with a 130 MHz LiNbO3 transducer.

Results/Discussion

With continuous sine waveforms, lower HD2(-43.3dB) and HD3(-41.5dB) were measured with the linearizer including power amplifier than those (HD2=-28.7dB and HD3=-29.4dB) of the power amplifier. For the pulse echo measurement, the lower 2nd harmonic distortion of the echo signals generated by the transducer with the linearizer and power amplifier (HD2=-24.2dB) was also achieved than that of the power amplifier alone (HD2=-16.9dB). These results demonstrate how the addition of the linearizer circuit improves the power amplifier performance for very high frequency (> 100MHz) transducer applications.

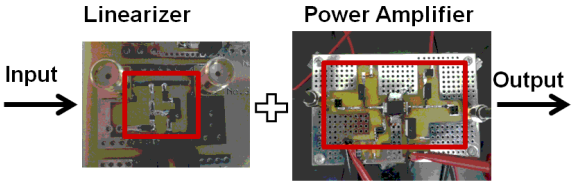

Fig. 1. Architecture of a linearizer circuit with power amplifier.

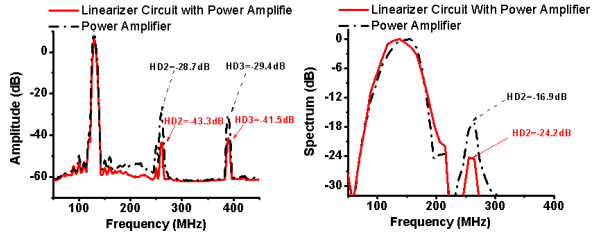

Fig. 2. (a) The comparison of the power spectrum data measured by spectrum analyzer between the linearizer circuit with the power amplifier (solid red line) and the power amplifier alone (dash-dot black line). (b) The comparison of the echo spectrum data using 130 MHz single element LiNbO3 transducer

IUS1-PC6-5

Bipolar Pulse Generator for Very High Frequency (> 100 MHz) Ultrasound Applications

Min Gon Kim[1], Hojong Choi[1], Hyung Ham Kim[1], K. Kirk Shung[1]; [1]*University of Southern California, USA*

Background, Motivation and Objective

Pulse generator (or pulser) is one of the major components that determine the spatial resolution of the ultrasound imaging system. It is particularly important for high frequency ultrasound imaging systems since the transmit pulse with short pulse length and wide band frequency characteristics is essential to obtain acceptable echo signal from the transducer. Commercially available pulse generators such as Panametrics ultrasonic analyzer (5900PR, Olympus NDT Inc.) have been extensively used for high frequency ultrasound imaging with single element transducers. However, for array based imaging systems, multiple compact sized pulse generators are required. We present a cost-effective and compact monocycle bipolar pulse generator for imaging with very high frequency (> 100 MHz) transducers.

Statement of Contribution/Methods

The proposed pulse generator circuit consists of a pulse forming network and a transistor driver that is made of a timing circuit and a speed up capacitor. It was implemented on the printed circuit board. For the pulse-echo measurement, the pulse generator was connected to the power amplifier (ENI 325LA, Electronic Navigation Industries) and diode-based expander (single diode pairs). A single pulse signal was used to excite a 1 mm diameter Lithium Niobate (LiNbO3) 140 MHz single element transducer with a f-number of 1.5, the received echo signal from the transducer was sent via the MOSFET-based limiter (IRF5801, International Rectifier) to the receive amplifier of the Panametrics 5900PR ultrasonic analyzer. Subsequently, the echo waveform was recorded in the oscilloscope (LC534, LeCroy) using a Labview program.

Results/Discussion

The designed pulse generator could produce a monocycle bipolar pulse with the center frequency of 220 MHz, -6dB bandwidth of 100% and the peak-to-peak amplitude of 2V as shown in Figure 1(a). Compared to the Panametrics 5900PR transmitter, the pulser can generate less ringing effect as shown in Figure 1(b), which may greatly improve the axial resolution of the very high frequency transducer. For the transducer that triggered by the pulse generator, the -6dB bandwidth of received echo signal was improved by 121% compared to the Panametrics 5900PR transmitter. Therefore, the designed pulse generators may be used for the array based high frequency imaging systems.

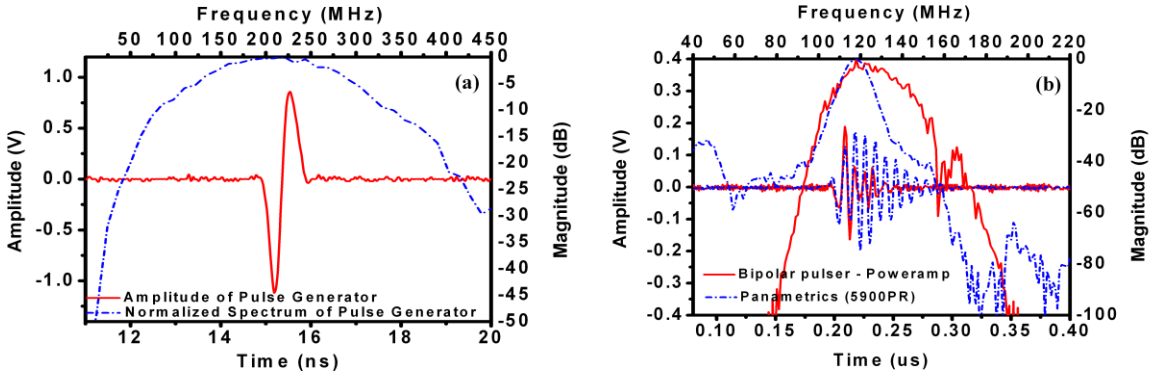

Fig. 1: (a) The pulse signal with the peak-to-peak amplitude of 2V and its spectrum with the center frequency of 220 MHz, -6dB bandwidth of 100% generated by the pulse generator. (b) The echo response comparison between the proposed pulse generator with -6dB bandwidth of 25.1% and Panametrics 5900 transmitter with -6dB bandwidth of 11.3% without receiver's amplification.

IUS1-PC6-6

A Novel Bipolar Pulse Generator for High-frequency Ultrasound System

Jian-Xing Wu[1], Yi-Chun Du[2], Chia-Hung Lin[3], Pei-Jarn Chen[2], Tainsong Chen[1]; [1]*Department of Biomedical Engineering, National Cheng Kung University, Tainan, Taiwan,* [2]*Department of Electrical Engineering, Southern Taiwan University of Science and Technology, Tainan, Taiwan,* [3]*Department of Electrical Engineering, Kao-Yuan University, Kaohsiung, Taiwan*

Background, Motivation and Objective

Pulse generator is the critical component in all ultrasound systems for driving a piezoelectric transducer to medical or nondestructive testing (NDT) applications. The transducer in ultrasound system was driven by a pulse train generator, which delivers high-voltage bipolar or unipolar pulse train. Several recent papers have discussed both the importance and the design of unipolar and biopolar pulse generator for ultrasound applications. Bipolar voltage pulse has lower unwanted DC and low-frequency component could decrease the leakage current. Also, its peak-to-peak pulse voltage could achieve twice of the voltage rating of the coaxial cable connecting the generator and the transducer. In current

commercial ultrasound systems, bipolar Pulse generators are commonly used; however, it still had some disadvantages like longer pulse length, which limited the driving frequency and affect the signal performance. This paper purposed a novel design of bipolar pulse generator based on a novel dual P-N channel MOSFET and FPGA timing control.

Statement of Contribution/Methods

The design used dual P-N channel MOSFET and timing controller based on FPGA to provide shorter pulse length. Bipolar pulse generator proposed in this paper could provide approximately 10ns pulse length and multi-cycle pulses with center frequency over 60 MHz achieving to a 50 ohm load. The performance was also compared to the commercial devices including Panametrics 5900 Pulser/Receiver (Olympus NDT Inc., Waltham, MA) and MD1213 Pulser (Supertex Inc., Sunnyvale, CA) in the same testing condition. The results showed that our design generated a 10ns 100Vpp monocycle pulse, the 5900PR generated a 100 Vpp 30ns negative spike, and the MD1213 generated a 30ns 100Vpp monocycle pulse, respectively. Unamplified received echoes from our design, MD1213 and Panametrics 5900PR are shown in Fig. 1. The results indicated the new design is efficient for triggering 50MHz transducer.

Results/Discussion

This study proposes a novel design for bipolar pulse generator with FPGA controlling. It could produce multi-cycle pulses with center frequency over 50 MHz and shorter pulse length. This design also preserved the low-cost advantage compared to other commercial design of bipolar pulse generator. It is suitable for high-frequency ultrasound Doppler and B-mode imaging applications.

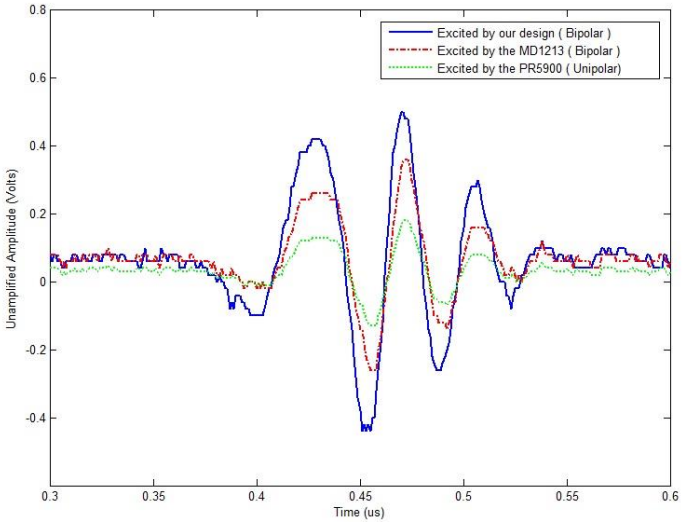

IUS1-PC6-7

Design of 80 MHz Linear Transducer Array for Breast Cancer Biopsy

Thomas Cummins[1], Hojong Choi[1], Hyung Ham Kim[1], K. Kirk Shung[1]; [1]*Biomedical Engineering, University of Southern California, USA*

Background, Motivation and Objective

In the United States, over 1.6 million breast biopsy procedures are performed each year. During the biopsy procedure, the biopsy needle is usually guided by the conventional low frequency (5 to 10 MHz) imaging. We propose a miniaturized 80 MHz linear array integrated within a core biopsy needle to provide ultra-high resolution images of breast tissue. High-frequency ultrasound imaging at the tip of the biopsy needle may allow radiologists to identify small structures such as microcalcifications, ducts and cancerous masses inside of fatty breast tissue at the closest proximity to the lesion. It will enhance the accuracy of the biopsy by visualizing the region of interest with high resolution images. Conventional low frequency (5 to 10 MHz) linear arrays for breast imaging do not provide enough spatial resolution and currently available high frequency (30 to 60 MHz) needle type single element transducers are not practical for real-time imaging. High-frequency ultrasound images obtained right at the lesion may allow radiologists to identify features not previously seen during the conventional biopsy guidance and achieve more targeted biopsies.

Statement of Contribution/Methods

The array is designed to fit within a 10AWG core biopsy needle with the imaging plane parallel to the long axis of the needle. We optimized this array's performance using KLM modeling, finite element analysis and two-way sound field simulation to determine the array geometry for this application. In addition to the array design, the packaging of such a compact device necessitated using a miniature 64-channel transmission line electronic component that can be bonded to the array easily and still fit within the biopsy needle.

Results/Discussion

We chose to design a 64-element single crystal PMN-PT array with 1.1λ pitch, elevation height of 1.0mm with the designed imaging depth of up to 3mm and -6dB axial and lateral resolution of 66μm and 43μm, respectively. KLM modeling showed the single element -6dB bandwidth to be 31% and finite element modeling yielded a single element impedance value of 370 Ω at 80MHz. This high frequency needle array will provide a close-up view of the tissue about to be sampled with the biopsy needle and thus allow radiologists to choose the most suspicious breast tissue.

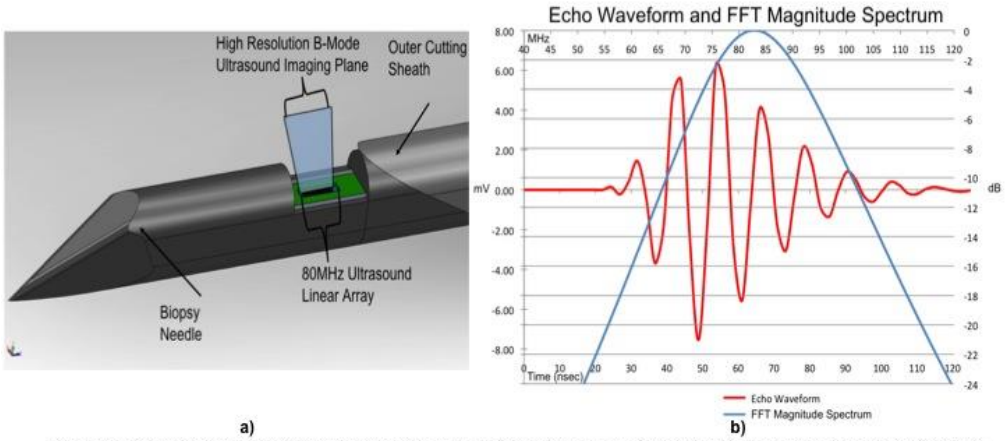

Figure 1: a) Concept rendering of biopsy needle array and **b)** KLM simulation of echo waveform and FFT magnitude spectrum of single array element.

IUS1-PC6-8

DEVELOPMENT OF LOW-NOISE WIDEBAND RECEIVER FOR INTRAVASCULAR AND PHOTOACOUSTIC IMAGING

Ju-Young Moon[1], Hea Min Kim[2], Jae Hee Song[1], Jun Su Lee[2], Jin Ho Chang[1,2]; *[1]Medical Solutions Institute, Sogang Institutes of Advanced Technology, Sogang University, Seoul, Korea, Republic of, [2]Interdisciplinary Program of Integrated Biotechnology, Sogang University, Seoul, Korea, Republic of*

Background, Motivation and Objective

Combining IVUS (Intravascular Ultrasound) and IVPA (Intravascular Photoacoustic) imaging systems is beneficial for diagnosis of atherosclerosis, i.e., assessment of plaque vulnerability. The IVUS/PA imaging is performed by transmitting and receiving high frequency ultrasound (HFU) in the range of 20 MHz to 80 MHz or more. Since HFU transducers for IVUS/PA imaging typically have a low sensitivity, the amplitude of received signals needs to be increased by at least 40 dB. However, it is challenging to implement a low-noise wideband receiver with a high amplification gain by off shelf components. This paper presents the analog frontend receiver developed for IVUS/PA imaging.

Statement of Contribution/Methods

The developed receiver consisted of matching and protection circuit, two low-noise amplifiers (AD8000, Analog Devices Inc.), one variable gain amplifier (AD8337, Analog Devices Inc.), and one analog low-pass filter. The high gain while low noise capability was achieved by using two 20-dB low-noise amplifiers for 40-dB amplification. Also, the filter-structured conjugate matching method was employed for the input/output impedance matching of each component on the receiver. By doing so, the wideband flat gain feature could be attained. The performances of the developed receiver were evaluated by measuring the amplification gain over frequencies and by comparing its SNR with that of the receive module in a commercial pulser/receiver system (UT340, UTEX Scientific Instruments Inc.). For the experiment, US and PA images of a 0.12 mm diameter wire were acquired using a custom-made 48 MHz PVDF single element transducer. For the US image, the transducer was excited by the transmit module in a UT340.

Results/Discussion

Fig. 1(a) shows the amplification gain of the developed receiver while the gain of the variable gain amplifier was kept 5 dB: operating frequency range of more than 120 MHz, gain flatness of less than 1 dB over 100 MHz, maximum gain of 41 dB. Also, the SNRs of US and PA images (Fig. 1(b), (c)) acquired by the developed receiver were 36.5 dB and 34.5 dB, respectively, while those by the UT340 (Fig. 1(d), (e)) were 29.7 dB and 19.5 dB. From the results, it was verified that the developed receiver is capable of improving SNR of US and PA images by at least 6.8 dB, compared with the commercial receiver and it is suitable for combined IVUS/PA imaging.

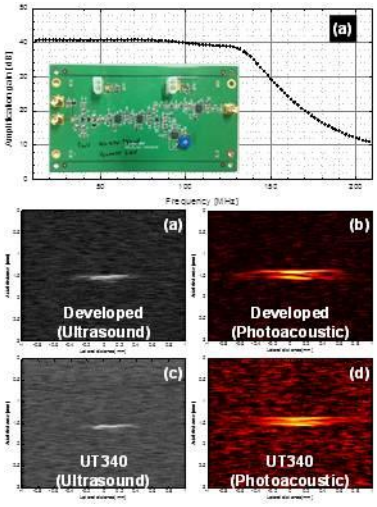

Materials and Defect Characterization

Forum Hall

Wednesday, July 24 2013, 01:00 pm - 04:30 pm

Congress Hallair: **Edward Haeggstrom**
University of Helsinki

IUS2-PC1-1

A method of evaluating CTE of TiO_2-SiO_2 ultra-low-expansion glasses by the ultrasonic microspectroscopy technology

Mototaka Arakawa[1], Yuji Ohashi[1], Jun-ichi Kushibiki[1]; [1]*Tohoku University, Sendai, Japan*

Background, Motivation and Objective

Ultra-low-expansion (ULE) glasses with a coefficient of thermal expansion (CTE) within 0±5 ppb/K at desired operating temperatures are required for substrates of mirrors and photomasks in extreme ultraviolet lithography (EUVL) systems. TiO_2-SiO_2 ULE glass is one of the candidate. The CTE of TiO_2-SiO_2 ULE glass becomes zero around room temperature by adjusting the concentration of TiO_2 around 7 wt%.

We developed an indirect ultrasonic measurement method and a practical system for super-precisely measuring CTE for the glass by the ultrasonic microspectroscopy (UMS) technology. CTE is evaluated by measuring the velocity of leaky surface acoustic waves (LSAWs), V_{LSAW}, excited and propagated on a water-loaded specimen surface or the longitudinal velocity, V_l, propagating along thickness direction of a specimen.

In this paper, we discuss the evaluation method of CTE of the glass by comparing the measurement results of V_{LSAW} and V_l.

Statement of Contribution/Methods

Two TiO_2-SiO_2 glass specimens (P and M) were prepared from two ingots with different grades (premium and mirror, respectively), and their surfaces were almost parallel to the striae plane. The period of striae is about 0.16 mm. Both surfaces were optically polished. The specifications of these ingots for CTE are provided in the catalog that the absolute value is 0±30 ppb/K and the homogeneities are within 10 ppb/K for the premium-grade ingot and 15 ppb/K for the mirror-grade ingot.

Results/Discussion

We measured V_{LSAW} and V_l for the specimens by the UMS technology. The results are shown in Fig. 1. The maximum differences of V_{LSAW} and $V_l$are 6.38 m/s and 1.52 m/s for specimen P and 4.25 m/s and 1.18 m/s for specimen M, respectively. The corresponding CTE distributions were estimated to be 27.6 ppb/K and 4.2 ppb/K for specimen P and 18.4 ppb/K and 3.2 ppb/K for specimen M, respectively, from the calibration lines we obtained.

CTE distributions estimated by V_{LSAW} were 6-7 times larger than those estimated by V_l for both specimens. V_{LSAW} can detect the distibution caused by striae accurately. While, V_l are averaged propeties along the thickness direction of the specimen. Therefore, CTE variations caused by striae on the specimen surface or in the glass ingots could not be detected accurately. V_{LSAW} measurements are extremely useful for development of EUVL-grade TiO_2-SiO_2 glass.

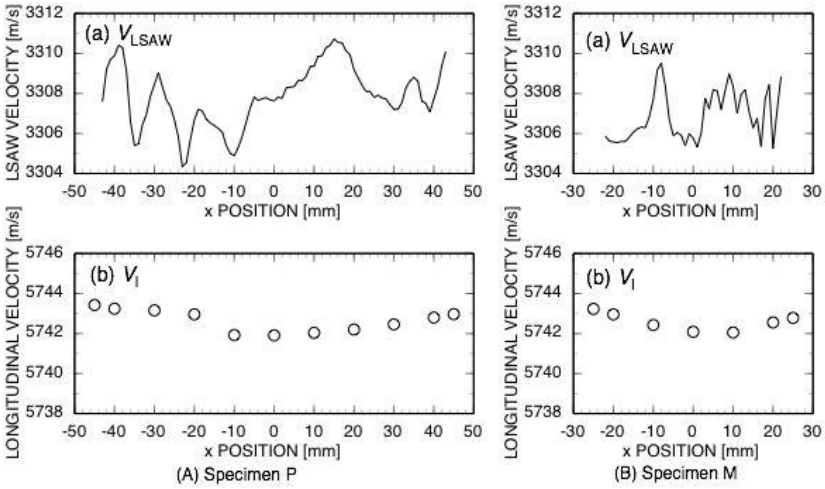

Fig. 1. LSAW and longitudinal velocity distributions for C-7972 specimens.

IUS2-PC1-2

Ultrasonic triaxial anvil setup for measuring longitudinal and shear wave velocities of rocks under controlled pressure

Ronnie Karlqvist[1], Ilkka Lassila[1], Edward Hæggström[1], Lauri Pesonen[2]; [1]*Deparment of Physics, Division of Materials Physics, University of Helsinki, Helsinki, Finland,* [2]*Deparment of Physics, Division of Geophysics and Astronomy, University of Helsinki, Helsinki, Finland*

Background, Motivation and Objective

Reliable interpretation of seismic surveys and loggings requires that the seismic velocities and anisotropies of the bedrock are taken into account. Velocity anisotropy in rocks can reach 30%, which at 1 km depth could lead to a 300 m error in estimated reflector location if one assumes isotropic velocity. Improved accuracy in determining reflector locations reduces the drilling effort in ore exploration.

Statement of Contribution/Methods

Our custom-built ultrasonic triaxial anvil setup permits measuring longitudinal (1 MHz center frequency) and shear wave (1.1 MHz center frequency including 0° and 90° polarizations) sound velocities in cubic rock samples (25 mm) under crustal-pressures (up to 300 MPa) in three directions (X, Y, and Z) simultaneously. We present the velocities and the anisotropies of eleven Precambrian rock samples from the FIRE-reflection profile in Central Finland using this novel setup.

Results/Discussion

Previous results from uniaxial time-of-flight measurements done at low pressure are compared with the results obtained with our triaxial anvil setup at high pressure. Measuring under different loads allow us to investigate how pore closure affects sound wave velocities. Comparing the triaxial anisotropy data with the uniaxial data from the same samples also reveals how the increased load affects the anisotropy.

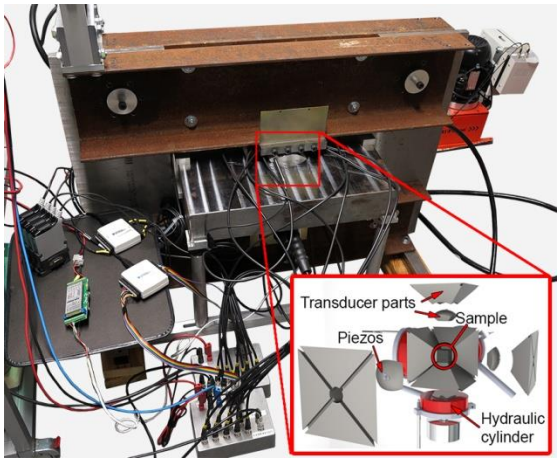

IUS2-PC1-3

Gelation process and silicone hardening kinetics using dynamic acousto-elastic testing method

Chloé Trarieux[1], Marielle Defontaine[1], Hélène Moreschi[1], Jean-François Tranchant[2], **Samuel Callé[1]**; *[1]UMRS Imagerie et cerveau - INSERM U930, Université François Rabelais, Tours, France, [2]Département Innovation Matériaux et Technologies, LVMH Recherche, Saint Jean de Braye, France*

Background, Motivation and Objective

Monitoring the physical properties of materials during processing is a real challenge in many industrial sectors such as food-processing, cosmetics or concrete. In this way, ultrasonic techniques provide an interesting option (cost-effective, contact-free and non-destructive), well-adapted to on-line measurements. The Dynamic Acousto-Elastic Testing (DAET) technique, particularly adapted to study complex media (granular, multiphasic media), has been developed to characterize nonlinear (NL) viscoelastic properties of fluids and solids. This work aims to study the feasibility of monitoring phase-change processes using DAET.

Statement of Contribution/Methods

The DAET method consists in coupling two acoustical waves: a sinusoidal low-frequency (LF, a few kHz) acoustic wave successively compresses and expands the medium which is probed by ultrasound (US, 1 MHz) pulses. A PMMA box, immersed in water and placed in the interaction area, is filled with the tested medium. The US pulses time-of-flight modulations (TOFM) and relative amplitude modulations (RAM) induced by the LF external stress are related to the nonlinear viscoelastic properties of the medium. TOFM and RAM curves are plotted as a function of instantaneous LF pressure amplitude. From these rheograms, nonlinear elastic and viscous (dissipative) parameters are extracted, and particularly the nonlinear elastic parameter B/A, proportional to the slope of the TOFM *vs* LF pressure curve. In addition to NL parameters, non-stressed time-of-flight and attenuation parameters were also monitored, related to the linear elastic and viscous moduli.Two different kinetics have been studied: a gelation process (gelatin from porcine skin, type A) and a silicone hardening (silicone elastomer, Silastic).

Results/Discussion

As presented on Figure 1, measurements on silicone present a decrease (from 14.1 to 13.8) and a stabilization of the NL parameter B/A as a function of time, depending on the hardening degree of the silicone. The linear and NL measurements on silicone have exhibited a good reproducibility, contrary to results on gelatin which have shown a weak reproducibility of the NL parameter. This is principally due to the high noise level (B/A of the gelatin close to B/A in water) and the influence of temperature, which has no effect on the silicone hardening kinetics (ambient temperature).

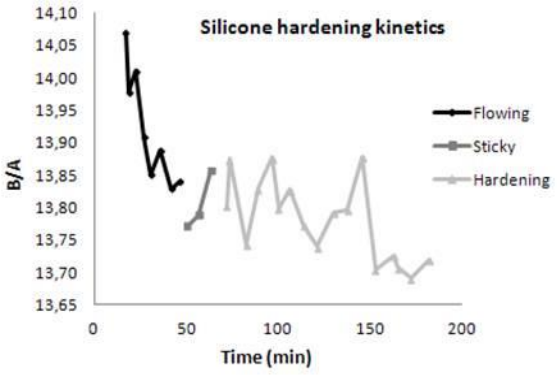

IUS2-PC1-4

Characterization of micro and nanolayers using frequency domain laser-ultrasound

Clemens Grünsteidl[1], Istvan Veres[1], Thomas Berer[1], Jürgen Roither[1], Todd Murray[2], Peter Burgholzer[1]; [1]*Research Center for Non Destructive Testing GmbH, Linz, OÖ, Austria,* [2]*University of Colorado at Boulder, Boulder, CO, USA*

Background, Motivation and Objective

Thin films can protect from corrosion and high temperatures or provide a functional surface. This made them essential components in displays, magnet disks or solar panels, for example. Non-destructive testing (NDT) of these layers can guarantee their performance and optimize their production. Since their properties might differ significantly from the properties of bulk materials, the description of this variation is of great practical interest. Recent developments address this task with frequency domain laser-ultrasound. This non-contact method provides high signal-to-noise ratios at low optical powers, which is crucial for NDT of sensitive layers. Our frequency domain laser-ultrasound setup can excite and detect surface acoustic waves (SAWs) up to 1GHz which allows us to investigate metallic layers down to the 100nm range.

Statement of Contribution/Methods

SAWs up to 1 GHz are generated thermo-elastically by the output of an erbium doped fiber amplifier which is fed by an intensity modulated laser diode. The generated SAWs are detected using a path stabilized Michelson interferometer coupled into a high frequency lock-in amplifier (LIA). A gimbal mirror spatially scans the propagating waves and the dispersion relation of the sample is calculated from the detected variation of the phase. To overcome the 200MHz bandwidth limit of the LIA we use an additional signal generator and standard high frequency components to fold the electric signal down to a detectable frequency. Using this "super heterodyne" principle we detected SAWs up to 1GHz and determined the dispersion relations of SiO_2 and Si samples coated with Mo. We also developed a numerical solution for the dispersion relations of coated substrates. For evaluation, we fitted this model to the measured data which yielded in thickness and Young's modulus of the coatings.

Results/Discussion

We investigated Mo layers with thicknesses between 200nm and 3µm on Si or SiO_2 substrate. The figure shows measured SAW velocities and the fitted theoretical dispersion curve for a Mo layer on SiO_2. Theory and experiment show good agreement over the measured frequency range (50-650 MHz) and result in a thickness of 531nm. The experimentally found values for Young's moduli of different layer thicknesses allow us to discuss a correlation of elastic properties and thickness of the layers.

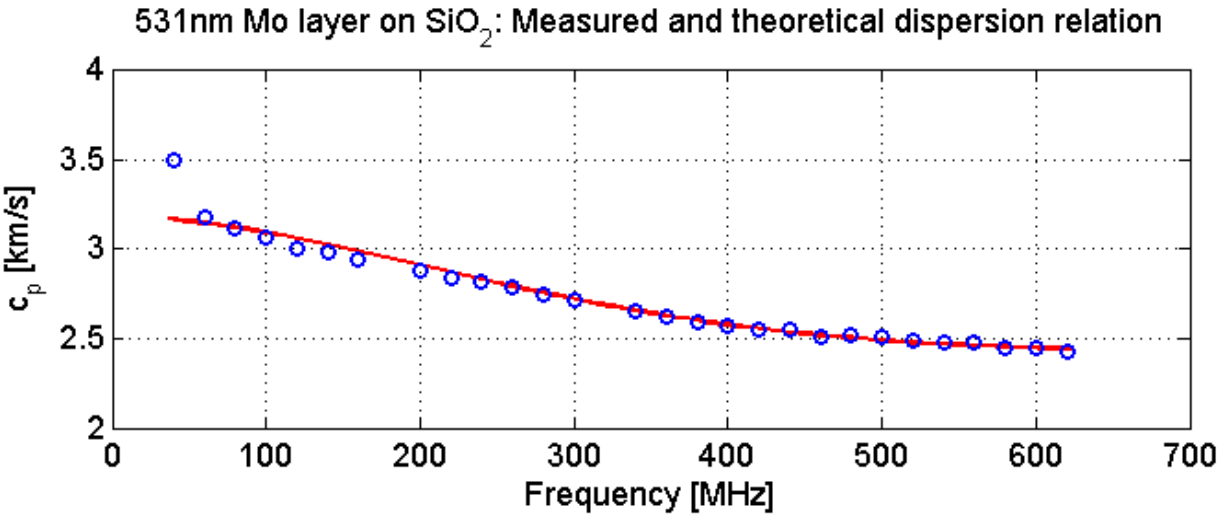

IUS2-PC1-5

Measurement of Local Wood Velocities by Acoustic Microscopy

Dawei Wu[1], Paul Harris[1]; [1]*CallaghanInnovation, Lower Hutt, Wellington, New Zealand*

Background, Motivation and Objective

In recent years genetic and silvicultural advances, and the economic pressure for an early harvesting age has had a profound impact on wood quality- lower overall modulus of elasticity (MOE) and with higher percentages of juvenile wood (wood having undesirable traits including a low MOE, a high propensity to warp, and a low tensile strength). Xray diffraction shows that a high microfibral angle of the cell S2 layer results in low wood MOE and hence acoustic velocities. At low ultrasonic frequencies techniques have been developed e.g. WoodSpec, to study average wood properties for sample dimensions of several cm's. In this work we explore the use of an acoustic microscope to image the cells themselves with an aim to ultimately obtain the local anisotropic elastic properties for areas of dimensions of less than 100µm, and to determine the distribution of these properties within the annular rings and tree height.

Statement of Contribution/Methods

A single-element transducer with a 400MHz center frequency and a sapphire point focus lens was mounted on a precision (1µm resolution) linear xyz stage. A home-made high frequency imaging system was used to drive the transducer and to acquire positioning data and ultrasonic signals. A carefully prepared and polished Cedar sample was immersed in a water bath and vacuumed to ensure there was no air trapped within the wood cells. Following initial z focussing adjustment xy scanning of the wood sample was undertaken.

Initial V(z) measurements using a 400MHz tone burst was used with a 1µm step in the z direction at the desired locations (determined from the acquired image) within the annular ring. In normal practise the inverse Fourier transform of the magnitude of the V(z) curve is used to give the longitudinal (v_l) and transverse (v_t) velocities, with the Rayleigh (v_R) velocity determined directly from successive peaks of the V(z) curve. WoodSpec was used to determine the average longitudinal and transverse velocities for the Cedar wood from which the micrscope sample was taken.

Results/Discussion

The high resolution ultrasonic image shows that for our Cedar sample the size of the cell is typically 30µm and the thickness of the cell wall typically 7µm. The results are in good agreement with those obtained by optical microscopy. Scanning the annular rings shows that the cells vary in dimensions across the earlywood/latewood regions. It is known that the average velocities vary greatly from pith to cambium which provides a convenient wide spread in data for wood with the same genetic, silvicultural and growing conditions to allow a relationship between WoodSpec and the microscope measurements to be developed.

IUS2-PC1-6

Non-contact ultrasonic inspection of CFRP prepregs for aeronautical applications during lay-up fabrication.

Maria Dolores Fariñas[1], Esmeralda Cuevas[2], Monica Garcia Merino[3], Tomas Gomez Alvarez-Arenas[1]; *[1]Spanish National Scientific Research Council (CSIC), Madrid, Madrid, Spain, [2]TECNATOM, San Sebastian de los Reyes, Madrid, Spain, [3]TECNATOM, Sansebastian de los Reyes, Madrid, Spain*

Background, Motivation and Objective

Use of composite materials in the aeronautical industry is in continuous advance due to the increasing demand of novel materials able to meet economic, security and design goals that are also becoming more demanding. In a similar way, challenges faced by the inspection techniques are growing at the same pace. For thermosetting polymers, inspection before curing is being considered as an alternative as it offers the possibility to repair or discard unsound material with a potential cost reduction.

Statement of Contribution/Methods

Material inspection during prepreg lay-up fabrication is extremely challenging. First, fabrication requirements determine that the material cannot be touched. Second, the attenuation of ultrasound waves in the uncured material is expected to be extremely high and to increase very fast with the frequency. Third, the ultrasonic properties of the material are expected to be strongly affected by the presence of lacks of compaction that may appear during the fabrication. However, most of them are not real defects as they are completely removed during curing. Fourth, the material has to be inspected along with the mold or lay-up surface where it is fabricated.

First, a detailed study of the properties of the uncured prepregs was performed. Then, these properties were used to model the ultrasonic propagation through the aluminum mold+lay-up laminate to determine the optimum inspection configuration. Consequently, a technique based on the use of low-frequency (0.25 MHz), high-sensitive (-23 dB) and wideband (70%) air-coupled transducers operated on through transmission mode by a commercial NDT pulser/receiver is proposed as a solution able to test this material and to comply with fabrication restrictions. Several samples (300 x 300 mm and up to 30 layers) were fabricated following different compaction schemes. Some of them included Teflon insertions to simulate the presence of defects. Inspections were carried out with the proposed technique during the fabrication to test the influence of both the number of layers and the compaction processes the material is subjected to.

Results/Discussion

The initial study of prepregs revealed ultrasound velocity and attenuation values at 0.5 MHz about 900-1200 m/s and 450-600 Np/m, respectively (while for the cured material we obtained 2800 m/s and 15 Np/m at 0.7 MHz, respectively). Material inspection during lay-up fabrication revealed that depending on the compaction of the laminate the ultrasonic attenuation varies from 0.3 dB/layer up to 10 dB/layer at 0.25 MHz. This determines the maximum thickness of the laminate that can be inspected, that for well compacted laminates can reach up to 90 layers. C-scans clearly revealed the presence of Teflon insertions by an increase of the transmission loss by 8 dB. In conclusion, it is shown that the proposed technique and configuration is able to efficiently test prepreg lay-up laminates directly on the aluminum mold where they are fabricated.

IUS2-PC1-7

The Acoustic Method of the Noncontact Determination of Thin Films Conductivity

Iren Kuznetsova[1], Boris Zaitsev[2], Vladimir Anisimkin[1], Andrey Teplykh[2], Alexander Shikhabudinov[2], Vladimir Kolesov[1], Valery Yakunin[3]; *[1]Kotel'nikov Institute of RadioElectronics and Engineering of RAS, Moscow, Russian Federation, [2]Saratov branch, Kotel'nikov Institute of RadioElectronics and Engineering of RAS, Saratov, Russian Federation, [3]Physics Department, Moscow State University, Moscow, Russian Federation*

Background, Motivation and Objective

At present the works concerning with synthesis of novel materials possessing by given characteristics as well as by possibility of their change under external actions are actively carried out. Sometimes the traditional methods of their investigation are not suitable because the new materials may have the active surface and interact with measuring instrument. Such interaction leads to the change of the properties of the material under study and distorts the measurement results. In this connection this work is devoted to the development of the noncontact acoustic method of the determination of the surface conductivity of diamond-like materials.

Statement of Contribution/Methods

The noncontact determination of the conductivity and permittivity was performed by using the structure containing the piezoelectric plate and the investigated sample separated from the plate by air gap. The piezofield of the propagating acoustic wave penetrated through the gap in the material under study and leaded to the change of the wave velocity and attenuation. The degree of these changes allowed to determine the necessary information about the electrical properties of studied materials. We investigated the samples of diamond-like films deposited on the plates of lithium niobate of Y-cut and silicon. The sample was placed in the space between interdigital transducers. The necessary value of gap was provided by the special strips of aluminum foil with the given thickness. We used the shear-horizontal acoustic wave of zero order (SH0) which propagated in structure "Y-X lithium niobate plate – air gap – sample". The phase shift and change in insertion loss of the output signal were measured by meter of S-parameters for different values of the gap between the plate and sample. The obtained experimental data allowed to determine the change in velocity and attenuation of SH0 wave as function of the value of gap. Then the theoretical analysis of the characteristics of SH0 wave in the structure "Y-X lithium niobate plate – air gap – sample with a layer of arbitrary conductance" was carried out. The comparison of the theoretical and experimental data allowed to determine the surface conductivity of the diamond-like films under study.

Results/Discussion

As a result of the performed experiments the values of the changes in velocity and attenuation of SH0 wave as functions of the gap for the investigated diamond-like films grown on the samples of lithium niobate and silicon at the different technological conditions were obtained. Theoretical analysis allowed to build up the families of the dependencies of changes in the velocity and attenuation of SH0 wave in the structures under study as functions of the gap value. Here the value of the surface conductivity used as parameter. These dependencies allowed to find the surface conductivity of the investigated diamond-like films grown at the different technological conditions.

The work is supported by the Russian Foundation of Basic Researches.

IUS2-PC1-8

Comparison of slowness curves of Lamb wave with elastic moduli and crystal structure in silicon wafers

Gyeongwon Yun[1], Kyung-Min Kim[1], Yuji Roh[1], Youngjae Min[1], Jeong-Ki Lee[2], Young H. Kim[1]; *[1]Physics and Earth Science, Korea Science Academy of KAIST, Busan, Korea, Republic of, [2]RIC for Safety Diagnosis in Heavy Chemical Facilities, Chonnam National University, Yeosu, Korea, Republic of*

Background, Motivation and Objective

Lamb wave propagation in anisotropic plates is complex due to the geometric feature and material properties. Various modes of Lamb wave can propagate along the plates with different phase velocities. In anisotropic plate, these are dependent on the propagation direction, and can be used as a tool for identification of crystal structure.

Statement of Contribution/Methods

In this experiment, [100], [110] and [111] single crystal silicon wafers of thickness of 525±25 μm were used as anisotropic plates. Ultrasonic wave of 10 MHz was obliquely incident on the wafers in order to generate Lamb wave in the plate. Leaky Lamb wave reflected from the edge of wafer was detected by same transducer using pulse-echo setup. Incident angle was changed, and phase velocities of Lamb wave were determined by Snell's law. Phase velocities as a function of propagation direction were determined by rotating specimen.

Results/Discussion

The results were shown in polar coordinate: θ, *r* and brightness are representing propagation direction, slowness (inverse of phase velocity) and amplitude of leaky LW, respectively. Obtained slowness curves from [100], [110] and [111] silicon wafers were shown in figure and compared with calculated elastic moduli. Slowness values obtained by computer simulation were also marked on the experimental results. It was found that the slowness curves of LW showed good agreements with elastic constants and crystal structure of anisotropic silicon plates. In addition, It was also found that LW measurement was more sensitive to the [111] crystal structure. As conclusion, slowness curves of LW can be an identification tool for crystal structure.

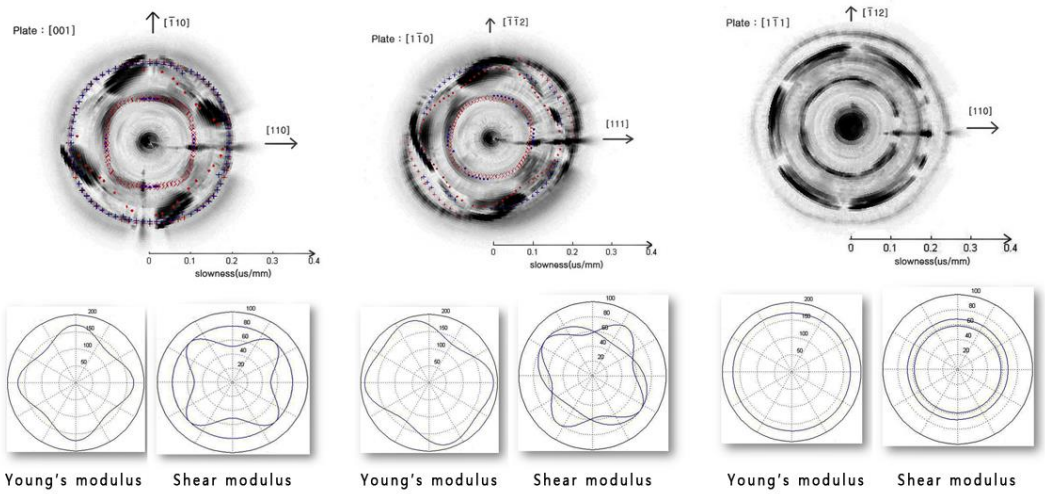

Ultrasonics in Liquids and Air

Forum Hall

Wednesday, July 24 2013, 01:00 pm - 04:30 pm

Congress Hallair: **William Wright**
University College Cork

IUS2-PC2-1

Flexural Mode Metal Cap Transducer Design for Specific Frequency Air Coupled Ultrasound Generation

Tobias Eriksson[1], Steve Dixon[1], Nishal Ramadas[1]; [1]*Physics Department, University of Warwick, United Kingdom*

Background, Motivation and Objective

The problem of generating ultrasound in fluid media due to the large impedance mismatch has been treated in the literature, but remains a topic of interest as new and more application specific solutions are proposed and tested. Flexural mode vibrations of piezoelectrically actuated metal caps have been used routinely to make low frequency (typically 40 kHz) air coupled transducers for simple distance measurements. Such transducer types have many distinct advantages, including an integrated metal buffer, good fluid coupling for both generation and detection of ultrasonic waves, and large amplitude signals for a small driving voltage, which are highly relevant to many application areas. In this work, we investigate the design of arbitrary and specifically higher frequency (> 100 kHz) flexural metal cap probes.

Statement of Contribution/Methods

The analytical model of vibrating circular plates was used to get an overview of the resonant modes and how they depend on the plate geometry and material. A more realistic system was investigated by finite element modelling (FEM). FEM was used to optimise the complete transducer design, including both the piezoelectric element and metal cap. Finally, a prototype transducer was built, consisting of an aluminium cap with an 11 mm diameter radiating face, and a piezoceramic disk with a 3.2 mm radius and a 0.5 mm thickness. The surface displacement of the radiating front face of the prototype was measured with a laser vibrometer, and the mode shapes were thus determined. A variety of other tests including pulse-echo experiments, radiated ultrasonic beam profile measurements using a microphone detector, and electrical impedance measurements were undertaken on the prototype device, and its performance compared to a commercially available low frequency flexure type transducer.

Results/Discussion

The prototype transducer has a dominant, 2nd harmonic, axisymmetric mode at 140 kHz, with a central peak-to-peak displacement amplitude of 50 nm for a 1.0 V continuous driving voltage. The results from the prototype transducer are in good qualitative agreement with both the FEM model and the analytical theory of vibrating plates. The modal frequencies of the prototype transducer are shifted by approximately 20% from those predicted by FEM, which could be explained by imperfect manufacturing. In general, the results to date show that it is possible to produce effective, high frequency, flexural transducer designs for air coupled ultrasonic application.

IUS2-PC2-2

Multi-Channel Indoor Wireless Data Communication Using High-k Capacitive Ultrasonic Transducers in Air

Wentao Jiang[1], William Wright[1]; [1]*Electrical and Electronic Engineering, University College Cork, Cork, Co. Cork, Ireland*

Background, Motivation and Objective

Using modulated ultrasound in air is an alternative method for short-range wireless communication instead of the radio frequency (RF) band. Ultrasound has several advantages over RF in that it produces no interference with other electronic devices and is inherently secure in an indoor environment as the transmissions are difficult to intercept from outside the room, thus increasing indoor wireless network security and preventing long range eavesdropping techniques such as Bluesniping. Previous work using ultrasound has used various modulation schemes to produce data rates of up to 200 kbps over distances of a few meters. The main limitations of the ultrasonic techniques are due to a lack, until recently, of ultrasonic transducers that can operate efficiently in air with sufficient sensitivity and bandwidth, which has limited the channel capacity of the system.

Statement of Contribution/Methods

A pair of broad-band air-coupled capacitive ultrasonic transducers, with metallized PET membranes and pitted silicon backplates coated with high-k HfO_2 dielectric layer for enhanced performance, was used in a prototype wireless ultrasonic data communication system to transmit modulated signals through multiple parallel channels. The channel responses were tested to determine the available transmission bandwidth. Amplitude Shift Keying (ASK) and other modulation schemes were then implemented successfully using the multiple channels. The capacitive ultrasonic transducers had a usable bandwidth of up to 1 MHz, allowing many parallel data streams to be sent simultaneously over short distances. Unlike previous work, the system was completely wireless, with synchronization achieved by ultrasonic means instead of a hardwired link.

Results/Discussion

Data rates of over 400 kbps were achieved, which is more than twice that previously reported in the literature. Transmission over distances of several meters was also possible. In addition, true wireless operation was demonstrated using various ultrasonic wireless handshaking methods, and their effectiveness was compared. System performance metrics including Signal-to-Noise Ratio (SNR) and Bit Error Rate (BER) were analysed and compared across the parallel channels, and for the different modulation schemes.

IUS2-PC2-3

Low Frequency Wave Propagation in Cylindrical Elasto-Viscoelastic Trilayer in the Presence of Free Gas

Semyon Levitsky[1], Rudolf Bergman[1]; [1]*Mathematics, Shamoon College of Engineering, Beer-Sheva, Negev, Israel*

Background, Motivation and Objective

Propagation of waves in multilayered systems was the subject of a great number of studies during recent years. Among others, acoustic properties of trilayers have attracted considerable attention because important applications in industry, chemical technology, petroleum production. Despite the major of studies were focused on the wave dynamics of solid structures, the solid-liquid-solid trilayers with ideal or pure viscous (Newtonian) liquid inside the waveguide have been considered as well. Wave propagation in such system in the case of polymeric liquid can be essentially influenced by the liquid rheology, which differs from a pure viscous behaviour, and by free gas traces characteristic for high-

molecular liquids. The objective of the study is to describe the combined effect of liquid rheology and gas microbubbles on sound dispersion and attenuation in a cylindrical trilayer in the low frequency range.

Statement of Contribution/Methods

The studied trilayer consists from two coaxial thin elastic cylindrical shells. The gap between the shells is filled with viscoelastic liquid, containing gas microbubbles. It is supposed that volume concentration of free gas is small, the microbubbles are size distributed, and the losses in the wave stem from both liquid-shell and liquid-bubble dynamic interaction. Rheology of polymeric liquid is described by generalized Maxwell model with Newtonian viscous term, responsible for low-molecular solvent contribution in the stress tensor. Dynamic equations for thin elastic shells are formulated within Kirchhoff-Love approximation; hydrodynamics of liquid flow in the gap in the wave is described using quasi-one-dimensional approach.

Results/Discussion

Solution of the formulated dynamic equations is searched in the form of an axially symmetric wave and leads to dispersion equation, accounting for structure coupling, fluid rheology and free gas presence in liquid. It was solved numerically for different combinations of the system parameters with a special emphasis on the liquid rheology and free gas effect. The results indicate that manifestation of liquid's rheology yields sound speed growth and attenuation reduction, as compared with a similar pure viscous liquid, and can change the dispersion sign in a small frequency interval. Free gas has an opposite effect on the wave parameters and leads to decrease of the sound speed and attenuation growth. Size distribution of bubbles in the studied frequency range has only minor effect on the wave propagation, so the basic characteristic parameter of the mixture in this range is the gas volume fraction. All data are highly influenced by the shells and gap widths - the wave speed is less and the attenuation is larger for more flexible waveguide walls. Results of the study indicate that the waveguide provides an attractive configuration for acoustic measurements and can find application, for instance, at free gas diagnostics in polymer technology.

IUS2-PC2-4

Theoretical Analysis and Experimental Validation of the Scholte Wave Propagation in Immersed Plates for the Characterization of Viscous Fluids

Aline Emy Takiy[1], Luis Elvira[2], Silvio César Garcia Granja[1], Ricardo Tokio Higuti[1], Claudio Kitano[1], Óscar Martínez-Graullera[2], Francisco Montero de Espinosa[2]; *[1]Universidade Estadual Paulista - Unesp, Brazil, [2]Centro de Acústica Aplicada y Evaluación No Destructiva, Spain*

Background, Motivation and Objective

The study of interfacial waves has attracted interest in the scientific community by their propagation features and potential applications in non-destructive evaluation (NDE) and characterization of liquids. At the interface between a solid and a fluid, mechanical waves called Stoneley-Scholte waves or simply Scholte waves, can propagate. For the especial case of a solid material having a plate-like geometry, the wave obtained from the elastic equations is called quasi-Scholte mode in the literature. For all these interfacial propagations modes, the wave energy in the fluid is confined in the region near to the surface of the plate. The wave attenuation is mainly due to viscous shear effects in the fluid near the solid phase instead of leakage energy away from the plate by elastic transmission. The analysis of this propagating mode is an attractive alternative to determine the bulk longitudinal velocity and attenuation in the liquid, which provide valuable information about the liquid properties. This feature can be explored in the fluid characterization, due to the high sensitivity associated with the interaction between the wave and the fluid.

Statement of Contribution/Methods

In this work, phase and group velocity dispersion and attenuation curves, as a function of frequency, of guided waves propagating in a solid plate immersed in a viscous fluid, are theoretically obtained. The viscous fluid was modeled using the Navier-Stokes equation and the global matrix method was used to model the multilayered media consisting of liquid-plate-liquid. From this model both Lamb waves and quasi-Scholte modes are obtained as equation solutions. Experiments were carried out by using a thin stainless steel plate partially immersed in a liquid inside a container and perpendicular to the liquid surface. A transducer operating in pulse-echo is coupled to the end at the centre of the upper edge of the plate, giving rise to multimodal propagation in the plate. The contact angle between the transducer and the plate is chosen to minimize indesired propagating modes (symmetric modes). The container fluid level is slowly varied by adding or removing liquid.

Results/Discussion

From the acquired waveforms, the modes attenuation and velocity curves is obtained as a function of frequency, and there was very good agreement with the theoretical results. Investigations about the plate size and liquid sample volume needed for an accurate liquid analysis is carried out.

IUS2-PC2-5

Thermal Studies of a Plate Waveguide Bundle for use in Ultrasonic Flow Metering Applications

Michael Laws[1], Sivaram Nishal Ramadas[1], Steve Dixon[1]; *[1]Department of Physics, University of Warwick, United Kingdom*

Background, Motivation and Objective

Ultrasonic flow meters are becoming increasingly common as they offer many benefits, such as limited disruption to the flow, zero pressure drop and wide turn down ratio. However a major disadvantage of this type of device is an inability of the piezoelectric element to function at elevated temperatures. A thermal buffer is often used in high temperature applications to protect the active piezoelectric element. In our earlier publication, we presented an ultrasonic flow measurement transducer assembly, which incorporates a buffer consisting of a bundle of thin stainless steel plate waveguides. This allows a larger energy transfer than a single plate, whilst limiting the dispersion of a controlled input pulse, as the ultrasonic waves will propagate in Lamb-like modes within the thin plates. It is this low dispersion property that is important in the practical application of a thermal buffer in general, and specifically if we are to obtain ultrasonic signals which can be used to accurately measure a fluid flow.

Statement of Contribution/Methods

In order to effectively use a waveguide buffer device in an ultrasonic flow meter, we need to know the temporal profile of the ultrasonic wave and its dispersion characteristics along the waveguide. Thermal experiments (using a heat gun and a hot oil bath) were carried out in order to set up a temperature gradient, from temperatures up to ~600 K to ambient temperature, along the length of the plate waveguide allowing the effect of temperature on wave dispersion to be monitored. The ultrasonic pulse shape was monitored using a laser vibrometer sensitive to the out-of plane displacement of the end of the waveguide. A thermal camera has also been used simultaneously, to bserve the temperature profile in the waveguide bundle prototype. The heat dissipation characteristics have also been modelled using finite element software, and various plate designs have been considered to allow the bundle to more effectively dissipate heat. Additionally, the effect of these modified plate geometries on the propagation and dispersion properties of an ultrasonic pulse was also studied.

Results/Discussion

The waveguide design has been shown to act as an effective thermal buffer, and it is able to function at elevated temperatures (up to around 600 K), while reducing the temperature at the transmitting end to approximately ambient. This type of device could allow a wider use of standard ultrasonic flow meter transducers in harsh environments. We have also begun to optimise the design of the individual plates to achieve high transmission, low dispersion and good heat dissipation.

Simulation and Evaluation of Fan-Shaped Beam Ultrasound Transducers for Multiphase Flow Process Tomography

Sascha Langener[1], Thomas Musch[1], Helmut Ermert[1], Michael Vogt[1]; [1]*Dept. of Electrical Engineering and Information Technology, Ruhr-University Bochum, Bochum, Germany*

Background, Motivation and Objective

The measurement of volume fractions of different components in multiphase flow is of great interest in many industrial applications such as oil production. Ultrasound based methods, including ultrasound tomography, have a great potential for the differentiation of liquid and gaseous phases. A well-established method is the fan-shaped backprojection tomography. In this approach, multiple ultrasound transducers are arranged along the circumference of the measurement pipe for measurements inside a thin cross-sectional image plane. The transducers are designed for a narrow radiation beam along the azimuth direction and for a diverging fan-shape beam in the lateral direction. Rectangular transducers with a large aperture size in azimuth and a small aperture size in circumferential direction are a possible approach, but suffer from a poor efficiency. Alternatively, large rectangular piezoelements equipped with a cylindrical acoustic lens can be utilized, but transducers of these kinds disadvantageously extend into the pipe.

Statement of Contribution/Methods

In this contribution, a different design of ultrasound transducers for fan-shaped tomography, which are based on a piezoceramic element in the shape of a hollow cylinder segment, is presented. The transducer is attached to the outer face of the measurement pipe, and ultrasound waves are focused onto its inner wall, what gives the desired fan-shape beam pattern in the flowing medium. The length of the hollow cylinder, i.e. the aperture length in azimuth direction, is chosen such that the Fresnel length is larger than the diameter of the pipe in order to minimize the diffraction loss for ultrasound transmission to transducers at the opposite side of the pipe.

A geometrical straight line analysis, considering reflection and refraction, has been performed to evaluate the transducer design. Different transducer configurations have been analyzed in detail by means of Finite Element Method (FEM) simulations. The proposed transducer concept has also been implemented in a setup working at 1 MHz center frequency, for measurements in an acrylic glass pipe (4 mm wall thickness, 110 mm inner diameter). For the assessment of the 3D beam pattern inside the pipe and of the system's point spread function (PSF), echoes from spherical phantoms as single point-like scattering objects at varying positions in the image plane have been acquired and analyzed in the time- and frequency-domain.

Results/Discussion

The implemented transducer design was aimed at a (-6 dB) beam spread angle of 60°, what has been confirmed by simulations, giving a beam width of 58°. The angle is in a good agreement with measurement results.

Experimental physical acoustics

Forum Hall

Wednesday, July 24 2013, 01:00 pm - 04:30 pm

Congress Hallair: **Victor Krylov**
Loughborough University

IUS3-PC-1

Orientation control of ZnO films by highly-energetic positive ion irradiation using RF substrate bias sputtering

Shinji Takayanagi[1], Takahiko Yanagitani[2], Mami Matsukawa[1]; [1]*Graduate School of Science and Engineering, Doshisha University, Kyotanabe, Kyoto, Japan,* [2]*Graduate School of Engineering, Nagoya Institute of Technology, Nagoya, Aichi, Japan*

Background, Motivation and Objective

c-Axis normal (0001) oriented ZnO films are used for piezoelectric devices such as Rayleigh SAW filters. [1] On the other hand, c-axis parallel (11-20) or (10-10) oriented ZnO films are suitable for use as shear mode and sezawa mode SAW devices. [1] In polycrystalline film growth, the close-packed (0001) plane of ZnO tends to orient parallel to the substrate plane because of its thermodynamic stability. In contrast, we have demonstrated that the c-axis parallel orientation was induced by highly-energetic O^- ion bombardments to the substrate during the film deposition. [2] We proposed RF substrate bias method to enhance ion irradiation in last year. In this study, quantitative information of relationship between the RF bias power, amount of ion flux, ion energy and crystalline orientation of ZnO was investigated.

Statement of Contribution/Methods

We measured the amount of ion flux and ion energy which enter the substrate by using an energy analyzer with a Q-mass spectrometer. 2 MHz RF power was applied to the substrate holder during RF sputtering deposition to enhance the positive ion bombardment. Ar/O_2 gas ratio was set to 1/3. ZnO films were grown on silica glass substrates by using an RF bias sputtering method. The orientations were determined by XRD.

Results/Discussion

Fig. 1(a) shows the energy distributions of O_2^+ positive ions which enter the substrate during the deposition with RF bias. Both the amount of ion flux and ion energy drastically increased as RF bias power increased. O^- negative ions were also investigated, but such drastic changes were not observed. Fig. 1(b) shows the XRD patterns. (0002) peak was observed without RF bias. In contrast, usual (0001) orientation changed into the (11-20) preferred orientation with RF bias power of 10 W, where the peak value of O_2^+ energy was 180 eV. Then, the (10-10) preferred orientation appeared with RF bias power of 20 W at O_2^+ energy of 250 eV. These changes of the preferred orientation from (0001) to (10-10) correspond with the descending order of the surface atomic density. This means that the densely-packed plane is easily damaged with the ion irradiation. Highly-energetic ion irradiation by RF bias sputtering is useful for orientation control of polycrystalline films.

[1] S. Takayanagi, et al., *IEEE IUS2013*, Submitted.

[2] S. Takayanagi, et al., *Appl. Phys. Lett.*, **101**, 232902 (2012).

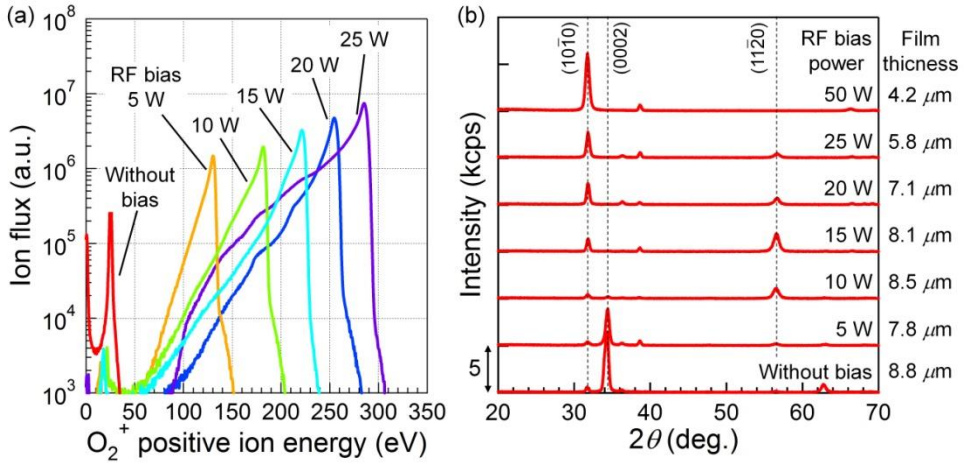

Fig. 1 (a)Energy distributions of O_2^+ positive ions which enter the substrate during the deposition with 2 MHz RF bias, and (b) XRD patterns of the ZnO film samples.

IUS3-PC-2

Piezoelectric crystal $La_3Ta_{0.5}Ga_{5.3}Al_{0.2}O_{14}$: growth, crystal structure perfection, piezoelectric and acoustic properties

Dmitrii Roshchupkin[1], Dmitrii Irzhak[1], Olga Ploticyna[1], Evgeny Emelin[1], Sergey Sakharov[2], Oleg Buzanov[2]; [1]*Institute of Microelectronics Technology and High-Purity Materials Russian Academy of Sciences, Russian Federation,* [2]*FOMOS Materials, Russian Federation*

Background, Motivation and Objective

$La_3Ta_{0.5}Ga_{5.3}Al_{0.2}O_{14}$ (LGTA) crystal is a new advanced piezoelectric crystal for high-temperature acoustoelectronic applications. LGTA is a non-ordering crystal of langasite family with point group symmetry 32 the same as piezoquartz. LGTA crystal has the high electric resistance at high temperature, which is important for high-temperature BAW and SAW applications.

Statement of Contribution/Methods

3-inch LGTA crystal was grown along the {11.0} axis using Czochralski technique. The parameters of the crystal unit cell were measured by XRD: $a=b$=8.2908 Å, c=5.1440 Å. The crystal structure perfection was studied using X-ray topography. Only growth banding was revealed in the crystal.

The piezoelectric constants d_{11}=6.45455×10^{-12} C•N^{-1} and d_{14}=–5.11735×10^{-12} C•N^{-1} were measured using high-resolution X-ray Laue-diffraction in the conditions of the opposite piezoelectric effect. In this case the applying of an external electric field to the crystal leads to the change of interplanar spacing, and as a result leads to the change of the angular position of the Bragg peak.

For investigation of bulk and surface acoustic waves properties of LGTA crystal the scanning electron microscopy (SEM) and X-ray diffraction methods were used. SEM was used for visualization of BAW and SAW propagation in LGTA, for measurements of power flow angles. Figure shows the SEM microphotograph of the BAW-resonator based on *Y*-cut of LGTA crystal. The BAW-resonator was excited at resonance excitation frequency f=5.16 MHz. X-ray diffraction was used to measure the velocity of SAW propagation in different cuts of LGTA crystal. SAW propagation in the crystal leads to sinusoidal modulation of a crystal lattice and as a result causes the diffraction satellites on the both sides of the Bragg peak. The intensities and angular divergence between diffraction satellites on the rocking curve are determined by the SAW amplitude and wavelength.

Results/Discussion

The complex investigations of an advanced piezoelectric LGTA crystal were carried out using the scanning electron microscopy and different X-ray diffraction techniques.

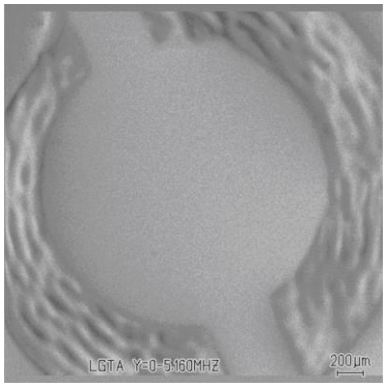

IUS3-PC-3

Amplitudes of transverse waves in the acoustical birefringence in [110] Silicon single crystal

Hye-Jeong Kim[1], Seho Kwon[1,2], Young H. Kim[1]; *[1]Physics and Earth Science, Korea Science Academy of KAIST, Busan, Korea, Republic of, [2]Seoul National University, Seoul, Korea, Republic of*

Background, Motivation and Objective

Wave velocities are dependent on the propagation direction in an anisotropic solid, and transverse waves can propagate with different wave velocities for certain propagation direction. The particle displacements are determined by propagating transverse wave mode. In the present work, the waves velocities and amplitudes of transverse waves were investigated when transverse wave with arbitrary direction of particle displacement propagate in anisotropic solids.

Statement of Contribution/Methods

Acoustic birefringence of bulk transverse wave propagating through [110] silicon single crystal is studied. There are two transverse wave modes when the wave is applied along [110] direction in single crystal. Transverse wave is generated by using 20 MHz frequency transducer whose delay line is 7 μs. For delicate control of vibration axis position, the [110] silicon single crystal is attached to rotary table with angle indicator. By pulse/echo method, the same transducer detects elastic transverse wave which is reflected and turns back from the opposite boundary of the sample. Waveforms are obtained by rotating initial vibration axis from [001] axis to opposite arrangement (180° from initial axis).

Results/Discussion

The experiment showed that initial transverse wave whose particle displacement is arbitrarily applied is decomposed into these two transverse wave modes in [110] silicon single crystal. Amplitudes of decomposed transverse wave modes depend on the particle displacement of initial transverse wave applied. Amplitude of each mode tends to be larger when initial vibration axis is near the mode axis. The experiment follows the general vector decomposition trend when the angle is calibrated for 4°. However, As a result of amplitude analysis, [001] wave mode has larger amplitude while [110] wave mode was smaller than vector decomposition's estimation. Maximum amplitude of each wave mode is also different, unlike optical polarization. Wave mode with faster wave velocity tends to have relatively large amplitude. It is thought that energy transfer process is distorted by two modes' velocity difference, and amplitude deviation from vector decomposition tends to compensate velocity difference between two transverse wave modes. Possible mechanism might be related to wave energy transfer and conservation.

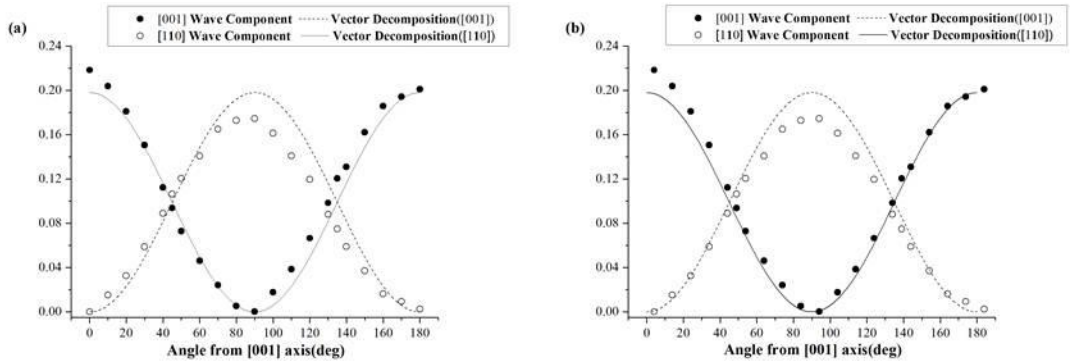

IUS3-PC-4

Experimental investigation of BAW propagation in Lithium Tantalate Oxide under the influence of uniaxial pressure and dc electric field

Arseny Telichko[1,2], Boris Sorokin[1], Gennady Kvashnin[1]; [1]*Technological Institute of Superhard and Novel Carbon Materials, Russian Federation,* [2]*Moscow Institute of Physics and Technology, Russian Federation*

Background, Motivation and Objective

Lithium Tantalate Oxide (LTO) single crystal has strong piezoelectric effect, low attenuation up to microwave frequencies, and is commonly used in many acoustoelectronic devices and sensors. Second-order elastic constants (SOEC) and piezoelectric constants of LTO have been well studied now. But the set of third-order elastic constants (TOEC) and non-linear piezoelectric constants were not investigated yet. Note that high-order elastic constants are important in the design of acoustic sensors for pressure, temperature or acceleration detection. The aim of this work was to obtain a set of non-linear electromechanical parameters of the LTO.

Statement of Contribution/Methods

In this work the dc electric field *E* and uniaxial pressure *P* dependencies of bulk acoustic waves (BAW) velocities in LTO were measured. Preliminary a set of BAW velocities *v* has been obtained in order to calculate exactly all the SOEC and piezoelectric constants of our crystals. BAW velocities and its variations under the *E* or *P* influence were measured by echo pulse method. The uniaxial pressure was applied by INSTRON 5965 electromechanical pressure apparatus up to 30 MPa. Displacement of time-flight echo pulse caused by the application of uniaxial pressure was measured by Tektronix oscilloscope DPO 71254B for a number of BAW modes and *P* application directions. Pressure force was applied along lateral directions to the BAW propagation vector, and modes without piezoelectric activity were studied only. To increase the sensitivity of the method, the reflected pulses to be measured were chosen as far as possible from probing pulse. Velocity variations were proportional to the *P* magnitude, when pressure was changed at measuring range up to 30 MPa. As a result the *P* controlling coefficients of BAW modes for based and rotated cuts were obtained.

The electric field dependencies *v* (*E*) were studied too for a number of BAW modes and different directions of the *E* influence. The magnitude of dc electric field was changed up to 5 kV/cm. The voltage was applied from the high-voltage source to the specimen through buffer capacity. The similar echo pulse method was used. The *E* and *P* controlling coefficients were used to calculate the LTO non-linear electromechanical parameters.

Results/Discussion

The values of BAW velocities and its variations under the *E* or *P* influence for basic and rotated cuts of LTO single crystal were determined. The linear *E* or *P* dependences of BAW phase velocities for both experiments were observed. Relations between the *P* controlling coefficients and linear combination of SOEC and TOEC have been obtained. Similar relations in case of dc electric field influence have been calculated too. Set of SOEC and piezoelectric constants as well as non-linear electromechanical parameters of LTO were calculated.

IUS3-PC-5

A Study in Wedge Waves with Applications in Delay-line

Po-Hsien Tung[1], Che-Hua Yang[1]; [1]*Graduate Institute of Mechanical and Electrical Engineering, National Taipei Univ of Technology, Taipei, ---, Taiwan*

Background, Motivation and Objective

This study is focused on wedge waves with applications in delay-line. Wedge waves are guided acoustic waves propagating along the tip of a wedge. Wedge waves has large motion amplitude and low energy attenuation when tip with small truncation. The difficulty of traditional probe measurement is hard to avoid noise from coupling agent and to raise spatial resolution by contact area.

Statement of Contribution/Methods

As shown in Fig.1, the experiment configuration consists of a 5MHz shear wave transducer and a wedge delay-line transducer for ultrasonic excitation and detection. In this research, the wedge delay-line transducer is composed of a 2.25MHz shear piezoelectric transducer and an aluminum wedge with apex angle 60 degree. The signal is detected by different contact angle between wedge delay-line transducer and specimen.

Results/Discussion

Fig. 2 shows the waveforms of the anti-symmetric flexural mode of wedge waves under contact angle start from 35 degree to 90 degree with an interval angle is 5 degree. The amplitude of anti-symmetric flexural mode is found to increase as the contact angle increases. The result shows when contact angle is approaching to 90 degree, the in-plane shear wave can be observed with best SNR. The feature can be used to mode selection by specific contact angle.

The wedge delay-line transducer are characterized experimentally. While the wedge delay line is in a configuration of contact angle near 90 degree, the detection for the in-plane shear wave is found to be very efficient. Advantages of wedge delay-line transducer include point-wise contact area, no coupling agent needed and mode selection by specific contact angle. This research aims at the development of a new signal-detection method based on wedge delayline.

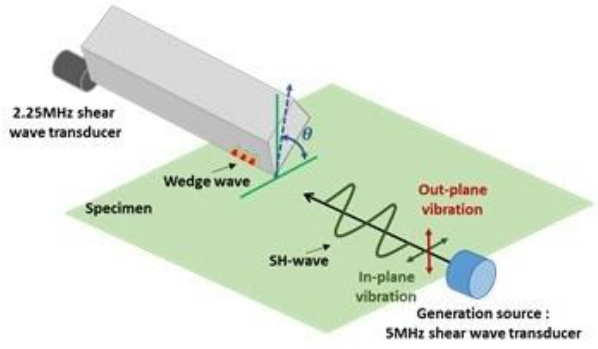

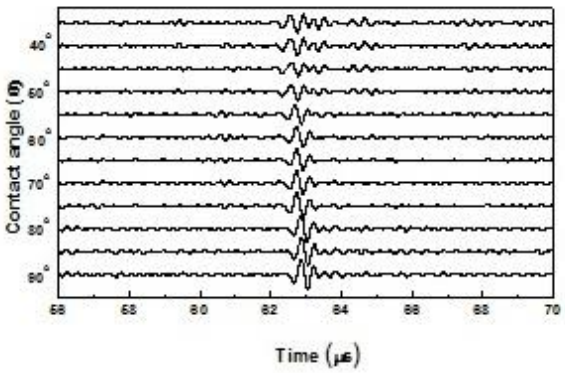

IUS3-PC-6

Writing and Reading Indentation in frequency space of acoustic resonators

Fujio Tsuruoka[1]; [1]*Kurume university, Kurume, Fukuoka, Japan*

Background, Motivation and Objective

Piezoelectric plate resonantly oscillates with the frequencies described with its dimensions. Piezoelectric particles have been known to resonantly oscillate, though, with smaller Q-values compared with plate. The ensemble of piezoelectric powders, whose dimensions are slightly different from each other, shows the resonant frequency spectrum that spread wide and moderately. When large amplitude oscillations, which bring about some change of their oscillation characteristics, is excited in a certain frequency part of resonators, some traces or indentation in the absorption spectrum might be left. These phenomena have been observed in the light absorption area and named spectral hole burning.

Statement of Contribution/Methods

We experimentally observed these phenomena and studied their mechanism or what change was introduced into resonators. In Fig. 1, we showed the results on $KBrO_3$ powder sample, which was prepared through grain destruction. Their dimensions are between 105 and 125 [μm] in diameter and the particle number was in the order of 10^6. The amplitude of the applied pulsed RF electric field was 200 [V/mm] and the pulse width 100 [μs]. Total pulse number was 10^3. We can recognize the trace or indentation at the frequency that coincides with the carrier frequency 11.5 [MHz] of applied pulse

Results/Discussion

The indentation formations were found to reflect sample preparation procedure. The shapes of indentation were different between as-received or deformed samples. We recognized that the indentation or the change of oscillation characteristics comes from crystal deformation introduced by large amplitude oscillation. We considered the mechanism of crystal deformation or dislocation induced model. The crystal oscillation damping increases in particles with lower dislocation-density, and decreases in particles with the higher one. We show and discuss also the results in which sequenced pulses were applied.

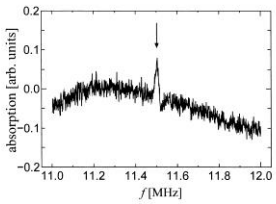

Fig. 1. Indentation written by RF pulses.

IUS3-PC-7

Impact-absorbing effect by applying ultrasonic vibrations to high-tensile steel plate

Atsuyuki Suzuki[1], Takahiro Onitake[2], Kanji Ikunaka[3], Jiromaru Tsujino[4]; *[1]Mechanical and Electrical Engineering, Tokuyama College of Technology, Shunan, Yamaguchi, Japan, [2]Tokuyama College of Technology, Shunan, Yamaguchi, Japan, [3]Tokuyama College of Technology, Japan, [4]Kanagawa University, Yokohama, Kanagawa, Japan*

Background, Motivation and Objective

The Blaha effect is a phenomenon in which the stress induced during the plastic deformation of metals decreases with the application of ultrasonic vibrations. This effect is currently employed in industrial operations such as bending. Now, we note that the rigidity of a traditional crushable zone does not change instantaneously. In this light, in this study, we aim to develop an impact-absorbing system based on the Blaha effect that can change the rigidity of crushable zones instantaneously in the event of a traffic accident. Ultrasonic vibrations reduce not only the stress but also the springback amount. If the decrease in the latter effectively prevents the rebound of the colliding object, damage after rebounding will be reduced.

Statement of Contribution/Methods

We have previously reported on the impact-absorbing characteristics when applying ultrasonic vibrations to aluminum alloy plates. However, we did not report any data regarding the impact force. In this study, the impact force was measured by using a load cell. The diameter and resonant frequency of the bolt-clamped Langevin type transducer (BLT) are 56 mm and approximately 17 kHz, respectively. We measured the impact-absorbing characteristics and springback amount when applying ultrasonic vibrations to high-tensile steel plates. High-tensile steel has been widely used in recent years to realize lightweight automobiles. The vibration characteristics of the transducer were also measured using a laser Doppler vibrometer and an impedance analyzer.

Results/Discussion

We developed an experimental device to confirm the impact-absorbing effect when applying ultrasonic vibrations. We measured the impact-absorbing characteristics, springback amount, and vibration characteristics. The following main results were derived from this study:

(1) The impact force was reduced by up to 7% by the application of ultrasonic vibrations.

(2) The springback amount was reduced by up to 30% by the application of ultrasonic vibrations.

(3) The deformation amount increased by up to 26% with the application of ultrasonic vibrations.

(4) The ultrasonic transducer was driven as designed. The effect of ultrasonic vibrations can be further enhanced by clamping a crumple specimen on the transducer and making the nose shape of the transducer rounded.

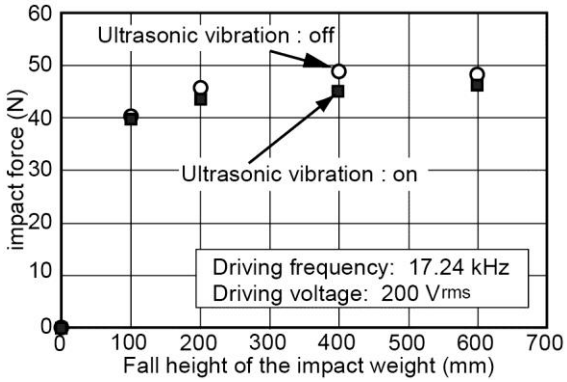

IUS3-PC-8

Noncontact flexural vibration modal testing of metallic cylinders using the electromagnetic acoustic coupling principle

Chan Il Park[1], Hongjin Kim[2], Yoon Young Kim[2], Jin Ho Lee[1]; *[1]Korea Institute of Nuclear Safety, Korea, Republic of, [2]Seoul National University, Korea, Republic of*

Background, Motivation and Objective

This investigation develops an eddy current method to excite and sense flexural vibrations of metallic cylinders in a noncontact manner without any mechanical movement of actuating units. The eddy current method has been used widely in many applications including damping generation and vibration reduction, but it was rarely used for the generation of mechanical vibrations of a structure for noncontact modal testing.

Statement of Contribution/Methods

The key in this method is to use a specially-configured figure-of-eight coil that supplies a dynamic magnetic field onto the cylinder and to install two permanent magnets inside the coil with specific polarities. Unlike existing eddy current methods, the present method does not require any mechanical motion of actuating units due to the specially-configured actuating magnet circuit. Numerical simulations showed that the direction of the Lorentz force generated by the magnetic circuit is in the desired direction.

Results/Discussion

The validity of the developed eddy current excitation method was first checked in the noncontact flexural modal testing of a slender aluminum pipe. The practicality of the developed the eddy current method was demonstrated by exciting a vehicle propeller shaft having a high bending rigidity and then obtaining its frequency response functions.

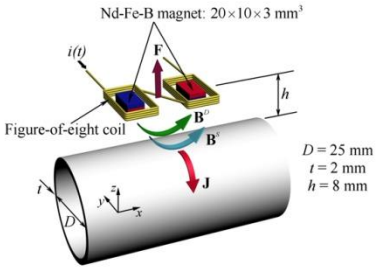

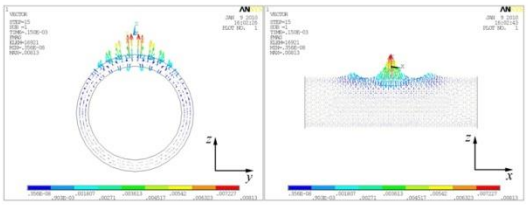

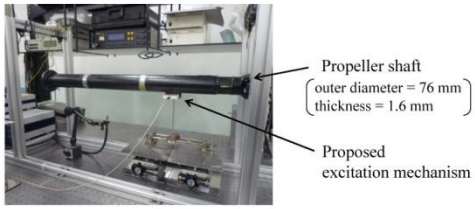

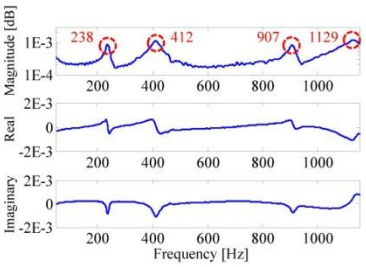

Mode	Natural frequency [Hz]	
	Proposed transducer	Impact hammer
1	238	238
2	412	408
3	907	910
4	1129	1132

IUS3-PC-9

Ultrasonic power measurement by calorimetric method using water as heating material -Investigation on thermal effects other than ultrasound -

Takeyoshi Uchida[1], Tsuneo Kikuchi[1]; *[1]National Metrology Institute of Japan (NMIJ), AIST, Tsukuba, Ibaraki, Japan*

Background, Motivation and Objective

Recently, high power ultrasounds higher than tens of watt have come into use in medical therapeutic field. The total power of ultrasound emitted by the medical equipment is one of key quantities closed related to the human safety. Traditionally, radiation force balance (RFB) is one of the most accurate methods of measuring ultrasonic power. However, it is difficult to measure ultrasonic power higher than around 20 W because an absorbing target is thermally damaged. Therefore, alternative measurement technique has become required. We have been developing ultrasonic power measurement technique by calorimetric method using water as heating material. In this paper, we investigated the effects of heat generation of ultrasonic transducer, heat loss of water vessel, and dissolved oxygen (DO) level of water on calorimetric method.

Statement of Contribution/Methods

We fabricated a cylindrical water vessel for accurate ultrasonic power measurement by calorimetric method. There is 10 mm air layer in the wall of the vessel. Thickness of inner wall is 0.8 mm which is smaller enough than the ultrasonic wavelength to avoid the loss of ultrasound in wall. The transducer is attached in the vessel wall parallel to water surface. The vessel is covered with a thermal insulator. By the structure, almost ultrasound energy contributes to increase the water temperature. The effect of heat generation of the transducer on the measured values by calorimetric method was investigated by comparison with those by RFB. Therefore, we fabricated two types of the transducer with different heat generation. Also, heat loss of the vessel was investigated by using the vessel with and without thermal insulator. Effect of DO level in water on calorimetric method was investigated by using saturated water more than DO level of 8 mg/L and degassed water less than DO level of 2mg/L.

Results/Discussion

The difference between ultrasonic power measured by calorimetric and RFB method was changed by using the transducers with different heat generation. The results show that excessively high ultrasonic power was measured owing to effect of heat generation of the transducer. Relative standard deviation of measured values by calorimetric method was decreased from 20 % to 5 % by using the vessel covered with thermal insulator. The results show that repeatability of measurement was improved owing to thermal insulator. Ultrasonic power measured by calorimetric method used degassed water was about 6 % smaller than those of saturated water. This cause was attributed to the difference in specific heat capacity between saturated and degassed water. We will present the accurate measurement of calorimetric method including the investigation of specific heat capacity of saturated and degassed water.

IUS3-PC-10

Visualization of temperature elevation in ultrasonic beam from circular piston

Jungsoon Kim[1], **Moojoon Kim[2]**, Myoungseok Kim[2], Kanglyel Ha[2], Seonae Hwangbo[3], Mincheol Chu[3]; *[1]Tongmyong University, Korea, Republic of, [2]Pukyong National University, Korea, Republic of, [3]Korea Research Institute of Standards and Science, Korea, Republic of*

Background, Motivation and Objective

There have been extended studies on the temperature elevation due to high power ultrasound in dissipative medium. However, most of the studies have been carried out in theoretical investigation. That is because measuring the thermal distribution is not easy in the case of a gel state or a soft tissue.

Statement of Contribution/Methods

In this study, the temperature elevation was investigated in a dissipative medium using agar and sucrose with the thermochromic particle. As the ultrasonic source, a plane circular piezoelectric transducer was used. A thermochromism layer of 100 μm was inserted between two agar layers with sucrose as shown in Fig.1. To obtain the acoustic attenuation of the medium, sucrose was mixed with the agar.

Results/Discussion

As an example, the temperature elevation pattern caused by ultrasound was changed by the ultrasonic irradiation time as shows in Fig. 2. In this case, the concentration of sucrose was 30 wt%, and the frequency of ultrasound was 650 kHz. The temperature elevation patterns were investigated with different attenuations of the acoustic medium. The experimental results were compared with the theoretical ones.

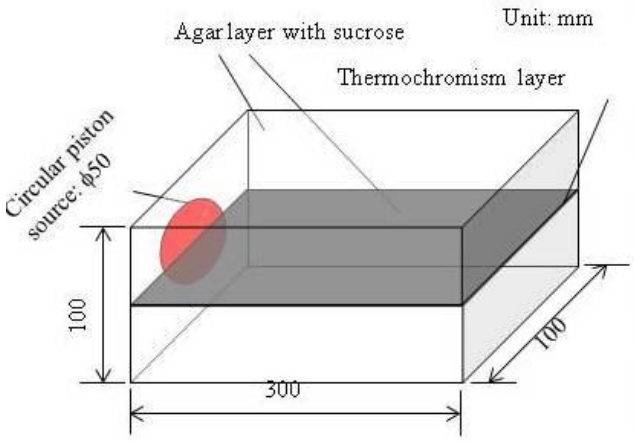

Fig. 1

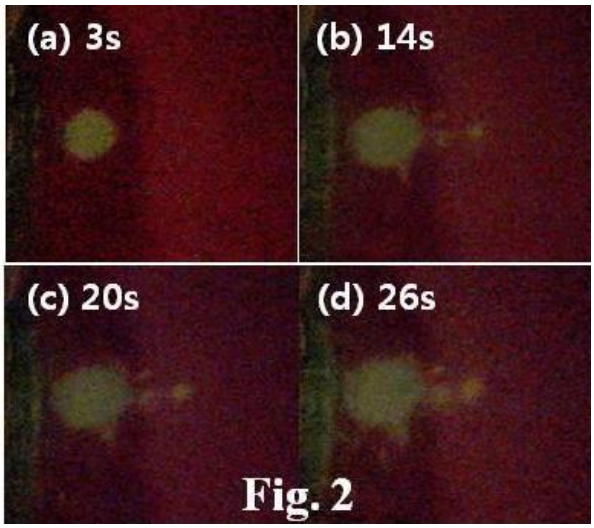

Fig. 2

IUS3-PC-11

Thermodynamic method for measuring the B/A nonlinear parameter under high pressure

Piotr Kielczynski[1], Marek Szalewski[1], Andrzej Balcerzak[1], Krzysztof Wieja[1], Aleksander Rostocki[2], Ryszard Siegoczynski[2]; *[1]Polish Academy of Sciences, Warsaw, Poland, [2]Warsaw University of Technology, Poland*

Background, Motivation and Objective

The nonlinearity parameter B/A is a measure of the nonlinearity of the equation of state for a fluid. It plays a significant role in acoustics, biology and medicine. The nonlinearity parameter is important because it determines distortion of a finite amplitude wave propagating in the fluid. Moreover, it can be related to the molecular dynamics of the medium and it can provide information about structural properties of medium, internal pressures, inter-molecular spacing, etc. Importance of the B/A parameter increases with the development of high-pressure technologies. The experimental techniques for the B/A parameter measurement can be classified by the two basic approaches: thermodynamic method and finite-amplitude method. In the first method, B/A is evaluated from the definition using measurements of the sound velocity as a function of pressure and temperature. The second method is based on the analysis on waveform distortion due to harmonics generation during wave propagation.

Statement of Contribution/Methods

Thermodynamic method is the most reliable method for measuring the nonlinearity parameter B/A. This method requires accurate measurement of the ultrasonic wave velocity in the liquid in a wide range of pressure and temperature. Computerized high-pressure measuring setup, designed and constructed by the authors, was used for the ultrasonic measurements.

The ultrasonic wave velocity was measured by using the time of flight method. The time of flight of the ultrasonic pulses was evaluated by applying the cross-correlation method.

Results/Discussion

Isotherms of ultrasonic wave velocity in triolein and isotherms of density were measured as a function of hydrostatic pressure from atmospheric to 600 MPa and at temperatures ranging from 10 °C to 40 °C, (f = 5 MHz). In the applied pressure range, the occurrence of phase transitions in triolein was stated.

To calculate the parameter B/A it is necessary to know the following thermodynamic parameters: coefficient of thermal expansion, specific heat at constant pressure and derivatives of the wave velocity on pressure and temperature. Required partial derivatives are calculated numerically using measured isotherms of velocity and density. This allowed to calculate the value of the nonlinear parameter B/A for triolein in a wide range of pressures (up to 600 MPa).

The usefulness of the ultrasonic thermodynamic method to evaluate the nonlinear parameter B/A was stated. The values of B/A are found to decrease monotonically with increasing pressure. Conversely, the nonlinear parameter B/A increases monotonically with temperature. It was found that a value of the nonlinearity coefficient B/A differs for the low-pressure phase and for the high-pressure phase in triolein, that is a novelty.

The measuring ultrasonic high-pressure setup and applied procedure have been employed successfully to the measurement of the nonlinear parameter B/A for a wide range of pressures and temperatures.

IUS3-PC-12

Ultrasonic investigation of physicochemical properties of liquids under high pressure

Piotr Kielczynski[1], Marek Szalewski[1], Andrzej Balcerzak[1], Krzysztof Wieja[1], Aleksander Rostocki[2], Ryszard Siegoczynski[2], Stanislaw Ptasznik[3]; *[1]Polish Academy of Sciences, Warsaw, Poland, [2]Warsaw University of Technology, Poland, [3]Institute of Agricultural and Food Biotechnology, Poland*

Background, Motivation and Objective

High pressure research of the physicochemical properties of liquids has been stimulated by the fast development of such technologies as biodiesel production, high-pressure food processing and conservation, modification of biotechnological properties. Monitoring and studying liquid viscosity and ultrasonic wave velocity in liquids as a function of pressure and temperature enable to evaluate many important physicochemical parameters of liquids. These methods allow also insight into the phenomena governing the microstructural modifications occurring in treated substances, i.e. phase transitions. The knowledge of physicochemical properties (e.g. density, compressibility or free volume) of pressurized substances is essential for understanding, design and control of the process technology.

Statement of Contribution/Methods

Established by the authors original Bleustein-Gulyaev (B-G) wave method has been applied for the measurement of the viscosity under high pressure. The sensor consists of the B-G wave waveguide made of PZT piezoceramics and sending-receiving PZT transducer. For measurements of the phase velocity of longitudinal ultrasonic waves, the authors have constructed the computerized setup especially designed to obtain a low level of parasitic ultrasonic signals. The ultrasonic wave velocity was measured by using the time of flight method. The time of flight of the ultrasonic pulses was evaluated by applying the cross-correlation method.

Results/Discussion

Measurements were conducted on the example of triolein (TAG), that is an important constituent of oils and fats. Longitudinal ultrasonic wave phase velocity, viscosity, and density of TAG have been measured. Measurements were conducted in a wide range of hydrostatic pressure, from atmospheric up to 650 MPa, and in the temperature range from 10 °C to 40 °C, (f = 5 MHz). Discontinuities of measured values as a function of pressure are the evidence of existence of phase transitions. Measured values of sound velocity, viscosity and density versus pressure have been used to calculate several important physicochemical parameters, e.g. compressibility, intermolecular free length, free volume, relaxation time, etc.

Direct measurements of the physicochemical properties of liquids are very difficult under conditions of high pressure. The sound velocity is closely linked with these properties and can be measured relatively easily and with high accuracy over wide ranges of pressure and temperature. Evaluation of the mentioned above physicochemical parameters of liquids is important not only from the cognitive point of view, but can also be useful for practical purposes to estimate the quality of edible oils. To the authors′ best knowledge the results obtained in this work are a novelty and have not been reported in the scientific literature.

Novel Resonators & Innovative Techniques

Forum Hall

Wednesday, July 24 2013, 01:00 pm - 04:30 pm

Congress Hallair: **Gernot Fattinger**
Triquint Semiconductor

IUS4-PC1-1

Metal Contact Print lithography for Fabricating High Frequency Surface Acoustic Wave Device with Heavy Electrode Loading Effect

Yung-Chun Lee[1], Tsung-Ming Chou[2]; [1]*Mechanical Engineering, National Cheng Kung University, Tainan, Taiwan, Taiwan,* [2]*Mechaical Engineering, National Cheng Kung University, Taiwan*

Background, Motivation and Objective

Surface acoustic wave (SAW) devises play an important role in current telecommunication technologies as well as many other applications. The operating frequency is getting higher and higher up to few to even few tens of GHz. Conventional methods for producing high-frequency SAW devices are limited and very expensive, and hence are not available to the majority of research society. In this paper, we present a simple but powerful method, named metal contact printing lithography, for fabricating high-frequency SAW devices operating at GHz region. Based on this new method, we are able to investigate and experimentally determine a pronounced loading effect in IDTs when the ratio of metal film thickness to wavelength is high. This new finding is important to the design, modeling, and application of high-frequency SAW Devices.

Statement of Contribution/Methods

Metal contact printing lithography (MCPL) utilizes a silicon mold as a template for first replicating a PDMS stamp and then transferring a metal film from to the PDMS stamp to a substrate. It can achieve small line-width patterning using only common equipments, ordinary laboratory environment, and simple processes. In this paper, we have modified and improved several key steps in the MCPL processes for fabricating IDT electrodes on a 128o y-cut LiBbO3 substrate. A number of one-port SAW resonators and two-port SAW filters with a central frequency from 1 to 4 GHz are successfully prepared. As shown in Fig.1 is a SEM image of fabricated IDT electrodes with a line-width of 500 nm and a central frequency around 2 GHz.Their electrical performance are also experimentally verified.

Results/Discussion

Because of the fabricating capabilities, we are able to investigate the metal film loading effects in high-frequency IDTs. Using one-port resonators as example, we have fabricated several samples with the same line-width and specifications but different metal film thicknesses. The correlation between the effective surface wave velocity and the ratio of film-thickness to wavelength si experimentally determined and is shown in Fig. 2, along with the theoretical predictions made by perturbation theory and finite-element method. To our surprise, neither methods can correctly predict the experimental results, which mean new model and analyzing method are needed for these high-frequency SAW devices in the future.

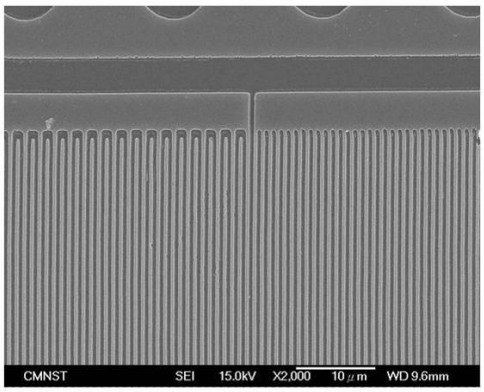

Fig. 1

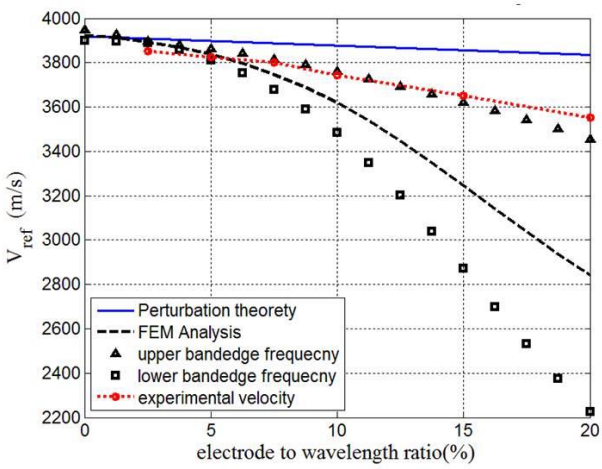

Fig. 2

IUS4-PC1-2

Laser Induced Forward Transfer: a Novel Technique for Piezoelectric MEMS Micromachining

Fabio Di Pietrantonio[1], Domenico Cannatà[1], Massimiliano Benetti[1], Enrico Verona[2], Valentina Dinca[3], Maria Dinescu[3]; [1]*Institute of Acoustics and Sensors, National Research Council of Italy CNR, Rome, Italy,* [2]*Institute for Photonics and Nanotechnologies, National Research Council of Italy CNR, Rome, Italy,* [3]*National Institute for Lasers, Plasma and Radiation Physics, Magurele, Romania*

Background, Motivation and Objective

Micro-electro-mechanical systems (MEMS) resonators based on piezoelectric materials are a class of highly miniaturized devices that open exceptional possibilities for creating miniature-scale precision oscillators at low cost. In particular, Film Bulk Acoustic Resonators, Lamb wave resonators and Contour Mode Resonators are examples of piezoelectric MEMS (pMEMS) devic-es made of a piezoelectric suspended membrane with metal electrodes. These structures are cur-rently fabricated by bulk or surface micromachining by using wet or dry etching, which are time consuming techniques that require high compatibility between the materials used and, hence, represent a limitation for the integration of pMEMS resonators with standard CMOS fabrication technologies. Furthermore, in the fabrication of pMEMS ladder filters, the need to manufacture resonators with different

resonant frequencies on the same substrate is an important issue. In this work, we used Laser Induced Forward Transfer (LIFT), a versatile direct write technique for spa-tially selective printing, to transfer a piezoelectric platelet on a silicon substrate. The objective is the development of a fabrication method of pMEMS that permits to overcome the limitations of etching techniques and to obtain different resonant frequencies on the same substrate.

Statement of Contribution/Methods

In order to fabricate the piezoelectric platelet a metallic electrode (350 x 350 μm^2) was patterned by photolithography on a quartz substrate. A piezoelectric c-axis oriented film (ZnO, AlN) was deposited by reactive magnetron sputtering and wet etched, in order to pre-pattern a 450 x 450 μm^2 square. Then, the metallic bottom electrode was deposited on the surface of the piezoelectric film to fabricate a metal/piezo/metal multi-layered platelet. Finally, the structure was transferred by a Nd:YAG laser using 266 nm wavelenght and 1 pulse on a conductive silicon wafer (Fig. 1) and measured with a Network Analyzer to evaluate the electro-mechanical properties of the platelet.

Results/Discussion

The deposition of a multi-layered piezoelectric platelet was implemented by LIFT on a silicon substrate. The transferred material showed acoustic properties comparable with those of the do-nor material demonstrating that LIFT technique is a promising method for micromachining pie-zoelectric thin film and hence, pMEMS devices.

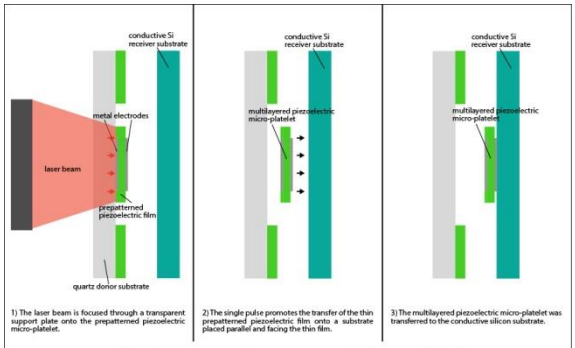

Fig. 1: Schematic representation of LIFT

IUS4-PC1-3

Improvement of Insertion Loss of Band Pass Tunable Filter using SAW Resonators and GaAs Diode Variable Capacitors

Michio Kadota[1], Yasuyuki Ida[2], Tetsuya Kimura[2], Masayoshi Esashi[1], Syuji Tanaka[1]; *[1]Tohoku University, Japan, [2]Murata Mfg. Co. Ltd., Japan*

Background, Motivation and Objective

Ultra wide band resonators are important devices to realize tunable filters with a wide band tunable range for mobile phones with multi-bands and cognitive radio systems. Authors realized the band pass tunable filter changing continuously from 1734 to 1844 MHz (6.1%) applying surface acoustic wave (SAW) resonators and Si diode variable capacitors as shown in Fig.1(1). But its insertion loss was large because a Q of the Si diode variable capacitors was very low as 1 at 1.8GHz(1). This time, the authors try to improve the insertion loss of the tunable filter.

Statement of Contribution/Methods

Compared with the Si diode variable capacitor, a GaAs diode variable capacitor has a high Q as 40 at 1.8GHz. The authors fabricated a PCB of a tunable filter using 2 SAW resonators and the GaAs diode variable capacitors instead of the Si diode variable capacitors. Fig. 2 shows frequency characteristics changing continuously by applying the voltage to the GaAs diode variable capacitors. Solid and broken lines show the measured and calculated characteristics, which were calculated considering residual inductances on the print circuit boad.

Results/Discussion

Compared with Fig.1, the insertion losses were drastically improved 12 dB in the maximum and the frequency characteristics are almost equal to the calculated ones, because of the calculation considering the residual inductances. The tunable range was also improved from 6.1% to 6.8 %. The Q of the GaAs is higher than that of the Si one. So, it is expected that a tunable filter with a wider tunable range in high frequency would be realized using the GaAs diode variable capacitors, if the high frequency SH0 plate wave resonator (2) with ultra wide bandwidth would be fabricated.

References

(1)M. Kadota etal: IUS, P1D6, 2011.

(2)M. Kadota etal: IUS, P1H, 2012 (in press).

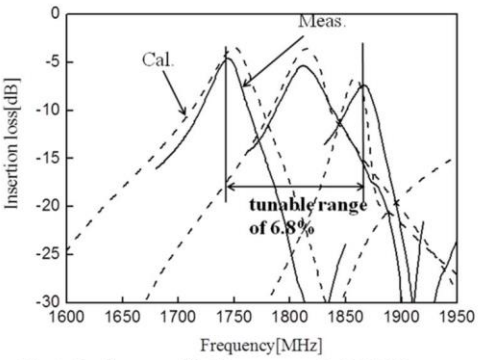

Fig. 2 Band pass tunable filter composed of 2 SAW resonators and GaAs diode variable capacitors with high Q.

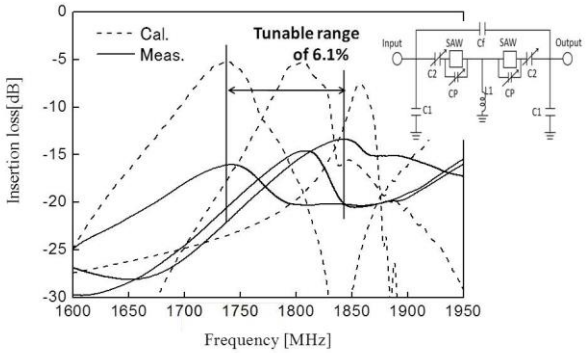

Fig. 1 Band pass tunable filter composed of 2 SAW resonators and Si diode variable capacitors (Cp and C2).

IUS4-PC1-4

High frequency SMR-BAW resonator on AlN thin film

Michael Dvoesherstov[1], Valentine Cherednick[1], Sergey Bosov[1]; *[1]Nizhny Novgorod state University, Russian Federation*

Background, Motivation and Objective

Heteroepitaxial structures (0002)AlN/Si(111) grown by molecular beam epitaxy (MBE), are promising for the manufacturing of microwave SMR-BAW resonators operating in the frequency range of 10 GHz. A thickness of the aluminum nitride film is about 0.2 microns for this frequency. Currently, MBE technology has been significantly optimized, thus providing a high-quality thin film (0002)AlN piezoelectric structures. According to the data of X-ray diffraction layer AlN diagnosed by the peak (0002) 2θ = 36.0°, which corresponds to the orientation of the film of aluminum nitride in the Miller indices (0002), i.e. c-axis is normal to the film surface. The measured width of the peaks (0002)AlN on the angle of rotation of the crystal (the width of the rocking curve) FWHM = 0.4o, indicating good crystal properties of the grown film. MBE method also allows you to get almost atomically smooth surface of the film. The roughness of the surface of the film grown by this method was Sq = ± 3 nm. The total RMS roughness in the frame 0.9x0.9 mm^2 is Sq = 18 nm.

Statement of Contribution/Methods

Technology of SMR-BAW microwave resonator manufacturing consists of the following opera-tions1: 1 - growing heteroepitaxial structure AlN/Si(111) by MBE, 2 - formation of the lower Mo electrode and an acoustic reflector (alternating SiO_2/Mo layers) by magnetron sputtering, 3 - bonding the obtained structure to the substrate holder at the reflector side, 4 - mechanical grinding of the silicon substrate up to 100 µm, 5 - plasmachemical etching of the silicon substrate up to its complete removing, 6 - magnetron sputtering of the upper Mo electrode on the surface of the AlN layer, 7 - forming of the upper electrode topology in the form of a coplanar transmission line by photolithography.

Results/Discussion

The resonator has the following sizes: thickness of the AlN film 0.22 µm, thickness of the top Mo electrode 0.069 µm, thickness of the bottom Mo electrode 0.07 µm. Asymmetric acoustic reflector[2] consists of alternating SiO_2/Mo layers (not quarter wavelength), allowing to reflect both the longitudinal and shear waves, where the thicknesses of the layers were t_L = 0.11 µm and t_H = 0.24 µm (for SiO_2 and Mo respectively). Microwave characteristics were measured by a vector network analyzer ROHDE&SCHWARTZ ZVB-20 using microprobes Z Probes Cascade Microtech of ACP40-GSG-100 type. The measured frequency of the parallel resonance fp = 9.88 GHz, the effective coupling coefficient K^2_{eff} = 6.5%, quality factor of the parallel resonance Qp = 150.

M. A. Allah, R. Thalhammer et al., " Solidly mounted BAW resonators with layer-transferred AlN using sacrificial Si surfaces", Solid-State Electronics, vol. 54, p.p. 1041–1046, 2010.

2 S.Jose., A.Jansman, R.Hueting, " A design procedure for an acoustic mirror providing dual reflection of longitu-dinal and shear waves in Solidly Mounted BAW Resonators (SMRs)", International Ultrasonics Symposium Proceedings, p. 2111, 2009.

IUS4-PC1-5

Performance of BAW Resonators at Cryogenic Temperatures

Eduard Rocas[1], Carlos Collado[1], Jordi Mateu[1,2], Alberto Hueltes[1], Jordi Verdú[3], James C. Booth[4], Robert Aigner[5]; *[1]Universitat Politècnica de Catalunya (UPC), Spain, [2]Centre Tecnològic de Telecomunicacions de Catalunya (CTTC), Spain, [3]Adaptive MicroNanoWave Systems Group, Ecole Polytechnique Fédérale de Lausanne (EPFL), Switzerland, [4]National Institute of Standards and Technology (NIST), USA, [5]TriQuint Semiconductor, USA*

Background, Motivation and Objective

An accurate knowledge of the material properties is crucial to BAW technology to ensure a good match between design and fabrication. Of especial importance are the temperature dependent material properties, as the devices have to work properly within a broad range of temperatures.

The objective of this work is to go beyond the usual temperature range for commercial applications and explore the functioning of the BAW resonator down to cryogenic temperatures, to get the whole picture at understanding the physical tendency of the main parameters with temperature. This can ensure the proper functioning for specific applications where the device is exposed to extreme temperature variations. Moreover, it can provide clues to some of the unresolved issues on the current technology, such as quality factor limiting origin.

Statement of Contribution/Methods

We perform broadband S-parameters measurements at temperatures from 293 K down to 40 K by use of a cryogenic probe station. We perform an Open-Short-Load (OSL) calibration at each temperature by characterizing each standard at 293 K and including a temperature dependent model for the Load.

Finally, the measurements are analyzed by use of a parameter extraction procedure to obtain the parameters of the Van-Dyke model at each temperature, to get meaningful data. The quality factor is also independently obtained directly from the reflection coefficient measurements.

Results/Discussion

The results show that the BAW resonators behave very well, and with no signs of substantial degradation, even down to 40 K. More specifically, the parallel resonance (fp) is seen to decrease at a faster rate than the series resonance (fs) when down in temperature (Fig. 1a, Fig. 1b), thus denoting an increased effective coupling coefficient at low temperature (Fig. 1c) due to the effect of the electrostatic capacitance (C0) (Fig. 1f).

Interestingly enough, the quality factor at fp (Qp) decreases dramatically at low temperature (Fig. 1d), which is related to the increase of the mechanical losses (Rm). On the contrary, the quality factor at fs (Qs) slightly increases at low temperatures (Fig. 1d) due to both the electric losses (Rs) and Rm effects (Fig. 1e).

From the results we can conclude that SMR-type BAW resonators show a proper functioning even at cryogenic temperatures and vacuum environments down to 10^{-6} Torr.

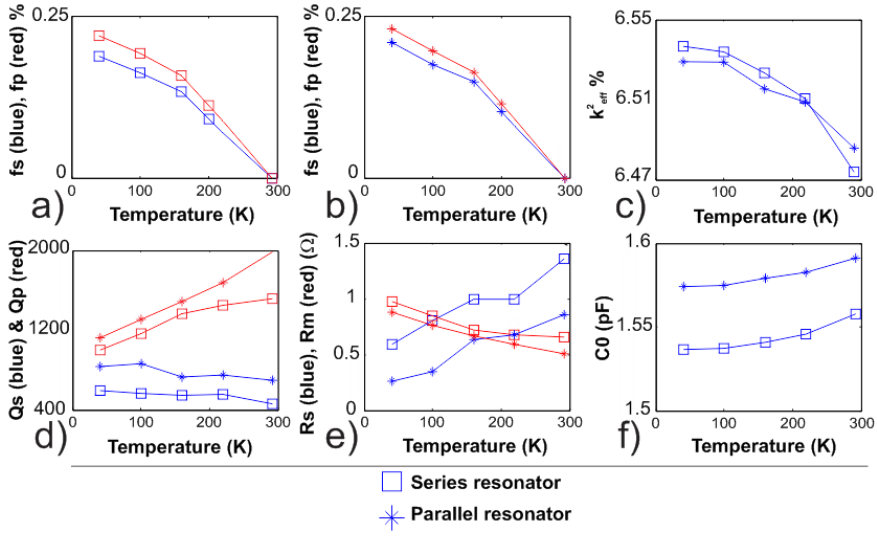

IUS4-PC1-6

GPS/GLONASS Filter using the Stoneley Wave for High Reliability Applications

Masakazu Mimura[1], Mari Saji[1], Kentaro Funahashi[1], Takashi Yamane[1], Daisuke Tamazaki[1], Norio Taniguchi[1], Hajime Kando[1]; [1]*Murata Manufacturing Co., Ltd., Japan*

Background, Motivation and Objective

Satellite positioning systems such as GPS and GLONASS are used for automotive navigation system globally. In those systems, RF filters are inevitable in receiver portion of the equipments and high reliability which satisfies automotive standards is required for these filters.

Boundary acoustic wave devices feature high reliability such as resistance against high humidity because their metal electrodes are completely covered with dielectric materials in comparison with SAW devices. A new GPS/GLONASS filter with very small size and high reliability has been developed by using a new boundary acoustic wave mode. For GPS/GLONASS filters, narrow bandwidth and steep cut off frequency response are required.

Authors have reported SH-type boundary acoustic wave resonators on SiN/SiO_2/electrodes/$LiNbO_3$ (LN) structure [1]. However, their electromechanical coupling coefficient (k^2) is too large to design such narrow bandwidth filters. Therefore, we tried to apply the Stoneley wave on around 128° Y-X LN which is not used in practical use. This wave mode is expected to have smaller k^2 and higher Q-value.

Statement of Contribution/Methods

In the case of the Stoneley wave substrate, the SH-type wave acts as a spurious response. We calculated the dependency of the k^2 of both the Stoneley wave and the SH-type wave on cut angle of LN, and the good cut angle, in which the k^2 of the SH-type is almost zero and that of the Stoneley wave is moderate, could be found at 120° Y-cut.

Next, the thickness of metal electrodes and the SiO_2 layer were optimized considering the acoustic reflection coefficient, the temperature coefficient of frequency and the k^2.

One port resonators were fabricated using those conditions and suitable values of 5.2 % of the k^2 and the good maximum Q-value of 1400 was obtained experimentally.

Results/Discussion

Fig. 1 shows the measured transmission characteristics of the developed ladder type GPS/GLONASS filter using the Stoneley wave resonators.

Small insertion loss of 1.2 dB in GPS band and 1.8 dB in GLONASS band and good shape factor have been achieved.

Several reliability tests such as humidity and thermal shock were carried out and it was confirmed that the developed filter realizes automotive class high reliability performances.

References

[1] M. Mimura, et al., Jpn. J. Appl. Phys. Vol. 51, pp. 07GC13 (2012).

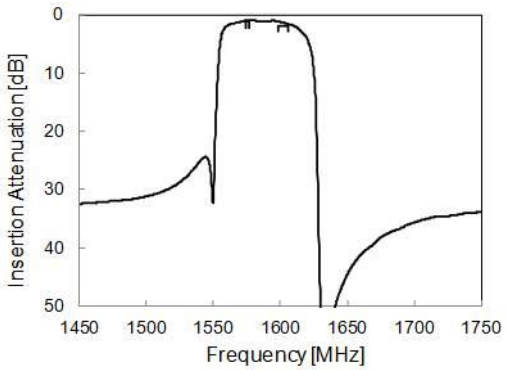

Fig. 1

IUS4-PC1-7

High Frequency Resonators with wide bandwidth using SH0 Mode Plate Wave in LiNbO3 Thin Plate

Michio Kadota[1], Yasuhiro Kuratani[2], Tetsuya Kimura[2], Masayoshi Esashi[1], Syuji Tanaka[1]; [1]*Tohoku University, Japan,* [2]*Murata Mfg. Co. Ltd., Japan*

Background, Motivation and Objective

Ultra wide band resonators are important devices to realize tunable filters with a wide band tunable range.(1) Authors fabricated 2 type structures of SH0 mode plate wave resonators composed of one intergidital transducer (IDT) on one surface (one sided IDT) and each IDT on both surface of a plate (both sided IDTs) as shown in Fig.1.(1) They showed ultra wide bandwidths of 26 and 29 %, respectively. However, their resonant frequencies (fr) are low as 1.8 MHz and they have large transverse mode ripples between fr and ant-resonant frequency (fa) as shown in Fig.1.(1)

Statement of Contribution/Methods

SH0 mode plate wave resonators composed of one sided IDT structure were fabricated by composing an Al IDT on a thin 30ºYX-LiNbO3 plate (500nm thickness) on Si substrate like a MEMS structure. An electrode was composed of an apodized IDT to suppress the transverse mode ripples and each grating reflector at both side of the IDT. The IDT metalization ratio is 0.34 to obtain a wide bandwidth.

Results/Discussion

Fig. 2 shows frequency characteristics of the resonators of fr of 440 and 550 MHz. They have an ultra wide band of 22 % and a large impedance ratio of 80 dB. In addition, the transverse mode ripples were suppressed. Their bandwidth and impedance ratio are little narrower and smaller than those in Fig.1 because of using one sided IDT type structure and the apodized IDT. Though, this time, small ripples higher than fa due to an upper stop band frequency at open grating or an S0 mode are observed, they could be resolved by designing an electrode or a plate thickness. The high frequency SH0 mode plate wave resonators with wide bandwidth and without the transverse mode ripples were realized for the first time. They are expected for a tunable filter in white band frequency.

Reference

(1)M. Kadota etal: IUS, P1H, 2012 (in press).

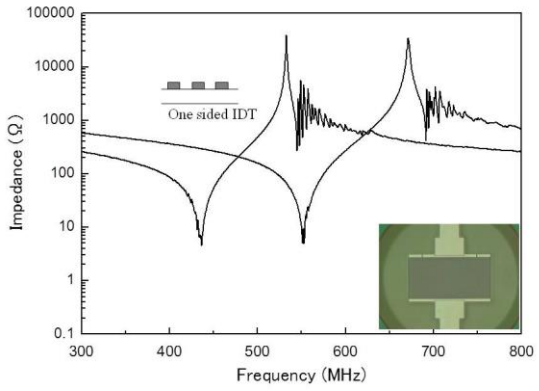

Fig.2 Frequency characteristics of high resonant frequency (440 and 550 MHz) SH0 mode plate wave resonators.

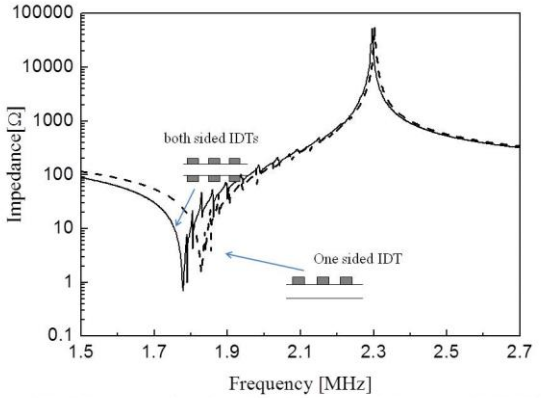

Fig.1 Frequency characteristics of low resonant frequency (1.8 MHz) SH0 mode plate wave resonators.

Propagation & Materials

Forum Hall

Wednesday, July 24 2013, 01:00 pm - 04:30 pm

Congress Hallair: **Maximilian Pitschi**
TDK Corporation

IUS4-PC2-1

Microwave Acoustic Properties of Diamond Single Crystal as a Substrate for High-overtone Bulk Acoustic Resonator

Boris Sorokin[1], Gennady Kvashnin[1], Sergey Burkov[2], Georgy Gordeev[1,3], **Arseny Telichko[1,3]**, Aleksandr Volkov[1], Vitaly Bormashov[1], Mikhail Kuznetsov[1]; *[1]Technological Institute of Superhard and Novel Carbon Materials, Russian Federation, [2]Siberian Federal University, Russian Federation, [3]Moscow Institute of Physics and Technology, Russian Federation*

Background, Motivation and Objective

High-overtone Bulk Acoustic Resonator (HBAR) operating on microwave frequencies belongs to the class of composite solid state devices which differ from conventional piezoelectric resonators owing to the miniature size and high quality factor *Q*. A good acoustic quality of substrate has a key significance as far as bulk acoustic wave is almost full concentrated inside the substrate. Diamond has a unique combination of properties as highest acoustic velocity, high thermo conductivity and excellent resistivity to the chemical and radiation damage. But there are no data on diamond single crystal application as the HBAR's substrate. The aim of this investigation consisted of the microwave acoustic properties studying of synthetic diamond single crystal and possible application as a substrate of acoustoelectronic devices.

Statement of Contribution/Methods

Piezoelectric structures Mo/AlN/Mo/diamond structures were obtained by magnetron sputtering method. Diamond type IIa single crystals were grown by HPHT method. The main attention was paid to the quality of AlN film, which was studied by X-ray diffraction using Cu K_α radiation and scanning electron microscopy. As a substrate the double-side polished wafers (~0.4 mm thickness) were fabricated of the (100) diamond single crystal. Substrate faces were prepared with better than 5′ deviation from [100] crystalline direction, and were polished to obtain the roughness better than 10 nm controlled by AFM method. The HBAR acoustic properties were studied on Network Analyzer E5071C and M-150 Multipurpose Probing System intended for the reflection coefficient S_{11} and impedance measurements. The piezoelectric transducer of 0.8 microns AlN film could be used in a super high frequency band, so the frequency dependence of the acoustic loss was examined in a wide range from 300 MHz up to 16 GHz.

The frequency Δf between two adjacent acoustic overtones can be calculated by the simple relation as $\Delta f = V_L/2d$, where V_L is the phase velocity of longitudinal bulk acoustic wave and d is the substrate thickness. The Δf measurements were shown a close accordance with calculated values of (100) diamond single crystal.

Results/Discussion

The Mo/AlN/Mo/diamond piezoelectric layered structure has been developed, and its acoustic properties at microwave frequencies have been investigated. It was found that diamond single crystal can be successfully used as a high *Q* perspective substrate for HBAR, operating on microwave frequencies. Frequency dependence of *Q* factor has been investigated, and $Q \approx 3700$ at 16 GHz. As a result the $Q*f \approx 6*10^{13}$ relation has been fulfilled for a named microwave band.

The best quality of the future BAW devices based on diamond single crystal could be provided by the diamond polishing process development as well as the special choice of the metals with improved conducting and acoustical properties.

IUS4-PC2-2

Experimental and theoretical investigation of guided acoustic wave properties in in-plane c-axis ZnO films

Shinji Takayanagi[1], Abdelkrim Talbi[2], Olivier Bou Matar[2], Nicolas Tiercelin[2], Mami Matsukawa[1], Philippe Pernod[2], Vladimir L. Preobrazhensky[2]; *[1]Graduate School of Science and Engineering, Doshisha University, Kyotanabe, Kyoto, Japan, [2]LIA LEMAC-LICS, Institute of Electronics, Microelectronics and Nanotechnology, PRES University Lille North of France, EC Lille, Villeneuve d'Ascq Cedex, France*

Background, Motivation and Objective

ZnO piezoelectric films are widely used for high frequency guided acoustic wave devices. In most cases the out of plane c-axis ZnO films were used. On the other hand, we successfully fabricated in-plane c-axis ZnO films[1] on different substrates including glass and Si. The in-plane c-axis of the ZnO film results in unique anisotropy of elastic properties enabling to generate multimode surface acoustic waves (SAWs). Values of electromechanical coupling coefficient K^2, up to 6% for some SAW modes and up to 13% for the first symmetrical Lamb wave mode, can be achieved. The high K^2 and multimode generation are very important for applications based on acousto-electric, acousto-optic and magneto-acoustic interactions. In this study, we investigated the potentiality of the in-plane c-axis ZnO films for guided acoustic waves including SAWs and Lamb waves.

Statement of Contribution/Methods

First, the in-plane c-axis ZnO films (2.2 μm) were grown on a Mo (100 nm)/Si substrate (380 μm) by an RF magnetron sputtering[1]. Next, Au/Ti IDTs with the wavelength of 12 μm were fabricated on the samples. We prepared four samples with ψ angle of 0°, 30°, 60° and 90°, which is defined as an angle between the in-plane c-axis direction and the IDT fingers. Insertion losses of these samples were measured by a network analyzer to investigate the propagation characteristics of SAWs. Theoretical analyses were also performed to evaluate the potentialities of such structures for Lamb wave generation.

Results/Discussion

Fig. 1(a) shows the insertion loss characteristic obtained in the sample with ψ angle of 90°. Rayleigh-SAW and Sezawa-SAW excitations were observed at the center frequency f_1 of 255 MHz and f_2 of 394 MHz, respectively. As ψ approached to 0°, SAW excitations weakened because the piezoelectric constant e_{33} of ZnO had a smaller effect on the longitudinal wave excitation. Fig. 1(b) shows K^2 for Lamb waves calculated for in-plane and out of plane c-axis ZnO films. We can note that the in-plane structure without bottom electrode exhibits the highest value of K^2 and can be of great interest for the applications cited above. The fabrication process of such structure is in progress. The high frequency magneto-elastic coupling will be investigated in multilayered structure including in-plane c-axis ZnO membrane and magnetostrictive film.

[1] S. Takayanagi, et al., Appl. Phys. Lett. **101**, 232902 (2012).

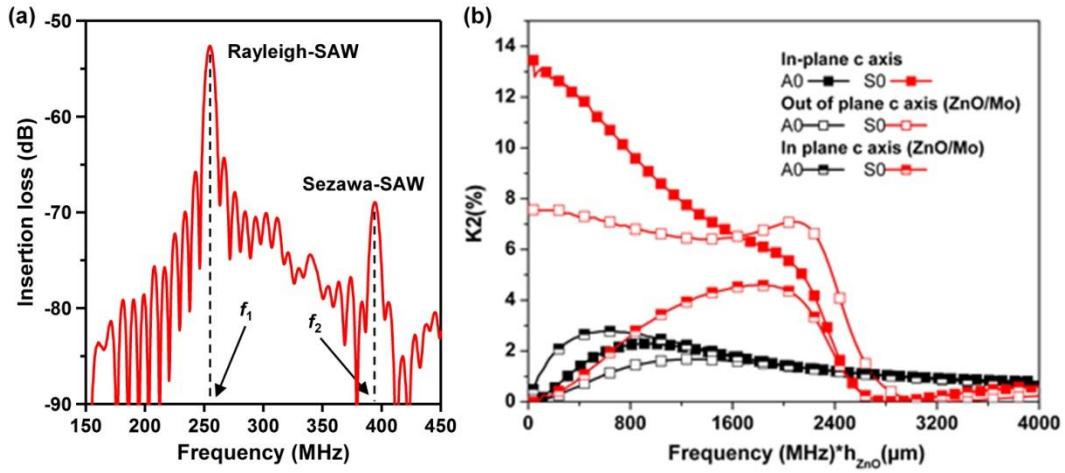

Figure 1 (a)Insertion loss characteristic observed in the Au/Ti IDT/in-plane c-axis ZnO (ψ=90º)/Mo/Si substrate structure, and (b)theoretical analyses of electromechanical coupling coefficient for Lamb wave modes.

IUS4-PC2-3

Legendre and Laguerre polynomial approach for modeling of wave propagation in layered magneto-electro-elastic media

Olivier Bou Matar[1], **Noura Gasmi[1]**, Huan Zhou[1], Marc Goueygou[1], Abdelkrim Talbi[1]; *[1]International Associated Laboratory LICS/LEMAC, IEMN UMR CNRS 8520, PRES Lille Nord de France, ECLille, Villeneuve d'Ascq, France*

Background, Motivation and Objective

The large magnetoelectric coefficient in composites composed of piezoelectric and piezomagnetic layers, compared to the one of single phase materials, has attracted a large amount of studies. These multiferroic materials are now widely used in the development of sensors, actuators and storage devices. In these devices, not only static stress can be exploited to control the magnetic properties, but also elastic waves. The growth of such applications requires the development of tools to simulate elastic wave propagation in multilayered piezoelectric-piezomagnetic composites. Methods based on a matrix formalism have been proposed to study the dispersion curves of elastic waves in layered media. However, the search of roots implied by these methods may be a difficult task.

Statement of Contribution/Methods

To overcome these drawbacks, we use a combined Legendre-Laguerre polynomial expansion method to compute the propagation constants and the mode shapes. The exponential convergence of the scheme is demonstrated in the case of Love wave propagation in a thin film deposited on a substrate, and the method is validated using two benchmarks taken from the literature.

Results/Discussion

The proposed method is used to investigate a tunable magneto-elastic thin film SAW device constituted of a 2.7 um SiO2 film, covered by a 200 nm magneto-elastic film, deposited on a LiNbO3 substrate. The velocity for waves propagating along the easy axis direction of the magneto-elastic thin film, as a function of frequency is displayed in Fig. 1 for two external magnetic field values. It appears that the tunability of the first mode, the Rayleigh mode, is considerably lower than the one of the second mode, a shear horizontal mode. The profiles of the displacement components at a frequency of 300 MHz are shown in Fig. 2.

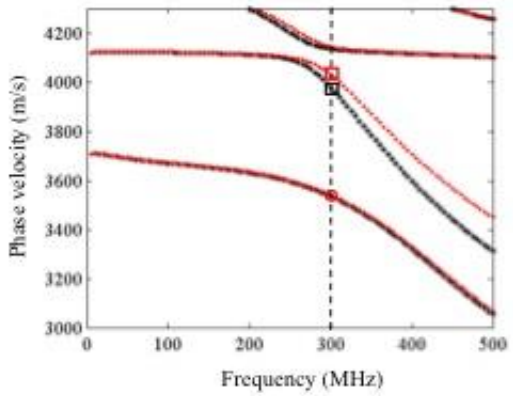

Fig. 1: Phase velocity as a function of frequency for a film of SiO_2/$TbCo_2$-FeCo deposited on a X-cut $LiNbO_3$ substrate for two external magnetic field values: 1 kOe (stars) and 250 Oe (diamonds).

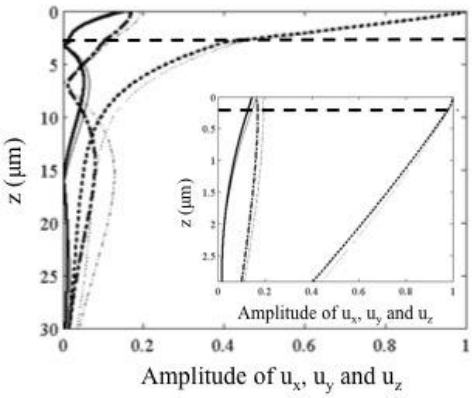

Fig. 2: Amplitude of the displacement components of the first order mode for two amplitude of the static magnetic field applied perpendicularly to the easy axis: 250 Oe (thick line) or 1000 Oe (thin lines).

IUS4-PC2-4

Material Parameters of Ca3TaGa3Si2O14 Single Crystal Revisited

Andrey Sotnikov[1,2], Hagen Schmidt[1], Manfred Weihnacht[1], Oleg Buzanov[3], Sergey Sakharov[3]; *[1]IFW Dresden, Dresden, Germany, [2]A.F.Ioffe Physical-Technical Institute, St. Petersburg, Russian Federation, [3]JCS Fomos-Materials, Moscow, Russian Federation*

Background, Motivation and Objective

Piezoelectric Ca3TaGa3Si2O14 (CTGS) belongs together with Ca3NbGa3Si2O14 (CNGS), Sr3NbGa3Si2O14 (SNGS) and Sr3TaGa3Si2O14 (STGS) to a group of ordered single crystals from the langasite family. CTGS has the same trigonal symmetry as quartz (point group 32) and, as usual for langasite family crystals, demonstrates a distinctly higher electromechanical coupling coefficients as compared to quartz. Other important features are the absence of a structural phase transition below its melting point and the availability of high quality large crystals grown by the Czochralski technique at relatively low cost of raw materials. To the best of our knowledge, CTGS material data sets including elastic, piezoelectric, and dielectric constants have been reported only in two papers using both pulse-echo [1] and resonance techniques [2]. Notice that the published values of some elastic constants and e14 piezoelectric coefficient are contradictory. In this communication, we report on the measurement of the elastic, piezoelectric and dielectric constants of CTGS.

Statement of Contribution/Methods

CTGS single crystals were grown using the Czochralski technique. The elastic and piezoelectric constants were derived from the velocity data of bulk acoustic waves measured by the high-precision pulse-echo method at a frequency of 10 MHz using crystals cubes (8x8x8 mm3) of the appropriate crystallographic orientations. SAW velocity measurements using a laser pulse excitation method were performed as an additional way to extract elastic constants. The dielectric permittivity was obtained using thin X-, Y- and Z crystalline plates (8x8x0.5 mm3) and standard capacitance technique.

Results/Discussion

Using the pulse-echo ultrasonic technique, the room temperature velocities of the longitudinal and the shear acoustic waves propagating in five crystallographic directions of CTGS single crystals have been measured. This method was combined with a special SAW velocity measurement technique. The complete set of room temperature elastic, piezoelectric and dielectric constants of CTGS was obtained and compared with the published data.

[1] Yu.V. Pisarevsky, B.V. Mill, N.A. Moiseeva, A.V. Yakimov "Ordered Ca3TaGa3Si2O14 crystals: growth, electromechanical and optical properties", Proc. 18 Eur. Freq. and Time Forum, pp. 216-219 (2004).

[2] X. Shi, D. Yuan, X. Yin, A. Wei, S. Guo, F. Yu "Crystal growth and dielectric, piezoelectric and elastic properties of Ca3TaGa3Si2O14 single crystal", Solid State Comm., 142, 173-176 (2007).

IUS4-PC2-5

Longitudinal-Type Leaky Surface Acoustic Wave on $LiNbO_3$ with High-Velocity Thin Film

Fumiya Matsukura[1], Masato Uematsu[1], Keiko Hosaka[1], Shoji Kakio[1]; *[1]Interdisciplinary Graduate School of Medicine and Engineering, University of Yamanashi, Japan*

Background, Motivation and Objective

The longitudinal-type leaky surface acoustic wave (LLSAW) has attracted interest owing to its high phase velocity close to that of a longitudinal bulk wave. However, an LLSAW has huge inherent attenuation owing to the continuous radiation of the bulk wave. Kakio, one of the authors, and Abe proposed a reverse proton exchange (RPE) layered structure on a $LiNbO_3$ (LN) substrate to reduce the attenuation of an LLSAW, which markedly improved the insertion loss and resonance properties of the LLSAW [1]. A feature of the layered structure is that the velocity on the surface layer is higher than that on the elastically softened substrate. Therefore, by loading with a dielectric thin film with a higher velocity than that of the substrate, the loss reduction of the LLSAW can be expected. In this study, an aluminum nitride (AlN) thin film was adopted as a high-velocity thin film, and the propagation properties of an LLSAW on LN substrates, in which an amorphous AlN (a-AlN) thin film was loaded, were investigated theoretically and experimentally.

Statement of Contribution/Methods

First, the elastic constants c_{11} and c_{44} in an a-AlN thin film deposited by RF magnetron sputtering were determined from the measured phase velocities of two SAW modes with mutually perpendicular particle motion. Next, the LLSAW attenuation on X36°Y-LN and YZ-LN was calculated using the determined constants. Then, the propagation properties of an LLSAW on X36°Y-LN were measured using an interdigital transducer (IDT) pair. A single-electrode IDT pair with a period λ of 20 μm was fabricated using a 0.01λ-thick-Al film. To evaluate the propagation loss *PL*, samples with propagation path lengths of L=25λ and 50λ were fabricated. Then, an a-AlN thin film was deposited on the IDT pair and the metallized propagation path.

Results/Discussion

For the deposited a-AlN thin film, c_{11} and c_{44} were determined to be 2.69×10^{11} and 1.13×10^{11} N/m^2, which were 78% and 96% of those of a single-crystal AlN thin film, respectively. From the theoretical calculation, it was found that the LLSAW attenuation can be reduced to zero by loading with an a-AlN thin film with a thickness of above h/λ=0.065 for X36°Y-LN. Furthermore, for YZ-LN, zero attenuation was obtained at a film thickness of less than half of that for X36°Y-LN. By loading with an a-AlN thin film with 0.12λ film thickness, the measured *PL* on X36°Y-LN was decreased from 0.26 dB/λ for the sample without a film to 0.15 dB/λ. When the film thickness was increased to 0.175λ, *PL* was slightly increased to 0.17 dB/λ, although the minimum insertion loss decreased. Therefore, it was found that the bulk wave radiation loss was also reduced by loading with an a-AlN thin film.

[1] S. Kakio and M. Abe: Jpn. J. Appl. Phys. **51** (2012) 07GC17.

IUS4-PC2-6

Evaluation of Piezoelectric Ta_2O_5 Thin Films Deposited on Sapphire Substrates

Shunsuke Iwamoto[1], Ryosuke Saigusa[1], Shoji Kakio[1]; *[1]Interdisciplinary Graduate School of Medicine and Engineering, University of Yamanashi, Japan*

Background, Motivation and Objective

Piezoelectric thin films with high coupling, high stability, low loss, and high phase velocity are required for the development of high-performance piezoelectric devices, such as surface acoustic wave (SAW) and film bulk acoustic resonator devices. An X-axis-oriented Ta_2O_5 piezoelectric thin film is a relatively new material and has a strong piezoelectric property similar to that of ZnO thin films and a high dielectric constant. In this study, Ta_2O_5 thin films were deposited on sapphire (Al_2O_3) substrates, from which single crystallization due to epitaxial growth can be expected, using an RF magnetron sputtering system with long-throw sputter cathodes, and the crystalline and Rayleigh-type SAW (R-SAW) propagation properties of the thin films were evaluated.

Statement of Contribution/Methods

Ta_2O_5 thin films were deposited on the *c*- and R-planes of Al_2O_3 substrates (*c*-, R-plane samples). An RF power of 150 W was applied to a Ta metal target. The gas flow rates of Ar and O_2 were 30 and 10 ccm, respectively, while the atmosphere gas pressure was fixed at 0.75 Pa. The substrate temperature was set to 800 °C. The deposition time was 4-8 h and the deposition rate was 0.43-0.75 μm/h. The degree of orientation and the crystallization of samples were evaluated from X-ray diffraction (XRD), pole figure, and

transmission electron microscope (TEM) patterns. To measure the SAW properties, interdigital transducers with a period λ of 20 µm and 30 split-finger pairs were fabricated on the deposited film using an Al film.

Results/Discussion

From the XRD patterns, the preferential (200)-axis orientation was observed for the R-plane sample. On the other hand, for the *c*-plane sample, not only the (200)-axis orientation but also the (203)-axis orientation of hexagonal Ta_2O_5 (δ-Ta_2O_5) was observed. From the spotted patterns in the pole figure and the TEM pattern, in which the poles were arranged to form the vertices of a hexagon, the possibility of the crystallization of δ-Ta_2O_5 in the *c*-Al_2O_3 substrate plane due to epitaxial growth was shown. From the measured SAW properties, the zeroth and first modes of the R-SAW were observed for both samples. For the first mode of the R-SAW on the R-plane sample, a coupling factor of 1.78% and a phase velocity of 4,895 m/s were obtained for a normalized thickness of 0.225. Unfortunately, no increase in coupling factor was observed upon the crystallization of hexagonal Ta_2O_5 because δ-Ta_2O_5 belongs to the 6/*mmm* point group without piezoelectricity.

IUS4-PC2-7

Derivation of accurate tensor data of materials in SAW devices by solving a parameter identification problem using an enhanced eigenvalue analysis of an infinite array model

Gerold Grünauer[1,2], Markus Mayer[1], Matthias Knapp[1], Philipp Jaeger[1], Thomas Ebner[1], Karl Wagner[1], Hans Josef Pesch[2]; *[1]TDK Corporation, Germany, [2]Universität Bayreuth, Germany*

Background, Motivation and Objective

Accurate ab initio simulations are a valuable tool for the development of SAW based filter products. However, the accuracy of every simulation is inherently limited by the quality of the provided material data. The material tensors from literature in general do not lead to a satisfying simulation quality for material systems fabricated with specific production processes. Possible reasons are that the employed crystals are not single crystals, or that thin layers are involved.

Hence, material data should be determined from measurements of test devices manufactured by the actual process.

In this work the material parameters are determined by solving a parameter identification problem based on measured velocities / resonance frequencies within SAW delay lines / resonators and periodic FEM modal analysis simulations thereafter.

Statement of Contribution/Methods

A surrogate model approach for solving the material parameter identification problem was developed. The surrogate models are created using an extended FEM program. At first, the FEM system is solved exactly. Afterwards it estimates new eigenvalues, representing the SAW velocities / resonance frequencies, efficiently using sparse matrix techniques using the already computed first FEM results. In order to fit the material parameters to measurements, surrogate models for various geometries (delay lines and/or resonators) and temperatures are computed. The material parameters, including stiffness, piezoelectric coupling factors, dielectric constants, density and their respective temperature coefficients are afterwards fitted using the surrogate models to the measured values. After the optimization, the maximum expected errors of the new material parameters are computed using the measurement errors.

Results/Discussion

Using the new parameter identification algorithm, material tensor data and their respective temperature coefficients have been determined for a silicon nitride passivation layer in dependence of various process parameters with a maximum relative error of ±2% for each constant. The surrogate model optimization approach using an eigenvalue estimator offers a fast, flexible, user-friendly and reliable method to fit the material parameters in complex measurement setups.

IUS4-PC2-8

Accurate determination of thin film properties using SAW differential delay lines

Matthias Knapp[1], Gerold Grünauer[1], Philipp Jäger[1], Günter Scheinbacher[1], Ingo Bleyl[1], Leonhard Reindl[2]; *[1]TDK Corporation, München, Germany, [2]Albert-Ludwigs-Universität Freiburg, Institut für Mikrosystemtechnik, Freiburg, Germany*

Background, Motivation and Objective

Modern surface acoustic wave (SAW) filters use dielectric layers for different purposes like passivation to humidity, temperature compensation, frequency trimming or wave guiding.

Therefore, an accurate knowledge of the electro-acoustic properties of these dielectric layers is important for filter design and optimization.

It is the objective of this study to establish a method to determine the film properties like density and the stiffness tensor. To improve the accuracy, all deteriorating effects coming from e.g. metal electrodes for wave excitation needs to be eliminated.

The validation of the method is done by analyzing Si3N4 films on LiNbO3 substrates.

Statement of Contribution/Methods

In this work the phase velocity dispersion of layered structures is evaluated using differential delay lines. With this approach, the impact of material properties and the geometry of the metal electrodes in the transducers is eliminated from the evaluation.

First, the group velocity is calculated from the measured signals of the delay lines. Afterwards the phase velocity is calculated from the phase spectrum using the already determined group velocity.

The material properties of the overlayer can now be extracted from the non-linear phase velocity dispersion using a Finite-Element-based optimization of the layer density and the stiffness tensor.

Results/Discussion

The method is applied to a layered system consisting of a LiNbO3 substrate with a Si3N4 layer. The chosen substrates were LiNbO3 rot 128°-YX for the Rayleigh wave and LiNbO3 rot 64°-YX for the shear wave. Different Si3N4 layers were produced and evaluated with variable deposition processes.

The phase velocity could be determined with an accuracy of less than +-0.5m/s. The material properties of the dielectric layer were extracted and correlated with process variations.

CMUTs

Forum Hall

Wednesday, July 24 2013, 01:00 pm - 04:30 pm

Congress Hallair: **William Wright**
University College Cork

IUS5-PC-1

Application of CMUT as immunoassay sensor

Dovydas Barauskas[1], Asta Makaraviciute[2], Almira Ramanaviciene[2], Darius Virzonis[1], Gailius Vanagas[1], Arunas Ramanavicius[2]; [1]*Panevezys Institute, Kaunas University of Technology, Panevezys, Lithuania,* [2]*Faculty of Chemistry, Vilnius University, Lithuania*

Background, Motivation and Objective

Conventional use of CMUT in sensing applications involves mass resonance sensing approach, which gives extreme sensitivity in the gaseous medium due to low moving mass and good resonance quality. We demonstrated the CMUTs previously as immunoassay sensors, however reliable measurement in the real time remains challenging because of complex requirements for the sensor surface modification, bringing the analyte in the contact with the sensor surface and controlling the measurement conditions, especially as affinity reactions take place in liquid environment. The mass resonance sensing requires CMUT to be dry to maintain the adequate resonance quality. Therefore in this work we aim to analyze the impact of the experimental conditions to the informative content of the specific antigen-antibody interaction.

Statement of Contribution/Methods

We designed and fabricated the 1.3x1.3 mm CMUT arrays for 20 MHz frequency in air (see the micrograph of an array). For the immunoassay tests we used antigen-antibody system of bovine leukemia virus glycoprotein gp51 (Ag) and polyclonal antibodies against gp51 (Ab). Ag after the immobilization step was allowed to react with analyte, in this case, Ab. Two techniques of Ag immobilization were compared: a) gold-covered CMUT array surface was modified by the self assembled monolayer (SAM) of 11-mercaptoundecanoic acid and Ag was immobilized via EDC/NHS chemistry; b) direct Ag adsorption on the sensor surface with subsequent glutaraldehyde cross-linking. Sensors were DI water rinsed after each deposition, immobilization or interaction step. Resonance frequency and electromechanical resistance was measured after each processing step, so the sensor loading dynamics was completely traceable.

Results/Discussion

We observed the decrease of the resonance frequency (due to mass loading) up to 12 kHz after Ag immobilization and up to 33 kHz after affinity reaction. At the same time the decrease of the electromechanical resistance up to 25 Ω and up to 28 Ω was measured. More than double the difference of the frequency shift between Ag immobilization and affinity reaction steps is explained by the threefold antigen and antibody mass difference. Using SAM for antigen immobilization gave controversial results, since changes in resonant frequency was positive in some cases. The influence of elasticity of dry proteins is discussed.

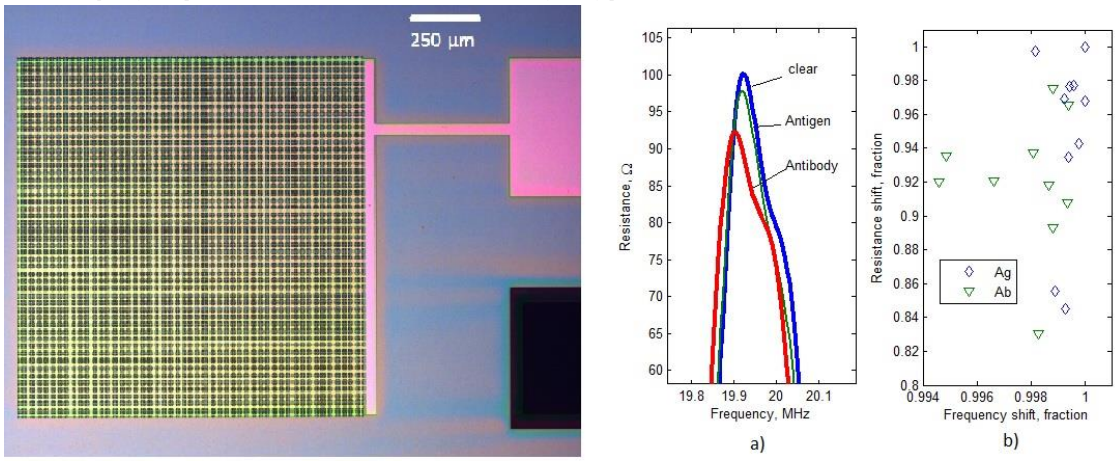

Left: micrograph of the CMUT arrray; Right: a) frequency spectra during different measurement steps; b) phase picture of frequency/resistance shifts over 10 CMUT arrays.

IUS5-PC-2

08:31 am **2-D Row-Column CMUT Arrays with an Open-Grid Support Structure**

Thomas Lehrmann Christiansen[1], Christian Dahl-Petersen[1], Jørgen Arendt Jensen[2], Erik Vilain Thomsen[1]; [1]*Department of Micro- and Nanotechnology, Technical University of Denmark, Kgs. Lyngby, Denmark,* [2]*Center for Fast Ultrasound Imaging, Dept. of Elec. Eng., Technical University of Denmark, Kgs. Lyngby, Denmark*

Background, Motivation and Objective

Capacitive micromachined ultrasonic transducers (CMUTs) require both well defined mechanical properties and high electric field strengths, the latter being achieved by using high voltages and small gaps between the electrodes of the CMUT. Therefore, designs have been proposed which incorporate both nano-scale gaps, thick insulation oxides supporting high voltages, and single crystalline plates through wafer bonding for precise control of the mechanical properties. However, for 2-D arrays, such designs incorporate through-wafer vias (TWVs) requiring high aspect ratio etching and via filling, severely complicating the fabrication process. Our objective is to propose a design with which 2-D arrays with row-column addressing can be fabricated in a 5 mask process utilizing an open-grid support structure that omits the use of TWVs without compromising the above mentioned qualities.

Statement of Contribution/Methods

The row-column CMUT design is illustrated in the figure. Two silicon on insulator (SOI) wafers (wafer A and B) with 20 µm device layers are used. On wafer A, a 164 nm oxide layer is grown. After a masked oxide etch, a second 136 nm oxidation is performed for pull-in isolation, yielding a vacuum gap height of 89 nm. Rows of bottom electrodes and posts are then etched in the oxide and the silicon device layer through a masked deep reactive ion etch (DRIE). Masked DRIE is also used for creating columns of top electrodes in the device layer of wafer B. After direct bonding of the two wafers, the handle of wafer B is thinned down to 40 µm in KOH, followed by a masked DRIE of the support structure. The final mask is used for defining aluminium contact pads for wire bonding.

Results/Discussion

The design allows the fabrication of nanometer precision gaps by using oxidation, and all DRIE uses oxide layers as etch stops. All electrical potentials are supported by the buried oxide layers and the CMUT electrodes are made from single crystalline silicon with a well defined thickness. The open-grid support structure defines the 180 µm square elements and enables the fabrication of bottom electrodes with no physical contact to the top electrode, thus avoiding oxide breakdown at high voltages. The support structure also implies that the bonding is non-critical and that no TWVs are needed. More detailed characterization results from the fabricated devices will be presented at the conference.

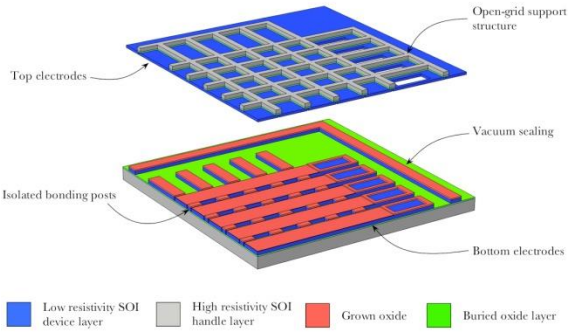

IUS5-PC-3

08:32 am **Interdigitated CMUT for Low Intensity Focused Ultrasound Delivery of Drugs**

Paul Cristman[1], Kwan-Kyu Park[1], Michael Mandella[2], Olav Solgaard[1], Christopher Contag[2], B. (Pierre) T. Khuri-Yakub[1]; [1]*E. L. Ginzton Laboratory, Stanford University, USA,* [2]*Pediatrics, Stanford University, USA*

Background, Motivation and Objective

Early stage cancer detection is critical for successful treatment. One promising advance has been the creation of molecular contrast agents. For better signal quality there is a need to improve contrast agent delivery, activation, and uptake. Often the signal quality is improved by systemic delivery of a relatively high dose of the agent to the entire body. Systemic delivery and large doses have caused toxicity and other problems when translating from animals to humans. One option is to apply low intensity focused ultrasound directly to the region to be imaged. Low intensity focused ultrasound has been used for years to aid local drug delivery. This technique could enable contrast agents to be applied locally and in smaller doses. The goal of this work is to combine an interdigitated capacitive micromachined ultrasonic transducer (CMUT) with a miniature dual axis confocal (DAC) fluorescence microscope. The DAC microscope is used to image fluorescent contrast agents that bind specifically to cancer cells. The field of view of the DAC microscope is limited to a depth of 300 µm making the application of ultrasound energy difficult. In order to overlap the acoustic pressure field with the optical field and not interfere with the lens optics interface waves must be exploited.

Statement of Contribution/Methods

Interdigitated CMUTs have been used for a range of applications including sensing, mixing, and pumping. For this application a circularly symmetric interdigitated CMUT with an open center lumen for the optics is used to focus the interface waves into the field of view of the optics. We have fabricated a wide variety of interdigitated CMUT designs with ring pitches ranging from 40 µm to 80 µm. At 5 MHz these devices have shown good focusing and peak pressure over 50 kPa at the surface of the element.

Results/Discussion

To test the basic concept the CMUT device was used to improve the signal quality of fluorescent dyes on a bench top fluorescent microscope on samples with and without ultrasound treatment. For the first tests the CMUT device was encapsulated using a thin polyurethane coating to keep it from shorting when immersed in the fluorescent dye solution. Tests using chicken breast tissue showed samples exposed to ultrasound had an increase in the average and maximum fluorescence compared to samples with no ultrasound.

Work supported by NIH Project: 5U54CA136465

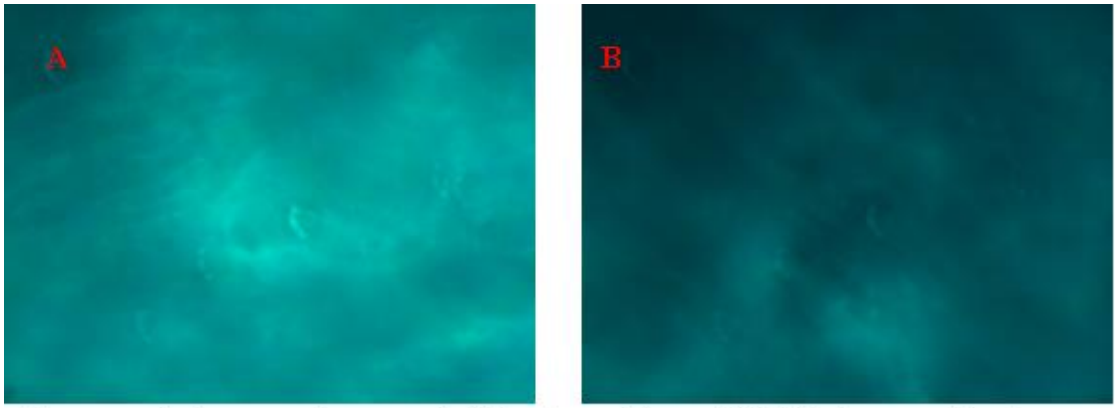

Fluorescent microscope images of chicken breast tissue A) With ultrasound for 5 minutes average signal 93 a.u. maximum signal 149 a.u. B) No ultrasound soak for 5 minutes average signal 51 a.u. maximum signal 93 a.u.

IUS5-PC-4

08:33 am **Characterization of a mid-volume fabrication process for CMUT development**

Anartz Unamuno[1], Martin Friedrichs[1], Werner Jeroch[1], Heinrich Grüger[1]; [1]*Fraunhofer IPMS, Germany*

Background, Motivation and Objective

The first steps taken towards widening the access to low/mid-volume fabrication of CMUTs are presented here. Too often, promising developments in research or industrial (SMEs) environment fail to reach the market due to limitations in the access to high quality low/mid-volume fabrication facilities. In this work, a possible CMUT integration has been conceptualized, fabricated and characterized and a 1D CMUT array is used to demonstrate the capabilities of the facility and the selected fabrication process.

Statement of Contribution/Methods

A 1D CMUT array was built based on a sacrificial release technology available within the fabrication facilities at Fraunhofer IPMS. Mechanical deflection measurements of the elements within the array and array-to-array (within wafer) will be performed using white light interferometry, proving the homogeneity across the array and within the wafer. Electrical impedance measurements in air will also be performed and reported.

Results/Discussion

The first lot of a new process to build CMUTs is being run through the fabrication facilities at Fraunhofer IPMS, where a 1D CMUT array has been implemented as a demonstrator. Figure 1 shows a X-SEM image of an element of the 1D CMUT array. Wafer maps of mechanical deflection due to stress and atmospheric pressure will be shown, describing the process homogeneity of the elements across the array and across the array. In addition, electrical impedance results will be mapped for CMUT elements.

The work here presented aims to prove the capabilities of Fraunhofer IPMS for low/mid-volume fabrication of CMUTs. The chosen process could provide operating frequency ranges between 100's of KHz and 10's of MHz, that could be adjusted for each application.

Figure 1: X-SEM image of a wafer processed at Fraunhofer IPMS, showing a cut through a single CMUT element.

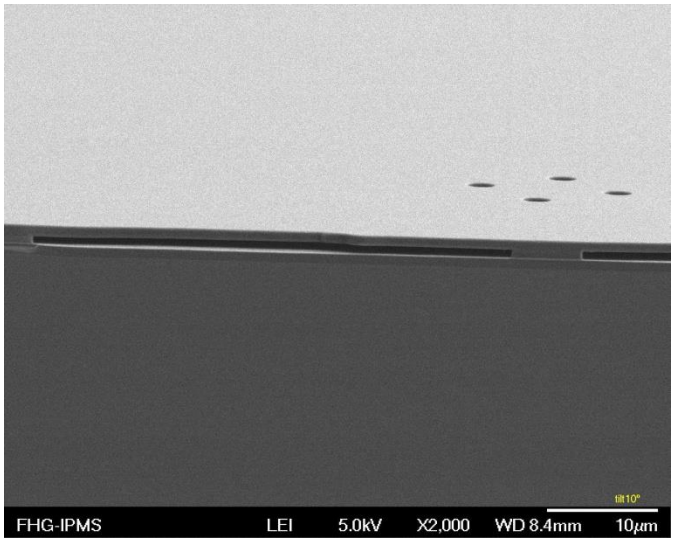

IUS5-PC-5

08:34 am **A Tethered Front-Plate Electrode CMUT for Broadband Air-Coupled Ultrasound**

William Wright[1], Sean McSweeney[1]; [1]*Electrical and Electronic Engineering, University College Cork, Cork, Co. Cork, Ireland*

Background, Motivation and Objective

Capacitive micromachined ultrasonic transducers (CMUTs) typically consist of a back-plate electrode on a substrate wafer, separated from a front-plate electrode by a small cavity. Various micromachining and wafer bonding techniques of CMUT manufacture have been described previously in the literature. When operating in air, the majority of these CMUTs are highly resonant and the CMUT structures are usually sealed. However, for air-coupled applications, this sealing is not strictly necessary, allowing other more open CMUT structures to be explored. Parameters that influence CMUT bandwidth include the front-plate electrode mass and stiffness, the compliance of the electrode gap, and front-plate damping. A novel CMUT structure specifically for air-coupled operation was investigated, consisting of an open-edged front-plate electrode that was tethered at only a few points around its periphery. The front-plate was made from aluminium to give a lower mass and stiffness in comparison to more conventional front-plate materials, and perforated to increase the overall squeeze-film damping and hence the bandwidth of the device.

Statement of Contribution/Methods

A series of devices was manufactured in a standard CMOS process using a sacrificial polyimide etch to leave a free-standing aluminium front-plate electrode of thickness 1.0µm with a nominal electrode gap of 1.5µm. The square devices ranged in size up to 800µm x 800µm, with a number of thin tethers along the device edges attaching the front-plate electrode to the substrate. This produced a novel CMUT structure that was open at the edges, with a low front-plate stiffness and high squeeze-film damping. A 1-D analytical model was formulated to predict the response of the devices, and compared to the electrical response and ultrasonic response of the manufactured CMUT.

Results/Discussion

The structures were not optimized, but initial results on the prototypes were promising. The devices had a pull-in voltage of only 5 V and a nominal capacitance of 70 pF. The devices were tested as transmitters and receivers over a 20 mm path in air, using a well-characterized broadband transducer as a standard transmitter or receiver. The tethered CMUTs had a center frequency of 250 kHz with a usable bandwidth of over 1 MHz in air, giving a Q-factor of significantly less than 1. However, the devices were not very efficient, with an insertion loss of almost 70 dB and highly damped as expected. The 1-D analytical model also gave reasonably good agreement with the experimental measurements.

IUS5-PC-6

08:35 am **Characterization and operation of different CMUT membranes for gas-flow sensing applications**

Alessandro Caspani[1], Giacomo Langfelder[1], Paolo Minotti[1], Antonio Longoni[1], Jaakko Saarilahti[2]; [1]*Dipartimento di Elettronica, Informazione e Bioingegneria, Politecnico di Milano, Milano, Italy,* [2]*VTT Technical Research Centre of Finland, Espoo, Finland*

Background, Motivation and Objective

Capacitive Micromachined Ultrasonic Transducers (CMUT) allow the emission and detection of ultrasounds (US) and can find application in several fields (medical imaging, flow control, gesture recognition). Careful process tuning is fundamental in defining the devices performance and repeatability. The work presents a thorough electromechanical characterization of different CMUT membranes optimized for gas-flow sensing, and shows US measurements for the different devices.

Statement of Contribution/Methods

Membranes are designed with different diameters (40 to 60 µm) and material stacks (silicon nitride, polysilicon and aluminum), vacuum sealing the cavity with porous polysilicon. Electromechanical characterization is performed to validate the modeling and check the process repeatability. Fig. 1a shows admittance curves for different DC voltages of one membrane, from which its resonance frequency is found. The measurement is repeated for all the devices: Fig. 1b plots the evaluated peak frequency as a function of the membrane diameter.

Results/Discussion

CMUTs are then calibrated in terms of sensitivity to ultrasonic pressure generated by a reference source (Ultran NCT5-D3). The electronics to read the current induced by membrane vibrations is based on an integrator-differentiator scheme that implements a wide-bandwidth (80 MHz) transimpedance gain.

Fig. 2a shows the voltage generating the source burst, and the corresponding signal detected by the CMUT at its peak frequency in air. Fig. 2b shows the amplitude of the signal received by the CMUT as a function of the distance from the source, for two voltages applied at the membrane. Results match the predictions in terms of propagation delay and attenuation, confirming the possibility to operate CMUT systems as gas-flow sensors.

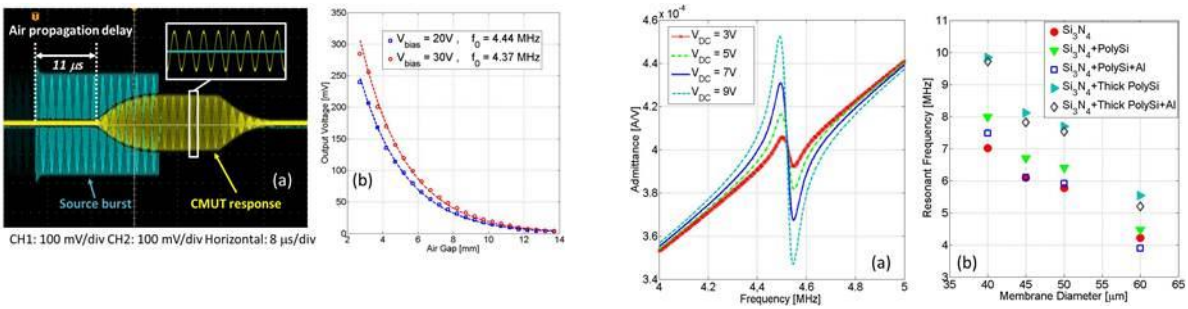

IUS5-PC-7

08:36 am **Experimental evaluation of CMUTs with vented cavities under varying pressure**

Nikhil Apte[1], **Kwan Kyu Park**[1], Butrus T. Khuri-Yakub[1]; [1]*E. L. Ginzton Laboratory, Stanford University, Stanford, California, USA*

Background, Motivation and Objective

Previously, we proposed CMUTs with pressurized cavities to operate over a wide pressure range (up to many atmospheres). One way to pressurize the cavity is by venting it to the ambient air, and thus equalizing the pressure across the CMUT plate. This approach ensures the CMUT plate would have a steady DC operating point under any pressure. Also, such a structure can withstand any pressure without the danger of mechanical failure. One application for such devices is air flow measurement in harsh environments with widely varying pressures and temperatures. A pair of CMUTs with vented cavities can be used in a pitch-catch setup in such an environment to measure air flow. The objective of this work is to fabricate CMUTs with vented cavities and to analyze their behavior under high ambient pressure in a pitch-catch setup.

Statement of Contribution/Methods

We fabricated a variety of CMUTs with vented cavities. The CMUTs had a plate thickness ranging from 10 µm up to 20 µm, gap height varying from 3 µm up to 11 µm, and plate radius varying from 500 µm up to 1500 µm. The CMUTs were fabricated using the wafer bonding technique. Highly conductive silicon plates were bonded on pre-defined cavities. The CMUTs were vented using through-wafer vias under the cavities. The number and location of the venting vias were also varied.

The fabricated CMUTs were mounted on chip carriers and initially tested under a laser Doppler vibrometer at 1 atm pressure. A pair of CMUTs from a selected design was then tested in a pitch-catch setup. This CMUT design had a 750 µm radius, and a 20 µm thick plate. The CMUTs were vented with 21 vias of 40 µm diameter through the substrate. The pair was mounted on a fixture inside a pressure chamber and the pressure was varied from 1.01 bar (1 atm) up to 20 bar, and the pitch catch signal was recorded.

Results/Discussion

We observe that this structure has two operating frequencies. One operating frequency is slightly higher than the resonant frequency of the plate (125 kHz). The signal from this mode gets weaker at higher pressures, and also the frequency and fractional bandwidth of this mode decreases with increasing pressure. In contrast, the signal from another mode at lower frequency becomes stronger with increasing pressure. The frequency and bandwidth of this mode remain quite stable. We are currently investigating these two modes of operation for such a CMUT structure.

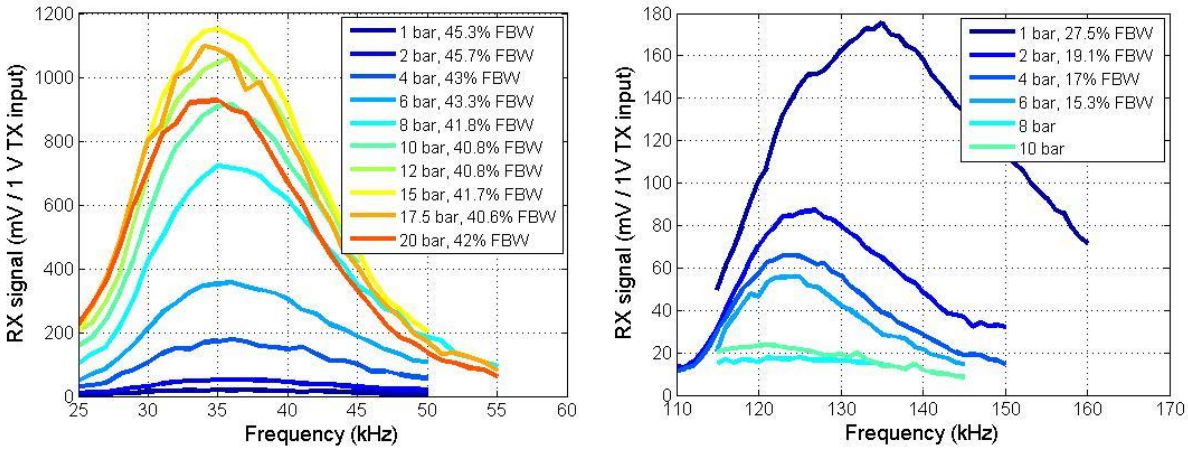

Fig. 1 Pitch-catch frequency spectrum

IUS5-PC-8

08:37 am **Pre-Charged CMUTs with Efficient Zero-Bias Voltage Operation for Medical Applications**

Abhijeet Kshirsagar[1], Alexander Sampaleanu[1], Roger Zemp[1]; [1]*Department of Electrical & Computer Engineering, University of Alberta, Edmonton, Alberta, Alberta, Canada*

Background, Motivation and Objective

Capacitive micro-machined ultrasonic transducers (CMUTs) require a dc bias voltage to establish an electric field across the two electrodes for operation. In pre-collapse mode, CMUTs typically operate more efficiently at larger applied bias voltages. However, the need to apply a DC bias during CMUT operation also imposes additional challenges, such as increased complexity in circuitry design, and the need for protective schemes to comply with electrical safety regulations for medical applications. These drawbacks become increasingly apparent as the CMUT snapdown voltage (and hence the required DC bias for more efficient operation) increases.

Traditionally, dielectric charging has been viewed as an undesirable feature of CMUTs, since charging can alter performance of devices and lead to permanent membrane collapse. We use a beneficial aspect of dielectric charging in CMUTs and demonstrate CMUTs that may be pre-charged such that the collapse voltage is shifted. At zero applied bias voltage they experience a much higher transmit power and receive sensitivity due to the trapped dielectric charge providing an intrinsic rather than external bias. While pre-charging strategies have previously been proposed, previous studies did not test long-term reliability of zero-bias operation and were not for diagnostic frequency devices. This is surprising since avoiding high voltages in medical applications is particularly critical.

Statement of Contribution/Methods

CMUTs have been fabricated using a modified sacrificial release process that we have previously reported. A Keithley Semiconductor Characterization System was used to measure capacitance vs. voltage curves at intervals during the charging process ensure the shift in the snapdown voltage reached desired levels. Vibrometer and hydrophone measurements were also taken before and after CMUT charging to measure dynamic displacement and pressure signals, respectively. Charging was accomplished by collapsing the devices and holding them at >150% of their snapdown voltage for a prolonged time. After charging, displacement and pressure measurements were taken in both air-coupled and immersion operation over extended time periods to characterize the lifetime of efficient zero-bias operation.

Results/Discussion

Uncharged CMUTs exhibited collapse voltages around 30V and zero-bias displacement of around 570pm in response to a 10V pseudo-random signal. After being charged by being held in collapse mode continuously over ~16 hours, the same CMUTs were observed to have a snapdown voltage of closer to 50V, and the same signal caused a displacement of over 8.5nm, an output almost 15 times higher than that of pre-charged CMUTs. Preliminary results show that after days of pre-collapse operation, membrane displacement at zero-bias decreased only marginally. Our approach offers advantages especially for medical applications where high bias voltages are undesirable for patient safety.

IUS5-PC-9

08:38 am **Traceable characterization of cMUT membrane motion**

Tor Paulin[1], Anton Nolvi[1], Ville Heikkinen[1], Ivan Kassamakov[2], Edward Hæggström[1]; [1]*Department of Physical Sciences, University of Helsinki, Helsinki, Uusimaa, Finland,* [2]*Helsinki Institute of Physics, University of Helsinki, Helsinki, Uusimaa, Finland*

Background, Motivation and Objective

Silicon micro-machining permits tailoring the membranes of cMUTs. The membrane motion determines transducer performance. In a thrust towards traceable characterization of cMUT membrane movement we compared a full field 3D imaging technique with a rastered laser doppler vibrometry (LDV) technique. 3D profiles of a moving cMUT membrane oscillating at 2.72 MHz were measured using stroboscopic scanning white light interferometry (SSWLI). In SSWLI pulsed illumination is synchronized with sample oscillation. SSWLI characterizes in-plane and out-of-plane sample motion. A broadband, rapidly switchable and stable, light source is essential. Such sources can't be bought.

Our custom hybrid source comprises a non-phosphor white light LED (L-513NPWC-15D) combined with a cyan LED (EL-333-2UBGC/S400-A4) and a beam splitter (NT46-669). The emis-sion was adjusted by regulating the input current to have a broad Gaussian spectrum and to avoid interferogram ringing. Our source features a peak wavelength of 504 ± 1.0 nm, FWHM of 46 ± 1.5 nm, and a minimum pulse width FDHM of 8.42 ± 0.10 ns. Our custom-built LED driver has an integrated MOSFET driver (IXDD415SI).

Statement of Contribution/Methods

Device: a cMUT was operated (30 VDC bias, 2.5 VAC), in the lab. A controlled phase angle was introduced between the cMUT drive signals and the source. LDV data was recorded as follows; the cMUT membrane was manually scanned using a translation stage and displacement data recorded with an oscilloscope, whereas SSWLI data was recorded as follows; changes in topography in pixels corresponding LDV measurements were recorded and compared pixel-by-pixel to the LDV data. Measurement time: 20min (24 scans, SSWLI), and 3 min (6 points, LDV).

A sine was fitted to both SSWLI (24 measurements at intervals of 30 degree phase shift) and LDV measurements (single point) at 6 points. The precision for the sine fits (95% confidence interval) was 17.6 nm (SSWLI) and 0.29 nm (LDV). The measured amplitude difference, comparing SSWLI with LDV, at these points was 10 ± 20 nm.

Results/Discussion

We characterized a cMUT membrane oscillating at 2.72 MHz with 10 ± 20 nm precision. This is important because some defects are invisible in LDV point- or/and static 3D measurements. Our achievement advances the quality control of US transducers by enabling high frequency dynamic characterization with nm precision.

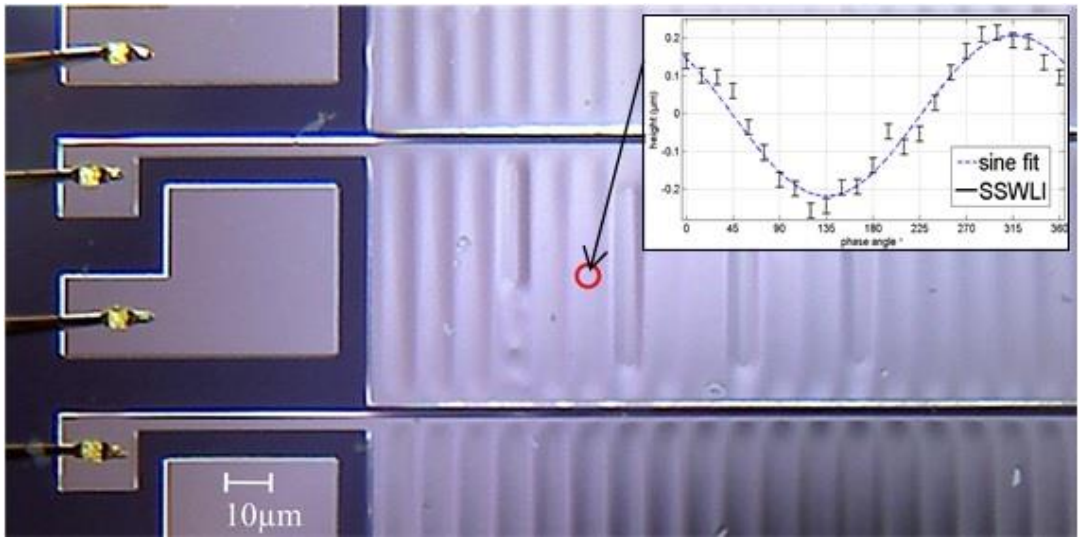

IUS5-PC-10

08:39 am **Fabrication of CMUTs with substrate-embedded springs**

Byung Chul Lee[1], **Amin Nikoozadeh[1]**, Kwan-Kyu Park[1], Butrus T. Khuri-Yakub[1]; *[1]E.L. Ginzton Laboratory, Stanford University, USA*

Background, Motivation and Objective

We have previously reported on a CMUT with substrate-embedded springs called post-CMUT (PCMUT). The PCMUT decouples the spring constant and the mass of the system by realizing the former using relatively long and narrow posts. The PCMUT improves on the fill factor and average volume displacement of the conventional CMUT as shown in our previous work using 3-D FEA. We have also demonstrated the functionality of the PCMUT using a simple fabrication process, however, this process suffered from several issues including post height non-uniformity. This work reports on second-generation PCMUT devices designed according to our FEA simulation results and manufactured using an improved fabrication process flow.

Statement of Contribution/Methods

Our first-generation PCMUT fabrication process did not yield uniform post height nor offered a clear path toward making 2-D arrays. Hence, we are developing a new fabrication process to address these issues. The proposed fabrication process is composed of three critical steps: deep reactive-ion etching (DRIE) of posts (i.e., springs), wafer bonding of two silicon-on-insulator (SOI) wafers, and precision wafer polishing.

The process starts with an SOI substrate wafer having a device layer of 50 ìm. This wafer is oxidized and patterned to define the PCMUT cavities. Then, the wafer goes through a second thermal oxidation that defines the cavity height. Next, shallow trenches are etched into the device layer using a reactive-ion etching process in order to maintain device symmetry and avoid undesired operation modes. Silicon posts and bottom electrode isolation pattern are then defined using a DRIE process by etching through the 50-ìm device layer. Particular attention should be given to this step since the posts are one of most important components of a PCMUT. After a short oxidation to passivate the exposed sidewalls, another SOI wafer is bonded to the substrate SOI wafer using a fusion bonding process under vacuum. The handle of the bonded SOI wafer is then polished to a final thickness of 20 ± 1 ìm for the stiff section of the PCMUT top plate. Then, the remaining handle layer and the box layer of the SOI wafer is patterned and etched to define the top plate. The 250-nm thick device layer of this SOI wafer constitutes the edge section of the top plate. Finally, the electrical connections to top and bottom electrodes are created using silicon and oxide etching and aluminum deposition steps.

Results/Discussion

82-element 1-D arrays, 2×2 2-D arrays, high-intensity focused ultrasound (HIFU) arrays, and test structures were fabricated using the proposed process flow. Electrical input impedance measurements in air confirmed the functionality of the fabricated devices. However, our first attempt resulted in low yield due to poor wafer bonding quality. We are currently working on improving the bonding quality in our second run to increase the yield.

This work is supported by the National Institutes of Health and Analog Devices.

08:40 am **Void-Free Direct Bonding of CMUT Arrays with Single Crystalline Plates and Pull-In Isolation**

Thomas Lehrmann Christiansen[1], Jørgen Arendt Jensen[2], Erik Vilain Thomsen[1]; [1]*Department of Micro- and Nanotechnology, Technical University of Denmark, Kgs. Lyngby, Denmark,* [2]*Center for Fast Ultrasound Imaging, Dept. of Elec. Eng., Technical University of Denmark, Kgs. Lyngby, Denmark*

Background, Motivation and Objective

Capacitive micromachined ultrasonic transducers (CMUTs) can be fabricated using direct bonding of two silicon wafers, one of which has an oxide layer with etched cavities. However, in order to avoid short circuiting during pull-in, a second oxide is often made at the bottom of the cavities by performing a second oxidation after the cavity etch. Yet, this creates protrusions at the cavity edges, see figure, resulting in bonding issues for closely spaced cavities. Subsequent steps must therefore be used to remove these protrusions, which may limit the yield. Alternatives such as placing the pull-in insulation on the plate is undesirable as the residual oxide stress will counteract the advantages of having single crystalline plates. Our objective is to demonstrate how void-free bonding of CMUTs with single crystalline plates and pull-in isolation can be achieved by simply defining the oxide cavities on the plate and the pull-in isolation on the substrate wafer.

Statement of Contribution/Methods

CMUT arrays containing 324, 2304 or 9216 circular or square cavities with a diameter/side length of 72 µm and a pitch of 92 µm were fabricated using both a double oxidation process and the process proposed herein (to the left and right, respectively, in the figure). In the first process, a 403 nm oxide was grown on the substrate wafer followed by cavity definition using lithography and dry etching of the oxide. Subsequently, the wafer was re-oxidized giving 195 nm insulation oxide in the bottom of the cavities. This double oxidation generated protrusions measured to be in the order of 30 nm in height, consistent with simulations in Silvaco Athena 5.20.0.R. An RCA clean was done prior to fusion bonding to a silicon on insulator (SOI) wafer with 2 µm device layer followed by 70 minutes of annealing at 1100 °C. Finally, the SOI handle was removed in a deep reactive ion etch. Our proposed process was identical except that the cavities were defined on the SOI wafer and the insulation oxide was grown on the substrate wafer.

Results/Discussion

The top left part of the figure shows multiple detached top plates on the double-oxidized CMUTs after removing the handle down to the buried oxide resulting in a bonding yield of 7 %. As opposed to this, a 100 % bonding yield is seen for the proposed process (top right in the figure). Note that this is achieved without additional processing steps and without altering the CMUT structure.

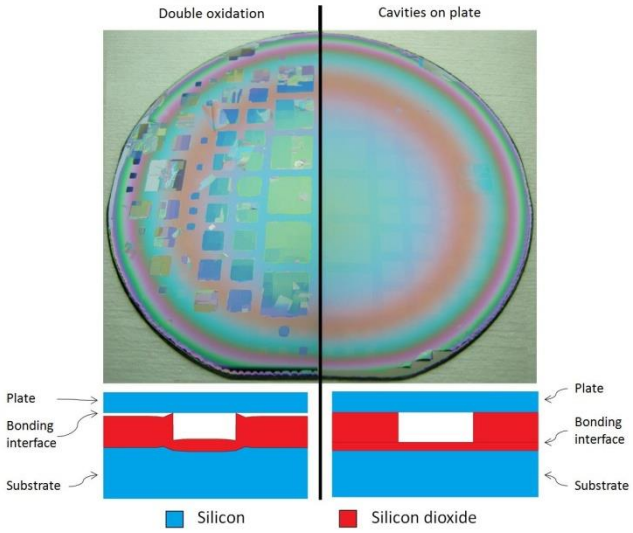

Blood flow and vector velocity imaging applications

CONGRESS HALL

Thursday, July 25 2013, 08:30 am - 10:00 am

Congress Hallair: **Alfred Yu**
The University of Hong Kong

IUS1-K1-1

In vivo transthoracic ultrafast Doppler imaging of Left intraventricular blood flow pattern

Bruno-Felix osmanski[1], Mathieu Pernot[1], Mathias Fink[1], Emmanuel Messas[2], Mickael Tanter[1]; *[1]Institut Langevin, ESPCI ParisTech, CNRS UMR7587, Inserm U979, UniversitÃ© Paris 7, Paris, Ile de France, France, [2]Hospital européen Georges Pompidou, France*

Background, Motivation and Objective

Mechanistic heart diseases can affect intraventricular blood flow pattern. Standard ultrasound Doppler lacks frame rate and sensitivity leading to a description of blood flow patterns only in ejection and diastasis phase. Our motivation is to use ultrafast circular wave imaging for 2D mapping of blood flow in the left ventricle during the whole cardiac cycle without any use of contrast agent. The high spatio temporal sampling permits to rely on more effective wall filtering, increase sensitivity and resolution to map pre-ejection, early diastole and late diastole phase. The study of these patterns could increase accuracy of the diagnosis.

Statement of Contribution/Methods

The experiment is carried out on healthy human volunteers (N=3) monitored by an ECG. The transducer array (64 elts, 2.75MHz, 0.28 µm pitch) is placed against the chest. The heart is imaged from the apex (four chambers view) at ultrafast frame rate (2.4KHz) using 2 cylindrical waves emitted from virtual point sources (focal depth -2 mm) placed behind the probe during a complete cardiac cycle (1s). Coherent summation of the backscattered echoes are performed for the 2 successive transmits. For each pixel of the 2D image a Doppler signal of 2400 time samples is obtained after adaptive high pass filtering (Butterworth with different cutoff frequency along the cardiac cycle).

Results/Discussion

During pre-ejection we notice high turbulences (fig1.A) then flow speed increases during the ejection phase (fig 1.B), we notice some aliasing near the aortic root. After the opening of the mitral valve (MV) we see a flow going toward the apex (fig 1.C), then a vortex appears during the diastasis (fig 1.D). We also noticed a dramatic increase of speed toward the apex in the late diastole (fig 1.E) before the closure of the MV. Same features were observed for all volunteers.

The high framerate of ultrafast imaging permitted an accurate clutter filtering on intraventricular flows. Although a comprehensive validation study is required, ultrafast imaging offers the possibility of studying a number of unexplored aspects of intraventricular flow dynamics. Previous work with microbubbles on porcine heart have shown that patterns of pre-ejection in 2D can be important to quantify the effect of electromechanical disorders on intracardiac rheology. Ultrafast Doppler could lead to similar information without microbubble injection.

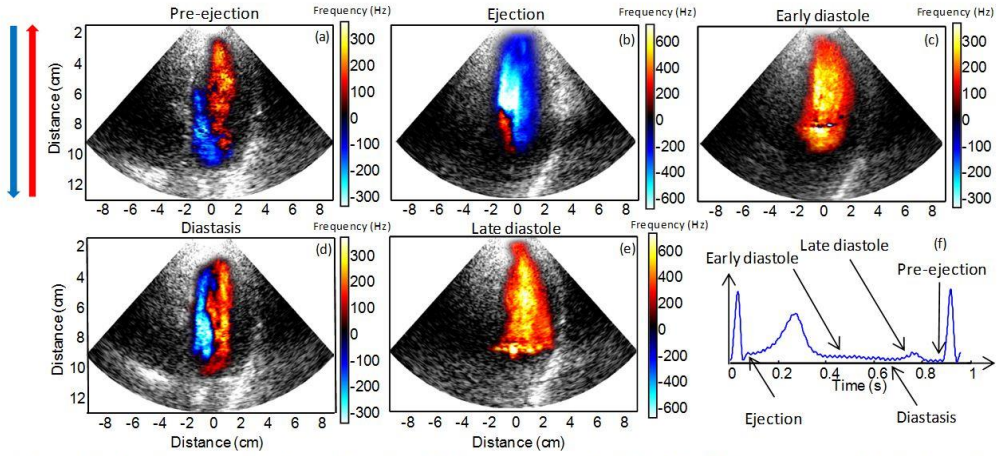

Figure: Color Doppler images of (a) Pre-ejection phase, (b) Ejection phase, (c) Early diastole, (d) Diastasis, (e) Late Diastole. The color Doppler is displayed with standard convention: Blood flowing respectively toward and downward the probe are displayed in respectively red and blue. (f) Patient ECG.

IUS1-K1-2

Intraoperative vector flow imaging of the heart

Kristoffer Hansen[1], Mads Pedersen[1], Hasse Møller-Sørensen[2], Jesper Kjærgaard[3], Jens Christian Nilsson[2], Jens Lund[4], Jørgen Jensen[5], Michael Nielsen[1]; *[1]Department of Radiology, Copenhagen University Hospital, Copenhagen, Denmark, [2]Department of Cardiothoracic Anesthesiology, Copenhagen University Hospital, Copenhagen, Denmark, [3]Department of Cardiology, Copenhagen University Hospital, Copenhagen, Denmark, [4]Department of Cardiothoracic Surgery, Copenhagen University Hospital, Copenhagen, Denmark, [5]Technical University of Denmark, Center for Fast Ultrasound Imaging, Denmark*

Background, Motivation and Objective

The objective of this study was to estimate cardiac blood flow intraoperatively using the vector flow method Transverse Oscillation (TO), which provides quantitative, real-time, angle-independent blood flow estimates. Velocity estimates obtained with conventional ultrasound are one-dimensional and angle-dependent, making it difficult to measure the complex cardiac blood flow. This can lead to erronous measurements in standard examinations and limits the usabilty in certain complex cardiac geometries.

Statement of Contribution/Methods

TO is implemented on a commercial scanner (Pro Focus 2202 UltraView, BK Medical) with a linear transducer (Type: 8670, BK Medical). During surgery three patients were scanned directly on the heart over the aortic valve, the pulmonary artery and the right atrium. For comparison, simultaneous measurements were obtained with conventional spectral Doppler (SD) and intravenous catheter thermodilution technique (TD).

Results/Discussion

The examinations revealed early systolic vortical flow filling of the aortic sinuses, central antegrade flow and retrograde wall-near flow in the ascending aorta. Vector flow estimates of the ascending aorta were compared to SD and TD. Peak systolic velocities were underestimated by 18% compared to SD and cardiac output was underestimated by 16% compared to TD. A clock-wise secondary flow was present in the ascending aorta during late systole and early diastole, and stable vortices were created in the aortic sinuses during diastole. During systole, central antegrade flow with retrograde wall-near flow were observed in the pulmonary artery and the flow patterns during closure of the pulmonary valve were visualized. For one patient the right atrium was examined and a stable vortex was seen during the entire cardiac cycle.

This is the first time vector flow measurements have been obtained of cardiac flow. TO can potentially reveal new information of cardiovascular physiology and blood flow dynamics, and become a valuable tool in e.g. cardiac output estimation, valve surgery and assessment of congenital heart defects and acquired heart diseases.

Fig. 1: Systolic antegrade flow in the ascending aorta is seen with retrograde flow along the vessel walls and vortices in the aortic sinuses. The colormap and arrows indicate velocity and direction of the blood flow.

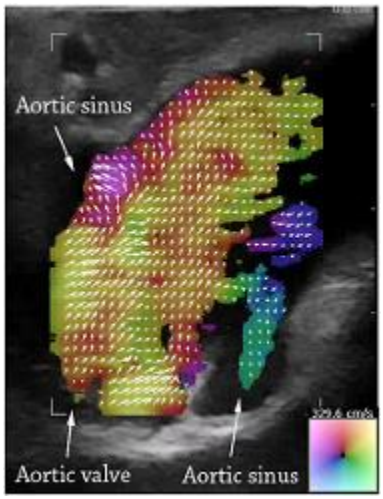

IUS1-K1-3

Getting intraventricular velocity vector fields from color Doppler: a simplified effective method

Damien Garcia[1], Louis Le Tarnec[1], Jean Sharestan[2], Dominique Auger[2], François Tournoux[2]; *[1]RUBIC - Research Unit of Biomechanics & Imaging in Cardiology, CRCHUM - Research Centre, University of Montreal, Montreal, Quebec, Canada, [2]Department of echocardiography, CHUM - University of Montreal Hospital, Montreal, Quebec, Canada*

Background, Motivation and Objective

Comprehensive intracardiac velocity mapping can be measured by phase-contrast magnetic resonance (MR). MR techniques, however, cannot be part of routine clinical set-up. In parallel to MR, echo-particle image velocimetry (echo-PIV) has been proposed to decipher the velocity vector field in the left ventricle. Echo-PIV applied on contrast enhanced echocardiographic images is able to track ultrasound speckle displacements. This technique requires a continuous intravenous infusion of contrast agent to reach an image quality suitable for motion tracking, which limits its application in everyday clinical practice. Recently, Garcia *et al.* [*IEEE TMI* 29, 2010] and Uejima *et al.* [*UMB* 36, 2010] proposed original intraventricular vector flow mapping (IV^2FM) techniques based on conventional color Doppler echocardiography. The objective of this study was to update Garcia's IV^2FM method to make it faster, more clinically-compliant and readily available for clinical studies.

Statement of Contribution/Methods

Clinical color Doppler images of the left ventricle were acquired in patients in the apical 3-chamber long-axis view with a Vivid ultrasound scanner (GE Healthcare). The Doppler raw data were extracted using the clinical GE workstation EchoPAC and denoised by a robust & unsupervised penalized least-squares method [Muth *et al.*, *MedIA* 15, 2011]. A fast coarse segmentation was performed to delineate the region-of-interest. An optimization method was then used in the polar coordinate system: the cross-beam angular velocity components were determined by minimizing a functional depending on the flow divergence and on the boundary cross-beam velocities. The polar velocity vector components were finally transformed to Cartesian coordinates and IV^2FM images were created by overlaying the vector fields over B-mode images (see Fig).

Results/Discussion

Application of the updated technique in several patients shows that IV^2FM is clinically simple, effective and little operator-dependent. Using this technique, intraventricular vortices can be easily detected using the Q-criterion or other techniques (see Fig). Color Doppler IV^2FM remains to be compared *in vivo* with MR velocimetry. The clinical relevance of such a tool for a better assessment of the diastolic dysfunction is presently under investigation.

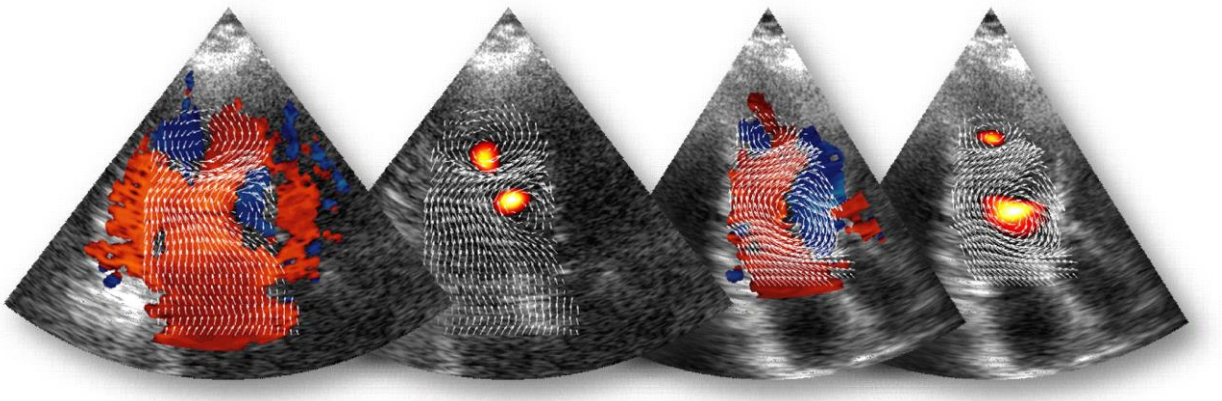

Fig. 1 – IntraVentricular Vector Flow Mapping by color Doppler. Illustration in 2 patients. The vector field is overlaid with 1) the Doppler data, 2) the vortex detection Q-criterion.

IUS1-K1-4

The computer simulation of microscopic interactions of RBC aggregation based on the depletion model under pulsatile flow

QI KONG[1], YING LI[2], TAE-HOON BOK[1], KWEON-HO NAM[1], DONG-GUK PAENG[1]; *[1]Ocean System Engineering, JEJU National University, Korea, Republic of, [2]Biomedical Engineering, University of Southern California, USA*

Background, Motivation and Objective

In a blood vessel, the main scatterers of Ultrasound (US) waves are the red blood cells(RBCs) and their aggregation. The depletion model proposes RBC aggregation formed from osmotic attractive forces due to polymer depletion, which overcome electrostatic repulsion due to RBC surface charge. Previous studies of simulation model under steady flow elucidated the relationship between shear rate and RBC aggregation. But shear rate could not fully explain the cyclic variation of backscattered power from blood under pulsatile flow. The flow acceleration was suggested as another hemodynamic factor to affect the RBC aggregation.

Statement of Contribution/Methods

In the current study, a two-dimensional particle model capable of RBC mimicking the main characteristics of RBC aggregation kinetics was proposed to elucidate the relationship between microscopic RBC interactions and macroscopic rheological behavior. The mechanical model of RBCs is depletion model under pulsatile flow. There are 596 RBCs randomly placed in a vessel (0.1X1mm) in the model driven by hydrodynamic force, aggregation force and elastic force. The mean flow velocity at the center of the tube was 2cm/s and the variation was 0.5~1.5cm/s and stoke rate was changed from 60 to 80 beats per minute (bpm).

Results/Discussion

The results show mean aggregated size (MAS) was increased as velocity amplitude variation was changed from 0.5 to 1.5cm/s. The maximum MAS happened when the aggregated number decreased. Another finding was that the time to reach the maximum of RBC MAS is shorter as stroke rate was increased from 60 to 80 bpm. In addition, MAS variation was related with mean velocity, and hematocrit. The numerical simulation showed 'Bright collapsing ring' during systole as shown in Figure 1, which is in good agreement with the experimental measurements and all simulation results were summarized in Table 1. Acknowledgement: This research was supported by NIPA-2013-H0401-13-1007.

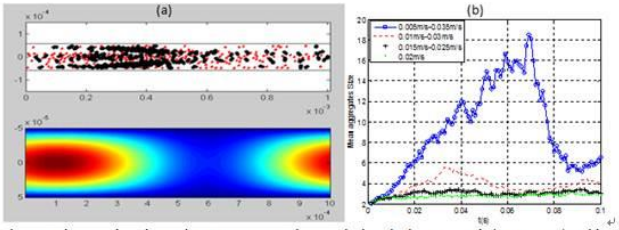

Fig. 1: The results showed RBC aggregation variation is in a vessel (0.1X1mm) with 40% hematocrit in the model and flow velocity profile at one time (a). Mean aggregated size(MAS) was changed as a function of time at different velocities (b).

Table. 1: Descriptive Statistics of mean aggregated size and aggregated number variation in the different condition of velocity amplitude deviation, mean velocity, stroke rate and hematocrit.

	Variation Range	Mean aggregated size (Maximum, $10^{-10}m^2$)	Aggregated number (Maximum)
Flow velocity amplitude	1~3cm/s	1.5~9	120~140
Mean velocity	2~10cm/s	1.5~10	120~140
Stroke rate	60~80bpm	5.5~9	80~140
Hematocrit	6%~40%	2.5~10	30~140

IUS1-K1-5

Optimization of transverse oscillating fields for vector velocity estimation with convex arrays

Jørgen Arendt Jensen[1]; *[1]Center for Fast Ultrasound Imaging, Dept. of Elec. Eng., Technical University of Denmark, Kgs. Lyngby, Denmark*

Background, Motivation and Objective

Vector velocity imaging using the transverse oscillation (TO) approach has recently been introduced on the market. The current method employs linear array transducers, which limits the field of view. A further development with increased field of view and penetration depth is, thus, needed for e.g. abdominal scanning. This can be attained using convex array transducers. The paper presents optimization schemes for TO fields for convex probes and evaluates their performance using Field II simulations.

Statement of Contribution/Methods

The TO approach introduces a transverse oscillation for estimating the lateral velocity component. A weakly focused field is transmitted and focused in receive with an apodization curve containing two separated peaks. Two beams are made during receive: the in-phase and the 90 degrees phase shifted quadrature beam. Fourier transforming the point spread function should thereby give a one sided spectrum for both temporal and spatial frequencies. Phase errors between the two beam results in energy appearing in the spectrum at negative spatial frequencies, which can bias the estimates of the lateral velocity component. The TO lateral wavelength λ_x is predicted from the distance between peaks, scan depth, and wavelength, and determine the focusing delays to form the two beams. The simple equation underestimates λ_x, and simulations must be made to obtain a one-sided spectrum due to the complex interaction between focusing, apodization, and wavelength. A design procedure based on Field II simulations is suggested to reduce standard deviation and bias of the estimates. The criteria for optimality is the ratio between the energy in the right half plane to the left plane of the spectrum. A 5 MHz 192 elements convex array probe (pitch 0.33 mm) is used. An F-number of 5 is used in transmit and two 32 element wide peaks are used in receive separated by 96 elements between peaks. Parabolic velocity profiles are simulated at beam-to-flow angles from 90 to 45 degrees in steps of 15 degrees. 2,000 pulse-echo lines are made for each angle, and 125 profiles are estimated for each angle using 16 emissions per estimate.

Results/Discussion

The basic equation for λ_x gives 1.14 mm at 40 mm, and 1.54 mm from the simulated point spread function. This results in a bias of 35% as λ_x directly scales the estimated velocities. Optimizing the focusing yields a λ_x of 1.49 mm. The energy ratio is reduced from -14.6 dB to -19.8 dB and the spectral bandwidth from 142.3 m^{-1} to 135.4 m^{-1}. λ_x is maintained between 1.47 and 1.70 mm from 25 mm to 70 mm and is increased to 2.8 mm at a depth of 100 mm. Parabolic profiles are estimated using 16 emissions. The optimization gives a reduction in standard deviation from 8.5% to 5.9% with a reduction in bias from 35% to 1.02 % at 90 degrees (transverse flow) at a depth of 40 mm. When the angle changes from 90 to 45 degrees the std is increased from 5.9% to 12.7% due to the increase in the axial velocity component.

IUS1-K1-6

Vascular Resistivity Imaging using Ultrafast Doppler : application to the 2D cerebral mapping of preterm infant vascular indexes

Charlie Demene[1], Mathieu Pernot[1], Valerie Biran[2], Marianne Alison[3], Mathias Fink[1], Olivier Baud[2], Mickael Tanter[1]; *[1]Institut Langevin, ESPCI ParisTech, CNRS UMR7587, Inserm U979, Universite Paris7, Paris, France, [2]Réanimation et Pédiatrie Néonatales, Hôpital Robert Debré, Paris, France, [3]Département d'imagerie médicale, Hôpital Robert Debré, Paris, France*

Background, Motivation and Objective

Preterm infant are in a large extent subject to neurological disorders resulting from injuries during brain development. Among the most common lesions, intraventricular hemorrhage and hypoxia-ischemia involve the vascular network and can lead to severe complications such as periventricular leukomalacia, while ultrasound modalities encounter difficulties to give good prognostic parameters. Ultrafast Doppler imaging through the fontanel, used regularly during preterm infant monitoring, could give early insights on changes in Cerebral blood flow, and help to detect those incidents. In this study we investigate the use of this technique to build 2D maps of resistivity/pulsatility index over the entire vascular network in a single cardiac cycle.

Statement of Contribution/Methods

Ultrafast Doppler Imaging uses the recently introduced compound ultrasound plane wave imaging technique enabling both the detection of small vessels (~100 µm) and the acquisition of the complete blood flow speed profile over the entire field of view in a single cardiac cycle, which would not be possible with a conventional focused Doppler sequence. UD Imaging was implemented and validated using an Aixplorer® (Supersonic Imagine, France) and a linear ultrasonic transducer (192 elements, 0.2mm pitch, 6 MHz). Ultrafast Doppler acquisitions were obtained in parasagittal and coronal sections for 10 preterm infants, using a dedicated ultrasound Plane Wave Compound sequence, enabling to acquire 3500 images in 1 sec. For each acquisition, in every pixel an a posteriori pulse wave Doppler like spectral profile is computed and the resistivity index is calculated.

Results/Discussion

Results showed that the extraction of peak systolic and end diastolic flow speeds in every location of the imaged vascular network was possible with quantitative values in agreement with the litterature (R.I = 0,8 +/- 0.1 in the anterior cerebral artery, RI < 0,2 in veins). Examples showed that this index mapping was reflecting changes in preterm cerebral hemodynamics in agreement with what was observed on a pulse wave Doppler profile. Parametric mapping via Ultrafast Doppler imaging could be a very useful prognostic tool for preterm infant monitoring, but also a ground breaking tool for functional imaging of the infant brain activity.

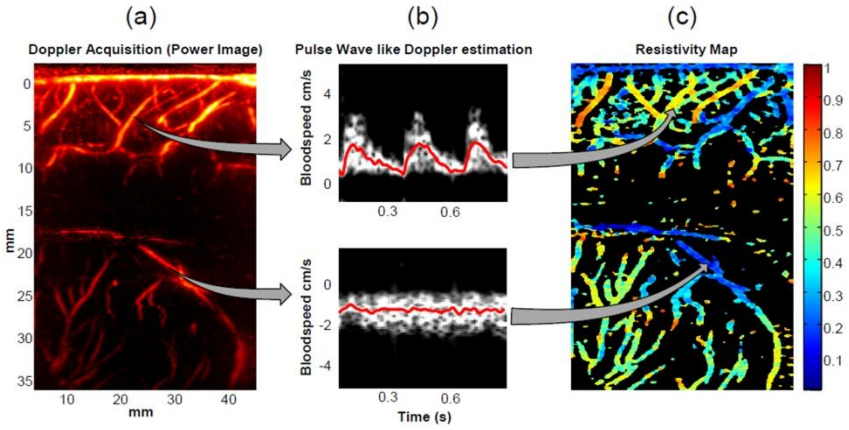

Figure: From an Ultrafast Doppler Acquisition lasting 1s, it is possible to compute a posteriori in each pixel (a) a spectrogram of the Doppler signal (b) from which a central frequency can be calculated (red line). From this central Doppler frequency, converted in blood flow speed, a resistivity index can be assessed in every pixel, enabling to build a Resistivity map over the entire image (c). On this example, a pulsatile artery appears orange (0.7) on the resistivity map, whereas a non pulsatile vein appears blue (0.1).

Elastography of blood and vessels

M4

Thursday, July 25 2013, 08:30 am - 10:00 am

Congress Hallair: **Charles Cain**
University of Michigan

IUS1-K2-1

Validation of 2D Ultrasound Elastography in Large Vessels

Richard G.P. Lopata[1], Mathijs F.J. Peters[1], Frans N. van de Vosse[1], Marcel C.M. Rutten[1]; [1]*Biomedical Engineering, Eindhoven University of Technology, Eindhoven, Netherlands*

Background, Motivation and Objective

Ultrasound (US) is increasingly used to estimate local strains and mechanical properties of tissue and organs, such as breast tumors, arteries and the heart. Many available methods, each with their own advantages, often exhibit large variations when compared. Validation of strain and elastography results is not trivial. In this study, 2D elastography in large vessels (aortas) is performed *in vitro* and validated for the first time by means of the gold standard: classic bi-axial tensile testing (TT).

Statement of Contribution/Methods

Nine healthy porcine aortas were prepared and pressurized from 0 to 130 mmHg in 10 mmHg steps. 2D ultrasound RF data were acquired with a MyLab70 scanner (Esaote, NL) equipped with a linear array probe. Data were analysed using a 2D coarse-to-fine strain estimation algorithm (Lopata et al. 2009), yielding time series of local diameters of the vessel, and thus the circumferential strain. The circumferential wall stress was calculated using Laplace's law. The resulting stress-strain data were fitted with a neo-Hookean model, accounting for isotropic elastic behaviour at large deformations, and rendered the shear modulus (G). The *in vivo* axial aortic stretch is unknown. Hence, the aortas were tested for a relatively low (10%) and high (30%) axial stretch. Next, the aortas were cut into 15 mm x 15 mm samples and tested in a bi-axial tensile tester (CellScale, Canada). Again, the samples were stretched 10% and 30% axially, after which a cyclic deformation was applied in the originally circumferential direction. The shear modulus was estimated using the resulting stress-strain curves.

Results/Discussion

Typical stress-strain curves for both experiments show good agreement (Fig. 1A). The shear modulus as obtained with ultrasound was 208 kPa ± 28 kPa, whereas the tensile test resulted in 216 kPa ± 33 kPa. This corresponds with a Young's modulus of E = 400 kPa ± 40 kPa, at 80-120 mmHg blood pressure. For comparison, the Bland-Altman plot is given in Fig. 1B.

A good agreement was found between the ultrasound elastography method and the bi-axial tensile tests. Little difference was found in estimated shear moduli for 10% and 30% axial stretch. The stress-strain curves have an increasing slope, implying that a non-linear material description might be useful in future studies. Ultimately, *in vivo* assessment of G would enable comparison between patients with aneurysms.

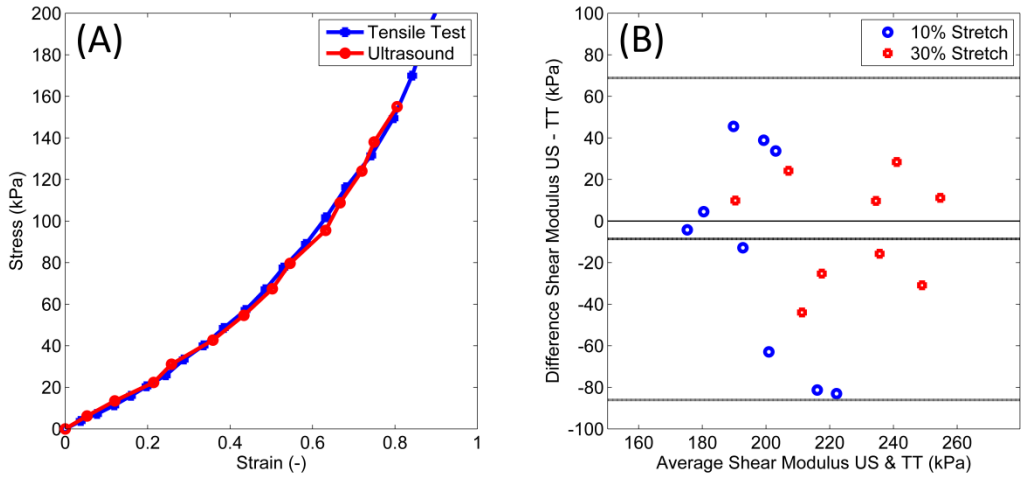

IUS1-K2-2

Speckle Tracking Strain Estimation of a Carotid Artery Plaque Phantom - Validation via Sonomicrometry

Erik Widman[1], Kenneth Caidahl[2], Jan D'hooge[3], Brecht Heyde[3], Matilda Larsson[1]; [1]*Department of Medical Engineering, KTH Royal Institute of Technology, Stockholm, Sweden,* [2]*Department of Molecular Medicine and Surgery, Karolinska Institute, Stockholm, Sweden,* [3]*Lab on cardiovascular imaging & dynamics, Department of Cardiovascular Sciences, Catholic University of Leuven, Leuven, Belgium*

Background, Motivation and Objective

Carotid artery plaque characterization is critical for the prevention of ischemic events. Since plaque stiffness has shown to correlate with plaque vulnerability, quantification of plaque strain throughout the heart cycle would be a useful diagnostic tool. Our previous work encompassed the development and validation of a 2D speckle tracking (ST) algorithm to evaluate arterial stiffness by measuring strain in the carotid artery wall in silico, in vitro, and in vivo. The focus of previous studies has been to quantify plaque strain in the radial direction but lack validation against a ground truth measurement. Our objective was to validate radial and longitudinal strain in plaques via sonomicrometry (sono), and compare the measured plaque and arterial wall strain.

Statement of Contribution/Methods

Three carotid artery phantoms with soft wall inclusions, mimicking a vulnerable plaque, were constructed (10% polyvinyl alcohol (PVA), 3% graphite) by exposing the vessel and plaque to three and one freeze-thaw cycles (12h freeze, 12h thaw) respectively, see Fig. 1a. The phantoms were embedded in a tissue mimicking mixture (3% Agar, 4% graphite) at approximately 1cm depth with a pump (CompuFlow 1000 MR) connected to the phantom lumen simulating the carotid blood flow. B-mode cineloops (GE Vivid E9, 9LD linear transducer, 10 MHz, 42 fps) recorded the vessel movement at 20 and 30 mL/s peak flows. The radial and longitudinal deformation of the plaque and vessel wall was estimated by an in house 2D ST (kernel size 5x2 wavelengths) algorithm throughout two consecutive cycles. The region of interest was adjusted according to the plaque size. Sono crystals were placed on the plaque and vessel wall and used as a reference of truth.

Results/Discussion

Fig. 1b and 1c show sample radial and longitudinal strain curves of a phantom with 20mL/s lumen flow with good agreement between sono and ST. A strong correlation was found at radial (r=0.67, p=0.03) and longitudinal peak systolic strain (r=0.84, p<0.001) between sono and ST. The plaque exhibited 47,3% (SD 27,4%) greater radial and 62,3% (SD 83,5%) longitudinal peak strain than the arterial wall when measured with ST. These preliminary data show that it is possible to measure radial and longitudinal strain in plaques; however, more extensive analysis is required as is the feasibility in vivo.

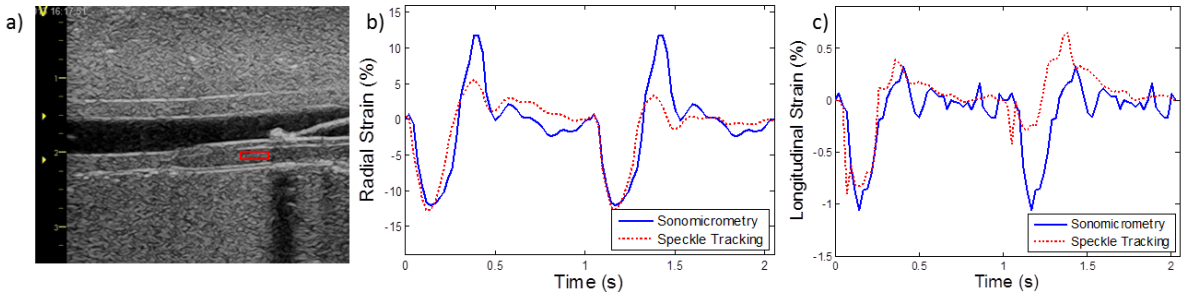

Figure 1 a) B-mode image of vessel phantom with a soft plaque inclusion to the right in the posterior wall. The red box indicates the ROI for the speckle tracking algorithm. b) Radial and c) longitudinal strain curves of the plaque during 2 heart cycles from speckle tracking and sonomicrometry.

IUS1-K2-3

A fast 2D tissue motion estimator based on the phase of the intensity enables visualization of the propagation of the longitudinal movement in the carotid artery wall

Tobias Nilsson[1], Åsa Rydén Ahlgren[2], John Albinsson[1], Simon Segstedt[1], Jan Nilsson[2], Tomas Jansson[1], Hans W Persson[1], Magnus Cinthio[1]; *[1]Electrical Measurements, Faculty of Engineering, LTH, Lund University, Sweden, [2]Department of Clinical Sciences Malmö, Lund University, Sweden*

Background, Motivation and Objective

A fast 2D motion estimator applied on ultrasound B-mode images has been developed and evaluated. As oppose to most other methods this method does not utilize block-matching or iterative solutions. The method is thus computationally efficient and suitable for real-time motion estimation over the entire image. Further the method has enabled visualization of the propagation of the longitudinal movement in the carotid artery wall.

Statement of Contribution/Methods

The 2D motion estimator converted the B-mode intensity to phase information in the vertical and horizontal directions. For each direction, the intensity was first differentiated and the Hilbert transform was applied to extract the spatial phase. Then the average temporal phase difference between two frames and the average spatial phase gradient was calculated using a convolution with a 2D kernel of ones (~1x1mm). The motion of each pixel was then calculated as the ratio between these matrices. The method has been evaluated on 1) phantom measurements and 2) in vivo on the carotid artery wall of 17 subjects, where measurements of the longitudinal displacement of the intima-media complex were compared to our previously validated method.

Results/Discussion

The error of the phantom measurements was 1.6±15.7% (velocities between 5-10 mm/s; approx. 9.5 million estimations). In the in vivo measurements the mean difference (validated-proposed) was 18±44µm. Several different phases of the longitudinal propagation, which seem to be connected to the multi-phasic pattern of the longitudinal movement, can be seen. All phases of the longitudinal propagation seem to originate from the direction of the heart. Figures A-D show four consecutive frames (fame rate 54 Hz) where two phases of the propagation of the longitudinal movement can be visualized (the direction of the heart is to the right). In conclusion, conversion of B-mode intensity to spatial phase information enables fast tissue motion estimation in two dimensions. The method is simple and well suited for real time implementation for tracking in entire images in various applications. An interesting application is the visualization of the propagation of the longitudinal movement in the carotid artery wall which, to our knowledge, has not been visualized before. All phases of the longitudinal movement during a cardiac cycle seem to originate from the direction of the heart.

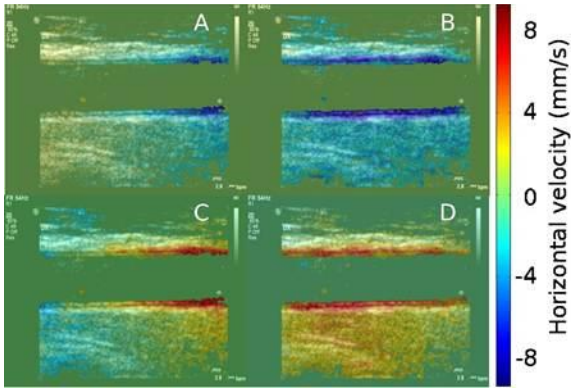

IUS1-K2-4

Measurement of longitudinal and circumferential waves in tubes and artery excited with ultrasound radiation force

Matthew Urban[1], Ivan Nenadic[1], Cristina Pislaru[1], James Greenleaf[1]; [1]*Department of Physiology and Biomedical Engineering, Mayo Clinic College of Medicine, Rochester, MN, USA*

Background, Motivation and Objective

Objective: Increased arterial stiffness is associated with increased risk of cardiovascular events. Radiation force methods have been developed to investigate the longitudinal wave speeds of the artery with high spatial and temporal resolution. The artery is anisotropic so to fully characterize its material properties, we need to examine longitudinal and circumferential wave speeds.

Statement of Contribution/Methods

Methods: We used ultrasound radiation force to generate propagating waves in the wall of rubber tubes and an excised pig carotid artery and measured the wave motion using compounded plane wave imaging. To study the tubes we used two Verasonics systems equipped with linear array transducers (L7-4, Philips Healthcare, Andover, MA). The transducers were placed 90° with respect to each other to obtain different views along the tube wall. One transducer applied a radiation force push and then both systems were used to detect the wall motion of the tube. One system was used for the artery experiment. The group velocity of the longitudinal wave, c_l, was measured along the length of the vessel/tube. The motion near the radiation force push location was analyzed to measure the speed of the circumferential wave. A Fourier transform was taken and the frequency of the peak motion was extracted. This frequency, f_c, is inversely proportional to the transit time needed for the wave to travel around the circumference of the cylinder such that the circumferential speed is $c_c = \pi D f_c$, where D is the outer diameter of the cylinder. We varied the transmural pressure over ranges of 10-30 mmHg and 20-200 mmHg for the tubes and artery, respectively.

Results/Discussion

Results: We confirmed the presence of circumferential waves by pushing on a tube with one transducer and measuring with the other transducer at 90°. We compared c_l and c_c in the tubes and found very good agreement in tube 1 and a bias in tube 2 (Fig. 1(a)). It was expected that both wave speeds would be similar because the material is isotropic. The c_l and c_c values for the artery shown in Fig. 1(b) show similar trends but the c_c values are lower than the c_l values.

Conclusion: We were able to measure values of c_l and c_c in tubes and arteries. The speeds measured in isotropic tubes were similar. The values of c_c in an excised artery were shown to be lower than the values of c_l. [This work was supported in part by grant EB002640 from NIH.]

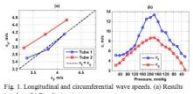

Fig. 1. Longitudinal and circumferential wave speeds. (a) Results in tubes. (b) Results in artery.

IUS1-K2-5

A Harmonic Tracking Method for Improved Visualization of Arterial Structures with Acoustic Radiation Force Impulse Imaging

Joshua Doherty[1], Jeremy Dahl[1], Jason Allen[2,3], Katherine Ham[2], Gregg Trahey[1,4]; [1]*Biomedical Engineering Department, Duke University, Durham, North Carolina, USA,* [2]*Department of Cardiology, Duke University Medical Center, Durham, North Carolina, USA,* [3]*Department of Community and Family Medicine, Duke University Medical Center, Durham, North Carolina, USA,* [4]*Department of Radiology, Duke University Medical Center, Durham, North Carolina, USA*

Background, Motivation and Objective

Increased arterial wall thickness is correlated with a higher prevalence of clinical cardiovascular events. By differentiating stiff arterial walls from softer, surrounding tissues, Acoustic Radiation Force Impulse (ARFI) imaging has shown improved visualization of arterial boundaries compared to B-mode imaging. Measurements of arterial thickness with ARFI imaging, however, are challenged by clutter that makes it difficult to delineate the blood-vessel interface, particularly at the proximal wall.

Statement of Contribution/Methods

We developed a novel pulse inversion harmonic tracking method to monitor the transient deformation response from an impulsive acoustic radiation force excitation. Using custom designed pulse sequences, quadruple sets of spatially-matched 1) fundamental B-mode, 2) harmonic B-mode, 3) fundamental ARFI, and 4) harmonic ARFI images of a carotid artery were obtained at multiple locations in six human subjects. A certified reader performed measurements of the carotid intima-media-thickness (IMT) in B-mode images and the adventitia-intima-media-thickness (AIMT) in ARFI images of both the proximal and distal walls in 14 quadruple image sets using a semi-automated carotid measurement analyzer.

Results/Discussion

Compared to B-mode images, ARFI images provide improved visualization of the distal wall boundaries (see Fig. 1). With an increased sensitivity to blood flow, the harmonic ARFI images provide the best delineation of the proximal wall and blood-vessel interface. Improvements in harmonic ARFI images are consistent with reduced clutter observed in matched harmonic B-mode images. On average, the ARFI measurement of AIMT was 0.96±0.34 mm larger than the B-mode IMT measurement. The lateral arterial length amenable for analysis was larger in ARFI images compared to B-mode images ($p=0.03$ proximal wall, and $p=0.01$ distal wall). Due to poor image quality, the reader was unable to measure the proximal wall thickness in 57‰ of fundamental B-mode, 43‰ of harmonic B-mode, 21‰ of fundamental ARFI, and 7‰ of harmonic ARFI images. While the ARFI AIMT measurement differs from conventional IMT measurements, these results suggest that harmonic ARFI imaging may provide a more reliable method for monitoring arterial thickening to predict the occurrence of clinical events.

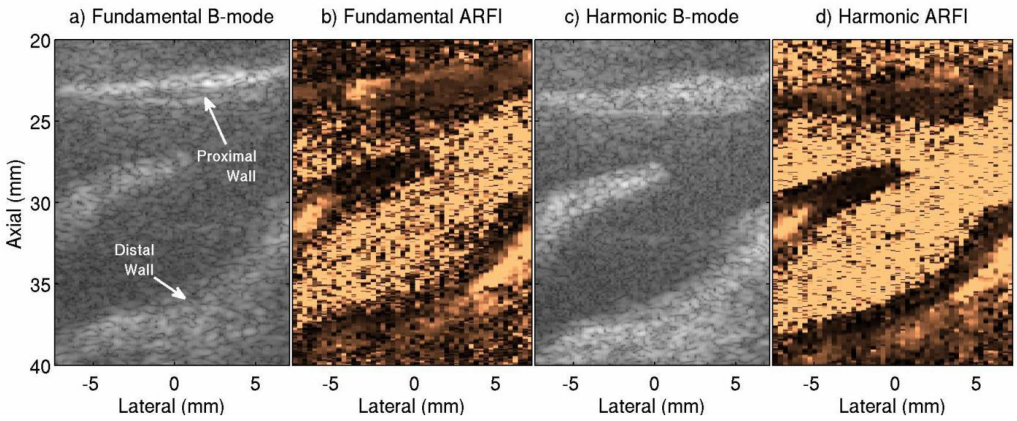

Fig 1: Spatially matched B-mode and ARFI images for both the fundamental and harmonic methods, of an *in vivo* carotid artery bifurcation. Improved visualization of the distal wall is demonstrated with both ARFI images compared to the B-mode images. The harmonic ARFI image shows improved sensitivity to blood flow and improved visualization of the proximal wall.

IUS1-K2-6

Cross Validation of Supersonic Shear Imaging (SSI) with Classical Rheometry during Blood Coagulation over a very large Bandwidth

Miguel Bernal[1], Jean-Luc Gennisson[1], Patrice Flaud[2], Mathias Fink[1], Mickael Tanter[1]; *[1]Institut Langevin – Ondes et Images, ESPCI ParisTech, CNRS UMR7587, INSERM U979, Paris, France, [2]2 Matière et Systèmes Complexes, CNRS UMR7057, Université Paris VII Denis Diderot, Paris, France*

Background, Motivation and Objective

Deep venous thrombosis (DVT) affects millions of people worldwide. Its diagnosis and treatment depends on clot's age which is closely related to its viscoelastic properties. These properties could be assessed noninvasively using SSI. The aim of this study is i) to validate SSI with classical rheometry during blood coagulation, ii) to study the best rheological model fitting this process.

Statement of Contribution/Methods

Classical rheometry and SSI were used in this study to characterize the elasticity (μ) and viscosity (η) of blood clots. Blood was collected from pigs and anticoagulated using EDTA. Coagulation was initiated using calcium ions. Shear waves over a bandwidth between 70 to 300 Hz, were induced with 100 μs tonebursts of 8 MH . The displacements generated were measured using ultrafast imaging at a rate of 2 kHz. Shear wave speed was recovered using a time of flight algorithm. Classical rheometry using a Haake Mars II was done simultaneously on the same blood sample (2.9 ml) between 0.25 and 25 Hz. An oscillatory shear was imposed with low amplitude (5%) to insure the linearity of the viscoelastic response of the blood. Using the values for G' and G" the theoretical shear wave speeds were calculated for frequencies between 0.25 and 25 Hz. Maxwell, Voigt and Zener models were fitted to the dispersion data combining the two methods to retrieve viscoelasticity.

Results/Discussion

Shear wave speed showed a marked increase with time of coagulation for all the frequencies, from around 0.5 m/s at the beginning of coagulation to 0.9 after 2 hours. The Zener model (μ_1, μ_2, η) showed to be the best fit on the data out of the 3 models, as shown in Fig 1. Maxwell (μ_M, η_M) and Voigt (μ_V, η_V), although they did a good job at higher frequencies (70 Hz and up), they fail to characterize the lower frequencies. Shear elasticity and viscosity increased with coagulation time from μ_1=167 kPa, μ_2=138 kPa and η=1.38 Pa·s at beginning of coagulation to 341 kPa, 391 kPa and 1.59 Pa·s, respectively, after 50 minutes of coagulation. After two hours, the values had increased to 351 kPa, 472 kPa and 1.56 Pa·s, respectively.

The combination of these two techniques allowed the characterization of the viscoelastic properties of blood clots in a very large frequency range between 0.25 Hz and 300 Hz. The two techniques showed very good agreement suggesting that SSI could be used to study the rheological properties of soft solids.

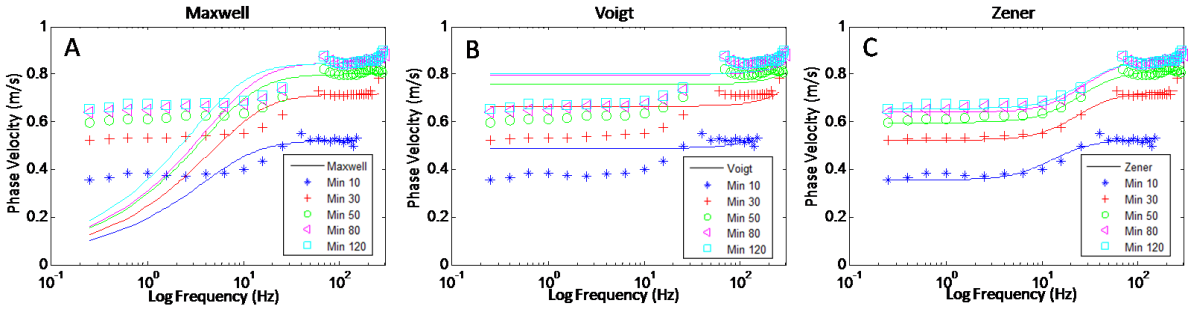

Metrology and sonoporation

M5

Thursday, July 25 2013, 08:30 am - 10:00 am

Congress Hallair: **Jeffrey Ketterling**
Riverside Research

IUS1-K3-1

Application of Complex Deconvolution to Correct for Non-Uniform Hydrophone Sensitivity for the Measurement of Acoustic Output Parameters

Keith Wear[1], Paul Gammell[2], Subha Maruvada[1], Yunbo Liu[1], Gerald Harris[1]; [1]*Center for Devices and Radiological Health, US Food and Drug Administration, Silver Spring, MD, USA,* [2]*Gammell Applied Technologies, USA*

Background, Motivation and Objective

Hydrophones are used to measure pressure waveforms from ultrasound transducers. The standard method for estimation of pressure is to divide the hydrophone output voltage by the hydrophone sensitivity at the "acoustic working frequency," but this approach ignores frequency dependence of hydrophone sensitivity. A more accurate method is to perform a complex deconvolution between the hydrophone output voltage and the hydrophone frequency-dependent complex sensitivity. We previously developed a method for measuring magnitude and phase of hydrophone sensitivity using time delay spectrometry (TDS) (Wear et al. IEEE Trans UFFC, 58, 2325-2333, 2011). This method may be applied to assess the effects of deconvolution on consistency of measurements of peak compressional pressure (p+), peak rarefactional pressure (p-, related to mechanical bioeffects), and pulse intensity integral (PII, related to thermal bioeffects).

Statement of Contribution/Methods

In the first set of experiments, swept-frequency (0–40 MHz) TDS was used to measure complex sensitivities of 8 hydrophones used in medical ultrasound exposimetry. These included PVDF spot-poled membrane (4), needle (2), capsule (1), and fiber-optic (1) designs. TDS measurements were performed using 5 broadband source transducers (center frequencies: 2, 5, 10, 30, 50 MHz) to obtain complex sensitivities from 1-40 MHz. In the second set of experiments, the 8 hydrophones were used to measure a 4-cycle, 3 MHz pressure waveform mimicking a pulsed Doppler waveform with significant harmonic content up to 40 MHz. p+, p-, and PII for the 8 hydrophones were measured using 1) the standard approach and 2) deconvolution (using complex sensitivities measured in the first set of experiments). Variability in measurements (across all 8 hydrophones) was described by the coefficient of variation (COV = standard deviation / mean).

Results/Discussion

The figure shows hydrophone output (left column) and deconvolved RF (right column) for 3 hydrophones. Average measurements (across all 8 hydrophones) of pulse parameters were 4.0 MPa (p+), 2.2 MPa (p-), and 0.18 mJ/cm2 (PII). Compared with the standard method, deconvolution reduced COV of p+ from 25% to 8% and reduced COV of PII from 36% to 13%. Deconvolution had a small effect on COV of p-. In conclusion, deconvolution significantly improves consistency of acoustic output measurements.

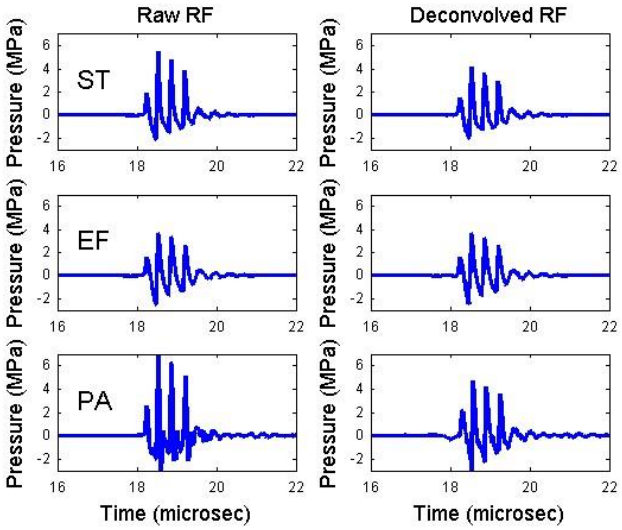

IUS1-K3-2

Quantitative Measurement of Focused Ultrasound Pressure Field by Background-subtracted Shadowgraph

Shin Yoshizawa[1], Ryo Miyasaka[1], Mohd Syahid[1], Shin-ichiro Umemura[1]; [1]*Tohoku University, Japan*

Background, Motivation and Objective

High-intensity focused ultrasound (HIFU) is a non-invasive treatment modality for solid tumors. An accurate and fast measurement of the three-dimensional pressure filed of the focused ultrasound is important to ensure and improve the therapeutic ultrasound system. The most common way of the acoustic field measurement is with a mechanically scanned hydrophone. Optical ultrasonic field mapping has the advantages of the measurement speed and its nature of not by interfering with the acoustic field compared with the hydrophone measurement. In this study, the focused ultrasound pressure field was reconstructed from background-subtracted shadowgraph images.

Statement of Contribution/Methods

Figure 1 shows the experimental setup to take the shadowgraph images. A spherical transducer was placed in a water tank and driven at a frequency of 1.14 MHz. An expanded and collimated green laser passed through the ultrasound field. The shadowgraph images were taken with a CCD camera which focused on a holographic diffuser. The optical phase modulation due to the acoustic pressure was considered for the optical measurement. Furthermore, neglecting the effect of the optical diffraction and assuming the optical deflection angle due to the ultrasound pressure distribution is sufficiently small, the integration of the acoustic pressure along the optical propagation axis was calculated from shadowgraph images with and without ultrasound exposure. The pressure field was reconstructed from the projected acoustic fields by CT algorithm.

Results/Discussion

The optical reconstruction well reproduced the pressure field measured with a hydrophone when the pressure amplitude at the focal point was less than 1 MPa. Increasing the acoustic pressure over 2 MPa, the reconstruction underestimated the pressure. Since the distance between the ultrasound propagation region and the optical focal plane corresponding to the position of the diffuser was measured easily and accurately, the focused ultrasound pressure field at pressure amplitude less than 1 MPa was successfully reconstructed without calibration. It would make it possible to optically measure the pressure field at larger pressure amplitude if the effect of the optical diffraction was considered by iterative calculation of the optical intensity modulation at the position of the diffuser owing to the optical phase modulation.

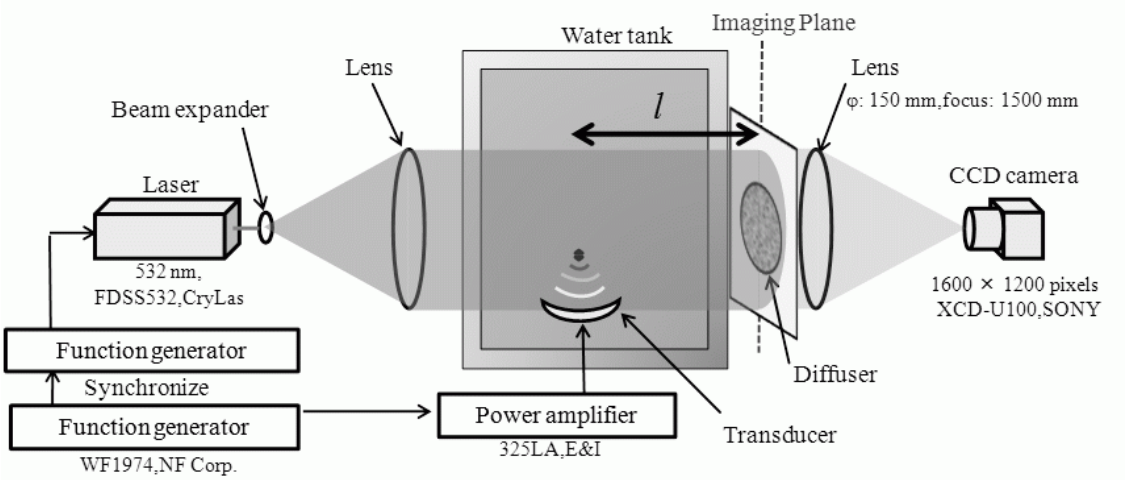

Figure 1 Experimental setup

IUS1-K3-3

Improved Finite Amplitude Insertion Substitution technique for acoustic nonlinearity parameter measurement

Bajram Zeqiri[1], Lise Retat[2], Pierre Gelat[1], Gail ter Haar[2]; *[1]Acoustics and Ionising Radiation Division, National Physical Laboratory, Teddington, Middlesex, United Kingdom, [2]Therapeutic Ultrasound Team, Institute of Cancer Research, Sutton, Surrey, United Kingdom*

Background, Motivation and Objective

The acoustic non-linearity parameter, commonly referred to as B/A, is a crucial parameter which dictates the way in which a finite amplitude acoustic wave distorts during propagation within any medium. At elevated acoustic pressure amplitudes, as distortion leads to the generation of higher harmonics of the fundamental frequency that are subject to greater absorption, B/A also plays a key role in terms of influencing thermal effects within biological media. Accurate knowledge of this parameter is therefore required to provide confidence in applied theoretical models that predict heat deposition for clinical procedures such as High Intensity Focused Ultrasound.

Statement of Contribution/Methods

The Finite Amplitude Insertion Substitution (FAIS) has been developed as a method which can be practically applied for B/A determination of tissues(1). The technique involves determining, for very slightly acoustically distorted waveforms, the degree of second harmonic generated during propagation through any test sample, relative to level generated through a reference medium (water) whose B/A value has been well characterized. Since the original paper, a number of variants of the technique have been implemented primarily to overcome the effects of acoustic diffraction. However, all of these methods ignore finite amplitude distortion of the acoustic wave which emerges from the test sample, and subsequently propagates to the device used to record the acoustic wave, either a second transducer or a hydrophone.This paper describes a refinement of the FAIS technique which includes modeling of the impact of finite amplitude distortion from the rear of the sample on B/A measurements.

Results/Discussion

Involving the application of a 2 MHz acoustic field, the study has demonstrated that, under certain conditions, ignoring this contribution can lead to an error in the measured B/A value in excess of 10%. The actual magnitude of the error depends on the acoustic properties of the material under test, particularly the frequency dependent attenuation coefficient. Another novel feature of the work presented is the use of a large area receiver in the form of a broadband membrane hydrophone of active element diameter 30 mm. This has enabled the effects of acoustic diffraction to be minimized, allowing measurements to be performed with the receiver positioned within the transducer near-field. B/A measurements are presented on two fluids commonly employed as reference materials within the technical literature: corn oil and ethylene glycol; as well as samples of an agar-based tissue-mimicking material. A systematic measurement uncertainty assessment will be presented alongside recommendations for optimized nonlinearity parameter measurement protocols.

(1) Xui-Feng Gong, Zhe-ming Zhu, Tao Shi and Jian-hong Huang, "Determination of the acoustic nonlinearity parameter in biological media using FAIS and ITD, J. Acoust. Soc. Am., 86, 1, 1-5, 1989.

IUS1-K3-4

Real-Time Imaging of Plasma Membrane Dynamics in Sonoporation: From Perforation to Recovery

Yaxin Hu[1], Jennifer M. F. Wan[2], Alfred C. H. Yu[1]; *[1]Medical Engineering Program, The University of Hong Kong, Pokfulam, Hong Kong, [2]School of Biological Sciences, The University of Hong Kong, Pokfulam, Hong Kong*

Background, Motivation and Objective

To properly harness sonoporation for therapeutic applications, it is unarguably vital to characterize the fundamental biophysical processes involved. Of particular relevance are two membrane-level processes that epitomize the notion of sonoporation: 1) how membrane perforation is induced by ultrasound-microbubble interactions, and 2) how the membrane remodels itself following an episode of sonoporation. Acquiring direct observations of these processes is however not a straightforward task (ironically, these membrane-level events have yet to be convincingly demonstrated in-situ). In this investigation, our aim is to acquire the first series of direct evidence on the time course of membrane perforation and recovery in sonoporation. In particular, we seek to unravel the time-varying surface topography of sonoporated cell membrane in-situ.

Statement of Contribution/Methods

A real-time imaging platform for monitoring of cell-microbubble interactions was first developed, and it was a composite system that coupled a 1 MHz ultrasound module to a laser scanning confocal microscope. A nose-cone shaped waveguide (1" diameter, 7.5 cm height) was devised to align the ultrasound beam focus to the microscope's imaging plane. This waveguide was angled at 45 deg. with respect to the imaging plane normal. A custom-made cell chamber was mounted onto the imaging plane, and it housed a 20x28 mm observation window with acoustically thin top and bottom layers (<0.16 mm thick). MRC5 fetal fibroblasts were seeded onto the bottom layer of the observation window, and their plasma membrane was fluorescently labeled using the CellMask Orange dye at 2.5 ug/ml concentration. Lipid-shelled microbubbles (Targeson) were then introduced on a 1:1 cell/bubble ratio, and they were allowed to passively settle onto the fibroblast monolayer. After that, a single ultrasound pulse (1 MHz frequency, 10 cycles, 0.75 MPa in situ peak negative pressure) was applied to instigate microbubble pulsation and collapse. Over this process, the surface topography of fibroblast membrane at positions with microbubbles was imaged in real-time using the confocal microscope. Pore size and recovery time were quantified from the acquired cineloops.

Results/Discussion

Localized perforation of cell membrane was synchronized with the time course of microbubble collapse. The pore size was highly time-dependent: it expanded for a limited time after microbubble collapse (up to 7 um diameter), after which resealing started to take place. The pore size was generally greater than the microbubble (mean diameter: 2.2 um). Membrane striation was also evident away from the perforation site: this signifies an increased membrane tension. During recovery, the perforation site exhibited a contractile ring morphology, and the endoplasmic reticulum was found to be actively participating in the resealing process. These findings demonstrate that membrane-level processes in sonoporation are highly dynamic.

IUS1-K3-5

Relation between cell membrane tension and repair of membrane damaged during sonoporation

Yuto TANAKA[1], Nobuki KUDO[1]; [1]*Graduate School of Information Science and Technology, Hokkaido University, Sapporo, Hokkaido, Japan*

Background, Motivation and Objective

Repair of a cell membrane damaged during sonoporation depends on membrane tension, and a difference in membrane tension has a great effect on sonoporation efficiencies in *in vitro* and *in vivo* conditions. In this study, cell membrane tension was controlled by changing osmotic pressure of the culture medium, and the effect of cell membrane tension was investigated by fluorescence microscopic observations of cells during sonoporation.

Statement of Contribution/Methods

Human prostate cancer cells (PC-3) were cultured on a coverslip, and the coverslip with cells facing down was attached to an observation chamber created in the bottom of a water bath (Fig. 1a). The observation chamber was filled with an isotonic or non-isotonic solution supplemented with 5 μg/ml propidium iodide (PI), which permeates only through damaged cell membranes and produces red fluorescence. Hanks' balanced salt solution was used as the isotonic solution. A hypertonic solution was prepared by addition of 0.2 g NaCl to a 50-ml isotonic solution, and a hypotonic solution was prepared by mixing the same volumes of 1.3 mM $CaCl_2$ solution and the isotonic solution. The solutions were also supplemented with the ultrasound contrast agent Levovist. After sufficient time to allow bubbles to come into contact with cells (30 min), the cells were exposed to a single shot of 10-cycle ultrasound pulse of 1 MHz in center frequency and 1.3 MPa in peak-negative pressure. Occurrence of cell membrane damage was discerned by increase in PI fluorescence inside the cells, and success or failure in membrane repair was discerned by a transient or persistent increase in fluorescence intensity. The repair rate was calculated as the number of repaired cells divided by the number of damaged cells.

Results/Discussion

Fig. 1b shows the repair rates of cells treated under the three conditions of osmolality. The repair rate under a hypertonia condition was significantly higher than the rates under the other two conditions. These results indicate that a decrease in cell membrane tension promotes repair of membranes damaged during sonoporation. However, there was no significant difference between iso- and hypotonic conditions, suggesting that decreased Mg^{2+} concentration in a hypotonic solution has a positive effect on membrane repair (R.A. Steinhardt, Ann. N. Y. Acad. Sci. 1066(2005) 152-165).

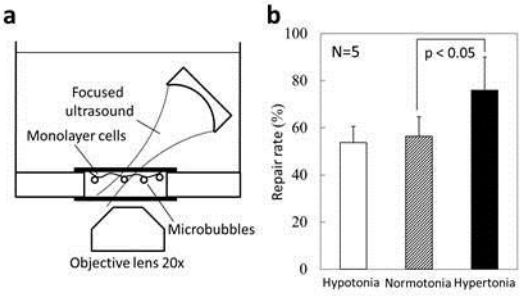

Fig. 1. (a) Experimental setup of the observation (b) Repair rates of cells treated under various conditions of osmolality. Error bar represents SD.

IUS1-K3-6

Sonoporation-Induced Endoplasmic Reticulum Stress: Signaling Pathway Analysis

Wenjing Zhong[1], Xian Chen[1], Pingping Jiang[2], Jennifer M. F. Wan[2], Peng Qin[3], **Alfred C. H. Yu**[1]; [1]*Medical Engineering Program, The University of Hong Kong, Pokfulam, Hong Kong,* [2]*School of Biological Sciences, The University of Hong Kong, Pokfulam, Hong Kong,* [3]*Department of Instrumentation Science and Engineering, Shanghai Jiaotong University, Shanghai, China, People's Republic of*

Background, Motivation and Objective

Sonoporation can induce a complex range of biological consequences beyond a transient porosity change at the membrane level. In particular, at a subcellular level, the functioning of various organelles may become disrupted. This work represents the first demonstration that the endoplasmic reticulum (ER) (an organelle responsible for protein folding, lipid synthesis, and calcium regulation) may be actively involved in mediating post-sonoporation cellular response.

Statement of Contribution/Methods

We have assayed for various ER-related proteins using Western blot analysis. HL-60 cell suspensions were used as the cell model, and sonoporation was applied to them using an immersion-based, secure-sealed exposure chamber with calibrated pressure profiles as obtained from needle hydrophone recordings. These waveform parameters were used: 1 MHz frequency, 1 kHz PRF, 100-cycle pulses, 1 min. duration. The measured in-situ acoustic field conditions were: 0.45 MPa peak negative pressure, 41 J/cm2 spatial-averaged energy density (i.e. a mild dosage). Targeson microbubbles were added to the cell chamber to serve as cavitation nuclei. Post-exposure cell samples were harvested at different times (2, 4, 8, 12, 24 h). Various ER proteins of these cells were analyzed with respect to sham control: 1) protein folding enzymes (PDI, Ero1); 2) ER membrane stress sensors (PERK, IRE1); 3) ER-induced pro-apoptotic signals (CHOP, JNK). To examine the correspondence of our Western blot assay with post-exposure mitochondrial stress, confocal microscopy was performed on the mitochondrial outer membrane (MOM) potential using the TMRE dye.

Results/Discussion

Normal functioning of the ER in sonoporated HL-60 cells was generally disrupted. ER enzymes with vital role in oxidative protein folding were upregulated. Stress sensor proteins located on the ER membrane were also activated following sonoporation. This is accompanied by an increased expression of their downstream effectors that are known to relay pro-apoptotic signals to the mitochondria. In line with these observations, MOM depolarization was observed on a time-lapsed basis. Taken together, our findings show that showing that an ER stress response can be elicited in sonoporated cells. They serve to highlight the need for further efforts to more controllably achieve sonoporation whilst curtailing its downstream bioeffects.

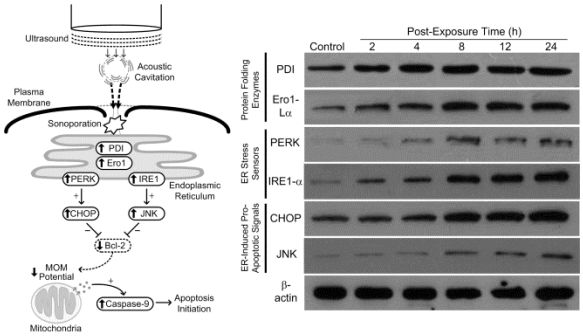

Arrays and Wave Propagation

NH

Thursday, July 25 2013, 08:30 am - 10:00 am

Congress Hallair: **Edward Haeggstrom**
University of Helsinki

IUS2-K-1

Automatic Ultrasonic Robotic Array

Gordon Dobie[1], Walter Galbraith[1], Charles MacLeod[1], Rahul Summan[1], Gareth Pierce[1], Anthony Gachagan[1]; [1]*University of Strathclyde, United Kingdom*

Background, Motivation and Objective

A novel, autonomous reconfigurable ultrasonic phased array inspection robot for non-destructive evaluation (NDE) is presented. The robotic system significantly reduces manual labour over current inspection regimes, as well as enabling inspection of inaccessible/hazardous areas such as those found in the nuclear and petrochemical industries. It offers three quantitative benefits: improved inspection accuracy, improved safety and reduced inspection costs. The current major innovation is in embedding ultrasonic phased array technology into a small form-factor robotic vehicle, overcoming issues in ultrasonic coupling, miniaturised electronics and robot positioning.

Statement of Contribution/Methods

The paper presents an overview of the robot specification and system architecture along with details of a specific inspection scenario where the robot is required to inspect a saddle weld found in reheat bifurcation. This weld was formed from the intersection of two 60 mm thick steel pipes with diameters 500 and 300 mm. The robot is capable of tracking the weld from either pipe, projecting an ultrasonic beam normal to the direction of travel. The design of a 2 MHz, 16 element embedded phased array controller is presented. A timing model of the controller details the throughput required to enable the robot to perform ultrasonic inspection while tracking the weld at 20 mm/s. The paper also considers robot positional estimation. The nature of the inspection prohibits the use of external positioning systems and so the system is limited to on-board sensors, namely wheels encoders, a six axis inertial sensor and a surface feature tracking camera. A Bayesian filter was used to fuse measurements from each of the positional sensors. An absolute tangential positional accuracy of 10 mm with a relative error of less than 2 mm was required. Moreover, the robot distance from the weld must be maintained with an accuracy of 2 mm.

Results/Discussion

The results section focuses on the characterisation of inspection performance, driven in part by the ultrasonic phased array controller and robot positional estimation. A-Scans are presented to show the SNR of each array channel which was approximately 14 dB when measuring the back wall echo. It is shown that ultrasonic scan rate is limited by 802.11g wireless transmission from the robot to the host computer. Strategies to minimise data transfer are discussed, notably the onboard processing of scans to minimise data transfer to the host during the inspection. The robot's on-board positioning system was characterised using a metrology based- laser tracker and shown to conform to the required specification.

IUS2-K-2

Tomographic Array Design for Online, Non-invasive, Non-intrusive, Measurement of Magnox Slurry during Nuclear Decommissioning

David Matthew Joseph Cowell[1], Peter Raymond Smith[1], Steven Freear[1]; [1]*School of Electronic Engineering, Ultrasound Group, Leeds, West Yorkshire, United Kingdom*

Background, Motivation and Objective

Conducting ultrasound measurements in a nuclear environment necessitates a non-invasive and non-intrusive transducer design, capable of operating through thick walled stainless steel vessels. Decommissioning of legacy infrastructure requires transducers capable of retro fitting. Achieving spatial measurements across vessel or pipe cross-sections requires a tomographic approach, typically using multiple invasive or intrusive point source transducers with a fanbeam profile enabling point to multipoint measurements. Non-invasive point source transducers are unable to create fanbeams within the vessel. Differing path lengths within the vessel wall combined with the ultrasonic velocity mismatch between the wall and vessel contents creates a plane wave ultrasound beam within the vessel which is unsuitable for tomography. The objective of this study is to create a non-invasive transducer array with the spatial diversity to allow point to multipoint measurement.

Statement of Contribution/Methods

A non-intrusive array design methodology, overcoming the inherent focusing effects of curved inner pipe surface, is proposed and illustrated through the design, manufacture and testing of an 18 virtual point tomographic array on a stainless steel 168.3 mm pipe with 19 mm thick walls. The pipe transfers magnesium oxide (Magnox) slurry during nuclear decommissioning activities. A point to multi-point transducer arrangement is achieved through the creation of virtual sources, located on the inner surface of the pipe wall. Transducers are arranged at discrete angles around the virtual point such that refraction at the inner pipe surface creates multiple beams, each directed at individual, virtual points, to create point to multi-point measurements (Fig 1a). The transducer array is constructed using an Electrical discharge machined (EDM) support with random 1-3 piezo-composite transducers. Finite element verification of the design and piezo-composite is conducted using PZFlex and the manufactured array (fig 1b) is experimentally characterized.

Results/Discussion

As the virtual sources are spaced at 20°, the transducers are angled at 45° to create refracted beams at 0° and 10°. Fig 1c shows the hydrophone measured beam profile of a virtual source with beams at 0° and 10°. Fig 1d shows the experimental time domain response for the two highlighted measurements paths.

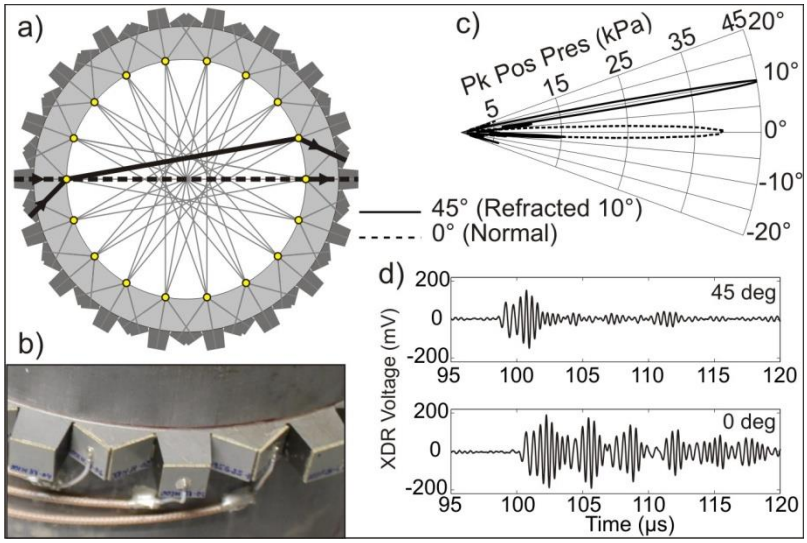

IUS2-K-3

Investigation of the Synthetic Aperture Focusing Technique resolution for heavy rotor forging ultrasonic inspection

Karl T. Fendt[1,2], Hubert Mooshofer[2], Stefan J. Rupitsch[1], Reinhard Lerch[1], Helmut Ermert[1,3]; [1]*Chair of Sensor Technology, University of Erlangen, Erlangen, Germany,* [2]*Siemens AG, Corporate Technology, Munich, Germany,* [3]*High Frequency Engineering Research Group, Ruhr-University Bochum, Bochum, Germany*

Background, Motivation and Objective

Increasing requirements for the quality of heavy rotor forgings in the energy industry have led to advancements in non destructive inspection techniques for application prior to further machining. Ultrasonic inspection with longitudinal waves, being the most suitable method for testing large (1.5 m diameter and more) forgings, has been extended to multiple inspection angles and automated inspection. This allows for the application of Synthetic Aperture Focusing Technique (SAFT) to the obtained ultrasound data. As conventional defect sizing techniques are resolution limited for small defects, knowledge of the resolution is necessary. For a circular 360° scan and a transducer with a finite divergence angle the resulting point spread function and the corresponding spatial resolution are highly dependent on the radial position of the point scatterer, due to the change of effective synthetic aperture size (see Fig. 1). In this contribution we present a resolution simulation procedure for the comparison to reconstructions based on actual inspection data.

Statement of Contribution/Methods

The applied methods are as follows: (i) Elastodynamic far field formulas for circular and rectangular transducers are used to calculate the transmit/receive characteristics and to consecutively approximate the spatial impulse response by calculating the echo signal of an ideal point scatterer at different radial positions. (ii) The simulated data is then converted into an analytic signal. (iii) SAFT with a side lobe suppressing weight function is applied. The result is a dataset of point spread functions at different radial positions.

Results/Discussion

Simulations of the SAFT point scatterer images for circular scan paths and various beam angles are conducted and the radial dependency is examined. Validity of the results is shown by comparison with data from actual inspections. Shown below are exemplary SAFT images of a 0° normal beam probe inspection of a rotor disc with a machined defect (Fig. 1), and the corresponding simulation (Fig. 2) of a point scatterer at the same location. The mean full width at half maximum for the 1mm diameter defect is 3.3 mm, only slightly larger than the simulated point spread function mean FWHM of 3.12 mm.

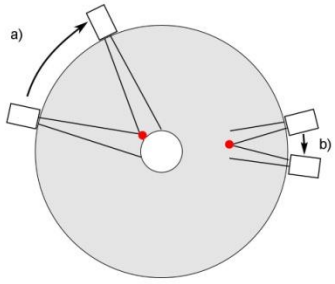

Fig. 1: Schematic illustrating the radial dependence of the effective aperture size, a) for a central point and b) for a peripheral point

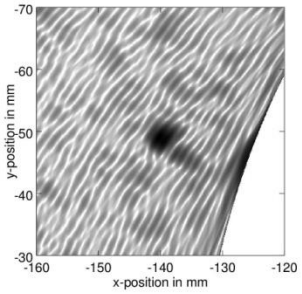

Fig. 2: Measurement - SAFT processed data of a 1 mm diameter flat bottom bore located near center

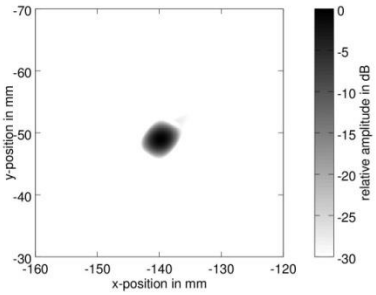

Fig. 3: Simulation - SAFT processed point scatterer image at the same radial position as the flat bottom bore in Fig. 1

IUS2-K-4

Discussion on the crossings and maxima of the Lamb waves

Istvan A Veres[1], Thomas Berer[1,2], Clemens Grünsteidl[1], Peter Burgholzer[1,2]; [1]*Research Center for Non-Destructive Testing GmbH, Linz, Austria,* [2]*Christian Doppler Laboratory for Photoacoustic Imaging and Laser Ultrasonics, Linz, Austria*

Background, Motivation and Objective

Lamb waves in isotropic plates possess fascinating properties: specific components of the surface displacements vanish at particular values of the phase velocity, for example. This happens for the symmetric branches when the phase velocity becomes equal to the longitudinal bulk wave velocity and the normal component of the displacements vanishes. The longitudinal component, on the other hand, vanishes for both symmetric and antisymmetric branches at Lame's equivoluminal modes when $c_p=\sqrt{2}c_S$, where c_S is the shear bulk wave velocity. Practical implications of such behavior are significant: maximal normal components of the displacements at the surface (with no longitudinal component) maximizes the transmission, hence the sensitivity of a sensor, for example. Longitudinally dominated surface displacements (with vanishing normal components) can reduce the leakage into the embedding medium allowing longer inspection distances.

Statement of Contribution/Methods

Here, we will reinterpret this behavior with the help of the crossings of the uncoupled dilatational and shear modes based on Mindlin's approach. Mindlin has shown that for the dispersion curves of an isotropic plate with free boundaries these modes become the bounds and the crossings of the symmetric and antisymmetric branches coincide with the crossings of these bounds if both modes are even or odd. We will show, that at these crossings specific components of the surface displacements vanish: for one mode the longitudinal component and for the other mode the normal component. Therefore, these crossings not only describe the previously obtained maxima and minima of the surface displacements but also lead to further points of the dispersion relation with similar behavior.

Results/Discussion

Practical implications are demonstrated experimentally [Fig.(a)] and numerically [Fig.(b)]. The dispersion relation of an aluminum plate was evaluated by a combination of spatio-temporal scan and 2D Fourier transform. The maximal normal displacements are well visible for Lame's modes due to the strong magnitudes of the Fourier transform. In the vicinity of the longitudinal bulk wave velocity c_L the symmetric modes become longitudinally dominated; the wave modes in this region are hardly visible. The variation of the displacements is shown for a symmetrical (S_2) and for an antisymmetrical (A_3) modes in Fig.(b).

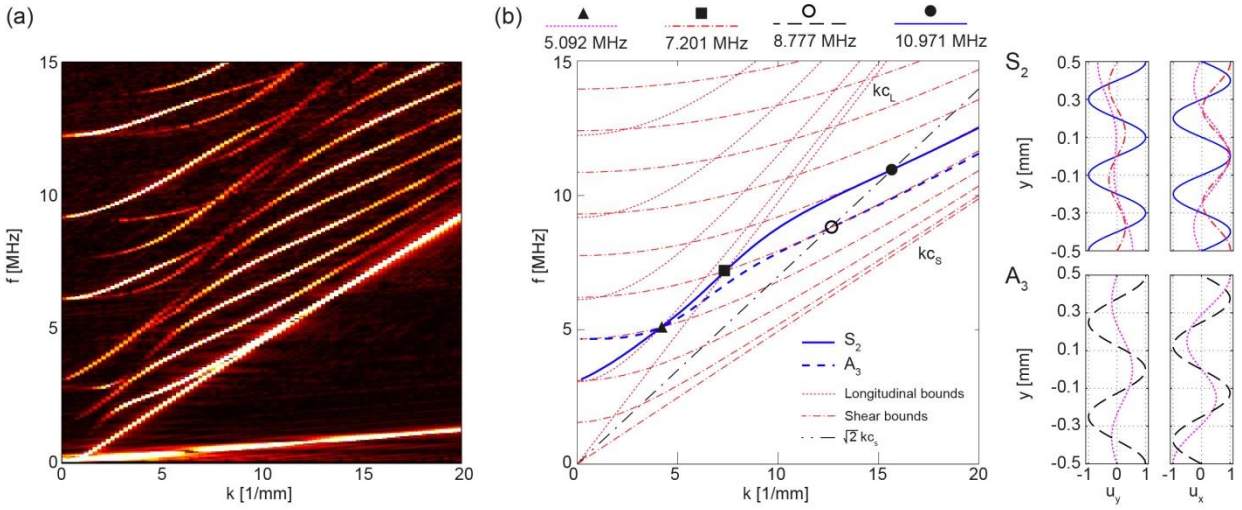

IUS2-K-5

Dipole and Monopole actuator for underground application

Abderrhamane ounadjela[1,2], Henri Pierre Valero[3], Jean christophe Auchere[4]; *[1]Sonic, Schlumberger, Fuchinobe, Kanagawa, Japan, [2]Sonic, Schlumberger, fuchinobe, Kanagawa, Japan, [3]Sonic, Schlumberger, Sagamihara-Shi, Kanagawa, Japan, [4]Sonic, Schlumberger, Sagamihara-shi, Kanagawa, Japan*

Background, Motivation and Objective

A new seismic source has been developed to answer to the increasing demand of the oil and gas reservoir management. This technology allows during the exploration to provide fundamental information about the reservoir topology, particularly to delineate the gas/oil/water contact interfaces and the fractures present in the reservoir. During the production phase, this type of source can either be used in an observation or in the production well to monitor the fluid front in the reservoir. In the past this type of technology has been limited by the depth of inves-tigation and the resolution. By placing the hardware close to the zone of interest, and thanks to this new source design, the acquired data are processed with a good signal/noise and resolution.

Statement of Contribution/Methods

This technology relies on a downhole seismic source clamped on the borehole wall, in order to optimize the energy transmitted into the formation. Because the borehole diameter is limited, the motors are placed along the tool axis, and the motor motion or force are transmitted either radially or axially following the desired mode of propagation. A dipole mode propagates when the motor are driven out of phase while the monopole mode is triggered with the motors vibrat-ing in phase. Because this source is mainly reactive, a new power electronic has been developed to supply the electrical energy through a conventional downhole cable. The best results are obtained with a sweep frequency signal or an M-sequence coded signal.

Results/Discussion

This technology relies on a downhole seismic source clamped on the borehole wall, in order to optimize the energy transmitted into the formation. Because the borehole diameter is limited, the motors are placed along the tool axis, and the motor motion or force are transmitted either radially or axially following the desired mode of propagation. A dipole mode propagates when the motor are driven out of phase while the monopole mode is triggered with the motors vibrat-ing in phase. Because this source is mainly reactive, a new power electronic has been developed to supply the electrical energy through a conventional downhole cable. The best results are obtained with a sweep frequency signal or an M-sequence coded signal.

Results and discussion

By the nature of the operation, the tool has been designed to withstand harsh environment and to be easily customized to an oil/gas production monitoring. Extensive lab experiments have allowed characterizing the mechanical and acoustic behavior of this device. The tool has a broad operation bandwidth up to 1 KHz without spurious modes. A field test has been performed in Connecticut, USA and various data sets have been acquired. At each station the monopole and the dipole mode have been fired, allowing thus to highlight a particular zone by performing a beam steering at the signal processing stage. Examples of this data will be presented highlighting performance of this new acoustic device.

Ultrasonic measurement of micrometric wall-thickness loss due to corrosion inside pipes

Julio Cezar Adamowski[1], Nicolas Perez[2], Flavio Buiochi[1], Carlos Patusco[3], Claudio Camerini[3]; *[1]Mechatronics, Universidade de Sao Paulo, Sao Paulo, SP, Brazil, [2]Centro Universitario de Paysandu, Universidade de La Republica, Paysandu, Uruguay, [3]CENPES, PETROBRAS, Rio de Janeiro, RJ, Brazil*

Background, Motivation and Objective

Pipelines are subject to wall-thickness loss due to corrosion along time. Ultrasonic pulse-echo techniques are widely used for thickness measurement achieving a high resolution. However, the precision of measurement is highly dependent on temperature and on the ultrasonic system (transducer assembly, electronics and signal processing). This work presents the temperature correction strategy of an ultrasonic measurement system to obtain a 1- µm precision in a pipeline corrosion long-lasting monitoring.

Statement of Contribution/Methods

This work presents the temperature correction strategy of an ultrasonic measurement system to obtain a 1- µm precision in a pipeline corrosion long-lasting monitoring. The experimental setup comprises an array of eight ultrasonic transducers (5 MHz, 10-mm diameter) operating in pulse-echo mode with a water coupling layer. The wall-thickness is evaluated by processing the first three echoes of the received ultrasonic signal. The first echo was reflected by the external wall (water layer) and the last two are internal reflections. The temperature of the water layer is measured with a digital thermometer (0.01°C resolution). The ultrasonic signal is acquired with a sampling frequency of 50 MHz, corresponding to a thickness resolution of about 60 µm in carbon steel. To achieve a resolution of 0.6 µm, a low-pass interpolation algorithm of 100 points is used. The time delay between the internal echoes is obtained by the zero crossing of the Hilbert transform of the cross correlation between the two internal reflections. A signal/noise ratio of 90 dB is used to obtain a resolution of 0.6 µm in the wall-thickness measurement. This ratio is obtained by using low noise electronics and signal averaging. The main strategy for temperature compensation is based on the fact that the coupling layer has a constant thickness during a long period of time (year) at a given temperature. At a range of temperatures, the strategy enables to relate the variation of time of flight in the coupling layer to the variation of time of flight in the pipe wall. This relation can be described by a polynomial function which includes a variation on propagation velocity and thermal expansion.

Results/Discussion

Long term corrosion tests were conducted at the Corrosion Laboratory, IPT (Institute for Technological Research, Sao Paulo, Brazil), using an electrolytic bath with 3 different current densities (1.6, 5.0 and 10 mA/cm2), along 10 months. Good agreement was found between the theoretical corrosion rate and the results of the ultrasonic measuring system. Field tests on oil pipelines will begin in the first semester of this year.

Piezoelectric Ultrasonic Transducers and Applications

T1

Thursday, July 25 2013, 08:30 am - 10:00 am

Congress Hallair: **Jean-Francois Saillant**
Areva

IUS5-K-1

Evaluation of the Pyroelectric Response of Embedded Piezoelectrics by Means of a Nyquist Plot

Gunnar Suchaneck[1], Agnes Eydam[1], Gerald Gerlach[1]; [1]*Solid State Electronics Lab, TU Dresden, Dresden, Germany*

Background, Motivation and Objective

In the so-called laser intensity modulation method, periodical heating of the sample top surface generates well-defined thermal waves, which propagate in the sample and cause local changes in temperature, thermoelastic strains, pyroelectric response etc. Recording the pyroelectric response of the already electroded piezoelectric transducer is therefore a suitable non-destructive technique to evaluate the polarization state of piezoelectrics embedded in metals, ceramics, polymers etc.

Statement of Contribution/Methods

The frequency response of non-resonant, linear systems with a periodic pulse signal (signal amplitude A, zero point equilibrium) is represented in the frequency domain by a function $H(i\omega)$ at each modulation frequency ω in terms of gain $|H(i\omega)| = \sqrt{\mathrm{Re}(H)^2 + \mathrm{Im}(H)^2} = A_{out}/A_{in}$ and phase shift $\varphi = \arctan[\mathrm{Im}(H)/\mathrm{Re}(H)]$. Frequency response is often analyzed by plotting the real and imaginary parts of the pyroelectric current in Cartesian coordinates on a parametric plot with frequency as a parameter (Nyquist plot). In our case, we have to take into account, that with increasing frequency thermal losses are decreased whereas the pyroelectric response is increased. Contrarily to well known dielectric relaxation, we have to consider therefore a frequency response $H(i\omega) = 1\text{-}H(i\omega)_{diel}$.

Results/Discussion

The simple Debye relation $H(i\omega) = i\omega\tau/(1+i\omega\tau)$, where τ is the relaxation time of thermal losses, gives already a satisfactory agreement with experiments for Macro-Fiber Composite (MFC) piezoelectric transducers consisting of rectangular piezoceramic rods sandwiched between layers of adhesive, electrodes and polyimide film (Fig. 1).

More advanced models will be considered to describe the pyroelectric response of piezoelectric plates embedded in low-temperature cofired ceramics, piezofibers embedded in epoxy resign and polyimide covered piezoelectric transducers embedded in die-casted aluminum.

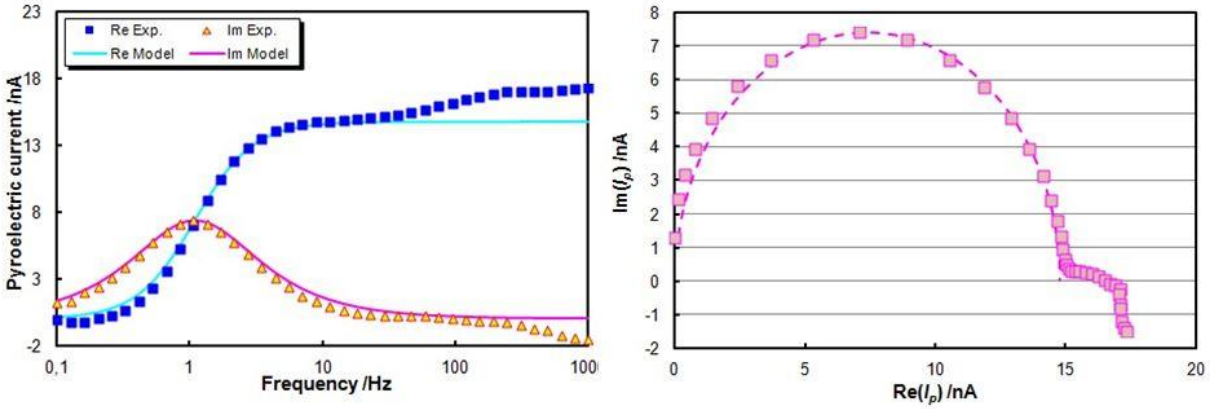

Fig.1: Pyroelectric current spectrum and Nyquist plot of the pyroelectric response of a commercial MFC transducer (Smart Materials GmbH).

IUS5-K-2

2D Array Transducer with a Conductive Backing

Jeongdong Woo[1], Wonseok Lee[2], Sanggon Lee[2], Hyungkeun Lee[1], Byungkook Bae[1], Eunhee Shin[1], Sunghag Kim[1], Yongrae Roh[2]; [1]*Alpinion Medical Systems Ltd., Korea, Republic of,* [2]*School of Mechanical Engineering, Kyungpook National University, Daegu, Daegu, Korea, Republic of*

Background, Motivation and Objective

Typical piezoelectric 2D array transducers have a large number of channels. In order to alleviate the difficulty in fabricating so many channels, most of the 2D array transducers reported so far have been made to consist of several sub-array modules. However, even if sophisticated process-es were employed to align and bond the modules in an exact pattern, the effects of the gap be-tween the modules are inevitable. The problem can be resolved by machining the whole 2D array on a piezoelectric plate as a single unit. Last year, we presented fabrication of whole 64,,e64 ele-ments on a single PMN-PT plate. However, it was very difficult to achieve good uniformity in sensitivity over the elements. Further, acoustic backing could not be so good as that for typical module type transducers. Hence, in this work, a new conductive backing has been developed to resolve the fabrication difficulty and to improve the transducer performance.

Statement of Contribution/Methods

As shown in Fig. 1, conductive pillars were molded in polymeric matrix following the processes similar to those for fabricating 1-3 piezocomposites. Many combinations of different pillar and matrix materials were tried to find the one to achieve the best acoustic performance (high imped-ance and attenuation), manufacturability, and channel uniformity of the backing. Final selection was graphite (Modern Carbon, Korea) for the pillars and epoxy (DP420 from 3M) mixture with tungsten powders for the matrix.

Manufactured backing sizes 23mm„e23mm„e3mm. The conduc-tive backing is attached to the rear surface of a PMN-PT crystal plate to work as both an electric wire plate and an acoustic backing. A hard PCB is attached to the other surface of the conductive backing to protect the backing and to ease the wiring of signal circuits to the conduc-tive backing.

Results/Discussion

Once the stack composed of the PMN-PT plate and the conductive backing is ready, the other processes to fabricate the 2D array transducer are similar to those for conventional linear arrays, which are much simpler than those for the module type transducer. Fabricated 64„e64 transducer has a center frequency at 3.5 MHz and fractional bandwidth of 75%. In terms of sensitivity uni-formity, standard deviation over the entire 4,096 array was 0.81dB at maximum without tuning circuits, which is significant improvement over the module type transducer.

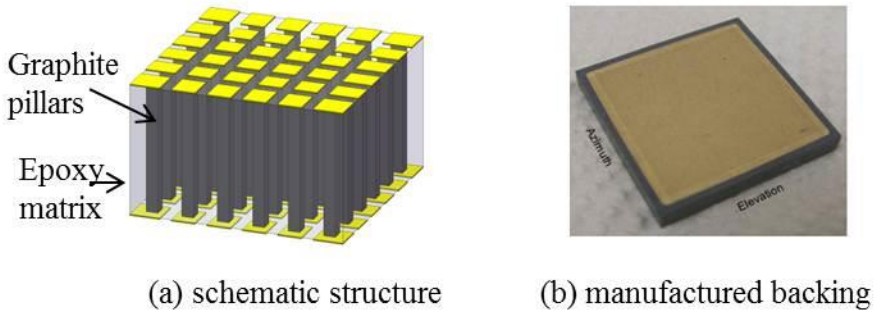

Fig. 1. Conductive backing

IUS5-K-3

Design and Fabrication of a New Multi-Active Layered Transducer with a Novel Single Copper Layered FPCB

Eunhee Shin[1], Susung Lee[2], Sangseok Lee[2], Jongkil Kim[2], Yongrae Roh[3]; *[1]Probe_Acoustic, Alpinion Medical Systems, Seoul, Korea, Republic of, [2]Alpinion Medical Systems, Korea, Republic of, [3]School of Mechanical Engineering, Kyungpook National University, Daegu, Korea, Republic of*

Background, Motivation and Objective

A multi-active layered transducer has multiple layers of a piezoelectric material as the active layer of the transducer. The multi-active layered structure improves the acoustical and electrical performance of an ultrasonic transducer by tailoring its impedance to the imaging circuits, resulting in better image quality for medical sonography. A multi-active layered design is an especially good structure for a phased array transducer at low frequency, with a small aperture size, and high element count. However, the multi-active layered structure is not widely used because of difficulty in fabrication.

Statement of Contribution/Methods

Multi-active layered transducers are generally composed of odd numbers of piezoelectric layers to simplify the electrical connections. Among the odd-numbered layered structures, 3 layers is the simplest, but even a 3.5MHz transducer requires piezoelectric layers that are very thin (<100um) and fragile. The odd-numbered layered structures also demand a unique electrode interconnection scheme, including wrapping the electrodes around the edges of the layers. Hence, in this paper, a two-active layer structure with a novel single copper layered flexible printed circuit board (FPCB) has been developed as in Fig. 1 to resolve the problem, i.e. to reduce the fabrication difficulty while achieving similar improvement in the transducer performance to those of odd-numbered layered structures.

Results/Discussion

A two-active layered phased array transducer which has 3.5 MHz center frequency, 0.15 mm pitch, and 128 elements has been designed and simulated using a finite-element analysis program (PZFlex). The transducer has two thin PZT layers, two front impedance matching layers, and a backing load. The two PZT layers are connected by the novel single copper layered FPCB. Detailed structure of the transducer has been optimized to achieve the widest bandwidth possible, and the transducer has a higher sensitivity (>5dB) and a wider bandwidth (+10%) than those of a comparable single active layer transducer. An experimental two-active layered transducer has been fabricated following the design, and the measured sensitivity agrees with the design within 0.2 dB difference, which confirms the efficacy of the new structure.

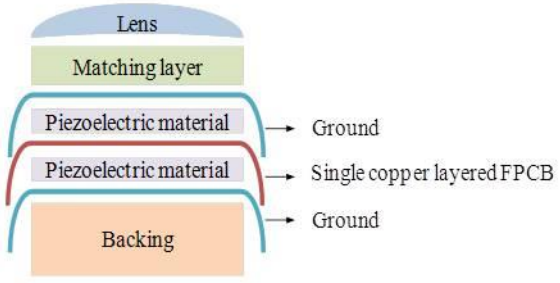

Fig. 1. Structure of two-active layered transducer

IUS5-K-4

Parabolic transducer array for ultrasonic energy harvesting inside an MRI machine.

Victor Klymko[1], Maurice Roes[2], Jeroen van Duivenbode[2], Elena Lomonova[2]; [1]*Electrical Engineering, Eindhoven University of Technology, Eindhoven, Netherlands,* [2]*Eindhoven University of Technology, Netherlands*

Background, Motivation and Objective

During an MRI scan, various sensors are placed on the patient's body to register his motion, temperature, etc.. We present a work-in-progress experimental setup with the goal to wirelessly power motion and temperature sensors that are located on the patient by using an ultrasonic wave. The ultrasonic energy is chosen to eliminate interference with the magnetic fields of the MRI machine.

Statement of Contribution/Methods

In this experimental work, an array of piezoelectric transducers is used to focus acoustic energy on a single transducer that acts as a receiver. The transmitting transducers are located along the parabolic shape that fits inside the MRI machine torus interior. The receiver is placed at the focal point of the parabola, 34 cm away from its surface, where the chest of the patient is thought to be. The focal distance is adjustable by changing the curvature of the parabola. In the prototype receiver, the acoustic energy is converted into electric energy and dissipated on a resistive load.

Results/Discussion

Our measurements show that the parabola-shaped transducer array is capable of focusing the ultrasonic wave at the distance of 19 λ, far beyond the near field of a single transducer. With 100 mW of input electric power applied to 4-element transducer array, the harvested electric power at the receiver is 8 μW. With the same input power at a single transmitting transducer, the harvested power is 5 μW. Increasing the number of elements in the transmitter array and implementation of the phased array can further improve acoustic wave focusing and efficiency of the system.

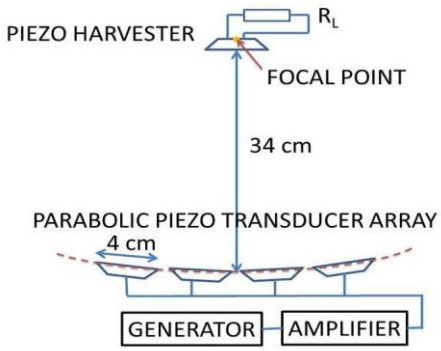

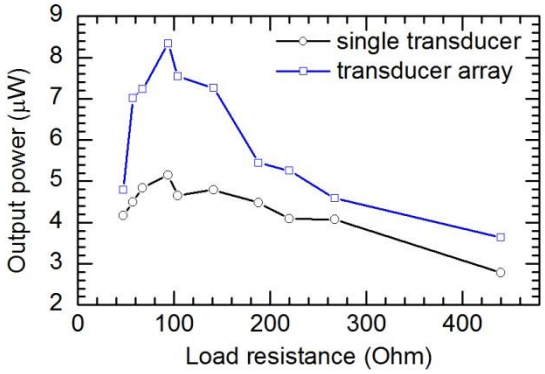

IUS5-K-5

Wide Aperture Convex Array Transducer with PMN-PT Piezoelectric Single Crystals

Heewon Kim[1], Susung Lee[1], Sangwoong Lee[1], Boyeon Cho[1], Nelson Oliver[2], Wonho Noh[1]; [1]*Probe, Alpinion medical systems, Seoul, Korea, Republic of,* [2]*None, Beaverton, Oregon, USA*

Background, Motivation and Objective

The piezoelectric single crystal PMN-PT has lower acoustic impedance and higher electromechanical coupling coefficient than conventional piezoelectric materials. For these reasons, the single crystal can be a good resolution to enhance the sensitivity and frequency bandwidth of ultrasonic transducers. However the single crystal has certain size limitation, difficult manufacturability and higher electrical impedance, too. Thus many transducer manufacturers commonly use the single crystal for a small aperture and lower frequency transducer design like a phased array transducer. In this paper, however, the single crystal is applied to a wide aperture convex transducer design that has a bigger aperture size (60 mm radius of curvature, 192 channels) and a higher center frequency (≥ 4MHz) than the general phased array transducers.

Statement of Contribution/Methods

In order to achieve the wide aperture, two small single crystal plates are combined together to compose one transducer. Two thin plates of the PMN-PT crystal are aligned very accurately to each other and molded together to work like a single unit eventually. Detailed structure of the transducer has been designed through finite element (FE) modeling and simulation. Unique manufacturing processes have been developed to fabricate prototypes of the transducer.

Results/Discussion

Figure 1 shows measured performance of the transducer: -6dB center frequency is 4.3MHz, -6dB fractional bandwidth is 89%, and -20dB pulse length is less than 4 cycles. The prototypes also show good uniformity in the performance over its entire channels, which confirm the validity of present fabrication technology. These results allow us to expand the range of single crystal application to ultrasonic transducers.

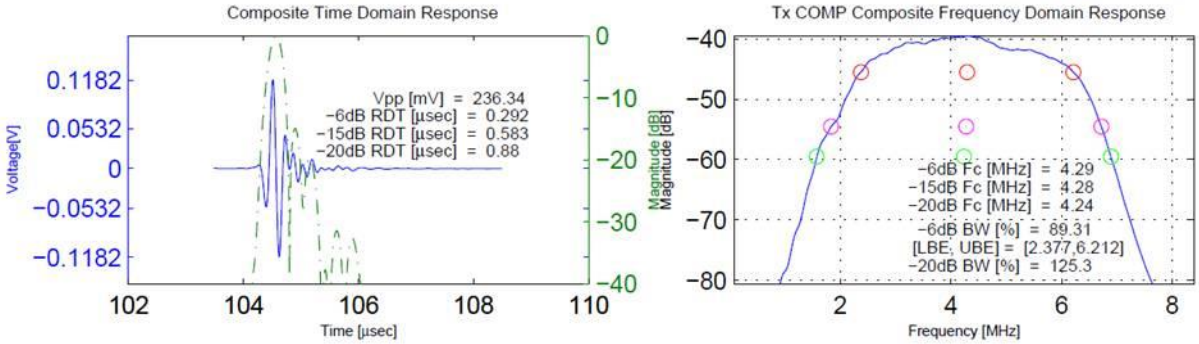

Fig. 1. Performance of the wide aperture convex array transducer.

IUS5-K-6

Experimental and Theoretical Evaluation of a Low-Cost, 15 MHz Fingerprint Piezo-Composite for Ultrasonic Imaging

Holly Lay[1], Devin Delong[1], Joseph Zeichman[1], Andrea Casanova[1], Yanli Xie[1], Rainer Schmitt[1]; [1]*Sonavation Inc, USA*

Background, Motivation and Objective

In previous work we have shown the usability of low-cost piezo-composites in acoustic impediography[1]. In this paper, we evaluate the use of both FEM (PZFlex)[2] and impulse-response methods (Field II) in predicting the performance of a 15 MHz acoustic impediography sensor. While FEM modelling techniques do a better job of replicating the boundary conditions and edge effects which impact the acoustic field, the necessary complexity can lead to long computation times and model size limits. In contrast, while impulse-response models do not fully replicate the physical characteristics of the system, their rapid computation time can allow many possible configurations to be compared in a relatively short amount of time. By comparing these models with experimental results, we are able to assess their relative strengths, allowing more efficient use of both experimental and simulation time.

[1]RM Schmitt, J Owen, "Impediography: Imaging Surface Acoustic Impedance Using 1-3 Piezo-Composite for Integrated Fingerprinting," Proceedings of the IEEE ECTC symposium 2011, pg. 1296-1300

[2]See accompanying abstract: FEM/BEM Model Evaluating Ultrasonic Imaging for High Frequency 15 MHz Ultrasound in 3D

Statement of Contribution/Methods

Our array was designed with a 50.8 µm pitch (500 DPI). The array elements were connected in pairs to produce a linear array suitable for imaging at 15 MHz. To test the array, a custom printed circuit board was designed to connect 64 elements of the array to the Verasonics acquisition system. An imaging phantom was made consisting of a 300 µm diameter steel needle suspended in a gelatine mold parallel to and 4.5 mm above the surface of the transducer. The Verasonics system was used to focus the beam at 4.5 mm and the echoes were recorded. PZFlex and Field II were then used to create virtual models of our sensor and the resulting time-domain responses compared to experimental imaging.

Results/Discussion

Comparing the experimental results to the Field II simulations (figure 1), it can be seen that the Field II shows good correspondence on general pulse shape and beam pattern, but does not fully model the impact on the axial and lateral resolution due to cross-talk and boundary conditions. However, by using the more rigorous PZFlex model to calibrate the Field II simulation, it becomes a powerful tool for rapid experimental validation.

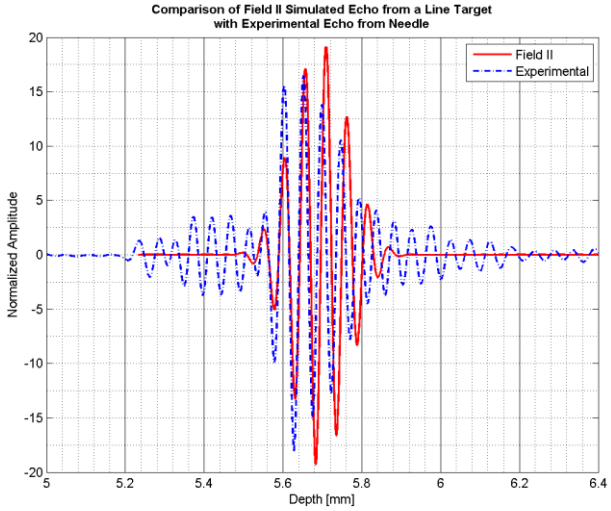

Emerging Technologies

T2

Thursday, July 25 2013, 08:30 am - 10:00 am

Congress Hallair: **Jan Kuypers**
Sands 9, Inc.

IUS4-K-1

Ultra-high Q.f product laterally-coupled AlN/Silicon and AlN/Sapphire High Overtone Bulk Acoustic Wave Resonators

Alexandre Reinhardt[1], Marie Thérèse Delaye[1], Julie Abergel[1], Veronika Kovacova[1], Marjolaine Allain[1], Laurence Andreutti[1], Denis Mercier[1], Jeremy Georges[1], Pierre Patrick Lassagne[1], Emmanuel Defaÿ[1], Nicolas Chretien[2], Thomas Baron[2], Gilles Martin[2], Eric Lebrasseur[2], Sylvain Ballandras[2], Luc Chommeloux[3], Jean-Marc Lesage[4]; *[1]CEA, Leti, Grenoble Cedex, France, Metropolitan, [2]Institut FEMTO-ST, Besançon, France, Metropolitan, [3]Senseor, Mougins, France, Metropolitan, [4]DGA, CELAR, Rennes, France, Metropolitan*

Background, Motivation and Objective

High-Overtone Bulk Acoustic Resonators (HBAR) have the capability to provide very sharp resonances directly at GHz frequencies. As such, they are seen as promising structures for direct frequency generation in GHz oscillators. The highest quality factor for such structures was reported exactly two decades ago by Kline and Lakin and reached 68,000 at 1.6 GHz, for an AlN on Sapphire resonator. Until now, this record Q.f product of 1.1 10^{14} has not been reproduced. More recently, laterally-coupled HBAR resonators have been proposed in order to provide a fully differential structure which naturally selects only a few overtones of the resonator response. First attempts lead by Gachon *et al.* in 2011 used thinned lithium niobate layers transferred on quartz substrate, and operated between 300 and 700 MHz. In this work, we investigate the use of sputtered AlN thin films as the piezoelectric layer and silicon or sapphire substrates in order to increase the operation frequency of laterally-coupled HBARs between 2 and 5 GHz.

Statement of Contribution/Methods

HBAR resonators have been fabricated on doubled side polished silicon and Z-cut sapphire substrates, on which a thin SiO2 film has been deposited before sputtering Molybdenum electrodes, the AlN piezoelectric film and again top Molybdenum electrodes. A SiN film was added before the deposition of Aluminum contact pads. The electrodes define two resonators with only a small gap ranging from 1 to 10 µm to provide a large acoustic coupling suitable for attaining a narrow filter bandwidth. These filters were then tested on wafer to evaluate insertion losses and bandwidth, from which a quality factor is extracted.

Results/Discussion

Insertion losses were found to lie between 5 and 25 dB. Unloaded quality factors reached 4,000 at 2.5 GHz and 2,000 at 4.3 GHz on silicon substrates, leading to a constant Q.f product close to 10^{13} Hz, which is the limit usually attributed to silicon. On the other hand, as shown below, filters fabricated on sapphire substrates exhibited quality factors of 31,000 at 2.5 GHz and 25,000 at 4.3 GHz, leading after twenty years to a Q.f product close to 1.1 10^{14} Hz. However, the fact that these quality factors do not scale with frequency indicate that viscoelastic losses are not the limiting factor and that there is still room for improvement.

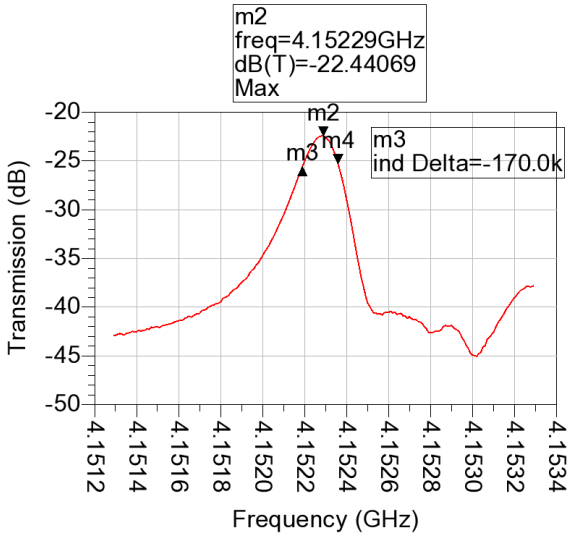

IUS4-K-2

Light-driven nano-machines: from ultra-cold resonators to opto-mechanical memories

Wolfram Pernice[1]; *[1]Institute of Nanotechnology, Karlsruhe Institute of Technology, Eggenstein-Leopoldshafen, Baden-Württemberg, Germany*

Background, Motivation and Objective

Transduction of nanomechanical resonators presents significant challenges for traditional approaches due to impedance mismatch and diffraction limited optical resolution. In this respect integrated optical methods provide an attractive alternative for nanoscale actuation and readout due to the fact that nanophotonic devices are size-matched to nanomechanical resonators. The resulting field of integrated optomechanics is therefore receiving increasing attention for fundamental physics as well as novel applications in ultra-sensitive detection and all-optical sensing. Furthermore, by employing principles of integrated optics on-chip signal processing can be employed to enhance the functionality of nanomechanical sensors. At the same time, leveraging the additional mechanical degree of freedom for nanophotonics provides a new route for tunable optical devices.

Statement of Contribution/Methods

Results/Discussion

In this talk I will present resent progress in the field of integrated optomechanics with respect to two regimes of optical operation. Exploiting optomechanical feedback by embedding the mechanical resonator into an optical cavity allows for both enhancing or suppressing nanomechanical motion depending on the detuning with respect to the cavity resonance. On the one hand, optomechanical damping can thus be employed to achieve low phonon occupation numbers, which has recently led to the preparation of an optomechanical resonator in its quantum ground state. On the other hand, optomechanical amplification allows for reaching high mechanical displacement, sufficient to overcome inherent potential barriers in multi-stable devices. This feedback scheme allows for the realization of all-optically driven mechanical memories that are non-volatile and suitable for both mechanical and optical multi-plexing.

IUS4-K-3

MODELLING OF INTER-DIGITATED TRANSDUCER FOR HIGH-ORDER CONTOUR MODE RESONATORS

Renyuan Wang[1], Sunil A. Bhave[1], Kushal Bhattacharjee[2]; [1]*ECE, Cornell University, Ithaca, NY, USA,* [2]*RF Micro Devices, Inc., Greensboro, NC, USA*

Background, Motivation and Objective

LiNbO3 contour-mode resonators (CMR) have potential to achieve multi-frequency wide-band-pass filters. IDT position on them can significantly affect their performance [1]. We present a model that analytically & intuitively explains behavior with IDT@anti-nodes(AN) vs @nodes(N). The model is verified with measurements.

Statement of Contribution/Methods

Fig. 1 shows the measured admittance of CMR with identical design except the IDT locations (AN vs N). The key feature of N IDT is it doesn't couple to the 11th S0 mode. Instead, it excites adjacent even order modes. In contrast, the AN IDT excites the 11th mode while suppressing other modes. This contradicts SAW IDT impulse model [2,3]. The CMR's sharply defined mechanical boundaries cause multiple wave reflections which interfere with themselves. Our model accounts for this effect and the coupling between RF field and mechanical mode, to simultaneously explain both AN & N response.

Consider N IDT with 2Np+1 fingers and a period of λo/2. IDT freq response is (1). The last part in (1) captures interferences of reflected waves in CMR, α is the loss from reflection. I(f) is the IDT response derived from impulse model (2), W(f) is the IDT element factor. From the model, the odd order modes of the N IDT in Fig. 1 are suppressed (Fig. 2a), as they falls at "0"s of H(f); while the even order modes are excited. This closely matches the measurement. In contrary, the AN IDT (Fig. 2b) suppresses all mechanical modes, except the 11th mode, which explains the spur-free AN spectrum.

Results/Discussion

We derived a universal model for analyzing IDT of MEMS resonators. Our model is applicable to any CMR technology including PZT, AlN and AlScN.

1 R. Wang, S. A. Bhave, K. Bhattacharjee, MEMS 2013.

2 M. Kadota, et al., Tran. UFFC, 1269-1279, 49 (2002).

3 R. Tancrell, M. Holland, IEEE Proc. of the IEEE, 393-409, 59 (1971).

$$H(f)=W(f)*I(f)*\mathrm{Re}\left[\left(1+\alpha e^{-j\frac{2\pi f}{f_0(N_p+0.5)}}\right)/\left(1-\alpha^2 e^{-j\frac{2\pi f}{f_0(2N_p+1)}}\right)\right] \quad (1)$$

$$I(f)=\sum_{-N_p}^{N_p}(-1)^n e^{-j\pi n\frac{f}{f_0}} \quad (2)$$

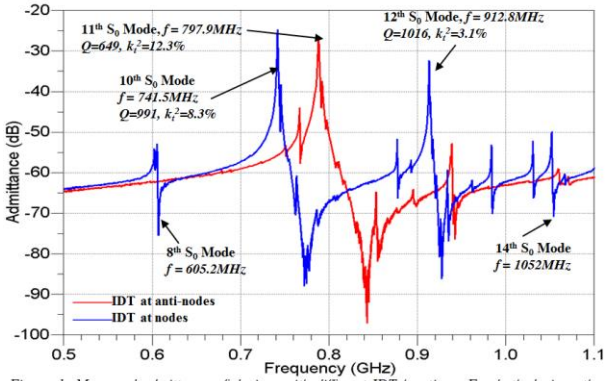

Figure 1: Measured admittance of devices with different IDT locations. For both devices, the IDT period ($\lambda_0/2$), metallization ratio and total width are 3.8um, 1 and 11$\lambda_0/2$.

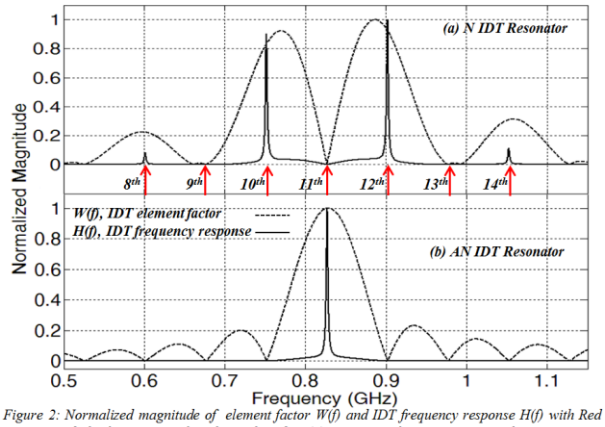

Figure 2: Normalized magnitude of element factor W(f) and IDT frequency response H(f) with Red arrows mark the frequencies of mechanical modes; (a) Response of N IDT resonator shown in Fig. 1; (b) Response of AN IDT resonator shown in Fig. 1.

IUS4-K-4

Oscillator-based strain gauges employing surface acoustic wave resonators for wireless sensor network

Tomokatsu Konno[1], Motoaki Hara[1], Hiroki Kuwano[1]; [1]*Department of Nanomechanics, Tohoku University, Sendai-shi, Miyagi-ken, Japan*

Background, Motivation and Objective

Nowadays, aging of public infrastructures such as tunnels or highways have been becoming a serious problem. Wireless stress monitoring can give a new solution to manage the risk. Assuming that the wireless monitoring system is applied to such giant infrastructures, it is difficult to read out the data from each sensor node using an interrogator. So, it is required for sensor nodes to send the data autonomously and also construct a mesh network each other.

Statement of Contribution/Methods

We develop the oscillator-based strain monitoring system for wireless sensor network using surface acoustic wave (SAW) resonator as shown in Fig. 1. The SAW resonator operates as not only a frequency reference for the oscillator but also a strain sensor head. Therefore the strain applied to the SAW resonator is detected as a shift of oscillation frequency (Δf). In our system, two oscillators with same SAW resonator are integrated. The frequency shift due to the strain can be extracted by the down conversion technique. Using this technique, disturbance from environment (f_d) such as temperature or humidity against the SAW resonance can be cancelled, and S/N ratio is improved.

Results/Discussion

Figure 2 shows the relationship between the strain and frequency shifts of the oscillator and the resonator. It was confirmed from Fig. 2 that the shift of the oscillation frequency was proportional to the applied strain based on variation of the resonant frequency of the resonator. Moreover, it was confirmed from this figure that our sensor had linear relation even in 10^{-6} order strain. This result is much lower than the minimum measurable limit in the commercial strain gauge using piezoresistance, which is 10^{-5} order.

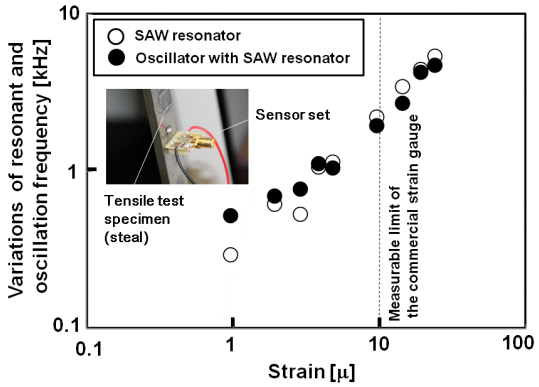

Fig.2

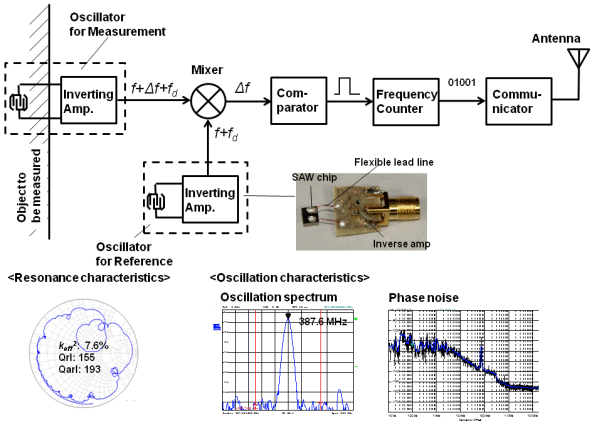

Fig. 1

IUS4-K-5

Chip Scale Sonic Communication Using AlN Transducers

Jason Hoople[1], Justin Kuo[1], Serhan Ardanuç[1], Amit Lal[1]; [1]*SonicMEMS Laboratory, School of Electrical and Computer Engineering, Cornell University, Ithaca, NY, USA*

Background, Motivation and Objective

The ability to scan an ultrasound beam has proved indispensable in several field including; ultrasonic imaging of tissue, non-destructive evaluation, and sonar ranging and communication. Here we demonstrate for the first time using thin film piezoelectric pixels on silicon chips to use ultrasonic pulses for on-chip communication. This on-chip ultrasonic communication would be reconfigurable offering programmable interconnects to communicate in 3D for inter-chip and intra-chip communication. In this paper, we present the first step towards this on-chip sonar by successfully demonstrating sonic communication between two aluminum nitride transducers fabricated by Sandia National Lab's RF MEMS process. This work opens up new vistas for computer architecture and low power computing using ultrasound. Thin film piezoelectric transducers allow for GHz pulse transmission which correlates to giga-bit per second communication on chip. This would allow the SONAR arrays to communicate information in parallel at very high speeds.

Statement of Contribution/Methods

The Sandia National Lab's RF MEMS process has been used to fabricate bulk micro-resonators and surface acoustic wave devices for RF filters and frequency references, for good devices an isolation step is used to keep energy within the device rather than lost to the bulk. We use the same fabrication processes for such devices without the isolation step to leave the piezoelectric structures on the substrate. In this configuration what is traditionally a loss mechanism is now the communication channel. An array of 100 micrometer square pixels spaced 200 micrometers apart was fabricated as seen in the microscope capture with schematic cross section as shown in Figure 1b and Figure 1c respectively.

Results/Discussion

An AlN pixel is driven with a 20 ns pulsed RF signal of 900 MHz. The neighboring pixel is connected to an RF amplifier and the voltage signal is measured. The measured amplitude and time of arrival for the receive signal matched what was predicted by PZFlex model. For 1 Vpp pulses, 100 μV receive pulses arrived at the detector 1.2 mm away. A low noise amplifier with a gain of 19 dB was used for easy pulse detection (Figure 1d). Extending the pulse width from 20 ns to 80 ns caused the corresponding change in the receive signal. RF frequencies in the range of 700 MHz to 1 GHz propagate well to the receive pixel (i.e. 50 to 100 μV).

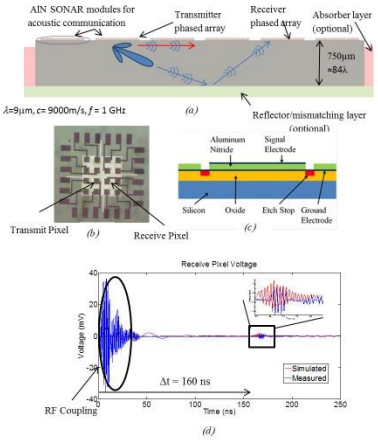

Figure 1: (a) Sonar schematic (b) microscope image of device (c) schematic cross section of single AlN pixel (d) Experimental and simulated results of receive pixel voltage corresponding to RF pulse from transmit pixel

Brain imaging

CONGRESS HALL

Thursday, July 25 2013, 10:30 am - 12:00 pm

Congress Hallair: **Wilko Wilkening**
Siemens Medical Solution

IUS1-L1-1

Functional Ultrasound Imaging of Brain Activity

Mickael Tanter[1]; [1]*Institut Langevin, ESPCI, Paris, France*

Background, Motivation and Objective

Functional imaging modalities such as fMRI or optical imaging identify regions of brain activity by measuring changes in blood flow thanks to the neurovascular coupling. Paradoxically, Ultrasound was not present in the field of Neuroscience till recently, whereas it is the most used modality for blood flow imaging in clinics. The reason for this was the poor sensitivity of Doppler ultrasound limiting blood flow imaging to large arteries. Ultrafast Doppler imaging based on plane wave imaging breaks this barrier and enabled recently the emergence of fUltrasound (by analogy to fMRI).

Statement of Contribution/Methods

fUltrasound (fUS) is able to provide unique whole brain images with unprecedented resolutions (100 µm and 200 ms on small rodents, 250 µm and 1s in clinical applications). Rodent examples such as the functional imaging of cerebral blood volume during epileptic seizures, whisker or odor stimulations first emphasizes the potential of this new imaging modality to provide completely new information for the understanding of brain.

Results/Discussion

fUS is a great tool for neuroimaging on small animals as it already helps both to answer unsolved questions and image the functional activity of to date unexplored brain regions. It should become a a full-fledged imaging modality of neuroscience as it provides the first whole brain and portable neuroimaging modality for awake and freely moving animal studies. Beyond small animal imaging, clinical fUS should become an alternative to fMRI in particular applications, such as newborns or preterm infants both for neonatal seizure monitoring or cognitive science studies. It could also become a powerful portable tool for neuroimaging during peroperative surgery on adults.

IUS1-L1-2

Automatic Mouse Embryo Brain Ventricle Segmentation from 3D 40-MHz Ultrasound Data

Jen-Wei Kuo[1], Yao Wang[1], Orlando Aristizabal[2], Jeffrey A. Ketterling[2], **Jonathan Mamou**[2]; [1]*Department of Electrical Engineering, Polytechnic Institute of New York University, Brooklyn, NY, USA,* [2]*F. L. Lizzi Center for Biomedical Engineering, Riverside Research, New York, NY, USA*

Background, Motivation and Objective

Volumetric analysis of brain ventricles is important to the study of normal and abnormal devel-opment of the central nervous system of mouse embryos. High-frequency ultrasound (HFU) is frequently used to image embryos because HFU is real-time, non-invasive, and provides fine-resolution images. However, manual segmentation of ventricles from 3D HFU volumes remains challenging and time consuming. Therefore, an automatic segmentation algorithm is needed.

Statement of Contribution/Methods

Volumetric ultrasound data were acquired *in utero* and *in vivo* from pregnant mice using a 5-element 40-MHz annular array. A 5-channel pulser was used to consecutively excite each array element. The 25 resulting transmit/receive signals were digitized and processed using delay-and-sum beamforming which yielded a depth of field sufficient to cover the entire head of the em-bryo. Active shape model (ASM) is a candidate segmentation method because it effectively "learns" the mean shape and shape variations from the training data. However, large training sets and dense sets of feature points (FPs) along region boundaries are required; these cannot easily be obtained from 3D HFU images. Therefore, a segmentation algorithm that augments ASM by using a detail-preserving reference shape and region growing was developed. During training, a set of corresponding FPs was extracted and the eigenvectors that describe the principal variation modes of FPs were determined. A reference shape that preserved shape details was also obtained from the training data. To segment a 3D HFU volume, the eigenvectors were used to find the initial FP positions using ASM and the reference shape was registered to the HFU volume using FPs. Finally, the registered reference shape was refined using a region-growing method con-straining the boundary deviation from the initial segmentation.

Results/Discussion

The algorithm was applied to 12.5-day-old embryos (6 training; 3 testing) and the Dice similarity coefficient (DSC) was used to quantitatively compare automatic and manual segmentation. The average DSC was 0.84 (superior to 0.78 obtained using region-growing alone). Our algorithm also showed better performance than region growing in preserving details and preventing leakage (Fig. 1). Our method could streamline current HFU longitudinal studies of brain development that require manual segmentation.

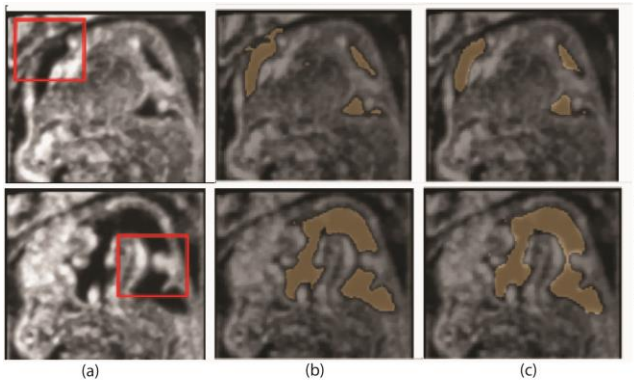

Fig. 1: (a) Lateral- (top panel) and Mid- (bottom panel) sagittal sections through the head of a 12 day old mouse embryo. Red rectangle indicates the undefined edge of the lateral ventricle (top panel) and the thin connection between the aqueduct and the fourth ventricle (bottom panel). (b) Delineation of the brain ventricles using traditional region growing segmentation algorithm. (c) Delineation of the brain ventricles using our ASM algorithm showing segmentation of lateral ventricle without leakage artifact (top panel). Our ASM algorithm is sensitive enough to segment out fine, low contrast regions of the brain ventricles such as the channel connecting the aqueduct and the fourth ventricle (bottom panel).

IUS1-L1-3

Functional Ultrasound Imaging of the Brain Resting State

Bruno-Felix osmanski[1], Sophie Pezet[2], mathias Fink[1], Zsolt Lenkei[2], Mickael Tanter[1]; *[1]Institut Langevin, ESPCI ParisTech, CNRS UMR7587, Inserm U979, UniversitÃ© Paris 7, Paris, Ile de France, France, [2]Laboratoire de Neurobiologie CNRS UMR7637, France*

Background, Motivation and Objective

In blood flow imaging, the high spatio temporal sampling of ultrafast plane wave imaging leads to a high sensitivity Power Doppler image called Ultrafast Doppler (UD). Thanks to the neurovascular coupling, repeating UD images gives access to brain neuronal activity and leads to the concept of Functional Ultrasound (fUS). We propose here to use fUS to map the functional connectivity of a rat brain at rest: The resting state (RS). The RS has been studied extensively in fMRI to describe the brain neuronal functional and structural connectivity in healthy and diseased subjects such as in Parkinson's or Alzheimer's disease. In RS, the neurovascular coupling leads to weak random cerebral blood volume (CBV) fluctuations around 0.1Hz. The objective is to make the proof of concept of RS fUS.

Statement of Contribution/Methods

The experiment was carried out using a 15MHz probe on 5 anesthetized rats with thinned skull. We used a standard fUS sequence: We repeated UD images (computed with 200 frames composed five angles (-4,-2,0,2,4) repeated with a 500Hz frame rate) with a 0.5Hz framerate to sample RS random fluctuations during 10 minutes.

Results/Discussion

By spotting a region (S1HL), extracting its temporal CBV variations and correlating it with all the other regions we can highlight neuronal connectivity of S1HL (fig a). Figure b shows the good match of the two temporal signals of two contra lateral correlated regions. A finest analysis was then done by applying a singular value decomposition of RS spatio-temporal dynamics and extracting the different "neuronal coupling modes" of the brain. Figure c to e show the first three modes.

As variations of CBV are weak (~5 %PD), blood pulsatility is a major issue in fMRI. Due to its high frequency (3Hz for rats) the variations of CBV within a heart cycle are aliased and decrease fMRI sensitivity. fUS permits to overcome this issue by insonifying the brain continuously at 500Hz. We tested it with only a short acquisition (40s) due to the high data volume. After wall filtering, the pulsatility can be filtered. Because of the higher sensitivity and time resolution of fUS, the first two "neuronal coupling mode" can be retrieved (fig f and g).

fUS was shown able to measure the weak neurovascular coupling of brain RS. Contrary to fMRI which has a limited framerate of 0.5Hz, fUS imaging overcomes the problem of blood pulsatility in RS strongly improving its sensitivity.

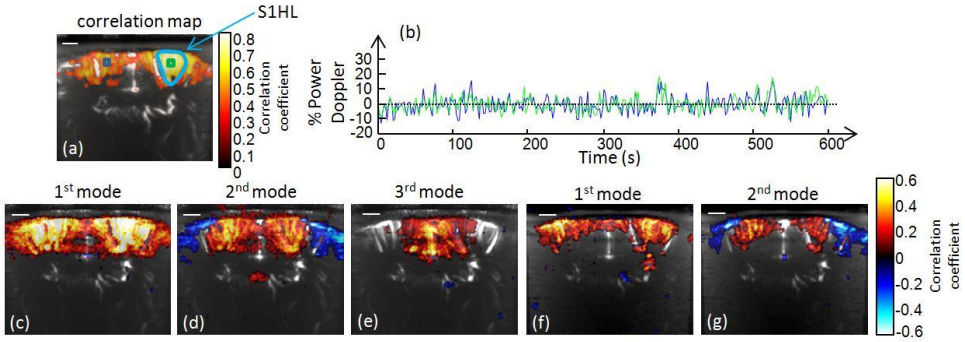

Figure: (a) Correlation map with the S1HL (bregma -1.5) temporal variation of CBV showing neuronal connection between S1HL and other regions. The vascularization is represented in gray scale. (b) CBV temporal variations of two regions. The respectively blue and green curves are extracted from respectively the blue and the green regions shown on (a). The %power Doppler evolution is calculated from the base line. (c) to (e) Three first "neuronal coupling mode" computed with a singular value decomposition (SVD) using standard fUS sequence during 10minutes. (f) and (g) The two first "neuronal coupling mode" computed with a SVD using continuous fUS sequence during 40s.

IUS1-L1-4

Rapid *in vivo* Imaging of Amyloid Plaques using Ultrasound-Induced Blood Brain Barrier Opening and MRI Gd-Staining

Mathieu Santin[1,2], Thomas Debeir[3], **Lori Bridal[4]**, Thomas Rooney[3], Marc Dhenain[1]; *[1]MIRCen, URA 2210 CEA/CNRS, Fontenay-aux-Roses, France, [2]Centre de Neuroimagerie de Recherche – CENIR, Institut du Cerveau et de la Moelle Epinière – ICM, Paris, France, [3]TSU Aging, Sanofi, France, [4]CNRS UMR 7623, France*

Background, Motivation and Objective

Alzheimer's disease (AD) is characterized by two complementary microscopic brain lesions: amyloid plaques and neurofibrillary tangles. They occur up to 20 years before the first clinical signs of the disease. Imaging amyloid plaques is critical to follow-up treatments and for an early diagnostic of AD. The approach developed here used NMR contrast agents combined to a transient blood-brain barrier (BBB) with ultrasound and microbubbles. Under the action of an ultrasound beam, microbubbles oscillate and allow the opening of the BBB. The aim of this work was thus to develop a new protocol (US-Gd-staining) to detect amyloid plaques after intra-venous (IV) injection of NMR contrast agent and BBB opening with ultrasound and microbubbles.

Statement of Contribution/Methods

This study was done using 6 APP/PS1 transgenic mice (8 to 17 months-old) exhibiting cerebral amyloid plaques and 6 control (littermate, PS1) plaque-free mice. A 1-MHz unfocused ultrasound transducer was used throughout this study (Imasonic). Near field distance, beam diameter and acoustic pressure were calibrated in a water tank filled with degassed and deionized water. The transducer was placed in a water tank under the animal's head. BBB opening was obtained by means of a controlled acoustic excitation at 1.1 MPa produced by the transducer and 200µL of encapsulated gas microbubbles (Sonovue, Bracco) injected IV.

NMR contrast agent (Dotarem, Guerbet) was also IV-injected. 3D Gradient-echo High-resolution (29µm) NMR images were recorded in 32 min.

The ability to detect amyloid plaques with this method was compared with detection of amyloid plaques with previously developed methods based on intracerebroventricular (ICV) injection of Dotarem.

Results/Discussion

US-Gd-staining, but also in vivo ICV-Gd-staining largely increased the signal to noise ratio in the brain of mice.

No hypointense spots which could be falsely identified as plaques were detected within the brain of amyloid-free litter-mate mice with the two methods described. No plaques could be detected *in vivo*- without the use of NMR contrast agent. In transgenic mice, hypointense spots could be detected in the cortex of all animals imaged with *in vivo* US-Gd-staining and *in vivo* ICV-Gd-staining protocols. The hypointense spots were confirmed as amyloid plaques with immunohistochemistry. These lesions were identified even in the youngest mice used in this study (8-months old).

To our knowledge this is the first study showing the feasibility of amyloid plaque imaging in mouse with a peripheric injection of NMR contrast agent and the non invasive opening of the BBB by US. This suggests that, in humans, contrast agents that can cross the BBB will allow the detection of amyloid plaques by MRI. In vivo US-Gd-staining should also permit a better follow-up of new therapies targeting amyloid in murine models of AD.

IUS1-L1-5

High-Frequency Ultrasound for In Vivo, 3D Imaging and Analysis of Mouse Embryo Brain Development

Orlando Aristizabal[1,2], Jonathan Mamou[3], Daniel H. Turnbull[1,2], **Jeffrey A. Ketterling[3]**; *[1]Kimmel Center for Biology and Medicine at the Skirball Institute of Biomolecular Medicine, New York, NY, USA, [2]Department of Radiology, New York University School of Medicine, New York, NY, USA, [3]Lizzi Center for Biomedical Engineering, Riverside Research, New York, NY, USA*

Background, Motivation and Objective

In utero imaging methods that are high throughput and high resolution are urgently required to analyze the dynamics of brain growth and patterning in mouse embryos, which are extensively utilized to study mammalian brain development. To address this need, a 5-ring, 38 MHz annular-array ultrasound imaging system was developed to obtain 3D data from individual, in utero embryos in close to 2 minutes, and data from 4-6 embryos in each pregnant mouse in less than 30 minutes. The approach was previously validated with a smaller number of embryos over 4 days of growth. Here, detailed studies of volumetric changes associated with mouse brain development were performed by acquiring 3D data from 148 embryos spanning five days from the early-to-mid gestational stages of E10.5-14.5.

Statement of Contribution/Methods

After synthetically focusing the digitized array data, 3D image stacks were imported into visualization software (Amira) for volumetric visualization, segmentation and quantitative analysis. Before segmentation, the data were processed with a 3D Gaussian filter and a contrast-limited adaptive histogram equalization filter. Semi-automatic segmentation of the head and brain ventricles was then performed with a 3D threshold detection algorithm. After segmenting the contours, the head and ventricles were reconstructed in 3D (Fig.), and

volume and surface areas were computed for each embryo data set. The data were then analyzed to establish quantitative parameters of normal brain development such as surface area and volume, as well as other morphometric parameters such as the pontine flexure angle.

Results/Discussion

Ventricular volume peaked at E11.5, increasing by close to 75% from E10.5 to 11.5, and then decreasing slowly until E14.5. The ventricular volume was close to 15% of the head volume at E10.5, and decreased over the developmental stages up to E14.5. As a quantitative index of embryonic stage, measurements of the pontine flexure angle in mid-sagittal sections showed a steady linear decrease between E10.5 and E13.5, and then remained constant between E13.5 and E14.5. The results demonstrate that high-frequency ultrasound can be used for high-throughput, in vivo 3D, longitudinal imaging of mouse embryos and may permit the creation of atlases of mouse brain development and more accurate staging of age.

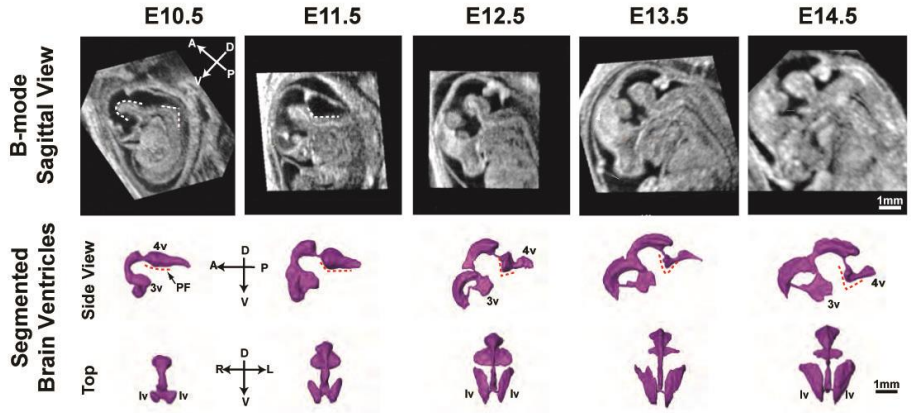

Therapy monitoring and evaluation

M4

Thursday, July 25 2013, 10:30 am - 12:00 pm

Congress Hallair: **Jean-Yves Chapelon**
INSERM

IUS1-L2-1

Acoustic Angiography of Tumor Vascular Perfusion Following High Intensity Focused Ultrasound Ablation

Linsey Phillips[1], K. Heath Martin[1], Ryan Gessner[1], Paul Dayton[1]; [1]*University of North Carolina at Chapel Hill, USA*

Background, Motivation and Objective

High intensity focused ultrasound (HIFU) is known to cause irreversible tissue ablation, and is currently under pre-clinical (U.S., Europe) and clinical (China, Europe) evaluation for the treatment of many types of solid tumors. HIFU in combination with microbubbles is known to enhance the volume and rate of tissue ablation. As a result of HIFU, blood perfusion of the tissue is diminished, but is dependent on the intensity of the HIFU. The effect of microbubbles on vascular perfusion after HIFU has not been well characterized. We hypothesized that microbubbles would further reduce the viable vasculature inside of tumors. The goal of this study was to evaluate changes in tumor perfusion due to microbubbles under a lower, and potentially safer, level of HIFU.

Statement of Contribution/Methods

Herein we applied a high resolution, high SNR acoustic angiography technique to evaluate tumor perfusion before and after the application of HIFU either in the presence or absence of microbubbles. All studies were institutional animal care and use committee approved. Contrast-enhanced, 3-D, acoustic angiographic images were acquired via a dual-frequency US transducer (transmit at 4 MHz, receive at 30 MHz) as described previously in rats bearing flank fibrosarcoma tumors (diameter = 13.1 ± 1.7mm). HIFU at 125 W/cm2 (1 MHz, 2 MPa, 10% duty cycle, 1 Hz PRF) was applied in 5 second bursts to each of 36 spots in a 6x6mm^2 area centered in the tumor (n=7). A subset of rats (n=4) received an infusion of 1.5x10^9 microbubbles during HIFU. Contrast agent signal was quantified throughout the tumor volume as a measure of vascular perfusion.

Results/Discussion

HIFU in the absence and presence of microbubbles respectively resulted in 34.8% ± 16.7% and 66.2% ± 15.2% mean reductions in the perfused volume of the tumors. This study confirms that HIFU with microbubbles reduces vascular perfusion beyond HIFU alone, and this reduction can be achieved at only 125 W/cm^2 (2 MPa) whereas ~10,000 W/cm^2 are typically applied clinically. Our method of acoustic angiography can also yield quantitative size and morphology parameters of the blood vessels before and after HIFU enabling a quantitative ultrasonic assessment of how microbubbles, in conjunction with HIFU, affect the tumor microvasculature.

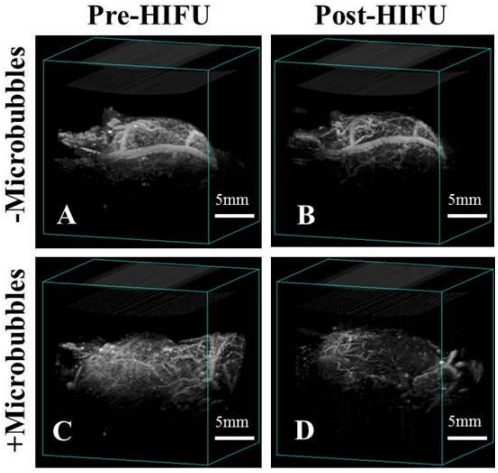

Fig. 1: Acoustic angiography maps of the tumor vasculature prior to (A,C) or after (B,D) HIFU ablation in the absence (A,B) or presence (C,D) of microbubble contrast agents.

[1]R. C. Gessner, et al "Mapping Microvasculature with Acoustic Angiography Yields Quantifiable Differences between Healthy and Tumor-bearing Tissue Volumes in a Rodent Model", Radiology., vol. 264, p. 733-740, 2012.

IUS1-L2-2

Analysis of Relationship between Thermal Dose and Mapped Decorrelation of RF Echoes Induced by High-Intensity Focused Ultrasound

Ryo Takagi[1], Ryo Matsuzawa[2], Takashi Shishitani[2], Shin Yoshizawa[2], Shin-ichiro Umemura[1]; [1]*Graduate School of Biomedical Engineering, Tohoku University, Japan,* [2]*Graduate School of Engineering, Tohoku University, Japan*

Background, Motivation and Objective

Ultrasonic detection of focal tissue coagulation thermally induced by high-intensity focused ultrasound (HIFU) has been difficult without the involvement of microbubbles.

In our previous study, motion-compensated detection of tissue coagulation using correlation between subimages at different times was suggested. The coagulation was detected as decorrelation of RF signals in this method. The decorrelation can be caused by both irreversible (e.g. coagulation) and reversible (e.g. thermal expansion) change, which should be investigated for the feasibility of this method as the real-time monitoring of HIFU treatment. In this study, we investigated the relationship between the mapped correlation coefficient and the irreversible and reversible change.

Statement of Contribution/Methods

In each of two RF echo image frames of tissue at different times during HIFU treatment, a small image block was chosen, and normalized correlation was calculated between them. The image block was fixed in the reference image frame while it was moved around in the other image frame. The decrease in the maximum correlation from unity could give the estimate of coagulation of the tissue corresponding to the image block. The temperature in the focal spot was measured, and the timing of tissue coagulation was estimated

by using the concept of thermal dose and was compared with the mapped correlation coefficient. Chicken fillets were used as a tissue phantom which was exposed to HIFU with an F-number of 1 at 1.13MHz in degassed water at 35 degree.

Results/Discussion

Figure.1 shows that the relationship between the correlation coefficient map (decorrelated pixels) and the temperature at the focal spot. As shown in Fig.1, the number of decorrelated pixels increased monotonously before the thermal dose reached the theoretical threshold of necrosis, and then saturated after it exceeded the threshold. This implies that the correlation coefficient map can be useful to detect tissue coagulation although it may also be affected by its reversible change. The effect by the reversible change on the correlation coefficient map need to be eliminated to improve the accuracy of the real-time monitoring of HIFU treatment.

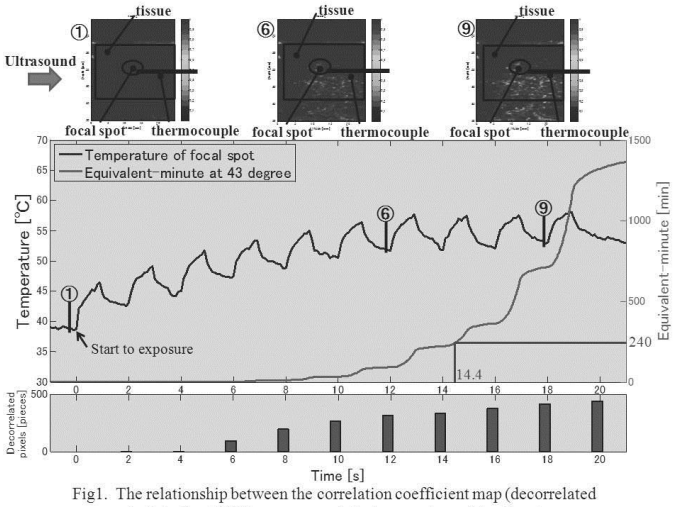

Fig1. The relationship between the correlation coefficient map (decorrelated pixels) after HIFU exposure and the temperature of focal spot

IUS1-L2-3

Quantitative Ultrasound Assessment of Ultrasound Therapy in Rodent Mammary Tumors: In Vivo and Ex Vivo Results

Jeremy Kemmerer[1], Goutam Ghoshal[2], Chandra Karunakaran[1], Michael Oelze[1]; [1]*University of Illinois at Urbana-Champaign, USA,* [2]*Acoustic MedSystems Inc., USA*

Background, Motivation and Objective

High-intensity focused ultrasound (HIFU) is a promising means of non-invasive therapy for the treatment of tumors. Monitoring and assessment challenges for HIFU therapy remain, however, and ultrasound is under investigation to accomplish non-invasive treatment feedback. In this study, quantitative ultrasound (QUS) was investigated for acute HIFU therapy assessment in a rat model mammary tumor.

Statement of Contribution/Methods

In this study, 40 rodent mammary tumors were exposed to focused ultrasound produced by a 1-MHz single-element transducer (f/1.1) at three spatial-peak temporal-average intensity levels (335, 360, and 502 W/cm2). Ultrasound assessment scans were performed on each tumor before and again immediately after HIFU exposure using clinical (Ultrasonix L14/5, 3-8 MHz) and small-animal high-frequency (VisualSonics MS-200, 8-15 MHz) ultrasound systems. Tissue damage from the therapy was also quantified with H&E staining, TTC vital staining, and thermocouple data. For comparison purposes, 12 additional tumors were excised and scanned using a 20-MHz single element transducer before and again immediately after treatment in a 60 ºC saline bath for 30 minutes to determine both scattering and attenuation changes with thermal insult. For the excised tumors, a bandwidth of 7 to 25 MHz was used for backscatter analysis.

Results/Discussion

Backscatter coefficient (BSC) and integrated backscatter coefficient (IBSC) estimates were generated in vivo for each tumor, both before and after treatment. A statistically significant ($p<0.05$) difference was observed in the change in IBSC with treatment for the first exposure group (335 W/cm2) compared to controls. However, no statistically significant differences were observed in IBSC estimates for exposures two and three compared to controls. In ex vivo tumor samples a statistically significant difference (increase) in BSC was observed between pre-treatment and post-treatment scan data above a frequency of 13 MHz and a statistically significant increase in attenuation was observed with treatment.This study demonstrated increases in the BSC in rodent mammary tumors with therapy in both ex vivo, water bath exposures and in vivo, HIFU exposures. In vivo results suggest that QUS sensitivity to HIFU therapy depends on exposure conditions, and that peak pressure was a better indicator than intensity of this sensitivity. This work was supported by NIH Grant R01-EB008992.

IUS1-L2-4

Real-time 2-D elasticity imaging and monitoring of HIFU treatment using Harmonic Motion Imaging for focused Ultrasound (HMIFU)

Gary Hou[1], Jean Provost[1], **Julien Grondin**[1], Shutao Wang[1], Fabrice Marquet[1], Elisa Konofagou[1]; [1]*Columbia University, USA*

Background, Motivation and Objective

Harmonic Motion Imaging for Focused Ultrasound (HMIFU) is a recently developed high-intensity focused ultrasound (HIFU) treatment monitoring method. HMIFU utilizes an Amplitude-Modulated (f_{AM}= 25 Hz) HIFU beam to induce a localized focal oscillatory motion, which is simultaneously estimated and imaged by HMI. HMIFU has been previously shown the feasibilities in silico, *in vitro*, and *in vivo* using both a 1-D and 2-D system for elasticity imaging and monitoring of HIFU treatment. The objective of this study is to develop a new 2D HMIFU framework with online feedback ability to translate HMIFU toward a clinical setting.

Statement of Contribution/Methods

In this study, a 93-element HIFU transducer (f_{center} = 4.5MHz) was used to induce a focal displacement while a coaxially-aligned 64-element phased array (f_{center} = 2.5MHz) was operated using a four-board Verasonics ultrasound system for radio-frequency (RF) channel data acquisition and beam-forming. An unfocused transmit sequence was used to perform imaging at 1000 frames/second, in a field of view of 30 degrees with 32 lateral beams. Beamforming was performed using a new method consisting of multiplying a

reconstruction matrix by the RF data matrix (Hou et al., in preparation). The reconstruction matrix is a sparse matrix containing the contribution of each point of the RF data matrix to the points of the beamformed signals at 80 MHz sampling frequency using a delay-and-sum algorithm. Axial HMI displacements were then estimated from the beamformed RF signals using a 1-D normalized cross-correlation method and streamed to a graphic user interface up to 5 frames/sec. All the data processing was performed on a Graphical Processing Unit (GPU) and it was shown that the displacement data can be streamed at rate of 1 Hz to 5 Hz.

Results/Discussion

As a feasibility study, a 200-ms HMIFU excitation at the acoustic power of 6 W was performed in a 15 kPa gelatin phantom and a 1-minute ablation monitoring was performed on an *in vitro* canine liver specimen. A focal spot (4 mm in axial and 2 mm in lateral) at the focusing depth of 7 cm was localized, where the estimated focal displacements in six different locations in the gelatin phantom varied within 47.7±7.4 µm. Ablation monitoring also showed a decrease of -2.80±0.32 µm after HIFU treatment, indicating the method's capability of estimating and monitoring stiffness changes in real time. Current ongoing studies include HIFU monitoring in *ex vivo* canine liver specimens and transgenic pancreatic tumor mice *in vivo*. This study was funded by NIH R01EB014496.

IUS1-L2-5

Adaptive motion compensation for in-vivo ultrasound temperature estimation

Mahdi Bayat[1], John R. Ballard[1], Emad S. Ebbini[1]; *[1]Electrical and Computer Engineering, University of Minnesota, Minneapolis, MN, USA*

Background, Motivation and Objective

Recent works have shown promising results in estimating small localized temperature changes (e.g. during sub-therapeutic HIFU operation) in vivo using speckle tracking. However, natural motion and deformation of the tissue could result in severe errors in the estimated temperature profiles. Two dimensional filtering inspired by the bioheat equation was shown to partially mitigate these effects, but it is ineffective when the spatial frequencies of the deformations are within the same bandwidth of the temperature-induced strains. We present a new adaptive technique which is capable of largely suppressing the interference without sacrificing the dynamics of the temperature change.

Statement of Contribution/Methods

A new adaptive interference cancellation method was applied to displacement data obtained using speckle tracking on RF imaging data of sub-therapeutic HIFU in the hind limb of Copenhagen rats *in vivo*. The animals were under anesthesia without breathing control, which resulted in sporadic gasping during data collection. The coefficients of the adaptive filter were determined from preheating displacement data before the HIFU shots were applied. This was achieved by identifying the sources of interference from strain data, e.g. nearby blood vessels and foci of muscle contraction due to gasping. During the sub therapeutic shot, the data from selected points and trained coefficients were used to suppress the effect of natural motions using a spatial interference cancellation filter.

Results/Discussion

Figure 1 shows the temperature profile at a point within the targeted region with and without applying the interference cancellation. The profiles show three gasps that resulted in temperature change artifacts of ≈2.5 °C. The application of the adaptive filter effectively removes this artifact as can be seen from the solid curve and the temperature error profile. These results demonstrate the adaptive filter's ability to reduce the effects of natural tissue motion and deformation even when they share the same bandwidth with the temperature change field (e.g. gasping artifact). Monitoring the tissue displacements/strains prior to the application of heating and the identification of the interfering sources allow for the design of robust adaptive filters capable of the removal of artifacts without affecting the dynamics of the estimated temperature change.

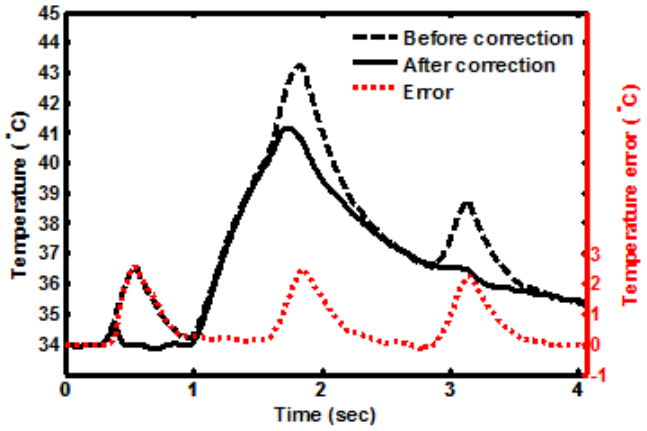

Figure 1: Temperature profile of a point in the targeted area

IUS1-L2-6

Localized Motion Imaging for Coagulation Monitoring using Acoustic Radiation Force

Ryosuke Aoyagi[1], **Takashi Azuma**[1], Hirofumi Nakamura[1], Keisuke Fujiwara[2], Hideki Takeuchi[2], Kazunori Itani[2], Kiyoshi Yoshinaka[3], Akira Sasaki[1], Shu Takagi[1], Yoichiro Matsumoto[1]; *[1]The University of Tokyo, Japan, [2]Hitachi Aloka Medical, Japan, [3]The National Institute of Advanced Industrial Science and Technology, Japan*

Background, Motivation and Objective

Localized Motion Imaging (LMI) to detect stiffness change caused by High Intensity Focused Ultrasound (HIFU) is described. In LMI, we used an amplitude-modulated (AM) HIFU to generate localized tissue oscillation caused by acoustic radiation force at the focal point. By measuring the amplitude ratio of tissue oscillation before and after coagulation, we can detect the thermal coagulation area. In this study, a two dimensional coagulation mapping using LMI capable to apply for a therapeutic assessment after treatment was demonstrated.

Statement of Contribution/Methods

In LMI, AM frequency was optimized to achieve a high spatial resolution and high sensitivity to detect the beginning of coagulation based on the consideration of oscillation localizing as parameters of shear-wave wavelength and HIFU beam width. We used porcine liver samples as tissue samples. HIFU frequency and beam width at focal point in lateral direction were 2.2 MHz and 1 mm. AM frequency of HIFU in LMI was 67 Hz. The HIFU intensity for heating was 1 kW/cm2 with exposure time of 15 s. On the other hand, HIFU intensity for LMI was 0.5 kW/cm2 with exposure time of 1 s. Temperature increase by this condition in LMI was estimated 13°C. In LMI process, an one-dimensional displacement distribution was estimated from a cross correlation between two consecutive echo signals in the time axis. To measure two-dimensional view of LMI, a mechanical lateral scan was performed. The lateral scan pitch and the range of the scan area were 1 and 20 mm, respectively.

Results/Discussion

Using LMI displacement maps before and after coagulation, an amplitude decrease area map was obtained. Since tissue stiffness increases with thermal coagulation, the amplitude decrease area means estimated coagulated area. The LMI image showed a conical shape coagulated area as shown in the figure, that is typical lesion shape caused by HIFU. This shape and size of estimated area roughly agreed with an actual cross-sectional image after sample cutting. In the deep part, LMI results showed over estimation in size. One possible reason of this effect was caused by decrease of the radiation force due to an attenuation increase at the coagulated area.

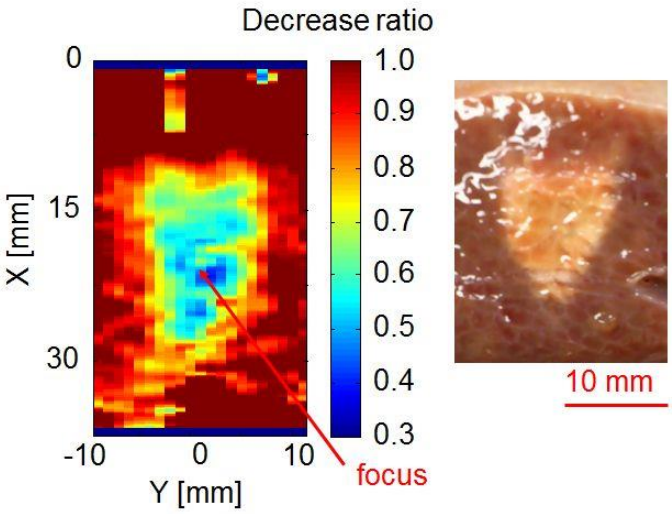

Bone characterization

M5

Thursday, July 25 2013, 10:30 am - 12:00 pm

Congress Hallair: **Pascal Laugier**
Université Paris VI

IUS1-L3-1

Characterization of circumferential guided waves in shells with complex cross-sections: application to a bone-mimicking elliptical phantom

Pierre Nauleau[1], Mathieu Chekroun[1], Quentin Grimal[1], Jean-Gabriel Minonzio[1], Claire Prada[2], Pascal Laugier[1]; [1]*Laboratoire d'imagerie parametrique (UPMC Paris6 - CNRS UMR7623), Paris, France,* [2]*Institut Langevin (ESPCI Université Paris7 - CNRS UMR 7587), Paris, France*

Background, Motivation and Objective

Estimate of material and geometric properties of the cortical femoral neck might improve fracture risk prediction. Measuring dispersion curves of circumferential waves guided in the cortical shell of the femoral neck can yield estimates of these properties. We have shown that such curves could be retrieved using the DORT method in the cases of an empty (Nauleau et al. J. Acoust. Soc. Am. 2012) and of a fluid-filled (Nauleau et al. IEEE IUS 2012) bone-mimicking cylinder of circular cross-section. The femoral neck cross-section is better approximated by an ellipsis than a circle. Thus, this study presents an extension of the DORT method to measure guided wave dispersion curves of elliptical bone phantoms.

Statement of Contribution/Methods

A cylindrical 1mm-thick bone-mimicking tube of elliptical cross-section was investigated. The water-filled tube was immersed in a water bath. Its scattering response was acquired using a 1MHz transmit-receive 128-element focused array. FDTD simulations were performed to serve as a noise-free reference. At each frequency, received signals are backpropagated. Local maxima of the backpropagated wavefield are interpreted as apparent radiation points of circumferential waves. For a circular cross-section, the position of these points can be easily linked to guided wave phase velocities. For other geometries, this relation is not trivial. We proposed a new method, based on the analysis of the radiation of the guided waves seen by the probe, to derive this relation. This method, which can be used for complex geometries, was applied here to an ellipsis.

Results/Discussion

Three branches were obtained (Fig.1). They were identified as modes A0, S0, A1 by comparison with theoretical curves of a free plate.

This study shows that guided wave dispersion curves can be measured with a good precision for an elliptical bone phantom. The validity of the method for an elliptical cross-section represents a significant step toward the extension of the method to realistic femoral neck cross-sections.

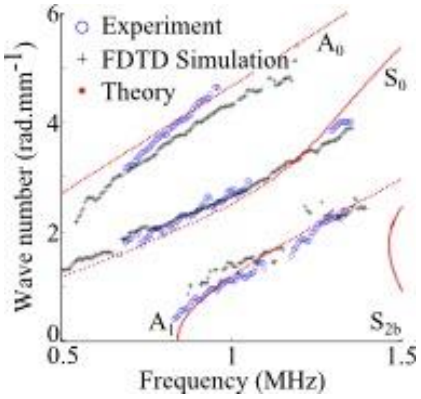

IUS1-L3-2

Incorporation of explicit transmission coefficients in the wave propagation model enhances the results of Bayesian analysis of fast and slow wave propagation in cancellous bone

Amber Nelson[1], Mark Holland[1], Jonathan Katz[1], **James Miller**[1]; [1]*Washington University in St. Louis, Saint Louis, MO, USA*

Background, Motivation and Objective

Fast and slow wave propagation in cancellous bone is a challenging coupled-mode problem. In previous reports, we demonstrated that Bayesian probability theory combined with a simple wave propagation model permits estimation of fast and slow wave velocity and slope of attenuation (nBUA) even in cases where the two waves overlap significantly. As an approach for obtaining additional information that might improve the potential of bone sonometry for monitoring osteoporosis, the **goal** of the present work was to enhance the propagation model by including the functional forms for the fast and slow wave transmission coefficients at the interfaces.

Statement of Contribution/Methods

In earlier work, we showed that the simple model below makes it possible to estimate velocities c_{fast} and c_{slow}, slopes of attenuation β_{fast} and β_{slow}, and the frequency independent prefactors A_{fast} and A_{slow}.

$$\text{Output}(f) = \text{Input}(f)[A_{fast}\exp(-\beta_{fast}fd)\exp(i2\pi fd/c_{fast}) + A_{slow}\exp(-\beta_{slow}fd)\exp(i2\pi fd/c_{slow})]$$

The present work enhances this model by accounting for transmission into and out of water-immersed cancellous bone specimens of length *d*, resulting in an explicit dependence of the *A*'s on the complex impedances *Z*.

$A_{fast} = [2Z_{ref} / (Z_{ref}+Z_{fast})]\times[2Z_{fast} / (Z_{fast}+Z_{ref})]$ and $A_{slow} = [2Z_{ref} / (Z_{ref}+Z_{slow})]\times[2Z_{slow} / (Z_{slow}+Z_{ref})]$

where each Z is of the form $Z = [\rho c(1+\alpha^2/k^2)^{-1}][1+i\alpha/k]$ and $\alpha = \beta f$.

For this coupled-mode system, this enhanced model provides a method for estimating the effective mass densities for fast and slow wave propagation. Studies were carried out on 72 sites from 8 specimens of cancellous bone obtained from human cadavers, as well as on a series of test objects of known properties.

Results/Discussion

Propagation through cancellous bone yielded effective mass densities ρ_{fast} and ρ_{slow} for the fast and slow wave modes while at the same time producing values for velocities, slopes of attenuation, and frequency independent prefactors consistent with those obtained with the simpler model. Interpretation of these effective densities will require further evaluation, but results shown in the figure below suggest that these quantities correlate with microCT-derived parameters while providing potentially valuable new information. [NIH/NIAMS grants R01AR057433 and P30AR057235]

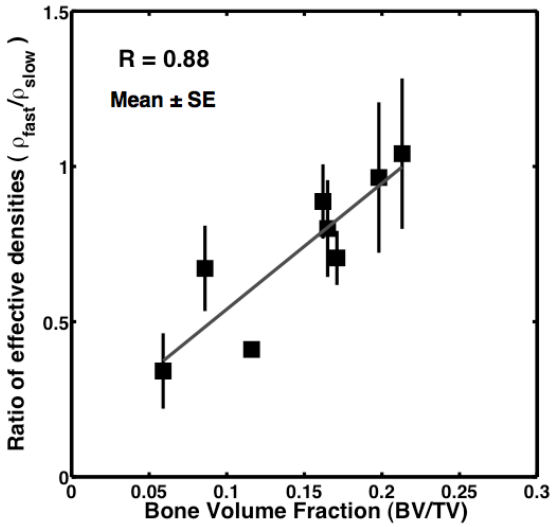

IUS1-L3-3

Estimation of fast and slow wave properties in cancellous bone using Prony's method and curve fitting

Keith Wear[1]*; [1]Center for Devices and Radiological Health, US Food and Drug Administration, Silver Spring, MD, USA*

Background, Motivation and Objective

Two longitudinal waves are predicted in poroelastic media by Biot's theory and are observed in through-transmission experiments on cancellous bone. The Modified Least Squares Prony's (MLSP) method has been shown to be effective for decomposing overlapping waves into fast and slow components (Wear, Ultrasound Med. Biol., 36, 276-287, 2010). The objective of this work is to augment the MLSP method with nonlinear curve fitting (MLSP+CF) in order to improve accuracy of estimates of fast and slow wave amplitude, attenuation coefficient, and velocity (6 parameters).

Statement of Contribution/Methods

MLSP is used to compute initial guesses to be used as inputs for curve-fitting. Correlations between amplitude and attenuation estimates are exploited to accelerate the initial coarse curve-fitting stage by reducing the search space from 6 to 4 dimensions. In the second curve-fitting stage, wave parameter estimates are refined by varying one parameter at a time and searching at high resolution to find values that minimize root-mean-square error (RMSE) between the measured bone transfer function and a parametric model bone transfer function that assumes linear-with-frequency attenuation coefficients and Kramers-Kronig relationship between attenuation and velocity. MLSP+CF is tested on 1) through-transmission measurements (500 kHz) in which polycarbonate produces the fast wave and Zerdine produces the slow wave, and 2) simulations (500 kHz) based on published values for wave parameters from human femur. In both cases, fast and slow waves overlapped by approximately half of a pulse duration.

Results/Discussion

For experiments in Polycarbonate/Zerdine (velocities = 2206, 1542 m/s; attenuation slopes = 3.2, 13.8 dB/cmMHz), RMSE's of parameter estimates were 3 m/s, 4 m/s, 0.4 dB/cmMHz, and 1.2 dB/cmMHz respectively. For simulation in human femur (SNR = 40 dB; velocities = 1511, 2036 m/s; attenuation slopes = 5.2, 42.8 dB/cmMHz), RMSE's of parameter estimates were 1 m/s, 4 m/s, 0.4 dB/cmMHz, and 1.7 dB/cmMHz respectively. The MLSP+CF method provides sufficient accuracy and precision for many applications such that experimental error is a greater limiting factor than estimation error. The MLSP+CF method is flexible with respect to the functional form of the parametric model for the bone transfer function.

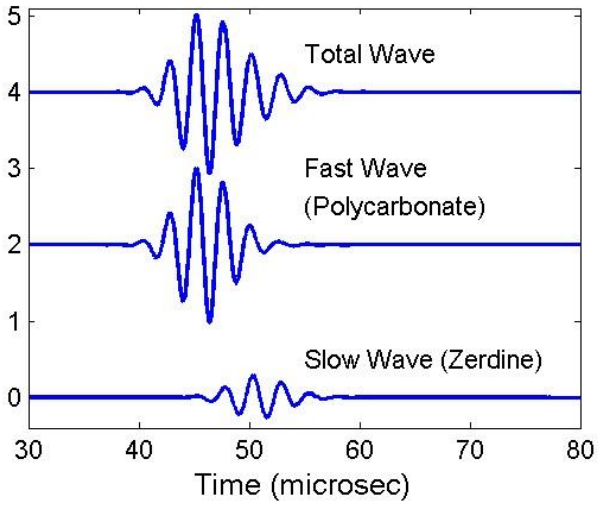

IUS1-L3-4

Two wave phenomenon in a child radius model

Fuminori Fujita[1], Katsunori Mizuno[2], Isao Mano[1], Mami Matsukawa[1]; [1]*Wave Electronics Research Center, Doshisha University, Japan,* [2]*Institute of Industrial Science, the University of Tokyo, Japan*

Background, Motivation and Objective

Longitudinal wave in cancellous bone separates into fast and slow waves depending on the alignment of trabeculae. The fast wave mainly propagates along the trabeculae, whereas slow wave mainly propagates in the soft tissue (bone marrow) [Hosokawa J.A.S.A., (1997)]. The structural anisotropy, which is strongly related to bone strength, can also be assessed using the two-wave phenomenon [Breban, Bone (2010)]. Monitoring of bone strength is important for bone growth in early life. However, two wave phenomenon in the children′s bones have not been investigated yet, because of the complicated wave propagation in the small bone. In this study, we have experimentally studied two wave phenomenon in a child radius model made of bovine trabecular bone surrounded by a cortical layer.

Statement of Contribution/Methods

Ultrasonic pulse measurements were performed using a PVDF focus transmitter (Custom made, Toray) and a hand-made flat PVDF receiver. A single sinusoidal pulse at 1 MHz was sent through a specimen composed of a elliptic cylinder, surrounded by a cortical bone layer. The size of the specimen was after that of the child radius. By changing the incident angle θ of wave to the specimen (0 degree is the direction of minor axis of the specimen), ultrasonic wave passed through the specimen was observed. 3D images of the specimen were obtained using an X-ray micro-CT (Shimadzu).

Results/Discussion

The trabeculae in the sample aligned strongly in one direction. Case (b) in Fig. 1 showed the clear separation of fast and slow waves. Two-waves also seemed to exist in a child radius model (case (c)), however, circumferential waves in the cortical layer were possibly included. Actually, in case (d), where wave does not propagate through a polystyrene foam inside the cortical cylinder, small circumferential waves were observed. The fast wave in the child radius model was confirmed from the residual wave (case (e)) between the wave of the model (case (c)) and the circumferential wave (case (d)). Here, the arrival time of fast wavefront was 0.3 μs faster than that of the circumferential wave. The arrival times of fast and circumferential waves changed due to the incident angle. More detailed studies of the effect of circumferential wave is required for the understanding of this phenomenon and future application to the *in vivo* assessment of child bone.

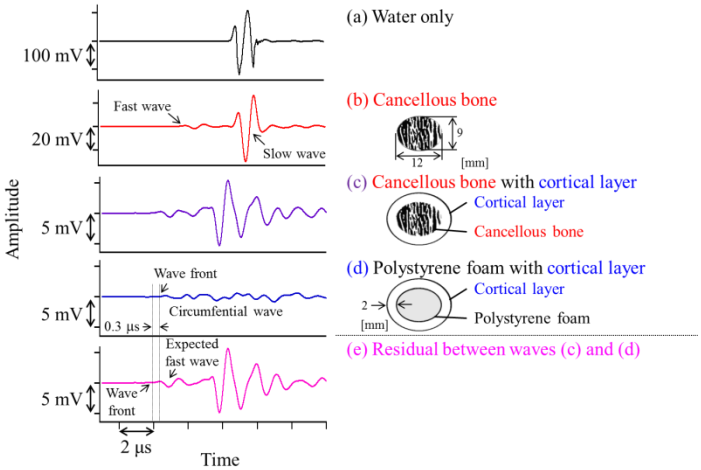

Fig.1 Typical experimental waveforms ($\theta = 0^{o}$) and the image of each specimen. Wave (d) is a child radius model.

IUS1-L3-5

Velocities, attenuations and insights on propagation paths for the fast and slow waves in numerical anisotropic porous media

Fabien Mézière[1], Marie Muller[1], Emmanuel Bossy[1], Arnaud Derode[1]; [1]*Institut Langevin, ESPCI ParisTech, Paris, France*

Background, Motivation and Objective

Bone microarchitecture is very complex, showing structural anisotropy, randomness and scattering. As mechanical waves, ultrasound could be a useful tool to assess fracture risk. However the physics of ultrasound propagation in cancellous bone remains poorly understood, particularly the occurrence and properties of two longitudinal waves.

In a previous study we demonstrated that the two-wave phenomenon can be qualitatively reproduced numerically, with simple random model media. Here, our aim is to go further, measure ultrasonic parameters and confront them to theoretical results. We also take advantage of the flexibility of numerical simulations to better understand the generation of fast and slow waves.

Statement of Contribution/Methods

The 3D models introduced previously consist of ellipsoidal scatterers randomly distributed in water with an orientation ensuring structural anisotropy, as in cancellous bone. A finite-difference scheme simulates elastic wave propagation, with no absorption. In this work, we estimate velocities and attenuations of the coherent (i.e., ensemble-averaged) wave, whatever the number of modes involved. Moreover, we investigate propagation in samples where either the fluid is replaced by vacuum (see (b) in the figure) or the solid matrix by a perfectly rigid structure (c). In particular, the phase of each displacement wave is measured at the interface between the solid and fluid media.

Results/Discussion

In both situations (b) and (c), only one wave is observed: in situation (b) (resp. (c)), the wave velocity is close to that of the fast (resp. slow) wave in (a). These results suggest that the propagation of each wave is determined by the structure of each phase, with a speed affected by geometric aspects such as tortuosity. The results are first analysed in the context of Biot's theory, which provides a classical framework to describe propagation in porous media. The measured velocities are found to be consistent with Biot's theory, as well as the phase shift between the displacements: the fast (resp. slow) wave measured in the solid and that measured in the fluid are in phase (resp. phase opposition). However, Biot's theory fails to predict attenuation, likely to be governed by scattering. Alternative multiple scattering models are discussed.

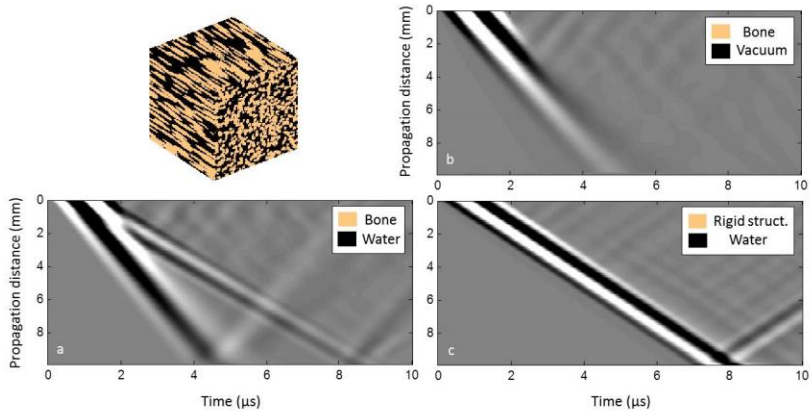

Top left: 3D numerical sample composed of ellipsoidal scatterers, with a 50% solid fraction (orange)
a) two waves propagating in a medium made of bone and water
b) water is replaced with vacuum. Only one wave is supported, with a velocity close to that of the fast wave in a)
c) the solid phase is a rigid structure. Only one wave is observed, with a velocity close to that of the slow wave in a)

IUS1-L3-6

A New Ultrasonic Method for Lumbar Spine Densitometry

Francesco Conversano[1], Ernesto Casciaro[1], Roberto Franchini[1], Giulia Soloperto[1], Antonio Greco[1], Eugenio Quarta[2], Laura Quarta[2], Maurizio Muratore[2], Sergio Casciaro[1]; [1]*Institute of Clinical Physiology, National Research Council, Lecce, Lecce, Italy,* [2]*O.U. of Rheumatology, "Galateo" Hospital, ASL-LE, San Cesario di Lecce, Lecce, Italy*

Background, Motivation and Objective

Osteoporosis is the most common bone disease, causing increased bone fragility and augmented fracture risk, with related huge social and economic costs. The most effective way to reduce these costs would be an earlier osteoporosis diagnosis through population mass screenings. Unfortunately, the only method to reliably predict main osteoporotic fractures is currently represented by bone mineral density (BMD) measurements performed on lumbar vertebras or femur through dual-energy X-ray absorptiometry (DXA), which cannot be used for population screenings because of radiation-related issues.

We developed a new ultrasound (US)-based approach to bone densitometry of lumbar spine and femur, capable of providing diagnostic accuracies comparable to DXA investigations without employing X-rays.

Aim of this work is to carry out a first clinical validation of this novel approach applied to spinal densitometry.

Statement of Contribution/Methods

A total of 290 female patients were enrolled for this study (45-75 years of age, body mass index (BMI)<40 kg/m^2, medical prescription for a spinal DXA, informed consent). All the patients underwent two different investigations: a lumbar spine DXA (Hologic Discovery W scanner) and an US scan of the same vertebras, performed with a commercially-available echograph configured for the acquisition of both echographic images and unfiltered radiofrequency signals. US data analysis was carried out through our new algorithm, whose main features include: a) measurements are always performed on a specific region of interest of the vertebra, identified on the basis of both morphologic and spectral characteristics; b) analysis takes into account patient BMI; c) the algorithm is integrated with a reference database containing model acquisitions for each combination of anatomical site, patient age and sex. Accuracy of final algorithm output, represented by the same diagnostic parameters of a DXA investigation (BMD, T-score, Z-score), was evaluated through a direct comparison with DXA results.

Results/Discussion

For 84.5% of the patients US diagnosis (osteoporotic, osteopenic, healthy) coincided with the corresponding DXA one. Assessing diagnostic accuracy as a function of patient BMI, we obtained: 85.2% for patients with BMI<25 (n=162), 87.2% for those having 25<BMI<30 (n=86) and 76.2% for those with 30<BMI<40 (n=42). Regarding diagnostic accuracy as a function of patient age, we found: 83.1% for patients in the range 45-55 y (n=71), 84.9% in 56-65 y (n=166), 84.9% in 66-75 y (n=53). For each group of patients with both

age and BMI in the same ranges, Pearson correlation coefficient (r) between DXA and US results was calculated for each of the 3 diagnostic parameters: all the obtained values were in the range 0.61-0.84 ($p<0.001$).

The proposed approach represents the first US method for osteoporosis diagnosis which is directly applicable on spine and has the potential to be effectively used for population mass screenings.

Propagation in Liquid and Polymers

NH

Thursday, July 25 2013, 10:30 am - 12:00 pm

Congress Hallair: **Michal Bezdek**
Endress+Hauser Flowtec AG

IUS2-L-1

Temperature uniformity of microdroplet heated by Rayleigh Surface Acoustic Wave in view of biological reaction

Thibaut Roux-Marchand[1], Denis Beyssen[1], Frederic Sarry[1]; [1]*Institut Jean Lamour, CNRS, Vandoeuvre les Nancy, France*

Background, Motivation and Objective

Rayleigh Surface Acoustic Waves (R-SAW), which are widely used as analog filters, are nowadays employed in microfluidic applications. R-SAWs, which present an elliptical displacement, become a leaky-SAW when they encounter droplet loaded on the wave path. A longitudinal wave is then radiated into the liquid. This induces, according to the wave's power and frequency, an internal streaming, droplet's heating, motion of droplet and atomization.

Using the R-SAW technique, biological reaction such as DNA amplification by PCR and hybridization should be performed. In recent work we have shown that R-SAWs don't affect the PCR biological species. More, we have shown that R-SAWs can heat the micro-droplets up to the needed maximum PCR temperature with viscous liquids. However, no study focuses on the uniformity of the microdroplet temperature, which is very important for lot of biological and chemical reactions, particularly the PCR. In this way we have designed a specific chip to obtain fast and precise temperature cycles. Hence the study of the temperature uniformity of the microdroplet has been checked to precisely ascertain the microdroplet temperature.

Statement of Contribution/Methods

There are different techniques for temperature measurements available, contact as well as non-contact methods. For R-SAW PCR devices, only non-contact methods like infrared thermography may be used so as to not interfere with the reaction. Our approach is to record the temperature of a microdroplet heated by R-SAW with an infrared camera (FLIR SC5600).

The emissivity of each solution has been collected before using thermalised structure, a black body, the solution and the infrared camera. The microdroplet temperature value and its uniformity, expressed by the temperature standard deviation, are then studied as a function of the power injected to IdTs. The effect of the wave frequency on the temperature uniformity is also studied as well as the microdroplets volume.

Results/Discussion

When increasing the power injected to IdT, the amplitude of R-SAW grows and the energy transferred to microdroplet increases. Thus the microdroplet average temperature is enhanced but the standard deviation also increases. The more the droplet is heated, the worst the uniformity is. To limit this behavior, we study the frequency effect of R-SAW. By decreasing it, the standard deviation is also reduced leading to a better uniformity.

We tested also the effect of the microdoplet volume. We mainly remark that, for a fixed power, the standard deviation rises when the volume increases. Indeed, with same power, it is more difficult to heat a bigger volume. So the temperature disparity enhances which leads to a greater standard deviation and a worse uniformity.

Thus, to develop a future lab on chip assisted by R-SAW with a microdroplet heater function, the microdroplet volume must be rather low and the exciting frequency of the device will be as low as possible to enhance the temperature uniformity.

IUS2-L-2

Impact of transducers configuration in a pilot sonoreactor used for nanocellulose production by ultrasound-assisted TEMPO oxidation

Eric Loranger[1], André-Olivier Piché[1], Claude Daneault[2]; [1]*Chemical engineering, Lignocellulosic Materials Research Centre - UQTR, Trois-Rivieres, Quebec, Canada,* [2]*Chemistry and physics, Lignocellulosic Materials Research Centre - UQTR, Trois-Rivieres, Quebec, Canada*

Background, Motivation and Objective

In the pulp and paper industry, it is generally believed that nanocellulose will open new market and increase mills profitability. Our research group as shown that the TEMPO-Sodium bromide-Sodium hypochlorite oxidation system can be further optimized with the use of low frequency ultrasound. Therefore, a pilot scale flow-through sonoreactor (sonoreactor 1) compatible with such oxidation was developed and studied. Trials from a previous paper have shown increased efficiency in comparison to the laboratory scale and in effort to further optimize the system; a new sonoreactor (sonoreactor 2) with variable transducer configuration was fabricated (see figure). The objective of this work is to study the sonochemical efficiency of the new transducer configuration and the impact on the oxidation efficiency.

Statement of Contribution/Methods

Potassium iodide oxidation (Weissler method) was used to determine the free radicals produced from ultrasonic cavitation at different frequency (40, 68 and 170 kHz), different power (250 to 1000 W) and transducers configuration (face to face, orthogonal, star pattern). The same experimental conditions were also used to carry out oxidation of once-dried bleached Kraft pulp at 1% consistency using two chemical dosage ratios (TEMPO-Sodium bromide-Sodium hypochlorite). The new sonoreactor experiments were done for a solution volume of 38 L, a flow rate of 38 LPM, natural water pH 7, 25°C temperature and 90 min reaction time.

Results/Discussion

From the Weissler method experiments, free radicals production was found to be dependent on the transducers configuration. For a given frequency and power, the production rate is respectively greater for the star pattern, orthogonal and face to face configuration. At 170 kHz, the frequency with the highest free radical production, the orthogonal configuration show a 30% increase with respect to the face to face configuration while the star pattern show a 25% over the orthogonal configuration. However, the increased free radical production was found to have a more subtle effect on the oxidation efficiency, thus carboxylate content of the pulp. Face to face configuration is somewhat beneficial while orthogonal configuration is detrimental. The discrepancies between these results show that the oxidation reaction is indeed catalysed by free radical but to a certain extent.

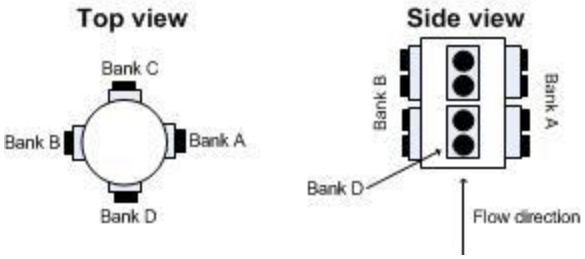

IUS2-L-3

Ultrasonic studies of polymer composites with inorganic nanotubes

Vytautas Samulionis[1], Juras Banys[1], Šarunas Svirskas[1], Antoni Sanchez-Ferrer[2], Raffaele Mezzenga[2], Tony McNally[3], Beatriz Mayoral[3]; *[1]Physics Faculty of Vilnius University, Vilnius, Lithuania, [2]ETH Zurich, Zurich, Switzerland, [3]Queen's University, Belfast, United Kingdom*

Background, Motivation and Objective

During last years it was demonstrated that formation of fullerene-like and nanotube structures is not specific to carbon, but is a generic property of layered materials, such as MoS_2. Such inorganic nanotubes can be used for fabrication of various composites based on polymer materials, because they exhibit a good homogeneity and solubility of the composite material. Properties of polymers can be strongly modified by adding different filaments such as nanowires or nanotubes. Composite materials made of polymers with functional nanofillers can become a perspective alternative for conventionally used materials in industry and science. Ultrasonic waves as non-destructive testing technique is used for determination of elastic properties of polymers and polymer composites. This method allows to obtain information about vibrating particles of a media and how it is influenced by addition of another material in the host lattice of polymer. Ultrasonic spectroscopy allows to observe and evaluate processes that govern their ultrasonic behaviour and to depict variation of these processes because of the change of the filler concentration.

Statement of Contribution/Methods

In this contribution we present the temperature measurements of longitudinal ultrasonic velocity and attenuation in two types of polymer composites with inorganic nanotubes: polyurea elastomers and polycaprolactone (PCL). The temperature dependencies of longitudinal ultrasonic velocity and attenuation, of these nanocomposites based on inorganic MoS_2 nanotubes or $Mo_6S_2I_8$ nanowires have been studied in wide temperature range including glass transitions. Ultrasonic measurements were carried out using automatic computer controlled pulse-echo ultrasonic system. The system have large dynamic range and large input ultrasonic power, therefore the large ultrasonic attenuation values could be measured.

Results/Discussion

In both investigated composite materials ultrasonic studies revealed large ultrasonic attenuation maxima - of the order: $\alpha \approx 15\text{-}30\ cm^{-1}$ for polyurea elastomers [1] and $\alpha \approx 8\text{-}10\ cm^{-1}$ for PCL at 10 MHz frequency - which appeared above the glass transition temperature T_g of the polymer matrix. It was shown that the shape and position of these attenuation peaks was influenced by the presence of inorganic MoS_2 nanotubes or $Mo_6S_2I_8$ nanowires. The increase of ultrasonic velocity because of reinforcement of composites also was observed.

Acknowledgements: The work was supported by the COST Action MP0902 (COINAPO - Composites of inorganic nanotubes and polymers) and Lithuanian Research Council under project MIP-068/2012.

References: [1] V. Samulionis, J. Banys, A. S¨cnchez-Ferrer and R. Mezzenga, Ultrasonic Characterization of Dynamic Elastic Properties of Polymer Composites with Inorganic Nanotubes, Sensors & Transducers **12**, 66 (2011).

IUS2-L-4

Multiple roundtrip SH-SAW liquid sensor using c-axis parallel oriented ZnO films on silica glass pipe

Yoshiya Kato[1], Takahiko Yanagitani[2], Kosuke Imamura[1], Shinji Takayanagi[1], Mami Matsukawa[1]; *[1]Doshisha University, Kyotanabe, Kyoto, Japan, [2]Nagoya Institute of Technology, Nagoya, Aichi, Japan*

Background, Motivation and Objective

SH-SAW device can be a sensor operating in the liquid, because SH-SAW propagates at liquid/solid interface without energy leakage to the liquid. c-axis parallel oriented ZnO films can excite SH-SAW and they can be grown on any substrates without the epitaxial technique.

On the other hand, due to the small diffraction loss, the ball SAW sensor realizes ultramultiple roundtrips which enable high-sensitive detection of small changes in the propagation path. SAW exciting with large overlap length shows less diffraction loss on the small curvature surface, and then SH-SAW propagating on pipe structure can realize a high-sensitive liquid sensor.

In this study, we investigated the SH-SAW liquid sensor consisting of the IDT/c-axis parallel oriented ZnO film/silica glass planar substrate or pipe structure.

Statement of Contribution/Methods

A numerical simulation of the IDT/c-axis parallel oriented (11-20) ZnO (0°, 90°, 55°) ($H/\lambda = 0.21$)/silica glass substrate structure showed the highest K^2 value. The viscosity of the glycerin solution was measured using a planar silica glass substrate with metallized propagation path to avoid effect of electrical conductivity of the solution (Fig. 1 (a)). Then ZnO films whose c-axis oriented (b) vertical or (c) parallel to the tube axis were deposited on the pipe surface as shown in Fig. 1. Propagation characteristic of the multiple roundtrip SH-SAW on the pipe surface, which was partly immersed in liquid was investigated. The time response waveform was obtained by inverse Fourier transform of a reflection coefficient S_{11} measured by a network analyzer. By comparison of the amplitude of the first lap with the third lap, we measured the propagation loss with or without the glycerin solution.

Results/Discussion

In the planar sensor, the phase velocity of SH-SAW monotonically decreased with the increase of liquid viscosity as shown in Fig. 1 (a). Discrepancy between the experimental plot and the theoretical curve is probably due to the viscoelastic effect of the liquid.

Figure 1 (b) and (c) show the three roundtrips of Rayleigh SAW or SH-SAW on the pipe surface, respectively. The losses due to the liquids were found to be (b) 63 dB/m and (c) 7 dB/m, which indicates that SH-SAW propagating on the pipe surface in the liquid has small propagation loss. Therefore a high-sensitive liquid sensor using multiple roundtrips SH-SAW on the pipe structure is expected.

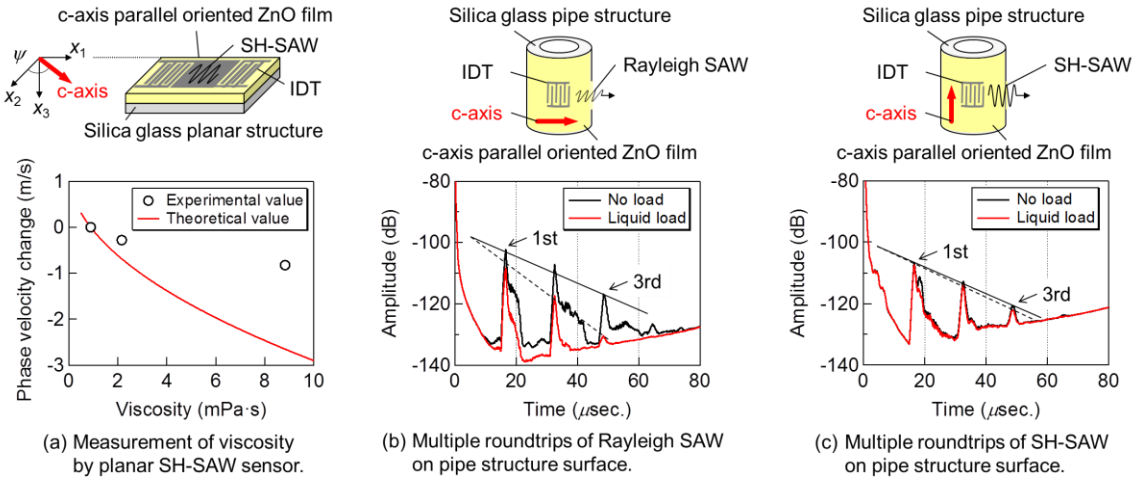

Fig. 1 Propagation characteristics of SH-SAW and Rayleigh SAW.

IUS2-L-5

Viscoelastic behavior monitoring of curing geopolymers by ultrasonic rheology

Julien Rouyer[1], Arnaud Poulesquen[1], Fabien Frizon[1]; [1]*DEN/DTCD/SPDE/LP2C, CEA Marcoule, Bagnols sur Cèze, Gars, France*

Background, Motivation and Objective

Ultrasonic waves have a great potential of showing up the evolution of viscoelastic parameters during a setting process. The suggested method is based on the exploitation of the ultrasonic shear waves reflection phenomenon from an interface which consists in an elastic reference medium and a viscoelastic material of interest: geopolymers. These polymers are inorganically synthesized by the alkaline activation of an aluminosilicate source (metakaolin) in an aqueous solution. This work aims to understand the geopolymerization mechanisms from the early fresh paste up to the hardened state.

Statement of Contribution/Methods

A dedicated self-made cell was built to transmit a broadband pulse (1-2.25-5 MHz) through the reference elastic material (plexiglas or stain steel) to study reflected shear wave from the interface.

An important issue of this method is the accurate determination of the phase angle θ and the reflectivity coefficient r which are directly linked to the viscoelastic evolution and, thus, to physicochemical properties. The high rate of digitalization (4 GHz) enables a fine temporal resolution.

Due to the exothermic dissolution of the metakoalin, a slight increase in temperature (about 1.5°C) generates a small error in phase angle measurements. A correction based on a thermal diffusion model (FEM) is employed in order to take into account the thermal effect in the wave propagation.

Results/Discussion

Shear elastic modulus (G^*) and viscoelastic parameters (G' and G'') over the curing process were obtained. Thus the percolation time was obtained for different curing temperature.

Ultrasonic rheology is based on the elastic shear wave propagation leading to low particle motion compared with displacement occurring in conventional rheology. Ultrasonic results were compared with standard dynamic rheology performed at 1 rad/s. Both methods contribute to a better understanding of the viscoelastic behaviour: the one focused mainly on the individual effects occurring with a unique particle, the other integrates collective effects providing a macroscopic perspective.

(a) (b)

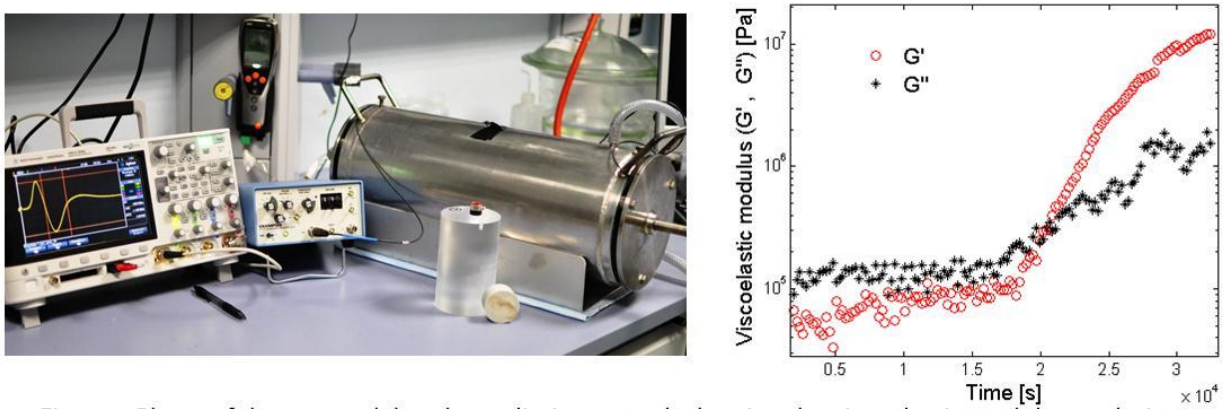

Figures: Photo of the system (a) and a preliminary result showing the viscoelastic modulus evolution during the phase of geopolymer hardening (b).

IUS2-L-6

Statistical signal processing for ultrasonic particle characterization

Sebastian Wöckel[1], Robert Weser[2], Ulrike Hempel[1], Benno Wessely[2]; [1]*ifak e.V. Magdeburg, Germany*, [2]*TU Dresden, Germany*

Background, Motivation and Objective

The quality control of suspensions in industrial processes needs the characterization of different particle parameter. In case of a high particle concentration and an opaque medium ultrasonic measurements are capable to deliver additional information, which are not accessible by conventional optical methods. Thus, common ultrasonic transmission mode spectroscopy uses the frequency dependent attenuation to gain information on particle dimension, distribution and concentration. Due to the increased attenuation, caused by high particulate content, such methods require a small measuring gap, usually in the range of a few millimeters. Alternatively, this article presents a simple method for omitting the gap by taking advantage of the 'particle-born' scattering sound signal.

Statement of Contribution/Methods

The current approach bases on the scattering on randomly moving particles in high concentrated suspensions. The time dependent standard deviation of multiple consecutive scattered sound waves is used, that represent a level for the back-scattering amplitude σmax and its decrease over time $\Delta\sigma$. It correlates with the particle size and concentration and delivers equivalent information like the attenuation calculated by conventional extinction measurements. The statistical signal processing ensures a representative imaging of the moving particle collective. Since no attenuation is derived, in first step, the method does not need any further information on the media or the ultrasonic system. Rather, the decrease of the standard deviation - as a simple parameter - is used which does not equal the attenuation but delivers an equivalent information on the (sound degrading) influence of particles especially in case of high concentration.

Results/Discussion

Influence of particle size and concentration on the backscattering behavior is studied experimentally using two samples of glass particles dispersed in water, differing in particle size. Non-intrusive measurements are performed and evaluated at wavelength with weak scattering. For empirical validation, the exponential decrease of the standard deviation was compared with the attenuation measured with a commercial transmission-mode ultrasonic spectrometer up to a mass content of 50 wt.%. Based on the two samples it is exemplified, that even for small particles and high concentrations the two simple parameters can be extracted from the backscattering signals. The exponential decrease of the standard deviation can be processed like an equivalent attenuation profile, which holds information on the particle concentration. The amplitude is a qualitative indicator correlating amongst others with the particle size.

Concluding, the novelty of the presented approach is the application of statistical feature extraction of the backscattered ultrasonic signal to characterize suspensions with high particle content.

Acoustic tweezers 1

T1

Thursday, July 25 2013, 10:30 am - 12:00 pm

Congress Hallair: **Christine Demore**
University of Dundee

IUS3-L-1

Study the deformability of red blood cell by a single-beam acoustic tweezer

Ying Li[1], Kwok Ho Lam[1], Changyang Li[1], Rose Wenby[2], Herbert J. Meiselman[2], K. Kirk Shung[1]; *[1]NIH Transducer Resource Center and Department of Biomedical Engineering, University of Southern California, Los Angeles, CA, USA, [2]Physiology and Biophysics, Keck School of Medicine, University of Southern California, Los Angeles, CA, USA*

Background, Motivation and Objective

The deformability of red blood cell (RBC) is essential for completing the function of blood circulation because RBCs are of 8μm diameter and must be flexible enough to pass through narrow capillaries smaller than 3μm. However, RBC deformability varies from cell to cell depending on their "age" and surrounding medium. Present techniques either could not access the information from an individual cell or is very time consuming. In this paper, a novel method for studying the deformability of RBCs is presented. The proposed method could measure several cells at the same time, and the time required per measurement could be as short as a few second. To put it to practice, the temperature dependence of RBC deformability was assessed.

Statement of Contribution/Methods

In this study, the gradient force at the focal point generated by a 200 MHz acoustic tweezer transducer was used to deform RBCs. The acoustic tweezer transducer was fabricated by press-focusing of a lithium niobate disc. As shown in Fig.1, experiment was performed in a chamber filled with Alsever's solution. Three RBCs were attached to the bottom of chamber and placed at approximately 50 μm away from the focus of the acoustic tweezer. RBCs were observed to elongate when the transducer was turn on. The gradient force was optimized by varying excitation conditions so that the RBCs could only be deformed but not moved away by the force. A Matlab code was developed to detect the boundary of cells, and calculate the maximum chord (MC) of the boundary. The extension ratio (ER) of RBCs was defined as the ratio between the final MC and the initial MC. ERs of three RBCs were recorded at room temperature (24^0C), 37^0C, 40^0C, and 48^0C, respectively.

Results/Discussion

Average ER of three RBCs at 37^0C was found to be 1.12±0.03 which was close to that at 24^0C (1.11±0.02). However, the average ER decreased to 1.05±0.03 at 40^0C and then further decreased to 1.02±0.04 at 48^0C. It was interesting to observe that ER would increase back to 1.08±0.03 when the cells were cooled from 40^0C to 37^0C. However, the ER would not rebound again after heating the cells at 48^0C for 5 min. It suggests that the RBCs permanently lose their deformability at 48^0C for 5min. This result is consistent with previous observations. In summary, a novel and efficient method to study the deformation of the individual RBC was introduced and its feasibility to study RBC deformability was demonstrated.

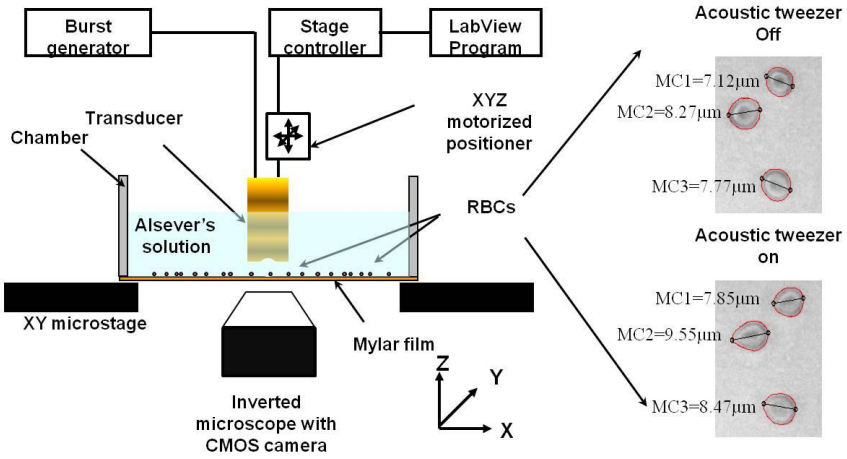

Fig.1 Experimental configuration for studying the deformability of RBCs with acoustic tweezers (T=37^0C)

IUS3-L-2

Manipulation of Microspheres and Microbubbles in an Octagonal Sonotweezers

Anne Bernassau[1], Charles Courtney[2], James Beeley[1], Bruce Drinkwater[3], David Cumming[1]; *[1]University of Glasgow, United Kingdom, [2]University of Bath, United Kingdom, [3]University of Bristol, United Kingdom*

Background, Motivation and Objective

Techniques that allow the manipulation of particles by non-invasive means are desired to facilitate biological applications. Propagating wave devices with four or fewer transducers have been used to demonstrate patterning and displacement of microspheres. However, due to the low number of degrees of freedom, pattern shapes and displacement are limited.

In this paper, an octagonal array of elements surrounding a fluid filled chamber is used to trap, pattern and displace microspheres and microbubbles. The octagonal device that is presented allows various patterns to be formed from the interference of travelling waves. Two cases are studied for patterning: when all the transducers are excited in phase; and

when the transducers are excited with a phase delay in the tweezer system. Furthermore, by varying the relative phase of the sinusoidal excitation of the transducer elements, it is possible to translate the position of the acoustic pressure patterns within the operating area of the device.

Statement of Contribution/Methods

Synchronisation between channels was achieved using two arbitrary waveform generators providing four output channels each allowing independent control of the amplitude, phase and frequency. The system is controlled by a virtual control panel developed in Labview, which allows real time voltage, frequency and phase control. The interface allows interactive and precise positioning and manipulation of the entities.

Results/Discussion

All patterning and displacement experiments were performed using 10 µm diameter polystyrene microspheres (Polysciences, Germany) and SonoVue microbubbles (Bracco, UK). Lines, squares or more complex shapes patterning can be obtained by exciting two, four, six or eight transducers, respectively. Furthermore, when exciting all eight transducers in phase, the nodes form a circular trap, with an acoustic pressure maximum at the centre. By changing the phase of the eight transducers in accordance, a pressure minimum at the centre is obtained that is suitable for tweezing. The tweezing action was demonstrated by translating the position of the central node.

In conclusion, we have presented an octagonal sonotweezer that can provide multiple patterning shapes in one device by changing the number, arrangement and applied-signal phase of pairs of transducers that are simultaneously excited. A computer interface that was developed for the tweezers system enabled different patterns of micro particles to be achieved by combining different pairs of transducers, and by delaying the phase of the transducer excitation around the tweezers system. The octagonal sonotweezers has demonstrated precise positioning and manipulation control of microspheres and microbubbles at different location on a surface, and allows higher spatial resolution compared to previous devices. Excellent agreement between computer simulation and experimental results has been demonstrated.

IUS3-L-3

Acoustic tweezer with a LiNbO3 200 MHz single element transducer for membrane manipulation of cancer cells

Jae Youn Hwang[1], Changyang Lee[1], Kwok Ho Lam[1], Hyung Ham Kim[1], Jungwoo Lee[2], K. Kirk Shung[1]; *[1]Biomedical Engineering, University of Southern California, Los Angeles, CALIFORNIA, USA, [2]Kwangwoon University, Korea, Republic of*

Background, Motivation and Objective

A number of tools such as optical tweezers, magnetic tweezers, and micro-pipettes have been developed to impart mechanical disturbances to a variety of cells for better understanding of mechanotransduction signaling in cells and to allow fine manipulation of cells. Recently, acoustic tweezers have emerged as an alternative tool to do so. Although the acoustic tweezers have several advantages over other methods including non-invasiveness, stronger trapping force, and less cell damage, their full potential remains to be explored. In this paper, we demonstrate the utility of acoustic tweezers with a high-frequency single element ultrasound transducer in cell manipulation and mechanotransduction studies.

Statement of Contribution/Methods

An acoustic tweezer with a press-focused 200 MHz single element LiNbO3 transducer was used to trap a 5 µm fibronectin-coated polystyrene microbead, which allows it to be attached to the membrane of a breast cancer cell. Local membrane elasticity of the cells was quantified by the degree that the membrane was stretched as the microbead, which was tightly bound to the cell membrane, was pulled by the acoustic tweezer.

Results/Discussion

The maximum membrane stretched length was found to increase as acoustic intensity (voltage input to the transducer) was increased, thus demonstrating the feasibility of characterizing mechanical properties of cells by acoustic tweezers [Fig. 1.(a)]. Furthermore, intracellular calcium signaling events in these breast cancer cells were examined while the microbead was bound to the cell membrane since calcium signaling was known to change as a cancer cell responded to extracellular disturbances. Significant calcium elevations were found resulted from the attachment of the microbead to the cell membrane [Fig. 1.(b)]. These results show that acoustic tweezer has the potential to become a valuable tool in cellular biology.

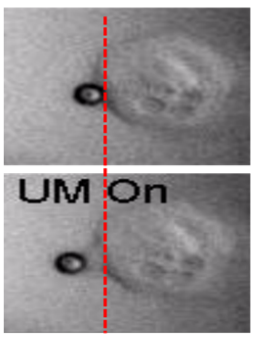

(a)

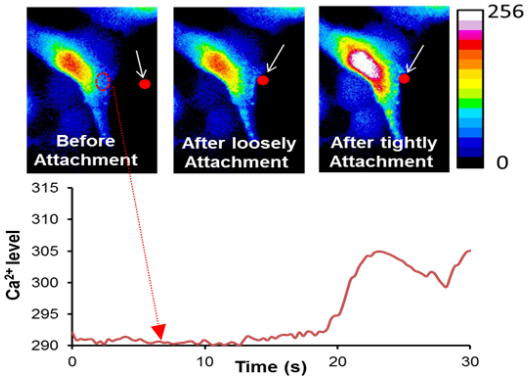

(b)

Fig. 1. Cell membrane manipulation by acoustic tweezers: (a) Cell membrane stretching by cell-attached microbead trap (below). (b) Calcium ion (Ca^{2+}) elevation from attaching a fibronectin-coated polystyrene microbead to cell membrane. Arrows indicate the microbead. The graph represents the temporal Ca^{2+} changes in the region selected by the dotted circle.

IUS3-L-4

Threshold detection for surface mode of an attached bubble by using laser Doppler vibrometer

Yukihiro Kagawa[1], Shunichi Morioka[1], Kenji Yoshida[1], Daisuke Koyama[1], Yoshiaki Watanabe[1]; *[1]Doshisha University, Japan*

Background, Motivation and Objective

A bubble during the ultrasound irradiation exhibits a breathing mode oscillation with expanses and shrinks keeping a spherical shape. When the amplitude of sound pressure exceeds a certain value, a bubble exhibits a non-spherical oscillation called as a surface mode. This study proposed a measurement system using a laser Doppler vibrometer (LDV) and summarized conditions in which an attached bubble begins to show a surface mode.

Statement of Contribution/Methods

It is difficult to acoustically evaluate the surface mode by such as a hydrophone because a radiated wave from a bubble is too small. However it is expected that LDV enables to detect the surface mode because a velocity of bubble surface can be directly measured. A generation of subharmonic component is used as an index of a surface mode, because it is a specific component in the surface mode based on the theory of the parametric excitation. [1] A velocity signal is measured by focusing a laser on the top surface of bubble. The spot radius of the laser is 1.5 µm smaller compared to bubble radius (20 to 200 µm). A bubble attached to glass is exposed to acoustic standing wave. By a Fourier transform after a time integration, we obtain fundamental and subharmonic components of a displacement amplitude (ΔR_f, $\Delta R_{f/2}$) of the bubble oscillation. A high speed camera is simultaneously used to confirm extreme bubble deformation.

Results/Discussion

It was typically confirmed that $\Delta R_{f/2}$ drastically increased when sound pressure P exceeded a certain value P_a. The appearance of a surface mode at $P \geq P_a$ was demonstrated by imaging of high speed camera. Thus, it was confirmed that the generation of $\Delta R_{f/2}$ at P_a is resulted from the surface mode. In contrast, ΔR_f linearly increased at $P<P_a$. It is known that a value of ΔR_f not P deeply relates with the occurrence of a surface mode according to theoretical calculation of a free bubble based on the parametric excitation [1]. So, we defined ΔR_f at P_a as a threshold value ΔR_t exciting a surface mode and showed ΔR_t-R_0 curve in Fig.1, where R_0 represents an initial radius. These results could be fitted by the expression of $\Delta R_t = A R_0^{-B}$ and it revealed a strong correlation (r^2>0.61). These results suggest that the threshold condition where an attached bubble begins to show a surface mode can be experimentally evaluated by using a LDV.

[1] D.Y.Hsieh,et.al, J. Acoust. Soc. Am., Vol. 56, No. 2, 392-393 (1974)

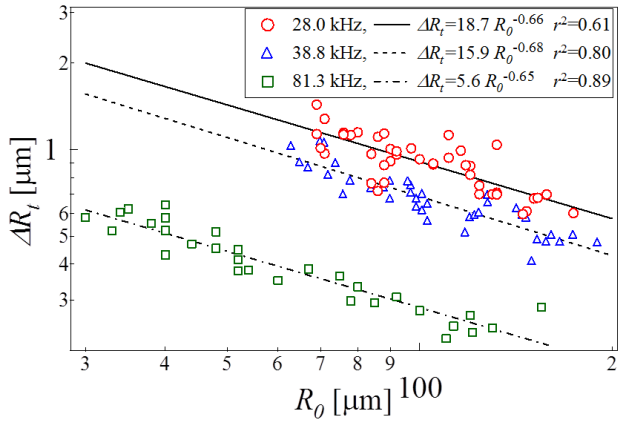

Fig.1 ΔR_t which is a threshold value of fundamental displacement amplitude of a bubble oscillation at $P=P_a$ versus an initial radius versus R_0 under the irradiation of 28.0, 38.8 or 81.3 kHz standing wave. Every determination coefficient r^2 of fitted curves is larger than 0.61 and coefficients B seemed not to depend on the driving frequency.

IUS3-L-5

The physical acoustics of acoustic tweezers

Bruce Drinkwater[1], Paul Wilcox[2], Charles Courtney[3], Alon Grinenko[2], Sandy Cochran[4], Christine Demore[4], David Cumming[5], Martyn Hill[6]; *[1]Mechanical Engineering, University of Bristol, Bristol, Bristol, United Kingdom, [2]University of Bristol, United Kingdom, [3]University of Bath, United Kingdom, [4]University of Dundee, United Kingdom, [5]University of Glasgow, United Kingdom, [6]University of Southampton, United Kingdom*

Background, Motivation and Objective

The operating principles of acoustic tweezers have attracted significant recent research. In parallel, applications of this technology are growing rapidly. For an acoustic tweezer to be dexterous it must be able to not only to trap particles, but to manipulate them flexibly, for example by moving different particles or groups of particles independently and producing a variety of particle distributions. This paper will survey the physical principles behind these developments: acoustic radiation forces on particles large and small, the design of dexterous tweezers and the control of acoustic fields and hence the forces and dexterity possible.

Statement of Contribution/Methods

Two key concepts are explored, firstly the modelling of acoustic forces on arbitrary shaped and sized particles of arbitrary composition. This requires numerical methods such as finite volume models that include all the relevant physics. Various assumptions are possible under certain circumstances such that simple analytical models can be used. However, biological applications involving soft and asymmetrical particles (i.e. cells) necessitates these more comprehensive numerical models or a clear understanding of the assumptions inherent in the simpler analytical models. The second concept is the use of arrays of active elements that enable a wide variety of acoustic pressure fields to be generated. Critically, arrays enable reconfigurability so that a given device can generate multiple and movable field patterns - it is this that leads to dexterous manipulation. Importantly, the design of these devices requires them to be non-resonant in at least one dimension so that the fields are not dependent solely on device geometry.

Results/Discussion

In this paper it is shown that the acoustic radiation force on particles of arbitrary size and shape can be modeled using finite volume time domain methods. It is also shown that in many practically significant cases, much simpler analytical models can be used with only a small loss of accuracy. Maximum dexterity is only obtained if an arbitrary acoustic field is generated within the device and this requires solution of an inverse problem: how to best excite the sources to achieve the desired field? Ideas from optical tweezers such as vortex fields are also shown to be applicable to acoustic devices as they enable trapping, translation and rotation. A number of possible applications of the emerging dexterous acoustic tweezers, such as new bio-assays based on the response of cells to an external force and tissue engineering are also described. Finally, future prospects are discussed, with particular attention to the complimentary developments of optical tweezers and how together these devices might find even more widespread application.

Microacoustic Sensors

T2

Thursday, July 25 2013, 10:30 am - 12:00 pm

Congress Hallair: **Clemens Ruppel**
TDK Corporation

IUS4-L-1

Infra-Red Thermography for spatially resolved measurements of the temperature distribution on the Acoustic Wave devices

Thibaut Roux-Marchand[1], omar Elmazria[1], Frederic Sarry[1]; [1]*Institut Jean Lamour, CNRS, Vandoeuvre les Nancy, France*

Background, Motivation and Objective

The evolution of communication systems leads to an increase in operating frequency and thus a size reduction of elementary devices. Concerning Surface Acoustic Wave (SAW) devices, key elements of these systems, this size reduction induces a localized increase in temperature that may limit the reliability of the devices or at least changes its operation frequency, especially for the substrates with high TCF values [1].

Therefore, the aim of this work is to investigate the potential of Infra-Red Thermography (IRT) as non-contacting and non-destructive methods to investigate the reliability of uncoated SAW devices and also to discriminate the thermal heating due to acoustic wave propagation and the heating due to RF power.

Statement of Contribution/Methods

Experimental set-up consists of an Infra-Red Camera (FLIR SC5600) positioned above the samples with a temperature resolution lower than 30mK, spatial resolution of 5 µm and a recording speed of 100 images per second. We choose two bulk materials with different propagation loss coefficient: 128°Y-X Lithium Niobate which has low coefficient and Y-cut Langasite with relatively high coefficient. Rayleigh SAW is generated through an IdT connected to a high frequency power source using RF probe. This leads to directly test the device on the wafer.

Results/Discussion

When using a low propagation loss material as Lithium Niobate, the heating due to the acoustic wave propagation is very weak and dominated by Joule effect. In this case, it is required to use a RF power pulse to minimise the Joule effect. Concerning crystal with relatively high losses, the discrimination between acoustic wave and RF power heating is illustrated in the figure:

a) IR image of the substrate when RF power is OFF.

b) RF power is ON and frequency corresponds to centre frequency of the SAW device. One can observe the heating due to RF power in the right, the heating due to acoustic beam in centre, but also the heating due to the reflection of acoustic wave in the edge of the wafer (left).

c) RF power is ON and the frequency is outside the band pass of the SAW device. Only the Joule effect is observed.

These results clearly show the IRT could be a powerful tool to enhance SAW devices design particularly when small size of device is combined with high power requirements.

[1] C. Huck, “Liquid crystal thermography on coated SAW devices”, Proceeding of IUS 2012, in press, 2012

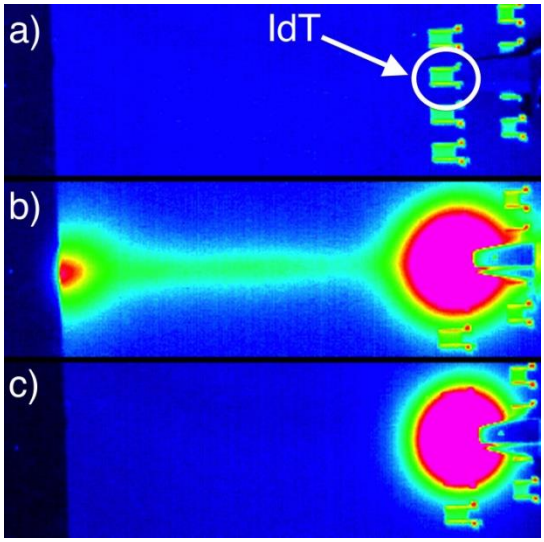

IUS4-L-2

SAW Strain Sensors - High Precision Strain Sensitivity Investigation on Chip-Level

Jochen Hempel[1], Roderich Zeiser[2], Dominik Finke[1], Michael Berndt[2], Jürgen Wilde[2], Leonhard Reindl[1]; [1]*Department of Microsystems Engineering, IMTEK, University of Freiburg, Laboratory for Electrical Instrumentation, Germany,* [2]*Department of Microsystems Engineering, IMTEK, University of Freiburg, Laboratory for Assembly and Packaging Technology, Germany*

Background, Motivation and Objective

State of the art SAW strain sensors have a vast range of application as passive wireless sensing devices. In order to meet the requirements in measurement applications, it is mandatory to know the sensor performance as precise as possible. So far, the strain sensitivity is determined by bending or stretching a multilayer setup, consisting of a SAW strain sensor glued on a carrier material [1-4]. Thus, the real induced strain and its effective orientation is not precisely known.

Statement of Contribution/Methods

In the presented work, a measurement setup was developed for inducing axially homogeneous strain into the SAW strain sensor on chip-level. A tensile test machine was used for applying the strain into the sensor substrate, parallel and perpendicular to the sensor orientation. A temperature variation up to 85 °C was performed, for analyzing the temperature dependency of the chip-level sensor sensitivity. The sensor response was measured and analyzed with a network analyzer while the load was applied. The sensor sensitivity and cross sensitivity were computed from the sensor response and the induced strain.

The 3D deformation of the sensor substrate due to the applied strain was measured with a high precision optical measurement system, based on digital image correlation (DIC). The sensor sub-strate deformation was compared with the simulated sensor deformation, using a 3D FEM. In conclusion, the measured and simulated sensor substrate deformations were compared with the reference strain value from the tensile test machine.

Results/Discussion

The results of these unique and reliable experiments will be presented. These will contribute to a better understanding of SAW strain sensor performance and the consolidation of passive wireless SAW strain sensors for high precision measurement applications.

[1] B. Donohoe, D. Geraghty, and G.E. O'Donnell, „Wireless Calibration of a Surface Acoustic Wave Resonator as a Strain Sensor", IEEE Sensors Journal, Vol.11, No. 4 (April 2011): 1026 –1032, doi:10.1109/JSEN.2010.2070492.

[2] R. Konno et al., „A Highly Sensitive Strain Sensor Using Surface Acoustic Wave and Its Evaluation for Wireless Batteryless Sensor Network", in 2007 IEEE Sensors, 2007, 796 –799, doi:10.1109/ICSENS.2007.4388520.

[3] Haekwan Oh et al., „Development of a High-sensitivity Strain Measurement System Based on a SH SAW Sensor", Journal of Micromechanics and Microengineering, Vol. 22, No. 2 (February 1, 2012): 025002, doi:10.1088/0960-1317/22/2/025002.

[4] Vasundara V. Varadan et al., „Wireless Passive IDT Strain Microsensor", Smart Materials and Structures, Vol. 6, No. 6 (December 1, 1997): 745, doi:10.1088/0964-1726/6/6/012.

IUS4-L-3

Investigation of Delay Path Modifications of SAW Sensors

Mandek Richardson[1], Sina Koochakzadeh[1], Kamlesh Suthar[2], Subramanian K. R. S. Sankaranarayanan[2], **Venkat Bhethanabotla[1]**; *[1]Chemical & Biomedical Engineering, University of South Florida, Tampa, Florida, USA, [2]Center for Nanoscale Materials, Argonne National Laboratories, USA*

Background, Motivation and Objective

Surface Acoustic Wave (SAW) biosensors monitor the interaction between a receptor and its target in real time, through changes in the properties of the traveling wave (i.e., frequency, phase, and amplitude). Key biosensing issues include selectivity, sensitivity, response and recovery times, and detection limit. Binding of undesirable moieties such as non-specific proteins to the sensor surface poses a serious limitation on performance. Rayleigh wave driven acoustic streaming has the potential to detach and remove the non-specifically bound (NSB) proteins from the device surface. Operating in the liquid environment presents another performance issue due to high insertion loss. Incorporation of reflective gratings , grooves and corrugated surfaces , and the application of a waveguide have been utilized to lower insertion loss.

Statement of Contribution/Methods

In this study, we compare finite-element simulations and experiments on SAW devices whose delay path has been modified to include an array of microcavities. Two different substrates commonly used in biosensors were studied, ST-Quartz and 36° YX LiTaO3.

Results/Discussion

From simulations, we find that microcavities optimized for a particular substrate and wave mode decrease insertion loss and increase sensitivity to mass loading. Rayleigh waves in ST Quartz are seen to attenuate the propagation of higher frequency components and increase out of band rejection. Our analysis of displacement vector plots for the microcavity structures indicate that these improvements are brought about by a larger coherent reflection of the incident wave and subsequent reduced conversions into bulk shear modes which radiate into the substrate. These findings can be applied to an improved filter design for use in communication applications, as well. Devices containing microcavities were fabricated based on results from these simulations. Experiments were performed to determine the effect of microcavities on insertion loss and sensitivity to mass loading and compared to what was obtained through simulations. These findings will be discussed in this presentation.

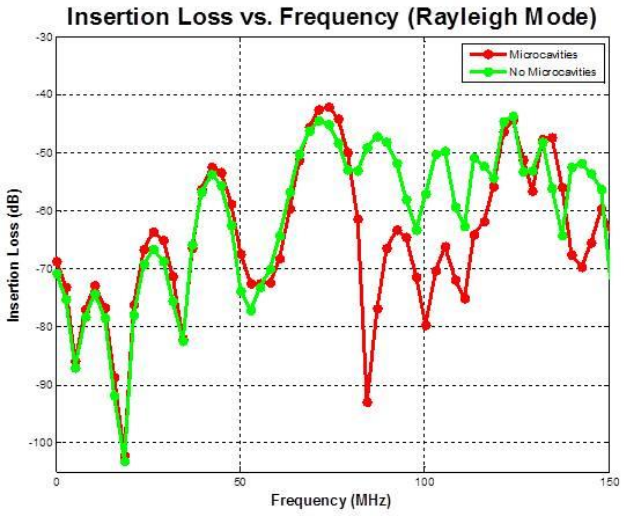

IUS4-L-4

Detection of antigen-antibody reaction by thickness-shear mode resonators consisting of c-axis parallel oriented ZnO films

Kenji Yoshida[1], Takahiko Yanagitani[2], Takayuki Kawamoto[1,3], Sho Sasaki[3], Masatoshi Oba[3], Yoshiya Kato[1], Shinji Takayanagi[1], Yoshiaki Watanabe[1]; *[1]Doshisha University, Japan, [2]Nagoya Institute of Technology, Japan, [3]OMRON, Japan*

Background, Motivation and Objective

Our goal is to develop simple measurement system enabling quantitative detection of biochemical reaction with high sensitivity and accuracy. It is well-known that mass loading due to the reaction can be detected by a Quartz crystal microbalance (QCM). The sensitivity of QCM depends on quartz thickness, and therefore the sensitivity is limited because of the thick quartz. Thin film resonator with thickness-shear mode which makes it possible to operate in liquid phase is promising for high sensitive bio-sensor. We prepared pure thickness-shear mode resonator consisting of c-axis parallel ZnO films, and detected a protein by using antigen-antibody reaction. The detection limit of the protein concentration was also investigated.

Statement of Contribution/Methods

As shown in Fig.1(a), the sensor had multi-layer structure consisting of upper electrode (Au/Ti), piezoelectric thin film (ZnO), lower electrode (Ti/Au/Ti) and reinforced layer (SiO2/Si/SiO2). A biomarker for arterial sclerosis was used as the antigen, and antigen-antibody reaction was detected by the sensor. The antibody was fixed on the upper electrode via self-assembled monolayers. The antigen-antibody reaction should decrease the resonant frequency of the sensor due to the mass loading of the antigen. We constructed the flow system including the sensor tip to automatically monitor the frequency shift in real time. The fundamental resonant frequency was measured from the frequency characteristic of reflection coefficient obtained by a network analyzer.

Results/Discussion

Fig.1(b) shows the typical time variation of the resonant frequency. The measurement was performed in the following procedure, (1) fixation of anti-body, (2) flowing the solution including antigen, (3) replacement by buffer solution, and (4) dissociating antigen-antibody binding. Comparing state (1) with (3), the frequency shift due to the mass loading of the antigen is clearly detected. With the increase of the concentration of the antigen from 0.001 to 10 μg/mL, we found that the frequency shift increased from several hundred Hertz to several kilo Hertz. The detection limit was determined by the frequency shift in the solution including no antigen. The obtained limit of 10 ng/mL was 30000 times smaller than the standard concentration in the blood. These results show that the proposed sensor is effective for the practical use.

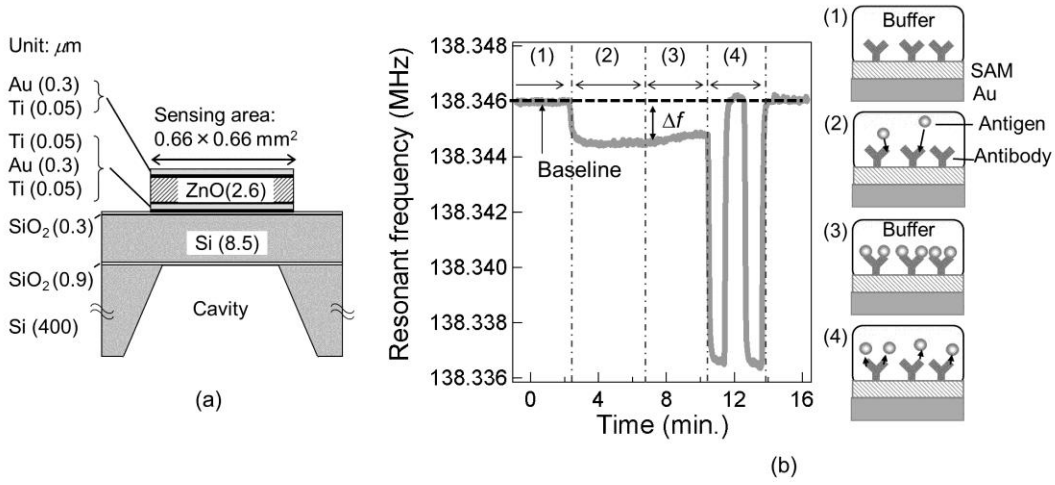

Figure 1 (a) Multi-layer structure of prototype sensor. (b) Frequency shift Δf caused by mass loading effect of antigens.

IUS4-L-5

Fast and sensitive H_2 detection by ball surface acoustic wave (SAW) sensor with porous Pd-Pt alloy film

Toshihiro Tsuji[1], Ryosuke Mihara[1], Tomohiro Saito[1], Satoshi Hagihara[1], Toru Oizumi[1], Nobuo Takeda[1], Tsuneo Ohgi[2], Takayuki Yanagisawa[2], Shingo Akao[1,2], Noritaka Nakaso[2], Kazushi Yamanaka[1]; *[1]Tohoku University, Japan, [2]Toppan Printing Co. Ltd., Japan*

Background, Motivation and Objective

H_2 sensor is essential in the safe use of H_2 gas as a clean energy [1]. Sensitive sensors operating at room temperature have been studied for monitoring with low power consumption [1-3]. We developed the ball surface acoustic wave (SAW) H_2 sensor that enhances the sensitivity using multiple roundtrip propagation of SAW (Fig. 1), and achieved the widest detection concentration range from 10 ppm to 100% using Pd-Ni alloy film [4], where Ni prevents the phase transition of Pd under high H_2 concentration [1]. However, the response times of [4], recent planar SAW sensor [6] and resistive sensor using Pd/CNT [5] are hundreds of seconds for low concentration H_2 (100 ppm), which is not fast enough for the safe use of H_2.

Statement of Contribution/Methods

In this study, we develop a fast and sensitive ball SAW sensor with porous Pd-Pt alloy film to solve this problem, where Pt is used not only to suppress the phase transition but also to catalyze the dissociation of H_2 molecule to H atoms. The porous Pd-20%Pt alloy film with 40 nm thickness was fabricated on a langasite ball SAW device (150 MHz, φ3.3 mm) using rf co-sputtering. H_2 diluted by N_2 was measured at 35°C by an amplitude change of the roundtrip waveform at the 10th turn. We defined the response time as the rise time from 10% to 90%.

Results/Discussion

Clear amplitude responses were obtained to the concentration from 1000 ppm to 20 ppm (Fig. 2). Each response was proportional to the square root of the concentration, leading to the detection limit of 3.7 ppm. The square root relationship could be explained by Sievelts' law where the solubility of a diatomic gas in metal is proportional to the square root of the partial pressure. We compared the concentration dependences of the response time with literatures [2-6] (Fig. 3). The response time of the present sensor was 15 s for 100 ppm, which was 5 times shorter than the shortest values of previous H_2 sensors [5, 6]. In conclusion, we successfully developed not only sensitive but also the fastest H_2 sensor operating at room temperature by the ball SAW sensor with porous Pd-Pt alloy film.

References
[1] R. C. Hughes and W. K. Schubert, J. Appl. Phys. 71 (1992) 542.
[2] D′Amico et. al., Proc. IEEE. Ultrasonic symposium (1982) 308.
[3] Jakubik et. al., Sens. Actuators B 82 (2002) 265.
[4] Yamanaka et. al., IEEE Trans. Ultrason. Ferroelectr. Freq. Control. 53 (2006) 793.
[5] Ju et. al., Sens. Actuators B 146 (2010) 122.
[6] Wang et. al., Sens. Actuators B173 (2012) 710.

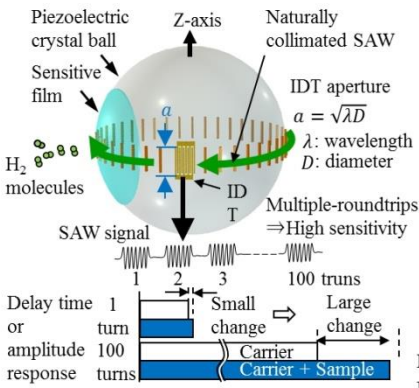

Fig.1 Principle of ball SAW sensor

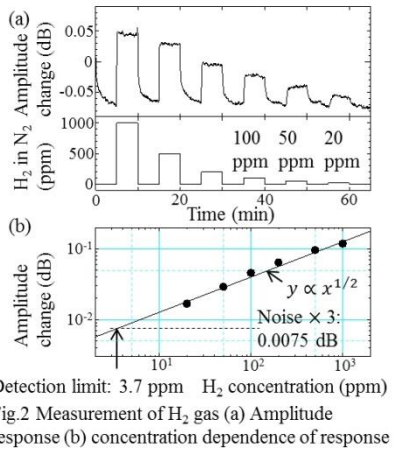

Fig.2 Measurement of H_2 gas (a) Amplitude response (b) concentration dependence of response

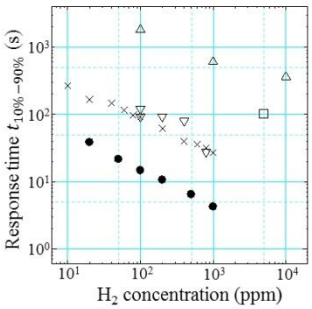

Fig.3 Comparison of concentration dependence of response time with literatures. ●: ball SAW (porous Pd-Pt film), △: planar SAW (Pd film) [2], □: planar SAW sensor (Pd + CuPc film) [3], ▽: planar SAW (InOx film) [6], ×: resistive (CNT with Pd nano-particles) [5]

IUS4-L-6

Experimental investigation of a novel SAW strain sensor with inbuilt temperature measurement capability

Alice Fischerauer[1], Christian Schwarzmueller[1], Gerhard Fischerauer[1]; [1]*Chair of metrology and control engineering, Universität Bayreuth, Germany*

Background, Motivation and Objective

The measurement of mechanical strain is usually influenced by temperature and humidity. This is certainly true of SAW strain sensors. As a consequence, one must measure the temperature and humidity in the sensor environment in addition to the strain. Recently, the authors have proposed a novel SAW strain sensor with inbuilt temperature measurement capability, which has the potential of providing the needed information at no extra cost[1]. This contribution focuses on experiments aiming at characterizing the influence of temperature and humidity on the transmission coefficient S_{12} of the novel sensor. This includes both the static behavior and dynamic effects, i. e., temperature variations when the sensor is subjected to constant strain.

Statement of Contribution/Methods

The device layout of the SAW strain sensor leads to a transmission coefficient spectrum $S_{12}(f)$ with features, such as minima and maxima in the magnitude plot, which depend characteristically on temperature and strain. Hence, by evaluating the magnitude spectrum $|S_{12}(f)|$ at a few distinct frequencies, both quantities can be extracted from the response of a single two-port device (Fig. 1). To demonstrate this, a device was characterized under longitudinal and shear stress at various temperature and humidity conditions. In addition, in order to explore the capability of the device to additionally act as gas sensor, the interdigital transducers were coated with a functional thin film and the effects of this on the strain sensitivity of the sensor were studied.

Results/Discussion

The measurement results obtained with a demonstrator device reveal a unique response of the magnitude spectrum $|S_{12}(f)|$ to temperature and strain variations. The measured frequencies of the minima in $|S_{12}(f)|$ show a pronounced sensitivity to strain. Furthermore, the measurements clearly indicate the buildup of additional internal stresses in a $LiNbO_3$ device when it is subjected to strain in combination with temperature ramps; this effect is attributed to pyroelectricity. The full version of this contribution will report on these results and on the influence of a thin semiconducting film on the device performance.

[1]A. Fischerauer, G. Fischerauer, "A novel highly sensitive SAW strain sensor with inbuilt temperature measurement," Proc. IEEE IUS, Dresden, Oct. 8–10, 2012, in print

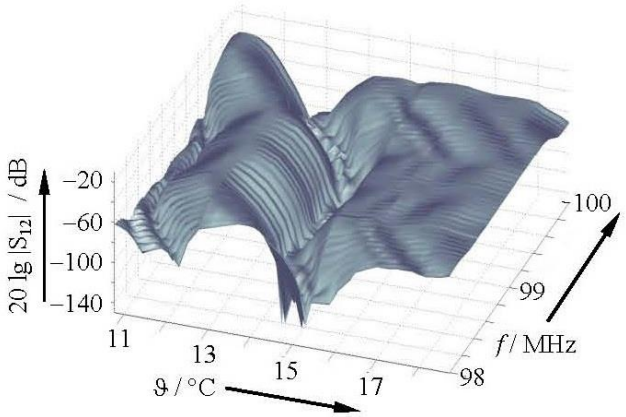

Fig. 1: Measured transmission coefficient magnitude $|S_{12}(f, \vartheta)|$ of the proposed sensor on 128°rotY, X-$LiNbO_3$ at constant uniaxial stress ($T_{xx} \approx 2.6$ N/mm²).

Histotripsy and cavitation

CONGRESS HALL

Thursday, July 25 2013, 02:00 pm - 03:30 pm

Congress Hallair: **Ralf Seip**
Philips Research North America

IUS1-M1-1

Active Removal of Residual Bubble Nuclei Following a Cavitation Event

Alexander P. Duryea[1], Charles A. Cain[1], William W. Roberts[1,2], Hedieh A. Tamaddoni[1], Timothy L. Hall[1]; *[1]Biomedical Engineering, University of Michigan, Ann Arbor, Michigan, USA, [2]Urology, University of Michigan, Ann Arbor, Michigan, USA*

Background, Motivation and Objective

Residual microscopic bubble nuclei can persist for 10s or even 100s of ms following a cavitation event. These bubbles may limit the efficiency of ultrasound therapies such as shock wave lithotripsy (SWL) and histotripsy, as they act to attenuate pulses that arrive subsequent to their formation. In the present study we explore a strategy for the active removal of residual bubble nuclei following a cavitation event, using a low amplitude ultrasound burst to stimulate bubble coalescence.

Statement of Contribution/Methods

All experiments were conducted in degassed water and monitored using high speed photography at 20 kfps. The following general pulse scheme was used: **(A) Cavitation Initiation Pulse:** A cavitational bubble cloud was initiated by a 1 MHz therapy transducer using a very short intense pulse (P- > 30 MPa); **(B) Nuclei Removal Pulse:** Residual bubble nuclei were sonicated using a 2 ms pulse from a separate 350 kHz unfocused transducer to stimulate coalescence. Nuclei removal pulses with amplitudes ranging from 0 to 750 kPa were tested; **(C) Interrogation Pulse:** The presence of residual nuclei following the coalescence pulse was probed using a second lower amplitude pulse from the therapy transducer sufficient to cause microscopic nuclei to expand and be more easily detected via high speed imaging. This pulse amplitude was found not to initiate any visible cavitation bubbles independently. The backlit area of shadow from the expanded bubbles was calculated to quantify efficacy of nuclei removal. Five trials were performed for each amplitude.

Results/Discussion

The control case (nuclei removal pulse amplitude = 0) generated a bubble shadow area of 0.64 ± 0.08 mm^2. For nuclei removal pulse amplitudes of 50 to 150 kPa, minimal coalescence was observed in high speed video; correspondingly, the area of bubbles excited by the interrogation pulse did not differ significantly from control ($p > 0.08$). Pronounced bubble coalescence was observable for nuclei removal pulses ≥250 kPa, with the extent of coalescence increasing with pulse amplitude. Bubble shadow area was significantly reduced relative to control in these cases ($p \leq 0.02$). Mechanistically, the Secondary Bjerknes force is hypothesized to provide the attractive force between bubble nuclei in this study. Modeling indicates this force is sufficient to achieve bubble coalescence on the time and amplitude scales investigated.

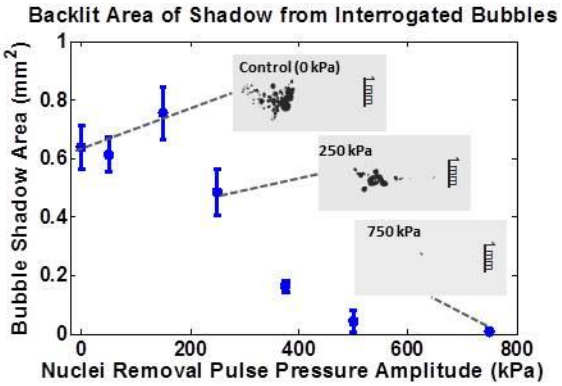

IUS1-M1-2

In-Vivo Transcostal Histotripsy Therapy without Aberration Correction

Yohan Kim[1], **Eli Vlaisavljevich**[1], Gabe Owens[2], Steven Allen[1], Charles Cain[1], Zhen Xu[1]; *[1]Biomedical Engineering, University of Michigan, Ann Arbor, MI, USA, [2]Department of Pediatrics, Division of Pediatric Cardiology, University of Michigan, Ann Arbor, MI, USA*

Background, Motivation and Objective

This study evaluates the feasibility of in vivo transcostal histotripsy therapy without using aberration correction. In a previous ex vivo investigation, histotripsy was shown to be capable of creating precise lesions through the ribs without aberration correction, as long as the main focal beam pressure exceeds the cavitation threshold while secondary lobes are below the threshold. This study attempts to validate this capability in vivo and assess the thermal effects of histotripsy therapy on overlying tissues when no aberration correction is used.

Statement of Contribution/Methods

Pigs weighting 40-50 kg were treated non-invasively through acoustic windows with full ribcage coverage in three pigs and with no rib obstruction in two pigs. Treatments were applied by a 750 kHz transducer 150 mm in diameter with 120 mm of focal length. To ensure that only the main beam exceeded the cavitation threshold and minimize grating lobe effects, the input pressure was gradually increased until a hyperechoic cavitation cloud was observed within the main focal zone using real-time ultrasound imaging. Thermocouples were inserted in the overlying tissue to measure the temperature increase. Lesions were created by mechanically scanning the transducer focus to a 5x5x5 mm grid with 1 mm spacing between adjacent points. Each point was sonicated by 5-cycle pulses at 16-19 MPa peak negative pressures and repetition rates of 200 Hz for 20 s.

Results/Discussion

Hyperechoic bubble clouds were generated within the main focus in all experiments, and no bubbles outside the focal zone were observed on ultrasound imaging (Fig 1a). Comparable lesions of approximately 1.2 x 1.7 cm were produced in the liver through windows with full rib coverage and with no ribs in the pathway (Fig 1b). Histological analysis showed complete tissue fractionation within the treatment region. Maximal temperature increase measured in the overlying tissue covering the ribs was 4.1 ± 1.1 C (Fig 1c). No damage to the ribs or overlying tissues was detected by gross morphology or MRI. Our initial results suggest that histotripsy therapy can generate precise lesions through the ribs without aberration correction. Temperature increases induced to overlying tissues remained below the thermal damage threshold. Transcostal histotripsy therapy could be useful for many applications such as hepatic, pancreatic and cardiac ablation.

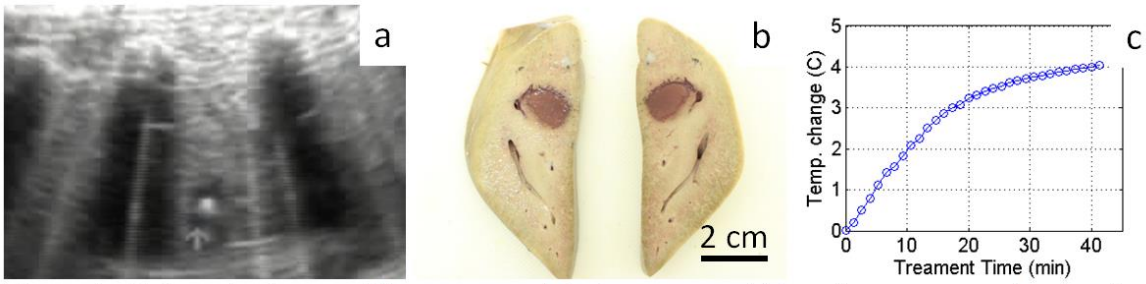

Figure 1. (a) B-mode ultrasound image captured during transcostal histotripsy treatment showing the hyperechoic cavitation bubble cloud (indicated by the arrow) generated in porcine liver. Shadows are clearly visible under the rib bones due to the reflection and attenuation of the signal. (b) Gross morphology of porcine liver samples treated transcostally showed consistent tissue fractionation and sharp boundaries surrounding the focal area. (c) Plot of the mean temperature increase on the ribs during histotripsy treatment. Maximum temperatures measured were below the threshold for thermal damage.

IUS1-M1-3

Feasibility of non-thermal brain ablation for noninvasive surgery in a large animal model under passive cavitation monitoring

Costas Arvanitis[1], Natalia Vykhodtseva[1], Margaret Livingstone[2], Nathan McDannold[1]; *[1]Radiology, BWH, Harvard Medical School, Boston, Massachusetts, USA, [2]Neurobiology, Harvard Medical School, Boston, USA*

Background, Motivation and Objective

Transcranial MRI-guided focused ultrasound (TcMRgFUS) thermal ablation in the brain has reached clinical trials. A current limitation is that this method cannot be applied in some brain regions without overheating the skull. Here, to overcome this limitation, "non-thermal" ablation induced by low power sonications with an ultrasound contrast agent was evaluated.

Statement of Contribution/Methods

Four macaques were sonicated at 2-4 regions adjacent to the optic tract using a clinical TcMRgFUS system (ExAblate 4000, 220 kHz, InSightec), originally developed for thermal ablation in the brain. The acoustic power level (3.5-6.4 W, estimated peak negative pressure amplitude: 420-560 kPa), was set to be just above the inertial cavitation threshold measured at each target using passive cavitation detectors. Burst sonications (10 ms, 1 Hz PRF) were applied for 5 min and combined with either 20 µl/kg IV bolus or infusions of Definity microbubbles. The acoustic emissions were recorded during the sonications, and spectral analysis was performed for each burst every 100 µs. Emissions signals were integrated over frequency bands reflecting broadband, harmonic and sub/ultraharmonic emissions and then normalized to data obtained without microbubbles. After sonication, the brains were evaluated in MRI and histology.

Results/Discussion

The mean inertial cavitation threshold in the brain, as indicated by the concurrent appearance of sub/ultra-harmonic and broadband emissions, was 430±90 kPa. During the 5 min sonications with bolus injection, strong broadband emissions were present initially, which decayed over time – sometimes rapidly and completely extinguished. However, with infusion, sustained harmonic emissions and broadband spikes (N>20) were recorded throughout the sonication. In each location, broadband emissions of at least 5 Np•Hz were observed. Harmonic emissions were proportional to the peak negative pressure. Interestingly, bellow the inertial cavitation threshold, the harmonic emissions appeared to increase during the 10 ms bursts. Histological analysis revealed discrete lesions (infarction) in all targeted regions, while the adjacent optic tract appeared mostly intact. The lesions were constrained to the targeted areas, which were hypointense in T2*-weighted MRI. Small regions of blood-brain barrier disruption and petechaie about 1 cm along the US beam-path were seen, but no severe lesions were detected.

These preliminary data demonstrate that transcranial passive cavitation monitoring can be used to establish the cavitation threshold at deep brain targets to ensure ablation during sonication with microbubbles. While future work is needed to reduce the effects along the beam path, this work is promising and could offer a potential way to expand the "treatment envelop" where TcMRgFUS ablation can be applied.

IUS1-M1-4

Enhanced *In Vivo* and *In Vitro* High Intensity Focused Ultrasound Ablation via Phase-shift Nanodroplets Compared to Microbubbles

Linsey C. Phillips[1], Connor Puett[1], Paul S. Sheeran[1], Kelsie F. Timbie[2], Richard J. Price[2], G. Wilson Miller[2], Paul A. Dayton[1]; *[1]University of North Carolina at Chapel Hill, USA, [2]University of Virginia, USA*

Background, Motivation and Objective

Both perfluorocarbon nanodroplets and microbubbles have been proposed as agents for enhanced thermal ablation by high intensity focused ultrasound (HIFU). HIFU ablation of uterine fibroids is FDA-approved. Pre-clinical evaluation of HIFU for treatment of a variety of tumors, including breast, prostate, brain, pancreas, bone, and liver, is underway in the U.S., Europe, and Asia. Major obstacles associated with HIFU tumor ablation are superficial skin burns and long treatment times. Microbubbles (MB) are known to enhance HIFU ablation, but often result in enhanced superficial heating also. We have designed a dual-perfluorocarbon nanodroplet (ND) that induces heating only at the focus and has the added advantages of extended circulation lifetime, and a lower acoustic threshold to induce heating.

Statement of Contribution/Methods

Microbubbles (2.1 ± 0.5 µm) and nanodroplets (240 ± 65 nm) were prepared in house as previously described[1] then incorporated into tissue-mimicking albumin-acrylamide phantom material. Phantoms were sonicated at 1 MHz by an MR-compatible transducer (TIPs, Philips, or RKO-100, FUS Instruments). Ablation lesion volume and ND vaporization field volume were both assessed as a function of continuous wave HIFU pressure and pulse length *in vitro*. *In vivo* ablations were performed in rat liver. Thermal enhancement was assessed by MR thermometry via phase mapping of the proton resonance frequency shift.

Results/Discussion

In vitro, NDs required half as much pressure (2 MPa) to induce lesion formation compared to controls (4 MPa). MBs caused excess surface heating during HIFU whereas HIFU of NDs primarily resulted in heating at the acoustic focus (Fig. 1). Maximal temperature rise at the target was enhanced by 16.9% and 37.0% by MB and ND respectively. *In vivo*, the NDs circulated and remained viable for at least 40 minutes, during which time all HIFU (15 W, 15 s) lesions produced were constant in size (~7mm). Without NDs, significantly greater power (25 W) and twice as much time (30 s) was required to induce an ablation lesion in the liver, demonstrating their ability to more safely shorten ablation procedures.

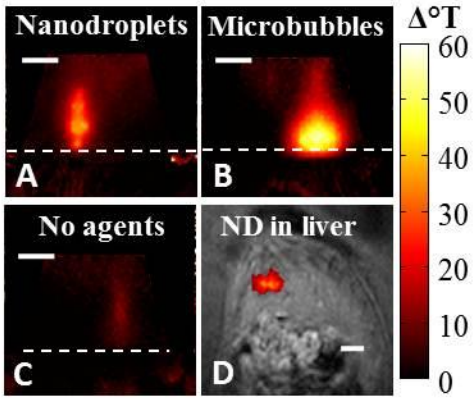

Fig. 1: MR temperature maps of HIFU ablation in acrylamide albumin phantoms containing nanodroplets (A), microbubbles (B), or no agents (C). The corresponding temperature map at the HIFU focus inside the rat liver. (White dotted lines indicate the location of the surface of the phantom, and each solid bar represent 5mm.)

[1]P. S. Sheeran, "Design of ultrasonically-activatable nanoparticles using low boiling point perfluorocarbons", Biomaterials, vol. 33, p. 3262-3269, 2012.

IUS1-M1-5

Ultrafast monitoring of liquid droplet vaporization

Claudia Errico[1], Olivier Couture[1,2], Alice Bretagne[1], Alan Urban[1], Patrick Tabeling[1,2], Mickael Tanter[1,3]; *[1]ESPCI, France, [2]CNRS, France, [3]INSERM, France*

Background, Motivation and Objective

Composite droplets can deliver large payloads in-situ with the spatial and temporal resolution of a clinical ultrasound scanner (Couture et al. Medical Physics 2012). Such technique could help tissue tattooing for tumor identification during surgery, but it could also deliver drugs at therapeutic concentrations. In this context, it would be important to develop an accurate monitoring method of the droplet's vaporization to assess the total dose. To provide such feedback, we have defined an ultrafast imaging sequence that can reveal the release of the composite droplets in-vivo with a millisecond time-resolution over an entire image.

Statement of Contribution/Methods

Monodisperse composite droplets were produced by injecting a nanoemulsion of water droplets and perfluorohexane within an external flow of water inside a microfluidic system. Fifty million droplets were introduced in the femoral vein of a rat. A 5 MHz transducer array (128 elements) was aligned over the liver of the rat. The array was connected to an ultrafast clinical scanner (SuperSonic Imagine, France), which was programmed to take a sequence combining a set of release focused pulses and a set of ultrafast plane waves images at 260 Hz frame rate.The release pressures were varied from 1.2 to 4.4 MPa-PNP. The resulting images were filtered to remove slow-moving tissue and to highlight the conversion of the droplets from liquid to gas. The same experiments were performed in Opticell plates filled with a dilute concentration of composite droplets (1/200) and placed perpendicularly to the plane of imaging of the same transducer.

Results/Discussion

A processing equivalent to ultrafast Doppler was performed to isolate fast decorrelation of the echoes within the site of release. Rapid changes were exclusively observed at 3.5 and 4.4 MPa PNP. The decorrelation contrast with respect to surrounding tissue was 20 dB. These hyperechoic regions appeared within 10 ms after the release pulses. Their presence was perfectly correlated with the observable delivery of fluorescein in the rat's liver.

In-vitro, the phenomena was observed at a faster rate. A strongly hyperechoic region was detected after release and was seen to rise over time within the Opticell plate as the resulting gas float toward the top. The hyperechoic regions on the ultrafast decorrelation images were successfully used as feedback by the sonographer to determine the success of the release. Such ultrafast monitoring is a specific phenomena that precisely provides either a confirmation or a refutation of the release.

IUS1-M1-6

Nanodroplet-Mediated Ultrasound Therapy for Targeted Cell Ablation

Eli Vlaisavljevich[1], Yasemin Durmaz[1], Adam Maxwell[2], Mohamed El-Sayed[1], Zhen Xu[1]; *[1]University of Michigan, USA, [2]University of Washington, USA*

Background, Motivation and Objective

Histotripsy is an ultrasound ablation method that fractionates tissue by controlling cavitation. Microbubble contrast agents can be combined with ultrasound for targeted ablation. However, microbubbles are too large to extravasate tumor vasculature to target cancer cells. We hypothesize that our nanodroplets can cross leaky tumor vessels to bind to targeted cancer cells. Acoustically vaporized nanodroplets act as cavitation nuclei at significantly reduced pressure to facilitate targeted histotripsy cancer ablation. Here we present our first effort to investigate the potential of nanodroplet-mediated histotripsy for targeted cell ablation.

Statement of Contribution/Methods

Nanodroplets of 200 nm in diameter were synthesized with a perfluoropentane core encapsulated in a cross-linked polymer shell. First, the peak negative pressure (p-) threshold to expand a bubble from 100-500 nm to 50 Î¼m was simulated at 0.2, 0.5, and 1.1 MHz using a single 2-cycle pulse. Second, to validate the simulation results, a layer of red blood

cells (RBC) mixed with nanodroplets was embedded in gels and exposed a 2-cycle pulse using a 0.5MHz focused transducer, and the resulting microbubbles and RBC disruption were imaged by a high speed camera. A total of 2000 ultrasound pulses were used at PRFs of 5, 10, 50, and 100Hz with p- up to 25 MPa.

Results/Discussion

The simulation shows that the p- threshold increased substantially with increasing frequency (Fig 1A). For example, the p- threshold using an initial 200nm bubble is 1.7, 6.3, and 21.3 MPa at 0.2, 0.5, and 1.1MHz, respectively. Experimental results closely matched simulation demonstrating a cavitation threshold ~7 MPa at 0.5MHz. The resulted microbubbles expanded to >50 Î¼m and collapsed within 100 Î¼s. Pulses at 10Hz PRF yielded the most consistent, well-defined ablation of the RBC phantoms compared to the other parameter combinations tested (Fig 1C). Without nanodroplets, no microbubbles or damage were observed at p- up to 25 MPa. This work demonstrates that the combination of nanodroplet and histotripsy produces cell ablation at a significantly lower pressure than using histotripsy alone, and therefore suggests the potential of this technique for targeted cancer ablation.

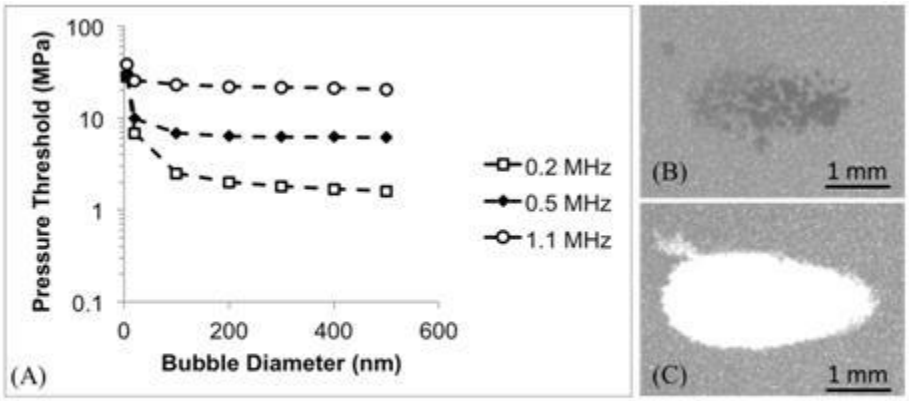

Fig 1. A) The simulated peak negative pressure (p-) threshold to expand a bubble from a diameter of 100-500 nm to 50 um in tissue. **B)** Microbubbles (dark) generated from nanodroplets in a gel phantom using p- of 15 MPa and PRF of 10 Hz. **C)** Correspondingly, RBC's within the microbubble region were destroyed (white).

Targeted contrast agents

M4

Thursday, July 25 2013, 02:00 pm - 03:30 pm

Congress Hallair: **Lori Bridal**
Univ. Pierre and Marie Curie, France

IUS1-M2-1

Quantification of targeted microbubbles in contrast enhanced ultrasound

Verya Daeichin[1], Zeynettin Akkus[1], Klazina Kooiman[1], Johan G. Bosch[1], Andrew Needles[2], Antonius F.W. van der Steen[1,3], Nico de Jong[1,3]; *[1]Thoraxcenter Biomedical Engineering, Erasmus MC, Rotterdam, Netherlands, [2]VisualSonics Inc., Toronto, Canada, [3]Interuniversity Cardiology Institute of the Netherlands, Utrecht, Netherlands*

Background, Motivation and Objective

Using targeted ultrasound contrast agent (t-UCA), molecular markers associated with diseases can be quantified noninvasively. Techniques used for quantifying t-UCA assume that all non-bound microbubbles (MB) are taken out of blood pool few minutes after injection. However, differences in physiology, diseases, and experimental conditions can increase longevity of unbound MB. In such conditions, unbound MB will falsely be quantified as t-UCA. We have developed a novel technique to distinguish and classify bound from unbound MB.

Statement of Contribution/Methods

Salivary glands of diseased mice were imaged using Vevo 2100 scanner. Boluses of 100 µL of MicroMarker MB targeted to angiogenesis markers and untargeted MB were injected separately. 10 minutes after injecting MB, 8 seconds long side-by-side B-mode and contrast images were recorded with a flash pulse in the middle to destroy MB in the imaging plane. In the post-processing steps, first tissue motion was compensated using block matching (BM) and multidimensional dynamic programing (MDP) techniques [1]. Then to preserve only stationary contrast signals a minimum intensity projection (MinIP) was applied on frames before and after the flash pulse. And, after-flash MinIP was subtracted from before-flash MinIP. This way, tissue artifacts in contrast images were reduced and signals from stationary MB were enhanced. In the next step, t-UCA candidates were detected by matching with artificial bubble templates. Finally templates of 0.1×0.1 mm around detected objects were tracked in subgroups of 20 frames using BM and MDP [2] to classify the candidates as unbound or bound MB based on their displacement.

Results/Discussion

Fig 1 shows an example of images before (c, d) and after (e, f) applying our method. Without analyses there are many control MB 10 minutes after injection which would be falsely considered as bound MB (Fig 1d). However, only few MB were classified as bound MB in the untargeted group after applying our technique (fig 1e). Using our method ratio of intensities in salivary gland for images with targeted MB (e) vs. untargeted MB (f) was improved 7 times compared to unprocessed images (c, d).

We have developed a novel image processing technique to automatically distinguish and classify bound t-UCA and unbound ones.

References

[1] Z. Akkus et al., Medical Imaging, 2012.

[2] A. Hoogi et al., Ultrasound Med. Biol., 2012.

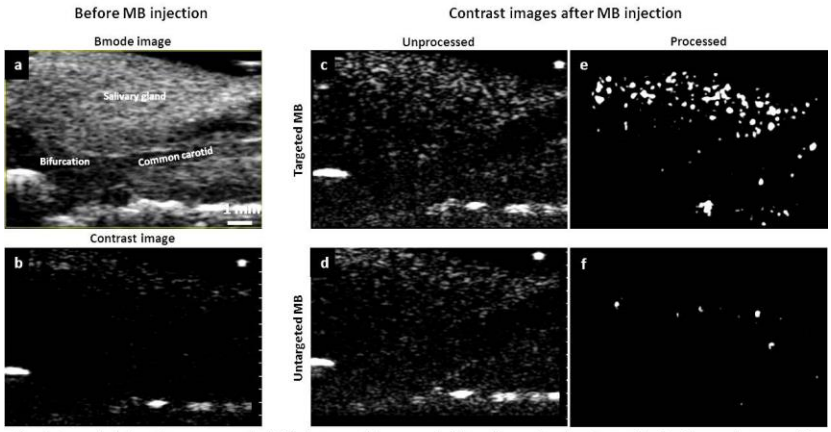

Fig. 1. B-mode (a) and contrast-mode (b-f) ultrasound images of right salivary gland and carotid of a diseased mouse. b is contrast image before injecting the microbubbles, c and d are single frame unprocessed images 10 minutes after injecting targeted (c) and control (d) microbubbles and their processed images(e, f).

This research was supported by the Center for Translational Molecular Medicine and the Netherlands Heart Foundation (PARISK).

IUS1-M2-2

Resonant frequency shift of quartz crystal microbalance caused by the specific adsorption of targeted microbubbles

Ryosuke Shimoya[1], Takashige Muramoto[1], Kenji Yoshida[1], Yoshiaki Watanabe[1]; *[1]Doshisha University, Japan*

Background, Motivation and Objective

Targeted microbubbles would be applied to molecular imaging and drug delivery system. For practical use, it is necessary to evaluate quantitatively the specific adsorption of the bubbles to the target site. Surface plasmon resonator (SPR) can detect molecular interactions and evaluate their affinity and reaction speed. However, SPR cannot provide the

bubble information such as their size and concentration because the penetration depth of evanescent wave is smaller than diameter of bubbles. This study proposes the method with quartz crystal microbalance (QCM) working as a thickness shear mode resonator. QCM possibly enables to obtain the bubble information because its resonant characteristics should be changed by microbubbles disturbing the oscillation of QCM.

Statement of Contribution/Methods

We attempted to attach biotinylated phospholipid bubbles (BB) specifically to QCM electrode via streptavidin-biotin bond. The average diameter of bubbles was about 2 µm. Bubble suspension was deposited for 300 seconds on the electrode surface. The resonant frequency of QCM was measured by a network analyzer. Third order harmonic of 15 MHz was monitored. The frequency shift before and after the deposit of the suspension was observed. As control experiments, we examined control bubble suspension without biotin (CB) and biotinylated lipid solution including no bubbles (LI). In addition, we quantitatively measured the frequency shift depending on the concentration of BB.

Results/Discussion

Figure 1 shows the resonant frequency shift caused by BB, CB, and LI. BB largely decreased the resonant frequency compared with CB (ΔF_{BB}=151.6±7.6 Hz, ΔF_{CB}=8.1±9.5 Hz). This demonstrated the specific binding of bubbles to QCM electrode. Compared BB with LI (ΔF_{LI}=83.1±6.1 Hz), it was proved that internal gas included by bubbles affects the frequency shift in addition to the mass effect of shell of the bubble. Moreover, we confirmed that the resonant frequency decreased with the increase of concentration of BB. The frequency shift seemed to be saturated at about -250 Hz in high concentration because the adsorbed amount of bubbles approached the maximum. These results indicated that the measurement using QCM is available for the evaluation of targeting ability of microbubbles.

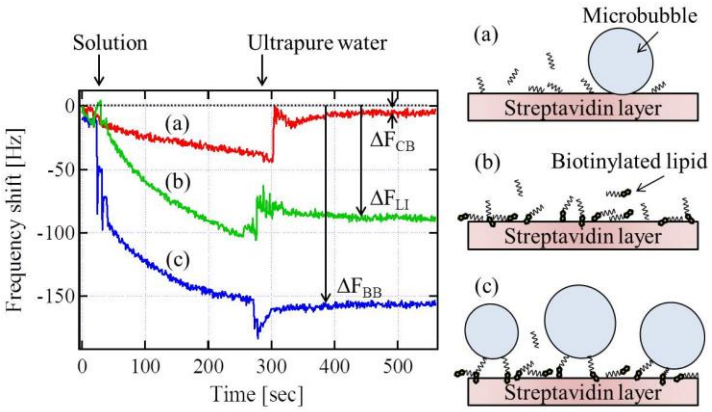

Fig. 1 Resonant frequency shift caused by attachment of (a) control bubbles, (b) lipid solution, and (c) biotinylated bubbles. The solution was added at 0 seconds and replaced with ultrapure water at 300 seconds.

IUS1-M2-3

Decorrelation-based Adherent Microbubble Identification as a Faster Alternative to Singular Spectrum-based Targeted Molecular Imaging (SiSTM) of Large Blood Vessels

Shiying Wang[1], F. William Mauldin, Jr. [1], John A. Hossack[1]; [1]*Biomedical Engineering, University of Virginia, Charlottesville, VA, USA*

Background, Motivation and Objective

Ultrasound-based targeted molecular imaging has potential for early detection of atherosclerosis. Current strategies employ non-linear extraction followed by frequency-based filtering to suppress signals from tissue and freely flowing microbubbles (MBs) while maintaining the desired adherent microbubble (AMB) signal. However, in large vessels, separation efficacy is limited due to non-linear signal components in the vessel wall reflection and overlapping frequency spectra between signals from the vessel wall and AMBs. We recently proposed singular spectrum-based targeted molecular imaging (SiSTM), which uses changes in statistical dimensionality – quantified by normalized singular spectrum area (NSSA) – to more effectively isolate the AMB signal. Unfortunately, the NSSA calculation employs a computationally intensive singular value decomposition, which may preclude real-time implementation. We have shown that the NSSA signature of AMBs results from frame-to-frame echo decorrelation. The goal of this work is to determine the relationship between NSSA and echo decorrelation, and to develop decorrelation-based signal separation of AMBs in large vessels (distinct from "loss of correlation" results from bursting MBs).

Statement of Contribution/Methods

Flow phantoms were constructed with 4.2 mm diameter lumens. Channels were incubated with 50 µg/mL streptavidin for 5 h and then with 5% bovine serum albumin for 3 h. Biotinylated lipid shelled MB (~ 2.3 µm) solution (5×10^5 mL^{-1}) was drew through the channels. Custom SiSTM beam sequences were programmed on a Verasonics scanner using an ATL L12-5 38mm transducer. Plane wave imaging pulses (4.09 MHz, 50 Hz frame rate) were interspersed with focused radiation pulses (800 Hz PRF, MI < 0.09, MBs did not burst). Both NSSA and decorrelation were calculated from focused RF data.

Results/Discussion

Without physiological motion, NSSA and decorrelation had a quadratic relationship (Adjusted-R^2 = 0.87). This relationship was sustained at different flow velocities (2.4, 4.8 and 7.2 cm/s; Adjusted-R^2 > 0.8). Processing based on decorrelation exhibited approximately 10-fold less time than that based on NSSA. The results demonstrate that decorrelation-based signal separation of AMBs in large vessels is feasible with less computational complexity and similar efficacy to NSSA-based method.

Grant: US NIH R01 HL111077

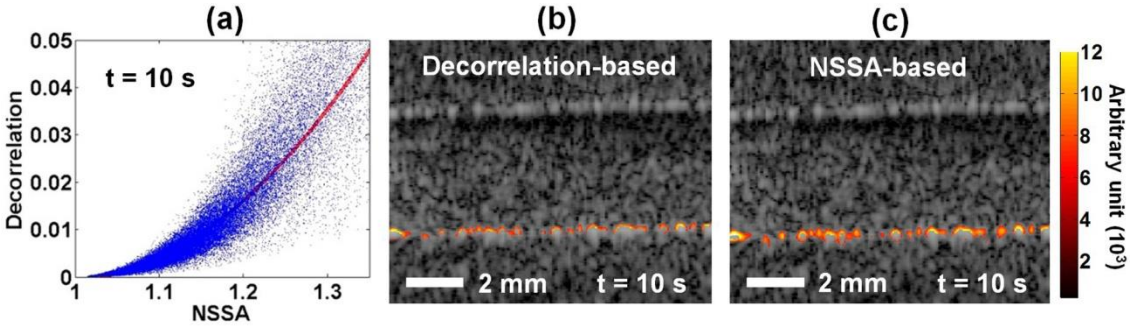

Figure (a) Relationship between NSSA and decorrelation. Red line shows the quadratic fit (Adjusted-R^2 = 0.87). (b) B-mode image overlaid with colored image showing location and intensity of AMBs (Decorrelation-based AMBs detection). (c) B-mode image overlaid with colored image showing location and intensity of AMBs (NSSA-based AMBs detection). MB solution was flowing from left to right at a flow velocity of 7.2 cm/s.

IUS1-M2-4

Quantitative Functional Assessment of Tumor Microenvironment using Contrast Enhanced Ultrasound and Photoacoustic Imaging

Melissa Yin[1], Minalini Lakshman[2], F. Stuart Foster[1,3]; [1]*Sunnybrook Research Institute, Toronto, Ontario, Canada,* [2]*FUJIFILM VisualSonics, Inc., Toronto, Ontario, Canada,* [3]*Medical Biophysics, University of Toronto, Toronto, Ontario, Canada*

Background, Motivation and Objective

Cancer cells are differentiated from normal cells by a number of genetically altered characteristics, one being the ability to induce abnormal angiogenesis. However, these specific traits are also regulated by tumor microenvironmental factors such as hypoxia. Alterations in the tumor microenvironment generally confer with aggressive cancer phenotypes, raising the need for in vivo and non-invasive methods of tracking these changes. Contrast enhanced ultrasound (CEUS) in combination with photoacoustic (PA) imaging serve as promising candidates – one has the ability to measure tissue perfusion, where as the other can be used to monitor oxygen saturation. In this study we investigate drug induced alterations to the tumor microenvironment, and validate the sensitivity of CEUS and PA imaging with histology.

Statement of Contribution/Methods

Primary orthotopic tumors were surgically implanted in nude SCID mice using the 231/LM2-4 breast cancer cell line. Mice with tumors of an approximate volume of 200mm3 were given either a single dose of 50mg/kg of Oxi-4503 or 0.9% saline (N=6/group). US imaging was performed using the VevoLAZR system with integrated PA probe at 21MHz; pre- and 4 hours post-vascular shut down. Relative tissue oxygen saturation was measured with PA imaging, and indices of relative blood volume and flow were assessed with CEUS. Post-sacrifice, tumour tissue was excised and fixed for histology.

Results/Discussion

Functional changes in the tumor vasculature were evident in the drug treated mice at 4 hours post-treatment as shown by a decrease in average blood volume (-82.1%), flow (-80.5%), and oxygen saturation (-37.2%) (see figure of sample tumor). Results for all parameters were statistically significant compared to pre-treatment. Similar degree of changes was not observed in the control group, which showed a decrease of 16.6% in blood volume, 8.7% in blood flow, and 0.008% in tumor oxygenation. Histological confirmation of subsequent molecular changes included CD31 staining for vessels distribution and CA9 staining for hypoxia. A higher level of hypoxia expression was found in the Oxi-4503 treated tumors, with increased areas of positive CA9 staining observed at the tumor core, confirming imaging data. Taken together, CEUS and PA imaging are potentially a sensitive tool for quantitative functional assessments of breast tumor models.

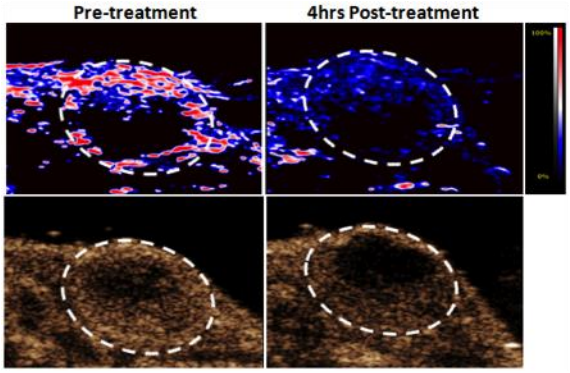

IUS1-M2-5

Cell Sorting Using Targeted Biotinylated Albumin Microbubbles

Yu-Ren Liou[1], Yu-Hsin Wang[1], Pai-Chi Li[2]; [1]*National Taiwan University, Taiwan,* [2]*Electrical Engineering, National Taiwan University, Taipei, Taiwan*

Background, Motivation and Objective

Cell analysis often requires isolation of certain cell types. Various separating methods have been applied to cell sorting, including florescence-activated cell sorting (FACS) and magnetic-activated cell sorting (MACS). However, these conventional approaches need to exert additional force on the cell, thus facing the risk of cell damage. In this study, we hypothesize that biotinylated albumin microbubbles (MBs) conjugated with antibodies (i.e., targeting MBs, or tMBs) can be used for cell separation from the solution by buoyancy of the MBs. Specifically, biotin is conjugated to the albumin shell by covalent bond (biotin tMBs) to strengthen the interaction between albumin shell and the antibodies.

Statement of Contribution/Methods

Biotin-(NHS)-ester in dimethyl sulfoxide at 20 mg/ml is added to 10 mg/ml human serum albumin in PBS (pH=8.0) to achieve a ratio of 10 molecules of biotin-ester per molecule of protein. The components are incubated on a shaker for two hours at room temperature. Biotin-labeled bubbles are prepared by a sonication method with a ratio of one biotin-labeled HSA to three unlabeled HSA. Excess unbound biotin is removed by washing three times with PBS. Next, biotin-MBs are incubated with avidin and the MDA-MB-231 breast cancer cells are incubated with biotin-antiCD44, respectively. Albumin without biotinylation is used as control MBs.

Results/Discussion

The upper suspension from the cell pellet is separated and cell number is counted. The results show that only the avidin-biotin-MBs suspends the MDA-MB-231 cells, in which the cell umber of the upper suspension (about 137.5*104 cells/mL) is six times higher than the one of the pellet (23.5*104 cells/mL). Biotinylation of MBs does not suspend the cells with only 7*104 cells/mL in the upper suspension and most of the cells (241.5*104 cells/mL) deposit as the pellet. Control MBs fail to sort the cells with or without avidin. Our biotinylated albumin MBs conjugated with specific tags successfully separated cells. Although the conventional method to make tMBs is incorporating avidin into the shell of albumin MBs and then coupling antibodies by using the biotin-avidin system, these avidin tMBs failed to sort the suspended cells. Finally, our biotin tMBs cannot suspend cells larger than 2000 μm2 in area, because the buoyancy limitation.

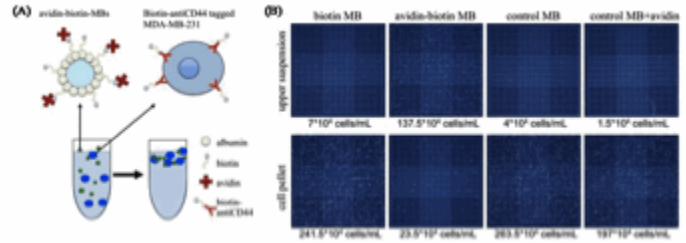

(A) The scheme of using biotin tMBs for cell separation. (B) The cell number of the upper suspension and the deposited pellet after MBs treatment.

IUS1-M2-6

Vaporization phenomena for ultrasound phase change nanodroplets assessed via high speed optical microscopy

Paul S. Sheeran[1], Terry O. Matsunaga[2], Paul A. Dayton[1]; [1]*Joint Department of Biomedical Engineering, University of North Carolina and North Carolina State University, Chapel Hill, NC, USA,* [2]*Department of Medical Imaging, University of Arizona, USA*

Background, Motivation and Objective

Many studies have proposed phase-change contrast agents (PCCAs) that vaporize to form bubbles ideal for contrast and cavitation. Understanding the phenomena involved with droplet vaporization to determine possible bioeffects (such as shear stresses) will have a profound impact on designing agents to be effective in desired applications. Even when formed with volatile components, droplet vaporization can require pressures higher than commonly used for microbubble imaging - increasing the possibility for secondary effects such as bubble destruction and fusion. In addition, the volatility of the core perfluorocarbon plays a significant role in the mechanical forces produced by droplet expansion. In this study, we use ultra-high-speed microscopy to explore for the first time the vaporization phenomena of decafluorobutane (DFB) droplets at clinically relevant frequencies and pressures.

Statement of Contribution/Methods

DFB droplets were formulated by a previously developed ′microbubble condensation′ method. Emulsions were injected into microcellulose tubing in a 37Â°C degassed water bath and placed at the co-focus of the ultrasound transducer and microscope. Droplets in the focal volume were vaporized using single pulses of adjustable intensity at 1 and 8 MHz delivered from a focused piston transducer. Vaporization dynamics were captured using an ultra-high-speed framing camera (SIMD24, Specialised Imaging) capable of up to 20 million frames per second and analyzed offline.

Results/Discussion

DFB droplets vaporize more rapidly than reported values for perfluoropentane droplets, and nanodroplet vaporization begins as early as the first rarefactional phase. Bubbles reach their final size within 200 ns, and are immediately subject to compression and rarefaction from the continuing pulse. As a result, many newly-formed bubbles are destroyed during the subsequent compressional phase. DFB microdroplets, in contrast, vaporize violently over the course of several microseconds, and the resulting bubbles showed characteristic over-expansion and resonant oscillatory settling (Fig. 1) to a final size. Radial velocities reached values on the order of 10 m/s during vaporization. Results also show that the bubbles produced from microdroplets tend to fuse with nearby bubbles as a result of secondary radiation force during subsequent rarefactional cycles.

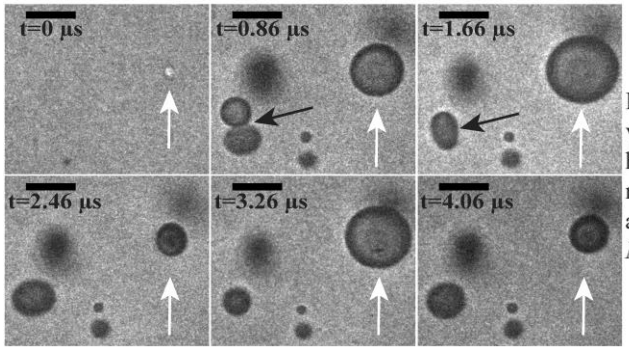

Figure 1. Droplets exposed to 8 MHz, 2 cycle pulse are vaporized to form microbubbles. Even after the pulse has ended, instances of bubble fusion (black arrow) and resonant oscillation as a result of expansion (white arrow, approx. oscillation at 625 kHz) can be observed. *Note: Scale bar = 10 μm.*

Photoacoustic imaging systems and signal processing

M5

Thursday, July 25 2013, 02:00 pm - 03:30 pm

Congress Hallair: **Emmanuel Bossy**
Institut Langevin ESPCI

IUS1-M3-1

Performance Characterisation of a new Clinical Spectroscopic Epiphotoacoustic Scanner

Erwin Alles[1], David Harris-Birtill[1,2], Michael Jaeger[3], Jeffrey Bamber[1]; [1]*Joint Department of Physics and CRUK-EPSRC Cancer Imaging Centre, Institute of Cancer Research and Royal Marsden NHS Foundation Trust, Sutton, Surrey, United Kingdom,* [2]*Hamlyn Centre for Robotic Surgery, Imperial College London, London, United Kingdom,* [3]*Institute of Applied Physics, University of Bern, Bern, Switzerland*

Background, Motivation and Objective

Reflection-mode epiphotoacoustic (epiPA) imaging combines the resolution and penetration of ultrasound (US) with the spectral properties of optical absorption imaging, and enables imaging of a wider range of organs than photoacoustic (PA) tomography. The image quality of a PA system is determined by both its ultrasonic and optical properties, and is affected by optical scattering and absorption. Consequently, the light delivery geometry could affect the image quality. In this work, a new clinical spectroscopic epiPA scanner was developed, and its performance evaluated and optimised in terms of resolution, signal to noise (SNR) and signal to clutter ratio (SCR).

Statement of Contribution/Methods

A clinical US scanner (Zonare Z.One + 9-14 MHz linear array) was combined with a tuneable laser (Quantel Brilliant B + Rainbow OPO, 685 – 950 nm) or a Q-switched laser (ElEn, 1064 nm) for fully automated clinical duplex spectroscopic epiPA and US imaging. Light is delivered through a bifurcated fibre-optic bundle, the ends of which flank the US transducer. An optimisation gantry facilitated accurate control of bundle separation, height and angle.

Using the tips of graphite rods (377 ± 5.6 µm in diameter) as PA "point" sources, arranged in a one-dimensional array and either submerged in Intralipid® solutions mimicking the optical scattering in human tissue or placed beneath chicken breast, the three-dimensional point-spread function (PSF), SNR and SCR of the system were determined for multiple source locations, wavelengths and optical fibre angles.

Results/Discussion

A clinical spectroscopic epiPA system was built that exhibits, in all experiments, PSFs with small spatial extents, especially laterally (399 ± 80 µm) and axially (340 ± 20 µm) (Fig.1). The elevational extent was found to vary with imaging depth, similar to the mechanical focus of the US transducer array. In purely scattering media (Intralipid® at 700, 800 and 900 nm), no significant optimum was observed in peak pressure amplitude, SNR, SCR or PSF extent for illumination angles between 57.5° and 75°. In absorbing media (chicken breast, Intralipid® at 1064 nm), a weak optimum was observed in only the peak pressure amplitude at an angle coinciding with the shortest optical path to the rod tips. The absence of a strong optimum implies that practicality is the main concern when designing the clinical scan-head geometry.

Fig. 1

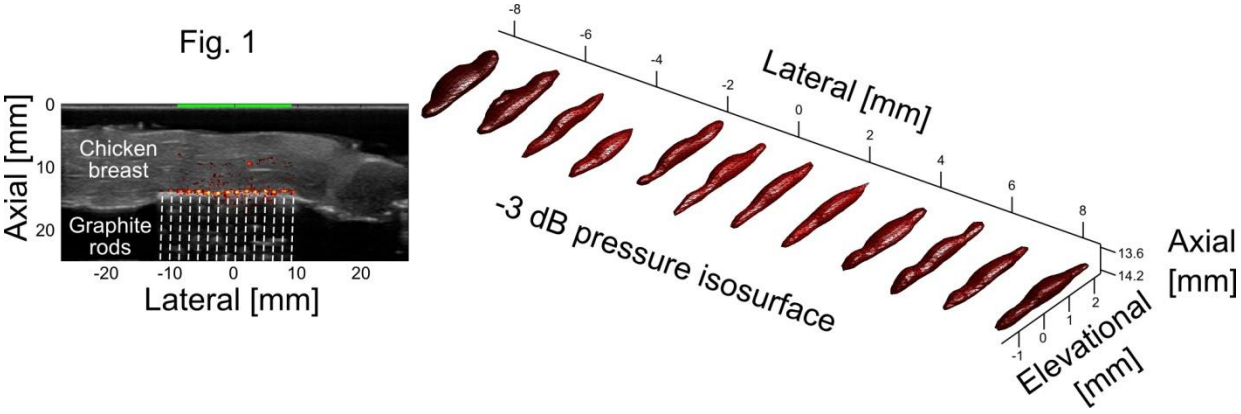

IUS1-M3-2

Reduction of clutter in medical epiphotoacoustic images using acoustic radiation force-based localized vibration tagging (ARF-LOVIT)

Michael Jaeger[1], Martin Frenz[1], **Jeffrey Bamber**[2]; [1]*Institute of Applied Physics, University of Bern, Bern, Switzerland,* [2]*Joint Department of Physics and CR-UK & EPSRC Cancer Imaging Centre, Div. of Radiotherapy & Imaging, The Institute of Cancer Research and The Royal Marsden NHS Foundation Trust, Sutton, Surrey, United Kingdom*

Background, Motivation and Objective

For versatile medical photoacoustic (PA) imaging an epiphotoacoustic (ePA) technique is preferred to avoid strongly attenuating media such as bone or gas. Unfortunately, the ePA approach causes severe clutter from strong PA emissions close to the probe, which limits useful clinical imaging to depths of 1cm or less. Deformation compensated averaging, which exploits clutter decorrelation during tissue strain, has achieved signal-to-clutter ratio (SCR) improvements in clinical ePA imaging of about three (Jaeger et al. J Biomed Opt; 17, 1-8, 2012) but larger gains are needed if the noise-limited imaging depth is to be acheived. Here we test a new method for clutter reduction.

Statement of Contribution/Methods

The new method uses vibration-induced localised displacements to "tag" PA signals at their place of origin, enabling signal identification and, in theory, full clutter cancellation if ideal conditions are met. Experiments were conducted with gelatine phantoms containing TiO_2 optical scatterers, cellulose ultrasound scatterers and India ink for optical absorption. Localised vibration tagging (LOVIT) was induced by acoustic radiation force (ARF) using a cylindrical 2MHz transducer. Sequences of pairs of PA images were acquired using a Zonare z.one® ultrasound (US) scanner with an ELEN 1064nm-wavelength 7ns-pulse Q-switched Nd:YAG laser, a first image prior to an ARF push and a second with an ARF push to produce a localised displacement. Different pairs were for different locations of the push focus, scanned in steps of 2 mm laterally and 5 mm axially.

Results/Discussion

In the figure, a) is a phantom section corresponding to the imaging plane showing 2mm diameter optically absorbing (India ink) and hypoechoic (no cellulose) gelatine cylinders, imitating blood vessels on US in b). c) is the best ePA image without clutter reduction. d) is an ARF-LOVIT image obtained by mosaicking results from many push focus locations where, at each location, a difference (push minus no-push) image was calculated with normalisation to ensure equal noise level for conventional and ARF-LOVIT images. ARF-LOVIT repeatedly demonstrated greatly improved SCR and imaging depth over conventional ePA imaging. Many LOVIT implementations are possible and the method may offer benefits in conventional US and other images such as optical coherence tomography if clutter limits image contrast.

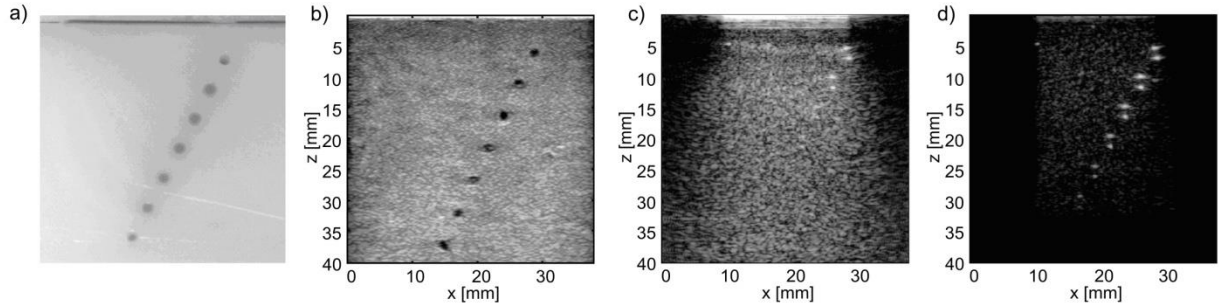

IUS1-M3-3

Spectrum analysis of photoacoustic signals for characterizing tissue microstructure

Parag V. Chitnis[1], Jonathan Mamou[1], Ashwin Sampathkumar[1], Ernest J. Feleppa[1]; [1]*F. L. Lizzi Center for Biomedical Engineering, Riverside Research, USA*

Background, Motivation and Objective

Quantitative-ultrasound (QUS) estimates obtained from echo data, e.g., spectral slope (SS), spectral intercept (SI), and effective scatterer size, can differentiate between diseased and healthy tissue. However, QUS estimates are sensitive to tissue microstructure, but do not provide molecular specificity, which could further improve tissue classification. We investigated the feasibility of obtaining quantitative photoacoustic (QPA) estimates for simultaneously providing sensitivity to microstructure and optical specificity for distinguishing among tissue constituents.

Statement of Contribution/Methods

QPA estimates were tested on an agar phantom containing three types of black polyethylene spheres (0.5% v/v) that were 42, 58, 116 µm in size. Two 10-mm inclusions, one consisting of 42-µm particles and other of 58-µm particles, were surrounded by 116-µm particles. A 532-nm laser with pulse duration of 5 ns and pulse energy of 6 mJ excited the photoacoustic (PA) response. A 26-MHz (-3-dB bandwidth of 20 MHz), F2 transducer with a 12.5-mm focal length was scanned in 100-µm steps to acquire 3D PA data. Spectra were computed from PA signals in a 1-mm window centered at the focus. Moving-window averaging smoothed the spectral data along both scan dimensions. The 3-dB band of the spectrum was used to obtain three QPA estimates: SS, SI, and estimated absorber size (EAS). SS and SI were computed using a linear-regression approximation to the normalized spectrum. EAS was computed by fitting the normalized spectrum to the single-sphere analytical solution. Normalization involved division of the measured spectrum by a spectrum obtained from a homogenous 58-µm-particle phantom, and multiplication by the modeled response from those particles. Mean values were computed using 2.5-mm square regions-of-interest in C-mode maps of local QPA-estimate values.

Results/Discussion

The C-mode images of QPA-estimate values showed both inclusions, which were not depicted in conventional B-mode images (See Figure). EAS estimate values had a standard deviation that was 1% to 6% of the corresponding means, which was considerably lower than the standard deviations of SS and SI estimates (See Table); this result suggests that EAS is a more-robust classification parameter. This work was supported in part by NIH grant EB015856.

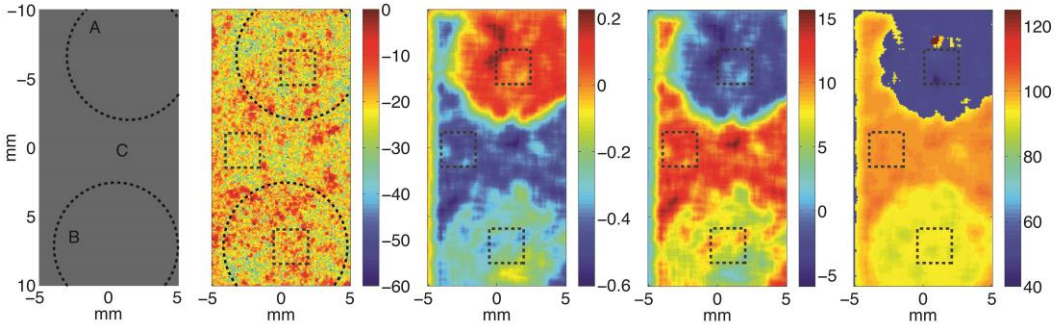

(a) Cartoon of the phantom. (b) C-mode map of the RF envelope at z = 12.5 mm (dB). (c) Spectral-slope map (dB/MHz). (d) Spectral-intercept map (dB). (e) Map of estimated absorber size (µm). The table below shows mean of QPA estimates obtained from three ROIs shown above.

Nominal diameter (µm)	Spectral slope (dB/MHz)	Spectral intercept (dB)	Estimated absorber size (µm)
42	0.05±0.06	-1.4±1.5	51±3
58	-0.27±0.06	7.0±1.5	92±1
116	-0.43±0.04	11.3±1.1	101±1

IUS1-M3-4

Photoacoustic Coded Excitation using Pulse Position Modulation

Martin F. Beckmann[1], Georg Schmitz[1]; [1]*Chair of Medical Engineering, Ruhr-Universität Bochum, Bochum, NRW, Germany*

Background, Motivation and Objective

Solid state laser systems are commonly employed for photoacoustic imaging, but cheap and handy pulsed laser diodes are an attractive alternative. They emit low pulse energies, but fast averaging is possible due to high achievable repetition rates in order to improve the Signal to Noise ratio (SNR).

While averaging is limited by the time of flight of the acoustic signal, photoacoustic coded excitation (PACE) can be used to overcome this limitation. Optical orthogonal codes are used to great effect in optical signal transmission. These codes are based upon varying temporal spacing between laser pulses, which makes them easy to generate. Therefore, we examine the performance of these PACE codes based on pulse position modulation (PPM).

Statement of Contribution/Methods

PPM codes rely on varying time distances between successive laser pulses. By varying time differences, the autocorrelation side lobes of the PPM code, which are a measure for the amount of distortion caused by the coding, can be kept very low. For short codes or high sampling rates, low maximum autocorrelation side lobe amplitudes equal to the single pulse amplitude are possible.

The gain in SNR was calculated theoretically and compared to previously published sequences. The theoretical results were verified in a simulation. In addition, experiments using a Sonix RP (Ultrasonix, L14 5/38, 7.2 MHz) clinical ultrasound system and a laser diode (808 nm, 530 nJ) were performed. Code length, pulse repetition frequency and time distances were varied.

Results/Discussion

PPM codes achieve a coding gain that exceeds that of previously reported codes. For long codes the performance drops. For example, a coding gain of 8.5 dB and more (depending on timing constraints) is possible for a pulse repetition frequency of 500 kHz, an imaging depth of 5 cm and short codes while Legendre sequences or Golay codes only approach 6.2 dB for very large code lengths (see Fig. 1). Additionally, the code consists of positive elements only, no separation is therefore necessary.

Because the reconstruction is not perfect, side lobes induced by the code can degrade image quality. These will be larger than for Legendre sequences. The Experiments indicate that the predicted gain may not be fully reached due to this. Nevertheless, the high SNR gain at short code lengths renders the PPM code a good choice for very low SNR applications at high image frame rates.

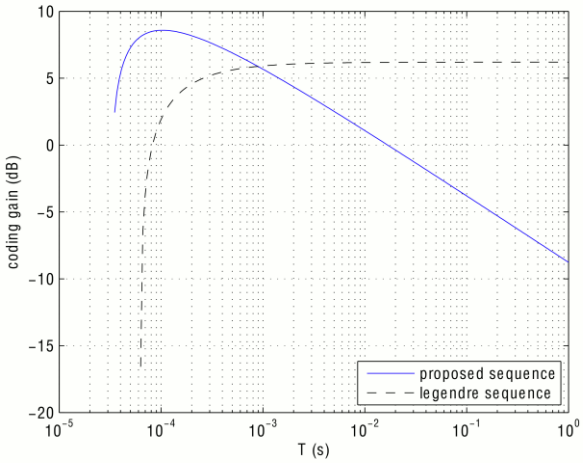

Figure 1: Coding gain performance of proposed sequence for a PRF of 500 kHz, imaging depth of 5 cm and time step adjustments of 150 ns per pulse.

IUS1-M3-5

Photoacoustic Flow Measurement with Ultra-High Temporal Resolution by Coded Excitation

Haichong Zhang[1], Kengo Kondo[1], Makoto Yamakawa[2], Tsuyoshi Shiina[1]; [1]*Human Health Science, Graduate School of Medicine, Kyoto University, Kyoto, Japan,* [2]*Advanced Biomedical Engineering Research Unit, Kyoto University, Kyoto, Japan*

Background, Motivation and Objective

Photoacoustic (PA) imaging is an emerging imaging technology combining optical imaging with ultrasound. There has been a strong demand for PA flow imaging of contrast agents such as blood or nano-particles for observing the disease process or drag delivery. In conventional PA flow imaging, however, the temporal resolution is limited by the acoustic time-of-flight (TOF), which is the highest possible frame rate, and the sensitivity is determined by the signal-to-noise ratio (SNR). We propose coded excitation to achieve photoacoustic flow imaging with ultra-high temporal resolution above the barrier of the acoustic TOF and high sensitivity.

Statement of Contribution/Methods

Periodically and unipolarly implemented m-sequence (PUM) was chosen as the code for coded excitation. The frame-rate, which was limited by the acoustic TOF, can be maximized up to the pulse repetition frequency (PRF) since the start point of decoding can be set in any code in the periodic sequence. Therefore, velocities can be acquired at shorter intervals, and higher temporal resolution is achieved. Moreover, the SNR can be improved by compressing coded signals. Here, we demonstrate the feasibility through an experiment. A black wire is moved by a motor at designated speed while being irradiated with a 532 nm Nd:YVO4 pulse laser (Fig. 1a). The velocity of the moving object is calculated by measuring the displacement of two signals using cross-correlation. Thirty-one-bit PUM was employed with a PRF of 100 kHz, and the coded and non-coded results were compared, assuming the acoustic TOF is 310 µs (the time for one PUM sequence).

Results/Discussion

The non-coded signals did not estimate velocity well, and there were numerous outliers because of the poor SNR (the averaged SD (standard deviation) of the estimated velocity was 19.88 mm/s). Coding significantly improved the SNR, so that the estimated velocity agreed well with the true designated velocity (Fig. 1b) (the averaged SD of the estimated velocity was 1.24 mm/s). In addition, we confirmed a shorter interval of temporal velocity change from the coded results (Fig. 1c). The velocity sampling period of coded signals was 10 µs, while that of non-coded signals was 310 µs. This indicates that slight flow variations, which could not be observed without coding, can be detected by coded excitation.

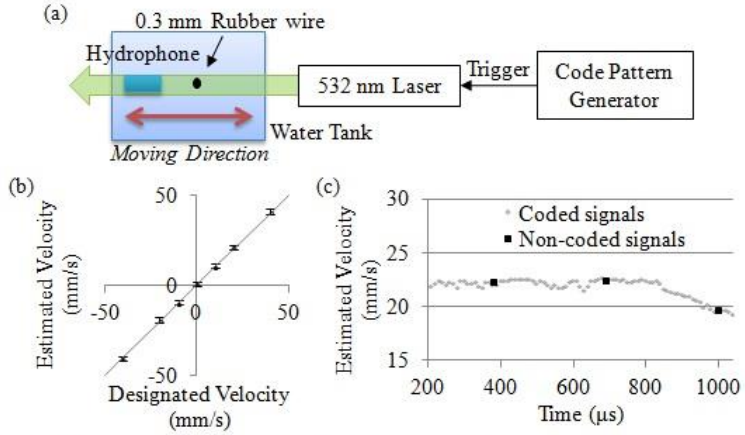

Fig. 1. Photoacoustic flow measurement. (a) System geometry. (b) Estimated velocity of coded signals; the solid line plots the true values. (c) Temporal velocity change of coded and non-coded signals when object moves at 20 mm/s.

IUS1-M3-6

Dependence of photoacoustic amplitude-temperature curves with the absorbers and illumination conditions

Olivier Simandoux[1], Amaury Prost[1], Emmanuel Bossy[1]; [1]*Institut Langevin, ESPCI ParisTech, CNRS, INSERM ERL U979, Paris, France*

Background, Motivation and Objective

Photoacoustic sensing has been proposed in recent years as a mean for temperature monitoring in biological tissues, with potential application to thermal therapy monitoring. It is classically assumed that the photoacoustic signal amplitude follows the tissue temperature via the temperature dependence of the Gruneisen coefficient. Although this is often true for appropriate conditions, including stress and heat confinement, our goal in this work is to show experimentally that this is not the case in some realistic situations: theoretical results (submitted for publication, not discussed here) suggest that the temperature-dependence of photoacoustic signals depends on the laser fluence and the size of the colloidal absorbers.

Statement of Contribution/Methods

A 20 MHz photoacoustic microscope was used to detect signals from water-filled tubes immersed in a temperature-monitored water tank. Micrometers, nanometers and molecular size absorbers were diluted in water to obtain absorbing solutions of equivalent optical densities. For various laser fluences, the photoacoustic signals amplitudes were measured as a function of temperature, for values ranging from 1°C to 20°C.

Results/Discussion

Our results show that the solutions with microns, nanometers or molecular dyes have very different photoacoustic amplitude dependences on the medium equilibrium temperature. We also show that this dependence is strongly affected by the laser fluence. In fig. 1 normalized photoacoustic signals amplitudes from a molecular blue dye solution (dots) and a black India ink (crosses) containing hundred nanometers particles, are represented versus the medium equilibrium temperature. Two different regimes may be observed: for molecular size absorbers, for which the medium may be considered as micro-homogoneously absorbing, the temperature dependence follows the dependence of the Gruneisen coefficient with temperature, as has been classically assumed in published works. On the other hand, local temperature rise on large enough colloidal absorbers clearly modifies the observed temperature dependence. As a consequence, photoacoustics-based thermometry approaches based in particular on metallic nanoparticles may have to take into account parameters such as the fluence and/or particles size to derive temperature changes from photoacoustic signals.

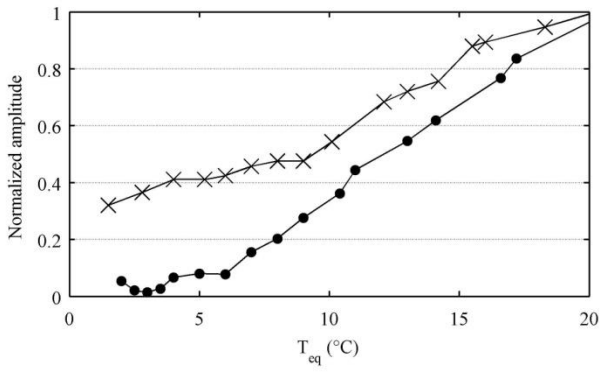

CMUTs

NH

Thursday, July 25 2013, 02:00 pm - 03:30 pm

Congress Hallair: **Omer Oralkan**
North Carolina State University

IUS5-M-1

CMUTs development progress review for medical applications

Mathieu Legros[1], Cyril Meynier[2], Nicolas Sénégond[2], Pascal Chatain[2], David Voisin[2]; *[1]R&D Department, VERMON S.A., Tours, France, [2]VERMON S.A., France*

Background, Motivation and Objective

Emerging applications in medical ultrasound progressively require probe designs with advanced performances or features. Probes fabrication sometimes becomes a challenge to address and satisfy all aspects requested by these new applications. CMUTs (Capacitive Micromachined Ultrasound Transducers) are an attractive technology for novel medical modalities. Intrinsic performances and high-level integration of CMUTs open also new opportunities for medical diagnosis. The industrial advantages and drawbacks of this transduction technology over its competitive piezoelectric materials are now clearly identified, and both transductions become complementary technologies able to address any medical ultrasound applications.

Statement of Contribution/Methods

After a short introduction, the talk will describe the different tasks covering the fabrica-tion of CMUT probes, from modeling, wafers design and manufacture, to the interconnect and packaging operations, including the development of transmit and receive electronics. Through different concrete examples based on original manufactured CMUT probes, we will give an overview of the specific performances of capacitive transduction. We'll browse all applications where VERMON was involved in the design or the realization of CMUT probes. The efforts to connect 1D arrays for medical imaging to standard ultrasound system will be reviewed. Then, CMUT opportunities and our recent development for medical applications such as high density arrays, novel 1D-array designs, miniaturized and therapy transducers, will be presented. Front-end integration was also investigated for most of the fabricated probes, and we will share our vision of interfacing CMUT transducers with dedicated electronics.

Results/Discussion

Using our CMUT development platform, we have demonstrated a large range of medical applications for CMUTs. Open problems and challenges for CMUT probes manufacturing, and next generation probes can be summarized through this presentation. CMUTs have to be seen as a polyvalent toolbox, which can make the portfolio of ultrasound applications grow.

IUS5-M-2

Development of a miniaturized 1D linear-array cMUTs for interstitial Ultrasound therapy

William Apoutou N'DJIN[1], Michael CANNEY[1,2], Cyril MEYNIER[3], Françoise CHAVRIER[1], Cyril LAFON[1], An NGUYEN-DINH[3], Alexandre CARPENTIER[2], Jean-Yves CHAPELON[1]; *[1]Inserm, U1032, LabTau, Lyon, F-69003, France ; Université de Lyon, Lyon, F-69003, France, [2]Carthera, Brain and Spine Institute, Paris, France, [3]Vermon SA, Tours, France*

Background, Motivation and Objective

Delivery of High Intensity Ultrasound from interstitial applicators has the potential to enable greater spatial control of the heat deposition, faster treatment rates and larger volumes of tissue to be treated as compared to existing interstitial heating applicators. Capacitive Micromachined Ultrasound Transducers (cMUT) exhibit several potential advantages such as the possibility for extreme miniaturization, inherit broad bandwidth, and high electro-acoustic efficiency. Although cMUTs have been mostly developed for imaging purposes, their characteristics can also be interesting for therapeutic ultrasound applications in comparison with conventional piezo technologies. Previous studies have shown the feasibility of using mono-element cMUT transducers or cMUT imaging arrays in continuous wave mode for generating high intensity ultrasound.

Statement of Contribution/Methods

Here a new miniaturized cMUT linear-array is presented that was developed for minimally-invasive interstitial therapeutic applications. A thin 1D planar-array, 32.4-mm long and 0.8-mm wide, was built with 12 electrically independent rectangular elements, each with a surface area of 2.7 × 0.8 mm2. The acoustical characteristics of this miniature cMUT linear-array were investigated experimentally and compared with simulations. Simulations were also performed to evaluate the ability to generate thermal ablations in soft tissues with several configurations: (i) 1 miniature linear array, (ii) a combination of multiple linear arrays positioned on a cylindrical catheter. With this later configuration, the feasibility of conformal interstitial ultrasound treatments was investigated by integrating human brain metastasis geometries segmented from clinical MR-images as target volumes.

Results/Discussion

First experimental characterizations showed that each single element of the 1D cMUT array had a frequency-bandwidth at -3dB of >12 MHz. At 6 MHz, a single element was able to generate in water a maximum peak pressure of >0.5 MPa which was, according to modeling, compatible with High Intensity Ultrasound application in soft tissues (surface intensity: 10W/cm2). The pressure field distribution measured for a single element was well collimated in the sagittal plan and no electro-mechanical coupling was observed between neighboring elements. In simulations, the ability to use various power levels and frequencies on independent elements and combinations of multiple linear-arrays offered sufficient flexibility to achieve a wide variety of thermal ablation patterns in 3D. Simulated ablation volumes could be controlled to cover accurately non-symmetrical volumes of brain metastasis. The miniaturized 1D linear-array cMUTs developed in this work shows interesting characteristics, which may open new perspectives for conformal interstitial thermal therapy. This work has been supported by the French National Research Agency (ANR TecSan, 2010).

IUS5-M-3

Design, Modeling and Characterization of a 35 MHz Linear CMUT Array

Toby Xu[1], Coskun Tekes[1], Sarp Satir[2], Evren Arkan[1], F. Levent Degertekin[1]; *[1]G.W. Woodruff School of Mechanical Engineering, Georgia Institute of Technology, Atlanta, GA, USA, [2]School of Electrical & Computer Engineering, Georgia Institute of Technology, Atlanta, GA, USA*

Background, Motivation and Objective

With its many applications from small animal imaging to intravascular ultrasound (IVUS), design and fabrication of high frequency phased arrays is still a significant challenge. CMUTs are particularly suitable for this application with their ease of fabrication and IC integration [1]. Here we discuss the design, large signal modeling, fabrication and experimental characterization of high frequency CMUTs arrays using a 35MHz linear CMUT array as an example.

Statement of Contribution/Methods

The 12 element 35MHz center frequency linear CMUT array for side looking IVUS application is surface micro machined using a low temperature silicon nitride membrane process. Each element consists of 40 individual 20x20µm membranes with a 50nm vacuum gap. The array size is 300x1000µm with an element to element pitch of 25µm, which is suitable for phased array applications (Fig 1. b). A novel large signal CMUT array transmit model [2] was used to predict the frequency response of the array for different DC and AC drive signals. The array elements are characterized for uniformity, frequency response and beam pattern.

Results/Discussion

Impedance measurements in air show 90kHz standard deviation around the resonance frequency of 38.7MHz at 80V (90% of collapse voltage). The hydrophone measurements with 25V short pulses with 80V DC bias show center frequency of 35.6MHz and -3dB bandwidth of 10MHz (Fig. 1a). As shown in the same figure, the frequency response is predicted remarkable well by the transient CMUT model when the experimental pulse was used as the input. The acoustic cross-talk behavior that causes dips in the frequency response near 53.5MHz is also well predicted by the model which used a 3x3 membrane partial-array geometry. The predicted radiation pattern indicated the suitability of the array for phased array imaging.

High frequency surface micro-machined CMUT arrays can be designed and modeled accurately for typical large input signals used for imaging. Reasonable collapse voltage levels and high uni-formity can be achieved with small gaps (35-50nm) using sacrificial release process. Experimental results on a 35MHz linear array verify this overall approach for CMUT based high frequency array design and fabrication.

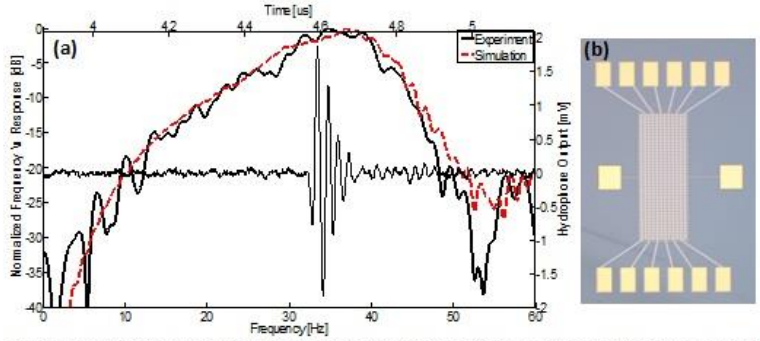

Figure. 1: (a) Experimental TX#7 and simulation (3x3 membranes) frequency and transient response (b) Micrograph of fabricated high frequency CMUT device on Silicon.

[1]Zahorian, J.; Hochman, M.; Xu, T.; Satir, S.; Gurun, G.; Karaman, Mustafa; Degertekin, F., "Monolithic CMUT-on-CMOS integration for intravascular ultrasound applications," *Ultrasonics, Ferroelectrics and Frequency Control, IEEE Transactions on*, vol.58, no.12, pp.2659,2667, December 2011
[2] S. Satir, J. Zahorian, F.L. Degertekin., "Transmit Optimization of CMUTs in Non-Collapse Mode using a Transient Array Model," Proc. of IEEE Ultrasonics Symposium, 2012

IUS5-M-4

Multi-Frequency CMUT Arrays for Imaging-Therapy Applications

Abhijeet Kshirsagar[1], Alexander Sampaleanu[1], Walied Moussa[2], Roger Zemp[1]; *[1]Department of Electrical & Computer Engineering, University of Alberta, Edmonton, Alberta, Alberta, Canada, [2]Department of Mechanical Engineering, University of Alberta, Edmonton, Alberta, Alberta, Canada*

Background, Motivation and Objective

Novel multi-frequency CMUT arrays with interlaced low and high-frequency elements are investigated for novel imaging-therapy applications. Our interlaced CMUTs are designed with device dimensions smaller than operating wavelengths. This permits low- and high-frequency CMUT cells to be interlaced monolithically on a scale smaller than the array wavelengths. This dense interlacing scheme thus offers the promise of co-registered dual-frequency-band operation with minimal deleterious grating lobes and with maximal overlap of low- and high-frequency beams.

Statement of Contribution/Methods

Feasibility of multi-frequency CMUTs for both imaging and therapy is demonstrated. Finite element simulations are used to predict device performance before and after protective coating with Parylene-C. Simulated results were compared with experimental measurements. Interlaced array element transducers are fabricated using a modified sacrificial release process. Acoustic measurements (immersion testing) of 1.5MHz and 7MHz sub-array elements driven separately and together are compared. The effect of DC bias voltage on the bandwidth of the devices is studied and the field profile and directivity of elements and focused arrays are reported. Nonlinear coupling effects between different-frequency CMUT elements is experimentally studied and shown to be an important consideration in operation and future design.

Results/Discussion

Fabricated devices exhibit close to expected performance in terms of snapdown voltage and resonant frequencies. Acoustic pressures of 1.5MHz devices can reach nearly 1MPa at the surface of the array when driven in CW mode, meaning that high-intensities for therapy should be achievable with focusing, especially with future large arrays. Present studies are conducted using small feasibility 7x7mm dies. Interlaced CMUTs offer the possibility of ultrabroad effective fractional bandwidth with -6dB sensitivity spanning from ~1MHz in the low-frequency band up to ~12MHz in the high-frequency band. Such sensitivity over both low and high frequencies is difficult to achieve using other present monolithic ultrasound transducer technology to our knowledge. Multi-frequency CMUTs arrays can be used for future ultra-high-resolution ultrasound or photoacoustic imaging technology, or imaging-therapy systems, among other possible applications.

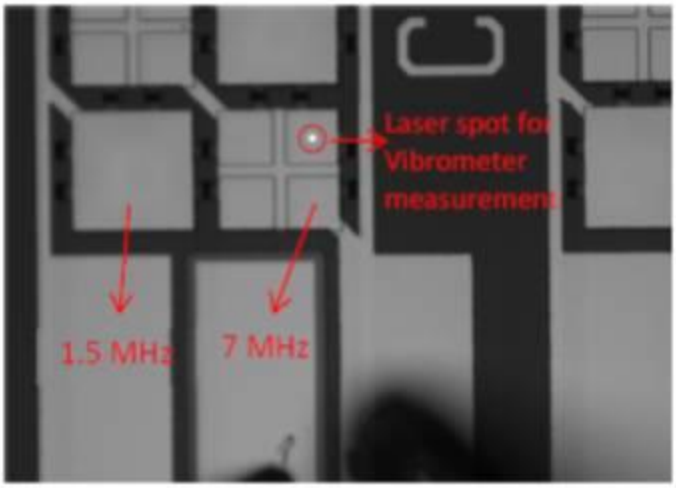

IUS5-M-5

Full Synthetic Aperture 3D Ultrasound Imaging Schemes with Top Orthogonal to Bottom Electrode (TOBE) 2D CMUT Arrays

Roger Zemp[1], Alexander Sampaleanu[2]; [1]*University of Alberta, Edmonton, Alberta, Canada,* [2]*University of Alberta, Canada*

Background, Motivation and Objective

Recently we introduced a unique top-orthogonal-to-bottom electrode (TOBE) 2D capacitive micromachined ultrasound transducer (CMUT) architecture capable of 3D ultrasound imaging with only N transmit/receive channels and N bias channels for addressing an NxN array. By biasing only one column at a time and routing transmit-receive signals along rows, dominant single-element operation was demonstrated due to the fact that only the element at the intersection of the active row and column experienced both signal and bias while other element actuation was negligible. Principal disadvantages of previous TOBE pulse sequence are that only a single column is effectively active and there is no active (but rather retrospective) elevational transmit focusing, leading to poor signal-to-noise ratio. Additionally, previously proposed schemes, while offering dynamic focusing capabilities, lacked the ability to perform full synthetic aperture imaging. We demonstrate this capability in TOBE CMUTs for the first time.

Statement of Contribution/Methods

Previously proposed approaches used the same single column biased for both transmit and receive operations. Here we propose the possibility of changing the bias pattern after a transmit event and prior to reception during the dead-time associated with pre-amp saturation-recovery. For each transmit event, columns are biased in an on/off pattern chosen from S-sequences which are rows of a binary NxN Hadamard S-Matrix. Immediately after a transmit pulse, bias voltages are switched to a different S-sequence. A complete set of S-sequences on both transmit and receive constitutes sufficient data for full synthetic aperture focusing once a matrix based decoupling algorithm is applied.

Results/Discussion

Because for each transmit/receive S-sequence, there are (N+1)/2 columns biased at a time, this scheme offers up to (N+1)/2 times the amount of transmit signal and up to (N+1)/2 times the amount of receive signal over N bias sequences compared to our previously suggested TOBE imaging schemes. The feasibility of the proposed technique is demonstrated using Field II simulations, then experimentally in small 30x30 CMUT arrays interfaced to a Verasonics Data acquisition system. Our work represents the first demonstration of full 3D synthetic aperture imaging possible with a 2D array addressable only by top electrode rows and bottom electrode columns. The reduced complexity of interconnects may lead to very large TOBE CMUT arrays for whole breast ultrasound imaging and other applications.

Acoustic tweezers 2

T1

Thursday, July 25 2013, 02:00 pm - 03:30 pm

Congress Hallair: **Bruce Drinkwater**
University of Bristol

IUS3-M-1

Independent manipulation of multiple microparticles using circular ultrasonic arrays

Charles Courtney[1], Christine Demore[2], Hongxiao Wu[2], Paul Wilcox[3], Alon Grinenko[3], Chun-Kiat Ong[3], Sandy Cochran[2], Bruce Drinkwater[3]; *[1]Department of Mechanical Engineering, University of Bath, Bath, Somerset, United Kingdom, [2]Institute for Medical Science and Technology, University of Dundee, Dundee, United Kingdom, [3]Department of Mechanical Engineering, University of Bristol, Bristol, United Kingdom*

Background, Motivation and Objective

The ability to trap and manipulate objects on the micro-metre scale has attracted interest in the biosciences and for micro-fabrication. While optical tweezers are well established, analogous systems using ultrasound are in their relative infancy. However, the use of ultrasonic manipulation offers the ability to work with larger objects than optical systems, including agglomerates of biological cells. Previously the authors have demonstrated trapping and manipulation of microparticles in two dimensions using Bessel-function acoustic pressure fields. The objective of the work reported here was to increase functionality by manipulating multiple particles independently and increasing the working volume within which this manipulation can take place.

Statement of Contribution/Methods

For small dense particles in water, a standing acoustic field forces the particles away from antinodes in the pressure field and towards nodes. This can be exploited by generating fields with nodes surrounded by regions of higher pressure amplitude to form traps. A device capable of producing arbitrary fields in a fluid filled chamber, and updating them in real time, allows dexterous manipulation of these traps. Arrays allow generation of arbitrary fields over a region determined by the pitch of the elements, with aliasing degrading control outside this region. A circular array forming the periphery of the fluid chamber results in a region of control whose radius is proportional to the number of elements and the wavelength in the fluid, λ. For a previous array with 16 elements, this radius was 0.9λ; for the 64-element device reported here it is 3.7λ.

The array was fabricated from an electroded piezoelectric ring which was diced into 64 elements, with both absorbing backing and anti-reflective matching layers. The device is operated at f = 2.4 MHz, the thickness extensional mode of the elements, to maximise pressure amplitudes. This corresponds to λ = 0.62 mm in water. By varying the amplitude and phase of the signal applied to each element, it is possible to generate various traps in the fluid-filled chamber.

Results/Discussion

Bessel functions are a form of solution to the wave equation that allows circular traps to be produced. A first-order Bessel function was generated by incrementing the phase delay of each element, such that the total phase shift around the ring was $\delta\varphi = 2\pi$, and a 45 μm diameter polystyrene microsphere was trapped. The trap was moved within the central 3.7λ (2.3 mm) radius region by applying further phase delays. Multiple traps were generated by applying a linear superposition of the excitation signals required for each individual trap. With this method, two independent traps were used to manipulate then bring together two microspheres. The new array thus demonstrates both dexterity and an enlarged region of control.

IUS3-M-2

Microbubble Manipulation Using Ultrasound Standing Wave between Two Sets of Parallel Transducers

Kazuhito Inoue[1], Hironobu Kaji[1], Rei Masuda[1], Hiroyuki Ushijima[1], Takashi Azuma[1], Kiyoshi Yoshinaka[2], Mitsuhisa Ichiyanagi[3], Shu Takagi[1], Yoichiro Matsumoto[1]; *[1]Mechanical Engineering, the University of Tokyo, Bunkyo-ku, Tokyo, Japan, [2]National Institute of Advanced Industrial Science and Technology, Tsukuba, Ibaraki, Japan, [3]Engineering and Applied Science, ", Sophia University, Chiyoda-ku, Tokyo, Japan*

Background, Motivation and Objective

In the field of biotechnology, the method for manipulating micro-particle remotely has been developed and practically used in recent years. If this micro-manipulation can apply to microbubbles (MBs), they will contribute to the mechanism investigation on the drug delivery system or the gene transfer. In a previous work, MBs were manipulated precisely by using optical tweezers. This method is limited to in vitro case because the laser cannot transmit through thick cell layers. On the other hand, there are many papers presenting the MBs manipulation with acoustic radiation force that is called Bjeknes force. However, this force cannot manipulate MBs precisely like optical tweezers. In this research, to develop the MB manipulation method with Bjeknes force, we try to control the position of MBs in a two dimensional ultrasound field.

Statement of Contribution/Methods

Bubbles in the ultrasound field are subjected to the Bjeknes force. In standing wave field, this force drives bubbles to certain direction that is to the antinode if bubbles are smaller than resonant radius and that is to the node if bubbles are larger. Our method aimed that MBs are trapped at the antinode or the node and manipulated with moving the position of the antinode or node. We prepared the device which had four flat transducers with the frequency of 2 MHz on all side of a square column to make ultrasound standing wave field. We confirmed that ultrasound field inside the device made a latticed pattern by computing and Schlieren picture. The position of the antinode or node could be moved with the frequency shift.

Results/Discussion

MBs were trapped at certain position and lined up into a lattice pattern after making ultrasound standing wave field shown in Fig. 1. The position was thought to be antinode since the interval between the crowds of MBs was approximately 0.38 mm which corresponded with the half of wave length. Moreover, we could manipulate the crowds of MBs to the desired direction with frequency shift. However, some MBs could not move to the desired direction because they hopped to the neighbor antinode in the opposite direction of the flow. This was because the standing wave field was distorted with the amplitude error of each transducer. A precise amplitude control of each transducer is one of possible solutions. In addition, we will measure trapping force and evaluate the accuracy of manipulation in the future.

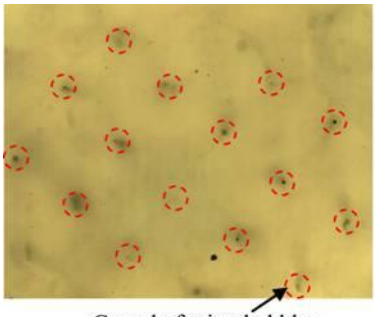

Fig. 1

IUS3-M-3

Breast Cancer Cell Manipulation with a Highly Focused High Frequency Ultrasonic Transducer

Hyung Ham Kim[1], Kwok Ho Lam[1], Changyang Lee[1], Jae Youn Hwang[1], Jungwoo Lee[2], K. Kirk Shung[1]; *[1]Department of Biomedical Engineering, University of Southern California, Los Angeles, California, USA, [2]Department of Electronic Engineering, Kwangwoon University, Seoul, Korea, Republic of*

Background, Motivation and Objective

Single beam acoustic tweezers have been introduced lately for micro-particle manipulation. Of particular interest is that such tweezers may be implemented with a single element transducer producing a single acoustic beam rather than multiple beams or standing waves, allowing ease of implementation and the flexibility of extension to different dimensions. Cell manipulation includes but not limited to trapping, seeding and sorting. The highly focused beam in the lateral direction is one of the key factors making the trapping effect possible. We report that a single acoustic beam produced by a low f-number (0.75), high frequency (30 MHz) is capable of trapping and moving a MCF-7 breast cancer cell.

Statement of Contribution/Methods

We designed and fabricated 30 MHz lithium niobate (LiNbO3) single element transducers. Double matching layers, i.e. silver epoxy for 1st matching and Parylene C for 2nd matching and a backing medium made by conductive silver epoxy were optimized by KLM modeling. In the fabrication, after lapping and bonding each layer, a circular-shaped acoustic stack with the diameter of 4.0 mm was press-focused on a stainless steel ball bearing of 3.0 mm radius to implement the f-number 0.75 (= 3.0/4.0). A finished transducer was placed on top of the MCF-7 breast cancer cells immersed in the phosphate-buffered saline solution. Tone bursts of 30 MHz with the peak-to-peak voltage of 15.8V, 500 cycles per pulse and pulse repetition frequency of 200 Hz were applied to the transducer to trap and move a MCF-7 cell. The whole process of cell manipulation was recorded by a CCD camera mounted on the microscope.

Results/Discussion

The -3 dB lateral beamwidth of a finished transducer was 36.9 μm at 30 MHz, which was adequate to generate the trapping force for a 13 μm sized breast cancer cell. As shown in Figure 1, it successfully demonstrates that a single acoustic beam created by a highly focused transducer with such a low f-number is capable of manipulating a breast cancer cell on a plane perpendicular to the beam direction. It proves the capability of acoustic tweezers for cell trapping and delivery. The configuration of transducers, e.g. center frequency, aperture size, or focal depth, can be easily scaled upon the characteristics of cells.

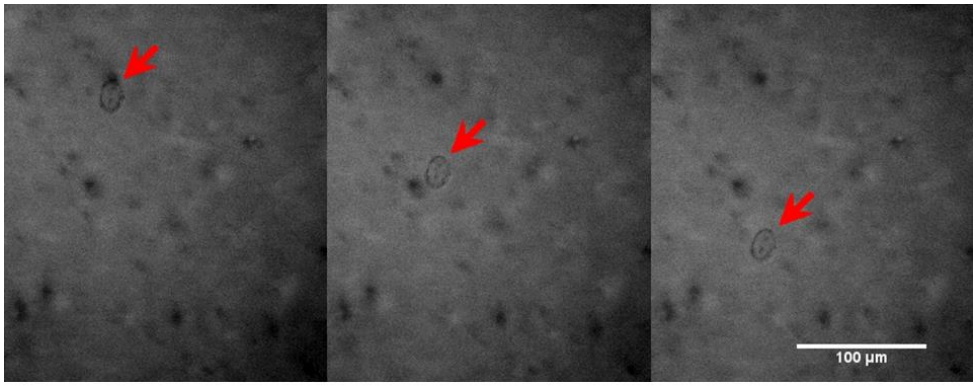

(a) (b) (c)

Figure 1. A MCF-7 breast cancer cell trapped and moved by a single acoustic beam at 30 MHz produced by a highly focused (f-number 0.75) 30 MHz single element transducer: time interval between each picture is 1 s.

IUS3-M-4

Thick Film PZT Transducer Arrays for Particle Manipulation

Yongqiang Qiu[1], Sylvia Gebhardt[2], Han Wang[1], Aleksandrs Bolhovitins[1], Christine Démoré[1], Andreas Schönecker[2], Sandy Cochran[1]; *[1]Institute for Medical Science and Technology, University of Dundee, Dundee, United Kingdom, [2]Fraunhofer Institute for Ceramic Technologies and Systems, Dresden, Germany*

Background, Motivation and Objective

The use of a 1-D ultrasonic transducer array under electronic control to manipulate particles laterally in water through the effects of potential and kinetic energy density gradients in the ultrasonic field has already been demonstrated by Kozuka *et al.* in 1998 and Glynne-Jones *et al.* in 2012. The same concept could also be extended to 2-D arrays to achieve more flexible operation. However, the manufacture of reliable, miniaturized 2-D arrays brings challenges in fabrication processes based on traditional machining. As an alternative, thick film technologies have significant advantages, e.g. in simplifying fabrication, with potential for bulk production of disposable devices for life sciences and healthcare applications.

Statement of Contribution/Methods

Here we report recent progress in screen printing of 1-D 30-element and 2-D 36-element (6×6) matrix ultrasonic arrays for microparticle manipulation. Patterned thick film layers were screen printed and sintered on an Al_2O_3 substrate in a sequence comprising bottom electrode, PZT, top electrode, isolation layer (2-D array only) and electrode fan-out tracks. The PZT was printed with multiple layers. The transducer arrays are controlled electronically using FPGA (Field Programmable Gate Array) technology, and coupled to a glass capillary or a chamber with a glass reflector to set up ultrasound standing waves in the fluid layer of the microfluidic system. Impedance spectrometry and laser vibrometry were used to evaluate the array performance. Finite element analysis software package, PZFlex, was used to predict the ultrasonic pressure distribution and particle trapping sites in the fluid layer, with experimental verification performed by levitating and manipulating 10 µm fluorescent microspheres.

Results/Discussion

The overall thickness of screen-printed thick film PZT of approximately 140 µm gave a device resonant frequency of about 7.5 MHz, including the Al_2O_3 substrate and electrode layers. The relative dielectric constant $\varepsilon_R^S = 2253 \pm 100$, and the loss tangent $\tan\delta = 0.0915 \pm 0.005$. Electrical impedance spectra measured by the impedance analyser and experimental laser vibrometer outputs correspond to PZFlex simulation results and there is also correspondence between the modelled particle trapping sites and experimental measurements. The microsphere manipulation experiments show the thick film PZT arrays have potential in ultrasonic particle manipulation, and should enable life scientists to manipulate individual cells or groups of cells to specific positions for a range of applications.

IUS3-M-5

A study of nanoparticle manipulation using ultrasonic standing waves

Paul van Neer[1], Armin Rasidovic[1], Arno Volker[1]; [1]*TNO, Netherlands*

Background, Motivation and Objective

There has been considerable interest in the noninvasive manipulation of particles in dispersions during the last 15 years. Among the methods reported are those based on magnetic and electrical fields, centrifuges, optical tweezers and acoustic radiation force. The latter is particularly interesting as it allows for the manipulation of particles based on their density, compressibility and/or size. The majority of the acoustic research has been focused on particles above a few µm. In the current work we investigate the manipulation of particles in the range of 100 nm to 1 µm using ultrasonic standing waves, where the fundamental frequency and their 3rd and 5th harmonics are combined to maximize the force on the particles.

Statement of Contribution/Methods

The setup consisted of a small rectangular cell. Within the cell, two sides of piezo material were meticulously aligned (square: 30 x 30 mm^2, center frequency 2 MHz). The distance between the piezo slabs was 9 mm. One piezo slab was excited using continuous sinusoids with frequencies around 2, 4 and 6 MHz; the frequencies were chosen such that the power transfer was maximized. The liquid in the tank consisted of SiO_2 nanoparticle dispersions with varying mean sizes: 100 nm, 500 nm, 1000 nm and 10 µm. The concentration of the particles was 0.03 mass%.

Results/Discussion

When the ultrasound was switched off, the nanoparticle dispersion appeared as a milky white substance. When the ultrasound was switched on, the particles move to the nodes of the standing wave field (see the figure for 500 nm nanoparticles). The distance between the planes in which the particles are concentrated corresponded to half the wavelength.

Good separation was achieved in roughly 1s, 5s and 10s for the 10 µm, the 1 µm and the 500 nm particles, respectively. No separation was observed for the 100 nm particles, which was likely caused by mixing due to acoustic streaming of the liquid and compounded by Brownian motion. The peak power dissipated into the piezo slabs was 6W. Due to the small size of the cell and the fairly high losses in the piezo material, the temperature increased considerably during the experiments (1.3°C/min).

Nanoparticles down to 500 nm were successfully manipulated using the radiation force induced by ultrasonic standing waves. Regarding 100 nm particles, the mixing effects due to acoustic streaming prevented successful manipulation.

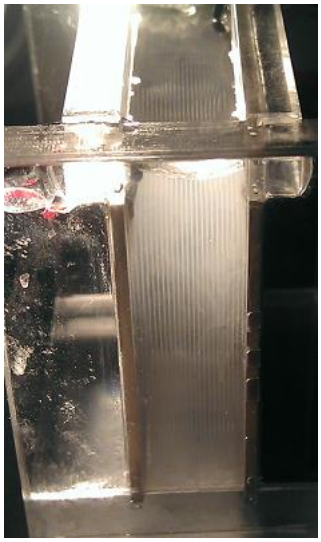

IUS3-M-6

Acoustic radiation force on cylindrical particles near subwavelength slits

Chen Wang[1,2], Feiyan Cai[1], Weijia Su[2], Hairong Zheng[1]; *[1]Shenzhen Institutes of Advanced Technology, Chinese Academy of Sciences, China, People's Republic of, [2]Sino-Dutch Biomedical and Information Engineering School, Northeastern University, China, People's Republic of*

Background, Motivation and Objective

It is well known that an object in acoustic field absorbing or reflecting sound energy can be subjected to the acoustic radiation force (ARF), which has potential applications for particle manipulation, acoustic separation, biosensor, and so on. There has been considerable progress in the study of ARF on objects in various free acoustic fields. However, seldom work has concerned with the ARF on objects in structured field. In this letter, we investigate the ARF exerted on a cylindrical particle near subwavelength slits both theoretically and experimentally.

Statement of Contribution/Methods

The system consists of a steel cylinder with radius R located near a slit with width D which is made of two pieces of aluminum plate of width W and thickness T placed in one plane. These parameters are set as D=2R, W=50R, T=5R, respectively. By using the two-dimensional finite-difference-time-domain (FDTD) method with four absorbing boundary conditions, we calculate the transmission spectrum of the slit firstly. Then combining the 2D FDTD method with the momentum-flux tensor, we obtain the ARF exerting on a steel cylinder at the point of 0.2R from the center line of the slit surface. Our experiment system is similar to the theoretical model. On one side of the slit there is a flat transducer with the central frequency of 100KHz, and on the other side of it there is a steel cylindrical particle (1cm in both diameter and length) which is suspended with a string. Both the transducer and the system are in a large water tank. Outside the water tank, there is a video camera for observing the trapping phenomenon.

Results/Discussion

Fig.1 shows the numerical results. There is a transmission peak at frequency of 0.98(c/R) due to the resonance of the slit in the direction of thickness. Interestingly, at the resonance frequency, the ARF on particle near the slit is negative and the magnitude of this force is larger than that of particle at free space. In experiment, we observe the phenomena of the cylindrical steel particle attracted toward the slit at the resonance frequency. However, when the transducer emits another frequency or the structure of slits changes slightly, this trapping effect can't appear. The structured field of the subwavelength slit can exert a strong trapping force on object, which may have potential application in microparticle detector.

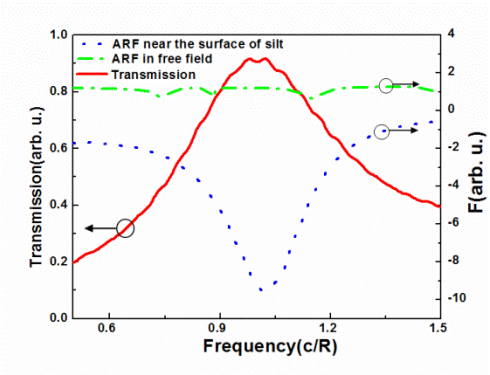

Advanced Modeling and Design

T2

Thursday, July 25 2013, 02:00 pm - 03:30 pm

Congress Hallair: **Ken-ya Hashimoto**
Chiba University

IUS4-M-1

Analysis of Rayleigh Wave Radiations from Leaky SAW Resonators

Shogo Inoue[1], Kentaro Nakamura[1], Hidetaro Nakazawa[1], Jun Tsutsumi[1], Masanori Ueda[1], Yoshio Satoh[1]; *[1]Microdevice Research & Development Department, TAIYO YUDEN CO., LTD., Akashi, Hyogo, Japan*

Background, Motivation and Objective

Filters and duplexers consist of leaky SAW resonators on around 42° Y-cut $LiTaO_3$ substrates are widely used in wireless communication devices. Low-loss filters/duplexers are strongly demanded since the lower insertion loss directly contributes to the longer operating time and higher receiver sensitivity of the mobile devices. The optical probe measurements have revealed some acoustic loss mechanisms in leaky SAW resonators including the side radiations of leaky SAW and the Rayleigh wave radiations [1]. However, the cause of the Rayleigh wave radiations has not been clarified yet. This paper analyzes and characterizes the Rayleigh wave radiations by using the scanning laser interferometer and the developed analytical model to simulate the radiations.

Statement of Contribution/Methods

First, the Rayleigh wave radiations from the leaky SAW resonators in 2 GHz range on 42° Y-cut $LiTaO_3$ substrates were measured and the frequency response of the leaked energy was investigated by using the optical interferometer. Then, the simple and fast analytical model was developed to simulate the Rayleigh wave radiations. In the model, the spot sources of Rayleigh wave were placed in the end gap between the IDT electrodes and dummy electrodes. The model intends that the leaky SAW is converted to the Rayleigh wave due to the scattering in the end gap and the converted Rayleigh wave propagates as a circular wave from the end gap.

Results/Discussion

Fig. 1(a) shows one measurement result for the test resonator. The transverse and oblique radiations at an angle of 90° and 40° were visualized. It was found that the frequency response of leaked energy exhibited the periodicity. Fig. 1(b) shows the simulation result which corresponds to the measurement shown in Fig. 1(a). The radiation patterns in the measurement and simulation match very well. The periodic frequency response of leaked energy was also precisely simulated with the developed model. These results suggest that the scattering of leaky SAW in the end gap would generate the Rayleigh wave radiations.

Reference

[1] J. Koskela et al., "Acoustic Loss Mechanisms in Leaky SAW Resonators on Lithium Tantalate," *Proc. IEEE Ultrason. Symp.*, pp. 209–213, 2000.

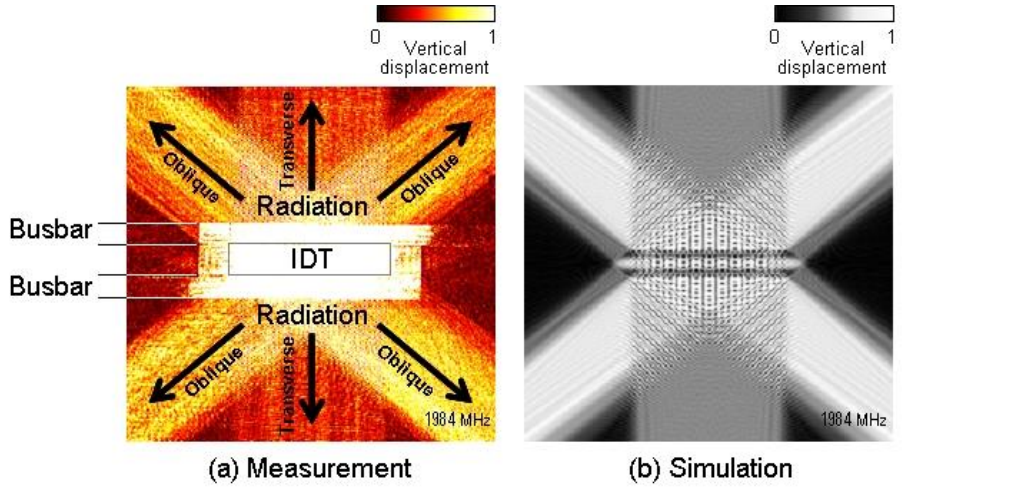

Fig. 1 Measured and simulated Rayleigh wave radiations from Leaky SAW resonator.

IUS4-M-2

Impact of Surface Periodic Grating on FBAR Structures to Spurious Transverse Resonances

Jiansong Liu[1], Tatsuya Omori[1], Changjun Ahn[1], Ken-ya Hashimoto[1]; *[1]Graduate School of Engineering, Chiba University, Chiba-shi, Chiba, Japan*

Background, Motivation and Objective

The main resonance of FBAR Structure is caused by the thickness extension vibration. However, the composite structure also acts as a waveguide, and laterally propagating plate modes, namely Lamb modes, cause unwanted spurious resonances. Therefore, their suppression without deteriorating the main resonance is one of the major concerns for designing RF BAW resonators. This study is aimed at discussing applicability of the Bragg reflection in a periodic grating placed on the top electrode of the FBAR structure in order to forbid lateral propagation of the S_1 mode.

Statement of Contribution/Methods

The finite element method (FEM) is employed for the analysis of Lamb wave propagation in the structure. In the analysis, the number of periods is set finite, and both ends are terminated by the absorption mechanism. With this setup, the lateral propagation of eigen modes can be identified from the existence of spurious resonances, while the lateral energy confinement can be evaluated qualitatively by the use of *Q* factor of the main resonance.

Results/Discussion

The investigation is performed for two representative structures, namely, Mo/ZnO/Mo and Ru/AlN/Ru, on which the first-order symmetric Lamb mode exhibits the ″Type-I″ and ″Type-II″ dispersion, respectively. Fig. 1(a) shows, as an example, calculated admittance of the Mo/ZnO/Mo structure without the surface grating in decibels. Series of spurious resonances are seen at frequencies above the main resonance. They are due to lateral propagation of eigen Lamb modes. Fig. 1(b) shows the admittance of the Mo/ZnO/Mo structure with Mo surface grating. It is clear that transverse spurious resonances are completely suppressed by the placement of surface grating. A clean resonance is obtainable provided that the grating period and height are set so that the stop band covers the frequency range where the lateral mode resonances occur.

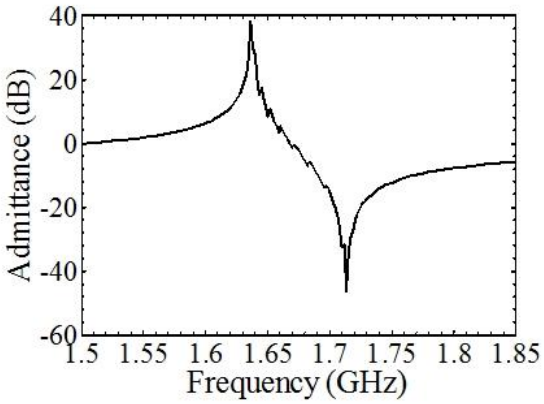

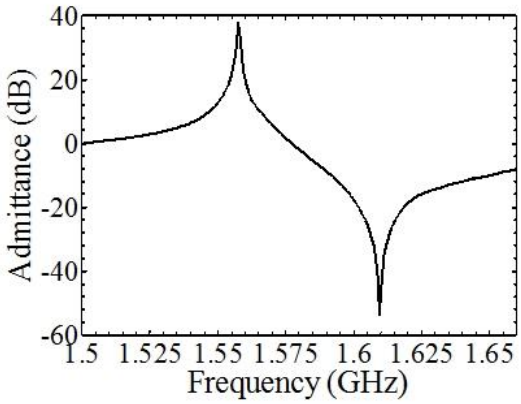

Fig.1(a). Calculated admittance of the Mo/ZnO/Mo structure
Fig.1(b). Calculated admittance of the Mo/ZnO/Mo structure with Mo surface grating

IUS4-M-3

Analysis of Heat Dissipation Improvement using the Bonded Wafer in the CSSD Structure

Takayuki Suzuki[1], Toshio Nishizawa[1], Osamu Kawachi[1]; *[1]TAIYO YUDEN Mobile Technology Co., Ltd., Japan*

Background, Motivation and Objective

In the small SAW (Surface Acoustic Wave) Duplexer, it is very important to improve the heat dissipation. For SAW Duplexer using RF front-end, especially in Tx side, self-heating by high input power on the inter-digital transducers (IDTs) is a big issue. We have proposed heat dissipation improvement by Chip Size SAW Device (CSSD) structure.[1] In the CSSD structure, heat dissipation was improved adding a new path that is the die to the package through the sealing material. However, additional improvement for the heat dissipation was needed.

Statement of Contribution/Methods

The bonded wafer technology has improved the heat dissipation effect. It can be realized the big improvement, especially insertion loss under the high power applied condition was achieved by using bonded wafer technology and CSSD structure, where the thermal conductivity of Sapphire is 33W/(m*K), that is more than 7 times larger than LiTaO3 of 4.6W/(m*K). Furthermore, it is considered that the heat of the die surface is easy to diffuse to the package through the bumps or back of the die.

Results/Discussion

In the case of the LiTaO3 die, the heat was accumulated in the center of the die. On the other hand, in the case of the bonded wafer, the die temperature was quite lower than the LiTaO3 die and also thermally-uniform due to the better thermal conductivity.

The bonded wafer has been confirmed a significant heat dissipation improvement.

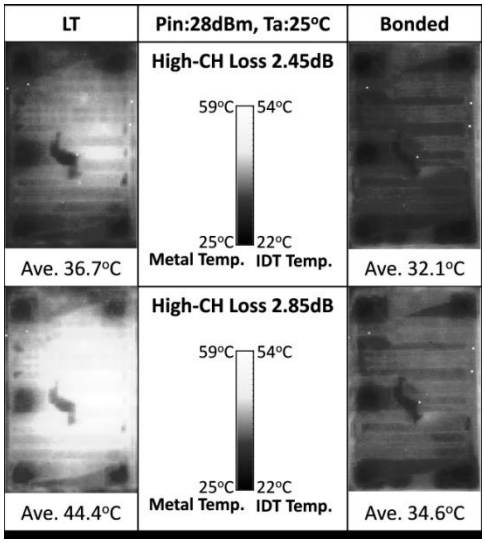

IUS4-M-4

Rigorous COM and P-matrix approaches to simulation of third-order intermodulation distortion and triple beat in SAW filters

Markus Mayer[1], Andreas Mayer[2], Elena Mayer[2], Werner Ruile[1], john johnson[1], Ingo Bleyl[1], Karl Wagner[1]; *[1]TDK corporation, Germany, [2]HS Offenburg, Germany*

Background, Motivation and Objective

With increasing number of simultaneously used frequency bands linearity requirements in SAW filters are tightened, while at the same time continuing miniaturization leads to an increase of power densities.

Therefore accurate simulations of nonlinear effects in SAW filters are needed, which allow to identify critical substructures and to find countermeasures.

Recently, nonlinearities in SAW filters have been identified to be of acoustic nature [Inoue et al. 2012]. Approaches based on COM, P-matrix and Mason models have been devised.

Statement of Contribution/Methods

In this work a set of nonlinear coupled COM equations for interacting frequency components of the wave field is derived from first principles. The formalism is presented for intermodulation distortions of third order (IMD3) and triple beat. The resulting COM equations are translated to the P-matrix formalism, where care is taken to obtain a correct frequency dependence. The resulting scheme depends on a single, frequency-independent, constant, which can be determined quantitatively from linear and nonlinear material constants (tensor data) of the substrate.

Results/Discussion

At first a comparison of the nonlinear COM- and P-matrix approaches is given, which shows equivalence of the methods. Then the P-matrix approach is applied to single filters and duplexers on LiTaO3 (YXl)/42.

Both IMD3 and Triple Beat show good agreement with measurement. A single nonlinear constant suffices for different frequency ranges.

IUS4-M-5

A Mixed PML/FEA Method for Realistic SAW Resonators Design and Understanding.

Karim Dbich[1], Thierry Laroche[1], William Daniau[1], Sylvain Ballandras[1], Karl Wagner[2], Markus Mayer[2]; *[1]Femto-ST, France, [2]TDK corporatoin, Germany*

Background, Motivation and Objective

The efficiency of Surface Acoustic Waves (SAW) resonators has been largely improved by applying the well known Finite Element Analysis/Boundary Element Method (FEA/BEM) [1]. In most of the cases, the effects of realistic parameters (i.e., numerical aperture, the guidance gradient between buses and grating or the finite size of the resonator...) are neglected. To address that problem, other numerical methods based on Coupling of Mode or P-Matrix model were developed for a realistic study of SAW resonators [2]. However, none of them pay attention to the whole set of parameters.

Statement of Contribution/Methods

In this presentation, we propose a complete and rigorous numerical method based on the mixed FEA/BEM approach suited to realistic SAW resonator configuration by adding Perfectly Matched Layer (PML). Previous 3D-models considered periodicity conditions in both the wave propagation direction and the transverse one. These models lead to infinite grating and to undesirable interactions with unreal neighbors. The PML method developed in a previous work[3] is introduced here to avoid these problems. Thus, we are able to simulate SAW devices with finite lateral dimensions as depicted in Fig. 1 or with finite number of electrodes. An energetic approach based on the Poynting vector computation is also demonstrated. It allows to determine for instance the beam steering or the damping due to velocity gradient.

Results/Discussion

A 3D-model is developed for an entire characterization of SAW resonators (Fig. 1). The numerical methods presented here are applied in order to improve the design of a realistic configuration based on a specific cut of Quartz and massive metallic grating as electrodes. The effect of aperture of computation area and busbars is discussed. The energetic radiation is also quantified in the major direction of the resonator.

[1]S. Ballandras et al.,"Finite-element analysis of periodic piezoelectric transducers", J. Appl Phys, 93, 702–711, 2003

[2]M. Solal et al.,"A P-Matrix based model for SAW grating waveguides taking into account modes conversion at the reflection", IEEE trans. UFFC, 51, 2004

[3]K. Dbich et al.,"An optimal 2D and 3D modeling of finite SAW and BAW devices based on perfectly matched layer method" EFTF, 2012.

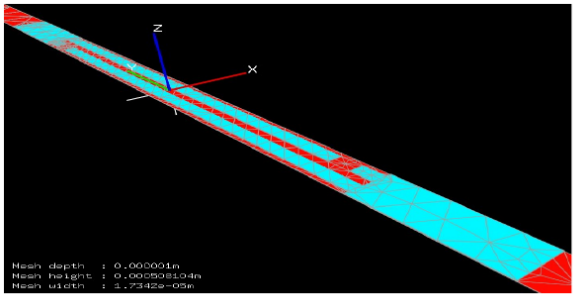

Fig. 1: 3D-model for practical SAW devices. The cyan parts stand for the massive electrodes deposited on the piezoelectric active material depicted in red. The power supply buses are modeling at the extremities of the electrodes. The boundary conditions in the y-direction are completed by PML and a periodicity condition is set on the x-boundaries.

IUS4-M-6

Paraxial RF Acoustics: Simple and Exact Description of Laser-Beam-Like Lamb and Rayleigh Waves by the Complex-Source-Point Method

Matt Eichenfield[1]; [1]*Sandia National Laboratories, USA*

Background, Motivation and Objective

The laser is one of the most useful technological tools in history, yet much of its utility could not be realized without the ability to deterministically create tightly-focused beams and to predict how these beams will propagate through optical systems. Transducers that produce focused surface acoustic waves (SAWs) have been described in the literature for some time, but the description of the fields has been limited to tractable forms applicable in the far-field limit or exact but cumbersome forms, usually cast in the form of green's functions or Kirchoff integrals. This prevents the kind of simple and intuitive calculations available for laser beams, such as ABCD matrices, to be used in analogous acoustic systems.

Statement of Contribution/Methods

Here it will be shown that an extremely simple conformal mapping, which has been named the Complex-Source-Point (CSP) method in analogy to optics, allows an elegant, compact, and exact description of Gaussian acoustic beams using nothing more than the ordinary solution to Lamb's problem of plane waves propagating in an infinite slab. The acoustic beams, as illustrated in figure 1, resemble focused laser beams and, like laser beams, can be used to describe the focusing of energy in diffraciton-limited volumes.

Results/Discussion

The propagation of CSP beam solutions will be described analytically and verified by numerical FEM solution of the acoustic wave equation in both an isotropic thin plate and an anisotropic thin plate with hexagonal crystal symmetry. It will further be shown how these CSP solutions can be used to describe paraxial acoustic Lamb and Rayleigh waves; this which enables the (considerable) theory developed to describe the propagation of laser beams through optical systems to be directly applied to SAW and Lamb wave systems. Finally, it will shown how these simple CSP solutions can guide design of interdigital transducers in piezoelectric material systems, with particular attention paid to uniaxial piezoelectric materials such as AlN, CdSe, and PZT-4.

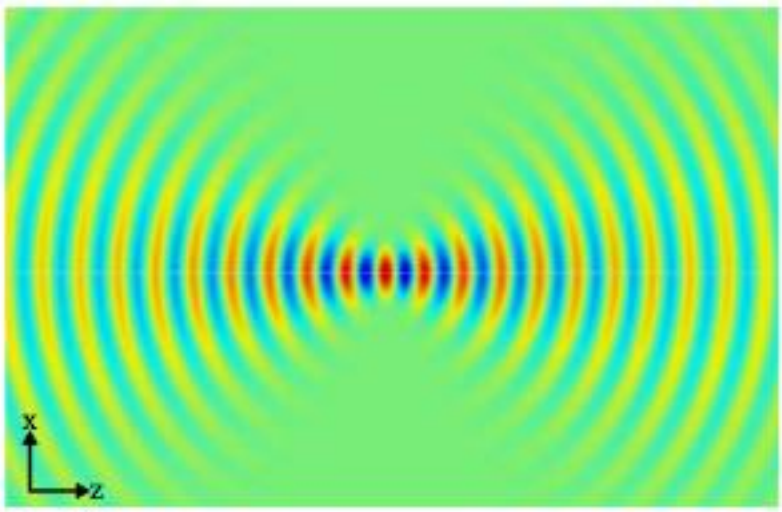

New imaging methodologies and high frequency imaging

Forum Hall

Thursday, July 25 2013, 01:00 pm - 04:30 pm

Congress Hallair: **Michalakis Averkiou**
University of Cyprus

IUS1-PD1-1

Electromechanical Wave Imaging of Atrial Fibrillation in Humans: A Feasibility Study

Alexandre Costet[1], Jonathan Lu[2], Elisa Konofagou[1]; [1]*Biomedical Engineering, Columbia University, New York, NY, USA,* [2]*Medicine Cardiology, Columbia University, New York, NY, USA*

Background, Motivation and Objective

Atrial fibrillation (AF) is the most common type of arrhythmia and is responsible for 15-20% of strokes. Persistent AF is treated with cardioversion which uses either antiarrhythmic drugs or a direct-current approach to return to normal sinus rhythm. Electromechanical Wave (EW) Imaging (EWI) is a direct ultrasound-based imaging technique that can map the transmural electromechanical activation in all four chambers in vivo. In this feasibility study, we explore novel EWI processing techniques based on analysis of the frequency content of the axial incremental strain curves. We show that EWI can differentiate between healthy and AF subjects and that EWI can provide important insight into the prediction of successful direct-current cardioversion procedures.

Statement of Contribution/Methods

Four patients (n=4) with AF and admitted for cardioversion and four healthy subjects (n=4) were recruited for this study. A Verasonics system (Verasonics, Redmond, WA) with a 2.5-MHz phased array was used to perform EWI transthoracically in free-breathing and conscious subjects using an unfocused beam sequence at 2000 frames/s in the standard apical views. Axial incremental displacement and strains were estimated using RF-cross-correlation with a window size of 6.2 mm (10 wavelengths) and a window shift of 0.612 mm (90% overlap), and a least-squares kernel size of 5.0mm, respectively. The atrial myocardium was segmented and frequency analysis of the corresponding incremental axial strain curves was performed using a modified Goertzel algorithm. Dominant frequencies were extracted from the frequency spectra and converted to cycle lengths. Finally, histograms of the distribution of cycle lengths across the atria were generated.

Results/Discussion

In healthy patients, the histogram peaks corresponded to cycle lengths which correlated with the measured heart rate of 50-80 beats per minute (i.e. 752-1205 ms). In AF patients, histogram peaks corresponded to shorter cycle lengths (150-400ms) and the detected peaks were either wideband (50 100ms width) and centered on multiple cycle lengths or narrowband (10-30ms width) and centered on a single cycle length. The shape of the histogram correlated with the success of the direct-current cardioversion procedures as histograms with single narrow peaks (n=2) resulted in successful cardioversions whereas histograms with numerous wide peaks (n=2) resulted in unsuccessful cardioversions.

Novel frequency-based processing of the EWI images provided new insight into AF and cardioversion. EWI was capable of differentiating between normal rhythm and AF. In healthy subjects, frequency analysis showed that the cycle length distribution histogram peak correlated with the heart rate. In AF patients, the shape of the histogram correlated with success of the cardioversion. These findings indicate the potential of EWI in imaging AF and more specifically in predicting the success of cardioversion treatment.

IUS1-PD1-2

Harmonic generation with a dual frequency pulse

Christina Keravnou[1], Michalakis Averkiou[1]; [1]*Department of Mechanical and Manufacturing Engineering, University of Cyprus, Nicosia, Cyprus*

Background, Motivation and Objective

Many methods have been published that propose single or multi-frequency pulse sequences for ultrasound nonlinear imaging. Nonlinear imaging relies on pulsing schemes like pulse inversion (PI), power modulated pulse inversion (PMPI), and power modulation (PM), to extract certain harmonic components [1]. In this work, a new method is presented for nonlinear imaging which uses dual frequency pulses at frequencies f and $2f$.

Statement of Contribution/Methods

The proposed imaging pulse, in addition to the fundamental frequency f, also contains the weighted and phase-shifted second harmonic $2f$. Since the two frequency components have different focusing gain and attenuation, it is possible to design for a specific pulse at the focus by changing the coefficients b_1 and b_2 of the two frequencies ($b_1 + b_2 = 1$). All nonlinear combinations (harmonics, sum frequencies, difference frequencies, etc) are multiples of f (f, $2f$, $3f$, $4f$, …). The performance and limitations of the new method were evaluated for nonlinear tissue imaging. Measurements of nonlinear propagation of dual frequency pulses in a tissue mimicking fluid were collected and analyzed. The measurements were compared with theoretical predictions based on a time-domain numerical solution of the KZK parabolic wave equation. Typical pulsing schemes (PI, PMPI, and PM) were constructed with the dual frequency pulse in order to isolate certain nonlinear components.

Results/Discussion

The measurements were in good agreement with the theoretical simulations. As shown with theoretical simulations in Fig. 1, the pulsing schemes with the dual frequency pulse ($0<b_1<1$) have different harmonic components than with single frequency pulse ($b_1=0$ or $b_1=1$). While with single frequency pulses only PM and PMPI contained a nonlinear fundamental signal, with the new dual frequency pulse, PI now contains a nonlinear fundamental signal [Fig. 1(a)] while it's second harmonic [Fig. 1(b)] is only slightly decreased. Similar trends are seen for the 3rd and 4th harmonics [Fig.1(c) and (d)]. The proposed pulse may be beneficial for ultrasound systems that are capable of implementing PI and not PM or PMPI due to hardware limitations. With dual frequency PMPI, the nonlinear fundamental is also increased.

[1] A. Averkiou, "Tissue harmonic ultrasonic imaging," *Comptes Rendus-Academie des Sciences - Series 4: Physics, Astrophysics*, 2(8),1139-51,2001

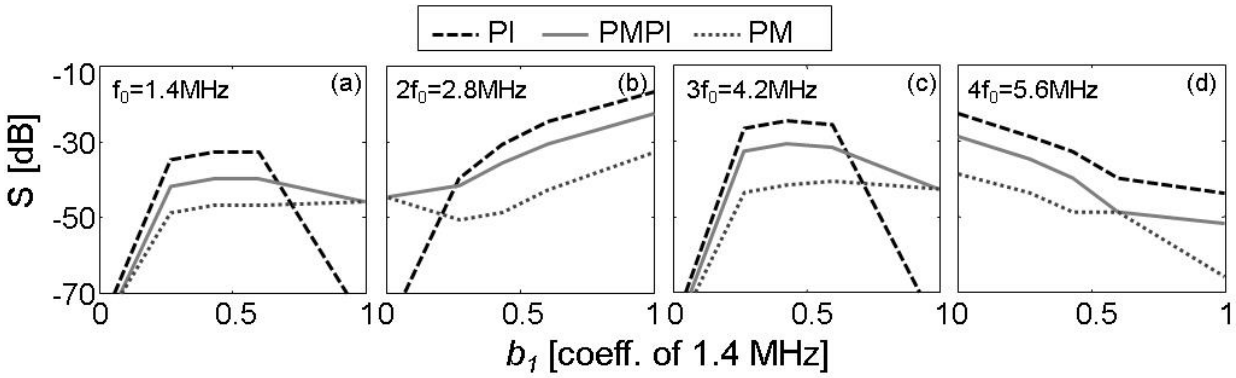

Fig. 1: Effect of the weight (b_1) of fundamental frequency on nonlinear signal generation for four harmonic components (b_1 =1: single frequency at 1.4MHz, b_1 =0: single frequency at 2.8MHz)

IUS1-PD1-3

Real-time pulse compression imaging on base-band data

Alessandro Ramalli[1], Francesco Guidi[1], Enrico Boni[1], Piero Tortoli[1]; [1]*Department of information engineering, University of Florence, Florence, Italy*

Background, Motivation and Objective

In ultrasound imaging, pulse compression methods based on the transmission of "long" coded pulses can be used to improve the penetration depth while preserving a good axial resolution. The performance of these algorithms is strongly affected by the frequency dependent attenuation causing mismatch of the receiver filter. Furthermore, the coded waveform phase may be distorted by dynamic focusing but filtering the received signal before the beamformer is very computationally expensive. In this paper we report on a low-cost real-time pulse compression system operating on beamformed, demodulated and down-sampled data.

.

Statement of Contribution/Methods

The arbitrary waveform generators of the ultrasound open system ULA-OP (MSDLab, Florence, Italy) are programmed to transmit linear frequency modulated chirps with 3-5 MHz bandwidth and 5-10 µs duration, tapered by a 10% Tukey window, to the linear array probe LA533 (Esaote, Italy). The received echo-signals are sampled at 50Msps, dynamically beamformed, quadrature demodulated and down-sampled to produce 512 samples in each pulse repetition interval. These samples are Fourier transformed by the on-board DSP through an efficient 1024-point FFT. The corresponding complex spectrum is multiplied by filter coefficients directly computed from the transmitted waveform, mismatched by a selectable weighting window and quadrature demodulated at programmable frequency. The latter can be set to compensate the expected mean-frequency shift due to tissue frequency-dependent attenuation in the region of interest (ROI).

The resulting data is finally inverse-transformed to the time domain, log compressed, transferred to the PC and displayed in real time as standard B-Mode images.

.

Results/Discussion

ULA-OP is programmed to produce interleaved real-time B-mode images for tone-burst and linear chirp excitations.

The figure shows sample images. A better dynamic range is highlighted in the right image, in which the penetration depth is increased without affecting resolution and contrast. Several examples and quantitative results in terms of SNR, resolution and contrast will be presented, showing that the operator can further improve the images in a specific ROI, by playing with the bandwidth, the demodulation frequency and the probe aperture.

.

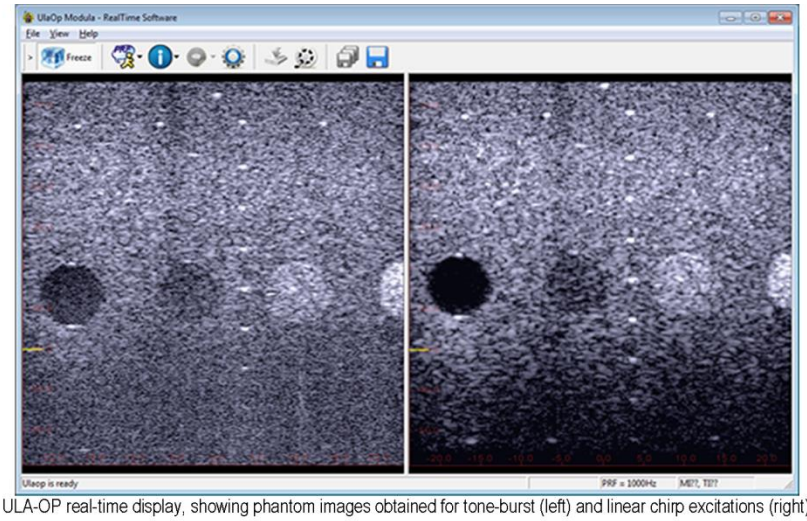

ULA-OP real-time display, showing phantom images obtained for tone-burst (left) and linear chirp excitations (right). In both cases a 16-element active aperture and a 12 V transmission amplitude was used.

IUS1-PD1-4

Automated Counting of Venous Gas Emboli in Post-SCUBA Dive Echocardiography

Virginie Papadopoulou *[1,2], Joe How Hui *[1], Costantino Balestra[2,3], Walter Hemelryck[2,4], Peter Germonpre[4], Robert J. Eckersley[5], Meng-Xing Tang[1]; *[1]Department of Bioengineering, Imperial College London, London, United Kingdom, [2]Environmental & Occupational Physiology Laboratory, Haute Ecole Paul Henri Spaak, Brussels, Belgium, [3]DAN Europe Research Division, Belgium, [4]Centre for Hyperbaric Oxygen Therapy, Military Hospital Brussels, Brussels, Belgium, [5]Imaging Sciences & Biomedical Engineering Division, King's College London, London, United Kingdom*

Background, Motivation and Objective

Decompression sickness (DCS) is a pathophysiology caused by bubbles which grow in the body during or after a reduction in ambient pressure that can affect divers, astronauts, pilots and compressed air workers. Adverse effects have been reported even for those who follow the decompression procedures produced by current decompression algorithms conservatively and Venous Gas Emboli (VGE) are observed after most SCUBA dives. There is a need to make quantitative measurement of the bubbles generated during decompression in order to help develop improved decompression algorithms. In particular, quantification techniques on post-dive B-mode ultrasound monitoring of bubbles in the heart have to be developed since current assessment procedures rely on trained experts to attribute severity grades.

The main objective of this project is to develop an automated VGE assessment method based on detecting and counting bubbles in real-time.

Statement of Contribution/Methods

Ultrasound B-mode sequences were acquired post-dive from 10 volunteers. Data was collected both pre and post flexion. An automated bubble recognition algorithm was developed and implemented in MatLab.

The cone-shaped field of view is first extracted, before a series of intensity thresholdings, top-hat filtering and morphological openings are used to segment the heart from the image. The right heart where VGE normally circulate, as well as the left heart where they sometimes appear in the presence of shunts, are then identified from the cross shape anatomical feature used to separate the four cardiac chambers. The heart rate and cardiac cycle information are used to select the frames where the valves are fully open. The bubbles can then be labelled and counted after an ultrasound speckle removal procedure. The automated method was compared to manual assessment done by expert raters.

Results/Discussion

The results show that the developed automated method is able to successfully segment the B-mode data of the heart into two regions of interest consisting of the right and left chambers. Initial comparison of the results with the manual method shows good agreement with the assessment from expert raters. This suggests that this method could become a powerful tool for quantitative evaluation of the validity of decompression algorithms.

Figure 1: Original image and with bubbles framed in green and indicated by arrows.

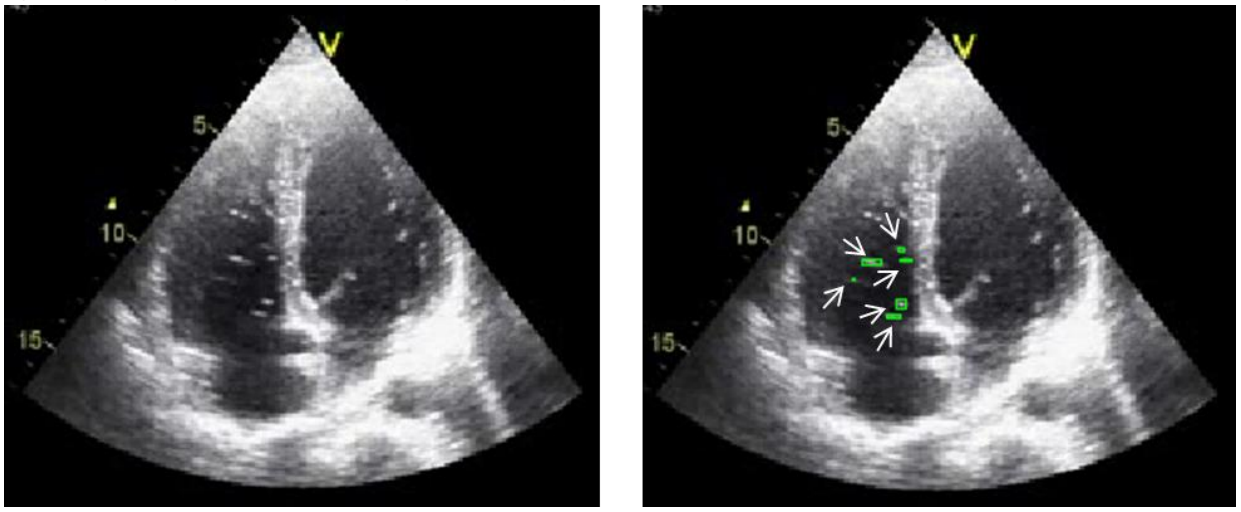

IUS1-PD1-5

Phase aberration effects on beam shape evaluated with particle motion in an elastic phantom

Sara Aristizabal[1], Carolina Amador[1], James F Greenleaf[1], Matthew W. Urban[1]; *[1]Physiology and Biomedical Engineering, Mayo Clinic College of Medicine, Rochester, Minnesota, USA*

Background, Motivation and Objective

Sound speed inhomogeneities in soft tissues lead to phase shifts in ultrasound waves propagating from the transducer to the focal region, and therefore defocus the ultrasound beam, reducing spatial resolution and image contrast of the image. This study describes the use of particle motion resulting from focused acoustic radiation force through different excised animal tissue layers to quantify the level of distortion of the ultrasound beam.

Statement of Contribution/Methods

Studies were conducted in a calibrated elastic phantom (CIRS, Inc., Norfolk, VA). The tissues used in this study, porcine belly skin, subcutaneous fat, and muscle were separated and placed on top of the elastic phantom. The layers were skin alone, fat alone, muscle alone, a double layer of fat, and a skin-fat-muscle combination. Saline was placed in a well on the phantom before being covered with the tissue layers.

A Verasonics ultrasound system (Verasonics, Inc., Redmond, WA) equipped with a linear array transducer (L7-4, Philips Healthcare, Andover, MA) operating at center frequencies of f_0 = 2.50, 3.00, 3.46, 4.09, 4.50, and 5.00 MHz was used. For all the variations of f_0, a beam of 300 μs duration focused at a depth of 40 mm from the transducer produced particle motion in the direction of the beam. The beam shape was evaluated from the distribution of particle motion, which was estimated by 2D auto-correlation of the compounded echoes from three different angled plane waves detected at an effective frame rate of 3.33 kHz.

For all the combinations of f_0, the beam shape without the tissue layers was determined using a thresholding operation to create a mask. For all the subsequent measurements with tissue layers, the particle velocity for each pixel inside this mask was recorded and used for calculations.

Results/Discussion

The median particle velocity decreased as various layers were added on the top of the phantom (Fig. 1(a)). Changes in f_0 also affected the particle velocity amplitude. We found that 5.00 MHz provides the largest change in amplitude. Figure 1(b) shows the normalized median particle velocity, and it was observed that using 3 MHz provided the lowest percentage of amplitude reduction. . Finally, the standard deviation of the particle velocity increased upon adding layers as shown in Fig. 1(c). [This study was supported by NIH grant DK092255.]

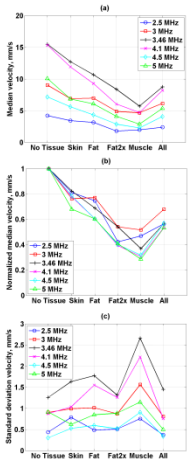

Figure 1: a) Median of the particle velocity, **b)** Normalized median of the particle velocity, **c)** Standard deviation of the particle velocity within the beam shape mask made when there was no tissue present for different combinations of tissue layers and ultrasound frequencies.

IUS1-PD1-6

Tissue imaging using the transmission of 100-MHz-range ultrasound through a fused quartz fiber

Takasuke Irie[1], Tomohito Hasegawa[1], Kouichi Itoh[2], Norio Hirota[3], Norio Tagawa[4], Masasumi Yoshizawa[5], Tadashi Moriya[6], Takashi Iijima[7]; *[1]Microsonic Co., Ltd., Tokyo, Japan, [2]Hitachi-Omiya Saiseikai Hospital, Ibaraki, Japan, [3]Hirota Institute for Surgical Pathology, Tochigi, Japan, [4]Tokyo Metropolitan University, Tokyo, Japan, [5]Metropolitan College of Industrial Technology, Tokyo, Japan, [6]Professor Emeritus of Tokyo Metropolitan University, Tokyo, Japan, [7]National Institute of Advanced Industrial Science and Technology, Ibaraki, Japan*

Background, Motivation and Objective

The tissue diagnosis in the current pathological examination has two drawbacks. (1) It takes time because it requires a tissue sample obtained by the biopsy and the observation using an optical microscope, and (2) it gives burden on the patient. The main objective of the study is to enable an operator to observe directly microscopic images of the tissue without taking out the tissue sample from patient. To achieve the objective, we are developing a needle type ultrasonic microscope that uses a thin fiber as an ultrasound probe.

Statement of Contribution/Methods

In this paper, we describe that the microscopic C-mode image of a tissue sample was obtained using a penetration method. In the experiment, we used a system consisting of a pulser/receiver (Panametrics model 5900PR), a 220-MHz-transducer (Panametrics model V2113) for transmitting and receiving, an oscilloscope (Tektronix TDS5104B), Personal Computer (including a NI LabVIEW for image construction), X/Y-axis stage controller, a fused quartz fiber (49 mm length, approximately 0.8-0.9 mm diameter, one side of the fiber has a flat surface, and the other side has a concave surface), and a tissue sample (mucosal layer of the stomach with approximately 10 µm thickness). The tissue sample fixed on a glass was placed at the focal point of ultrasonic beam in water. In the C-mode imaging, the scanning interval of the ultrasonic beams was 5 µm, and the scanning widths in X and Y directions were 1 mm and 1 mm, respectively. Lateral resolution of the image was measured using a 13 µm (diameter) stainless steel mesh.

Results/Discussion

A C-mode image of the tissue sample (mucosal layer of the stomach with approximately 10 µm thickness) was obtained in the penetration method (Fig.1), and an image of the stainless steel mesh was also obtained. It was shown that the lateral resolution of the image was approximately up to 13 µm. As the results of the experiments, we expect that the microscopic image of the human tissue can be seen directly.

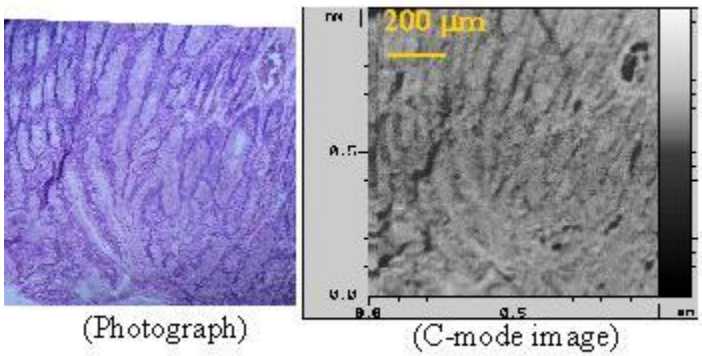

Fig.1 Images of mucosal layer of the stomach

IUS1-PD1-7

Visualization of cancer distribution for living tissues using acoustic impedance microscope

Sachiko Yoshida[1], Hikari Yamada[1], Yasunori Shioki[1], Makoto Yagihashi[2], Kazuto Kobayashi[3], Seiji Yamamoto[4], Naohiro Hozumi[1]; *[1]Toyohashi University of Technology, Japan, [2]Nagoya Municipal Industrial Research Institute, Japan, [3]Honda Electronics Co. Ltd., Japan, [4]Hamamatsu University. School of Medicine, Japan*

Background, Motivation and Objective

Two-dimensional acoustic impedance imaging is useful for observation of tissue conditions without chemical fixation or histochemical processing. Previously, we showed that direct or immnological heavy metal binding to particular proteins of cerebellar tissues made them featuring as higher acoustic impedance, and visualized their distribution in the tissues acoustically. In this report, we would propose a new technique of the acoutic impedance imaging to visualize cancer cells in living sliced organs.

Statement of Contribution/Methods

Zn^{2+} ions are required for dividing cells as an important element of cell mitogenic proteins, zinc finger proteins. Some types of cancers, for example, hepatoma and brain tumor, accumulate applied Zn^{2+} in their organs.

STAM mouse is an useful model animal of non-alcoholic steatohepatitis (NASH) based hepatocellular carcinoma (HCC) generation. After 16 weeks old, many tumors develop and grow in liver. We prepared fresh slices of 17 week-STAM mouse liver and treated them with 200 μM $ZnSO_4$ solution. Their acoustic impedances were observed with 120 MHz transducer using acoustic microscope HMS-1000 (Honda Electronics Co. Ltd.). The slices and reference water were mounted on a hydrophilic silane-treated flat culture dish made of 0.7 mm thick polystylene. Either silane treatment or vaccum ultraviolet (VUV) treatment was useful for stabilization of acoustic measurement. Observed slices were fixed and stained with anti-glypican 3 antibodies in order to confirm the HCC distribution traditionally.

Results/Discussion

The acoustic images of rat healthy liver slices showed hepatic lobules and blood vessels clearly. In HCC mouse liver slices, round tumor tissue was observed with high impedance (fig.1). After Zn^{2+} application, some regions in the tumor increased their impedance in zigzag lines (fig.2). Subtraction image showed the increased region in the tumor (fig.3). Immunohistochemical staining with glypican 3 antibodies showed the HCC distributed there in the tumor.

We conclude that some specific metal-treatment would become a new technique for the visualization of cancer cells in the living organs acoustically.

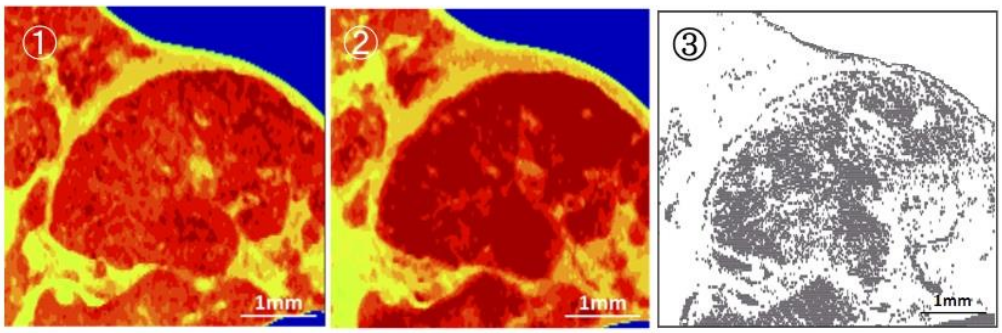

IUS1-PD1-8

In vivo analysis of adult zebrafish ventricular functions by high frequency ultrasound tissue Doppler imaging during heart regeneration phase

Ta-Han Su[1], Ting-Yu Liu[1,2], Chih-Chung Huang[1]; *[1]Department of Electrical Engineering, Fu Jen Catholic University, Taiwan, [2]Graduate Institute of Applied Science and Engineering, Fu Jen Catholic University, Taiwan*

Background, Motivation and Objective

The adult zebrafish has recently become an important animal model for studying human pathologies in many preclinical applications. Zebrafish can fully regenerate its heart even after 20% of its ventricle has been removed, which has prompted many scientists to study zebrafish cardiovascular regeneration. To date, histological specimens is the most common method used to observe the zebrafish cardiac morphology. Recently, high frequency ultrasound (HFUS) has been used to observe the structure and blood flow of zebrafish heart. However, determination of the ventricular functions also depends on measuring the myocardial deformation and motion speed, particularly during the heart regeneration phase. Therefore, the purpose of this study was development a HFUS tissue Doppler imaging for observing the zebrafish cardiac function during ventricular myocardium regeneration. The emphasis was on obtaining information about the myocardium velocity and the corresponding time series variations in cardiac cycle.

Statement of Contribution/Methods

Figure 1(a) shows the block diagram of 50 MHz HFUS tissue Doppler imaging system. The location of target tissue can be found from B-mode imaging. Subsequently, the blood flow and tissue velocities were obtained individually by tissue Doppler imaging. The procedure of ultrasound signal processing is shown in Fig. 1(b). All experiments were carried out using adult A/B line zebrafish.

Results/Discussion

Figure 1(c) shows the typical HFUS color Doppler M-mode images of zebrafish ventricle for non-injury (day 0), ventricle resection after one day (day1), and ventricle resection after seven day (day7). Colored areas present tissue velocity of myocardium motion in the heart walls and anechoic regions (near by color area) indicate intracardiac blood pool. The quantitative analysis of myocardium velocity and the corresponding time series variations in cardiac cycle during heart regeneration are shown in Fig 1(d). Experimental results showed that the myocardium motion speed was increased during systole in order to keep the cardiac output, and therefore the peak flow velocity was maintained during ventricle injury. It is anticipated that this novel device could provide many useful information for studying the cardiac function of zebrafish during heart regeneration.

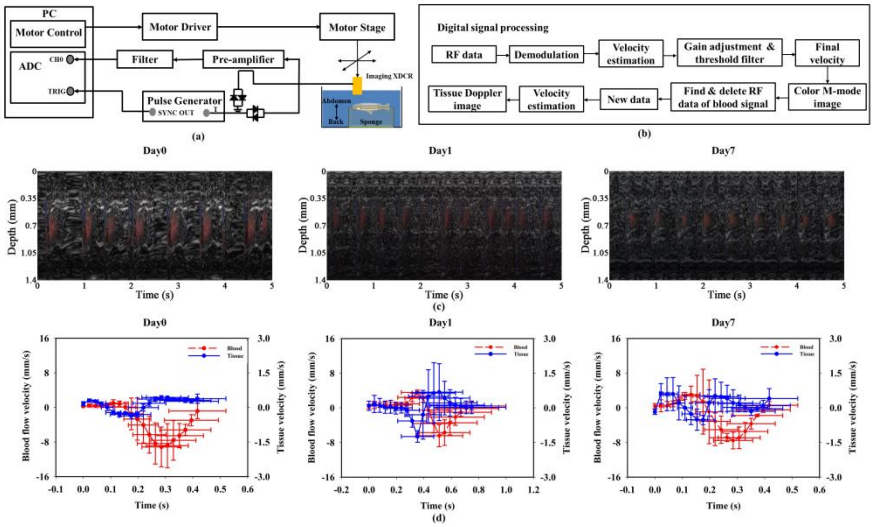
PC
Motor Control
ADC
CH0
TRIG
Motor Driver
Filter
Pre-amplifier
Pulse Generator
SYNC OUT
Motor Stage
Imaging XDCR
Abdomen
Back
Sponge
(a)
Digital signal processing
RF data
Demodulation
Velocity estimation
Gain adjustment & threshold filter
Final velocity
Color M-mode image
Find & delete RF data of blood signal
New data
Velocity estimation
Tissue Doppler image
(b)
Day0
Day1
Day7
Depth (mm)
Time (s)
(c)
Blood flow velocity (mm/s)
Tissue velocity (mm/s)
Blood
Tissue
(d)

New applications of vector velocity imaging

Forum Hall

Thursday, July 25 2013, 01:00 pm - 04:30 pm

Congress Hallair: **Abigail Swillens**
Ghent University

IUS1-PD2-1

High-speed vector motion imaging with diverging circular waves: *in vitro* study using a spinning disc phantom

Daniel Posada[1], Shahrokh Shahriari[1], Boris Chayer[2], Guy Cloutier[2], Hervé Liebgott[3], Damien Garcia[1]; *[1]RUBIC - Research Unit of Biomechanics & Imaging in Cardiology, CRCHUM - Research Centre, University of Montreal Hospital, Montreal, Quebec, Canada, [2]LBUM - Laboratory of Biorheology and Medical Ultrasonics, CRCHUM - Research Centre, University of Montreal Hospital, Montreal, Quebec, Canada, [3]Creatis-LRMN, CNRS UMR 5220, INSERM U630, Université Lyon 1, INSA-Lyon, Villeurbanne, France*

Background, Motivation and Objective

Analysis and quantification of both myocardial and intracardiac flow motions by (tissue) Doppler ultrasound are of major interest for early detection of heart failure and are becoming part of routine clinical set-up. The non-invasive measures yielded by conventional Doppler, however, are incomplete since only the velocity components along the ultrasound beam direction are captured. In addition, because one usually needs to cover a large sector in cardiac imaging, frame rates (typically <50 fps) offered by standard focusing are generally too low to fully describe the intracavitary blood flow and tissue motion. For the same latter reason, alternate techniques such as speckle tracking and/or echo-PIV (particle image velocimetry) are also currently limited by a reduced frame rate. The objective of this *in vitro* study was to demonstrate the capability of ultrafast circular wave imaging to provide accurate time-resolved vector flow mapping over a wide deep sector. Circular wave imaging was chosen in the context of potential cardiac applications, where small intercostal acoustic windows and wide regions-of-interest are required.

Statement of Contribution/Methods

A 10 cm-diameter ultrasound disc phantom spinning at 50 to 300 rpm was insonified at > 1000 fps by diverging circular waves using a Verasonics scanner and a 2.5 MHz probe (64 elements, pitch = 0.32 mm). The backscattered RF signals were beamformed and laterally oversampled using the 2.5-D Kirchhoff migration [Gazdag *et al*., *P IEEE* 72, 1984]. The migrated RFs were then time-gain compensated and B-mode polar images were created using standard envelope detection through a Hilbert transform. The 2-D polar velocity fields were determined using an adaptive coarse-to-fine PIV process based on ensemble correlation and were validated with a robust penalized least squares approach [Garcia, *Exp Fluids* 50, 2011]. The velocity vector components were finally transformed to Cartesian coordinates.

Results/Discussion

Accurate velocity fields were returned by high-speed vector motion imaging with diverging circular waves (Fig. 1). The normalized root mean squared errors between the ground-truth and the ultrasound-derived vector fields were <15%. Although these findings remain to be further validated, our results show that ultrafast circular wave imaging can provide accurate vector motion imaging for cardiac applications.

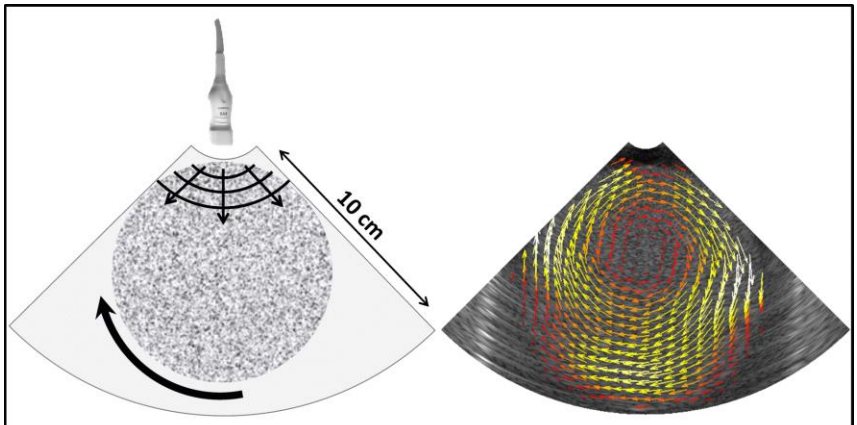

Fig. 1 – High-speed vector motion imaging by circular wave insonifications. *In vitro* studies were performed in a spinning disc phantom. The vector velocity fields were determined using an adaptive multigrid PIV process.

IUS1-PD2-2

Non-invasive Measurement of Pressure Gradients in Pulsatile Flow using Ultrasound

Jacob Bjerring Olesen[1], Marie Sand Traberg[1], Michael Johannes Pihl[1], Jørgen Arendt Jensen[1]; *[1]Center for Fast Ultrasound Imaging, Dept. of Elec. Eng., Technical University of Denmark, Denmark*

Background, Motivation and Objective

This paper demonstrates how pressure gradients in a pulsatile flow environment can be measured non-invasively using ultrasound data. Local pressure gradients in hemodynamics can provide important information for diagnosing various cardiovascular diseases such as atherosclerosis. The gradients can be used as an indication on how changes in the flow, for instance caused by plaque formation, affect the risk of embolism. Current measures of pressure gradients are acquired using catheters inserted into a larger artery and threaded to the region of interest. Although this procedure is reported reliable and of low risk, it remains an invasive procedure that exposes risk of infection to the patients.

Statement of Contribution/Methods

The proposed method relies on vector velocity fields acquired from ultrasound data. 2-D flow data are acquired at 20 frames/sec using the Transverse Oscillation approach. Pressure gradients are calculated from the measured velocity fields using the Navier-Stokes equation for an incompressible Newtonian fluid. The velocity fields are measured for pulsatile flow on a carotid bifurcation phantom (Shelley Medical Imaging Technologies, Canada) with a 70% constriction on the internal branch. Scanning is performed with a 5 MHz BK8670 linear transducer using a BK Medical 2202 UltraView Pro Focus scanner. The calculated pressure gradients are validated through a finite element simulation of the flow model. The geometry of the flow simulation model is reproduced using MRI data, thereby providing identical flow domains in measurement and simulation.

Results/Discussion

The figure presents the measured magnitude of the fluids velocity (red line) and its pressure gradients (blue line) during pulsating flow. The data are measured at the centre of the vessel constriction and the figure shows pressure gradients varying from 0-110 kPa/m. The graph reveals that pressure gradients are strongly sensitive to temporal variations in the velocity, thus, a high temporal sampling rate is required when measuring pressure gradients. The standard deviation and bias of the estimator are calculated during steady flow conditions and yield 48% and -10%, respectively, given in reference to the peak pressure gradient. The results demonstrate that pressure gradients can be estimated non-invasively by use of 2-D velocity fields acquired using an ultrasound scanner.

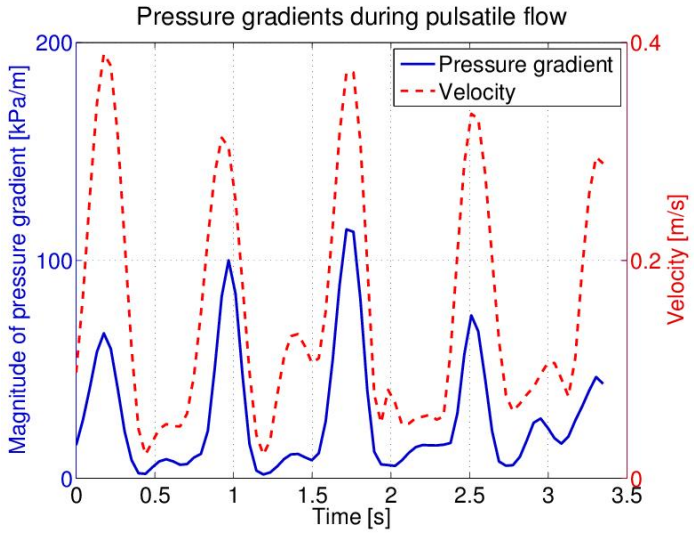

IUS1-PD2-3

Vector Volume Flow in Arteriovenous Fistulas

Peter Møller Hansen[1], Jacob Bjerring Olesen[2], Michael Johannes Pihl[2], Søren Heerwagen[1], Mads Møller Pedersen[1], Marianne Rix[3], Lars Lönn[1], Jørgen Arendt Jensen[2], Michael Bachmann Nielsen[1]; *[1]Dep. of Radiology, Copenhagen University Hospital, Copenhagen OE, Denmark, [2]Center for Fast Ultrasound Imaging, Dept. of Elec. Eng., Technical University of Denmark, Kgs. Lyngby, Denmark, [3]Dep. of Nephrology, Copenhagen University Hospital, Copenhagen OE, Denmark*

Background, Motivation and Objective

The objective of this paper is to demonstrate how Vector Flow Imaging (VFI) can be used to directly measure the volume flow in an arteriovenous fistula. VFI is an angle independent ultrasound technique that provides quantitative information about velocity and direction of the blood flow in a vessel. The native arteriovenous (AV) fistula is the preferred vascular access for hemodialysis. 40 % - 60 % of hemodialysis patients will experience fistula failure during the first 18 months after creation of the fistula. It is therefore essential to continuously monitor these vessels and several methods are currently in use, but these are either invasive, e.g. Ultrasound Dilution Technique (UDT), or based on conventional Doppler ultrasound technique. The latter is very difficult to use directly on the fistula due to the superficial localization of the vessel and the angle dependency of the technique.

Statement of Contribution/Methods

VFI is implemented on a commercial scanner (UltraView 800, BK Medical) with a linear transducer (8670, BK Medical). Four patients were scanned with VFI directly on their functioning AV-fistulas. Each fistula was scanned transversely to measure the diameter of the vessel, and longitudinally to record VFI-data, see figure. The scans were performed just prior to insertion of the hemodialysis needles and start of the dialysis. During dialysis the flow was measured with UDT. From the recorded VFI-data and the geometry of the vessel, volume flow in the fistula was calculated and compared with the UDT measurements.

Results/Discussion

Patient 1: VFI volume flow = 824 mL/min, UDT volume flow = 717 mL/min.

Patient 2: VFI volume flow = 1035 mL/min, UDT volume flow = 1595 mL/min.

Patient 3: VFI volume flow = 411 mL/min, UDT volume flow = 555 mL/min.

Patient 4: VFI volume flow = 431 mL/min, UDT volume flow = 430 mL/min.

The calculated VFI volume flow results deviate 0 % to 35 % from the measured UDT results, and indicate that it is possible to obtain a reasonable volume flow measurement directly from an AV-fistula with a conventional ultrasound scanner. The angle independence of VFI makes it easy to use, compared to Doppler, and in addition to volume flow, VFI can provide further information about flow phenomena in the fistulas, not detected by conventional Doppler. This can make VFI an important tool for diagnostic examination and monitoring of AV-fistulas and other blood vessels.

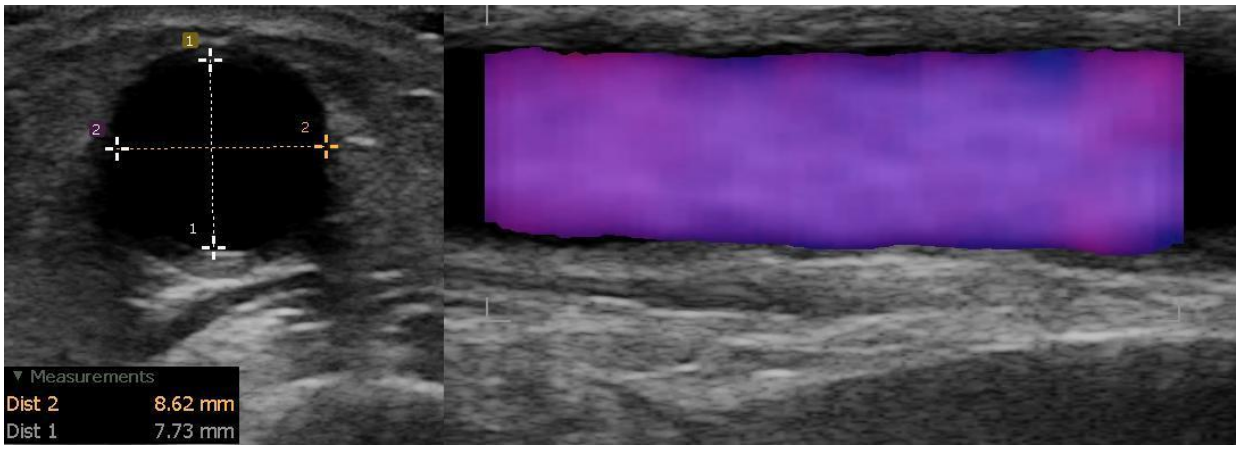

IUS1-PD2-4

Speckle-Enhanced Cardiac Blood Flow Imaging with High Frame Rate Ultrasound

Hiroki Takahashi[1], Hideyuki Hasegawa[1], Hiroshi Kanai[2]; *[1]Graduate School of Biomedical Engineering, Tohoku University, Japan, [2]Graduate School of Engineering, Tohoku University, Japan*

Background, Motivation and Objective

Recently, echocardiographic particle image velocimetry (E-PIV) technique was developed to show velocity vectors and streamlines of blood flow in the human heart based on motions of echo speckles. E-PIV, however, requires intravenous injection of contrast agent to enhance ultrasonic echoes. An alternative method was developed to visualize blood flow in the carotid artery by imaging echo speckles from blood particles using high frame rate ultrasound (Hasegawa and Kanai, Proc. IEEE Intn'l Ultrason. Symp., 2010). However, in cardiac ultrasound, ultrasound attenuation is significant due to longer propagation path. Therefore, it is difficult to enhance weak echoes from blood particles in the heart without averaging echo signals for number of frames to achieve a high temporal resolution. In this study, we overcome such problem to realize cardiac blood flow imaging with enhanced echo speckle.

Statement of Contribution/Methods

As illustrated in Fig. (a), ultrasonic RF echo signals in the left ventricle of three chamber view of a 25-year-old healthy male were measured at very high frame rate of 1010 Hz by parallel receive beamforming for cardiac measurement (Hasegawa and Kanai, J. Med. Ultrason., 2011) to continuously observe echoes from the same blood particles between frames. Coded excitation and pulse compression with 5-bit Barker code were used to increase signal-to-noise ratios (SNRs) of weak echoes from blood particles (about 14 dB increase in SNRs). Beamformed RF signals with pulse compression were high pass filtered in the direction of frame to suppress echoes from slowly moving tissue. Furthermore, the spatially coherent signal components were extracted from filtered signals in two consecutive frames to enhance echoes from blood particles.

Results/Discussion

Figure (b) shows a B-mode image in ejection phase and Fig. (c) shows a flow image obtained by the proposed method, which visualizes speckle-like patterns of echoes from blood particles inside the left ventricle. Moreover, flow vectors were estimated based on speckle tracking of echo signals as shown in Fig. (d). Motions of speckles and vectors directing to the aortic valve showed that blood in the left ventricle was ejected to the aorta. These in vivo experimental results show a potential of the proposed method for non-invasive imaging of blood flow at high temporal resolution of a few milli-seconds.

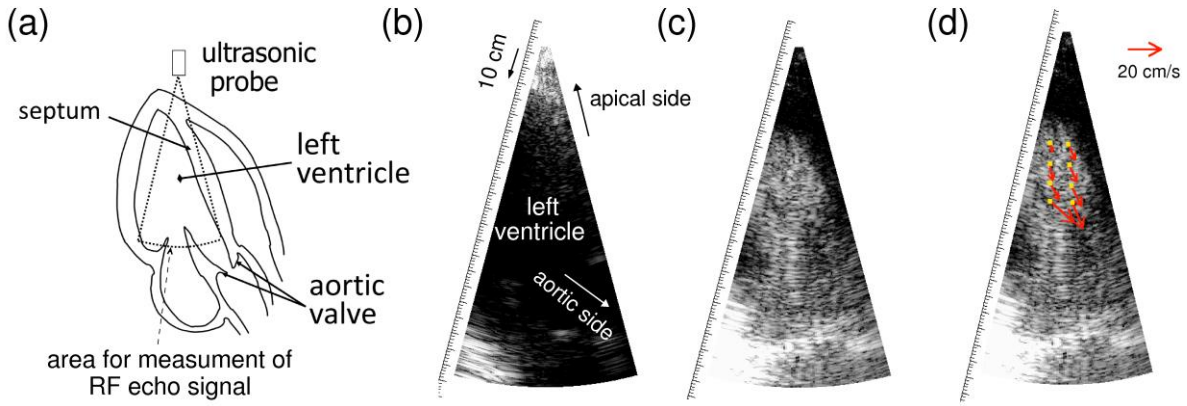

IUS1-PD2-5

A particle-based simulation tool for ultrasound blood flow imaging: validation of high-speed echo-PIV

Shahrokh Shahriari[1], Damien Garcia[1]; *[1]RUBIC - Research Unit of Biomechanics & Imaging in Cardiology, CRCHUM - Research Centre, University of Montreal Hospital, Montreal, Quebec, Canada*

Background, Motivation and Objective

The inability to determine cross-beam velocities with Doppler-echo leaded to the development of echographic particle image velocimetry (echo-PIV). This technique currently suffers from having low temporal resolution due to the wave excitation based on focused beam formation. High-quality vector flow imaging needs development of high-speed

imaging techniques. This work aims to provide a new simulation environment for ultrasound flow imaging through smoothed particle hydrodynamics (SPH), a state-of-the-art computational method for modeling fluid flows. This tool was used to analyze the potential of high-speed echo-PIV in physiological flows.

Statement of Contribution/Methods

In the context of ultrasound imaging, high temporal resolution is achievable by plane wave excitation. We evaluated the echo-PIV technique using a particle-based simulation environment integrating linear acoustics and fluid dynamics. Field II was used as a scattering acoustic model. A given arrangement of point scatterers mimicking blood components were insonified with ultrasound plane waves and the backscattered RF signals were analyzed.

To get rid of the drawbacks related to standard mesh-based computational fluid dynamics (CFD), we developed a simulation environment based on SPH, a mesh-free Lagrangian CFD method. In SPH, the fluid is divided into a set of particles and the physical properties of each particle are calculated based on the properties of its neighboring particles. By contrast with standard CFD methods, fluid-acoustic coupling is effortless since the SPH particles can be used directly as sound scatterers.

A physiological Womersley flow was insonified perpendicularly by acoustic plane waves at the rate of >1000 fps. The RF signals were beamformed using Kirchhoff migration. The velocity fields were then determined using iterative multigrid PIV processing on the RF images.

Results/Discussion

The velocity profiles derived by high-speed echo-PIV were very concordant with those yielded by the SPH particles (NRMSE = 12%, see Fig). Though these findings remain to be confirmed *in vitro*, our results show that high-speed echo-PIV provides accurate measures of cross-beam velocities. Because a large number of frames are available, it is anticipated that advanced RF and PIV processing (compounding, ensemble correlation) may further improve the accuracy of high-speed echo-PIV.

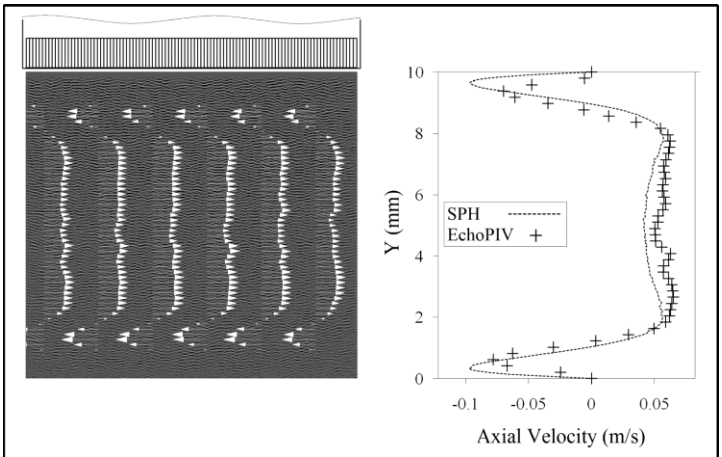

Fig. 1 - Ultrafast echo-PIV validated by SPH. Velocity profiles in an oscillating pipe flow: comparison between ground-truth SPH and high-speed echo-PIV.

IUS1-PD2-6

Physiological flow characterization in elastic vessel phantom using Ultrasonic Particle Image Velocimetry

Ming Qian[1], Lili Niu[2], Congzhi Wang[3], Yang Xiao[4], Weibao Qiu[4], Hairong Zheng[3]; *[1]Shenzhen Institutes of Advanced Technology, Chinese Academy of Sciences, Shenzhen, Guangzhou, China, People's Republic of, [2]Shenzhen Institutes of Advanced Technology, Chinese Academy of Sciences, Shenzhen, Guangdong, China, People's Republic of, [3]Chinese Academy of Sciences, China, People's Republic of, [4]Chinese Academy of Sciecnes, China, People's Republic of*

Background, Motivation and Objective

Cardiovascular disease is the leading cause of deaths worldwide. Arterial stiffness and its hemodynamic consequences are both considered as essential predictors of cardiovascular risks. The fluid-structure interaction in human arterial system is complex, and how arterial stiffness influences hemodynamics needs more detailed research. We previously used Ultrasonic Particle Image Velocimetry (EchoPIV) method to quantitatively and non-invasively characterize the velocity distribution both in vitro and in vivo experiments. In this study, we constructed physiological flow circulation by pumping fluid through elastic artery phantom, and measured flow characteristics including pressure, flow velocity, and wall shear rate when the arterial stiffness changed. The effect of arterial stiffness on flow characteristics is discussed.

Statement of Contribution/Methods

Arterial phantoms that had elastic modules of 168.52, 248.79, and 310.28 kPa were fabricated and assembled in fluid circuit, physiological flow were generated in phantoms by blood pump, and EchoPIV method is used to measure flow characteristics for comparative tests. The phantoms had the same geometry of 6mm inner diameter, 2mm wall thickness, and 160mm length. The Harward blood pump was maintained at 15 ml/stroke, 1 beat/s, and systole/diastole ratio of 35/65. B-mode images were acquired at a frame rate of 213 Hz using onixRP ultrasound system with a 128-element transducer with central transmit frequency of 10 MHz. The vessel motion was evaluated by measuring the inner diameter from image sequence in a whole the cardiac cycle. The flow pressure was read by pressure sensor mounted at the inlet. EchoPIV and ultrasonic Doppler methods were applied to hemodynamic research regarding flow velocity and shear rate.

Results/Discussion

First, increased vessel stiffness causes degraded vasomotion and elevated pulse pressure, indicating degrading function of blood pumping. The diameter variation ratios were respectively 26.7%, 20.0%, 13.3%. The measured pulse pressures were respectively 15.5, 17.5, 21.0 kPa. Second, Peak velocity measured by Doppler and EchoPIV has bias less than 5% during the whole cardiac cycle. The EchoPIV results show parabolic velocity profiles. The measured peak velocities were 61.58, 53.72, and 46.44 cm/s respectively, and stiffer vessel has smaller peak-to-peak value of velocity. The difference is slight for shear rate in all measures due to relatively small stiffness differences of the three phantoms. In sum, vessel stiffness has influence on vasomotion, flow pressure, flow velocity, and shear rate. The results in this study may help understand the interaction between hemodynamics and wall mechanics.

Medical system design

Forum Hall

Thursday, July 25 2013, 01:00 pm - 04:30 pm

Congress Hallair: **Andrzej Nowicki**
Polish Academy of Sciences

IUS1-PD3-1

A Modulated Excitation Imaging System for Micro-Ultrasound

Weibao Qiu[1], Yanyan Yu[2], Fu Keung Tsang[2], Ming Qian[1], Hairong Zheng[1], Lei Sun[2]; *[1]Paul C. Lauterbur Research Center for Biomedical Imaging, Shenzhen Institutes of Advanced Technology, Chinese Academy of Sciences, Shenzhen, China, People's Republic of, [2]Interdisciplinary Division of Biomedical Engineering, The Hong Kong Polytechnic University, Hong Kong*

Background, Motivation and Objective

Micro-ultrasound (micro-US) is an invaluable technique to delineate small living structures with fine spatial resolution. It has been applied for evaluating the eye, skin, blood vessel, etc. However, high frequency ultrasound suffers from significantly large attenuation. The penetration depth is a consequently serious problem for micro-US utilities. This paper presents the development of a novel system with modulated excitation techniques to extend penetration depth for various micro-US investigations.

Statement of Contribution/Methods

The waveform for modulated excitation imaging usually requires amplitude and frequency modulation (Chirp excitation) or phase modulation (Barker excitation and Golay excitation) of sinusoidal carrier signal. A programmable high voltage arbitrary waveform generator was developed to generate various arbitrary waveforms for different modulated excitation imaging. A programmable field programmable gate array (FPGA), and a high speed digital-to-analog converter (DAC) combined with amplifiers are used for high voltage arbitrary waveform generation. High precision ultrasound signal amplification and acquisition, real-time image processing, and fast data transfer were achieved in a high speed imaging receiver. It includes front-end electronics, analog-to-digital converter (ADC), FPGA, and high speed computer interfaces, which allows to process the images in real-time with high programmability and flexibility.

Results/Discussion

Fig. 1(a-f) shows the prototype of the proposed programmable modulated excitation imaging system. The amplitude of the arbitrary waveform is over 60 Vpp. The gain of the imaging receiver is 36 dB in the frequency range of 20-80 MHz. The noise floor and the dynamic range of the receiver are about 50 μV, and 56 dB respectively. The speed of data transfer is higher than 150 MByte/s in case of PCIE interface, which allows very high speed imaging. Test results show that the proposed modulated excitation imaging system can acquire up to 20dB SNR improvement and 83% increase of penetration depth in contrast to traditional short pulse imaging method. In vivo experimental test on the dorsal skin of a human hand, which is shown in Fig. 1(g-h), demonstrates good performance of the programmable modulated excitation imaging system.

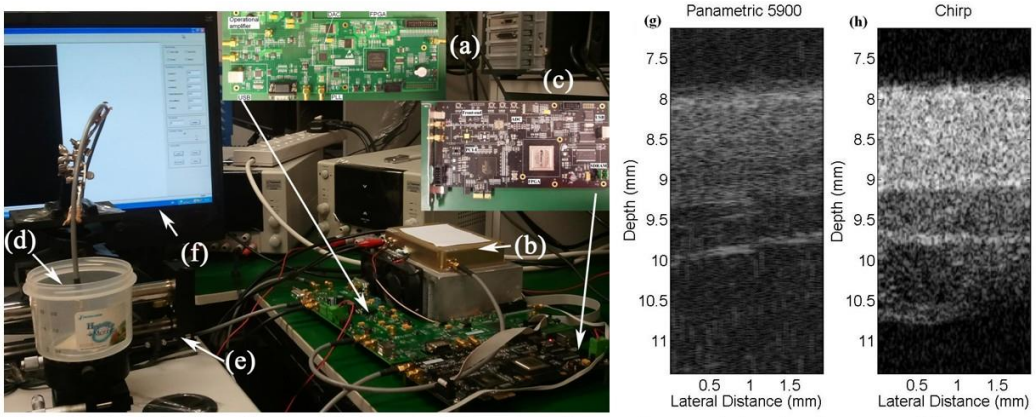

Fig. 1. The setup for the modulated excitation imaging system and *in vivo* images of the dorsal skin of a human hand. (a-b) 8-layer PCB of the arbitrary waveform generator. (c) 8-layer PCB of the imaging receiver. (d) Transducer. (e) Linear motor. (f) Customized console software. (g) The image of short pulse imaging. (h) The image of chirp based modulated excitation imaging.

IUS1-PD3-2

A Novel High-frequency Endoscopic Ultrasound System for Colorectal Cancer Diagnosis

Cheng LIU[1], Weibao QIU[2], Yan CHEN[3], Yanyan YU[1], Jiyan DAI[3], Lei SUN[1]; *[1]Interdisciplinary Division of Biomedical Engineering, Faculty of Engineering, The Hong Kong Polytechnic University, Hong Kong SAR, China, People's Republic of, [2]Paul C. Lauterbur Research Center for Biomedical Imaging, Shenzhen Institutes of Advanced Technology, Chinese Academy of Sciences, Shenzhen, China, People's Republic of, [3]Department of Applied Physics, Faculty of Applied Science and Textiles, The Hong Kong Polytechnic University, Hong Kong SAR, China, People's Republic of*

Background, Motivation and Objective

The fact that only 39% of pre-cancerous colorectal tumors are detected at an early stage is the main factor that leads to metastasis and high mortality rate. The invasion depth of early colorectal cancer limits to superficial layers of colorectal wall with few vascular and lymphatic vessels. Colonoscopy is clinically performed for screening, during which biopsy may be conducted; however, colonoscopy is limited to surface, which is insufficient for pre-cancerous diagnosis. Endoscopic ultrasound (EUS) has been widely used to assess tumor penetration and metastasis risk for determining the treatment strategy. With high-frequency transducer (20MHz-30MHz), EUS is capable of delineating the mucosa-

submucosa layer of normal human colon with micron-scale resolution anatomical information; however, the current high-frequency EUS is still insufficient to distinguish cancer from polyp and adenoma due to the lack of patho-physiological information. An open high-frequency EUS system, compatible with regular endoscope, which allows acquisition of radio frequency (RF) data for acoustic tissue characterization and combination with other functional imaging modalities (e.g. photoacoustic imaging) may bring values to diagnose early stage colorectal malignancies.

Statement of Contribution/Methods

The development of a novel high-frequency endoscopic ultrasound system which allows quantitative acoustic tissue characterization and easy fusion of multiple functional modalities for complementary structural & patho-physiological information is presented in this paper. A compact and cost-effective system, which was based on electronic components and printed circuit board (PCB), was designed to implement reconfigurable hardware circuitry, flexible imaging control, programmable processing algorithms and raw RF data acquisition. The system employed a high-performance Field programmable gate array (FPGA) as a core microprocessor to accomplish flexibility, diversity, and real-time imaging. Low noise electronics were used to support large signal-to-noise ratio (SNR) and high precision data acquisition. Two high speed data transfer schemes, the PCI Express (PCIe) interface and USB, were implemented in this system for fast data transmission. Processed images or unprocessed raw RF data could be stored, displayed and post-processed in PC. A miniaturized 30 MHz single element mechanical side-view endoscopic ultrasound transducer was fabricated using PMN-0.28PT single crystal.

Results/Discussion

Testing results showed that the system could detect a minimum signal of 25 μV, allowing a 50 dB dynamic range at 45 dB gain, with a frequency range from 20 MHz to 100 MHz. Finally, phantom imaging, *in vivo* imaging of normal colon in ICR mouse and New Zealand White rabbit model were conducted to demonstrate the performance of the system.

IUS1-PD3-3

Implementation of a Novel High Frequency Ultrasound Device for Guiding Epidural Anesthesia-In Vivo Animal Study

Po-Yang Lee[1,2], Chih-Chung Huang[2], Huihua K. Chiang[3]; *[1]Graduate Institute of Applied Science and Engineering, Fu Jen Catholic University, Taiwan, [2]Department of Electrical Engineering, Fu Jen Catholic University, Taiwan, [3]Institute of Biomedical Engineering, National Yang-Ming University, Taiwan*

Background, Motivation and Objective

Epidural anesthesia (EA) is a common surgical operation in clinical anesthesia. An epidural needle is inserted from the backside of patient into epidural space (ES) where an anesthetic drug is injected by anesthetist during operation. A successful EA is highly dependent on the experience of the operator because the epidural needle insertion is a blind technique. In order to reduce the risk of accidental dural puncture, a novel method which combination of a high frequency ultrasound (HFUS) needle transducer and epidural catheter has been proposed for guiding EA insertion in our previous study [1]. Since HFUS exhibits a higher spatial resolution, the locations of different structures can be observed clearly via ultrasound A-mode image. In order to implement this concept for clinical applications, a ultrasound-embedded epidural needle guide device based on FPGA electronic circuit was developed in present study.

Statement of Contribution/Methods

Figure 1(a) shows the block diagram of the ultrasound-embedded epidural needle guide device. It is a custom-designed portable system for real-time display the 40 MHz ultrasound A-mode image during the epidural needle insertion. It includes a HFUS pulser/receiver, A/D converter (sampling frequency of 200 MHz), FPGA (CyclineII-EP2C5T144, Altera), and LCD display module. The measured data can be also stored for off-line analysis. A photo of current system is shown in Fig.1 (b). The in vivo experiments were carried out using porcine model. Figure 1 (c) shows the photo of animal experiment which a needle transducer was placed into the hollow chamber of a Tuohy needle for guiding the epidural needle insertion.

Results/Discussion

Fig. 1(d) shows a typical A-mode image of ES during needle insertion. The backscattering signals received during the advancement of the ultrasound-embedded epidural needle transducer toward the ES. The locations of arachnoid, dura mater, epidural space, and ligamentum flavum can be observed clearly on the LCD module during surgical operation. It is anticipated that this novel device could reduce failed epidural blocks and complications caused by dural puncture.

[1] H.K. Chiang et al."Novel Epidural Needle with Embedded High-frequency Ultrasound Transducer: Epidural Access in Porcine Model", Anesthesiology.2011;114:1320.

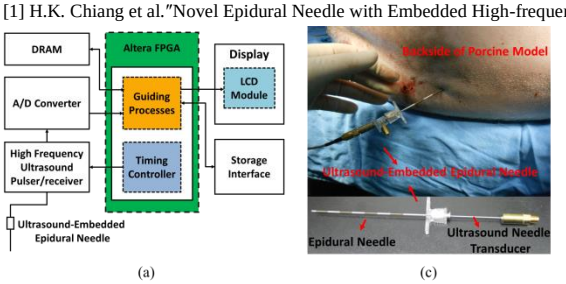

Fig. 1

IUS1-PD3-4

Ultrasonically Marked Instruments for Ultrasound-Guided Interventions

Jay Mung[1], **Francois Vignon**[2], Ramon Erkamp[2], Doug Stanton[2], Ameet Jain[2]; *[1]Sinc Labs, LLC, USA, [2]Philips Research North America, USA*

Background, Motivation and Objective

Needles and catheters are poorly visualized under ultrasound due to their specular nature, reflecting beams away from the imaging probe. Echogenic coatings and steered imaging beams have improved visualization but the improvement they offer is limited and steered beams fail on curved and phased array geometries, when the needle approach is perpendicular to the image plane, and when the tool is slightly off the imaging plane.

It has been proposed to embed ultrasound receivers near the tip of interventional tools. These sensors receive and beamform signals coming from the imaging probe as it acquires the image, yielding <0.5mm accuracy position information even when the needle tip is invisible (Figure).

This paper presents the acoustical characterization of PZT sensors for acoustical marking of needles and catheters. PZT-equipped tools are also presented and the tracking capability is demonstrated ex vivo.

Statement of Contribution/Methods

High-frequency (>10MHz) PZT disks and tubes of different form factors (Sonic Concepts and Philips) were acoustically characterized. SNR, waveform, and directivity of the sensors were tested in water under imaging by an S5-1 probe (Philips, 2.4MHz center frequency, MI = 1.1). Acoustically marked biopsy needles and catheter guidewires were manufactured. Ex-vivo tracking experiments of needles in pork loin with the C5-1 probe (Philips) were also performed to qualitatively test tracking robustness.

Results/Discussion

Maximum SNRs of >50dB were found with all sensors in the water tank. Complex directivity patterns were observed varying with sensor size and shape: several directivity peaks may be found on a given sensor due to mode conversion inside the sensor and excitation of the materials's g31 coefficient. Small disks (<1mm diameter) were found to be most appropriate with flattest directivity. Ex vivo experiments demonstrated reliable tracking of an ultrasound-equipped needle at depths >10cm. The figure presents experimental results for acoustical characterization of a 1mm diameter, 30MHz PZT disk and ex vivo tracking of the same sensor embedded in a 16g biopsy needle.

In conclusion, it is feasible to manufacture PZT-equipped instruments exhibiting good tracking accuracy and robustness.

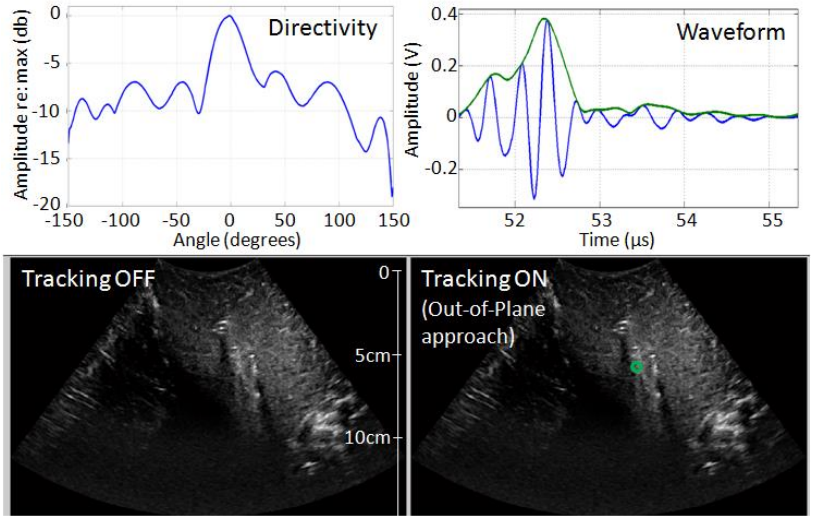

IUS1-PD3-5

GPU-Based Real-Time Imaging Software Suite for Medical Ultrasound

Jung Woo Choe[1], **Amin Nikoozadeh[1]**, Ömer Oralkan[2], Butrus Khuri-Yakub[1]; *[1]E. L. Ginzton Laboratory, Stanford University, USA, [2]Electrical and Computer Engineering, North Carolina State University, USA*

Background, Motivation and Objective

Previously we have developed real-time volumetric ultrasound imaging software on a multi-core CPU platform, and presented imaging results using annular, rectangular, and linear capacitive micromachined ultrasonic transducer (CMUT) arrays. However, the frame rate obtained using this software was not sufficient for some applications requiring high frame rates, such as cardiac imaging. In addition, it was not suitable for more compute-intensive jobs, for example, real-time volume-rendering. To overcome these limitations, we developed a new GPU-based software suite. This software aims to provide a fast real-time imaging platform for various probe geometries and imaging schemes.

Statement of Contribution/Methods

The imaging software receives the raw RF data from a data acquisition system, and processes them on the GPU to reconstruct volumetric images in real-time. The most general-purpose imaging program displays three cross-sectional images for arbitrary probe geometry and various imaging schemes including conventional beamforming, synthetic beamforming, and plane-wave compounding. The other imaging programs in the software suite, derived from the general-purpose program, are optimized for their own purposes, such as displaying a rotating B-mode plane and its maximum intensity projection (MIP), photoacoustic imaging, and real-time volume-rendering.

Results/Discussion

Real-time imaging was successfully demonstrated using each of the imaging programs in the software suite. In an imaging experiment with a 64-element annular CMUT array, the GPU-based software displayed three cross-sectional images at a rate of 45 frames per second, using synthetic beamforming and Hadamard coding schemes. This rate is 4.5 times higher than that of our previous CPU-based software.

[Software displaying a rotating B-mode image and its MIP]

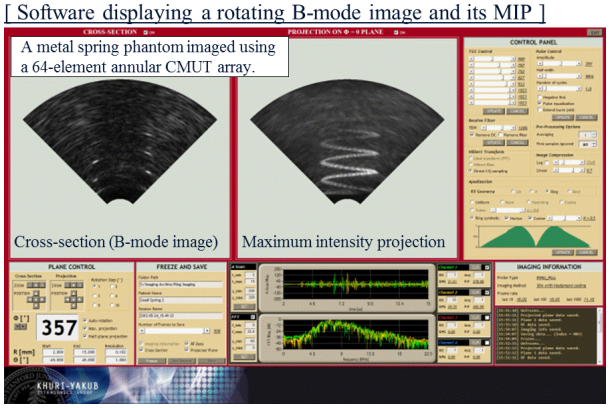

[The Software Suite]

Imaging programs	The most general-purpose imaging program, displaying three arbitrary cross-sectional images
	Software showing one B-mode image rotating about the axis
	Software displaying one rotating B-mode image and its maximum intensity projection (MIP)
	Photoacoustic and ultrasound dual-mode imaging program
	Volume imaging software with real-time volume-rendering
	Ultrafast flow imaging software (*under development*)
Non-imaging programs	4-channel real-time RF data viewer
	TX controller for a Verasonics system, used in drug delivery and HIFU applications
	A Matlab program to view and analyze saved images from real-time imaging

IUS1-PD3-6

Smartphone-based Portable Ultrasound Imaging System: Primary Results

Kyucheol Kim[1], Minjae Kim[1], Hyunseok Joo[1], Wooyoul Lee[1], Changhan Yoon[1], Tai-kyong Song[1], Yangmo Yoo[1,2]; *[1]Department of Electronic Engineering, Sogang University, Seoul, Korea, Republic of, [2]Interdisciplinary Program of Integrated Biotechnology, Sogang University, Seoul, Korea, Republic of*

Background, Motivation and Objective

There is a growing need of portable ultrasound imaging systems since it can allow clinicians to access and diagnose a patient at the scene of an accident or at the patient's bedside due to their improved accessibility. Portable ultrasound imaging systems have been developed based on application-specific integrated circuits (ASICs). However, this ASIC approach is typically beneficial to well-defined targeted applications such that its usefulness for POC systems would be limited. The recent advance in application processors (APs) and graphics processing units embedded in smartphones can facilitate smartphone-based portable ultrasound imaging systems.

Statement of Contribution/Methods

In this paper, the feasibility of the smartphone-based portable ultrasound imaging system is demonstrated where the high-end Android smartphone (i.e., Samsung's Galaxy Note II) is used for performing core ultrasound B-mode signal and image processing (e.g., quadrature demodulation and scan conversion). The Samsung's Galaxy Note II has the Exsynos4412 Quad-core 1.6-GHz AP and 5.5-inch high-definition AMOLED display. The Java language was used with the Eclipse 4.2.1 Java development open source program. To efficiently incorporating ultrasound signal and image processing on the smartphone, a quadrature bandpass filter with poly-phase structures was applied. For demonstrating its performance, beamformed ultrasound data were captured from a commercial ultrasound system (V10, Samsung Medison, Seoul, Korea).

Results/Discussion

In this paper, the feasibility of the smartphone-based portable ultrasound imaging system is demonstrated where the high-end Android smartphone (i.e., Samsung's Galaxy Note II) is used for performing core ultrasound B-mode signal and image processing (e.g., quadrature demodulation and scan conversion). The Samsung¡¯s Galaxy Note II has the Exsynos4412 Quad-core 1.6-GHz AP and 5.5-inch high-definition AMOLED display. The Java language was used with the Eclipse 4.2.1 Java development open source program. To efficiently incorporating ultrasound signal and image processing on the smartphone, a quadrature bandpass filter with poly-phase structures was applied. For demonstrating its performance, beamformed ultrasound data were captured from a commercial ultrasound system (V10, Samsung Medison, Seoul, Korea).

(a)

Processing block	Execution time [ms]
Quadrature bandpass filtering	450
Envelop detection	20
Fractional decimation	18
Time gain compensation	4
Log compression	27
Scan conversion	600
Total	1,119

(b)

Figure 1. (a) a reconstructed ultrasound B-mode image displayed on the Samsung Galaxy Note II and (b) execution time for each processing block.

IUS1-PD3-7

Optimization of real-time ultrasound PCIe data streaming and OpenCL processing for SAFT imaging

Mateusz Walczak[1], Marcin Lewandowski[1], Norber Zolek[1]; *[1]Department of Ultrasound, Institute of Fundamental Technological Research PAS, Warsaw, Poland*

Background, Motivation and Objective

A real-time implementation of the SAFT imaging methods is a big engineering challenge due to the required extremely high data bandwidth and performance of data processing. Nowadays, only the complex structures of FPGAs and GPUs offer a processing power sufficient to implement such tasks.

The Universal Ultrasound Platform built by our group will enable implementation of the SAFT methods and other complex algorithms of ultrasound signal processing. The developed RX64 card provides the acquisition as well as streaming of 64 parallel ultrasound channels through the PCIe 2.0 8-lane interface.

The objective of the conducted tests was to determine a nominal data throughput of the RX64->CPU->GPU communication and a performance of processing of the SAFT reconstruction algorithms which were implemented on GPU in OpenCL.

Statement of Contribution/Methods

The acquisition RX64 card was built based on the FPGA Altera Stratix 4 which provides transfer of digital data from 64 A/D converters to the DDR3 memory buffer. Then, the data are transferred through the PCIe interface to the CPU RAM memory. Data streaming from the module is performed by the DMA (Direct Memory Access) resulting in high throughput and low CPU load. The next step is a data transfer from the CPU to the GPU memory. An optimal use of the OpenCL functions eliminates additional copying the data within the CPU memory; therefore a direct use of a memory region which was allocated by the transfer from the RX64 is possible. Due to interoperability the resultant buffer can be directly transferred to a display using the OpenGL libraries after implementation of the processing in the OpenCL.

The OpenCL kernel which was implemented in order to reconstruct the SAFT with apodization function, received demodulated signals of ultrasound echoes (hardware demodulated in the FPGA). The stored data from 128 channels were streamed from the RX64. Afterwards they were reconstructed on the GPU card.

Results/Discussion

All tests were performed on the PC with the Intel i7-960 (3.2 GHz) processor with 6 GB of RAM, ASUS-P5T7WS motherboard and a GPU NVIDIA GTX580 on Microsoft Windows 7 64-bit operating system.

The applied asynchronous transfer of data between the RX64 CPU and RAM has reached 3GB/s (theoretical limit is 3.8GB/s). Transfer time of a single frame of the SAFT acquisition using 128 channels, sampling at 65MSPS, imaging depth of 19 cm (128ch x 16kS x 2B = 4MB) was approximately 1.3 ms. That provides the acquisition frame rate of up to 769 Hz to the CPU memory. The transfer of data from the CPU memory to the GPU memory was 5.2GB/s The obtained real rate of the data transfer from the CPU to the GPU and reconstruction of the 256x256 pixels LRI (Low Resolution Image) on a single GPU card was approximately 450 Hz.

The results show that the developed concept of the system based on the communication through the PCIe interface and processing on the GPU enables practical implementation of the SAFT imaging in the real-time for systems of the 64-128 channel range.

IUS1-PD3-8

Cumulative method of image reconstruction in synthetic aperture. Theory and experimental results

Janusz Wojcik[1], Ihor Trots[1], Andrzej Nowicki[1], **Marcin Lewandowski[1]**; *[1]Department of Ultrasound, Institute of Fundamental Technological Research PAS, Warsaw, Poland*

Background, Motivation and Objective

The Synthetic Aperture (SA) method provides a new solution in ultrasound diagnostics and has particular importance in applications where frame rate and image resolution are crucial. Our new approach named Cumulative Synthetic Transmit Aperture (CSTA) allows optimizing SA in terms of the memory size and computational power.

With the advent of GPU (graphics processor unit) processing era real-time the SA processing became feasible. However, required memory transfer starts to be a limiting factor. Proposed CSTA algorithm requires 25 times less memory than reference STA method for 64 elements transducer. This makes feasible a low-power implementation of CSTA on embedded GPU.

Statement of Contribution/Methods

In theoretical development of the CSTA algorithm the Rayleigh-Sommerfeld solutions to boundary-value problem of Dirichlet for the Helmholtz equation were used. The distinctive feature of the CSTA is accumulating echoes of subsequent transmissions in only one matrix, sufficient for data acquisition and image synthesis. In traditionally applied STA a separate acquisition matrices for each transmission are created and next for each acquisition only a fragments of the images are reconstructed from the subsequent matrices.

For both STA and CSTA methods the L=64 elements linear array was synthesized. The receiving sequence Lr for both, STA and CSTA, was equal to full aperture of 64 elements. The transmitting groups were also the same and equal to 16 For CSTA the scanning step was equal to the number of transmitting transducers (16), it means that for one acquisition matrix four transmission were executed. For standard STA the scanning step was equal to 2 elements, 25 transmissions and 25 acquisition matrices were built up. Experimental data from a tissue phantom were obtained with the Ultrasonix SonixTouch research scanner and specially crafted scripts.

Results/Discussion

The comparison of reconstructed 2D images using both methods, as well as and their cross-sections in linear and logarithmic scales are presented. The obtained CSTA images clearly show comparable resolution and contrast to the reference STA, while the memory/processing cost is at least 20 times lower.

IUS1-PD3-9

Optimization of a Magnetic Linear Transducer Actuator Using Computational Fluid Dynamics

John Pitre Jr. [1], Grant Kruger[2,3], Leo Koziol[3,4], Alan Vollmer[3,4], William Weitzel[3,4], Joseph Bull[1]; *[1]Biomedical Engineering, University of Michigan, Ann Arbor, Michigan, USA, [2]Mechanical Engineering, University of Michigan, Ann Arbor, Michigan, USA, [3]Nephrology, VA Medical Center, Ann Arbor, Michigan, USA, [4]Internal Medicine, University of Michigan, Ann Arbor, Michigan, USA*

Background, Motivation and Objective

In order to improve single element ultrasound imaging and Doppler flow measurements for superficial vascular applications, we have designed a magnetic linear transducer actuator. Our overarching objective is to develop a low-cost ultrasound data acquisition system for point-of-care medical applications. The actuator consists of a scan head carrying a single element ultrasound transducer. The scan head is driven along a linear or curvilinear path by an electromagnetic force. As it scans, it moves through an acoustic coupling fluid which exerts a drag force on it. In order to achieve the high frame rates necessary for imaging, we conducted this study to evaluate and minimize the effects of drag in this prototype device.

Statement of Contribution/Methods

In order to quantify the drag forces experienced by the magnetic actuator scan head, we have formulated a theoretical model of the device. Using COMSOL Multiphysics, we solve the Navier-Stokes equations in order to obtain the flow field and drag forces generated by the movement of the scan head. We investigated the effects of three parameters on the drag and lift forces: the velocity and shape of the scan head and the distance h_{gap} separating it from the housing walls. For the scan head velocity, we simulated three frame rates: 10, 20, and 30 frames per second. Our study also investigated three scan head shapes: blunt, semi-rounded, and fully rounded. Finally, we implemented a parametric sweep on the value of h_{gap} to quantify its effect.

Results/Discussion

Our model provides quantitative predictions of drag forces in the device. Our results show that the scan head shape has little effect on drag. In contrast, we can greatly reduce drag by increasing h_{gap}. In addition, the velocity field reveals interesting flow phenomena including periodic vortex shedding and trailing vortex cells. This vortex shedding increases drag and produces an oscillating lift force. This could contribute to unwanted vibration of the scan head. In conclusion, our analysis indicates that scan head shape contributes less to drag than gap clearance over a range of suitable frame rates. Furthermore, our analysis uncovered an additional source of force and motion from the shedding vortices. We are incorporating these new findings into our transducer actuator design.

This work was supported in part by a grant from the Coulter Foundation and NIH grant 1R41HL112517.

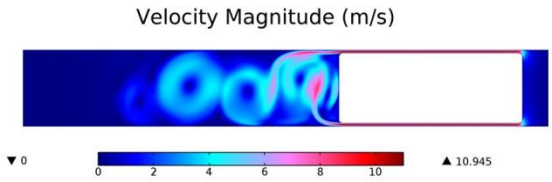

Bone characterization

Forum Hall

Thursday, July 25 2013, 01:00 pm - 04:30 pm

Congress Hallair: **Keith Wear**
US Food and Drug Administration

IUS1-PD4-1

Estimation of Wave Propagation inside Human Body while Walking and Running - Measurement of Vibration on Body Surface and 3-D Simulation

Yoshiki Nagatani[1,2], Isao Mano[2], Mami Matsukawa[2]; *[1]Department of Electronics, Kobe City College of Technology, Kobe, Japan, [2]Wave Electronics Research Center, Doshisha University, Kyoto, Japan*

Background, Motivation and Objective

In order to estimate the waves propagating inside human body, we have constructed a 3-D human body model which contains acoustic parameters (Abstract Book of 2012 IEEE IUS, p.529). By impressing a single pulse to human calcaneus using piezoelectric transducer, we showed that similar characteristics of two-group propagation in human inferior limb could be seen in both measurement and simulation. The simulation result revealed that the primary group propagates in bone portion (tibia, fibula, and femur) and the secondary group mainly propagates in soft tissue. However, the validity of the initial transmitted waveform was not clear. In this report, therefore, the estimation of wave propagation inside human body while walking or running was investigated.

Statement of Contribution/Methods

In order to observe the acoustic wave evoked by walking or running, the experimental measurements were performed. The vibration on the body surface were received by an acceleration sensor located on the greater trochanter. The participant with bare feet walks or runs on the floor, then the temporal waveforms were recorded by an oscilloscope. The participants were instructed to touch their heels to the floor while both walking and running. The mean intervals of each step were 0.50 seconds while walking and 0.26 seconds while running, respectively.

Results/Discussion

Figures (a) show the typical examples of observed waveforms within one step of walking and running. While the wavelength of the waveform of running was shorter than that of walking, the amplitude was much larger. The shorter pulse may come from the quicker performance of running motion, which results in faster velocity of leg part and higher impact of calcaneus to floor.

Figure (b) shows the sum of squares of acceleration waveforms, indicating the mean and standard deviation of ten trials. The results clearly shows that the total energy of propagation wave of running movement is much greater (about 10 times) than that of walking. Considering our previous finding that a pulse wave from calcaneus propagates in both bone part and soft tissue before arriving at greater trochanter (as shown in Figs.(c)), the observed results may be proportional to the amount of wave which propagated inside bone. The precise investigation of this new point of view brings us the information about the load to bone, and also will help us to estimate the regrowth of bone.

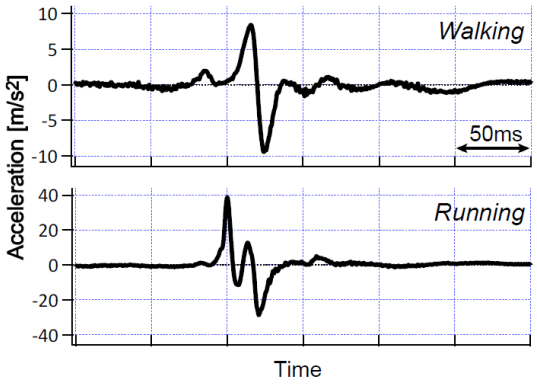

(a) Examples of Acceleration Waveforms Observed at Greater Trochanter

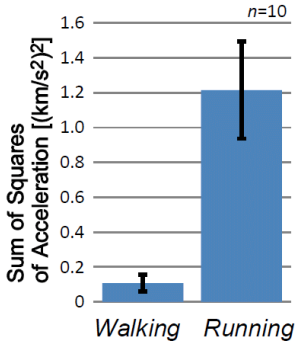

(b) Sum of Squares of Acceleration Waveforms

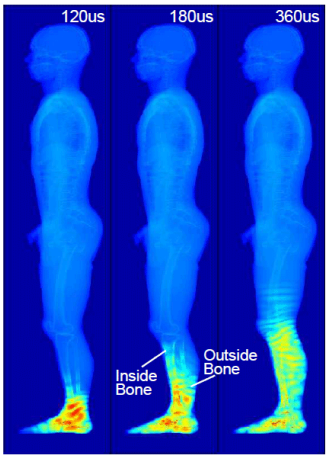

(c) Simulation of Wave Propagation (Single pulse was impressed to heel)

IUS1-PD4-2

Effect of collagen crosslinks on wave velocity in bone measured by a micro-Brillouin scattering technique

Ryo Tsubota[1], Shinya Murata[1], Mami Matsukawa[1], Mitsuru Saito[2], Keishi Marumo[2], Kazufumi Yamamoto[3]; *[1]Wave Electronics Research Center, Doshisha University, Kyotanabe, Kyoto, Japan, [2]Orthopaedic Surgery, Jikei University school of Medicine, Tokyo, Japan, [3]JA Shizuoka Kohseiren Enshu Hospital, Hamamatsu, Shizuoka, Japan*

Background, Motivation and Objective

Aging effects on the collagen in bone, such as oxidation and saccharification, induce advanced end products (AGEs). The abnormal AGEs crosslinks in bone are known to result in the decrease of mechanical strength. In this study, we have investigated the effects of artificial AGEs crosslinks on the longitudinal wave velocity in cortical bone using a micro-Brillouin scattering technique (μ-BR). The local wave velocities in a small area have been studied, considering the effect of AGEs crosslinks.

Statement of Contribution/Methods

The mid-shaft of a 32 month-old bovine femurs was cut into 4 film specimens (10 mm×5 mm) which were perpendicular to the radial direction. The specimen thicknesses were about 70 µm. For AGEs formation, specimens were incubated in a phosphate buffered saline (PBS) solution, with D-(-)-Ribose, Protease Inhibitor Cocktail Set III (without EDTA) and Penicillin-Streptomycin, for 14 days at 37 °C. Reference specimens were also incubated in a pure PBS solution. They were also kept at 37 °C for 14 days. Then, the amount of collagen in bone was calculated by measuring hydroxyproline by high-performance liquid chromatography. Longitudinal wave velocities in the bone axis or tangential directions were measured by µ-BR. The µ-BR system is composed of a tandem Fabry-Perot interferometer, a solid-state laser. An optical microscope system enables the measurement in a small area (diameter: 8 µm). The wave velocity in a specimen was defined as the average velocity value at 9 different positions in the specimen.

Results/Discussion

Figure 1 shows wave velocity changes in the bone axis direction. The velocities decreased in all incubated specimens more than 5 %. In the tangential direction, the decrease was around 5 %. These tendencies were not observed in the measurement of the reference specimens. In addition, the volume of AGEs crosslinks increased in all incubated specimens. Next, we investigated the velocity changes as a function of time to make sure the relation between velocity and crosslinking. The velocity was stable in the initial state but decreased monotonously as a function of time. The velocity decrease shows that AGEs crosslinks might alter the bone elastic property. Brillouin scattering can give us the velocity in a minute area. The results are not dependent of the bone microstructure and seem to show the changes in bone matrix.

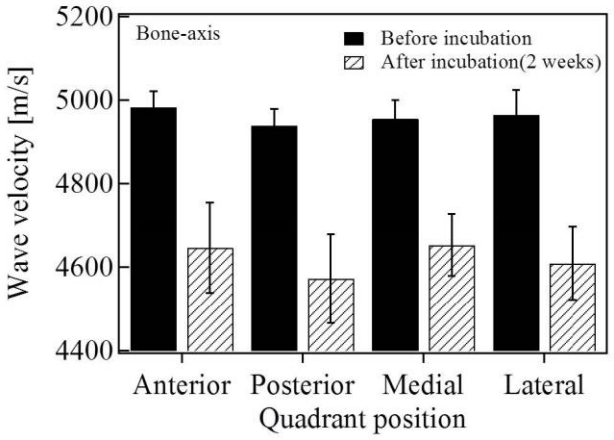

Fig.1 Wave velocity changes in bone axis direction.

IUS1-PD4-3

A novel procedure using multi-modal axial transmission for the characterization of elastic and geometrical properties of cortical bone

Josquin Foiret[1], **Jean-Gabriel Minonzio[1]**, Pascal Laugier[1], Maryline Talmant[1]; *[1]LIP, UPMC - CNRS, Paris, France*

Background, Motivation and Objective

To date, the only parameter evaluated in clinical ultrasound axial transmission (AT) is the speed of the first arriving signal. Recently the technique has evolved to a more sophisticated approach consisting in measuring multiple guided modes. This multi-modal AT has the potential to yield estimates of clinically relevant cortical bone properties. Last year, we reported successful estimates of cortical thickness (Ct.Th) on several ex vivo human radii, the elastic properties being fixed (Foiret et al., 2012 IUS). The present work aimed at assessing the whole inversion procedure on ex vivo human radius specimens with respect to a combined estimation of Ct.Th and elastic properties.

Statement of Contribution/Methods

The spectrum of guided waves was measured in five human radius specimens with a compact probe (directly in contact with the bone) dedicated for clinical use. The entire procedure can be summarized in three steps:

1/ a signal processing adapted to the multi-transmitter/multi-receceiver measurement configuration, based on singular value decomposition of the matrix response at each frequency

2/ identification of each measured trajectories of the spectrum to a Rayleigh-Lamb branche of a plate model

3/ inversion scheme by adjusting the geometric and elastic parameters of a plate model.

Steps 2 and 3 use a homogeneous free anisotropic plate model, described by four elastic parameters (bulk shear VT, compression along axis VL3, compression across axis VL1 velocities, Poisson ratio n) in addition to the thickness. The inversion scheme is designed to minimize the difference by considering simultaneously all measured trajectories.

High resolution computed tomography HR-pQCT measurements yielded a reference value of Ct.Th (Ct.Thref).

Results/Discussion

The S0, S1, A1 and S2 modes were preferentially observed in the thickness range of the specimens, in agreement with the modes excitability of the free plate.The results summarized in Table I show an overall good agreement between estimated Ct.Th and Ct.Thref while the elastic parameters were found to be consistent with the values found in the bone literature. The results highlight the potential of the approach based on the multi-modal analysis of guided waves to provide estimates of clinically relevant bone properties.

Specimen #	$Ct.Th_{ref}$ (mm)	Ct.Th (mm)	ν	V_T (m.s-1)	V_{L1} (m.s-1)	V_{L3} (m.s-1)
268D	1.1 ± 0.2	1.0	0.55	1680	2700	3840
251D	1.5 ± 0.2	1.4	0.53	1550	2570	4010
218D	1.5 ± 0.3	1.6	0.41	1860	3490	4130
227D	1.7 ± 0.3	1.7	0.49	1820	3250	3960
267D	2.7 ± 0.3	2.7	0.40	1910	3500	3870

IUS1-PD4-4

Multi-mode guided wave measurements in axial transmission on tubular bone-mimicking phantoms

Jean-Gabriel Minonzio[1], Josquin Foiret[1], Petro Moilanen[2], Jalmari Pirhonen[2], Zuomin Zhao[3], Maryline Talmant[1], Jussi Timonen[2], Pascal Laugier[1]; *[1]LIP, UPMC - CNRS, Paris, France, [2]Department of Physics, University of Jyväskylä, Jyväskylä, Finland, [3]Department of Electrical Engineering, University of Oulu, Oulu, Finland*

Background, Motivation and Objective

The context of this study is the evaluation of bone strength by guided mode measurements in axial transmission. As guided modes are sensitive to cortical elasticity and thickness, they are good candidates for providing clinically useful information on bone strength. Much work has been carried out with bone mimicking plates, much less with bone mimicking tubes. Bone-mimicking tubes with geometrical dimensions typical of those of human bones were measured in this study with the goal of investigating the effect of surface curvature on guided mode measurements. One of the important questions is whether the measured spectrum of guided modes can still be approximated by a plate model.

Statement of Contribution/Methods

Experimental wavenumbers of guided modes were obtained in the 0.4 – 2 MHz frequency bandwidth using a singular value decomposition approach developed previously by our group for a multi-emitter and multi-receiver probe. Minimization of the difference between experimental data and the theoretical result based on a free isotropic plate model, yields then estimates of the waveguide thickness and bulk velocities.

Experiments were carried out on five custom-made tubes, without and with a soft-tissue-mimicking coating. The tubes, with an external radius of curvature of 8 mm and wall thickness of 1 to 5 mm, were made of an isotropic absorbing bone-mimicking composite material (epoxy mixed with aluminum oxide powder), with shear and compression bulk velocities of cT = 1550 m.s-1 and cL = 3000 m.s-1 , respectively, and a density of ρ = 2.3 g.cm-3. The 5 mm thick soft coating (2.5 mm thick) was made of a mixture of silicone rubber and glycerol with a bulk compression velocity of cL = 1250 m.s-1 and a density of ρ = 1.1 g.cm-3.

Results/Discussion

Experimental wavenumbers were found to be in good agreement with those of the isotropic plate model. The main observation was that the curvature of the tube (measured either with or without the soft coating) had a weak impact on the guided modes in the frequency bandwidth considered.

In all cases difference between the reference and optimized thickness was less than 0.1 mm. In the thick tubes (2-5 mm), difference between the reference and optimized bulk wave velocities was less than 100 m.s-1. In the thinnest tube (1mm), that difference was about 300 m.s-1.

Our results indicate that the plate model is suitable for estimating the properties of tubes made of the same material, but have a different thickness. They also illustrate the potential of axial transmission to obtain estimates of clinically relevant bone strength factors such as the geometry and elasticity of the cortical shell.

IUS1-PD4-5

Variations in Reflection Properties of Fast and Slow Longitudinal Waves in Cancellous Bone with Boundary Condition

Atsushi Hosokawa[1]; *[1]Department of Electrical and Computer Engineering, Akashi National College of Technology, Akashi, Japan*

Background, Motivation and Objective

Fast and slow longitudinal waves propagating in cancellous bone can reflect at the boundaries of the cortical bone and bone marrow layers, but the reflection properties of these waves have not significantly been clarified. The purpose of this study is to numerically investigate the variations in the reflection properties with the boundary condition.

Statement of Contribution/Methods

The reflected waveforms at normal incidence to the boundaries of 100% and 0% bones (solid bone and water) were simulated using a finite-difference time-domain (FDTD) method with microcomputed tomographic (μCT) models of bovine cancellous bone filled with water. The reflection coefficients were calculated by comparing with the waveform simulated for the model with an artificial absorbing boundary.

Results/Discussion

The simulated results are shown in Figs. 1 and 2, as a function of cancellous bone porosity. In Fig. 1, the reflection coefficients of the fast wave at the 0% bone boundary are greater than those at the 100% bone boundary. In Fig. 2, the reflection coefficients of the slow wave at the 100% bone boundary are greater. These results agree with the fact that the fast and slow waves propagate mainly in the parts of the trabeculae and pores, respectively. For both waves, the porosity dependences of the reflection coefficients are observed to change with the boundary. The reflected wave at the boundary can be divided into 2 waves propagating in the trabecular and pore parts, and therefore, both the fast and slow incident waves can be converted to both the fast and slow reflected waves. It is considered that the wave conversions can be associated with the reflection properties, particularly the fast wave reflection at the 100% bone boundary and the slow wave reflection at the 0% bone boundary.

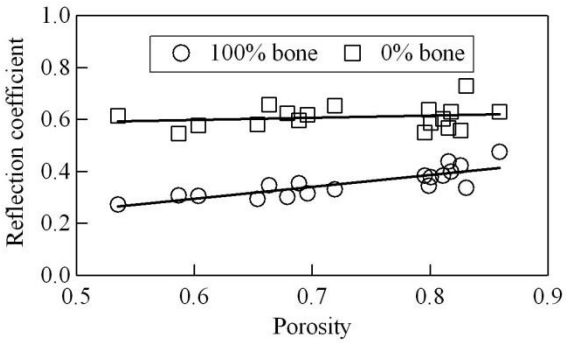

Fig. 1 Reflection coefficients of the fast wave.

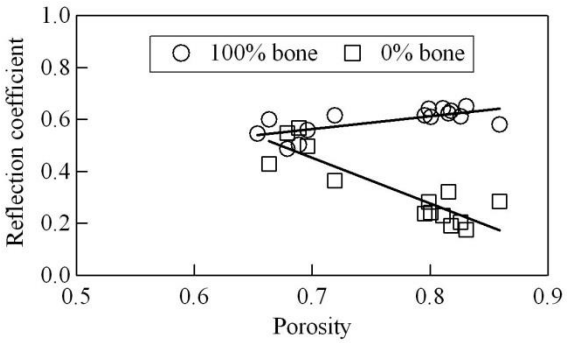

Fig. 2 Reflection coefficients of the slow wave.

IUS1-PD4-6

Photo-Acoustic Phase-Delayed Excitation of Guided Waves in Coated Bone Phantoms

Petro Moilanen[1], Ari Salmi[2], Pasi Karppinen[2], Vantte Kilappa[1], Zuomin Zhao[3], Risto Myllylä[3], Edward Hæggström[2], Jussi Timonen[1]; *[1]Department of Physics, University of Jyväskylä, Jyväskylä, Finland, [2]Department of Physics, University of Helsinki, Helsinki, Finland, [3]Department of Electrical Engineering, University of Oulu, Oulu, Finland*

Background, Motivation and Objective

Photo-acoustic skeletal quantitative ultrasound enables assessment of the fundamental flexural guided wave (FFGW), consistent with the F(1,1) tube mode, in bone through a coating of soft tissue. There is, however, interference due to ultrasound propagation in the soft tissue surrounding the bone. We aim to reduce this interference by using phase-delayed ultrasound excitation.

Statement of Contribution/Methods

The photo-acoustic phase-delayed excitation was tested experimentally on coated bone phan-toms. Four axisymmetric bone phantoms, made of a solid composite material (aluminum oxide and epoxy), featured wall thicknesses ranging from 1 to 4 mm. An elastomer coating (mixture of silicone rubber and glycerol; 5 mm thick) mimicked a layer of soft tissue on top of the bone. A fiber head composed of an array of four equally spaced (3.5 mm) optical fibers (0.4 mm diameter) was employed as the phase-delayed source. The fibers were illuminated by pulsed laser diodes (905 nm wavelength) with a tunable delay. Ultrasound was received by a small (10 mm diameter) custom-made piezo transducer from the top surface of the coating, 20-50 mm apart from the closest fiber. The recorded signals were analyzed using 2D-FFT.

Results/Discussion

Tuning of the phase-delay enabled selection of the mode(s) excited. FFGW was detected at a frequency band of 20-40 kHz when the power ratio between FFGW and interference was tuned to a local maximum (Fig. 1). This tuning removed interference and improved the signal-to-noise ratio of the FFGW mode by 10 to 20 dB. Phase-velocity of FFGW featured good consistency with theoretically predicted wall thickness sensitivity (Fig. 2). These results thus suggest that photo-acoustic phase-delayed excitation enables in vivo assessment of cortical thickness based on FFGW.

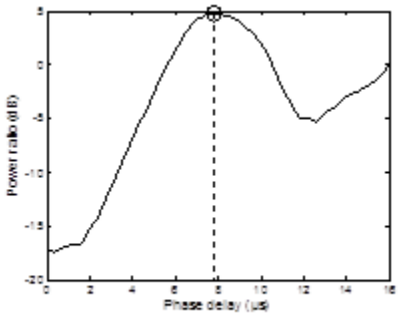

Fig. 1: (a) Optimal phase delay was chosen based on the local maximum in power ratio. Result is shown for a 2 mm tube.

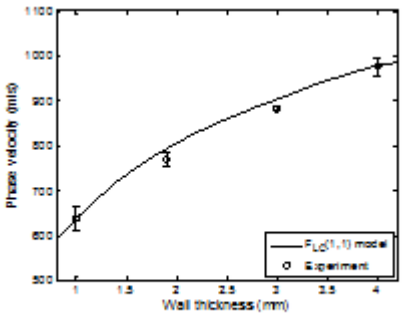

Fig. 2: Thickness dependence of experimental FFGW phase velocity (markers). The solid line is theoretical prediction.

IUS1-PD4-7

Finite difference elastodynamic code and semi-analytic diffraction coupling: an efficient approach to simulate in-vivo ultrasonic inspection of bone

Didier Cassereau[1], **Pierre Nauleau**[1], Aniss Bendjoudi[2], Emmanuel Bossy[2], Jean-Gabriel Minonzio[1], Pascal Laugier[1], Quentin Grimal[1]; *[1]Laboratoire d'imagerie parametrique (UPMC Paris6 - CNRS UMR7623), Paris, France, [2]Institut Langevin (ESPCI Université Paris7 - CNRS UMR 7587), Paris, France*

Background, Motivation and Objective

Ultrasonic inspection of bones is essential to get some information about the mechanical properties of the internal bone structure, and consequently evaluate the fracture risk. The numerical simulation of the interaction of the ultrasonic beam with bone helps the understanding of the complex phenomena that occur in such applications. For this purpose, elastodynamic Finite Difference Time Domain (FDTD) codes, which can take into account the complexity of the bone structure (in terms of its geometry as well as its spatial heterogeneities), are often used.

A sufficiently small spatial grid size is required to model the geometry accurately and to avoid numerical dispersion. In cases where the propagation in soft tissues must be modeled over many wavelengths (e.g. in in-vitro experiments in water tanks, in measurement of the hip region), the resulting computation time can be prohibitively high.

Statement of Contribution/Methods

In order to reduce the computation costs, we propose a coupling of two numerical approaches: (1) the propagation in soft tissues, modeled as a homogeneous fluid for the sake of simplicity, is calculated using standard diffraction formalism (http://iadc.info.espci.fr/dc/pass); (2) the propagation within and in the vicinity of bone structures is computed with FDTD (SimSonic, http://www.simsonic.fr). The method is applied to the ultrasonic inspection of circular and elliptical tubular bone phantoms, which are idealized models of the femoral neck.

Results/Discussion

We show how this coupling is performed and validated, and illustrate the gain in terms of the total computation time and memory resources needed. This gain can reach a ratio of more than 30 in quite standard situations, and this makes the difference between reasonable and impossible simulations.

Based on this coupled numerical scheme, we use the DORT approach (Prada et al., J. Acoust. Soc. Am 1998) with a phased-array probe, where each element is used in emission successively, therefore resulting in a complete transmit/receive simulation. Finally, from this set of transmit/receive signals, we can calculate the dispersion curves. The latter can subsequently be used to obtain some information about the thickness and mechanical properties of the inspected bone phantoms. In this presentation, we will expose the different steps of the coupled simulation approach and its validation based on the comparison of calculated and theoretical dispersion curves.

IUS1-PD4-8

Simultaneous Assessment of Bone Thickness and Velocity for Ultrasonic Computed Tomography Using Transmission-Echo Method

Rui Zheng[1], **Philippe LASAYGUES[1]**; [1]*Laboratory of Mechanics and Acoustics, CNRS, Marseille, France*

Background, Motivation and Objective

Ultrasonic computed tomography (UCT) has been applied to image internal structures and estimate cortical thickness and velocity of long bones such as tibia and fibula *in vitro*. To set up the initial models to be used by reconstruction, transmitted and echo signals collected from a pair of aligned transducers can be combined and implemented to simultaneously assess acoustic velocity and thickness of cortex. The goal of this study is to investigate the feasibility and robustness of the transmission-echo (TE) method applied to velocity and thickness estimation of double-layered thin bone samples, which is performed as a mimic model of long bones measured in UCT.

Statement of Contribution/Methods

Nine groups of samples with different combination of cortical thickness were assembled and one pair of immersion transducers with nominal frequency 1MHz was used for the experiments. The thickness of all samples is smaller than one wavelength referring to cortical bone tissue and ranged from 0.98 to 2.32 mm. For each group, one transmitted signal and two echo signals from both transducers were acquired and used for the further signal analysis. The TOF (time of flight) of seven pulses contained by transmitted, echo and reference signals were estimated by the wavelet-based processing (WBP) method and then used for the calculation of thickness and velocity. Among all measurements, three groups with the least thickness (~0.33 wavelength) are failed for the estimation, two groups with the most thickness (>0.6 wavelength) provide the best estimation, and other groups are only successful on the velocity estimation. For cortical thickness estimation, the mean relative error (referring to caliper measurement) of the "proper" samples, whose thickness is larger than half wavelength, is 5.68%, however the samples with thickness smaller than half wavelength cannot be accurately calculated. For acoustic velocity estimation, the TE method shows better performance, most samples can be measured, and the relative error (referring to the results measured by echo method and single sample) is as low as 4.64%.

Results/Discussion

The results demonstrate that the TE method has the potential to simultaneously assess bone thickness and velocity in the condition of UCT. The measurements show good agreement with others performed by conventional methods. However when the samples are too thin, the thickness measurement will be failed due to severe interference caused by large wavelength. On the other hand, the velocity estimation is less influenced by sample thickness, which will be an advantage on providing reliable background information for imaging. Summarily, the TE method can be applied to determine the inversion parameters before imaging, yet more effort should be attributed to the detailed studies of experimental parameters and conditions such as the applied ultrasound wavelength, the interference of other waves.

Therapy II

Forum Hall

Thursday, July 25 2013, 01:00 pm - 04:30 pm

Congress Hallair: **Emad Ebbini**
University of Minnesota

IUS1-PD5-1

Contrast-Enhanced Ultrasound Imaging for the Detection of Transient Dynamics of Blood-Brain Barrier Opening Induced by Focused Ultrasound

Ching-Hsiang Fan[1], Wun-Hao Lin[1], Chien-Yu Ting[1], Wen-Yen Chai[2], Hao-Li Liu[2], Tzu-Chen Yen[3], Chih-Kuang Yeh[1]; *[1]Biomedical Engineering and Environmental Science, National Tsing Hua University, Taiwan, [2]Department of Electrical Engineering, Chang-Gung University, Taiwan, [3]Department of Nuclear Medicine, Chang Gung University College of Medicine and Memorial Hospital, Taiwan*

Background, Motivation and Objective

Focused ultrasound (FUS) with microbubbles (MBs) has been shown to induce local blood-brain barrier (BBB) opening, enhancing therapeutic agents into the brain. Previous works showed FUS BBB-opening may accompanied with vessel constriction, and may lead to regional blood flow and perfusion change under various FUS condition. In this study, we propose the use of destruction/ reperfusion (D/R) technique in contrast-enhanced (CE) ultrasound imaging to monitor transient perfusion change after FUS BBB-opening and also to characterize the dependence of the perfusion change to FUS exposure level.

Statement of Contribution/Methods

Six Sprague-Dawley rats were performed with craniotomy prior FUS exposures. A confocally-arranged holder integrated a single-element 2.25-MHz FUS transducer and a 21-MHz linear array probe (Vevo2100 imaging system) was designed. The FUS (0.9 to 1.3 MPa, duty cycle: 0.1 %, and sonication time: 60s) was delivered to the left hemisphere following MB injection to induce intact or hemorrhagic BBB-opening. A series of D/R B-mode images (nonlinear contrast mode) were acquired and the corresponding time-intensity curves (TICs) were constructed. The TICs were then performed with sigmoidal function fitting and the derivative parameter (e.g., rate constant) dependent to flow velocity was identified. The dynamic CE-MRI images were also acquired to depict kinetics of permeability change (Ktrans) for comparison.

Results/Discussion

We observed that FUS BBB-opening induces transient perfusion changes, and the perfusion of the FUS-exposed areas decreased apparently, which may be due to local vasoconstriction. The distributions of flow velocity were highly correlated with the Evens Blue staining sections and Ktrans mapping (fig. A-C). The perfusion change (subtraction rate constant maps between pre- and post-sonication) was related to FUS exposure levels (fig. B), and the TICs reflect the RBC extravasations and seems to be effective to depict the BBB-opening level (either intact or hemorrhagic).

We successfully demonstrated that the CE D/R technique can serve as a useful tool to transiently monitor FUS-induced BBB-opening, and potentially to characterize the occurrence of microhemorrhages. Applications include applying such immediate-feedback control tool for safety issue by preventing the induction of hemorrhage during FUS treatment.

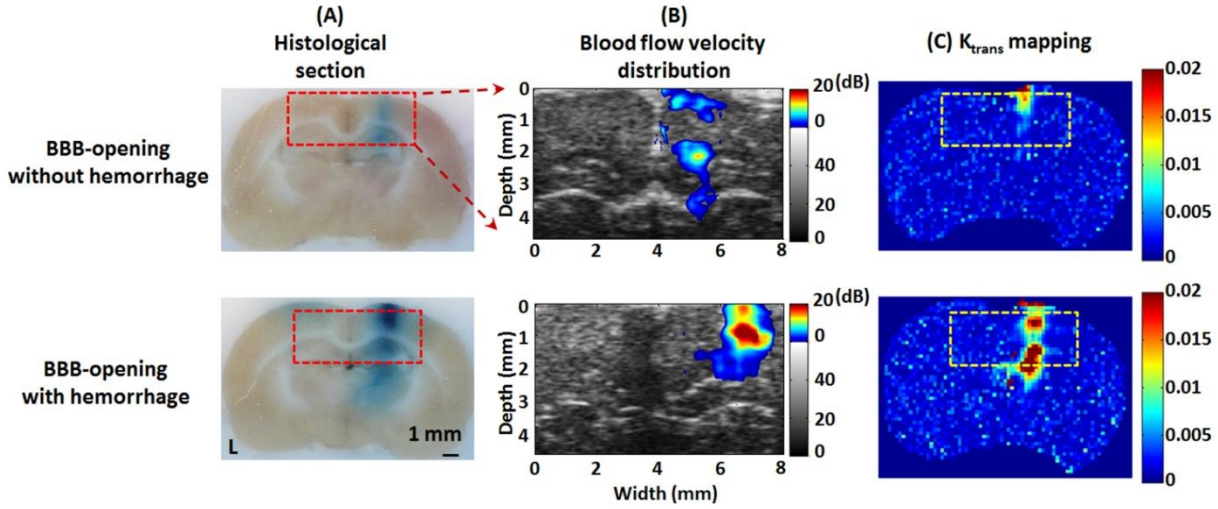

IUS1-PD5-2

High-Sensitivity Distribution Mapping of Iron, Zinc and Copper during SPIO-Microbubbles Facilitated Focused Ultrasound Induced Blood-Brain Barrier Opening via Laser Ablation/Inductively Coupled Plasma Mass Spectrometry

Ching-Hsiang Fan[1], Chien-Yu Ting[1], Yi-Kong Hsieh[1], Hao-Li Liu[2], Chu-Fang Wang[1], Chih-Kuang Yeh[1]; *[1]Department of Biomedical Engineering and Environmental Sciences, National Tsing Hua University, Hsinchu, Taiwan, [2]Department of Electrical Engineering, Chang-Gung University, Taoyuan, Taiwan*

Background, Motivation and Objective

Focused ultrasound (FUS) with microbubbles (MBs) has been approved to achieve the local blood-brain barrier disruption (BBBD), increasing therapeutic agents into brain. Previous reports have demonstrated the use of medical imaging (ultrasound, CT, MRI, SPECT, or PET) to observe the redistribution of the delivered substance. However, the

redistribution of the element such as zinc or copper has not yet been discovered, nor its effects and roles to CNS after sonications. Laser ablation/inductively coupled plasma mass spectrometry (LA-ICP-MS) is a sensitive analytical technique and capable of quantitatively providing solid inorganic matrices distribution in tissues. In this study, we used LA-ICP-MS to explore its feasibility on detecting the delivered iron (i.e., SPIO-conjugated MBs) and its redistribution after magnetic targeting (MT), as well as the element redistribution.

Statement of Contribution/Methods

Six Sprague-Dawley rats were used. The 1-MHz FUS (acoustic energy = 0.7 MPa, duty cycle = 5%, sonication = 2 min) was exposed to left brain of animals after SPIO-MBs injection to induce BBBD (SPIO payload was 200 ± 19.6 μg by ICP-AES). A 0.5 T permanent magnet was attached to the rat′s scalp for performing MT. The spatial elemental maps were performed with the LA-ICP-MS system excited by 213 nm Nd-AG laser (energy = 1.6 mJ, frequency = 10 Hz, scanning speed = 90 μm/s). The distribution and concentration of elements including iron, copper, and zinc were analyzed.

Results/Discussion

Results demonstrated that LA-ICP-MS performs high sensitivity in the detection of the element distribution in the brain. The iron mapping revealed that the SPIOs were highly concentrated at FUS exposed and MT site. Quantitative elemental analysis showed that the MT further increase local SPIO concentration at the BBBD site from a 7.7- and 21.5-fold increase compared to the control brain. No obvious local zinc and copper deposition in sonication regions after sonication.

This study showed the potential of LA-ICP-MS for providing highly-sensitive detection method of solid inorganic matrices in brain tissues, and is also beneficiary in detecting trace element redistribution. Moreover, concurrent the use of SPIO-MBs with MT further enhanced the SPIO delivery into the BBBD area. Future work includes using SPIO-MBs as a surrogate tracer to estimate drug delivery efficiency during BBBD.

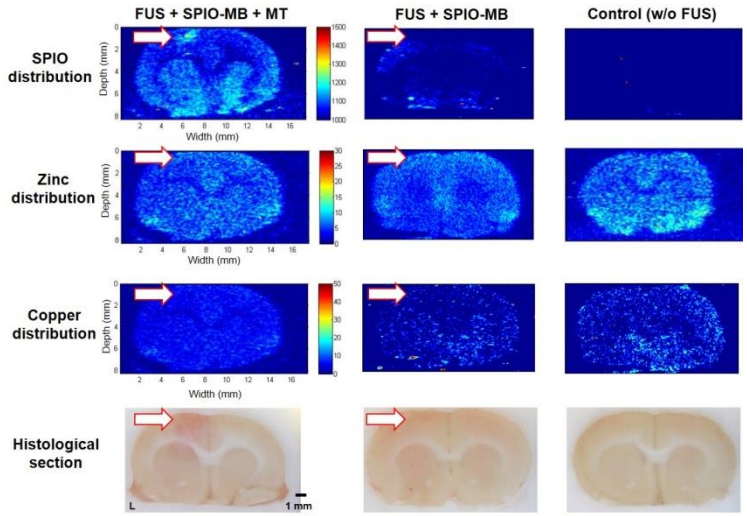

IUS1-PD5-3

Intrinsic Contrast Based Ultrasound Time Intensity Curve Analysis for Monitoring Focused-Ultrasound Induced Blood-Brain-Barrier Disruption

Nai-Ying Kuo[1], Po-Hsun Wang[1], Hao-Li Liu[2], Meng-Lin Li[1,3]; *[1]Electrical Engineering, National Tsing Hua University, Taiwan, [2]Electrical Engineering, Chang Gung University, Taiwan, [3]Institute of Photonics Technologies, National Tsing Hua University, Taiwan*

Background, Motivation and Objective

Recently, focused ultrasound (FUS) has been proved to be able to open the blood brain barrier (BBB) temporarily, locally, and reversibly, which can increase the performance of the treatment. However, FUS can be harmful if the applied acoustic pressure is too high. Therefore, an imaging technique that can monitor the dynamic response of FUS-induced BBB opening in real time is desirable.

Statement of Contribution/Methods

In this study, we propose an intrinsic contrast based ultrasound time intensity curve (TIC) technique for real-time monitoring the dynamic response of FUS-induced BBB opening on a rat model. The BBB were disrupted by 1-MHz FUS in a tone-burst mode (repetition rate: 1Hz, duration: 90 seconds/spot, cycles: 10,000) with the company of microbubbles (Sonovue). Cases with and without cerebral microhemorrhage when performing FUS-incuded BBB opening were investigated. At 40-MHz imaging frequency, the changes of signal intensity in the sonicated brain area mainly resulted from the changes in cerebral blood flow at the BBB foci, and hemorrhage would also contribute to the signal enhancement. The TIC then could be used to analyze the variation of the cerebral blood flow and hemorrhage during FUS-induced BBB opening.

Results/Discussion

Our results showed that in the cases without microhemorrhage, the TICs of the left (sonicated) and the right (control) brain had no specific tendency but the TICs of the right brain were higher than those of the left brain at least over 60 minutes, suggesting that FUS possibly induced vasoconstriction, and thus caused reduction of blood volume or ischemia at the sonication foci. In the case with microhemorrhage, the ultrasonic intensity of the left brain sharply increased immediately after the sonication while that of the right brain stayed on the baseline. The TICs of microhemorrhage would finally converge to the baseline or saturate in a higher level. The hemorrhage provided much more influence on the TIC than vasomotion, and the convergences of the TIC might reflect to the clearance of the hemorrhage. Overall, it is shown that the TIC technique provide a unique opportunity to characterize the degree of hemorrhage by analyzing the intrinsic contrast based TICs. More studies are required to explore the mechanism of these TIC responses. Contrast enhanced MRI and photoacoustic microscopy will be used to confirm the results in the future.

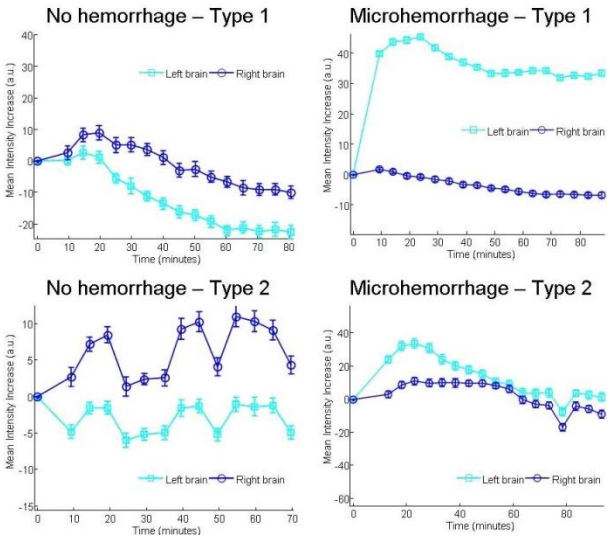

IUS1-PD5-4

Intra-cerebral diffusion of Irinotecan and Temozolomide after US-induced opening of the blood-brain barrier with an unfocused ultrasound device in rabbits

Kevin BECCARIA[1,2], Michael CANNEY[2], Lauriane GOLDWIRT[3], Christine FERNANDEZ[3], Julie PIQUET[4], Cyril LAFON[5,6], Jean-Yves CHAPELON[5,6], Alexandre CARPENTIER[1,7]; *[1]Neurosurgery Department, Pitie-Salpetriere Hospital, Paris, France, [2]CarThera Research Team, Paris, France, [3]Pharmacology Department, Pitie-Salpetriere Hospital, Paris, France, [4]Laboratory of Biosurgical Research, Universite Paris Descartes, Sorbonne Paris Cite, Paris, France, [5]Inserm, U1032, LabTau, Lyon, France, [6]Lyon 1 University, Lyon, France, [7]Sorbonne University, Paris 6 School of Medicine, Paris, France*

Background, Motivation and Objective

The blood-brain barrier (BBB) is a physiological impediment to the intra-cerebral diffusion of drugs in the treatment of primitive brain tumors. In this work, we assessed the intra-cerebral diffusion of Irinotecan (CPT11) and Temozolomide (TMZ) after US-induced BBB opening with an unfocused ultrasound transducer.

Statement of Contribution/Methods

Seventeen White New Zealand rabbits were sonicated on a region of the right hemisphere after craniotomy and in the presence of SonoVue (0.03 mL) while seventeen others served as controls and had only right craniotomy, without sonication and without SonoVue injection. US-induced BBB opening of sonicated rabbits was performed by pulsing a 1 MHz planar ultrasound transducer with a duty cycle of 2.5% and an in situ acoustic pressure level of 0.6 MPa. Twenty rabbits received CPT11 (6mg/kg) and fourteen rabbits received TMZ (75mg/m2). Two different timings of drug injection were assessed. In the first protocol (â€œH0.5â€ •, n=16), the drug was injected at T-5min, blood was harvested at T+25min and the animals were sacrificed at T+30min. In the second protocol (â€œH0.75â€ •, n=18), the drug was injected at T+15min, blood was harvested at T+40min and the animals were sacrificed at T+45min. The blood and intra-cerebral concentrations of CPT11 and TMZ were measured by Ultra-Performance Liquid Chromatography (UPLC).

Results/Discussion

Intra-cerebral concentrations of both TMZ and CPT11 were enhanced in regions where the BBB was opened in comparison to the contralateral hemisphere in both protocols ($p<0.01$ and $p<0.0001$ for CPT11, and $p=0.02$ and $p=0.03$ for TMZ, at H0.5 and H0.75 respectively). The same significant difference was observed when the concentration of drug in the rabbits with BBB opening was compared against the group without opening ($p<0.001$ and $p<0.0001$ for CPT11, and $p<0.01$ and $p=0.02$ for TMZ, at H0.5 and H0.75 respectively). Intra-cerebral diffusion of drugs in control hemispheres was considered as spontaneous diffusion. It was on average 2.5% for CPT11 and 34% for TMZ. After opening of the BBB, intra-cerebral diffusion of drugs was increased by +159% for CPT11 and by +23% for TMZ. Intra-cerebral diffusion of both CPT11 and TMZ was systematically significantly improved in the cortex ($p<0.05$), but it was more heterogeneous in the deep brain. No significant difference was observed between the non-sonicated hemispheres of treated and control rabbits.

Intra-cerebral diffusion of both Irinotecan and Temozolomide can be enhanced after US-induced opening of the BBB with our unfocused ultrasound transducer. Work supported by CarThera SAS.

IUS1-PD5-5

Active Control of Bubble Liposome through Artificial Capillary by Using Matrix Array Transducer

Ren Koda[1], Naoto Hosaka[1], Shinya Onogi[1], Takashi Mochizuki[1], Kohji Masuda[1], Ryo Suzuki[2], Kazuo Maruyama[2]; *[1]Tokyo Univ. of A & T, Japan, [2]Teikyo Univ., Japan*

Background, Motivation and Objective

We have ever reported our attempts to control microbubbles (MBs) using the primary and secondary acoustic force for active control in artificial blood vessels. Recently, we have demonstrated active path selection of MBs by using a matrix array transducer to produce multiple focal points. However, we used the MBs which were mimicking of ultrasound contrast agent, they had been developed for industrial purpose and then were not possible to be used for medicine. On the other hand, bubble liposomes (BLs) had been developed being safe *in vivo* and easily modifying targeting ligand. In this study, we investigated the BLs control in multi-bifurcated flow of artificial blood vessel with multiple focal points of US.

Statement of Contribution/Methods

We used the liposomes (BLs) entrapping perfluoropropane gas with the average diameter of 500 nm. Also we prepared an artificial blood vessel according to a capillary model, which was made of poly (vinyl alcohol) with the path width of 0.7 - 1.4 mm. A matrix array transducer (Tr) was set to propel the streaming of BLs to a desired path in the capillary. Tr has air-backed 64 PZT elements with the aperture of 23.9 x 23.9 mm^2, the size of each element of 2.9 x 2.9 mm^2, respectively. Tr was driven by a continuous square wave with frequency of 1 MHz, where the drive unit was required to produce that with minimum delay pitch of 5 ns. We calculated delay time of divided in two parts with 32 elements to produce two focal points of ultrasound.

Results/Discussion

Fig.1(a) shows the microscopic image of BLs thorough the bifurcations overlapped sound pressure distribution from Tr. The positions of two focal points of P and Q were set according to the capillary structure. The maximum sound pressure was about 150 kPa-pp. Flow velocity was set 40 mm/sec. The microscopic image of MBs was also shown in Fig.1(b) to compare BLs behavior to our previous research. In Fig.1(b), the streaming of MBs was smoothly propelled to a desired path (Path B). On the other hand, the streaming of BLs was viscously propelled to Path B. The differences were seemed to be come from the shell properties of BLs and MBs. BLs are much tied each other because of surface interaction of the lipid membrane and then caused a resistance to flow. In conclusion, active control of BLs was confirmed by using a matrix array transducer. We are going to measure controllability of BLs quantitatively for precise evaluation.

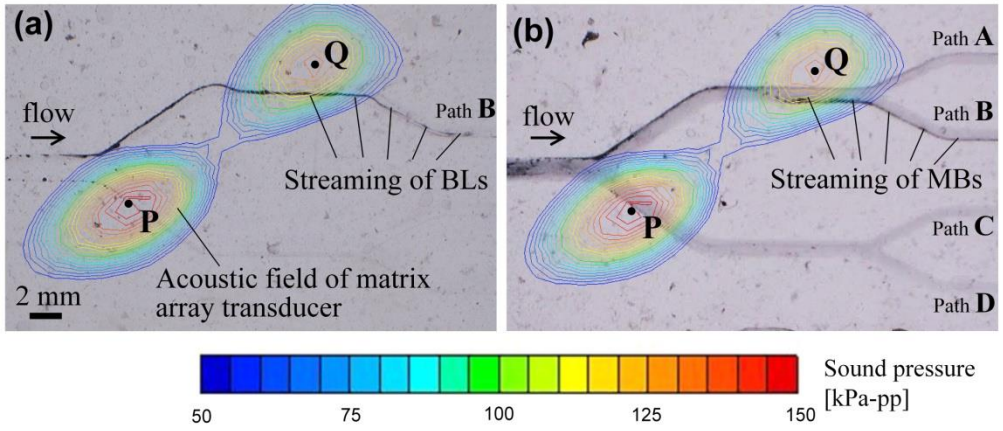

Fig. 1: Microscopic results with the distribution of sound pressure targeted at P and Q. (a)BLs, (b)MBs

IUS1-PD5-6

Nonlinear mixing of two ultrasonic beams for transcranial sonothrombolysis

Hermes Kamimura[1], Pedro Pinto[2], Theo Pavan[1], Octávio Pontes-Neto[2], Antonio Carneiro[1]; [1]*Department of Physics, University of São Paulo, Ribeirão Preto, São Paulo, Brazil,* [2]*Department of Neuroscience and Behavioral Sciences, University of São Paulo, Ribeirão Preto, São Paulo, Brazil*

Background, Motivation and Objective

The enhancement of the fibrinolytic effect of rtPA under ultrasonic radiation - called sonothrombolysis - has been explored in the treatment of stroke. The use of ultrasound (US) in the MHz range for this technique is recommended because lower frequencies (kHz range) promote better dissolution of clots and better penetration in the skull but it is still debated if they may increase bleeding rates due to thermal effects and standing waves formation in the brain. In the study presented here, we set two cofocused ultrasonic beams in the MHz range aiming to generate a focused low-frequency component (kHz) on the thrombus for its dissolution.

Statement of Contribution/Methods

A 2-element confocal US transducer was placed in front of an acrylic cylinder (125x3x95mm) used to simulate a skull. Initially, the transducer was driven by a signal of 3.2 MHz with the amplitude modulated (AM) at 20 kHz. In a second experiment, the elements were driven by 2 signals with frequencies of $3.2 \pm \Delta f/2$ MHz, where Δf = 20 kHz. A laser Doppler vibrometer (Ometron VQ-500-D-V) mapped the Δf–component of the acoustic field based on the acousto-optics phenomenon. The US transducer and the cylinder were moved in a raster pattern to form the images of the acoustic fields. Additionally, the same experiment was performed with a 2.25 MHz planar transducer modulated at 20 kHz (AM).

Results/Discussion

Fig.1 shows the acoustic fields at 20 kHz for the planar and confocal transducers. Standing waves were observed when AM-mode was used for both the planar and focal transducers. The Standing Wave Ratios (SWR) - the mean pressure in the antinodes divided by the mean pressure in the nodes - were 3.99, 1.18 and 0.95 for the planar (P), focal (F), and confocal (C) transducer, respectively. The effectiveness of the methods in focusing the beams is measured by the ratio (R) of the maximum pressures by the average pressures for each transducer, R_P = 37.9, R_F = 44.8, and R_C = 60.3. The nonlinear mixing of the two ultrasonic beams suppressed the standing wave formation in the kHz range and focused the kHz-field in the focal zone. The narrow kHz field may limit the damage (hemorrhage) of the surrounding tissue by avoiding thermal effects or cavitation in unwanted regions. Furthermore, it allows multifrequency excitation of the blood clot by combining frequencies in the driven signals, which has potential therapeutic applications for sonothrombolysis.

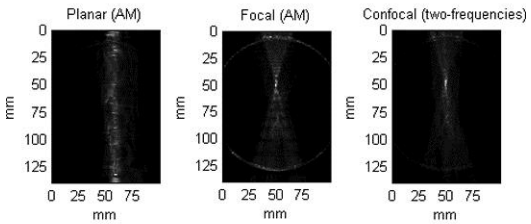

Fig. 1: 20-kHz-fields for the planar and confocal transducer. Standing waves are observed in the AM-mode images. The use of two-frequencies strengthened the 20 kHz acoustic field in the focal zone.

IUS1-PD5-8

Controlled induction of mechanical bioeffects with pulsed ultrasound and chemical agents

Ken-ichi Kawabata[1], Rei Asami[1], Reiko Ashida[2]; [1]*Medical Systems Research Department, Central Research Laboratory, Hitachi, Ltd., Kokubunji, Tokyo, Japan,* [2]*Departments of Cancer Survey and Gastrointestinal Oncology, Osaka Medical Center for Cancer and Cardiovascular Diseases, Higashinari, Osaka, Japan*

Background, Motivation and Objective

There have been many studies on non-invasive tumor treatments using ultrasound bioeffects. Until recently, cavitational bioeffects have not been playing major roles in the studies. Histotripy is expected to widen the applicability of cavitational bioeffects especially mechanical ones. It utilizes extremely intense (typically more than 10 kW/cm^2) and short pulse waves for reproducible cavitation induction. The idea of histotripsy is great and proved to work magnificently. Still, its applicability would be significantly increased if required intensity can be reduced. Reduced intensity would lead to a reduced size of the transducer and increased targetability in deep regions in the body.

We propose a method of inducing mechanical effects by precursors to generate microbubbles. Our method differs from histotripsy, which uses bubbles induced from dissolved gas species in tissues.

In this paper, results on preliminary *ex vivo* studies on 'low intensity' site-selective tissue structure destroying with locally injected chemicals will be presented.

Statement of Contribution/Methods

Microbubble precursors were prepared as emulsions by an extruder method from mixtures of perfluoropentane / perfluorohexane and an aqueous phospholipid suspension. Freshly excised chicken breast tissues were used as samples. A 0.5 ml aliquot of emulsions containing ca. 0.1 mg of perfluorocarbons were injected into samples and they were exposed to pulses of focused ultrasound at 1 MHz in a water tank. Typical acoustic conditions were as follows: pulse intensity = 2 kW/cm^2, duration = 200 cycles, repetition frequency = 0.5 kHz, exposure time = 30 sec.

Results/Discussion

It was confirmed by both gross and microscopic observations that ultrasound exposure with conditions described in the Methods section destructs structures of tissue samples completely. The acoustic intensity threshold required for such structure destruction was found to be about 1 kW/cm^2. Increasing the intensity increased the speed for the destruction. Moreover, it was suggested that structure-destroyed tissues aid to destroy surrounding regions. After treating a site, another ultrasound exposure to the surrounding area destroyed tissues if the focus was set to overlap with the pre-treated site. Such enlargement of tissue-destructed area was possible even to areas where precursors had not been injected. Thus, regions without injected precursors are also targetable in our method. Since precursor-injected regions as well as cavitation induction were visualized by ultrasound imaging, our method can give a highly controllable treatment modality with relatively mild ultrasound conditions. Our approach would be applicable for the treatment of deep-seated and hypovascular tumors such as pancreatic cancer.

IUS1-PD5-9

Three-dimensional design of acoustic field to trap higher amount of microbubbles in flow using a matrix array transducer

Naoto Hosaka[1], **Kohji Masuda**[1], Ren Koda[1], Takashi Mochizuki[1], Shinya Onogi[1]; [1]*Tokyo Univ. of A&T, Japan*

Background, Motivation and Objective

In therapeutic applications using microbubbles under ultrasound exposure, as the purpose of improvement of thermal efficiency in HIFU, because of the diffusion of in vivo microbubbles, it is difficult to enhance the local density of microbubbles near the desired target area. Thus we challenged to produce a three-dimensional acoustic field to trap higher amount of microbubbles in flow.

Statement of Contribution/Methods

We used a flat matrix array transducer including 64 PZT elements on the surface, which was newly developed to guarantee steerable area and to produce a continuous wave, where the waveform is different from HIFU therapy. We prepared a thin channel made of poly(ethylene glycol), which was fixedly floated from the bottom of a water tank, to suggest the behavior of microbubbles in a capillary of an internal organ. We observed the channel through the transparent bottom plate of the tank by using a microscope. The flow velocity of microbubbles (average diameter of 4 μm) suspension was 10 mm/s. We designed various shapes of acoustic fields, which were produced by setting delay time in 64 elements individually, where the maximum acoustic intensity was unified.

Results/Discussion

To evaluate the trapped area of microbubbles quantitatively, we calculated by processing successive microscopic images. As shown in Fig, microbubbles were propelled by primary acoustic force and trapped in the middle of the channel. Comparing the trapped areas in the horse shoe and the ring shapes of acoustic field, the former trapped area was obviously more than the latter one, where the acoustic energy in the latter one was considered to be more dispersed than that in the former one. The result indicates that there should be an appropriate shape to trap microbubbles according to the distribution of microbubbles in flow. Here it must be noted that though the behavior of microbubbles in a thin channel is not equal to that in an actual capillary, density distribution of trapped microbubbles can be predicted where small vessels are concentrated. In conclusion, we have confirmed that there is a relation between the trapping performance of microbubbles and the shape of acoustic field.

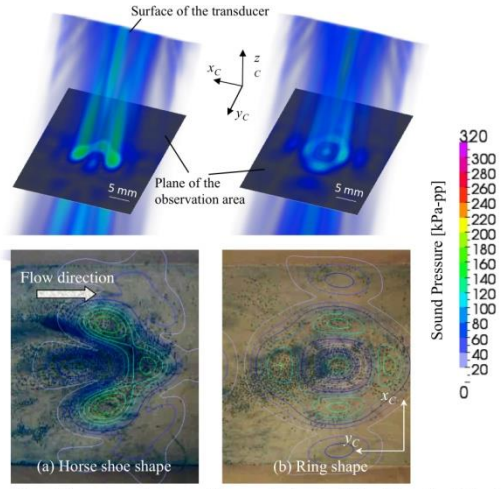

Fig. Microscope images of trapped microbubbles 30 s after injection under exposure of two shapes of acoustic field (flow velocity 10 mm/s).

IUS1-PD5-10

A Novel Use of Chitosan Combines with Ultrasound for Body Weight and Local Fat Controlled in Mice.

Ai-Ho Liao[1], **Wan-Chun Ma[1]**; *[1]Graduate Institute of Biomedical Engineering, National Taiwan University of Science and Technology, Taiwan*

Background, Motivation and Objective

Recently, ultrasound has been used for reduction of localized adiposities in human. In this study, chitosan, an important product in the treatment of hyperlipidemic diseases and fatty liver, combines with ultrasound to control weight loss and local fat pad in mice was evaluated.

Statement of Contribution/Methods

ICR female mice (47-56g) were randomly divided into four groups: (1) control group (C); (2) only ultrasound (U) (3) only chitosan group (CIS); (4) chitosan combine with ultrasound group (CU). The body weight measurements, evaluations of fat pad and abdominal subcutaneous fat thickness by US imaging were performed before and after treatment. Plasma total, HDL-cholesterol, total triglyceride and plasma LDL-cholesterol concentrations off the blood samples from all mice were measured.

Results/Discussion

The mean thicknesses of the epididymal fat pad were 3.67 and 3.53 mm prior to the treatment interventions (Fig. 1A-B), and 3.93, 2.50 mm after treatment (Fig. 1C-D) in the C and CU groups, respectively. The reductions in epididymal fat pad thicknesses were greater in the CU group (-28.2%) than other groups. The reduction in the size of adipocytes in the epididymal fat pads (Fig. 1E-F) was 32.8um markedly greater in the CU group than 72.1um in the C group and the accumulation of fat vacuoles (arrows) in the liver was clearly decreased in the CU and compared with the C groups (Fig. 1G-H). CU group decreased triglyceride and low density lipoprotein cholesterol by 25% and 26%. This method could reduce the thickness of local fat and decrease the plasma levels significantly.

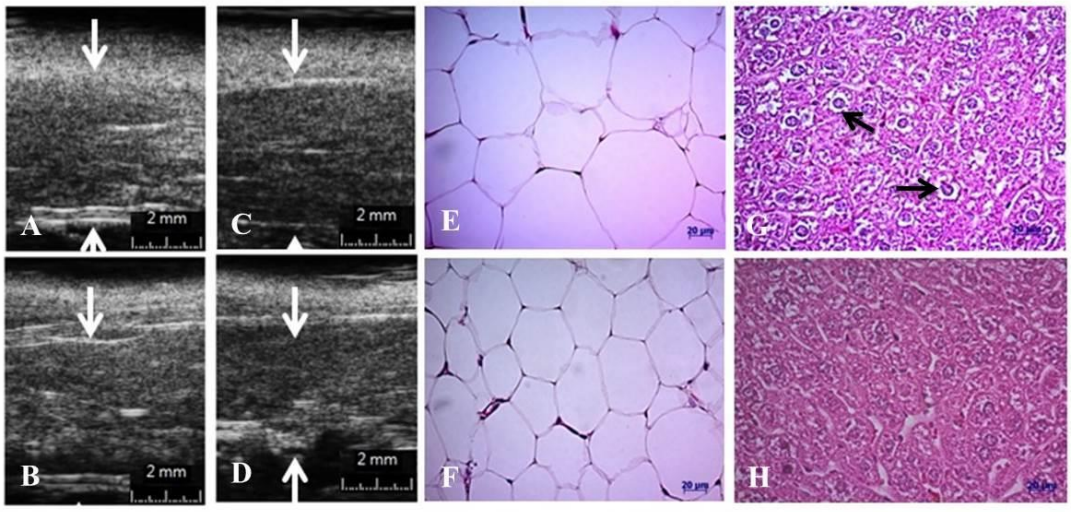

IUS1-PD5-11

Efficient Generation of Cavitation Bubbles in Rose Bengal Solution by Ultrasound Exposure with Negative- Followed by Positive-Peak-Pressure Emphasized Waves

Jun Yasuda[1], Ayumu Asai[1], Shin Yoshizawa[1], Shin-ichiro Umemura[2]; *[1]Department of Communication Engineering, Tohoku Univ., Sendai, Miyagi pref., Japan, [2]Department of Biomedical Engineering, Tohoku Univ., Sendai, Miyagi pref., Japan*

Background, Motivation and Objective

In therapeutic application of acoustic cavitation bubbles, generating them at high efficiency is important.

In our previous study, we have suggested the second-harmonic superimposition method, in which N- and P-waves emphasizing either the peak negative or positive pressure, respectively, are synthesized and the exposure with N- immediately followed by P-waves (NP sequence) can generate cavitation bubbles efficiently. In the medical ultrasound field, the effect of cavitation bubbles can be applied to HIFU treatment, lithotripsy and histotripsy.

It has also been shown that rose bengal (RB) can reduce the cavitation threshold and has potential as a sonochemically active agent for cancer treatment.

In this study, the amount and behavior of the cavitation bubbles generated by such an NP sequence in a RB aqueous solution are investigated.

Statement of Contribution/Methods

The RB solution was injected into the optically transparent gel and the cavitation bubbles generated in the solution were observed by using a high-speed camera. Three different concentrations of RB solution, 10, 1, 0.1 mg/kg, and distilled water were used. The ultrasonic intensities from 15 kW/cm^2 to 40 kW/cm^2 at the fundamental frequency was 0.8 MHz were used for the exposure..

Results/Discussion

Figure 1 shows the high-speed camera pictures and the time history of the cavitation area. The cavitation area was calculated from the high-speed images. The captured images were binarized and the number of pixels of the cavitation area was counted and then, the cavitation area was calculated by multiplying the detected number of pixels by the area of one pixel.

No cavitation bubbles were observed in the case of distilled water. Due to the reduction of the cavitation threshold by RB, the cavitation area generated by the N waves became larger as the concentration of the solution was higher.

On the other hand, the amounts after the exposure to P waves did not seem to depend on the concentration.

The experimental results show NP sequence can generate cavitation bubbles at high efficiency in the case of only 0.1 mg/kg of RB solution and more cavitation bubbles can be generate by higher concentration solution.

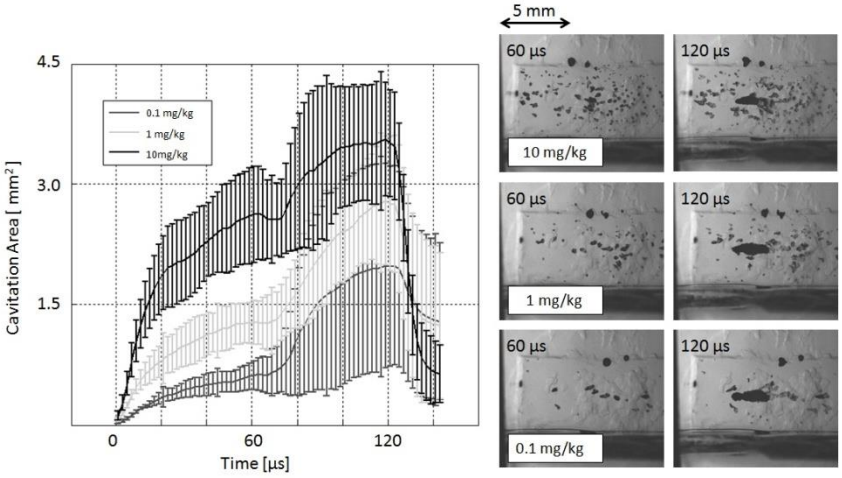

Figure 1 Time History of Cavitation Area and High-Speed Camera pictures

IUS1-PD5-12

Ultrasonic Monitoring of Cavitation-Induced Damage in Articular Cartilage

Christoffer Fridlund[1], Heikki Nieminen[1], Edward Hæggström[1]; [1]*Department of Physics, University of Helsinki, Finland*

Background, Motivation and Objective

We have shown that 20 kHz intense ultrasound (HIU, 76 W/cm^2) may permit drug delivery into articular cartilage (AC) [1]. Here we investigated at 5 different time points, using SAM, damage to AC that we ascribe to cavitation occurring during HIU.

Statement of Contribution/Methods

This study is important, because cavitation that may occur during HIU drug delivery needs to be monitored. This study shows that quantitative US can monitor cavitation-related damage in AC.

We prepared an osteochondral plug (N = 1, 28 mm in diameter) from a femoral condyle of a young cow. A 20 MHz SAM (Olympus Probe V317, 26.4 mm focal length) recorded 2D images from AC during a sequence of sonications (VibraCell 750 VC HIU system, f = 20 kHz, 12.7 mm tip diameter, 1 mm sample-sonicator distance). B-mode images (1.5 x 50 µm^2 pixel size) were acquired at 0, 10, 30, 120 and 300 s time points during a HIU sonication. A 18 mm long scan was done across the sonicated spot. The temperature of the immersion liquid was 21.5 ± 0.2°C (n = 5) and 21.1 ± 0.1°C (n = 5) before and after the scans, respectively.

We assessed the surface integrity of AC by detecting changes in acoustic reflection from the cartilage surface (at 10 MHz) and in URI[2].

Results/Discussion

As compared to 0 s, the amplitude reflection coefficients decreased by 0.3 ± 6.5%, -1.5 ± 8.9%, -8.8 ± 10.1%, -22.6 ± 33.7% at 10, 30, 120 and 300 s, increase in uncertainty due to a 0.5 mm wide crater formation. Moreover, the URI changed, 1.1 ± 0.5 µm, 1.6 ± 0.7 µm, 1.8 ± 0.7 µm and 6.6 ± 2 µm at the sonication center (2.5 mm segment of B-scan).

Changes in surface reflection are detected by SAM after a 10 s sonication burst of 880 J. As collagen degeneration reduces surface reflection[3] and URI increases with sonication time, our result implies that damage is induced by cavitation. Therefore, USM could be used to monitor cavitation-induced damage to AC during ultrasonic drug delivery.

[1]H. J. Nieminen et al, "Ultrasonic transport of particles into articular cartilage and subchondral bone" IEEE USI, October 8-10 2012, Dresden, Germany, ID 616

[2]H. Niu et al, "Ultrasonic reflection coefficient and surface roughness index of OA articular cartilage: relation to pathological assessment", BMC Musculoskeletal Disorders 2012.

[3]H. J. Nieminen et al, "Real-time ultrasound analysis of articular cartilage degradation in vitro", UMB, vol. 28 Issue 4, 2002.

Fig. 1: Relative decrease in surface reflection as compared to 0 s

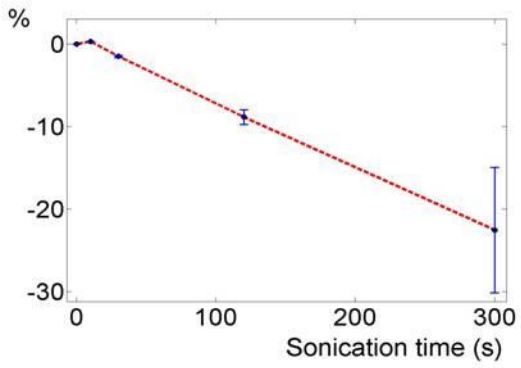

Acoustic tweezers 3

Forum Hall

Thursday, July 25 2013, 01:00 pm - 04:30 pm

Congress Hallair: **Charles Courtney**
University of Bath

IUS3-PD1-1

3D standing waves in polymer-based microfluidic chips for acoustic particle manipulation

Itziar González[1], Almudena Cabañas[2], Adela Castillejo[3], Jose Luis Soto[3], María Tijero[4], Javier Berganzo[5], Mounir Bouali[6], Alain Martin[7], Victor Acosta[8]; *[1]Ultrasonidos, Consejo Superior de Investigaciones Científicas, madrid, madrid, Spain, [2]Multi, University of Manchester, Manchester, United Kingdom, [3]Oncología Biomolecular, Hospital Universitario de Elche, Elche, Alicante, Spain, [4]Group Microsystems, Ikerlan, Mondragón, Guipuzcoa, Spain, [5]Dpt of Microsystems, Ikerlan, Mondragón, Guipuzcoa, Spain, [6]Microfluidics, Universidad de Mondragón, Mondragón, Guipuzcoa, Spain, [7]Microfluidcs, Universidad de Mondragón, Mondragón, Guipuzcoa, Spain, [8]Ultrasonidos, consejo superior de invetigaciones cientificas, madrid, madrid, Spain*

Background, Motivation and Objective

Background: novel polymeric-based ultrasonic devices were developed by the authors and applied to perform extraction of circulating tumor cells from peripheral blood samples. They provided efficiency levels lower than 70%, which demands new optimized designs for the clinical application of these .

Motivation and Objective: the development of optimized polymeric microresonators as a low-cost platfform using ultrasounds for early detection and extraction of CTCs in human blood samples with efficiency levels higher than 90% is the goal of this free-label technology for its clinical application.

Statement of Contribution/Methods

This work presents a comparative study of different polymeric microdevices in which some physical and geometric properties are varied to analyze their influence on the efficiency of cell/particle collection on flowing suspensions. The polymer-based chips were firstly designed and developed for particle micromanipulation on flwoing samples. In these systems of low acoustic impedance, the whole structure (including the chip and the ultrasonic actuator laterally attached to it) behaves as a 3D resonator, providing different pressure node locations of treatment where particles collect inside the channel at different frequencies. These locations can be displaced varying the frequency in a narrow range around a central value. In previous works the authors demonstrated the feasibility of these devices to extract tumor cells from human blood samples, achieving efficiency levels below 75%,which demands new optimized de-signs for clinical applications.

For such purpose, a comparative analysis among new chips with different substrates has been performed for the first time to analyze their influence on the particle collection. These devices include a polymeric chip with a SU-8 layer containig the channel over a substrate approximately 3 times thicker,so a significant percentage of the acoustic vibrations are established within this thick layer, whose upper surface is directly under the channel, so those vibration modes establsihed in the chip substrate are expected to affect strongly the acoustic field distribution inside the fluid phase.

Three chips have been developed with substrates of PMMA, PYREX and PMMA cracked in regular lines respectively, and their effects on the pressure distribution inside the channel have been separately investigated by direct observations on their channels.

Results/Discussion

Different results of particle collection have been found for the three chip designs at the same resonance frequencies. Lower voltages applied on the PZ actuator have been required to collect the particle in the chip with a cracked PMMA- substrate, which could be related to those 3D modes removed in this new “broken structure” of the thick substrate layer. These rseults make our new designs point the direction of optimization to achieve a higher efficiency of separation in the polymeric based cell manipulators

IUS3-PD1-2

Measuring Acoustic Forces Using Holographic Optical Tweezers

Philip Bassindale[1], Dave Phillips[1], Adrian Barnes[1], Bruce Drinkwater[1]; *[1]University of Bristol, Bristol, United Kingdom*

Background, Motivation and Objective

Acoustic standing waves at frequencies in excess of 1 MHz may be used to trap and manipulate particles on length scales on order of 10 μm or less. Devices that use this principle have been successfully used to trap particles in both 1 and 2 dimensions. Previous experimental measurement and verification of the trapping potentials (forces) has relied on two methods: fitting the motion of a particle to the equations of motion or by balancing the acoustic force against an external flow. These methods require assumptions to be made about the local force distribution. In this work we have developed a hybrid acoustical-optical trapping system able to determine the local trapping forces to pN resolution with a spatial resolution of a few microns.

Statement of Contribution/Methods

A 1D acoustic trap operating at 7 MHz was constructed from opposed piezoelectric elements to produce linear shaped traps separated by a distance of approximately 120 μm. Silica spheres of 5 μm diameter were accumulated in these traps and the trapping forces exerted on them were determined by reference to an optical trap created with a holographic tweezer acting on the same particle. The optical trap was modelled as a simple harmonic oscillator and its stiffness independently determined by tracking the particle’s position and using equipartition theory. The acoustic trapping forces were then determined by translating the optical trap through the acoustic field and observing the particle displacement with respect to the centre of the optical trap.

Results/Discussion

Our results demonstrate that we can measure, with good spatial resolution, the trapping forces exerted by the acoustic field to a resolution of better than 1 pN. The results agree with previous measurements of the trapping forces. In addition to the trapping forces we observe previously undetected constant offset forces that we attribute to acoustic streaming of the fluid. We show that this streaming is dependent on how well the piezoelectric crystals are frequency matched and show how it can be changed and reduced by control of the acoustical output of the transducers. We discuss how these methods may be extended to force measurements in 2D traps.

IUS3-PD1-3

Particle Trapping Study in Multiple-focus Acoustic Field

Yanyan Yu[1], Weibao Qiu[2], Lei Sun[1]; [1]*Interdisciplinary Division of Biomedical Engineering, The Hong Kong Polytechnic University, Hong Kong,* [2]*Paul C. Lauterbur Research Center for Biomedical Imaging, Shenzhen Institutes of Advanced Technology, Chinese Academy of Sciences, Shenzhen, China, People's Republic of*

Background, Motivation and Objective

Current various practical applications recommend the simultaneous trapping of many particles rather than one particle only, including sorting small particles, controlling multi-molecular complexes, particle-patterning technology etc. Although the multiple-focus acoustic field created by 50MHz phased array transducer has been proposed in a previous paper [1], the ultrasonic attenuation in the particles and acoustic streaming effect have not been taken into consideration. These influences are very crucial to evaluate whether radiation force is big enough to do multiple-trapping. In this paper, both ultrasonic attenuation in the particles and acoustic streaming effect are evaluated and compared with radiation force.

Statement of Contribution/Methods

According to the law of conservation, the radiation force is computed by the momentum transfer for the particles with diameter size varied from 240μm to 360μm on the multiple-focus acoustic field. The influence of ultrasonic attenuation is evaluated with consideration of scattering ray successive reflecting within the particles. Besides, to investigate the acoustic streaming effect, we introduce the approach studied by Stokes' law to estimate the axial streaming velocities.

Results/Discussion

Assuming acoustic impedance of the particle 1.4 MRayls, sound speed of the surrounding medium and the particle 1500m/s and 1450 m/s, density of the particle 950kg/m^3, attenuation coefficient of particles 1.5 dB/cm/MHz. Fig.1(a) shows the momentum transfer direction across the beam axis before the focal point. The axial radiation force with and without the consideration of acoustic attenuation is shown in Fig.1(b). Fig.1(c) indicates drag force due to acoustic streaming velocity combined with axial radiation.

The results demonstrate that although the acoustic attenuation effect leads to lessening trapping effect beyond trapping point, it slightly increases the trapping effect before trapping point. In addition, it can be seen that the drag force due to acoustic streaming is much smaller than the force caused by trapping force.

[1]Y. Yu et al, IEEE Ultrasonics Symposium, 2011.

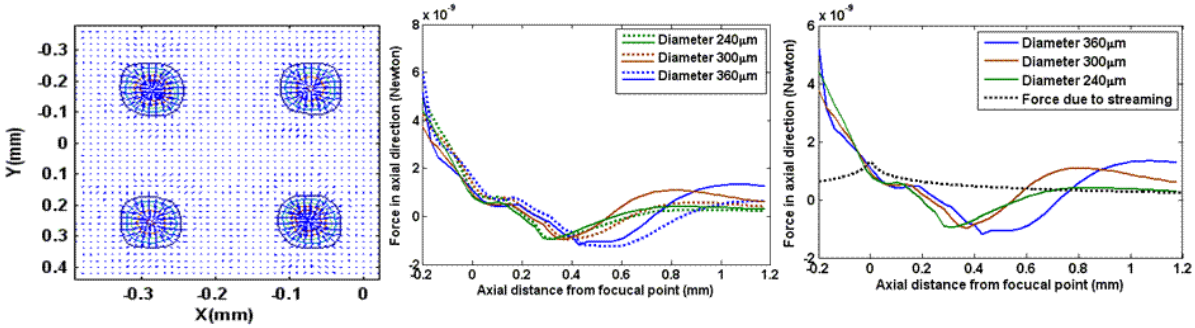

Fig.1 (a) Shows the momentum transfer across the beam axis. (b) Shows the axial radiation force across the one of the four beam propagation direction for the particles with diameter varied from 240μm to 360μm. The solid shows the force with consideration of ultrasonic attenuation, the dashed lines indicate the force without attenuation. (c) Drag force due to acoustic streaming velocity combined with radiation force along the axial direction.

IUS3-PD1-4

Acoustic radiation force on a cluster of rigid particles in viscoelastic medium

Valeriy Andreev[1], Andrey Shanin[1], Ekaterina Atletova[1], Igor Demin[2], Oleg Rudenko[1]; [1]*Moscow State University, Russian Federation,* [2]*University of Nizhniy Novgorod, Russian Federation*

Background, Motivation and Objective

Microcalcifications are an important diagnostic sign of breast cancer, highlighting tumor progression in the early stages, when the disease is asymptomatic. Calcium salts are deposited in the soft tissue, often forming clusters of individual microparticles. Such formations are identified on mammography and are found on most of mammograms. The size, form, and density of microcalcifications are varied significantly and can serve as characteristic signs of the disease. Sensitivity and resolution of conventional ultrasonic devices are not sufficient for detection of microcalcifications. We propose to induce a radiation force in a suspicious volume by the focused ultrasound. The presence of solid microparticles will increase the radiation force and results in excitation of shear wave of higher amplitude.

Statement of Contribution/Methods

The finite element method was used for calculation of radiation force acting on a rigid particle of arbitrary shape. The calculations were performed for different ratios of particle size to the ultrasonic wavelength and ratios of a particle density to the density of soft tissue. The effect of orientation of the particles in a form of the elongated ellipsoid with respect to the incident wave was studied. The radiation force on the aggregate of particles was calculated taking into account the rescattering of ultrasonic waves.

Results/Discussion

It was found the characteristic distance between the particles at which radiation force becomes nonlinear function of particle density.

Experiments were performed in gel phantoms with embedded solid microparticles in a form of sphere and cubes. Radiation force was produced by focused ultrasonic beam with use of Verasonics system. The displacements of the particles were measured with cross-correlation method. Experimental results are in a good agreement with the calculation data.

IUS3-PD1-5

Precipitation method for nano particle using focused ultrasound

Moojoon Kim[1], **Jungsoon Kim[2]**, Kanglyeol Ha[1], Seonae Hwangbo[3], Mincheol Chu[3]; *[1]Pukyong National University, Korea, Republic of, [2]Tongmyong University, Korea, Republic of, [3]Korea Research Institute of Standards and Science, Korea, Republic of*

Background, Motivation and Objective

Recently, several studies show that ultrasound wave can agglomerate and precipitate the suspended particles in the waste water from quarries. That effect can be explained by the ultrasonic cavitations on the suspension. The high temperature and high pressure state due to the ultrasonic cavitation effect increases the chemical activity of ion. That effect changes the zeta potential of the particles, and then the suspended particles can be agglomerated without any additional chemicals. However, it is hard to agglomerate the particles uniformly because the ultrasonic field distribution in the water tank is not homogeneous in the conventional methods.

Statement of Contribution/Methods

In this study, we suggest a cylindrical piezoelectric transducer to precipitate the nano particles uniformly. The suspension of TiO_2 was circulated through the center of a cylindrical piezoelectric transducer as shown in Fig.(a). The ultrasound from the transducer is focused in the glass tube where the suspension flows. The major diameter of TiO_2 is 25 nm and the concentration of the suspension was 0.01 wt%.

Results/Discussion

The nano particles started to precipitate 40 minutes after ultrasound irradiation. To compare with other ultrasonic methods, the precipitated states from each method 60 hours after ultrasound irradiation are shown in Fig. (b). In this figure, H, F, and B are horn type with 20 kHz, focused type with 500 kHz, and bath type with 40 kHz, respectively.

This method could be applied not only to the purification system for radioactive contamination water but also to the recovery of value-added resources.

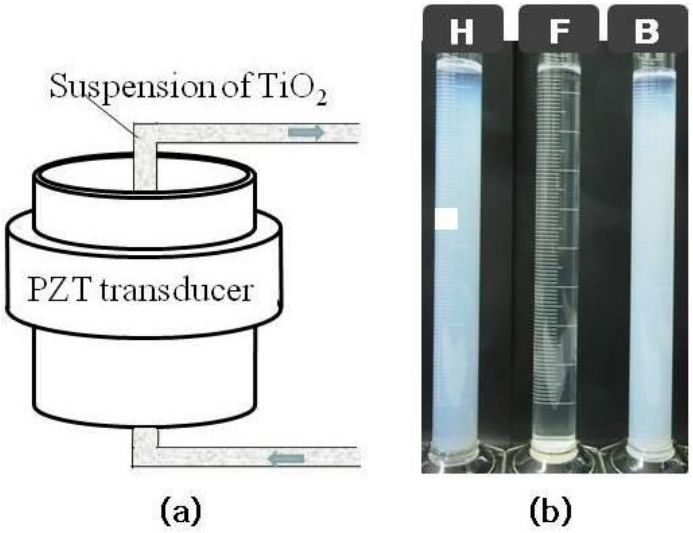

IUS3-PD1-6

Nanoparticle dispersion by focused ultrasound from cylindrical transducer

Moojoon Kim[1], **Seonae Hwangbo[2]**, Jungsoon Kim[3], Kanglyeol Ha[1], Mincheol Chu[2]; *[1]Pukyong National University, Korea, Republic of, [2]Korea Research Institute of Standards and Science, Korea, Republic of, [3]Tongmyong University, Korea, Republic of*

Background, Motivation and Objective

Over the past several years, there has been increasing interest in dispersion methods using ultrasonic power for nanoparticle dispersion, since the materials dispersed by this method are much purer than those by other methods. However, conventional ultrasonic homogenizers are not appropriate for nanoparticle dispersing because they have low resonant frequency of several tens kHz. Moreover, we can't control the locations of cavitations because it is hard to expect the acoustic field in the water tank with limited size.

Statement of Contribution/Methods

To produce a focused ultrasound field, an ultrasonic dispersion system is fabricated using a cylindrical piezoelectric vibrator. The cylindrical vibrator has an inner radius of 38.5 mm, an outer radius of 46.5 mm, and a height of 19.2 mm. The polarization direction of the transducer is along the radius of the cylinder. A glass tube whose thickness, diameter, and length are 0.3, 5.5, and 35 mm, respectively, was placed at the center of the inner space of the transducer along the length. The ultrasound wave from the vibrator was focused in the center of the glass tube. Ultrasound cavitations due to the high pressure amplitude dispersed the nanoparticle in the aqueous suspension.

Results/Discussion

The particle size distributions of TiO_2 were measured using the particle counters CPC 5.403 (GRIMM Aerosol Technik) as shown in figure. In this figure, left one is the result before the ultrasonic dispersion. Number of major particle size (40nm) increased by dispersion of particles with submicron size in right one. The agglomerated particles in the range of submicron or over were dispersed by ultrasonic cavitations and the number of major particles increased as shown in figure. We also compared the efficiency of this method with that of other ultrasonic dispersion methods such as ultrasonic horn and ultrasonic cleaning bath.

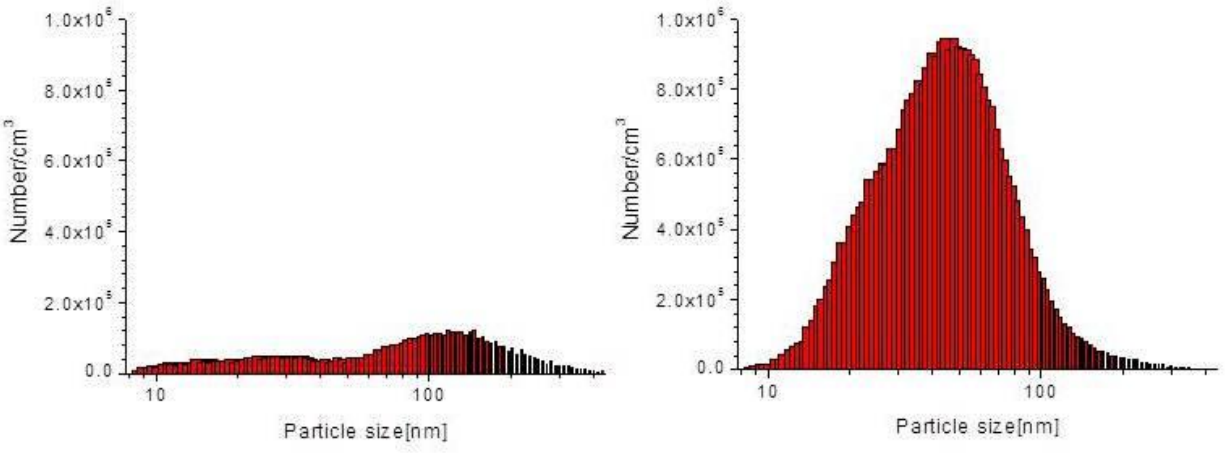

IUS3-PD1-7

Multi-Particle Trapping and Patterning using a Single Ultrasound Beam

Changyang Lee[1], Jong Seob Jeong[2], Jae Youn Hwang[1], Jungwoo Lee[3], K. Kirk Shung[1]; [1]*Department of Biomedical Engineering, University of Southern California, Los Angeles, USA,* [2]*Department of Medical Biotechnology, Dongguk University, Seoul, Korea, Republic of,* [3]*Department of Electronic Engineering, Kwangwoon University, Seoul, Korea, Republic of*

Background, Motivation and Objective

Optical tweezers have been employed in various biomedical applications where they are typically used for manipulating a single micro-object. Optical tweezers using dynamic holographic optical trapping was able to trap invasively multi-particles and form certain patterns. Multi-trapping optical systems offered new opportunities and applications for biotechnology. In spite of the impressive performance of these systems, they are all bulky and require complicated optical instruments. Previous research on acoustic tweezers showed that a single element focused ultrasound transducer could manipulate a single micro- particle in lateral direction. This paper demonstrates the trapping of multi-particles in a circular pattern of micro-particles using a ring-type single element ultrasound transducer. Experimental results show the potential capability of acoustic tweezers as a multi-particle manipulator and a device of pattern formation.

Statement of Contribution/Methods

A focused 24 MHz ring type single element transducer of f-number 1 was designed for multi-particle trapping experiments. The transducer was positioned perpendicular to thin mylar membrane at the focal point. Oleic acid lipid droplets of 50 μm were suspended underneath a thin mylar membrane in deionized water. The experimental arrangement is shown in figure 1(a).

Results/Discussion

Trapping pattern of lipid droplets was monitored with a microscope, when a focused ring transducer was driven with a sinusoidal burst signal at resonance frequency. Circular pattern trapping of 50 μm lipid particle was successfully demonstrated by this transducer in figure 1(b). The multi-lipid particles were able to be manipulated to form a circular pattern.

These results demonstrate that single beam acoustic tweezer is capable of manipulating and formatting patterns of small particles.

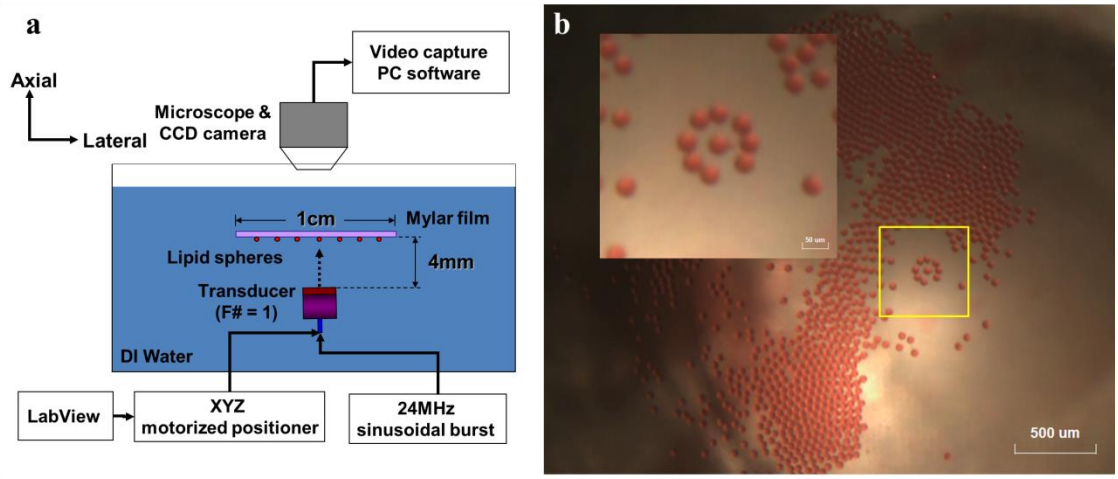

Figure 1. (a) Trapping Set-Up (b) Circular Pattern Trapping of 50um Lipid Particles

Phononic crystals 2

Forum Hall

Thursday, July 25 2013, 01:00 pm - 04:30 pm

Congress Hallair: **Roy Olsson**
Sandia National Laboratories

IUS3-PD2-1

Fourier Series Representation of the Dispersion of Coupled-Resonator Acoustic Waveguides

Jose Maria Escalante[1], Alejandro Martinez[1], **Vincent Laude[2]**; *[1]Nanophotonics Technology Center, Universidad Politecnica de Valencia, Valencia, Spain, [2]Institut FEMTO-ST, Centre National de la Recherche Scientifique, Besançon, Franche-Comté, France*

Background, Motivation and Objective

Most phononic crystal waveguides are formed from line defects opening transmission channels within an otherwise completely opaque complete band gap. Their dispersion is usually multimodal and dramatic interference effects can appear between different guided bands, leading to mini-band gaps, avoided crossings, or band repellings. Another guiding mechanism that has been less examined is the coupling of defect cavities. These structures, coupled-resonator acoustic waveguides (CRAW), provide us with an increased flexibility in the engineering of their dispersion relation, by design of the cavities and of their coupling strength. In this paper, we discuss the CRAW relation dispersion in the context of coupled cavities managed in phononic crystals and show that it can be approximated by a fast converging Fourier series expansion.

Statement of Contribution/Methods

The idea of CRAW managed in phononic crystals followed by analogy with coupled-resonator optical waveguides (CROW) managed in photonic crystals. Propagation in CROW has been described using the tight-binding (TB) approximation for cavities. We extend the TB approximation to the case of CRAW in phononic crystal and further investigate an alternative dispersion model that is based on the view of coupled cavities as a linear chain of coupled harmonic oscillators, similar to the description of phonon propagation in a one-dimensional lattice of atoms. The discussion is illustrated numerically with the case of CRAW managed in a two-dimensional square-lattice solid-solid phononic crystal of tungsten inclusions in a silicon matrix (see the inset in the figure).

Results/Discussion

Both models predict frequency as a function of wavenumber in the form of a Fourier series expansion. Of the two models, however, only the TB approximation gives an explicit expression for the Fourier coefficients, but it is found not to exactly reproduce the computed dispersion relation (computation: crosses; TB approximation: solid line; blue: $\Lambda=2a$; orange: $\Lambda=3a$). The 1D-lattice of coupled resonators model, in contrast, has *a priori* unspecified coefficients that can be fitted against the computed dispersion relation. It is found that only a very limited number of Fourier coefficients are necessary to reproduce the exact dispersion, a clear indication that the influence of distant resonators decreases very fast with their separation.

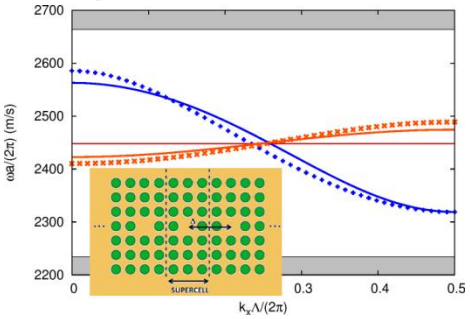

IUS3-PD2-2

Study of surface elastic wave propagation in 2D array with various lattices symmetries based on cylindrical and conical Ni pillars on piezoelectric crystal

Abdelkrim Talbi[1], Yu Du[1], Abdelali Mrabti[2], Noura Gasmi[1], Jeremy Streque[1], Ali Soltani[2], Jean-Claude Gerbedeon[1], Abdllatif Akjouj[2], Yann Pennec[2], Baron Djafari Rouhani[2], Olivier Boumatar[1], Philippe Pernod[1]; *[1]LIA LICS/LEMAC, IEMN, UMR 8520,ECLille, PRES Universite Lille Nord de France, 59652 Villeneuve dAscq, France, [2]IEMN, UMR CNRS 8520, Université de Lille 1, PRES Universite Lille Nord de France 59655 Villeneuve dA, France*

Background, Motivation and Objective

Recently, investigations of SAW propagation in 2D Phononic crystals (PC) have attracted significant attention due to its potential applications, especially in wireless communication, transducer and sensor system. Such structure enables designers to control the elastic properties of materials resulting in forbidden frequency bands, anomalous dispersion and near-zero group velocity, etc. These characteristics are of a great interest to achieve advanced transfer functions for micro electroacoustic and useful signal processing tools, ect. Very recently, theoretical and experimental demonstrations of cylindric Ni pillars array forming square lattices PCs for SAW in piezoelectric crystals have been reported (khelif et al PRB 2010), taking advantage of the direct measurement of SAW transmission through the PC using IDTs. In most study, the electrical measurement was restricted to the transmission to demonstrate the existence of band-gaps. The transmission alone doesn't reveal a direct information on the wave interaction with the PC. In this study, we investigate in depth the origin of band-gaps in SAW-PCs system with various lattices symmetries and pillars shape using measurements of transmission, reflection and delay time.

Statement of Contribution/Methods

First we perform by means of a 3D FEM method to calculate SAW band structures in lattices with different symmetries (square, triangular, and hexagonal), in order to obtain large frequency band gap principally for surface modes. We investigated the evolution of ABG obtained with different geometrical shapes of Ni pillars (including cylinder and conical) organized following lattices cited above on the surface of Y-128 (LiNbO3) crystal cut. In a second time, experimental samples of PCs made of 2.6 um thick Ni pillars according to the specifications defined above were elaborated and as shown figure 1.

Results/Discussion

From theoretical point of view, as the shape of the pillars change from cylindrical to conical, the band-gap shifts down in frequency and is widening. Figure 1 shows the transmission and delay time measured for the device composed of cylindrical Ni pillars array with square lattice. We can notice clearly the existence of absolute band gaps. We can also observe the peaks corresponding the the pillars resonance and antiresonance, this is well confirmed if we consider the measurement of delay time.

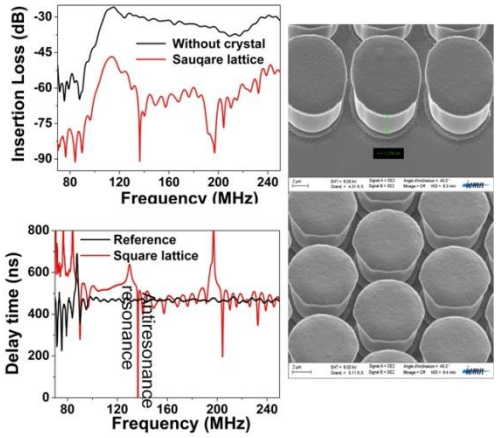

Figure 1: Transmission and delay time for SAW devices with and without crystal for the case of square lattice. Example of SEM image of PCs Crystals with Ni pillars

IUS3-PD2-3

Experimental investigation of the propagation of Lamb Wave in nanostructured silicon plates

Remi Marchal[1], Bernard Bonello[2], Olga Boyko[3], Jinfeng Zhao[3]; *[1]INSP, University Pierre et Marie Curie, France, [2]INSP, CNRS and University Paris 6, France, [3]University Pierre et Marie Curie, France*

Background, Motivation and Objective

We present experimental studies of the propagation of zero order anti-symmetric Lamb modes in nanostructured silicon plates. This is illustrated with two systems. First, we studied the dynamic of localization of a defect mode in a 2D cavity, with honey comb symmetry. Then we present the mapping of the displacements field within acoustical gradient index lenses formed by holes in Si plates (Fig. 1).

Statement of Contribution/Methods

An all optical experimental setup allowed us to generate Lamb waves and to mon-itor them with a Michelson interferometer.Generation of elastic waves in silicon is based on thermoelastic effects. Nd-YAG laser with pulses as short as 35ps at 532nm is used to heat the surface. The short heating produced by the absorption of light generates thermoelastic stresses and strains that act as an ultrasonic source . The heating shape, a circular spot or a line, allowed generating respectively circular waves or plane waves. In both cases, Lamb waves with frequencies from 1MHz up to 80MHz (in silicon plate of thickness ~150microns) are generated. The elastic wavelength of the source can be tuned through a heating pattern obtained by imaging an amplitude grating with a lens. With this kind of heating profile, a strong efficiency in the generation of a monochromatic Lamb mode A0 is obtained

Results/Discussion

The displacements on the surface of the sample are monitored with a Michelson interferometer based on a He-Neon laser and a microscope objective focusing onto a spot of about 8ìm in diameter. The Michelson interferometer is stabilized for linearity of both the amplitude and the phase. The absolute precision on the displacement is evaluated to be about 1-2pm. The microscope objective is mounted on motorized stages able to map the out-of-plane displacements onto 25x25mm².

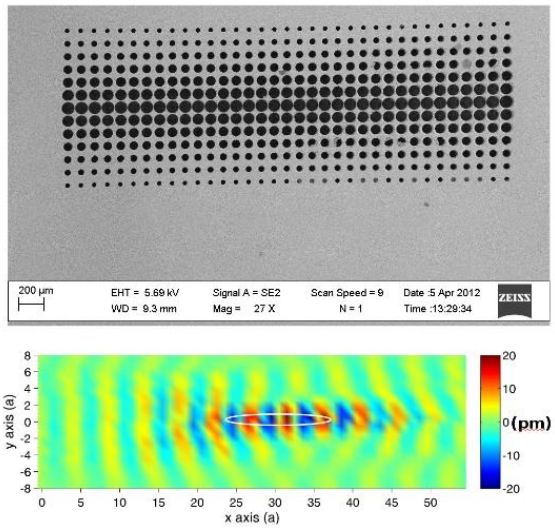

IUS3-PD2-4

Tunable Locally Resonant Band Gaps for Surface Acoustic Waves and Lamb Waves in a Phononic Crystal

Noura Gasmi[1], Abdelkrim Talbi[1], Yu Du[1], Marc Goueygou[1], Olivier Bou Matar[1]; *[1]International Associated Laboratory LICS/LEMAC, IEMN UMR CNRS 8520, PRES Lille Nord de France, ECLille, Villeneuve d'Ascq, France*

Background, Motivation and Objective

Phononic crystals may have potential applications in numerous technological domains. For ex-ample, by modifying the surrounding medium of a conventional Lamb wave resonator using phononic crystal structures with complete phononic band gaps the leakage of waves out of a resonator can be suppressed and the quality factor of the resonant mode can be improved. A recent study has demonstrated that optimal improvement of the quality factor is obtained when the con-sidered resonant mode is in the middle of the phononic band gap. So, a tuning capability of this phononic bang gap will open the possibility to optimize the micromechanical resonator for a chosen resonant mode by adjusting the resonant mode position exactly in the middle of a band gap.

Statement of Contribution/Methods

We consider RF phononic crystal resonators based on a two-dimensional array of cylindrical pillars, made of magneto-acoustic material, on a slab or a semi-infinite substrate. As in such sys-tems band gaps originate from local resonances of the individual cylindrical pillars, they highly depend on their elastic properties which are very sensitive to the magnetic state of the magneto-acoustic material and on the applied external magnetic field. This leads to a fully non contact tuning of the resonators.

Results/Discussion

A device made of TbCo/FeCo pillars positioned on a square lattice on a LiNb03 substrate is numerically optimized considering magneto-acoustic coupling induced by giant magnetostriction, Spin Reorientation Transition (where the dynamic elasticity modulus for the corresponding quasi-phonon mode vanishes in theory) and magneto-acoustic resonance (when the frequencies and the wave vectors of phonons and magnons coincide). Numerical simulations (band structure calculation and transmission co-efficient) are performed by using a 3D finite element method. Potential application to magnetic field sensor will also be presented.

IUS3-PD2-5

Band gap and local resonances of Love waves in a piezoelectric substrate coated with phononic guiding layer

Tsung-Tsong Wu[1], Chun-Shao Liu[1], Ting-Wei Liu[1]; *[1]Institute of Applied Mechanics, National Taiwan University, Taiwan*

Background, Motivation and Objective

Recently, propagation of Rayleigh or Lamb waves in a substrate with finite depth phononic holes or pillars have been studied and showed the existence of either partial or complete band gaps in such phononic coated structures. Different from the aforementioned studies, this paper investigates the band gaps and local resonances of Love wave (polarization of the wave perpendicular to the sagittal plane) in a piezoelectric substrate coated with a phononic guiding layer. The phononic layer is consisted of a thin layer and periodic stubbed rectangular pillars.

Statement of Contribution/Methods

The piezoelectric substrate we chose in the numerical study was ST-cut quartz and the thin guiding layer was silica. To understand the influence of the pillars¡¦ height on the dispersion of Love wave, we conducted a series of numerical calculations using the finite element (FE) method. On the other hand, to understand the dependency of the gap width on the geometry of rectangular pillars, we fixed the height of the pillar at h and varied the width of the pillars from 0.25 to 0.5 a. In addition, the influence of attaching a heaver mass on top of the pillars on the local resonant frequency is also investigated.

Results/Discussion

The results showed strong level repulsion existed between the twisting and bending local resonant Love modes in Silica/ST-cut quartz phononic structure. It was also found that the gap width can be enlarged by increasing the width of the rectangular pillars, while the local resonant frequency can be controlled by changing the height of the pillars or attaching a heavier mass on top of the pillars. Results on the transmission of Love waves through a 10-layer PC showed good agreements with the band structures obtained from the eigenmode analyses.

IUS3-PD2-6

Band gap behavior of phononic strip with MEMS materials

hammouche khales[1], Rafik Serhane[1], Abdelkader Hassein-Bey[2], Abdelkrim Khelif[3]; *[1]MEMS & Sensors group, CDTA, Baba Hassen, Algiers, Algeria, [2]FUNDAPL, Faculty of Sciences, Saad Dahlab University, Blida, Blida, Algeria, [3]FEMTO-ST Institut, CNRS UMR 6174, Besançon, Besançon, France*

Background, Motivation and Objective

We study the band gap behavior of PC strip waveguides made with MEMS materials. The structure considered is joined unit cells, with inclusions on substrate, repeated periodically to forms PCs waveguides. This is a useful structure for vibration isolation and energy loss re-duction in frequency devices, which received high interest recently.

Statement of Contribution/Methods

The influence of materials contrast and the forms of inclusions on the band gap formation is considered. We investigate the influence of material contrast and the geometrical characteristic on 1D phononic crystal with dimension properties in the same order of system periodicity (Figure 1). We focus on the materials commonly used in microfabrication, such as W, Ni, Cu, and Al as inclusions materials, and silicon as substrate material. The behavior of band gaps, as function of the relative height and the relative radius of the inclusions is discussed by analyzing the dispersion curves obtained using FEM simulation.

Results/Discussion

Figure 2 describe the highest band gap ratio obtained for different materials in silicon strip. The optimum band gap ratio is obtained for W and Ni inclu-sions on silicon substrate. This ratio is of 17% and 13% respectively for W and Ni inclusions. First, the mass density and the acoustic velocity contrast, between the inclusions and substrate, are the key of the opening of the gap bandwidth. Second, the effect of the geometrical parametric inclusions on the PC strip band gap is investigated. The effect of the inclusions on strip on the band gap is the existence of two types of band gaps. The first is around the Bragg frequency, and the other type is related to the structures resonances of the inclusions.

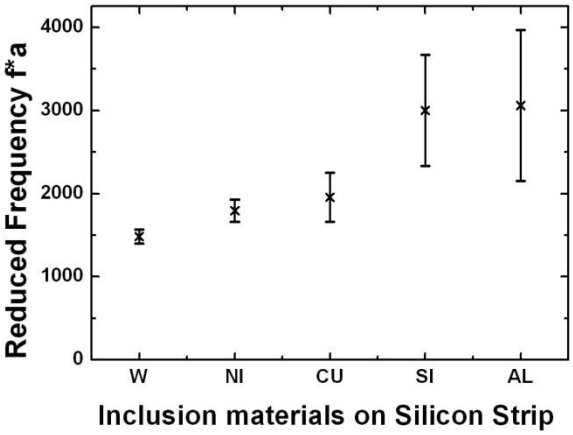

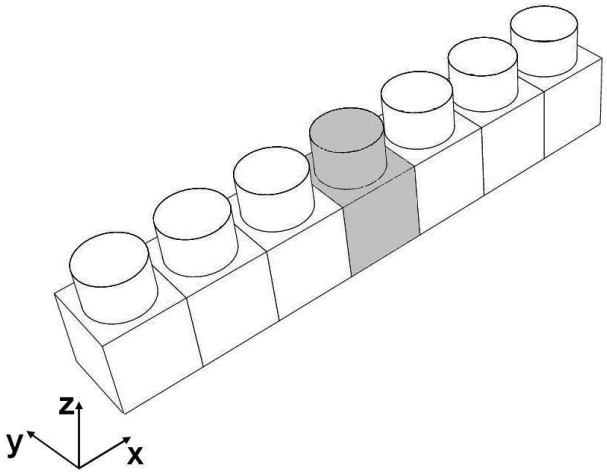

IUS3-PD2-7

Band Gaps and Resonances in Periodic Graphite-like Structures

Zi-Gui Huang[1], Chun-Fu Su[2]; [1]*Department of Mechanical Design Engineering, National Formosa University, Yun-lin County, Taiwan,* [2]*National Formosa University, Taiwan*

Background, Motivation and Objective

Graphene structures are a popular single-layer nanomaterial. Numerous relevant academic and industrial studies are conducted every year. Compared with the spherical chain atoms of the three-dimensional graphene-like structure, the two-dimensional graphene-like structure adopts a column form shown in Fig. 1. We observed the band gap variations for systems of various sizes using the XY model, and found that although the overall size is hypothetical instead of in the nanoscale, its integrity is complete.

Statement of Contribution/Methods

Using the frequency analysis results provided by the finite-element software, the ZnO material parameters can be substituted into the model easily to determine the oscillation characteristics and band gaps of the two-dimensional graphene-like structure.

Results/Discussion

This study constructs a new phononic crystal acoustic wave device that adopts a graphene-like structure and is composed of piezoelectric ZnO material. We employed the finite-element method to determine periodic boundary conditions. Following Bloch¡¦s theorem, we analyzed the acoustic wave propagation of the proposed graphene-like structure in the frequency domain to understand the band gap effect and oscillation behavior. We also investigated the band gap variation and modal distortion tendencies of the piezoelectric ZnO material in the two-dimensional graphene-like structure under the condition of changing chain structure diameters and bonding rod widths between the atoms columns to develop an optimal acoustic wave device.

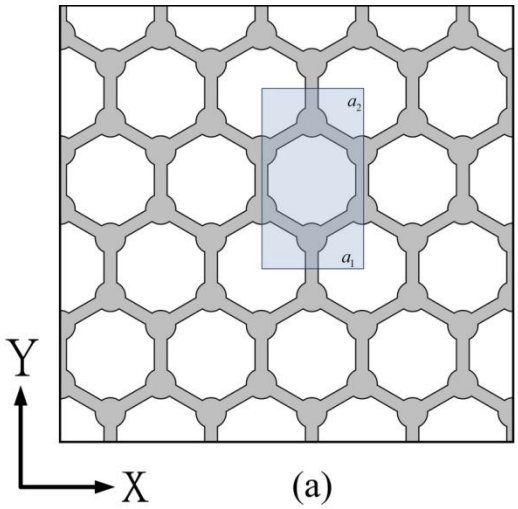

Microwave Acoustic Sensors

Forum Hall

Thursday, July 25 2013, 01:00 pm - 04:30 pm

Congress Hallair: **Victor Plessky**
GVR Trade SA

IUS4-PD-1

Analysis of Quality Factor of Quartz-Crystal Tuning Fork Using Thermoelastic Coupling Equations and L-shaped Bar Model with Torsion Spring

Keisuke Sugiura[1], Hideaki Itoh[2]; *[1]Faculty of engineering, Shinshu university, Nagano, Nagano, Japan, [2]Shinshu university, Japan*

Background, Motivation and Objective

Analysis of the damping coefficient of the cantilever beam undergoing flexural vibration was done by Zener using thermoelasticity.[1] However, although the comparison between calculated and measured values about the damping coefficient was made, not about quality factor (Q value or Q). The equations of motion and heat conduction of the cantilever beam were derived from a viewpoint of thermoelasticity, Q value of the quartz-crystal tuning fork was calculated using the cantilever beam model, and the comparison between calculated and measured values was made.[2] Moreover, there was a research in which the dynamic capacitance of the electrical equivalent circuit of the quartz-crystal tuning fork was given by L-shaped bar model which was depicted by the right half of the tuning fork since the arms of the tuning fork vibrated symmetrically each other and an arm and the base of the tuning fork were connected by means of a torsion spring.[3] In this research, it turned out that a torsion spring caused a certain loss so that the efficiency of vibration of the tuning fork became always under that of cantilever beam. From this fact, we suppose that the torsion spring also affects Q value of the tuning fork.

Statement of Contribution/Methods

Q value formula is derived from the equations of motion and heat conduction of quartz-crystal tuning fork from a viewpoint of thermoelasticity using L-shaped bar model and the comparison between the calculated and measured Q values is conducted.

Results/Discussion

Q value of quartz-crystal tuning fork calculated by L-shaped bar model was smaller about 10% and approached to be closer to the measured one than that of cantilever beam model. These results are shown in Table I. Table I shows the comparison between calculated Q values of a cantilever-beam and L-shaped bar models and the Winkler coefficient R of the torsion spring of L-shaped bar model and measured Q values against the ratio of the width h to the length l of the arm of the tuning fork. It is thought that the existence of the torsion spring results in larger displacement of the arm of the tuning fork than that of cantilever beam so that Q value

decreases because of the influence of thermoelasticity as shown in Table I.

[1] C. Zener, Phys. Rev., vol.52, 230, 1937.

[2] H. Itoh and Y. Tamaki, Jpn. J. Appl. Phys., vol.48, 07GF03, 2009.

[3] T. Ishikawa and H. Itoh, IEEE International Ultrasonics Symposium, to be published, 2012.

Table I Comparison between calculated and measured Q values

	Cantilever	L-shaped Bar		Measured
h/*l*	Q value	*R* [N·m]	Q value	Q value
0.0654	2.81×10^4	0.413	2.58×10^4	2.41×10^4
0.0947	1.24×10^5	0.442	1.12×10^5	7.09×10^4
0.0966	1.41×10^5	1.36	1.34×10^5	1.07×10^5
0.121	3.11×10^5	2.53	2.57×10^5	1.71×10^5
0.0953	1.27×10^5	2.75	1.15×10^5	8.00×10^4

IUS4-PD-2

Microacoustic voltage transformer with bandpass filter characteristics

Milena Moreira[1,2], Johan Bjurström[1], Ventsislav Yantchev[1], Ilia Katardjiev[1]; *[1]Uppsala University, Sweden, [2]University of Campinas (Unicamp), Brazil*

Background, Motivation and Objective

Passive RFID tags acquire energy from the interrogation signal which is rectified and accumulated over time. Voltage amplification is achieved by employing a network of rectifying devices (charge pumps). However, the efficiency of such charge pumps decreases with the degree of amplification.

In a different context, remotely triggered switches (RTS) are needed in remotely controlled devices such as wake up radios. The idea is to make use of the energy of the interrogation signal to trigger a low threshold electronic switch. Since the power levels at practical distances are insufficiently low the energy is accumulated over a period of time and stored into a capacitor. A voltage transformer is needed to increase the output voltage and hence the energy accumulated. Addressing is achieved by frequency coding which requires the use of additional bandpass filters. Current solutions thus suffer from high cost and insufficient performance.

Statement of Contribution/Methods

In this work we present a new device which represents a micro-acoustic bandpass filter with a large ratio between input and output impedances. Accordingly, it has both transformer and filter (transfilter) characteristics, which in view of its low fabrication cost makes it suitable for the above applications.

The transfilter is a 2-port Lamb wave resonator based on c-textured AlN thin films although in general it can employ any other type of wave, say, SAW, to achieve a high impedance ratio and good filtering.

Results/Discussion

The S21 transfer function (fig.1) shows that the device behaves as a bandpass filter with a center frequency of 889 MHz and an insertion loss of about -5dB. The input and output impedances measured at center frequency are 25Ω and 2600Ω, respectively, which yields a voltage transformer ratio of about 10 (fig.2).

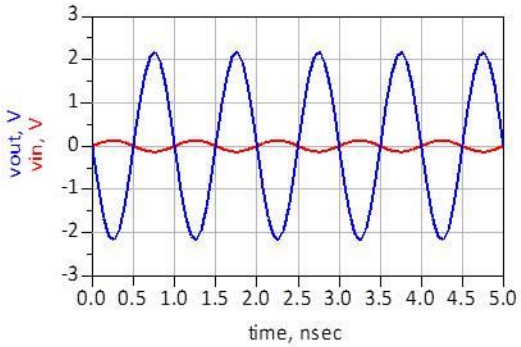

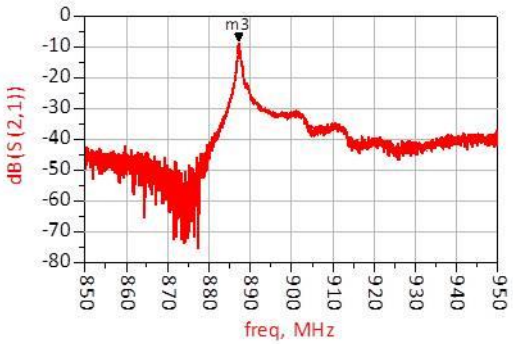

IUS4-PD-3

Stress Sensitivity of SAW Rayleigh Waves on Lithiumniobate and its Application in Pressure Sensor Design

Gudrun Bruckner[1], Jochen Bardong[1], Johannes Schicker[1], Venjamin Stojanov[2], Peter Schlumpf[2]; [1]*Sensor Development, Carinthian Tech Research AG, Villach, 9524, Austria,* [2]*Unisensor, Switzerland*

Background, Motivation and Objective

Surface acoustic wave (SAW) devices are since long known for their passive sensing capability. They are therefore qualified candidates for implantable physical sensors for different medical applications. Compared to quartz, which has been frequently used for wireless force, pressure or strain sensors, lithiumniobate (LN) provides a better coupling coefficient and therefore longer reading distances while the bigger temperature sensitivity can be compensated by differential measurements. In addition it allows operating the devices in the ISM Band at 2.45 GHz, which is essential for implantable devices as the operating frequency should be maximized to minimize the size of the SAW device and the antenna.

Statement of Contribution/Methods

For a reliable sensor design the stress sensitivity of the selected substrate has to be known. We have used a combination of experimental investigation and FEM simulations to obtain the required sensitivity data for the lithiumniobate cuts LN YZ with Euler angles of (0°,90°,90°) and LN 128 (0°, 38°,0°). A dedicated test bench has been constructed to measure the influence of applied force on the S-parameters of SAW samples. The sensitivity to stress and strain was derived by measuring the time response of delay lines versus varying forces and correlating these results with the strain or stress values obtained from the FEM simulation of the corresponding mechanical geometry. Both substrates showed linear behavior as demonstrated for LN YZ in figure 1 where the data of ten independent measurements are plotted.

Results/Discussion

The obtained stress sensitivity and was used in designing, fabricating and testing a delay line based membrane pressure sensor with temperature compensation (figure 2), proposed for epidural or subdural brain pressure monitoring.

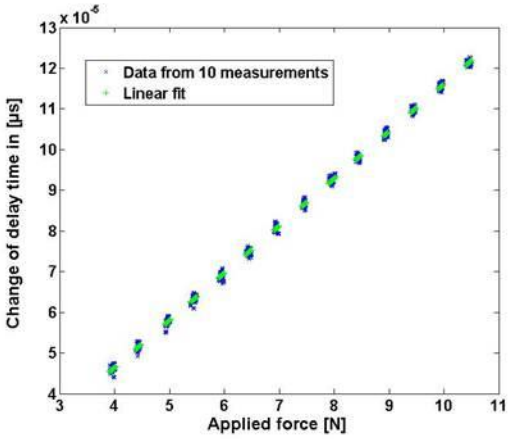

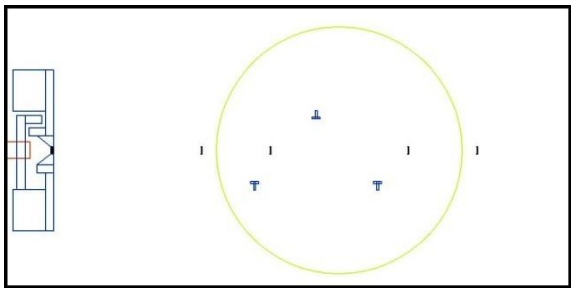

IUS4-PD-4

Surface Acoustic Wave Biosensor based on Odorant Binding Proteins Deposited by Laser Induced Forward Transfer

Fabio Di Pietrantonio[1], Massimiliano Benetti[1], Domenico Cannatà[1], Antonio Varriale[2], Sabato D'Auria[2], Alexandra Palla-Papavlu[3], Pere Serra[3], Enrico Verona[4]; [1]*Institute of Acoustics and Sensors, National Research Council of Italy, Rome, Italy,* [2]*Institute of Protein Biochemistry, National Research Council of Italy, Naples, Italy,* [3]*Departament de Física Aplicada i Òptica, Universitat de Barcelona, Barcelona, Spain,* [4]*Institute for Photonics and Nanotechnologies, National Research Council of Italy, Rome, Italy*

Background, Motivation and Objective

In the last decade, surface acoustic wave (SAW) biosensors immobilizing biologic molecules have attracted great attention for bio/sensing applications. In particular, detection of odorant molecules by SAW biosensor array based on odorant-binding proteins (OBPs) has been recently demonstrated [1]. In this work, we present a SAW biosensor based on wild type OBPs from pig (pOBP) deposited by laser-induced forward transfer (LIFT) technique. The proposed solution exploits the well-known features of SAW based sensors in conjunction with the adaptable selectivity of the OBPs and the flexibility and homogeneity of the depositions obtainable with the LIFT technique.

Statement of Contribution/Methods

The biosensors consist of 2-port SAW resonators operating at about 393 MHz and implemented on quartz (ST cut, x-propagation). The electrodes are made of Al film covered by a thin Au film (2 nm thick) used to promote the adhesion of proteins. The pOBPs were prepared as reported in [1] and were printed by LIFT onto SAW devices with a Yb:KYW laser, under optimized conditions of fluence, glycerol content in the protein solution, etc.. Differential frequency responses were obtained using the SAW biosensor and an uncoated reference SAW device as frequency control elements in the feedback path of two RF oscillators.

Results/Discussion

The SAW biosensor was tested in nitrogen upon exposure to concentrations of R-(–)-1-octen-3-ol and R-(–)-carvone vapors that are two odorants largely used in food industry. The response curve of the sensors are linear and, sensitivities of 20.7 Hz/ppm and of 13.9 Hz/ppm are obtained, respectively, for octenol and carvone. An example of time response to 13 ppm of octenol is reported in Fig. 1. The results obtained by LIFT are comparable to those obtained using the droplet method deposition [1], demonstrating the feasibility of the LIFT technique for the fabrication of SAW biosensors based on OBPs.

[1] F. Di Pietrantonio, D. Cannatà, M. Benetti, E. Verona, A. Varriale, M. Staiano, and S. D'Auria, "Detection of odorant molecules via surface acoustic wave biosensor array based on odorant-binding proteins," Biosensors and Bioelectronics, vol. 41, pp. 328-334, 2013.

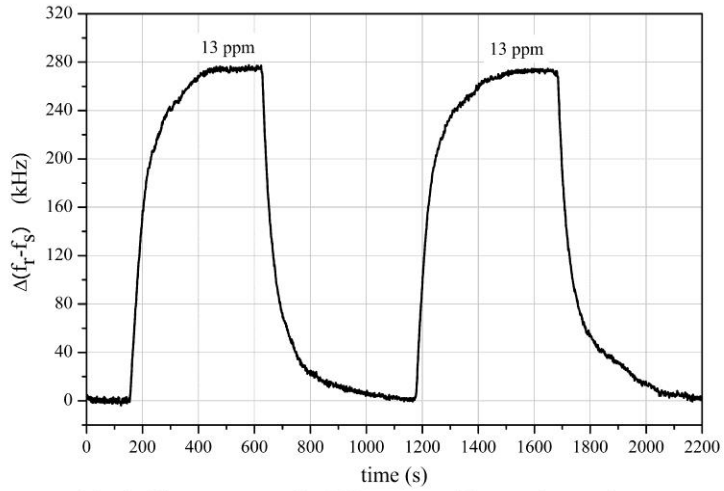

Fig. 1: Time response of pOBP sensor to 13 ppm of octenol.

IUS4-PD-5

A room temperature SAW based ethanol gas sensors

Wen Wang[1], Shitang He[1], **Haoliang Hu[2]**; *[1]Institute of Acoustics,Chinese Academy of Sciences, Beijing, Beijing, China, People's Republic of, [2]Institute of Acoustics, Chinese Academy of Sciences, Beijing, China, People's Republic of*

Background, Motivation and Objective

Surface acoustic wave (SAW) gas sensor have many unique properties as their small size, low cost, satisfactory sensitivity and reliability. This paper develops a novel room temperature cryptophane-A coated SAW sensor for ethanol gas sensing. High sensitivity, excellent reproducibility, and good linearity were observed in the gas sensor experiment.

Statement of Contribution/Methods

The present SAW gas sensor system utilizes a difference structure of dual-resonator-oscillator. The supermolecule of cryptophane-A was used as the sensitive interface towards ethanol gas owing to its amazing affinity. The selective and reversible interaction between the cryptophane-A and ethanol gas modulates the SAW phase velocity, which can be read out by recording the frequency change of the oscillator. Couple of modes (COM) model was performed to the SAW device simulation prior to fabrication.

Results/Discussion

Two parallel resonators with operation frequency of 300MHz one a same ST-X quartz wafer were fabricated by using a standard lithographic technique, and acted as the feedback element of the oscillator. The developed gas sensor system with a nickel-plated aluminum gas chamber was shown in Fig. 1(a). Fig. 1 (b) shows the measured frequency response of the SAW resonator, low insertion loss of ~5dB and high Q-value of ~3000 were observed. The cryptophane-A was coated on the SAW propagation path of the SAW resonator by using the spin coating of a mixtures of cryptophane-A, tetrahydrofuran, and SU8-3000 followed by curing. Before gas sensing, the frequency stability of the dual-resonator-oscillator was evaluated as shown in Fig. 1(c). Fig. 2 shows a typical response profile obtained from six consecutive 50 s on–off exposures to 1% of CH4, larger sensor response and excellent repeatability were observed.

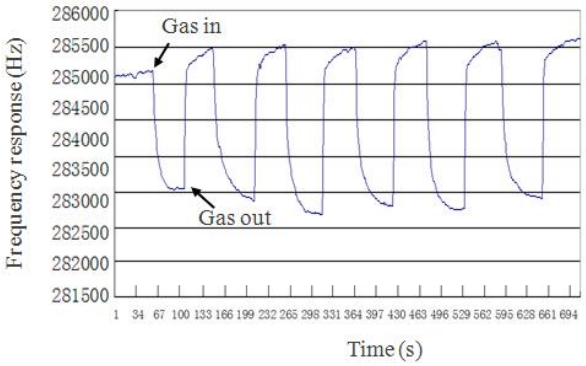

Fig. 2 SAW gas sensor experiment towards ethanol gas

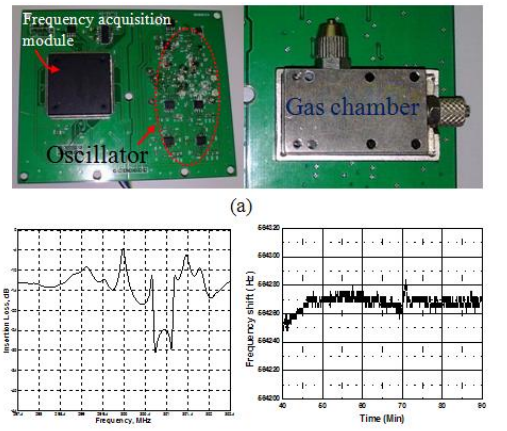

Fig. 1(a) the developed SAW gas sensor system, (b) measured frequency response of the SAW resonator, (c) frequency stability evaluation of the oscillator

IUS4-PD-6

Optimization of gold film thickness for SH-SAW biosensor on quartz

Mikihiro Goto[1,2], Hiromi Yatsuda[1], Jun Kondoh[2]; *[1]Japan Radio Co., Ltd., Fujimino-Shi, Saitama, Japan, [2]Graduate School of Science and Technology, Shizuoka University, Hmamatsu, Shizuoka, Japan*

Background, Motivation and Objective

Recently, an innovation platform for the detection and identification of the infectious agents that can be used by the patients has been required. There are various important requirements for the sensor platform, such as portable, cost per test, maximum achievable sensitivity and specificity, ease of use and so on. The authors have developed the surface acoustic wave (SAW) based biosensor on quartz which propagation area covered with a gold film [1], [2]. However, there are only few papers which have studied optimization of the gold film thickness of SAW biosensor on quartz.

Statement of Contribution/Methods

In order to optimize the gold film thickness of shear horizontal (SH) SAW biosensors on quartz, we have studied influence of liquid by numerical calculation method. The effect of the immunization reaction can be equivalent to viscosity changes of a liquid. The numerical calculation method which was proposed by Campbell and Jones has been generally used to obtain SAW propagation characteristics. On the other hand, in this paper, a numerical calculation method for propagation characteristics, which was a modified Campbell and Jones method involving influence of liquid viscosity was applied to quartz. As the SH-SAW on 36Y-90X quartz is pure SH-SAW, due to the shear horizontal nature, the SAW on it has only one displacement. The SH displacement at the surface drives shear fluid movement by viscosity coupling, which eventually results in additional increment of the propagation loss. Optimization of gold film thickness for the SH-SAW that structure of liquid/gold-film/36Y-90X quartz was discussed using the calculated velocities and attenuations of the SH-SAW.

Results/Discussion

The viscosity sensitivities of the SH-SAW with liquid were calculated as a function of the normalized gold film thickness, h/λ. The largest viscosity sensitivity of the SH-SAW is obtained when the gold thickness is about 0.015λ. On the other hand, the phase and amplitude changes are measured in the actual system [1], [2]. The phase and amplitude changes that are determined by the effective length of the SH-SAW delay-line depend on the gold film thickness. In our calculation, the maximum phase and amplitude changes are obtained at the gold film thickness of 0.03λ. Also at that thickness, the minimum error of the phase and amplitude changes due to thickness variation is achieved. In this paper, some experimental results using SH-SAW sensors on quartz with different gold film thickness are also shown for comparison with the numerical calculation results.

[References]

[1] M. Goto, et al., Proc. IEEE Ultrasonics Symp., 2010 p.736.

[2] M. Goto, et al., Proc. IEEE Ultrasonics Symp., 2012 5J-6.

IUS4-PD-7

Design of a coupled resonator 3dB Power Divider based on BAW Technology

Mercedes Jimenez[1], Edén Corrales[1], Pedro de Paco[1], Óscar Menéndez[1]; *[1]Telecommunications and Systems Engineering, Universitat Autonoma de Barcelona, Cerdanyola del Valles, Spain*

Background, Motivation and Objective

A power divider is a passive component that splits the input signal into two or more signals of lower power level. The most common type is an equal power division with 3dB output power level reduction.

Bulk Acoustic Wave (BAW) filters offer high performance and high level of miniaturization. Coupled Resonators Filters (CRF) are one of the existing BAW filter configurations. The Mason model is useful to study the CRF performance.

This paper describes an innovative 3dB power divider based on three CRF sections.

Statement of Contribution/Methods

The CRF sections are electrically connected through the lower electrodes (Figure 1). The upper electrodes of each section are used as the input port and the two output ports. An equivalent behavior between the electric and mechanical fields is produced in the power divider regarding a single CRF.

Design techniques used for two-port CRF filters are extended here to a power divider. The synthesis is based on the coupling matrix approach for multiple coupled resonators with multiple outputs. The proposed 3-port network is designed with a Chebyshev filter response for the transmission responses S_{21} and S_{31}.

Results/Discussion

A power divider for application on W-CDMA receivers is designed at 2140 MHz assuming SMR resonators. Figure 2 shows the simulations results of the example. An order 4 equi-ripple Chebyshev response can be distinguished. The power divider has been designed with 15 dB return loss in all the passband (60 MHz).

The use of BAW technology overcomes the miniaturization issue. On the designed example the input section area (A_i) is 1.9e-8 m^2 and for output sections (A_o) is 9.6e-9 m^2. The proposed structure simplifies the fabrication because, except for the thickness of the uppermost electrode layer (t_{up}), the rest are uniform.

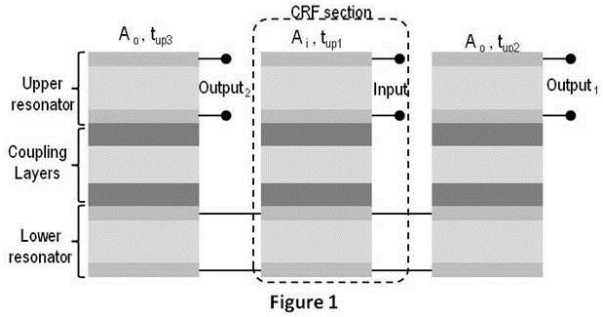

Figure 1

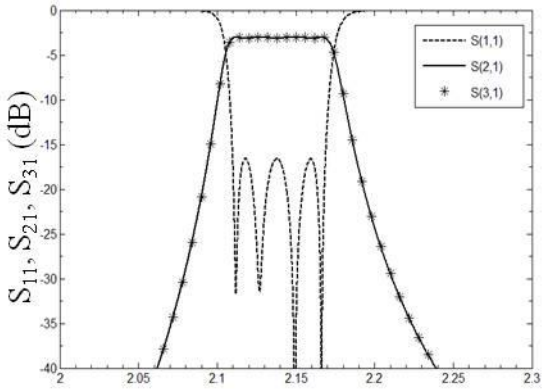

Figure 2

IUS4-PD-8

Wavelet versus Fourier for Wireless SAW sensors resonance frequency measurement

Pascal Rischette[1], Angel Scipioni[2], Omar Elmazria[3], Hamid Mjahed[3], Gérard Prieur[3]; *[1]Research Center of the French Air Force, France, [2]GREEN, France, [3]Institut Jean Lamour, France*

Background, Motivation and Objective

SAW resonators are more and more used as wireless and batteryless sensors. Both time domain and frequency domain readers are in competition to determine the resonance frequency of the sensor (f_r). The frequency domain method shows the advantage to use standard and then low cost components, but suffers from a low accuracy. If from a theoretical point of view, the smallest value of the spectral resolution is given by the Fourier transform (FT), the situation is significantly different when considering the experimental conditions. In fact, the transition from theory to practical experience inevitably introduces the notion of observation window T_0. Therefore, in a digital system, instead to be considered as infinitesimally small, the spectral resolution ΔF is constant and defined by $\Delta F = 1/T_0$.

This paper aims at exploring an alternative way offering more degrees of freedom, which consists to implement a time-based approach by using the wavelet transform (WT).

Statement of Contribution/Methods

The idea of this method is to perform a continuous WT on a lag of the signal with just few periods. The calculation of the WT modulus maxima shows that they appear at the extrema of the signal if a well-adapted wavelet is considered (Fig. 1). Thus, we show that the use of the WT leads to a simple calculation of half-period from which f_r. can be easily deduced.

Results/Discussion

The main advantages of WT are:

– Only 5% to 10% of the complete signal is required since only few periods are sufficient to get the frequency.

- The spectral resolution becomes variable unlike Fourier approach, and is directly related to the sampling frequency F_e.

An extension of the method allows distinguishing between two cases:

– The frequency f_r of the SAW is variable: we give the necessary conditions to obtain a better spectral resolution than the FT.

–f_r is fixed: we calculate an upsampling factor R obtained by the splines method and by the Shannon theorem.

Thus, we propose an expression for the factor R depending on the oscillation frequency f_r and above all on the desired spectral resolution ΔF.

For f_r = 5 MHz, T_0 = 15 µs, F_e = 2.5 GHz, we get the following spectral resolutions:

– ΔF = 66 kHz by FT,

– ΔF = 10 kHz by WT without upsampling,

– ΔF = 2 kHz by WT with an upsampling ratio R = 5.

A comparison of the two methods allows us to estimate the optimal implementing by evaluating their relative performances.

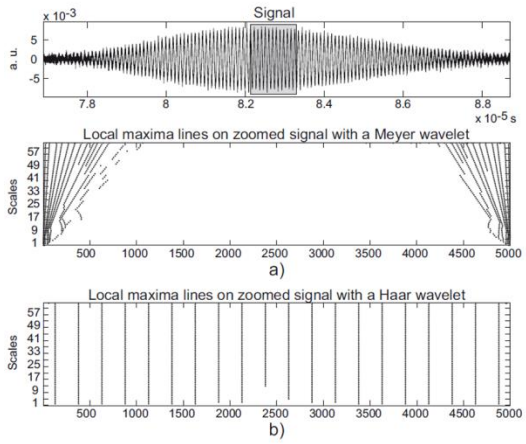

Fig. 1. The analyzed signal and modulus maxima lines of the continuous wavelet transform for: a) a bad wavelet, b) a good wavelet.

Transducer Design and Modeling

Forum Hall

Thursday, July 25 2013, 01:00 pm - 04:30 pm

Congress Hallair: **Reinhard Lerch**
Friedrich-Alexander-Universität Erlangen-Nuremberg

IUS5-PD-1

Estimation of multiple unknown constructive internal parameters from broadband "black box" models for matched contact piezoelectric probes

Abelardo Ruíz[1], Luis Alberto Castellanos[2], **Antonio Ramos[1]**, David K. Anthony[1], Hector Calas[3]; *[1]Ultrasonic Systems, CSIC, Madrid, Spain, [2]R&D, Matersys Group S.A, Mexico DF, Mexico, [3]Tecnatom S.A., S. Sebastian de los Reyes, Madrid, Spain*

Background, Motivation and Objective

Deep probe knowledge is mandatory to solve an old designers problem: to optimize the global responses in ultrasonic transceivers for Non-Destructive Evaluation (NDE) and Medical Imaging (MI). But, the construction details are practically unknown for the user in commercial probes. A prediction of these data is necessary for the numerical simulation tasks needed to electronically improve the final performance (efficiency, dynamic range and resolution) of ultrasonic transceivers. Genetic Algorithms (GA) have been used already in this field: a) for conjecturing, from experiments, which had been the effective design data of a constructed broadband un-matched probe [1], and b) for theoretically designing (narrowband / open-circuit) matched airborne probes [2], without experimental contrasting. Here, a GA-based procedure is aimed for "a posteriori" estimation of 5 internal constructing parameters, in broadband piezoelectric probes matched to radiation medium, and under a realistic spike excitation

Statement of Contribution/Methods

An original GA procedure is described for "inverse"-prediction of internal data in probes mechanically matched in their faces, which is based on a matrix model of matched ultrasonic transmitters. The Emission transfer function (ETF) module (considered under a spike driving) and peaks zones of the real & imaginary curves of input electrical admittance (Yin), calculated and measured in a real probe, are used to define the algorithm fitness function

Results/Discussion

Five unknown probe parameters: acoustic impedances of piezoceramic Zo, matching layer Zc, and backing Zb; layer thickness tc, and piezoelectric constant h33, were found with our GA approach. The agreement in resulting Yin curve was used as an index of estimation success (Fig. 1). Considering the noisy nature of transient measurements of ETF and the little distortions in practical experimental Yin, reasonable good results were obtained in parameters estimation, and in experimental - estimated comparison of ETF & Yin curves. This proves that our GA procedure behaves as a very valuable tool to discover hidden design data in NDE & MI matched ultrasonic probes

[1] A. Ruiz et al, Ultrasonics 42 (2004) 459–463
[2] S. Saffar et al. Ultrasonics 52 (2012) 169–185

Fig.1 Experimental and AG estimated curves:
a) Emitting Transfer Function (ETF)
b) Admittance Modulus (Yin)

.

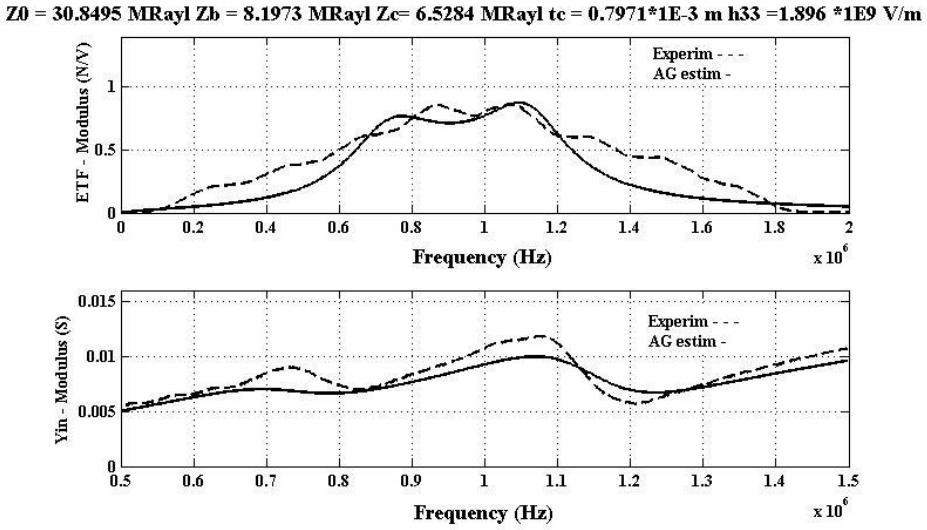

IUS5-PD-2

Determination of All the Complex Material Constants of the Piezoelectric Single Crystals PMN-28%PT by a New Automated Iterative Method

Yongrae Roh[1], Jinwook Kim[1], Cheeyoung Joh[2]; *[1]School of Mechanical Engineering, Kyungpook National University, Daegu, Korea, Republic of, [2]Agency for Defence Development, Korea, Republic of*

Background, Motivation and Objective

In recent years, extensive researches have been performed on the PMN-PT single crystals owing to their superior electromechanical properties compared with conventional piezoceramics. Their high electromechanical coupling factor and high energy density provide larger bandwidth and reduced size for acoustic and ultrasonic transducers in various applications. For both fundamental study and device design purposes with the single crystals, however, it is necessary to have a complete set of material constants. Further, precise design and analysis of the piezoelectric devices necessitates complex material constants because the imaginary terms contain the information on the loss mechanism of the material. Although material constants of PMN-PT single crystals in real numbers have been reported in several literatures, their full complex properties have not been investigated, yet.

Statement of Contribution/Methods

A number of methods, such as static and quasi-static, resonance, pulse-echo ultrasonic techniques and their combinations have been used to identify the material constants of piezoelectric crystals. Each method has its own advantages and limitations over the other methods. For instance, the conventional resonance measurement can provide the material constants in real numbers only, and cannot consider the effects of loss inside the material. In this work, a new automated iterative method has been developed to determine the complex material constants of PMN-28%PT single crystals that were grown by the Bridgman method to have tetragonal 4mm symmetry. Five resonator specimens of different configurations were used to analyze distinctive impedance and admittance spectra of each resonant mode. All the complex material constants were determined through nonlinear regression of the complex impedance and admittance spectra of the resonators as functions of frequency.

Results/Discussion

Table 1 summarizes all the complex material constants including six elastic compliance constants, three piezoelectric constants, and two dielectric constants determined in this work. The efficacy of the new characterization method and the accuracy of the determined material constants were verified through comparison of measured impedance spectra of the resonators with those calculated numerically with the determined constants, which showed excellent agreement.

Table 1. Determined complex material constants of the PMN-28%PT crystals.

Elastic compliance constants [10^{-12} m^2/N]	s_{11}^E	40.6 - *i* 0.15	Piezoelectric strain constants [10^{-12} C/N]	d_{31}	-548 + *i* 0.85
	s_{12}^E	-21.0 + *i* 0.14		d_{33}	1280 - *i* 15.4
	s_{13}^E	-19.7 + *i* 0.25		d_{15}	171 - *i* 6.66
	s_{33}^E	48.4 - *i* 1.03	Dielectric constants [10^{-9} F/m]	$\varepsilon_{11}^T/\varepsilon_0$	17.4 - *i* 0.89
	s_{44}^E	14.9 - *i* 0.09		$\varepsilon_{33}^T/\varepsilon_0$	44.3 - *i* 1.18
	s_{66}^E	27.5 - *i* 0.93			

IUS5-PD-3

Combined physical and statistical modeling of laser induced ultrasound signals from thin light absorbing films

Tomas Linder[1], Erika Svanström[1], **Johan E. Carlson**[2]; *[1]EISLAB, Lulea University of Technology, Lulea, Sweden, [2]Div. of Systems and Interaction, Lulea University of Technology, Lulea, Sweden*

Background, Motivation and Objective

A thermoelastic model of laser-generated acoustic pressure waves from thin layers of optically absorbing media (PET) is compared with measurements to determine the voltage responses from a polymer (PVDF) transducer. A physical model is first developed to predict the acoustic pressure wave generated in the thin film. The second step is then to link the transducer output voltage to the pressure wave, i.e. to account for the combined effects of the propagation medium and the transducer's electro-mechanical transfer function. The results are then compared with experimental measured output voltages, $v(t)$.

The overall objective is to be able to predict the output voltage resulting from exciting a thin PET layer with known material characteristics, with a short laser pulse, thus facilitating the customization and optimization of such optoacoustic setups.

Statement of Contribution/Methods

The properties of the thin film were varied in a designed experiment consisting of 9 different configurations and replicates, resulting in a total of 14 experiments. For each of the configurations, the theoretical sound pressure, $p(t)$, was determined by solving the 1D photoacoustic wave equation for thermoelastic expansion in a light-absorbing layer of a laser pulse. The link between the modeled pressure and the measured transducer output voltage $v(t)$, were then established through a multivariate calibration scheme.

Results/Discussion

The figure shows one example of the measured and modeled voltages, respectively, given the acoustic pressure, $p(t)$, determined from the material properties of the thin PET film. The paper presents the corresponding results for all PET film configurations, along with an analysis of the uncertainty and predictive performance of the multivariate calibration scheme. We also show how the process can be reversed, i.e. how the theoretical sound pressures can be estimated from the measured voltage signals.

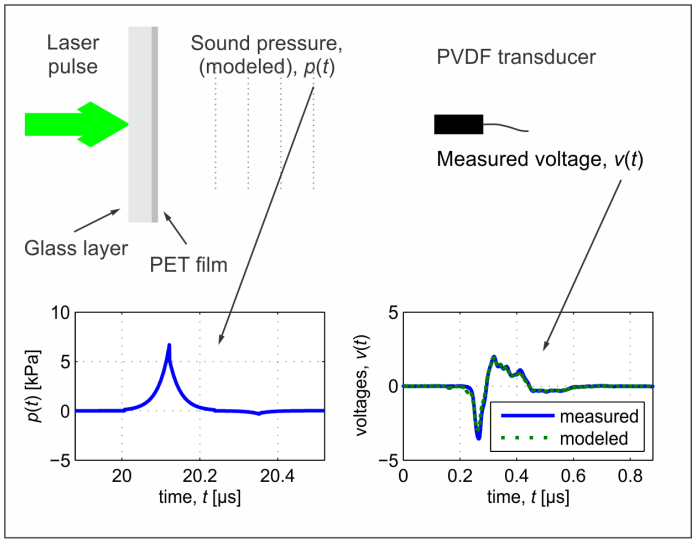

IUS5-PD-4

Thermal Stability Investigation of 1-3 Piezocomposites for Underwater Transducers

Erman Uzgur[1], Geoff Steel[1], Chris Gibbs[1]; [1]*Maritime Services, BAE Systems, Portsmouth, Hampshire, United Kingdom*

Background, Motivation and Objective

Thermal management is an important parameter for ultrasonic transducers. High power applications require a knowledge of loss and heating in the structure. 1-3 piezocomposites are widely used in design of transducers in BAE systems for underwater applications but the effects of driving the composite transducers at high power levels need further investigation. These may include likely destructive effects on the composite and behavior of insulating layers such as backings, matching layer and over-mould. Thermal issues have to be examined and controlled by experimental prototyping first and then proper modelling and simulation for future transducer design and manufacturing.

Statement of Contribution/Methods

In this study, thermal stability of 1-3 piezocomposite underwater transducers were examined by experimental prototyping first and then electromechanical modelling and simulations.

Piezocomposites were manufactured by the classical dice and fill method. Miniaturized thermistors were embedded in various thicknesses of backing material as well as to the surface of the ceramic for the purpose of monitoring the temperature change during operation.

After testing admittance and underwater properties of transducers, heating effects were examined under different driving conditions.

Experimental results were compared with simulations carried out by a transmission line model.

Finally, a new transducer design to control the thermal dissipation in transducer was introduced, manufactured and tested.

Results/Discussion

Simulation results were in good agreement with experiments. It was found that internal heating of the backing material due to sound absorption was greater than heating by conduction from the ceramic. As a result, backing material characteristics are the main restrictions for the maximum power applied to the transducer rather than active piezoelectric material itself.

Simulations showed that with new thermally controlled transducer design, applied power can be doubled without any heating problem.

IUS5-PD-5

Calculation of diffraction loss between non-co-axial ultrasonic transducer configurations

Abhinav Gupta[1], Maik Hoffmann[2], Mario Kupnik[2]; [1]*Indian Institute of Technology, Kharagpur, India,* [2]*Brandenburg University of Technology (BTU), Cottbus, Germany*

Background, Motivation and Objective

Theoretical and experimental methodologies are presented for determining the diffraction loss between circular ultrasonic transducers of finite size with the main focus on generic non-coaxial configurations. Our main objective in this work is to provide and validate a closed-form equation for the diffraction loss, including the derivation. This will be valuable for numerous practical applications. Examples are arbitrary pitch-catch-based acoustic measurement systems, such as anemometers and ultrasonic flow meters; hydrophone measurements; and transducer characterization systems.

Statement of Contribution/Methods

In contrast to existing approaches [e.g. K. Beissner, ACUSTICA, vol. 49, pp.: 212-217, 1981] the transducers can be located off-center with an arbitrary tilt angle between the two transducer planes. Thus, our obtained quadruple integral expression can be seen as a valuable extension and with today's computers it can be efficiently solved by means of numerical integration. The expression for pressure at any point due to a transducer with either a pressure released or rigid baffle was obtained by using the according Rayleigh-Sommerfeld integrals [G. Kino, Acoustic waves, 1987]. Then, we performed the surface integral on these expressions for finding the acoustic pressure at the receiving transducer. By using superposition we generalized the approach for the non-coaxial configuration with arbitrary tilt angle. We tested the approach by modeling circular piston transducers and bending-plate transducers in (0,1) mode. We investigated and compared several numerical integration methods available in the commercially available software package Mathematica (v8). The main focus was on identifying an efficient and accurate way of solving the expression.

Results/Discussion

The best performance was obtained with the Levin method and the faster, but less accurate, adaptive Monte Carlo method. The computation time ranges from a couple of minutes to several hours on a regular 64-Bit quad-core machine depending on both the configuration geometry and whether one comes close to the near field region. In a first step, we verified our method by comparing to exact solutions from existing expressions, i.e. co-axial configurations without tilt. Our expression delivered identical solutions. Then, we

calculated the diffraction loss for various non-coaxial configurations with and without tilt and for validation we compared the results to measurements obtained from two ultrasonic transducers. We present several graphs that prove good agreement over a wide range of transducer locations and tilt angles, which validates our model. For example, for an angular variation of the configuration ranging from 0° to 90° tilt angle, the deviation was only 2.4% in average with a standard deviation of 4.9%. The generic nature of our integral expression ensures its wide and simple applicability for efficient diffraction loss calculations.

IUS5-PD-6

Membrane design of an all-optical ultrasound receiver

Suzanne Leinders[1], Wouter Westerveld[2], Jose Pozo[3], Paul Urbach[2], Nico de Jong[1], Martin Verweij[1]; *[1]Lab. of Acoustical Wavefield Imaging, Delft University of Technology, Delft, Netherlands, [2]Optics Research Group, Delft University of Technology, Delft, Netherlands, [3]Nano-instrumentation Department, Technical Sciences TNO, Delft, Netherlands*

Background, Motivation and Objective

Intravascular ultrasonography is nowadays widely used in the diagnostics of cardiovascular disease to assess the level of occlusion caused by atherosclerotic plaque. Diagnostic images could be obtained by bringing a catheter, containing the ultrasonic transducer, into the artery. However, respiratory motion can displace the catheter tip as much as 6 mm, resulting in serious deterioration of images. To improve the image quality, it is advantageous to use an array of many transducer elements in the arterial direction. Because the available size on the catheter tip is limited to 1 mm x 2 mm, there is a need for the miniaturization of the elements.

Statement of Contribution/Methods

We propose a novel type of ultrasound receiver array based on chip technology, in which one receiver element consists of an optical microring resonator that is integrated on an acoustical membrane (see Fig. 1). Incident ultrasonic waves deform the membrane, which induces strain in the Silicon microring resonator. This strain induces a shift in its optical resonance frequency, which is recorded. Integrated optical multiplexers allow simultaneous interrogation of many elements via as few as two optical fibers. This technology allows for a small footprint (e.g., 50 µm x 75 µm per element) and hence, for maximizing the amount of elements in the catheter.

Results/Discussion

To optimize the acoustical sensitivity of the receiver, finite element modeling using COMSOL Multiphysics has been performed. The influence of the size and thickness of the membrane on the acoustical behavior was investigated using both static and time domain analysis. To be able to give an proof of principle, we determined the frequency response of three prototype membranes (SiO2 with 2.5 µm thickness and 30 µm, 40 µm and 50 µm radius). The model shows that the 40 µm receiver has a resonance frequency in water of 1.6 MHz and a sensitivity of 3.4 microstrain/kPa. In combination with a strain sensor as in Ref. 2 and an optical detector with a reso-lution of 1 pm, a minimum detection level of 590 Pa is obtained.

The results lead to the conclusion that this technology is a suitable candidate for miniaturized non-electrical ultrasound receivers.

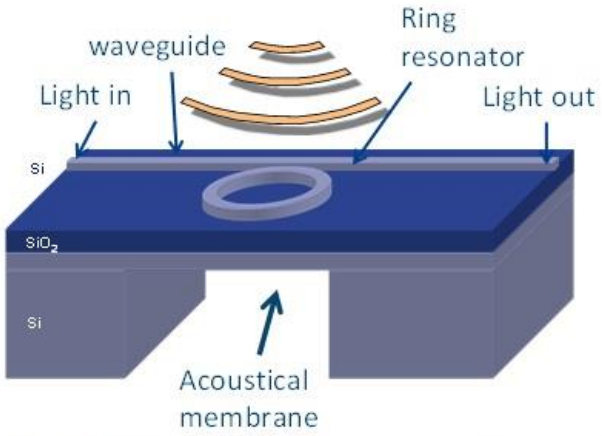

Fig. 1: Sketch of the proposed ultrasound receiver element

IUS5-PD-7

Coupled Vibration Analysis for a Piezoelectric Array element Using Superposition Method

Daeseung Kim[1], Myungdeok Kim[2], Kookjin Kang[2], Keonho Son[2]; *[1]New Business Department, Alpinion Medical Systems, Korea, Republic of, [2]Alpinion Medical Systems, Korea, Republic of*

Background, Motivation and Objective

The coupled vibration was analyzed for a piezoelectric array element of two-dimensional structure whose vibration can be described by two coupled differential equations with coupled boundary conditions. The exact solutions satisfying both equations of motion and boundary conditions are not available. Therefore, the approximate solutions were obtained using the superposition method suggested for the accurate vibration analysis of the elastic structures.

Statement of Contribution/Methods

To this end, the mechanical and electric displacements were represented in terms of the Levy-type solutions satisfying the differential equations, and then, the mechanical and electrical boundary conditions were satisfied approximately by summing the stress and the electric potential obtained from the displacements. The frequency spectrum and the electro-mechanical coupling factor of the element varying the width/thickness ratio were calculated and compared with the results of the finite element analysis and experiment.

Results/Discussion

As the ratio of thickness to width increases, the fundamental frequency and the electro-medhanical coupling factor of the array element increase. The theoretically calculated results has shown good agreement with the results of the finite element analysis. The superposition method was verified to provide the accurate analysis for a piezoelectric array element.

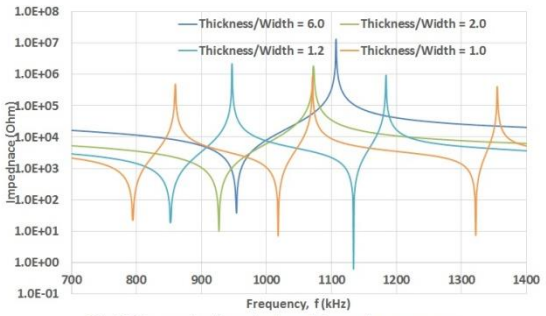

Fig.1 Theoretically calculated impedance curves according to the aspect ratio, thickness/width

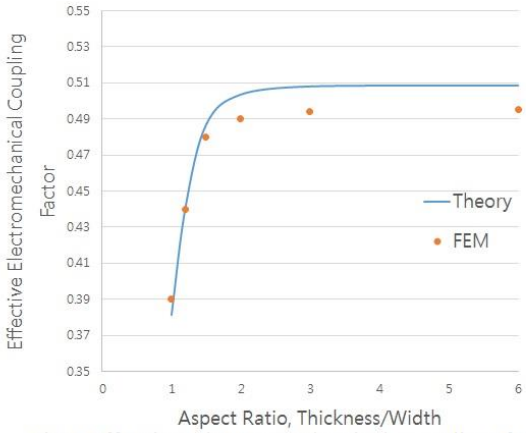

Fig.2 Effective electromechanical coupling factor according to the aspect ratio, Thickness/Width

IUS5-PD-8

Design and modelling of an integrated device for acoustic resonance spectroscopy

Megha Agrawal[1], Ying Zhou[1], Jayesh R. Bellare[2], Ashwin A. Seshia[1]; *[1]University of Cambridge, United Kingdom, [2]Indian Institute of Technology, Bombay, India*

Background, Motivation and Objective

This paper investigates the design and modelling of an integrated device for acoustic resonance spectroscopy (ARS). ARS is a technique to characterize samples using piezoelectric transducers whereby a signature of a specimen of interest is obtained through the acoustic resonance spectrum. By integrating the transducers together with a sample handling system, an integrated platform may be realised that reduces some of the geometrical variability associated with the measurement. Further, miniaturisation of such platforms can be achieved using MEMS technology thereby enabling scaling of device dimensions to investigate smaller specimens while simultaneously operating at higher frequencies.

Statement of Contribution/Methods

In this paper, we propose an integrated device where the transducers are mounted in close proximity with the specimen to be analysed (e.g. by integrating ultrasound transducers within a microfluidic channel). A finite element (FE) model and a simplified analytical model have been constructed to predict the acoustic response of a sample embedded in such a device configuration. A representative FE simulation is performed in COMSOL by embedding the transmitting and receiving piezo-material in various fluid media. Resonant frequencies associated with the measurement can be extracted from this data.

Results/Discussion

The response of various media modelled through FEA matches with analytical predictions for a range of biological media. A variety of biological media may be distinguished by using the measured resonant frequencies as a signature of relevant physical characteristics. This study establishes the modelling basis of an integrated acoustic resonant spectrometer that may then be extended to examine the impact of geometrical scaling on system resolution.

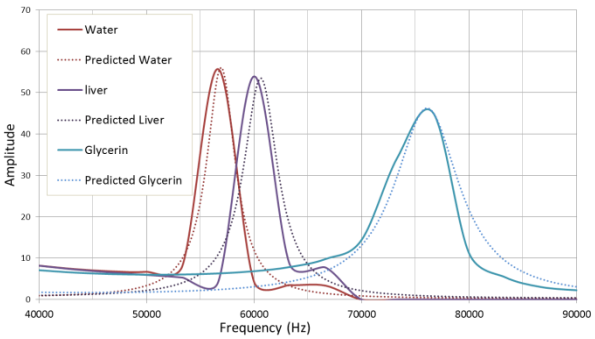

Fig 2: Modelled frequency for various media showing a good match between the response predicted by finite element analysis and analytical modelling.

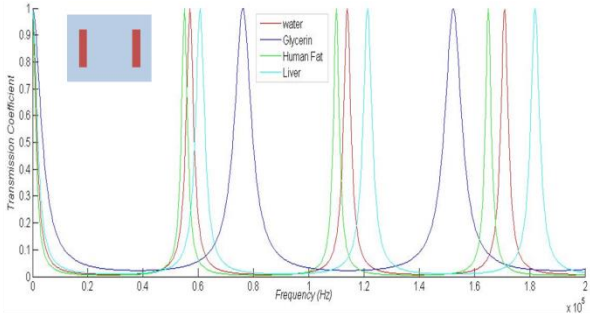

Fig 1: PZT-Fluid-PZT system. Analytical model for transmission coefficient is plotted for various media. Inset shows the schematic design (not drawn to scale)
Blue represents fluid and red represent piezoelectric transducer blocks
(PZT5A, diameter=8mm;thickness=0.3mm. Distance between transducers=13mm)

IUS5-PD-9

Modeling of CMUTs with Square Anisotropic Plates

Mette Funding la Cour[1,2], Thomas Lehrmann Christiansen[2], Christian Dahl-Petersen[2], Jørgen Arendt Jensen[1], Erik Vilain Thomsen[2]; *[1]Center for Fast Ultrasound Imaging, Dept. of Elec. Eng., Technical University of Denmark, Kgs. Lyngby, Denmark, [2]Department of Micro- and Nanotechnology, Technical University of Denmark, Kgs. Lyngby, Denmark*

Background, Motivation and Objective

Precise modeling of capacitive micromachined ultrasonic transducers (CMUT) is important for an efficient design process. Most analytical approaches use the isotropic plate equation to obtain the deflection *w(x,y)*. However, when the plate consists of silicon, which is an anisotropic material, this needs to be taken into account. We have previously calculated the plate bending for an anisotropic plate with circular geometry and have now expanded the theory to include square plates.

Statement of Contribution/Methods

A CMUT can mechanically be described as a square plate of sidelength *2L*, thickness *h*, exposed to a uniform load *p*. Having a square plate makes analytical calculations complicated and approximate methods must be used. The Galerkin method is used to find approximate expressions for the deflection of a thin anisotropic square plate. A differential operator is defined from the full anisotropic plate equation and the Galerkin system of equations can then be defined. The deflection profile is approximated by a polynomial series which is inserted into the Galerkin system, giving a linear equation system that can be solved.

Results/Discussion

Trial functions are used to find the deflection. When a square (100) silicon plate is aligned to the <110> direction (the flat), the symmetry is simplified from a tetragonal to a cubic structure and a simple expression for the deflection is obtained.

The figure shows a comparison between the analytical solution using the Galerkin method for a square plate of silicon (001), the isotropic solutions corresponding to [100] or [110] directions, finite element (FEM) simulations made using the full anisotropic stiffness tensor in COMSOL and a deflection profile measurement on a fabricated CMUT, 65x65 µm wide and 2.5 µm thick plate. The calculated deflections are normalized to the FEM center deflection, and the measured deflection is normalized to itself to be able to compare the profiles. Excellent agreement is shown between the anisotropic case and both FEM and measurement with a deviation of less than 0.7 % from FEM and 2 % from the measurements for the distance between [-0.5,0.5]. The isotropic approach leads to errors in the center deflection of around 10 %. Using the anisotropic expression for the deflection the parameters in a lumped element model for the CMUT are presented and used for prediction of e.g. bandwidth and resonance frequency.

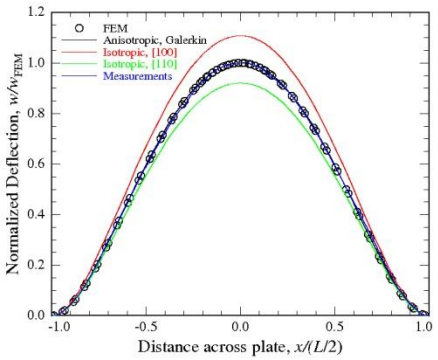

IUS5-PD-10

Modelling of Electric Field and Stress in Piezoelectric Composite under Bending Load in Quasi-static Conditions

Guillaume Beckers[1], Bruno Dehez[2]; [1]*Centre for Research in Mechatronics, Université Catholique de Louvain (UCL), Belgium,* [2]*Université Catholique de Louvain (UCL), Belgium*

Background, Motivation and Objective

Piezoelectric benders are laminated structures composed of passive and active layers made in elastic and piezoelectric materials respectively. Those structures have many applications as actuator or sensor in various field where a high dynamic is necessary in a compact device. Benders have been widely studied but most of models don't take in consideration the evolution of the electric field in layer's thickness and its impact on the stress in the piezoelectric material. A finite-element model of a monomorph shows the maximum value of the electrical field is more than 15 percent higher than the average value. It demonstrates the interest of taking into account the evolution of the electric field and its impact on the stress for actuator and sensors sizing.

Statement of Contribution/Methods

In this study, constitutive equations of laminated structures are developped based on the static equilibrium of forces and moments. Cross sections are supposed to remain planar after deformation. Bonding between layers is supposed to ensure strain continuity. Moreover, the model incorporates the effect of the transverse stress. Evolution of the electric field and its impact on the stress are supposed to have second order effects on the strain. Those assumptions give an electric field that varies linearly accross the piezoelectric layer and which is different of zero in the non-electrically loaded layers.

The analytical model obtained is then compared to a finite-element model of a monomorph loaded by an electrical field and mechanical load. Both models are compared for a given set of parameters.

Results/Discussion

The comparison shows a good fit of finite-element analysis and analytical models. Fig. 1 shows the relative error on the longitudinal stress is reduced of more than 10 percent and the relative error on the electric field along the x-axis is less than 1.5 percent. Huge peak occurs because at some point the stress is null. The proposed analytical model shows a significant improvement in stress and electric field evaluation giving quite accurate values for those two critical physical quantity for actuator and sensor sizing.